

Nikolay I. Klev

---

Multiphase Flow Dynamics 2

Nikolay I. Kolev

# **Multiphase Flow Dynamics 2**

Thermal and Mechanical Interactions

3rd Edition

With 309 Figures

Nikolay Ivanov Kolev, PhD., DrSc.

Möhrendorferstr. 7

91074 Herzogenaurach

Germany

Nikolay.Kolev@herzovision.de

Library of Congress Control Number: 2007923416

ISBN 978-3-540-69834-0 Springer Berlin Heidelberg New York

ISBN 978-3-540-22107-4 2nd Edition Springer Berlin Heidelberg New York

This work is subject to copyright. All rights are reserved, whether the whole or part of the material is concerned, specifically the rights of translation, reprinting, reuse of illustrations, recitation, broadcasting, reproduction on microfilm or in other ways, and storage in data banks. Duplication of this publication or parts thereof is permitted only under the provisions of the German Copyright Law of September 9, 1965, in its current version, and permission for use must always be obtained from Springer-Verlag. Violations are liable to prosecution under German Copyright Law.

Springer is a part of Springer Science+Business Media

[springer.com](http://springer.com)

© Springer-Verlag Berlin Heidelberg 2002, 2005 and 2007

The use of general descriptive names, registered names, trademarks, etc. in this publication does not imply, even in the absence of a specific statement, that such names are exempt from the relevant protective laws and regulations and therefore free for general use.

Production: Integra Software Services Pvt. Ltd., Pondicherry, India

Cover design: Erich Kirchner, Heidelberg

Printed on acid-free paper SPIN: 11926139 45/3100/Integra 5 4 3 2 1 0

*To Iva, Rali and Sonja with love!*



*Autumn in Bulgaria, Oct. 2005, Nikolay Ivanov Kolev, 36× 48cm oil on linen*



## A few words about the third extended edition

The reader will find in the third edition the information already included in the second one improved and extended in several places. Only the differences will be mentioned here.

Chapter 1 contains additionally important velocity scales definition frequently used in defining flow pattern maps. Additional information is available for flow pattern in rod bundles. Chapter 2 is extended with a provision of constitutive relationships for the lift- and virtual mass forces. The drag force section is updated with recent information. Discussion is provided for the uncertainty of the film-gas forces. Chapter 3 contains additionally the Rehmes method for computation of: pressure drop of flow in channels with arbitrary cross section; pressure drop in rod bundles axial and cross flow; pressure drop of spacers for rod bundles of nuclear reactors. Chapter 5 considering entrainment in annular two-phase flow is updated. Discussion is provided in entrainment increase in boiling channels, residual film thickness during dry out, entrainment increase due to obstacles. Estimation of the uncertainty of the existing state of the art is performed based on dry out process in boiling channel. Chapter 6 considering deposition in annular flow is updated. Discussion is provided on the influence of the nucleate boiling inside the film and on the heat transfer due to the bouncing of the droplets onto the hot wall. Estimation of the uncertainty of the existing state of the art is performed based on dry out process in boiling channel. Chapter 15 considering the bubble departure mechanism on heated wall is updated. The theory is extended to subcooled liquid. Chapter 16 considering nucleate boiling is updated. Additional information coming from boiling of fluids with nano-particles confirm the sound physical basics of the authors method. Additional information is provided for nucleation site density at high pressure. Chapter 18 considering boiling of subcooled liquid is updated. Chapter 19 considering forced convection boiling is updated. The 2005 look-up-table by Groeneveld et al. is demonstrated to be an excellent scaling base for critical heat flux in bundles for variety of geometries and conditions. Chapter 24 considering condensation at cooled walls is updated. Test examples are provided for demonstration of the application of the theory.

As in the previous edition, due to the large number of the color pictures in Chapters 14 of volume 1 and Chapter 26 of this volume they are included as a PDF-files in the attached CD. Chapter 26 of this volume is completely rewritten. First, Section 26.2 contains a quick look of the IVA computer code with several interesting demonstration of the power of the technology described in this three Volumes work. A list of references is provided in Sections 26.3 and 26.4 documenting the IVA-code development and validation. Review of the state of the

art of the instability analyses of boiling systems is provided and interesting comparison of the modern IVA-predictions with large scale AREVA- experiments is provided in Section 26.6.3. Powerful demonstration of the methods for analysing pressure wave propagations in single and two-phase systems is given by comparison with the Interatome experiments from 1983 performed on simple and complex pipe-networks, Section 26.8.3. Section 26.15 contains comparison with 333 experiments for variety of bundles, flow regimes including dry out, steady state and transients. It clearly demonstrates the power of the method and its well defined uncertainty to simulate boiling processes in complex geometry.

And finally, Section 26.21 contains the discussion regarding: Is it possible to design universal multiphase flow analyser? It contains my personal vision for future development of the multiphase fluid dynamics.

Erlangen, September 2006

Nikolay Ivanov Kolev

# Summary

This monograph contains theory, methods and practical experience for describing complex transient multi-phase processes in arbitrary geometrical configurations. It is intended to help applied scientists and practicing engineers to understand better natural and industrial processes containing dynamic evolutions of complex multi-phase flows. The book is also intended to be a useful source of information for students in the high semesters and in PhD programs.

This monograph consists of three volumes:

Vol. 1 Fundamentals (14 Chapters and 2 Appendixes), 750 pages + 322 pages + movies on CD-ROM

Vol. 2 Mechanical and thermal interactions (26 Chapters), 912 pages

Vol. 3 Selected chapters: turbulence, gas absorption and release by liquid, diesel fuel properties, 300 pages

In Volume 1 the concept of three-fluid modeling is presented in detail "from the origin to the applications". This includes derivation of local volume- and time-averaged equations and their working forms, development of methods for their numerical integration and finally finding a variety of solutions for different problems of practical interest.

Special attention is paid in Volume 1 to the link between the partial differential equations and the constitutive relations called closure laws without providing any information on the closure laws. Volume 2 is devoted to these important constitutive relations for mathematical description of the mechanical and thermal interactions. The structure of the volume is in fact a state-of-the-art review and selection of the best available approaches for describing interfacial transfer processes. In many cases the original contribution of the author is incorporated in the overall presentation. The most important aspects of the presentation are that it stems from the author's long years of experience developing computer codes. The emphasis is on the practical use of these relationships: either as stand-alone estimation methods or within a framework of computer codes.

In particular, Volume 2 contains information on how to describe the flow patterns and the specific mechanical and thermal interactions between the velocity fields in flight. In Chapter 1 the flow regime transition criteria in transient multi-phase flows are presented for the cases of pool flow, adiabatic flow, channel flow in vertical pipes, channel flow in inclined pipes, heated channels, porous media, particles in film boiling and rod bundles. The idea of flow pattern boundaries depending on the transient evolution of the particle number and particle size is pre-

sented. Chapter 2 collects information about modeling the drag forces on a single bubble, a family of particles in a continuum, droplets in a gas, solid particles in a gas in the presence of liquid, solid particles in a liquid in the presence of a gas, solid particles in a free particles regime, solid particles in bubbly flow, solid particles in a densely packed regime, annular flow, inverted annular flow, stratified flow in horizontal or inclined rectangular channels and stratified flow in horizontal or inclined pipes. Chapter 3 presents information about the friction pressure drop in single- and multi-phase flow. Historically algebraic correlations for describing the velocity difference preceded the development of interfacial interaction models. The large number of empirical correlations for the diffusion velocities for algebraic slip models for two- and three-phase flows is provided in Chapter 4. Chapters 5 and 6 are devoted to the entrainment and deposition in annular two-phase flow, respectively. Chapter 7 gives an introduction to the fragmentation and coalescence dynamics in multi-phase flows. Acceleration-induced droplet and bubble fragmentation is described in Chapter 8. Chapter 9 is devoted to the turbulence-induced particle fragmentation and coalescence and Chapter 10 to the liquid and gas jet disintegration. Chapter 11 presents the state of the art on the fragmentation of melt in coolant in a variety of its aspects. Chapter 12 presents nucleation in liquids. Chapter 13 presents different aspects of the bubble growth in superheated liquid and the connection to computational system models. Condensation of pure steam bubbles is considered in Chapter 14. New information with respect to the bubble departure diameter and nucleate boiling is presented in Chapters 15 and 16, respectively. An interesting result of the theory presented in these chapters is the prediction of a critical heat flux without empirical correlation for critical heat flux as a result of the mutual bubble interaction for increasing wall superheating. Applying the theory for the inverted problem of the flashing of superheated water in pipes as given in Chapter 17 surprisingly supported the validity of the new approach. The state of the art in boiling theory is presented in Chapters 18 to 21 where boiling in subcooled liquid, natural convection film boiling, critical heat flux, forced convection film boiling, and film boiling on vertical plates and spheres is presented. The emphasis is on the elaboration of all coupling terms between the fluids, and between the wall and fluid required for closure of the overall description. Chapter 22 provides information on all heat and mass transfer processes across a droplet interface starting with the nucleation theory, and going through the droplet growth, self-condensation stop, heat transfer across a droplet interface without mass transfer, direct contact condensation of pure steam on a subcooled droplet, spontaneous flushing of a superheated droplet, evaporation of a saturated droplet in superheated gas, and droplet evaporation in a gas mixture. A similar approach is applied to the description of the interface processes at a film-gas interface in Chapter 23 with a careful treatment of the influence of the turbulent pulsation on the interfacial heat and mass transfer. A set of empirical methods for prediction of condensation on cooled walls with and without a non-condensable is presented in Chapter 24. Chapter 25 provides information on the implementation of the discrete ordinate method for radiation transport in multi-phase computer codes. In this chapter the dimensions of the problem, the differences between micro and macro interactions and the radiation transport

equation are discussed. Then the finite volume representation of the radiation transport is given and different aspects of the numerical integration are discussed. The computation of some material properties is discussed. Then three specific radiation transport cases of importance for the melt-water interaction are discussed in detail: a spherical cavity of gas inside a molten material; concentric spheres of water droplets, surrounded by vapor surrounded by molten material; clouds of spherical particles of radiating material surrounded by a layer of vapor surrounded by water. For the last case the useful *Lanzenberger* solution is presented and its importance is demonstrated in two practical cases.

The book ends with Chapter 26, which provides information on how to verify multi-phase flow models by comparing them with experimental data and analytical solutions. The complexity of the problems is gradually increased from very simple ones to problems with very complex melt-water interaction multi-fluid flows with dynamic fragmentation and coalescence and strong thermal and mechanical interactions. In particular the following cases are described and compared with the prediction using the basics presented in different chapters of this book: material relocation – gravitational waves (2D), U-tube benchmarks such as adiabatic oscillations, single-phase natural convection in a uniformly heated vertical part of a U-tube, single-phase natural convection in a uniformly heated inclined part of a U-tube, single-phase natural convection in a U-tube with an inclined part heated by steam condensation, steady state single-phase nozzle flow, pressure waves in single phase flow, 2D gas explosion in a space filled previously with gas, 2D gas explosion in space with internals previously filled with liquid, film entrainment in pipe flow, water flashing in nozzle flow, pipe blow-down with flashing, single pipe transients, complex pipe network transients, boiling in pipes and rod bundles, critical heat flux, post critical heat flux heat transfer, film boiling, behavior of clouds of cold and very hot spheres in water, experiments with dynamic fragmentation and coalescence like the FARO L14, 20, 24, 28, 31 experiments, PREMIX 13, 15, 17, 18 experiment, RIT and IKE experiment. In addition an application of a powerful method for investigation of the propagation of input and model uncertainties on the final results by using the Monte Carlo method and regression analysis is demonstrated for the prediction of non-explosive melt-water interactions. Benchmarks for testing the 3D capabilities of computer codes are provided for the rigid body steady rotation problem, pure radial symmetric flow, radial-azimuthal symmetric flow. Examples of very complex 3D flows are also given such as small break loss of coolant, asymmetric steam-water interaction in a vessel, and melt relocation in a pressure vessel.

Chapter 26 of this volume together with Chapter 14 of Volume 1 are presented on the compact disc (CD) attached to Volume 1. The reader can read these two documents with Acrobat Reader software, which is freely available on the internet. In addition many animated sequences (movies) have been presented on the CD. The reader can execute them directly from the already-opened document with Acrobat Reader by simply double clicking on the figures numbers marked in blue. HTML documents are then executed using any Web browser available on the local computer of the reader. The reader can see also these movies with any other software able to open animated GIF files, for instance with PaintShopPro software.

# Table of contents

Chapter 14 of volume 1 and Chapter 26 of volume 2 are available in pdf format on the CD-ROM attached to volume 1. The system requirements are Windows 98 and higher. Both pdf files contain links to computer animations. To see the animations, one double clicks on the active links contained inside the pdf documents. The animations are then displayed in an internet browser, such Microsoft Internet Explorer or Netscape. Alternatively, gif-file animations are also provided.

<b>1</b>	<b>Flow regime transition criteria</b>	<b>1</b>
1.1	Introduction	1
1.2	Pool flow	3
1.3	Adiabatic flows	6
1.3.1	Two important velocity scales	6
1.3.2	Channel flow – vertical pipes	9
1.3.3	Channel flow – inclined pipes	13
1.4	Heated channels	20
1.5	Porous media	21
1.6	Particles in film boiling	22
1.7	Rod bundles	23
	Nomenclature	25
	References	28
<b>2</b>	<b>Drag, lift and virtual mass forces</b>	<b>31</b>
2.1	Drag forces	31
2.1.1	Introduction	31
2.1.2	Drag coefficient for single bubble	32
2.1.3	Family of particles in continuum	35
2.1.4	Droplets-gas	39
2.1.5	Solid particles-gas in presence of liquid. Solid particles-liquid in presence of a gas	40
2.1.6	Annular flow	50
2.1.7	Inverted annular flow	59
2.1.8	Stratified flow in horizontal or inclined rectangular channels	60
2.1.9	Stratified flow in horizontal or inclined pipes	63
2.2	Lift force	68
2.3	Virtual mass force	72

Nomenclature.....	75
References .....	78
<b>3 Friction pressure drop .....</b>	<b>83</b>
3.1 Introduction.....	83
3.2 Single-phase flow.....	83
3.2.1 Circular pipes .....	83
3.2.2 Annular channels.....	86
3.2.3 Arbitrary channel form.....	86
3.2.4 Axial flow in rod bundles.....	87
3.2.5 Cross flow in rod bundles.....	91
3.2.6 Pressure drop at spacer for bundles of nuclear reactors .....	93
3.3 Two-phase flow.....	95
3.4 Heated channels .....	100
3.5 Three-phase flow.....	102
Nomenclature .....	105
References .....	106
<b>4 Diffusion velocities for algebraic slip models.....</b>	<b>109</b>
4.1 Introduction.....	109
4.2 Drag as a function of the relative velocity .....	110
4.2.1 Wall force not taken into account.....	110
4.2.2 Wall forces taken into account .....	114
4.3 Two velocity fields.....	115
4.3.1 Single bubble terminal velocity.....	115
4.3.2 Single particle terminal velocity.....	118
4.3.3 Cross section averaged bubble rise velocity in pipes – drift flux models.....	119
4.3.4 Cross section averaged particle sink velocity in pipes – drift flux models.....	136
4.4 Slip models.....	138
4.5 Three velocity fields – annular dispersed flow .....	140
4.6 Three-phase flow.....	141
Nomenclature.....	144
References .....	146
<b>5 Entrainment in annular two-phase flow.....</b>	<b>149</b>
5.1 Introduction.....	149
5.2 Some basics.....	150
5.3 Correlations.....	151
5.4 Entrainment increase in boiling channels.....	159
5.5 Residual film thickness at DO? .....	160
5.6 Entrainment increase due to obstacles .....	161
5.7 Size of the entrained droplets.....	161

Nomenclature .....	162
References .....	165
<b>6 Deposition in annular two-phase flow .....</b>	<b>169</b>
6.1 Introduction .....	169
6.2 Analogy between heat and mass transfer .....	169
6.3 Fluctuation mechanism in the boundary layer .....	171
6.4 <i>Zaichik's</i> theory .....	176
6.5 Deposition correlations .....	176
6.6 Leidenfrost heat transfer to droplet bouncing hot wall .....	180
Nomenclature .....	180
References .....	184
<b>7 Introduction to fragmentation and coalescence .....</b>	<b>187</b>
7.1 Introduction .....	187
7.2 General remarks about fragmentation .....	189
7.3 General remarks about coalescence .....	191
7.3.1 Converging disperse field .....	191
7.3.2 Analogy to the molecular kinetic theory .....	192
7.4 Superposition of different droplet coalescence mechanisms .....	196
7.5 Superposition of different bubble coalescence mechanisms .....	197
7.6 General remarks about particle size formation in pipes .....	198
Nomenclature .....	201
References .....	204
<b>8 Acceleration induced droplet and bubble fragmentation .....</b>	<b>207</b>
8.1 Critical <i>Weber</i> number .....	207
8.2 Fragmentation modes .....	216
8.3 Relative velocity after fragmentation .....	219
8.4 Breakup time .....	222
8.5 Particle production rate correlations .....	229
8.5.1 Vibration breakup .....	229
8.5.2 Bag breakup .....	229
8.5.3 Bag and stamen breakup .....	231
8.5.4 Sheet stripping and wave crest stripping following by catastrophic breakup .....	231
8.6 Droplets production due to highly energetic collisions .....	238
8.7 Acceleration induced bubble fragmentation .....	240
Nomenclature .....	243
References .....	245
<b>9 Turbulence induced particle fragmentation and coalescence .....</b>	<b>249</b>
9.1 Homogeneous turbulence characteristics .....	249
9.2 Reaction of a particle to the acceleration of the surrounding continuum .....	253



9.3	Reaction of particle entrained inside the turbulent vortex – inertial range.....	254
9.4	Stability criterion for bubbles in continuum.....	255
9.5	Turbulence energy dissipation due to the wall friction .....	259
9.6	Turbulence energy dissipation due to the relative motion.....	261
9.7	Bubble coalescence probability.....	262
9.8	Coalescence probability of small droplets.....	266
	Nomenclature .....	268
	References .....	270
<b>10</b>	<b>Liquid and gas jet disintegration.....</b>	<b>273</b>
10.1	Liquid jet disintegration in pools .....	273
10.2	Boundary of different fragmentation mechanisms .....	275
10.3	Size of the ligaments .....	277
10.4	Unbounded instability controlling jet fragmentation .....	278
10.4.1	No ambient influence .....	278
10.4.2	Ambient influence .....	280
10.4.3	Jets producing film boiling in the ambient liquid.....	282
10.4.4	An alternative approach .....	284
10.4.5	Jets penetrating two-phase mixtures.....	285
10.4.6	Particle production rate .....	285
10.5	Jet erosion by high velocity gas environment .....	285
10.6	Jet fragmentation in pipes .....	287
10.7	Liquid spray produced in nozzles .....	289
10.8	Gas jet disintegration in pools.....	289
	Nomenclature .....	292
	References .....	295
<b>11</b>	<b>Fragmentation of melt in coolant .....</b>	<b>297</b>
11.1	Introduction.....	297
11.2	Vapor thickness in film boiling.....	299
11.3	Amount of melt surrounded by continuous water .....	300
11.4	Thermo-mechanical fragmentation of liquid metal in water .....	301
11.4.1	External triggers.....	302
11.4.2	Experimental observations.....	307
11.4.3	The mechanism of the thermal fragmentation .....	312
11.5	Particle production rate during the thermal fragmentation.....	326
11.6	<i>Tang's</i> thermal fragmentation model .....	328
11.7	<i>Yuen's</i> thermal fragmentation model .....	330
11.8	Oxidation.....	331
11.9	Superposition of thermal fragmentation.....	332
11.9.1	Inert gases.....	332
11.9.2	Coolant viscosity increase .....	332
11.9.3	Surfactants.....	333
11.9.4	Melt viscosity .....	334

Nomenclature .....	334
References .....	337
<b>12 Nucleation in liquids .....</b>	<b>343</b>
12.1 Introduction .....	343
12.2 Nucleation energy, equation of <i>Kelvin</i> and <i>Laplace</i> .....	344
12.3 Nucleus capable to grow .....	345
12.4 Some useful forms of the <i>Clausius-Clapeyron</i> equation, measures of superheating .....	347
12.5 Nucleation kinetics .....	350
12.5.1 Homogeneous nucleation .....	350
12.5.2 Heterogeneous nucleation .....	351
12.6 Maximum superheat .....	357
12.7 Critical mass flow rate in short pipes, orifices and nozzles .....	360
12.8 Nucleation in the presence of non-condensable gases .....	361
12.9 Activated nucleation site density – state of the art .....	362
12.10 Conclusions and recommendations .....	368
Nomenclature .....	368
References .....	370
<b>13 Bubble growth in superheated liquid .....</b>	<b>375</b>
13.1 Introduction .....	375
13.2 The thermally controlled bubble growth .....	376
13.3 The <i>Mikic</i> solution .....	378
13.4 How to compute the mass source terms for the averaged conservation equations? .....	381
13.4.1 Non-averaged mass source terms .....	381
13.4.2 The averaged mass source terms .....	382
13.5 Superheated steam .....	384
13.6 Diffusion controlled evaporation into mixture of gases inside the bubble .....	385
13.7 Conclusions .....	386
Appendix 13.1 Radius of a single bubble in a superheated liquid as a function of time .....	386
Nomenclature .....	391
References .....	394
<b>14 Condensation of a pure steam bubble in a subcooled liquid .....</b>	<b>397</b>
14.1 Introduction .....	397
14.2 Stagnant bubble .....	397
14.3 Moving bubble .....	399
14.4 Non-averaged source terms .....	404
14.5 Averaged source terms .....	405
14.6 Change of the bubble number density due to condensation .....	406
14.7 Pure steam bubble drifting in turbulent continuous liquid .....	407

14.8	Condensation from a gas mixture in bubbles surrounded by subcooled liquid .....	409
14.8.1	Thermally controlled collapse .....	410
14.8.2	Diffusion controlled collapse .....	410
	Nomenclature .....	411
	References .....	415
<b>15</b>	<b>Bubble departure diameter.....</b>	<b>417</b>
15.1	How accurately can we predict bubble departure diameter for boiling? .....	417
15.2	Model development .....	420
15.3	Comparison with experimental data .....	425
15.4	Significance .....	429
15.5	Summary and conclusions .....	429
15.6	Extension of the theory to sub-cooled liquids .....	430
15.7	Influence of the wall material .....	433
	Nomenclature .....	434
	References .....	435
<b>16</b>	<b>How accurately can we predict nucleate boiling? .....</b>	<b>439</b>
16.1	Introduction .....	439
16.2	New phenomenological model for nucleate pool boiling .....	446
16.2.1	Basic assumptions .....	446
16.2.2	Proposed model .....	448
16.3	Data comparison .....	450
16.3.1	Nucleation site density at high pressures .....	453
16.4	Systematic inspection of all the used hypotheses .....	455
16.5	Significance .....	456
16.6	Conclusions .....	456
16.7	Extension to forced convection with nucleate boiling .....	457
	Appendix 16.1 State of the art of nucleate pool boiling modeling .....	460
	Nomenclature .....	465
	References .....	467
<b>17</b>	<b>Heterogeneous nucleation and flashing in adiabatic pipes.....</b>	<b>471</b>
17.1	Introduction .....	471
17.2	Bubbles generated due to nucleation at the wall .....	472
17.3	Bubble growth in the bulk .....	473
17.4	Bubble fragmentation and coalescence .....	473
17.5	Film flashing bubble generation in adiabatic pipe flow .....	475
17.6	Verification of the model .....	476
17.9	Significance and conclusions .....	481
	Nomenclature .....	482
	References .....	484

<b>18 Boiling of subcooled liquid .....</b>	<b>487</b>
18.1 Introduction .....	487
18.2 Initiation of visible boiling on the heated surface .....	487
18.3 Local evaporation and condensation .....	490
18.3.1 Relaxation theory .....	490
18.3.2 Boundary layer treatment .....	492
Nomenclature .....	495
References .....	496
<b>19 Natural convection film boiling .....</b>	<b>499</b>
19.1 Minimum film boiling temperature .....	499
19.2 Film boiling in horizontal upwards-oriented plates .....	500
19.3 Horizontal cylinder .....	501
19.4 Sphere .....	502
Nomenclature .....	502
References .....	504
<b>20 Forced convection boiling .....</b>	<b>505</b>
20.1 Convective boiling of saturated liquid .....	505
20.2 Forced convection film boiling .....	507
20.2.1 Tubes .....	507
20.2.2 Annular channel .....	509
20.2.3 Tubes and annular channels .....	510
20.2.4 Vertical flow around rod bundles .....	510
20.3 Transition boiling .....	511
20.4 Critical heat flux .....	512
20.4.1 The hydrodynamic stability theory of free convection DNB .....	513
20.4.2 Forced convection DNB and DO correlations .....	515
20.4.3 The 1995 and 2005 look-up tables .....	519
Nomenclature .....	524
References .....	526
<b>21 Film boiling on vertical plates and spheres .....</b>	<b>529</b>
21.1 Plate .....	529
21.1.1 Introduction .....	529
21.1.2 State of the art .....	530
21.1.3 Problem definition .....	531
21.1.4 Simplifying assumptions .....	532
21.1.5 Energy balance at the vapor-liquid interface, vapor film thickness, average heat transfer coefficient .....	535
21.1.6 Energy balance of the liquid boundary layer, layer thickness ratio .....	538
21.1.7 Averaged heat fluxes .....	541
21.1.8 Effect of the interfacial disturbances .....	542
21.1.9 Comparison of the theory with the results of other authors .....	543

21.1.10	Verification using the experimental data.....	545
21.1.11	Conclusions .....	546
21.1.12	Practical significance.....	546
21.2	Sphere .....	547
21.2.1	Introduction .....	547
21.2.2	Problem definition.....	547
21.2.3	Solution method .....	547
21.2.4	Model .....	547
21.2.5	Data comparison.....	556
21.2.6	Conclusions .....	559
Appendix 21.1	Natural convection at vertical plate .....	559
Appendix 21.2	Predominant forced convection only at vertical plate.....	560
	Nomenclature .....	561
	References .....	564
<b>22</b>	<b>Liquid droplets .....</b>	<b>567</b>
22.1	Spontaneous condensation of pure subcooled steam – nucleation .....	567
22.1.1	Critical nucleation size .....	568
22.1.2	Nucleation kinetics, homogeneous nucleation .....	570
22.1.3	Droplet growth .....	572
22.1.4	Self-condensation stop .....	574
22.2	Heat transfer across droplet interface without mass transfer.....	575
22.3	Direct contact condensation of pure steam on subcooled droplet .....	581
22.4	Spontaneous flashing of superheated droplet.....	583
22.5	Evaporation of saturated droplets in superheated gas .....	587
22.6	Droplet evaporation in gas mixture.....	589
	Nomenclature .....	594
	References .....	596
<b>23</b>	<b>Heat and mass transfer at the film-gas interface .....</b>	<b>599</b>
23.1	Geometrical film-gas characteristics .....	599
23.2	Convective heat transfer.....	601
23.2.1	Gas side heat transfer .....	601
23.2.2	Liquid side heat transfer due to conduction.....	604
23.2.3	Liquid side heat conduction due to turbulence.....	606
23.3	Spontaneous flashing of superheated film.....	613
23.4	Evaporation of saturated film in superheated gas.....	613
23.5	Condensation of pure steam on subcooled film .....	614
23.6	Evaporation or condensation in presence of non-condensable gases .....	615
	Nomenclature .....	617
	References .....	620
<b>24</b>	<b>Condensation at cooled walls.....</b>	<b>623</b>
24.1	Pure steam condensation .....	623
24.1.1	Onset of the condensation .....	623
24.1.2	Gravitation films on plates .....	623

24.1.2	Gravitation films on pipes .....	631
24.2	Condensation from forced convection two-phase flow at liquid film .....	632
24.2.1	Down flow of vapor across horizontal tubes .....	632
24.2.2	<i>Collier</i> correlation .....	632
24.2.3	<i>Boyko</i> and <i>Krjulin</i> approach .....	633
24.2.4	The <i>Shah</i> modification of the <i>Boyko</i> and <i>Krjulin</i> approach .....	634
24.3	Steam condensation from mixture containing non-condensing gases .....	634
24.3.1	Computation of the mass transfer coefficient .....	636
	Nomenclature .....	638
	References .....	640
<b>25</b>	<b>Discrete ordinate method for radiation transport in multi-phase computer codes.....</b>	<b>643</b>
25.1	Introduction.....	643
25.1.1	Dimensions of the problem .....	643
25.1.2	Micro- versus macro-interactions.....	644
25.1.3	The radiation transport equation (RTE).....	644
25.2	Discrete ordinate method .....	645
25.2.1	Discretization of the computational domain for the description of the flow .....	647
25.2.2	Finite volume representation of the radiation transport equation .....	648
25.2.3	Boundary conditions.....	653
25.3	Material properties .....	655
25.3.1	Source terms – emission from hot surfaces with known temperature .....	655
25.3.2	Spectral absorption coefficient of water .....	655
25.3.3	Spectral absorption coefficient of water vapor and other gases .....	660
25.4	Averaged properties for some particular cases occurring in melt-water interaction .....	660
25.4.1	Spherical cavity of gas inside a molten material .....	660
25.4.2	Concentric spheres of water droplets, surrounded by vapor, surrounded by molten material .....	661
25.4.3	Clouds of spherical particles of radiating material surrounded by a layer of vapor surrounded by water – <i>Lanzenberger's</i> solution .....	665
25.4.4	Chain of infinite number of <i>Wigner</i> cells .....	678
25.4.5	Application of <i>Lanzenbergers's</i> solution .....	679
	Nomenclature .....	681
	References .....	682
<b>Index .....</b>	<b>.....</b>	<b>685</b>

# 1 Flow regime transition criteria

*This Chapter presents a review of the existing methods for identification of flow patterns in two phase flow in pools, adiabatic and non-adiabatic channels, rod bundles and porous structures. An attempt is made to extend this information to be applicable in three-phase flow modeling. In addition the influence of the dynamic fragmentation and coalescence of the flow regimes is introduced.*

## 1.1 Introduction

Transient multi-phase flows with temporal and spatial variation of the volumetric fractions of the participating phases can be represented by *sequences* of geometrical *flow patterns* that have some characteristic length scale. Owing to the highly random behavior of the flow in detail, the number of flow patterns needed for this purpose is very large. Nevertheless, this approach has led to some successful applications in the field of multi-phase flow modeling. Frequently modern mathematical models of *transient flows* include, among others, the following features:

1. Postulation of a limited number of idealized flow patterns, with transition limits as a function of local parameters for *steady state* flow (e.g., see Fig. 1.1);
2. Identification of one of the postulated idealized *steady state* flow patterns for each time step;
3. Computation of a characteristic *steady state length scale of the flow patterns* (e.g., bubble or droplet size) in order to address further constitutive relationships for interfacial heat, mass, and momentum transfer.

Various transfer mechanisms between mixture and wall, as well as between the velocity fields, depend on the flow regimes. This leads to the use of regime dependent correlations for modeling of the interfacial mass, momentum and energy transfer. The transfer mechanisms themselves influence strongly the flow pattern's appearance. That is why the first step of the coupling between the system PDEs and the correlations governing the transfer mechanisms is the flow regime identification.

We distinguish between flow patterns appearing in *pool* flow and in *channel* flow. In pool flow,  $\gamma_v = 1$ , there is no influence of the walls on the flow pattern. In channel flows characterized by  $\gamma_v < 1$ , however, this influence can be very strong resulting in patterns like film flow, slug flow etc.

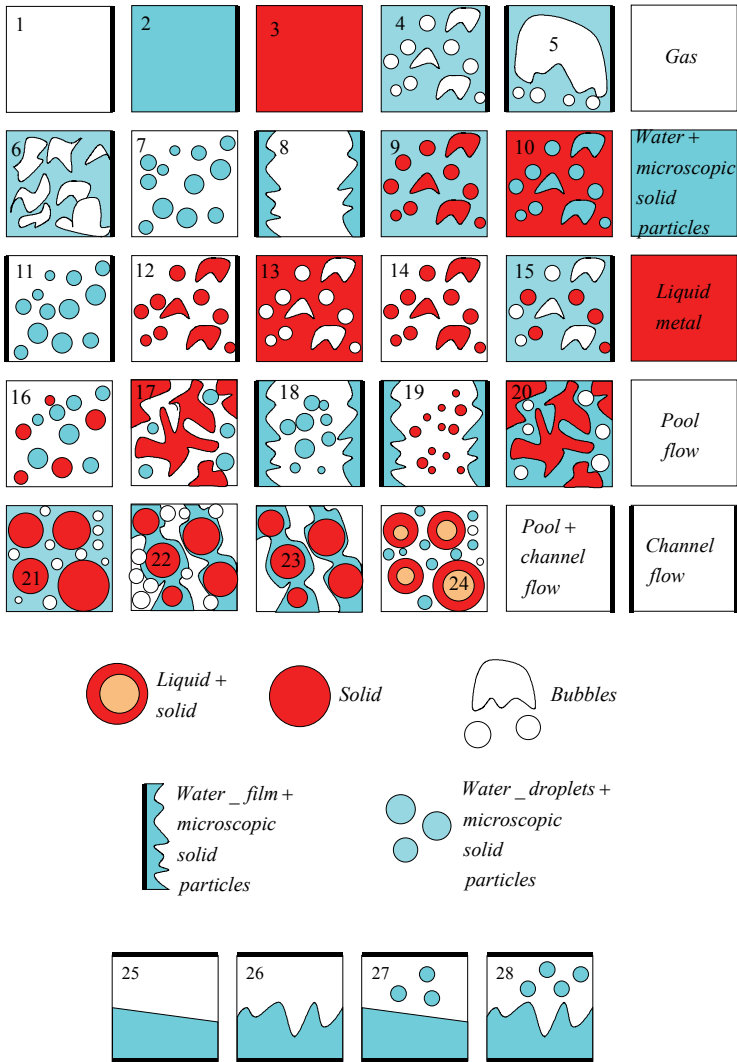


**Fig. 1.1** Multi-phase flow patterns

Some flow patterns can be trivially identified by knowing only the values of the local volume fractions of the fields,  $\alpha_i$ , and the consistency of the fields i.e.  $C_{li}$ , e.g. the single phase flows or flows consisting of three velocity fields with an initially postulated structure. For two interpenetrating velocity fields additional information is necessary to identify the flow pattern. There are analytical and experimental arguments for flow pattern identification which will be considered



here. The emphasis of this Chapter is on how dynamics influence the transitions from one flow pattern into the other.

## 1.2 Pool flow

In pool flows we distinguish two main flow patterns: continuous liquid and continuous gas, and one intermediate between them. Next we discuss the conditions for existence of the bubble flow. We will realize that the dynamic fragmentation and coalescence will have an influence on the transition criterion through the bubble size.

**Bubbly flow:** The existence of the bubbly flow in pools is discussed in this section.

*Non-oscillating particles:* Consider equally sized spherical particles forming a rhomboid array. The average distance between the centers of two adjacent particles with diameter  $D_d$  and volumetric fraction  $\alpha_d$  is then

$$\Delta \ell_d = D_d \left( \frac{\pi \sqrt{2}}{6 \alpha_d} \right)^{1/3}. \quad (1.1)$$

Here  $d$  stands for disperse. The *non-oscillating* particles will touch each other if

$$\Delta \ell_d = D_d. \quad (1.2)$$

This happens for a volume fraction of

$$\alpha_d = \frac{\pi}{6} \sqrt{2} \approx 0.74, \quad (1.3)$$

which is sometimes called in the literature the *maximum packing density* volume concentration. This consideration leads to the conclusion that bubble flow cannot exist for

$$\alpha_1 > 0.74, \quad (1.4)$$

and vice versa droplet flow cannot exist for

$$\alpha_1 < 0.26. \quad (1.5)$$

*Oscillating particles:* Oscillating particles will touch each other occasionally at larger average distance. This means that in strongly turbulent flows the existence of bubble flow should be expected to be limited by smaller volume fractions. In fact turbulent bubble flows in nature and technical facilities are observed up to

$$\alpha_1 < 0.25 \text{ to } 0.3, \quad (1.6)$$

*Taitel et al. (1980), Radovich and Moissis (1962), see in Mishima and Ishii (1984).* If the mean free path length of the oscillating particles is  $\ell_d^t$  the sphere of influence of this particle is  $D_d + \ell_d^t = D_d (1 + \ell_d^t / D_d)$ . In this case the particles may touch each other if

$$D_d (1 + \ell_d^t / D_d) = D_d \left( \frac{\pi \sqrt{2}}{6 \alpha_d} \right)^{1/3}, \quad (1.7)$$

or

$$\alpha_d = \frac{\pi}{6} \sqrt{2} / (1 + \ell_d^t / D_d) < 0.74, \quad (1.8)$$

and consequently

$$\ell_d^t / D_d > 0.44 \text{ to } 0.35. \quad (1.9)$$

*The influence of the particle size on the flow regime transition: Brodkey (1967)* shows that bubbles with radii smaller than

$$D_{\text{I,solid like}} = 0.63 \sqrt{\frac{2\sigma_2}{g\Delta\rho_{21}}} \approx 0.89 \lambda_{RT}, \quad (1.10)$$

where  $\lambda_{RT}$  is the *Raleigh-Taylor* wavelength defined as follows

$$\lambda_{RT} = \sqrt{\frac{\sigma_2}{g\Delta\rho_{21}}}, \quad (1.11)$$

behave as a solid sphere and the coalescence is negligible. This argument was used by *Taitel et al. (1980)* to explain the existence of bubble flow in regions up to

$$\alpha_1 < 0.54, \quad (1.12)$$

if strong liquid turbulence destroys bubbles to dimensions

$$D_1(\varepsilon_2, \dots) < D_{\text{I,solid like}} \quad (1.13)$$

where  $\varepsilon_2$  is the dissipation rate of the turbulent kinetic energy of the liquid.

### Conclusions:

a) In the concept of modeling dynamic fragmentation and coalescence, bubble flow is defined if we have at least one bubble in the volume of consideration,  $Vol_{\text{cell}}$ , i.e.

$$n_1 Vol_{\text{cell}} > 1, \quad (1.14)$$

otherwise both phases are continuous. This is the trivial condition. Here  $n_1$  is the number of bubbles per unit mixture volume.

b) For small bubble sizes,  $D_1(\varepsilon_2, \dots) < D_{1, \text{solid like}}$ , the bubbles behave as solid spheres and the coalescence probability is dramatically reduced. In this case bubble flow exists up to

$$\alpha_{1, B-Ch} = 0.54. \quad (1.15)$$

c) For larger bubble sizes,  $D_1(\varepsilon_2, \dots) > D_{1, \text{solid like}}$ , the transition between bubble and churn turbulent flow happens between

$$\alpha_{1, B-Ch} \approx 0.25 \text{ and } 0.54. \quad (1.16)$$

The size at which the lower limit holds is not exactly known. Assuming that this size is governed by a critical *Weber* number equal to 12 and using the bubble rise velocity in the pool as computed by *Kutateladze*

$$V_{1Ku} = \sqrt{2} \left[ g \sigma_2 (\rho_2 - \rho_1) / \rho_2^2 \right]^{1/4},$$

we obtain 6 times  $\lambda_{RT}$ . A linear interpolation between these two sizes gives

$$\alpha_{1, B-Ch} = 0.54 - 0.0567 (D_1 / \lambda_{RT} - 0.89). \quad (1.17)$$

The dependence of this transition criterion on the bubble size is remarkable. Modeling dynamic bubble size evolution gives different regime transition boundaries for different bubble sizes at the same gas volume fraction.

d) Churn turbulent flow exists between

$$0.54 < \alpha_1 < 0.74. \quad (1.18)$$

Note that the upper limit of the churn turbulent flow,  $\alpha_{1, Ch-A} = 0.74$ , seems to be a function of the *local Mach* number. The higher the *local Mach* number, the higher the upper limit due to the increasing turbulence. This consideration is supported by the position of the slip maximum as a function of the gas volume fraction in critical flow as measured by e.g. *Deichel* and *Winter* (1990). The investigation of *Ginsberg et al.* (1979) of flow behavior of volume-heated boiling pools shows that for fast transients the limit between bubble and churn turbulent flow and dispersed flow is higher. Thus one can assume that the upper limit is

$$\alpha_{1, Ch-A} = 0.74 + Ma(0.92 - 0.74) = 0.74 + 0.18Ma. \quad (1.19)$$

In accordance with this consideration, very slow flows do not have churn turbulent regimes and bubble flow goes directly into disperse droplet flow with increasing gas volume fraction.

## 1.3 Adiabatic flows

Boundary between flow-patterns are frequently expressed as a function of important velocity scales. Such velocity scales are the so called velocity of a *Taylor* bubble and the *Kutateladze* velocity. Next we briefly describe how they appear in the two-phase flow analysis.

### 1.3.1 Two important velocity scales

**Velocity of Taylor bubble:** For a free rising bubbles in liquid and free falling droplet in a gravitational field presented in Fig. 1.2 the drag force is equal to the buoyancy force

$$c_{cd}^d \frac{1}{2} \rho_c (w_c - w_{d\infty})^2 \pi D_{d\infty}^2 / 4 = (\pi D_{d\infty}^3 / 6) g \Delta \rho_{dc} .$$

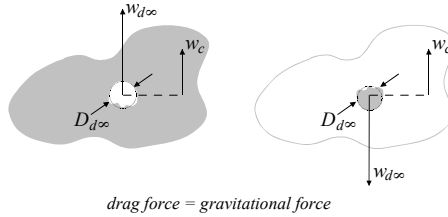


**Fig. 1.2** Free falling droplet in a gravitational field and free rising bubbles in liquid

For  $c_{cd}^d \approx \text{const}$  we have

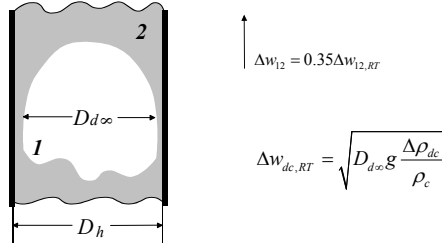
$$\Delta w_{dc} = \frac{1}{\sqrt{3c_{cd}^d}} \Delta w_{dc,RT} \approx \text{const} \Delta w_{dc,RT} ,$$

The so defined characteristic velocity is called *Taylor*-velocity

$$\Delta w_{dc,RT} = \sqrt{D_{d\infty} g \frac{\Delta \rho_{dc}}{\rho_c}} .$$

For *slug* in vertical pipes, see Fig. 1.3, where  $D_{d\infty} \approx D_h$  the slug rise velocity is experimentally found by *Dimitresku* (1943) and by *Davies* and *Taylor* (1950) to be dependent really on the pipe diameter

$$\Delta w_{12} = 0.35 \Delta w_{12,RT} .$$



*Dimitresku (1943), Davies und Taylor (1950)*

**Fig. 1.3** Free rising gas slug in pipe

**Kutateladze velocities:** For large bubbles where the size is comparable to the *Rayleigh-Taylor* instability wavelength for the case where gas and liquid are interpenetrating due to gravity

$$D_{d\infty} \approx \lambda_{RT} = \left[ \sigma_d / (g \Delta \rho_{dc}) \right]^{1/2}.$$

In this case the free rising bubble velocity in a pool or the free falling droplet velocity in a gas, see Fig. 1.4, is

$$\Delta w_{dc} = \frac{1}{\sqrt{3c_{cd}^d}} \left( \frac{\sigma_d g \Delta \rho_{dc}}{\rho_c^2} \right)^{1/4} \approx (\sqrt{2} \text{ to } 1.7) \left( \frac{\sigma_d g \Delta \rho_{dc}}{\rho_c^2} \right)^{1/4} = (\sqrt{2} \text{ to } 1.7) \Delta w_{dc,Ku}.$$

Here

$$\Delta w_{dc,Ku} = \left( \frac{\sigma_d g \Delta \rho_{dc}}{\rho_c^2} \right)^{1/4}$$

is called *Kutateladze* velocity, see *Kutateladze (1951)*. Note that

$$\frac{\Delta w_{dc,Ku}}{\Delta w_{dc,RT}} = \left( \frac{\lambda_{RT}}{D_{d\infty}} \right)^{1/2}.$$

One will immediately recognize the importance of the above discussed velocity scale if the phenomenon of flooding has to be simply described. Flooding is a limit to counter-current flow where the gas phase is flowing upwards and the liquid phase is stagnating.

**Flooding in vertical channels with large sizes:** For large pipes the flow pattern is schematically presented in Fig. 1.5. *Kutateladze (1951)* found that the condition for gas stagnation after injection through horizontal perforated plate in water is

$\left[ \alpha_1 w_{i0} / \left( \sqrt{2} \Delta w_{21, Ku} \right) \right]^{1/2} = \text{const}$ . The constant is reported by *Pushkina* and *Sorokin* (1969) to be 1.79,

$$(\alpha_1 w_1)_{\text{lim}} = 3.2 \sqrt{2} \Delta w_{21, Ku}.$$

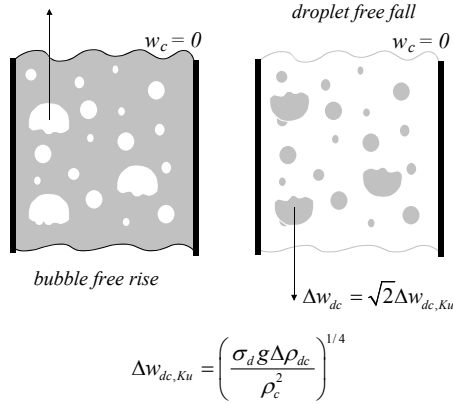


**Fig. 1.4** Free rising bubbles and free falling droplets

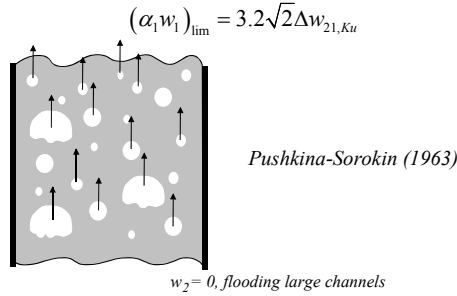


**Fig. 1.5** Flooding in large pipes: the gas phase blocks the down flow of the liquid

*Tien et al.* (1979) extended the validity of the *Pushkina* and *Sorokin* correlation to pipe diameter with different sizes as follows

$$\left[ \alpha_1 w_{i0} / \left( \Delta w_{21, Ku} \right) \right]^{1/2} + c_1 \left[ \alpha_2 w_{20} / \left( \Delta w_{12, Ku} \right) \right]^{1/2} = c_2 \tanh \left[ c_3 \left( D_h / \lambda_{RT} \right)^{1/4} \right],$$

where  $c_1 = 0.65$  to  $0.8$ ,  $c_2 = 1.79$  to  $2.1$ ,  $c_3 = 0.8$  to  $0.9$ .

**Flooding in vertical channels with small sizes:** *Wallis* (1969) p. 338, proposed the following relation defining the so called counter current flow limitation

$$\left[ \frac{\alpha_1 w_{10}}{\sqrt{D_h g \frac{\Delta \rho_{21}}{\rho_1}}} \right]^{1/2} + \left[ \frac{(1 - \alpha_1) w_{20}}{\sqrt{D_h g \frac{\Delta \rho_{21}}{\rho_2}}} \right]^{1/2} = C ,$$

$C = 0.775$ . For sharp ended pipes,  $C = 0.88$   $j_{20}^* < 0.3$ ,  $C = 1$  otherwise, *Hewitt* and *Wallis* (1963). There is variety of sophistications of this expression in the literature but its main structure remains as it is. In a cross section where the outflow liquid volume flow is equal to the inflow gas flow,  $\alpha_1 w_{10} = (1 - \alpha_1) w_{20}$ , see Fig. 1.6 left, we have

$$\alpha_1 w_{10} = (1 - \alpha_1) w_{20} = C^2 \frac{(D_h g \Delta \rho_{21})^{1/2}}{(\rho_1^{1/4} + \rho_2^{1/4})^2}$$

The relation between the flooding condition and the slug velocity is found by *Whalley* (1987) after setting  $\alpha_1 w_{10} = 0.35 \Delta w_{12, RT}$ . The result is

$$C = \sqrt{0.35} (1 + \rho_1^{1/4} / \rho_2^{1/4}) .$$

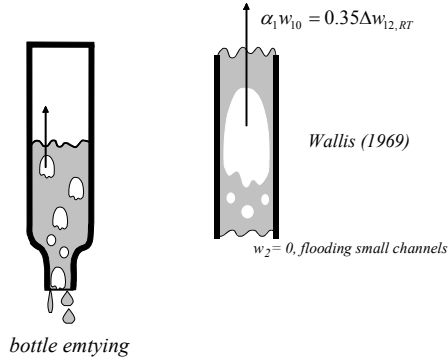


**Fig. 1.6** Flooding in small channels

### 1.3.2 Channel flow – vertical pipes

For vertical pipe flows the following regime boundaries are defined as follows:

**Bubble flow:** As for the pool flow, in the concept of modeling dynamic fragmentation and coalescence, bubble flow is defined if we have at least one bubble in the volume of consideration,  $Vol_{cell}$ , i.e.

$$n_1 Vol_{cell} > 1, \quad (1.20)$$

otherwise both phases are continuous.

- b) Figure 1.7 indicates that the *Rayleigh-Taylor* instability wavelength  $\lambda_{RT}$  is the appropriate scale for distinguishing whether the pipe diameter is small or large.

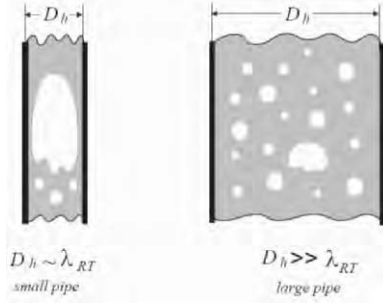


**Fig. 1.7** Criterion for distinguishing between small and large channels

Bubble flow exists in the region

$$0 < \alpha_1 < \alpha_{1,bubble \text{ to slug}} \quad \text{and} \quad D_h > D_{h,slug}. \quad (1.21)$$

where

$$D_{h,slug} = 19 \frac{\Delta \rho_{21}}{\rho_2} \lambda_{RT}, \quad \text{Taitel et al. (1980),} \quad (1.22)$$

$$\alpha_{1,bubble \text{ to slug}} = 0.54 \quad \text{for} \quad D_1(\varepsilon_2, \dots) < 0.89 \lambda_{RT}, \quad (1.23)$$

$$\alpha_{1,bubble \text{ to slug}} = 0.54 - 0.0567(D_1 / \lambda_{RT} - 0.89) \quad \text{for} \quad 0.89 \lambda_{RT} < D_1(\varepsilon_2, \dots) < 6 \lambda_{RT}, \quad (1.24)$$

$$\alpha_{1,bubble \text{ to slug}} \approx 0.25 \quad \text{for} \quad D_1(\varepsilon_2, \dots) \geq 6 \lambda_{RT} \quad (1.25)$$

**Slug flow:** Slug flow is defined as a train of large bubbles followed by mixtures of small bubbles and liquid or liquid only. The slug regime is never stationary. Slug flow exists if

$$D_h < D_{h,slug} \quad (1.26)$$

or if

$$D_h > D_{h,slug} \quad \text{and} \quad \alpha_{1,bubble \text{ to slug}} < \alpha_1 < \alpha_{1,slug \text{ to churn}}. \quad (1.27)$$

This condition reflects the fact that slug flow can be transformed into churn turbulent flow if the gas volume fraction averaged over the entire pipe length is larger



than those in the slug bubble section only. The gas volume fraction in the slug bubble section only is

$$\alpha_{1,\text{slug to churn}} = 1 - 0.813 \left\{ \frac{(C_0 - 1) |j| + 0.35 V_{TB}}{|j| + 0.75 V_{TB} b_1} \right\}^{0.75}, \quad (1.28)$$

*Mishima and Ishii* (1984). The drift flux distribution coefficient for slug flow is

$$C_0 = 1.2, \quad (1.29)$$

the slug (*Taylor* bubble) raising velocity is

$$V_{TB} = \sqrt{\frac{\rho_2 - \rho_1}{\rho_2} g D_h}, \quad (1.30)$$

the mixture volumetric flux is

$$j = \alpha_1 V_1 + (1 - \alpha_1) V_2, \quad (1.31)$$

and

$$b_1 = \left( \frac{\rho_2 - \rho_1}{\eta_2^2 / \rho_2} g D_h^3 \right)^{1/18}. \quad (1.32)$$

The correlation contains the length of the *Taylor* bubble

$$\sqrt{2 \ell_{TB} \Delta \rho_{21} g / \rho_2} = |j| + 0.75 V_{TB} b_1. \quad (1.33)$$

The error for computing  $\ell_{TB}$  is  $\pm 100\%$ . Thus, air-water flow in a pipe with diameter  $D_h = 0.027m$  at atmospheric conditions and phase volumetric flow rates of  $\alpha_1 V_1 = 0.2$  to  $2 m/s$ ,  $(1 - \alpha_1) V_2 = 0.2 m/s$ , is a slug flow with characteristic slug length of  $\ell_{TB} \approx 0.1$  to  $0.5m$ .

**Churn turbulent flow:** In accordance with *Mishima and Ishii* (1984) churn turbulent flow exists under the following conditions:

$$\alpha_1 > \alpha_{1,\text{slug to churn}} \text{ and } \left[ (D_h < D_{hc} \text{ and } V_1 < V_{11}) \text{ or } (D_h \geq D_{hc} \text{ and } V_1 < V_{12}) \right]. \quad (1.34)$$

Here

$$D_{hc} = \lambda_{RT} / \left[ (\alpha_1 - 0.11)^2 N_{\eta 2}^{0.4} \right], \quad (1.35)$$

and

$$N_{\eta 2} = \eta_2 / \sqrt{\rho_2 \sigma_2 \lambda_{RT}} \quad (1.36)$$

is the viscous number. The first criterion is applied to flow reversal in the liquid film section along large bubbles,

$$D_h < D_{hc} \text{ and } V_1 > V_{11}, \quad (1.37)$$

where

$$V_{11} = (1 - 0.11/\alpha_1) V_{TB}. \quad (1.38)$$

In this case the flow reversal in the liquid film section along the large bubbles causes the transition.

The second criterion is applied to destruction of liquid slugs or large waves by entrainment or deformation

$$D_h \geq D_{hc} \text{ and } V_1 > V_{12}. \quad (1.39)$$

where

$$V_{12} = \frac{V_{2Ku}}{\alpha_1 N_{\eta 2}^{0.2}}, \quad (1.40)$$

and

$$V_{2Ku} = [g\sigma_2(\rho_2 - \rho_1)/\rho_1^2]^{1/4}, \quad (1.41)$$

is the *Kutateladze* terminal velocity for free falling droplets in gas. The correlation holds for low viscous flows  $N_{\eta 2} < 1/15$  and relatively high liquid *Reynolds* number  $Re_{23} > 1635$ . In this case the churn flow bubble section following the slug disintegrates or the liquid waves and subsequent liquid bridges and slugs can be entrained as small droplets. This leads to the elimination of liquid slugs between large bubbles and to a continuous gas core. This is the criterion for transition from slug flow to annular-dispersed flow.

**Annular film flow:** The annular film flow is defined if

$$\alpha_1 > \alpha_{1,slug \text{ to churn}} \text{ and } [(D_h < D_{hc} \text{ and } V_1 > V_{11}) \text{ or } (D_h \geq D_{hc} \text{ and } V_1 > V_{12})]. \quad (1.42)$$

**Annular film flow with entrainment:** The annular film flow with entrainment is defined by *Kataoka* and *Ishi* (1982) as follows

$$D_h > D_{hc} \text{ and } \alpha_1 > \alpha_{1,slug \text{ to churn}} \text{ and } V_1 > V_{13} \text{ and } Re_{2\delta} = \rho_2 V_2 4\delta_2 / \eta_2 > 160. \quad (1.43)$$

Here  $\delta_2 = \frac{1}{2} D_h (1 - \sqrt{1 - \alpha_2})$  is the film thickness,

$$V_{13} = b_8 \frac{\sigma_2}{\eta_2 \alpha_1 \left( \frac{\rho_1}{\rho_2} \right)^{1/2}}, \quad (1.44)$$

$$b_8 = N_{\eta_2}^{0.8}, \quad \text{for } \text{Re}_{23} > 1635, \quad (1.45)$$

$$b_8 = 11.78 N_{\eta_2}^{0.8} / \text{Re}_{23}^{1/3} \quad \text{for } \text{Re}_{23} \leq 1635, \quad (1.46)$$

$$\text{Re}_{23} = (1 - \alpha_1) \rho_2 |V_{23}| D_h / \eta_2, \quad (1.47)$$

$$V_{23} = (\alpha_2 V_2 + \alpha_3 V_3) / (1 - \alpha_1). \quad (1.48)$$

### 1.3.3 Channel flow – inclined pipes

Compared with the vertical flow the flow in horizontal pipes possess two additional flow patterns - stratified flow and stratified wavy flow. For the computation of the relative velocities and pressure drop for these flow pattern the work by *Mamaev et al.* (1969) is recommended. *Mamaev et al.* considered stratified flow

possible for  $Fr < Fr_{crit}$ , where  $Fr = \frac{(\rho w)^2 v_h}{g D_h}$ ,  $v_h = X_1 v_1 + (1 - X_1) v_2$ . The critical

*Froude* number was obtained from experiments

$$Fr_{crit} = \left[ \left( 0.2 - \frac{2 \cos \varphi}{\lambda_{fr}} \right) / (1 - \beta)^2 \right] \exp(-2.5\beta),$$

where  $\beta = X_1 v_1 / v_h$ , and  $\lambda_{fr} = \lambda_{fr} \left( \frac{\pi (1 - \alpha_1) w_2 D}{\pi - \theta} \frac{k}{v_2}, \frac{k}{D} \right)$  is the liquid site wall fric-

tion coefficient computed using the *Nikuradze* diagram. *Weisman et al.* (1979), *Weisman and Kang* (1981) and *Grawford et al.* (1985) published a set of correlations for horizontal as well as vertical flows. Their correlations for horizontal flows are summarized at the end of this section.

Transition criteria are systematically elaborated by *Taitel and Dukler* (1976), *Rouhani and Sohal* (1983). The *Taitel* line of criteria development is presented here.

**Stratified flow:** Almost all results available in the literature provide a criterion for identification of the existence of the stratified flows based on the stability criterion Eq. (151b) from Chapter 2 in Volume 1 of this monograph

$$V_{1, \text{stratified}} - V_2 = \left[ g \cos(\varphi - \pi/2) (\rho_2 - \rho_1) \left( \frac{\alpha_1}{\rho_1} + \frac{1 - \alpha_1}{\rho_2} \right) \right]^{1/2} \frac{d\alpha_2}{d\delta_{2F}}, \quad (1.49)$$

where  $\delta_{2F}$  is the liquid thickness.  $\varphi$  is the angle defined between the upwards oriented vertical and the pipe axis – see Fig. 1.7. For a larger velocity difference the flow is no longer stratified and disintegrates into an intermittent flow like elongated bubble or slug or churn flow. For flow between two parallel plates

$$\frac{d\delta_{2F}}{d\alpha_2} = H, \quad (1.50)$$

where  $H$  is the distance between the two plates. For flows in a round tube, see Fig. 1.8, the angle  $\theta$  with the origin the pipe axis is defined between the upwards oriented vertical and the liquid-gas-wall triple point as a function of the liquid volume fraction given by the equation

$$1 - \alpha_2 = \frac{\theta - \sin \theta \cos \theta}{\pi}. \quad (1.51)$$

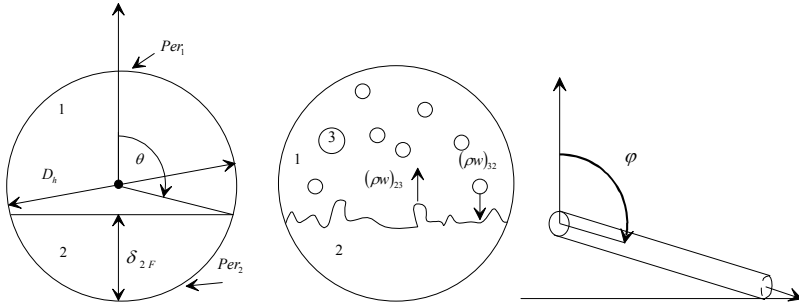


**Fig. 1.8** Definition of the geometrical characteristics of the stratified flow

Having in mind that

$$\delta_{2F} = \frac{1}{2} D_h (1 + \cos \theta) \quad (1.52)$$

we obtain

$$\frac{d\alpha_2}{d\delta_{2F}} = \frac{d\alpha_2}{d\theta} \bigg/ \frac{d\delta_{2F}}{d\theta} = \frac{4}{D_h} \frac{\sin \theta}{\pi}. \quad (1.53)$$

This criterion is in fact consistent with the *Kelvin-Helmholtz* gravity long wave theory -see *Milne-Thomson* (1968), or *Delhaye*, p. 90 (1981), or *Barnea and Taitel* (1994).

*Wallis and Dobson* (1973) compared the above equation with experimental data for channels with  $H$  ranging from 0.0254 to 0.305 m and corrected then by introducing a constant multiplier of 0.5. This result was in fact confirmed by *Mishima and Ishii* in 1980. These authors obtained for low pressure  $\frac{\alpha_1}{\rho_1} \gg \frac{1-\alpha_1}{\rho_2}$  the con-

stant 0.487. *Hohannessen* (1972) considered the situation depicted in Fig. 1.9 and defined the transition of the stratified flow as equality of the static pressures at the bottom of the pipe  $p_{2b,1}$  and  $p_{2b,2}$  taking into account the change of the gas pressure due to cross section decrease by using the *Bernouli* equation. *Taitel and Dukler* (1976), similarly to *Hohannessen* (1972), equalized the buoyancy pressure increment required to create solution disturbance with finite amplitude to the increase of the gas dynamic pressure and obtained after linearization the following multiplier  $\left(1 - \frac{\delta_{2F}}{H}\right)$  again testing the result for low pressure. Defining the *Taylor* bubble velocity for inclined pipe with

$$V_{TB}^* = \left[ \frac{\rho_2 - \rho_1}{\rho_2} D_h g \cos(\varphi - \pi/2) \right]^{1/2}, \quad (1.54)$$

the criterion for a pipe is then

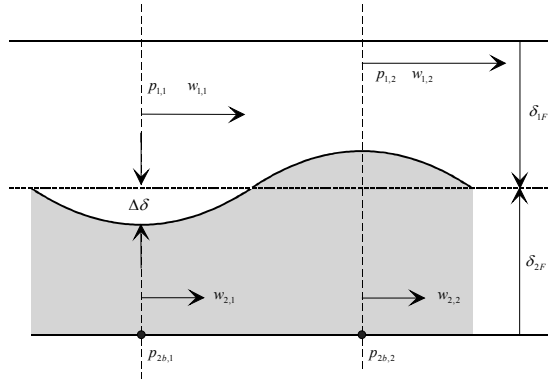


**Fig. 1.9** The definition of the variables for the Hohannessen stability criterion

$$V_{1, \text{stratified}} - V_2 = \frac{1}{2}(1 - \cos \theta) \left[ \frac{g(\rho_2 - \rho_1) \cos(\varphi - \pi/2) \left( \frac{\alpha_1}{\rho_1} + \frac{1 - \alpha_1}{\rho_2} \right)}{\frac{4}{D_h} \frac{\sin \theta}{\pi}} \right]^{1/2} \quad (1.55)$$

or

$$\frac{V_{1, \text{stratified}} - V_2}{V_{TB}^*} = \frac{1}{4}(1 - \cos \theta) \left[ \frac{\pi}{\sin \theta} \rho_2 \left( \frac{\alpha_1}{\rho_1} + \frac{1 - \alpha_1}{\rho_2} \right) \right]^{1/2}. \quad (1.56)$$

This criterion is valid for gravity driven liquid flow. *Johnston* (1985) compared the *Taitel* and *Dukler* result and found that the RHS of the above equation has to be multiplied with a factor ranging between 0.39 and 4 with 1 being a good choice. The accuracy of prediction varies from 2% for slow inclinations, 1/10, to 75% for 1/400 inclinations. *Anoda et al.* (1989) confirmed the validity of the above equation for large diameter pipes (0.18m) and large pressures (3 to 7.3 MPa).

*Bestion* (1990) reported data for stratification of horizontal flow for pressure range of 2 to 10 MPa. The data shows that if the liquid velocity is smaller than the bubble free rising velocity,  $V_2 < V_{Ku}$ , the flow is stratified.

**Stratified wavy flow:** The surface of the liquid remains *smooth* if the gas velocity remains below some prescribed value. *Mamaev et al.* reported in 1969 that waves started within  $0.01w_2 \leq w_1 \leq 3.33w_2$  and are always there for  $w_1 > 3.33w_2$ . *Taitel* and *Dukler* (1976) derived approximate expression for the gas velocity exciting waves

$$V_{1, \text{wavy}} - V_2 = \left[ \frac{4\eta_2 g(\rho_2 - \rho_1) \cos(\varphi - \pi/2)}{0.01\rho_2 \rho_1 V_2} \right]^{1/2}, \quad (1.57)$$

or after rearranging

$$\frac{V_{1, \text{wavy}} - V_2}{V_{TB}^*} = 20 \left( \frac{\rho_2}{\rho_1} \right)^{1/2} \left( \frac{\rho_2 V_2 D_h}{\eta_2} \right)^{-1/2}. \quad (1.58)$$

For larger gas velocity the surface of the liquid is *wavy* (stratified wavy flow).

**Annular flow – Fig.1.10:** The first requirement for the flow to be annular is that the film volume fraction is

$$\alpha_2 < 0.24, \quad (1.59)$$

see in *Taitel* (1990), p. 245. More information on the existence of the annular flow is contained in the *Weisman-Kang* flow map given below.

**Bubble flow:** *Taitel and Dukler (1976)* investigated gravity driven flow. The authors found the transition to dispersed bubble flow to occur if the liquid side share force due to turbulence equals the buoyancy force acting on the liquid. This results in the following criterion

$$V_{2,bubble} - V_2 = \left[ \frac{4F}{b} \frac{\alpha_1 g (\rho_2 - \rho_1) \cos(\varphi - \pi/2)}{\rho_2 c_{2w}} \right]^{1/2} \quad (1.60)$$

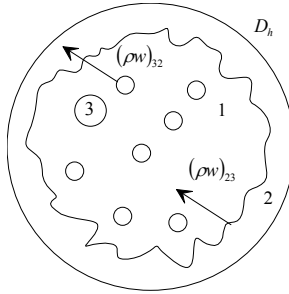


Fig. 1.10 Annular flow

where

$$c_{2w} = \frac{0.046}{\left( \frac{\rho_2 V_2 D_{h2}}{\eta_2} \right)^{1/5}}, \quad (1.61)$$

$$\frac{4F}{b} = 4 \frac{\pi D_h^2 / 4}{D_h \sin \theta} = \frac{\pi}{\sin \theta} D_h. \quad (1.62)$$

$F$  is the pipe cross section and  $b$  is the gas-liquid interface median if stratification is assumed. After rearrangement for pipe flow we obtain

$$V_{2,bubble} - V_2 = 8.26 \left[ \frac{\alpha_1 D_h g (\rho_2 - \rho_1) \cos(\varphi - \pi/2)}{\sin \theta \rho_2} \right]^{1/2} \left( \frac{\rho_2 V_2 D_{h2}}{\eta_2} \right)^{1/10}, \quad (1.63)$$

or

$$\frac{V_{2,bubble} - V_2}{V_{TB}^*} = 8.26 \left( \frac{\alpha_1}{\sin \theta} \right)^{1/2} \left( \frac{\rho_2 V_2 D_{h2}}{\eta_2} \right)^{1/10}. \quad (1.64)$$

For smaller gas velocities the bubble flow exists. For larger gas velocity the flow is intermittent regime.

### The *Weisman and Kang (1981)* empirical flow map

**Stratified-intermittent transition:** *Weisman* et al. (1979) defined the existence of the stratified flow if the liquid velocity is smaller than the prescribed value given below

$$\frac{\alpha_1 V_1}{V_{TB}} = 0.25 \left( \frac{\alpha_1}{\alpha_2} \frac{V_1}{V_{2, stratified}} \right)^{1.1}, \quad (1.65)$$

or

$$(\alpha V)_{2, stratified} = \left[ 0.25 V_{TB} (\alpha_1 V_1)^{0.1} \right]^{0.909}. \quad (1.66)$$

**Stratified wavy flow:** *Weisman* et al. (1979) proposed the following correlation

$$\left( \frac{\lambda_{RT}}{D_h} \right)^{0.4} \left( \frac{\alpha_1 \rho_1 V_1 D_h}{\eta_1} \right)^{0.45} = 8 \left( \frac{\alpha_1}{1 - \alpha_1} \frac{V_1}{V_2} \right)^{0.16} \quad (1.67)$$

i.e.

$$(\alpha V)_{1, wavy} = \left\{ 101.6 \frac{\eta_1}{\rho_1 D_h} \frac{1}{[(1 - \alpha_1) V_2]^{0.3556}} \left( \frac{D_h}{\lambda_{RT}} \right)^{0.889} \right\}^{1.55}. \quad (1.68)$$

For larger gas velocity the surface of the liquid is *wavy* (stratified wavy flow).

**Transition to annular flow:** The transition from stratified wavy to annular flow happens in convection regimes. This is the reason why the transition criterion is valid for horizontal as well for vertical flows. The transition conditions is defined by the *Weisman* et al. (1979) correlation

$$1.9 \left( \frac{\alpha_1}{1 - \alpha_1} \frac{V_{1, annular}}{V_2} \right)^{1/8} = \left( \frac{\alpha_1 V_{1, annular}}{V_{2Ku}} \right)^{0.2} \left( \frac{\alpha_1 V_{1, annular}}{V_{TB}} \right)^{0.36} \quad (1.69)$$

i.e. if

$$\alpha_1 V_{1, annular} > 4.37 \frac{V_{2Ku}^{0.46} V_{TB}^{0.83}}{[(1 - \alpha_1) V_2]^{0.287}}, \quad (1.70)$$

where

$$V_{2Ku} = \left[ g \sigma_2 (\rho_2 - \rho_1) / \rho_1^2 \right]^{1/4}, \quad (1.71)$$

the annular flow exists.



**Transition to bubble flow:** *Weisman* et al. (1979) defined the existence of the dispersed bubble regime by comparing the pressure drop with a value obtained by data comparison as follows

$$\frac{(dp/dz)_{20}}{g(\rho_2 - \rho_1)} = 2.89 \frac{\lambda_{RT}}{D_h}, \quad (1.72)$$

where

$$\lambda_{RT} = \left[ \sigma_{12} / (g \Delta \rho_{21}) \right]^{1/2}, \quad (1.73)$$

$$(dp/dz)_{20} = \frac{1}{2} \rho_2 \left( \frac{G}{\rho_2} \right)^2 \frac{\lambda_{R20}}{D_h}, \quad (1.74)$$

is the pressure drop due to friction computed for liquid flow having mass flow rate equal to the mixture mass flow rate

$$G = \sum_{l=1}^3 \alpha_l \rho_l w_l. \quad (1.75)$$

If

$$(dp/dz)_{20} > 2.89 \frac{\lambda_{RT}}{D_h} g(\rho_2 - \rho_1) \quad (1.76)$$

bubble flow exists. Otherwise we have intermittent flow. Using the *Blasius* formula for the friction coefficient

$$\lambda_{R20} = \frac{0.316}{\left( \frac{GD_h}{\eta_2} \right)^{1/4}}, \quad (1.77)$$

the above criterion can be rewritten as follows

$$\frac{GD_h}{\eta_2} > 5.26 \left[ \lambda_{RT} g \frac{D_h^2 \rho_2}{\eta_2^2} (\rho_2 - \rho_1) \right]^{4/7}. \quad (1.78)$$

*Weisman* and *Kang* (1981) reported a criterion for existence of dispersed bubble flow for vertical and inclined flows defined as follows

$$\frac{\alpha_1 V_{1,bubble}}{V_{TB}} = 0.45 \left( \frac{j}{V_{TB}} \right)^{0.78} \left[ 1 - 0.65 \cos(\varphi - \pi/2) \right], \quad (1.79)$$

where  $(\varphi - \pi/2)$  is the inclination angle. Solving with respect to  $\alpha_1 V_1$  requires some iterations starting with initial value

$$\alpha_1 V_{1,bubble} = (1 - \alpha_2) V_2 / \left\{ \frac{1}{0.45 V_{TB}^{0.22} [1 - 0.65 \cos(\varphi - \pi/2)]} - 1 \right\}. \quad (1.80)$$

For smaller gas velocities the bubble flow exists. For larger gas velocity the flow is in intermittent regime.

**Summary of the transition conditions:** The decision procedure for flow pattern recognition is defined as follows

- 1) Compute from Eq.(1.78)  $G_{dispersed}$ . If  $G > G_{dispersed}$  we have bubbly flow.
- 2) Compute  $(\alpha V)_{1,annular}$  from Eq. (1.70). If  $(\alpha V)_1 > (\alpha V)_{1,annular}$  we have annular flow.
- 3) Compute  $(\alpha V)_{2,stratified}$  from Eq. (1.66). If  $(\alpha V)_2 < (\alpha V)_{2,stratified}$  we have stratified flow.
- 4) Compute  $(\alpha V)_{1,wavy}$  from Eq. (1.68). If  $(\alpha V)_1 > (\alpha V)_{1,wavy}$  we have wavy flow.
- 5) Compute  $(\alpha V)_{1,bubble}$  from Eq. (1.80). If  $(\alpha V)_1 < (\alpha V)_{1,bubble}$  we have bubble flow.
- 6) In all other cases slug or plug flow is defined.

## 1.4 Heated channels

For heated channels the flow pattern maps for unheated flows have to be corrected after checking the heat transfer regime on the wall. If the heat flux on the wall exceeds the critical heat flux the inverted annular non-adiabatic flow occurs. There are investigations, which provide specific flow pattern transition criteria for non-adiabatic flow. Such an example is the study performed by *Doroschuk et al.* (1982), whose results are summarized in Table 1.1.

**Table 1.1** The *Doroschuk et al.* (1982) flow pattern boundaries for heated flow in a vertical pipe.  $D_h=0.0088m$

---

The identification criteria are verified for the following conditions:		
$10^6 \leq p \leq 10^7 Pa$ ,	$500 \leq G \leq 2500 kg/(m^2 s)$ ,	$-0.2 \leq X_{1,eq} \leq 0.6$ ,
$0 \leq \dot{q}_w'' \leq 0.5 \times 10^6 W/m^2$ , $X_{1,eq} = \frac{\sum X_i h_i - h'}{h'' - h'}$ , $X_1$ is the mass flow concentration of the vapor velocity field 1.		

---

One phase-to-subcooled nucleate boiling transition:

$$X_{1,eq} = -140 \left[ \frac{\dot{q}_w''}{G(h'' - h')} \right]^{1.1} \text{Re}_{20}^{0.2} \left( \frac{\rho_2}{\rho_1} \right)^{0.2}, \quad \text{Re}_{20} = GD_h / \eta_2,$$

*Tarasova* (1976), see in *Doroschuk et al.* (1982).

Bubble-to-slug flow transition:  $X_{1,eq} = 0$

Slug-to-churn flow transition

$$X_{1,eq} = c_1 Fr_{20}^{-0.25} \left( \frac{\rho_2}{\rho_1} \right)^{-0.05} - 0.76 \times 10^2 \left[ \frac{\dot{q}_w''}{G(h'' - h')} \right]^{0.25} \left( \frac{\rho_2}{\rho_1} \right)^{0.5}, \quad Fr_{20} = \frac{G}{gD_h \rho_2^2}.$$

Churn-to-annular, dispersed flow transition:

$$X_{1,eq} = c_2 \text{Re}_{20}^{-0.5} \left( \frac{\rho_2}{\rho_1} \right)^{-0.5}$$

Strong disturbance on the film-to-small ripples transition:

$$X_{1,eq} = c_3 We_{20}^{-0.25} \left( \frac{\rho_2}{\rho_1} \right)^{-0.35}, \quad We_{20} = \frac{G^2 D_h}{\rho_2 \sigma_2}$$

Rippled film-to-micro film transition:

$$X_{1,eq} = c_4 (We_{20} / \text{Re}_{20})^{-0.5} \left( \frac{\rho_2}{\rho_1} \right)^{0.25} \left( \frac{D_h}{0.008} \right)^{-0.25}$$

	$c_1$	$c_2$	$c_3$	$c_4$
tubes	0.05	130	3.5	0.11
annuli	0.08	120	3.0	0.07

## 1.5 Porous media

*Tung and Dhir* (1990) analyzed non-boiling gas-liquid flow in porous media consisting of solid particles with uniform diameter  $D_3$  assumed to form rhomboid arrays. The authors distinguish bubbly, annular and slug flow structure. Describing three-phase flow with solid particles requires also flow pattern transition criteria for the structure between the solid particles. That is why this information is of considerable interest for multi-phase flow modeling. The flow pattern criteria are functions of the gas volume fraction of the gas-liquid mixture only. For three velocity fields in which the third field consists of spheres the required gas-liquid void fraction is

$$\bar{\alpha}_1 = \frac{\alpha_1}{\alpha_1 + \alpha_2} . \quad (1.81)$$

**Table 1.2.** Flow regime limits as recommended by *Tung and Dhir* (1990)

The **bubble flow** regime is divided into two sub regimes  $\bar{\alpha}_1 \leq \bar{\alpha}_{10}$  and  $\bar{\alpha}_{10} \leq \bar{\alpha}_1 \leq \bar{\alpha}_{11}$ , where  $\bar{\alpha}_{10}$  and  $\bar{\alpha}_{20}$  are given by

$$\bar{\alpha}_{10} = \frac{\pi}{3} \frac{1 - \bar{\alpha}_1}{\bar{\alpha}_1} \bar{D}_1 (1 - \bar{D}_1) \left[ 6 \frac{\Delta \ell_3}{D_3} - 5(1 + \bar{D}_1) \right] \quad \text{as long as } \bar{\alpha}_{10} \geq 0$$

and

$$\bar{\alpha}_{11} = 0.6(1 - \bar{D}_1^2) \quad \text{as long as } \bar{\alpha}_{10} \geq 0.3 ,$$

where

$$D_1 = \min \left( \frac{1}{2} 2.7 \lambda_{RT}, \frac{1 - \alpha_3}{\alpha_3} D_3 \right)$$

is the bubble diameter

$$\bar{D}_1 = D_1 / D_3 ,$$

$$\frac{\Delta \ell_3}{D_3} = \left( \frac{\pi}{6} \frac{\sqrt{2}}{\alpha_3} \right)^{1/3} ,$$

and  $\Delta \ell_3$  is the average distance between two adjacent solid particles if they are assumed to be rhomboid arrays.

Pure **slug flow** occurs in the range of  $\bar{\alpha}_{12} \leq \bar{\alpha}_1 \leq \bar{\alpha}_{13}$ , where

$$\bar{\alpha}_{12} = \pi/6 \approx 0.52 \quad \text{and}$$

$$\bar{\alpha}_{13} = \pi\sqrt{2}/6 \approx 0.74 .$$

Pure **annular flow** is assumed to occur in the range of  $\bar{\alpha}_1 > \bar{\alpha}_{13}$ .

## 1.6 Particles in film boiling

The particles in film boiling are surrounded by a film with dimensionless thickness

$$\delta_{1F}^* = \frac{\delta_{1F}}{D_3}, \quad (1.82)$$

where  $\delta_{1F}^* > 0$ . The ratio of the volume of the sphere consisting of one particle and the surrounding film to the volume of the particle itself is

$$(\alpha_3 + \alpha_{1F}) / \alpha_3 = (D_3 + 2\delta_{1F})^3 / D_3^3 = (1 + 2\delta_{1F}^*)^3. \quad (1.83)$$

Therefore the vapor film volume fraction of the mixture is

$$\alpha_{1F} = \alpha_3 \left[ (1 + 2\delta_{1F}^*)^3 - 1 \right]. \quad (1.84)$$

Thus the condition that the films are not touching each other is

$$\alpha_3 + \alpha_{1F} = \alpha_3 (1 + 2\delta_{1F}^*)^3 < 0.25 \text{ to } 0.52 \quad (1.85)$$

depending of the diameter of the film-particle system. The application of the criteria already derived for gas-liquid flows in porous structures is also used by using as a controlling void fraction the local gas volume fraction in the space outside the film-particles volumes,

$$\bar{\alpha}_1 = \frac{\alpha_1 - \alpha_{1F}}{\alpha_1 - \alpha_{1F} + \alpha_2}. \quad (1.86)$$

The condition to have three-phase flow with continuous liquid and particles being in film boiling is then

$$\bar{\alpha}_1 < 0.74. \quad (1.87)$$

This is a very important result. It simply demonstrates that particles in film boiling can be surrounded by much less continuous liquid mass than required in case of no film boiling.

## 1.7 Rod bundles

**Bubble flow:** Venkateswararao et al. (1982) investigated two-phase flow in a vertical rod bundle and found that bubbles are seldom observed in the smallest gap between two rods. They migrate to the open area which exists between the rods. From this observation the authors recommend the upper limit of the bubble flow  $\alpha_{1,\text{bubble to slug}}$  to be valid only for the part of the cross section inside the inscribed circle between the neighboring rods. The local void fraction in this circle

$$\alpha_{1, RB} = f \alpha_1 \quad (1.88)$$

is  $f$  times greater than the averaged void fraction, where

$$f = \frac{\frac{4}{\pi} \left( \frac{\ell_{FR}}{D_{FR}} \right)^2 - 1}{\left( \sqrt{2} \frac{\ell_{FR}}{D_{FR}} - 1 \right)^2} \quad (1.89)$$

for a quadratic array, and

$$f = \frac{\frac{\sqrt{3}}{\pi} \left( \frac{\ell_{FR}}{D_{FR}} \right)^2 - \frac{1}{2}}{\left( 2 \frac{\sqrt{3}}{3} \frac{\ell_{FR}}{D_{FR}} - 1 \right)^2} \quad (1.90)$$

for a triangular array. Here  $\ell_{FR}$  and  $D_{FR}$  are the pitch and the rod diameter, respectively. Thus, the comparison of  $\alpha_{1, RB}$  with the limit,  $\alpha_{1, \text{bubble to slug}}$ , dictates whether bubble flow exists or not.

**Slug flow:** For slug flow in a vertical rod bundle there are no confining walls around the *Taylor* bubbles. The transition criteria in this case are quite different compared to the pipe flow. *Venkateswararao et al. (1982)* observed *Taylor*-like bubbles occupying almost the entire free space in the cell. At the same time the number of cells occupied by *Taylor* bubbles increases and eventually the concentration of the occupied cells is great enough to cause coalescence  $\alpha_{1, \text{slug coalescence}}$ .

For the quadratic rod array the authors recommend

$$\alpha_{1, \text{slug coalescence}} = \frac{\pi}{6 \cos \theta} \frac{\ell_{FR} + D_{FR}}{2 \ell_{FR} - D_{FR}}, \quad (1.91)$$

where

$$\theta = \arcsin \frac{\ell_{FR} - D_{FR}}{\ell_{FR} + D_{FR}}. \quad (1.92)$$

Similar is the expression for the triangular rod array.

*Mizutani, et al.* performed in 2006 air-water experiments at atmospheric pressure in 4x4-rod-bundle with 12mm transparent rods. Illustration of the results is given in Fig. 1.11.

The authors found that: (1) the region of slug flow in the  $(\alpha_1 w_1, \alpha_2 w_2)$ -flow pattern diagram is so narrow that it can be considered as a boundary between bubbly and churn flows; (2) the boundary between bubbly and churn flows is close to the boundary between bubbly and slug flows of the *Mishima and Ishii (1984)* flow pattern transition model, and (3) the boundary between churn and annular flows is well predicted by the *Mishima and Ishii (1984)* model.

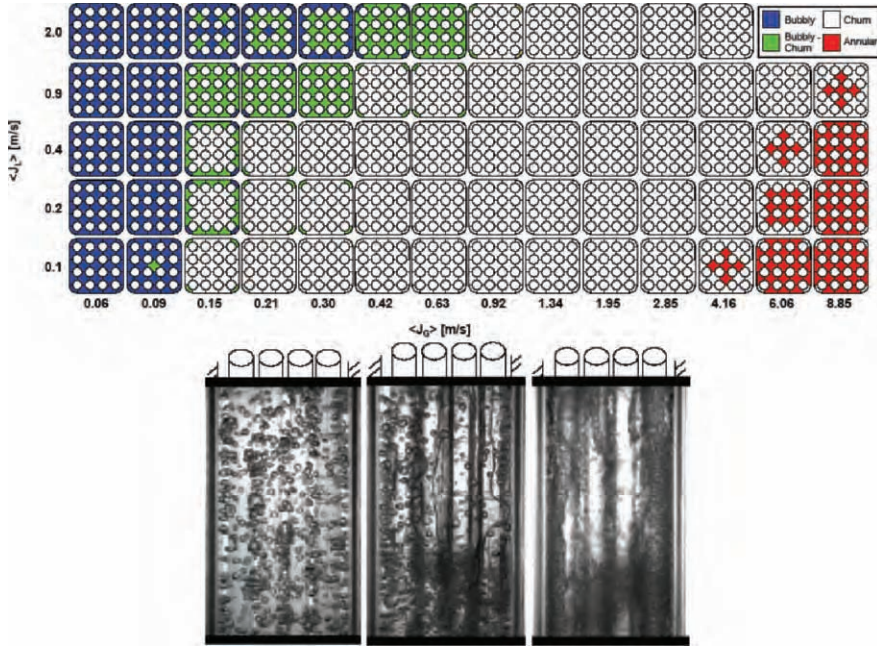


**Fig. 1.11** a) Flow pattern observed by Mizutani et al. 2006 in rod bundle. Regime parameter: air-water, atmospheric conditions. Photographs of the flow pattern at  $\alpha_2 w_2 = 0.9 \text{ m/s}$  ; b) bubbly flow  $\alpha_1 w_1 = 0.06 \text{ m/s}$  ; c) churn flow  $\alpha_1 w_1 = 0.42 \text{ m/s}$  ; d) churn to annular transition  $\alpha_1 w_1 = 8.85 \text{ m/s}$

## Nomenclature

### Latin

$C_{li}$	mass concentration of species $i$ inside the field $l$ , dimensionless
$C_0$	drift flux distribution coefficient, dimensionless
$D_d$	particle diameter (bubble, droplet, particle), $m$
$D_{1, \text{solid like}}$	bubbles with size less then this behave as a solid sphere, $m$
$D_h$	hydraulic diameter, $m/s$
$D_{FR}$	rod diameter, $m$
$Fr$	$= \frac{(\rho w)^2 v_h}{g D_h}, \text{ Froude number, dimensionless}$

---

$Fr_{20}$	$= \frac{G}{gD_h\rho_2^2}$ , <i>Froude number, dimensionless</i>
$G$	$= \sum_{l=1}^3 \alpha_l \rho_l w_l$ , <i>mass flow rate, kg/(m<sup>2</sup>s)</i>
$g$	<i>gravitational acceleration, m/s<sup>2</sup></i>
$H$	<i>distance between two parallel plates, m</i>
$h_l$	<i>specific enthalpy of the velocity field l, J/kg</i>
$h''$	<i>saturated vapor specific enthalpy, J/kg</i>
$h'$	<i>saturated liquid specific enthalpy, J/kg</i>
$j$	$= \alpha_1 V_1 + (1 - \alpha_1) V_2$ , <i>mixture volumetric flux, m/s</i>
$\ell_{FR}$	<i>pitch diameter, m</i>
$\ell_d^t$	<i>mean free path length of oscillating particles, m</i>
$\ell_{TB}$	<i>length of the Taylor bubble, m</i>
$Ma$	<i>local Mach number, dimensionless</i>
$N_{\eta 2}$	$= \eta_2 / \sqrt{\rho_2 \sigma_2 \lambda_{RT}}$
$n_1$	<i>number of bubbles per unit mixture volume, l/m<sup>3</sup></i>
$p$	<i>pressure, Pa</i>
$\dot{q}_w''$	<i>heat flux from the wall into the flow, W/m<sup>2</sup></i>
$Re_{20}$	$= GD_h / \eta_2$ , <i>Reynolds number, dimensionless</i>
$Vol_{cell}$	<i>cell volume, m<sup>3</sup></i>
$V_{1Ku}$	$= \sqrt{2} [g\sigma_2 (\rho_2 - \rho_1) / \rho_2^2]^{1/4}$ , <i>Kutateladze bubble rise velocity in a pool, m/s</i>
$V_{TB}$	$= \sqrt{\frac{\rho_2 - \rho_1}{\rho_2}} gD_h$ slug (Taylor bubble) raising velocity, <i>m/s</i>
$V_1$	<i>gas velocity, m/s</i>
$V_2$	<i>liquid velocity, m/s</i>
$V_{1, stratified}$	<i>gas velocity dividing the non-stratified from the stratified flow, m/s</i>
$V_{2, stratified}$	<i>liquid velocity dividing the non-stratified from the stratified flow, m/s</i>
$V_{1, annular}$	<i>gas velocity dividing the non-annular from the annular flow, m/s</i>
$V_{1, wavy}$	<i>velocity: for gas velocity larger than this velocity the surface of the liquid is wavy (stratified wavy flow), m/s</i>
$V_{2, bubble}$	<i>critical liquid velocity for transition into bubble flow, m/s</i>
$We_{20}$	$= \frac{G^2 D_h}{\rho_2 \sigma_2}$ , <i>Weber number, dimensionless</i>



---

$X_{1,eq}$	$= \frac{\sum X_l h_l - h'}{h'' - h'}$ , equilibrium mass flow concentration of the vapor velocity field, <i>dimensionless</i>
$X_1$	mass flow concentration of the vapor velocity field 1, <i>dimensionless</i>
$z$	axial coordinate, <i>m</i>

**Greek**

$\alpha_l$	local volume fractions of the fields <i>l</i> , <i>dimensionless</i>
$\alpha_d$	local volume fractions of the dispersed field <i>d</i> , <i>dimensionless</i>
$\alpha_{1,B-Ch}$	gas volume fraction that divides bubble and churn turbulent flow, <i>dimensionless</i>
$\alpha_{1,bubble\ to\ slug}$	gas volume fraction that divides bubble and slug flow, <i>dimensionless</i>
$\alpha_{1,slug\ to\ churn}$	gas volume fraction that divides slug and churn turbulent flow, <i>dimensionless</i>
$\beta$	$= X_1 v_1 / v_h$ , homogeneous gas mass fraction, <i>dimensionless</i>
$\gamma_v$	volume porosity – volume occupied by the flow divided by the total cell volume, <i>dimensionless</i>
$\Delta \ell_d$	averaged distance between the centers of two adjacent particles, <i>m</i>
$\Delta \ell_3$	average distance between two adjacent particles if they are assumed to be rhomboid arrays, <i>m</i>
$\delta_{2F}$	liquid thickness, <i>m</i>
$\lambda_{fr}$	friction coefficient, <i>dimensionless</i>
$\lambda_{RT}$	<i>Rayleigh-Taylor</i> wavelength, <i>m</i>
$\rho_1$	gas density, <i>kg/m<sup>3</sup></i>
$\rho_2$	liquid density, <i>kg/m<sup>3</sup></i>
$\rho w$	mixture mass flow rate, <i>kg/(m<sup>2</sup>s)</i>
$\sigma_2$	viscous tension, <i>N/m</i>
$\varepsilon_2$	dissipation rate of the turbulent kinetic energy of the liquid, <i>W/m<sup>3</sup></i>
$\eta_1$	dynamic gas viscosity, <i>kg/(ms)</i>
$\eta_2$	dynamic liquid viscosity, <i>kg/(ms)</i>
$v_h$	$= X_1 v_1 + (1 - X_1) v_2$ , homogeneous specific volume, <i>m<sup>3</sup>/kg</i>
$\theta$	angle with origin the pipe axis defined between the upwards oriented vertical and the liquid-gas-wall triple point, <i>rad</i>
$\varphi$	angle between the upwards oriented vertical and the pipe axis, <i>rad</i>

## References

- Anoda Y, Kukita Y, Nakamura N, Tasaka K (1989) Flow regime transition in high-pressure large diameter horizontal two-phase flow, ANS Proc. 1989 National Heat Transfer Conference, 6-9 Aug., Philadelphia, Pennsylvania, ISBN: 0-89448-149-5, ANS Order Number 700143
- Barnea D, Taitel Y (1994) Interfacial and structural stability of separated flow, *Int. J. Multiphase Flow*, vol 20 pp 387-414
- Bestion D (1990) The physical closure laws in the CHATHRE code, *Nuclear Engineering and Design*, vol 124 pp 229-245
- Brodkey RS (1967) *The phenomena of fluid motions*, Addison-Wesley Press
- Davies RM and Taylor GI (1950) The mechanism of large bubble rising velocity through extended liquids and through liquids in tubes, *Proc. R. Soc.*, vol 200A pp 375-390
- Deichel M, Winter ERF (1990) Adiabatic two-phase pipe flow at air-water mixtures under critical flow conditions, *Int. J. Multiphase Flow*, vol 16 no 3 pp 391-406
- Delhaye JM (1981) Basic equations for two-phase flow, in Bergles AE et al., Eds., *Two-phase flow and heat transfer in power and process industries*, Hemisphere Publishing Corporation, McGraw-Hill Book Company, New York
- Dimitresku DT (1943) Stroemung an einer Luftblase im senkrechten Rohr, *Z. angew. Math. Mech.*, vol 23 no 3 pp 139-149
- Doroschuk VE, Borevsky LY, Levitan LL (1982) Holographic investigation of steam-water flows in heated and unheated channels, 7th Int. Heat Transfer Conf. Munich TF15 pp 277-281
- Hewitt GF, Wallis GB (1963) Flooding and associated phenomena in falling film flow in a vertical tube, UKAEA Report, AERE R-4022
- Ginsberg T, Jones OC Jr, Chen JC (Mid-Dec. 1979) Flow behavior of volume-heated boiling pools: implication with respect to transition phase accident conditions, *Nuclear Technology*, vol 46 pp 391-398
- Grawford TJ, Weinberger CB, Weisman J (1985) Two-phase flow pattern and void fractions in downward flow. Part I: Steady state flow pattern, *Int. J. Multiphase Flows*, vol 11 no 2 pp 761-782. (1986) Part II: Void fractions and transient flow pattern, *Int. J. Multiphase Flows*, vol 12 no 2 pp 219-236
- Hohannessen T (1972) Beitrag zur Ermittlung einer allgemeingültigen Stroemungsbilder-Karte, SIA Fachgruppe fuer Verfahrenstechnik, Tagung vom 14. Dez. 1972, ETH Zuerich
- Johnston AJ (1985) Transient from stratified to slug regime in countercurrent flow, *Int. J. Multiphase Flow*, vol 11 no 1 pp 31-41
- Kataoka I, Ishii M (July 1982) Mechanism and correlation of droplet entrainment and deposition in annular two-phase flow. NUREG/CR-2885, ANL-82-44
- Kutateladze SS (1951) Gidrodinamicheskaja teorija izmenenija rejima kipiennja jidkosti pri svobodnoj konvekcii, *Izvestija akademii nauk SSSR, Otfelenie technicheskikh hanuk*, no 4 pp 529-536
- Mamaev WA, Odicharia GS, Semeonov NI, Tociging AA (1969) *Gidrodinamika gasogid-kostnych smesey w trubach*, Moskva
- Milne-Thomson LM (1968) *Theoretical hydrodynamics*, MacMillan & Co. Ltd., London
- Mishima K, Ishii M (Dec. 1980) Theoretical prediction of onset of horizontal slug flow, *Journal of Fluid Engineering*, vol 102 pp 441-445

- Mishima K, Ishii M (1984) Flow regime transition criteria for upward two-phase flow in vertical tubes, *Int. J. Heat Mass Transfer*, vol 27 no 5 pp 723-737
- Mizutani Y, Hosokawa S and Tomiyama A (July 17-20, 2006) Two phase flow patterns in a four by four rod bundle, *Proc. of ICONE14, Int. Conf. on Nuclear Engineering*, Miami, FA, USA
- Pushkina OL and Sorokin L (1969) Breakdown of Liquid Film Motion in Vertical Tubes, *Heat Transfer Soviet Research*, vol 1 pp 56-64
- Rouhani SZ, Sohal MS (1983) Two-phase flow patterns: A review of research results, *Progress in Nucl. Energy*, vol 11 no 3 pp 219-259
- Taitel Y (1990) Flow pattern transition in two - phase flow, *Proc. 9 th Int. Heat Transfer Conf.*, Jerusalem, Israel, ed. by G. Hetstroni, Hemisphere, New York etc., vol 1 pp 237-254
- Taitel Y, Bornea D, Dukler AE (1980) Modeling flow pattern transitions for steady upward gas-liquid flow in vertical tubes, *AIChE J.*, vol 26 no 3 p 345
- Taitel Y, Dukler AE (Jan. 1976) A model for predicting flow regime transitions in horizontal and near horizontal gas-liquid flow, *AIChE J.*, vol 22 no 1 pp 47-55
- Tien CL, Chung KL and Liu CP (1979) Flooding in counter-current flows. EPRI Report no EPRI NP-1283
- Tung VX, Dhir VK (1990) Finite element solution of multi-dimensional two-phase flow through porous media with arbitrary heating conditions, *Int. J. Multiphase Flow*, vol 16 no 6 pp 985-1002
- Venkateswararao P, Semiat R, Dukler AE (1982) Flow pattern transition for gas-liquid flow in a vertical rod bundle, *Int. J. Multiphase Flow*, vol 8 no 5 pp 509-524
- Wallis GB (1969) *One-Dimensional Two-Phase Flow*, McGraw-Hill
- Wallis GB, Dobson JE (1973) The onset of slugging in horizontal stratified air-water flow, *Int. J. Multiphase Flow*, vol 1 pp 173-193
- Weisman J, Duncan D, Gibson J, Grawford T (1979) Effect of fluid properties and pipe diameter on two - phase flow pattern in horizontal lines, *Int. J. Multiphase Flow*, vol 5 pp 437-462
- Weisman J, Kang Y (1981) Flow pattern transition in vertical and upwardly inclined lines, *Int. J. Multiphase Flow*, vol 7 pp 271-291
- Whalley PB (1987) Flooding, slugging and bottle emptying, *Int. J. Multiphase Flow*, vol 13 no 5 pp 723-728



## 2 Drag, lift and virtual mass forces

The pressure distribution around a particle moving in a continuum is non-uniform. Integrating the pressure distribution over the surface one obtains a resulting force that is different from zero. As shown in Vol. I, Chapter 6.2, the different spatial components of the integral correspond to different forces: drag-, lift and virtual mass forces. The averaging procedure over a family of particles gives some averaged forces which can be used in the computational analysis based on coarse meshes in the space. The purpose of this section is to summarize the empirical information for computation of the drag-, lift and virtual mass forces in multi-phase flow analysis.

### 2.1 Drag forces

#### 2.1.1 Introduction

Consider the discrete velocity field  $d$  surrounded by a continuum denoted by  $c$ . The force acting on a single particle multiplied by the number of particles per unit volume is

$$f_d^d = -\frac{\alpha_d}{\pi D_d^3 / 6} c_{cd}^d \frac{1}{2} \rho_{cd} |\Delta V_{cd}| \Delta V_{cd} \frac{\pi D_d^2}{4} = -\alpha_d \rho_{cd} \frac{1}{D_d} \frac{3}{4} c_{cd}^d |\Delta V_{cd}| \Delta V_{cd}. \quad (2.1)$$

Next we describe some experimentally observed effects influencing the *drag coefficient*  $c_{cd}^d$ .

It is well known from experimental observations that the drag coefficient depends on the radius, on the particle *Reynolds* number based on the absolute value of the relative velocity, and on whether the particle is solid, bubble, drop of pure liquid or drop of liquid with impurities of microscopic solid particles. Due to the *internal circulation* in the liquid or gas particle, its drag coefficient can be 1/3 of the corresponding drag coefficient of the solid particle with the same radius and *Reynolds* number. *Small impurities hinder the internal circulation* and lead to drag coefficients characteristic for solid particles.

Drag coefficients on deformed particles are 2 to 3 times larger than rigid sphere drag coefficients.

During the relative motion each particle deforms the continuum. *Increasing the concentration leads to increased resistance to the deformation in a restricted geometry*. This means that the mechanical cohesion of the family of particles with the surrounding continuum is stronger than the cohesion of the single particle

moving with the same relative velocity. In other words, the *drag coefficient* of a *single* particle with a given radius and *Reynolds* number is *less* than the drag coefficient of a particular particle with the same radius and *Reynolds* number, belonging to a *family of particles* collectively moved through the continuum.

The velocity  $V_{wake}$  at any location  $\delta$  behind a solid particle with diameter  $D_d$ , caused by its wake, e.g.

$$V_{wake} \approx \Delta V_{cd} / \left[ 0.2 + 0.24\delta / D_d + 0.04(\delta / D_d)^2 \right], \quad (2.2)$$

*Stuhmiller et al.* (1989), can influence the interaction of the following particle with the continuum. For one and the same concentration and form of the particles, the less the compressibility of the particle, the greater the drag coefficient.

### 2.1.2 Drag coefficient for single bubble

The drag coefficients in bubbly flow are governed by three dimensionless numbers: The *Reynolds* number for a single bubble,

$$Re = D_1 \rho_2 |\Delta V_{12}| / \eta_2, \quad (2.3)$$

the *Eötvös* number,

$$Eo = (D_1 / \lambda_{RT})^2, \quad (2.4)$$

where

$$\lambda_{RT} = [\sigma / (g \Delta \rho_{21})]^{1/2} \quad (2.5)$$

is the *Rayleigh-Taylor* instability wavelength and the *Morton* number

$$Mo = \frac{g \Delta \rho_{21}}{\sigma} \left( \frac{\eta_2^2}{\rho_2 \sigma} \right)^2. \quad (2.6)$$

*Geary* and *Rice* observed that the aspect ratio of a bubble defined as the high (minor axis) divided by the breadth (major axis) varies

$$\frac{h}{b} = \begin{cases} 1 & \text{for } Ta < 1 \\ \left\{ 0.81 + 0.206 \tanh \left[ 2(0.8 - \log_{10} Ta) \right] \right\}^3 & \text{for } 1 \leq Ta \leq 39.8 \\ 0.24 \times 1.6 & \text{for } Ta > 39.8 \end{cases}$$

depending of the following dimensionless number

$$Ta = \frac{|\Delta V_{12}|}{\sqrt{g \lambda_{RT}}} \frac{D_1}{\lambda_{RT}}.$$

The data base for this correlation was within  $1 \leq Ta \leq 50$ .

Next we will consider four regimes of mechanical flow-bubble interaction.

*Hadamard* (1911) and *Rybczynski* (1911) analyzing flow of a viscous fluid 2 around a sphere 1 having other viscosity for  $Re \ll 1$  succeeded in finding analytical stream functions inside and outside the sphere and computed a drag coefficient

$$c_{21}^d = \frac{3\eta^* + 2}{\eta^* + 1} \frac{8}{Re},$$

Depending on the viscosity ratio  $\eta^* = \eta_1/\eta_2$ . For infinite viscosity of the internal fluid which is equivalent to solid sphere the solution reduces to the famous Stokes solution  $c_{21}^d = 24/Re$ . For inviscid bubble  $c_{21}^d = 16/Re$ . As already mentioned, bubbles in liquids with impurities behave as a solid spheres.

1) For low relative velocities

$$Re \leq 16, \quad (2.7)$$

the force on a single particle depends linearly on the velocity difference, *Stokes* (1880). This regime is called the *Stokes* regime. The drag coefficient for this regime is computed as follows

$$c_{21}^d = 24/Re. \quad (2.8)$$

2) We have a *viscous* regime (the force depends non-linearly on the velocity difference) if the following condition is satisfied

$$Re > 16. \quad (2.9)$$

The drag coefficient for this regime is computed as follows

$$c_{21}^d = \frac{24}{Re} \left( 1 + 0.1 Re^{0.75} \right). \quad (2.10)$$

This is the *Ishii and Zuber* (1978) modification of the *Oseen* equation (1910)

$$c_{21}^d = \frac{24}{Re} \left( 1 + \frac{3}{16} Re \right) \quad (2.11)$$

modified later by *Schiller and Naumann* (1935) to

$$c_{21}^d = \frac{24}{Re} \left( 1 + 0.15 Re^{0.687} \right) \quad (2.12)$$

and valid for  $Re < 500$ . *Lahey et al.* (1980) proposed the dependence

$$c_{21}^d = 26.34 Re^m$$

with

$$m = -0.889 + 0.0034 Re + 0.0014 (\ln Re)^2.$$

For larger Reynolds number  $5 < Re \leq 1000$  *Michaelides* (2003) reported a correlation obtained by direct numerical simulation:

$$c_{cd}^d = \frac{2 - \eta_d / \eta_c}{2} c_{cd,0}^d + \frac{4 \eta_d / \eta_c}{6 + \eta_d / \eta_c} c_{cd,2}^d \quad \text{for } 0 \leq \eta_d / \eta_c \leq 2 ,$$

$$c_{cd}^d = \frac{4}{\eta_d / \eta_c + 2} c_{cd,2}^d + \frac{\eta_d / \eta_c - 2}{\eta_d / \eta_c + 2} c_{cd,\infty}^d \quad \text{for } 2 < \eta_d / \eta_c < \infty ,$$

where

$$c_{cd,0}^d = \frac{48}{\text{Re}} \left( 1 + \frac{2.21}{\sqrt{\text{Re}}} - \frac{2.14}{\text{Re}} \right) ,$$

$$c_{cd,2}^d = 17 \text{Re}^{-2/3} ,$$

$$c_{cd,\infty}^d = \frac{24}{\text{Re}} \left( 1 + \frac{1}{6} \text{Re}^{2/3} \right) ,$$

with subscripts  $c$  used for continuum and  $d$  for disperse. The correlation is useful also for droplets in gas.

These two regimes are known in the literature as "undisturbed particles" because the distortions of the particles are negligible. The correlations for the undisturbed particles given above are valid for a slightly contaminated system, *Tomiyama et al. (1990, 1995)*. For pure liquids the drag coefficient is given by *Tomiyama* as  $2/3$  of that for slightly contaminated liquids. The "distorted particles" regime is characterized by a vortex system developing behind the particle, where the vortex departure creates a large wake region which distorts the particle itself and the following particles.

3) We have a *distorted* bubble regime (the single particle drag coefficient depends only on the particle radius and fluid properties, but not on the velocity or viscosity) if the following condition is satisfied

$$\frac{24}{\text{Re}} (1 + 0.1 \text{Re}^{0.75}) \leq \frac{2}{3} D_1 / \lambda_{RT} < \frac{8}{3} . \quad (2.13)$$

The drag coefficient for this regime is computed as follows

$$c_{21}^d = \frac{2}{3} (D_1 / \lambda_{RT}) . \quad (2.14)$$

4) We have the regime of strongly deformed, *cap bubbles* if

$$D_1 / \lambda_{RT} \geq 4 . \quad (2.15)$$

*Tomiyama et al. (1995)* proposed an empirical correlation for the drag coefficient and generalized the distorted and the cup bubble regimes as follows:

$$c_{21}^d = \frac{8}{3} \frac{Eo}{Eo + 4} . \quad (2.16)$$



The data base for this correlation was reported to be for  $Re$  number up to  $10^5$  and for  $Eo$  number between  $10^{-2}$  and  $10^3$ , see Fig. 3 in *Tomiyama et al. (1995)*.

In a later work *Tomiyama (1998)* proposed a general correlation set for bubble drag coefficient:

For pure liquid

$$c_{21}^d = \max \left\{ \min \left[ \frac{16}{Re} (1 + 0.15 Re^{0.687}), \frac{48}{Re} \right], \frac{8}{3} \frac{Eo}{Eo + 4} \right\}. \quad (2.17)$$

For slightly contaminated liquid

$$c_{21}^d = \max \left\{ \min \left[ \frac{24}{Re} (1 + 0.15 Re^{0.687}), \frac{72}{Re} \right], \frac{8}{3} \frac{Eo}{Eo + 4} \right\}. \quad (2.18)$$

For contaminated systems

$$c_{21}^d = \max \left[ \frac{24}{Re} (1 + 0.15 Re^{0.687}), \frac{8}{3} \frac{Eo}{Eo + 4} \right]. \quad (2.19)$$

As noted by *Tomiyama* the system air-tap water may correspond to contaminated or slightly contaminated water. Water carefully distilled two or more times belongs to the pure liquid system. This correlations represents experimental data very well for  $10^{-2} < Eo < 10^3$  and  $10^{-3} < Re < 10^6$ , and  $10^{-14} < Mo < 10^7$ .

### 2.1.3 Family of particles in continuum

In order to calculate the drag coefficient for a family of particles in continuum, *Ishii and Chawla (1979)*, among others, use the same relationship as for a single particle, changing properly only the *effective continuum viscosity*  $\eta_m$  (similarity assumption)

$$\frac{\eta_m}{\eta_c} = \left(1 - \frac{\alpha_d}{\alpha_{dm}}\right)^{-2.5\alpha_{dm}\eta^*} \quad \eta^* = \frac{\eta_d + 0.4\eta_c}{\eta_d + \eta_c} \quad (2.20)$$

as a function of the volume concentration of the disperse phase and the *maximum packing*  $\alpha_{dm}$  - see Table 2.1.

**Table 2.1** Effective viscosity model

	Bubble in liquid	Drop in liquid	Drop in Gas	Solid Part. System
$\alpha_{dm}$	$\approx 1$	$\approx 1$	0.26 to 1	$\approx 0.62$
$\eta^*$	0.4	$\approx 0.7$	1	1
$\frac{\eta_m}{\eta_c}$	$(1 - \alpha_d)^{-1}$	$(1 - \alpha_d)^{-1.75}$	$\approx (1 - \alpha_d)^{-2.5}$ <i>Brinkman (1951)</i> <i>Roscoe (1952)</i>	$(1 - \frac{\alpha_d}{0.62})^{-1.55}$

The experiments with liquid - liquid used for verification of the drag coefficient are summarized below:

- Water dispersed in mercury column with diameter 0.1 m. The water was introduced through a perforated plate with diameters of the nozzles 0.1 m. The volume fraction of water was varied between 0 and 0.5.
- Isobutanol water, isobutyl kentone water, loluen water column with diameter 0.0476 m. The dispersed liquid was introduced into the column with orifices having diameter 0.0016 to 0.0032 m.
- Kerosene water column with diameter 0.015 m and nozzle diameter 0.0015 m for introduction of the dispersed phase. The volumetric fraction of the dispersed phase varied between 0.05 and 0.4.
- Kerosene neptane column with diameter 0.032 m. The volumetric fraction of the dispersed phase varied between 0.05 and 0.7.

Next we discuss how to compute the drag coefficient for a *gas-liquid* system in a pool ( $D_{hy} \gg D_l$ ) according to the recommendation of *Ishii* and *Chawla*, and extend their analysis to three-dimensional flow. In the three-phase case the forces have to be additionally corrected in order to take into account the influence of the third component. If we assume that the particles are completely surrounded by the continuum the correction for the influence of the third component can be easily introduced considering the bubbles and the continuous liquid as one mixture flowing through the fictitious channel volume fraction  $\alpha_1 + \alpha_2$ . The bubble concentration in this fictitious channel is

$$\alpha_d = \frac{\alpha_1}{\alpha_1 + \alpha_2}. \quad (2.21)$$

The assumption that the bubbles are completely surrounded by the continuum holds only if the size of the solid particles  $D_3$  is considerably smaller than the size of the bubbles  $D_l$ . For other cases additional experimental information is necessary to describe completely this phenomenon.

1) We have the *Stokes regime* (the force on a single particle depends linearly on the velocity difference *Stokes* (1880)) if the following condition is satisfied

$$Re < 16, \quad (2.22)$$

and

$$\frac{2}{3} D_l / \lambda_{RT} < (1 - \alpha_d)^{0.6} \frac{24}{Re}, \quad (2.23)$$

where

$$Re = D_l \rho_2 |\Delta V_{12}| / \eta_m. \quad (2.24)$$

The drag coefficient is computed as follows

$$c_{21}^d = 24 / Re . \quad (2.25)$$

The drag force is therefore

$$\mathbf{f}_{21}^d = -(18\alpha_d \eta_m / D_1^2)(\mathbf{V}_2 - \mathbf{V}_1) . \quad (2.26)$$

2) We have a viscous regime (the force depends non-linearly on the velocity difference) if the following condition is satisfied

$$Re > 16, \quad (2.27)$$

and

$$\frac{2}{3} D_1 / \lambda_{RT} < (1 - \alpha_d)^{0.6} \frac{24}{Re} (1 + 0.1 Re)^{0.75} . \quad (2.28)$$

The drag coefficient is computed as follows

$$c_{21}^d = \frac{24}{Re} (1 + 0.1 Re^{0.75}) , \quad (2.29)$$

which is as already mentioned the *Ishii* and *Zuber* (1978) modification of *Schiller* and *Nauman* (1935) valid for  $Re < 500$ . The drag force is therefore

$$\mathbf{f}_{21}^d = -(18\alpha_d \eta_m / D_1^2)(1 + 0.1 Re^{0.75})(\mathbf{V}_2 - \mathbf{V}_1) . \quad (2.30)$$

These two regimes are designated by *Ishii* and *Chawla* as "undisturbed particles" because the distortions of the particles are negligible. The "distorted particles" regime is characterized by a vortex system developing behind the particle, where the vortex departure creates a large wake region distorting the particle itself and the following particles.

3) We have a *distorted* bubble regime (the single particle drag coefficient depends only on the particle radius and fluid properties, but not on the velocity or viscosity) if the following condition is satisfied

$$(1 - \alpha_d)^{0.6} \frac{24}{Re} (1 + 0.1 Re^{0.75}) \leq \frac{2}{3} D_1 / \lambda_{RT} < \frac{8}{3} (1 - \alpha_d)^{0.87} . \quad (2.31)$$

The three components of the drag coefficient computed as follows

$$c_{21}^d = \frac{2}{3} (D_1 / \lambda_{RT}) \left( \frac{1 + 17.67 f^{6/7}}{18.67 f} \right)^2 ; f = (1 - \alpha_d)^{1.5} . \quad (2.32)$$

4) We have the regime of strongly deformed, *cap bubbles* if

$$\frac{2}{3} D_1 / \lambda_{RT} \geq \frac{8}{3} (1 - \alpha_d)^{0.87} . \quad (2.33)$$

The drag coefficient for this regime is

$$c_{21}^d = \frac{8}{3}(1 - \alpha_d)^2. \quad (2.34)$$

The drag force is therefore

$$\mathbf{f}_{21}^d = -\left[2\alpha_d(1 - \alpha_d)^2 \rho_2 / D_1\right] |\mathbf{V}_2 - \mathbf{V}_1| (\mathbf{V}_2 - \mathbf{V}_1). \quad (2.35)$$

For a flow in a pool this regime also exists for  $\alpha_d > 0.3$ .

The above described methods for computation of the bubble drag coefficient were verified as follows Ishii and Zuber (1978).

1. Air-water in column of 0.06 m diameter and bubble diameter of 0.00276 m in the region  $\alpha_2 V_2 = 0.44$  to 1.03 m/s,  $\alpha_1 V_1 = 0.073$  to 0.292 m/s,  $\alpha_1 = 0.05$  to 0.3. The error for the velocity measurements was reported of to be  $\pm 5\%$ .

2. Nitrogen - kerosene-neptane column with diameter 0.032 m where  $\alpha_1$  was varied between 0 and 0.8. Air water bubble in column of 0.051 m bubble diameter varying between 0.002 to 0.004 m. The air volumetric fraction was varied between 0 and 0.35.

3. Air-water bubble flow with bubbles produced by nozzles having diameters of 0.00004 to 0.000078 m. The air volumetric fraction was varied between 0 and 0.34. Air-water bubble in column of 0.051 m bubble diameter varying between 0.002 to 0.004 m. The air volumetric fraction was varied between 0 and 0.18, for stagnant water and  $\alpha_2 V_2 = -0.0541$  m/s.

Beside the above mentioned regimes in pool flow, for flow in confined geometry there are additionally three kinds of interaction between gas and continuous liquid namely *churn turbulent*, *slug* and *film flows*. The identification of these regimes is discussed in Chapter 1.

1) For the *churn turbulent flow* the drag coefficient is calculated as for the previously discussed cap bubble regime.

2) For the computation of the drag coefficient for the axial direction in the *slug flow in a pipe* Ishii and Chawla propose

$$c_{21}^d = 9.8(1 - \alpha_1)^3, \quad (2.36)$$

where

$$D_{TB} = D_1 = 0.9D_{hw}. \quad (2.37)$$

The drag force is therefore

$$\mathbf{f}_{21}^d = -\left[7.35\alpha_d(1 - \alpha_d)^3 \rho_2 / D_1\right] |\mathbf{V}_2 - \mathbf{V}_1| (\mathbf{V}_2 - \mathbf{V}_1). \quad (2.38)$$

This correlation was verified by experiments performed with:

1. Air low concentration solution of sodium sulfite  $Na_2SO_3$  in water. The column diameter was 0.07 to 0.6 m and the nozzle inlet diameter was 0.00225 to 0.04 m. The air void fraction was varied between 0.02 and 0.03.

2. Air-water column with diameter 0.06 m,  $\alpha_1 V_1 = 0.2198$  to  $0.367$  m/s,  $\alpha_2 V_2 = 0.44$  to  $1.03$  m/s and  $\alpha_1 = 0.1$  to  $0.35$ .

Note that slug flow does not exist in the pool flow.

**Flow in rod bundles:** Flow in cannels with complex geometry possess spatial velocity and concentration distributions. The cross section averaged velocities and void fractions are then depending on the geometry. Using a effective drag coefficient for single bubble or family of bubbles in free flow as a function of the cross section averaged velocities and void fractions is not recommended. Some authors started to modify existing correlations for such cases by applying computer codes with discretization not fine enough to resolve the profiles. *Rousseau* and *Houdayer* (1983) proposed for instance for *churn-turbulent* flow to use a modification of Eq. (2.32) which is preparedly derived for cup bubbles in the form

$$c_{21}^d = \frac{2}{3} (D_1 / \lambda_{RT}) 2.23 (1 - \alpha_1)^3 (1 - 0.75 \alpha_1)^2.$$

Such approach may not necessarily lead to universal correlations but to such applicable for the particular geometry only.

### 2.1.4 Droplets-gas

Next we compute the drag coefficient for a *droplets-gas* system in a pool ( $D_h \gg D_3$ ) according to the recommendation of *Ishii* and *Chawla*, and extending their analysis for three-dimensional flow. The effective viscosity for this case is

$$\frac{\eta_m}{\eta_l} = (1 - \alpha_d)^{-2.5}, \quad (2.39)$$

*Roscoe* and *Brit* (1952), *Brinkman* (1952), where

$$\alpha_d = \frac{\alpha_3}{\alpha_1 + \alpha_3}. \quad (2.40)$$

1) The drag coefficient for the *Stokes* regime

$$Re < 1, \quad (2.41)$$

is computed as follows

$$c_{13}^d = \frac{24}{Re}; Re = D_3 \rho_l \Delta V_{13} / \eta_m. \quad (2.42)$$

The drag force is therefore

$$\mathbf{f}_{13}^d = -(18 \alpha_d \eta_m / D_3^2) (\mathbf{V}_1 - \mathbf{V}_3). \quad (2.43)$$

The drag coefficient for the viscous regime

$$1 \leq Re < 1000 \quad (2.44)$$

is computed as follows

$$c_{13}^d = \frac{24}{Re} (1 + 0.1 Re^{0.75}) . \quad (2.45)$$

Therefore the drag force is

$$\mathbf{f}_{13}^d = -(18\alpha_d \eta_m / D_3^2) (1 + 0.1 Re^{0.75}) (\mathbf{V}_1 - \mathbf{V}_3) . \quad (2.46)$$

3) The drag coefficient for *Newton's regime* (for single particle - *Newton*)

$$Re \geq 1000 \quad (2.47)$$

is computed as follows

$$c_{13}^d = \frac{2}{3} (D_3 / \lambda_{RT}) \left( \frac{1 + 17.67 f^{6/7}}{18.67 f} \right)^2 ; \quad f = (1 - \alpha_d)^3 \quad (2.48)$$

The drag force is therefore

$$\mathbf{f}_{13}^d = -\frac{1}{2} \alpha_3 \rho_l \frac{1}{\lambda_{RT}} \left( \frac{1 + 17.67 f^{6/7}}{18.67 f} \right)^2 |\mathbf{V}_1 - \mathbf{V}_3| (\mathbf{V}_1 - \mathbf{V}_3) . \quad (2.49)$$

Again if solid particles participate in the flow we consider the gas-droplet flow as flowing in a fictitious channel with volume fraction of the all control volume and the volume fraction  $\alpha_1 + \alpha_3$  of the droplets in this channel is

$$\alpha_d = \frac{\alpha_3}{\alpha_1 + \alpha_3} . \quad (2.50)$$

This assumption holds if the size of the solid particles,  $D_3$ , is much smaller than the size of the droplets,  $D_2$ . Otherwise one needs additional experimental information to perform the correction. As already mentioned, small impurities  $C_{n3} > 0$ , hinder the internal circulation of the droplets and lead to drag coefficients characteristic for the *solid particles in a gas*.

### 2.1.5 Solid particles-gas in presence of liquid. Solid particles-liquid in presence of a gas

Depending on the volumetric concentration of the macroscopic solid particles (the third velocity field) we distinguish the following cases:

1) The solid particles are touching each other in the control volume

$$\alpha_3 = \alpha_{dm} . \quad (2.51)$$

2) The solid particles are free in the flow

$$\alpha_3 < \alpha_{dm} . \quad (2.52)$$

In the second case we distinguish two sub cases:

2a) The volume fraction of the space among the particles if they were closely packed,

$$\alpha_2^* = \frac{1 - \alpha_{dm}}{\alpha_{dm}} \alpha_3 , \quad (2.53)$$

is smaller then the liquid volume fraction

$$\alpha_2^* < \alpha_2 \quad \left( \alpha_3 \leq \frac{\alpha_{dm}}{1 - \alpha_{dm}} \alpha_2 \right) . \quad (2.54)$$

2b) The volume fraction of the space among the particles if they were closely packed is larger then the liquid volume fraction

$$\alpha_3 > \alpha_2 . \quad (2.55)$$

### 2.1.5.1 Solid particles: free particles regime

There is good experimental support for the two-phase regime: solid particle-gas, (2.31), or solid particles-liquid (2.32). We use further the notation  $d$  for discrete and  $c$  for continuous where  $d = 3$ .  $c$  can take values 1 or 2.

Following *Ishii* and *Chawla* in case of

$$\alpha_c + \alpha_d = 1 \quad (2.56)$$

we have:

a) The *Stokes* regime is defined by

$$Re \leq 1 . \quad (2.57)$$

The drag coefficient for this regime is

$$c_{cd}^d = 24 / Re , \quad (2.58)$$

where

$$Re = D_d \rho_c |\Delta V_{cd}| / \eta_m , \quad (2.59)$$

$$\eta_m = \eta_c \left( 1 - \frac{\alpha_d}{\alpha_{dm}} \right)^{-1.55} , \quad (2.60)$$

$$\alpha_{dm} = 0.62 . \quad (2.61)$$

The drag force is therefore

$$\mathbf{f}_{cd}^d = -(18\alpha_d \eta_m / D_d^2)(\mathbf{V}_c - \mathbf{V}_d). \quad (2.62)$$

*Ishii and Zuber* (1978) compared the prediction of this equation with experimental data for glass particles with diameter  $D_3 = 0.036 \text{ cm}$  in a tube with  $D_h = 10 \text{ cm}$  filled with a glycerin - water column. In the region of  $Re_\infty \approx 0.001$  to  $0.06$  and  $\alpha_3 = 0$  to  $0.45$  the authors reported excellent agreement.

b) Viscous regime is defined by

$$1 \leq Re < 1000. \quad (2.63)$$

The drag coefficient for this regime is

$$c_{cd}^d = \frac{24}{Re} (1 + 0.1 Re^{0.75}). \quad (2.64)$$

Therefore the drag force is

$$\mathbf{f}_{cd}^d = -(18\alpha_d \eta_m / D_d^2)(1 + 0.1 Re^{0.75})(\mathbf{V}_c - \mathbf{V}_d). \quad (2.65)$$

Note that for symmetric flow around a spheroid form with aspect ratio defined as

$$A = \text{semi-axes along the flow} / \text{semi-axes normal to the flow}, \quad (2.66)$$

*Militzer et al.* (1998) obtained

$$c_{cd}^d = \frac{4+A}{5} \left[ \frac{24}{Re} (1 + 0.15 Re^{0.687}) + \frac{0.42}{1 + 42500 Re^{-1.16}} \right] \\ (1 + 0.00094 Re / A - 0.000754 A Re + 0.0924 / Re + 0.00276 A^2). \quad (2.67)$$

c) *Newton's* regime is defined by

$$Re \geq 1000. \quad (2.68)$$

The drag coefficient for this regime is

$$c_{cd}^d = 0.45 \left( \frac{1 + 17.67 f^{6/7}}{18.67 f} \right)^2; \quad f = \sqrt{1 - \alpha_d} \frac{\eta_c}{\eta_m}. \quad (2.69)$$

The drag force is therefore

$$\mathbf{f}_{cd}^d = (0.3375 \alpha_d \rho_c / D_d) \left( \frac{1 + 17.67 f^{6/7}}{18.67 f} \right)^2 |\mathbf{V}_c - \mathbf{V}_d| (\mathbf{V}_c - \mathbf{V}_d). \quad (2.70)$$

Comparison with *Richardson and Zaki's* data for  $D_h = 0.062 \text{ m}$ ,  $D_s = 0.635 \text{ cm}$  for  $\alpha_3 = 0$  to  $0.4$  shows a good agreement.



### 2.1.5.2 Solid particles in bubbly flow

If a heated solid sphere is falling in a liquid the boiling around the sphere changes the pressure field and consequently the drag coefficient. The investigations for estimation of the drag coefficients under boiling conditions for arbitrary velocity differences are not complete and future investigations are necessary. *Zvirin* et al. (1990) published the following empirical method for computation of the drag coefficients in the limited region of *Reynolds* numbers and superheating:

$$c_{23}^d = c_{23,nb}^d / \left\{ 1.020 + 3.87 \times 10^{-5} [T_3 - T'(p)] \right\}^2, \quad (2.71)$$

where

$$\log c_{23,nb}^d = -4.3390 + 1.589 \log Re_{32} - 0.154 (\log Re_{32})^2, \quad (2.72)$$

is the drag coefficient measured for non-boiling conditions and

$$Re_{32} = D_3 \rho_2 |\Delta V_{32}| / \eta_2 \quad (2.73)$$

is the *Reynolds* number. The *Zvirin* et al. observations are valid in the following region  $10^4 < Re_{32} < 3.38 \times 10^5$ ,  $373 < T_3 < 973$  K.

For illustration if the temperature of the solid sphere is 973 K the drag coefficient is 8.8% lower than the value for the non-boiling case under atmospheric conditions and free falling. More complicated is the case if the free particles are part of a solid/liquid/gas mixture.

Consider first the bubble three-phase flow. As a first approximation we can assume that if the bubbles in the space among the particles are touching each other

$$\frac{\alpha_1}{\alpha_1 + \alpha_2} > 0.52 \quad (2.74)$$

the bubble three - phase flow cannot exist and vice versa if

$$\frac{\alpha_1}{\alpha_1 + \alpha_2} \leq 0.52 \quad (2.75)$$

the bubble three-phase flow is defined. For the time being no experimental information is available to confirm the value 0.52. In any case if three-phase bubble flow is identified we distinguish two sub cases. If the volume fraction of the space among the particles if they were closely packed is smaller than the liquid fraction

$$\alpha_2^* < \alpha_2 \quad (2.76)$$

the theoretical possibility exists that the particles are carried only by a liquid. This hypotheses is supported if one considers the ratio of the free setting velocity in gas and liquid

$$\frac{w_{31\infty}}{w_{32\infty}} = \sqrt{\frac{\rho_3 - \rho_1}{\rho_3 - \rho_2} \frac{\rho_2}{\rho_1}} \gg 1. \quad (2.77)$$

We see that, due to the considerable differences between gas and liquid densities, the particles sink much faster in gas than in a liquid. Thus, most probably the solid particles are carried by the liquid. In this case the mixture can be considered as consisting of gas and liquid/solid continuum. The drag force between gas and solid is zero and the drag force between solid and liquid is computed for

$$\alpha_d = \alpha_3 / (\alpha_2 + \alpha_3) \quad (2.78)$$

and

$$\Delta \mathbf{V}_{dl} = \mathbf{V}_3 - \mathbf{V}_2 \quad (2.79)$$

If the volume fraction of the space among the closely packed particles is larger then the liquid volume fraction

$$\alpha_2^* > \alpha_2 \quad (2.80)$$

only

$$\alpha_3 - \frac{\alpha_{dm}}{1 - \alpha_{dm}} \alpha_2 = \alpha_3 (1 - \alpha_2 / \alpha_2^*) = \alpha_{31} \quad (2.81)$$

are surrounded by gas. So we can compute the drag and the virtual mass force between one single solid particle and gas as for a mixture

$$\alpha_d = \frac{\alpha_{31}}{\alpha_1 + \alpha_{31}} \quad (2.82)$$

namely

$$c_{13o}^d = c_{cd}^d(\alpha_d, \Delta \mathbf{V}_{dc}, \dots) \quad (2.83)$$

$$c_{13o}^{vm} = c_{cd}^{vm}(\alpha_d, \Delta \mathbf{V}_{dc}, \dots) \quad (2.84)$$

and multiply this force by the number of particles which are surrounded by gas having volumetric fraction  $\alpha_{31}$ . The result is

$$c_{13}^d = \alpha_{31} c_{13o}^d, \quad (2.85)$$

$$c_{13}^{vm} = \alpha_{31} c_{13o}^{vm}. \quad (2.86)$$

The same has to be done for the calculation of the force between one single solid particle and liquid for the mixture  $\alpha_2 + \alpha_{32}$ ,

$$\alpha_d = \frac{\alpha_{32}}{\alpha_2 + \alpha_{32}}, \quad (2.87)$$

$$\Delta \mathbf{V}_{dc} = \mathbf{V}_3 - \mathbf{V}_2, \quad (2.88)$$

namely

$$c_{23o}^d = c_{cd}^d(\alpha_d, \Delta V_{dc}, \dots), \quad (2.89)$$

$$c_{23o}^{vm} = c_{cd}^{vm}(\alpha_d, \Delta V_{dc}, \dots), \quad (2.90)$$

where

$$\alpha_{32} = \alpha_3 - \alpha_{31} = \alpha_3 \alpha_2 / \alpha_2^* \quad (2.91)$$

and multiply this force by the number of the particles which are surrounded by liquid  $\alpha_{32}$

$$c_{23}^d = \alpha_{32} c_{23o}^d, \quad (2.92)$$

$$c_{23}^{vm} = \alpha_{32} c_{23o}^{vm}. \quad (2.93)$$

In case that the bubbles in the space between the particles are touching each other

$$\frac{\alpha_1}{\alpha_1 + \alpha_2} > 0.52 \quad (2.94)$$

the more likely flow pattern is *three-phase disperse flow*. In this case the gas - liquid flow relative to the solid particles resembles two-phase gas liquid flow in a channel. Therefore the drag forces exerted by the solid particles should be larger than the drag forces exerted by the solid phase in the case of missing liquid. A possible correction of the drag force coefficients is

$$c_{13}^d = (1 - \phi) c_{13o}^d, \quad (2.95)$$

$$c_{13}^{vm} = (1 - \phi) c_{13o}^{vm}, \quad (2.96)$$

$$c_{23}^d = \phi c_{23o}^d, \quad (2.97)$$

$$c_{23}^{vm} = \phi c_{23o}^{vm}, \quad (2.98)$$

where

$$\phi = \alpha_2 / (\alpha_1 + \alpha_2). \quad (2.99)$$

### 2.1.5.3 Solid particles: dense packed regime

If over a period of time the volume fraction of the solid particles is

$$\alpha_{3a} = \alpha_{dm}, \quad (2.100)$$

we have the constraint in the mass conservation equation

$$\frac{\partial}{\partial \tau}(\alpha_3 \rho_3) \leq 0. \quad (2.101)$$

This means that the mass conservation equation for the solid particles has the form

$$\nabla(\alpha_3 \rho_3 \mathbf{V}_3 \gamma) = \mu_3 - \alpha_3 \rho_3 \frac{\partial \gamma_v}{\partial \tau} \quad (2.102)$$

for

$$\tau = \tau_a + \Delta \tau, \quad \alpha_{3a}(\tau_a) = \alpha_{dm} \quad \text{if} \quad \frac{\partial}{\partial \tau}(\alpha_3 \rho_3) \geq 0 \quad (2.103)$$

and

$$\frac{\partial}{\partial \tau}(\alpha_3 \rho_3 \gamma_v) + \nabla(\alpha_3 \rho_3 \mathbf{V}_3 \gamma) = \mu_3 \quad (2.104)$$

for

$$\tau = \tau_a + \Delta \tau, \quad \alpha_{3a}(\tau_a) = \alpha_{dm} \quad \text{if} \quad \frac{\partial}{\partial \tau}(\alpha_3 \rho_3) < 0. \quad (2.105)$$

In other words if the maximum packed density in a particular computational cell is reached no further mass accumulation in the cell is possible. In this case the forces between continuum and particles can be computed using the results of *Ergun* (1952). *Ergun* generalized experimental results for pressure drop through packed beds ( $\mathbf{V}_3=0$ ) for

$$1 < \frac{1}{\alpha_3} \frac{\rho_1 D_3 |\Delta \mathbf{V}_{13}|}{\eta_1} \leq 4 \times 10^4 \quad (2.106)$$

and correlated them with the following equation

$$\frac{\partial p}{\partial z} = -150 \left( \frac{\alpha_3}{1 - \alpha_3} \right)^2 \frac{\eta_1}{D_3^2} V_1 - 1.75 \frac{\alpha_3}{1 - \alpha_3} \frac{\rho_1 |\mathbf{V}_1|}{D_3} V_1 \quad (2.107)$$

where  $l = 1$  or  $2$ ,  $\mathbf{V}_3 = 0$ ,

$$D_3 = \frac{Vol}{F_3} \frac{6}{\alpha_3}, \quad (2.108)$$

$F_3$  is the total geometric surface of the solid particles in the volume  $Vol$  of the mixture consisting of phase 1 and phase 3.

*Achenbach* (1993) reported a slightly modified *Ergun's* equation

$$\begin{aligned} \frac{\partial p}{\partial z} = & -160 \left( \frac{\alpha_3}{1-\alpha_3} \right)^2 \frac{\eta_l}{D_3^2} (V_l - V_3) \\ & - 0.6 \frac{\alpha_3}{1-\alpha_3} \frac{\rho_l |\Delta \mathbf{V}_{l3}|}{D_3} (V_l - V_3) \left( \frac{1-\alpha_3}{\alpha_3} \frac{\eta_l}{\rho_l D_3 |\Delta \mathbf{V}_{l3}|} \right)^{0.1} \end{aligned} \quad (2.109)$$

verified for  $\frac{\alpha_3}{1-\alpha_3} \frac{\rho_l D_3 \Delta V_{l3}}{\eta_l} \leq 10^5$ , see in *Achenbach* or in *VDI-Wärmeatlas* (1991).

The sum of the linear and the quadratic dependences of the forces on the velocity difference was first proposed by *Osborne Reynolds* (1900). The first term represents the viscous friction corresponding to *Poiseuille* flow (*Darcy's law*) and the second - the turbulent dissipation.

Rewriting *Ergun's* equation in terms of forces acting on phase l per unit mixture volume for  $V_3 \neq 0$  we obtain

$$\alpha_1 \frac{\partial p}{\partial z} = -\alpha_1 150 \left( \frac{\alpha_3}{1-\alpha_3} \right)^2 \frac{\eta_l}{D_3^2} (V_l - V_3) - \alpha_1 1.75 \frac{\alpha_3}{1-\alpha_3} \frac{\rho_l |\Delta \mathbf{V}_{l3}|}{D_3} (V_l - V_3) = f_{l3}^d. \quad (2.110)$$

Comparing the above equation with the definition equation of the drag coefficient we obtain

$$c_{l3}^d = \frac{200}{\frac{\alpha_1}{\alpha_3} \frac{D_3 |\Delta \mathbf{V}_{l3}|}{\rho_l \eta_l}} + \frac{7}{3}. \quad (2.111)$$

Note that this expression was derived for pure solid - continuum flow, which means

$$\alpha_3 + \alpha_1 = 1. \quad (2.112)$$

Expressions for drag coefficient in dense packed particles are obtained also by using the lattice Boltzmann method by *Koch* and *Hill* – see in *Michaelides* (2003) p. 233,

$$c_{l3}^d = c_{l3,0}^d + \left[ 0.0673 + 0.212\alpha_3 + 0.0232(1-\alpha_3)^{-5} \right] \frac{\rho_l D_3 |\Delta \mathbf{V}_{l3}|}{\eta_l},$$

where

$$c_{l3,0}^d = \frac{1 + 3(\alpha_3/2)^{1/2} + 2.11\alpha_3 \ln \alpha_3 + 16.14\alpha_3}{1 + 0.681\alpha_3 - 8.48\alpha_3^2 + 8.16\alpha_3^3}.$$

This correlation is reported to reproduce also the *Ergun*'s data. Note the contradiction for the influence of the Reynolds number comparing it with Eq. (2.111).

If the gas and the liquid are flowing around the densely packed particles the resistance forces between each of the phases 1 and the particles are considerably higher (see *Wyckoff* (1936)). Part of the liquid,  $\alpha_2^*$ , is bound between the particles by capillary force

$$\frac{\alpha_2^*}{1-\alpha_3} = \left[ \frac{\alpha_3^2}{(1-\alpha_3)^3} \frac{\sigma_2 \cos \phi_{23}}{D_3^2 \rho_2 g} \right]^{0.264} / 22 \equiv \alpha_{2r}^*, \quad (2.113)$$

*Brown* et al. (1950), and remains for given pressure drop across the distance of consideration. It can normally be removed by evaporation rather than drainage. Here  $\sigma_2$  is the surface tension and is  $\theta_{23}$  the wetting contact angle between the liquid and particles (typically 0.8 for water/steel and 1 for  $\text{UO}_2$ /water or sodium. Usually the drag forces are corrected by means of the so called viscous and turbulent permeability coefficients,  $k_1^l$ ,  $k_1^t$  respectively. *Lepinski* (1984) uses the following form of the modified *Ergun* equation

$$\begin{aligned} \frac{\partial p_1}{\partial z} + \rho_1 g + \frac{\alpha_1 \alpha_3^2}{(1-\alpha_3)^3} 150 \frac{\eta_1}{D_3^2 k_1^l} (w_1 - w_3) \\ + \frac{\alpha_1^2 \alpha_3}{(1-\alpha_3)^3} 1.75 \frac{\rho_1}{D_3 k_1^t} |w_1 - w_3| (w_1 - w_3) = 0. \end{aligned} \quad (2.114)$$

Again rewriting this equation in term of forces acting on phase  $l$  per unit mixture volume we obtain

$$\begin{aligned} \alpha_1 \frac{\partial p_1}{\partial z} + \alpha_1 \rho_1 g + \frac{\alpha_1^2 \alpha_3^2}{(1-\alpha_3)^3} 150 \frac{\eta_1}{D_3^2 k_1^l} (w_1 - w_3) \\ + \frac{\alpha_1^3 \alpha_3}{(1-\alpha_3)^3} 1.75 \frac{\rho_1}{D_3 k_1^t} |w_1 - w_3| (w_1 - w_3) = 0. \end{aligned} \quad (2.115)$$

Comparing with the definition equation for the drag force we find an expression defining the drag coefficients

$$c_{13}^d = \left( \frac{\alpha_1}{1-\alpha_3} \right)^3 \frac{200}{\frac{\alpha_1}{\alpha_3} \rho_1 \frac{D_3 |\Delta V_{13}|}{\eta_1} k_1^l} + \frac{7}{3 k_1^t}. \quad (2.116)$$

For  $\alpha_1 = 1 - \alpha_3$  and  $k_1^l$ ,  $k_1^t \equiv 1$  this is exactly the expression resulting from the original *Ergun* equation.

The relative permeabilities are function of the effective saturation,  $\alpha_{2eff}^*$

$$k_1^1 = (1 - \alpha_{2eff}^*)^3, \quad k_2^1 = \alpha_{2eff}^{*3}, \quad (2.117)$$

*Brooks and Corey* (1966),

$$k_1^t = (1 - \alpha_{2eff}^*)^5, \quad k_2^t = \alpha_{2eff}^{*5}, \quad (2.118)$$

*Reed* (1982) where

$$\alpha_{2eff}^* = \frac{\alpha_2^* - \alpha_{2r}^*}{1 - \alpha_{2r}^*} \quad \text{for } \alpha_2^* > \alpha_{2r}^*. \quad (2.119)$$

The true saturation is defined as

$$\alpha_2^* = \frac{\alpha_2}{1 - \alpha_3}. \quad (2.120)$$

In this case the virtual mass coefficient for the particles is

$$c_{23}^{vm} \approx \alpha_{2r}^* / \alpha_3. \quad (2.121)$$

*Tung and Dhir* (1990) described the steady-state incompressible two-phase flow through porous media ("saturated" - all of the liquid is moving) modifying the *Ergun* equation

$$\begin{aligned} \alpha_1 \frac{\partial p_1}{\partial z} + \alpha_1 \rho_1 g + \frac{\alpha_1 \alpha_3^2}{(1 - \alpha_3)^3} 150 \frac{\eta_1}{D_3^2 \bar{k}_1^1} (w_1 - w_3) \\ + \frac{\alpha_1^2 \alpha_3}{(1 - \alpha_3)^4} 1.75 \frac{\rho_1}{D_3 \bar{k}_1^t} |w_1 - w_3| (w_1 - w_3) \pm f_{21}^d = 0, \end{aligned} \quad (2.122)$$

where  $l = 1, 2$ . Comparing with the definition equation for the drag force we find expression defining the drag coefficients

$$c_{13}^d = \left( \frac{\alpha_1}{1 - \alpha_3} \right)^3 \left[ \frac{200}{\frac{\alpha_1}{\alpha_3} \rho_1 \frac{D_3 |\Delta \mathbf{V}_{13}|}{\eta_1}} \frac{1}{\alpha_1 \bar{k}_1^1} + \frac{7}{3} \frac{1}{(1 - \alpha_3) \alpha_1 \bar{k}_1^t} \right]. \quad (2.123)$$

*Tung and Dhir* distinguish bubbly, annular and slug flow structure of the gas-liquid mixture. The different relative permeability multipliers are summarized in Table 2.2. In case of bubble flow the bubble diameter and flow regime limits are computed as shown in Chapter 1.

**Table 2.2** Relative permeability multipliers as recommended by *Tung and Dhir* (1990)

For all flow regimes, the liquid relative permeability multipliers <i>are given by</i> $\bar{k}_2^l = \bar{k}_2^t = (1 - \bar{\alpha}_1)^3$
Gas relative permeability multipliers <i>a) Bubble flow, slug flow (<math>\bar{\alpha}_1 \leq \bar{\alpha}_{13}</math>):</i> $\bar{k}_1^l = \left( \frac{\alpha_3}{1 - \alpha_1} \right)^{4/3} \bar{\alpha}_1^3$ and $\bar{k}_1^t = \left( \frac{\alpha_3}{1 - \alpha_1} \right)^{2/3} \bar{\alpha}_1^3$ . <i>b) Annular flow (<math>\bar{\alpha}_{14} \leq \bar{\alpha}_1 \leq 1</math>):</i> $\bar{k}_1^l = \left( \frac{\alpha_3}{1 - \alpha_1} \right)^{4/3} \bar{\alpha}_1^2$ and $\bar{k}_1^t = \left( \frac{\alpha_3}{1 - \alpha_1} \right)^{2/3} \bar{\alpha}_1^2$ .

### 2.1.6 Annular flow

**Film-wall force:** The resisting force between wall and film per unit flow volume for *fully developed annular flow* is

$$f_{w2} = \frac{4}{D_h} \tau_{w2}, \quad (2.124)$$

where

$$\tau_{w2} = \eta_2 \left[ \frac{dw_2(r)}{dr} \right]_{r=R} = c_{w2} \frac{1}{2} \rho_2 w_2^2. \quad (2.125)$$

For laminar flow,

$$Re_2 = \rho_2 w_2 \delta_2 / \eta_2 \leq 400. \quad (2.126)$$

the assumption for a parabolic velocity profile leads to *Fanning*

$$c_{w2} = 4 / Re_2, \quad (2.127)$$

For turbulent flow,

$$Re_2 > 400, \quad (2.128)$$

the assumption for a 1/7 profile leads to

$$c_{w2} = 0.057 / Re_2^{1/4}. \quad (2.129)$$



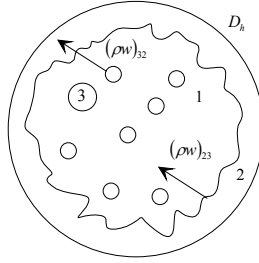


**Fig. 2.1** Annular flow

Of course 1/7 profile velocity profile is a first approximation. In fact for thin turbulent films the universal velocity profile is found by direct measurements of the turbulent structure by *Vassallo* (1999). *Vassallo* observed for larger film thickness bubble inclusions inside the film with a smooth transition from zero to one void fraction starting from the wall and crossing the wavy surface layer. The presence of the bubbles shifts the logarithmic part of the dimensionless velocity  $w^+ = 2.5 \ln y^+ + 5.5$  to lower values e.g.  $w^+ \approx 2.5 \ln y^+ + 1.2$  indicating increasing of the wall share stress  $\tau_2^{w\sigma}$ . Here  $w_2^+ = w_2 / w_{w2}^*$  and  $y^+ = y w_{w2}^* / \nu_2$  and  $w_{w2}^* = \sqrt{\tau_2^{w\sigma} / \rho_2}$ .

**Film-gas force:** The gas resisting force per unit flow volume between film and gas is

$$\begin{aligned} f_1^d &= -a_{12} \tau_{21} = -a_{12} c_{21}^d \frac{1}{2} \rho_1 |w_2 - w_1| (w_2 - w_1) \\ &= -\frac{2}{D_h} \sqrt{1 - \alpha_2} c_{21}^d \rho_1 |w_2 - w_1| (w_{2i} - w_1), \end{aligned} \quad (2.130)$$

where  $a_{12}$  is the interfacial area density

$$a_{12} = \frac{4}{D_h} \sqrt{1 - \alpha_2}. \quad (2.131)$$

*Nikuradze* (1933) proposed the following formula for computation of the friction coefficient in pipes

$$c_w = 0.005 \left( 1 + 300 \frac{k_s}{D_h} \right), \quad (2.132)$$

over the range,  $0.0001 \leq k_s / D_h \leq 0.03$  where  $k_s$  is the sand roughness grain size. *Wallis* (1969) proposed to use as a roughness the film thickness which results the following equation

$$c_{21}^d = 0.005 \left( 1 + 300 \frac{\delta_2}{D_h} \right) \approx 0.005 (1 + 75 \alpha_2), \quad (2.133a)$$

where the ratio is approximately

$$\frac{\delta_{1F}}{D_h} \approx \frac{\alpha_2}{4}. \quad (2.134)$$

*Moeck* and *Stachiewicz* (1972) based on air-water experiments at atmospheric pressure reported

$$c_{21}^d = 0.005 \left[ 1 + 545 (2\delta_2 / D_h)^{1.42} \right].$$

*Nigmatulin* et al. (1978), *Subbotin* et al. (1978) based on steam-water experiments at high pressure reported

$$c_{21}^d = 0.008 \left[ 1 + 210 (2\delta_2 / D_h)^{1.3} \right].$$

After 31 years this equation was compared with a modern data base including 200 points by *Fore* et al. (2000) and revised in order to increase the accuracy at low gas velocities. The final result is

$$c_{21}^d = 0.005 \left\{ 1 + 300 \left[ \left( 1 + \frac{17500}{\alpha_1 w_1 D_h / \nu_1} \right) \frac{\delta_2}{D_h} - 0.0015 \right] \right\}. \quad (2.133b)$$

The equation is verified within  $0.001 < \left( 1 + \frac{17500}{\alpha_1 w_1 D_h / \nu_1} \right) \frac{\delta_2}{D_h} < 0.1$  giving values of  $4.25 \times 10^{-3} < c_{21}^d < 0.153$  with an uncertainty of  $\pm 25\%$ .

*Hewitt* and *Govan* used instead of the coefficient 0.005 the modified *Blasius* formula

$$c_{21}^d = \frac{0.079}{Re_{13}^{1/4}} (1 + 75\alpha_2) \quad (2.135)$$

where

$$Re_{13} = (\alpha_1 \rho_1 w_1 + \alpha_3 \rho_3 w_3) D_h / \eta_1. \quad (2.136)$$

Actually the roughness is a function of the liquid Reynolds number  $Re_{2F} = \rho_2 w_2 \delta_2 / \eta_2$  and the *Kapiza* number  $Ka_2 = \sigma_2^3 / (\rho_2^3 g \nu_2^3)$ . *Alekseenko* et al. (1996) reported the following fitting of experimental data from several authors:

$$\frac{\delta_{1F,\max} - \delta_{1F,\max}}{\delta_{1F}} = 1 + \exp \left( -0.0012 Re_{2F} / Ka_2^{1/11} \right) - \exp \left( -0.4 Re_{2F} / Ka_2^{1/11} \right).$$

In accordance with this relation first if  $Re_{2F} / Ka_2^{1/11} > 10$  we have  $\delta_{1F,\max} - \delta_{1F,\max} = 2\delta_{1F}$  with other words, the wave amplitude equal to the film thickness and the above relations make physical sense. For lower films the roughness is smaller.

*Bharathan et al.* proposed the following equation (1978) which was *effectively* for churn flow

$$c_{21}^d = 0.005 + 14.14 \alpha_2^{2.03}. \quad (2.137)$$

An alternative empirical correlation of the interfacial friction factor was proposed by *Bharathan et al.* (1979)

$$c_{21}^d = 0.005 + A \delta^{*B}, \quad (2.138)$$

where the constants  $A$  and  $B$  are given by

$$\log_{10} A = -0.56 + 9.07 / D^*, \quad (2.139)$$

$$B = 1.63 + 4.74 / D^*. \quad (2.140)$$

The dimensionless film thickness  $\delta^*$  and diameter  $D^*$  are defined by

$$\delta^* = \delta_2 / \lambda_{RT}, \quad (2.141)$$

$$D^* = D_h / \lambda_{RT}. \quad (2.142)$$

*Govan et al.* (1991) provided experimental data for effectively churn and annular flow for  $\alpha_1 > 0.8$  and show that the *Bharathan* correlation gives much better agreement with the data whereas the *Wallis* correlation under predicts the data for  $\alpha_1 < 0.92$ . The values of the measured quantities  $f^d / \Delta w^2$  vary between 40  $\text{kg/m}^4$  for  $\alpha_1 \approx 0.8$  and  $\approx 2.5 \text{ kg/m}^4$  for  $\alpha_1 \approx 0.95$  for  $\alpha_2 \rho_2 w_2 = 31.8$  to 47.7  $\text{kg/(m}^2\text{s)}$ .

*Stephan and Mayinger* (1990) improved the *Barathan et al.* correlation based on high pressure experiments ( $p = 6.7 \cdot 10^5$  to  $13 \cdot 10^5 \text{ Pa}$ ,  $D_h = 0.0309 \text{ m}$ ,  $j_2 = 0.017$  to  $0.0035 \text{ m/s}$ ,  $j_1 = 5$  to  $18 \text{ m/s}$ ) as follows

$$c_{21}^d = \frac{0.079}{Re_1^{1/4}} (1 + 115 \delta^{*B}), \quad (2.143)$$

where

$$Re_1 = \rho_1 w_1 D_h / \eta_1, \quad (2.144)$$

$$B = 3.91 / (1.8 + 3 / D^*). \quad (2.145)$$

An alternative correlation is proposed by *Ambrosini et al.* (1991)

$$c_{21}^d = \frac{0.046}{Re_1^{1/5}} \left[ 1 + 13.8 (\rho_1 V_1^2 D_h / \sigma)^{0.2} Re_1^{-0.6} (\delta_{2F} V_1^* / \nu_1 - 200 \sqrt{\rho_1 / \rho_2}) \right], \quad (2.146)$$

$$V_1^* = \sqrt{\tau_{12} / \rho_1} = V_1 \sqrt{\frac{1}{2} c_{21}^d}, \quad (2.147)$$

$$\tau_{12} = \frac{1}{2} c_{21}^d \rho_1 V_1^2, \quad (2.148)$$

which describes data in the region  $c_{21}^d / (0.046 / \text{Re}_1^{1/5}) \approx 1$  to 10 within  $\pm 30\%$  error band.

*Nigmatulin* (1982) obtained good agreement between the above expressions for  $c_{w2}$  and experimental data for  $D_h = 0.0081$  to  $0.0318$  m and  $\text{Re}_2 = 5$  to  $1.5 \times 10^5$  for upstream air water and steam water flow. The experiments of *Nigmatulin* shows that between the film surface velocity and averaged film velocity the following relationship exists

$$w_{2i} = 2w_2 \text{ for } \text{Re}_2 < 400, \quad (2.149)$$

$$w_{2i} = 1.1w_2 \text{ for } \text{Re}_2 \geq 400. \quad (2.150)$$

In the same work the gas resisting force between film and gas is estimated to be

$$\begin{aligned} f_1^d &= -a_{12} \tau_{21} = -a_{12} c_{21}^d \frac{1}{2} \rho_1 |w_{2i} - w_1| (w_{2i} - w_1) \\ &= -\frac{2}{D_h} \sqrt{1 - \alpha_2} c_{21}^d \rho_1 |w_{2i} - w_1| (w_{2i} - w_1), \end{aligned} \quad (2.151)$$

and

$$c_{21}^d = 0.005 \left[ 1 + 16 (2\delta_2 / D_h)^{1/2} + 1.5 \times 10^3 (2\delta_2 / D_h)^2 \right]. \quad (2.152)$$

Here  $\delta_2$  is the film thickness

$$\delta_2 = D_h (1 - \sqrt{1 - \alpha_2}) / 2. \quad (2.153)$$

The  $f_{21}^d$  is computed in this way with an square mean error of 20%. The verification was performed by *Nigmatulin* with data for air-water and  $p = 2.7 \times 10^5$  Pa,  $D_h = 0.0318$  m and for steam - water and  $p = (10 \text{ to } 100) \times 10^5$  Pa and  $D_h = 0.0081$  and  $0.0131$  m.

*Ueda* (1981) proposed the following correlation for the computation of the drag coefficient in annular flow

$$\begin{aligned} c_{21}^d &= \text{const} \frac{1}{4} (2.85 - 2.10 \alpha_1^{2.20})^4 \left[ \frac{\rho_2 - \rho_1}{\rho_1} \frac{g D_{h21}}{(w_1 - w_2)^2} \right]^{0.7} \\ &\times \left[ \frac{\eta_1}{\eta_2} \frac{|w_1 - w_2|}{w_2} \right]^{0.1} \left[ \frac{|w_1 - w_2| D_{h21}}{\nu_1} \right]^{-0.2} \end{aligned} \quad (2.154)$$

where the

$$\text{const} \approx 2 \quad (2.155)$$

for horizontal flow and

$$D_{h21} = D_h \sqrt{1 - \alpha_2} . \quad (2.156)$$

Some authors successfully correlated experimental data for interfacial friction coefficient using instead the relative velocity between film and gas, only the film velocity

$$f_{21}^d = -a_{12} \rho_2 c_{21}^{d*} \frac{1}{2} w_2 |w_2| . \quad (2.157)$$

*Hugmark* (1973) correlated experimental data for film thickness of vertical upward flow as a function of film *Reynolds* number and summarized data for the relationships between drag coefficients and film thickness. Thus using this data base the relationship between liquid *Reynolds* number and drag coefficients is established. Later *Ishii* and *Gromles* correlated this relationship with the following correlation

$$\sqrt{c_{u1}^{d*} / 4} = k Re_{2F}^m \quad (2.158)$$

where

$$Re_{2F} = \rho_2 w_2 4 \delta_{2F} / \eta_2 \quad (2.159)$$

and  $k$  and  $m$  are given by

$$k = 3.73, \quad m = -0.47 \quad 2 < Re_{2F} < 100, \quad (2.160)$$

$$k = 1.962, \quad m = -1/3 \quad 100 < Re_{2F} < 1000, \quad (2.161)$$

$$k = 0.735, \quad m = -0.19 \quad 1000 < Re_{2F} . \quad (2.162)$$

The data base for the derivation of the correlation cover the range of

$$0.003 < \delta_{2F} / (D_h / 2) < 0.1. \quad (2.163)$$

Careful evaluation of the interface friction factor taking into account the momentum pre-distribution due to entrainment and deposition done by *Lopes* and *Dukler* (1986) shows that there is no unique relationships between  $c_{21}^d$  and  $Re_{2F}$ . The experimental data obtained by the *Lopes* and *Dukler* can be represented very well by the modified *Altstul* formula

$$c_{21}^d = \frac{1}{4} (3.331 \log Re_1 - 33.582)^{-2}, \quad (2.164)$$

for  $4 \times 10^4 < Re_1 \leq 8.5 \times 10^4$ , and

$$c_{12}^d = 0.014, \quad (2.165)$$

for  $8.5 \times 10^4 < Re_1 \leq 12 \times 10^4$ , where

$$Re_1 = \rho_1 (V_1 - V_{2i}) D_{hc} / \eta_1, \quad (2.166)$$

$$D_{hc} = D_h \sqrt{1 - \alpha_2} . \quad (2.167)$$

Variation within  $310 < Re_{23} = < 3100$ , where

$$Re_{23} = \rho_2 (\alpha_2 V_2 + \alpha_3 V_3) D_h / \eta_2 , \quad (2.168)$$

does not influence the results.

*Hanratty and Dykko* (1997) proposed the following correction of the drag coefficient computed for gas flow without film:

$$c_{12}^d = c_{1w}^d \left[ 1 + 1400 \frac{f(Re_{2F})}{Re_1^{0.9}} \frac{v_2}{v_1} \sqrt{\frac{\rho_2}{\rho_1}} \right] , \quad (2.169)$$

where

$$f(Re_{2F}) = \left[ \left( 0.34 Re_{2F}^{0.6} \right)^{2.5} + \left( 0.0379 Re_{2F}^{0.9} \right)^{2.5} \right]^{0.4} \quad (2.170)$$

$$Re_{2F} = \alpha_2 w_2 4 \delta_{2F} / v_2 , \quad Re_1 = \alpha_1 w_1 D_h / v_1 . \quad (2.171, 2.172)$$

For stand along use the authors reported  $\delta_{2F} V_2^* / v_2 = f(Re_{2F})$ ,  $V_2^* = \sqrt{\tau_{2,eff} / \rho_2}$ ,

$$\tau_{2,eff} = \frac{2}{3} \tau_{2w} + \frac{1}{3} \tau_2^{1\sigma} .$$

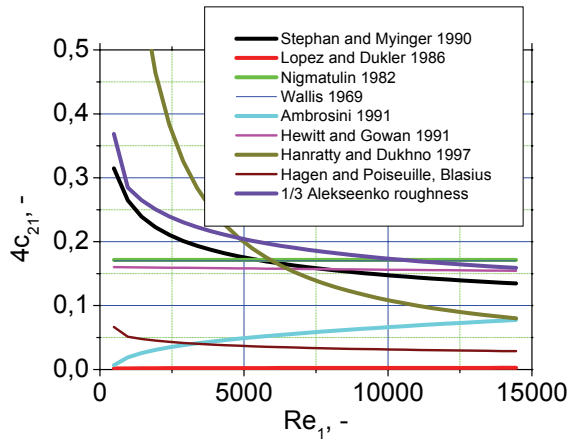


**Fig. 2.2** Gas-film friction coefficient as a function of the gas *Reynolds* number

Comparison between the predictions of different correlations as a function of the gas Reynolds number is given in Fig. 2.2. The correlations by *Wallis*, *Gowan* et al. and *Nigmatulin* do not differ from each other much. The prediction of the correlation by

the *Stephan* and *Maying* converges to the prediction of the above mentioned correlations for higher Reynolds number, but differs much for low Reynolds numbers. If one uses the formula of *Alekseenko* and take 1/3th of the film amplitude as effective roughness the *Nikuradze* formula predict results close to those predicted by *Stephan* and *Maying*. For comparison the prediction by the *Blasius* correlation for Reynolds number larger then 1187 and by the *Hagen* and *Poiseuille* correlation for lower Reynolds numbers is given also in Fig. 2.2. It is obvious that final state of the knowledge in this field is not achieved.

*Hulburt* et al. (2006) proposed for the first time a time-averaging of the friction forces considering the base waviness of the film (ripples) and the traveling waves (roll waves) depending on the local parameters. They estimated film thickness and the film averaged velocity using the following correlations:

$$\delta_{2F}^+ = 0.34 \text{Re}_{2F}^{0.6}, \quad w_2 = w_{12}^* (\delta_{2F}^+)^{2/3} \quad (2.173)$$

for laminar flow, *Asali* et al. (1985) and

$$\delta_{2F}^+ = 0.0379 \text{Re}_{2F}^{0.9}, \quad w_2 = w_{12}^* 9.5 (\delta_{2F}^+)^{1/10} \quad (2.174)$$

for turbulent flow, *Henstock* and *Hanratty* (1976), where  $\text{Re}_{2F} = w_2 4 \delta_{2F} / \nu_2$ ,  $w_{12}^* = \sqrt{\tau_1^{2\sigma} / \rho_2}$  and  $\delta_{2F}^+ = \delta_{2F} w_{12}^* / \nu_2$ . Using the *Andreussi*'s et al. (1985) observation that at about  $\text{Re}_{2F,cr} \approx 370$  corresponding to  $\delta_{cr}^+ \approx 8$  there is the onset of disturbances waves the authors correlated the standard deviation from the averaged film thickness data with

$$\sigma_\delta^+ = 0 \quad \text{for } \delta_{2F}^+ \leq \delta_{2F,crit}^+, \quad (2.175)$$

$$\sigma_\delta^+ = (\delta_{2F}^+ - \delta_{2F,crit}^+)^{0.9} \quad \text{for } \delta_{2F}^+ > \delta_{2F,crit}^+. \quad (2.176)$$

The *base* waves average peak thickness is approximated by  $\delta_{2F,base,max} = \frac{1}{2} \delta_{2F} + \Delta \delta_{2F,trav,max}$  and the average base wave roughness is approximated by  $\Delta \delta_{2F,base,max} = 0.6 \sigma_\delta^+$ . The *traveling* waves average peak thickness is approximated by  $\delta_{2F,trav,max} = \frac{1}{2} \delta_{2F} + \Delta \delta_{2F,trav,max}$  and the average traveling wave roughness is approximated by  $\Delta \delta_{2F,trav,max} = 2.1 \sigma_\delta^+$ . Then *Hulburt* et al. introduced the intermittency  $f_{int}$  defining in what portion of time at a local point the traveling wave is observed. Data for nitrogen-water at atmospheric pressure are correlated by

$$f_{int} = 0 \quad \text{for } \delta_{2F}^+ \leq 8, \quad (2.177)$$

$$f_{\text{int}} = 0.41 \left\{ 1 - \frac{\delta_{2F,cr}^+}{\delta_{2F}^+} + \frac{4}{\delta_{2F}^+} \left[ \exp\left(-\frac{\delta_{2F}^+ - 2}{4}\right) - \exp\left(-\frac{\delta_{2F,cr}^+ - 2}{4}\right) \right] \right\} \text{ for } \delta_{2F}^+ > 8. \quad (2.178)$$

The time averaged interfacial share stress is then  $\tau_1^{2\sigma} = f_{\text{int}} \tau_{1,trav}^{2\sigma} + (1 - f_{\text{int}}) \tau_{1,base}^{2\sigma}$ . *White* (2006) proposed the following approximation of the velocity profile with an offset depending on the type of the roughness

$$\frac{w(y)}{w^*} = \frac{1}{\kappa} \ln\left(\frac{yw^*}{\nu}\right) + B - \Delta B, \quad (2.179)$$

where  $\Delta B = \frac{1}{\kappa} \ln(1 + c_B k^+)$ ,  $k^+ = kw^*/\nu$ ,  $B = 5$ ,  $\kappa = 0.41$ ,  $c_B \approx 0.3$  for sand roughness,  $c_B \approx 0.8$  for stationary wavy wall data. The advantage of this approach is that it can be also used for description of the drag coefficient between liquid and gas wavy interface. Comparing with data *Hulburt et al.* (2006) proposed to use for gas interaction with the *base* waves  $c_{B,2F,base} \approx 0.8$  and for gas interaction with the *traveling* waves  $c_{B,2F,trav} \approx 4.7$  for which  $\Delta B \approx \frac{1}{\kappa} \ln\left(c_B \frac{kw^*}{\nu}\right)$ . The final approximate expression for prediction of the interfacial share stress  $\tau_1^{2\sigma} = \frac{1}{2} c_{12}^d \rho_1 (w_1 - w_1^{2\sigma})^2$  components was then

$$c_{12}(c_B, k_{rel}) = \left[ \frac{0.58}{-\frac{\ln k_{rel}}{(k_{rel} - 1)^2} - \ln c_B + 1.05 + \frac{1}{2} \frac{k_{rel} + 1}{k_{rel} - 1}} \right]^2 \quad (2.180)$$

where  $k_{rel} \approx 2\Delta\delta_{2F,max}/(D_h - \delta_{2F})$ . The friction velocity for the gas core is then  $w_1^* = \sqrt{\tau_1^{2\sigma}/\rho_1}$ .

Actually the idea to use the logarithmic velocity profile, Eq. 2.179, for the gas core interacting with the base waves come from *Antal et al.* in 1998. The authors used with  $B = 5.5$ ,  $\kappa = 0.41$ ,  $c_B \approx 1.05$  and for the dimensionless roughness

$$k^+ = 0.035 (\delta_{2F}^+)^2 (\rho_2/\rho_1)/(\rho_2/\rho_1)_{atm}, \quad (2.181)$$

and computed

$$\sqrt{\frac{8}{c_{12,base}^d}} = \frac{1}{\kappa} \ln\left(\frac{1}{2} \text{Re}_1 \sqrt{\frac{c_{12,base}^d}{8}}\right) + \frac{3}{2\kappa} + B - \Delta B. \quad (2.182)$$



The authors reported that the solution of this equation is well approximated by the expression obtained by *Lopez de Bertodano et al. (1997)*

$$c_{12,base}^d = 1.02 \left[ \log_{10} \left( \frac{2.51 \text{Re}_1}{\sqrt{8k^+ + 2.51}} \right) \right]^{-2.5}. \quad (2.183)$$

The relation of the base wave interfacial friction factor to those of the traveling waves was reported by *Antal et al. (1998)* to be

$$\left( \frac{c_{12,trav}^d}{c_{12,smooth}^d} - 1 \right) \bigg/ \left( \frac{c_{12,base}^d}{c_{12,smooth}^d} - 1 \right) = 10 \text{Re}_1^{-0.2}. \quad (2.184)$$

But the idea to timely average the contribution of both mechanisms is introduced first by *Hulburt et al.* as already mentioned before. The idea to consider the film as a consisting of base thickness and wavy layer is clearly derived by *Dobran* in 1983, who used  $\delta_{2F,crit}/D_h = 140 \left[ g D_h^3 \rho_2 (\rho_2 - \rho_1) / \eta_2^2 \right]^{0.5} \text{Re}_1^{-1.35}$  and introduced an eddy viscosity within this mixing layer  $\nu'_2 = \nu_2 \left[ 1 + 1.6 \times 10^{-3} (y^+ - \delta_{2F,crit}^+)^{1.8} \right]$  for  $\delta_{2F,crit}^+ < y^+ \leq \delta_{2F}^+$ . This method does not distinguish between the basic waves and traveling waves. *Dobran* assumed for  $y^+ < \delta_{2F,crit}^+$  the validity of the universal three layer velocity profile.

### 2.1.7 Inverted annular flow

During some processes (e.g. reflooding phase of loss-of-coolant accidents in water cooled nuclear reactors) the temperature of the heated surface may exceed the maximum film boiling temperature. Thus the situation may occur where the superheated vapor flows up around the heated surface and a subcooled or saturated liquid jet. Since the positions of liquid and vapor phases are exactly opposite to the ones in normal annular flow, this flow pattern is called inverted annular flow. The drag force acting on a liquid in a fully developed inverted annular flow can be calculated in accordance to *Aritomi et al. (1990)* as follows

$$f_{w2}^d = -a_{12w} \rho_1 c_{w2}^d \frac{1}{2} |w_1 - w_2| (w_1 - w_2) \quad (2.185)$$

where

$$a_{12w} = \frac{4}{D_{hw}} \sqrt{a_2}, \quad (2.186)$$

$$c_{w2}^d = 0.3164 / \text{Re}_{12}^{1/4}, \quad (2.187)$$

$$\text{Re}_{12} = (w_1 - w_2) D_{hw} \sqrt{\alpha_2} / \nu_1. \quad (2.188)$$

### 2.1.8 Stratified flow in horizontal or inclined rectangular channels

*Geometrical characteristics:* Stratified flow may exist in regions with such relative velocities between the liquid and the gas which does not cause instabilities leading to slugging. Some important geometrical characteristics are specified here - see Fig. 2.3.

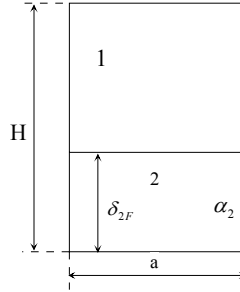


**Fig. 2.3** Definition of the geometrical characteristics of the stratified flow

The perimeter of the pipe is then

$$Per_w = 2(a + H), \quad (2.189)$$

and the wetted perimeters for the gas and the liquid parts are

$$Per_{1w} = a + 2(H - \delta_{2F}) = a + 2\alpha_1 H, \quad (2.190)$$

$$Per_{2w} = a + 2\delta_{1F} = a + 2\alpha_2 H. \quad (2.191)$$

The gas-liquid interface median is then  $a$ , and the liquid level

$$\delta_{2F} = \alpha_2 H. \quad (2.192)$$

The hydraulic diameters for the gas and the liquid for computation of the pressure drop due to friction with the wall are therefore

$$D_{h1} = 4\alpha_1 F / Per_{1w} = \frac{4\alpha_1 a H}{a + 2H\alpha_1}, \quad (2.193)$$

$$D_{h2} = 4\alpha_2 F / Per_{2w} = \frac{4\alpha_2 a H}{a + 2H\alpha_2}, \quad (2.194)$$

and the corresponding *Reynolds* numbers

$$Re_1 = \frac{\alpha_1 \rho_1 w_1}{\eta_1} \frac{4\alpha_1 a H}{a + 2H\alpha_1}, \quad (2.195)$$

$$Re_2 = \frac{\alpha_2 \rho_2 w_2}{\eta_2} \frac{4\alpha_2 aH}{a + 2H\alpha_2}. \quad (2.196)$$

Here  $F$  is the channel cross section and  $Per_{lw}$  and  $Per_{2w}$  are the perimeters wet by gas and film, respectively.

If one considers the core of the flow the hydraulic diameter for computation of the gas-liquid friction pressure loss component is then

$$D_{h12} = 4\alpha_1 F / (Per_{lw} + a) = \frac{2\alpha_1 aH}{a + H\alpha_1} \quad (2.197)$$

and the corresponding *Reynolds* number

$$Re_1 = \frac{\alpha_1 \rho_1 |w_1 - w_2|}{\eta_1} \frac{2\alpha_1 aH}{a + H\alpha_1}. \quad (2.198)$$

The gas-wall, liquid-wall and gas-liquid interfacial area densities are

$$a_{lw} = \frac{Per_{lw}}{F} = \frac{a + 2\alpha_1 H}{aH}, \quad (2.199)$$

$$a_{2w} = \frac{Per_{2w}}{F} = \frac{a + 2\alpha_2 H}{aH}, \quad (2.200)$$

$$a_{12} = \frac{a}{F} = \frac{1}{H}. \quad (2.201)$$

For the estimation of flow pattern transition criterion the following expression is sometimes required

$$\frac{d\alpha_2}{d\delta_{2F}} = \frac{1}{H}. \quad (2.202)$$

Using the geometric characteristics and the *Reynolds* numbers the interfacial interaction coefficients can be computing by means of empirical correlations. The wall-gas and the wall-liquid interaction can be modeled as

$$f_1^{w\sigma,d} = -a_{lw}\tau_{w1} = a_{lw}c_{w1}^d \frac{1}{2} \rho_1 |w_1| w_1 = \frac{a + 2\alpha_1 H}{aH} c_{w1}^d \frac{1}{2} \rho_1 |w_1| w_1, \quad (2.203)$$

$$f_2^{w\sigma,d} = -a_{2w}\tau_{w2} = a_{2w}c_{w2}^d \frac{1}{2} \rho_2 |w_2| w_2 = \frac{a + 2\alpha_2 H}{aH} c_{w2}^d \frac{1}{2} \rho_2 |w_2| w_2. \quad (2.204)$$

The gas resisting force between film and gas is

$$\begin{aligned} f_1^{2\sigma,d} &= -a_{12}\tau_{21} = -a_{12}c_{21}^d \frac{1}{2} \rho_1 |w_2 - w_1| (w_2 - w_1) \\ &= -\frac{1}{H} c_{21}^d \frac{1}{2} \rho_1 |w_2 - w_1| (w_2 - w_1). \end{aligned} \quad (2.205)$$

For single-phase pipe flow the friction force per unit flow volume is equivalent to the pressure drop per unit length. The friction force can be then expressed either in terms of the drag coefficient or in terms of the friction coefficient

$$\begin{aligned} f_l^{w\sigma,d} &= -a_{lw}\tau_{wl} = a_{lw}c_{wl}^d \frac{1}{2} \rho_l |w_l| w_l = \frac{a+2H}{aH} c_{wl}^d \frac{1}{2} \rho_l |w_l| w_l \\ &= \frac{1}{2} \rho_l |w_l| w_l \frac{\lambda_{fr,wl}}{D_h} = \frac{1}{2} \rho_l |w_l| w_l \frac{a+2H}{4aH} \lambda_{fr,wl}. \end{aligned} \quad (2.206)$$

Obviously the relation between the drag coefficient  $c_{wl}^d$  and the friction coefficient  $\lambda_{fr,wl}$  usually used in European literature is

$$c_{wl}^d = \frac{1}{4} \lambda_{fr,wl}. \quad (2.207)$$

The friction coefficient in a pipe with a technical roughness can then be used to compute

$$\lambda_{fr,wl} = \lambda_{fr,wl} (Re_l = \rho_l w_l D_h / \eta_l, \quad k / D_h), \quad (2.208)$$

from the *Nukuradze* diagram given in *Idelchik's* text book (1975).  $k$  is the roughness roughness of the pipe wall in  $m$ . In particular we will have

$$\lambda_{fr,w1} = \lambda_{fr,w1} (Re_1, \quad k / D_{h1}), \quad (2.209)$$

$$\lambda_{fr,w2} = \lambda_{fr,w2} (Re_2, \quad k / D_{h2}), \quad (2.210)$$

and

$$\lambda_{fr,12} = \lambda_{fr,12} (Re_{12}, \quad k_{wave} / D_{h12}). \quad (2.211)$$

In the later case  $k_{wave}$  is the wave amplitude at the liquid interface. *Houze* and *Dukler* (1965) observed on experiments with mechanically designed oscillating interface that the turbulence structure inside the gas is influenced by the frequency of the oscillations. At low frequency a drag reduction is observed. This is probably the reason for the low resistance that dolphins experience swimming in the sea. At high frequencies and low wave length the drag increases due to changes in the turbulence structure inside the gas boundary layer. This specific behavior was the reason why the authors warned from uncritical use of the equivalent roughness method for computing the interfacial drag coefficient.

*Lee* and *Bankoff* (1983) measured interfacial shear stresses in a nearly horizontal stratified steam - saturated water flow. According to their results, the interfacial friction factor during the buildup of the roll waves can be expressed as follows

$$c_{21}^d = 0.012 + 2.694 \times 10^{-4} \left( \frac{Re_2^*}{1000} \right)^{1.534} (Re_1^* - Re_1^{**}) / 1000, \quad (2.212)$$

where

$$Re_1^{**} = 1.837 \times 10^5 / Re_2^{0.184} \quad (2.213)$$

represents the critical gas *Reynolds* number at which the transition to the roll wave regime take place. Here

$$Re_1^* = \frac{\alpha_1 \rho_1 w_1}{\eta_1} F / Per_1, \quad (2.214)$$

$$Re_2^* = \frac{\alpha_2 \rho_2 w_2}{\eta_2} F / Per_2. \quad (2.215)$$

$F$  is the channel cross section and  $Per_1$  and  $Per_2$  are the wet perimeters of gas and film, respectively. Note the particular definition of the *Reynolds* numbers in the above correlation, instead of the hydraulic diameter the length scale is the cross section divided by the wet perimeter of the gas and film, respectively (the film *Reynolds* number was defined by *Lee* and *Bankoff* as mass flow rate per unit width of the film divided by the dynamic viscosity). The data base for Eq. (2.212) lies in the region  $2000 \leq Re_2 \leq 12000$ ,  $23000 \leq Re_1 < 51000$ .

### 2.1.9 Stratified flow in horizontal or inclined pipes

*Geometrical characteristics:* The geometric characteristics for round pipes are non linearly dependent on the liquid level, which makes the computation somewhat more complicated. Some important geometrical characteristics are specified here - see Fig. 2.4. The angle with the origin the pipe axis defined between the upwards oriented vertical and the liquid-gas-wall triple point is defined as a function of the liquid volume fraction by the equation

$$f(\theta) = -(1 - \alpha_2)\pi + \theta - \sin \theta \cos \theta = 0. \quad (2.216)$$

The derivative

$$\frac{d\theta}{d\alpha_1} = \frac{\pi}{2 \sin^2 \theta} \quad (2.217)$$

will be used later. Having in mind that

$$\frac{df}{d\theta} = 2 \sin^2 \theta \quad (2.218)$$

the solution with respect to the angle can be obtained by using the *Newton* iteration method as follows

$$\theta = \theta_0 - \frac{f_0}{df/d\theta} = \theta_0 + \frac{(1 - \alpha_2)\pi - \theta_0 + \sin \theta_0 \cos \theta_0}{2 \sin^2 \theta_0} \quad (2.219)$$

where subscript  $\theta$  stands for the previous guess. We start with an initial value of  $\pi/2$  (Kolev 1977). Biberg proposed in 1999 accurate direct approximation

$$\pi - \theta = \pi\alpha_2 + \left(\frac{3\pi}{2}\right)^{1/3} \left[1 - 2\alpha_2 + \alpha_2^{1/3} - (1 - \alpha_2)^{1/3}\right] \quad (2.219b)$$

with an error less then  $\pm 0.002rad$  or

$$\begin{aligned} \pi - \theta = \pi\alpha_2 + \left(\frac{3\pi}{2}\right)^{1/3} \left[1 - 2\alpha_2 + \alpha_2^{1/3} - (1 - \alpha_2)^{1/3}\right] \\ - \frac{1}{200} \alpha_2 (1 - \alpha_2) (1 - 2\alpha_2) \left\{1 + 4 \left[\alpha_2^2 + (1 - \alpha_2)^2\right]\right\}, \end{aligned} \quad (2.219c)$$

with an error less then  $\pm 0.00005rad$ .

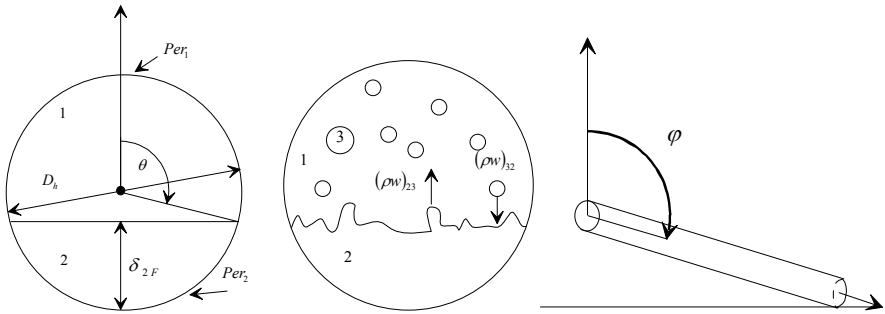


**Fig. 2.4** Definition of the geometrical characteristics of the stratified flow

The perimeter of the pipe is then

$$Per_{1w} = \pi D_h, \quad (2.220)$$

and the wetted perimeters for the gas and the liquid parts are

$$Per_{1w} = \theta D_h, \quad (2.221a)$$

$$Per_{2w} = (\pi - \theta) D_h. \quad (2.221b)$$

The gas-liquid interface median is then

$$b = D_h \sin(\pi - \theta) = D_h \sin \theta, \quad (2.222)$$

and the liquid level

$$\delta_{2F} = \frac{1}{2} D_h (1 + \cos \theta). \quad (2.223)$$

The hydraulic diameters for the gas and the liquid for computation of the pressure drop due to friction with the wall are therefore

$$D_{h1} = 4\alpha_1 F / Per_{1w} = \frac{\pi}{\theta} \alpha_1 D_h, \quad (2.224)$$

$$D_{h2} = 4\alpha_2 F / Per_{2w} = \frac{\pi}{\pi - \theta} \alpha_2 D_h, \quad (2.225)$$

and the corresponding *Reynolds* numbers

$$Re_1 = \frac{\alpha_1 \rho_1 w_1 D_h}{\eta_1} \frac{\pi}{\theta}, \quad (2.226)$$

$$Re_2 = \frac{\alpha_2 \rho_2 w_2 D_h}{\eta_2} \frac{\pi}{\pi - \theta}. \quad (2.227)$$

Here  $F$  is the channel cross section and  $Per_1$  and  $Per_2$  are the wet perimeters of gas and film, respectively.

If one considers the core of the flow the hydraulic diameter for computation of the gas-liquid friction pressure loss component is then

$$D_{h12} = 4\alpha_1 F / (Per_{1w} + b) = \frac{\pi}{\theta + \sin \theta} \alpha_1 D_h, \quad (2.228)$$

and the corresponding *Reynolds* number

$$Re_{12} = \frac{\alpha_1 \rho_1 |w_1 - w_2| D_h}{\eta_1} \frac{\pi}{\theta + \sin \theta}. \quad (2.229)$$

The gas-wall, liquid-wall and gas-liquid interfacial area density are

$$a_{1w} = \frac{Per_{1w}}{F} = \frac{4\alpha_1}{D_{h1}} = \frac{\theta}{\pi} \frac{4}{D_h}, \quad (2.230)$$

$$a_{2w} = \frac{Per_{2w}}{F} = \frac{4\alpha_2}{D_{h2}} = \frac{\pi - \theta}{\pi} \frac{4}{D_h}, \quad (2.231)$$

$$a_{12} = \frac{b}{F} = \frac{\sin \theta}{\pi} \frac{4}{D_h}. \quad (2.232)$$

*Ratel* and *Bestion* (2000) approximated this relation for smooth interface with

$$a_{12} \cong \frac{8}{\pi D_h} \sqrt{\alpha_2 (1 - \alpha_2)}. \quad (2.233)$$

For the estimation of the flow pattern transition criterion the following expression is sometimes required

$$\frac{d\alpha_2}{d\delta_{2F}} = \frac{4}{D_h} \frac{\sin \theta}{\pi}. \quad (2.234)$$

The wall-gas and the wall-liquid forces per unit mixture volume can then be computed as follows

$$f_1^{w\sigma,d} = -a_{1w}\tau_{w1} = a_{1w}c_{w1}^d \frac{1}{2} \rho_1 |w_1| w_1 = \frac{\theta}{\pi} \frac{4}{D_h} c_{w1}^d \frac{1}{2} \rho_1 |w_1| w_1, \quad (2.235)$$

$$f_2^{w\sigma,d} = -a_{2w}\tau_{w2} = a_{2w}c_{w2}^d \frac{1}{2} \rho_2 |w_2| w_2 = \frac{\pi - \theta}{\pi} \frac{4}{D_h} c_{w2}^d \frac{1}{2} \rho_2 |w_2| w_2. \quad (2.236)$$

The gas resisting force between film and gas is

$$\begin{aligned} f_1^{2\sigma,d} &= -a_{12}\tau_{21} = -a_{12}c_{21}^d \frac{1}{2} \rho_1 |w_2 - w_1| (w_2 - w_1) \\ &= -\frac{\sin \theta}{\pi} \frac{4}{D_h} c_{21}^d \frac{1}{2} \rho_1 |w_2 - w_1| (w_{2i} - w_1). \end{aligned} \quad (2.237)$$

One choice for computation of the drag coefficient is the correlation by *Lee and Bankoff* (1983).

*Ratel* and *Bestion* proposed in 2000 the following empirical correlation

$$c_{21}^d = 6 \times 10^{-8} Re_{10}^{1.75} \left( 1 + 0.035 Re_{10}^{0.97} Fr^{*-1.3} \frac{\alpha_2^{0.44}}{\alpha_1^{0.5}} \right), \quad (2.238)$$

where

$$Re_{10} = \frac{\rho_1 w_1 D_h}{\eta_1}, \quad (2.239)$$

$$Fr^* = \frac{g D_h}{w_1^2}, \quad (2.240)$$

valid for the range  $3.5 \times 10^5 < Re_{10} < 7 \times 10^5$ . Unfortunately the authors retrieved the correlation with a computer code using in the momentum equations the erroneous term

$$\alpha_1 \alpha_2 (\rho_2 - \rho_1) g D_h \frac{\partial \alpha_1}{\partial z},$$

instead of the correct term

$$\alpha_1 \alpha_2 (\rho_2 - \rho_1) g \frac{F}{b} \frac{\partial \alpha_1}{\partial z},$$

where  $F$  is the channel cross section and  $b$  is the gas-liquid interface median.



For single-phase pipe flow the friction force per unit flow volume is equivalent to the pressure drop per unit length. The friction force can be then expressed either in terms of the drag coefficient  $c_{wl}^d$  or in terms of the friction coefficient  $\lambda_{fr,wl}$

$$f_l^{w\sigma,d} = -a_{lw}\tau_{wl} = a_{lw}c_{wl}^d \frac{1}{2} \rho_l |w_l| w_l = \frac{4}{D_h} c_{wl}^d \frac{1}{2} \rho_l |w_l| w_l = \frac{1}{2} \rho_l |w_l| w_l \frac{\lambda_{fr,wl}}{D_h}. \quad (2.241)$$

Again as for rectangular channel we have

$$c_{wl}^d = \frac{1}{4} \lambda_{fr,wl} \quad (2.242)$$

and the procedure for computation of the forces applied to the rectangular channels can be used also for pipes.

Of course the approximation used by *Biberg* (1999) considers not the influence of the interfacial shear stress on the wall shear stress. Data comparison reported by *Biberg* (1999) demonstrated a systematic under prediction of the liquid volume fraction in averaged with -5.5% if using this approach. By careful elaboration of an approximation for the turbulent velocity profile in both fields *Biberg* (1999) come to the very important result

$$\frac{1}{\sqrt{\lambda_{fr,wl}}} = \frac{-1.8 \log \left[ \frac{6.9}{\text{Re}_l^*} + \left( \frac{k}{3.7 D_{hl}^*} \right)^{1.11} \right]}{1 + 2 \log(1 + b/\text{Per}_{lw}) \frac{w_1 - w_2}{w_1} \sqrt{\lambda_{fr,12}}}. \quad (2.243)$$

Here for free surface flow the equivalent hydraulic diameter is defined as

$$D_{hl}^* \approx \begin{cases} 8\delta_l/3 & \text{rectangular channel} \\ 4\alpha_l F / \text{Per}_{lw} & \text{pipe} \end{cases}, \quad (2.244)$$

and for closed duct flow as

$$D_{hl}^* \approx \begin{cases} 4\delta_l/3 & \text{rectangular channel} \\ 4\alpha_l F / (\text{Per}_{lw} + b) & \text{pipe} \end{cases}. \quad (2.245)$$

The *Reynolds* number  $\text{Re}_l^* = \rho_l |w_l| D_{hl}^* / \eta_l$  is computed with the corresponding equivalent hydraulic diameter.

## 2.2 Lift force

The force component acting on a dispersed particle perpendicular to the relative velocity direction is called lateral- or *lift force*. The lift force is zero for symmetric bodies exposed to symmetrical flow

$$\mathbf{f}_l^L = 0. \quad (2.246)$$

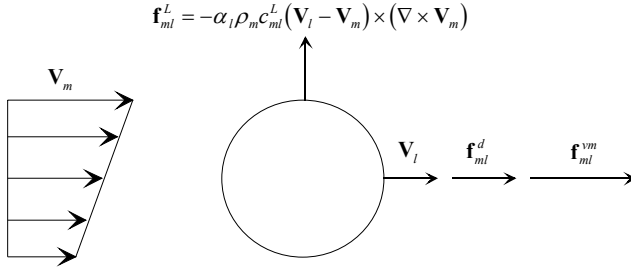


**Fig. 2.5** Drag, virtual mass, and lift forces acting simultaneously on the field  $l$

A symmetric body exposed to asymmetrical flow experiences a lateral force - see Fig. 2.5. The lift force is similar in nature to the aerodynamic lift of an airfoil, but differs in that it is a result of gradient in the continuum velocity field over a symmetric body rather than a uniform flow over an asymmetric airfoil. The general form of the lateral lift force for inviscid flows is given by *Drew and Lahey* (1987)

$$\mathbf{f}_{cd}^L = -\alpha_d \rho_c c_{cd}^L (\mathbf{V}_d - \mathbf{V}_c) \times (\nabla \times \mathbf{V}_c). \quad (2.247)$$

The scalar components for *Cartesian* and *cylindrical* coordinates are

$$f_{cd,r}^L = -\alpha_d \rho_c c_{cd}^L \left\{ (v_d - v_c) \left[ \frac{1}{r^\kappa} \frac{\partial}{\partial r} (r^\kappa v_c) - \frac{1}{r^\kappa} \frac{\partial u_c}{\partial \theta} \right] - (w_d - w_c) \left( \frac{\partial u_c}{\partial z} - \frac{\partial w_c}{\partial r} \right) \right\}, \quad (2.248)$$

$$f_{cd,\theta}^L = -\alpha_d \rho_c c_{cd}^L \left\{ (w_d - w_c) \left[ \frac{1}{r^\kappa} \frac{\partial w_c}{\partial \theta} - \frac{\partial v_c}{\partial z} \right] - (u_d - u_c) \left( \frac{1}{r^\kappa} \frac{\partial}{\partial r} (r^\kappa v_c) - \frac{1}{r^\kappa} \frac{\partial u_c}{\partial \theta} \right) \right\} \quad (2.249)$$

$$f_{cd,z}^L = -\alpha_d \rho_c c_{cd}^L \left\{ (u_d - u_c) \left[ \frac{\partial u_c}{\partial z} - \frac{\partial w_c}{\partial r} \right] - (v_d - v_c) \left( \frac{1}{r^\kappa} \frac{\partial w_c}{\partial \theta} - \frac{\partial v_c}{\partial z} \right) \right\}. \quad (2.250)$$

For axis-symmetric vertical developed flow in cylindrical pipe we have simply

$$f_{cd,r}^L = -\alpha_d \rho_c c_{cd}^L (w_d - w_c) \frac{\partial w_c}{\partial r}. \quad (2.251)$$

*Staffman* (1965, 1968) derived for negligible particle rotation, negligible particle *Reynolds* number and small gradients of the continuum velocity the analytical expression for the shear lift force

$$c_{21}^L = 3.084 v_2^{1/2} \left/ \left( D_1 \left| \frac{dw_2}{dr} \right|^{1/2} \right) \right. \quad (2.252)$$

Inside the boundary layer of bubbly flow having  $w_1 > w_2$  and  $\partial w_2 / \partial r < 0$  the lift force is ascertaining force for the bubbles toward the wall. Note that the spatial

resolution in discrete analyses has to be fine enough in order to accurately compute the rotation of the continuous velocity field. Bad resolution like those used in the so called sub-channel analyses produces only useless noise that makes the use of this force meaningless.

*Mei* (1992) proposed an expression that can be used for larger particle *Reynolds* numbers

$$c_{21}^L = Mei \ 3.084 v_2^{1/2} / \left( D_1 \left| \frac{dw_2}{dr} \right|^{1/2} \right), \quad (2.253)$$

where

$$Mei = (1 - 0.3314 \beta^{1/2}) \exp(-0.1 Re_{12}) + 0.3314 \beta^{1/2}, \quad Re_{12} \leq 40, \quad (2.254)$$

$$Mei = 0.0524 (\beta Re_{12})^{1/2}, \quad Re_{12} > 40, \quad (2.255)$$

and

$$Re_{12} = \Delta w_{12} D_1 / v_2, \quad (2.256)$$

$$\beta = \frac{D_1/2}{w_2 - w_1} \left| \frac{dw_2}{dr} \right|. \quad (2.257)$$

In a later work *Klausner et al.* (1993) found that the lift force on a bubble attached to a wall can be computed using

$$c_{21}^L = \frac{16}{3} 3.877 \beta^{3/2} (0.014 \beta^2 + Re_{12}^{-2})^{1/4}, \quad (2.258)$$

which is valid for larger *Reynolds* numbers than previous relation. In a later work *Mei and Klausner* (1995) proposed to use interpolation between the *Stafman's* results for small *Reynolds* numbers and *Auton's* results (1987), for large *Reynolds* numbers:

$$c_{21}^L = \frac{3}{8 \beta^{1/2}} \left\{ \frac{16}{9} \beta + \left[ \frac{1.72 J \sqrt{2 \beta / Re_{12}}}{Re_{12}^{1/2}} \right]^2 \right\}^{1/2}, \quad (2.259)$$

$$J = 0.6765 \left\{ 1 + \tanh \left[ 2.5 \left( \log_{10} \sqrt{2 \beta / Re_{12}} + 0.191 \right) \right] \right\} \\ \times \left\{ 0.667 + \tanh \left[ 6 \left( \log_{10} \sqrt{2 \beta / Re_{12}} - 0.32 \right) \right] \right\}. \quad (2.260)$$

*Moranga, Bonetto and Lahey* (1999) proposed

$$c_{21}^L = \left[ 0.12 - 0.2 \exp \left( -\frac{\text{Re}_{12} \text{Re}_{2rot}}{36 \times 10^4} \right) \right] \exp \left( \frac{\text{Re}_{12} \text{Re}_{2rot}}{3 \times 10^7} \right)$$

where  $\text{Re}_{2rot} = (\text{rot} \mathbf{V}_2) D_1^2 / \nu_2$  and  $\text{rot} \mathbf{V}_2$  is the local vorticity e.g.  $dw_2/dr$  in axially symmetric flow, see also *Lahey and Drew* (2001). This equation possesses a sign inversion at large Reynolds numbers. For bubbly flow of atmospheric conditions the order of magnitude of the lift coefficient is around 0.1.

They are other expression for the lift force on a single bubble. *Tomiyama et al.* (2002) measured trajectories of single bubbles in simple shear flows of glycerol-water solution. They obtained the following empirical correlation:

$$c_{21}^L = \min \left[ 0.288 \tanh(0.121 \text{Re}_{12}), f(E\ddot{o}_{1m}) \right] \quad \text{for } E\ddot{o}_{1m} < 4, \quad (2.261)$$

$$c_{21}^L = f(E\ddot{o}_{1m}) = 0.00105 E\ddot{o}_{1m}^3 - 0.0159 E\ddot{o}_{1m}^2 - 0.0204 E\ddot{o}_{1m} + 0.474 \quad (2.262a)$$

for  $4 \leq E\ddot{o}_{1m} \leq 10.7$ ,

$$c_{21}^L = -0.29 \quad \text{for } 10.7 < E\ddot{o}_{1m}, \quad (2.262b)$$

based of experiments within the region of parameters defined by  $1.39 \leq E\ddot{o}_{1m} \leq 5.74$ ,  $-5.5 \leq \log_{10} Mo_{12} \leq -2.8$ , and  $0 < |\nabla \times \mathbf{V}_2| \leq 8.3 s^{-1}$ . The lift coefficient varied in this region between about 0.3 and -0.3. Here a modified *Eöt-vös* and *Morton* numbers are used build with the horizontal bubble size

$$E\ddot{o}_{1m} = g(\rho_2 - \rho_1) D_{1,max}^2 / \sigma_{12}, \quad (2.263)$$

$$Mo_{12} = g(\rho_2 - \rho_1) \eta_2^4 / (\rho_2^2 \sigma_{12}). \quad (2.264)$$

The aspect ratio of the bubble is computed by using the *Wellek et al.* (1966) correlation

$$D_{1,max} / D_{1,min} = 1 + 0.163 E\ddot{o}_{1m}^{0.757}. \quad (2.265)$$

The lift coefficient for a bubble with diameter 3mm in an air-water system in accordance with *Tomiyama et al.* correlation equal to 0.288. *Zun* (1980) performed a measurements and estimated a value for small bubbles of about 0.3. *Naciri* (1992) experimentally measured the lift coefficient of a bubble in a vortex to be 0.25.

It should be emphasized that the above reviewed considerations are for single object in the share flow. The presence of multiple objects in the share flow is found to influence this force too.

The importance of the findings by *Tomiyama et al.* (2002) is in the observation that for large bubbles the lift force changes the sign. *Krepper et al.* (2005) observed experimentally that in vertical bubbly flow the void profile is depending on the bubble size spectrum. For spectrum with predominant small size bub-

bles a wall void peaking is observed. The level of the wall peaking depends of the turbulence in the liquid and on the stagnation pressure force. For spectrums having predominant large bubbles the central void packing is observed. This effect was reproduced by *Krepper* and *Egorov* (2005) by using lift force applied on multiple groups with  $c_{21}^L = 0.05$  for  $D_1 < 0.006m$  and  $c_{21}^L = -0.05$  for  $D_1 \geq 0.006m$ . The improvement was considerable going from 1 to 2 groups. None substantial change was reported if more then 8 size groups are used.

Using a combination of the radial liquid and gas momentum equations

$$p(r) = p(R) - (1 - \alpha_1) \rho_2 \overline{u'^2} - \int_R^r \frac{(1 - \alpha_1) \rho_2 (\overline{u'^2} - \overline{v'^2})}{r^*} dr^* . \quad (2.266)$$

and the measured fluctuation velocities in the radial and in the azimuthally direction *Wang* et al. (1987) explained why for upwards flows the bubble peaking is observed close to the wall. Later it was found that this is valid for bubbles with small sizes. Close to the wall the authors observed that a) the velocity gradient has a maximal, b) the velocity fluctuations have maximum and c) the static pressure has a minimum. Using the radial momentum equations for gas and liquids

$$-\alpha_1 \frac{\partial p}{\partial r} + \frac{1}{r} \frac{d}{dr} (\alpha_1 r \tau_{1,rr}) - \frac{1}{r} \alpha_1 \tau_{1,\theta\theta} + f_{21}^L = 0 , \quad (2.267)$$

$$-(1 - \alpha_1) \frac{\partial p}{\partial r} + \frac{1}{r} \frac{d}{dr} [r(1 - \alpha_1) \tau_{2,rr}] - \frac{1}{r} (1 - \alpha_1) \tau_{2,\theta\theta} - f_{21}^L = 0 , \quad (2.268)$$

it is possible to estimate the radial pressure distribution and the lift force, knowing from measurements the void and the velocity profiles with their fluctuations  $\tau_{1,rr} \approx 0$ ,  $\tau_{1,\theta\theta} \approx 0$ ,  $\tau_{2,rr} = -\rho_2 \overline{u_2'^2}$ ,  $\tau_{2,\theta\theta} = -\rho_2 \overline{v_2'^2}$ . This is the approach used by *Wang* et al. to gain expression for the lift force in bubbly flow based on groups of variables that are coming from the theory for the lift force on a single object. *Wang* et al. introduced the influence of the local volume fraction into the lift coefficient

$$c_{21}^L(\xi) = 0.01 + \frac{0.49}{\pi} \cot^{-1} \frac{\log \xi + 9.3168}{0.1963} , \quad (2.269)$$

as a function of

$$\xi = \exp(-\alpha_1) 2\beta \left( \frac{D_1}{D_{hyd}} \frac{1}{\text{Re}_{12}} \right)^2 \left( \frac{w_1}{\Delta w_{12\infty}} \right)^2 , \quad (2.270)$$

where

$$\Delta w_{12\infty} = 1.18 (g\sigma/\rho_2)^{1/4} . \quad (2.271)$$

This coefficient varies within 0.01 and 0.1 in accordance to the *Wang's* et al. data. The disadvantage of this approach is that due to the dependence  $\xi = \xi(D_{hyd})$  the correlation is depending on one global geometry characteristic and can not be applied locally.

For a down flow of buoyant bubbles the lift-force is directed toward the center of the pipe. As a result no wall peaking of the void fraction is experimentally observed in turbulent bubbly flow. The level of the wall peaking depends of the turbulence in the liquid and on the stagnation pressure force.

**Conclusions:** (a) The spatial resolution in finite volume analyses has to be fine enough in order to accurately compute the rotation of the continuous velocity field. Bad resolution like those used in the so called sub-channel analyses produces only useless noise that makes the use of this force meaningless. (b) There is no method known to me that is based on local conditions and that allows taking into account the effect of multiple objects on the lift force. (c) The other problem is that small bubbles will probably rotate and the application of lift force derived for non-rotating objects in share flows is questionable. (d) Heavy solid particles carried by gas are rather subject of lift force because they hardly will take the rotation of the surrounding continuum.

### 2.3 Virtual mass force

Consider the integral defined by Eq. (2.161) taken over the first term of Eq. (2.160)

$$\mathbf{f}_d^{vm} = -\alpha_d \rho_c c_d^{vm} \left[ \frac{\partial}{\partial \tau} \Delta \mathbf{V}_{cd} + (\mathbf{V}_d \cdot \nabla) \Delta \mathbf{V}_{cd} \right], \quad (2.272)$$

where the subscripts c and d mean continuous and disperse, respectively. The force  $\mathbf{f}_i^{vm}$  is the *virtual mass force* per unit mixture volume. Here the virtual mass coefficient is  $c_{ml}^{vm} = 1/2$ . The general form of the virtual mass force with the accuracy of an empirical coefficient was proposed first by *Prandtl* (1952), *Lamb* (1945) and *Milne-Thomson* (1968) in the same form. The scalar force components in *Cartesian* and in *cylindrical* coordinates are

$$f_{d,r}^{vm} = -\alpha_d \rho_c c_d^{vm} \left\{ \begin{array}{l} \frac{\partial}{\partial \tau} (u_c - u_d) + u_d \frac{\partial}{\partial r} (u_c - u_d) \\ + v_d \frac{1}{r} \frac{\partial}{\partial \theta} (u_c - u_d) + w_d \frac{\partial}{\partial z} (u_c - u_d) \end{array} \right\}, \quad (2.273)$$

$$f_{d,\theta}^{vm} = -\alpha_d \rho_c c_d^{vm} \left\{ \begin{array}{l} \frac{\partial}{\partial \tau} (v_c - v_d) + u_d \frac{\partial}{\partial r} (v_c - v_d) \\ + v_d \frac{1}{r^\kappa} \frac{\partial}{\partial \theta} (v_c - v_d) + w_d \frac{\partial}{\partial z} (v_c - v_d) \end{array} \right\}, \quad (2.274)$$

$$f_{d,z}^{vm} = -\alpha_d \rho_c c_d^{vm} \left\{ \begin{array}{l} \frac{\partial}{\partial \tau} (w_c - w_d) + u_d \frac{\partial}{\partial r} (w_c - w_d) \\ + v_d \frac{1}{r^\kappa} \frac{\partial}{\partial \theta} (w_c - w_d) + w_d \frac{\partial}{\partial z} (w_c - w_d) \end{array} \right\}. \quad (2.275)$$

The virtual mass force is experienced by the body as if it had an additional mass during its translation relative to the continuum. This explains the other name used for this force, *added mass force*. For larger particle concentrations,  $c_d^{vm}$  is a function of  $\alpha_l$ .

*Lamb* (1945) computed the virtual mass coefficient for a partials in potential flow with ellipsoidal shape defined by

$$\frac{x^2}{R_x} + \frac{y^2}{R_y} + \frac{z^2}{R_z} = 1, \quad (2.276)$$

where the lengths of the principle axis are  $R_x$ ,  $R_y$  and  $R_z$ , and the relative velocity is parallel to the x-axis as follows

$$c_{cd}^{vm} = \frac{a_0}{2 - a_0}, \quad (2.277)$$

$$a_0 = R_x R_y R_z \int_0^\infty \frac{d\lambda}{(R_x^2 + \lambda) \sqrt{(R_x^2 + \lambda)(R_y^2 + \lambda)(R_z^2 + \lambda)}}. \quad (2.278)$$

*Bournaski* (1992) evaluated some values as given in Table 2.1.

For single ellipsoid bubble with axis aspect ratio  $\chi$

$$c_{21}^{vm} = \frac{(\chi^2 - 1)^{1/2} - \cos^{-1} \chi^{-1}}{\cos^{-1} \chi^{-1} - (\chi^2 - 1)^{1/2} / \chi^2}, \quad \text{van Wijngaarden (1998)}. \quad (2.279)$$

**Table 2.3.** Virtual mass coefficients for an ellipsoid

Shape of particles	Translation parallel to axis		
	$x$	$y$	$z$
	$c_{cd,x}^{vm}$	$c_{cd,y}^{vm}$	$c_{cd,z}^{vm}$
$R_x = R_y = R_z$ , sphere	1/2	1/2	1/2
$R_x = R_y = R_z/2$ , rotary ellipsoid	0.704	0.704	0.210
$R_x = R_y = R_z/3$ , rotary ellipsoid	0.803	0.803	0.122
$R_x = R_y = R_z/4$ , rotary ellipsoid	0.859	0.859	0.081
$R_x = (2/3)R_y = R_z/2$ , unrotary ellipsoid	0.936	0.439	0.268
$R_x = R_y/2 = R_z/4$ , unrotary ellipsoid	1.516	0.398	0.126

*Lance* and *Bataille* (1991) reported experiments showing that for 5mm deforming bubble the virtual mass coefficient is in the region:  $1.2 < c_{21}^{vm} < 3.4$ . For family of spherical bubbles:

$$c_{21}^{vm} = \frac{1}{2}(1 + 2.78\alpha_1), \quad (2.280)$$

dilute bubble dispersion, interaction between two equally sized bubbles, *van Wijngaarden* (1976);

$$c_{21}^{vm} = \frac{1}{2} \frac{1 + 2\alpha_1}{1 - \alpha_1}, \quad (2.281)$$

no interaction with the neighboring bubbles, *Zuber* (1964);

$$c_{21}^{vm} = \frac{1}{2}(1 + 3\alpha_1), \quad \alpha \rightarrow 0, \quad (2.282)$$

*Zuber* (1964);

$$c_{21}^{vm} = \frac{1}{2}(1 + 3.32\alpha_1), \quad (2.283)$$

analogy to thermal conductivity in composite material, *Jeffrey* (1973);

$$c_{21}^{vm} = \frac{1}{2} \left[ \frac{1}{2} - 1.98 \ln(0.62 - \alpha_1) \right], \quad (2.284)$$

approximation for  $\alpha_1 \leq 0.35$ , *Biesheuvel* and *Spoelstra* (1989). *Kendoush* (2006) considered the separation of the velocity profile around a single sphere and obtained a virtual mass coefficient depending on the separation angle.



## Nomenclature

### Latin

$a_{1w}$	gas-wall interfacial area densities, $1/m$
$a_{2w}$	liquid-wall interfacial area densities, $1/m$
$a_{12}$	gas-liquid interfacial area densities, $1/m$
$b$	bubble breadth (major axis), $m$
$c_{cd}^L$	lateral or lift force coefficient for the force acting on the dispersed field $d$ which is submerged into the continuous field $c$ , <i>dimensionless</i>
$c_d^{vm}$	virtual mass force coefficient for the force acting on the dispersed field $d$ which is submerged into the continuous field $c$ , <i>dimensionless</i>
$c_{cd}^d$	dispersed phase drag coefficient due to continuum action, <i>dimensionless</i>
$c_{21}^d$	bubble drag coefficient due to liquid action, <i>dimensionless</i>
$c_{13}^d$	particle drag coefficient due to gas action, <i>dimensionless</i>
$c_{23,nb}^d$	particle drag coefficient due to liquid action measured for non-boiling condition, <i>dimensionless</i>
$c_{13o}^{vm}$	single particle virtual mass coefficient due to gas action, <i>dimensionless</i>
$c_{23o}^{vm}$	single particle virtual mass coefficient due to liquid action, <i>dimensionless</i>
$c_{13o}^d$	single particle drag coefficient due to gas action, <i>dimensionless</i>
$c_{23o}^d$	single particle drag coefficient due to liquid action, <i>dimensionless</i>
$c_{13}^{vm}$	$= (1 - \phi)c_{13o}^{vm}$ , particles virtual mass coefficient due to gas action, <i>dimensionless</i>
$c_{23}^{vm}$	$= \phi c_{23o}^{vm}$ , particles virtual mass coefficient due to liquid action, <i>dimensionless</i>
$c_{13}^d$	$= (1 - \phi)c_{13o}^d$ , particles drag coefficient due to gas action, <i>dimensionless</i>
$c_{23}^d$	$= \phi c_{23o}^d$ , particles drag coefficient due to liquid action, <i>dimensionless</i>
$c_{w1}^d$	gas drag coefficient due to wall-gas interaction, <i>dimensionless</i>
$c_{w2}^d$	liquid drag coefficient due to wall-gas interaction, <i>dimensionless</i>
$D_d$	dispersed particle diameter, $m$
$D_1$	bubble diameter, $m$
$D_3$	particle diameter, $m$
$D_{h1}$	hydraulic diameters for the gas, $m$
$D_{h2}$	hydraulic diameters for the liquid, $m$

$D_{h12}$	hydraulic diameter for computation of the gas friction pressure loss component in a gas-liquid stratified flow, $m$
$Eu$	$= (D_1 / \lambda_{RT})^2$ , <i>Eötvös number, dimensionless</i>
$Eö_{1m}$	$\equiv g(\rho_2 - \rho_1) D_{1,max}^2 / \sigma_{12}$ , <i>Eötvös number build with the horizontal bubble size, dimensionless</i>
$F$	channel cross section, $m^2$
$\mathbf{f}_l^L$	lateral or lift force acting on field $l$ , $N/m^3$
$\mathbf{f}_{cd}^L$	$\equiv -\alpha_d \rho_c c_{cd}^L (\mathbf{V}_d - \mathbf{V}_c) \times (\nabla \times \mathbf{V}_c)$ , lateral or lift force acting on the dispersed field $d$ which is submerged into the continuous field $c$ , $N/m^3$
$\mathbf{f}_d^{vm}$	$\equiv -\alpha_d \rho_c c_d^{vm} \left[ \frac{\partial}{\partial \tau} \Delta \mathbf{V}_{cd} + (\mathbf{V}_d \cdot \nabla) \Delta \mathbf{V}_{cd} \right]$ , lateral or virtual mass force acting on field $d$ , $N/m^3$
$\mathbf{f}_{w1}$	gas resisting force between wall and gas per unit flow volume, $N/m^3$
$\mathbf{f}_{w2}^d$	film resisting force between wall and film per unit flow volume, $N/m^3$
$\mathbf{f}_{21}^d$	bubble force per unit flow volume due to liquid-gas interaction, $N/m^3$
$\mathbf{f}_{13}^d$	particle force per unit flow volume due to liquid-gas interaction, $N/m^3$
$h$	bubble high (minor axis), $m$
$Mo$	$= \frac{g \Delta \rho_{21}}{\sigma} \left( \frac{\eta_2^2}{\rho_2 \sigma} \right)^2$ , <i>Morton number, dimensionless</i>
$Mo_{12}$	$\equiv g(\rho_2 - \rho_1) \eta_2^4 / (\rho_2^2 \sigma_{12})$ , <i>Morton number build with the horizontal bubble size, dimensionless</i>
$Per_w$	perimeter of the rectangular channel, $m$
$Per_{1w}$	wetted perimeters for the gas, $m$
$Per_{2w}$	wetted perimeters for the liquid, $m$
$p$	pressure, $Pa$
$R_x, R_y, R_z$	lengths of the principle axis of an ellipsoid bubble, $m$
$Re_{12}$	$\equiv D_1 \rho_2  \Delta w_{12}  / \eta_2$ , <i>Reynolds number for a single bubble based on bubble-liquid relative velocity, dimensionless</i>
$Re$	$= D_1 \rho_2  \Delta V_{12}  / \eta_2$ , <i>Reynolds number for a single bubble, dimensionless</i>
$Re_{13}$	$= (\alpha_1 \rho_1 w_1 + \alpha_3 \rho_3 w_3) D_h / \eta_1$ , <i>core Reynolds number, dimensionless</i>
$Re_1$	$= \rho_1 w_1 D_h / \eta_1$ , <i>gas Reynolds number, dimensionless</i>
$Re_2$	$= \rho_2 w_2 D_h / \eta_2$ , <i>liquid Reynolds number, dimensionless</i>
$Ta$	$= \frac{ \Delta V_{12} }{\sqrt{g \lambda_{RT}}} \frac{D_1}{\lambda_{RT}}$ , <i>dimensionless</i>
$V_{wake}$	velocity behind a solid particle, $m/s$

---

$\mathbf{V}$	velocity vector with components $u, v, w$ in $x, y, z$ (or $r, \theta, z$ ) directions, respectively, $m/s$
$\mathbf{V}_1$	gas velocity, $m/s$
$\mathbf{V}_2$	liquid velocity, $m/s$
$\mathbf{V}_3$	droplet velocity, $m/s$
$w_{31\infty}$	particle sink velocity in gas, $m/s$
$w_{32\infty}$	particle sink velocity in liquid, $m/s$
$w_1$	axial gas velocity, $m/s$
$w_2$	axial liquid velocity, $m/s$
$w_{2i}$	axial liquid film interface velocity, $m/s$
$z$	axial coordinate, $m$

### Greek

$\alpha_d$	particle volume fraction, <i>dimensionless</i>
$\alpha_{dm}$	volume concentration of the disperse phase and the maximum packing, <i>dimensionless</i>
$\alpha_3$	particle volume fraction, <i>dimensionless</i>
$\alpha_{2eff}^*$	effective saturation, <i>dimensionless</i>
$\beta$	$:= \frac{D_1/2}{w_2 - w_1} \left  \frac{dw_2}{dr} \right $ , parameter in the lift force correlations, <i>dimensionless</i>
$\gamma$	surface permeability - flow cross section divided by the overall cross section, <i>dimensionless</i>
$\nabla$	gradient
$\nabla V_{cd}$	velocity difference continuous minus disperse, $m/s$
$\nabla V_{13}$	velocity difference gas minus particle, $m/s$
$\Delta \tau$	time interval, $s$
$\partial$	partial differential
$\delta$	location, $m$
$\delta_{1F}$	film thickness, $m$
$\phi$	$= \alpha_2 / (\alpha_1 + \alpha_2)$ , liquid volume fraction inside the gas liquid mixture within the three fluid mixture, <i>dimensionless</i>
$\lambda_{RT}$	$= [\sigma / (g \Delta \rho_{21})]^{1/2}$ , Rayleigh-Taylor instability wavelength, $m$
$\eta_m$	effective continuum viscosity, $kg/(ms)$
$\eta^*$	viscosity coefficient, <i>dimensionless</i>
$\eta_d$	dispersed phase dynamic viscosity, $Pa \cdot s$
$\eta_c$	continuum dynamic viscosity, $Pa \cdot s$

$k_1^l, k_1^t$	viscous and turbulent permeability coefficients, respectively, <i>dimensionless</i>
$\lambda_{fr, wl}$	friction coefficient, <i>dimensionless</i>
$\mu_3$	field 3 mass generation per unit mixture volume, $kg/(sm^3)$
$\rho_1$	gas density, $kg/m^3$
$\rho_2$	liquid density, $kg/m^3$
$\rho_3$	particle density, $kg/m^3$
$\sigma_2$	liquid-gas surface tension, $N/m$
$\tau$	time, $s$
$\tau_{l, xy}$	share stress, force acting in $y$ -direction per unit surface perpendicular to $x$ -direction, $N/m^2$
$\tau_a$	time at the old time level, $s$
$\tau_{w2}$	liquid share stress caused by the wall friction, $N/m^2$
$\tau_{w1}$	gas share stress caused by the wall friction, $N/m^2$
$\tau_{12}$	$= \frac{1}{2} c_{21}^d \rho_1 V_1^2$ , gas side interfacial share stress at the liquid interface, $N/m^2$
$\theta_{23}$	wetting contact angle between the liquid and particles, $rad$

### ***Subscripts***

$c$	continuous
$d$	dispersed
$r$	in $r$ -direction
$\theta$	in $\theta$ -direction
$z$	in $z$ -direction
min	minimum
max	maximum
hyd	hydraulic

### ***Superscript***

$'$	fluctuation component
vm	virtual mass force
d	drag
L	lift

## **References**

- Achenbach E (1993) Heat and flow characteristics of packed beds, Experimental Heat Transfer, Fluid Mechanics and Thermodynamics, Kelleher M D et al. (eds) Elsevier

- Alekseenko SW, Nakoryakov VE and Pokusaev BG (1996) Wave flow of liquid films, Begel House, New York, ed. Fukano
- Ambrosini W, Andreussi P and Azzopardi BJ (1991) *Int. J. Multiphase Flow*, vol 17 no 4 pp 497-507
- Andreussi P, Asali JC and Hanratty TJ (1985) Initiation of roll waves in gas-liquid flows, *AIChE Journal* vol 31, pp 119-126
- Antal S, Kurul N, Podowski MZ and Lahey Jr RT (June 8-12, 1998) The development of multidimensional modeling capabilities for annular flows, Third Int. Conf. on Multiphase Flow, ICMF'98, Lion, France
- Aritomi M, Inoue A, Aoki S and Hanawa K (1990) Thermo- hydraulic behavior of inverted annular flow, *NED* vol 120 pp 281-291
- Asali JC, Hanratty TJ and Andreussi P (1985) Interfacial drag and film height for vertical annular flow, *AIChE Journal* vol 31 pp 895-902
- Auton RT (1987) The lift force on a spherical body in rotating flow, *J. Fluid Mechanics*, vol 183 pp 199-218
- Bharathan D, Richter HT and Wallis GB (1978) Air-water counter-current annular flow in vertical tubes, EPRI-NP-786
- Bharathan D, Wallis GB, Richter HT (1979) Air - water countercurrent annular flow. EPRI NP - 1165, Electric Power Research Inst., Palo Alto, California
- Biberg D (December 1999) An explicit approximation for the wetted angle in two-phase phase stratified pipe flow, *The Canadian Journal of Chemical Engineering*, vol 77 pp 1221-1224
- Biesheuvel A and Spoelstra S (1989) The added mass coefficient of a dispersion of spherical gas bubbles in liquid, *Int. J. Multiphase Flow*, vol 15 pp 911-924
- Bournaski E (1992) Numerical simulation of unsteady multiphase pipeline flow with virtual mass effect, *Int. J. for Numerical Methods in Engineering*, vol 34 pp 727-740
- Brinkman HC (1951) *J. Chem. Phys.*, vol 6 p 571
- Brinkman HC (1952) *J. Chem. Phys.*, vol 20 p 571
- Brooks RH and Corey AT (1966) Properties of porous media affecting fluid flow, *J. Irrig. and Drainage Div. Proc. ASChE*, vol 92, IR2 pp 61
- Brown GG et al. (1950) Unit operations, J. Wiley and Sons, Inc., New York, pp 210-228
- Dobran F (1983) Hydrodynamics of heat transfer analysis of two-phase annular flow with a new liquid film model of turbulence, *Int. J. of Heat and Mass Transfer*, vol 26 pp 1159-1171
- Drew DA, Lahey RT Jr (1987) The virtual mass and lift force on a sphere in rotating and straining flow, *Int. J. Multiphase Flow*, vol. 13 no 1, pp 113-121
- Ergun S (1952) Fluid flow through packed columns, *Chem. Eng. Prog.*, vol 48 no 2 pp 89-94
- Fore LB, Beus SG and Bauer RC (2000) Interfacial friction in gas-liquid annular flow: analogies to full and transition roughness, *International Journal of Multiphase Flow*, vol 26 pp 1755-1769
- Geary NW and Rice RG (Oct. 1991) Circulation in bubble columns: correlations for distorted bubble shape, *AIChE Journal*, vol 37 no 10 pp 1593-1594
- Govan AH, Hewitt GF, Richter HJ, and Scott A (1991) Flooding and churn flow in vertical pipes, *Int. J. Multiphase Flow*, vol 17 no 1 pp 27-44
- Hadamard JS (1911) Mouvement permanent lent d' une sphere liquide et visqueuse dans un liquide visqueux, *Compte-Rendus de l' Acad. Des Sci.*, Paris, vol 152 pp 1735-1738
- Hanratty TJ and Dykko LA (1997) Physical issues in analyzing gas-liquid annular flows, *Experimental Heat Transfer, Fluid Mechanics and Thermodynamics*, Eds.: Giot M, Mayinger F and Celata GP, pp 1127-1136

- Henstock WH and Hanratty TJ (1976) The interfacial drag and the height of the wall layer in annular flows," *AIChE Journal*, vol 22 pp 990-1000
- Houze N and Dukler AE (21-23 June 1965) The effect of a moving interface on gas phase turbulence, *Proc. Of the Symposium on Two Phase Flow*, Department of chemical engineering University of Exeter, Devon, England
- Hugmark GA (Sept. 1973) Film thickness, entrainment and pressure drop in upward annular and dispersed flow, *AIChEJ*, vol 19 no 5 pp 1062-1065
- Hurlburt ET, Fore LB and Bauer RC (July 17-20, 2006) A two zone interfacial shear stress and liquid film velocity model for vertical annular two-phase flow, *Proceedings of FEDSM2006 2006 ASME Joint U.S. - European Fluids Engineering Summer Meeting* July 17-20, Miami, FL, FEDSM2006-98512
- Idelchik IE (1975) *Handbook of hydraulic resistance*, Second Edition, Hemisphere, Washington, translated from Russian in 1986
- Ishii M and Chawla TC (Dec.1979) Local drag laws in dispersed two-phase flow, *NUREG/CR-1230*, ANL-79-105
- Ishii M and Zuber N (1978) Relative motion and interfacial drag coefficient in dispersed two - phase flow of bubbles, drops and particles, Paper 56 a, *AIChE 71st Ann. Meet.*, Miami
- Jeffrey D (1973) Condition to a random suspension of spheres, *Proc. R. Soc. London*, A335 pp 355-367
- Kendoush AA (July 17-20, 2006) Modification of the classical theory of the virtual mass of an accelerated spherical particle, *Proc. of the FEDSM2006, 2006 ASME Joint US-European Fluids Engineering Summer Meeting*, Miami, FL
- Klausner JF, Mei R, Bernhard D and Zeng LZ (1993) Vapor bubble departure in forced convection boiling, *Int. J. Heat Mass Transfer*, vol 36 pp 651-662
- Kolev NI (1977) Two-phase two-component flow (air-water steam-water) among the safety compartments of the nuclear power plants with water cooled nuclear reactors during loss of coolant accidents, PhD Thesis, Technical University Dresden
- Krepper E and Egorov Y (May 16-20, 2005) CFD-Modeling of subcooled boiling and application to simulate a hot channel of fuel assembly, *13<sup>th</sup> Int. Conference on Nuclear Engineering*, Beijing, China References 91
- Krepper E, Lucas D and Prasser H-M (2005) On the modeling of bubbly flow in vertical pipes, *Nuclear Engineering and Design*, vol 235 pp 597-611
- Lahey R Jr and Drew DA (2001) The analysis of two-phase flow and heat transfer using a multi-dimensional four field, two fluid model, *Nuclear Engineering and Design*, vol 204 pp 29-44
- Lamb H (1945) *Hydrodynamics*, Dover, New York
- Lamb MA (1945) *Hydrodynamics*, Cambridge University Press, Cambridge
- Lance M and Bataille J (1991) Turbulence in the liquid phase of a uniform bubbly airwater flow, *J. of Fluid Mechanics*, vol 22 pp 95-118
- Lee SC and Bankoff SG (1983) Stability of steam - water countercurrent flow in an inclined channel. *J. Heat Transfer*, vol 105 pp 713-718
- Lepinski RJ (Apr. 1984) A coolability model for postaccident nuclear reactor debries, *Nucl. Technology*, vol 65 pp 53-66
- Lopes JCB and Dukler AE (Sept.1986) Droplet entrainment in vertical annular flow and its contribution to momentum Transfer, *AIChE Journal*, vol 32 no 9 pp 1500-1515
- Lopez de Bertodano MA, Shi JF and Beus SG (1997) Air-water experiments for annular flow pressure drop in small pipe, *Nuclear Science and Engineering*, vol 126 pp 108-114
- Mei R (1992) An approximate expression for the shear lift force on spherical particle at finite Reynolds number, *Int. J. Multiphase Flow*, vol 18 no 1 pp 145-147

- Mei R and Klausner JF (1995) Shear lift force on spherical bubbles, *Int. J. Heat Fluid-Flow*, vol 15 pp 62-65
- Michaelides EE (March 2003) Hydrodynamic force and heat/mass transfer from particles, bubbles and drops – The Freeman Scholar Lecture, *ASME Journal of Fluids Engineering*, vol 125 pp 209-238
- Militzer J, Kann J M, Hamdullahpur F, Amyotte P R, Al Towel A M (1998) Drag coefficients of axisymmetric flow around individual spheroidal particles, *Powder Technol.*, vol 57 pp 193-195
- Milne-Thomson LM (1968) *Theoretical Hydrodynamics*, MacMillan & Co. Ltd., London
- Moeck ED and Stachiewicz JW (1972) A droplet interchange model for annular dispersed, two phase flow, *Int. J. Heat Mass Transfer*, vol 28 no 8 pp 1159-1171
- Moranga FJ, Bonetto FJ and Lahey KT Jr (1999) Lateral forces on spheres in turbulent uniform shear flow, *Int. J. Multiphase Flow*, vol 25 pp 1321-1372
- Naciri A (1992) Contribution à l'étude des forces exercées par un liquide sur une bulle de gaz: portance, masse ajoutée et interactions hydrodynamiques, Doctoral Dissertation, École Central de Lyon, France
- Nigmatulin B et al. (1978) Experimental investigation of the hydrodynamics of equilibrium dispersed-annular steam-water flow, *Teplofiz. Vys. Temp.*, vol 16 p 1258
- Nigmatulin BI (1982) Heat and mass transfer and force interactions in annular - dispersed two - phase flow, 7th Int. Heat Transfer Conf., Munich, pp 337-342
- Oseen CW (1910) Über die Stokessche Formel und über eine verwandte Aufgabe in der Hydrodynamik, *Ark. F. Math. Astron. Och. Fys.*, vol 6 no 29
- Prandtl L (1952) *Essentials of Fluid Dynamics*, Blackie & Son, Glasgow pp. 342
- Ratel G and Bestion D (2000) Analysis with CHATHARE code of the stratified flow regime in the MERESA hot leg entrainment tests, 38<sup>th</sup> European Two Phase Group Meeting, Karlsruhe
- Reed AW (Feb. 1982) The effect of channeling on the dryout of heated particulate beds immersed in a liquid pool, PhD Thesis, Massachusetts Institute of Technology, Cambridge
- Roscoe R (1952) *Brit. Appl. Phys.*, vol 3 p 26
- Roscoe R and Brit J (1952) *Appl. Phys.*, vol 3 p 267
- Rousseau JC and Houdayer G (1983) Advanced safety code CATHARE summary of verification studies on separate effects experiments, *Proc. NURETH-2*
- Rybczynski W (1911) On the translatory motion of a fluid sphere in viscous medium, *Bull. Acad. Sci., Krakow, Series A*, pp 40-46
- Schiller L and Naumann AZ (1935) *Z. Ver. Deut. Ing.*, vol 77 p 318
- Staffman PG (1965) The lift on a small sphere in a slow shear flow, *J. Fluid Mech.* vol 22 pp 385-400
- Staffman PG (1968) Corrigendum to "The lift on a small sphere in a slow shear flow", *J. Fluid Mech.* vol 31 pp 624
- Stephan M and Mayinger F (1990) Countercurrent flow limitation in vertical ducts at high system pressure, Hetstroni G (ed), *Proc. of The Ninth International Heat Transfer Conference*, Jerusalem, Israel, vol 6 pp 47-52
- Stokes GG (1880) *Mathematical and physical papers*, vol 1, Cambridge University Press, London
- Stuhmiller JH, Ferguson RE and Meister CA (November 1989) Numerical simulation of bubble flow, EPRI Research Project Report NP-6557
- Subbotin VI et al. (1978) Integrated investigation into hydrodynamics of annular dispersed steam-liquid flows, *Int. Heat Transfer Conf.*, vol 1 p 327
- Tomiyama A (June 8-12, 1998) Struggle with computational bubble dynamics, Third International Conference on Multiphase Flow, ICMF 98, Lyon, France,

- Tomiyama A, Matsuoka T, Fukuda T and Sakaguchi T (April 3-7, 1995) A simple numerical method for solving an incompressible two-fluid model in a general curvilinear coordinate system, Proc. of The 2nd International Conference on Multiphase Flow '95 Kyoto, Kyoto, Japan, vol 2 pp NU-23 to NU-30
- Tomiyama A, Sakaguchi T and Minagawa H (1990) Kobe University, private communication
- Tomiyama A et al. (2002) Transverse migration of single bubbles in simple shear flows, Chemical Engineering Science, vol 57 pp 1849-1858
- Tung VX and Dhir VK (1990) Finite element solution of multi-dimensional two-phase flow through porous media with arbitrary heating conditions, Int. J. Multiphase Flow, vol 16 no 6 pp 985-1002
- Ueda T (1981) Two-phase flow - flow and heat transfer, Yokendo, Japan (in Japanese)
- van Wijngaarden L (1976) Hydrodynamic interaction between the gas bubbles in liquid, J. Fluid Mechanics, vol 77 pp 27-44
- van Wijngaarden L (1998) On pseudo turbulence, Theoretical and Computational Fluid Dynamics, vol 10 pp 449-458
- Vassallo P (1999) Near wall structure in vertical air-water annular flows, International Journal of Multiphase Flow, vol 25 pp 459-476
- VDI-Wärmeatlas, VDI-Verlag, Düsseldorf (1991) 6. Aufl.
- Wallis GB (1969) One-dimensional two-phase flow, New York: McGraw Hill
- Wang SK, Lee SJ, Jones OC and Lahey RT Jr (1987) 3-D turbulence structure and phase distribution measurements in bubbly two-phase flows, Int. J. Multiphase Flow, vol 13 no 3 pp 327-343
- Wellek RM, Agrawal AK and Skelland AHP (1966) Shapes of liquid drops moving in liquid media, AIChE J. vol 12 p 854
- White FM (2006) Viscous fluid flow, 3rd ed, McGraw-Hill, New York
- Wyckoff RD and Botset HG (1936) Physics, vol 73 p 25
- Zuber N (1964) On the dispersed two-phase flow in the laminar flow regime, Chem. Eng. Science, vol 49 pp 897-917
- Zun I (1980) The transverse migration of bubbles influenced by walls in vertical bubbly flow, Int. J. Multiphase Flow, vol 6 pp 583-588
- Zvirin Y, Hewitt GF, Kenning DBR (1990) Boiling of free - falling spheres: Drag and heat transfer coefficients. Experimental Heat Transfer, vol 3 pp 185-214



## 3 Friction pressure drop

### 3.1 Introduction

The drag force acting on the velocity field that is in contact with the wall can be calculated in different ways. One of them is to model the two-dimensional flow with fine resolution of the boundary layer, then to differentiate the velocity profile of the field being in a contact with the wall, and finally to compute the tangential stress at the wall. Due to the complexity of the flow pattern this is difficult to do for all of them. That is why empirical methods are commonly used for practical applications.

### 3.2 Single-phase flow

The friction pressure loss computation for multi-phase flows uses the knowledge from the single-phase flow as a prerequisite. The pressure drop per unit length in a straight pipe with hydraulic diameter  $D_h$ , roughness  $k$  and length  $\Delta z$  is

$$\left( \frac{dp}{dz} \right)_R = \frac{1}{2} \rho |V| V \left( \frac{\lambda_R}{D_h} + \frac{\xi}{\Delta z} \right), \quad (3.1)$$

where

$$\lambda_R = \lambda_R(\text{Re} = \rho V D_h / \eta, k / D_h) \quad (3.2)$$

is the friction pressure loss coefficient.

#### 3.2.1 Circular pipes

For technical roughness the *Nikuradze* diagram, Fig. 3.1, given in *Idelchik's* text book (1975), is recommend.

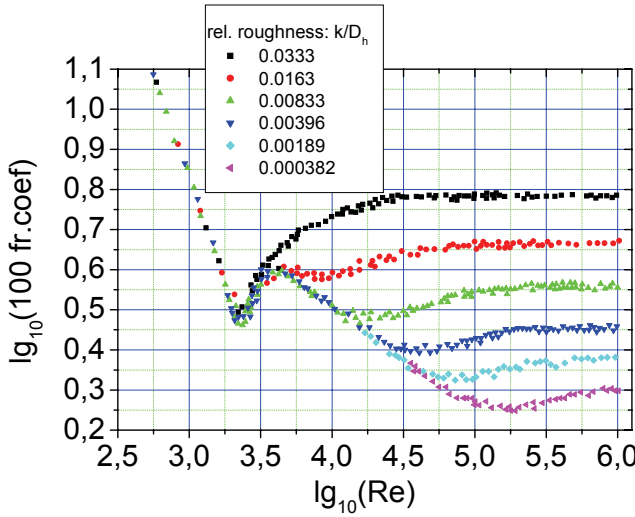


**Fig. 3.1** Nikuradze diagram for uniform grain roughness, *Idelchik's* (1975): Friction coefficient for internal pipe flow as a function of the flow *Reynolds* number. Parameter: roughness

The analytical approximations of this diagram are given below. First the minimum of  $\lambda_R$  is defined for  $k = 0$  as follows:

(a) For laminar flow i.e.  $Re < 2300$  the *Hagen* and *Poiseuille* law is valid

$$\lambda_R = 64 / Re. \quad (3.3)$$

(b) For the intermediate region,  $2300 < Re < 2818$ , an interpolation between the *Hagen* and *Poiseuille* and the *Altshul* formula

$$\lambda_R = 0.028(Re / 2300)^{2.667}, \quad (3.4)$$

is necessary.

(c) For the turbulent region the *Altshul* formula

$$\lambda_R = (1.8 \log Re - 1.64)^{-2}, \quad (3.5)$$

is recommend. For the case of  $k > 0$  four *Reynolds* numbers are computed in order to define different regions of the *Nikuradze* diagram

$$Re_0 = 754e^{0.0065/(k/D_h)}, \quad (3.6)$$

$$Re_1 = 1160 \left( \frac{D_h}{k} \right)^{0.11}, \quad (3.7)$$

$$Re_2 = 2090 \left( \frac{D_h}{k} \right)^{0.0635}, \quad (3.8)$$

$$Re_3 = 560 D_h / k. \quad (3.9)$$

The following approximations are recommended for the four regions of the *Nikuradze* diagram:

- (a) For  $Re < Re_0$  or  $Re_0 > Re_1$ , use the *Hagen* and *Poiseuille* formula;
- (b) For  $Re_0 < Re < Re_1$ , use the *Samoilenko* formula

$$\lambda_R = 4.4 / \left( Re^{0.595} e^{0.00275 D_h / k} \right). \quad (3.10)$$

- (c) For  $Re_1 < Re < Re_2$ , interpolation between  $\lambda_{R2}$  and  $\lambda_{R3}$  is used

$$\lambda_R = \lambda_{R3} + (\lambda_{R2} - \lambda_{R3}) / e^{\left[ 0.0017 (Re_2 - Re) \right]^2}, \quad (3.11)$$

where for  $k/D_h < 0.007$

$$\lambda_{R1} = 0.032, \quad (3.12)$$

$$\lambda_{R2} = 7.244 / Re_2^{0.643}, \quad (3.13)$$

$$\lambda_{R3} = \lambda_{R1}, \quad (3.14)$$

and for  $k/D_h \geq 0.007$

$$\lambda_{R1} = 0.0775 - 0.019 / (k / D_h)^{0.286}, \quad (3.15)$$

$$\lambda_{R2} = 0.145 (k / D_h)^{0.244}, \quad (3.16)$$

$$\lambda_{R3} = \lambda_{R1} - 0.0017. \quad (3.17)$$

- (d) For  $Re_2 < Re < Re_3$  the *Colebrook* and *Witte* formula is recommended

$$\frac{1}{\sqrt{\lambda_R}} = 1.74 - 2 \log \left[ \frac{1}{\sqrt{\lambda_R}} \frac{18.7}{Re} + 2 (k / D_h) \right]. \quad (3.18)$$

One can avoid the solution of the above equation with respect to  $\lambda_R$  by using the following approximation

$$\lambda_R = \lambda_{R2} (Re / Re_2)^n, \quad (3.19)$$

where

$$n = \left[ \log (\lambda_{R3} / \lambda_{R2}) \right] / \left[ \log (Re_3 / Re_2) \right], \quad (3.20)$$

and

$$\lambda_{R2} = 7.244 / Re_2^{0.643} \quad \text{for } k / D_h < 0.007, \quad (3.21)$$

$$\lambda_{R2} = 0.145 (k / D_h)^{0.244}. \quad (3.22)$$

*Haland* (1983) proposed a very accurate explicit replacement of the *Colebrook* and *Witte* formula

$$\frac{1}{\sqrt{\lambda_R}} = -1.8 \log \left[ \frac{6.9}{Re} + \left( \frac{k}{3.7 D_h} \right)^{1.11} \right]. \quad (3.18b)$$

which agrees with it to within  $\pm 1.5\%$  for  $4000 \leq Re \leq 10^8$  and  $k / D_h \leq 0.05$ .

(e) For  $Re > Re_3$  the *Prandtl - Nikuradze* formula is recommended,

$$\lambda_R = 1 / \left[ 1.74 + 2 \log(0.5 D_k / k) \right]^2. \quad (3.23)$$

Note that turbulent pipe flows with strong density variation across the boundary layer may change the pressure drop due to friction. For *supercritical fluids* in heated channels the density in the boundary layer is smaller than the density in the bulk resulting in reduction of the pressure drop,

$$\lambda_R = \lambda_{R, isotherm} \left[ \rho_{wall}(T_{wall}) / \rho_{bulk}(T_{bulk}) \right]^{-0.4},$$

*Kirilov et al.* (1990). This correlation is valid for  $p / p_{cr} = 1.016 \div 1.22$ ,  $Re = 8 \times 10^4 \div 1.5 \times 10^6$ .

### 3.2.2 Annular channels

For turbulent single phase flow in annular channels the information for circular pipes can be used by modifying the effective velocity as proposed by *Hartnett et al.* in 1962,

$$w_{eff} = \bar{w} \frac{1}{(1-r)^2} \left( 1 + r^2 + \frac{1-r^2}{\ln r} \right). \quad (3.24)$$

Here  $r = D_{in} / D_{out}$  is the ration of the inner and outer diameters.

### 3.2.3 Arbitrary channel form

*Rehme's equivalent annular zone*: If a rod is in a bundle of infinite number of parallel equidistant rods, a factious zone can be extracted building a channel at which outer boundary the share stress is zero. In this case again the ration of the inner and outer diameters  $r = D_{in} / D_{out}$  gives information about the non-homogeneity

velocity profile. For laminar flow *Rehme* found analytical solution of the *Poison* equation in 1971

$$\lambda_{fr} \text{Re} = Rm, \quad (3.25)$$

where the *Rehme*'s number is

$$Rm = \frac{64(r^2 - 1)^3}{3r^4 - 4r^2 - 4r^2 \ln r + 1}, \quad (3.26)$$

Eq. (26) in 1973. For the same case and turbulent flow *Rehme* obtained

$$\sqrt{\frac{8}{\lambda_{fr}}} = 2.5 \ln \left( \text{Re} \sqrt{\frac{\lambda_{fr}}{8}} \right) + 5.5 - G^*, \quad (3.27)$$

where

$$G^* = \frac{3.966 + 1.25r}{1 + r} + 2.5 \ln [2(1 + r)], \quad (3.28)$$

Eq. (31) in 1973. For infinite number of rods with diameter  $D_{rod}$  with axis to axis distance (pitch)  $p_{triang}$  in a bundle the ratio  $r$  for triangular arrangement is

$$r = \frac{p_{triang}}{D_{rod}} \sqrt{\frac{2\sqrt{3}}{\pi}}, \quad (3.29)$$

and for square arrangement

$$r = \frac{p_{trans}}{D_{rod}} \frac{2}{\sqrt{\pi}}. \quad (3.30)$$

The dependence on  $P/D$  can be farther simplified for specific cases, e.g. for triangular rod bundles of infinite extension

$$\lambda_{fr} / \lambda_{fr, pipe} = 1.045 + 0.071(p_{triang} / D_{rod} - 1) \quad \text{for} \quad \text{Re} = 10^4, \quad (3.31)$$

$$\lambda_{fr} / \lambda_{fr, pipe} = 1.036 + 0.054(p_{triang} / D_{rod} - 1) \quad \text{for} \quad \text{Re} = 10^5. \quad (3.32)$$

### 3.2.4 Axial flow in rod bundles

#### 3.2.4.1 Integral approach

Rod bundles are used as design geometry for generating heat in nuclear reactors. *Voj* and *Scholven* (1974) demonstrated that the hydraulic diameter is not the only geometry parameter influencing the pressure drop. The particular arrangement is of great importance.

*Square* and *triangle* arrangements are most popular. An example how the pressure drop for triangular bundles deviates from the *Hagen* and *Poiseuille* and *Blasius* laws is given below *triangle* rod arrangement in a bundle with the following characteristics: rod diameter 6mm, distance between the rod axes 7.9mm, distance between the rod axes and the wall 7.6mm, distance between the internal parallel walls of the shroud 105mm, flow cross section 4745mm<sup>2</sup>, wetted perimeter 3547mm and hydraulic diameter 5.351mm.

$$\lambda_{fr} = 140/\text{Re} \quad (\lambda_{fr} = 64/\text{Re}, \text{Hagen and Poiseuille}) \text{ for } \text{Re} \leq 2300, \quad (3.33)$$

$$\lambda_{fr} = 0.590/\text{Re}^{0.303} \quad (\lambda_{fr} = 0.316/\text{Re}^{0.25}, \text{Blasius}) \text{ for } \text{Re} > 2300. \quad (3.34)$$

This represents the cross section averaged pressure drop. The particular axial pressure drop in subchannels is different depending on their lateral position even at the same hydraulic diameters of the subchannels. This is an indication for the limitation of any subchannel analyses. *Rehme* (1968) found for the same bundle but with a distance between the rod axes and the wall 7.71mm that in the turbulent region the data are close to the *Blasius* correlation.

Laser Doppler anemometer measurements in triangle rod arrangement in a bundle with the following characteristics: 127-rods with diameter 9.1mm and length 2.44m, distance between the rod axes 12.2mm, distance between the rod axes and the wall 6.65mm, distance between the internal parallel walls of the shroud 140mm, flow cross section 8714mm<sup>2</sup>, wetted perimeter 4116mm, hydraulic diameter 8.469mm and 11 honeycomb spacers with 10mm high are reported by *Lestinen* and *Gang* in (33). The overall pressure loss friction coefficient in the turbulent region was between 21 and 16.

*Cheng* and *Todreas* (1986) reported subchannel friction factors for hexagonal rod bundles given in the following table.

$\lambda_{fr} = c_1 + c_2 (p_{triang} / D_{rod} - 1) + c_3 (p_{triang} / D_{rod} - 1)^2$					
Pitsch/ Diameter	Flow regime	Subchan- nel type	$c_1$	$c_2$	$c_3$
$1 \leq p_{triang} / D_{rod} \leq 1.1$	laminar	interior	26	888.2	-3334
		edge	26.18	554.5	-1480
	turbulent	interior	0.09378	1.398	-8.664
		edge	0.09377	0.8732	-3.341
$1.1 \leq p_{triang} / D_{rod} \leq 1.5$	laminar	interior	62.97	216.9	190.2
		edge	44.4	256.7	-267.6
	turbulent	interior	0.1458	0.03632	-0.03333
		edge	0.1413	0.04199	-0.04428

The boundary between laminar and transition flow and between transition and turbulent are given by the authors

$$\log_{10} (\text{Re}_{lam}/300) = 1.7 (p_{triang} / D_{rod} - 1), \quad (3.35)$$

$$\log_{10} (\text{Re}_{turb}/10000) = 0.7 (p_{triang} / D_{rod} - 1). \quad (3.36)$$

Inside the transition region the friction coefficient is

$$\lambda_{fr} = \lambda_{fr,lam} (1 - \Psi)^{1/3} + \lambda_{fr,turb} \Psi^{1/3}, \quad (3.37)$$

where

$$\Psi = \frac{\log_{10} \text{Re} - \log_{10} \text{Re}_{lam}}{\log_{10} \text{Re}_{turb} - \log_{10} \text{Re}_{lam}}. \quad (3.38)$$

### 3.2.4.2 Subchannel approach by Klaus Rehme

Since 1960 flows in bundles are analyzed as consisting of several parallel flows in the so called parallel subchannels which if collected together represent the flow space inside the bundle. An approximation for computing a single phase pressure drop in a bundle for flow with constant density can be derived by recognizing that the pressure drop over length  $\Delta z$  is common for all parallel channels

$$\Delta p = \lambda_{fr} \frac{1}{2\rho} \left( \frac{\dot{m}}{F} \right)^2 \frac{\Delta z}{D_h} = \lambda_{fr,i} \frac{1}{2\rho} \left( \frac{\dot{m}_i}{F_i} \right)^2 \frac{\Delta z}{D_{h,i}}. \quad (3.39)$$

Here the mass flow trough a single channel

$$\frac{\dot{m}_i}{F_i} = \frac{\dot{m}}{F} \sqrt{\frac{\lambda_{fr}}{\lambda_{fr,i}} \frac{D_{h,i}}{D_h}}, \quad (3.40)$$

is a function of the cross sections  $F_i$ , hydraulic diameter  $D_{h,i}$  and friction factor  $\lambda_{fr,i}$  of the channel. Recognizing that the total mass flow is the sum of the sub-channel mass flows

$$\dot{m} = \sum_{i=1}^{i_{\max}} \dot{m}_i, \quad (3.41)$$

the relation for the effective friction coefficient

$$\frac{1}{\sqrt{\lambda_{fr}}} = \sum_{i=1}^{i_{\max}} \frac{1}{\sqrt{\lambda_{fr,i}}} \frac{F_i}{F} \sqrt{\frac{D_{h,i}}{D_h}}, \quad (3.42)$$

is easily obtained by *Rehme* (1973) and used by many authors later (see for instance *Wilkie* (1980)). For laminar flow using the *Stokes* relation

$$\lambda_{fr,i} = \frac{64}{\frac{\dot{m}_i}{F_i} \frac{D_{h,i}}{\eta}}, \quad (3.43)$$

and after some rearrangement *Rehme* obtained

$$\lambda_{fr} \text{Re} = Rm, \quad (3.44)$$

where the *Rehme's* factor

$$Rm = \frac{64}{\sum_{i=1}^{i_{\max}} \left( \frac{D_{h,i}}{D_h} \right)^2 \frac{F_i}{F}}, \quad (3.45)$$

Eq. (25) in 1973, is only dependent on the geometry. For turbulent flow *Rehme* uses the *Maubach's* correlation for friction coefficient (1970) in the form

$$\sqrt{\frac{8}{\lambda_i}} = 2.5 \ln \left( \frac{D_{h,i}}{2} \frac{w_i}{\nu} \sqrt{\frac{\lambda_i}{8}} \right) + 5.5 - G_i, \quad (3.46)$$

which is based on the validity of the *Nikuradse's* velocity profile at the wall [44].

Here  $G_i = \frac{w_{i,\max} - w_i}{\sqrt{\tau_{w,i}/\rho}}$  characterizes the heterogeneity of the velocity profile depending on the channel geometry ( $G_i = 3.966$  for  $\text{Re} < 10^6$ ). In terms of the bundle Reynolds number the equation reads

$$\sqrt{\frac{8}{\lambda_{fr,i}}} = 2.5 \ln \left[ \text{Re} \sqrt{\frac{\lambda_{fr}}{8}} \frac{1}{2} \left( \frac{D_{h,i}}{D_h} \right)^{3/2} \right] + 5.5 - G_i. \quad (3.47)$$

After replacing in the definition equation for the effective friction factor *Rehme* obtained the very interesting expression

$$\sqrt{\frac{8}{\lambda_{fr}}} = A \left[ 2.5 \ln \left( \text{Re} \sqrt{\frac{\lambda_{fr}}{8}} \right) + 5.5 \right] + G^*, \quad (3.48)$$

in which

$$A = \left( \sum_{i=1}^{i_{\max}} \frac{F_i}{F} \sqrt{\frac{D_{h,i}}{D_h}} \right), \quad (3.49)$$



$$G^* = \sum_{i=1}^{i_{\max}} \frac{F_i}{F} \sqrt{\frac{D_{h,i}}{D_h}} \left\{ 2.5 \ln \left[ \frac{1}{2} \left( \frac{D_{h,i}}{D_h} \right)^{3/2} \right] - G_i \right\}, \quad (3.50)$$

are geometric factors only. *Rehme* demonstrated then that  $A = f(Rm)$  and  $G^*(Rm)$  only. This approach is verified by comparison with very large data base for variety of channel forms.

### 3.2.5 Cross flow in rod bundles

Two types of arrangement are usually considered in the technology (a) in-line arrangement and staggered arrangement with the narrowest cross section perpendicular to the flow direction and (b) staggered arrangement with the narrowest cross section along the diagonal, defined by the following geometrical scales:

$a = p_{trans} / D_{rod}$ , relative transverse (lateral) spacing (square arrangement),

$b = p_{long} / D_{rod}$ , relative longitudinal spacing (square arrangement) and

$c = p_{triang} / D_{rod} = \sqrt{(a/2)^2 + b^2}$ , relative diagonal spacing (triangle arrangement).

The velocity varies across the bundle. Therefore two characteristic velocities are usually selected for description of the pressure drop: the undisturbed velocity  $w_{undisturbed}$  (as flow occupies the channel without rods) and the maximum velocity is the velocity at the minimum cross section

$$w_{\max} = \frac{a}{2(c-1)} w_{undisturbed}. \quad (3.51)$$

The hydraulic diameter is

$$D_h = \frac{4Vol}{wetted\ surface} = \left( \frac{4ab}{\pi} - 1 \right) D_{rod}, \quad (3.52)$$

For equidistant triangular arrangements  $p_{long} = p_{trans} \sqrt{3}/2$  and

$$D_h = \frac{2\sqrt{3}p_{triang}^2 - \pi D_{rod}^2}{\pi D_{rod}}. \quad (3.53)$$

Over the distance  $\Delta x$ ,

$$N = \Delta x / p_{long} \quad (3.54)$$

rods are placed. *Gunter* and *Shaw* proposed in 1945 to use a correlation for computation of the pressure drop per single row and then to multiply the result by the number of transversal rows

$$\Delta p = \zeta \frac{1}{2} \rho w_{\max}^2 N. \quad (3.55)$$

The single row pressure drop coefficient is found to be

$$\zeta = \frac{b}{\text{Re}_x^m} \left( \frac{D_{h,w}}{D_{rod}} \right)^{0.4}, \quad (3.56)$$

where

$$\text{Re}_x = D_h \rho |w_{\max}| / \eta, \quad (3.57)$$

$b = 180$ ,  $m = 1$  for laminar flow,  $b = 2.26$ ,  $m = 0.145$  for turbulent flow.

Dwyer et al. (1956) p. 1845 performed measurements for single phase flow in triangular array up to  $\text{Re} = \rho w_{\max} D_{rod} / \eta < 10^6$  and found

$$\zeta = \left[ 1.23 + 0.11 / (p_{triang} / D_{rod} - 1)^{1.08} \right] / \text{Re}^{0.15}. \quad (3.58)$$

Bötenbach (1975) p. 233 modified the Dwyer's friction coefficient by using data of several authors to

$$\zeta = \left[ 1.35156 + 0.49244 / (p_{triang} / D_{rod} - 1)^{1.0788} \right] / \text{Re}^{0.17838}. \quad (3.59)$$

The correlation is reported to reproduce the available data for staggered arrangement with maximum deviation of  $\pm 29\%$ . Subbotin et al. (1975) reported data for cross flows over triangular rod arrangement. They correlated their data with

$$\zeta = 50 / \left[ \text{Re} (p_{triang} / D_{rod} - 1) \right] \quad \text{for laminar flow, } \text{Re} (p_{triang} / D_{rod} - 1) \leq 40, \quad (3.60)$$

$$\zeta = 3 / \left[ \text{Re} (p_{triang} / D_{rod} - 1) \right]^{0.25} \quad \text{for turbulent flow, } \text{Re} (p_{triang} / D_{rod} - 1) > 40. \quad (3.61)$$

Gaddis and Gnielinski (1985) reproduced a data base consisting of about 2500 points for  $N \geq 5$  within an error band of 35% with the correlations set given below. For laminar flow,  $\text{Re} \leq 10$ , the pressure loss coefficient is

$$\zeta_{lam} = \frac{c_{lam} c_{w,lam}}{\text{Re}} \pm 25\%, \quad (3.62)$$

where for type a) arrangement

$$c_{lam} = \frac{280\pi \left[ (b^{0.5} - 0.6)^2 + 0.75 \right]}{(4ab - \pi) a^{1.6}}, \quad (3.63)$$

and for type b) arrangement

$$c_{lam} = \frac{280\pi \left[ (b^{0.5} - 0.6)^2 + 0.75 \right]}{(4ab - \pi)c^{1.6}}. \quad (3.64)$$

For turbulent flow,  $Re > 10000$ , the authors obtained for type a)

$$\zeta_{turb} = \frac{c_{w,turb}}{Re^{0.1b/a}} \left\{ \left[ 0.22 + 1.2 \frac{(1 - 0.94/b)^{0.6}}{(a - 0.85)^{1.3}} \right] 10^{0.47(b/a - 1.5)} + 0.03(a - 1)(b - 1) \right\}, \quad (3.65)$$

and for type b)

$$\zeta_{turb} = \frac{c_{w,turb}}{Re^{0.25}} \left[ 2.5 + 1.2/(a - 0.85)^{1.06} + 0.4(b/a - 1)^3 - 0.01(a/b - 1)^3 \right]. \quad (3.66)$$

A general form of the final correlation is then proposed within  $1 < Re < 3 \times 10^5$  for type a)

$$\zeta = \zeta_{lam} + \zeta_{turb} \left[ 1 - \exp\left(-\frac{Re + 1000}{2000}\right) \right], \quad (3.67)$$

and for type b)

$$\zeta = \zeta_{lam} + \zeta_{turb} \left[ 1 - \exp\left(-\frac{Re + 200}{1000}\right) \right]. \quad (3.68)$$

The corrector for the change of the viscosity at the wall for the laminar and turbulent flow is

$$c_{w,lam} = \left( \frac{\eta_w}{\eta} \right)^{\frac{0.57}{[(4ab/\pi - 1)Re]^{0.25}}} \quad \text{for more the 10 rows}, \quad (3.69)$$

$$c_{w,turb} = \left( \frac{\eta_w}{\eta} \right)^{0.14}, \quad (3.70)$$

respectively. Here  $Re_x = D_{rod} \rho |w_{max}| / \eta$ .

### 3.2.6 Pressure drop at spacer for bundles of nuclear reactors

Spacers for rod bundles in nuclear reactors are intended to keep the rods on their specified positions. They are very specific in their geometry reflecting the contradictory requirement (a) to reduce the pressure drop and (b) to increase the margin

to dry out or to departure from nucleate boiling regime by increasing the tubulization. In general each spacer blocks part of the cross section the reason why as a first approximation the pressure loss coefficient in  $\Delta p \approx \zeta_{spacer} \rho w_0^2 / 2$  can be computed as

$$\zeta_{spacer} = 0.5 \left(1 - \frac{F_0}{F_1}\right)^{0.75} + \left(1 - \frac{F_0}{F_2}\right)^2 + \tau \left(1 - \frac{F_0}{F_1}\right)^{0.375} \left(1 - \frac{F_0}{F_2}\right) + \lambda_{fr,sp} \frac{L_{sp}}{D_{h,sp}}, \quad (3.71)$$

where  $\tau = (2.4 - \bar{l}) \times 10^{-\phi(\bar{l})}$ ,  $\bar{l} \approx \frac{L_{sp}}{D_{h,sp}}$ ,  $\phi(\bar{l}) = 0.25 + 0.535 \frac{\bar{l}^8}{0.5 + \bar{l}^8}$  (Idelchik 1996).

The indices indicate: 1 before the spacer, 2 after the spacer and 0 spacer.  $L$  and  $D$  are the length and the hydraulic diameter of the spacer, respectively. The  $F$ 's are the flow cross sections. The above equation demonstrates that the pressure loss coefficient is depending on flow plugging due to the spacer,  $\zeta_{spacer} = f(1 - \gamma_{z,spacer})^n$ . *Rehme* (1972a, 1977) found in 1973–1977, that

$$\zeta_{spacer} = (6 \div 7) (1 - \gamma_{z,spacer})^2 \text{ for } Re > 5 \times 10^4, \quad (3.72)$$

where  $\gamma_{z,spacer} = F_0/F_1 = F_0/F_2$ . For smaller Reynolds number there is a dependence on the Reynolds number computed using the hydraulic diameter of the spacer region,  $\zeta_{spacer} / (1 - \gamma_{z,spacer})^2 = f(Re)$  given graphically for variety of spacer grid types in *Rehme* (1972a). The function takes values between 7 and 15.

Note that each producer is measuring the hydraulic characteristic of his own spacer. Some examples are given below.

*Voj and Scholven* (1974) measured pressure drop on spacers for triangle rod arrangement in a bundle with the characteristics: rod diameter 6mm, distance between the rod axes 7.9mm, distance between the rod axes and the wall 7.6mm, distance between the internal parallel walls of the shroud 105mm, flow cross section 4745mm<sup>2</sup>, wetted perimeter 3547mm and hydraulic diameter 5.351mm. With a spacer made by connected 10mm short pipes to each other the authors found that the blockage ratio influences the pressure drop

$$\Delta p = \zeta_{spacer} \frac{1}{2} \frac{G^2}{\rho_2}, \text{ where } \zeta_{spacer} = f(Re, \gamma_{blockage}). \quad (3.73)$$

Here the liquid Reynolds number is  $Re = G D_h / \eta_2$ . The blockage ratio  $\gamma_{blockage} = 1 - \gamma_{z,spacer}$  is defined as the flow cross section of the spacer divided by the flow cross section of the undisturbed flow.

The authors found that in the turbulent region the dependence on the blockage rate is like

$$\zeta_{spacer} \approx (C + B/\text{Re}^m) \gamma_{blockage}^{3.5} \quad (3.74)$$

	$\zeta_{spacer}$	
$\gamma_{lockage}$	$\text{Re} \leq 6000$	$\text{Re} > 6000$
0.737	$273.6/\text{Re}^{0.45}$	$3.3 + 0.2 \times 10^5/\text{Re}^{1.05}$
0.640	$73.9/\text{Re}^{0.4}$	$1.4 + 0.3 \times 10^5/\text{Re}^{1.2}$
0.500	$14.8/\text{Re}^{0.3}$	$0.85 + 1.1 \times 10^5/\text{Re}^{1.5}$

For  $\text{Re} \geq 5 \times 10^4$   $\zeta_{spacer} \approx (0.291 \div 0.293) \gamma_{blockage}^{3.5}$ . The increase of the vertical size of the spacer from 10mm to 15mm resulted in increased pressure drop  $\zeta_{spacer} \approx 0.337 \gamma_{blockage}^{3.5}$ . Honeycomb spacers cause smaller resistance retaining this dependence. Changing vertical size of the spacer from 8mm to 15mm resulted in increased pressure drop  $\zeta_{spacer} \approx 0.236 \gamma_{blockage}^{3.5}$  to  $\zeta_{spacer} \approx 0.322 \gamma_{blockage}^{3.5}$ .

*Leung and Hotte* (1997) proposed

$$\zeta_{spacer} = a \left[ \tan \left( \frac{\pi}{2} \gamma_{blockage}^2 \right) \right]^b, \quad (3.75)$$

where  $a$  varies between 7.59 and 11.86, and  $b$  between 0.92 and 1.47. Obviously the *Hotte* proposal does not take into account the Reynolds number dependence.

*Caraghiaur et al.* (2004) analyzed experimentally the single phase pressure loss of the SVEA-64 spacer on bundle with 88 rods (9.62mm rod diameter, 1.32 pitch to diameter ratio, 1.305 and 1.264 wall to diameter ratio, 9mm corner radius, 1.894m rod length, 2400mm<sup>2</sup> flow cross section and 9.96mm hydraulic diameter). The liquid Reynolds number was varied from  $9.6 \times 10^3$  to  $48.8 \times 10^3$ . The result is

$$\zeta_{spacer} = 3.6/\text{Re}^{0.14}. \quad (3.76)$$

*Unal et al.* (1994) reported data for a spacer for 3x3 bundle in *two phase* dispersed droplet flow being between 2 and 1.5 for Reynolds numbers varying between 2000 and 10000. He used

$$\zeta_{spacer} = 0.1/\text{Re}^{0.3}. \quad (3.77)$$

### 3.3 Two-phase flow

**Circular pipes:** The modeling of the two-phase friction pressure drop in a pipe started with the work by *Lockhart and Martinelli* (1949). The authors defined the following auxiliary variables: The pressure gradient of the liquid flowing alone in the same tube

$$\left( \frac{dp}{dz} \right)_{R2} = \frac{1}{2} \frac{(\alpha_2 \rho_2 V_2)^2}{\rho_2} \frac{\lambda_{R2}}{D_h}, \quad (3.78)$$

where

$$\lambda_{R2} = \lambda_{R2}(\text{Re}_2 = \alpha_2 \rho_2 V_2 D_h / \eta_2, k / D_h); \quad (3.79)$$

The pressure gradient of the gas flowing alone in the same tube

$$\left( \frac{dp}{dz} \right)_{R1} = \frac{1}{2} \frac{(\alpha_1 \rho_1 V_1)^2}{\rho_1} \frac{\lambda_{R1}}{D_h} \quad (3.80)$$

where

$$\lambda_{R1} = \lambda_{R1}(\text{Re}_1 = \alpha_1 \rho_1 V_1 D_h / \eta_1, k / D_h); \quad (3.81)$$

The pressure drop for two phase flow is related either to

$$\left( \frac{dp}{dz} \right)_R = \Phi_1^2 \left( \frac{dp}{dz} \right)_{R1} \quad (3.82)$$

or to

$$\left( \frac{dp}{dz} \right)_R = \Phi_2^2 \left( \frac{dp}{dz} \right)_{R2}. \quad (3.83)$$

The ratio

$$X_{LM} = \Phi_1^2 / \Phi_2^2 = \left( \frac{dp}{dz} \right)_{R2} / \left( \frac{dp}{dz} \right)_{R1} \quad (3.84)$$

is called the *Lockhardt and Martinelli* factor in honor of the authors. In case of the validity of the *Blasius* formula  $X_{LM}$  reduces to

$$X_{LM} = X_u = \left( \frac{\rho_1}{\rho_2} \right)^{1/2} \left( \frac{\eta_2}{\eta_1} \right)^{0.1} \left( \frac{1 - X_1}{X_1} \right)^{0.9}, \quad (3.85)$$

see Hetstroni (1982). Comparing with experimental data for air-water horizontal flow near to atmospheric pressure the authors found

$$\Phi_1^2 = 1 + CX_{LM} + X_{LM}^2, \quad (3.86)$$

$$\Phi_2^2 = 1 + \frac{C}{X_{LM}} + \frac{1}{X_{LM}^2}, \quad (3.87)$$

where  $C$  has the following values

- $C = 20$  for turbulent liquid and turbulent gas,
- $C = 12$  for laminar liquid and turbulent gas,
- $C = 10$  for turbulent liquid and laminar gas, and
- $C = 5$  for laminar liquid and laminar gas.

Other simple approximations can be found in the literature in the form

$$\Phi_2^2 = 1/(1 - \alpha_1)^m, \quad m = 1.75 \text{ to } 2. \quad (3.88)$$

*Ransom et al.* (1988) recommended for  $C$  the following continuous approximation

$$C = \max \left\{ 2, \left( 28 - 0.3\sqrt{G} \right) / \exp \left[ \frac{(\log Y^* + 2.5)^2}{2.4 - 10^{-4}G} \right] - 2 \right\}, \quad (3.89)$$

$$Y^* = \frac{\rho_1}{\rho_2} \left( \frac{\eta_2}{\eta_1} \right)^{0.2}. \quad (3.90)$$

Thus if the gas is the continuous phase

$$\left( \frac{dp}{dz} \right)_R = c_{1w} |V_1| V_1, \quad (3.91)$$

where

$$c_{1w} = c_{1w}^* \Phi_1^2, \quad (3.92)$$

$$c_{2w} = 0, \quad (3.93)$$

$$c_{1w}^* = \frac{1}{2} \frac{(\alpha_1 \rho_1)^2}{\rho_1} \left( \frac{\lambda_{R1}}{D_h} + \frac{\xi}{\Delta z} \right) \quad (3.94)$$

and if the liquid is the continuous phase we have

$$\left( \frac{dp}{dz} \right)_R = c_{2w} |V_2| V_2, \quad (3.95)$$

where

$$c_{2w} = c_{2w}^* \Phi_2^2, \quad (3.96)$$

$$c_{1w} = 0, \quad (3.97)$$

$$c_{2w}^* = \frac{1}{2} \frac{(\alpha_2 \rho_2)^2}{\rho_2} \left( \frac{\lambda_{R2}}{D_h} + \frac{\xi}{\Delta z} \right). \quad (3.98)$$

Later *Martinelli* and *Nelson* (1948) introduced the following additional variables used successfully for description of friction pressure loss in two-phase steam-water flows at arbitrary parameter: The frictional pressure drop of the liquid following alone in the tube with flow rate equal to the total flow rate of the two phase flow

$$\left( \frac{dp}{dz} \right)_{R20} = \frac{1}{2} \frac{G^2}{\rho_2} \left( \frac{\lambda_{R20}}{D_h} + \frac{\xi}{\Delta z} \right), \quad (3.99)$$

where

$$\lambda_{R20} = \lambda_{R20} \left( Re_{20} = D_h |G| / \eta_2, k / D_h \right), \quad (3.100)$$

and the ratio

$$\Phi_{20}^2 = \left( \frac{dp}{dz} \right)_R / \left( \frac{dp}{dz} \right)_{R20}, \quad (3.101)$$

called later the *Martinelli-Nelson* multiplier. The relationship between  $\Phi_{20}^2$  and  $\Phi_2^2$  for the *Blasius* regime was analytically found

$$\Phi_{20}^2 = (1 - X_1)^{1.75} \Phi_2^2. \quad (3.102)$$

Later the *Martinelli-Nelson* method was provided with a more accurate database and approximation of  $\Phi_{20}^2$  as a function of the local flow parameter. *Hewitt* makes the following proposal for the most accurate approximation of the available experimental data - see *Hetstroni* (1982):

(a) In case of  $\eta_2 / \eta_1 < 1000$ , the *Friedel* (1979b) correlation should be used:

$$\Phi_{20}^2 = E + 3.21FH / \left( Fr^{0.0454} We^{0.035} \right), \quad (3.103a)$$

where

$$E = (1 - X_1)^2 + X_1^2 \frac{\rho_2}{\rho_1} \frac{\lambda_{10}}{\lambda_{20}}, \quad (3.104)$$

$$\lambda_{10} = \lambda_{10} \left( \frac{\rho w D_h}{\eta_1}, \frac{k}{D_h} \right), \quad (3.105)$$

$$\lambda_{20} = \lambda_{20} \left( \frac{\rho w D_h}{\eta_2}, \frac{k}{D_h} \right), \quad (3.106)$$

[in case of validity of the *Blasius* relation  $\lambda_{10} / \lambda_{20} \approx (\eta_1 / \eta_2)^{1/4}$ ],



$$F = X_1^{0.78} (1 - X_1)^{0.224}, \quad (3.107a)$$

$$H = \left( \frac{\rho_2}{\rho_1} \right)^{0.91} \left( \frac{\eta_1}{\eta_2} \right)^{0.19} \left( 1 - \frac{\eta_1}{\eta_2} \right)^{0.7}, \quad (3.108a)$$

$$Fr = \frac{(G / \rho)^2}{g D_h}, \quad (3.109)$$

$$We = G^2 D_h / (\rho \sigma). \quad (3.110)$$

This correlation approximates 25 000 experimental points for vertical upwards co-current flow and for horizontal flow with 30 to 40% standard deviation for one- and two-component flow. For vertical downwards flow the correlation obtain the following modifications

$$\Phi_{20}^2 = E + 48.6 F H \quad Fr^{0.03} / We^{0.12}, \quad (3.103b)$$

$$F = X_1^{0.8} (1 - X_1)^{0.29}, \quad (3.107b)$$

$$H = \left( \frac{\rho_2}{\rho_1} \right)^{0.9} \left( \frac{\eta_1}{\eta_2} \right)^{0.73} \left( 1 - \frac{\eta_1}{\eta_2} \right)^{7.4}. \quad (3.108b)$$

Details regarding this work can be found in *Friedel* (1979a, 1980).

(b) In case of  $\eta_2 / \eta_1 \geq 1000$  and  $G > 100$ , the *Baroczy* correlation from 1965 modified by *Chisholm* (1983) should be used

$$\Phi_{20}^2 = 1 + (Y^2 - 1) \left\{ B [X_1 (1 - X_1)]^{0.875} + X_1^{1.75} \right\}. \quad (3.111)$$

Here  $B$  is computed as function of the dimensionless number

$$Y = \sqrt{\frac{\rho_2}{\rho_1} \left( \frac{\eta_1}{\eta_2} \right)^{0.25}} \quad (3.112)$$

as follows

$9.5 \geq Y$		$9.5 < Y < 28$		$Y \geq 28$
$G \leq 500$	$B = 4.8$	$G \leq 600$	$B = \frac{520}{Y \sqrt{G}}$	$B = \frac{15000}{Y^2 \sqrt{G}}$
$500 < G < 1900$	$B = 2400/G$	$G > 600$	$B = 21/Y$	
$1900 \leq G$	$B = 55/\sqrt{G}$			

(c) In the case of  $\eta_2/\eta_1 \geq 1000$  and  $G \leq 100$ , the *Martinelli* correlation is recommended.

**Annular channels:** *Yano and Aritomi* (2004) found for air-water flow in annular channels that the constant  $C$  in Eq. (3.32) should be 22.5. Their experiments are in the region of  $j_2 = 0.08$  to  $0.12$  m/s,  $j_1 = 30$  to  $50$  m/s, in a annular channel with  $12.1$  mm inner diameter and  $19.8$  mm, outer diameter, and  $2.7$  m length. The inlet pressure was  $0.27$  MPa and the outlet pressure  $0.1013$  MPa.

**Bubbly flow:** *Avdeev* (1982, 1983a) proposed to consider bubbly boundary layer as a surface with equivalent roughness being part of the local bubble size  $k = 0.257 D_b$  for use in the modified *Colebrook* (1939) relation

$$\frac{1}{\sqrt{\lambda_{fr}}} = 1.74 - 2 \log \left( \frac{k}{R_h} + \frac{49}{\text{Re}^{0.91}} \right) = 1.74 - 2 \log \left( 0.514 \frac{D_i}{D_h} + \frac{49}{\text{Re}^{0.91}} \right).$$

**Pressure drop at spacer for bundles of nuclear reactors:** *Yano and Aritomi* (2004) performed experiments in the region of  $j_2 = 0.08$  to  $0.12$  m/s,  $j_1 = 30$  to  $50$  m/s, in a annular channel with  $12.1$  mm inner diameter and  $19.8$  mm, outer diameter, and  $2.7$  m length resulting in pressure loss between  $1500$  and  $4500$  Pa. The inlet pressure was  $0.27$  MPa and the outlet pressure  $0.1013$  MPa. The blockage ratio of the spacer was varied between  $0.15$  and  $0.212$ . The empirical correlation representing their data within  $\pm 10\%$  error band is

$$\Delta p = 0.97 \left( 2\delta_{spacer}/D_h \right)^{-0.05} \exp \left( -0.8 \delta_{gap}/D_h \right) \frac{1}{2} \rho_1 w_1^2 \left( 4\delta_{gap}/D_h \right)^{2/7} \Phi_{1,tt}^2, \quad (3.113)$$

where

$$\Phi_{1,tt}^2 = 1 + 22.5 X_{LM} + X_{LM}^2, \quad (3.114)$$

$\delta_{spacer}$  is the thickness of the spacer and  $\delta_{gap}$  is the gap clearance between the spacer and the wall surface.

### 3.4 Heated channels

The above algorithm is valid strictly for an *adiabatic* flow. For a *boiling* flow in a heated channel, the application of the above correlations is justified, if there is no *sub cooled boiling* with a net steam volume fraction different from zero. In the last case the friction pressure drop *increases* several times compared to the adiabatic case with the same mass flow rate. This cannot be taken into account by the above mentioned methods. For the estimation of the pressure loss in case of sub cooled

boiling it is worth to paying attention to *Nigmatulin's* works (1982), relying on the several successful comparisons with experimental data. For the computation of the friction pressure gradient

$$\left(\frac{dp}{dz}\right)_R = \frac{4}{D_h} \tau \quad (3.115)$$

in the direction  $z$ , *Avdeev* proposes the method described in 1983b, 1986. *Staengl* and *Mayinger* [17] (1989) recommend for the sub cooled boiling the use of *Friedel's* correlation together with their correlation for prediction of the drift flux parameter given in Chapter 4. For the pressure loss they reported a standard deviation of  $\pm 25\%$ .

*Zheng* et al. (1991) proposed a new empirical correlation for prediction of the frictional pressure drop per unit length for heated channels in the form

$$\left(\frac{dp}{dz}\right)_R = \frac{\lambda_R}{D_h} \frac{1}{2} \rho |V| V, \quad (3.116)$$

where the friction coefficient is computed as follows

$$\lambda_R = \lambda_R(Re = D_h |G| / \eta_{eff}, k / D_h), \quad (3.117)$$

where the effective viscosity is

$$\begin{aligned} \eta_{eff} / \eta_2 = & (1 - X_1)^{3.67} + \frac{\eta_1}{\eta_2} X_1^{2.43} + 3.2727 \times 10^6 \left(\frac{p}{p_{cr}}\right)^{2.48} \\ & \times \left(1 - \frac{p}{p_{cr}}\right)^{9.07} We^{-0.97} X_1^{0.001} (1 - X_1)^{0.4} \end{aligned} \quad (3.118)$$

Here the *Weber* number

$$We = G^2 La / (\rho_1 \sigma) \quad (3.119)$$

is computed using the *Laplace* constant

$$La = \sqrt{2} \lambda_{RT}, \quad (3.120)$$

and modified in the case of rough pipes

$$We_{rough} = \frac{\lambda_{1,rough}}{\lambda_{2,smooth}} We. \quad (3.121)$$

This correlation was compared with 7172 data in the region  $D_h = 0.003$  to  $0.1\text{ m}$ ,  $p = 1$  to  $200\text{ bar}$ ,  $G = 290$  to  $10\,000\text{ kg/(m}^2\text{s)}$ . The comparison shows that 70 to 90 % of the data are within the  $\pm 30\%$  error band and presents some improvement of with respect to the *Friedel's* correlation for mass flow rates below  $4560\text{ kg/(m}^2\text{s)}$ .

This correlation is valid for heat transfer regimes without boiling crisis. In the case that the local heat transfer is associated with dry heated surface the authors recommend to use the following two-phase multiplier for Eq. (3.46)

$$\Phi_{20}^2 = \left( \frac{\eta_1}{\eta_2} \right)^{0.2} \left( \frac{\rho_1}{\rho_2} \right)^{0.8} \left[ 1 + X_1 \left( \frac{\rho_2}{\rho_1} - 1 \right) \right]^{1.8} \quad (3.122)$$

For heated pipes with internal structure promoting swirls and droplet deposition at the wall in all heat transfer regimes the authors proposed to use the *Martinelli - Nelson* method with the following two-phase friction multiplier

$$\Phi_{20}^2 = 1 + X_1 \left( \frac{\rho_2}{\rho_1} \frac{\lambda_1}{\lambda_2} - 1 \right) + 2.351 X_1^{2.637} (1 - X_1)^{0.565} \frac{\rho_2}{\rho_1}. \quad (3.123)$$

The correlation was compared with 1018 data for  $D_h = 0.01325$  and  $0.02181$  m, rib height of  $0.000775$  and  $0.0011$  m, incline  $56.9$  and  $48.7^\circ$ , vertical pipes,  $p = 20$  to  $210$  bar,  $G = 300$  to  $1500$  kg/(m<sup>2</sup>s). 85% of the data are in the 30% error band.

Knowing the frictional pressure loss we can compute the *dissipation rate of the kinetic energy of turbulence* the field  $l$  per unit volume of the mixture by multiplying the friction pressure gradients by the corresponding velocities in each direction, add the thus-obtained products, and obtain

$$\alpha_l \rho_l \varepsilon_l = \left[ u \left( \frac{dp}{dr} \right)_R + v \left( \frac{1}{r^\kappa} \frac{dp}{d\theta} \right)_R + w \left( \frac{dp}{dz} \right)_{R,l} \right] \quad (3.124)$$

This is an important characteristic for a flow in a confined geometry. It contains information about the *characteristic size and frequency of the turbulent eddies*, which are of interest for the flow structure identification as well as for the heat and mass transfer modeling.

### 3.5 Three-phase flow

There are only a few investigations on frictional pressure drop in the three-phase flows. For liquid - solid two phase pressure drop due to friction *Sakagushi et al.* (1989) correlated their own experimental data for vertical flow within an error band of  $\pm 2\%$  as follows

$$\left( \frac{dp}{dz} \right)_R = \frac{1}{2} \rho_2 w_2^2 \frac{\lambda_{R2}}{D_h} \Phi^2 \quad (3.125)$$

where

$$\lambda_{R2} = \lambda_{R2} \left( \frac{k}{D_h}, \frac{\rho_2 w_2 D_h}{\eta_2} \right), \quad (3.124)$$

$$\Phi^2 = 1 + \min \left[ 120, 5.28 \times 10^3 \left( 0.08 - \frac{D_3}{D_h} \right) \left( \frac{w_2}{\Delta w_{23\infty}} \right)^{-2.8} \right] \alpha_3, \quad (3.125)$$

for  $\frac{D_3}{D_h} \leq 0.08$  and

$$\Phi^2 = 1 \quad (3.126)$$

for  $\frac{D_3}{D_h} > 0.08$ .

For liquid - solid - gas flow *Tomyama* et al. (1990) approximate with the following correlation the experimental data obtained in the *Sakagushi's* laboratory for gas phase in a form of a bubbles  $\alpha_1 < 0.3$  with standard deviation of  $\pm 10\%$

$$\left( \frac{dp}{dz} \right)_R = \frac{1}{2} \rho_2 (\alpha_2 w_2)^2 \frac{\lambda_{R2}}{D_h} \left( 1 + 350 \sqrt{\frac{\alpha_1}{\text{Re}_2 Fr_2}} / [0.98(1 - \alpha_1)(1 - \alpha_3)^{3.8}] \right), \quad (3.127)$$

where the *Blasius* formula for computation of the liquid only friction coefficient

$$\lambda_{R2} = 0.3164 / \text{Re}_2^{1/4}, \quad (3.128)$$

with

$$\text{Re}_2 = \alpha_2 \rho_2 w_2 D_h / \eta_2, \quad (3.129)$$

was used and

$$Fr_2 = \frac{(\alpha_2 w_2)^2}{g D_h}. \quad (3.130)$$

The data belong to the following region  $0 \leq \alpha_1 w_1 \leq 0.121$ ,  $0.488 \leq \alpha_2 w_2 \leq 1.02$ ,  $0 \leq \alpha_3 w_3 \leq 0.0375$ ,  $p \approx 10^5$ ,  $\rho_3 = 2400 \div 2640$ ,  $0.0209 \leq D_h \leq 0.0504$ ,  $0.00115 \leq D_3 \leq 0.00416$ .

For higher void fraction  $\alpha_1 > 0.3$  *Minagawa* (1990) observed a flow pattern similar to the slug flow in the two-phase flow. It is remarkable that for both regimes, bubble and slug flow, the particles are completely surrounded by liquid. For the liquid - solid - gas slug flow *Minagawa* proposed the following correlation.

$$\left( \frac{dp}{dz} \right)_R = \Phi^2 \left( \frac{dp}{dz} \right)_{32} \quad (3.131)$$

where

$$\Phi^2 = 1 + \frac{\text{const}}{X} + \frac{1}{X^2}, \quad (3.131)$$

$$X^2 = \frac{(dp/dz)_{32}}{(dp/dz)_{10}}, \quad (3.132)$$

$$\left(\frac{dp}{dz}\right)_{32} = \Phi_{32}^2 \left(\frac{dp}{dz}\right)_2, \quad (3.133)$$

$$\Phi_{32}^2 = 1 + 400\alpha_3 / \left\{ \left[ \left( 1 + \frac{D_3}{D_h / 0.038} \right)^{3.62} \right] \left( \frac{w_2}{\Delta w_{32\infty}} \right)^{2.8} \right\}, \quad (3.134)$$

$$\left(\frac{dp}{dz}\right)_{10} = \frac{1}{2} \rho_1 (\alpha_1 w_1)^2 \frac{\lambda_{10}}{D_h}, \quad (3.135)$$

$$\lambda_{10} = \lambda_{10} \left( \frac{k}{D_h}, \frac{\alpha_1 \rho_1 w_1 D_h}{\eta_1} \right), \quad (3.136)$$

$$\left(\frac{dp}{dz}\right)_2 = \frac{1}{2} \rho_2 w_2^2 \frac{\lambda_0}{D_h}, \quad (3.137)$$

$$\lambda_2 = \lambda_2 \left( \frac{k}{D_h}, \frac{\rho_2 w_2 D_h}{\eta_2} \right) \quad (3.138)$$

$D_h$	$D_3$	const	$\bar{\Delta}\%$
0.0209	0.00114	57.7	18.3
	0.00257	40.1	18.1
	0.00417	49.8	20.1
	0.00296 (AL)	52.4	23.0
0.0307	0.00114	49.1	11.7
	0.00257	55.9	21.3
	0.00417	47.9	11.8
	0.00296 (AL)	50.9	28.8
0.0507	0.00114	113	20.5
	0.00257	105	30.0

## Nomenclature

### Latin

$C$	constant
$c_w$	modified friction coefficient, $kg/m^3$
$D_{BE}$	outer rod diameter, $m$
$D_h$	hydraulic diameter, $m$
$\left(\frac{dp}{dz}\right)_R$	pressure drop per unit length, $Pa/m$
$\left(\frac{dp}{dz}\right)_{R1}$	pressure gradient of the gas flowing alone in the same tube, $Pa/m$
$\left(\frac{dp}{dz}\right)_{R2}$	pressure gradient of the liquid flowing alone in the same tube, $Pa/m$
$Fr$	$= \frac{(G/\rho)^2}{gD_h}$ , total flow <i>Froude</i> number, <i>dimensionless</i>
$G$	mass flow rate, $kg/(m^2s)$
$k$	roughness, $m$
$La$	$= \sqrt{2}\lambda_{RT}$ , <i>Laplace</i> constant, $m$
$p$	pressure, $N/m^2$
$p_{cr}$	critical pressure, $N/m^2$
$Re$	<i>Reynolds</i> number, <i>dimensionless</i>
$S_{BE}$	averaged distance between the rods in triangular array arrangement, $m$
$V$	velocity, $m/s$
$We$	$= G^2 La / (\rho_l \sigma)$ , modified <i>Weber</i> number for smooth pipe, <i>dimensionless</i>
$We_{rough}$	$= \frac{\lambda_{1,rough}}{\lambda_{2,smooth}} We$ , modified <i>Weber</i> number for rough pipe, <i>dimensionless</i>
$We$	$= G^2 D_h / (\rho \sigma)$ , total flow <i>Weber</i> number, <i>dimensionless</i>
$X_{LM}$	<i>Lockhardt</i> and <i>Martinelli</i> factor, <i>dimensionless</i>
$X_l$	<i>l</i> field mass fraction, <i>dimensionless</i>
$z$	axial coordinate, $m$

### Greek

$\alpha_l$	<i>l</i> field volume fraction, <i>dimensionless</i>
$\Delta z$	pipe length, $m$
$\Delta r$	distance, $m$
$\delta_{spacer}$	thickness of a spacer for nuclear reactor rod bundle

---

$\delta_{gap}$	gap clearance between the spacer for nuclear reactor rod bundle and the wall surface
$\varepsilon_l$	dissipation rate of the kinetic energy of turbulence the field $l$ per unit volume of the mixture, $W/m^3$
$\phi_1^2$	gas only two phase friction multiplier, <i>dimensionless</i>
$\phi_2^2$	liquid only friction multiplier, <i>dimensionless</i>
$\eta_{eff}$	effective dynamic viscosity, $kg/(ms)$
$\lambda_{R10}$	friction coefficient for the total mass flow rate considered as gas, <i>dimensionless</i>
$\lambda_{R20}$	friction coefficient for the total mass flow rate considered as liquid, <i>dimensionless</i>
$\lambda_R$	friction pressure loss coefficient, <i>dimensionless</i>
$\xi$	local pressure loss coefficient, <i>dimensionless</i>
$\tau$	share stress, $N/m^2$
$\rho_l$	$l$ field density, $kg/m^3$
$\rho$	density, $kg/m^3$

### Subscripts

1	gas
2	liquid
3	field 3

### References

- Avdeev AA (1982) Teploenergetika vol 3 p 23
- Avdeev AA (1983a) Gidrodynamika turbulentnyih techeniy puzyrkovoj dwuchfasnoj smesi, Teplofizika visokih temperature, vol 21 no 4 pp 707-715
- Avdeev AA (1983b) Hydrodynamics of turbulent bubble two phase mixture, High Temperature Physic, vol 21 no 4 pp 707-715, in Russian
- Avdeev AA (1986) Application of the Reynolds analogy to the investigation of the surface boiling in forced convection, High Temperature Physics, vol 24 no 1 pp 111 - 119, in Russian.
- Böttenbach H (1975) Strömungswiderstand von quer- und längstangeströmten Stabbündeln, Atomkernenergie vol 26 no 4 pp 229-234
- Caraghiaur D, Frid W, Tillmark N (October 4-8, 2004) Detailed pressure drop measurements in single and two phase adiabatic air-water turbulent flows in realistic BWR fuel assembly geometry with spacer grids, The 6th International Conference on Nuclear Thermal Hydraulics, Operations and Safety (NUTHOS-6) Nara, Japan, Paper ID N6P207



- Cheng SK and Todreas NE (1986) Hydrodynamic models and correlations for bare and wire-wrapped hexagonal rod bundles – bundle friction factors, subchannel friction factors and mixing parameters, Nucl. Eng. Design vol 92 pp 227-251
- Chisholm D (1983) Two-phase flow in pipelines and heat exchanger, George Godwin, London and New York, p 110
- Colebrook CF (1939) Turbulent flow in pipes with particular reference to the transition region between the smooth and the rough pipe laws, J. Institution Civil Engineers
- Dwyer OE et al. (Oct. 1956) Cross flow of water trough a tube bank at Reynolds numbers up to a million, Industrial and Engineering Chemistry, vol 48 no 10 pp 1836-1846
- Friedel L (1979a) Improved friction pressure drop correlation for horizontal and vertical two-phase flow, 3R international, vol 18 no 7 pp 485-491 or in European two-phase flow meeting, Ispra
- Friedel L (1979b) New friction pressure drop correlations for upward, horizontal, and downward two - phase pipe flow. Presented at the HTFS Symposium, Oxford, September 1979 (Hoechst AG Reference No. 372217/24 698)
- Friedel L (1980) Pressure drop during gas/vapor-liquid flow in pipes, Int. Chemical Engineering, vol 20 pp 352-367
- Gaddis ES and Gnielinski V (Jan. 1985) Pressure drop in cross flow across tube bundles, International Chemical Engineering, vol 25 no 1 pp 115
- Gunter A Y, Shaw WA (1945) A general correlation of friction factors for various types of surfaces in cross flow, ASME Trans., vol 57 pp 643-660
- Haland SE (1983) Simple and explicit formulas for the friction factor in turbulent pipe flow, J. Fluids Eng., vol 98 pp 173-181
- Hartnett, JP et al. (1962) *Trans. ASME*, Ser. C, vol 84-1, pp 82
- Hetstroni G (1982) Handbook of multiphase systems. Hemishere Publ. Corp., Washington etc., McGraw-Hill Book Company, New York etc.
- Idelchik IE (1975) Handbook of hydraulic resistance, Second edition, Hemisphere, Washington, 1986, translation o a Russian edition
- Idelchik IE (1996) Handbook of hydraulic resistance, 3<sup>rd</sup> Edition, Begell House, Inc. p. 219
- Kirilov PL, Yur'ev YuS an Bobkov VP (1990) Handbook of thermal-hydraulic calculations, in Russian, Energoatomizdat, Moscow, Russia, pp 130-132
- Lestinen V and Gang P (Oct. 3-8, 1999) Experimental and numerical studies of the flow field characteristics of VVER-440 fuel assembly, Ninth Int. Top. Meeting on Nuclear Thermal Hydraulics, NURETH-9, San Francisco, California
- Leung LKH and Hotte G (September 7-9, 1997) A generalized prediction method for single-phase pressure drop in a string of aligned CANDU-type bundles, Proc. 20<sup>th</sup> CNS Simulation Symp., Niagara-on-the-Lake
- Lockhart RW, Martinelli RC (1949) Proposed correlation of data for isothermal two-phase, two- component flow in pipes, Chem. Eng. Prog., vol 45 no 1 pp 39-48
- Martinelli RC, Nelson DB (1948) Prediction of pressure drop during forced circulation boiling of water, Trans. ASME, vol 70, p 695
- Maubach K (1970) Reibungsgesetze turbulenter Strömungen, Chemie-Ing. Technik vol 42 no 15 pp 995-1004
- Minagawa H (1990) Pressure drop for liquid - gas - solid - slug flow, Kobe University, private communication

- Nigmatulin BI (1982) Heat and mass transfer and force interactions in annular - dispersed two - phase flow, 7th Int. Heat Transfer Conf., Munich, pp 337-342
- Nikuradse J (1932) Gesetzmässigkeiten der turbulenten Strömung in glatten Röhren, Forsch.-Arb.-Ing.-Wesen, VDI Forschungsheft no 336
- Ransom VH et al. (1988) RELAP5/MOD2 Code Manual Volume 1: Code Structure, System Models, and Solution Methods, NUREG/CR-4312 EGG-2396, rev 1, pp 209-216
- Rehme K (1968) Widerstandsbeiwert des Na-2 Abstandshalters GfK/PSB-Notiz Nr. 208/68
- Rehme K (1971) Laminar strömung in stabbundeln, Chemie-Ing-Tech, vol 43 pp 962-966
- Rehme K (1972a) Pressure drop correlations for fuel element spacers, Nuclear Technology, vol 17 pp 15-23
- Rehme K (1972b) Pressure drop performance of rod bundles in hexagonal arrangements, Int. J Heat Mass Transfer, vol 15 pp 2499-2517
- Rehme K (1973) Simple method of predicting friction factors of turbulent flow in non-circular channels, Int. J. Heat and Mass Transfer, vol 16 pp 933-950
- Rehme K (1977) Pressure drop of spacer grids in smooth and roughened rod bundles. Nuclear Technology, vol 31 pp 314-317
- Rehme K (1978) The structure of turbulent flow trough a wall subchannel of rods bundle, Nucl. Eng. and Design, vol 45 pp 311-323
- Sakagushi T, Minagawa H, Tomyama A, Shakutsui H (1989) Characteristics of pressure drop for liquid - solid two - phase flow in vertical pipes, Reprint from Memories of the faculty of engineering, Kobe University, no 36 pp 63-90
- Staengel G, Mayinger F (March 23-24, 1989) Void fraction and pressure drop in subcooled forced convective boiling with refrigerant 12, Proc. of 7th Eurotherm Seminar Thermal Non-Equilibrium in Two-Phase Flow, Roma, pp 83-97
- Subbotin VI et al. (1975) Hydrodynamic and heat exchange in nuclear energy facilities, Moskva, Atomisdat (in Russian)
- Tomyama A, Sakagushi T, Minagawa H (1990) Kobe University, private communication
- Unal C et al. (1994) Pressure drop at rod-bundle spacers in the post-CHF dispersed flow, Int. J. Multiphase Flow, vol 20 no.3 pp 512-522.
- Voj P and Scholven K (Juni 1974) Druckverlustmessungen und Abstandshaltergittern für SNR-300-Brennelement, Techischer Bericht ITB 74.34
- Wilkie D (Aug. 1980) Effect of dimensional variation of the effective friction factor of pin-cluster fuel ellemnts, Nucl. Energy, no 4 pp 283-289
- Yano T and Aritomi M (October 4-8, 2004) Local pressure drops for a ring-type spacer in vertical annular channel, The 6th International Conference on Nuclear Thermal Hydraulics, Operations and Safety (NUTHOS-6), Nara, Japan., Paper ID. N6P033
- Zheng Q et al. (1991) Druckverlust in glatten und innenberippten Verdampferrohren, Wärme- und Stoffübertragung, vol 16 pp 323-330

## 4 Diffusion velocities for algebraic slip models

### 4.1 Introduction

Historically stationary bubble flows or particle flows in pipes are investigated by measuring the volumetric flows of gas and liquid among the other flow characteristics. These measurements are easily recomputed in terms of relative cross section averaged volume fluxes or relative velocities. The obtained results for the relative velocities are frequently compared with the bubble free rise velocity or particle free fall velocity. We consider next bubbles and solid particles in a continuum as particles and their free rising and free settling velocities in stationary continuum will be called simple free particle velocities. It was found that the free particle velocity is a function of the particle size. The next interesting finding was that the cross section averaged relative velocity differs from the free particle velocity which can be explained by the non-uniformity of the velocity and volume concentration profiles depending on the particle-continuum density ratio, orientation of the pipe flow and local parameters. Much later careful measurements provided a data base for the velocity and concentration profiles in pipes. The obtained experimental information is usually generalized by empirical correlations. Some of them are purely empirical while others are based on sound mathematical principles of averaging. The correlations are very useful inside the measurement data banks for steady state flow. In the past usually mixture momentum equations are used for computation of the mixture momentum and the redistribution of the momentum was simulated by using this empirical information. Later this approach was extended to transient pipe flows and then to 3D flows. This approach is very useful if the simulated processes are slowly changing. For fast processes the instant momentum redistribution of the mixture momentum leads to non-adequate process description especially in cases of very strong interfacial heat and mass transfer. For this case the complete set of momentum equations has to be integrated and the drag coefficients have to be provided. Usually the drag coefficients measured for steady flows are used in the latter approach. If one has a method to compute the drag coefficients from the correlation for steady state relative velocities the collected correlation data bank is then a reliable data base also for the drag coefficients. In this chapter we will provide first an approximation for computation of steady state drag coefficients from relative velocity measurements for single particles and for flows. Then we will present a collection of correlation for different cases. The correlation can be used as already mentioned

- a) for steady state flows in addition to the mixture momentum equation completing the description of the mechanical interaction,
- b) for slow transient flows in addition to the mixture momentum equation completing the description of the mechanical interaction,
- c) for strong transient flows in form of drag coefficients used in the separated momentum equations.

In pool flows with low particle concentration the drag coefficients for single particles are the proper choice. For a cloud of particles the drag forces have to be modified taking into account the increased adhesion to the continuum. One should never forget that the drag forces for single particles are only the first choice for pipe flows. The better choice is the effective drag force based on drift flux models.

## 4.2 Drag as a function of the relative velocity

### 4.2.1 Wall force not taken into account

We start with the simplified momentum equations for the continuous and the disperse phase, denoted with  $c$  and  $d$ , respectively, neglecting compressibility, interfacial mass transfer, the spatial acceleration and the viscous terms

$$\alpha_c \rho_c \frac{\partial w_c}{\partial \tau} + \alpha_c \nabla p + \alpha_c \rho_c g - f_d^d - f_d^{vm} = 0, \quad (4.1)$$

$$\alpha_d \rho_d \frac{\partial w_d}{\partial \tau} + \alpha_d \nabla p + \alpha_d \rho_d g + f_d^d + f_d^{vm} = 0, \quad (4.2)$$

where the drag force per unit mixture volume

$$f_d^d = -\alpha_d \rho_c \frac{3}{4} \frac{c_d^d}{D_d} |\Delta w_{cd}| (w_c - w_d), \quad (4.3)$$

and the virtual mass force per unit mixture volume

$$f_d^{vm} = -\alpha_d \rho_c c_d^{vm} \frac{\partial}{\partial \tau} (w_c - w_d) \quad (4.4)$$

are functions of the relative velocities. All parameters in the above equations are cross section averaged. We multiply Eq. (4.1) by  $\alpha_d \rho_d$ , Eq. (4.2) by  $\alpha_c \rho_c$  and subtract the thus obtained equations. The result is

$$\alpha_c \rho_c \alpha_d \rho_d \frac{\partial}{\partial \tau} (w_c - w_d) + (\alpha_c \alpha_d \rho_d - \alpha_d \alpha_c \rho_c) \nabla p - (\alpha_c \rho_c + \alpha_d \rho_d) (f_d^d + f_d^{vm}) = 0. \quad (4.5)$$

Dividing the thus obtained equation by  $\alpha_c \rho_c \alpha_d \rho_d$  and replacing the forces defined by Eqs. (4.3) and (4.4) we obtain

$$(1 + bc_d^{vm}) \frac{\partial}{\partial \tau} \Delta w_{cd} + \left( \frac{1}{\rho_c} - \frac{1}{\rho_d} \right) \nabla p + b \frac{3}{4} \frac{c_d^d}{D_d} |\Delta w_{cd}| \Delta w_{cd} = 0, \quad (4.6)$$

or

$$\frac{\partial}{\partial \tau} \Delta w_{cd} + a \Delta w_{cd} = a \Delta w_{cd, \tau \rightarrow \infty}, \quad (4.7)$$

where

$$a = b \frac{3}{4} \frac{c_d^d}{D_d} |\Delta w_{cd}| / (1 + bc_d^{vm}), \quad (4.8)$$

$$b = \frac{\alpha_c \rho_c + \alpha_d \rho_d}{\alpha_c \rho_d}, \quad (4.9)$$

$$\Delta w_{cd, \tau \rightarrow \infty} = - \left( \frac{1}{\rho_c} - \frac{1}{\rho_d} \right) \nabla p / \left( b \frac{3}{4} \frac{c_d^d}{D_d} |\Delta w_{cd}| \right). \quad (4.10)$$

We see from the Eq. (4.6) that the effect of the virtual mass force is to increase the effective particle inertia. For initial condition

$$\tau = 0, \quad (4.11)$$

$$\Delta w_{cd} = \Delta w_{cd,0}, \quad (4.12)$$

the analytical solution of the above equation for constant pressure gradient and for  $\tau = \Delta \tau$  is

$$\Delta w_{cd} = \Delta w_{cd, \tau \rightarrow \infty} + (\Delta w_{cd,0} - \Delta w_{cd, \tau \rightarrow \infty}) e^{-a \Delta \tau}. \quad (4.13)$$

We see that for

$$\Delta \tau \rightarrow \infty, \quad (4.14)$$

$$\Delta w_{cd} \rightarrow \Delta w_{cd, \tau \rightarrow \infty} \quad (4.15)$$

the velocity difference approaches the steady state velocity difference.

Equation (4.13) is valid for all direction. For the steady state case and vertical flow Eq. (4.1) reduces to

$$\nabla p = -\rho_c g + f_d^d / \alpha_c. \quad (4.16)$$

Substituting Eq. (4.16) into Eq. (4.10) we obtain

$$\frac{\alpha_c + \alpha_d}{\alpha_c} \rho_c \frac{3}{4} \frac{c_d^d}{D_d} \Delta w_{cd, \tau \rightarrow \infty}^2 = g(\rho_d - \rho_c), \quad (4.17)$$

and

$$f_d^d = -\frac{\alpha_c \alpha_d}{\alpha_c + \alpha_d} g(\rho_d - \rho_c). \quad (4.18)$$

The latter equation is the well-known forces balance equation for a free falling sphere for  $\alpha_c \rightarrow 1$ ,  $\alpha_d \rightarrow 0$ .

Note that Eq. (4.17) is valid also if we take into account the wall friction force.

For the vertical flow the drag coefficient can be computed from Eq. (4.17) resulting in

$$c_d^d = \frac{4}{3} D_d g \frac{|\rho_d - \rho_c|}{\rho_c} \frac{\alpha_c}{\alpha_c + \alpha_d} / \Delta w_{cd\infty}^2. \quad (4.19)$$

As already mentioned in the introduction, the steady state drag coefficient can be used also in the transient solution – Eq.(4.13). The coefficient  $a$  then takes the form

$$a = \frac{(\alpha_c \rho_c + \alpha_d \rho_d) |\rho_d - \rho_c|}{\rho_c \rho_d (\alpha_c + \alpha_d)} g / [\Delta w_{cd\infty} (1 + b c_d^{vm})]. \quad (4.20)$$

Remember that in this case  $\Delta w_{cd\infty}$  is the steady state free settling velocity for the family of solid spheres or the free rising velocity for a family of bubbles.

The usual method for deriving the terminal speed of a spherical particle falling (or rising) under gravity is to consider the balance between *buoyancy and drag forces*, see Fig. 4.1.

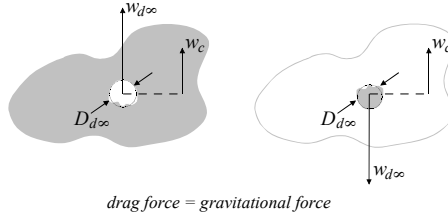


**Fig. 4.1** Free falling droplet in a gravitational field and free rising bubbles in liquid

Employing the drag coefficient for a particle in an infinite medium  $c_{d,single}^d$ , we have

$$\frac{4}{3} \pi r_d^3 g |\Delta \rho|_{cd} = c_{d,single}^d \pi r_d^2 \frac{1}{2} \rho_c \Delta w_{cd\infty,single}^2 \quad (4.21)$$

or

$$c_{d,single}^d = \frac{4}{3} D_d g \frac{|\Delta \rho|_{cd}}{\rho_c} / \Delta w_{cd\infty,single}^2. \quad (4.22)$$

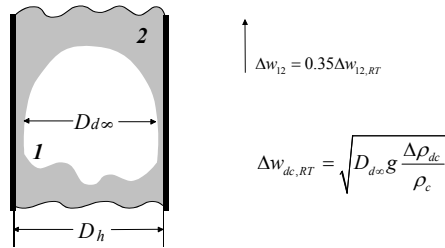
$\Delta\rho$  is the density difference. For the case of a drag coefficient not depending on the bubble form the above equation reduces to

$$\Delta w_{cd\infty, single} = const \sqrt{D_d g \frac{|\Delta\rho|_{cd}}{\rho_c}}. \quad (4.23)$$

It is fundamental velocity scaling parameter in bubbly and slug flow. For slug flow, see Fig. 4.2, the slug bubble diameter is comparable with the hydraulic diameter and therefore

$$\Delta w_{cd\infty, single} = const \sqrt{D_h g \frac{|\Delta\rho|_{cd}}{\rho_c}}, \quad (4.24)$$

see *Dimitresku (1943)*,  $const = 0.35$ .



*Dimitresku (1943), Davies und Taylor (1950)*

**Fig. 4.2** Free rising gas slug in pipe

For large bubbles as presented in Fig. 4.3, which the sizes are comparable with the *Rayleigh-Taylor* instability length

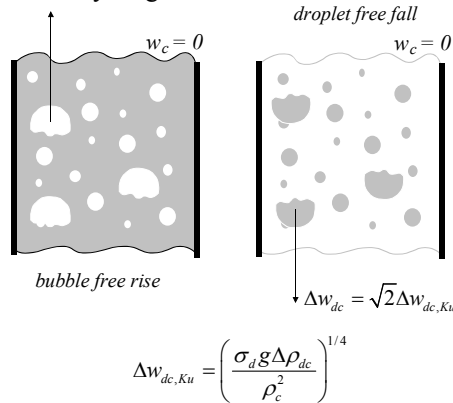


**Fig. 4.3** Free rising bubbles and free falling droplets

$$\lambda_{RT} = \sqrt{\frac{\sigma_2}{g(\rho_2 - \rho_1)}}, \quad (4.25)$$

Kutateladze [39] (1951) obtained

$$\Delta w_{cd\infty, single} = const \sqrt{\sqrt{\frac{\sigma_2}{g(\rho_2 - \rho_1)}} g \frac{|\Delta \rho|_{cd}}{\rho_c}} = const \left( \frac{\sigma g \Delta \rho_{cd}}{\rho_c^2} \right)^{1/4}. \quad (4.26)$$

More information about the constants will be given later on in this Chapter. Equation (4.22) is in fact Eq. (4.19) for disappearing concentration of the dispersed phase. Equation (4.19) is more general. Eliminating the group

$$\frac{4}{3} D_d g \frac{|\Delta \rho|_{cd}}{\rho_c} = c_{d, single}^d \Delta w_{cd\infty, single}^2 \quad (4.27)$$

from Eqs. (4.19) and (4.22) results in

$$c_d^d = c_{d, single}^d \frac{\alpha_c}{\alpha_c + \alpha_d} \left/ \left( \frac{\Delta w_{cd\infty}}{\Delta w_{cd\infty, single}} \right)^2 \right. \quad (4.28)$$

This result demonstrates that the single particle drag coefficient has to be modified in order to obtain an effective drag coefficient for clouds of mono-disperse particles. *Richardson* and *Zaki* proposed in 1954 to correlate experimental data with the function

$$\frac{\Delta w_{cd\infty}}{\Delta w_{cd\infty, single}} = \alpha_c^n. \quad (4.29)$$

where  $n$  is depending on the particle-continuum system and local parameters. Using Eq. (4.29) Eq. (4.28) takes the form

$$c_d^d = \frac{c_{d, single}^d}{(\alpha_c + \alpha_d) \alpha_c^{2n-1}}. \quad (4.30)$$

Note that the drag coefficient may also depend on the relative velocity. This makes iteration necessary to compute the drag coefficient. To avoid this, the *Wallis* collection of correlations given in the Section 4.3 is recommended.

## 4.2.2 Wall forces taken into account

We consider a steady state, one-dimensional, fully developed flow, consisting of two velocity fields designated with  $c$  and  $d$  without any mass sources. The continuous field wets the pipe wall. After inserting the pressure gradient from the mixture momentum equation



$$\frac{dp}{dz} + \rho g + f_{wc} = 0 \quad (4.31)$$

into the momentum equation for the continuous velocity field

$$\alpha_c \left( \frac{dp}{dz} + \rho_c g \right) + f_{wc} + \alpha_d \rho_c \frac{3}{4} \frac{c_d^d}{D_d} |\Delta w_{cd}| (w_c - w_d) = 0 \quad (4.32)$$

and solving with respect to  $c_d^d$  we obtain

$$c_d^d = \frac{4}{3} D_d \frac{\alpha_c \Delta \rho_{cd} g + f_{wc}}{\rho_c |\Delta w_{cd}| (w_d - w_c)} . \quad (4.33)$$

Thus, using correlations for the wall friction force  $f_{wc}$  and a drift flux correlation (or other type of correlations) for computing of the relative velocity  $\Delta w_{dc}$ , we can easily compute from the above equation the drag coefficient  $c_d^d$ .

## 4.3 Two velocity fields

### 4.3.1 Single bubble terminal velocity

*Wallis* (1974) approximated the experimental observations of a number of authors for the terminal speed of bubble by the algorithm presented in Table 4.1. The dimensionless terminal velocity

$$V^* = \Delta w_{dc,\infty} \left( \frac{\rho_c^2}{\eta_c g \Delta \rho} \right)^{1/3} \quad (4.34)$$

is approximated as a function of the dimensionless bubble size

$$r^* = \frac{D_d}{2} \left( \frac{\rho_c g \Delta \rho}{\eta_c^2} \right)^{1/3} , \quad (4.35)$$

and the *Arhmedes* number

$$Ar = \sqrt{\frac{\sigma^3 \rho_c^2}{\eta_c^4 g \Delta \rho}} . \quad (4.36)$$

In a later work *Wallis et al.* (1976) provided for this regions also the corresponding drag coefficients which are also summarized in Table 4.1. They are function of the *Reynolds* and *Weber* numbers defined as follows

$$Re_d = D_d \rho_c \Delta w_{dc} / \eta_c , \quad (4.37)$$

$$We_d = D_d \rho_c \Delta w_{dc}^2 / \sigma . \quad (4.38)$$

**Table 4.1.** The terminal speed of bubble  $V^*$  Wallis (1974), and the corresponding drag coefficients  $c_1^d$  Wallis et al. (1976)

Re- gion	Range	$V^*$	$c_1^d$	Range
1	$r^* < 1.5$	$r^{*2} / 3$	$\frac{16}{Re_d}$	$Re_d < 2.25$
2A	$1.5 \leq r^* < \min(13.4, r_{2A \rightarrow 3}^*)$	$0.408 r^{*1.5}$	$\frac{13.6}{Re_d^{0.8}}$	$2.25 \leq Re_d < 2068$ $We_d < 4$
2D	$13.4 \leq r^* < r_{2D \rightarrow 3}^*$	$\frac{1}{9} r^{*2}$	$\frac{73}{Re_d}$	$Re_d \geq 2068$ $We_d < 4$
3	$r_{2D \rightarrow 3}^* \leq r^* < r_{3D \rightarrow 4}^*$	$Ar^{1/3} \sqrt{2/r^{*2}}$	$We_d = 4$	
4	$r_{3D \rightarrow 4}^* \leq r^* < r_{4 \rightarrow 5}^*$	$\sqrt{2} Ar^{1/6}$	$\frac{We_d}{3}$	$We_d < 8$
5	$r_{4 \rightarrow 5}^* \leq r^*$	$\sqrt{r^*}$	$\frac{8}{3}$	

The boundary of the ranges are defined as follows

$$r_{2A \rightarrow 3}^* = \sqrt{\frac{\sqrt{2}}{0.408}} Ar^{1/6} = 1.862 Ar^{1/6}, \quad (4.39)$$

$$r_{2D \rightarrow 3}^* = (9\sqrt{2})^{2/5} Ar^{2/15} = 2.77 Ar^{2/15}, \quad (4.40)$$

$$r_{3D \rightarrow 4}^* = Ar^{1/3}, \quad (4.41)$$

$$r_{4 \rightarrow 5}^* = 2 Ar^{1/3}. \quad (4.42)$$

The first range is for sufficiently small bubbles ( $D_I$  less than  $0.0005m$ ), where *the viscous forces dominate inertia* forces and the rise velocity can be predicted from the theory of the "*creeping flow*" as long as the interface remains spherical.

In the second region the bubbles behave approximately as solid particles.

In Region 3 *the shape of the bubbles departs significantly from sphericity*, they move in a helical or zigzag path, and the velocity decreases as the "effective radius",  $r_I$ , increases. The effective radius is the radius of a sphere which would have the same volume as the dispersed globule.

In the Region 4 (bubble diameter approximately  $0.001$  to  $0.02m$ ) the terminal bubble velocity

$$\Delta w_{dc,\infty} = Ku V_{Ku} \quad (4.43)$$

is independent on size and is proportional to the *Kutateladze* terminal velocity

$$V_{Ku} = \left[ g \frac{\Delta \rho_{cd}}{\rho_c} \left( \frac{\sigma}{g \Delta \rho_{cd}} \right)^{1/2} \right]^{1/2} = \left( \frac{\sigma g \Delta \rho_{cd}}{\rho_c^2} \right)^{1/4} \quad (4.44)$$

The coefficient is

$$Ku = \sqrt{2} . \quad (4.45)$$

The inclination of the pipe can be taken into account by taking into account only the component of the gravity acceleration being parallel to the pipe axis

$$V_{Ku}^* = \left( \frac{\sigma g \cos \varphi \Delta \rho_{cd}}{\rho_c^2} \right)^{1/4} . \quad (4.46)$$

where  $\varphi$  is the angle between the positive flow direction and the upwards directed vertical. The *Kutateladze* terminal velocity is frequently used as a scaling factor for correlating the so called weighted mean drift velocity in the drift flux theory for bubbly flow.

The collective motion of bubbles in this region for  $\alpha_1 < 0.25$  to 0.30 is called by *Ishii* and *Chawla* motion of distorted particles. The collective motion of bubbles in this region for  $\alpha_1 > 0.25$  to 0.30 is named churn-turbulent flow.

In the Region 5 the bubbles are very large assuming *spherical cap* shape and a flat base. In many publications such a bubble is named *Taylor* bubble. Both viscous and surface tension forces can be neglected and the rise velocity is given by a balance between form-drag and buoyancy. The analytical result derived by *Davis* and *Taylor* for this regime is equivalent to

$$\Delta w_{dc,\infty} \equiv V_{TB} = \sqrt{D_h g \Delta \rho_{cd} / \rho_c} . \quad (4.47)$$

The inclination of the pipe can be taken into account by taking into account only the component of the gravity acceleration being parallel to the pipe axis

$$\Delta w_{dc,\infty} \equiv V_{TB}^* = \sqrt{D_h g \cos \varphi \Delta \rho_{cd} / \rho_c} . \quad (4.48)$$

where  $\varphi$  is the angle between the positive flow direction and the upwards directed vertical. The *Taylor* terminal velocity is frequently used as a scaling factor for correlating the so called weighted mean drift velocity in the drift flux theory for slug flows. Note that the ratio

$$\frac{V_{Ku}^*}{V_{TB}^*} = \left( \frac{\sigma}{D_h^2 g \cos \varphi \Delta \rho_{cd}} \right)^{1/4} = \sqrt{\frac{\lambda_{RT}}{D_h}} . \quad (4.49)$$

The collective motion of bubbles in this regime in channels is named *slug flow*. For vessels with diameters much larger than  $40 \lambda_{RT}$  the slug bubbles can not be sustained due to the interfacial instability and they disintegrate to cap bubbles, *Kataoka* and *Ishii* (1987).

The rise velocity of a group of bubbles is less than the terminal rise velocity of one single bubble due to the mutual interference of the bubbles. *Zuber* and *Findlay* propose the following relationship

$$\Delta w_{dc\infty} = \Delta w_{dc\infty, \text{single}} \alpha_c^{n-1}. \quad (4.50)$$

where  $n = 3$  for Regions 1 and 2,  $n = 5/2$  for churn-turbulent flow. For the churn-turbulent flow *Ishii* (1977) and *Ishi* and *Mishima* (1980) propose  $n = 2.75$ . For the same region *Clark* and *Flemmer* (1985) measured in a vertical 0.1 m - diameter pipe  $n = 1.702$ . The differences between the different authors can be explained by the differences of the pipe diameters for which the data are obtained, which influence the distribution profile of the void fraction. *Wallis*, p.178, (1969) proposes the following relationship

$$n = 4.7 \frac{1 + 0.15 Re_{d\infty}^{0.687}}{1 + 0.253 Re_{d\infty}^{0.687}}, \quad (4.51)$$

where

$$Re_{d\infty} = \rho_c D_d \Delta w_{dc, \infty} / \eta_c. \quad (4.52)$$

Thus the relationship (4.30) is slightly modified

$$c_{cd}^d = \frac{c_{cd, \infty}^d}{(\alpha_d + \alpha_c) \alpha_c^{2n-3}}. \quad (4.53)$$

If for the computational simulation of pool bubbly flow the used discretization mesh size is in the order of magnitude of a few bubble diameters one can use the above method.

### 4.3.2 Single particle terminal velocity

Consider a family of solid particles with a representative volume median diameter  $D_d$ , which are further denoted as *discrete field d* moving in a continuum liquid, denoted further as a *continuum c*. The mixture flows in a channel with a hydraulic diameter  $D_h$ . In this case the maximal volumetric fraction which can be occupied by solid spheres is

$$\alpha_d \leq \alpha_{d \max} \quad (\alpha_{d \max} = \pi / 6 \cong 0.52). \quad (4.54)$$

To describe the *relative velocity of the solid particles* we use a similar approach to that in Section 3.1 - first estimation of the terminal speed of a single particle in an infinite continuum, and thereafter using it for the estimation of the terminal speed of a group of particles. Again the result is used to compute the terminal speed. The data are approximated by the following set of correlations – see *Wallis* (1974):

$$V^* = \frac{2}{9} r^{*2} \quad r^* < 1.5 \text{ (entirely viscous flow)} \quad (4.55)$$

$$V^* = 0.307 r^{*1.21} \quad 1.5 \leq r^* < 10 \quad (\text{inertia forces become important}) \quad (4.56)$$

$$V^* = 0.693 r^{*0.858} \quad 10 \leq r^* < 36 \quad (\text{reflects the effect of vortex shading}) \quad (4.57)$$

$$V^* = 2.5 \sqrt{r^*} \quad 36 \leq r^* \text{ (fully-developed turbulent wake).} \quad (4.58)$$

The falling velocity of a *group of particles* is less than the terminal falling velocity of one single particle due to the mutual interference of the particles. For this case *Richardson and Zaki*, p. 47 proposed in 1954 to use in Eqs. (4.29, 4.30) the following exponents

$$n = 4.65 + 19.5 D_d/D_h, \quad Re_d < 0.2, \quad (4.59)$$

$$n = (4.35 + 17.5 D_d/D_h) Re_d^{-0.03}, \quad 0.2 \leq Re_d < 1, \quad (4.60)$$

$$n = (4.45 + 18.0 D_d/D_h) Re_d^{-0.1}, \quad 1 \leq Re_d < 200, \quad (4.61)$$

$$n = 4.45 Re_d^{-0.1}, \quad 200 \leq Re_d < 500, \quad (4.62)$$

$$n = 2.39, \quad 500 < Re_d. \quad (4.63)$$

*Rowe* (1987) found a convenient empirical equation for the estimation of the *Richardson-Zaki* exponent

$$n = 2.35 \frac{2 + 0.175 Re_{d\infty}^{3/4}}{1 + 0.175 Re_{d\infty}^{3/4}} \quad (4.64)$$

representing the data with standard deviation of  $\pm 0.02$ .

*Zwirin et al.* (1989) experimentally observe that the free settling velocity of particles in liquid, having averaged temperature greater than the liquid saturation temperature, is higher than the free settling velocity of particles with temperature lower than the saturated temperature

$$V/V_{T < T'} = 1.02 + 3.87 \cdot 10^{-5} (T - T') \quad (4.65)$$

for  $373 < T < 973.14 \text{ K}$ .

### 4.3.3 Cross section averaged bubble rise velocity in pipes – drift flux models

#### 4.3.3.1 Basics

Computing the weighted mean velocity defined by

$$w_d = \frac{\frac{1}{A} \int_A \alpha_{d,local} w_{d,local} dA}{\frac{1}{A} \int_A \alpha_{d,local} dA}, \quad (4.66)$$

which appears in the cross section averaged conservation equations results in the expression

$$w_d = C_0 j + V_{dj}^*. \quad (4.67)$$

$j$  is the volumetric flux of the mixture which is equivalent to the center of volume velocity of the mixture. Here the *distribution parameter*

$$C_0 = \frac{\frac{1}{A} \int_A \alpha_{d,local} j_{local} dA}{\left( \frac{1}{A} \int_A j_{local} dA \right) \left( \frac{1}{A} \int_A \alpha_{d,local} dA \right)}, \quad (4.68)$$

and the weighted mean drift velocity

$$V_{dj}^* = \frac{\frac{1}{A} \int_A \alpha_{d,local} V_{dj,local} dA}{\left( \frac{1}{A} \int_A \alpha_{d,local} dA \right)}, \quad (4.69)$$

are averages over the cross section of the channel. The local drift velocity of the dispersed phase is defined with respect to the total volume flux

$$V_{dj,local} = w_{d,local} - j. \quad (4.70)$$

This expression has been known in the literature as the *Zuber and Findlay* model since 1965— see *Zuber and Findlay* (1965). A large number of publication exists on correlating experimental data with the so called distribution parameter  $C_0$  and the weighted mean drift velocity  $V_{dj}^*$ . We will give a summary reviewing this literature in this chapter for gas liquid flows.

#### 4.3.3.2 Some useful relationships

Solving the equation system consisting of the definition equations for the dispersed phase velocity  $w_d = C_0 [\alpha_d w_d + (1 - \alpha_d) w_c] + V_{dj}^*$  and the mass flow rate  $\rho w = \alpha_d \rho_d w_d + (1 - \alpha_d) \rho_c w_c$  with respect to the cross section averaged velocities results in

$$w_c = \frac{\rho w (1 - \alpha_d C_o) - \alpha_d \rho_d V_{dj}^*}{(1 - \alpha_d) [\rho_c (1 - \alpha_d C_o) + \alpha_d \rho_d C_o]}, \quad (4.71)$$

$$w_d = \frac{\rho w - (1 - \alpha_d) \rho_c w_c}{\alpha_d \rho_d}. \quad (4.72)$$

The relative velocity is therefore

$$\Delta w_{dc} = \frac{V_{dj}^* - (1 - C_o) w_c}{1 - \alpha_d C_o}. \quad (4.73)$$

Defining the averaged volumetric flow concentration

$$\dot{\alpha}_d = \frac{j_d}{j}, \quad (4.74)$$

the drift flux equation takes the form

$$\frac{\dot{\alpha}_d}{\alpha_d} = C_0 + \frac{V_{dj}^*}{j}, \quad (4.75)$$

or

$$\alpha_d = \frac{\dot{\alpha}_d}{C_0 + \frac{V_{dj}^*}{j}}. \quad (4.76)$$

The velocity ratio takes the form

$$\frac{w_d}{w_c} = \frac{1 - \alpha_d}{\frac{1}{C_0 + V_{dj}^* / j} - \alpha_d}. \quad (4.77)$$

The above relations are very useful for comparison of information from different publications on this issue.

*Zuber and Findlay* (1965) clearly demonstrated that the reason for success of correlating data is in using flow regime dependent correlations. As we will show in the following literature review there are also the so called general drift flux correlations, some of them containing smooth change over the flow pattern boundaries

Having the drift flux parameter we compute easily from Eqs. (4.71) through (4.74) the field velocities and the relative velocity, respectively. If separated momentum equations are used the cloud drag coefficient can be easily computed by using Eqs. (4.19) and (4.33).

### 4.3.3.3 Bubble or churn-turbulent flow

Zuber and Findlay (1965) demonstrated that for adiabatic flows the data of several authors can be generalized with the following expressions

$$w_d = C_0 j + 1.53 V_{Ku} \quad (4.78)$$

For bubble flow or churn-turbulent flow the distribution parameter is

$$C_0 = 1.2 \quad (4.79)$$

The distribution parameter may take values less than 1 for wall void picking profiles and values up to 1.5 for strong center line picking of the void fraction. For slug flow observed for values of

$$\alpha_1 \approx 0.26 \quad (4.80)$$

the recommended expression is

$$w_d = C_0 j + 0.35 V_{TB} \quad (4.81)$$

The correlations are valid for co-current up flow. It seems that for small diameters

$$D_h < 19.1 \left( \frac{\sigma}{g \cos \phi \Delta \rho_{cd}} \right)^{1/2}, \quad (4.82)$$

or

$$D_h / \lambda_{RT} < 19.5 \quad (4.83)$$

the slug flow is always the expected regime. Note that Kataoka and Ishii (1987) used instead of 19.5 the value of 40.

Coddington and Macian compared in the year 2000 a set of empirical correlation for  $0.1 \leq p \leq 15 \text{ MPa}$ ,  $1 \leq G \leq 2000 \text{ kg} / (\text{m}^2 \text{ s})$ , channel length between 1.7 and 3.7 m, for pipes and rod bundles with rod diameters 9.5, 10.7, 12.2, 12.3 mm, and hydraulic diameters between 4 and 13 mm, with uniform and variable axial heat distribution, subcooling between 118 and 0 K, and heat fluxes between 5 and  $3377 \text{ kW} / \text{m}^2$ . The results for the mean absolute error and the standard deviation of the absolute error are given in Table 4.2.

This very informative study confirms once again the sound physical basics of the Zuber and Findlay correlation.

Lellouche (1974) correlated the void cross section distribution parameter with

$$C_0 = 1 / [A_o + (1 - A_o) \alpha_1^{\beta_o}], \quad (4.84)$$



**Table 4.2.** Wide range void fraction correlation

Correlation	Year	Data Source	Aver. err.	Stand. dev. in %
<i>Zuber-Findlay</i>	1965	Tube	-0.025	11.4
<i>Ishii</i>	1977	Tube	0.048	12.6
<i>Gardner</i>	1980	Tube	0.056	11.1
<i>Liao, Parlos and Griffith</i>	1985	Tube	0.028	9.4
<i>Takeochi</i>	1992	Tube	0.040	8.3
<i>Sun</i>	1980	RB+Tube	-0.041	11.4
<i>Jowitt</i>	1981	RB	0.057	11.6
<i>Sonnenburg</i>	1989	RB+Tube	0.049	9.7
<i>Toshiba</i>	1989	RB	0.019	10.3
<i>Dix</i>	1971	RB	-0.010	9.2
<i>Bestion</i>	1985	RB+Tube	0.018	8.8
<i>Chexal-Lellouche</i>	1992	RB+Tube	-0.017	7.8
<i>Inoue</i>	1993	RB	0.003	8.3
<i>Maier and Coddington</i>	1996	RB	-0.002	7.1

RB: Rod Bundle

where

$$\begin{aligned}
 k_l &= 0.833, \\
 A_o &= k_l + (1 - k_l) p / 22115000, \\
 B_o &= \frac{1}{1 - A_o} (1 + 1.57 \rho_1 / \rho_2),
 \end{aligned}$$

and the weighted mean drift velocity with

$$V_{lj}^* = 1.41 V_{Ku}. \quad (4.85)$$

The correlation is valid for co-current up flow.

*Clark and Flemmer* (1985) reported a correlation for bubble flow in vertical tube with hydraulic diameter  $D_h = 0.1m$ . The void cross section distribution parameter is correlated taking into account the void fraction dependence which was already discussed by *Zuber* but not established for practical applications: For up flows

$$C_0 = 0.934(1 + 1.42\alpha_1), \quad (4.86)$$

and for down flow with

$$C_0 = 1.521(1 - 3.67\alpha_1), \quad (4.87)$$

The weighted mean drift velocity is correlated again as proposed by *Zuber*  $V_{lj} = 1.53 V_{Ku}$ , for both cases.

*Ishii* (1977) reported a correlation for bubble flow ( $w_2 > 0.5$ ) in a vertical tube. For a round tube the void cross section distribution parameter is correlated with

$$C_0 = 1.2 - 0.2\sqrt{\rho_1 / \rho_2} , \quad (4.88)$$

for a rectangular channel with

$$C_0 = 1.35 - 0.35\sqrt{\rho_1 / \rho_2} , \quad (4.89)$$

and the weighted mean drift velocity is correlated with

$$V_{1j}^* = \sqrt{2} (1 - \alpha_1)^{1.75} V_{Ku} , \quad (4.90)$$

for both cases. For churn-turbulent bubbly flow *Ishii* uses the *Zuber-Findlay* expression with constant,  $\sqrt{2}$ ,  $V_{1j}^* = \sqrt{2} V_{Ku}$ . For slug flow *Ishii* uses the *Zuber-Findlay* expression  $V_{1j}^* = 0.35 V_{TB}$ . *Imura et al.* (2006) used 2 for the exponent instead 1.75.

In a later work *Kataoka and Ishii* (1987) investigated pool flows. They used the same void cross section distribution parameter for a round tube and a rectangular channel as before but introduced viscosity dependence in the weighted mean drift velocity as follows. For the low viscous case characterized by

$$N\eta_2 \leq 2.25 \times 10^{-3} , \quad (4.91)$$

$$N\eta_2 = \eta_2 / \sqrt{\rho_2 \sigma_2 \lambda_{RT}} \quad (\text{Viscous number}), \quad (4.92)$$

and small diameters

$$D_h^* \leq 30 , \quad (4.93)$$

where

$$D_h^* = D_h / \lambda_{RT} , \quad (4.94)$$

the weighted mean drift velocity is correlated with

$$V_{1j}^* = 0.0019 D_h^{*0.809} (\rho_1 / \rho_2)^{-0.157} N\eta_2^{-0.562} V_{Ku} . \quad (4.95)$$

For large diameters

$$D_h^* > 30 , \quad (4.96)$$

the weighted mean drift velocity is correlated with

$$V_{1j}^* = 0.03 (\rho_1 / \rho_2)^{-0.157} N\eta_2^{-0.562} V_{Ku} . \quad (4.97)$$

For the high viscous case characterized by

$$N\eta_2 > 2.25 \times 10^{-3} , \quad (4.98)$$

the weighted mean drift velocity is reported for large diameters

$$D_h^* > 30, \quad (4.99)$$

and is

$$V_{1j}^* = 0.92 (\rho_1 / \rho_2)^{-0.157} V_{Ku}. \quad (4.100)$$

The accuracy of the void fraction prediction reported by the authors is  $\pm 20\%$  for  $\alpha_1 w_1 = 0.1$  to  $2.5$ ,  $D_h = 0.01$  to  $0.6$ ,  $p = (1 \text{ to } 25)10^5 \text{ Pa}$  for air-water,  $p = (1 \text{ to } 182)10^5 \text{ Pa}$  for steam-water.

#### 4.3.3.4 Bubble flow in an annular channel

*Staengel* and *Mayinger* (1989) reported for this case the following correlation the void cross section distribution parameter with

$$C_0 = \alpha_1 \left[ 1 + 1.409 Fr^{-0.01} \left( 1 - \frac{h' - h_2}{h'' - h'} \right)^{0.164} \left( \frac{\rho_1}{\rho_2} \right)^{0.694} \left( \frac{1 - X_1}{X_1} \right)^{0.864} \left( 1 - \frac{p}{p_{cr}} \right)^{0.124} \right], \quad (4.101)$$

where

$$\alpha_1 = \frac{1}{1 + \frac{1 - X_1}{X_1} \frac{\rho_1}{\rho_2}}, \quad (4.102)$$

$$Fr = \frac{G^2}{g D_h \rho_2^2}, \quad (4.103)$$

$$X_1 = \frac{\alpha_1 \rho_1 w_1}{G}, \quad (4.104)$$

and the weighted mean drift velocity with

$$V_{1j}^* = 1.18 V_{Ku}. \quad (4.105)$$

The correlation is obtained for subcooled boiling of  $CCL_2F_2$  in a channel with  $D_h = 0.014$ , for the parameter region  $10 \leq T' - T_2 \leq 50 \text{ K}$ ,  $12 \cdot 10^5 \leq p \leq 40 \cdot 10^5 \text{ Pa}$ ,  $500 \leq G \leq 3000 \text{ kg/(m}^2\text{s)}$ .

#### 4.3.3.5 Slug flow in a tube

As already mentioned the free rising Taylor bubble velocity is used as a velocity scale for the weighted mean drift velocity for slug flow in a tube.

*Dimitresku* (1943) correlated the void cross section distribution parameter with

$$C_0 = 1.2, \quad (4.106)$$

and the weighted mean drift velocity with

$$V_{1j}^* = 0.351 V_{TB}^* . \quad (4.107)$$

The correlation was validated for

$$\frac{\rho_2 j D_h}{\eta_2} > 8000 , \quad (4.108)$$

and volume of *Taylor* bubble  $> (0.4 D_h)^3$ . *Zuber* and *Findlay* (1965) confirmed the data for  $D_h \leq 0.05$ . For larger diameters,  $D_h > 0.05$ , *Delhaye* et al. (1981) proposed to use

$$V_{1j}^* = 0.56 V_{TB}^* . \quad (4.109)$$

*Wallis* (1969) observed the dependence on the bubble to pipe radius as follows

$$V_{1j}^* = V_{TB}^* \quad (4.110)$$

for

$$D_1 < D_h / 8 , \quad (4.111)$$

and

$$V_{1j}^* = 1.13 V_{TB}^* e^{-D_1 / D_h} \quad (4.112)$$

for

$$D_h / 8 < D_1 < 0.6 . \quad (4.113)$$

*Kuroda* - see in *Sakagushi* et al. (1987) correlated the weighted mean drift velocity with

$$V_{1j}^* = \left\{ 0.35 - \frac{0.25}{\left[ \left( \sqrt{Bo} - 1.9 \right) / 2.12 \right]^{2.67} + 1} \right\} V_{TB}^* \quad (4.114)$$

where

$$Bo = \rho_2 g D_h^2 / \sigma . \quad (4.115)$$

*Bendiksen* (1985) investigated vertical flow within  $0 < 4/Eo < 0.6$  and correlated the weighted mean drift velocity with

$$V_{1j}^* = 0.344 \frac{1 - 0.96^{-0.0165 Eo}}{(1 - 0.52 e^{-0.0165 Eo})^{3/2}} \sqrt{1 + \frac{20}{Eo} \left( 1 - \frac{6.8}{Eo} \right)} V_{TB}^* \quad (4.116)$$

where

$$Eo = \frac{g \Delta \rho_{21} D_h^2}{\sigma} \quad (4.117)$$

is the pipe Eötvös number. *Bendiksen* observed that the void cross section distribution parameter is different for laminar

$$C_0 = 2.29 \left[ 1 - \frac{20}{Eo} (1 - e^{-0.0125 Eo}) \right], \quad (4.118)$$

and turbulent flow

$$\frac{\log Re + 0.309}{\log Re - 0.743} \left[ 1 - \frac{2}{Eo} (3 - e^{-0.025 Eo} \log Re) \right], \quad (4.119)$$

where

$$Re = \rho_2 j D_h / \eta_2. \quad (4.120)$$

*Bendiksen* observed that for large *Froude* numbers  $Fr > 3.5$  where  $Fr = j / V_{TB}$  there is no strong influence of the inclination on the distribution parameter  $C_o \approx 1.19$  to  $1.2.$ , but for  $Fr < 3.5$  the distribution parameter may vary within 20%  $C_o \approx 1$  to  $1.2.$

#### 4.3.3.6 Annular flow

*Ishii* (1977) correlated the void cross section distribution parameter for annular flow with

$$C_0 = 1 + \frac{1 - \alpha_1}{\alpha_1 + \left[ \frac{1 + 75(1 - \alpha_1)}{\sqrt{\alpha_1}} \frac{\rho_1}{\rho_2} \right]^{1/2}}, \quad (4.121)$$

and the weighted mean drift velocity with

$$V_{1j}^* = 8.16 (C_o - 1) \alpha_2^{1/2} V_{TB}. \quad (4.122)$$

*Imura* et al. (2006) used a simplified form for the distribution coefficient

$$C_0 = 1 + (1 - \alpha_1) / \left[ \alpha_1 + 4 (\rho_1 / \rho_2)^{1/2} \right].$$

For

$$|j_1| < V_{TB} \left( \frac{1}{C_0} - 0.1 \right) \quad (4.123)$$

*Ishii* reported the existence of churn turbulent flow.

*Delhaye et al.* (1981) correlated the void cross section distribution parameter with

$$C_0 = 1, \quad (4.124)$$

and the weighted mean drift velocity with

$$V_{1j}^* = 23 \sqrt{\frac{\eta_2 \alpha_2 w_2}{\rho_1 D_h} \frac{\rho_2 - \rho_1}{\rho_2}}. \quad (4.125)$$

#### 4.3.3.7 Annular dispersed flow

*Imura et al.* (2006) used the *Ishi's* correlation the void cross section distribution parameter for annular dispersed flow in the form

$$C_0 = 1 + \alpha_2 / \left[ \alpha_1 + 4(\rho_1 / \rho_2)^{1/2} \right]$$

and the weighted mean drift velocity in the form

$$V_{1j}^* = 8.16(C_0 - 1)\alpha_2^{1/2}V_{TB} + \frac{\alpha_3}{\alpha_1 + \alpha_3} \sqrt{2} \left( \frac{\sigma g \cos \varphi \Delta \rho_{31}}{\rho_1^2} \right)^{1/4}.$$

#### 4.3.3.8 Mist flow

In accordance with *Imura et al.* (2006) the void cross section distribution parameter for annular dispersed flow is  $C_0 = 0$  and weighted mean drift velocity

$$V_{1j}^* = \alpha_3 \sqrt{2} \left( \frac{\sigma g \cos \varphi \Delta \rho_{31}}{\rho_1^2} \right)^{1/4}.$$

#### 4.3.3.9 Full-range drift-flux correlation

There are successful attempts to generalize data for all flow regimes in a pipe flow by the so called full-range drift flux correlations. Three of the best examples will be given below.

**The Holmes correlation from 1981:** *Holmes* (1981) correlated the void cross section distribution parameter with

$$C_0 = 1 / \left[ A_o + (1 - A_o) \alpha_1^{B_o} \right]. \quad (4.126)$$

Here

$$A_o = 1 - 0.328 (1 - 1.5228 \cdot 10^{-3} p) F^2,$$

$$\begin{aligned}
B_o &= B_1 B_2 / [1 + F(B_2 - 1)], \\
B_1 &= 2.94 + 7.763 \cdot 10^{-4} p + 9.702 \cdot 10^{-6} p^2, \\
B_2 &= \sqrt{\rho_2 / \rho_1}, \\
G_1 &= 251.7 + 232.7 p^{1/2} + 18.39 p, \\
G_2 &= -4.8 + 6650 \rho_1 / \rho_2 + 7.62 p^{1/2} + 14.20 p, \\
G_{HS} &= 1 / \sqrt{|x_1 / G_2^2 + (1 - x_1) / G_1^2|}, \\
F &= 1 / e^{20683.9 |G| G_{HS}}.
\end{aligned}$$

The weighted mean drift velocity was correlated with

$$V_{1j}^* = \frac{(1 - \alpha_1 C_o) C_o K(\alpha_1)}{\sqrt{\rho_1 / \rho_2 \alpha_1 C_o + 1 - \alpha_1 C_o}} V_{Ku}. \quad (4.127)$$

The transition limits are given as follows:  $\alpha_1^*$  for bubble-to-film flow and  $\alpha_2^*$  for slug-to-annular flow. The limits are set as follows  $\alpha_1^* = 0.18$ ,  $\alpha_2^* = 0.45$ .

**The Chexal et al. correlation from 1989:** Chexal et al. (1989) correlated the void cross section distribution parameter with

$$C_o = Fr C_{ov} + (1 - Fr) C_{oh} [1 + \alpha_1^{0.05} (1 - \alpha_1)^2]. \quad (4.128)$$

Here

$0 \leq \alpha_1 \leq \alpha_1^*$	$K(\alpha_1) = 1.53 C_o$
$\alpha_1^* \leq \alpha_1 \leq \alpha_2^*$	$K(\alpha_1) = \frac{\frac{1.53}{C_o} (\alpha_2^* - \alpha_1)^2 + Ku (\alpha_1^* - \alpha_1)^2}{(\alpha_2^* - \alpha_1)^2 + (\alpha_1 - \alpha_1^*)^2}$
$\alpha_2^* \leq \alpha_1 \leq 1$	$K(\alpha_1) = Ku$

$Ku = w_1 / V_{Ku}$	(Kutateladze number) $K(Ku)$
$\leq 2$	0
4	1
10	2.1
14	2.5
20	2.8
28	3.0
$\geq 50$	3.2

The Froude number is computed as follows

$$Re_1 > 0$$

$$Fr = (\pi - 2\varphi^*) / \pi \quad \text{for } (0 \leq \varphi^* \leq \pi/2).$$

$$Re_1 < 0$$

$$Fr = 1 \quad \text{if } \varphi^* < \frac{8}{9} \frac{\pi}{2},$$

$$Fr = (\pi/2 - \varphi^*) / (\frac{1}{9} \frac{\pi}{2}) \quad \text{for } (\frac{8}{9} \frac{\pi}{2} < \varphi^* \leq \frac{\pi}{2}).$$

$\varphi^*$  = pipe orientation angle measured from vertical ( $0 \leq \varphi \leq \pi/2$ ).  $\varphi^* = 0$  for vertical pipe,  $\varphi^* = \pi/2$  for horizontal pipe. Here  $C_{ov}$  is valid for vertical flow.  $C_{oh}$  for horizontal co current flow and is defined as for vertical flow but using absolute values of the volume fluxes  $j_1$  and  $j_2$ .

$$Re_1 > 0$$

$$C_{ov} = C_{ov}^+$$

where

$$C_{ov}^+ = L / [A_o + (1 - A_o)\alpha_1^{B_o}]$$

$$Re_1 < 0$$

$$C_{ov} = \max \left[ C_{ov}^+, \frac{V_{1j}^o (1 - \alpha_1)^{0.2}}{|j_1| + |j_2|} \right]$$

where

$$B_o = (1 + 1.57 \rho_1 / \rho_2) / (1 - k_1),$$

$$L = [1 - \exp(-C_1 \alpha_1)] / [1 - \exp(-C_1)],$$

$$C_1 = 4p_{kr}^2 / [p(p_{kr} - p)],$$

$$A_o = k_1 + (1 - k_1)(\rho_1 / \rho_2)^{1/4},$$

$$k_1 = \min(0.8, A_1),$$

$$A_1 = 1 / [1 + \exp(-Re/60000)],$$

$$Re = Re_1 \quad \text{if } Re_1 > Re_2 \quad \text{or } Re_1 < 0,$$

$$Re = Re_2 \quad \text{if } Re_1 \leq Re_2.$$

The local gas superficial *Reynolds* number is defined as follows

$$Re_1 = \alpha_1 \rho_1 w_1 D_h / \eta_1.$$

The local liquid superficial *Reynolds* number is defined as follows

$$Re_2 = \alpha_2 \rho_2 w_2 D_h / \eta_2.$$



The weighted mean drift velocity was correlated by *Chexal* et al. as follows.

$$V_{1j}^* = FrV_{1jv} + (1 - Fr)V_{1jh} \quad (4.129)$$

for co-current up flow.

$$V_{1j}^* = FrV_{1jv} + (Fr - 1)V_{1jh}$$

for co current down flow.  $V_{1jh}$  considers only co-current horizontal flow ( $j_1 > 0, j_2 > 0$ ) and is evaluated using the same equation as for the vertical flow using positive values of  $j_1$  and  $j_2$ .

$$V_{1jv} = V_{1jv}^o C_9,$$

$$V_{1jv}^o = 1.41 C_2 C_3 C_4 V_{Ku}.$$

Computation of the  $C_2$  factor:

$$\begin{aligned} \rho_2 / \rho_1 &> 18, \\ C_5 &= \sqrt{150 \rho_1 / \rho_2}, \quad C_6 = C_5 / (1 - C_5), \\ C_5 &\geq 1, \quad C_2 = 1, \\ C_5 &< 1, \quad C_2 = 1 / [1 - \exp(-C_6)], \\ \rho_2 / \rho_1 &\leq 18, \\ C_2 &= 0.4757 [\ln(\rho_2 / \rho_1)]^{0.7}. \end{aligned}$$

Computation of the  $C_4$  factor:

$$\begin{aligned} D_2 &= 0.09144 \text{ (normalizing diameter)}, \\ C_7 &= (D_2 / D_h)^{0.6}, \quad C_8 = C_7 / (1 - C_7), \\ C_7 &\geq 1, \quad C_4 = 1, \\ C_7 &< 1, \quad C_4 = 1 / [1 - \exp(-C_8)]. \end{aligned}$$

Computation of the  $C_3$  and  $C_9$  factors:

$$\begin{aligned} &\text{Co-current up flow (} Re_1 > 0, Re_2 > 0 \text{)} \\ C_9 &= (1 - \alpha_1)^{k_1}, \\ C_3 &= \max \left[ 0.5, 2e^{(-|Re_2|/60000)} \right], \\ &\text{Co-current down flow (} Re_1 < 0, Re_2 < 0 \text{)} \\ C_9 &= \min \left[ 0.7, (1 - \alpha_1)^{0.65} \right], \\ C_3 &= 2(C_{10} / 2)^{B_2}, \end{aligned}$$

where

$$C_{10} = 2 \exp \left[ \frac{|Re_2|}{350000} \right]^{0.4} - 1.75 |Re_2|^{0.03} \exp \left[ - \left( \frac{D_1}{D_h} \right)^2 \frac{|Re_2|}{50000} \right] + \left( \frac{D_1}{D_h} \right)^{0.25} |Re_1|^{0.001},$$

and  $D_1 = 0.0381$  (normalizing diameter),

$$B_2 = 1 / \left[ 1 + 0.05 \left( \frac{|Re_2|}{350000} \right) \right]^{0.4}.$$

Counter-current flow ( $Re_1 > 0$ ,  $Re_2 < 0$ ) : Two solution for the void fraction,  $\alpha_{11}, \alpha_{12}$ . The desired void fraction,  $\alpha_1$  known a priori, is used to select the appropriate  $C_3$  as follows: for

$$\begin{aligned} \alpha_1 &= \max(\alpha_{11}, \alpha_{12}) \\ C_3 &= 2(C_{10} / 2)^{B_2}, \end{aligned}$$

for

$$\begin{aligned} \alpha_1 &= \min(\alpha_{11}, \alpha_{12}), \\ C_3 &= \min \left\{ 2 \left( \frac{C_{10}}{2} \right)^{B_2}, 2 \left[ \left( \frac{C_{10}}{2} \right)^{B_2} \left( \frac{j_2}{j_2^*} \right) + \left( 1 + \frac{|Re_2|}{60000} \right) \left( 1 - \frac{j_2}{j_2^*} \right) \right] \right\}. \end{aligned}$$

$j_2^*$  is  $j_2$  on the counter-current flow limiting (CCFL) line corresponding to  $j_1$  and is calculated using

$$\begin{aligned} C_3 &= \min \{ 2(C_{10} / 2)^{B_2} \}, \\ C_9 &= (1 - \alpha_1)^{k_1}. \end{aligned}$$

On CCFL line  $dj_1 / d\alpha_1 = 0$ .

*Kawanishi et al. (1990)* compared the prediction of  $\alpha_1$  with 1353 data points for  $p < 180 \cdot 10^5$ ,  $D_h \leq 0.61$ . The error band was  $\pm 30.7\%$ .

**The Kawanishi et al. correlation from 1990:** Kawanishi et al. (1990) correlated the void cross section distribution parameter with

$$j \leq -3.5 \quad C_0 = 1.2 - 0.2 \sqrt{\rho_1 / \rho_2}, \text{ Ishii (1977) for round tube,} \quad (4.130)$$

$$-3.5 < j \leq -2.5 \quad C_0 = 0.9 + 0.1 \sqrt{\rho_1 / \rho_2} - 0.3(1 - \sqrt{\rho_1 / \rho_2})(2.5 + j) \quad (4.131)$$

$$-2.5 < j < 0 \quad C_0 = 0.9 + 0.1 \sqrt{\rho_1 / \rho_2} \quad (4.132)$$

$$0 \leq j \quad C_0 = 1.2 - 0.2 \sqrt{\rho_1 / \rho_2}, \text{ Ishii (1977) for round tube,} \quad (4.133)$$

The weighted mean drift velocity was correlated with

$$j \leq 0 \quad V_{1j}^* = \sqrt{2} V_{Ku}, \quad \text{Zuber and Findlay (1965)} \quad (4.134)$$

$$0 < j < 0.24 \quad \text{Interpolate between } V_{1j} \text{ for } j \leq 0 \text{ and } V_{1j} \text{ for } j = 0.24. \quad (4.135)$$

$$j \geq 0.24 \\ p \leq 15 \times 10^5$$

$$D_h \leq 0.05 \quad V_{1j}^* = 0.35 V_{TB}, \quad \text{Zuber and Findlay (1965)} \quad (4.136)$$

$$0.05 < D_h \leq 0.46 \quad V_{1j}^* = 0.52 V_{TB}, \quad (4.137)$$

$$0.46 < D_h \quad V_{1j}^* = 0.52 V_{TB, D_h=0.46}, \quad (4.138) \\ 15 \times 10^5 < p \leq 180 \times 10^5$$

$$D_h \leq 0.02 \text{ m} \quad V_{1j}^* = 0.35 V_{TB}, \quad \text{Zuber and Findlay (1965)} \quad (4.139)$$

$$0.02 < D_h \leq 0.24 \quad \text{Interpolate between} \\ V_{1j}^* \text{ for } D_h = 0.02 \text{ and } V_{1j}^* \text{ for } D_h = 0.24. \quad (4.140)$$

$$0.24 < D_h \leq 0.46 \quad V_{1j}^* = 0.048 \sqrt{\frac{\rho_2}{\rho_1}} V_{TB} \quad (4.141)$$

$$0.46 < D_h \quad V_{1j}^* = 0.048 \sqrt{\frac{\rho_2}{\rho_1}} V_{TB} \text{ for } D_h = 0.46. \quad (4.142)$$

*Kawanishi et al. (1990)* compared the prediction of  $\alpha_1$  with 1353 data points for  $p < 180 \times 10^5$ ,  $D_h \leq 0.61$ . The error band was  $\pm 16.8\%$  which makes the correlation more accurate than that of *Chexal et al. (1989)* for this region.

***Liao, et al. (1985) correlation:*** The *Liao, et al. (1985)* correlation taken from *Coddington and Macian (2000)* consists of two regions: For bubbly flow

$$j_2 > 2.34 - 1.07 \left( \frac{g \sigma \Delta \rho_{21}}{\rho_2^2} \right)^{1/4}, \quad (4.143)$$

$$C_0 = 1, \quad (4.144)$$

$$V_{1j}^* = 1.53(1 - \alpha_1)^2 V_{Ku} . \quad (4.145)$$

For churn turbulent flow

$$C_0 = \left\{ 1.2 - 0.2 \sqrt{\frac{\rho_1}{\rho_2}} [1 - \exp(-18\alpha_1)] \right\} , \quad (4.146)$$

which is the *Ishii* (1977) correlation for around tube modified by *Liao* et al. (1985) with the multiplier  $1 - \exp(-18\alpha_1)$ . For the weighted mean drift velocity the gas density was used in the denominator in the *Kutatededze* number (scaling with the free falling droplet velocity)

$$V_{1j}^* = 0.33 \left( \frac{g \sigma \Delta \rho_{21}}{\rho_1^2} \right)^{1/4} . \quad (4.147)$$

For annular flow  $|j_1| > V_{TB} \left( \frac{1}{C_0} - 0.1 \right)$ , the authors used the *Ishii* (1977) results as follows: For the distribution parameter

$$C_0 = 1 + \frac{1 - \alpha_1}{\alpha_1 + \left[ \frac{1 + 75(1 - \alpha_1) \frac{\rho_1}{\rho_2}}{\sqrt{\alpha_1}} \right]^{1/2}} , \quad (4.148)$$

and for the weighted mean drift velocity

$$V_{1j}^* = 8.16(C_0 - 1)(1 - \alpha_1)^{1/2} V_{TB} . \quad (4.149)$$

**Gardner [10] correlation (1980):**

$$\frac{\alpha_1}{\sqrt{1 - \alpha_1}} = 11.2 \left( \frac{j_1}{V_{ku}} \rho_1 w_2^2 \sqrt{\frac{g \Delta \rho_{21}}{\sigma_2^3}} \right)^{2/3} . \quad (4.150)$$

**Maier and Coddington correlation (1986):** The best fit of the data is given by the *Maier and Coddington* (1986) correlation

$$C_0 = 1.0062 + 2.57 \times 10^{-9} p , \quad (4.151)$$

$$\begin{aligned} V_{1j}^* &= 0.8 - 1.23 \times 10^{-7} p + 5.63 \times 10^{-15} p^2 \\ &+ G \left( 1.05 \times 10^{-3} - 8.81 \times 10^{-11} p + 6.73 \times 10^{-19} p^2 \right) . \end{aligned} \quad (4.152)$$

#### 4.3.3.10 Horizontal stratified flow

*Fraß* and *Wiesenberger* (1976) obtained a correlation for stratified horizontal flow valid for high pressures 40 to 160 bar:

$$S = \left( 0.38 Fr_2^{-3/2} + 1.2 \right) \left( \frac{X_1}{1 - X_1} \frac{\rho_2}{\rho_1} \right)^{0.76}, \quad (4.153)$$

where

$$Fr_2 = \frac{(\rho w)^2 v_2}{g D_h}. \quad (4.154)$$

#### 4.3.3.11 Mamaev et al. method for inclined pipes

**Stratified flow:** For the computation of the relative velocities and pressure drop for this flow pattern the work by Mamaev et al. (1969) is recommended.

$$\alpha_1 = 1 - A^{0.4} \quad \text{for } 0 \leq A \leq 0.18, \quad (4.155)$$

$$\alpha_1 = 0.615(1 - A) \quad \text{for } 0.18 < A \leq 1, \quad (4.156)$$

where

$$A = \lambda_{fr} (1 - \beta)^2 Fr_{crit} / (-2 \cos \varphi). \quad (4.157)$$

Note that Mamaev et al. considered stratified flow possible for  $Fr_h < Fr_{crit}$ , where

$Fr_h = \frac{(\rho w)^2 v_h^2}{g D_h}$ ,  $v_h = X_1 v_1 + (1 - X_1) v_2$ . The critical Froude number was obtained from experiments

$$Fr_{crit} = \left[ \left( 0.2 - \frac{2 \cos \varphi}{\lambda_{fr}} \right) / (1 - \alpha_1)^2 \right] \exp(-2.5 \alpha_1), \quad (4.158)$$

where  $\alpha_1 = X_1 v_1 / v_h$ , and  $\lambda_{fr} = \lambda_{fr} \left( \frac{\pi(1 - \alpha_1)}{\pi - \theta} \frac{w_2 D}{v_2}, \frac{k}{D_h} \right)$  is the liquid site wall friction coefficient computed using the Nikuradze diagram.

**Slug flow, churn-turbulent flow, or bubbly flow:** For the computation of the relative velocities and pressure drop for this flow pattern the work by Mamaev et al. (1969) is again recommended. The volume fraction is then

$$\alpha_1 = 0.81 \alpha_1 \left[ 1 - \exp(-2.2 Fr_{crit}^{1/2}) \right], \quad (4.159)$$

where the required variables are computed as in the previous section. This correlation goes together with the friction pressure drop correlation obtained by the authors

$$\left(\frac{dp}{dz}\right)_{fr} = \lambda_{fr} \frac{1}{2D} [\alpha_1 \rho_1 w_1^2 + (1 - \alpha_1) \rho_2 w_2^2] \Phi_{2o}, \quad (4.160)$$

where

$$\lambda_{fr} = \lambda_{fr} \left[ \frac{X_1 w_1 + (1 - X_1) w_2}{X_1 / \rho_1 + (1 - X_1) / \rho_2} \frac{w_2 D_h}{v_2}, \frac{k}{D_h} \right], \quad (4.161)$$

$$\Phi_{2o} = \left\{ 1 + 0.78 \dot{\alpha}_1 \left[ 1 - \exp(-2.2 Fr_{crit}^{1/2}) \right] - 0.22 \dot{\alpha}_1 \left[ 1 - \exp(-15 \rho_2 / \rho_1) \right] \right\} / (1 - \dot{\alpha}_1). \quad (4.162)$$

#### 4.3.4 Cross section averaged particle sink velocity in pipes – drift flux models

In this case we calculate the drift flux parameter using the appropriate correlation from Table 4.3.

**Table 4.3.** Drift flux parameters for a mixture of liquid and solid particles ( $\alpha_{d \max} < \pi / 6$ )

Concentration (distribution) parameter  $C_o$       Weighted mean drift velocity

$$V_{dj}^* = -const V_T, \text{ where}$$

$$V_T = \sqrt{g D_h \frac{\rho_d - \rho_c}{\rho_c}}$$

$$const = \dots$$

*Covier and Azis (1972)*

$$1.2$$

$$1.77 \text{ (Newton regime, } C^d = 0.44 \text{ )}$$

*Oedjoe and Buchman (1966)* for flow of water slurries of coal,  
 $D_d = 0.062$  to  $0.0318$  and gravel,  $D_d = 0.0047$  to  $0.0138$

$$1.2$$

$$0.88$$

*Wallis (1969)*

$$1.2$$

$$V_{dj}^* = (1 - \alpha_d)^{2.39} V_{dj, \alpha_d=0}^*$$

*Sakaguchi et al. (1990),*  
 $0.8 \leq C_o \leq 1.4$

$$[1 + \frac{-1.39 \frac{j_{c,w_d=0}}{j_{cd}} + 2.48 \frac{D_d}{D_{hcd}} + 0.488}{\left(\frac{\alpha_d}{0.01}\right)^{1.2} + 1}] \quad V_{dj}^* = -C_o j_{c,w_d=0}$$

$$[1.213 - 0.294(w_c - w_d) / \Delta w_{cd\infty}]$$

where

$$j_{c,w_d=0} = \Delta w_{cd\infty} \frac{\alpha_c^m}{\alpha_d^n},$$

$$m = \left[ -0.457 \left( \frac{D_d}{D_h} \right)^{0.7} + 1.31 \right] / \alpha_d^{1.2},$$

$$n = -0.797 \frac{D_d}{D_h} + 0.732,$$

$$\Delta w_{cd} = \sqrt{\frac{4}{3} \frac{D_d}{c_{cd}^d} \frac{\rho_d - \rho_c}{\rho_c} g},$$

$$c_{dc}^d = \frac{24}{\text{Re}_{dc}} (1 + 0.15 \text{Re}_{dc}^{0.687})$$

$$+ \frac{0.42}{1 + 42500 \text{Re}_{dc}^{-1.16}}.$$

For  $\alpha_d < 0.005$  one should use  $C_o = 1$  and  $j_{c,w_d=0} = \alpha_c \Delta w_{cd\infty}$ . The experimental data base includes diameters 0.00114, 0.00257 and 0.00417 *m* for aluminum ceramic particles with density 2270, 2380 and 2400, respectively, and diameter 0.00296 for aluminum particles with density 2640. The pipe diameters are 0.0209, 0.0306, 0.0508. The solid volumetric fraction was  $0.005 < \alpha_3 < 0.1$ , the superficial liquid velocity  $0.193 < j_c < 1.51$ , and the superficial solid particle velocity  $0.000450 < j_d < 0.0407$ .

We see from Table 4.3 that *Covier* and *Azis* and *Oedjoe* and *Buchman* used as a weighted mean drift velocity the free-setting velocity of single solid particles. *Wallis* introduced the correction for the influence of neighbor particles in a confined flow.

*Sakaguchi et al.* (1986, 1987) rewrite the original *Zuber* drift flux correlation (4.67) in terms of the velocities

$$w_d = \frac{C_o(1-\alpha_d)w_c}{1-\alpha_d C_o} + \frac{V_{dj}^*}{1-\alpha_d C_o}, \quad (4.163)$$

calculate the liquid flux for which the solid particle velocity,  $w_d$ , is equal to zero

$$j_{d,w_d=0} = (1-\alpha_d)w_{c,w_d=0} = -\frac{V_{dj}^*}{C_o} \quad (4.164)$$

called suspension volumetric flux of the liquid phase, and rewrite the *Zuber* drift flux correlation in terms of the suspension volumetric flux of the liquid

$$w_d = C_o(j - j_{d,w_d=0}). \quad (4.165)$$

The analog to Eq. (4.165) in terms of the suspension volumetric flux of the liquid phase is

$$\frac{\Delta w_{cd}}{\Delta w_{cd\infty}} = [(1-C_o)\frac{w_c}{\Delta w_{cd\infty}} + C_o\frac{j_{d,w_d=0}}{\Delta w_{cd\infty}}]/(1-\alpha_d C_o) \quad (4.166)$$

*Sakaguchi et al.* proposed instead of the use the *free settling velocity* as a main parameter in the drift flux description, to use the *suspension volumetric* flux of the liquid phase. The relationship between this velocity and the *weighted mean drift velocity* is given with Eq. (4.164). The experimental data of *Sakagushi* are correlated by means of the correlations given in Table 4.3. They are obtained by using the *fast closing valves* method to measure the volumetric fraction of each phase. The experimental data for the particles volumetric fraction are approximated with an index of deviation of +10.6 and -8.61%. Comparing with the data of other authors, *Sakagushi* shows that they are correlated with an index of deviation +57.3 and -311%. Using *Sakaguchi's* correlation from Table 4.3 we can rewrite Eq. (4.166) in the following form

$$\frac{\Delta w_{cd}}{\Delta w_{cd\infty}} = [(1-C_o)\frac{w_c}{\Delta w_{cd\infty}} + C_o\frac{\alpha_c^m}{\alpha_d^n}]/(1-\alpha_d C_o) \quad (4.167)$$

## 4.4 Slip models

The critical two phase is co-current flow. Some authors used in this case successfully slip correlation describing the gas-to-liquid velocity ratio  $S$  as a function of the local parameters. In what follows we give some of them.

*Kolev* (1982) propose the following form of empirical correlation



$$S = w_1 / w_2 = 1 + \frac{(n+1)^{n+1}}{n^n} X_1 (1 - X_1)^n \left[ (\rho_2 / \rho_1)^m - 1 \right]. \quad (4.168)$$

Here  $m$  determines the magnitude of the maximum of  $S$  and  $n$  the position at the  $X_l$  coordinate where this maximum occurs

$$S = 1 + \frac{X_1}{X_{1m}} \left( \frac{1 - X_1}{1 - X_{1m}} \right)^{\frac{1 - X_{1m}}{X_{1m}}} \left[ (\rho_2 / \rho_1)^m - 1 \right] \quad (4.169)$$

where

$$S = S_{\max} = (\rho_2 / \rho_1)^m \quad (4.170)$$

for

$$X_l = X_{1m}. \quad (4.171)$$

This relationship gives the maximum possible slip ratios for gas mass flow concentration greater than 0.5, and divides the regions of experimentally observed and not observed slip ratios for  $X_l$  less than 0.5. The measurements for critical air - water made by *Deichsel* and *Winter* (1990) for  $T = 293 \text{ K}$  and  $p = (1.65, 2.65, 3.37, 4.15) 10^5$  are represented successfully using the above equation and  $X_{1m} \approx 0.1$ ,  $m \approx (0.18, 0.17, 0.16, 0.14)$ , respectively.

One year later *Petry* (1983) reported a similar relationship correlating data for two-phase flow of R12 in capillary tubes

$$\log S = 1/[A (\log X_l)^2 + B \log X_l + C], \quad (4.172)$$

where  $A = 6.3014$ ,  $B = 25.5632$ ,  $C = 23.3784$ . This correlation gives  $S_m = 5.5$  at  $X_{1m} = 0.013$ . Similar to those authors a correlation was proposed by *Michaelides* and *Parikh* (1982)

$$S = 1 + \frac{X_1}{X_{1m}} \exp \left[ (X_{1m} - X_1) / X_{1m} \right] \left[ (\rho_2 / \rho_1)^m - 1 \right] \quad (4.173)$$

where

$$m = 1/2, \quad (4.174)$$

$$X_{1m} = 1/C = 0.1. \quad (4.175)$$

$C$  was experimentally observed in the region 7 to 15. A probably more general form is

$$S = 1 + \left( \frac{X_1}{X_{1m}} \right)^\kappa \exp \left[ (X_{1m} - X_1) / X_{1m} \right] \left[ (\rho_2 / \rho_1)^m - 1 \right] \quad (4.176)$$

where

$$\kappa > 1. \quad (4.177)$$

The fact that there is a maximum of the  $S(X_1)$  function is confirmed by *Grieb* (1989) showing the change of the flow pattern from continuous liquid to continuous gas with liquid entrainment. *Hug* and *Loth* (1992) proposed a new semi-empirical correlation for  $S_2$

$$S_2 = (\rho_2 / \rho_1) 2X_1 (1 - X_1) / \left\{ 2X_1 (1 - X_1) + \left[ 1 + 4X_1 (1 - X_1) \left( \frac{\rho_2}{\rho_1} - 1 \right) \right]^{1/2} - 1 \right\}. \quad (4.178)$$

This simple correlation gives a comparable result to the very complicated and extensively tested EPRI correlation (1989) and approximate reasonably air - water data for mass flow rates  $G = 50$  to  $1330 \text{ kg/(m}^2\text{s)}$  at atmospheric pressure.

*Deichsel* and *Winter* (1990) found indirect experimental evidence that in the critical cross section the local critical flow at every point of the cross section is nearly homogeneous. They found that there is a profile of the gas volumetric fraction which can be described as follows

$$\alpha_1(r) = \alpha_{1,r=0} - (\alpha_{1,r=0} - \alpha_{1,r=R_h})(r / R_h)^n, \quad (4.179)$$

where

$$\alpha_{1,r=0} = 1 - (1 - \alpha_1)^{3.1}, \quad (4.180)$$

$$\alpha_{1,r=R_h} = 1 - (1 - \alpha_1)^{\alpha_1/3}, \quad (4.181)$$

$$n = 1.015 / (1.015 - \alpha_1). \quad (4.182)$$

The authors assumed that at each point of the critical cross section the flow velocity is equal to the sound velocity and computed the slip as the ratio of the cross section averaged gas velocity to the cross section averaged liquid velocity

$$S = \frac{1 - \alpha_1}{\alpha_1} \left[ \int_A a_h(\alpha_1, p) \alpha_1(r) dA \right] / \left\{ \int_A a_h(\alpha_1, p) [1 - \alpha_1(r)] dA \right\}. \quad (4.183)$$

## 4.5 Three velocity fields – annular dispersed flow

Consider the mixture of gas, film and droplets. The relative droplets velocity with respect to the gas in accordance with *Kataoka* and *Ishii* (1982)

$$\Delta w_{13} = w_1 - w_3 = (D_3 / 4) \left\{ [g(\rho_3 - \rho_1)]^2 / (\eta_1 \rho_1) \right\}^{1/3} (1 - \alpha_d)^{1.5}, \quad (4.184)$$

depends on the volume averaged droplet size. Here

$$\alpha_d = \alpha_3 / (1 - \alpha_2) \quad (4.185)$$

is the volume *concentration of droplets in the gas-droplets mixture*. In annular-dispersed flow, most droplets are in a wake regime due to their relatively small size. That is why one can consider approximately the flow consisting of a core having a volume fraction and a density of

$$\alpha_{core} = \alpha_3 + \alpha_1, \quad (4.186)$$

$$\rho_{core} = \alpha_d \rho_3 + (1 - \alpha_d) \rho_1, \quad (4.187)$$

respectively, and a film. This allows us to compute the drift flux parameter for an annular flow using *Ishii's correlation* (1977)

$$C_{core} = 1 + \alpha_2 / \left[ \alpha_{core} + \sqrt{(1 + 75\alpha_2) \rho_{core} / (\sqrt{\alpha_{core}} \rho_2)} \right], \quad (4.188)$$

$$V_{corej} = (C_{core} - 1) \sqrt{(\rho_2 - \rho_{core}) D_{hy} g \alpha_2 / (0.015 \rho_2)}, \quad (4.189)$$

and thereafter to compute the film velocity

$$w_2 = \frac{\rho w (1 - \alpha_{core} C_{core}) - \alpha_{core} \rho_{core} V_{corej}}{(1 - \alpha_{core}) [\rho_2 (1 - \alpha_{core} C_{core}) + \alpha_{core} \rho_{core} C_{core}]}. \quad (4.190)$$

Having the relative velocity  $\Delta w_{13}$ , we compute the gas velocity from the definition of the c.m. velocity, namely

$$w_1 = (\rho w - \alpha_2 \rho_2 w_2 + \alpha_3 \rho_3 \Delta w_{13}) / (\alpha_1 \rho_1 + \alpha_3 \rho_3). \quad (4.191)$$

Having the actual field velocities and the c.m. velocity, the diffusion velocities are easily obtained from the definition equations.

In case of dispersed flow (*gas and particles only*) the gas velocity is

$$w_1 = (\rho w + \alpha_3 \rho_3 \Delta w_{13}) / (\alpha_1 \rho_1 + \alpha_3 \rho_3) \quad (4.192)$$

Similarly we can model the flow if the gas phase or if the second field carry out solid particles. In both cases the particle diameter is an input parameter.

## 4.6 Three-phase flow

Depending on the volumetric concentration of the macroscopic solid particles (the third velocity field) we distinguish the following cases:

1. The *solid particles are touching each other* in the control volume

$$\alpha_3 = \alpha_{dm}. \quad (4.193)$$

In this case we suppose that the *friction* between wall and particles and among the particles itself *obstructs their movement*

$$V_3 = 0. \quad (4.194)$$

In this case it is not possible to have simultaneously a droplet field. In the free space between the particles, a mixture of liquid and gas can flow. It is convenient in such cases to simply correct the volumetric porosities, the permeabilities, and the hydraulic diameters, and to describe the flow of gas-liquid mixture through the free space.

2. The *solid particles are free in the flow* and the volume fraction of the space between them if they were closely packed,

$$\alpha_2^* = \frac{1 - \alpha_{dm}}{\alpha_{dm}} \alpha_3, \quad (4.195)$$

is *smaller* than the liquid volume fraction

$$\alpha_2^* < \alpha_2. \quad (4.196)$$

In this case the question arises how the particles are distributed in the mixture. The ratio of the free settling velocities in gas and liquid

$$\sqrt{\frac{\rho_3 - \rho_1}{\rho_3 - \rho_2} \frac{\rho_2}{\rho_1}}$$

gives an idea how to answer this question. We see that, due to considerable differences between gas and liquid densities, the *particles sink much faster in gas than in the liquid*. Thus most probably the solid particles are carried out by the liquid, which corresponds to the experimental observations. In this case one can consider the flow consisting of gas, droplets, and a fictitious liquid velocity field consisting of the liquid field and the macroscopic solid particles field, having a density of

$$\rho_2' = (\alpha_2 \rho_2 + \alpha_3 \rho_3) / \alpha_2' \quad (4.197)$$

volume concentration in the mixture of

$$\alpha_2' = \alpha_2 + \alpha_3. \quad (4.198)$$

mixture mass flow rate and velocity of the fictitious mixture of the velocity fields 2 and 3,  $V_2'$ . Further our task reduces to the estimation of the momentum redistribution between the components 2 and 3, which means calculation the velocities  $V_2'$  and  $V_3$ . For this purpose we use either

$$V_2 = V_2' - \frac{\alpha_3 \rho_3}{\alpha_2 \rho_2 + \alpha_3 \rho_3} \Delta V_{23}, \quad (4.199)$$

$$V_3 = V_2 - \Delta V_{23} \quad (4.200)$$

estimating  $\Delta V_{23}$  empirically, or a proper correlation from Table 4.3, and the proposal made by Giot see in *Hetstroni* (1982) and *Sakagushi* et al. (1986). Both authors assume that the particles behave as they are moving in a fictitious channel with hydraulic diameter

$$D_{hcd} = D_h \sqrt{1 - \alpha_1 - \alpha_3} \quad (4.201)$$

filled with liquid, a local volumetric particles concentration of

$$\alpha_c = \frac{\alpha_2}{\alpha_2 + \alpha_3}, \quad (4.202)$$

and a density of the continuous and discrete phase

$$\rho_c = \rho_2, \quad (4.203)$$

$$\rho_d = \rho_3. \quad (4.204)$$

3. The *solid particles are free in the flow*

$$\alpha_3 > \frac{\alpha_{dm}}{1 - \alpha_{dm}} \alpha_2 \quad (4.205)$$

and the volume fraction of the space between them if they were closely packed is larger then the liquid volume fraction

$$\alpha_2^* > \alpha_2. \quad (4.206)$$

This means that part of the particles,  $\alpha_{31}$

$$\alpha_3 - \frac{\alpha_{dm}}{1 - \alpha_{dm}} \alpha_2 = \alpha_3 (1 - \alpha_2 / \alpha_2^*) \quad (4.207)$$

are surrounded by gas. Probably in this case the particles surrounded by gas will settle down and will be carried out mechanically by the other particles carried out by the liquid. The question arises how to compute their velocity. As a first approximation one can correct the density of the particles surrounded by the liquid, with the weight of the rest of the particles

$$\rho_3^* = \rho_3 \alpha_3 / \left( \frac{\alpha_{dm}}{1 - \alpha_{dm}} \alpha_2 \right) = \rho_3 \alpha_2^* / \alpha \quad (4.208)$$

and proceed as in the previous case. But this question has to be clarified experimentally, which has not been done as far as the author knows.

## Nomenclature

### Latin

$Ar$	$= \sqrt{\frac{\sigma^3 \rho_c^2}{\eta_c^4 g \Delta \rho}}$ Archimedes number, <i>dimensionless</i>
$Bo$	$= \rho_2 g D_h^2 / \sigma$ , Bond number, <i>dimensionless</i>
$C_0$	distribution parameter
$c_l^d$	drag coefficient acting on the field $l$ , <i>dimensionless</i>
$c_{d, single}^d$	drag coefficient for a particle in an infinite medium, <i>dimensionless</i>
$Eo$	$= \frac{g \Delta \rho_2 D_h^2}{\sigma} = (D_h / \lambda_{RT})^2$ , pipe Eötvös number, <i>dimensionless</i>
$Fr$	$= \frac{G^2}{g D_h \rho_2^2}$ , square of Froude number based on the liquid density, <i>dimensionless</i>
$Fr_h$	$= \frac{(\rho w)^2 v_h^2}{g D_h}$ , square of Froude number based on the mixture density, <i>dimensionless</i>
$f_l^d$	drag force acting on the field $l$ per unit mixture volume, $N/m^3$
$f_l^{vm}$	virtual mass force acting on the field $l$ per unit mixture volume, $N/m^3$
$g$	gravity acceleration, $m/s^2$
$h$	specific enthalpy, $J/kg$
$j$	volumetric flux of the mixture - equivalent to the center of volume velocity of the mixture, $m/s$
$N\eta_2$	$= \eta_2 / \sqrt{\rho_2 \sigma_2 \lambda_{RT}}$ , liquid viscous number, <i>dimensionless</i>
$p$	pressure, $Pa$
$Re_d$	$= D_d \rho_c \Delta w_{dc} / \eta_c$ , Reynolds number for dispersed particle surrounded by continuum, <i>dimensionless</i>
$S$	$= w_1 / w_2$ , slip (velocity ratio), <i>dimensionless</i>
$r^*$	$= \frac{D_d}{2} \left( \frac{\rho_c g \Delta \rho}{\eta_c^2} \right)^{1/3}$ , bubble size, <i>dimensionless</i>
$T$	temperature, $K$
$V^*$	$= \Delta w_{dc, \infty} \left( \frac{\rho_c^2}{\eta_c g \Delta \rho} \right)^{1/3}$ , terminal velocity, <i>dimensionless</i>

---

$V_{Ku}$	$= \left( \frac{\sigma g \Delta \rho_{cd}}{\rho_c^2} \right)^{1/4}$ , <i>Kutateladze</i> terminal velocity of dispersed particle in continuum, <i>m/s</i>
$V_{TB}^*$	$= \sqrt{D_h g \cos \varphi \Delta \rho_{cd} / \rho_c}$ , <i>Taylor</i> terminal velocity, <i>m/s</i>
$V_{dj}^*$	weighted mean drift velocity, <i>m/s</i>
$We_d$	$= D_d \rho_c \Delta w_{dc}^2 / \sigma$ , <i>Weber</i> number for dispersed particle surrounded by continuum, <i>dimensionless</i>
$v_h$	$= X_1 v_1 + (1 - X_1) v_2$ , homogeneous mixture specific volume, <i>m<sup>3</sup>/kg</i>
$w_l$	cross section averaged axial velocity of field <i>l</i> , <i>m/s</i>
$w_d$	weighted mean velocity, <i>m/s</i>
$X_1$	$= \frac{\alpha_1 \rho_1 w_1}{G}$ , gas mass flow concentration, <i>dimensionless</i>

### Greek

$\alpha_l$	volume fraction of field <i>l</i> , <i>dimensionless</i>
$\dot{\alpha}_d$	$= \frac{j_d}{j}$ , averaged volumetric flow concentration of the field <i>d</i> , <i>dimensionless</i>
$\dot{\alpha}_1$	$= \frac{1}{1 + \frac{1 - X_1}{X_1} \frac{\rho_1}{\rho_2}}$ , averaged volumetric flow concentration of the gas, <i>dimensionless</i>
$\alpha_{core}$	$= \alpha_3 + \alpha_1$ , core volume fraction: droplet + gas, <i>dimensionless</i>
$\alpha_{dm}$	particle volume fraction at which the solid particles are touching each other in the control volume, <i>dimensionless</i>
$\Delta w_{cd}$	velocity difference: continuum minus disperse, <i>m/s</i>
$\Delta w_{cd\infty}$	steady state free settling velocity for the family of solid spheres or the free rising velocity for a family of bubbles, <i>m/s</i>
$\Delta w_{cd,0}$	velocity difference at zero time, <i>m/s</i>
$\Delta w_{cd,\tau \rightarrow \infty}$	steady state velocity difference, <i>m/s</i>
$\Delta \rho_{cd}$	density difference: continuum minus disperse, <i>kg/m<sup>3</sup></i>
$\Phi_{2o}$	two phase friction multiplier, <i>dimensionless</i>
$\varphi$	angle between the positive flow direction and the upwards directed vertical, <i>rad</i>
$\lambda_{RT}$	$= \sqrt{\frac{\sigma_2}{g(\rho_2 - \rho_1)}}$ , <i>Rayleigh-Taylor</i> instability length, <i>m</i>

$\rho_l$	density of field $l$ , $kg/m^3$
$\rho_{core}$	$= \alpha_d \rho_3 + (1 - \alpha_d) \rho_1$ , core density: droplet + gas, $kg/m^3$
$\rho_w$	mixture mass flow rate, $kg/(m^2s)$
$\sigma$	gas-liquid surface tension, $N/m$
$\eta$	dynamic viscosity, $kg/(ms)$

### ***Subscripts***

1	field 1
2	field 2
3	field 3
c	continuum
d	disperse
cr	critical
core	droplets + gas in annular flow

### ***Superscripts***

'	saturated liquid
"	saturated vapor

## **References**

- Bendiksen KH (1985) On the motion of long bubbles in vertical tubes, *Int. J. Multiphase Flow*, vol 11 pp 797 - 812
- Chexal B, Lellouche G, Horowitz J and Healzer J (Oct. 10-13, 1989) A void fraction correlation applications, *Proc. of the Fourth International Topical Meeting on Nuclear Reactor Thermal- Hydraulics*. Mueller U, Rehme K, Rust K, (eds) G Braun Karlsruhe Karlsruhe, vol 2 pp 996-1002
- Clark NN and Flemmer RL (1985) Predicting the holdup in two-phase bubble up flow and down flow using the Zuber and Findlay drift flux model, *AIChE J.*, vol 31 no 3 March, pp 500-503
- Coddington P and Macian R, (2000) A study of the performance of void fraction correlations used in the context of drift-flux two phase flow models, Internet publication of the *Proceedings of Trends in Numerical and Physical Modeling for Industrial Multiphase Flows*, 27<sup>th</sup> - 29<sup>th</sup> September, Corse, France
- Covier GW and Azis K (1972) *The flow of complex mixtures in pipes*, Von Nostrand Reinhold, p 469
- Deichsel M and Winter ERF (1990) Adiabatic two-phase pipe flow at air-water mixtures under critical flow conditions, *Int. J. Multiphase Flow*, vol 16 no 3 pp 391-406
- Delhay JM, Giot M, and Riethmueller ML (1981) *Thermodynamics of two-phase systems for industrial design and nuclear engineering*. Hemisphere Publ. Corp., Mc Graw-Hill Book Company



- Dimitresku DT, (1943) Stroemung an einer Luftblase im senkrechten Rohr, Z. angew. Math. Mech., vol 23 no 3 pp 139-149
- Fraß F and Wiesenberger J (September 1976) Druckverlust und Phasenverteilung eines Dampf/Wasser-Gemisches in horizontaldurchströmten Rohr, BWK, vol 28 no 9
- Gardner C G (1980) Fractional vapor content of a liquid pool through which vapor is bubbled, Int. Journal of Multiphase Flow, vol 6 pp 399-410
- Grieb G (June 1989) New slip correlation of forced convection two - phase flow, Nucl. Energy, vol 28 no 3 pp 155-160
- Hetstroni G (1982) Handbook of multiphase systems. Hemisphere Publ. Corp., Washington etc., McGraw-Hill Book Company, New York etc.
- Holmes JA (13-15 Sept. 1981) Description of the drift flux model in the LOCA-Code RELAP-UK. Heat and Fluid Flow in Water Reactor Safety. Manchester,
- Hug R and Loth J (Jan.-March 1992) Analytical two phase flow void prediction method, J. Thermophysics, vol 6 no 1 pp 139-144
- Imura K, Yoshida K, Kataoka I and Naitoh M (July 17-20, 2006) Subchannel analysis with mechanistic methods for thermo-hydro dynamics in BWR fuel bundles, Proc. of ICONE14, Int. Conf. on Nuclear Engineering, Miami, FA, USA
- Ishii M (1977) One dimensional drift-flux model and constitutive equations for relative motion between phases in various two-phase flow regimes. ANL-77-47 Argonne National Laboratory, Argone
- Ishii M and Mishima K (Dec. 1980) Study of two-fluid model and interfacial area. NUREG/CR-1873, ANL-80-111
- Kataoka I and Ishii M (July 1982) Mechanism and correlation of droplet entrainment and deposition in annular two-phase Flow. NUREG/CR-2885, ANL-82-44
- Kataoka I and Ishii M (1987) Drift flux model for large diameter pipe and new correlation for pool void fraction, Int. J. Heat and Mass Transfer, vol 30 no 9 pp 1927-1939
- Kawanishi K, Hirao Y and Tsuge A (1990) An Experimental Study on Drift Flux Parameters for Two-Phase Flow in Vertical Round Tubes, NED, vol 120 pp 447-458
- Kolev NI (1982) Modeling of transient non equilibrium, non homogeneous systems, Proc. of the seminar "Thermal Physics 82 (Thermal Safety of VVER Type Nuclear Reactors)", Karlovy Vary, May 1982, Czechoslovakia, vol 2 pp 129-147 (in Russian).
- Kutateladze SS (1951) Gidrodinamicheskaja teorija izmenenija rejima kipenija jidkosti pri svobodnoj konvekcii, Izvestija akademii nauk SSSR, Otfelenie technicheskikh hanuk, no 4 pp 529-536
- Lellouche GS (1974) A model for predicting two-phase flow, BNL-18625
- Liao LH, Parlos A and Griffith P (1985) Heat transfer, carryover and fall back in PWR steam generators during transients, NUREG/CR-4376, EPRI NP-4298
- Maier D and Coddington P (1986) Validation of RETRAN-03 against a wide range of rod bundle void fraction data, ANS Transactions, vol 75 pp 372-374
- Michaelides E and Parikh S (1982) The prediction of critical mass flux by the use of Fanno lines, Nucl. Eng. Des., vol 71 pp 117-124
- Mamaev WA, Odicharia GS, Semeonov NI, Tociging AA (1969) Gidrodinamika gasogid-kostnych smesey w trubach, Moskva
- Oedjoe D and Buchman BH (1966) Trans. Inst. Chem. Eng., vol 44 no 10 p 364
- Petry G (1983) Two - phase flow of R12 in capillary tubes under the critical flow state. Ph. D. Thesis, Technical University of Munich, Germany
- Richardson JF and Zaki WN (1954) Sedimentation and fluidization: Part I, Trans. Instrn. Chem. Eng., vol 32 pp 35-53

- Rowe PN (1987) A convenient empirical equation for the estimation of the Richardson-Zaki exponent, *Chem. Eng. Science*, vol 42 no 11 pp 2795-2796
- Sakaguchi T, Minagawa H, and Sahara K (March 22-27, 1987) Estimation of volumetric fraction of each phase in gas-liquid-solid three-phase flow, *Proc. of the ASME-JSME Thermal Engineering Joint Conference*, Honolulu, Hawaii, pp 373-380
- Sakaguchi T, Minagawa H, Kato Y, Kuroda N, Matsumoto T, and Sohara K (1987) Estimation of in-situ volume fraction of each phase in gas-liquid-solid three-phase flow, *Trans. of JSME*, vol 53 no 487 pp 1040-1046
- Sakaguchi T, Minagawa H, Tomiama A, and Sjakutsui H (Jan.1990) Estimation of volumetric fraction in liquid - solid two - phase flow, *Trans. JSME*, vol 56 no 521 pp 5-10 (in Japanese)
- Sakaguchi T et al. (1986) Volumetric fraction of each phase in gas-liquid and liquid-solid two-phase flow, *Memories of the faculty of engineering, Kobe University*, no 33 pp 73-102
- Staengel G and Mayinger F (March 23-24, 1989) Void fraction and pressure drop in sub-cooled forced convective boiling with refrigerant 12, *Proc. of 7th Eurotherm Seminar Thermal Non-Equilibrium in Two-Phase Flow*, Roma pp 83-97
- Wallis GB (1969) *One dimensional two-phase flow*, New York: McGraw Hill
- Wallis GB (1974) The terminal speed of single drops or bubbles in an infinite medium, *Int. J. Multi phase Flow*, vol 1 pp 491-511
- Wallis GB, Richter H J, and Kuo J T (Dec.1976) The separated flow model of two-phase flow, *EPRI NP-275*
- Zuber N and Findlay JA (Nov. 1965) Average volumetric concentration in two-phase flow systems, *Trans. ASME, J.of Heat Transfer*, vol 84 no 4 pp 453-465
- Zwirin Y, Hewitt GF and Kenning DB (1989) Experimental study of drag and heat transfer during boiling on free falling spheres, *Heat and Technology*, vol 7 no 3-4 pp 13-23

## 5 Entrainment in annular two-phase flow

### 5.1 Introduction

Entrainment is a process defined as mechanical mass transfer from the continuous liquid velocity field into the droplet field. Therefore entrainment is only possible if there is a wall in the flow, i.e. in channel flow or from the surfaces in pool flows. The surface instability on the film caused by the film-gas relative velocity is the reason for droplets formation and their entrainment.

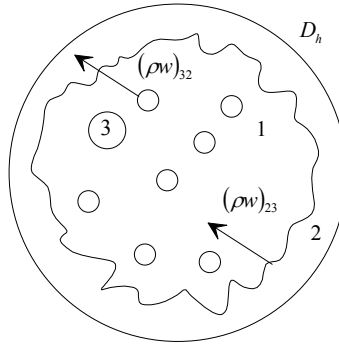


**Fig. 5.1** Annular flow

The entrainment is quantitatively described by models for the following characteristics:

- (1) Identification of the conditions when the entrainment starts;
- (2) The mass leaving the film per unit time and unit interfacial area,  $(\rho w)_{23}$ , or the mass leaving the film and entering the droplet field per unit time and unit mixture volume,  $\mu_{23}$

$$\mu_{23} = a_{12} (\rho w)_{23} \quad (5.1)$$

where  $a_{12}$  is the interfacial area density, i.e. the surface area between gas and film per unit mixture volume;

- (3) Size of the entrained droplets.

Note that there is no general correlation for entrainment and deposition up to now. In what follows we summarize some results presented in the literature for quantitative modeling of these processes.

## 5.2 Some basics

*Taylor*, see Batchelor (1958) or Taylor (1963) obtained the remarkable result for the interface averaged entrainment velocity

$$u_{23} = \text{const} \left( \rho_1 / \rho_2 \right)^{1/2} \Delta V_{12} \lambda_m^* f_m^* \quad (5.2)$$

where  $\lambda_m^*$ , defined by

$$2\pi\lambda_m^* = \lambda_m \rho_1 \Delta V_{12}^2 / \sigma, \quad (5.3)$$

and  $f_m^*$ , defined by

$$2f_m^* = f_m / \left[ \left( \rho_1 / \rho_2 \right)^{1/2} \rho_1 \Delta V_{12}^3 / \sigma \right], \quad (5.4)$$

are the dimensionless wavelength and the frequency of the fastest growing of the unstable surface perturbation waves which are complicated functions of the *Taylor* number based on relative velocity,

$$Ta_{12} = \left( \rho_2 / \rho_1 \right) \left[ \sigma / \left( \eta_2 \Delta V_{12} \right) \right]^2, \quad (5.5)$$

where  $f_m^* \leq \sqrt{3}/9$  and  $0.04 \leq \lambda_m^* f_m^* \leq \sqrt{3}/6$  for  $10^{-5} \leq Ta_{12} \leq 10^4$  and  $\lambda_m^* f_m^* = \sqrt{3}/6$  for  $Ta_{12} > 10^4$ . Comparison with experimental data for engine spray where  $\Delta V_{12} = V_2$ , indicates that  $\frac{1}{2} / (\text{const } \lambda_m^* f_m^*)$  is of order of 7, see *Bracco* (1985). This means

$$u_{23} \approx 14 \left( \rho_1 / \rho_2 \right)^{1/2} \Delta V_{12}. \quad (5.6)$$

Following *Schneider* et al. (1992) and assuming that (a) the surface entrainment velocity is equal to the liquid side surface friction velocity,

$$u_{23} = u_2^{*1\sigma} = \left( \tau_2^{1\sigma} / \rho_2 \right)^{1/2}, \quad (5.7)$$

and (b) the liquid side surface shear stress is equal to the vapor side shear stress due to the gas flow

$$\tau_2^{1\sigma} = c_{12}^d \frac{1}{2} \rho_1 \Delta V_{12}^2, \quad (5.8)$$

we obtain a result

$$u_{23} = \left( \frac{c_{12}^d}{2} \right)^{1/2} (\rho_1 / \rho_2)^{1/2} \Delta V_{12}, \quad (5.9)$$

which is close to *Taylor's* solution.

The internal turbulent pulsation can also cause surface entrainment not influenced by the gas environment directly. Mathematically it can be expressed as

$$u_{23} = u_2^{*1\sigma} + u_2' = \left( c_{12}^d \frac{1}{2} \rho_1 \Delta V_{12}^2 / \rho_2 \right)^{1/2} + cV_2. \quad (5.10)$$

Here the interface averaged fluctuation velocity  $u_2' = cV_2$  is proportional to the jet velocity. The proportionality factor can be of the order of 0.1, see *Faeth* (1995). With the *Braco's* constant this expression results in

$$u_{23} = u_2^{*1\sigma} + u_2' = 14 \left( \frac{\rho_1}{\rho_2} \right)^{1/2} \Delta V_{12} + 0.1 V_2. \quad (5.11)$$

For film flows it was early recognized that the film have to be wavy to pump energy into the crests of the waves,  $Re_{2\delta} = \rho_2 w_2 \delta_2 / \eta_2 > 203$ , *Miles* (1960), and the gas velocity have to exceed some value  $(w_1 \eta_1 / \sigma_2)(\rho_1 / \rho_2)^{1/2} > 2.46 \times 10^{-4}$  *Wallis* (1969), in order to remove the unstable droplets from the film.

### 5.3 Correlations

This Section contains a set of empirical correlation used in the literature for modeling the entrainment mass flow rate.

**The Nigmatulin correlation:** *Nigmatulin* (1982) and *Nigmatulin et al.* (1995) analyzed experimental data for entrainment for non-heated flow in the region  $3 < We_{12} < 10$ ,  $3 \times 10^3 < (Re_{2\delta} = \rho_2 w_2 \delta_2 / \eta_2) < 1.5 \times 10^4$  and  $10 < \rho_2 / \rho_1 < 100$  and for heated flow with  $G = 500$  to  $2000 \text{ kg/(m}^2\text{s)}$ ,  $w_1 = 3$  to  $40 \text{ m/s}$  and  $\dot{q}_{w2}'' = 0.1$  to  $3.6 \text{ MW/m}^2$  and obtained the following

$$\frac{(\rho w)_{23}}{\alpha_2 \rho_2 w_2} = 29 \frac{We_{Zeichik}}{Re_2} \left( \frac{\rho_2}{\rho_1} \right)^{1/2} \left( \frac{\delta_{2F}}{D_h} \right), \quad (5.12)$$

where the shear stress  $\tau_2^{1\sigma}$  in the *Weber* number is computed as given in Chapter 2. The data are reproduced by the *Nigmatulin* correlation with an error of  $\pm 20\%$ .

*Nigmatulin* reported also information about the equilibrium entrained mass fraction of the total liquid mass,  $E_\infty$ , defined as follows

$$1 - E_\infty = 3.1 Y^{-0.2} \quad \text{for } Y \leq 8000 \quad (5.13)$$

$$1 - E_\infty = 1700 Y^{-0.9} \quad \text{for } Y > 8000 \quad (5.14)$$

where

$$Y = c_1 c_2 (\rho_{core} / \rho_2) (\eta_2 / \eta_1)^{0.3} Fr_1 Eo, \quad (5.15)$$

$$Fr_1 = V_1^2 / (g D_h), \quad (5.16)$$

$$Eo = (D_h / \lambda_{RT})^2, \quad (5.17)$$

$$\lambda_{RT} = (\sigma / g \Delta \rho_{21})^{1/2}, \quad (5.18)$$

$$c_1 = \Delta \rho_{21} / \rho_1 \quad \text{for } \Delta \rho_{21} / \rho_1 \leq 10, \quad (5.19)$$

$$c_1 = 1 \quad \text{for } \Delta \rho_{21} / \rho_1 > 10, \quad (5.20)$$

$$c_2 = 0.15 \quad \text{for } Eo^{1/2} \geq 20, \quad (5.21)$$

$$c_2 = 1 \quad \text{for } Eo^{1/2} < 20. \quad (5.22)$$

The data base for this correlation is: (a) air-water,  $p = 0.18$  to  $0.3$  MPa,  $G = 90$  to  $2140$  kg/(m<sup>2</sup>s),  $X_I = 0.08$  to  $0.8$ ,  $V_I = 16$  to  $80$  m/s; (b) steam - water,  $p = 2$  to  $16$  MPa,  $G = 253$  to  $4000$  kg/(m<sup>2</sup>s),  $X_I = 0.08$  to  $0.9$ . This correlation gives the best agreement compared to other correlations existing up to 1995.

**The Zaichik inception model:** *Zaichik* et al. provided in 1998 the following criterion for the inception of the entrainment

$$\frac{We_{Zeichik}}{Re_{2F}} = \frac{1}{4} \frac{\tau_2^{1\sigma} \eta_2}{\sigma_2 \rho_2 w_2} = 2.5 \times 10^{-5} + \frac{6 \times 10^{-4}}{(Re_{2F} - 160)^{0.6}} \quad (5.23)$$

which represents excellent data in the region  $160 < Re_{2F} < 2000$ . Here the interfacial share stress  $\tau_2^{1\sigma}$  is computed using the *Nigmatulin's* model given in Ch. 2.

**The Kataoka and Ishii model:** *Kataoka* and *Ishii* (1982) found that entrainment starts if the following condition is fulfilled

$$Re_{2F} > Re_{2Fc}. \quad (5.24)$$

Then the authors distinguish two entrainment regimes depending on whether the droplet field is under-entrained or over-entrained with respect to the equilibrium condition. The entrained mass fraction of the total liquid mass flow that defines the boundary between these two regimes is defined by the following correlation

$$E_{\infty} = \tanh\left(7.25 \times 10^{-7} We_{Ishii}^{1.25} Re_{23}^{1/4}\right). \quad (5.25)$$

The above correlation for  $E_{\infty}$  was verified with data in the region  $2 \times 10^4 < We_{Ishii}^{1.25} Re_{23}^{1/4} < 8 \times 10^6$ ,  $1 < p < 4 \text{ bar}$ ,  $0.0095 < D_h < 0.032 \text{ m}$ ,  $320 < Re_2 < 6400$ ,  $\alpha_1 V_1 < 100 \text{ m/s}$ . In this region of parameters the maximum value of the dimensionless entrainment  $(\rho w)_{23} D_h / \eta_2$  was  $\approx 20$ . The *under-entrained regime* (entrance section and smooth injection of liquid as a film causing excess liquid in the film compared to the equilibrium condition) is defined by

$$Re_2 > Re_{2\infty}. \quad (5.26)$$

In this regime the entrainment mass flow rate is described by the following correlation which was published in Kataoka and Ishii in 1983

$$(\rho w)_{23} = \frac{\eta_2}{D_h} \left[ \begin{aligned} &0.72 \times 10^{-9} Re_{23}^{1.75} We_{Ishii} (1 - E_{\infty})^{0.25} \left(1 - \frac{E}{E_{\infty}}\right)^2 \\ &+ 6.6 \times 10^{-7} (Re_{23} We_{Ishii})^{0.925} (1 - E)^{0.185} \left(\frac{\eta_1}{\eta_2}\right)^{0.26} \end{aligned} \right]. \quad (5.27)$$

For the *over-entrained regime* (entrainment is caused by shearing-off of roll wave crests by gas core flow) defined by

$$Re_2 \leq Re_{2\infty} \quad (5.28)$$

the entrainment mass flow rate is correlated by Kataoka and Ishii (1983) as follows:

$$(\rho w)_{23} = \frac{\eta_2}{D_h} 6.6 \times 10^{-7} (Re_{23} We_{Ishii})^{0.925} (1 - E)^{0.185} \left(\frac{\eta_1}{\eta_2}\right)^{0.26}. \quad (5.29)$$

Lopez de Bertodano et al. (1998) recommended in 1998 to replace the correlation by Kataoka and Ishii with the following correlation

$$(\rho w)_{23} = \frac{\eta_2}{D_h} \left\{ 4.47 \times 10^{-7} [(Re_{2F} - Re_{2Fc}) We_{Lopez}] \right\}^{0.925} \left(\frac{\eta_1}{\eta_2}\right)^{0.26}. \quad (5.30)$$

This correlation gives the same results as the Kataoka and Ishii correlation for low pressure and relative low mass flow rates but better agreement with the data for high pressure and large gas mass flow rates.

The *diffusion droplet deposition rate* has been investigated by several authors and reliable data are available. The most frequently used in the literature is Paleev and Filipovich's correlation (1966), which is used by Kataoka and Ishii slightly modified

$$(\rho w)_{32} = (\eta_3 / D_h) 0.022 (\eta_1 / \eta_3)^{0.26} (Re_{23} - Re_2)^{0.74} \quad (5.31)$$

for existing droplets, i.e. for  $\alpha_3 > 0.0001$ . The *Kataoka - Ishii* model was based on data in the following region  $277 < Re_{23} < 5041$ ,  $1414 < We_{Ishii} < 9602$ ,  $0.0095 < D_h < 0.032$ .

**The *Whalley et al.* model:** *Whalley et al.* (1974) propose for the entrainment and deposition mass flow rates

$$(\rho w)_{32} = f \rho_{3c}, \quad (5.32)$$

$$(\rho w)_{23} = f \rho_{3c,eq}, \quad (5.33)$$

respectively, where  $\rho_{3c} = \frac{\alpha_3}{\alpha_1 + \alpha_3} \rho_3$  is the homogeneous droplet concentration in  $kg/m^3$  in the vapor core. The deposition coefficient  $f$  is found to be function of particle size, which itself depends on the surface tension and other local parameters. In order to avoid the computation of the particle size *Whalley et al.* plotted  $f$  versus the surface tension and found a dependence that was later correlated by *Katto's* (1984) as given in Table 6.1 in the next Section. Since the amount of deposition is equal to that of entrainment at the equilibrium state, the same " $f$ " is used in Eqs. (5.32) and (5.33). The data collected by *Hutchinson and Whalley* (1973) for the equilibrium droplet concentration  $\rho_{3c,eq}$  are found to be function of the interfacial share stress

$$\tau^* = \tau_{12} \delta_2 / \sigma. \quad (5.34)$$

Here,  $\delta_2$  is the film thickness,  $\sigma$  the surface tension and  $\tau_{12}$  the interfacial stress. with analytical expressions. *Tomiya et al.* (1988) approximated them with

$$\rho_{3c,eq} = 186.349 \tau^{*2} + 0.185919 \tau^* - 0.0171915 \quad \tau^* \leq 0.047 \quad (5.34)$$

$$\rho_{3c,eq} = 96.6903 \tau^{*2} + 10.55840 \tau^* - 0.3097050 \quad 0.047 < \tau^* \leq 0.100 \quad (5.35)$$

$$\rho_{3c,eq} = 51.6429 \tau^{*2} + 27.13020 \tau^* - 1.6586300 \quad 0.100 < \tau^* \leq 0.300 \quad (5.36)$$

$$\rho_{3c,eq} = 145.8329 \tau^{*2.13707} \quad 0.300 < \tau^* \quad (5.37)$$

Note that *Saito et al.* (1978) proposed earlier

$$\begin{aligned} \rho_{3c,eq} = & 2.141 \times 10^4 \tau^{*5} - 8.135 \times 10^3 \tau^{*4} + 8.84 \times 10^2 \tau^{*3} \\ & + 1.925 \times 10 \tau^{*2} - 0.171 \tau^* - 2.65 \times 10^{-4} \quad \tau^* \leq 0.1 \end{aligned}$$

$$\begin{aligned} \rho_{3c,eq} = & 4.681 \times 10 \tau^{*5} - 1.01 \times 10^2 \tau^{*4} + 6.351 \times 10 \tau^{*3} \\ & - 9.901 \times 10 \tau^{*2} + 8.97 \tau^* - 0.376 \quad 0.1 < \tau^* \end{aligned}$$



The interfacial stress is given by the following equations

$$\tau_{12} = \frac{\lambda_{R12}}{8} \rho_{core} j_{core}^2 \quad \text{Wallis (1970)} \quad (5.39)$$

where

$$j_{core} = \alpha_1 w_1 + \alpha_3 w_3 \quad (5.40)$$

is the core (gas + droplet) superficial velocity,

$$\rho_{core} = (\alpha_1 \rho_1 w_1 + \alpha_3 \rho_3 w_3) / j_{core} \quad (5.41)$$

is the core density,

$$\lambda_{R12} = \lambda_{R1} (1 + 360 \delta_2 / D_h) \quad (5.42)$$

is the gas-film friction coefficient,

$$\lambda_{R1} = \begin{cases} 64 / \text{Re}_{core} & \text{Re}_{core} \leq 2000 \\ 0.3164 / \text{Re}_{core}^{1/4} & \text{Re}_{core} > 2000 \end{cases} \quad (5.43)$$

is the friction coefficient computed using the core *Reynolds* number defined as follows

$$\text{Re}_{core} = (\alpha_1 \rho_1 w_1 + \alpha_3 \rho_3 w_3) D_h / \eta_1. \quad (5.44)$$

*Saito et al.* (1978) used for air 310 instead 360 in the equation for the friction coefficient. The film thickness  $\delta_2$  is evaluated with the triangular relationship

$$\left( \frac{dp}{dz} \right)_2 = \frac{4\delta_2}{D_h} \left( \frac{dp}{dz} \right)_{Tph} \quad (5.45)$$

in accordance with *Turner and Wallis* (1965), where

$$\left( \frac{dp}{dz} \right)_{Tph} \approx 4\tau_{12} / D_h \quad (5.46)$$

is the two-phase friction pressure drop per unit length in the core,

$$\left( \frac{dp}{dz} \right)_2 = \frac{1}{2} \rho_2 w_2^2 \lambda_{R2} / D_h \quad (5.47)$$

is the friction pressure drop per unit length in the film. Here the film friction coefficient

$$\lambda_{R2} = \lambda_{R2} (\text{Re}_2, k / D_h) \quad (5.48)$$

is estimated using *Hewitt's* analysis (1961). If three fluid models are used the film thickness is a natural results of the integration of the mass conservation equations for the particular wetted geometry.

**The Sugawara model:** For the range of application  $p = 2.7 \times 10^5$  to  $90 \times 10^5$  Pa and *Reynolds* number  $Re_1 = 3 \times 10^4$  to  $7 \times 10^5$  *Sugawara* (1990) proposes the following entrainment correlation:

$$(\rho w)_{23} = 1.07 \left( \frac{\tau_{12} \delta_{2eq}}{\sigma} \right) \left( \frac{V_1 \eta_2}{\sigma} \right) \left( \frac{\rho_2}{\rho_1} \right)^{0.4}, \quad (5.49)$$

where

$$\delta_{2eq} = k_2 \quad \text{for } Re_1 > 10^5, \quad (5.50)$$

$$\delta_{2eq} = k_2 (2.136 \log_{10} Re_1 - 9.68) \quad \text{for } Re_1 \leq 10^5, \quad (5.51)$$

is the wavelength and

$$k_2 = 0.57 \delta_2 + 21.73 \times 10^3 \delta_2^2 - 38.8 \times 10^6 \delta_2^3 + 55.68 \times 10^9 \delta_2^4 \quad (5.52)$$

is hydrodynamic equivalent wave roughness as obtained by *Wurtz* (1978).

The entrainment correlation was verified in conjunction with the deposition correlation given in Table 6.1 in the next Section. The applicability of this equation is limited in the region pressure:  $p = 1 \times 10^5$  to  $70 \times 10^5$  Pa,  $Re_1 = \frac{V_1 D_h}{\nu_1} = 10^4$  to  $10^6$  and  $\frac{\alpha_3}{\alpha_1 + \alpha_3} \frac{\rho_3}{\rho_1}$  from 0.04 to 10.

**The Ueda model:** *Ueda* (1981) proposed a simple model for the entrainment based on his experiments with air-water and air - alcohol

$$(\rho w)_{23} = 3.54 \cdot 10^{-3} U^{0.57} \quad \text{for } 120 < U < 5000 \quad (5.53)$$

where

$$U = \frac{\tau_{12}}{\sigma_2} \left( \frac{\alpha_2 w_2}{\sigma_2} \right)^{0.6}. \quad (5.54)$$

For  $U < 120$  linear interpolation to  $(\rho w)_{23} = 0$  at  $U = 0$  can be used.

**The Hewitt and Gowan model:** A model was proposed by *Hewitt* and *Govan* (1989). For *entrainment* the authors recommend the *Govan et al.* correlation (1988)

$$(\rho w)_{23} = 0, \quad \text{for } Re_2 < Re_{2\infty} \quad (5.55)$$

$$(\rho w)_{23} = 5.75 \times 10^{-5} \alpha_1 \rho_1 w_1 \left[ (Re_2 - Re_{2\infty})^2 \frac{\eta_2^2}{D_h \sigma} \frac{\rho_2}{\rho_1^2} \right]^{0.316}, \quad (5.56)$$



*Schadel* et al. summarized their data for entrainment by the following correlation

$$(\rho w)_{23} = c_{23} w_1 (\rho_1 \rho_2)^{1/2} \eta_2 (Re_2 - Re_{2\infty}) \quad (5.60)$$

or

$$(\rho w)_{23} = c_{23} \frac{\eta_2}{D_h} \rho_1 w_1 D_h \left( \frac{\rho_2}{\rho_1} \right)^{1/2} (Re_2 - Re_{2\infty}), \quad (5.61)$$

where the coefficient  $c_{23}$  is given in the Table 5.1. Note that this coefficient is not dimensionless. For the deposition the authors recommend the correlation given in Table 6.1. *Schadel* et al. correlations for entrainment and deposition are based on data for air/water vertical flow in the following region:  $0.0254 \leq D_h \leq 0.0572$ ,  $20 < w_1 < 120$  m/s,  $12 < \alpha_2 \rho_2 w_2 < 100$  kg/(m<sup>2</sup>s).

*Tomiyama and Yokomiyo* (1988) found experimentally that behind spacer grids in nuclear reactor cores, the value of  $f$  increases with the increase of the pulsation components of the gas velocity.

Note that all of the entrainment models are proposed with a counterpart deposition model.

At the end a word of conscious: *Kawara* et al. (1998) compared 9 correlations for entrainment obtained by different authors or teams. They found differences of six orders of magnitude at low entrainment ratios and three orders of magnitude at high entrainment ratios.

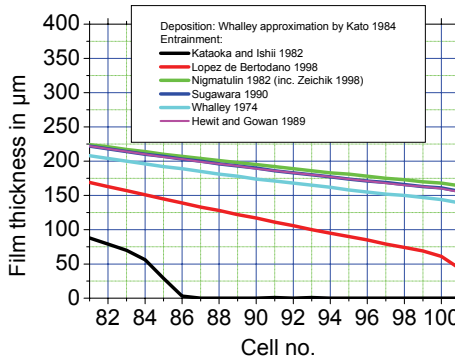


**Fig. 5.2** Film thickness as a function of the distance from the entrance. Boiling water in vertical circular pipe, Bennett et al. (1967): Vertical pipe, 0.01262m inner diameter, 5.5626m length, uniformly heated with 199kW, inlet water flow from the bottom: 68.93bar and 538.90K

The practical implication of this fact is demonstrated by computing the parameters in boiling pipe with boundary conditions reported by *Bennet et al.* (1967) for test nr. 5253. We make 6 computations using one of the entrainment models discussed here. The results regarding the film thickness are presented on Fig. 5.2. Diminishing film thickness causes overheating of the pipe. Such overheating has to be avoided in technical facilities. In the real experiment the dry out of the film occurred at 8/10 of the total pipe length which is the beginning of the x-axis of Fig. 5.2. The largest entrainment, and therefore the closest to the observed result, is predicted by the *Kataoka and Ishii's* correlation.

Therefore a final state of this research field is still not reached.

## 5.4 Entrainment increase in boiling channels

There are two important characteristics of the annular flow in boiling channels. The possibility at specific operating conditions for diminishing of the film may cause increase the wall temperature which for imposed constant heat flux may result to melting of the surface and its failure. This phenomenon, known as burn out or dry out is important for the safety of boiling system.

Boiling films manifest few additional phenomena controlling the film dynamics that are not present in adiabatic films. The steam mass flow generated at the wall surface contributes substantially to the fragmentation of the liquid by two mechanisms: At low film velocity if the bubble departures diameter is larger than the film thickness the bubble burst cause additional entrainment. At high film velocities the bubble departure diameter is small but there is a vapor net flow perpendicular to the wall crossing the film. This may cause additional entrainment. In addition the vapor blows into the gas core and dumps the penetration of the gas pulsation into the boundary layer.

*Milashenko et al.* collected in 1989 data for boiling flow in a 0.0131m inside diameter pipe of 0.15 and 1m heated lengths. Setting the deposition rate  $\mu_{32}$  equal to zero the authors correlated their data for an effective entrainment by the following correlation

$$\mu_{23\_boiling\_film} + \mu_{23\_adiabat} - \mu_{32} = \frac{1.75}{\pi D_h} \alpha_2 \rho_2 w_2 \left( \dot{q}_{w2}'' 10^{-6} \frac{\rho''}{\rho'} \right)^{1.3}, \quad (5.63)$$

indicating a strong dependence on the wall heat flux. Note that the asymptotic value for zero heat flux will produce zero effective entrainment which can not be true. Nevertheless this is the ultimate prove that boiling process influence the effective entrainment. Probably better scaling velocity of the additional to the adia-

batic entrainment is  $w_{1\_blow} = \frac{\mu_{21}}{\rho_1} \frac{D_{heat}}{4}$ , which will be linearly dependent on

$w_{1\_blow} = \dot{q}_{w2}'' / (\rho_1 \Delta h)$  for saturated film. This explains why *Milashenko et al.* (1989) are forced to introduce the constant  $10^{-6}$  being of order of  $1/\Delta h$ . Therefore

$$\mu_{23\_boiling\_film} = f \rho_2 \frac{\mu_{21}}{\rho_1} \frac{D_{heat}}{4}$$

with function  $f < 1$  that remains to be found is probably the better physical basis for data correlation. My own comparison with the Bennett's data for dry out in a pipe indicated that  $f$  is of the order of 0.02. *Kodama and Kataoka* reported in 2002 a dimensional correlation for the net entrainment rate due to the bubble break up with accuracy up to a constant that have to be derived from experiments

$$\begin{aligned} & (\rho w)_{23\_boiling\_film} + (\rho w)_{23\_adiabat} - (\rho w)_{32} \\ &= const \frac{\dot{q}_{w2}''}{\Delta h \rho''} \exp \left[ -\frac{\delta_2 \sqrt{\tau_{2w} / \rho_2}}{158.7 (\eta'' / \eta')^{2.66} 30 w_2} \right]. \end{aligned} \quad (5.62)$$

We see here that the group  $w_{1\_blow} = \dot{q}_{w2}'' / (\rho_1 \Delta h)$  is used correctly but again for adiabatic flow the asymptotic is not correct.

## 5.5 Residual film thickness at DO?

Using correlation for entrainment and deposition gained from adiabatic experiments results obviously to over prediction of the deposition and under prediction of the entrainment. The results of such computations are always predicting some film thickness at places where the wall has to be dry. This lead some authors to introduce some critical film thickness depending on the local parameter as already mentioned in the introduction. Regarding the experimental evidence: At the dry out *Milashenko et al.* experimentally observed in 1989 a residual film mass flow rate of 0.02kg/s. *Adamsson and Anglart* (2004) used in their computational analyses the number  $\delta_{2,crit} = 9 \times 10^{-7} m$  for one rod bundle type and  $\delta_{2,crit} = 7 \times 10^{-5} + 2.86 \times 10^{-7} (G - 360)$  for others. Regarding the dry out film thickness *Groeneveld* [32] 2001 reported that in all of his dry out experiments (more then 30 years experimental research) a complete drying of the film was observed which contradicts to *Milashenko et al.* 1989.

**Conclusion:** The influence of the boiling film on enhancing of the entrainment and suppression of the deposition has to be taken in any case into account. Then the film nucleate boiling has to be exanimate for departure from nucleate boiling (DNB). If there are no local conditions for DNB then the DO requires dry film. This logic allows finite film thickness and boiling crisis simultaneously in cases of DNB.

## 5.6 Entrainment increase due to obstacles

Regarding the influence of the flow obstacles attached to a surfaces on the entrainment *Guguchkin* et al. reported in 1985 "...for smooth surface-buckling the intensity of the entrainment depends on the radius of the buckling, for sharp obstacles - from the blockage ratio. Even small sharp blockages may increase the entrainment several times compared to the same situation for smooth surface...". Systematic experiments are not available.

## 5.7 Size of the entrained droplets

*Kataoka* et al. (1983) correlated the droplet size after the entrainment with a large experimental data base for air-water at low pressure  $p \approx 1.2 \text{ bar}$ :  $10 < Re_2 < 9700$ ,  $2.5 < Re_1 < 17 \times 10^4$ ,  $3 < We_{31} < 20$ . Note that the dimensionless numbers used below

$$Re_1 = \alpha_1 \rho_1 V_1 D_h / \eta_1, \quad (5.66)$$

$$Re_2 = \alpha_2 \rho_2 V_2 D_h / \eta_2, \quad (5.67)$$

and

$$We_{31} = \rho_1 (\alpha_1 V_1)^2 D_{3E} / \sigma, \quad (5.68)$$

are based on superficial velocities. The final correlation for the median particle size in an always observed log-normal distribution is

$$We_{31} = 0.01 Re_1^{2/3} \left( \frac{\rho_1}{\rho_2} \right)^{-1/3} \left( \frac{\eta_1}{\mu_2} \right)^{2/3}, \quad (5.69)$$

with the ratio of the maximum to median size  $D_{3,\max} / D_{3E} = 3.13$ .  $We_{31}$  takes values between 3 and 20 in the considered region and is accurate within  $\pm 40\%$ . In contrast to pool flow, the walls influence the processes in the channel. For this reason the averaged stable droplet diameter in channel flow depends on the hydraulic diameter of the channel,  $D_h$ . Note the difference between the *Kataoka* et al. correlation and the proposed ones by other authors, e.g. the correlation proposed by *Azzopardi* et al. (1980)

$$We_{31} = 1.9 Re_1^{0.1} \left( \frac{\rho_1}{\rho_2} \right)^{0.6} \left( \frac{\rho_1 (\alpha_1 V_1)^2 D_h}{\sigma} \right)^{2/3}, \quad (5.70)$$

or those proposed by *Ueda* (1981)

$$\frac{\rho_1 V_1^2 D_{3E}}{\sigma} = 0.68 \left( \sigma^{0.1} D_h^{-1/4} \right) \frac{\rho_1 V_1 D_h}{\eta_1} \left( \frac{\rho_1 V_1^2 D_h}{\sigma} \right)^{0.4}, \quad (5.71)$$

(not dimensionless) verified in the region  $3000 < \rho_1 V_1 D_h / \eta_1 < 50000$ .

Recently *Ambrosini et al.* (1991) proposed a new correlation for the droplet size in pipes in the presence of film at the wall

$$\frac{D_{3\infty}}{\delta_2} = 22 \left( \frac{\sigma}{\rho_1 c_{12}^d V_1^2 \delta_2} \right)^{0.5} \left( \frac{\rho_1}{\rho_2} \right)^{0.83} \exp \left[ 0.6 \alpha_3 D_h / D_{3\infty} + 99 / \left( \rho_1 V_1^2 D_h / \sigma \right) \right], \quad (5.72)$$

where  $\delta_2$  is the film thickness,  $c_{12}^d$  the gas-film drag coefficient. Here 1 stands for gas, 2 for film and 3 for droplets. The data correlated are in the region  $\alpha_2 \rho_2 V_2 + \alpha_3 \rho_3 V_3 \approx 40$  to  $140 \text{ kg}/(\text{m}^2 \text{s})$ ,  $V_2 \approx 22$  to  $67 \text{ m/s}$ , and the results are in the region of  $D_2 \approx 0.025$  to  $0.2 \text{ mm}$ . Note that Eq. (5.72) attempts to correlate integral results of simultaneously happening fragmentation and coalescence, which - as shown in Section 7.6 - is not correct.

## Nomenclature

### Latin

$a_{12}$	interfacial area density, i.e. the surface area between gas and film per unit mixture volume, $\text{m}^2/\text{m}^3$
$c_{12}^d$	vapor side shear stress coefficient at the liquid surface due to the gas flow, <i>dimensionless</i>
$c_1$	$= \Delta \rho_{21} / \rho_1$
$const$	constant, <i>dimensionless</i>
$D_h$	hydraulic diameter, $m$
$\left( \frac{dp}{dz} \right)_2$	friction pressure drop per unit length in the film, $\text{Pa}/m$
$\left( \frac{dp}{dz} \right)_{Tph}$	two phase friction pressure drop per unit length in the core, $\text{Pa}/m$
$E$	$= \frac{\alpha_3 \rho_3 w_3}{\alpha_2 \rho_2 w_2 + \alpha_3 \rho_3 w_3}$ , mass fraction of the entrained liquid, entrainment, <i>dimensionless</i>
$E_\infty$	equilibrium mass fraction of the entrained liquid, entrainment, equilibrium entrainment, <i>dimensionless</i>



---

$Eo$	$= (D_h / \lambda_{RT})^2$ , <i>Eötvös number, dimensionless</i>
$Fr_1$	$= V_1^2 / (gD_h)$ , <i>gas Froude number, dimensionless</i>
$f$	<i>deposition coefficient, dimensionless</i>
$f_m^*$	<i>frequency of the fastest growing of the unstable surface perturbation waves, dimensionless</i>
$G$	<i>mass flow rate, kg/(m<sup>2</sup>s)</i>
$j_{core}$	$= \alpha_1 w_1 + \alpha_3 w_3$ <i>core (gas + droplet) superficial velocity, m/s</i>
$k_2$	<i>film wavelength, m</i>
$p$	<i>pressure, Pa</i>
$Re_1$	$= \alpha_1 \rho_1  w_1  D_h / \eta_1$ , <i>local gas film Reynolds number based on the hydraulic diameter, dimensionless</i>
$Re_{1, strat}$	$= \frac{\alpha_1 \rho_1  w_1 - w_2  D_h}{\eta_1} \frac{\pi}{\theta + \sin \theta}$ , <i>local gas film Reynolds number based on the gas hydraulic diameter for stratified flow, dimensionless</i>
$Re_2$	$= \alpha_2 \rho_2  w_2  D_h / \eta_2$ , <i>local film Reynolds number based on the hydraulic diameter, dimensionless</i>
$Re_{2\delta}$	$= \rho_2 w_2 \delta_2 / \eta_2$ , <i>local film Reynolds number based on the liquid film thickness, dimensionless</i>
$Re_{2\infty}$	$= Re_{23}(1 - E_\infty)$ , <i>local equilibrium film Reynolds number based on the hydraulic diameter, dimensionless</i>
$Re_{23}$	$= \rho_2 (1 - \alpha_1)  w_{23}  D_h / \eta_2$ , <i>total liquid Reynolds number, dimensionless</i>
$Re_{2F}$	$= \rho_2 w_2 4\delta_{2F} / \eta_2$ , <i>local film Reynolds number, dimensionless</i>
$Re_{2Fc}$	$= 160$ , <i>critical local film Reynolds number, dimensionless</i>
$Re_{core}$	$= (\alpha_1 \rho_1 w_1 + \alpha_3 \rho_3 w_3) D_h / \eta_1$ , <i>core Reynolds number, dimensionless</i>
$Ta_{12}$	$= (\rho_2 / \rho_1) \left[ \sigma / (\eta_2 \Delta V_{12}) \right]^2$ , <i>Taylor number based on relative velocity, dimensionless</i>
$\dot{q}_{w2}''$	<i>heat flux, MW/m<sup>2</sup></i>
$U$	$= \frac{\tau_{12}}{\sigma_2} \left( \frac{\alpha_2 w_2}{\sigma_2} \right)^{0.6}$ , <i>group used in the Ueda correlation</i>
$u_2^{*1\sigma}$	$= (\tau_2^{1\sigma} / \rho_2)^{1/2}$ , <i>liquid side surface friction velocity, m/s</i>
$u_2'$	$= cV_2$ <i>interface averaged fluctuation velocity, m/s</i>
$u_{23}$	<i>interface averaged entrainment velocity, m/s</i>
$V_1$	<i>gas velocity, m/s</i>
$V_2$	<i>jet velocity, continuum liquid velocity, m/s</i>

- $V_{1,wave}$  for gas velocity larger then  $V_{1,wave}$  the horizontal pipe flow is no longer stratified with smooth surface, *m/s*
- $V_{1,stratified}$  for gas velocity larger then  $V_{1,stratified}$  horizontal pipe flow is no longer stratified, *m/s*
- $We_{Ishii} = \frac{\rho_1(\alpha_1 w_1)^2 D_h}{\sigma_2} \left( \frac{\rho_2 - \rho_1}{\rho_1} \right)^{1/3}$ , *Weber number for the Ishii entrainment correlation, dimensionless*
- $We_{Lopez} = \frac{\rho_1 w_1^2 D_h}{\sigma_2} \left( \frac{\rho_2 - \rho_1}{\rho_1} \right)^{1/2}$ , *Weber number for the Lopez et al. correlation, dimensionless*
- $We_{Zeichik} = \frac{\tau_2^{1\sigma} \delta_{2F}}{\sigma_2}$ , *Weber number for the Zeichik et al. correlation, dimensionless*
- $We_{12} = \frac{\rho_1 D_h \Delta V_{12}^2}{\sigma_2}$ , *Weber number, dimensionless*
- $We_{31} = \rho_1 (\alpha_1 V_1)^2 D_{3E} / \sigma$ , *Weber number, dimensionless*
- $w_{23} = \frac{\alpha_2 w_2 + \alpha_3 w_3}{1 - \alpha_1}$ , *center of volume velocity of film and droplet together, m/s*
- $w_1$  axial cross section averaged gas velocity, *m/s*
- $w_2$  axial cross section averaged film velocity, *m/s*
- $w_3$  axial cross section averaged droplets velocity, *m/s*
- $X_l$  gas mass flow divided by the total mass flow, *dimensionless*
- $Y = c_1 c_2 (\rho_{core} / \rho_2) (\eta_2 / \eta_1)^{0.3} Fr_l Eo$

### Greek

- $\alpha_1$  gas volume fraction, *dimensionless*
- $\alpha_2$  film volume fraction, *dimensionless*
- $\alpha_3$  droplets volume fraction, *dimensionless*
- $\Delta V_{12}$  relative velocity, *m/s*
- $\Delta w_{12} = w_1 - w_2$ , *relative velocity, m/s*
- $\delta_{2F} = D_h (1 - \sqrt{1 - \alpha_2}) / 2$ , *film thickness in annular flow, m*
- $\delta_{2eq}$  equilibrium thickness, *m*
- $\eta_1$  gas dynamic viscosity, *kg/(ms)*
- $\eta_2$  liquid dynamic viscosity, *kg/(ms)*
- $\lambda_{R12}$  gas-film friction coefficient, *dimensionless*

---

$\lambda_{R1}$	friction coefficient, <i>dimensionless</i>
$\lambda_{R2}$	$= \lambda_{R2} (Re_2, k / D_h)$ , film friction coefficient, <i>dimensionless</i>
$\lambda_m^*$	wavelength of the fastest growing of the unstable surface perturbation waves, <i>dimensionless</i>
$\lambda_{RT}$	$= (\sigma / g \Delta \rho_{21})^{1/2}$ , Rayleigh-Taylor wavelength, <i>m</i>
$\mu_{23}$	mass leaving the film and entering the droplet field per unit time and unit mixture volume, <i>kg/(m<sup>3</sup>s)</i>
$\rho_1$	gas density, <i>kg/m<sup>3</sup></i>
$\rho_2$	liquid density, <i>kg/m<sup>3</sup></i>
$\rho_{core}$	$= (\alpha_1 \rho_1 w_1 + \alpha_3 \rho_3 w_3) / j_{core}$ , core density, <i>kg/m<sup>3</sup></i>
$\rho_{3c}$	$= \frac{\alpha_3}{\alpha_1 + \alpha_3} \rho_3$ , mass of droplets per unit volume of the gas-droplet mixture assuming equal velocities, <i>kg/m<sup>3</sup></i>
$(\rho w)_{23}$	entrainment mass flow rate, mass leaving the film per unit time and unit interfacial area, <i>kg/(m<sup>2</sup>s)</i>
$(\rho w)_{32}$	deposition mass flow rate, mass leaving the droplet field per unit time and unit interfacial area and deposited into the film, <i>kg/(m<sup>2</sup>s)</i>
$\sigma$	surface tension, <i>N/m</i>
$\tau_2^{1\sigma}$	liquid side surface shear stress
$\tau_{12}$	interfacial stress, <i>N/m<sup>2</sup></i>
$\tau^*$	$= \tau_{12} \delta_2 / \sigma$ , interfacial stress, <i>dimensionless</i>
$\theta$	angle with origin of the pipe axis defined between the upwards oriented vertical and the liquid-gas-wall triple point, <i>rad</i>

## References

- Adamsson C and Anglart H (October 4-8, 2004) Dry out predictions in BWR fuel assemblies with spacers, The 6th International Conference on Nuclear Thermal Hydraulics, Operations and Safety (NUTHOS-6) Nara, Japan, Paper ID. N6P265
- Ambrosini W, Andreussi P, Azzopardi BJ (1991) A physical based correlation for drop size in annular flow, Int. J. Multiphase Flow, vol 17 no 4 pp 497-507
- Azzopardi BJ, Freeman G, King D J (1980) Drop size and deposition in annular two- phase flow, UKAEA Report AERE-R9634
- Batchelor GK (Editor) (1958) Collected works of Taylor GI, Cambridge Univ. Press, Cambridge, MA
- Bennett AW et al. (1967) Heat transfer to steam-water mixtures flowing in uniformly heated tubes in which the critical heat flux has been exceeded, AERE-R5373

- Bracco FV (Feb. 25 - March 1, 1985) Modeling of engine sprays, Proc. International Congress & Exposition Detroit, Michigan, pp 113-136
- Faeth GM (April 3-7 1995) Spray combustion: A review, Proc. of The 2nd International Conference on Multiphase Flow '95 Kyoto, Kyoto, Japan
- Govan AH, Hewitt GF, Owen DG, Bott TR (1988) An improved CHF modelling code, 2nd UK National Heat Transfer Conference, Glasgow
- Groeneveld DC (2001) Private communication
- Guguchkin VV, Nigmatulin BI, Markovich EE, Vasilev NI, Arestenko YuP and Ivanovskaya VI (1985) Peculiarities in droplet movement and bubbles in wall region. Theses of a report presented at VII All-Union Conf. on Two Phase Flow in Power Machines and Apparatus, Leningrad, vol 3 pp 316-317
- Hewitt GF (1961) Analysis of annular two phase, application of the Dukler analysis to vertical upward flow in a tube, AERE-R3680
- Hewitt GF, Govan AH (March 23-24, 1989) Phenomenological modelling of non-equilibrium flows with phase change, Proc. of 7th Eurotherm Seminar Thermal Non-Equilibrium in Two-Phase Flow, Roma, pp 7-27
- Hutchinson P, Whalley PB (1973) Possible characterization on entrainment in annular Flow, Chem. Eng. Sci., vol 28 p 974
- Kataoka I, Ishii M (July 1982) Mechanism and correlation of droplet entrainment and deposition in annular two-phase flow. NUREG/CR-2885, ANL-82-44
- Kataoka I, Ishii M (March 20-24, 1983) Entrainment and deposition rates of droplets in annular two-phase flow, ASME-JSME Thermal Engineering Joint Conference Proceedings, Honolulu, Hawaii, vol 1 pp 69-80, Eds. Yasuo Mori, Wen-Jei Yang
- Kataoka I, Ishii M, Mishima K (June 1983) Transaction of the ASME, vol 5 pp 230-238
- Katto Y (1984) Prediction of critical heat flux for annular flow in tubes taking into account of the critical liquid film thickness concept, Int. J. Heat Mass Transfer, vol 27 no 6 pp 883-890
- Kawara Z, Kataoka I, Serizawa A, Ko YJ and Takahashi O (August 23-28, 1998) Analysis of forced convective CHF based on two-fluid and three-fluid model, Heat Transfer 1998, Proc. Of the 11<sup>th</sup> IHTC, Kyongju, Korea, vol 2 pp 103-108
- Kodama S and Kataoka I (April 14-18, 2002) Study on analytical prediction of forced convective CHF in the wide range of quality, Proceedings of ICONE10, 10TH International Conference on Nuclear Engineering Arlington, VA, USA, Paper nr ICONE1022128
- Lopes JCB, Dukler AE (Sept. 1986) Droplet entrainment in vertical annular flow and its contribution to momentum transfer, AIChE Journal, vol 32 no 9 pp 1500-1515
- Lopez de Bertodano MA, Assad A, Beus S (1998) Entrainment rate of droplets in the ripple-annular regime for small vertical ducts, Third International Conference on Multiphase Flow, ICMF'98, Lyon, France, June 8-12, CD Proceedings
- Milashenko VI, Nigmatulin BI, Petukhov VV and Trubkin NI (1989) Burnout and distribution of liquid in evaporative channels of various lengths. Int. J. Multiphase Flow vol 15 no 3 pp 393-402
- Miles JW (1960) The hydrodynamic stability theory of a thin film in uniform shearing motion, J. of Fluid Mechanics, vol 8 part 4 pp 593-611
- Nigmatulin BI (1982) Heat and mass transfer and force interactions in annular - dispersed two - phase flow, 7-th Int. Heat Transfer Conference Munich, pp 337 - 342

- Nigmatulin BI, Melikhov OI, Khodjaev ID (April 3-7, 1995) Investigation of entrainment in a dispersed-annular gas-liquid flow, Proc. of The 2nd International Conference on Multiphase Flow '95 Kyoto, Japan, vol 3 pp P4-33 to P4-37
- Owen GD, Hewitt GF (1987) An improved annular two-phase flow model, 3rd BHRA Int. Conf. on Multiphase Flow, The Hague
- Paleev II, Filipovich BS (1966) Phenomena of liquid transfer in two-phase dispersed annular flow. Int. J. Heat Mass Transfer, vol 9 p 1089
- Saito T, Hughes ED and Carbon MW (1978) Multi-fluid modeling of annular two-phase flow, Nuclear Engineering and Design vol 50 pp 225-271
- Schadel SA, Leman GW, Binder JL, Hanratty TJ (1990) Rates of atomization and deposition in vertical annular flow, Int. J. Multiphase Flow, vol 16 no 3 pp 363-374
- Schneider JP, Marchiniak MJ, Jones BG (Sept. 21-24, 1992) Breakup of metal jets penetrating a volatile liquid, Proc. of the Fifth Int. Top. Meeting On Reactor Thermal Hydraulics NURETH-5, vol 2 pp 437-449
- Sugawara S (1990) Droplet deposition and entrainment modeling based on the three- fluid model, Nuclear Engineering and Design, vol 122 pp 67-84
- Taylor GI (1963) Generation of ripples by wind blowing over a viscous fluid, in "The scientific papers of Sir Geoffrey Ingham Taylor", Cambridge University Press, vol 3 Ch 25 pp 244-254
- Tomiyama A, Yokomiyo O (February 1988) Spacer - effects on film flow in BWR fuel bundle, J. Nucl.Sc.Techn., Atomic Energy Society of Japan, vol 25, no 2, pp 204-206
- Tomiyama A et al. (Dec. 1988) Method of critical power prediction based on film flow model coupled with subchannel analyses, J. of Nucl. Science and Technology, vol 25 no 12 pp 914-928
- Turner JM, Wallis GB (1965) An analysis of the liquid film annular flow, Dartmouth College, NYO-3114-13
- Ueda T (1981) Two-phase flow - flow and heat transfer, Yokendo, Japan, in Japanese
- Wallis GB (1969) One-dimensional two-phase flow, McGraw-Hill, NY, Sec. 12
- Wallis GB (1970) Annular two-phase flow, Part I, A Simple Theory, J. Basic Eng., vol 92 p 59
- Whalley PB et al. (1974) The calculation of critical heat flux in forced convection boiling, Proc. 5th Int. Heat Transfer Conf., Tokyo, vol 4 pp 290-294
- Wurtz J (1978) An experimental and theoretical investigation of annular steam-water flow in tubes and annuli at 30 to 90bar, RISO report no 372
- Zaichik LI, Nigmatulin BI, Aliphenkov VM (June 1998) Droplet deposition and film atomization in gas-liquid annular flow, Third International Conference on Multiphase Flow, ICMF'98, Lion, France



## 6 Deposition in annular two-phase flow

### 6.1 Introduction

Droplets in the gas core may follow the turbulent gas pulsation depending on their size, Fig. 6.1. Therefore some kind of turbulent diffusion from regions of high droplet concentrations into the region with smaller concentration is possible if the droplets are small enough. The deposition of droplets on the walls is defined as a process of transfer of droplets from the gas bulk flow to the wall leading to increase of the film wall thickness. If the gas core is turbulent there is in any case droplet deposition on the wall.

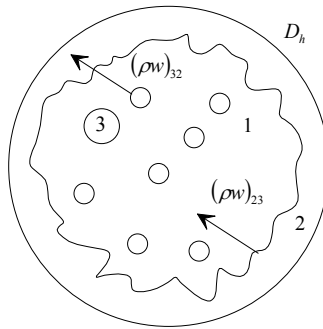


Fig. 6.1 Annular flow

### 6.2 Analogy between heat and mass transfer

Historically there are several empirical attempts in the literature to model this process. Most of the reported methods rely on the analogy between heat and mass transfer. The droplet mass flow rate is defined as a droplet diffusion process

$$(\rho w)_{32} = K_{32} (\rho_{3c} - 0) = K_{32} \rho_{3c} . \quad (6.1)$$

Here  $(\rho w)_{32}$  is the deposition mass flow rate in  $kg/(m^2s)$ .  $K_{32}$  is commonly reported in the literature as a droplet mass transfer coefficient.

$$\rho_{3c} = \frac{\alpha_3}{\alpha_1 + \alpha_3} \rho_3$$

is the mass concentration of droplets in the droplet-gas mixture per unit core volume (droplets + gas), i.e. in  $kg/m^3$ . This quantity is called sometimes in the literature the droplet mass density. The starting point is the well-known *Colburn* correlation for heat transfer in a pipe

$$Nu = \frac{hD_h}{\nu} = 0.023 \left( \frac{VD_h}{\nu} \right)^{0.8} Pr^{1/3}. \quad (6.2)$$

The analogy between heat and mass transfer gives

$$\frac{K_{32}D_h}{D'_3} = 0.023 Re_1^{0.8} \left( \frac{\nu'_1}{D'_3} \right)^{1/3} \quad (6.3)$$

Here

$$Re_1 = \rho_1 V_1 D_h / \eta_1 \quad (6.4)$$

is the gas *Reynolds* number,  $\nu^t$  is cinematic turbulent viscosity of gas and  $D'_3$  is turbulent diffusion constant of the droplets through the gas. Solving with respect to the droplet mass transfer coefficient and dividing by the gas velocity results in

$$\frac{K_{32}}{V_1} = 0.023 Re_1^{-1/5} \left( \frac{\nu'_1}{D'_3} \right)^{-2/3} \frac{\nu'_1}{V_1}. \quad (6.5)$$

Assuming  $K_3 \approx K_1$ ,  $\nu'_1 \approx \nu_1$ ,  $D'_3 \approx D_1$  and  $\nu'_1/D'_3 \approx Pr_1$  (questionable) and substituting in Eq. (6.1) we obtain

$$(\rho w)_{32} = 0.023 V_1 Re_1^{-1/5} Pr_1^{-2/3} \rho_{3c} = K_{32} \rho_{3c}, \quad (6.6)$$

The analogy eliminated the need to estimate the turbulent diffusion constant of the droplets through the gas

$$D'_3 = \frac{1}{3} \ell_3 u'_3, \quad (6.7)$$

which is associated with the estimation of the mean free path  $\ell_3$  in which the droplet changes its direction by colliding with a turbulent eddy and of the droplet pulsation velocity  $u'_3$ . The analogy is also applicable only for very small particles, which follow immediately the gas pulsations. Table 6.1 gives different empirical correlations and the region of validation of each correlation.



## 6.3 Fluctuation mechanism in the boundary layer

### 6.3.1 Basics

Next we consider the fluctuation mechanism in the boundary layer more carefully. Many authors reported that for gas flow with particle loads the particle concentration profiles are flat e.g. Hay et al. (1996). Therefore the concentration in the boundary layer is frequently assumed as equal to the volume averaged local concentration in the pipe. Having in mind that  $\alpha_3/(\alpha_1 + \alpha_3)$  is the volumetric concentration of the particles per unit core volume (gas + droplet), and  $u_3$  is the boundary layer particle velocity in radial direction, the droplet mass deposited into the film per unit surface and unit time is then

$$(\rho w)_{32} = u_3 \rho_3 \alpha_3 / (\alpha_1 + \alpha_3) = u_3 \rho_{3c} . \quad (6.8)$$

The mass entering the film per unit time and unit mixture volume is

$$\mu_{32} = a_{12} (\rho w)_{32} . \quad (6.9)$$

For channels with defined hydraulic diameter,  $D_h$ , the interfacial area density is

$$a_{12} = \frac{4}{D_h} \sqrt{1 - \alpha_2} . \quad (6.10)$$

The relation between the boundary layer particle velocity in radial direction and the local fluctuation particle velocity depends on the distribution of the fluctuation of the particle velocities and on the probability of the rebound from the wall. Zaichik et al. (1998) assumed *Gaussian* distribution and obtained after averaging

$$u_3 = \frac{1 - \chi}{1 + \chi} \sqrt{\frac{2}{\pi}} u'_3 . \quad (6.11)$$

The authors tacked into account also the probability of the particle rebound from the wall  $\chi$  called also *reflection coefficient*. Here  $\chi = 0$  means no rebound,  $\chi = 1$  complete reflection. It is experimentally observed that droplets heating dry walls or thin films remains in the film but if they impact a thick film they rebound. Guguchkin et al. (1985) reported that the droplet velocity has to be larger than 4,7m/s to cause rebound. Alipchenko et al. (2003) made the reflection coefficient  $\chi = 1 - \exp(-3We_{2F})$  a function of the film *Weber* number build with the

sum of the interface share stresses  $We_{2F} = (\tau_{2w} + \tau_{12})\delta_{2F}/\sigma_{21}$ , satisfying the condition  $\chi \rightarrow 0$ ,  $We_{2F} \rightarrow 0$  and  $\chi \rightarrow 1$ ,  $We_{2F} \rightarrow 1$ .

The result obtained by *Hanratty* and *Dykho* (1997)  $u_3 = u'_3/\sqrt{2\pi}$ , corresponds to  $\chi = 1/3$ . The result used by *Matsuura* et al. (1995)  $u_3 = u'_3/4$  corresponds to  $\chi \approx 0.52$ . Therefore in general

$$(\rho w)_{32} = K_{32}\rho_{3c}. \quad (6.12)$$

Thus we see the physical meaning of the deposition mass transfer coefficient

$$K_{32} = K_{32}(u'_3). \quad (6.13)$$

*Matsuura* et al. (1995) assumed that the droplet fluctuation velocity is proportional to the gas fluctuation velocity in the gas boundary layer

$$u'_3 \approx C'_{31}u'_1. \quad (6.14)$$

The missing information in the considerations by *Matsuura* et al. (1995) is the fact that the capability of the droplets to follow the gas turbulent pulsations depends on their size. Usually the capability of the droplets to follow the gas turbulent pulsations is expressed by the particle relaxation time

$$\Delta\tau_{13} = \frac{\rho_3 D_3^2}{18\eta_1\psi(\text{Re}_{13})}. \quad (6.15)$$

For the *Stokes* regime  $\psi(\text{Re}_{13}) = 1$ . For larger velocity differences

$$\psi(\text{Re}_{13}) = 1 + 0.15\text{Re}_{13}^{0.687} \text{ for } \text{Re}_{13} \leq 10^3, \quad (6.16)$$

$$\psi(\text{Re}_{13}) = 0.11\text{Re}_{13}/6 \text{ for } \text{Re}_{13} > 10^3, \quad (6.17)$$

*Zaichik* et al. (1998). Integrating over the time interval  $\Delta\tau$  the simplified particle momentum equation written for the interaction between the continuum eddy and the particle results in

$$C'_{31} := u'_3/u'_1 = 1 - e^{-\Delta\tau/\Delta\tau_{13}}. \quad (6.18)$$

For  $\Delta\tau \ll \Delta\tau_{13}$ ,  $C'_{31} \approx (1 + \Delta\tau_{13}/\Delta\tau)^{-1}$ . The ratio  $C'_{31}$ , called *response coefficient*, characterizes the ability of the particles to response on a pulsation of the continuum. The very small particles quickly response to the gas pulsations. Large particles, if stable, remain unaffected by the gas turbulence.

Combining the information collected so far we obtain the general expression

$$(\rho w)_{32} = \frac{1-\chi}{1+\chi} \sqrt{\frac{2}{\pi}} (1 - e^{-\Delta\tau/\Delta\tau_{13}}) u'_1 \rho_{3c}. \quad (6.19)$$

The time interval  $\Delta\tau$  is the minimum of the life time of the large eddy inside the gas flow

$$\Delta\tau_{le} = 0.37 k_1 / \varepsilon_1 \quad (6.20)$$

and the time between two particle collisions  $\Delta\tau_{33,col}$ . Therefore two regimes of deposition are expected: regime (a) at low particle concentration in which the collisions do not play any role and regime (b) at high particle concentration in which the motion is interrupted by collisions. The droplet-droplet collision time can be approximated by

$$\Delta\tau_{33,col} \approx (D_3 / \Delta V_{33}) / \alpha_3 ,$$

indicating that increasing concentration decrease the collision time and therefore decrease the response coefficient. The product of the response coefficient and the droplet density in the gas-droplet mixture varies little in this region giving deposition mass flow rate almost not depending on the concentration as observed experimentally by *Schadel et al.* (1990) and *Owen and Hewitt* (1987). We own this theoretical explanation to *Hanratty and Dykko* (1997).

Thus, if the gas fluctuation velocity is known, the deposition mass flow rate can be computed.

The data obtained for gas fluctuation velocity normal to the wall in pipes can be also used for flow parallel to a rod bundles due to the systematical experimental observations reported by *Rehme* (1992) p. 572: "...The experimental eddy viscosities normal to the wall are nearly independent on the relative gap width and are comparable to the data of circular tubes by *Reichardt* close to the walls..."

To compute the gas fluctuation velocity two approaches can be used: a) The turbulence of the continuum is modeled by e.g.  $k-\varepsilon$  formalism or similar approaches; b) The steady state velocity distribution for single gas flow is used to compute characteristic fluctuation components in the wall boundary layer. The second approach is widely used in the engineering practice with the disadvantage that transient development of the turbulence characteristics is ignored. Furthermore the local geometry singularities generating additionally turbulence and its decay in the flow can not be correctly taken into account.

### 6.3.2 Deposition to boiling films

Flow boiling in channels, rod bundles etc. is important in the technology. In film flow boiling vapor is generated at the film-wall interface. The vapor creates two phase unstable structure that eventually break up and release the vapor into the gas core flow. Therefore there is an impact on the gas boundary layer close to the interface resembling blowing of gas from the film/gas interface. This phenomenon hinders deposition. Assuming that all generated vapor enters the bulk flow perpendicular to the wall we have for the effective gas velocity

$$u_{1\_blow} = \frac{D_{heat}}{4} \frac{\mu_{21}}{\rho_1}.$$

If  $u_{1\_blow} > u'_1$  the deposition is effectively non existing. If  $u_{1\_blow} < u'_1$  the effective gas fluctuation velocity is reduced to  $u'_1 - u_{1\_blow}$ . Note that for isotropic turbulence the fluctuating velocity components  $u'$  is random deviates of a *Gaussian* probability distribution

$$f(u') = \frac{1}{\sigma_{u'} \sqrt{2\pi}} e^{-\frac{1}{2} \frac{u'^2}{\sigma_{u'}^2}},$$

with zero mean and variance

$$\sigma_{u'}^2 = u'^2 = 2k/3.$$

In this case the statistical average of the difference  $u'_1 - u_{1\_blow}$ ,

$$\int_{u_{1\_blow}}^{\infty} (u'_1 - u_{1\_blow}) f(u'_1) du'_1 = \sigma_{u'} \psi,$$

where

$$\psi = \frac{1}{\sqrt{2\pi}} \exp \left[ -\frac{1}{2} \left( \frac{u_{1\_blow}}{\sigma_{u'}} \right)^2 \right] - \frac{1}{2} \left( \frac{u_{1\_blow}}{\sigma_{u'}} \right) \operatorname{erfc} \left( \frac{u_{1\_blow}}{\sqrt{2} \sigma_{u'}} \right),$$

*Pei* (1981), is of practical importance for describing boiling critical heat flux in bubbly and in dispersed film flows. *Doroschuk and Levitan* (1971), *Guguchkin et al.* (1985) reported data that prove that the vapor blow from the film into the gas bulk reduce deposition. *Doroschuk and Levitan* (1971) derived a condition at which the droplets are not reaching the wall by equalizing the lift force in the boundary layer to the resistance force. *Milashenko et al.* (1989) recommended ignoring the deposition in boiling flows.

### 6.3.3 Steady state boundary layer treatment

*Order of magnitude estimate:* The scale of the averaged velocity fluctuation in a pipe can be evaluated by the cross section averaged kinetic energy of gas turbulence. In analogy to pipe flow we may use the *Chandesris et al.* (2005) results for the equilibrium kinetic energy in the gas  $k_{1,\infty} \approx c_k \bar{w}^2 \operatorname{Re}_1^{-1/6}$ , where  $c_k$  is 0.0306, 0.0367, 0.0368 for channels, pipes and rod bundles respectively. Using  $V'_1 \approx \sqrt{(3/2)k_{1,\infty}}$  we obtain for the non boiling film

$$(\rho w)_{32,adiabat,\infty} \approx \operatorname{const} \left( 1 - e^{-\Delta \tau_{1e}/\Delta \tau_{13}} \right) \bar{w}_1 \operatorname{Re}_1^{-1/12} \rho_{3e},$$

where  $const \approx \frac{1-\chi}{1+\chi} \sqrt{\frac{3}{\pi}} c_k < 0.19$ . In addition, the constant has to reflect also the difference between the averaged gas turbulence and those close to the film interface. Note the ignorable dependence of  $Re_1$ .

*Vames* and *Hanratty* (1988) reviewed turbulent measurements in a pipe including well known measurements of *Laufer's* (1952, 1953) and reported that close to the wall  $r \rightarrow R$  the fluctuation velocity is  $u' \approx 0.9u^*$  the characteristic time scale of turbulent pulsation  $\Delta\tau_e = 0.046 D_h / u^*$  and the eddy diffusivity is  $\nu' = 0.037 u^* D_h$  (note that  $\nu' = u'^2 \Delta\tau_e = 0.0414 u^* D_h$ ). Based on this, *Matsuura* et al. (1995) used in their deposition model the fact that the gas fluctuation velocity in lateral direction is 90% of the gas friction velocity

$$V_1' = 0.9V_1^* . \quad (6.21)$$

The interfacial shear stress  $\tau_{12} = (\lambda_{fr,12}/8) \rho_1 V_1'^2$  and the gas friction velocity at the interface  $V_1^* = \sqrt{\tau_{12}/\rho_1} = V_1' \sqrt{(\lambda_{fr,12}/8)}$ , for turbulent gas boundary layer can be estimated by using the *Blasius* formula  $\lambda_{fr,12} = 0.3164/Re_1^{1/4}$ . Consequently

$$(\rho w)_{32} = const \left(1 - e^{-\Delta\tau_{1e}/\Delta\tau_{13}}\right) \rho_{3c} V_1' Re_1^{-1/8} \quad (6.22)$$

$const \approx \frac{1-\chi}{1+\chi} 0.143 < 0.143$ . Using the *Blasius* formula in case of film flow gives smaller friction coefficient then experimentally observed. From the other site, it is not known how the flexible water interface influences the local fluctuations. *Matsuura* et al. arrived to the following relation

$$(\rho w)_{32} = 0.038 \rho_{3c} V_1' Re_1^{-1/8} , \quad (6.23)$$

which does not show the dependence on the particle size.

The ratio  $K_{32}/V_1^*$  is found to be a function of the dimensionless relaxation time  $\Delta\tau_{13}^+ = \Delta\tau_{13} V_1'^2 / \nu_1 = \Delta\tau_{13} \tau_{12} / \eta_1$  if  $\Delta\tau_{13}^+ < 30$  decreasing to a *Brownian* diffusion coefficient with decreasing relaxation time, *Liu* and *Agarwal* (1974). For  $\Delta\tau_{13}^+ > 30$  the ratio is found to be approximately

$$K_{32}/V_1^* = 0.15 , \text{ Liu and Agarwal (1974).} \quad (6.24)$$

For inclined pipes, the gravitational component contributes also to the sedimentation velocity.

## 6.4 Zaichik's theory

Zaichik et al. (1998) succeeded for the first time to derive expression based on the turbulence fluctuation theory in dispersed flows

$$(\rho w)_{32} = \rho_{3c} V_1^* f. \quad (6.25)$$

Here

$$f = \frac{0.247}{(1 + 0.54 \Delta \tau_{13}^{*1/3}) \left[ 1 + 1.44 \left( \frac{\Delta \tau_{13}^*}{1 + 0.54 \Delta \tau_{13}^{*1/3}} \right)^{1/2} \right]}, \quad (6.26)$$

$$\Delta \tau_{13}^* = \Delta \tau_{13} \frac{D_3}{2} / V^*. \quad (6.27)$$

Substituting the *Blasius* expression for the gas friction velocity into the *Zaichik* formula results in

$$(\rho w)_{32} = 0.2 \rho_{3c} V_1 \text{Re}_1^{-1/8} f. \quad (6.28)$$

## 6.5 Deposition correlations

Comparing with the correlation in Table 6.1 we see that *Nigmatulin* properly correlate in 1982 the data by using  $(\rho w)_{32} \propto \alpha_3 \rho_3 V_1 \text{Re}_1^{-1/8}$ . The *Paleev* and *Filipovich* correlation contains the dependence  $(\rho w)_{32} \propto (\alpha_3 \rho_3 w_3)^{3/4}$  which is close to the theoretical one but does not have the slight dependence on the *Reynolds* number and on the particle size explicitly. The *Lopes* and *Dukler* correlation from 1986 possesses the proper dependence  $(\rho w)_{32} \propto V_1^*$  by taking into account the dependence on the particle size.

**Table 6.1.** Deposition correlations

*Paleev* and *Filipovich* (1966):

$$(\rho w)_{32} = 0.022 \rho_1 V_1 \text{Re}_1^{-1/4} \left( \frac{\alpha_3 \rho_3}{\alpha_1 \rho_1} \right)^{0.74}$$

validated for air - water mixture at  $p \approx 10^5 \text{ Pa}$ ,  $0.1 < \alpha_3 \rho_3 < 1.3$   $3 \times 10^4 < \text{Re}_1 < 8.5 \times 10^4$ . Sometimes Zaichik et al. (1998) this correlation is used in slightly modified form

$$(\rho w)_{32} = \frac{\eta_3}{D_h} 0.022 \left( \frac{\eta_1}{\eta_3} \right)^{1/4} \left( \frac{\alpha_3 \rho_3 w_3 D_h}{\eta_3} \right)^{3/4}.$$

The authors proposed in the same work a correlation for the splitting of the liquid:

$$E_\infty = 0.985 - 0.44 \log_{10} \left[ 10^4 \frac{\alpha_1 \rho_1 w_1 + \alpha_3 \rho_3 w_3}{\rho_2 \alpha_1 \rho_1 w_1} \left( \frac{\eta_2 w_1}{\sigma} \right)^2 \right],$$

$$\text{valid in } 1 \leq 10^4 \frac{\alpha_1 \rho_1 w_1 + \alpha_3 \rho_3 w_3}{\rho_2 \alpha_1 \rho_1 w_1} \left( \frac{\eta_2 w_1}{\sigma} \right)^2 \leq 1000.$$

*Sugawara* (1990):

$$(\rho w)_{32} = 0.009 \text{Pr}_1^{-2/3} V_1 \text{Re}_1^{-1/5} \left( \frac{\rho_{3c}}{\rho_1} \right)^{-0.5} \rho_{3c}$$

validated for steam - water flows in the region  $1 \times 10^5 < p < 70 \times 10^5$  Pa,  $0.04 < \frac{\rho_{3c}}{\rho_1} < 10$ ,  $10^4 < \text{Re}_1 < 10^6$ .

*Nigmatulin* (1982):

$$\frac{(\rho w)_{32}}{\alpha_3 \rho_3 V_3} = 0.008 \text{Re}_1^{-0.12} \left( \frac{\alpha_1}{\alpha_1 + \alpha_3} \right)^{-0.16} f$$

where

$$f = \sigma^* \text{ for } \sigma^* > 1,$$

$$f = \sigma^{*1/2} \text{ for } \sigma^* \leq 1,$$

$$\sigma^* = 0.16 \frac{\sigma}{V_1 \sqrt{\eta_1 \eta_2}} \left( \frac{\rho_1}{\rho_2} \right)^{1/4}.$$

Validated for  $p = (10 \text{ to } 100) \times 10^5$  Pa,  $D_h = 0.013$  m,  $0.2 \leq \sigma^* \leq 10$ ,  $0.01 \leq \rho_1 / \rho_2 \leq 0.1$ ,  $10^4 < \text{Re}_1 < 10^5$ . Error for  $(\rho w)_{32} / \alpha_3 \rho_3 V_3$ : +35%, -40%

*Katto* (1984):

$$(\rho w)_{32} = 0.405 \sigma^{0.915} \rho_{3c} \text{ for } \sigma < 0.0383$$

$$(\rho w)_{32} = 9.480 \times 10^4 \sigma^{4.7} \rho_{3c} \text{ for } \sigma \geq 0.0383$$

*Owen and Hewitt* (1987):

$$(\rho w)_{32} = \frac{0.18}{\sqrt{\frac{\rho_1 D_h}{\sigma}}} \rho_{3c}, \text{ for } \frac{\rho_{3c}}{\rho_1} < 0.3$$

$$(\rho w)_{32} = \frac{0.083}{\sqrt{\frac{\rho_1 D_h}{\sigma}}} \left( \frac{\rho_{3c}}{\rho_1} \right)^{-0.65} \rho_{3c} \text{ for } \rho_{3c} \geq 0.3$$

validated for air-genkane, fluorheptane, air-water, steam-water, and  $p < 110 \times 10^5$  Pa.

*Lopes and Dukler (1986):*

$$(\rho w)_{32} = K_3 \rho_{3c} V_1^*$$

where

$$V_1^* = \sqrt{\tau_{12} / \rho_1}$$

is the friction velocity,

$$\tau_{12} = \frac{1}{2} \frac{c_{12}^d}{4} \rho_1 (V_1 - V_{2i})^2$$

is the interfacial shear stress

$$c_{12}^d = (3.331 \ln \text{Re}_1 - 33.582)^{-2} \text{ for } 4 \times 10^4 < \text{Re}_1 < 8.5 \times 10^4$$

and

$$c_{12}^d = 0.056 \text{ for } 8.5 \times 10^4 < \text{Re}_1 < 12 \times 10^4,$$

is the approximation of the data of *Lopes and Dukler* for the friction coefficient,

$$\text{Re}_1 = \rho_1 (V_1 - V_{2i}) D_{hc} / \eta_1$$

is the gas Reynolds number and

$$D_{hc} = D_h \sqrt{1 - \alpha_2}$$

is the gas core diameter. The experimental data for the modified mass transfer coefficient  $K_3$  are a unique function of the dimensionless particle relaxation time

$$\tau^+ = \frac{1}{18} \frac{\rho_3}{\rho_1} \left( \frac{\rho_1 V_1^* D_3}{\eta_1} \right)^2$$

in the range  $10^{-2} < \tau^+ < 10^6$  the data are represented by

$$K_3 = 2 \times 10^{-5} \text{ for } \tau^+ < 0.2 \text{ (Brownian diffusion),}$$



$$K_3 = 4.93 \times 10^{-4} (\tau^+)^{1.99} \text{ for } 0.2 < \tau^+ < 25,$$

$$K_3 = 0.3 \text{ for } 25 < \tau^+.$$

Schadel et al. (1990)

$$(\rho w)_{32} = \frac{0.034}{D_h^{0.6}} \frac{\alpha_3 \rho_3 V_3}{\alpha_1 V_1} \text{ for } \frac{\alpha_3 \rho_3 V_3}{\alpha_1 V_1} < \frac{0.078}{D_h^{0.6}}$$

$$(\rho w)_{32} = \frac{0.021}{D_h^{0.6}} \text{ for } \frac{\alpha_3 \rho_3 V_3}{\alpha_1 V_1} \geq \frac{0.078}{D_h^{0.6}}$$

$0.0254 < D_h < 0.05715 \text{ m}$ ,  $19.5 < V_l < 115 \text{ m/s}$ , vertical air / water flow.

At the end a word of conscious: *Kawara* et al. (1998) compared 11 depositions coefficients obtained by different authors or teams. They found differences up to two orders of magnitude depending on the local droplet concentration. Therefore a final state of this research field is still not reached.

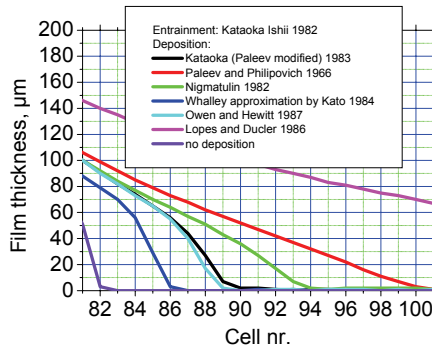


**Fig. 6.2** Film thickness as a function of the distance from the entrance. Boiling water in vertical circular pipe, Bennett et al. (1967): Vertical pipe, 0.01262m inner diameter, 5.5626m length, uniformly heated with 199kW, inlet water flow from the bottom: 68.93bar and 538.90K

The practical implication of this fact is demonstrated by computing the parameters in boiling pipe with boundary conditions reported by *Bennet* et al. (1967) for test nr. 5253. We make 7 computations using one of the deposition models discussed here. The results regarding the film thickness are presented on Fig. 6.2. Diminishing film thickness causes overheating of the pipe. Such overheating has to be avoided in technical facilities. In the real experiment the dry out of the film occurred at 8/10 of the total pipe length which is the beginning of the x-axis of Fig. 6.2. The smallest deposition, and therefore the closest to the observed result, is predicted by the *Kato*'s correlation. Note that we do not take into account the deposition suppression due to boiling of the film as discussed in Ch. 6.3.2 which is

obviously important. Repeating the computation with virtually no deposition gives the best results. Note that *Hoyer* and *Stepniewski* reported already in 1999 that deposition suppression due to boiling is important for dry out prediction at high void fractions boiling flows.

## 6.6 Leidenfrost heat transfer to droplet bouncing hot wall

In many technological facilities the droplets carried by the steam can influence the cooling of the very hot surfaces. Conceptually it happens in the situation where the conditions for the entrainment are better then the conditions for deposition. In this case there is no net film thickness but there is effective contact of the droplet with the wall over the time  $\Delta\tau_{3w} = \pi\sqrt{\rho_3 D_3^3 / (16\sigma_3)}$ , *Bolle* and *Moureau* (1986). The same authors reported that the base diameter change over this period following  $(D_{w3}/D_3)^2 = 6.97(\tau - \tau^2)$ . Assuming that the pressure difference in the film thickness is controlled by the momentum of the impinging droplet and the heat conduction through the vapor film is the limiting heat transferred mechanism *Guo* and *Mishima* (2002) derived an expression for the averaged heat flux over single droplet impact:

$$q_{\text{wall to single droplet}} = \frac{\pi}{4} \lambda_1 (T_w - T') \Delta\tau_{3w} D_3^2 \left[ \frac{32}{9} \frac{\rho_1 \rho_3 [\Delta h + c_{p1} (T_1 - T')]}{\eta_1 \lambda_1 (T_w - T') \Delta\tau_{3w} D_3} u_{3w} \right]^{1/4}.$$

The averaged heat flux due to droplet-wall contact is therefore

$$\dot{q}_{w3}'' = \frac{(\rho w)_{32}}{\rho_3 \pi D_3^3 / 6} q_{\text{wall to single droplet}}.$$

The impinging velocity can be approximated by  $u_{3w} \approx (\rho w)_{32} / (\alpha_3 \rho_3)$ . The cooling of the hot wall in this case is done by the direct heat transfer from the wall to the gas and by the wall-droplet heat transfer  $\dot{q}_{w3}''$ . The later is very important especially for low mass flows and low pressures, *Guo* and *Mishima* (2002). At high wall temperatures the radiation heat transfer has also to be taken into account.

## Nomenclature

### Latin

$a_{12}$  interfacial area density, i.e. the surface area between gas and film per unit mixture volume,  $m^2/m^3$

---

$c_{12}^d$	vapor side shear stress coefficient at the liquid surface due to the gas flow, <i>dimensionless</i>
$c_1$	$= \Delta\rho_{21} / \rho_1$
$const$	constant, <i>dimensionless</i>
$D_h$	hydraulic diameter, <i>m</i>
$\left(\frac{dp}{dz}\right)_2$	friction pressure drop per unit length in the film, <i>Pa/m</i>
$\left(\frac{dp}{dz}\right)_{Tph}$	two-phase friction pressure drop per unit length in the core, <i>Pa/m</i>
$E$	$= \frac{\alpha_3 \rho_3 w_3}{\alpha_2 \rho_2 w_2 + \alpha_3 \rho_3 w_3}$ , mass fraction of the entrained liquid, entrainment, <i>dimensionless</i>
$E_\infty$	equilibrium mass fraction of the entrained liquid, entrainment, equilibrium entrainment, <i>dimensionless</i>
$Eu$	$= (D_h / \lambda_{RT})^2$ , <i>Eötvös</i> number, <i>dimensionless</i>
$Fr_1$	$= V_1^2 / (g D_h)$ , gas <i>Froude</i> number, <i>dimensionless</i>
$f$	deposition coefficient, <i>dimensionless</i>
$f_m^*$	frequency of the fastest growing of the unstable surface perturbation waves, <i>dimensionless</i>
$G$	mass flow rate, <i>kg/(m<sup>2</sup>s)</i>
$j_{core}$	$= \alpha_1 w_1 + \alpha_3 w_3$ core (gas + droplet) superficial velocity, <i>m/s</i>
$k_2$	film wavelength, <i>m</i>
$p$	pressure, <i>Pa</i>
$Re_1$	$= \alpha_1 \rho_1  w_1  D_h / \eta_1$ , local gas film <i>Reynolds</i> number based on the hydraulic diameter, <i>dimensionless</i>
$Re_{1, strat}$	$= \frac{\alpha_1 \rho_1  w_1 - w_2  D_h}{\eta_1} \frac{\pi}{\theta + \sin \theta}$ , local gas film <i>Reynolds</i> number based on the gas hydraulic diameter for stratified flow, <i>dimensionless</i>
$Re_2$	$= \alpha_2 \rho_2  w_2  D_h / \eta_2$ , local film <i>Reynolds</i> number based on the hydraulic diameter, <i>dimensionless</i>
$Re_{2\delta}$	$= \rho_2 w_2 \delta_2 / \eta_2$ , local film <i>Reynolds</i> number based on the liquid film thickness, <i>dimensionless</i>
$Re_{2\infty}$	$= Re_{23}(1 - E_\infty)$ , local equilibrium film <i>Reynolds</i> number based on the hydraulic diameter, <i>dimensionless</i>
$Re_{23}$	$= \rho_2 (1 - \alpha_1)  w_{23}  D_h / \eta_2$ , total liquid <i>Reynolds</i> number, <i>dimensionless</i>
$Re_{2F}$	$= \rho_2 w_2 4\delta_{2F} / \eta_2$ , local film <i>Reynolds</i> number, <i>dimensionless</i>
$Re_{2Fc}$	$= 160$ , critical local film <i>Reynolds</i> number, <i>dimensionless</i>

- $Re_{core} = (\alpha_1 \rho_1 w_1 + \alpha_3 \rho_3 w_3) D_h / \eta_1$ , core *Reynolds* number, *dimensionless*  
 $Ta_{12} = (\rho_2 / \rho_1) \left[ \sigma / (\eta_2 \Delta V_{12}) \right]^2$ , *Taylor* number based on relative velocity, *dimensionless*  
 $\dot{q}_{w2}''$  heat flux,  $MW/m^2$   
 $U = \frac{\tau_{12}}{\sigma_2} \left( \frac{\alpha_2 w_2}{\sigma_2} \right)^{0.6}$ , group used in the *Ueda* correlation  
 $u_2^{*1\sigma} = (\tau_2^{1\sigma} / \rho_2)^{1/2}$ , liquid side surface friction velocity,  $m/s$   
 $u_2'$  =  $cV_2$  interface averaged fluctuation velocity,  $m/s$   
 $u_{23}$  interface averaged entrainment velocity,  $m/s$   
 $V_1$  gas velocity,  $m/s$   
 $V_2$  jet velocity, continuum liquid velocity,  $m/s$   
 $V_{1,wave}$  for gas velocity larger then  $V_{1,wave}$  the horizontal pipe flow is no longer stratified with smooth surface,  $m/s$   
 $V_{1,stratified}$  for gas velocity larger then  $V_{1,wave}$  horizontal pipe flow is no longer stratified,  $m/s$   
 $We_{Ishii} = \frac{\rho_1 (\alpha_1 w_1)^2 D_h}{\sigma_2} \left( \frac{\rho_2 - \rho_1}{\rho_1} \right)^{1/3}$ , *Weber* number for the *Ishii* entrainment correlation, *dimensionless*  
 $We_{Lopez} = \frac{\rho_1 w_1^2 D_h}{\sigma_2} \left( \frac{\rho_2 - \rho_1}{\rho_1} \right)^{1/2}$ , *Weber* number for the *Lopez* et al. correlation, *dimensionless*  
 $We_{Zeichik} = \frac{\tau_2^{1\sigma} \delta_{2F}}{\sigma_2}$ , *Weber* number for the *Zeichik* et al. correlation, *dimensionless*  
 $We_{12} = \frac{\rho_1 D_h \Delta V_{12}^2}{\sigma_2}$ , *Weber* number, *dimensionless*  
 $w_{23} = \frac{\alpha_2 w_2 + \alpha_3 w_3}{1 - \alpha_1}$ , center of volume velocity of film and droplet together,  $m/s$   
 $w_1$  axial cross section averaged gas velocity,  $m/s$   
 $w_2$  axial cross section averaged film velocity,  $m/s$   
 $w_3$  axial cross section averaged droplets velocity,  $m/s$   
 $X_I$  gas mass flow derived by the total mass flow, *dimensionless*  
 $Y = c_1 c_2 (\rho_{core} / \rho_2) (\eta_2 / \eta_1)^{0.3} Fr_1 Eo$

**Greek**

$\alpha_1$	gas volume fraction, <i>dimensionless</i>
$\alpha_2$	film volume fraction, <i>dimensionless</i>
$\alpha_3$	droplets volume fraction, <i>dimensionless</i>
$\Delta V_{12}$	relative velocity, <i>m/s</i>
$\Delta w_{12}$	$= w_1 - w_2$ , relative velocity, <i>m/s</i>
$\delta_{2F}$	$= D_h(1 - \sqrt{1 - \alpha_2})/2$ , film thickness in annular flow, <i>m</i>
$\delta_{2eq}$	equilibrium thickness, <i>m</i>
$\eta_1$	gas dynamic viscosity, <i>kg/(ms)</i>
$\eta_2$	liquid dynamic viscosity, <i>kg/(ms)</i>
$\lambda_{R12}$	gas-film friction coefficient, <i>dimensionless</i>
$\lambda_{R1}$	friction coefficient, <i>dimensionless</i>
$\lambda_{R2}$	$= \lambda_{R2}(Re_2, k/D_h)$ , film friction coefficient, <i>dimensionless</i>
$\lambda_m^*$	wavelength of the fastest growing of the unstable surface perturbation waves, <i>dimensionless</i>
$\lambda_{RT}$	$= (\sigma/g\Delta\rho_{21})^{1/2}$ , Rayleigh-Taylor wavelength, <i>m</i>
$\mu_{23}$	mass leaving the film and entering the droplet field per unit time and unit mixture volume, <i>kg/(m<sup>3</sup>s)</i>
$\rho_1$	gas density, <i>kg/m<sup>3</sup></i>
$\rho_2$	liquid density, <i>kg/m<sup>3</sup></i>
$\rho_{core}$	$= (\alpha_1\rho_1w_1 + \alpha_3\rho_3w_3)/j_{core}$ , core density, <i>kg/m<sup>3</sup></i>
$\rho_{3c}$	$= \frac{\alpha_3}{\alpha_1 + \alpha_3} \rho_3$ , mass of droplets per unit volume of the gas-droplet mixture assuming equal velocities, <i>kg/m<sup>3</sup></i>
$(\rho w)_{23}$	entrainment mass flow rate, mass leaving the film per unit time and unit interfacial area, <i>kg/(m<sup>2</sup>s)</i>
$(\rho w)_{32}$	deposition mass flow rate, mass leaving the droplet field per unit time and unit interfacial area and deposited into the film, <i>kg/(m<sup>2</sup>s)</i>
$\sigma$	surface tension, <i>N/m</i>
$\tau_2^{1\sigma}$	liquid side surface shear stress
$\tau_{12}$	interfacial stress, <i>N/m<sup>2</sup></i>
$\tau^*$	$= \tau_{12}\delta_2/\sigma$ , interfacial stress, <i>dimensionless</i>
$\theta$	angle with origin of the pipe axis defined between the upwards oriented vertical and the liquid-gas-wall triple point, <i>rad</i>

## References

- Alipchenko VM, Stonik OG, Zaichik LI, Antipin VA, Charlamov SM, Markovich DM, Mrlikhov OI, Nigmatulin RI, Soloviev SL (Oct. 5-9, 2003) Dry out prediction in bundle geometry, 10<sup>th</sup> Int. Top. Meeting on Nuclear Reactor Thermal Hydraulics (NURETH-10), Seoul, Korea
- Bennett AW et al. (1967) Heat transfer to steam-water mixtures flowing in uniformly heated tubes in which the critical heat flux has been exceeded, AERE-R5373
- Bolle L and Moureau JC (1986) Spray cooling at hot surface, in Hewitt JM, Delhay JM and Zuber N eds., Multiphase science and technology, Hemisphere Publishing, Washington, DC, vol 1
- Chandesris M, Serre G and Sagaut (2005) A macroscopic turbulence model for flow in porous media suited for channel, pipe and rod bundle flows, 4<sup>th</sup> Int. Conf. On Computational Heat and Mass Transfer, Paris
- Doroshuk VE and Levitan LL (1971) Investigation of droplet deposition from annular dispersed steam-water flow core a wall liquid film, Therm. Phys. High Temp., vol 9 pp 591-596
- Guguchkin VV, Nigmatulin BI, Markovich EE, Vasilev NI, Arestenko YuP and Ivanovskaya VI (1985) Peculiarities in droplet movement and bubbles in wall region. Theses of a report presented at VII All-Union Conf. on Two Phase Flow in Power Machines and Apparatus, Leningrad, vol 3 pp 316-317
- Guo Y and Mishima K (2002) A non-equilibrium mechanistic heat transfer model for post-dryout dispersed flow regime, Experimental Thermal and Fluid Science, vol 26 pp 861-869
- Hanratty TJ and Dykko LA (1997) Physical issues in analyzing gas-liquid annular flows, Experimental Heat Transfer, Fluid Mechanics and Thermodynamics, Eds.: Giot M, Mayinger F and Celata GP, pp 1127-1136
- Hay KJ, Liu ZC and Hanratty TJ (1996) Relation of deposition rates to drop size at large concentrations, Int. J. Multiphase Flow, vol 22 pp 829-848
- Hoyer N and Stepniewski M (Oct. 3-8, 1999) Dry out prediction in bundle geometry, 9<sup>th</sup> Int. Top. Meeting on Nuclear Reactor Thermal Hydraulics (NURETH-9), San Francisco, California
- Katto Y (1984) Prediction of critical heat flux for annular flow in tubes taking into account of the critical liquid film thickness concept, Int. J. Heat Mass Transfer, vol 27 no 6 pp 883-890
- Kawara Z, Kataoka I, Serizawa A, Ko YJ and Takahashi O (August 23-28, 1998) Analysis of forced convective CHF based on two-fluid and three-fluid model, Heat Transfer 1998, Proc. Of the 11<sup>th</sup> IHTC, Kyongju, Korea, vol 2 pp 103-108
- Laufer J (1952) Investigation of turbulent flow in a two-dimensional channel, NACA Report 1053
- Laufer J (1953) The structure of turbulence in fully developed pipe flow, NACA Report 1273
- Liu BYH and Agarwal JK (1974) Experimental observation of aerosol deposition in turbulent flow, in Aerosol Science, vol5, Pergamon Press, GB
- Lopes JCB and Ducler AE (Sept. 1986) Droplet entrainment in vertical annular flow and its contribution to momentum transfer, AIChE Journal, vol 32 no 9 pp 1500-1515
- Matsuura K, Kataoka I and Serizawa A (April 23-27, 1995) Prediction of droplet deposition rate based on Lagrangian simulation of droplet behavior, Proc. Of the 3<sup>rd</sup> JSME/ASME Joint International Conference on Nuclear Engineering, Kyoto, Japan, vol 1 pp 105-109

- 
- Milashenko VI, Nigmatulin BI, Petukhov VV and Trubkin NI (1989) Burnout and distribution of liquid in evaporative channels of various lengths. *Int. J. Multiphase Flow* vol 15 no 3 pp 393-402
- Nigmatulin BI (1982) Heat and mass transfer and force interactions in annular - dispersed two - phase flow, 7-th Int. Heat Transfer Conference Munich, pp 337 - 342
- Owen GD and Hewitt GF (1987) An improved annular two-phase flow model, 3rd BHRA Int. Conf. on Multiphase Flow, The Hague
- Paleev II and Filipovich BS (1966) Phenomena of liquid transfer in two-phase dispersed annular flow, *Int. J. Heat Mass Transfer*, vol 9 p 1089
- Pei BS (1981) Prediction of critical heat flux in flow boiling at low quality, PhD Thesis, University of Cincinnati, Cincinnati, Ohio
- Rehme K (1992) The structure of turbulence in rod bundles and the implications on natural mixing between the subchannels, *Int. J. Heat Mass Transfer*, vol 35 no 2 pp 567-581
- Schadel SA, Leman GW, Binder JL, and Hanratty TJ (1990) Rates of atomization and deposition in vertical annular flow, *Int. J. Multiphase Flow*, vol 16 no 3 pp 363-374
- Sugawara S (1990) Droplet deposition and entrainment modeling based on the three- fluid model, *Nuclear Engineering and Design*, vol 122 pp 67-84
- Vames JS and Hanratty TJ (1988) Turbulent dispersion of droplets for air flow in a pipes, *Experiments Fluids* vol 6 pp 94-104
- Zaichik LI, Nigmatulin BI and Alipchenko VM (June 8-12, 1998) Droplet deposition and film atomization in gas-liquid annular flow, Third International Conference on Multiphase Flow, ICMF'98, Lyon, France, CD Proceedings





## 7 Introduction to fragmentation and coalescence

### 7.1 Introduction

As already mentioned in Section 1.1, transient multiphase flows with temporal and spatial variation of the volumetric fractions of the participating phases can be represented by *sequences* of geometrical *flow patterns* that have some characteristic length scale. Owing to the highly random behavior of the flow in detail, the number of flow patterns needed for this purpose is very large. Nevertheless, this approach has led to many successful applications in the field of multiphase flow modeling. Frequently modern mathematical models of *transient flows* include, among others, the following features:

1. Postulation of a limited number of idealized flow patterns, with transition limits as a function of local parameters for *steady state* flow (e.g., see Fig. 1.1);
2. Identification of one of the postulated idealized *steady state* flow patterns for each time;
3. Computation of a characteristic *steady state length scale of the flow patterns* (e.g., bubble or droplet size) in order to address further constitutive relationships for interfacial heat, mass, and momentum transfer.

A steady state length scale should not be used for highly transient processes. *Mechanical disintegration* of fluid occurs in the flow over a *finite time*. In many transient processes, the characteristic time constant may be comparable with the time scale of the macroscopic process under consideration. There is a class of multi-phase flows for which the prediction of the transient flow pattern length scale is crucial. An example is the mathematical description of the interaction between molten metal and water or between a cold liquid and a hot liquid that is at a temperature much higher than the saturation temperature of the cold liquid. The mathematical description of violent explosions that occur during such interactions is possible only if the *dynamic fragmentation and coalescence* modeling corresponds to the real physics. Thus there is a need to model the continuous fragmentation and coalescence dynamics for multi-phase flows. Moreover, an adequate theory to predict the length scale of the flow structure should automatically provide information for the flow pattern identification. As already mentioned the opposite is the widespread practice today.

A possible formalism to model dynamic fragmentation and coalescence is the following. Describe multi-phase flows by means of three mutually interacting velocity fields, three abstract fluids having their own temperature and velocity.

Define the correspondence between the abstract fluids and the real physical world: (1) the first fluid,  $l = 1$ , as a gas; (2) the second fluid,  $l = 2$ , as a liquid; and (3) the third fluid,  $l = 3$ , as another liquid. Write the local volume and time average mass conservation equation for each velocity field – compare with Eq. (1.62) in Vol.1,

$$\frac{\partial}{\partial \tau}(\alpha_l \rho_l) + \nabla \cdot (\alpha_l \rho_l \mathbf{V}_l) = \mu_l. \quad (7.1)$$

Here  $\alpha_l$  is the averaged volumetric fraction,  $\rho_l$  is the density,  $\mathbf{V}_l$  is the velocity vector and  $\mu_l$  is the mass source density. Define the particle number density  $n_l$  as a volume-averaged number of discrete particles of the fluid  $l$  (e.g., bubbles or droplets) per unit flow volume, and write the local volume and time-averaged conservation equation for this quantity neglecting diffusion effects – compare with Eq. (1.109) in Vol.1,

$$\begin{aligned} \frac{\partial}{\partial \tau}(n_l \gamma_v) + \nabla \cdot (\mathbf{V}_l n_l) &= \gamma_v (\dot{n}_{l,kin} - \dot{n}_{l,coal} + \dot{n}_{l,sp}) \\ &\equiv \gamma_v n_l \left\{ \frac{1}{n_l} \dot{n}_{l,kin} + f_{l,sp} - \frac{1}{2} \left[ (f_{d,col}^s + f_{d,col}^{no}) P_{d,coal}^{no} + f_{d,col}^o P_{d,coal}^o \right] - f_{l,spectrum\_cut} \right\} \end{aligned}$$

for  $\alpha_l \geq 0$ . (7.2)

Here  $\dot{n}_{l,sp}$  is the particle production term, that is the increase in the number of particles per unit time and unit mixture volume due to mechanical fragmentation such as splitting (subscript *sp*), and  $\dot{n}_{l,coal}$  is the particle sink term, that is, the decrease, in the number of particles due to mechanical coalescence (subscript *coal*).  $\dot{n}_{l,kin}$  is the number of particles generated or lost per unit time and unit mixture volume due to evaporation and/or condensation.

The next important step in the modeling is the estimation of the length scale of the particles needed for computation of mass, momentum and energy transport between the velocity fields, given the number of particles per unit mixture volume,  $n_d$ , and their volume fraction  $\alpha_d$  in the flow mixture. It is possible to proceed in different ways, but one of them seems to be easy and practicable: We assume that the dispersed phase is *locally mono-disperse*, that is, that all particles in a control volume have the same size. In this case the product of the particle number density,  $n_d$ , and the volume of single particles,  $\pi D_d^3 / 6$ , assuming spherical shapes with constant diameter  $D_d$ , gives the volume fraction  $\alpha_d$ , and therefore

$$D_d = \left( \frac{6}{\pi} \frac{\alpha_d}{n_d} \right)^{1/3}. \quad (7.3)$$

As already shown in Kolev (1999) and the references given there, this method can be used to describe the dynamic evolution of the length scale of a

multi-phase structure. The success of the application depends on whether appropriate experimental information is available and, if it is available, on whether this information can be generalized to provide the source terms in Eq. (7.2).

A further sophistication of the theory needs the *multi-group approach* already successfully exercised in neutron physics in the last 50 years with a detailed description of the dynamic interaction among groups of particles. This very ambitious task is outside the scope of this work. A compromise between complexity and a practicable approach is shown in Chen et al. (1995), where a two-group approach for *macro*- and *microscopic* liquid metal particles in water-gas flows was used. Other promising examples for bubbly flow are reported in Tomiyama (1998), Antal et al. (2000), and Lo (2000).

In Chapters 7 to 9 we concentrate our attention on the available knowledge for computation of the particle production term  $\dot{n}_{l,sp}$ , and the particle sink term  $\dot{n}_{l,coal}$ . The number of particles born per unit time and unit mixture volume,  $\dot{n}_{l,kin}$ , due to evaporation and condensation is subject to the nucleation theory and will be discussed later.

The experimental observations useful for development of the fragmentation or coalescence model are classified here as follows:

1. Identification of the kind of process leading to fragmentation or coalescence;
2. Measurements of the size of the final products of the fragmentation or coalescence;
3. Definition of the final state of the fragmentation or coalescence process and measurement of the duration of the process.

The quantitatively estimated characteristics are functions of the local flow parameters and initial conditions. These characteristics are used to model the production and sink rates. These models are then used in the range of parameters for which they are valid in macroscopic fluid models.

The following discussion will be restricted to mono-disperse particles in a single computational cell. We will also discuss the implication of this assumption.

## 7.2 General remarks about fragmentation

There are different but partially overlapping processes leading to disintegration of the continuum and the formation of dispersed particles or leading to the disintegration of unstable droplet and the formation of finer particles as shown in Fig. 1.4 in Chapter 1:

The main characteristics of each fragmentation process are

1. the stable particle diameter after the fragmentation is finished,  $D_{d\infty}$ , and
2. the duration of fragmentation,  $\Delta\tau_{br}$ .

It is very important to note that  $D_{d\infty}$  is defined here for situations without particle coalescence.

After the fragmentation process we assume that

1. the total mass of the particles is the same as before the fragmentation,
2. all newly formed particles are at the same temperature.

Knowing  $D_{d\infty}$  we compute the particle number density after the fragmentation process using assumption 1,

$$n_{d\infty} = \alpha_d / (\pi D_{d\infty}^3 / 6) \quad (7.4)$$

and finally the time-averaged production rate

$$\dot{n}_{d,sp} \approx \frac{n_{d\infty} - n_d}{\Delta\tau_{br}} = \frac{n_d}{\Delta\tau_{br}} \left[ \left( \frac{D_d}{D_{d\infty}} \right)^3 - 1 \right]. \quad (7.5)$$

The production rate  $\dot{n}_{d,sp}$  can be written in the form

$$\dot{n}_{d,sp} = n_d f_{d,sp}, \quad (7.6)$$

where

$$f_{d,sp} = \left[ \left( \frac{D_d}{D_{d\infty}} \right)^3 - 1 \right] / \Delta\tau_{br}, \quad (7.7)$$

is the *fragmentation frequency* of a single particle. If  $D_d = D_{d\infty}$ , the fragmentation frequency is zero and therefore the production rate  $\dot{n}_{d,sp}$  is zero.

If the process is considered over a time interval  $\Delta\tau$  (e.g., computational time step) that is larger than the fragmentation period  $\Delta\tau_{br}$ , the  $\Delta\tau_{br}$  in Eq. (7.5) should be replaced by  $\Delta\tau$ , which in fact means that during the time interval  $\Delta\tau$  the particle fragmentation is completed and stable conditions are reached. Only if  $\Delta\tau \gg \Delta\tau_{br}$ , is it justified to use the steady state flow pattern length scale instead of the transient one.

For volumes with zero convective net flux and no coalescence, the steady-state value of  $n_d$  approaches  $n_{d\infty}$ , that is,  $D_d$  approaches  $D_{d\infty}$ . The situation changes if coalescence effects are included.

Obviously, we need  $D_{d\infty}$  and  $\Delta\tau_{br}$  to compute the average mono-disperse particle production rate  $\dot{n}_{d,sp}$ . The quantitative description of the above discussed 16 modes of fragmentation concentrates on providing information for  $D_{d\infty}$  and  $\Delta\tau_{br}$  for the particular conditions and geometry.

## 7.3 General remarks about coalescence

Fragmentation is one of the processes controlling the particle size. Not less important is the collision and coalescence of particles in a continuum. The collision is caused by existence of *spatial velocity differences among the particles themselves*. This spatial relative velocity is caused by different factors, e.g. non-linear trajectory of the particles, turbulent fluctuations etc. Not each collision leads necessarily to coalescence. Thus *modeling particle agglomeration means modeling of collision and coalescence mechanisms*. In the following we discuss a simple formalism for the mathematical description of particle collision and coalescence and the available formalized empirical information needed for practical application of the theory.

### 7.3.1 Converging disperse field

Because of various geometrical obstacles, boundary conditions or variety of interactions inside the flow the particles may change their velocity in magnitude and direction. Consider a cloud of particles moving from a center radially outwards. None of the particles will touch the other. In this case there is no collision. The condition for collision in a flow of dispersed particles without oscillation over the mean velocity values is that they are coming together. Mathematically it can be expressed as follows: It is only if the relative velocity

$$V^{rel} = \left| \max \left[ 0, \mathbf{V}_d(\mathbf{r} + \Delta \mathbf{r}) - \mathbf{V}(\mathbf{r}) \right] \right|, \quad (7.8)$$

is negative, collisions and therefore agglomerations may take place. Here  $\mathbf{r}$  is the position vector of the point having particle velocity vector  $\mathbf{V}_d$ . In this case

$$\nabla \mathbf{V}_d < 0. \quad (7.9)$$

Usually, for a practical computation,  $\Delta V_{dd}^{no} = V^{rel}$  should be averaged across the computational cell so that we have

$$\Delta V_{dd}^{no} \approx \left[ \left( \Delta x \frac{\partial u}{\partial x} \right)^2 + \left( \Delta y \frac{\partial v}{\partial y} \right)^2 + \left( \Delta z \frac{\partial w}{\partial z} \right)^2 \right]^{1/2}. \quad (7.10)$$

As in the molecular kinetic theory, the average distance between collisions, or the mean free path  $\ell_{col}$ , is given by the ratio of the distance of collisions  $V^{rel} \Delta \tau$  and the collision frequency along this distance

$$\ell_{col} \approx const \frac{1}{n_d \pi D_d^2}. \quad (7.11)$$

It is recommended to resolve this distance by the computation because along this distance the interaction happens and the velocity of the particles changes as follows

$$\Delta V_{dd}^{no} \approx \ell_{col} \nabla \mathbf{V}_d . \quad (7.12)$$

### 7.3.2 Analogy to the molecular kinetic theory

Usually the agglomerated particles per unit time and unit volume are defined as

$$\frac{dn_d}{d\tau} = \dot{n}_{d,coal} = -f_{d,coal} n_d / 2 , \quad (7.13)$$

where  $f_{d,coal}$  is the coalescence frequency of single particles with the dimension  $s^{-1}$ .  $\dot{n}_{d,coal}$  is the instant coalescence rate. The number of particles remaining after a time interval  $\Delta \tau$  per unit volume is easily obtained by integration of Eq. (7.13)

$$\int_{n_d}^{n_{d,\tau+\Delta\tau}} d \ln n_d = -\frac{1}{2} \int_{\tau}^{\tau+\Delta\tau} f_{d,coal} d\tau , \quad (7.14)$$

or

$$n_{d,\tau+\Delta\tau} = n_d e^{-f_{d,coal} \Delta\tau / 2} . \quad (7.15)$$

The time-averaged coalescence rate is therefore

$$\dot{n}_{d,coal} = \frac{n_d - n_{d,\tau+\Delta\tau}}{\Delta\tau} = n_d \left( 1 - e^{-f_{d,coal} \Delta\tau / 2} \right) / \Delta\tau . \quad (7.16)$$

The coalescence frequency is defined as the product of the collision frequency and the coalescence probability,  $f_{d,coal}^p$ ,

$$f_{d,coal} = f_{d,col} f_{d,coal}^p , \quad (7.17)$$

which expresses the fact that not each collision leads necessarily to coalescence. To model the coalescence means to find adequate physical models for  $f_{d,col}$  and  $f_{d,coal}^p$ , which is the purpose of this Section.

We start with the analogy to molecular kinetic theory and discuss the differences resulting from the different nature of the droplet agglomeration compared with the random molecular collision.

Postulate a hypothetical particle-continuum mixture in which the particles are colliding at random with the following properties (see *Rohsenow* and *Choi* (1961), p.487):

1. The particles are hard spheres, resembling billiard balls, having diameter  $D_d$  and mass  $m$ .
2. The particles exert no forces on each other except when they collide.
3. The collisions are perfectly elastic and obey the classical conservation laws of momentum and energy.
4. The particles are uniformly distributed through the gas. They are in a state of continuous motion and are separated by distances that are large compared with their diameter  $D_d$ .
5. All directions of particle velocity fluctuations are equally probable. The speed (magnitude of the velocity) of particles can have any value between zero and infinity.

One usually singles out a particle as it travels in a straight path from one collision to the next: its speed and direction of motion changes with each collision. Imagine that at a given instant all particles but the one in question are frozen in position and this particle moves with an averaged speed  $V^{rel}$ . At the instant of collision, the center-to-center distance of the two particles is  $D_d$ . The collision cross section of the target area of the particle is  $\frac{1}{4}\pi D_d^2$ . In time  $\Delta\tau$  the moving particle sweeps out a cylindrical volume of the length  $V^{rel}\Delta\tau$  and the cross section  $\frac{1}{4}\pi D_d^2$ . Any particle whose center is in this cylinder will be struck by the moving particle. The number of collisions in the time  $\Delta\tau$  is

$$n_d \frac{1}{4} \pi D_d^2 V^{rel} \Delta\tau, \quad (7.18)$$

where  $n_d$  is the number of particles present per unit volume, assumed to be uniformly distributed in space. The collision frequency of a single particle is defined as the number of collisions per unit time

$$f_{d,col} = n_d \frac{1}{4} \pi D_d^2 V^{rel} = \frac{3}{2} \frac{\alpha_d}{D_d} V^{rel}. \quad (7.19)$$

By multiplying the collision frequency of a *single* particle,  $f_{d,col}$ , with the number of particles per unit mixture volume we obtain the total collision frequency, i.e. the number of collisions per unit mixture volume and per unit time

$$\dot{n}_{d,col} = f_{d,col} n_d = n_d^2 \frac{\pi}{4} D_d^2 V^{rel}. \quad (7.20)$$

Assuming all particles move at *averaged space* velocities  $V^{rel}$  (*Clausius*) the result is

$$f_{d,col} = \frac{1}{0.75} n_d \frac{\pi}{4} D_d^2 V^{rel} = \frac{1}{0.75} \frac{3}{2} \frac{\alpha_d}{D_d} V^{rel}. \quad (7.21)$$

If the particles are assumed to possess a *Maxwellian relative speed distribution* the result is

$$f_{d,col} = \frac{1}{\sqrt{2}} n_d \frac{\pi}{4} D_d^2 V^{rel} = \frac{1}{\sqrt{2}} \frac{3}{2} \frac{\alpha_d}{D_d} V^{rel}. \quad (7.22)$$

The assumptions 1 and 3 do not hold for real liquid droplet collision because droplets are deformable, elastic and may agglomerate after random collisions. The collision frequency is not an independent function of the coalescence probability. The functional relationship is not known. That is why some authors correct the collision frequency with a constant less than one estimated by comparison with experiments, e.g. *Rosenzweig et al. (1980)* give for relatively low  $V^{rel}$  and non-oscillatory coalescence  $const = 0.0001$ . *Howarth (1967)* obtained a modified form of Eq. (7.22), which includes additionally the multiplier  $8/\sqrt{3\alpha_d}$ , namely

$$f_{d,col} = \frac{1}{\sqrt{2}} \frac{6\alpha_d}{D_d} V^{rel} 8/\sqrt{3\alpha_d} = \frac{\sqrt{24\alpha_d}}{D_d} V^{rel}. \quad (7.23)$$

The dependence of the collision frequency on  $\approx \alpha_d^m$  in the above equation is confirmed by experiments as follows. For droplets - *Howarth (1967)*  $\approx \alpha_d^{0.6}$ , for liquid - liquid droplets *Coulaloglu and Tavlarides (1976)*, *Madden (1962)*, *Komasawa et al. (1968)*  $\approx \alpha_d^{0.45}$ , and for bubbles *Sztatecsny et al. (1977)*  $\approx \alpha_d^{0.6}$ .

Similar considerations can be repeated for dispersed particles having diameters  $D_{d1}$ ,  $D_{d2}$  and particle densities  $n_{d1}$ ,  $n_{d2}$ . The result is

$$\dot{n}_{d,col} = n_{d1} n_{d2} \frac{\pi}{4} \left( \frac{D_{d1} + D_{d2}}{2} \right)^2 V^{rel}, \quad (7.24)$$

see the pioneer work of *Smoluchowski* in 1918.

*Hibiki and Ishii* used in 1999 the *Loeb* notation from 1927 of Eq. (7.19) modifying it as follows

$$f_{d,col} = \frac{F_{col}}{4(1-\alpha_d)} V^{rel}, \quad (7.25)$$

where

$$F_{col} \approx n_d 4\pi D_d^2 \quad (7.26)$$

is the interface available for collision per unit mixture volume.  $1-\alpha_d$  takes into account the reduction of the volume available for collisions. *Hibiki and Ishii (1999)* modified the above relation to



$$f_{d,col} = \frac{F_{col}}{4(\alpha_{d,max} - \alpha_d)} V^{rel} = \frac{\alpha_d}{\alpha_{d,max} - \alpha_d} \frac{6}{D_d} V^{rel} \quad (7.27)$$

by introducing the maximum allowable void fraction  $\alpha_{d,max} = 0.52$  for existence of bubbly flow. This modification ensures that the collision frequency increases to infinite if the bubble volume concentration reaches the maximum packing concentration.

Two spherical particles with initial size  $D_{d0}$  possess surface energy of  $E_{\sigma 0} = 2\pi D_{d0}^2 \sigma$ . After coalescence the new spherical particle has a size  $D_d = 2^{1/3} D_{d0}$ , and therefore less surface energy,  $E_{\sigma} = \pi D_d^2 \sigma$ . The difference is  $\Delta E_{\sigma} = E_{\sigma 0} - E_{\sigma} = 2\pi D_{d0}^2 (1 - 1/2^{1/3})$ . The kinetic energy forcing the large bubble to split in this case is there virtual mass kinetic energy,  $\Delta E_k = 2 \left[ \frac{1}{2} \rho_c (V^{rel})^2 \right] \frac{1}{2} \frac{\pi D_{d0}^3}{6}$ . For droplets this is simply the kinetic energy of the droplets before collision  $\Delta E_k = 2 \left[ \frac{1}{2} \rho_d (V^{rel})^2 \right] \frac{\pi D_{d0}^3}{6}$ .

The theoretical minimum for  $V^{rel}$  required to produce bubble coalescence is computed by equalizing the change of surface energy of the both particle to the kinetic energy lost during the coalescence of particles  $\Delta E_{\sigma} = \Delta E_k$ , and therefore

$$\frac{\rho_c D_{d0} (V^{rel})^2}{\sigma} = 24(1 - 1/2^{1/3}) = 4.95 \quad (7.28)$$

or

$$V^{rel} > \left( \frac{4.95\sigma}{\rho_c D_{d0}} \right)^{1/2}. \quad (7.29)$$

For droplets we have,

$$\frac{\rho_d D_{d0} (V^{rel})^2}{\sigma} = 6(1 - 1/2^{1/3}) = 2.476 \quad (7.30)$$

or

$$V^{rel} > \left( \frac{2.476\sigma}{\rho_d D_{d0}} \right)^{1/2}. \quad (7.31)$$

Comparing Eqs. (7.29) with (7.31) we realize that at the same relative velocities bubbles will coalesce less frequently then droplets having the same size.

The nature of  $V^{rel}$  depends

- (a) on the turbulent fluctuation of the particles,
- (b) on the difference of the relative velocities caused by the differences of the particle size, and
- (c) on the non-uniform velocity field.

Even using an average particle size, the second and the third components may differ from zero. We call the coalescence caused by reasons (a), (b), and (c), *oscillatory*, *spectral*, and *non-oscillatory* coalescence, respectively. While for the oscillatory coalescence the driving force moving the particles is exerted from the oscillating turbulent eddies and therefore pushing out the continuum between two particles and moving the particles apart (under some circumstances before they coalesce), for the spectral and the non-oscillatory coalescence the forces leading to collisions inevitably act toward coalescence – for contracting particle free path length. Therefore we have for the probability of the oscillatory coalescence

$$P_{d,coal}^o \leq 1, \quad d = \text{bubbles, droplets}, \quad (7.32)$$

and for non-oscillatory and spectral coalescence in the case of contracting particle free path length

$$P_{d,coal}^{no} = P_{d,coal}^s = 1, \quad d = \text{bubbles}, \quad (7.33)$$

$$-\infty < P_{d,coal}^{no} = P_{d,coal}^s \leq 1, \quad d = \text{droplets}. \quad (7.34)$$

The last condition reflects the fact that for high droplet - droplet relative velocities the splitting of the resulting unstable droplet is possible.

## 7.4 Superposition of different droplet coalescence mechanisms

Let us rewrite the final expression for the coalescence frequency for the average particle diameter  $D_d$

$$\begin{aligned} f_{d,coal} &= f_{d,col}^s P_{d,coal}^s + f_{d,col}^{no} P_{d,coal}^{no} + f_{d,col}^o P_{d,coal}^o \\ &= 4.9 \frac{\sqrt{\alpha_d}}{D_d} \left( \Delta V_{dd}^s P_{d,coal}^s + \Delta V_{dd}^{no} P_{d,coal}^{no} + V_d' P_{d,coal}^o \right) \\ &= 4.9 \frac{\sqrt{\alpha_d}}{D_d} \left[ \left( \Delta V_{dd}^s + \Delta V_{dd}^{no} \right) P_{d,coal}^{no} + V_d' P_{d,coal}^o \right] \end{aligned} \quad (7.35)$$

where

$$P_{d,coal}^{no} = 0, \quad \Delta V_{dd}^s + \Delta V_{dd}^{no} < \left( \frac{12\sigma}{\rho_d D_d} \right)^{1/2}, \quad (7.36)$$

$$P_{d,coal}^{no} = f \left( \Delta V_{dd}^s + \Delta V_{dd}^{no} \right) \approx \Delta m_{d1} / m_{d2}, \quad (7.37)$$

$$P_{d,coal}^o \approx 0, \quad \text{for } \Delta \tau_{col} / \Delta \tau_{coal} < 1, \quad (7.38)$$

$$P_{d,coal}^o \approx 0.032 \left( \Delta \tau_{col} / \Delta \tau_{coal} \right)^{1/3}, \quad \text{for } \Delta \tau_{col} / \Delta \tau_{coal} \geq 1, \quad (7.39)$$

$$\Delta \tau_{col} / \Delta \tau_{coal} = 1.56 \left( \frac{D_d \sigma_d}{3\rho_d + 2\rho_c} \right)^{1/2} / V_d'. \quad (7.40)$$

The first term in Eq. (7.35) takes into account the coagulation caused by differences in the particle size leading to a relative movement between the particles, the second takes into account the spatial change of the particle velocities, also responsible for dramatic coagulation in stagnation points, and the third term takes into account the turbulence induced coagulation. This method is very easy to implement in computer codes.

## 7.5 Superposition of different bubble coalescence mechanisms

The method already described for particles is also valid for bubble agglomeration. The frequency of coalescence of a single bubble is

$$\begin{aligned} f_{d,coal} &= f_{d,coal}^s P_{d,coal}^s + f_{d,coal}^{no} P_{d,coal}^{no} + f_{d,coal}^o P_{d,coal}^o \\ &= 4.9 \frac{\sqrt{\alpha_d}}{D_d} \left[ \left( \Delta V_{dd}^s + \Delta V_{dd}^{no} \right) P_{d,coal}^{no} + V_d' P_{d,coal}^o \right], \end{aligned} \quad (7.41)$$

where

$$P_{d,coal}^{no} = 0, \quad \Delta V_{dd}^s + \Delta V_{dd}^{no} < \left( \frac{24\sigma}{\rho_c D_d} \right)^{1/2}, \quad (7.42)$$

$$P_{d,coal}^{no} = 1, \quad \Delta V_{dd}^s + \Delta V_{dd}^{no} \geq \left( \frac{24\sigma}{\rho_c D_d} \right)^{1/2}, \quad (7.43)$$

$$P_{d,coal}^o \approx 0, \quad \text{for } \Delta \tau_{col} / \Delta \tau_{coal} < 1, \quad (7.44)$$

$$P_{d,coal}^o \approx 0.032 \left( \Delta \tau_{col} / \Delta \tau_{coal} \right)^{1/3}, \quad \text{for } 1 \leq \Delta \tau_{col} / \Delta \tau_{coal} \leq 3.149, \quad (7.45)$$

$$\Delta\tau_{col} / \Delta\tau_{coal} = 3.35 \times 10^{-13} \frac{\sigma_c^2}{\eta_c \rho_c (D_d V'_d)^3}. \quad (7.46)$$

The first term in Eq. (41) takes into account the coagulation caused by differences in the bubble size leading to relative bubble movement, the second takes into account the spatial change of the bubble velocities also responsible for dramatic coagulation in stagnation points, and the third term takes into account the turbulence induced coagulation.

## 7.6 General remarks about particle size formation in pipes

Droplets can be formed from a continuous liquid in channels due to different reasons:

- Transition from churn turbulent flow in which the liquid is the continuous phase into a disperse regime in which the liquid is disintegrated;
- Distortion of a jet in inverted annular flow due to hydrodynamic instability;
- Disintegration of hydrodynamic unstable drops into smaller droplets due to acceleration induced fragmentation as will be discussed in Chapter 8;
- Droplet entrainment from a film attached at the wall.

Let us now examine more precisely the basic physics of the particle size formation in pipes with film on the wall where entrainment and deposition of droplets takes place, see *Kolev* (1993).

As discussed in Chapter 5 the entrainment is quantitatively described by models for the following characteristics:

- (1) Identification of the conditions when the entrainment starts;
- (2) The mass leaving the film per unit time and unit interfacial area,  $(\rho w)_{23}$ , or the mass leaving the film and entering the droplet field per unit time and unit mixture volume,

$$\mu_{23} = a_{12}(\rho w)_{23} \quad (7.47)$$

where  $a_{12}$  is the interfacial area density, i.e. the surface area between gas and film per unit mixture volume;

- (3) Size of the entrained droplets.

For channels with defined hydraulic diameter the interfacial area density is

$$a_{12} = \frac{4}{D_h} \sqrt{1 - \alpha_2}. \quad (7.48)$$

The particle production rate in case of entrainment is

$$\dot{n}_{23} = \mu_{23} / \left( \rho_2 \frac{\pi}{6} D_{3E}^3 \right) = \frac{6}{\pi} \frac{4}{D_h} \sqrt{1 - \alpha_2} (\rho w)_{23} / (\rho_2 D_{3E}^3). \quad (7.49)$$

While the entrainment transports droplets from the film into the gas bulk flow, the deposition reverses this process and transports droplets from the bulk region into the film. Entrainment takes place only if certain conditions are fulfilled. In contrast the deposition is controlled by turbulent fluctuations (a kind of macroscopic turbulent diffusion) and lift forces due to velocity gradients and takes place under all conditions. While entrainment is quantitatively described by the above-mentioned three models, the deposition is described only by a model for the mass flow rate entering the film,  $(\rho w)_{32}$  - see Chapter 6. The mass entering the film per unit time and unit mixture volume is

$$\mu_{32} = a_{12} (\rho w)_{32}, \quad (7.50)$$

and the particle sink term for velocity field  $l = 3$  is

$$\dot{n}_{32} = \mu_{32} / \left( \rho_3 \frac{\pi}{6} D_3^3 \right) = \frac{6}{\pi} \frac{4}{D_h} \sqrt{1 - \alpha_2} (\rho w)_{32} / (\rho_3 D_3^3). \quad (7.51)$$

Thus, the net particle production rate due to entrainment and deposition is

$$\dot{n}_{23} - \dot{n}_{32} = \frac{6}{\pi} \frac{4}{D_h} \sqrt{1 - \alpha_2} \left[ (\rho w)_{23} / (\rho_2 D_{3E}^3) - (\rho w)_{32} / (\rho_3 D_3^3) \right], \quad (7.52)$$

where  $D_{3E}$  is the volume-averaged size of the droplets leaving the film. Obviously a proper description of the particle production rate needs proper prediction of the entrainment and deposition mass flow rate and the entrainment diameter of the droplets.

Finally, we write the conservation equation of the droplets, Eq. (1.109), in case of three-fluid gas-film-droplet flow neglecting the turbulent diffusion

$$\frac{\partial n_3}{\partial \tau} + V_3 \nabla n_3 = \dot{n}_{3,sp} - \dot{n}_{3,coal} + \dot{n}_{23} - \dot{n}_{32}. \quad (7.53)$$

Replacing the source terms by their equals, we obtain finally

$$\begin{aligned} \frac{\partial n_3}{\partial \tau} + V_3 \nabla n_3 = n_3 & \left\{ \left[ \left( \frac{D_3}{D_{3\infty}} \right)^3 - 1 \right] / \Delta \tau_{br} - f_{3,coal} / 2 \right\} \\ & + \frac{6}{\pi} \frac{4}{D_h} \sqrt{1 - \alpha_2} \left[ (\rho w)_{23} / (\rho_2 D_{3E}^3) - (\rho w)_{32} / (\rho_3 D_3^3) \right]. \end{aligned} \quad (7.54)$$

Obviously, for large hydraulic diameters  $D_h \rightarrow \infty$ , i.e. for pool flow, entrainment and deposition do not influence the particle number density.

For flow with constant droplet velocity  $V_3 \approx \text{const}$ , the droplet mass conservation equation simplifies to

$$\rho_3 \left( \frac{\partial \alpha_3}{\partial \tau} + V_3 \nabla \alpha_3 \right) = \mu_{23} - \mu_{32} = \frac{4}{D_h} \sqrt{1 - \alpha_2} \left[ (\rho w)_{23} - (\rho w)_{32} \right]. \quad (7.55)$$

Having in mind the relationship between particle number density, volume fraction of droplets and the droplet diameter

$$\frac{\pi}{6} D_3^3 = \alpha_3 / n_3, \quad (7.56)$$

we can write

$$\alpha_3 \left( \frac{\partial D_3}{\partial \tau} + V_3 \nabla D_3 \right) = \frac{D_3}{3} \left[ \frac{\partial \alpha_3}{\partial \tau} + V_3 \nabla \alpha_3 - \frac{\pi}{6} D_3^3 \left( \frac{\partial n_3}{\partial \tau} + V_3 \nabla n_3 \right) \right]. \quad (7.57)$$

Substituting into the above equation the right hand side (RHS) from Eqs. (7.54) and (7.55) one obtains the differential equation governing the particle size in the steady state flow

$$\alpha_3 \left( \frac{\partial D_3}{\partial \tau} + V_3 \nabla D_3 \right) = \frac{D_3}{3} \left[ \begin{aligned} & \frac{4}{D_h} \sqrt{1 - \alpha_2} (\rho w)_{23} \left( 1 - \frac{\rho_3}{\rho_2} \frac{D_3^3}{D_{3E}^3} \right) / \rho_3 \\ & - \alpha_3 \left\{ \left[ \left( \frac{D_3}{D_{3\infty}} \right)^3 - 1 \right] / \Delta \tau_{br} - f_{3,coal} / 2 \right\} \end{aligned} \right]. \quad (7.58)$$

Some plausible conclusions are immediately drawn from the above equation:

1. Deposition does not influence the particle size because the deposition terms cancel.
2. Entrainment, particle disintegration in gas, and coalescence are the three mechanisms influencing the particle size.
3. If the entrained droplets have a size equal to the droplet size of the core, i.e.  $D_{3E} \approx D_3$ , the entrainment does not influence the particle size because of

$$\lim \left( 1 - \frac{\rho_3}{\rho_2} \frac{D_3^3}{D_{3E}^3} \right) \rightarrow 0. \quad (7.59)$$

$$D_{3E} \rightarrow D_3$$

4. There is an exact relationship between the local droplet number density, i.e. local droplet diameter, for known volume fraction  $\alpha_3$  and the three participating mechanical phenomena, (a) droplet fragmentation, (b) coalescence of

droplets, and (c) entrainment, which is not independent of the initial and boundary conditions.

Consequently, for steady state flow it cannot be expected to obtain an exact correlation for the local droplet diameter, which depends only on the local conditions but not on the initial conditions.

Therefore correlations modeling droplet diameter in steady state pipe flows as a function of the local parameters only but not of the steady state boundary conditions should be used very carefully.

Obviously the need to increase the accuracy of the dynamic models for prediction of droplet sizes in pipes leads necessarily to the need of increasing accuracy of the models of the above-mentioned four mechanical phenomena.

For the case of the fully developed steady state flow Eq. (7.58) reduces to

$$D_3 = \left[ \frac{\frac{4}{D_h} \sqrt{1-\alpha_2} (\rho w)_{23} / \rho_3 + \alpha_3 (1 / \Delta \tau_{br} + f_{3,coal} / 2)}{\frac{4}{D_h} \sqrt{1-\alpha_2} (\rho w)_{23} / (\rho_2 D_{3E}^3) + \alpha_3 / (\Delta \tau_{br} D_{3\infty}^3)} \right]^{1/3}, \quad (7.60)$$

and for the case of the fully developed steady state flow without entrainment we obtain

$$D_3 = D_{3\infty} (1 + \Delta \tau_{br} f_{3,coal} / 2)^{1/3} > D_{3\infty}. \quad (7.61)$$

One should not be surprised that the final effective droplet size is larger than the stable size under the local flow conditions because the coalescence acts towards increasing it.

Note that the identification of the velocity fields as disperse require *initialization of the particle length scale* equal to some typical geometrical length scale of the confined channel, for example, the local hydraulic diameter.

## Nomenclature

### *Latin*

$a_{12}$	interfacial area density, i.e. the surface area between gas and film per unit mixture volume, $1/m$
$D_h$	hydraulic diameters, $m$
$D_d$	$= \left( \frac{6}{\pi} \frac{\alpha_d}{n_d} \right)^{1/3}$ , particle diameter assuming spherical shapes, $m$

$D_{d\infty}$	stable particle diameter after the fragmentation is finished, $m$
$D_{3E}$	equivalent diameter of the entrained droplet, $m$
$F_{col}$	$\approx n_d 4\pi D_d^2$ , interface available for collision per unit mixture volume, $m^2$
$f_{d,sp}$	fragmentation frequency of a single particle, $s^{-1}$
$f_{d,coal}$	$= f_{d,col} f_{d,coal}^p$ , coalescence frequency of single particles, $s^{-1}$
$f_{d,col}$	collision frequency, $s^{-1}$
$f_{d,coal}^p$	coalescence probability, $s^{-1}$
$\ell_{col}$	average distance between collisions, or the mean free path, $m$
$n_l$	particle number density: volume-averaged number of discrete particles of the fluid $l$ (e.g., bubbles or droplets) per unit flow volume, $m^{-3}$
$n_{d\infty}$	$= \alpha_d / (\pi D_{d\infty}^3 / 6)$ , particle number density after the fragmentation is finished, $m^{-3}$
$n_{d1}, n_{d2}$	particle densities of the two groups of particle with diameters $D_{d1}$ and $D_{d2}$ , respectively, $m^{-3}$
$\dot{n}_{l,sp}$	particle production term – increase in the number of particles per unit time and unit mixture volume due to mechanical fragmentation such as splitting (subscript $sp$ ), $m^{-3}s^{-1}$
$\dot{n}_{l,coal}$	particle sink term – the decrease in the number of particles due to mechanical coalescence (subscript $coal$ ), instant coalescence rate, $m^{-3}s^{-1}$
$\dot{n}_{l,kin}$	number of particles generated or lost per unit time and unit mixture volume due to evaporation and/or condensation, $m^{-3}s^{-1}$
$\dot{n}_{23}$	particle production rate in case of entrainment, $m^{-3}s^{-1}$
$\dot{n}_{32}$	particle sink term in case of deposition, $m^{-3}s^{-1}$
$P_{d,coal}^o$	$\leq 1$ , probability of the oscillatory coalescence, <i>dimensionless</i>
$P_{d,coal}^{no}$	probability of the non oscillatory coalescence, <i>dimensionless</i>
$P_{d,coal}^s$	probability of the spectral coalescence, <i>dimensionless</i>
$\mathbf{r}$	position vector
$\mathbf{V}_l$	velocity vector, $m/s$
$\mathbf{V}_d$	particle velocity vector
$V^{rel}$	$= \left  \max \left[ 0, \mathbf{V}_d(\mathbf{r} + \Delta \mathbf{r}) - \mathbf{V}_d(\mathbf{r}) \right] \right $ , particle velocity difference at two different points at the same time, $m/s$

### Greek

$\alpha_l$	averaged volumetric fraction, <i>dimensionless</i>
------------	--



$\alpha_{d,\max}$	=0.52, maximum allowable void fraction for existence of bubbly flow, <i>dimensionless</i>
$\Delta m_{d1}$	mass change of the target droplet $d1$ after colliding with the projectile droplet $d2$ having mass $m_{d2}$ , see Chapter 8 Section 6, <i>kg</i>
$m_{d2}$	mass of the single particle belonging to the second group of particles, <i>kg</i>
$\Delta V_{dd}^s$	artificial particle-particle relative velocity resulting from the assembly averaging of the relative velocities, <i>m/s</i>
$\Delta V_{dd}^{no}$	$= V^{rel}$ , particle-particle velocity difference averaged over the computational cell volume, <i>m/s</i>
$V'$	fluctuation particle velocity component, <i>m/s</i>
$\Delta \tau_{br}$	duration of fragmentation, <i>s</i>
$\Delta \tau_{col}$	duration of the contact of the particles due to collision, <i>s</i>
$\Delta \tau_{coal}$	time interval necessary to push out the medium between two colliding particles, sometimes called coalescence time, <i>s</i>
$\Delta \tau$	time interval, <i>s</i>
$\rho_l$	density, <i>kg/m<sup>3</sup></i>
$(\rho w)_{23}$	entrainment mass flow rate, mass leaving the film per unit time and unit interfacial area, <i>kg/(m<sup>2</sup>s)</i>
$(\rho w)_{32}$	deposition mass flow rate entering the film, <i>kg/(m<sup>2</sup>s)</i>
$\mu_l$	mass source density, <i>kg/(m<sup>3</sup>s)</i>
$\mu_{23}$	$= a_{12}(\rho w)_{23}$ mass entering the film per unit time and unit mixture volume, <i>kg/(m<sup>3</sup>s)</i>
$\mu_{32}$	$= a_{12}(\rho w)_{32}$ mass entering the film per unit time and unit mixture volume, <i>kg/(m<sup>3</sup>s)</i>
$\sigma$	liquid-gas surface tension, <i>N/m</i>

### Subscripts

$l$	= 1 first fluid – gas
	= 2 second fluid – liquid
	= 3 third fluid – another liquid
$d$	disperse
$c$	continuous
23	from 2 to 3
32	from 3 to 2

## References

- Antal SP, Ettorre SM, Kunz RF, Podowski MZ (27<sup>th</sup>-29<sup>th</sup> September, 2000) Development of a next generation computer code for the prediction of multi-component multi-phase flows, Internet publication of the Proceedings of Trends in Numerical and Physical Modeling for Industrial Multiphase Flows, Course, France
- Chen X, Yuen WW, Theofanous TG (1995) On the constitutive description of microinteractions concept in steam explosions, Proceedings of the Seventh International Topical Meeting on Nuclear Reactor Thermal Hydraulics NURETH-7, New York, USA, NUREG/CP-0142
- Coulaloglu CA, Tavlarides LL (1976) Drop size distribution and coalescence frequencies of liquid - liquid dispersions in flow vessels, A. I. Ch. E., vol 22 no 2 pp 289-297
- Hibiki T, Ishii M (August 15-17, 1999) Interfacial area transport of air-water bubbly flow in vertical round tubes, CD proc. of the 33<sup>rd</sup> Nat. Heat Transfer Conf., Albuquerque, New Mexico
- Howarth W J (1967) Measurement of coalescence frequency in an agitated tank, A. I. Ch. E. J., vol 13 no 5 pp 1007-1013
- Kolev NI (1993) Fragmentation and coalescence dynamics in multi-phase flows, Experimental Thermal and Fluid Science, vol 6 pp 211 - 251
- Kolev NI (October 3-8, 1999) Verification of IVA5 computer code for melt-water interaction analysis, Part 1: Single phase flow, Part 2: Two-phase flow, three-phase flow with cold and hot solid spheres, Part 3: Three-phase flow with dynamic fragmentation and coalescence, Part 4: Three-phase flow with dynamic fragmentation and coalescence – alumina experiments, Proc. of the Ninth International Topical Meeting on Nuclear Reactor Thermal Hydraulics (NURETH-9), San Francisco, California
- Komasawa S et al (February 1968) Behavior of reacting and coalescing dispersed phase in a stirred tank reactor, Journal of Chemical Engineering of Japan, vol 1 no 1 pp 208-211
- Lo S (27<sup>th</sup>-29<sup>th</sup> September, 2000) Application of population balance to CFD modeling of gas-liquid reactors, Internet publication of the Proceedings of Trends in Numerical and Physical Modeling for Industrial Multiphase Flows, Course, France.
- Loeb LB (1927) The kinetic theory of gases, Dover, New York
- Madden AJ (1962) Coalescence frequencies in agitated liquid-liquid systems, A. I. Ch. E. J., vol 8 no 2 pp 233-239.
- Rohsenow WM, Choi H (1961) Heat, mass, and momentum transfer, Prentice - Hall, Inc., Engelwood Cliffs, New Jersey
- Rosenzweig AK, Tronov VP, Perguschev LP (1980) Coalizencija kapel vody v melkodispersnyh emulsiyach tipa voda v nevti, Journal Prikladnoj Chimii, no 8 pp 1776-1780
- Smoluchowski M (1918) Versuch einer mathematischen Theorie der Koagulationskinetik kolloider Lösungen, Zeitschrift für Physikalische Chemie, Leipzig, Band XCII pp 129-168

- Sztatecsny K, Stöber K, Moser F (1977) Blasenkoaleszenz und - zerteilung in einem Rührkessel, Chem. Ing. Techn., vol 49 no 2 p 171
- Tomiyama A (June 8-12, 1998) Struggle with computational bubble dynamics, Third International Conference on Multiphase Flow, ICMF 98, Lyon, France



## 8 Acceleration induced droplet and bubble fragmentation

### 8.1 Critical *Weber* number

Consider pool flow, that is, flow without any wall influence. Fluid particles in multiphase mixtures experience forces acting to destroy them and forces acting to retain their initial form. The *hydrodynamic stability* limit is usually described by the ratio of the forces acting to destroy the particles, the shear forces  $\mathbf{t}\pi D_d^2$ , where  $\mathbf{t}$  is the tangential force per unit surface, and the forces acting to retain the particle form, for example, surface tension forces  $\sigma_d\pi D_d$  (see Figs. 8.1 and 8.2),

$$We_d = \text{Shear force/Surface tension force} = \mathbf{t}D_d^2 / (\sigma_d D_d) = \mathbf{t}D_d / \sigma_d. \quad (8.1)$$

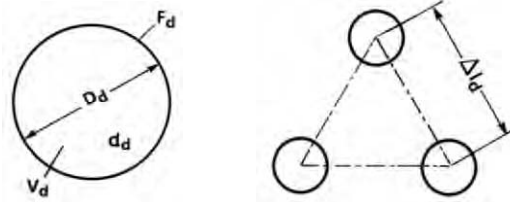


**Fig. 8.1** (a) Particle size. (b) Average distance between adjacent particles if they form a rhomboid array

This ratio is called the *Weber* number in honor of *Heinrich Weber* (1842-1913), who used it first. At the end of fragmentation, the *Weber* number is

$$We_{d\infty} = \mathbf{t}D_{d\infty} / \sigma_d \quad (8.2)$$

There are two considerations leading to a theoretical upper and lower limit of  $We_{d\infty}$ :

(a) *Triebnigg* (1929) was the first who equated the surface tension force to the shear force acting on the particles

$$\sigma_d\pi D_{d\infty} \approx c_{cd}^d \frac{1}{2} \rho_c (V_c - V_{d\infty})^2 \pi D_{d\infty}^2 / 4 \quad (8.3)$$

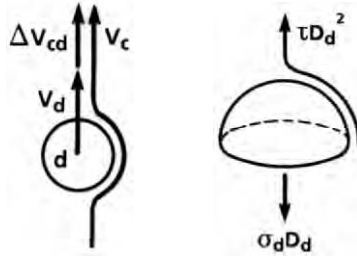


**Fig. 8.2** Hydrodynamic stability affecting forces

and obtained for the upper limit of the *Weber* number

$$We_{d\infty} \equiv \frac{\rho_c (V_c - V_{d\infty})^2}{\sigma_d / D_{d\infty}} \approx 8 / c_{cd}^d. \quad (8.4)$$

The drag coefficient for a solid sphere in the turbulent regime,  $c_{cd}^d$ , is  $\approx 0.4$ , and therefore the upper limit is

$$We_{d\infty} \approx 20. \quad (8.5)$$

Note that Eq. (8.5) does not reflect the experimentally observed dependence of  $We_{d\infty}$  on  $c_{cd}^d$  i.e.  $We_{d\infty}$  on  $Re_d = \rho_c D_{d0} \Delta V_{cd} / \eta_c$ , where  $\Delta V_{cd} = V_c - V_d$ , - see Lane (1951), Hanson (1963). Hinze (1949a) shows that during the fragmentation process the particle changes shape and experiences a considerably higher drag; therefore, in nature  $We_{d\infty}$  is less than 20.

b) The *Kelvin - Helmholtz* (KH) stability analysis provides the information necessary for the estimation of the lower limit of the *Weber* number. The *Kelvin - Helmholtz* instability is caused by the relative motion of two continuous phases - see in Chandrasekhar (1981). The most unstable wavelength is (for gas as a continuous phase)

$$\delta_{d,KH} \approx 3\pi (1 + \rho_c / \rho_d) \sigma_d / (\rho_c \Delta V_{cd\infty}^2). \quad (8.6)$$

-see Fig. 8.3

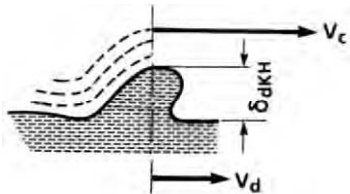


**Fig. 8.3.** The most unstable wavelength during relative motion of two continuous phases

If the entrained particle in this process has a size approximately equal to the most unstable wavelength

$$D_{d\infty} \approx \delta_{d,KH}, \quad (8.7)$$

the critical *Weber* number should be

$$We_{d\infty} \equiv \frac{\rho_c (V_c - V_{d\infty})^2}{\sigma_d / D_{d\infty}} \approx 3\pi (1 + \rho_c / \rho_d) \quad (8.8)$$

which e.g. for water droplets in gas means

$$We_{d\infty} \geq 9.52. \quad (8.9)$$

At very high relative velocities *Pilch* et al. (1981) indicated that inside the droplet the liquid boundary layer with thickness

$$\lambda_{bk} = 2\pi D_d \left( \frac{3 \text{Re}_d}{2\pi} \right)^{-1/2} \quad (8.10)$$

forms and has stabilizing effect acting against the *Kelvin - Helmholtz* instabilities. This was the reason for the recommendation made recently by *Dinh* et al. (1997) to limit the prediction of Eq. (8.8) by the water boundary layer thickness.

*Haas* (1964) provided experimental data for mercury droplets in air in the region

$$2000 < \text{Re}_d = \rho_c D_d \Delta V_{cd} / \eta_c < 17600 \quad (8.11)$$

and found that below  $We_{cd} \approx 5.2$  there is no breakup, and above  $We_{cd} \approx 6$ , there is. *Haas* found

$$We_{d\infty} \approx 5.6 \quad (8.12)$$

valid for experiments with initial *Weber* numbers ranging from 3.36 to 37.5, a region characterized by bag breakup. This seems to be the lower limit for the critical *Weber* number.

In fact, the experimental observations of several authors for low viscosity liquids provide a value of  $We_{d\infty}$  of about

$$5 < We_{d\infty} < 20 \quad (8.13)$$

with the most commonly used value being

$$We_{d\infty} \approx 12, \quad (8.14)$$

as shown in Fig. 8.5

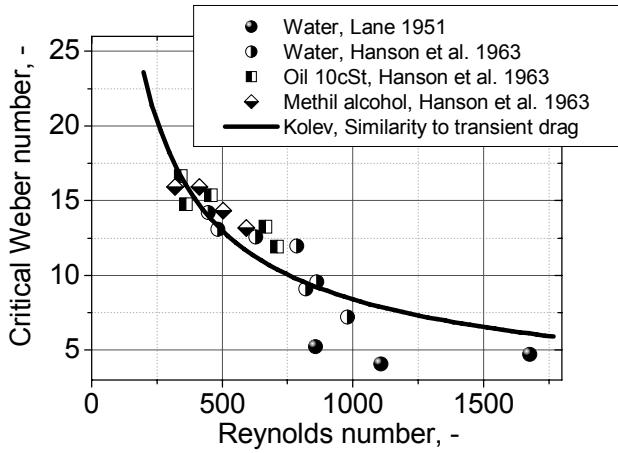


**Fig. 8.4** Variation of the critical *Weber* number  $We_{d\infty}$  for suddenly applied relative velocities with *Reynolds* number  $Re_d$

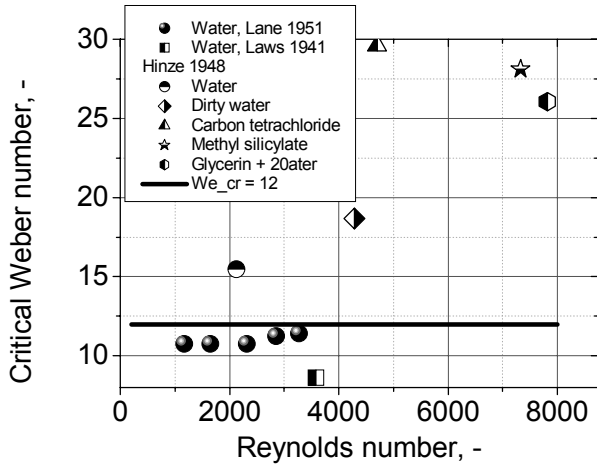


**Fig. 8.5** Variation of the critical *Weber* number  $We_{d\infty}$  for gradually applied relative velocities with *Reynolds* number  $Re_d$ . 1-Water, *Lane* 1951; 2-Water, *Laws* 1941; 3-7 *Hinze* 1948: Water; 4-Dirty water, 5-Carbon tetrachloride, 6-Methyl salicylate, 7-Glycerin+20 % water

Within the margin  $5 < We_{d\infty} < 20$  there is a dependence on the *Reynolds* number not considered into the above mentioned approaches. *Sarjeant* (1979)



summarized the data of *Hinze* (1949b), *Lane* (1951), *Hanson et al.* (1963), see Figs. 8.4 and 8.5, and found that for suddenly applied relative velocities within  $Re_d = 300$  and  $10^5$  where

$$Re_d = \rho_c D_d \Delta V_{cd} / \eta_c, \quad (8.15)$$

the critical *Weber* number varies as given in Fig. 8.4. The data given in Fig. 8.4 indicate proportionality with the transient drag. Comparing with the approximation of the lowest boundary of the transient drag for accelerating spheres as computed by *Brauer* (1992) we obtain

$$We_{d\infty} = 55 \left( \frac{24}{Re_d} + \frac{20.1807}{Re_d^{0.615}} - \frac{16}{Re_d^{2/3}} \right) \quad \text{for } 200 < Re_d < 2000, \quad (8.16)$$

and

$$We_{d\infty} \approx 5.48 \quad \text{for } 2000 < Re_d. \quad (8.17)$$

The value of  $Re_d \approx 200$  is chosen to take into account the observation of *Schröder* and *Kitner* (1965) reporting that a droplet oscillates only in the presence of a vortex tail behind the droplet, which requires a *Reynolds* number of 200 at least. This is the explanation why an upper limit of the critical *Weber* number is observed experimentally. The computer simulation reported by *Brauer* (1992) also supports this observation for flow around an accelerated sphere.

For gradually applied relative velocities *Taylor* (1949) provides a theoretical analysis leading to the critical *Weber* number that is about  $\sqrt{2}$  times greater than the critical *Weber* number for suddenly applied relative velocities which is not definitely confirmed from experiments. For a free falling droplet in a gravitational field that can be considered as gradual application of relative velocity, the drag force in Eq. (8.3) is equal to the buoyancy force

$$c_{cd}^d \frac{1}{2} \rho_c (V_c - V_{d\infty})^2 \pi D_{d\infty}^2 / 4 = (\pi D_{d\infty}^3 / 6) g \Delta \rho_{dc}. \quad (8.18)$$

Therefore

$$D_{d\infty}^2 g \Delta \rho_{dc} / \sigma_d = 6 \quad (8.19)$$

or having in mind that the terminal velocity of a large drop is about

$$\Delta V_{cd} \approx (\sqrt{2} \text{ to } 1.7) \left( \frac{\sigma_d g \Delta \rho_{dc}}{\rho_c^2} \right)^{1/4}, \quad (8.20)$$

$$We_{d\infty} \approx 4.8 \text{ to } 7.1. \quad (8.21)$$

*Magarvey* and *Taylor* (1956) observed that free falling water droplets with artificially produced initial diameter of 12 to 20 mm disintegrate before reaching

the "terminal velocity" corresponding to the initial drop size which should reduce the value estimated by means of Eq. (8.19). Equation (8.19) can be written in somewhat different form

$$(D_{d\infty} / \lambda_{RT})^2 = 6, \quad (8.22)$$

where

$$\lambda_{RT} = [\sigma_d / (g \Delta \rho_{dc})]^{1/2} \quad (8.23)$$

is the scale of the *Rayleigh - Taylor* instability wavelength for the case where gas and liquid are interpenetrating due to gravity. The above described approach considers the stability limit of the free falling liquid globules.

There is another point of view to approach this limit, namely, to consider the transition from churn turbulent bubble flow into dispersed flow – see left Fig. 8.6a.

For churn turbulent two - phase flow, the relative velocity between gas and liquid is nearly independent of the dispersed particle size, and is given by *Ishii* (1977)

$$|\Delta V_{13}| \approx \sqrt{2} (\sigma_3 g |\Delta \rho_{13}| / \rho_1^2)^{1/4}. \quad (8.24)$$

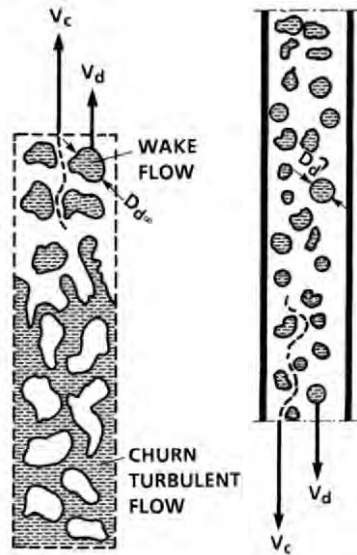


**Fig. 8.6** a) Transition from churn-turbulent to dispersed wake. b) Droplet fragmentation in channels

Here 1 stands for gas and 3 stands for liquid. For the wake flow regime of droplets in a gas, the relative velocity is

$$|\Delta V_{13}| \approx [g\Delta\rho_{13}^2/(\eta_1\rho_1)]^{1/3} D_3/4, \quad (8.25)$$

see in *De Jarlais et al.* (1986). Obviously at the transition between both regimes the relative velocity should be the same. *De Jarlais et al.* use this argument and after solving both equations for  $D_3$  they obtain the expression

$$D_3 = D_{d\infty} = 4[2\sigma_d/(g\Delta\rho_{dc})]^{1/2} \left\{ [\rho_c\sigma_d\sqrt{\sigma_d/(g\Delta\rho_{dc})}]^{1/2} / \eta_c \right\}^{-1/3} = 4\sqrt{2}\lambda_{RT}N_{\eta d}^{1/3}, \quad (8.26)$$

where  $d \equiv 3$ ,  $c \equiv 1$  and  $\lambda_{RT}$  is the *Rayleigh - Taylor* wavelength as defined with Eq. (8.23).

$$N_{\eta d} = \eta_c/(\rho_c\sigma_d\lambda_{RT})^{1/2} = Ar^{-1/2} \quad (8.27)$$

is the viscosity number. The experimental observation of the authors confirms that this expression approximates the maximum droplet size. Relative velocities larger than those predicted by Eq. (8.25) leads to further fragmentation governed by the fragmentation mechanism for pool flow as discussed before.

Comparing with experimental data, *Ruft* (1977) found that the constant  $4\sqrt{2}$  in Eq. (8.26) should be replaced by 20. The complete algorithm proposed by *Ruft* for free falling droplets representing the data in Fig. 8.7 is

$$(i) \left( \frac{\Delta\rho_{dc}}{\rho_c} \right)^2 / N_{\eta d}^4 < 10^7, \quad D_{d\infty} = 20N_{\eta d}^{1/3}\lambda_{RT}, \quad (We_{d\infty} \approx 40N_{\eta d}^{2/3}); \quad (8.28)$$

$$(ii) 10^7 \leq \left( \frac{\Delta\rho_{dc}}{\rho_c} \right)^2 / N_{\eta d}^4 < 10^9, \quad D_{d\infty} \approx 3\lambda_{RT}, \quad (We_{d\infty} \approx 6); \quad (8.29)$$

$$(iii) 10^9 \leq \left( \frac{\Delta\rho_{dc}}{\rho_c} \right)^2 / N_{\eta d}^4 < 3 \times 10^9 \text{ interpolation between (ii) and (iv); } (8.30)$$

$$(iv) 3 \times 10^9 \leq \left( \frac{\Delta\rho_{dc}}{\rho_c} \right)^2 / N_{\eta d}^4, \quad D_{d\infty} \approx 3.9\lambda_{RT}, \quad (We_{d\infty} \approx 7.75). \quad (8.31)$$

The 28 experimental data are in the region

$$90 \leq \left( \frac{\Delta\rho_{dc}}{\rho_c} \right)^2 / N_{\eta d}^4 < 10^{18}. \quad (8.32)$$

In this region the uncertainty is

$$3 \leq D_{d\infty} / \lambda_{RT} < 10. \quad (8.33)$$

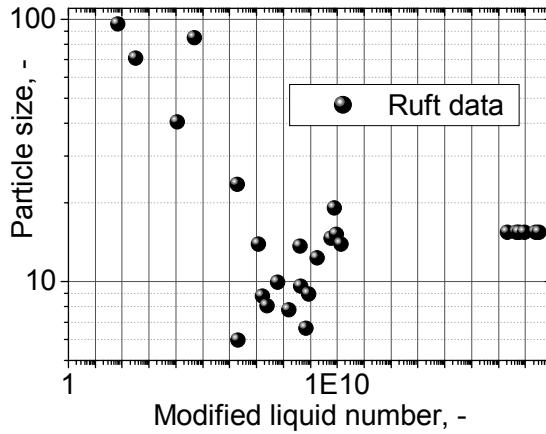


**Fig. 8.7** Dimensionless maximum droplet diameter  $(D_{d,max} / \lambda_{RT})^2$  as a function of a modified liquid number  $(\Delta\rho_{dc} / \rho_c)^2 / N_{\eta d}^4$

Using Eq. (8.20) the *Ruft* approximation can be expressed in terms of *Weber's* number as given in the brackets. Thus *Ruft's* recommendations should be considered in any case as an upper bound of the particle size for gradually applied relative velocity.

*Brodkey* (1967) and *Gelfand et al.* (1973) approximated the dependence of the critical *Weber* number on the viscosity, see Fig. 8.8, experimentally observed by *Haas* (1964), *Hanson et al.* (1963), *Hinze* (1955), *Hassler* (1971) by multiplying the critical *Weber* number for water by

$$1 + (1.077 \text{ to } 1.5) On_d^{(1.6 \text{ to } 1.64)} \quad (8.34)$$

where the *Ohnesorge* number is defined as follows

$$On_d = \eta_d / \sqrt{\rho_d D_d \sigma_d} = We_d^{1/2} / Re_d . \quad (8.35)$$

Summary: Thus, if

$$We_d > We_{d\infty} \quad \text{and} \quad Re_d > 200 .$$

a drop exposed on relative velocity is unstable. For *suddenly* applied relative velocity the recommended critical *Weber* number is

$$We_{d\infty} = 55 \left( \frac{24}{Re_d} + \frac{20.1807}{Re_d^{0.615}} - \frac{16}{Re_d^{2/3}} \right) [1 + 1.077 On_d^{1.64}] , \quad (8.36)$$

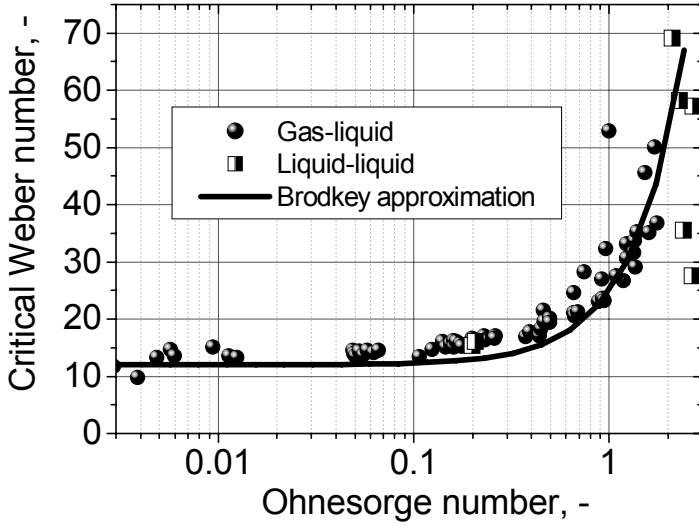


**Fig. 8.8.** Critical Weber number as a function of the *Ohnesorge* number (viscosity). Data for gas - liquid by *Hanson et al. (1963)*, *Haas (1964)*, *Hassler (1971)*, *Hinze (1955)*. Data for liquid-liquid by *Li and Folger, (1978)*. Approximation by *Brodkey (1967)*

for  $200 < Re_d < 2000$  and

$$We_{d\infty} = 5.48 \left[ 1 + 1.077 On_d^{1.64} \right], \quad (8.37)$$

for  $2000 \leq Re_d$ . As the experiments performed by *Hsiang and Faeth (1992)* show, there is no fragmentation if

$$On_d > 4, \quad (8.38)$$

see Fig. 8.8

For *gradually* applied relative velocity the critical *Weber* number is expected to be larger than the critical *Weber* number for *suddenly* applied relative velocity.

The decision which of both regimes should be taken, depends on the ratio of the velocity relaxation time,  $\Delta\tau_{\Delta V}$ , to the breakup time  $\Delta\tau_{br}$ . If  $\Delta\tau_{\Delta V} \gg \Delta\tau_{br}$  the condition for suddenly applied relative velocity should be used. If  $\Delta\tau_{\Delta V} \ll \Delta\tau_{br}$  the condition for gradually applied relative velocity is more appropriate. The estimation of  $\Delta\tau_{\Delta V}$  and  $\Delta\tau_{br}$  will be discussed later. Experimental data are needed in order to establish the behavior of the unstable droplet between the above discussed two extreme cases.

For free falling drops the method proposed by *Ruffi* is recommended.

### Important remarks about the size initialization by flow pattern transition:

The acceleration induced droplet fragmentation in channel flow, Fig. 8.6b, is preceded usually by the transition from the structure with continuous liquid to the structure with continuous gas - see Fig. 8.6a. This situation is easily identified if one *keeps a record of the flow pattern during the computational analysis*. Thus, if during the integration time step the liquid was continuous at the old time level and is getting dispersed at the new time level, the initial median size of the new born family of unstable drops is  $D_{d\infty}$  computed as follows:

- In case of transition from churn turbulent to annular-disperse two-phase flow, the mean size of the new born unstable droplets is well prescribed by Eq. (8.26) or Eq. (8.28).
- The transition from inverted annular flow into dispersed flow is visualized by jet disintegration in a pipe. For estimation of the initial size of the drops born the formalism proposed by *De Jarlais* et al. given Chapter 9 is recommended.
- If the relative velocity between gas and the new born droplets is larger than the critical one, the unstable droplets follow the dynamic fragmentation mechanism already described for pool flow.
- The splitting of the liquid between droplets and film at the transition to dispersed flow is not jet investigated. *Milashenko* et al. (1989) observed experimentally that such splitting exists.

## 8.2 Fragmentation modes

The sequences of pattern of deforming and fragmenting particles can be classified in groups called fragmentation modes. The qualitative description may vary depending on the different author's views but some important *common* features are confirmed by many authors. We use further the following verbal description of the different modes:

1. In the *vibration breakup* the droplet is excited by the gas vortex tail behind the drop to oscillate with its natural oscillation frequency and eventually to decompose into two or more large fragments.
2. *Bag breakup* is analogous to the bursting of soap bubbles blown from a soap film attached to a ring. A thin hollow bag is blown downstream while it is still attached to a more massive toroidal rim. The bag eventually bursts, forming a large number of small fragments; the rim disintegrates in a short time later, producing a small number of large fragments.
3. In the *bag and stamen breakup* a thin bag is blown downstream while being anchored to a massive toroidal rim. A column of liquid - *stamen* - is formed along the drop axis parallel to the approaching flow. The bag bursts first, rim and stamen follow.

4. In the *sheet stripping* a thin sheet disintegrates a short distance downstream from the drop. A coherent residual drop exists during the entire breakup process.
5. In the *wave crests stripping* small waves are formed on the windward surface of the drop. The wave crests are continuously eroded by the action of the flow field over the surface of the drop.
6. In the *catastrophic breakup* large amplitude, long wavelength waves ultimately penetrate the drop creating several large fragments before wave crest stripping can significantly reduce the drop mass.

The mode of the particle disintegration depends on the initial conditions before the fragmentation. The initial condition is characterized by the *Weber* number. Depending on the initial *Weber* number

$$We_d = \frac{\rho_c (V_c - V_d)^2}{\sigma_d / D_d} \quad (8.39)$$

the experimentally observed modes of fragmentation differ from each other.

*Anderson* and *Wolfe* (1965) divided the fragmentation mechanisms into two extreme modes: bag breakup and stripping breakup for following reason. The total drag force exerted on the drop consists of two components: (i) the pressure drag due to the pressure distribution over the surface of the drop and (ii) the friction drag due to viscous shear at the interface. The pressure drag at low relative velocities produces bag breakup, while the friction drag at high velocities produces stripping breakup. There are some other characteristic modes in between the above mentioned two extreme modes. *Pilch* et al. (1981) showed that the critical *Rayleigh-Taylor* (RT) instability wavelength

$$\lambda_d \approx 2\pi \left[ (1 - \rho_c / \rho_d) \rho_d a / \sigma \right]^{-1/2} \pi / 2 = 2\pi D_{d0} \left[ (1 - \rho_c / \rho_d) \frac{3}{4} c_{cd}^d We_{cd} \right]^{-1/2} \pi / 2, \quad (8.40)$$

where

$$a = \frac{3}{4} c_{cd}^d \frac{\rho_c}{\rho_d} \frac{\Delta V_{cd}^2}{D_d} \quad (8.41)$$

is the drop acceleration, and  $c_{cd}^d \approx 1.7$ , determines the range of the bag, bag and stamen breakup and sheet stripping: The *Weber* number  $\approx 14.4$  was predicted in order to have one unstable *RT* wave to fit on the deformed windward drop surface ( $\lambda_d \approx 2.3D_{d0}$ ) which is approximately the lower limit below which bag breakup is not observed. The *Weber* number of 57.8 is prescribed in order to have two unstable *RT* waves to fit on the deformed windward drop surface ( $2\lambda_d \approx 2.3D_{d0}$ ), which is approximately the lower limit below which bag and stamen breakup was not observed. The *Weber* number of  $\approx 130$  is predicted in order to have three

unstable  $RT$  waves to fit on the deformed windward surface ( $3\lambda_d \approx 2.3D_{d0}$ ) which is approximately the limit above which bag and stamen breakup was not observed. *The Weber number of 350 is the limit below which only primary breakup of the newly born fragments was experimentally observed.*

*Sarjeant* (1979), reviewing data of 10 literature sources, estimated the boundaries of the different regimes as follows:

1. Bag mode

$$We_{d\infty} < We_{cd} < 25, \quad (8.42)$$

confirmed also by *Krzczkowski* (1980),  $10 < We_{cd} < 20$  and by *Magarvey* and *Taylor* (1956) for free falling droplet, *Haas* (1980),  $5.6 < We_{cd} < 37.5$ . *Arcoumanis* et al. (1994) supported recently the upper limit of 25.

2. Umbrella mode

$$25 \leq We_{cd} < 50, \quad (8.43)$$

confirmed also by *Krzczkowski* (1980),  $20 \leq We_{cd} < 65$ . *Arcoumanis* et al. (1994) supported recently the upper limit of 65.

3. Stripping of the ligaments from the periphery of the deformed drop

$$50 \leq We_{cd} < 100; \quad (8.44)$$

4. Stripping of the ligaments from the periphery of the deformed drop and droplets from the crest of waves

$$100 \leq We_{cd} < 1000; \quad (8.45)$$

5. Stripping of droplets from the crests of waves on the windward face

$$1000 \leq We_{cd} < 10^5; \quad (8.46)$$

6. Initial stripping of droplets from the crests of waves on the windward face followed by perforation due to *Taylor* waves

$$10^5 \leq We_{cd} < 10^6; \quad (8.47)$$

Perforation due to *Taylor* waves

$$10^6 \leq We_{cd}. \quad (8.48)$$

*Gelfand* et al. (1974), *Pilch* et al. (1981) classified the experimentally observed modes of fragmentation as follows:

1. Vibration breakup

$$We_c < 12; \quad (8.49)$$



## 2. Bag breakup

$$12 \leq We_c < 50 \quad (8.50)$$

(experimentally confirmed by *Simpkins* and *Bales* (1972),  $7 \leq We_c < 50$ ;

## 3. Bag - and - stamen breakup

$$50 \leq We_c < 100; \quad (8.51)$$

## 4. Sheet stripping

$$100 \leq We_c < 350; \quad (8.52)$$

## 5. Wave crest stripping followed by catastrophic breakup

$$350 \leq We_c. \quad (8.53)$$

Obviously there are not clear boundaries between the different regimes which explains the differences due to the subjective judgment of the authors. *Gelfand* and *Pilch*'s proposal is formally supported by experimental data which change the character of break time as a function of *Weber* number at the above mentioned boundaries. That is why, for low viscous liquids, we recommend the method proposed by *Gelfand* et al. (1974) and *Pilch* et al. (1981).

In the region of

$$10^{-7} \leq 1/La_d < 5 \quad (8.54)$$

*Krizekowski* provided experimental evidence that the limits of the regimes are functions of  $1/La_d$ , where the relationship between the *Laplace* number and the already introduced *Ohnesorge* number is

$$1/La_d = On_d^2. \quad (8.55)$$

For  $1/La_d > 10^{-3}$  the influence of the liquid viscosity is negligible. For  $1/La_d > 10^{-3}$  the boundaries of the regimes increase with  $1/La_d$ . For such cases the classification by *Krizekowski* is useful.

### 8.3 Relative velocity after fragmentation

The stability criterion, Eqs. (8.36) and (8.37),  $We_{d\infty} = const$  refers to the final stable diameter,  $D_{d\infty}$ , and the *final fragment velocity*,  $V_{d\infty}$ , reached by the fragments after the fragmentation. Therefore, to predict  $D_{d\infty}$  knowing  $D_d$ ,  $V_d$ ,  $V_c$  one needs a method to predict  $V_{d\infty}$ .

Using the momentum equations of the continuum and of the dispersed phase, neglecting the inertial terms, dividing by the corresponding densities and

summing up the resulting equations, one obtains the following equation governing the relative velocity,  $\Delta V_{cd}$ ,

$$\left(1 + bc_{cd}^{vm}\right) \frac{\partial}{\partial \tau} \Delta V_{cd} + \left(\frac{1}{\rho_c} - \frac{1}{\rho_d}\right) \nabla p + b \frac{3}{4} \frac{c_{cd}^d}{D_d} |\Delta V_{cd}| \Delta V_{cd} = 0. \quad (8.56)$$

Here

$$b = (\alpha_c \rho_c + \alpha_d \rho_d) / \alpha_c \rho_c, \quad (8.57)$$

$c_{cd}^{vm}$  is the virtual mass coefficient which for droplets in gas is negligible but for liquid-liquid or bubble-liquid systems is very important.

For drag forces considerably larger than the pressure gradient forces the acceleration of a single droplet is computed using a simplified form of Eq. (8.56),

$$\frac{\partial}{\partial \tau} \Delta V_{cd} = -\Delta V_{cd} / \Delta \tau_{\Delta V}, \quad (8.58)$$

where

$$\Delta \tau_{\Delta V} = \frac{4}{3} \frac{1 + bc_{cd}^{vm}}{b} \frac{D_d}{c_{d\infty}^d} \left/ |\Delta V_{cd}| \right. \quad (8.59)$$

is used to estimate the linearized velocity relaxation time constant. The analytical solution of the above simplified equation is

$$\frac{\Delta V_{cd\infty}}{\Delta V_{cd}} = \frac{1}{1 + \frac{\Delta \tau}{\Delta \tau_{\Delta V}}}. \quad (8.60)$$

Eq. (8.56) is an equation of the *Riccati* type with respect to  $\Delta V_{cd}$  and possesses a hyperbolic solution. Substituting

$$a_1 = \left( b \frac{3}{4} \frac{c_{cd}^d}{D_{d\infty}} \right) \left/ (1 + bc_{cd}^{vm}) \right., \quad (8.61)$$

$$a_2 = \left( \frac{1}{\rho_c} - \frac{1}{\rho_d} \right) \nabla p \left/ (1 + bc_{cd}^{vm}) \right. \quad (8.62)$$

and using the initial condition  $\Delta V_{cd}(\tau) = \Delta V_{cd,0}$  we obtain the velocity difference  $\Delta V_{cd}$  after the time interval  $\Delta \tau$ .

$$\Delta V_{cd} = \frac{\Delta V_{cd,0} (a_1 a_2)^{1/2} + a_1 \tanh \left[ (a_1 a_2)^{1/2} \Delta \tau \right]}{(a_1 a_2)^{1/2} + a_1 \Delta V_{cd,0} \tanh \left[ (a_1 a_2)^{1/2} \Delta \tau \right]}, \quad (8.63)$$

see Kamke (1959). If the time interval is equal to the time needed to complete the fragmentation,  $\Delta\tau = \Delta\tau_{br}$ , Eq. (8.63) provides the velocity difference between the cloud of fragments and its surroundings at the end of the fragmentation. Note that the drag coefficient of the deforming particles divided by the changing diameter of the fragmented particles during the breakup period  $\Delta\tau_{br}$  is a complicated function of time

$$c_{cd}^d / D_d = f(\tau^*) \quad \text{for} \quad \tau < \tau^* < \tau + \Delta\tau_{br} \quad (8.64)$$

so that the averaged quotient is in any case greater than the final one

$$\overline{c_{cd}^d / D_d} > c_{cd}^d / D_d. \quad (8.65)$$

Krzczkowski (1980) provided very important measurements on the kinematics of the fragmentation. *A common feature of all types of fragmentation is that they start with a basic shape the so called "liquid disk".* Data for  $D_d / D_{d0}^v$  as a function of time are plotted for  $13.5 < We_{cd} < 101$ .

The Baines and Buttery (1978) experimental data for deformation preceding the breakup for liquid-gas ( $1.3 \times 10^3 \leq We_{cd} \leq 7.1 \times 10^5$ ) as well for liquid-liquid ( $2.5 \times 10^2 \leq We_{cd} \leq 3.9 \times 10^3$ ) are correlated by Pilch et al. (1981) with

$$D_d / D_{d0}^v - 1 \approx 1.4\Delta\tau^* - 0.3\Delta\tau^{*2}, \quad 0 \leq \Delta\tau^* \leq 2 \quad (8.66)$$

$$D_d / D_{d0}^v - 1 \approx 0.12 + 1.28\Delta\tau^* - 0.27\Delta\tau^{*2}, \quad 2 \leq \Delta\tau^* \leq 5.5 \quad (8.67)$$

where  $\Delta\tau^* = \tau\Delta V_{cd} (\rho_c / \rho_d)^{1/2} / D_{d0}^v$ .

Simpkins and Bales (1972) found experimentally that the drag coefficient for distorted drops is similar to the rigid sphere value for  $Re_d < 10^3$ . When compressibility effects become significant, a mean value of  $c_{cd}^d = 2.5$  is observed for  $10^3 < Re_d < 10^5$ . The later result is comparable to measurements taken from rigid disks in similar flow conditions. Pilch et al. (1981) reviewing experimental data from several authors found that drag coefficients for fragmenting drops are 2 to 3 times larger than the rigid sphere drag coefficient ( $\approx 2.5$  for compressible flow,  $\approx 1.54$  for fragmenting drops in incompressible flow). That is the reason leading some authors to look for an empirical description of the final fragment velocity by modifying solutions of the momentum equations using experimental data.

The fragmentation cloud velocity that is reached after completion of the breakup process for regimes (a) through (e) was correlated by Pilch et al., p.22, by a modified solution of the simple force balance equation ( $\tau = 0$ ,  $V_d = 0$ ;  $\tau = \Delta\tau_{br}$ ,  $V_d = V_{d\infty}$ ,  $V_c = const$ )

$$V_{d\infty} = V_c (\rho_c / \rho_d)^{1/2} \left( \frac{3}{4} c_{cd}^d \Delta \tau_{br} + 3b \Delta \tau_{br}^2 \right) \quad (8.68)$$

or

$$(V_c - V_{d\infty})^2 = V_c^2 \left[ 1 - (\rho_c / \rho_d)^{1/2} \left( \frac{3}{4} c_{cd}^d \Delta \tau_{br} + 3b \Delta \tau_{br}^2 \right) \right]^2. \quad (8.69)$$

The experimental data are reproduced using the tuning constants  $c_{cd}^d = 0.5$ ,  $b = 0.0758$  for incompressible ( $Ma < 0.1$ ), and  $c_{cd}^d = 1$ ,  $b = 0.116$  for compressible flow ( $Ma > 0.1$ ). The different form during the different deformation modes explains the differences in  $c_{cd}^d$ .

For the liquid - liquid system *Pilch et al. (1981)*, p.16, used

$$V_{d\infty} = V_c (\rho_c / \rho_d)^{1/2} \left( \frac{3}{4} c_{cd}^d \Delta \tau_{br} \right) / \left[ 1 + \frac{3}{4} c_{cd}^d \Delta \tau_{br} (\rho_c / \rho_d)^{1/2} \right] \quad (8.70)$$

or

$$(V_c - V_{d\infty})^2 = V_c^2 \left\{ 1 - (\rho_c / \rho_d)^{1/2} \left( \frac{3}{4} c_{cd}^d \Delta \tau_{br} \right) / \left[ 1 + \frac{3}{4} c_{cd}^d \Delta \tau_{br} (\rho_c / \rho_d)^{1/2} \right] \right\}^2. \quad (8.71)$$

Thus, for computation of the final velocity difference after the fragmentation, either the stepwise analytical solution (8.63) together with the deformation approximation (8.66, 8.67) for computing  $c_{cd}^d / D_d$  or the empirical correlation (8.68, 8.69) provided by *Pilch et al. (1981)*, which is simpler, should be used.

## 8.4 Breakup time

Next we concentrate our attention on the modeling of the time scale of the fragmentation process  $\Delta \tau_{br}$ , see Fig. 8.9

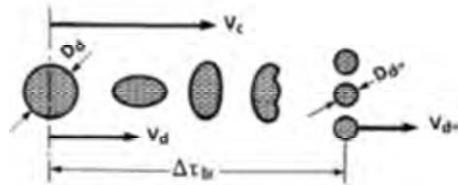


**Fig. 8.9** Definition of the parameters characterizing the break-up process

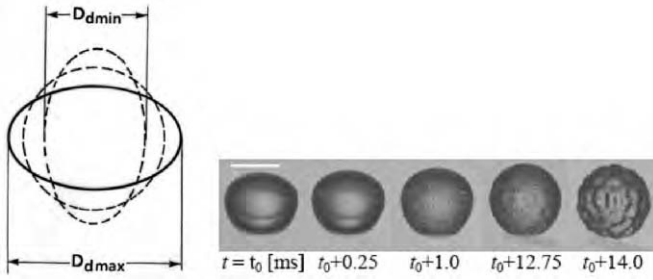


**Fig. 8.10** a) Particle vibration; b) *Kojo and Ueno* (2006): Water bubble vibration in 20 kHz ultrasonic field at atmospheric conditions. Scale bar in the left frame corresponds to 1.0 mm

The vibration breakup mechanism, see Fig. 8.10a, is probably the best analyzed fragmentation mechanism up to now. According to *Lamb* (1932), see in *Lamb* (1945), the natural frequency of the  $n$ -th order mode of a spherical drop or bubble (d) performing *oscillations* in continuum (c) is given by

$$(2\pi f_n)^2 = b \frac{8\sigma_d}{D_d^3} \frac{n(n+1)(n-1)(n+2)}{(n+1)\rho_d + n\rho_c}, \quad b \approx 1, \quad (8.72)$$

where  $n = 2, 3, \dots, n$ . *Kojo and Ueno* (2006) confirmed the validity of this equation for bubbles in liquid ( $b = 1$ ). An example of their observation is given in Fig. 8.10b. *Riso and Fabre* [58] reported in 1998 that bubbles in turbulent field manifest the strongest oscillation at the first mode ( $n = 2$ ). For droplets the first mode of oscillation ( $n = 2$ ) is the only one observed experimentally. The factor  $b$  should approach unity for small amplitude oscillations. *Schröder and Kitner* (1965) describe 132 data points for 19 disperse - continuum systems with the correlation

$$b = 1 - \frac{D_{d,\max} - D_{d,\min}}{2D_d^v} \approx 0.805D_d^{v0.225} \quad (8.73)$$

with an average error of 9.01 % - see Fig. 8.11. Here  $D_d^v$  is the volume-averaged diameter. The data cover the region  $0.01 < (D_d^v)^3 < 3$  and take values within

$$0.005 < \frac{b\sigma}{f_2^2(3\rho_d + 2\rho_c)} < 0.5. \quad \text{They observed oscillations only in the presence of}$$

a vortex tail which requires a *Reynolds* number of at least 200. *Hsiang and Faeth*, see in *Faeth* (1995) p. C0-7, summarized a relatively large data base on maximum drop deformation for steady disturbances, considering both drop-gas and drop-immiscible environments for

$$We_d \leq 20, \quad D_{d,\max} / D_{d,\min} = \left(1 + 0.07We_d^{1/2}\right)^3, \quad (8.74)$$

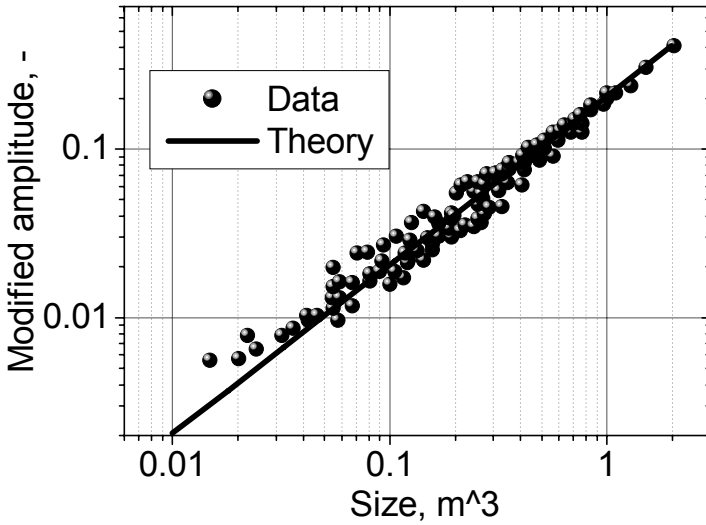


**Fig. 8.11** Amplitude corrected data  $b(\sigma_d / f_n^2) / (3\rho_d + 2\rho_c)$  vs. drop size  $D_d^3$ . Values of  $b$  from Eq. (8.79). *Schröder and Kitner* (1965)

and

$$D_{d,\max}^2 D_{d,\min} = (D_d^v)^3. \quad (8.75)$$

The time needed for breakup of an unstable, vibrating particle should therefore be of the order

$$\Delta\tau_{br} \approx 1 / f_2 \quad (8.76)$$

- see Fig. 8.11. This was first proposed by *Laftaye* (1943) as a rough estimate of the time of splitting-up for the vibration breakup. This, however is correct if the relative velocity is just equal to the critical speed

$$\Delta V_{cd}^* = \left( We_{d\infty} \frac{\sigma_d}{D_d \rho_c} \right)^{1/2}. \quad (8.77)$$

If the relative velocity exceeds the critical speed,  $\Delta V_{cd}^*$ , the splitting time is shorter than the time determined by the natural vibration period. The *Kelvin-Helmholtz* instability analysis, see *Hinze* (1949b) (1981) provides the period for the droplet fragmentation

$$\Delta\tau_{br}^* = \frac{\Delta\tau_{br}}{\delta_{dKH} \left[ \Delta V_{cd} (\rho_c / \rho_d)^{1/2} \right]} \approx \frac{\sqrt{3}}{2\pi} (1 + \rho_c / \rho_d) \approx 2.28, \quad (8.78)$$

that is the lowest limit of the experimentally observed fragmentation times. The expression  $\delta_{dKH} / \left[ \Delta V_{cd} (\rho_c / \rho_d)^{1/2} \right]$  has the dimension of a time and is usually used as a time scale for modeling of droplet fragmentation in the form  $D_d / \left[ \Delta V_{cd} (\rho_c / \rho_d)^{1/2} \right]$ . In this sense the time needed for the first mode of oscillation in accordance with Eq. (8.78) is

$$\frac{\Delta \tau_{br}}{D_d / \left[ \Delta V_{cd} (\rho_c / \rho_d)^{1/2} \right]} \approx \frac{\pi}{4} \left[ \frac{1}{b} \left( 1 + \frac{2}{3} \frac{\rho_c}{\rho_d} \right) We_{cd} \right]^{1/2}. \quad (8.79)$$

Having in mind that the vibration mode is observed for  $\approx 12 < We_{cd} < 18$ , the dimensionless breakup time should be expected to be of the order of

$$\Delta \tau_{br}^* = 6.6 \text{ to } 8.2 \quad (8.80)$$

for  $b \approx 1/2$ , which is in fact the upper limit for the fragmentation time observed in all sources known to the author.

*Pilch et al.* (1981) correlated experimental data for the total breakup period for droplets in gas from 8 sources, see Fig. 8.12, for the non- vibration modes (b) through (e) in the form

$$\Delta \tau_{br}^* = c (We_{cd} - We_{d\infty})^m, \text{ for } We_{cd}^* < We_{cd} < We_{cd}^{**} \quad (8.81)$$

where the dimensionless time  $\Delta \tau_{br}^*$  was defined as

$$\Delta \tau_{br}^* = \frac{\Delta \tau_{br}}{D_d / \left[ V_c (\rho_c / \rho_d)^{1/2} \right]}, \quad (8.82)$$

the critical *Weber* number,

$$We_{cd} = 12, \quad (8.83)$$

and the constants are

$c$	$m$	$We_{cd}^*$	$We_{cd}^{**}$	
7	0	1	12	Vibration mode
6	-1/4	12	18	Bag breakup
2.45	+1/4	18	45	Bag - and - stamen breakup
14.1	-1/4	45	351	Sheet stripping
0.766	+1/4	351	2670	Wave crest stripping followed by catastrophic breakup
5.5	0	2670	$\infty$	

The data base of *Sarjeant*, see Fig. 4 in *Sarjeant* (1979), confirms also Eq. (8.81) with some differences for the boundaries of the regimes. For *Weber* number  $> 500$   $c$  is estimated by *Hsiang* (see in *Faeth* (1995) p. C0-7, fig. 8) to be 5.

The accuracy of the data representation is of order of

$$\pm D_d / \left[ V_c (\rho_c / \rho_d)^{1/2} \right]. \quad (8.84)$$

Experimental data for the bag breakup are provided by *Haas* (1964). Using mercury drop in air *Haas* observed bag breakup in the region of  $5.6 < We_{cd} < 37.5$  and  $200 < Re_d < 17600$ . *Haas* provided measurements for the duration of the three stages of breakup (a) time for disk formation, (b) time for the bag formation and (c) time for the global breakup. The constant  $c$  in Eq. (8.81) derived from his data is  $\approx 2.3$  in

$$\Delta \tau_{br}^* \approx 2.3 We_{cd}^{1/4}. \quad (8.85)$$

The order of magnitude of the constant was confirmed later by the measurements of *Krzczkowski* (1980)

$$\Delta \tau_{br}^* \approx (1.9 \text{ to } 2.7) We_{cd}^{1/4}. \quad (8.86)$$

Note that the relationship for the fourth regime is based on the experimental observations made by *Simpkins* and *Bales* (1972) and other authors. The original relationship for the onset of *Taylor* instability of water droplets in gas, i.e. the least squares fit of the minimum value for the breakup time, is

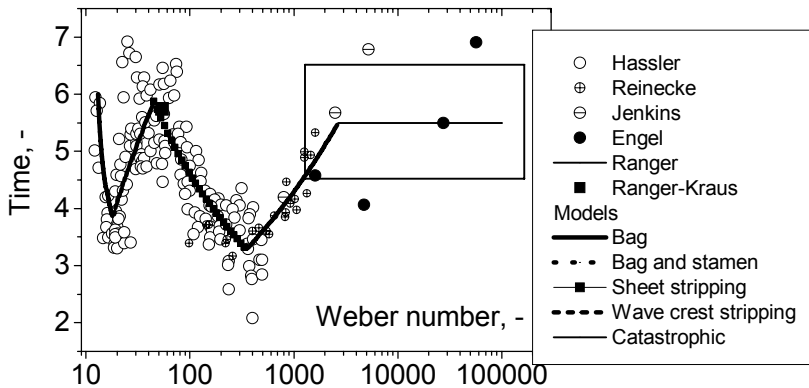


**Fig. 8.12** Total break-up time  $\Delta \tau_{br} \left[ V_c (\rho_c / \rho_d)^{1/2} \right] / D_d$  as a function of *Weber* number  $We_{cd}$  for gas-liquid systems. The summary was prepared by *Pilch* et al. in 1981



$$\frac{\Delta \tau_{br}}{D_d \left[ \Delta V_{cd} (\rho_c / \rho_d)^{1/2} \right]} = \frac{1}{2} 22 Bo_d^{-1/4} \approx 13.3 We_{cd}^{-1/4}, \quad (8.87)$$

where

$$Bo_d = \left[ \rho_d \frac{dV_d}{d\tau} (D_d / 2)^2 \right] / \sigma_d = \frac{3}{16} c_{cd}^d We_{cd} \quad (8.88)$$

and

$$c_{cd}^d = f(Re_{cd}), \quad \text{for rigid sphere, } Re_{cd} < 10^3, \quad (8.89)$$

$$c_{cd}^d = 2.5, \quad \text{for } 10^3 \leq Re_{cd} < 10^5. \quad (8.90)$$

The experimental data show that the breakup time is in any case less than the time prescribed by the equation

$$\frac{\Delta \tau_{br}}{D_d \left[ \Delta V_{cd} (\rho_c / \rho_d)^{1/2} \right]} \approx \frac{1}{2} 65 Bo_d^{-1/4} \approx 39.9 We_{cd}^{-1/4}. \quad (8.91)$$

The experimental data of *Krzczkowski* (1980) support the order of magnitude of the constant

$$\Delta \tau_{br}^* \approx (12 \text{ to } 22) We_{cd}^{-1/4}. \quad (8.92)$$

The reader should be careful when comparing such correlations because, as already mentioned, the definition of the end of the breakup process may differ depending on the author's subjective view. Next an example will be given.

For liquid-liquid systems, *Patel* and *Theofanous* (1981) modified the correlation by *Simpkins* and *Bales* (1972), Eq. (8.93), as follows

$$\frac{\Delta \tau_{br}}{D_d \left[ \Delta V_{cd} (\rho_c / \rho_d)^{1/2} \right]} = c We_{cd}^{-1/4}, \quad (8.93)$$

where  $c$  takes values between 0.9 and 3.6, which means that the dimensionless breakup time is an order of magnitude shorter than for the case of water - gas systems for the same *Weber* number. More recent experiments with a mercury-water system reported by *Yuen* et al. motivated a revision the equation (8.91) to

$$\frac{\Delta \tau_{br}}{D_d \left[ \Delta V_{cd} (\rho_c / \rho_d)^{1/2} \right]} \approx 14.8 Bo_d^{-1/4} \approx 17.8 We_{cd}^{-1/4}, \quad (8.94)$$

which is essentially the same as *Krzczkowski's* (1980) finding for gas-liquid systems. Recently *Chen* et al. [8] (1995) reported data for  $Bo_d = 10^2, 10^3, 10^4$  giving dimensionless fragmentation times 2.8, 1.6, and 0.9, respectively, which means

$$\Delta\tau_{br}^* \approx 9Bo_d^{-1/4} \approx 10.8We_{cd}^{-1/4}. \quad (8.95)$$

Obviously the spreading of the experimental data and the subjective judgment of the end of the fragmentation process explains the variation of the controlling constant.

*Gelfand et al. (1973)* proposed to take into account the viscosity of the droplets in the following manner

$$\Delta\tau_{br}^* = 4.5 \left( 1 + 1.2 On_d^{1.64} \right), \quad \text{for } We_d \leq 228 \quad (8.96)$$

where  $On_d$  is the *Ohnesorge* number. *Pilch et al. (1981)* envisage the possibility of taking the viscosity of the droplet into account by multiplying their correlation by  $1 + 1.2 On_d$ , where  $D_d$  is the instantaneous, deformed drop diameter measured normal to the approaching free stream. In a later work *Pilch and Erdman (1987)* used  $1 + 2.2 On_d$ . *Hsiang and Faeth (1992)* approximated provisionally their few data for  $On_d < 3.7$  and  $We_d < 10^3$  with the correction  $1/(1 - On_d/7)$  instead.

Let us summarize the results presented in this section: The final particle size for acceleration induced fragmentation is assumed to be the stable particle size governed by the stability criterion. The stability criterion is defined by the ratio of the shear force acting to destroy the particle and the surface tension force acting to retain the particle form. This ratio is found to be constant. The stability criterion contains the difference between the velocities of the continuum and of the particle adjusted after the fragmentation. This velocity difference is predicted either by analytical or by modified analytical solution of simplified momentum equations. The velocity difference computed by means of the stability criterion with the initial particle size is called *critical velocity*. The higher the relative velocity compared with the critical velocity the shorter the time interval in which the fragmentation occurs. There are 5 types of disintegration of particles exposed in continuum. The duration of the vibration type of fragmentation is estimated analytically. The duration of the other kinds of fragmentation is described empirically.

Knowing (i) the breakup time  $\Delta\tau_{br}^*$ , (ii) the final velocity difference between the stable particles and their environment,  $V_c - V_{d\infty}$ , and, (iii) using the hydrodynamic stability criterion Eqs. (8.36) and (8.37), we can compute the final maximum of the diameter of the fragments

$$D_{d\infty} \approx We_{d\infty} \sigma_d / \left[ \rho_c (V_c - V_{d\infty})^2 \right] \quad (8.97)$$

which is the first step of the modeling of the fragmentation process.

This method known as "maximum stable diameter concept" was introduced by *Pilch et al.* The maximum stable diameter concept is useful for estimating the largest stable fragment sizes resulting from droplet breakup, provided that the

initial *Weber* number exceeds about 350. The authors found that in this region the ratio of the maximum to the mass median fragment size is

$$D_{d\infty,\max} / D_{d\infty} = 2.04 \quad (8.98)$$

independent of the *Weber* number.

Thus, we recommend the *Pilch* et al. method for prediction of the mass median fragment size for *Weber* numbers exceeding 350. The successful comparison of this method given in Brauer (1992, 1981), p.111 Fig. 3.2, is valid for  $\approx 350 < We_{cd} < 10^5$ .

If the computed mass median fragment size for  $We_{cd} > 5.28$  after the fragmentation is larger than the initial drop size only vibration breakup can be expected.

## 8.5 Particle production rate correlations

Knowing the characteristics of the different fragmentation modes from experiments we can estimate approximately the particle production rate. Next we give the expressions for the production rates incorporating our knowledge of the different regimes of fragmentation.

### 8.5.1 Vibration breakup

Each vibration breakup leads to particle splitting. Therefore the particle production rate is

$$\dot{n}_{sp} \approx \frac{2n_d - n_d}{\Delta\tau_{br}} = n_d \frac{1}{\Delta\tau_{br}} = n_d f_{d,sp} \quad (8.99)$$

and the fragmentation frequency is simply the reciprocal value of the fragmentation period

$$f_{d,sp} = 1/\Delta\tau_{br}, \quad (8.100)$$

where  $\Delta\tau_{br}$  is computed using Eqs. (8.79) and (8.73).

### 8.5.2 Bag breakup

As shown by *Magarvey* and *Taylor* (1956) for free falling 15 mm water drops each bag breakup produces a spectrum of particle sizes that can be roughly divided into two groups:

1. Macroscopic particles produced by the rim breakup  $N_{dr}$  (e.g.  $N_{dr} \approx 2$  to 8) having 70 to 75% of the drop mass - see *Komabayasi et al.*, (1964) and *Gelfand et al.* (1976). For the following analysis we assume  $N_{dr} \approx 6$ . Assuming 75% the resulting particle size is

$$D_{dr} \approx \left( \frac{0.75}{N_{dr}} \right)^{1/3} D_d . \quad (8.101)$$

2. Microscopic particles produced by bag fragmentation  $N_{db} \approx 30$  to 100 as shown by *Fournier et al.* (1955), and *Magarvey and Taylor* (1956), having a size governed by the capillary surface waves amplitude. For the following analysis we assume  $N_{db} \approx 65$ . Assuming that the microscopic droplets have 25% of the initial mass we have for their size

$$D_{db} \approx \left( \frac{0.25}{N_{db}} \right)^{1/3} D_d . \quad (8.102)$$

Therefore the particle production rate is

$$\dot{n}_{sp} \approx \frac{n_d (N_{dr} + N_{db}) - n_d}{\Delta \tau_{br}} = n_d \frac{N_{dr} + N_{db} - 1}{\Delta \tau_{br}} = n_d f_{d,sp} , \quad (8.103)$$

and the fragmentation frequency is

$$f_{d,sp} = \frac{N_{dr} + N_{db} - 1}{\Delta \tau_{br}} \approx (N_{dr} + N_{db}) \frac{1}{\Delta \tau_{br}} \approx 70 / \Delta \tau_{br} , \quad (8.104)$$

where  $\Delta \tau_{br}$  is computed using Eq. (8.81).

The above information is sufficient to compute the resulting mass mean diameter

$$D_{d\infty} = D_d / (N_{dr} + N_{db})^{1/3} \approx D_d / 4.12 , \quad (8.105)$$

the *Souter* mean diameter

$$D_{d\infty}^{sm} = \left( \frac{N_{dr} D_{dr}^2 + N_{db} D_{db}^2}{N_{dr} + N_{db}} \right)^{1/2} = \left[ \frac{N_{dr} \left( \frac{0.75}{N_{dr}} \right)^{2/3} + N_{db} \left( \frac{0.25}{N_{db}} \right)^{2/3}}{N_{dr} + N_{db}} \right]^{1/2} D_d , \quad (8.106)$$

and finally the ratio

$$\begin{aligned}
 \left( \frac{D_{d\infty}^{sm}}{D_{d\infty}} \right)^2 &= \frac{N_{dr} \left( \frac{0.75}{N_{dr}} \right)^{2/3} + N_{db} \left( \frac{0.25}{N_{db}} \right)^{2/3}}{(N_{dr} + N_{db})^{1/3}} = \frac{N_{dr} \left( \frac{0.75}{N_{dr}} \right)^{2/3} + N_{db} \left( \frac{0.25}{N_{db}} \right)^{2/3}}{(N_{dr} + N_{db})^{1/3}} \\
 &= \frac{5 \left( \frac{0.75}{5} \right)^{2/3} + 65 \left( \frac{0.25}{65} \right)^{2/3}}{(5 + 65)^{1/3}} = 0.73
 \end{aligned} \tag{8.107}$$

which is important for computation of heat and mass transfer at the surface. Note that *Hsiang* and *Faeth* (1992) found experimentally  $0.83^2 = 0.79$  which is very close to the above estimate for this case.

Sophisticated application of this theory needs at least two velocity fields for the droplets description: microscopic and macroscopic, and more reliable experimental information about  $N_{db}$ .

### 8.5.3 Bag and stamen breakup

A similar approach to that used for the bag breakup is useful also for bag and stamen breakup. For this case  $N_{dr}$  should be interpreted as the number of fragments produced by the rim and stamen breakup.

### 8.5.4 Sheet stripping and wave crest stripping following by catastrophic breakup

The maximum of the fragment size for the sheet stripping and wave crest stripping followed by catastrophic breakup is well described by Eqs. (8.48) and (8.49). The ratio of the maximum to mass median fragment size has a constant value of 2.04 regardless of the initial *Weber* number for  $We_d > 300$ .

#### 8.5.4.1 Model without taking into account the primary breakup

Both mechanisms are associated with a very short breakup period, which is the reason for assuming that the production rate as a time function during  $\Delta\tau_{br}$  is equal to the averaged production rate, namely

$$\dot{n}_d \approx \frac{n_{d\infty} - n_d}{\Delta\tau_{br}} = n_d \left[ \left( \frac{D_d}{D_{d\infty}} \right)^3 - 1 \right] / \Delta\tau_{br} \approx n_d \left( \frac{D_d}{D_{d\infty}} \right)^3 \frac{1}{\Delta\tau_{br}}. \tag{8.108}$$

Next it will be shown that this expression is essentially equivalent to the one obtained by the assumption of linear reduction of the mass of the donor droplet with respect to the time.

It is convenient experimentally to measure the size or the mass of the remaining droplet and therefore

$$\frac{M_d}{M_{d0}} = f(\tau). \quad (8.109)$$

If the entrained fragment size is  $D_{d\infty}$ , the fragmentation source term can be computed as follows

$$\dot{n}_d = -\frac{n_d}{\rho_d \frac{\pi D_{d\infty}^3}{6}} \frac{dM_d}{d\tau} = -n_d \left( \frac{D_d}{D_{d\infty}} \right)^3 \frac{d}{d\tau} \frac{M_d}{M_{d0}}. \quad (8.110)$$

For linear mass reduction we have

$$M_d / M_{d0} = 1 - \tau / \Delta \tau_{br}, \quad (8.111)$$

$$\dot{n}_d = n_d \left( \frac{D_d}{D_{d\infty}} \right)^3 \frac{1}{\Delta \tau_{br}}. \quad (8.112)$$

If the entrained droplets have just the stable size at the local relative velocity  $V_{d\infty}$  which is close to the  $V_d$  we obtain

$$\frac{D_d}{D_{d\infty}} = \frac{We_d}{We_{d\infty}} \left( \frac{V_c - V_{d\infty}}{V_c - V_d} \right)^2 \approx \frac{We_d}{We_{d\infty}} \quad (8.113)$$

and therefore

$$\dot{n}_{d,sp} \approx n_d \left[ \left( \frac{We_d}{We_{d\infty}} \right)^3 - 1 \right] / \Delta \tau_{br}. \quad (8.114)$$

This approach is used by the author of this work in the computer code IVA3 (Kolev 1991a, 1991b, 1991c) and is recommended for  $We_c > 350$ .

For very high *Weber* numbers we have

$$\dot{n}_{d,sp} \approx \frac{n_d}{\Delta \tau_{br}} \left( \frac{We_d}{We_{d\infty}} \right)^3 \quad (8.115)$$

Note the difference between Eq. (8.115) and the intuitive proposal made by Kalinin (1970)

$$\dot{n}_{d,sp} \approx \frac{n_d}{\Delta \tau_{br}} \left[ \exp(-1/We_d) \right], \quad (8.116)$$

which is similar to Eq. (8.115) in the qualitative dependence on  $We_d$  but neglects the influence of the velocity ratio.

*Hsiang* and *Faeth* (1992) succeeded to correlate measurements for the final mass median diameter for all regimes of fragmentation which is dependent on the initial droplet size and *Reynolds* number

$$\frac{We_{d\infty}}{We_d} = 7.44 \left( \rho_d / \rho_c \right)^{1/4} / Re_d^{1/2} \quad (8.117)$$

for the region of the  $(\rho_d / \rho_c)^{1/4} We_d / Re_d^{1/2} \approx 0.3$  to 10,  $We_d = 0.5$  to 1000,  $Oh_d = 0.0006$  to 4,  $\rho_d / \rho_c = 580$  to 12 000, and  $Re_d = 300$  to 16 000. The data shows that the *Weber* number of the drop after the end of the breakup was generally greater than the critical *Weber* characteristic for the final particle diameter and the new adjusted velocity ( $We_{d\infty} > 13$ ). The *Souter* mean diameter was found to be 0.83 of the mass median diameter. Using this expression we obtain for the linearized fragmentation rate

$$\dot{n}_{d,sp} \approx \frac{n_{d\infty} - n_d}{\Delta \tau_{br}} = n_d 0.00243 (\rho_c / \rho_d)^{3/4} Re_d^{3/2} / \Delta \tau_{br}. \quad (8.118)$$

From Fig. (8.12) we see that

$$\Delta \tau_{br} \approx 5.5 D_d / \left[ \Delta V_{cd} (\rho_c / \rho_d)^{1/2} \right]. \quad (8.119)$$

Substituting into the above equation we finally obtain

$$\dot{n}_{d,sp} \approx n_d 0.00044 (\rho_c / \rho_d)^{5/4} \frac{\Delta V_{cd}}{D_d} Re_d^{3/2}. \quad (8.120)$$

#### 8.5.4.2 Models taking into account the primary breakup

Sheet stripping and wave crest stripping followed by catastrophic breakup are associated with a *primary breakup* leading to  $N'_d = 3$  to 5 fragments after  $\Delta \tau'_{br}$  for initial *Weber* number  $< 350$  defined by

$$\frac{\Delta \tau'_{br}}{D_d / \left[ \Delta V_{cd} (\rho_c / \rho_d)^{1/2} \right]} \approx 1 \text{ to } 1.5 \quad \text{for drop in gas} \quad (8.121)$$

and

$$\frac{\Delta \tau'_{br}}{D_d / \left[ \Delta V_{cd} (\rho_c / \rho_d)^{1/2} \right]} \approx 2 \quad \text{for drop in liquid.} \quad (8.122)$$

Therefore for  $0 < \Delta\tau \leq \Delta\tau'_{br}$  we have

$$\dot{n}_d \approx \frac{n_{d\infty} - n_d}{\Delta\tau'_{br}} \approx \frac{N'_d n_d - n_d}{\Delta\tau'_{br}} = n_d \frac{N'_d - 1}{\Delta\tau'_{br}} \approx n_d \frac{3}{\Delta\tau'_{br}}, \quad (8.123)$$

or

$$\dot{n}_d \approx n_d 2 \frac{\Delta V_{cd}}{D_d} (\rho_c / \rho_d)^{1/2} \quad (8.124)$$

for drop in gas and

$$\dot{n}_d \approx n_d \frac{3}{2} \frac{\Delta V_{cd}}{D_d} (\rho_c / \rho_d)^{1/2} \quad (8.125)$$

for liquid in liquid. The size of the newly produced unstable fragments is

$$D'_d = D_d / N_d'^{1/3}. \quad (8.126)$$

During this time  $\Delta\tau > \Delta\tau'_{br}$  fragments with diameter  $\lambda_{KH}$  are produced due to sheet stripping. Thus the maximum number of particles produced from the stripping of a single donor droplet is

$$\frac{D_d'^3 - D_{d\infty}^3}{\lambda_{KH}^3}. \quad (8.127)$$

Here we denote with  $D_{d\infty}$  the size of the donor particle remaining stable after the sheet stripping. The correlation of *Hsiang* and *Faeth* (1992) can be used also in this case.

Thus the rate of particle production during the time interval  $\Delta\tau_{br} - \Delta\tau'_{br}$  is

$$\begin{aligned} \dot{n}_d &\approx \frac{N'_d n_d \frac{D_d'^3 - D_{d\infty}^3}{\lambda_{KH}^3} - N'_d n_d}{\Delta\tau_{br} - \Delta\tau'_{br}} = N'_d n_d \frac{\left(\frac{D'_d}{\lambda_{KH}}\right)^3 - \left(\frac{D'_{d\infty}}{\lambda_{KH}}\right)^3 - 1}{\Delta\tau_{br} - \Delta\tau'_{br}} \\ &= N'_d n_d \frac{\frac{1}{N'_d} \left(\frac{D_d}{\lambda_{KH}}\right)^3 - \left(\frac{D'_{d\infty}}{\lambda_{KH}}\right)^3 - 1}{\Delta\tau_{br} - \Delta\tau'_{br}} \end{aligned} \quad (8.128)$$

The time-averaged production rate is therefore

$$\begin{aligned} \dot{n}_d &\approx \frac{n_d}{\Delta\tau_{br}} \left[ \left(\frac{D_d}{\lambda_{KH}}\right)^3 - N'_d \left(\frac{D'_{d\infty}}{\lambda_{KH}}\right)^3 - 1 \right] \\ &\approx n_d \frac{\Delta V_{cd}}{D_d} (\rho_c / \rho_d)^{1/2} \frac{1}{5.5} \left[ \left(\frac{D_d}{\lambda_{KH}}\right)^3 - 4 \left(\frac{D'_{d\infty}}{\lambda_{KH}}\right)^3 \right]. \end{aligned} \quad (8.129)$$



The total number of droplets after the fragmentation of a single droplet is

$$N'_d + N'_d \frac{D_d'^3 - D_{d\infty}^3}{\lambda_{KH}^3} \quad (8.130)$$

and the resulting mass median diameter is

$$D_{d\infty} = D_d \left( N'_d + N'_d \frac{D_d'^3 - D_{d\infty}^3}{\lambda_{KH}^3} \right)^{1/3} = \frac{D_d}{N_d'^{1/3}} \left\{ 1 + \left( \frac{D_d}{\lambda_{KH}} \right)^3 \left[ \frac{1}{N'_d} - \left( \frac{D_{d\infty}}{D_d} \right)^3 \right] \right\}^{1/3}. \quad (8.131)$$

#### 8.5.4.3 Other models

*Reineke* and *Waldman* (1970, 1975) recommended the following empirical equation to describe the change of the single drop mass

$$M_d / M_{d0} = \frac{1}{2} \left[ 1 - \cos \left( \pi \frac{\tau}{\Delta \tau_{br}} \right) \right], \quad 0 < \tau \leq \Delta \tau_{br} \quad (8.132)$$

due to sheet stripping. Here the dimensionless breakup time is assumed to be  $\Delta \tau_{br}^* \approx 4$  and primary breakup was not taken into account. For high pressure shock waves (200, 340 and 476 bar amplitudes) *Yuen* et al. (1994) provided experimental data for mercury-water systems which are described by the linear law

$$M_d / M_{d0} = 1 - \tau / \tau_{br} = 1 - \frac{1}{c} \tau W e_{cd}^{1/4}, \quad 0 < \tau \leq \Delta \tau_{br}^*, \quad (8.133)$$

see *Yuen* et al. (1992), Fig. 1, where  $\Delta \tau_{br} = \text{Eq. (8.95)}$ . In addition the authors demonstrated that the *Reineke* and *Waldman* correlation does not represent the *Yuen* et al. data, see Fig. 3 in *Yuen* et al. (1992), and demonstrated that linear dependence, Eq. (8.133) is the better one, compare with Fig. 1 in *Yuen* et al. (1992).

For the region of sheet stripping and wave crest stripping with catastrophic breakup, *Chu* and *Corrardini* (1984) proposed two models. The first model,

$$M_d / M_{d0} \approx \exp(-3c_1 \tau^{c_2} W e_{cd}^{c_3}) \quad (8.134)$$

where  $c_1 = 0.1708 - 0.149 (\rho_d / \rho_c)^{1/2}$ ,  $c_2 = 0.772$ , and  $c_3 = 0.246$ , describes the droplet diameters  $D_d$  as a function of the time since the beginning of the fragmentation,  $\tau$ . The second model (*Chu* and *Corrardini* 1986),

$$M_{d2} / M_{d1} \approx \left( 1 - c_0 \Delta \tau_{21}^{c_2} W e_{cd}^{c_3} \right)^3 \quad (8.135)$$

where  $c_0 = 0.1093 - 0.078 (\rho_d / \rho_c)^{1/2}$ , gives the relationship between two average particle masses  $M_{d2}$  and  $M_{d1}$  for two different times  $\tau_2$  and  $\tau_1$  during the fragmentation process. The database for the second model consists of the *Baines* and *Buttery* experimental data for  $We_{cd} \approx 200 - 3860$  (Baines and Buttery 1978).

Using Eq. (8.132), and assuming that the produced small particles have the size  $D_{d\infty}$ , the particle number production rate is

$$\dot{n}_{d,sp} = -\frac{n_d}{\rho_d} \frac{\pi D_{d\infty}^3}{6} \frac{dM_d}{d\tau} = n_d \frac{\pi}{8} \frac{\Delta V_{cd}}{D_d} (\rho_c / \rho_d)^{1/2} \left( \frac{D_d}{D_{d\infty}} \right)^3 \sin \left( \pi \frac{\tau}{\Delta \tau_{br}} \right) = n_d f_{d,sp} . \quad (8.136)$$

Note that the time used in this correlation is the time elapsed from the beginning of the fragmentation process which has to be kept in storage during computational analysis. This is very inconvenient. Using Eq. (8.133) we obtain

$$\dot{n}_{d,sp} = n_d \frac{\Delta V_{cd}}{D_d} (\rho_c / \rho_d)^{1/2} \left( \frac{D_d}{D_{d\infty}} \right)^3 \frac{1}{\Delta \tau^*} = n_d f_{d,sp} , \quad (8.137)$$

which is time independent and very convenient for use in computer codes.

Keeping in mind that the droplet surface per unit volume of the mixture,  $(F_d / Vol)$ , is about  $n_d \pi D_d^2$  the term

$$\dot{n}_{d,sp}'' = \frac{1}{2\Delta \tau_s^*} \frac{\Delta V_{cd}}{D_d^3 (\rho_d / \rho_c)^{1/2}} \sin \left( \pi \frac{\Delta \tau^*}{\Delta \tau_s^*} \right) \quad (8.138)$$

or

$$\dot{n}_{d,sp}'' = \frac{1}{\pi \Delta \tau_{br}^*} \frac{\Delta V_{cd}}{D_d^3 (\rho_d / \rho_c)^{1/2}} \quad (8.138)$$

for the high pressure liquid-liquid case, can be interpreted as the number of the entrained micro-droplets per unit surface of the macroscopic droplet (particle flow rate). So the idea naturally arises to model the surface particle flow rate not only at droplet surfaces but also at surfaces with arbitrary form, namely

$$\dot{n}_{d,sp} = (F_d / Vol) \dot{n}_{d,sp}'' . \quad (8.140)$$

As already mentioned, some authors prefer to use interfacial area concentration as the convected variable instead of the particle number density. For such an approach the generated interfacial area per unit time and unit mixture volume is easily computed multiplying the above equation with  $\pi D_{d\infty}^2$ . The result is

$$\dot{F}_d = (F_d / Vol) \frac{1}{2\Delta\tau_s^*} \frac{\Delta V_{cd}}{D_d^3 (\rho_d / \rho_c)^{1/2}} \sin\left(\pi \frac{\Delta\tau^*}{\Delta\tau_s^*}\right) \quad (8.141)$$

or

$$\dot{F}_d = (F_d / Vol) \frac{1}{\Delta\tau_{br}^*} \frac{\Delta V_{cd}}{D_d^3 (\rho_d / \rho_c)^{1/2}} \quad (8.142)$$

for high pressure liquid-liquid case. A similar expression,

$$\dot{F}_d = (F_d / Vol) 0.089 c_{cd}^{d\ 3/4} We_{cd}^{1/4} \frac{|\Delta V_{cd}|}{D_d (\rho_d / \rho_c)^{1/2}} \quad (8.143)$$

was proposed by *Pilch* and *Young* and used by *Young* (1989) in the computer code IFCI, where  $c_{cd}^d$  is the drag coefficient between continuum and droplet. This idea was used in terms of diameter change by *Young* (1989),

$$\dot{D}_d^{donor} = - \frac{\left[1 - (N'_d)^{-1/3}\right] \Delta V_{cd}^{donor}}{\Delta\tau'_{br} (\rho_d / \rho_c)^{1/2}}. \quad (8.144)$$

Two points should be considered in the application of the detailed sheet stripping models in system computer codes:

1. The detailed description of the sheet stripping needs additional computer storage to store the time when the sheet stripping process starts and the particle size at this moment in each computational cell (see the comments by *Fletcher* and *Anderson* (1990)), because the time in Eq. (8.116) is counted from the beginning of the sheet stripping in a *Lagrangian* manner.
2. At least two velocity fields for representation of macro- and microscopic droplets are formally needed in order to distinguish between the donor drop and the produced fragments. Within the donor drop field the primary breakup can be easily modeled if the time from the beginning of the sheet stripping reaches the time for primary breakup. Within the next actual time step  $\Delta\tau$  the particle production rate in the donor drop field is

$$\dot{n}_{d,sp}^{donor} = N'_d n_d^{donor} / \Delta\tau. \quad (8.145)$$

The further sheet stripping is allowed until the donor cell reduces its size to the size of the produced stable fragments. Another modeling approach is the use of the averaged production rate during the period  $\Delta\tau'_{br}$

$$\dot{n}_{d,sp}^{donor} = \frac{n_d^{donor} - N'_d n_d^{donor}}{\Delta\tau'_{br}} = n_d^{donor} \frac{1 - N'_d}{\Delta\tau'_{br}} = n_d^{donor} \frac{1 - N'_d}{\Delta\tau_{br}^*} \frac{\Delta V_{cd}^{donor}}{D_d^{donor} (\rho_d / \rho_c)^{1/2}}. \quad (8.146)$$

This idea was used in terms of diameter change by *Young* (1989)

$$\dot{D}_d^{donor} = - \frac{1 - N_d'^{-1/3}}{\Delta \tau_{br}^*} \frac{\Delta V_{cd}^{donor}}{(\rho_d / \rho_c)^{1/2}}. \quad (8.147)$$

Acceleration induced fragmentation seems to be the most frequently investigated fragmentation phenomenon and reliable data are available for practical *approximate* modeling of dynamic fragmentation.

The questions that are not resolved by this approach are the following: Acceleration induced fragmentation strongly depends on the relative velocities between neighboring velocity fields. The relative velocities are governed by the modeling of drag, lift, and virtual mass forces. Drag, lift, and virtual mass coefficients are usually measured and correlated for simple steady state flows. Little is known about the drag coefficients for transient conditions, for molten drops in water with strong evaporation, drag coefficients in mutual interpenetration of three fluids. This inevitably affects the accuracy of the prediction of the relative velocity and therefore the accuracy of the prediction of the dynamic fragmentation. Obviously improvement of the knowledge in these fields is necessary in order to increase the accuracy of the theoretical predictions.

## 8.6 Droplets production due to highly energetic collisions

Consider collision of two droplets with relative velocity of  $V^{rel} = \Delta V_{dd}^{no}$  being very high. The collision will inevitably lead to a strong instability of the resulting droplet and eventually to fragmentation of the resulting droplet. If after the collision of two droplets two new droplets are produced the coalescence frequency of a single droplet is equal to zero

$$(f_{coal}^p)^{no} = 0, \quad (8.148)$$

and there is no effective droplet production due to collision. If more than two droplets are produced the coalescence frequency of a single droplet due to collision is zero and there is a production of particles due to collision which may be expressed with negative coalescence frequency of a single droplet

$$f_{coal}^p < 0. \quad (8.150)$$

The interactions observed for colliding water droplets by *Ashgriz* and *Givi* (1987) may involve:

- 1) a bouncing collision;
- 2) a grazing collision, in which the droplets just touch each other slightly without coalescence;
- 3) a permanent coalescence;
- 4) temporally coalescence followed by separation in which satellite droplets are generated;

- 5) a shattering collision, occurring at high energy collisions, in which numerous tiny droplets are expelled radially from the periphery of the interacting drops.

An empirical description of the dynamics of such collisions for gas droplet suspensions was made by *Podovisotsky* and *Schreiber* (1984). According to the authors, a target droplet  $d1$  colliding with the projectile  $d2$  (smaller than the target droplet) undergoes a main change in mass, given as

$$\Delta m_{d1} / m_{d2} = 1 - 0.246 Re_{d12}^{0.407} Lp_{d1}^{-0.096} (D_{d1} / D_{d2})^{-0.278} - \Phi_{d12} \quad (8.151)$$

(for  $30 < Re_{d12} < 6000$ ;  $5 < Lp_{d1} < 3 \times 10^5$ ;  $1.9 < D_{d1} / D_{d2} \leq 12$ ), where  $m$  is the droplet mass;  $Re_{d12}$  is the *Reynolds* number for a small droplet penetrating into the larger droplet,

$$Re_{d12} = D_{d2} |V_{d2} - V_{d1}| \rho_d / \eta_d, \quad (8.152)$$

where  $D_{d2}$  is the droplet diameter,  $V_d$  is the droplet velocity,  $\rho_d$  is its density and  $\eta_d$  is the liquid particle viscosity;  $Lp_{d1}$  is the *Laplace* number, indicating a ratio between surface tension forces and viscous drag,

$$Lp_{d1} = D_{d1} \rho_d \sigma / \eta_d^2, \quad (8.153)$$

where  $\sigma$  is the surface tension between droplet and gas;  $\Phi_{d12}$  is a correction term accounting for the gas flow, given as

$$\Phi_{d12} = 0.00446 A \quad \text{for } A \leq 40.6, \quad (8.154)$$

$$\Phi_{d12} = 11.85 (0.01A)^{4.64} \quad \text{for } 40.6 \leq A \leq 120, \quad (8.155)$$

$$A = Re_{d12}^{0.285} Lp_{d1}^{0.2} (D_{d1} / D_{d2})^{0.4} We_{cd1}^{0.442}, \quad (8.156)$$

and  $We_{cd1}$  is the *Weber* number, indicating a ratio between the inertia force and the surface tension force,

$$We_{cd1} = \rho_c (V_c - V_{d1})^2 D_{d1} / \sigma, \quad (8.157)$$

where  $V_c$  is the local gas velocity. When

$$\Delta m_{d1} / m_{d2} = 1, \quad (8.158)$$

the droplets coalesce. When

$$0 < \Delta m_{d1} / m_{d2} < 1, \quad (8.159)$$

some of the projectile droplets are fragmented. For

$$-\Delta m_{d1} / m_{d2} < \Delta m_{d1} / m_{d2} < 0 \quad (8.160)$$

the projectile droplet is fully fragmented while the target droplet is fragmented partially or fully. Note that the condition

$$-\Delta m_{d1} / m_{d2} < \Delta m_{d1} / m_{d2} \quad (8.161)$$

is imposed by conservation of mass. We see that this interpretation of  $\Delta m_{d1} / m_{d2}$  resembles the coalescence probability

$$\left( f_{dcoal}^p \right)^{no} \approx \Delta m_{d1} / m_{d2} . \quad (8.162)$$

## 8.7 Acceleration induced bubble fragmentation

Bubbles can disintegrate due to different kinds of instabilities, e.g. acceleration or turbulence induced fragmentation. To model the dynamic fragmentation means to compute the bubble number production rate in Eq. (7.2), i. e. the estimation of the bubble diameter at the end of the fragmentation process,  $D_{d\infty}$ , and the estimation of the duration of the fragmentation,  $\Delta \tau_{br}$ . The production rate due to bubble splitting is computed by means of Eq. (7.11). The hydrodynamic stability criterion already introduced for droplets

$$We_{d\infty} = \rho_c (V_c - V_{d\infty})^2 D_{d\infty} / \sigma \approx const \quad (8.163)$$

for acceleration induced fragmentation is also valid for bubble fragmentation. The most frequently used value for the hydrodynamic stability criterion in the two-phase literature is

$$We_{d\infty} = \rho_c (V_c - V_{d\infty})^2 D_{d\infty} / \sigma \approx 12 \quad (8.164)$$

Next we discuss first the upper and then the lower values of  $D_{d\infty}$ .

There is a bubble flow regime (bubble diameter approximately 0.001 to 0.02 m) in which the terminal velocity

$$\Delta V_{cd\infty} = Ku V_K , \quad (8.165)$$

see *Wallis* (1969), is independent of the size and is proportional to the so called *Kutateladze* terminal velocity

$$V_K = \left[ \sigma g (\rho_c - \rho_d) / \rho_c^2 \right]^{1/4} , \quad Ku = \sqrt{2} . \quad (8.166)$$

Substituting Eq. (8.165) into Eq. (8.164) and solving for  $D_{d\infty}$  we obtain the upper limit of the bubble size in the flow

$$D_{d\infty, \max} \approx We_{d\infty} \frac{1}{2} \lambda_{RT} . \quad (8.167)$$

*Brodkey* (1967) found that bubbles having a diameter less than

$$D_{d\infty, \min} \approx 2.53 \frac{1}{2} \lambda_{RT} \quad (8.168)$$

behave as solid spheres and are not subject to further splitting. *Berenson* observed experimentally that during film boiling on horizontal surfaces the bubbles departing the film have a size

$$D_{d\infty, \min} \approx 4.7 \lambda_{RT} . \quad (8.169)$$

Thus, the stable bubble size after the fragmentation should be

$$D_{d\infty} \approx We_{d\infty} \frac{\sigma}{\rho_c (V_c - V_{d\infty})^2} , \quad (8.170)$$

within the bounds

$$D_{d\infty, \min} < D_{d\infty} < D_{d\infty, \max} . \quad (8.171)$$

Some authors have correlated the observed bubble diameters for steady state flows as a function of the local conditions. *Note that these correlations contain integral results of simultaneously happening fragmentation and coalescence.* Two examples are given below.

*Ahmad* (1970) correlated data modifying the maximum possible bubble diameter observed in the flow by using instead of  $We_{d\infty}=12$ , the following correlation

$$We_{d\infty} = \frac{1.8}{1 + 1.34(\alpha_c w_c)^{1/3}} = We_{d\infty}^* \quad \text{for } \alpha_d < 0.1 \quad (8.172)$$

$$We_{d\infty} = We_{d\infty}^* \left( \frac{9\alpha_d}{1 - \alpha_d} \right)^{1/3} \quad \text{for } 0.1 < \alpha_d < 0.99 . \quad (8.173)$$

*Kelly and Kazimi* (1982) modified this correlation to

$$\frac{D_{d0}}{\lambda_{RT}} = \frac{1.8}{1 + 1.34(\alpha_c w_c)^{1/3}} \quad \text{for } \alpha_d < 0.1 \quad (8.172b)$$

$$D_d = D_{d0} \left( \frac{9\alpha_d}{1 - \alpha_d} \right)^{1/3} \quad \text{for } 0.1 < \alpha_d < 0.99 . \quad (8.173b)$$

*Serizawa and Kataoka* (1987) correlated their data for the interfacial area concentration for vertical bubble flow in a pipe with 0.3 m diameter in the region  $\alpha_c w_c = 1$  to 5 m/s by the following correlation

$$\frac{6\alpha_d}{D_{d\infty}} = 1030\alpha_d^{0.87} (\alpha_c w_c)^{0.2} \quad \text{or} \quad (8.174)$$

$$D_{d\infty} = 0.00582\alpha_d^{0.13} / (\alpha_c w_c)^{0.2}. \quad (8.175)$$

Both correlations already contain the effect of the bubble splitting with increasing liquid velocity and of the coalescence with increasing gas volume fraction.

In what follows we estimate the period of the bubble splitting. By relative displacement of a body in an infinite continuum, compared with the size of the body, the continuum is deformed in front of, and around the body, and fills the region behind it. Similarly, bubbles displace liquid due to their relative motion with respect to the continuum. Bubble flows in which the bubble velocity differs from the liquid velocity possess natural fluctuations. We estimate the period of these fluctuations by dividing the average distance between two adjacent bubbles by the time needed for one bubble to sweep out this distance. The average distance between two adjacent bubbles,  $\Delta\ell_d$ , in a flow with bubble volume fraction  $\alpha_d$  is

$$\Delta\ell_d \approx D_d \left( \frac{\pi\sqrt{2}}{6\alpha_d} \right)^{1/3} \approx 0.9047 D_d / \alpha_d^{1/3}. \quad (8.176)$$

The time needed for one bubble to sweep out this distance is

$$\Delta\tau_d^{nat} \approx \Delta\ell_d / |\Delta V_{cd}| \approx \frac{0.9047 D_d}{|\Delta V_{cd}| \alpha_d^{1/3}}. \quad (8.177)$$

In fact the real picture is more complicated. The fluctuations are damped due to the bubble compressibility, and the bubbles are interacting with each other and with the eddies behind the bubbles.

Thus the natural fluctuation period in the bubble flow is of the order of

$$\Delta\tau_d^{nat} \approx \text{const} \frac{D_d}{|\Delta V_{cd}| \alpha_d^{1/3}}. \quad (8.178)$$

If the bubble is unstable,

$$We_d > We_{d\infty}, \quad (8.179)$$

the fragmentation is likely to happen within  $\Delta\tau_d^{nat}$  i.e.

$$\Delta\tau_{br} \approx \text{const} \frac{D_d}{|\Delta V_{cd}| \alpha_d^{1/3}}. \quad (8.180)$$



Thus, bubbles having relative velocity with respect to the surrounding liquid are unstable if  $We_d > We_{d\infty}$ , where  $We_{d\infty}$  is found to be equal 12 within the time interval  $\Delta\tau_{br}$  defined by Eq. (8.178). The final diameter after the fragmentation can be assumed equal to that defined by Eq. (8.170), within the limits given with the inequality (8.171).

*Gelfand et al.* (1974) found experimentally that bubbles behind the front of the waves are stable for  $We_{d\infty} < 5$ . *Gelfand et al.* [19] (1975) have successfully used the time scale

$$\Delta\tau_{br}^* = \frac{\Delta\tau_{br}}{\delta_{dKH} / \left[ \Delta V_{cd} (\rho_d / \rho_c)^{1/2} \right]} \approx 1 \quad (8.181)$$

for bubble fragmentation behind the front of the pressure wave.

There are some unresolved problems in this approach:

- Why should the swarm of bubbles with an unstable average diameter  $D_d$  after the fragmentation take just the stable averaged diameter  $D_{d\infty}$ ?
- How large is the constant in Eq. (8.180), or is it a constant at all?

Further experiments are needed to resolve this particular problem.

## Nomenclature

### Latin

$Ar$	<i>Archimedes number, dimensionless</i>
$Bo_d$	$= \left[ \rho_d \frac{dV_d}{d\tau} (D_d / 2)^2 \right] / \sigma_d = \frac{3}{16} c_{cd}^d We_{cd}$ , <i>Bond number, dimensionless</i>
$c_{cd}^d$	<i>drag coefficient, dimensionless</i>
$c_{cd}^{vm}$	<i>virtual mass coefficient, dimensionless</i>
$D$	<i>particle diameter, m</i>
$D_d^v$	<i>volume equivalent diameter for non-spherical particle, m</i>
$D_{d,max}$	<i>maximum diameter during the oscillation, m</i>
$D_{d,min}$	<i>minimum diameter during the oscillation, m</i>
$D_{dr}$	<i>particle diameter produced by the rim breakup, m</i>
$D_{db}$	<i>particle diameter produced by the bag breakup, m</i>
$D_{d\infty}^{sm}$	<i>Souter mean diameter, m</i>
$\dot{D}_d^{donor}$	<i>change of the donor particle diameter per unit time, m/s</i>

$D_{d\infty}$	stable particle diameter after the fragmentation is finished, $m$
$D_{d1}$	target droplet diameter, $m$
$D_{d2}$	projectile droplet diameter (smaller than the target droplet diameter), $m$
$d$	differential
$\dot{F}_d$	generated interfacial area per unit time and unit mixture volume, $m^2/(sm^3)$
$f_n$	natural frequency of the n-th order mode of a spherical drop or bubble performing oscillations in continuum, where $n = 2, 3, \dots, n$ , $1/s$
$f_{d,sp}$	$= 1/\Delta\tau_{br}$ , fragmentation frequency, $1/s$
$g$	gravitational acceleration, $m/s^2$
$La_d$	$= 1/On_d^2$ , Laplace number, <i>dimensionless</i>
$Lp_{d1}$	$= D_{d1}\rho_d\sigma/\eta_d^2$ , Laplace number, ratio between surface tension forces and viscous drag, <i>dimensionless</i>
$M_d$	mass of a single droplet, $kg$
$M_{d0}$	initial mass of a single droplet before fragmentation, $kg$
$Ma$	Mach number, <i>dimensionless</i>
$N_{\eta d}$	viscosity number, <i>dimensionless</i>
$N_{dr}$	macroscopic particles produced by the rim breakup, -
$N_{db}$	microscopic particles produced by bag fragmentation, -
$N'_d$	microscopic particles produced by primary breakup, -
$\dot{n}_{sp}$	particle production rate, $1/(m^3s)$
$\dot{n}_{d,sp}''$	number of the entrained micro-droplets per unit surface of the macroscopic droplet (particle flow rate), $1/(m^2s)$
$\dot{n}_{d,sp}^{donor}$	particle production rate in the donor drop field, $1/(m^3s)$
$On_d$	$= \eta_d/\sqrt{\rho_d D_d \sigma_d} = We_d^{1/2}/Re_d$ , Ohnesorge number, <i>dimensionless</i>
$Re$	Reynolds number, <i>dimensionless</i>
$Re_{d12}$	$= D_{d2} V_{d2} - V_{d1} \rho_d/\eta_d$ , Reynolds number for a small droplet penetrating into the larger droplet, <i>dimensionless</i>
$t$	tangential force per unit surface, $N/m^2$
$V$	velocity, $m/s$
$V_{d\infty}$	final fragment velocity, $m/s$
$We$	Weber number, <i>dimensionless</i>

### Greek

$\Delta m_{d1}$	mass change of the target droplet $d1$ after colliding with the projectile droplet $d2$ having mass $m_{d2}$ , $kg$
$m_{d2}$	mass of the projectile droplet, $kg$

---

$\Delta\rho_{dc}$	density difference, $kg/m^3$
$\Delta V_{13}$	velocity difference, $m/s$
$\Delta\tau_{\Delta V}$	linearized velocity relaxation time constant, $s$
$\Delta\tau_{br}$	fragmentation period, $s$
$\Delta\tau'_{br}$	duration of the primary breakup, $s$
$\Delta\tau^*$	time, <i>dimensionless</i>
$\delta_{d,KH}$	most unstable wavelength, <i>Kelvin-Helmholtz</i> wavelength, $m$
$\Phi_{d12}$	correction term accounting for the gas flow, <i>dimensionless</i>
$\sigma$	surface tension, $N/m$
$\tau$	time, $s$
$\lambda_{bk}$	liquid boundary layer thickness inside the droplet, $m$
$\lambda_{RT}$	$= [\sigma_d / (g\Delta\rho_{dc})]^{1/2}$ , scale of the <i>Rayleigh-Taylor</i> instability wavelength, $m$
$\rho$	density, $kg/m^3$
$\eta$	dynamic viscosity, $kg/(ms)$

### ***Subscripts***

0	initial, before fragmentation
1	gas
2	liquid
3	droplet, particles
c	continuous
d	disperse
$\infty$	at the end of the fragmentation
d1	target droplet
d2	projectile droplet (smaller than the target droplet)

## **References**

- Ahmad SY (1970) Axial distribution of bulk temperature and void fraction in a heated channel with inlet subcooling, *J. Heat Transfer*, vol 92 pp 595
- Anderson WH and Wolfe HE (1965) Aerodynamic breakup liquid drops - I. Theoretical, *Proc. Int. Shock Tube Symposium*, Naval Ordnance Lab. White Oak, Maryland, USA, pp 1145-1152
- Arcoumanis C, Khezzar L, Whitelaw DS and Warren BCH (1994) Breakup of Newton and non-Newton fluids in air jets, *Experiments in Fluids*, vol 17 pp 405-414

- Ashgriz N and Givi P (1987) Binary collision dynamics of fuel droplets, *Int. J. Heat Fluid Flow*, vol 8 pp 205-210
- Baines M and Buttery NE (Sept. 1978) Differential velocity fragmentation in liquid - liquid systems, RD/B/N4643, Berkley Nuclear Laboratories
- Brauer H (1992) Umströmung beschleunigter und verzögerter Partikel, *Wärme und Stoffübertragung*, vol 27 pp 93-101
- Brodkey RS (1967) *The phenomena of fluid motions*, Addison-Wesley Press
- Chandrasekhar S (1981) *Hydrodynamic and hydromagnetic stability*, Dover Publ. Inc., New York
- Chen X, Yuen WW and Theofanous TG (1995) On the constitutive description of microinteractions concept in steam explosions, *Proceedings of the Seventh International Topical Meeting on Nuclear Reactor Thermal Hydraulics NURETH-7*, New York, USA, NUREG/CP-0142
- Chu CC and Corradini MC (Nov.1984) Hydrodynamics fragmentation of liquid droplets, *ANS Transaction*, Wash. DC, vol 47
- Chu CC and Corradini MC (Febr. 2-6, 1986) One-dimensional model for fuel coolant fragmentation and mixing analysis, *Proceedings of the International ANS/ENS Topical Meeting on Thermal Reactor Safety*, San Diego, California, U.S.A., vol 1 pp II.2-1-II.2-10
- De Jarlais G, Ishii M and Linehan J (Febr. 1986) Hydrodynamic stability of inverted annular flow in an adiabatic simulation, *Transactions of ASME, Journal of Heat Transfer*, vol 108 pp 85-92
- Dinh AT, Dinh TN, Nourgaliev RR and Sehgal BR (19<sup>th</sup>-21<sup>th</sup> May 1997) Hydrodynamic fragmentation of melt drop in water, *OECD/CSNI Specialist Meeting on Fuel Coolant Interactions*, JAERI-Tokai Research Establishment, Japan
- Faeth GM (April 3-7, 1995) Spray combustion: a review, *Proc. of The 2nd International Conference on Multiphase Flow '95 Kyoto*, Japan
- Fletcher DF and Anderson RP (1990) A review of pressure-induced propagation models of the vapor explosion process, *Progress in Nuclear Energy*, vol 23 no 2 pp 137-179
- Fournier D'Albe EM and Hidayetulla MS (1955) *Quarterly Journal Royal Meteorological Society*, Kondon, vol 81 pp 610-613
- Gelfand BE, Gubin SA and Kogarko SM (1976) Various forms of drop fragmentation in shock waves and their spatial characteristics, *J. Eng. Phys.*, vol 27
- Gelfand BE, Gubin SA, Kogarko SM and Komar SP (1973) Osobennosti Razrusheniya Kapel Vijaskoi Zhidkosti v Udarnich Volnach (Feature of Viscous Liquid Drop Breakup Behind Shock Wave) *Inzenerno Physicheski Journal*, vol 25 no 3 pp 467-470
- Gelfand BE et al (1974) The main models of the drops breakup; *Inzenerno Physicheski Journal*, vol 27 no 1 pp 120-126
- Gelfand BE, Gubin SA et al (1975) Breakup of air bubbles in liquid, *Dokl. USSR Ac. Sci.*, vol 220 no 4 pp 802-804
- Haas F (November 1964) Stability of droplets suddenly exposed to a high velocity gas steam, *A.I.Ch.E. Journal*, vol 10 no 6 pp 920-924
- Hanson AR, Domich EG and Adams HS (August 1963) Shock tube investigation of the breakup of drop by air blasts, *Phys. Fluids*, vol 6 no 8 pp 1070 - 1080
- Hassler G (1971) *Untersuchungen zur Verformung und Auflösung von Wassertropfen durch aerodynamische Kräfte im stationären Luft - und Wasserstrom für Unterschallgeschwindigkeit*, Dissertation, Universität Karlsruhe

- Hinze JO (1949a) Critical speed and sizes of liquids globules, *Appl. Sci. Res.*, vol A1 pp 273-288
- Hinze JO (1949b) Forced deformation of viscous liquid globules, *Appl. sci. Res.*, vol A1 pp 263-272
- Hinze JO (1955) Fundamentals of hydrodynamics of splitting in dispersion processes, *AIChE Journal*, vol 1 pp 284-295
- Hsiang LP and Faeth GM (1992) Near-limit drop deformation and secondary breakup, *Int. J. Multiphase Flow*, vol 18 no 5 pp 635-652
- Ishii M (1977) One-dimensional drift-flux model and constitutive equations for relative motion between phases in various two-phase flow regimes, *ANL-77-47*
- Kalinin AV (May 1970) Derivation of fluid mechanics equations for two phase medium with phase change, *Heat Transfer - Sov. Res.* Vol 2 no 3
- Kamke E (1959) *Differentialgleichungen, Lösungsmethoden und Lösungen*, Bd.I *Gewöhnliche Differentialgleichungen*. Leipzig: Gees & Portig
- Kelly JE and Kazimi MS (1982) Interfacial exchange relations for two-fluid vapour-liquid flow, A simplified regime-map approach, *Nucl. Sci.*, vol 81 p 318
- Kojo T and Ueno I (7-12 May 2006) Oscillation mode transition of bubbles under large amplitude pressure field, *ECI International Conference on Boiling Heat Transfer Spoleto*
- Kolev NI (Sept. 1991a) A three-field model of transient 3D multi-phase three-component flow for the computer code IVA3, Part 1: Theoretical basics: Conservation and state equations, numerics. *Kernforschungszentrum Karlsruhe, KfK 4948*
- Kolev NI (Sept. 1991b) A three-field model of transient 3D multi-phase three- component flow for the computer code IVA3, Part 2: Models for interfacial transport phenomena. *Code Validation. Kernforschungszentrum Karlsruhe, KfK 4949*
- Kolev NI (Sept. 1991c) IVA3: Computer code for modeling of transient three dimensional three phase flow in complicated geometry, *Program documentation: Input description. Kernforschungszentrum Karlsruhe, KfK 4950*
- Komabayasi MT, Gonda T and Isono K (1964) Life time of water drops before breaking in size distribution fragment droplet, *J. Met. Soc. Japan*, vol 42 no 5 pp 330-340
- Krzczkowski S (1980) Measurement of liquid droplet disintegration mechanisms, *Int. J. Multiphase Flow*, vol 6 pp 227-239
- Laftaye G (1943) *Sur l'atomatisation d'un jet liquide*, *C. R. Acad. Sci.*, Paris 217 p 340
- Lamb MA (1945) *Hydrodynamics*. Cambridge, At the University Press
- Lane WR (June 1951) Shatter of drops in streams of air, *Ind. Eng. Chem.*, vol 43 pp 1312-1317
- Li MK and Folger HS (1978) Acoustic emulsification, Part 2. Breakup of large primary oil droplets in water medium, *J. Fluid Mech.*, vol 88 no 3 pp 513-528
- Magarvey RH and Taylor BW (Oct.1956) Free fall breakup of large drops, *Journal of Applied Physics*, vol 27 no 10 pp 1129 - 1135
- Milashenko VI, Nigmatulin BI, Petukhov VV and Trubkin NI (1989) Burnout and distribution of liquid in evaporative channels of various lengths. *Int. J. Multiphase Flow* vol 15 no 3 pp 393-402
- Patel PD and Theofanous TG (1981) Hydrodynamic fragmentation of drops, *J. Fluid Mech.*, vol 103 pp 307-323
- Pilch MM and Erdman CA (1987) Use of the breakup time data and velocity history data to predict the maximum size of stable fragments for acceleration-induced breakup of a liquid drops, *Int. J. Multiphase Flow*, vol 13 no 6 pp 741-757

- Pilch M, Erdman CA and Reynolds AB (Aug.1981) Acceleration induced fragmentation of liquid drops, Charlottesville, VA: Department of Nucl. Eng., University of Virginia, NUREG/CR-2247
- Podovisotsky AM and Schreiber AA (1984) Coalescence and break-up of drops in two-phase flows, *Int. J. Multiphase Flow*, vol 10 pp 195-209
- Reineke WG and Waldman GD (Aug. 11-13, 1970) An investigation of water drop disintegration in region behind strong shock waves, Third International Conference on Rain Erosion and Related Phenomena, Hampshire, England
- Reineke WG and Waldman GD (Jan. 20-22, 1975) Shock layer shattering of cloud drops in reentry flight, AIAA Paper 75-152, AIAA 13th Aerospace Sciences Meeting, Pasadena California
- Riso F and Fabre J (1998) Oscillation and breakup of bubbles immersed in turbulent field, *J. Fluid Mech.* vol 372 pp 323-355
- Ruft K (1977) Maximale Einzeltropfen bei stationärer Bewegung in einer niedrig-viscosen kontinuierlichen Phase, *Chemie Ingenieur Technik*, vol 49 no 5 pp 418-419
- Sarjeant M (4th-6th April 1979) Drop breakup by gas streams, Third European Conference on MIXING, Held at the University of York, England, pp 225-267
- Schröder RR and Kitner RC (Jan. 1965) Oscillation of drops falling in liquid field, *A.I.Ch.E. Journal*, vol 11 no 1 pp 5-8
- Serizawa A and Kataoka I (May 24-30, 1987) Phase distribution in two-phase flow, *Proc. ICHMT Int. Sem. Transient Two-Phase Flow*, Dubrovnik, Yugoslavia, Invited Lecture
- Simpkins PG and Bales EL (1972) Water-drop response to sudden accelerations, *J. Fluid Mech.*, vol 55 pp 629-639
- Taylor GI (1949) The shape and acceleration of a drop in a high - speed air stream, *Min. of Supply Paper AC10647/Phys. C69*. See also (1963) "Scientific Papers", Cambridge University Press, vol 3 pp 457-464
- Triebnigg H (1929) *Der Einblase- und Einspritzvorgang bei Dieselmotoren*, Vienna
- Wallis GB (1969) *One-dimensional two-phase flow*, New York: McGraw Hill
- Young MF (1989) Application of the IFCI integrated fuel-coolant interaction code to FITS-type pouring mode experiments, SAND 89 -1962C, Sandia National Laboratories
- Yuen WW, Chen X and Theofanous TG (Sept.21-24, 1992) On the fundamental micro-interactions that support the propagation of steam explosions, *Proc. at the Fifth Int. Top. Meeting on Reactor Thermal Hydraulics*, Salt Lake City, UT. NURETH-5, vol 11 pp 627-636
- Yuen WW, Chen X and Theofanous TG (1994) On the fundamental micro-interactions that support the propagation of steam explosions, *NED*, vol 146 pp 133-146

## 9 Turbulence induced particle fragmentation and coalescence

Particles in continuum react differently on the fluctuation of the mean continuum velocity. While bubbles follow quickly the continuum, heavy droplet may considerably delay following the continuum fluctuation. This makes the main difference in the criteria for fragmentation of bubbles and particles. In this Chapter we will give a brief characterization of the homogeneous isotropic turbulence, and then we will analyze the reaction capability of a particle to follow the changes in velocity of the surrounding continuum. We will derive expressions for the maximum relative velocity, which creates distortion and possible fragmentation. Finally we will look for quantitative information describing, as in the previous section, (a) the final diameter after the fragmentation,  $D_{d\infty}$ , and (b) the time interval in which the fragmentation occurs,  $\Delta\tau_{br}$ . The different components of the turbulent energy dissipation are analyzed. For channel flows expression are given for approximate estimation of the dissipation rate of the turbulent kinetic energy as a function of the frictional pressure drop. The dissipation rate of the turbulent kinetic energy due to relative phase motion is also analyzed. The probability of the bubble and droplet coalescence is then estimated.

### 9.1 Homogeneous turbulence characteristics

*Large scale motion:* Observing turbulent motion of continuum one realizes that random eddies overlay the mean flow. The eddies have different size  $\ell$  at this length scale. The largest scale of the eddies is limited by the geometrical boundary of the systems. In a pipe flow the natural limit is the pipe diameter

$$\ell \leq D_h. \quad (9.1)$$

Large scale eddies contain the main part of the turbulent kinetic energy. Viscous forces have no effect on the large scale motion. There is no energy dissipation. The large scale motion is characterized by the velocity difference over the scale of the eddies  $\ell$ ,  $V'_\ell$ . Usually the turbulence *Reynolds* number

$$\text{Re}'_\ell = \frac{V'_\ell \ell}{\nu} \quad (9.2)$$

is used for characterizing the turbulence.

*Small scale motion:* Small scale eddies with a size

$$\ell_e < \ell \quad (9.3)$$

contains only a small part of the kinetic energy of turbulent motion. There are characterized by

$$Re'_{\ell_e} = \frac{V'_\ell \ell_e}{\nu} . \quad (9.4)$$

*Viscous limit:* The size of a eddy characterized by

$$Re'_{\ell_0} = \frac{V'_{\ell_0} \ell_0}{\nu} \approx 1 \quad (9.5)$$

or

$$\ell_0 \approx \frac{\nu}{V'_{\ell_0}} \quad (9.6)$$

is called *inner scale* or *micro scale* of turbulence. Eddies with

$$\ell < \ell_0 \quad (9.7)$$

dissipate mechanical energy by viscous friction in internal energy (heat). Fluctuations with such sizes are gradually damped. The very nature of the turbulent motion is the continuous transfer of mechanical energy from larger to smaller eddies.

*Dimensional analysis for small scale motion:* We already stated that the turbulent motion of scale larger then the viscous limit does not depend on viscosity and is characterized by  $V'_\ell$ ,  $\ell_e$ ,  $\rho$ . Starting with this observation *Kolmogoroff* (1941, 1949) found that the only combination of these flow parameters having dimension of energy dissipated per unit time and per unit volume is  $\rho V'^3_{\ell_e} / \ell_e$ , or per unit time and unit mass

$$\varepsilon \approx \frac{V'^3_{\ell_e}}{\ell_e} . \quad (9.8)$$

The mechanical energy of turbulent dissipation per unit time and unit mass of the continuum  $\varepsilon$  is called *turbulence dissipation rate* in the following. Thus the velocity change over the distance  $\ell_e$

$$V'_\ell = (\varepsilon \ell_e)^{1/3} \quad (9.9)$$

increases with increasing energy dissipation. The characteristic time period of the fluctuation with given size  $\ell_e$  is then



$$\tau'_{l_e} = \frac{\ell_e}{V'_{l_e}} = \left( \frac{\ell_e^2}{\varepsilon} \right)^{1/3}. \quad (9.10)$$

The acceleration of the fluctuation with given size  $\ell_e$  is then

$$\frac{dV'_{l_e}}{d\tau} \approx \frac{V'_{l_e}}{\tau'_{l_e}} = \frac{\varepsilon^{2/3}}{\ell_e^{1/3}}. \quad (9.11)$$

Substituting the fluctuation velocity defined by Eq. (9.9) into the definition equations for the turbulent *Reynolds* number results in

$$Re'_{\ell_e} = \frac{V'_{\ell_e} \ell_e}{\nu} = \varepsilon^{1/3} \frac{\ell_e^{4/3}}{\nu}. \quad (9.12)$$

*Viscous limit as a function of the dissipation of the specific kinetic energy of turbulence:* Setting the turbulent *Reynolds* number equal to one defines the viscosity limit as follows

$$\ell_0 = \left( \frac{\nu^3}{\varepsilon} \right)^{1/4}, \quad (9.13)$$

$$V'_{\ell_0} \approx \frac{\nu}{\ell_0} = (\varepsilon \nu)^{1/4}. \quad (9.14)$$

The characteristic time period of the fluctuation with given size  $\ell_0$  is then

$$\tau'_{\ell_0} = \frac{\ell_0}{V'_{\ell_0}} = \left( \frac{\nu}{\varepsilon} \right)^{1/2}. \quad (9.15)$$

The acceleration of the fluctuation with given size  $\ell_0$  is then

$$\frac{dV'_{\ell_e}}{d\tau} \approx \frac{V'_{\ell_e}}{\tau'_{\ell_e}} = \frac{\varepsilon^{3/4}}{\nu^{1/4}}. \quad (9.16)$$

*Yaglom* found in 1949 the exact expression

$$\frac{dV'_{\ell_e}}{d\tau} = \sqrt{3} \frac{\varepsilon^{3/4}}{\nu^{1/4}}. \quad (9.17)$$

*Turbulent viscosity:* In analogy to the laminar flow

$$\varepsilon \approx \nu^t \left( \frac{V'_l}{\ell} \right)^2, \quad (9.18)$$

a effective dynamic viscosity of turbulence

$$\eta' = \rho V'_l \ell \quad (9.19)$$

can be defined. The effective kinematic viscosity of turbulence is then

$$\nu' = V'_l \ell. \quad (9.20)$$

The analogy to the molecular kinetics is obvious:  $V'_l$  corresponds to the molecule velocity and  $\ell$  to the mean free path. The ratio

$$\frac{\nu}{\nu'} = \frac{\nu}{V'_l \ell} = \frac{1}{Re'_\ell} \quad (9.21)$$

contains the information that the larger the turbulent *Reynolds* number the more negligible is the molecular viscosity compared to the turbulent viscosity.

There is also a deterministic way to Eq. (9.15). If we assume isotropic turbulence the definition of the turbulence dissipation rate, Eq. (5.156) in Chapter 5 of Volume 1 results in

$$\varepsilon = \frac{15}{2} \nu \left( \frac{\partial V'}{\partial r} \right)^2. \quad (9.22)$$

Taking  $\partial V' \approx V'_l$  and  $\partial r \approx \ell$  and rearranging we obtain

$$\frac{V'_l}{\ell} = \left( \frac{2}{15} \frac{\varepsilon}{\nu} \right)^{1/2}, \quad (9.23)$$

which is very similar to Eq. (9.15). This equation is frequently used in the literature for estimation the order of magnitude of the velocity fluctuation in the viscous turbulence regime

$$V'_\ell = \ell \left( \frac{2}{15} \frac{\varepsilon}{\nu} \right)^{1/2} \quad \text{for } \ell < \ell_0, \quad (9.24)$$

e.g. *Smoluchowski* (1918). This result is used in the literature for instance for modeling of rain droplet agglomeration. If we take as a characteristic distance the size of a particle inside a continuum then we have for  $D_d < \ell_0$

$$V'_{D_d} = D_d \left( \frac{2}{15} \frac{\varepsilon_c}{\nu_c} \right)^{1/2}, \quad (9.25)$$

$$\tau' = \frac{D_d}{V'_{D_d}} = \left( \frac{15}{2} \frac{\nu_c}{\varepsilon_c} \right)^{1/2}, \quad (9.26)$$

$$\frac{dV'_{D_d}}{d\tau} \approx \frac{V'_{D_d}}{\tau'} = \frac{2}{15} D_d \frac{\varepsilon_c}{\nu_c}. \quad (9.27)$$

## 9.2 Reaction of a particle to the acceleration of the surrounding continuum

We start with the simplified momentum equations for the continuous and the disperse phase, denoted with  $c$  and  $d$ , respectively, neglecting compressibility, interfacial mass transfer, the spatial acceleration and the viscous terms

$$\alpha_c \rho_c \frac{\partial w_c}{\partial \tau} + \alpha_c \nabla p + \alpha_c \rho_c g - f_d^d - f_d^{vm} = 0, \quad (9.28)$$

$$\alpha_d \rho_d \frac{\partial w_d}{\partial \tau} + \alpha_d \nabla p + \alpha_d \rho_d g + f_d^d + f_d^{vm} = 0, \quad (9.29)$$

where the drag force per unit mixture volume

$$f_d^d = -\alpha_d \rho_c \frac{3}{4} \frac{c_d^d}{D_d} |\Delta w_{cd}| (w_c - w_d), \quad (9.30)$$

and the virtual mass force per unit mixture volume

$$f_d^{vm} = -\alpha_d \rho_c c_d^{vm} \frac{\partial}{\partial \tau} (w_c - w_d) \quad (9.31)$$

are functions of the relative velocities. Dividing by the corresponding volume fraction and subtracting the equations we eliminate the pressure gradient

$$\rho_c \frac{\partial w_c}{\partial \tau} - \rho_d \frac{\partial w_d}{\partial \tau} + (\rho_c - \rho_d) g - \frac{1}{\alpha_c \alpha_d} f_d^d - \frac{1}{\alpha_c \alpha_d} f_d^{vm} = 0. \quad (9.32)$$

After some rearrangements we have

$$\begin{aligned} & \alpha_c (\rho_c - \rho_d) \frac{\partial w_c}{\partial \tau} + (\alpha_c \rho_d + \rho_c c_d^{vm}) \frac{\partial \Delta w_{cd}}{\partial \tau} + \alpha_c (\rho_c - \rho_d) g \\ & + \rho_c \frac{3}{4} \frac{c_d^d}{D_d} |\Delta w_{cd}| \Delta w_{cd} = 0. \end{aligned} \quad (9.33)$$

For a single particle in infinite continuum  $\alpha_c \rightarrow 1$  we have

$$(\rho_c - \rho_d) \frac{\partial w_c}{\partial \tau} + (\rho_d + \rho_c c_d^{vm}) \frac{\partial \Delta w_{cd}}{\partial \tau} + (\rho_c - \rho_d) g + \rho_c \frac{3}{4} \frac{c_d^d}{D_d} |\Delta w_{cd}| \Delta w_{cd} = 0. \quad (9.34)$$

If the acceleration of the continuum  $\partial w_c / \partial \tau$  is known the reaction of the particle is governed by the above equation. In a turbulent field the local acceleration of the continuum depends on the local turbulent characteristics and the size of the vortex. Neglecting the gravity and the virtual mass force Eq. (9.34) reduces to Eq. (32.2) by *Levich* (1962).

Equation (9.34) contains surprising information. Consider the case of no gravity and no friction

$$\frac{\partial \Delta w_{cd}}{\partial \tau} = \frac{\rho_d - \rho_c}{\rho_d + \rho_c c_d^{vm}} \frac{\partial w_c}{\partial \tau}. \quad (9.35)$$

For positive acceleration the velocity-difference may increase if the dispersed phase has larger density or decrease if the denser phase has lower density than the continuum density. This means that a bubble in water will rush into the direction of the acceleration of the water.

### 9.3 Reaction of particle entrained inside the turbulent vortex – inertial range

The relative velocity within the turbulent eddy: Assuming that the particles are large enough that the quadratic drag law holds we replace in Eq. (9.34)

$$\frac{\partial w_c}{\partial \tau} = \frac{\varepsilon_c^{2/3}}{\ell_{ec}^{1/3}} \quad (9.36)$$

$$\frac{\partial \Delta w_{cd}}{\partial \tau} = \frac{\Delta w_{cd}}{\tau'_{cd}} = \frac{\Delta w_{cd}^2}{\ell_{ec}} \quad (9.37)$$

$$\tau'_{cd} \approx \frac{\ell_{ec}}{\Delta w_{cd}} \quad (9.38)$$

as proposed by *Levich* (1962) and obtain

$$(\rho_c - \rho_d) \frac{\varepsilon_c^{2/3}}{\ell_{ec}^{1/3}} + (\rho_d + \rho_c c_d^{vm}) \frac{\Delta w_{cd}^2}{\ell_{ec}} + (\rho_c - \rho_d) g + \rho_c \frac{3}{4} \frac{c_d^d}{D_d} |\Delta w_{cd}| \Delta w_{cd} = 0 \quad (9.39)$$

or solved with respect to the relative velocity

$$\Delta w_{cd}^2 = (\rho_d - \rho_c) \frac{\varepsilon_c^{2/3} \ell_{ec}^{2/3} + g \ell_{ec}}{\rho_d + \rho_c c_d^{vm} + \rho_c \frac{3}{4} \frac{c_d^d}{D_d} \ell_{ec}}. \quad (9.40)$$

The velocity difference is obviously a function of the size of the eddy. The maximum of the relative velocity is reached if

$$\frac{d \Delta w_{cd}^2}{d \ell_{ec}} = 0, \quad (9.41)$$

that is if

$$\ell_{ec,\max} - \frac{g}{\varepsilon_c^{2/3}} a \ell_{ec,\max}^{1/3} - \frac{2}{3} a = 0, \quad (9.42)$$

Where

$$a = \frac{4}{c_d^d} D_d \left( \frac{\rho_d}{\rho_c} + c_d^{vm} \right). \quad (9.43)$$

The maximum relative velocity is then

$$\Delta w_{cd,\max}^2 = (\rho_d - \rho_c) \frac{\varepsilon_c^{2/3} \ell_{ec,\max}^{2/3} + g \ell_{ec,\max}}{\rho_d + \rho_c c_d^{vm} + \rho_c \frac{3}{4} \frac{c_d^d}{D_d} \ell_{ec,\max}}. \quad (9.44)$$

Neglecting the virtual mass force and the gravitation influence we obtain the *Levich* equation (33.9) in 1962. Note also by comparing with the *Levich* expression in 1962 that he uses turbulence energy dissipation per unit volume and we use turbulence energy dissipation per unit mass. In our notation the *Levich* expression reads

$$\Delta w_{cd,\max}^2 = \frac{\rho_d - \rho_c}{\rho_d} \frac{1}{3} \left( \frac{2^3}{3} \frac{1}{c_d^d} \frac{\rho_d}{\rho_c} \varepsilon_c D_d \right)^{2/3} \approx \frac{\rho_d - \rho_c}{\rho_d} \left( \frac{\rho_d}{\rho_c} \right)^{2/3} (\varepsilon_c D_d)^{2/3}. \quad (9.45)$$

Note that for particles in gas the neglecting of the virtual mass force is a good approximation but the neglecting of the gravitational influence is not always a good one.

Now consider again Eq. (9.9) for a velocity difference inside the continuum between two points having  $D_d$  distance between each other

$$V_{l_{ec}}'^2 = (\varepsilon_c D_d)^{2/3} \quad (9.46)$$

It is obvious that for  $\rho_d \gg \rho_c$  Eq. (9.44) gives much higher velocities than Eq. (9.46), see the discussion by *Kocamustafaogullari* and *Ishii* (1995) on p. 436. Therefore droplets in gas will still obey the mechanical stability criterion for inertial droplet fragmentation as discussed before but with velocity computed by Eq. (9.44). For the case of bubbles in continuum the stability criterion will be modified and additional information is required as discussed below.

## 9.4 Stability criterion for bubbles in continuum

Bubbles in a turbulent velocity field having sizes,  $D_d$ , larger than some characteristic size of the turbulent eddies,  $\ell_{ec}$ , are unstable and disintegrate. The

resulting bubble size distribution is likely to be similar to the distribution of the sizes of the turbulent eddies. The characteristic time period in which the disintegration occurs is likely to be equal to the characteristic time scale of the turbulent fluctuations. These are the main ideas leading to a successful quantitative description of turbulence induced bubble fragmentation. In what follows we look for quantitative information describing, as in the previous section, (a) the final diameter after the fragmentation,  $D_{d\infty}$ , and (b) the time interval in which the fragmentation occurs,  $\Delta\tau_{br}$ .

The introduction of the hydrodynamic stability criterion in this case, as for the acceleration induced fragmentation, is very useful. However, the nature of the force causing the bubble distortion is different. If the continuous velocity field,  $c$ , is highly turbulent, the force acting toward the bubble distortion is the turbulent shear force instead of the drag force - see Fig. 9.1. So the critical *Weber* number is defined as

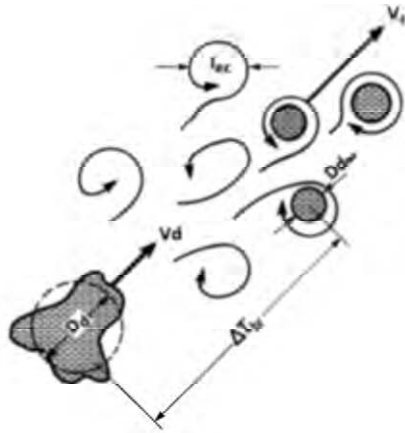


**Fig. 9.1** Characteristics of turbulence induced particle fragmentation

$We'_{d\infty}$  = turbulent shear force / surface tension force

$$= t\pi D_{d\infty}^2 / (\sigma_d \pi D_{d\infty}) \approx const, \quad (9.47)$$

where

$$t = \rho_c V_c'^2 \quad (9.48)$$

is the turbulent shear stress. It is customary to assume that the turbulence is locally isotropic and that the particle size lies in the inertial sub range. Using the *Kolmogoroff* (1941, 1949) hypothesis for an isotropic turbulent structure to compute  $V_c'$  for the lower end of the equilibrium range where the energy transfer through the spectrum is independent of the viscosity

$$V_c^2 = (1/c_1)^{2/3} (\ell_{ec} \varepsilon_c)^{2/3}, \quad (9.49)$$

where

$$(1/c_1)^{2/3} = 2 \quad \text{or} \quad c_1 = 0.3536, \quad (9.50)$$

and assuming that the maximum particle diameter,  $D_{d\infty}$ , is equal to the characteristic size of the turbulent eddies,  $\ell_{ec}$ , the *Weber* number can be expressed by

$$We'_{d\infty} = D_{d\infty}^{5/3} (\varepsilon_c / c_1)^{2/3} \rho_c / \sigma_d. \quad (9.51)$$

*Hinze* (1955) used *Clay's* data (1940) for a *liquid-liquid* system and found

$$We'_{d\infty} = 1.17. \quad (9.52)$$

*Thomas* (1981) reviewed several literature sources and after comparing with experimental data confirms the value 1.17.

Another argument supplying the order of magnitude of this constant comes from *Sevik* and *Park* (1973). They analyzed theoretically the splitting of dispersed particles in continuum using the following argument. According to *Lamb*, see in (1945), the natural frequency of the  $n$ -th order mode of a spherical drop or bubble (d) performing small amplitude oscillations in continuum (c) is given by Eq. (8.72). Due to the small amount of damping the amplitude of the response of a bubble to a steady-state sinusoidal external pressure increases enormously if one of the natural frequencies is reached. The characteristic frequency of the turbulent flow is given by

$$f = \sqrt{V'^2} / \ell_{ec}. \quad (9.53)$$

To obtain the *Weber* number at which particle breakup will occur, *Sevik* and *Park* set  $f$  equal to the natural frequency at the lowest fixed volume oscillation of the particle and  $\ell_{ec}$  equal to the particle diameter. The resulting critical *Weber* number for *liquid-liquid* systems with density ratio equal to one is 1.04, which is very close to the *Hinze's* result, and for *bubbles in water* is

$$We'_{d\infty} \cong 2.48. \quad (9.54)$$

This value describes very well the breakup of a *gas jet in a turbulent liquid stream* observed experimentally by *Sevik* and *Park*.

Thus the values for the critical *Weber* number

$$We'_{d\infty} = 1.17 \quad (9.55)$$

for *droplets in turbulent liquid* and

$$We'_{d\infty} \cong 2.48 \quad (9.56)$$

for *bubbles in turbulent liquid* can be considered reliable. Modification of Eq. (9.55) taking into account the viscosity of the dispersed system

$$We'_{d\infty} = 1.17 \left[ 1 + 1.077 On_d^{1.64} \right] \quad (9.56)$$

is also recommended.

For a particle concentration not affecting the main turbulent characteristics of the continuum i.e.  $\alpha_d \rightarrow 0$ , Eq. (9.51) solved for  $D_{d\infty}$

$$D_{d\infty} \approx (c_1 / \varepsilon_c)^{2/5} (We'_{d\infty} \sigma_d / \rho_c)^{3/5} \quad (9.57)$$

is all what we need to compute the particle size after the fragmentation as a function of the turbulence dissipation rate. Obviously increasing the turbulence dissipation rate leads to a decrease of the particle size which is the intuitively expected relationship.

The influence of the volumetric particle concentration and of the viscosity (Taylor 1935; Hinza 1955) of both fluids on the turbulent characteristics and therefore on the stable particle size is taken into account by *Calderbank* (1967) by introducing the correction factor,  $\alpha_c^n (\eta_d / \eta_c)^{0.25}$ , for liquid-liquid and bubble-liquid systems

$$D_{d\infty} \approx (c_1 / \varepsilon_c)^{2/5} (We'_{d\infty} \sigma_d / \rho_c)^{3/5} \alpha_c^n (\eta_d / \eta_c)^{0.25}, \quad (9.58)$$

where  $n \approx 0.45$  to  $0.65$ . A similar correction factor  $(100\alpha_c)^{0.15} (\eta_d / \eta_c)^{0.25}$  was introduced by *Meusel* (1989a) to take into account the interference of the particles in the flow. Note that Eq. (9.58) generalizes integral results of *simultaneously happening fragmentation and coalescence*.

The characteristic time constant for the fragmentation should be comparable with the period of oscillation of a single turbulent eddy

$$\Delta \tau_{br} \approx \Delta \tau' \approx \ell_{ec} / \sqrt{V_c^2} \approx D_{d\infty} / \sqrt{V_c^2} \approx (D_{d\infty}^2 / \varepsilon_c)^{1/3}. \quad (9.59)$$

We see that the key parameter for an estimation of the local particle size by turbulence induced fragmentation is the rate of the local dissipation of turbulent kinetic energy,  $\varepsilon_c$ , of the continuous velocity field.

To decide whether acceleration or turbulence induced fragmentation is the governing mechanism we compare the stable particle size computed using the critical *Weber* number for acceleration induced fragmentation  $We_{d\infty}$  as discussed in the previous Section with Eq. (9.58). If

$$\frac{We_{d\infty} \sigma_d}{\rho_c (V_c - V_d)^2} > (c_1 / \varepsilon_c)^{2/5} (We'_{d\infty} \sigma_d / \rho_c)^{3/5} \alpha_c^n (\eta_d / \eta_c)^{0.25} \quad (9.60)$$

turbulence induced droplet fragmentation is probably the predominant fragmentation mechanism, otherwise the acceleration induced droplet fragmentation is probably predominant. Eq. (9.60) needs experimental confirmation.



*Paranjape* et al. developed in 2003 a correlation for bubble breakup by impact of turbulent eddies in the form

$$\dot{n}_{d,sp} = C_{TI} \frac{1}{3} \frac{n_d}{D_d} V_c \sqrt{1 - 6/We} \exp(-6/We)$$

based on data for upwards and downwards air water flow in vertical pipes with 25.5 and 50.8mm ID for  $j_c = 0.62$  to 5m/s and  $j_d = 0.004$  to 1.977m/s at 6.9bar, where  $We = \rho_c w_c^2 D_d / \sigma > 6$ ,  $C_{TI} = 0.085$  for upward flow and 0.034 for downward flow. *Morel* et al. (2003) developed in the same time the following correlation for the above discussed case

$$\dot{n}_{d,sp} = 1.6 \frac{\varepsilon_c^{1/3} \alpha_d (1 - \alpha_d)}{D_d^{11/3}} \frac{\exp(-\sqrt{We'_d / We'_{d\infty}})}{1 + 0.42(1 - \alpha_d) \sqrt{We'_d / We'_{d\infty}}},$$

where  $We'_{d\infty} = 1.24$ ,  $\alpha_{d,max} = 0.52$ ,  $We'_d = 2D_d^{5/3} \varepsilon_c^{2/3} \rho_c / \sigma_d$ .

## 9.5 Turbulence energy dissipation due to the wall friction

Now let us consider the turbulence induced droplet fragmentation in channels. As for the turbulence induced droplet fragmentation in pool flow the stable droplet diameter can be computed by means of Eq. (9.57) or one of its modified forms. The key parameter here is the estimation of the rate of dissipation of the turbulent kinetic energy. For channel flow, the knowledge of the frictional pressure drop allows one to compute the dissipation rate of the turbulent kinetic energy and therefore to estimate the dynamic fragmentation source. For 3D flows in structures resembling a porous body, the frictional pressure drop is strongly related to the dissipation rate of the turbulent kinetic energy of the continuum, namely

$$\alpha_c \rho_c \varepsilon_c = u \bar{R}_u + v \bar{R}_v + w \bar{R}_w, \quad (9.61)$$

where  $u$ ,  $v$  and  $w$  are the mixture velocity components in  $r$ ,  $\theta$  and  $z$  directions and  $\bar{R}_u$ ,  $\bar{R}_v$  and  $\bar{R}_w$  are the pressure drops in each particular direction per unit length. In accordance with *Lockhart* and *Martinelli*

$$\bar{R}_u = \frac{1}{2} \frac{1}{\rho_c} (\rho u)^2 \Phi_{c0u}^2 (\lambda_{Ru} / D_{hu} + \xi_u / \Delta r), \quad (9.62)$$

$$\bar{R}_v = \frac{1}{2} \frac{1}{\rho_c} (\rho v)^2 \Phi_{c0v}^2 [\lambda_{Rv} / D_{hv} + \xi_v / (r^\kappa \Delta \theta)], \quad (9.63)$$

$$\bar{R}_w = \frac{1}{2} \frac{1}{\rho_c} (\rho w)^2 \Phi_{c0w}^2 (\lambda_{Rw} / D_{hw} + \xi_w / \Delta z), \quad (9.64)$$

$\rho$  is the mixture density and  $\Phi_{c0}^2$  are the two-phase multipliers for each particular direction and the friction factors  $\lambda_{Ru}$ ,  $\lambda_{Rv}$ ,  $\lambda_{Rw}$  are computed assuming that the total mass flow rate  $\rho V$  has the properties of the continuum,

$$\lambda_R = \lambda_R (\rho V D_h / \eta_c, \delta_k / D_h). \quad (9.65)$$

A simplified version of this approach for a pipe flow was used by *Rosenzweig et al.* (1980). These authors computed the dissipation rate caused by wall friction as follows:  $\varepsilon_c = \frac{1}{2} \frac{\lambda_R}{D_h} w_c^3$ , where  $\lambda_R \approx 0.3164 / Re_c^{1/4}$ ,  $Re_c = D_h w_c / \nu_c$ .

*Bello* (1968) computed successfully the stable bubble diameter in one-dimensional pipe flow using Eqs. (9.57) and (9.61) and

$$We'_{d\infty} \approx 0.437. \quad (9.66)$$

A slightly modified approach for pipes was used later by *Kocamustafaogullari et al.* in 1994. The particle size thus obtained is some averaged size for the cross section of the channel. In fact in channel flow the turbulence is generated mainly by the wall and the length scale of turbulence outside the laminar sublayer

$$\ell_{ec} \approx \text{const} \frac{r}{D_h} \left( \frac{\nu_c^3 V_c^{*3}}{D_d} \right)^{1/4}, \quad \text{Kolmogoroff (1949),} \quad (9.67)$$

depends on the distance from the tube axis,  $r$ . Here  $V_c^*$  is the friction velocity. Therefore in tubes one should expect a spectrum of the particle sizes depending on the distance from the wall.

Modeling of turbulence induced fragmentation (and coalescence) needs modeling of turbulence in multi-phase flows. For channel flow the knowledge of the frictional pressure drop allows to compute the dissipation rate of the turbulent kinetic energy and therefore to estimate the dynamic fragmentation sources. For pool flows or 3D flows in complicated geometries multi-phase turbulence modeling needs much more attention because a reliable model of turbulence does not yet exist. That is why the theoretical estimation of the dynamic fragmentation (and coalescence) characteristics is not possible today. Exceptions are some simple geometries or flows with small concentrations of the dispersed phase where the turbulence modeling consists mainly of one phase turbulence models or cases where the input of the mechanical dissipation energy per unit time from external sources is known (e.g. some chemical equipment).

## 9.6 Turbulence energy dissipation due to the relative motion

The wall friction is one cause for turbulence generation and dissipation. Another cause is the relative motion between particles and continuum. The dissipation rate of the turbulent kinetic energy in the wakes behind particles,  $d$ , can be estimated as the  $\beta_c$  part

$$\alpha_c \rho_c \varepsilon_c = \beta_c \alpha_d \rho_c \frac{3}{4} \frac{1}{D_d} \left( c_{cd,r}^d |u_c - u_d|^3 + c_{cd,\theta}^d |v_c - v_d|^3 + c_{cd,z}^d |w_c - w_d|^3 \right) \quad (9.68)$$

of the specific power needed to move the particles with relative velocity

$$|\Delta V_{cd}| = \left( \Delta u_{cd}^2 + \Delta v_{cd}^2 + \Delta w_{cd}^2 \right)^{1/2}. \quad (9.69)$$

Here  $\Delta u$ ,  $\Delta v$ , and  $\Delta w$  are the components of the vector  $\Delta \mathbf{V}$  in each particulate coordinate  $r$ ,  $\theta$  and  $z$ .

For low *Reynolds* number (laminar flow),  $0 < Re_{cd} < Re_{cd}^*$ , there is no energy dissipation due to particle produced turbulence

$$\beta_c \approx 0. \quad (9.70)$$

In the transition regime  $Re_{cd}^* < Re_{cd} < Re_{cd}^{**}$  of the periodic particle deformation

$$\beta_c \approx (Re_{cd} - Re_{cd}^*) / (Re_{cd}^{**} - Re_{cd}^*) \quad (9.71)$$

only a part of the kinetic energy is dissipated. For high *Reynolds* numbers  $Re_{cd} > Re_{cd}^{**}$ , the particles are stochastically deformed and the flow is turbulent wake flow in which the kinetic energy need to move the particles with respect to the continuum is totally dispersed

$$\beta_c \approx 1. \quad (9.72)$$

Equation (9.68) contains in its RHS the density of the continuum as a multiplier. For gas as a continuum phase the resulting RHS is much smaller than for liquid as a continuum phase, i.e. the bubbles themselves produce considerable turbulence in a liquid.

*Reichardt* (1942) derived theoretical equations for both limiting *Reynolds* numbers

$$Re_{cd}^* = 3.73 \left( \frac{\rho_c \sigma_c^3}{g \eta_c^4} \right)^{0.209} = 3.73 \left( \frac{\Delta \rho_{cd}}{\rho_c} Ar^2 \right)^{0.209} \quad (9.73)$$

and

$$Re_{cd}^{**} = 3.1 \left( \frac{\rho_c \sigma_c^3}{g \eta_c^4} \right)^{0.25} = 3.1 \left( \frac{\Delta \rho_{cd}}{\rho_c} Ar^2 \right)^{0.25}. \quad (9.74)$$

There is an alternative approach to compute the dissipation rate of the turbulent kinetic energy of turbulence in the liquid. *Bhavaraju et al. (1978)* developed an expression for the power input to gas sparked vessels, based on the expansion of bubbles as they ascend up a column from pressure  $p_2$  to  $p_1$ . The resulting expression can be generally written as

$$\alpha_c \rho_c \varepsilon_c = \alpha_d w_d g \frac{p_2}{p_1 - p_2} \ln \frac{p_1}{p_2}. \quad (9.75)$$

Let us summarize the results of this section. In a pool flow the turbulence is produced mainly due to (1) velocity gradients in space and (2) wakes behind the bubbles. For the estimation of the first component models are needed to describe the turbulence evolution of bubble flow in time and space. Such models are at the beginning of their development and no reliable method is known up to now to the author. For the estimation of the second component, Eq. (9.68) is recommended. With an approximate estimation of the dissipation rate of the turbulent kinetic energy, the stable diameter after the fragmentation can be estimated using Eq. (9.57) or (9.58), and for the breakup time Eq. (9.59) can be used.

For channel flow or flow in porous structures with significant wall friction the dissipation rate of the turbulent kinetic energy of the liquid is

$$\alpha_c \rho_c \varepsilon_c = \text{RHS of Eq. (9.61)} + \text{RHS of Eq. (9.68)}. \quad (9.76)$$

Here RHS stands for right hand side. After estimating  $\varepsilon_c$  the procedure to compute the production rate using Eq. (9.5) is the same as for pool flow.

## 9.7 Bubble coalescence probability

The probability of coalescence, sometimes called efficiency of coalescence of bubbles, is defined as a function of the ratio of the time interval within which the eddies are touching each other, called *collision time* interval  $\Delta \tau_{col}$  and the time interval required to push out the surrounding liquid and to overcome the strength of the capillary micro-layer between the two bubbles, called *coalescence time* interval  $\Delta \tau_{coal}$

$$\left( f_{d,coal}^p \right)^0 \approx f \left( \Delta \tau_{col} / \Delta \tau_{coal} \right). \quad (9.77)$$

An example of such functional relationship given by *Coulaloglu and Tavlarides (1977)*

$$\left(f_{d,coal}^p\right)^0 \approx \exp(-\Delta\tau_{coal} / \Delta\tau_{col}), \quad (9.78)$$

will be used here. Note that there are also other proposals for the functional dependence in the literature. Obviously coalescence is possible if there is enough contact time for completing the coalescence

$$\Delta\tau_{col} > \Delta\tau_{coal}. \quad (9.79)$$

If the bubbles are jumping apart before the liquid is pushed out completely between them and before the micro skin between them is broken there is effectively no coalescence. Usually the change of the velocity along the distance equal to the bubble size  $D_d$  is estimated by the *Kolmogoroff* velocity scale, Eq. (9.9),

$$V^{rel} \approx (D_d \varepsilon_c)^{1/3}. \quad (9.80)$$

Assuming that the bubble is following completely the turbulent fluctuation the collision time interval is then

$$\Delta\tau_{col} \approx D_d / V_d' = \frac{D_d^{2/3}}{\varepsilon_c^{1/3}}. \quad (9.81)$$

Thus the collision is completely controlled by the turbulence of the continuum.

What remains to be estimated is the coalescence time. The time needed to push out the liquid between the bubbles is approximated by *Thomas* (1981) by the time required to push out the liquid between two discs each of them of radius  $r$  (a classical lubrication problem)

$$\Delta\tau_{coal} = \frac{3\pi\eta_c r^4}{2F\delta^2}, \quad (9.82)$$

$r$  is the radius of common surface of the both bubbles at the moment of coalescence,

$$\delta \approx 10^{-7} m \quad (9.83)$$

is the radial film thickness between them and

$$F = 4\pi r^2 \sigma / D_d \quad (9.84)$$

is the force acting from inside of the bubble on the common surface that is equal to the pulsation pressure force

$$F \approx \rho_c D_d^2 V_d'^2 = \rho_c V_d'^2 D_d^2. \quad (9.85)$$

Solving the last two equations for  $D_d$  and substituting into Eq. (9.80) we obtain

$$\Delta\tau_{coal} = \frac{3}{32\pi} \eta_c \rho_c V_d'^2 D_d^2 \left( \frac{D_d}{\sigma\delta} \right)^2. \quad (9.86)$$

Having in mind Eq. (9.81) we have for the time ratio

$$\frac{\Delta \tau_{col}}{\Delta \tau_{coal}} = \frac{32\pi}{3} \frac{(\sigma\delta)^2}{\eta_c \rho_c (V'_d D_d)^3} = \frac{32\pi}{3} \frac{(\sigma\delta)^2}{\eta_c \rho_c D_d^4 \varepsilon_c} \quad (9.87)$$

or for the coalescence probability

$$(f_{d,coal}^p)^o \approx \exp(-\Delta \tau_{col} / \Delta \tau_{coal}) = \exp\left(-\frac{3}{32\pi\delta^2} \frac{\eta_c \rho_c D_d^4 \varepsilon_c}{\sigma^2}\right) \quad (9.88)$$

for  $\Delta \tau_{col} / \Delta \tau_{coal} \geq 1$ .

$$(f_{d,coal}^p)^o \approx 0, \quad (9.89)$$

for  $\Delta \tau_{col} / \Delta \tau_{coal} < 1$ . We see from this expression that the coalescence probability decreases with in-creasing the bubble diameter and with increasing the fluctuation velocity. There should be a limiting diameter called coalescence escape limit dividing the regimes of coalescence and no coalescence. It is computed from the condition

$$\Delta \tau_{col} / \Delta \tau_{coal} = 1, \quad (9.90)$$

namely

$$D_{d,lim} = \left[ \frac{32\pi (\sigma\delta)^2}{3 \eta_c \rho_c} \right]^{1/3} / V'_d, \quad (9.91)$$

or replacing by using Eq. (9.80) and solving with respect to the diameter

$$D_{d,lim} \approx \left( \frac{32\pi}{4} \right)^{1/4} (\sigma\delta)^{1/2} / (\eta_c \rho_c \varepsilon_c)^{1/4}. \quad (9.92)$$

Thus for

$$D_d > D_{d,min} \quad (9.93)$$

no coalescence is expected. This regime is called *coalescence escaping* regime. It is important to note that if the bubble diameters are larger than the coalescence escaping diameter, but lower than the critical bubble diameter

$$D_{d,min} < D_d < D_{d\infty} \quad (9.94)$$

there is neither fragmentation nor coalescence. Obviously, for small relative velocities causing bubble coalescence,  $D_{d,lim}$  can increase and take values larger than the stable bubble diameter  $D_{d\infty}$ . In this case coalescence and fragmentation

simultaneously take place. The values of the limiting relative bubble velocity,  $V_{\text{lim}}^{\text{rel}}$ , is easily obtained by equating  $D_{d,\text{lim}}$  and  $D_{d\infty}$

$$\left[ \frac{32\pi (\sigma\delta)^2}{3 \eta_c \rho_c} \right]^{1/3} / V'_{d,\text{lim}} = \frac{We_{d\infty} \sigma}{\rho_c (V_c - V_{d\infty})^2}, \quad (9.95)$$

or

$$V'_{d,\text{lim}} = \frac{\rho_c (V_c - V_{d\infty})^2}{We_{d\infty} \sigma} \left[ \frac{32\pi (\sigma\delta)^2}{3 \eta_c \rho_c} \right]^{1/3}. \quad (9.96)$$

This theory is already applied by *Thomas* (1981) for turbulence induced coalescence.

In reality *two regimes* of bubble formation with stable diameters are observed for turbulent two-phase flow. They depend on the amount of dissipated mechanical energy of turbulence. For low values, the controlling mechanism is the escaping from coalescence, and for greater values - the destroying of unstable bubbles.

Recently *Hibiki and Ishii* (1999) recommended to use the *Oolman and Blanch* (1968a, 1986b) results for thinning of the liquid film between bubbles of equal size

$$\Delta\tau_{\text{coal}} = \frac{1}{8} \left( \frac{\rho_c D_d^3}{2\sigma} \right)^{1/2} \ln \frac{\delta_{\text{init}}}{\delta_{\text{crit}}} = 0.814 \left( \frac{\rho_c D_d^3}{\sigma} \right)^{1/2}, \quad (9.97)$$

where the initial film thickness is

$$\delta_{\text{init}} = 10^{-4} m, \quad (9.98)$$

*Kirkpartick and Lockett* (1974), and the final thickness is

$$\delta_{\text{crit}} = 10^{-8} m, \quad (9.99)$$

*Kim and Lee* (1987). Using Eqs. (9.81) and (9.80) *Hibiki and Ishii* (1999) corrected the constant in the ratio

$$\frac{\Delta\tau_{\text{coal}}}{\Delta\tau_{\text{col}}} = 0.814 \left( \frac{\rho_c D_d}{\sigma} \right)^{1/2} V^{\text{rel}} = 0.814 \left( \frac{\rho_c^3 D_d^5 \mathcal{E}_c^2}{\sigma^3} \right)^{1/6} \quad (9.100)$$

to 1.29 by comparing with experiments and used finally the *Coulaloglu and Tavlarides* (1977) expression for the coalescence probability

$$f_{d,\text{coal}}^p \approx \exp(-\Delta\tau_{\text{coal}} / \Delta\tau_{\text{col}}) = \exp \left[ -1.29 \left( \frac{\rho_c^3 D_d^5 \mathcal{E}_c^2}{\sigma^3} \right)^{1/6} \right]. \quad (9.101)$$

which differs considerably from the *Thomas* (1981) expression

$$\left(f_{d,coal}^p\right)^o \approx \exp(-\Delta\tau_{coal} / \Delta\tau_{col}) = \exp\left(-\frac{3}{32\pi\delta^2} \frac{\eta_c \rho_c D_d^4 \varepsilon_c}{\sigma^2}\right). \quad (9.102)$$

Using Eq. (7.33) the *Hibiki* and *Ishii* final expression for the coalescence frequency due to turbulence in bubbly flow is given as

$$\left(f_{d,coal}^p f_{d,coal}^p\right)^o = const \frac{\alpha_d}{0.52 - \alpha_d} \frac{6}{D_d} V^{rel} \exp\left[-1.29 \left(\frac{\rho_c^3 D_d^5 \varepsilon_c^2}{\sigma^3}\right)^{1/6}\right]$$

for  $\Delta\tau_{col} / \Delta\tau_{coal} \geq 1$ , (9.103)

in which the empirical constant is introduced by comparison with experimental data.

*Paranjape* et al. developed in 2003 a correlation in the form

$$\left(f_{d,coal}^p f_{d,coal}^p\right)^o = \frac{1}{3} \left(\frac{6}{\pi}\right)^{2/3} n_d^{4/3} \alpha_d^{2/3} \left[ \frac{0.00141 V_c}{\alpha_{d,max}^{1/3} (\alpha_{d,max}^{1/3} - \alpha_d^{1/3})} \exp\left(1 - 0.3 \frac{\alpha_{d,max}^{1/3} \alpha_d^{1/3}}{\alpha_{d,max}^{1/3} - \alpha_d^{1/3}}\right) + 0.002 c_d^{drag} (V_d - V_c) \right]$$

based on data for upwards and downwards air water flow in vertical pipes with 25.5 and 50.8mm ID for  $j_c = 0.62$  to 5m/s and  $j_d = 0.004$  to 1.977m/s at 6.9bar, where  $\alpha_{d,max} = 0.75$ . The second term in the brackets takes into account the bubble coalescence due to wake entrainment. *Morel* et al. (2003) developed in the same time the following correlation for the above discussed case

$$\left(f_{d,coal}^p f_{d,coal}^p\right)^o = 2.86 \frac{\varepsilon_c^{1/3} \alpha_d^2}{D_d^{11/3}} \frac{\exp(-1.017 \sqrt{We'_d / We'_{d\infty}})}{\frac{\alpha_{d,max}^{1/3} - \alpha_d^{1/3}}{\alpha_{d,max}^{1/3}} + 1.992 \alpha_d \sqrt{We'_d / We'_{d\infty}}},$$

where  $We'_{d\infty} = 1.24$ ,  $\alpha_{d,max} = 0.52$ ,  $We'_d = 2D_d^{5/3} \varepsilon_c^{2/3} \rho_c / \sigma_d$ .

## 9.8 Coalescence probability of small droplets

Consider liquid droplets that follow the turbulent motion exactly. In this case the turbulent pulsation causes particle collisions and under some circumstances coalescence. As already discussed before, large particles delay in following the



pulsation in the gas continuum. Larger than a given size they do not react any more to the gas pulsations.

Again as for the bubbles coalescence, the assumption of small particles results in the use of Eqs. (9.80) and (9.81) for computation of the pulsation velocity and collision time. *Meusel* (1980, 1989b) proposed the following functional relationship for the coalescence probability

$$\left(f_{d,coal}^p\right)^0 \approx \text{const} \left(\Delta\tau_{col} / \Delta\tau_{coal}\right)^{1/3}, \quad \text{for } \Delta\tau_{col} / \Delta\tau_{coal} \geq 1, \quad (9.97)$$

where

$$\Delta\tau_{col} \approx D_d V^{rel} \quad (9.104)$$

is the time available for a possible collision, and  $\Delta\tau_{coal}$  is the time needed to complete the coalescence. *Meusel* found by comparison with experiments with bubble flows for the constant the following value

$$\text{const} = 0.032. \quad (9.105)$$

Next we estimate the coalescence time. The coalescence time for droplets should be comparable with the period of oscillation, Eqs. (8.72) and (8.73). We assume that after two droplets are touching each other the maximum unstable diameter is  $D_{d,max} \approx 2D_d$  - see the photographs of droplet collisions presented in Figs. 3a,b given by *Schelle* and *Leng* in (1971). The lowest limit for the diameter of the newly produced oscillating droplet is assumed to be  $D_{d,min} \approx D_d$ . For  $n = 2$  Eq. (8.72) results in

$$\Delta\tau_{coal} \approx 0.64 \left[ \frac{D_d^3 (3\rho_d + 2\rho_c)}{\sigma_d} \right]^{1/2}. \quad (9.106)$$

Therefore we have

$$\Delta\tau_{col} / \Delta\tau_{coal} \approx 1.56 \left[ \frac{\sigma_d}{D_d^3 (3\rho_d + 2\rho_c)} \right]^{1/2} / V^{rel}. \quad (9.107)$$

For comparison we give here the coalescence time for water droplets as correlated by *Jeffreys* and *Hawksley* (1965)

$$\Delta\tau_{coal} = 1.96\eta_2^{1/2} \Delta\tau_{1/2} \quad (\approx 1.01\Delta\tau_{1/2}), \quad (9.108)$$

where

$$\Delta\tau_{1/2} = 4.53 \times 10^5 \left[ \frac{\eta_d^{1/2} (\rho_d - \rho_c)^{1.2}}{\sigma^2} \left( \frac{T_d - 273.15}{25} \right)^{-0.7\eta_d^{1/2}} D_d^{0.021} \left( \frac{\sigma^2}{\eta_d^{1/5}} \right)^{0.55} \right]^{0.91} \quad (9.109)$$

is the half time period ( $\Delta\tau_{1/2} \rightarrow 10s$ ) (see Pfeifer and Schmidt 1978, p. 29). Obviously the experiment confirms the trend of the dependence of  $\Delta\tau_{coal}$  on  $D_d$ ,  $\rho_d$  and  $\sigma_d$ .

Again the key parameter controlling agglomeration is the dissipation rate of the turbulent kinetic energy,  $\varepsilon_c$ , of the continuous field.

## Nomenclature

### Latin

$c_{cd}^d$	drag coefficient, <i>dimensionless</i>
$c_{cd}^{vm}$	virtual mass coefficient, <i>dimensionless</i>
$D_h$	pipe diameter, <i>m</i>
$D_{d\infty}$	final diameter after the fragmentation, <i>m</i>
$D_d$	size of a particle inside a continuum, <i>m</i>
$D_{d,lim}$	coalescence escape limit diameter dividing the regimes of coalescence and no coalescence, <i>m</i>
$F$	force acting from inside of the bubble on the common surface
$f$	$= \sqrt{V'^2}/\ell_{ec}$ , characteristic frequency of the turbulent flow, <i>1/s</i>
$(f_{d,coal}^p)^o$	probability of coalescence, efficiency of coalescence, <i>dimensionless</i>
$\ell$	eddies size, <i>m</i>
$\ell_e$	small scale eddies (contains only a small part of the kinetic energy of turbulent motion), <i>m</i>
$\ell_0$	inner scale or micro scale of turbulence, <i>m</i>
$p$	pressure, <i>Pa</i>
$r$	radius of the common surface of two bubbles at the moment of coalescence, <i>m</i>
$Re_{\ell}'$	$= \frac{V_{\ell}'\ell}{\nu}$ , turbulence <i>Reynolds</i> number, <i>dimensionless</i>
$Re_{\ell_e}'$	$= \frac{V_{\ell_e}'\ell_e}{\nu}$ , turbulent <i>Reynolds</i> number, <i>dimensionless</i>
$\bar{R}_u, \bar{R}_v, \bar{R}_w$	pressure drops in each particular direction per unit length, <i>Pa/m</i>
$\mathbf{t}$	$= \rho_c V_c'^2$ , turbulent shear stress, <i>N/m<sup>2</sup></i>
$u, v, w$	mixture velocity components in <i>r</i> , $\theta$ and <i>z</i> directions, <i>m/s</i>
$V_{\ell}'$	velocity change over the distance $\ell_e$ , <i>m/s</i>
$V_c'$	spatial velocity fluctuation at the lower end of the equilibrium range, <i>m/s</i>

---

$V'_\ell$	velocity difference over the scale of the eddies $\ell$ for large scale motion, $m/s$
$V$	velocity, $m/s$
$We'_{d\infty}$	=turbulent shear force / surface tension force, critical <i>Weber</i> number, <i>dimensionless</i>

### **Greek**

$\alpha_d$	particle volume fraction, <i>dimensionless</i>
$\Delta\tau_{col}$	collision time, $s$
$\Delta\tau_{coal}$	coalescence time interval, $s$
$\Delta\tau_{br}$	time interval in which the fragmentation occurs, $s$
$\Delta w_{cd,max}$	maximum relative velocity, $m/s$
$\delta$	radial film thickness between two colliding bubbles, $m$
$\delta_{init}$	initial film thickness, $m$
$\delta_{crit}$	final thickness, $m$
$\varepsilon$	turbulence dissipation rate, mechanical energy of turbulence dissipated per unit time and unit mass of the continuum, $W/kg$
$\Phi_{c0}^2$	two-phase multipliers for each particular direction, <i>dimensionless</i>
$\rho$	density, $kg/m^3$
$\rho V$	total mass flow rate, $kg/(m^2s)$
$\lambda_{Ru}, \lambda_{Rv}, \lambda_{Rw}$	friction factors for each particular direction, <i>dimensionless</i>
$\eta$	dynamic viscosity, $kg/(sm)$
$\eta^t$	$= \rho V'_l \ell$ , effective dynamic viscosity of turbulence, $kg/(sm)$
$\nu^t$	$= V'_l \ell$ , effective kinematic viscosity of turbulence, $m^2/s$
$\tau'_{l_e}$	$= \frac{\ell_e}{V'_l}$ , characteristic time period of the fluctuation with given size $\ell_e$ , $s$

### **Subscripts**

$l$	= 1 first fluid – gas = 2 second fluid – liquid = 3 third fluid - another liquid
$d$	disperse
$c$	continuous

## References

- Bello JK (1968) Turbulent flow in channel with parallel walls, Moskva, Mir, in Russian
- Bhavaraju SM, Russel TWF, Blanch HW (1978) The design of gas sparged devices for viscous liquids systems, *AIChE J.*, vol 24 p 3
- Calderbank PH (October 1967) Gas absorption from bubbles, *The Chemical Engineer* CE209-CE233
- Clay PH (1940) Proceedings of the Royal Academy of Science (Amsterdam), Vol. 43 p 852
- Coulaloglu CA, Tavlarides LL (1977) Description of Interaction Processes in Agitated Liquid - Liquid Dispersion, *Chem. Eng. Sci.*, vol 32 p 1289
- Hibiki T, Ishii M (August 15-17, 1999) Interfacial area transport of air-water bubbly flow in vertical round tubes, CD proc. of the 33<sup>rd</sup> Nat. Heat Transfer Conf., Albuquerque, New Mexico
- Hinze JO (1955) Fundamentals of hydrodynamics of splitting in dispersion processes, *AIChE Journal*, vol 1 pp 284-295
- Jeffreys GV, Hawksley L (1965) Coalescence of liquid droplets in two-component - two-phase systems, *Amer. Inst. Chem. Engs. J.*, vol 11 p 413
- Kim WK, Lee KL (1987) Coalescence behavior of two bubbles in stagnant liquid, *J. Chem. Eng. Japan*, vol 20 pp 449-453
- Kirkpartick RD, Lockett MJ (1974) The influence of the approach velocity on bubble coalescence, *Chem. Eng. Sci.*, vol 29 pp 2363-2373
- Kocamustafaogullari G, Huang W D, Razi J (1994) Measurements and modelling of average void fraction, bubble size and interfacial area, *Nucl. Eng. Des.*, vol 148 p 437
- Kocamustafaogullari G, Ishii M (1995) Foundation of the interfacial area transport equation and its closure relations, *Int. J. Heat Mass Transfer*, vol 38 no 3 pp 481-493
- Kolmogoroff AN (1941) The local structure of turbulence in incompressible viscous fluid for very large Reynolds numbers, *C. R. Acad. Sci. U.S.S.R.*, vol 30 pp 825-828
- Kolmogoroff AN (1949) On the disintegration of drops in turbulent flow, *Doklady Akad. Nauk. U.S.S.R.*, vol 66 p 825
- Lamb MA (1945) *Hydrodynamics*. Cambridge, At the University Press
- Levich VG (1962) *Physicochemical hydrodynamics*, Prentice-Hall, Inc. Englewood Cliffs, N.J.
- Meusel W (1980) Einfluß der Partikelkoaleszenz auf den Stoffübergang in turbulenten Gas-flüssig-Systemen, Ph. D. Thesis, Ingenieurhochschule Köthen
- Meusel W (1989a) Beitrag zur Modellierung von Gas - Flüssigkeits - Reaktoren auf der Basis relevanter Mikroprozesse, Doctoral Thesis, Ingenieurhochschule Köthen
- Meusel W (1989b) Beitrag zur Modellierung von Gas - Flüssigkeits - Reaktoren auf der Basis relevanter Mikroprozesse, Doctoral Thesis, Ingenieurhochschule Köthen
- Morel C, Yao W and Bestion D (5-9 October 2003) Three dimensional modeling of boiling flow for NEPTUNE code, 10<sup>th</sup> Int. Top. Meeting on Nuclear Reactor Thermal Hydraulic (NURETH-10) Seul, Korea
- Oolman T, Blanch HW (1986a) Bubble coalescence in air-sparged bio-reactors, *Biotech. Bioeng.*, vol 28 pp 578-584
- Oolman T, Blanch HW (1986b) Bubble coalescence in stagnant liquids, *Chem. Eng. Commun.*, vol 43 pp 237-261

- Paranjape SS et al (5-9 October 2003) Interfacial structure and area transport in upward and downward two-phase flow, 10<sup>th</sup> Int. Top. Meeting on Nuclear Reactor Thermal Hydraulic (NURETH-10) Seoul, Korea
- Pfeifer W, Schmidt H (April 1978) Literaturübersicht zu den fluiddynamischen Problemen bei der Auslegung gepulster Siebböden-Kolonnen, Kernforschungszentrum Karlsruhe, KfK 2560
- Reichardt H (Mai/Juni 1942) Gesetzmäßigkeiten der freien Turbulenz, VDI-Forschungsh. Nr. 414, Beilage zu "Forschung auf dem Gebiet des Ingenieurwesens", Ausgabe B, Band 13
- Rosenzweig AK, Tronov VP, Pergushev LP (1980) Coalizencija Kapel Vody v Melkodispersnyh Emulsijach Tipa Voda v Nevti, Journal Prikladnoj Chimii, no 8 pp 1776-1780
- Schelle GF, Leng DE (1971) An experimental study of factors which promote coalescence of two colliding drops suspended in Water-I, Chemical Engineering Science, vol 26 pp 1867-1879
- Sevik M, Park SH (1973) The splitting of drops and bubbles by turbulent fluid flow, Trans. ASME J. Fluid Eng., vol 95 p 53
- Smoluchowski M (1918) Versuch einer mathematischen Theorie der Koagulationskinetik kolloider Lösungen, Zeitschrift für Physikalische Chemie, Leipzig Band XCII pp 129-168
- Taylor GI (1935) Proc. Roy. Soc. A, vol 151 p 429. See also (1950) The instability of liquid surface when accelerated in a direction perpendicular to their plane, Proc. Roy. Soc. A, vol 201 pp 192-196
- Thomas RM (1981) Bubble coalescence in turbulent flows, Int. J. Multiphase Flow, vol 6 no 6 pp 709-717
- Yaglom AM (1949) Doklady AN SSSR, vol 67 no 5



## 10 Liquid and gas jet disintegration

### 10.1 Liquid jet disintegration in pools

The mathematical description of jet breakup has attracted the attention of outstanding scientists in the past. Lord *Rayleigh* analyzed for the first time in 1878 the instability of jets. *Nils Bohr* extended *Rayleigh's* analysis to include viscous effects, in a prize winning paper on the evaluation of the surface tension in 1909. *Constantin Weber* went on to obtain the breakup length for a viscous jet in 1936. *Wolfgang von Ohnesorge* classified in 1936 his experimental observation with a high speed camera (200 to 12 000 frames per second) of four different regimes of jet breakup, introduced a dimensionless number quantifying the properties of the jet and described successfully two jet transition boundaries. *Weber* in 1936 and later *Taylor* in *Batchelor* (1958) introduced in addition to the previous analyses the influence of the environment on the jet breakup. These are the fundamental works in jet fragmentation theory used in almost all later works on this topic. In recent time the nozzle geometry is found to influence strongly the jet dynamics. Geometries not allowing the establishment of a turbulent boundary layer produce more stable jets than those which promote turbulent boundary layers at the jet interface - see *Iciek* (1982).

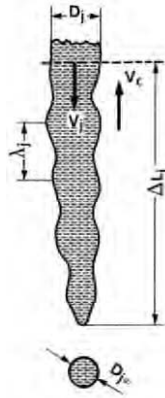


**Fig. 10.1** Characteristics of jet disintegration in a pool

A jet disintegrates due to internally or externally excited and unboundedly growing instabilities, due to surface entrainment or due to all mechanisms working together with different strength. The products of the fragmentations are primary ligaments which may continue to fragment to secondary droplets.

We use the *Ohnesorge* classification of the jet fragmentation mechanism (see Fig. 10.1).

- 0) Slow dropping from the nozzle under the gravity influence without jet formation (depends on the density ratio);
- I) Cylindrical jet disintegration due to symmetric interface oscillations as discussed by *Rayleigh* (later called varicose regime). In this regime the relative velocity has no influence and increasing jet velocity causes increasing penetration length.
- II) Jet disintegration due to asymmetric waves which deform the core to the snake-like shape as discussed by *Weber* and *Haenlein* (called sinuous jet breakup);
- III) Jet atomization due to internal turbulization and surface entrainment.

The dimensionless numbers required to describe jet dynamics are given below.

$\Delta L_j / D_j$  relative jet penetration length

$$We_j = \rho_j V_j^2 D_j / \sigma, \text{ jet Weber number}$$

$$We_{cj} = \rho_j \Delta V_{cj}^2 D_j / \sigma, \text{ continuum Weber number based on the relative velocity}$$

$$Fr_{cj} = \Delta V_{cj}^2 / (g D_j), \text{ Froude number based on the relative velocity, appropriate for jets causing boiling at the interface so that the environment velocity is governed by buoyancy driven convection}$$

$$Fr_j = V_j^2 / (g D_j), \text{ Froude number based on the jet velocity, appropriate for gravitationally driven jets}$$

$$Ta_{cj} = (\rho_j / \rho_c) \left[ \sigma / (\eta_j \Delta V_{cj}) \right]^2, \text{ Taylor number based on relative velocity}$$

$$Ta_c = (\rho_j / \rho_c) \left[ \sigma / (\eta_j V_c) \right]^2, \text{ Taylor number based on the continuum velocity}$$

$$Lp_j = \rho_j \sigma_j D_j / \eta_j^2, \text{ Laplace number}$$

$$Re_j = \rho_j V_j D_j / \eta_j, \text{ liquid jet Reynolds number}$$

$$On_j = We_j^{1/2} / Re_j = 1 / Lp_j^{1/2} = \eta_j / (D_j \sigma_j \rho_j)^{1/2}, \text{ jet Ohnesorge number (Ruft 1972)}$$

$$On_{j\lambda} = \eta_j / (\lambda_{RT} \sigma_j \rho_j)^{1/2}, \text{ jet viscosity number based on Rayleigh-Taylor instability wavelength}$$

$$On_j^* = (3\eta_j + \eta_c) / (D_j \sigma_j \rho_j)^{1/2}, \text{ modified Ohnesorge number}$$

$$On_c = \eta_c / (D_j \sigma_j \rho_c)^{1/2}, \text{ ambient Ohnesorge number}$$

Here we denote with  $j$  the first continuum and with  $c$  the second continuum. The jet penetration length,  $\Delta L_j$ , is defined as the length for complete disintegration measured from the nozzle outlet. Note that the jet velocity,  $V_j$ , is not necessarily



equal to the relative velocity between the jet and the environment,  $\Delta V_{cj}$ . Both velocities are equal for relatively slow jet penetration in a stagnant continuum.

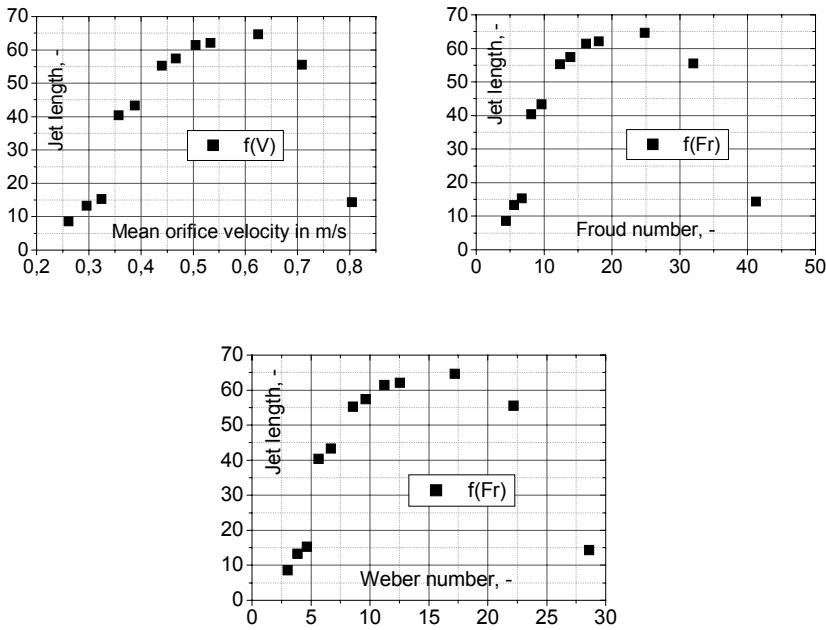


**Fig. 10.2** Jet penetration length  $\Delta L_j / D_j$  as a function of jet velocity in three different presentations. Liquid-liquid jet fragmentation experiment by Meister and Scheele. Heptane in water:  $D_j = 0.0016\text{m}$ ,  $\eta_j = 0.000393\text{Pa s}$ ,  $\rho_j = 683\text{kg/m}^3$ ,  $\sigma_j = 0.0362\text{N/m}$

Figure 10.2 digitized from Meister and Scheele (1969) gives possible regimes of jet breakup. The penetration length  $\Delta L_j / D_j$  is presented as a function of the nozzle velocity (alternatively as a function  $Fr_j$ , or  $We_{ej} = We_j$  for liquid jet penetration from the bottom of a reservoir filled with stagnant liquid.

To model jet fragmentation for engineering applications we need to know

- the boundaries of the different fragmentation mechanisms,
- the size of the generated particles, and
- the dependence of the jet penetration length on the jet velocity and other local parameters.

## 10.2 Boundary of different fragmentation mechanisms

- The regime (0) is seldom interesting for practical application.

- b) The transition from regime (I) to regime (II) can be deduced from the *Ohnesorge* diagram (1936)

$$Re_j = 46 / On_j^{4/5}. \quad (10.1)$$

- c) In the same work *Ohnesorge* found for the transition between regime (II) and regime (III)

$$Re_j = 270 / On_j^{4/5}. \quad (10.2)$$

This transition criterion was modified in 1947 by *Merrington* and *Richardson*,  $Re_j = 300 / On_j^{4/5}$ , in 1954 by *Tanzawa* and *Toyoda*,  $Re_j = 370 / On_j^{0.318}$ , and later by *Grant* and *Middleman* (1966) based on their own experiments,  $Re_j = 325 / On_j^{0.28}$ . The transition boundary from sinuous to turbulent jets was demonstrated to happen for  $Re_j \approx (2 \text{ to } 5) \times 10^4$ , for water which corresponds to the *Ohnesorge* experiment performed in 1931 and the result obtained by *Lienhard* and *Day* compare with Fig.5 in [19] where  $Re_j \approx (4 \text{ to } 6) \times 10^4$ . For liquid-liquid systems additional dependence of the ambient condition was reported by *Takahashi* and *Kitamura* (1971, 1972),

$$Re_j = (98 / On_c^{0.11}) / On_j^{0.30}. \quad (10.3)$$

*Grant* and *Middleman* (1966) indicated that it may depend on the system geometry which can promote or dampen turbulence in the jet surface. *Iciek* (1982) reported a data set for nozzles with different geometries that strongly supports this conclusion. *Faeth* [1995, p. C0-11, fig.15] demonstrated experimentally that the liquid jet *Reynolds* number, and the nozzle length to diameter ratio, govern the internal structure of the jet turbulence. For

$$L_{nozzle} / D_j < 5, \quad (10.4)$$

the jet remain laminar. The higher the nozzle length the better the turbulence develops.

In regime (II) the influence of the ambient conditions starts to play an important role. It is known that water jets with coaxial gas injection producing gas velocity equal to the jet velocity are more stable than jets with the same velocity in stagnant gas. The transition to regime (III) can be accelerated if the ambient relative velocity increases. It is associated by some authors with some critical *Weber* number. *Fenn* and *Middleman* found experimentally that for ambient *Weber* number

$$We_{ej} < 5.3, \quad (10.5)$$

there is no influence of the ambient aerodynamic pressure forces on the fragmentation. For larger  $We_{ej}$  the surrounding continuum conditions begin to reduce the core breakup length.

*Smith* and *Moss* [see Fig. 8] found in 1917 experimenting with mercury in aqueous solutions that for

$$We_{cj} > 100 \quad (10.6)$$

atomization starts. In the atomization regime increasing relative velocity decreases the penetration length. The atomization is associated with dramatic surface droplet entrainment. *De Jarlais* et al. (1986) found that at

$$On_{j\lambda}^{0.8} Ta_{cj}^{1/2} \leq 1 \quad \text{for } On_{j\lambda} < 1/15, \quad (10.7)$$

and

$$0.1146 Ta_{cj}^{1/2} \leq 1 \quad \text{for } On_{j\lambda} \geq 1/15, \quad (10.8)$$

roll wave entrainment starts. Higher relative velocities cause droplet entrainment which thin the jet. Breakup may occur in such cases before the core exhibits any sinuous jet behavior.

### Conclusions:

1. Use Eq.(10.1) to recognize the transition varicose/sinuous.
2. Use Eq.(10.2) or its recent modifications to recognize the transition sinuous/atomization.
3. Check by Eq.(10.5) whether the ambient conditions are important.
4. Check by Eqs.(10.7) and (10.8) whether surface entrainment starts.
5. Decide in favor of the regime that is most stable at the given local conditions.

## 10.3 Size of the ligaments

The size of the dropping liquid is observed by *Ohnesorge* (1936) to be in order of

$$Lp_j \approx 0.01 \text{ to } 1. \quad (10.9)$$

The size of the ligaments resulting from primary breakup for inviscid fluid is estimated by *Rayleigh*

$$D_{d\infty} / D_j = 9.02. \quad (10.10)$$

*Thimotika* found in 1935 theoretically that the jet properties influence the size of the ligaments for the varicose and sinuous breakup as follows

$$D_{d\infty} / D_j = 13 On_j^{1/2}. \quad (10.11)$$

Recently the size of the gross ligaments resulting from the primary varicose or sinuous breakup has been correlated by *Teng* et al. (1995) by considering the influence of the ambient continuum properties in addition to the jet properties as follows

$$D_{d\infty} / D_j = 1.88 \left( 1.1303 + 0.0236 \ln On_j^* \right) \left( 1 + On_j^* \right)^{1/6}. \quad (10.12)$$

This correlation was compared with data for seventeen *Newtonian* and power-law/*Newtonian* liquid-in-liquid systems. The averaged deviation was 8.1 and 5.1%, respectively. For water jets in air, the averaged deviation was 1.6%. The secondary breakup stability criterion corresponds to that already discussed assuming the new born primary drop has 0.9 from the jet velocity as experimentally measured by *Faeth* in (1995).

Turbulence inside the jet can produce surface instabilities and therefore surface entrainment. This fact is widely used in different technologies to fragment jets in smaller particles. Simple approach to the size of the particles jumping apart the surface,  $D_{d\infty}$ , is to equate the pulsation pressure at the interface,  $\frac{1}{2}\rho_j V_j^2 \pi D_{d\infty}^2 / 4$ , to the surface tension force,  $\pi D_{d\infty} \sigma$ , which results in the *Weber* number stability criterion based on the pulsation velocity equal to 8. In fact, as already discussed in Section 9.4, this is of the order of 1.17 to 2.48, and therefore,  $\rho_j V_j^2 D_{d\infty} / \sigma \approx (1.17 \text{ to } 2.48)$ . Having in mind that the pulsation velocity is only a part of the jet velocity,  $V_j' \approx 0.07 V_j$ , see *Faeth* (1995), we obtain simply

$$D_{d\infty} / D_j \approx (240 \text{ to } 500) / We_j, \quad (10.13)$$

which is not a function of the jet diameter. This simple estimation is in quite good agreement with the experimental observation reported by *Faeth* (1995)

$$D_{d\infty} / D_j \approx 133 / We_j^{0.74}, \quad (10.14)$$

which shows some dependence of the jet diameter.

Thus, I recommend to take as a final size after the primary and secondary fragmentation the minimum of all relevant mechanisms. The justification is: If the inertia fragmentation produces the smaller particles they will be stable in the environment. If the relative velocity method predicts the smaller particle size the primary entrained droplet will further fragment to reach a stable state following relative velocity fragmentation.

## 10.4 Unbounded instability controlling jet fragmentation

### 10.4.1 No ambient influence

*Lord Rayleigh* found in 1878 by perturbation analysis for the varicose mode of water jet breakup

$$\Delta L_j / D_j = \text{const } We_j^{1/2}, \quad (10.15)$$

where  $\text{const} = 8.46$  for  $Le_j^{1/2} \gg 1$ . The experiments performed by *Smith* and *Moss* [p 388] in 1917 shows that the constant is

$$const = 13. \quad (10.16)$$

*Weber* (1936) analyzed in 1931 the stability in the varicose mode of vibrations. His remarkable result for the fragmentation time is

$$\Delta \tau_j = \ln \left[ D_j / (2\lambda_0) \right] \left( \rho_j D_j / \sigma_j \right)^{1/2} D_j (1 + 3On_j) \quad (10.17)$$

or having in mind that  $\Delta \tau_j = \Delta L_j / V_j$

$$\begin{aligned} \Delta L_j / D_j &= \ln \left[ D_j / (2\lambda_0) \right] \left( We_j^{1/2} + 3We_j / Re_j \right) \\ &= \ln \left[ D_j / (2\lambda_0) \right] (1 + 3On_j) We_j^{1/2}, \end{aligned} \quad (10.18)$$

where the symbol  $\lambda_0$  denotes the initial deviation from the non-disturbed jet radius and  $\ln \left[ D_j / (2\lambda_0) \right]$  is assumed to be equal 12. This result compares well with data for  $10^{-4} \leq \frac{1}{9} / On_j^2 < 10^4$ . Remarkably, the result reduces to the *Rayleigh* equation (10.15) with a constant very similar to those previously estimated by *Smith* and *Moss* (1917). *Grant* and *Middleman* (1966) found experimentally that the excitation of interface instability is also a function of the jet properties and fitted their data with the correlation

$$\ln \left[ D_j / (2\lambda_0) \right] = 7.68 - 2.66 \ln On_j. \quad (10.19)$$

The authors correlated their own experimental data in the region of  $2 < We_j^{1/2} + 3We_j / Re_j < 200$  with the slightly modified form of the *Weber* result, namely

$$\Delta L_j / D_j = 19.5 \left[ (1 + 3On_j) We_j^{1/2} \right]^{0.85} \quad (10.20)$$

for  $Re_j < 325 / On_j^{0.28}$ , and

$$\Delta L_j / D_j = 8.51 \left( We_j^{1/2} \right)^{0.64} \quad (10.21)$$

for larger jet *Reynolds* numbers - turbulent jets. For the last regime *Iciek* (1982) obtained a slightly modified form

$$\Delta L_j / D_j = 11.5 \left( We_j^{1/2} \right)^{0.62} \quad (10.22)$$

on the base of an additional 56 data points.

### 10.4.2 Ambient influence

*Taylor*, see in *Batchelor* (1958), starts with the continuity equation for a steady state jet

$$d \left( V_j D_j^{*2} \right) / dz = -4 D_j^* u_{j\sigma} \quad \text{or} \quad dD_j^* / dz = -2 u_{j\sigma} / V_j \quad (10.23)$$

Here  $D_j^*$  is a function of  $z$ ,  $V_j$  is the jet velocity, assumed to be constant, and  $u_{j\sigma}$  is the interface averaged entrainment velocity. The continuity equation, integrated for  $z = 0$ ,  $D_j^* = D_j$  and  $z = \Delta L_j$ ,  $D_j^* = 0$  and constant  $V_j$  and  $u_{j\sigma}$ , gives

$$\Delta L_j / D_j = \frac{1}{2} V_j / u_{j\sigma}. \quad (10.24)$$

The interface averaged entrainment velocity is computed as

$$u_{j\sigma} = \text{const} \left( \rho_c / \rho_j \right)^{1/2} \Delta V_{cj} \lambda_m^* f_m^* \quad (10.25)$$

where  $\lambda_m^*$ , defined by

$$2\pi \lambda_m^* = \lambda_m \rho_c \Delta V_{cj}^2 / \sigma, \quad (10.26)$$

and  $f_m^*$ , defined by

$$2f_m^* = f_m / \left[ \left( \rho_c / \rho_j \right)^{1/2} \rho_c \Delta V_{cj}^3 / \sigma \right], \quad (10.27)$$

are the dimensionless wavelength and the frequency of the fastest growth of the unstable surface perturbation waves which are complicated functions of  $Ta_{cj}$ , being  $f_m^* \leq \sqrt{3}/9$  and  $0.04 \leq \lambda_m^* f_m^* \leq \sqrt{3}/6$  for  $10^{-5} \leq Ta_{cj} \leq 10^4$  and  $\lambda_m^* f_m^* = \sqrt{3}/6$  for  $Ta_{cj} > 10^4$ . Substituting Eq. (10.25) in Eq. (10.24) results in

$$\Delta L_j / D_j = \frac{1}{2} V_j / \left[ \text{const} \lambda_m^* f_m^* \left( \rho_c / \rho_j \right)^{1/2} \Delta V_{cj} \right], \quad (10.28)$$

which is a remarkable result. Comparison with experimental data for engine spray where  $\Delta V_{cj} = V_j$ , indicates that  $\frac{1}{2} / (\text{const} \lambda_m^* f_m^*)$  is of order of 7, see *Bracco* (1985). Rewritten in terms of *Weber's* numbers the *Taylor* equation takes the form

$$\Delta L_j / D_j = 7 We_j^{1/2} / We_{cj}^{1/2}. \quad (10.29)$$

*Epstein* and *Fauske* (1985) investigated theoretically the stability of a liquid jet in a continuum, making the following assumptions: The wavelength of the surface disturbance is small compared with the diameter of the jet. Considering linear *Kelvin*

- *Helmholtz* stability of three parallel inviscid streams of jet, steam film and liquid, the authors obtained the following expression for the jet penetration distance:

$$\Delta L_j / D_j = \frac{\sqrt{3}}{2} (1 + \rho_c / \rho_j) / (\rho_c / \rho_j)^{1/2}. \quad (10.30)$$

which for  $\rho_c \ll \rho_j$  reduces to the *Taylor* result for  $\Delta V_{cj} = V_j$  giving the lowest possible estimate for the constant  $\sqrt{3}/2$ . *Nigmatulin* et al. (1993) reported similar analysis for cylinder geometry coming to an expression very similar to the above mentioned *Rayleigh* result. The authors showed that the *Epstein* and *Fauske* analysis holds for jet diameters larger the 1 cm, see [1985, p 94] and pointed out the importance of the accurate estimation of the surrounding continuous medium in case of film boiling. *De Jarlais* et al. (1986) investigated jet disintegration in confined pipe geometry. The authors find that the confinement influences the disintegration process and corrected the existing correlation for jet fragmentation by introducing the factor  $(1 - \alpha_j)$ , which reduces to unity for jets in an infinite environment. The obtained correlations are: For  $We_{cj} / (1 - \alpha_j)^2 < 5.3$ , the modified *Weber* result was recommended

$$\Delta L_j / D_j = 12 (1 + 3On_{j\lambda}) We_j^{1/2}, \quad (10.31)$$

and for  $We_{cj} / (1 - \alpha_j)^2 \geq 5.3$  the *Grant* and *Middleman* (1966) result was recommended

$$\Delta L_j / D_j = 35 (1 + 3On_{j\lambda}) We_j^{1/2} / [We_{cj} / (1 - \alpha_j)^2]^{0.645}. \quad (10.32)$$

The last correlation contains elements from *Weber*'s and from *Taylor*'s theory.

There are similar correlations to *Taylor*'s, giving decreasing  $\Delta L_j / D_j$  with increasing  $We_{cj}$  and taking into account the viscosity, e.g.

$$\Delta L_j / D_j = 50.3 On_j^{0.192} / \left[ (\rho_c / \rho_j)^{1/2} We_{cd}^{0.83} \right]. \quad (10.33)$$

Conclusion: For the time being the following approach seems to be meaningful.

(1) Compute the ambient *Weber* number defining the transition into atomization as follows

$$We_{cj}^* = 49 / \left[ (7.68 - 2.66 \ln On_j) (1 + 3On_j) \right]^2. \quad (10.34)$$

This is a very interesting result. It simply says that for non-viscous jets the transition's ambient *Weber* number is of the order of  $We_{cj}^* \approx \rho_j / \rho_c$ , which means that

jets in gas environment experience transitions into the atomization regime for much higher relative velocities than jets in liquids.

(2) For  $We_{cj} \leq We_{cj}^*$  use the *Weber* solution with the *Smith* and *Moss* coefficient for non-atomization regimes,

$$We_{cj}^* = (7.68 - 2.66 \ln On_j) (1 + 3On_j) We_j^{1/2}. \quad (10.35)$$

(3) For  $We_{cj} > We_{cj}^*$  use the *Taylor* solution with the *Braco* constant, that is Eq. (10.29) to estimate the coherent jet length during atomization.

### 10.4.3 Jets producing film boiling in the ambient liquid

Now we consider a situation which differs from the above discussed. Consider a jet of molten metal, e.g. iron penetrating water and causing considerable evaporation. In this case the jet surrounding continuum is vapor. Following *Schneider et al.* (1992) and assuming that (a) the surface entrainment velocity is equal to the jet side surface friction velocity,

$$u_{j\sigma}^* = u_{j\sigma} = (\tau_{j\sigma} / \rho_j)^{1/2}, \quad (10.36)$$

and (b) the jet side surface shear stress is equal to the vapor side shear stress due to buoyancy driven upwards gas flow

$$\tau_{j\sigma} = c_{ld}^d \frac{1}{2} \rho_1 \Delta V_{lj}^2 \approx (D_j^* / 4) (\rho_2 - \rho_1) g, \quad (10.37)$$

the jet mass conservation equation reduces to

$$dD_j^* / dz = -2u_{j\sigma} / V_j = -2 \left[ (D_j^* / 4) (\rho_2 - \rho_1) g / \rho_j \right]^{1/2} / V_j, \quad (10.38)$$

or after integrating for  $z = 0$ ,  $D_j^* = D_j$  and  $z = \Delta L_j$ ,  $D_j^* = 0$  and constant  $V_j$

$$\Delta L_j / D_j = 2Fr_j / \left[ (\rho_2 - \rho_1) / \rho_j \right]^{1/2}. \quad (10.39)$$

Low pressure experiments performed by *Saito et al.* (1988) show that the penetration length of the very hot jet into coolant with strong evaporation tends to increase with the jet velocity. These authors correlated their data with the expression

$$\Delta L_j / D_j = 2.1 Fr_j^{1/2} / (\rho_2 / \rho_j)^{1/2} \quad (10.40)$$

for  $Fr_j < 5 \times 10^3$ , which is surprisingly close to the analytical solution. For application we recommend not to neglect the vapor density because it will restrict the validity of *Saito's* finding only to low pressure. The correlation with film boiling



(10.40) predicts larger penetration lengths than experimentally observed for adiabatic liquid-liquid penetration - see *Sun* 1998

$$\Delta L_j / D_j = 1.45 Fr_j^{1/2} / (\rho_c / \rho_j)^{1/2}$$

valid for  $90 < Fr_j < 2 \times 10^3$ . *Schneider* et al. (1992) provided a theoretical explanation of the observations made by *Saito* et al. Interface jet entrainment caused by

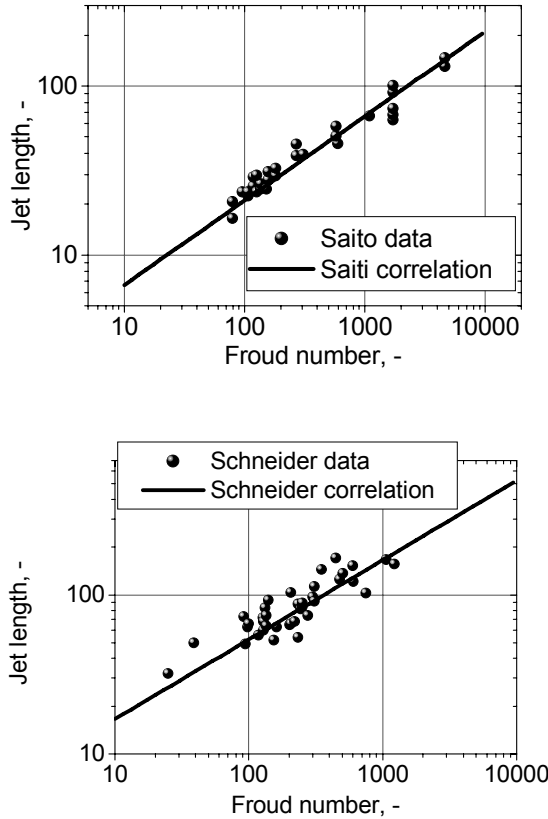


**Fig. 10.3** (a) Film boiling jet penetration length  $(\Delta L_j / D_j)(\rho_c / \rho_j)^{1/2}$  as a function of the Froude number  $Fr_j$ . (b) Film boiling jet penetration length  $\Delta L_j / D_j$  as a function of the Froude number  $Fr_j$ . Comparison between the prediction of the Saito correlation with the experimental data of Saito and Schneider

the surrounding vapor phase was made responsible for this process as discussed above. In a similar way as the above the authors obtained the analytical equation

$$\Delta L_j / D_j = \frac{1}{2} Fr_j^{1/2} \left\{ \left[ 1 + 1 / \left( \frac{2}{5} Fr_j^{1/2} (\rho_2 / \rho_j)^{1/2} \right) \right]^{8/5} - 1 \right\} \quad (10.41)$$

which can successfully be approximated by *Saito's* empirical equation. Equation (10.41) is experimentally verified to  $Fr_j < 1400$  or  $We_j < 67$  - see Fig. 10.3. In accordance with *Saito* and *Schneider's* experiments for  $\rho_2 < \rho_j$ , the denser the jet surrounding continuum, 2, the smaller the jet penetration distance  $\Delta L_j$ .

Note: *Saito's* type of correlations has to be used only for jets causing film boiling. Do not use them in other cases.

#### 10.4.4 An alternative approach

The success of the simple *Taylor-Scheider* approach is very promising also for non boiling environment. The internal turbulent pulsation can cause also surface entrainment not influenced by the environment directly. That is why I recommend to use in the mass conservation equation the interface averaged entrainment velocity

$$u_{j\sigma} = u_\sigma^* + u_j' = \left( c_{cd}^d \frac{1}{2} \rho_c \Delta V_{cj}^2 / \rho_j \right)^{1/2} + cV_j. \quad (10.42)$$

Here the interface averaged pulsation velocity  $u_j' = cV_j$  is proportional to jet velocity. The proportionality factor can be of the order of 0.1, see *Faeth* (1995). The approximate solution of the mass conservation equations looks like

$$\Delta L_j / D_j = \frac{1}{2} V_j / u_\sigma^* = \frac{1}{2} V_j / \left\{ \left( c_{cd}^d / 2 \right)^{1/2} (\rho_c / \rho_j)^{1/2} \Delta V_{cj} + cV_j \right\}. \quad (10.43)$$

Equation (10.43) can be expressed in terms of *Weber* numbers

$$\Delta L_j / D_j = \frac{1}{2} We_j^{1/2} / \left[ \left( c_{cd}^d / 2 \right)^{1/2} We_{cj}^{1/2} + cWe_j^{1/2} \right]. \quad (10.44)$$

The above simple equations have some surprising properties. Neglecting the influence of the internal jet turbulence,  $c = 0$ , we obtain an equation very similar to the *Taylor* result, compare also with Eq. (2) published by *Buerger* et al. (1993), for parallel flow surface instability. The friction drag coefficient depends on the interface waviness, which itself depends on the ambient relative velocity, and is expected to be less than 0.33. The constant 7, experimentally obtained by *Braco* in the *Taylor* equation, corresponds to the friction coefficient  $c_{cd}^d \approx 0.01$ . For jets in stagnant environment,  $\Delta V_{cj} \approx V_j$ , the above equation resembles the *Epstein* and *Fauske* (1985) equation. For strong turbulized jets,  $\left( c_{cd}^d / 2 \right)^{1/2} (\rho_c / \rho_j)^{1/2} \Delta V_{cj} \ll cV_j$ , and where

$c$  is order of unity,  $\Delta L_j / D_j = 1 / (2c)$  is as expected, very short. Equating the predictions of Eqs. (10.35) and (10.44)

$$We_{cj}^* = (c_{cd}^d / 2) \left\{ 1 / \left[ 2(7.68 - 2.66 \ln On_j)(1 + 3On_j) \right] - cWe_j^{1/2} \right\}^2 \quad (10.45)$$

we find the transition to atomization boundary.

#### 10.4.5 Jets penetrating two-phase mixtures

If a jet is penetrating a two-phase mixture in a sandwich structure, consisting of gas layers with overall thickness  $\alpha_1^* \Delta L_j$ , and liquid layers with overall thickness  $(1 - \alpha_1^*) \Delta L_j$ , where  $\alpha_1^* = \alpha_1 / (1 - \alpha_1)$ , the penetration length is

$$\Delta L_j / D_j = \frac{1}{2} V_j / \left\{ \begin{aligned} &\alpha_1^* (c_{ld}^d / 2)^{1/2} (\rho_1 / \rho_j)^{1/2} \Delta V_{1j} \\ &+ (1 - \alpha_1^*) (c_{2d}^d / 2)^{1/2} (\rho_2 / \rho_j)^{1/2} \Delta V_{2j} + cV_j \end{aligned} \right\}. \quad (10.46)$$

#### 10.4.6 Particle production rate

The application of these correlations in the form of rate correlation in a space resembling a pool can be performed using Eq. (7.2) as follows. As already mentioned if the number of particles in the volume under consideration is less than one, the fluid should be considered as continuous,  $c$ . After a distance  $\Delta L_j$ , the jets disintegrate in particles having size  $D_{d\infty}$ . Obviously a “marked control volume”, being in the continuum jet and traveling the distance  $\Delta L_j$  with the velocity  $V_j$ , should experience fragmentation. It means that the time interval needed by this “marked control volume” to disintegrate is of the order of  $\Delta L_j / V_j$ . This is approximately the characteristic time interval in which the jet fragmentation is completed  $\Delta \tau_{br} \approx \Delta L_j / V_j$ . Using this time and  $D_{d\infty}$  we can estimate the particle production rate by means of Eq. (7.11).

### 10.5 Jet erosion by high velocity gas environment

There are some attempts in the literature to describe entrainment from liquid film for very high gas velocity. Next, we give two possible approaches proposed by Mayer (1961) and Chawla (1975, 1976).

*Mayer* (1961) investigated the interaction of a high velocity gas stream with a large liquid surface. For capillary surface waves (ripples), the change of the amplitude,  $A$ , with the time was described by

$$\frac{dA}{d\tau} = \frac{A}{\Delta\tau}, \quad (10.47)$$

where the frequency of the waves is a function of their wavelength besides other parameters

$$\frac{1}{\Delta\tau} = c_1 \sqrt{\pi/2} \frac{\rho_1 \Delta V_{12}^2}{\sqrt{\sigma/\rho_2}} \frac{1}{\delta^{1/2}} - 8\pi^2 \frac{\eta_2}{\rho_2} \frac{1}{\delta^2}, \quad (10.48)$$

using for the *sheltering* parameter  $c_1 = 0.3$ . Here  $\Delta\tau$  is the time constant of the process and  $\delta$  is the wavelength. *Mayer* (1961) found that if the generated wavelengths are greater than a minimum value obtained by the condition  $1/\Delta\tau = 0$ ,

$$\delta > \delta_{\min} = 2\pi\sqrt{16} \left( \frac{\eta_2 \sqrt{\sigma/\rho_2}}{c_1 \rho_1 \Delta V_{12}^2} \right)^{2/3}, \quad (10.49)$$

the capillary wave will grow unboundedly and the wave is eroded as a ligament from which droplets of size proportional  $\delta$ ,

$$D_{3E} \approx c_2 \delta, \quad (10.50)$$

with  $c_2 \approx 0.14$  are entrained. The average size of the entrained particles was found to be

$$\overline{D_{3E}} = 9\pi\sqrt[3]{16}c_1 \left( \frac{\eta_2 \sqrt{\sigma/\rho_2}}{c_1 \rho_1 \Delta V_{12}^2} \right)^{2/3}. \quad (10.51)$$

The constants  $c_1$  and  $c_2$  are derived from a single experimental point. Later, *Wolfe* and *Anderson* (1965) compared *Mayer's* theory with their own data in the region

$$9 \times 10^{-5} < 9\pi\sqrt[3]{16}c_1 \left( \frac{\eta_2 \sqrt{\sigma/\rho_2}}{c_1 \rho_1 \Delta V_{12}^2} \right)^{2/3} < 0.0011, \quad (\text{see also Fig. 12 in } Wolfe \text{ and } Anderson \text{ 1965}) \quad (10.52)$$

and found for the sheltering parameter  $c_1 = 0.18$ .

In the sense of *Mayer's* theory the average number of the entrained droplets per unit surface is

$$\dot{n}_{23}'' = \frac{1}{\delta^2 \Delta\tau(\delta)}, \quad (10.53)$$

where  $\bar{\delta} = \overline{D_{3E}}$  from Eq. (10.51),  $\Delta\tau$  is computed using Eq. (10.48). The erosion mass flow rate is then

$$(\rho w)_{23} = \rho_2 \frac{\pi}{6} \delta^3 \dot{n}_{23}^* = \rho_2 \frac{\pi}{6} \frac{\delta}{\Delta\tau(\delta)}. \quad (10.54)$$

Chawla (1975, 1976) analyzed the instabilities of the interface of a gas jet entering a liquid and the resulting droplets entrainment. He found that when the amplitude of the disturbance becomes large enough, the liquid at the wave crests (protruded into the gas jets) is torn off by the gas jet. The size of the resulting droplets is governed by *Kelvin-Helmholz* instabilities

$$D_{3E} \approx c_0 \delta_{3E} + c_1 \delta_{3E}^*, \quad (10.55)$$

where

$$We_{12E} = \delta_{3E} \rho_1 \Delta V_{12}^2 / \sigma_2 = 3\pi (1 - Ma^2)^{1/2}, \quad Ma < 1, \quad (10.56)$$

$$We_{12E}^* = \delta_{3E}^* \rho_1 \Delta V_{12}^2 / \sigma_2 = \frac{2\pi}{0.803} (\rho_1^* / \rho_2)^{1/5}, \quad Ma = 1. \quad (10.57)$$

Here,  $Ma = \Delta V_{12} / V_1^*$  is the local *Mach* number and  $\rho_1^*$ ,  $V_1^*$  are critical density and sonic gas velocity at the throat conditions for sonic gas jets, respectively. The constants  $c_0 \approx 1.5$ , and  $c_1 \approx 27.14$  are estimated by comparison with experimental data. Thus for low *Mach* numbers the stability criterion is

$$We_{12E} \approx 14. \quad (10.58)$$

It seems that there is a lack of reliable data for the development of a more reliable correlation for high gas velocity entrainment.

## 10.6 Jet fragmentation in pipes

The liquid jet disintegration is also a kind of transition of flow with continuous liquid into flow with dispersed liquid. De Jarlais et al. (1986) considered the hydrodynamic stability of inverted annular flow in an adiabatic situation as a jet disintegration problem in channels - see Fig. 10.4.

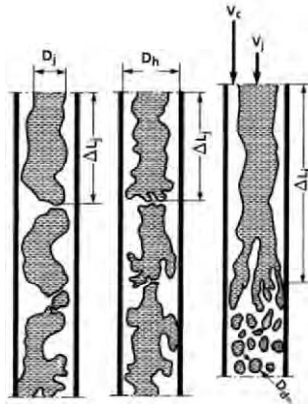


**Fig. 10.4** Jet fragmentation in channels

After reviewing the jet stability literature and comparing with their own experimental data, the authors proposed the following correlation which represents their data for the jet core breakup length. For

$$We_{ej} / \alpha_c^2 < 1.73 \quad (10.59)$$

$$\Delta L_j / D_j = 480 We_j^{1/2} / Re_j^{0.53}, \quad (10.60)$$

where  $Re_j = \rho_j V_j D_j / \eta_j$  is the liquid jet *Reynolds* number and  $We_j = \rho_j V_j^2 D_j / \sigma$  is the liquid jet *Weber* number. The averaged wavelength was found to be

$$\lambda_j \approx 5.8 D_j. \quad (10.61)$$

For

$$We_{ej} / \alpha_c^2 \geq 1.73 \quad (10.62)$$

$$\Delta L_j / D_j = 685 (We_j^{1/2} / Re_j^{0.53}) / (We_{ej} / \alpha_c^2)^{0.645}, \quad (10.63)$$

where  $We_{ej} = \rho_c \Delta V_{ej}^2 D_h / \eta_c$  is the gas *Weber* number. The average wavelength,  $\lambda_j$ , was found to be

$$\lambda_j \approx 7.6 (We_{ej} / \alpha_c^2)^{-1/2}. \quad (10.64)$$

Again the time needed for the fragmentation is

$$\Delta \tau_{br} \approx \Delta L_j / \Delta V_{ej}. \quad (10.65)$$

Thus the particle production rate in this case is

$$\dot{n}_3 \approx \alpha_j / \left( \frac{\pi}{4} D_j^2 \lambda_j \Delta \tau \right). \quad (10.66)$$

The entrainment of micro-droplets from the surface of the jet was also a subject of investigation by the above mentioned authors but the obtained information is not sufficient for reliable conclusions to be drawn.

## 10.7 Liquid spray produced in nozzles

Forcing liquid through specifically designed nozzles various types of sprays can be produced. Sprays consist of a range of droplet sizes and shape depending on the nozzle geometry. *Hollow cones sprays* are produced by inserting liquid tangentially into a swirl chamber or by grooved vanes directly upstream of an orifice. The swirling liquid exits the orifice as a ring of droplets. *Full cone sprays* are produced by forcing liquid through stationary vanes that add turbulence. Gas-atomizing nozzles use a gas jet to break up the liquid into fine droplets at higher velocity. The parameter that is generally used to characterize sprays is the *Sauter* mean diameter, defined as a droplet size whose surface area is average surface area over all droplets in the spectrum. *Estes and Mudawar* (1995) proposed the following correlation for estimation of the *Sauter* mean diameter

$$\frac{D_{d\infty}}{D_{nozzle}} = 3.07 \left( \frac{\rho_c^{0.5} D_{nozzle}^{1.5} \Delta p}{\sigma_d^{0.5} \eta_d} \right)^{-0.259}$$

The droplet velocity exiting the nozzle in liquid atomized sprays can be estimated by the method proposed by *Ghodbane and Holman* (1991).

## 10.8 Gas jet disintegration in pools

There are many industrial processes in which gas is injected into a liquid. For mathematical modeling of such processes one needs quantitative information on how gas injected into the liquid through an orifice behaves. This information can be used as a boundary condition for modeling the processes in the volume of interest. That is why in this section we concentrate our attention on gas jet disintegration produced by orifices.

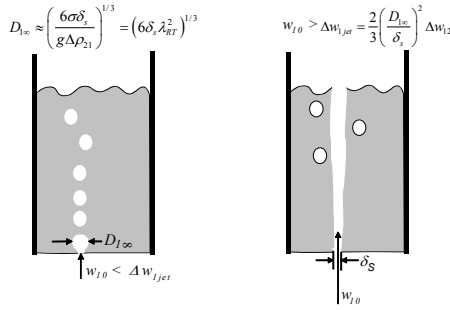


**Fig. 10.5** Gas injection into a pool of liquid: a) small gas mass flows; b) large gas mass flow – jet formation

Consider vertical gas injection into a stagnant liquid pool as presented in Fig. 10.5. The gas velocity at the orifice is  $V_{10}$  and the orifice diameter  $D_{10}$ . The volumetric gas flow is

$$\dot{V}_{10} = F_0 V_{10}, \quad (10.67)$$

where  $F_0 = \pi D_0^2 / 4$  is the cross section of the orifice. The cross section of the pool above the orifice is  $F$ , the gas volume fraction immediately after the orifice is  $\alpha_1$  and at the bubble velocity  $V_{1\infty}$ . For approximately constant pressure we have

$$\alpha_1 V_{1\infty} = \frac{F_0}{F} V_{10}. \quad (10.68)$$

In the following we are interested in the diameter of the *largest* bubble,  $D_{1\infty}$  which can be in static equilibrium. For this purpose we write a simple momentum balance: buoyancy force = surface force i.e.

$$\frac{\pi D_{1\infty}^3}{6} g (\rho_2 - \rho_1) = \pi D_{10} \sigma \quad (10.69)$$

or

$$D_{1\infty} = \left( \frac{6\sigma D_{10}}{g \Delta \rho_{21}} \right)^{1/3}. \quad (10.70)$$

see *Fritz and Ende* (1966).

*Kutateladze and Styrikovich* (1958) observed experimentally

$$D_{1\infty} \approx \left( \frac{4\sigma D_{10}}{g \Delta \rho_{21}} \right)^{1/3}. \quad (10.71)$$

Obviously  $D_{1\infty}$  should be at least of the order of  $D_{10}$ , i.e.



$$D_{1\infty} < \left( \frac{\sigma}{g\Delta\rho_{21}} \right)^{1/2} < \lambda_{RT}. \quad (10.72)$$

The simple momentum balance, Eq. (10.69), is not sufficient to describe the real bubble size after the jet fragmentation which is smaller than the largest bubble diameter defined by Eq. (10.71). The effect of the gas momentum is not taken into account. *Davidson* and *Harrison*, see in 1963, obtained an empirical correlation which takes into account the influence of the volumetric gas flow on  $D_{1\infty}$

$$\pi D_{1\infty}^3 / 6 \approx 1.138 \dot{V}_{10}^{6/5} / g^{3/5}. \quad (10.73)$$

Later work by *Darton* et al. (1977) supported the order of magnitude of the constant but changed the value from 1.138 to 2.27 in the above equation (10.73). Similar conclusions are reached by *Davidson* and *Schüler*, see in *Davidson* and *Harrison* (1963)

$$\pi D_{1\infty}^3 / 6 = \left( \frac{4\pi}{3} \right)^{1/4} \left[ \frac{15\eta_2 \dot{V}_{10}}{2g(\rho_2 - \rho_1)} \right]^{3/4}. \quad (10.74)$$

The next step of sophistication of the theory is to use the steady state momentum balance in the form: buoyancy + momentum = drag + virtual mass force + surface force, i.e.

$$\begin{aligned} & \frac{\pi D_{1\infty}^3}{6} [g(\rho_2 - \rho_1) + \rho_1 V_{10}^2] \\ &= 3\pi\eta_2 D_{10} V_{10} \left[ 1 + 0.1(D_{10}\rho_2 V_{10} / \eta_2)^{3/4} \right] + \frac{1}{2} \frac{\pi D_{1\infty}^3}{6} \rho_2 V_{10} \frac{V_{10}}{D_{1\infty}} + \pi D_{10} \sigma \end{aligned} \quad (10.75)$$

and to solve the resulting transcendental equation with respect to  $D_{1\infty}$ . Further improvement of the theory is reported by *Ruft* (1972) who developed a semi-empirical model modifying the above equation and by *Geary* and *Rice* (1991). *Geary* and *Rice* proposed a theory of transient departure which describes the available experimental data without any adjustable parameter. The final analytical solution is voluminous and will not be repeated here. Nevertheless we recommend this solution as the most accurate to describe jet fragmentation by an orifice.

The number of bubbles generated at the orifice per unit time is easily computed by dividing the volumetric gas flow rate  $\alpha_1 V_{1\infty}$  by the volume of the single bubble

$$\dot{n}_{1,sp} = \alpha_1 V_{1\infty} / \frac{\pi D_{1\infty}^3}{6} = \frac{F_0}{F} V_{10} / \frac{\pi D_{1\infty}^3}{6}. \quad (10.76)$$

The time in which the bubble remains attached at the orifice is

$$\Delta \tau_{br} = \frac{\pi D_{1\infty}^3}{6} / \dot{V}_{10}. \quad (10.77)$$

If the raising velocity of the bubbles after the fragmentation is equal to the *Kutateladze* velocity

$$\Delta V_{12\infty} = \sqrt{2} \left[ \frac{\sigma g (\rho_2 - \rho_1)}{\rho_2^2} \right]^{1/2} \quad (10.78)$$

the bubble leaving the orifice should travel the distance  $\Delta V_{12\infty} \Delta \tau_{br}$  during  $\Delta \tau_{br}$ . If this distance is smaller than the bubble diameter after the fragmentation, i.e.

$$\Delta V_{12\infty} \Delta \tau_{br} < D_{1\infty} \quad (10.79)$$

or

$$\frac{V_{10}}{\Delta V_{12\infty}} > \frac{2}{3} \left( \frac{D_{1\infty}}{D_0} \right)^2, \quad (10.80)$$

bubbles are no longer formed individually, but the gas leaves the orifice in the form of a jet which eventually breaks into individual bubbles. This line of argument was first proposed by *Kutateladze* and *Styrikovich* (1958).

Summarizing the results discussed in this section we can say that:

1. To have a jet behind the orifice a critical gas velocity should be exceeded in order that the orifice provides more volumetric flow than that which can be transferred away by buoyancy driven bubble raise;
2. The generated number of bubbles per unit mixture volume is uniquely defined if the stable bubble size after the fragmentation, the dimensions of the orifice and of the pool, and the volumetric gas flow through the orifice are known.

## Nomenclature

### Latin

$A$	amplitude, $m$
$D$	diameter, $m$
$\overline{D_{3E}}$	average size of the entrained particles, $m$
$D_{d\infty}$	size of the ligaments resulting from primary breachup, $m$
$D_{10}$	orifice diameter, $m$
$d$	differential
$F_0$	$= \pi D_0^2 / 4$ , cross section of the orifice, $m^2$

---

$f_m^*$	dimensionless frequency of the fastest growing of the unstable surface perturbation waves
$Fr_{cj}$	$= \Delta V_{cj}^2 / (gD_j)$ , <i>Froude</i> number based on the relative velocity, appropriate for jets causing boiling at the interface so that the environment velocity is governed by buoyancy driven convection, <i>dimensionless</i>
$Fr_j$	$= V_j^2 / (gD_j)$ , <i>Froude</i> number based on the jet velocity, appropriate for gravitationally driven jets gravitational acceleration, <i>dimensionless</i>
$Lp_j$	$= \rho_j \sigma_j D_j / \eta_j^2$ , <i>Laplace</i> number, <i>dimensionless</i>
$Ma$	local <i>Mach</i> number, <i>dimensionless</i>
$\dot{n}_{23}''$	average number of the entrained droplets per unit surface, $1/m^2$
$\dot{n}_{1,sp}$	number of bubbles generated at the orifice per unit time, $1/s$
$\dot{n}_3$	particle production rate, $1/(sm^3)$
$On_j$	$= We_j^{1/2} / Re_j = 1 / Lp_j^{1/2} = \eta_j / (D_j \sigma_j \rho_j)^{1/2}$ , jet <i>Ohnesorge</i> number, <i>dimensionless</i>
$On_{j\lambda}$	$= \eta_j / (\lambda_{RT} \sigma_j \rho_j)^{1/2}$ , jet viscosity number based on <i>Rayleigh-Taylor</i> instability wave length, <i>dimensionless</i>
$On_j^*$	$= (3\eta_j + \eta_c) / (D_j \sigma_j \rho_j)^{1/2}$ , modified <i>Ohnesorge</i> number, <i>dimensionless</i>
$On_c$	$= \eta_c / (D_j \sigma_j \rho_c)^{1/2}$ , ambient <i>Ohnesorge</i> number, <i>dimensionless</i>
$Re_j$	$= \rho_j V_j D_j / \eta_j$ , liquid jet <i>Reynolds</i> number, <i>dimensionless</i>
$Ta_{cj}$	$= (\rho_j / \rho_c) [\sigma / (\eta_j \Delta V_{cj})]^2$ , <i>Taylor</i> number based on relative velocity, <i>dimensionless</i>
$Ta_c$	$= (\rho_j / \rho_c) [\sigma / (\eta_j V_c)]^2$ , <i>Taylor</i> number based on the continuum velocity, <i>dimensionless</i>
$u_{j\sigma}$	interface averaged entrainment velocity, $m/s$
$u_\sigma^*$	jet side surface friction velocity, $m/s$
$u'_j$	interface averaged pulsation velocity, $m/s$
$V$	velocity, $m/s$
$V_j$	jet velocity, $m/s$
$V_{10}$	gas velocity at the orifice, $m/s$
$\dot{V}_{10}$	$= F_0 V_{10}$ , volumetric gas flow, $m^3/s$
$V_1^*$	critical sonic gas velocity at the throat conditions for sonic gas jets, $m/s$
$V_{1\infty}$	bubble velocity, $m/s$

$We_j = \rho_j V_j^2 D_j / \sigma$ , jet *Weber* number, *dimensionless*

$We_{ej} = \rho_j \Delta V_{ej}^2 D_j / \sigma$ , continuum *Weber* number based on the relative velocity, *dimensionless*

### **Greek**

$\alpha$  volume fraction, *dimensionless*

$\alpha_1$  gas volume fraction, *dimensionless*

$\Delta L_j$  length for complete disintegration measured from the nozzle outlet, *m*

$\Delta V_{ej}$  relative velocity between the jet and the environment, *m/s*

$\Delta \tau_{br} \approx \Delta L_j / V_j$ , characteristic time interval in which the jet fragmentation is completed, *s*

$\Delta \tau_{br} = \frac{\pi D_{10}^3}{6} / \dot{V}_{10}$ , time in which the bubble remains attached at the orifice, *s*

$\Delta L_j / D_j$  relative jet penetration length, *dimensionless*

$\delta$  wavelength, *m*

$\lambda_{RT} = [\sigma_d / (g \Delta \rho_{dc})]^{1/2}$ , scale of the *Rayleigh - Taylor* instability wavelength, *m*

$\lambda_0$  initial deviation from the non-disturbed jet radius, *m*

$\lambda_m^*$  dimensionless wavelength frequency of the fastest growing of the unstable surface perturbation waves

$\lambda_j$  average wave length, *m*

$\eta$  dynamic viscosity, *kg / (ms)*

$\rho$  density, *kg/m<sup>3</sup>*

$(\rho w)_{23}$  erosion mass flow rate, *kg/(sm<sup>2</sup>)*

$\rho_1^*$  critical density at the throat conditions for sonic gas jets, *kg/m<sup>3</sup>*

$\sigma$  surface tension, *N/m*

$\tau$  time, *s*

$\tau_{j\sigma}$  vapor side shear stress, *N/m<sup>2</sup>*

### **Subscripts**

$\Delta$  difference

*j* jet

*c* continuum

1 gas

2 liquid

3 droplet

## References

- Batchelor GK (ed) (1958) Collected works of Taylor GI, Cambridge Univ. Press, Cambridge, MA
- Bohr N (1909) Determination of the surface-tension of water by method of jet vibration, Phil. Trans. Roy. Soc. London, Series A., vol 209 p 281
- Bracco FV (Feb. 25 - March 1, 1985) Modeling of engine sprays, Proc. International Congress & Exposition Detroit, Michigan, pp 113-136
- Buerger M, von Berg E, Cho SH, Schatz A, (October 25-29, 1993) Modeling of jet breakup as a key process in premixing, Proc. of the Int. Seminar on The Physics of Vapor Explosions, Tomakomai, pp 79-89
- Chawla TC (1975) The Kelvin - Helmholtz instability of gas - liquid interface, J. Fluid Mechanics, vol 67 no 3 pp 513-537
- Chawla TC (1976) Drop size resulting from breakup of liquid-gas interfaces of liquid submerged subsonic and sonic gas jets, Int. J. Multiphase Flow, pp 471-475
- Darton RC, La Nauze RD, Davidson JF and Harrison D (1977) Bubble growth due to coalescence in fluidized beds, Trans. I. Chem. E., vol 55 pp 274-280
- Davidson JF and Harrison D (1963) Fluidized particles, Cambridge University Press, London
- De Jarlais G, Ishii M and Linehan J (Febr. 1986) Hydrodynamic stability of inverted annular flow in an adiabatic simulation, Transactions of ASME, Journal of Heat Transfer, vol 108 pp 85-92
- Eppstein M and Fauske K (August 4-7, 1985) Steam film instability and the mixing of core-melt jets and water, ANS Proceedings, National Heat Transfer Conference, Denver, Colorado, pp 277-284
- Estes KA and Mudawar I (1995) Correlation of Sauter mean diameter and critical heat flux for spray cooling of small surfaces, International Journal of Heat and Mass Transfer, vol. 38 no 16 p 2985-2996
- Faeth GM (April 3-7, 1995) Spray combustion: a review, Proc. of The 2nd International Conference on Multiphase Flow, Kyoto, Japan
- Fenn III RW and Middleman S (1969) Newtonian jet stability: The role of air resistance, AIChE Journal, vol 15 no 3 pp 379-383
- Fritz W and Ende W (1966) Über den Verdampfungsvorgang nach kinematographischen Aufnahmen an Dampfblasen. Phys. Z., vol 37 pp 391-401
- Geary NW and Rice RG (Feb. 1991) Bubble size prediction for rigid and flexible sparkers, AIChE Journal, vol 37 no 2 pp 161-168
- Ghodbane M and Holman JP (1991) Experimental study of spray cooling with Freon-113, International Journal of Heat and Mass Transfer, vol 34 no 4/5 pp1163-1174
- Grant RP and Middleman S (July 1966) Newton Jet Stability, AIChEJ, vol 12 no 4 p 669
- Iciek J (1982) The hydrodynamics of free, liquid jet and their influence on direct contact heat transfer - I, II, Int. J. Multiphase Flow, vol 8 no 3 pp 239-260
- Kutateladze SS and Styrikovich MA (1958) Hydraulics of gas-liquid systems, Moscow, Wright Field transl. F-TS-9814/V
- Lienhard JH and Day JB (1970) The breakup of superheated liquid Jets, ASME J. Basic Eng., vol 92 pp 511-522
- Mayer E (Dec. 1961) Theory of liquid atomization in high velocity gas streams, ARS Journal, vol 31 pp 1787 - 1785

- Meister BJ and Scheele GF (1969) *AIChEJ* vol 15 pp 689 - 699
- Merrington AC and Richardson EG (1947) The breakup of liquids jets, *Proc. Phys. Soc.*, vol 59 pp 1-13
- Nigmatulin BI, Melikhov OI, and Melikhov VI (Oct.25-29, 1993) Breakup of liquid jets in film boiling, *Proc. of Int. Sem. on The Physics of Vapor Explosions*, Tomakomi, pp 90-95
- Ohnesorge W (1936) Die Bildung von Tröpfen an Düsen und die Auflüssiger Strahlen, *Z. Angew. Math. Mech.*, vol 16 pp 335-359
- Rayleigh L (1878) On the instability of jets, *Proc. London Math. Soc.*, vol 10 p 7
- Ruft K (1972) Bildung von Gasblasen an Düsen bei konstantem Volumendurchsatz, *Chemie-Ing. Techn.* vol 44 no 24 pp 1360-1366
- Saito M, Sato K and Imahori S (July 24-July 27, 1988) Experimental studi on penetration of water jet into Freon-11 and Liquid Nitrogen, *ANS Proc. 1988 Nat. Heat Transfer Conference.*, HTS-Vol.3, Houston, Texas, pp 173-183
- Schneider JP, Marchiniak MJ, Jones BG (Sept. 21-24, 1992) Breakup of metal jets penetrating a volatile liquid, *Proc. of the Fifth Int. Top. Meeting On Reactor Thermal Hydraulics NURETH-5*, vol 2 pp 437-449
- Smith SWJ and Moss H (1917) Experiments with mercury jets, *Proc. Roz. Soc.*, vol A/93 pp 373-393
- Sun PH (November 4-6, 1998) Molten fuel-coolant interactions induced by coolant injection into molten fuel, *SARJ98: The Workshop on Severe Accident Research held in Japan* Tokio, Japan
- Takahashi T and Kitamura Y (1971) *Kogaku Kogaku*, vol 35 p 637
- Takahashi T and Kitamura Y (1972) *Kogaku Kogaku*, vol 36 p 912
- Tanzawa Y and Toyoda S (1954) *Trans. J.S.M.E.* vol 20 p 306
- Teng H, Kinoshita CM and Masutani SM (1995) Prediction of droplet size from the breackup of cylindrical liquid jet, *Int. J. Multiphase Flows*, vol 21 no 1 pp 129-136
- Thimotika H (1935) *Proc. Roy. Soc.*, vol.150 p 322: (1936) vol 153 p 302
- Weber C (1936) Zum Zerfall eines Flüssigkstrahles, *Z. Angew. Math. Mech.*, vol 11 pp 136-154
- Wolfe HE and Anderson WH (1965) Aerodynamic breakup of liquid drops, II. Experimental, *Proc. Int. Shock Tube Symposium*, Naval Ordinance Lab. White Oak, Maryland, USA

# 11 Fragmentation of melt in coolant

## 11.1 Introduction

Let us start with some definitions necessary to understand the content of this Chapter:

- a) The term *melt* is used here for liquid having solidification temperature higher than the film boiling temperature of the surrounding coolant.
- b) *Coolant* is the liquid surrounding the melt.
- c) *Mechanical fragmentation* is fragmentation not influenced by local heat and mass transfer processes.
- d) *Thermo-mechanical fragmentation* is mechanical fragmentation additionally amplified by the local heat and mass transfer.
- e) *Events distorting the film boiling process* are interface instabilities caused by
  - inherent vapor-coolant instability and
  - externally introduced pressure pulses.
- f) *Inherent vapor-coolant instability* is an interface instability caused by
  - mechanical fragmentation of the initially unstable particle leading to intimate melt/coolant contact during the fragmentation,
  - transition from film boiling to transition boiling, and
  - cavitation of vapor bubbles in subcooled liquid in the immediate neighborhood to the particle being in film boiling.
- g) *Contact heat transfer* is a local contact between melt and liquid coolant.

If once established stationary, film boiling at the surface of a liquid sphere is a very stable process. Events distorting the film boiling process may lead to intimate melt-coolant contact resulting in effective energy transfer between the hot droplet and the surrounding coolant. The mechanical feed-back to the droplet leads to additional surface fragmentation which is called thermo-mechanical fragmentation. The result is generation of local pressure pulses. If the same happens not only with a single drop but with a family of melt drops, the resulting pressure pulse may contain considerably more energy than the single drop event.

In order to estimate the risk of the steam explosion for nuclear reactors by postulated severe accidents leading to melt-coolant interaction, to know how the thermo-mechanical fragmentation works is very important. Because of the complexity of the mechanisms involved considerable amount of literature appeared during the last 40 years. The purpose of this Chapter is to review the experimental observation and to derive practically useful estimation methods for quantitative analysis of the steam explosion risk based on the experimental observation. In what follows we will discuss separate effects of these phenomena and the way they can be quantitatively described.

Whether non-stable melt being in film boiling will behave as mechanically fragmenting in vapor or in liquid depends on the thickness of the vapor film. *Epstein and Fauske* (1985) provided an expression derived from instability analysis of both surfaces which can be used to distinguish between thick and thin vapor films

$$\delta_{1F,critc} = 3 \frac{\rho_3 - \rho_1}{\rho_3} \frac{\sigma_3}{\rho_1 \Delta V_{31}^2}. \quad (11.1)$$

For  $\delta_{1F,fc} < \delta_{1F,critc}$  the influence of the vapor film on the fragmentation can be neglected and liquid metal/coolant is the appropriate mode of mechanical interaction. As already mentioned primary mechanical fragmentation of a non-stable particle in film boiling may lead to intimate melt/water contact and therefore may introduce some thermal fragmentation. *Knowles* (1985) found theoretically that the pressure impulse required for vapor collapse is a function of the film thickness. This was experimentally confirmed by *Naylor* (1985).

The film boiling at spheres is well understood as demonstrated in Chapter 21 by comparison with about 2000 experimental data points in different two-phase flow environments - continuous or dispersed liquids. In the next section we are rather interested on the approximated estimation of the average film thickness. The reasons why the estimation of the average film thickness is important are:

For given void fraction in three-phase flow, part of the void is attached to the droplets surfaces and other part is in form of bubbles between the molten droplets. The local volume concentration in the space continuously occupied by water naturally provides a criterion whether the water will remain continuous or get dispersed. Some important consequences result from this observation for the practical analysis:

- a) The pressure wave propagation is known to be much less damped in systems in which the water forms a continuum. Acoustically water/gas discontinuity acts as reflectors to pressure waves. Thus, events initiating external pressure pulses in continuous liquid may lead to explosions, which is not the case when such events happens in a gas environment. We call mixtures having molten particles and being surrounded by continuous water *potentially explosive mixtures*. Whether they are really explosive depends on many other parameters beside the local geometry flow pattern.



- b) The heat and mass transfer processes at the molten particle interface in case of continuous liquid is completely described by the film boiling description methods. The part of the void drifting as bubbles between the films is subject to additional water/vapor heat and mass transfer. This subject is discussed in details in Chapters 13 and 14.
- c) The mechanical fragmentation mechanism is much stronger for melt/liquid systems than for melt/gas systems.

## 11.2 Vapor thickness in film boiling

Consider clouds of hot spheres characterized by volume fraction, diameter, and particle number density designated with  $\alpha_3, D_3, n_3$ , respectively. The mass generated due to film boiling per unit mixture volume and unit time is designated with  $\mu_{21}$ . The film thickness at the equator  $\delta_{1F}$  has to satisfy the continuity condition

$$\pi D_3 \delta_{1F} \rho_1 \langle w_1 \rangle_1 = \frac{\mu_{21}}{n_3} = \frac{\mu_{21}}{\alpha_3} \frac{\pi D_3^3}{6}. \quad (11.2)$$

Here

$$\langle w_1 \rangle_1 \approx \frac{\Delta \rho_{21} g \cos(\mathbf{g}, \Delta \mathbf{V}_{23}) D_3^2}{12 \eta_1} \left( \frac{\delta_{1F}}{D_3} \right)^2 + \frac{3}{4} \Delta V_{23} \quad (11.3)$$

is the vapor velocity averaged over the film thickness computed for particle having large size compared to the film thickness.  $\cos(\mathbf{g}, \Delta \mathbf{V}_{23})$  is the cosine of the angle between the gravitational acceleration and the relative velocity vector particle-water and

$$\Delta V_{32} = \sqrt{\Delta u_{32}^2 + \Delta v_{32}^2 + \Delta w_{32}^2} \quad (11.4)$$

is the magnitude of the velocity difference. The resulting cubic equation

$$\frac{\rho_1 \Delta \rho g \cos(\mathbf{g}, \Delta \mathbf{V}_{23})}{12 \eta_1} \delta_{1F}^3 + \frac{3}{4} \Delta V_{23} \rho_1 \delta_{1F} - \frac{\mu_{21}}{\alpha_3} \frac{D_3^2}{6} = 0, \quad (11.5)$$

rewritten in the compact form

$$\left( \frac{\delta_{1F}}{\delta_{1F,nc}} \right)^3 + r \frac{\delta_{1F}}{\delta_{1F,nc}} - 1 = 0, \quad (11.6)$$

has the following real solution

$$\frac{\delta_{1F}}{\delta_{1F,nc}} = a^{1/3} - \frac{1}{3} r a^{-1/3}. \quad (11.7)$$

Here

$$r = \frac{\delta_{1F,nc}}{\delta_{1F,fc}} = \frac{9}{2} \left( \frac{\alpha_3 \rho_1}{\mu_{21} D_3^2} \right)^{2/3} \Delta V_{23} \left[ \frac{2\eta_1}{g \cos(\mathbf{g}, \Delta \mathbf{V}_{23}) (\rho_2 - \rho_1)} \right]^{1/3} \quad (11.8)$$

is the ratio of the film thickness for natural convection only, e.g. for  $\Delta V_{23} < 0.001$

$$\delta_{1F,nc} = \left[ \frac{2D_3^2 \mu_{21} \eta_1}{\alpha_3 g \cos(\mathbf{g}, \Delta \mathbf{V}_{23}) \rho_1 (\rho_2 - \rho_1)} \right]^{1/3}, \quad (11.9)$$

and for predominant forced convection

$$\delta_{1F,fc} = \frac{2}{9} \frac{D_3^2 \mu_{21}}{\alpha_3 \rho_1 \Delta V_{23}}, \quad (11.10)$$

and

$$a = \frac{1}{2} + \frac{1}{18} \sqrt{3(4r^3 + 27)}. \quad (11.11)$$

The stronger the film boiling, the thicker the vapor film surrounding the drop, the more stable the droplet.

### 11.3 Amount of melt surrounded by continuous water

The particles in film boiling are surrounded by a film with dimensionless thickness

$$\delta_{1F}^* = \frac{\delta_{1F}}{D_3}, \quad (11.12)$$

where  $\delta_{1F}^* > 0$  as already discussed in the previous section. The ratio of the volume of the sphere consisting of one particle and the surrounding film to the volume of the particle itself is

$$(\alpha_3 + \alpha_{1F}) / \alpha_3 = (D_3 + 2\delta_{1F})^3 / D_3^3 = (1 + 2\delta_{1F}^*)^3. \quad (11.13)$$

Therefore the gas volume fraction of the film is

$$\alpha_{1F} = \alpha_3 \left[ (1 + 2\delta_{1F}^*)^3 - 1 \right]. \quad (11.14)$$

The condition to have three-phase flow with continuous liquid and particles being in film boiling is

$$(\alpha_1 - \alpha_{1F}) / (\alpha_1 - \alpha_{1F} + \alpha_2) < 0.52. \quad (11.15)$$

This is a very important result. It demonstrates simply that particles in film boiling can be surrounded by much less continuous liquid mass than required in case of no film boiling.

As already mentioned, *this conclusion has strong implication on the mechanical fragmentation condition* simply allowing the molten particles to experience fragmentation in continuous liquid by far less liquid required. Thus, only the  $f_3^+$  part of the particles  $n_3$  per unit mixture volume experiences melt/water fragmentation while the  $1 - f_3^+$  part the particles experiences melt gas fragmentation. A practicable approach is to define inside a computational cell

$$f_3^+ = 1 \quad \text{for} \quad (\alpha_1 - \alpha_{1F}) / (\alpha_1 - \alpha_{1F} + \alpha_2) < 0.52, \quad (11.16)$$

$$f_3^+ = 0 \quad \text{for} \quad (\alpha_1 - \alpha_{1F}) / (\alpha_1 - \alpha_{1F} + \alpha_2) \geq 0.52. \quad (11.17)$$

## 11.4 Thermo-mechanical fragmentation of liquid metal in water

The scale of the thermo-mechanical fragmentation is much smaller than those for which averaged conservation equations are usually applied. Therefore the description of the thermo-mechanical fragmentation is in fact associated with providing constitutive physics for source terms for the averaged equations. Thermo-mechanical fragmentation is experimentally observed within systems in which the microscopic relative phase velocity is so small that pure mechanical fragmentation is impossible. In pressure wave systems with melt and water as a constituents, in which mechanical fragmentation is possible pure mechanical fragmentation mechanism does not provide the complete description of the thermal energy release. The reader can find interesting discussions on this topic in *Ando and Caldarola (1982), Ando (1984), Arakeri et al. (1978), Bankoff and Yang (1989), Bjorkquist (1975), Bjornard (1974), Burger et al. (1991), Chen et al. (1995), Dullforce et al. (1986), Fletcher and Thyagaraja (1989), Inoue and Aritomi (1989), Henkel (1987), Kim et al. (1989), Medhekar et al. (1989), Saito et al. (1988), Spencer et al. (1985), Young (1987), Young (1990), Zimmer et al. (1989), Zyskowski (1975).*, among many others, and in the references given therein.

For the discussion in this Section we consider the velocity field 3 to be a liquid metal.

The initial conditions under which thermo-mechanical liquid metal fragmentation were experimentally observed are summarized below.

## 1. Coexistence of melt and coolant

$$\alpha_2 > 0, \alpha_3 > 0. \quad (11.18)$$

## 2. Continuous liquid and particles in film boiling

$$(\alpha_1 - \alpha_{1F}) / (\alpha_1 - \alpha_{1F} + \alpha_2) < 0.52. \quad (11.19)$$

Experiments show that the lower the particle and vapor volume fraction the higher the probability of thermo-mechanical fragmentation. Such systems are called *lean systems*.

3. Surface of the melt is in liquid state. The fragments after thermo-mechanical fragmentation were usually smooth, indicating that fragmentation occurred while the particles were still molten, *Kim et al. (1989)*.
4. The droplet surface temperature is higher than the minimum film boiling temperature  $T_{3i} > T_{FB, \min}$ .
5. The initial droplet size is considerably greater than the size of the final fragments.

All of these conditions must be satisfied in order to have thermo-mechanical fragmentation. Under the above conditions and if physical mechanisms are acting to establish contact between melt and liquid coolant, the thermal fragmentation occurs. The mechanisms can be classified as

- a) due to imposed surface instability, or as
- b) due to inherent surface instability, e.g. mechanical fragmentation followed by melt/liquid coolant contact immediately after the fragmentation event, transition from film to nucleate boiling.

Next we discuss some of these conditions in more detail.

## 11.4.1 External triggers

### 11.4.1.1 Experimental observations

As already mentioned, if the droplet surface temperature is higher than the minimum film boiling temperature  $T_3^\sigma > T_{FB, \min}$ , mechanical fragmentation was observed only with additional pressure pulses disturbing the film called trigger pressure pulse

$$\frac{dp}{d\tau} > \left| \frac{dp}{d\tau} \right|_{\text{trigger}}. \quad (11.20)$$

The lowest limit of the pressure gradient causing film distortion has not been systematically investigated. Experimental evidence shows that it is a function of the melt surface temperature - the higher the surface temperature of the melt, the higher the pressure pulse needed to destroy the film.

*Ando and Caldarola* (1982) produced thermal fragmentation on molten copper droplets in water at atmospheric pressure by using pressure pulses of 4.5-9.5 *bar* with approximately triangle form and impulse 50 to 160 *Pa s*. The authors observed two types of fragmentation, *delayed*, caused by impulses of 10 to 70 *Pa s*, and *prompt*, caused by impulses between 70 and 160 *Pa s*. The delay time varies between 2900 and 700  $\mu s$  for the delayed fragmentation and between 300 and 100  $\mu s$  for the prompt fragmentation, respectively.

**Table 11.1** Experimentally observed trigger pressure change

$\left  dp / d\tau \right _{\text{trigger}}$ <i>Pa / s</i>	$\Delta p_{\text{pulse}}$ <i>MPa</i>	$\Delta \tau_{\text{pulse}}$ $\mu s$	Authors, ref.	Rem.
$\approx 10^{12} \pm 20\%$	$\approx 1$	1	<i>Nelson and Buxton</i>	4 <i>cm</i> bridge wire $\Delta \tau_{\text{pulse}} \Delta p_{\text{pulse}} \approx 1 \text{ Pa s}$
$\approx 5 \times 10^{10} \pm 20\%$	$\approx 10$	20	(1980)	detonator $\Delta \tau_{\text{pulse}} \Delta p_{\text{pulse}} \approx 200 \text{ Pa s}$
$(4 \text{ to } 8) \times 10^9$	0.2 to 0.4	50	<i>Kim et al.</i> (1989)	$\Delta \tau_{\text{pulse}} \Delta p_{\text{pulse}} \approx 15 \text{ Pa s}$
$\approx 5 \times 10^9$			<i>Peppler et al.</i> (1991)	depends on the form of the produced pulse
$(4 \text{ to } 7.6) \times 10^9$	0.45 to 0.95	62	<i>Ando and Caldarola</i> (1982)	cooper droplets, triangle pulse form $\Delta \tau_{\text{pulse}} \Delta p_{\text{pulse}} \approx 43.4 \text{ Pa s}$
$\approx 5 \times 10^9$	4	0.8	<i>Huhtiniemi et al.</i> (1997)	gas chamber $\Delta \tau_{\text{pulse}} \Delta p_{\text{pulse}} \approx 3.2 \text{ Pa s}$
$\approx 6 \times 10^7$	3	0.05	<i>Chapman et al.</i> (1997)	electromagnetic movable piston $\Delta \tau_{\text{pulse}} \Delta p_{\text{pulse}} \approx 0.15 \text{ Pa s}$
$(1 \text{ to } 4) \times 10^{12}$	2.5 to 8	1 to 7	<i>Buetner and Zimanowski</i> (1998)	triangle pulse form $\Delta \tau_{\text{pulse}} \Delta p_{\text{pulse}} \approx 8 \text{ to } 15 \text{ Pa s}$

*Knowles* (1985) suggested the following criterion for vapor collapse:

$$\Delta \tau_{\text{pulse}} \Delta p_{\text{pulse}} \approx \delta_F \frac{1}{2} \rho_2 a_2 \cdot \quad (11.21)$$

where  $a_2$  is the coolant sound velocity.

*Naylor* (1985) reported experimental data supporting this criterion. As an example for the order of magnitude estimate consider film boiling of water at atmospheric pressure for film thickness of 0.0001 m. The required pressure impulse is then  $\Delta\tau_{pulse}\Delta p_{pulse} \approx 130 Pa \cdot s$ .

Thus the data in the table can be interpreted only by knowing the local conditions and the film thickness which have to be destabilized in order to cause thermal fragmentation.

### 11.4.1.2 Theory

Because the work by *Naylor* (1985) will play an important role in the following discussion we summarize the most important result of this work. If two continua having common interface are accelerated perpendicular to the interface and if the viscous effects are negligible, the initial disturbance with wavelength  $\lambda_0$  will grow as follows

$$\frac{\lambda}{\lambda_0} = \cosh \frac{\tau}{\Delta\tau_{RT}}, \quad (11.22)$$

where the growing time constant is

$$\Delta\tau_{RT} \approx \left[ a \frac{2\pi}{\lambda_{RT}} \frac{\rho_2 - \rho_1}{\rho_2 + \rho_1} \right]^{-1/2}. \quad (11.23)$$

$a$  is the normal interface acceleration pointing from the heavier to the lighter continuum, and

$$\lambda_{RT} \sim 2\sqrt{3}\pi \left[ \frac{\sigma_2}{a(\rho_2 - \rho_1)} \right]^{1/2} \quad (11.24)$$

is the wavelength of the fastest growing oscillation. *Belman* and *Pennington* obtained in (1954) an additional term in the time constant as given below

$$\Delta\tau_{RT} \approx \lambda_{RT} / V_{2,jets} \approx \left[ a \frac{2\pi}{\lambda_{RT}} \frac{\rho_2 - \rho_1}{\rho_2 + \rho_1} - \left( \frac{2\pi}{\lambda_{RT}} \right)^3 \frac{\sigma_2}{\rho_2 + \rho_1} \right]^{-1/2}, \quad (11.25)$$

which is often neglected in practical analyses.

The nature of the interface acceleration can be different. Some examples are

- a) acceleration due to shock wave propagation which we call *global acceleration*, and
- b) acceleration due to bubble collapse, which we call *local acceleration*.

The global acceleration causes changes of the average velocity differences  $\frac{d}{d\tau}(\Delta V_{12})$ , and the local acceleration causes changes in the local interface velocity, e.g. during bubble collapse  $\left| \frac{d^2 R}{d\tau^2} \right|$ .

For the discussion of the thermal fragmentation we will make use also of the velocity of the wave normal to the interface which we will call coolant micro jet velocity

$$V_{2,jets} = \left[ 2\pi a \lambda_{RT} \frac{\rho_2 - \rho_1}{\rho_2 + \rho_1} \right]^{1/2} = 2\pi \left[ a \frac{3\sigma_2 (\rho_2 - \rho_1)}{(\rho_2 + \rho_1)^2} \right]^{1/4}. \quad (11.26)$$

#### 11.4.1.2.1 Global coolant/vapor interface instability due to phase acceleration

If we consider the film surrounding the particle in the case of film boiling, only distortions having wavelengths shorter than the “bubble” diameter,  $D_3 + 2\delta_{1F}$ , are able to destroy the film. *Gelfand* et al. (1977) analyzed experimentally and theoretically the distortion of bubbles with different densities behind the front of pressure waves. Idealizing the bubble as a cube, the authors applied to the surfaces normal to the pressure wave direction the *Rayleigh-Taylor*, and for the parallel surfaces the *Kelvin - Helmholtz* instability criteria to explain the distortion conditions. Extending this analysis to the gas-water interface in our case, we have a stable film if

$$D_3 + 2\delta_{1F} > \pi \left[ 24 \frac{\sigma_2}{\frac{d}{d\tau}(\Delta V_{12})(\rho_2 - \rho_1)} \right]^{1/2} \quad (11.27)$$

and

$$D_3 + 2\delta_{1F} > \frac{2\pi\sigma(\rho_2 + \rho_1)}{\Delta V_{12}\rho_2\rho_1}. \quad (11.28)$$

Keeping in mind the simplified momentum difference Eq. (8.56),

$$\frac{d}{d\tau}(\Delta V_{21}) \approx - \left( \frac{1}{\rho_2} - \frac{1}{\rho_1} \right) \nabla p \approx \frac{\rho_2 - \rho_1}{\rho_2\rho_1} \nabla p, \quad (11.29)$$

the first *Taylor* instability criterion takes the form

$$D_3 + 2\delta_{1F} > \pi \left[ 24 \frac{\sigma_2\rho_2\rho_1}{(\rho_2 - \rho_1)^2 \nabla p} \right]^{1/2} \quad (11.30)$$

or

$$\nabla p > 24\pi^2 \frac{\rho_2 \rho_1}{(\rho_2 - \rho_1)^2} \frac{\sigma_2}{(D_3 + 2\delta_{1F})^2}. \quad (11.31)$$

If the pressure pulse propagation velocity through the mixture is  $a_m$ , the spatial component of the total pressure change with the time is

$$a_m \nabla p > 24\pi^2 a_m \frac{\rho_2 \rho_1}{(\rho_2 - \rho_1)^2} \frac{\sigma_2}{(D_3 + 2\delta_{1F})^2}. \quad (11.32)$$

The criterion given by this equation contains useful information:

1. For atmospheric pressure and  $D_3 + 2\delta_{1F}$  of the order of 1 mm, small particles concentration for which the mixture sound speed is equal to liquid sound speed,  $a_m = a_2$ , we obtain

$$24\pi^2 a_m \frac{\rho_2 \rho_1}{(\rho_2 - \rho_1)^2} \frac{\sigma_2}{(D_3 + 2\delta_{1F})^2} \approx 1.5 \times 10^7 \text{ Pa/s}, \quad (11.33)$$

which explains the experimentally observed values given in Table 11.1.

2. The linear dependence of the spatial pressure change  $a_m \nabla p$  on the surface tension given by Eq. (11.32) is also supported by the experiments of *Ando* and *Caldarola* (1982).
3. The higher the surface tension, the higher the trigger pressure gradient. The linear dependence of the spatial pressure change  $a_m \nabla p$  on the surface tension given by Eq. (11.32) is also supported by the experiments of *Ando* and *Caldarola* (1982). The increasing oxide content at increasing temperature for liquid copper droplets reduces the surface tension and therefore reduces the threshold pressure impulse required for thermal fragmentation.
4. The higher the system pressure, the higher  $\frac{\rho_2 \rho_1}{(\rho_2 - \rho_1)^2}$  i.e. the steam to liquid acceleration is smaller for the same pressure gradient and therefore the higher the trigger pressure gradient.
5. The smaller the melt particle size, the higher the trigger pressure gradient (experimentally supported by *Fröhlich*, see fig. 5 in (1991)).
6. The trigger pressure pulse increases with decreasing film thickness [experimentally confirmed by *Fröhlich* (1991)].
7. Equation (11.29) explains why  $|dp/d\tau|_{\text{trigger}}$  depends on the spatial form of the trigger pulse - the dependence on  $\nabla p$ . Obviously the application of the condition (11.32) for practical computational analysis needs good spatial resolution in order to estimate accurately the local value of the pressure gradient.



#### 11.4.1.2.2 Local coolant/vapor interface instability due to film collapse

As will be discussed in the chapter “Interface instabilities due to bubble collapse”, the interface acceleration during film collapse in subcooled coolant leads to interface instabilities. The condition that the interface instability wavelength is smaller than the particle size leads to an interesting expression for the so called *threshold pressure*

$$p_{2,th} > p_1 + \frac{2\sigma_2}{R_3} \left( \pi^2 \frac{3}{2} \frac{\rho_2}{\rho_2 - \rho_1} - 1 \right). \quad (11.34)$$

The threshold pressure condition contains an important message: The threshold pressure increases with decreasing particle size due to the term  $\frac{2\sigma_2}{R_3}$ , and with increasing system pressure due to the term  $\frac{\rho_2}{\rho_2 - \rho_1}$ .

The reestimation of the existing data and future experiments should be performed in order to establish a reliable database for the criterion (11.32).

### 11.4.2 Experimental observations

The internal triggers may originate due to different reasons classified as follows:

1. The reduction of the melt surface temperature below the minimum film boiling temperature leads to transition boiling. Fragmentation is caused due to
  - a) instabilities induced by bubble formation and departure,
  - b) micro-shocks caused by liquid entering the volumes that are made free after the bubbles departure, and
  - c) local thermal stresses caused by the local differences in the temperature at the particle surface.
2. Spontaneous vapor condensation (cavitation) in subcooled water.
3. Geometry dependent pressure wave formation and interactions. In order to describe this process, adequate geometry description of the system is necessary associated with appropriate spatial resolution of the pressure waves. The computational models can be tested using well defined pressure wave propagation experiments not necessary associated with melt/water interactions. The mechanism of the thermo-mechanical fragmentation is then described with the information provided in chapter external triggers.
4. Particles reaching the bottom or an obstacle in a liquid state may serve as a trigger by the mechanism of the so called entrapment - see *Mitsumura et al. 1997*.

### 11.4.2.1 Interface solidification and availability of internal triggers

#### 11.4.2.1.1 Solidification macro time scale of the system

We now consider the condition that the surface of the molten drop has to be in a liquid state in order to allow further fragmentation of the droplet. For such processes the external cooling due to film boiling and radiation causes solidification starting at the surface and penetrating into the drop. Therefore, if the drop possesses a specific entropy below  $s_3''$ , the crust on the surface is already formed and the probability that the droplet will be destroyed due to thermo-mechanical fragmentation is very low. Therefore the first order approximation for the condition allowing fragmentation is that the locally average field specific entropy is greater than the liquidus entropy of the molten drop,

$$s_3 > s_3'' . \quad (11.35)$$

This approximate criterion is very convenient for application in computer codes. Note that there is a spatial temperature profile inside the drop which explains the term approximate. In addition, this criterion neglects the solidification delay.

Next we will estimate under which condition melt penetrating the water may create internal triggers due to entrapment using a simple lumped parameter approach. If particles of melt enter a water reservoir with water depth  $L_{pool\_depth}$  one can estimate the time within the particle reaches the bottom of the reservoir

$$\Delta \tau_{life\_time} = \frac{L_{pool\_depth}}{\Delta w_{32}} . \quad (11.36)$$

Here  $\Delta w_{32}$  is the average velocity with which the droplet crosses the water. If there are some obstacles normal to the flow direction  $L_{pool\_depth}$  should represent the distance between water level and these obstacles. Particles reaching the bottom or an obstacle in a liquid state may serve as a trigger for the mechanism of the so called entrapment - see *Mitsumura et al. 1997*.

For nuclear reactor systems the melt possesses temperatures considerably higher than the critical temperature of water and therefore the film boiling and radiation are the heat transfer controlling mechanism at non-disturbed droplet interfaces. Thus the heat flux emitted from the surface is

$$\dot{q}_3^{\sigma 2} = k_{SB} \left[ T_3^{\sigma 4} - T'(p)^4 \right] + h_{FB} \left[ T_3^{\sigma} - T'(p) \right] . \quad (11.37)$$

The characteristic time elapsed from the beginning of the melt-coolant mixing process to the formation of the crusts at the interface having the solidus-liquid temperature is computed from equating the heat flux released from the interface and the heat flux coming from the droplet bulk to the interface computed by the short time solution of the *Fourier* equation

$$\dot{q}_3^{\sigma 2} = (T_3 - T_{3\sigma}) \sqrt{\frac{3}{\pi}} \frac{\lambda_3 \rho_3 c_{p3}}{\tau} . \quad (11.38)$$

The result is

$$\Delta \tau_{crust} \approx \frac{3}{\pi} \lambda_3 \rho_3 c_{p3} \left\{ \frac{T_3 - T''' }{k_{SB} [T_3''' - T'(p)]^4 + h_{FB} [T_3''' - T'(p)]} \right\}. \quad (11.39)$$

Thus the approximate condition to expect entrapment triggers is

$$\Delta \tau_{crust} > \Delta \tau_{life\_time}, \quad (11.40)$$

or

$$\frac{3}{\pi} \frac{\lambda_3 \rho_3 c_{p3} \Delta w_{32}}{L_{pool\_depth}} \left\{ \frac{T_3 - T''' }{k_{SB} [T_3''' - T'(p)]^4 + h_{FB} [T_3''' - T'(p)]} \right\}^2 > 1. \quad (11.41)$$

#### 11.4.2.1.2 Micro time scale of the system

As already mentioned, primary mechanical breakup of a non-stable particle in film boiling may lead to intimate melt/water contact and therefore introduce some thermal fragmentation which may serve as a local trigger.

Mechanical fragmentation of melt entering a water pool is possible if the time required for mechanical fragmentation is less than the time to reach surface solidification. As already discussed in Chapter 8, there are different regimes of mechanical fragmentation. The data collection of *Pilch et al.* from 1981, see Fig.8.2, shows that the dimensionless fragmentation time

$$\Delta \tau_{br}^* = \frac{\Delta \tau_{br}}{\frac{D_3}{|\Delta V_{3c}|} \sqrt{\frac{\rho_3}{\rho_c}}} \quad (11.42)$$

varies between 2 and 7. Note that for thin vapor layers in film boiling, which is usually the case, the continuum density is effectively equal to the coolant density. Thus the condition to have primary breakup before reaching the obstacle is

$$\Delta \tau_{crust} > \Delta \tau_{life\_time} > \Delta \tau_{br}. \quad (11.43)$$

#### 11.4.2.2 Transition boiling

The reduction of the melt surface temperature below the minimum film boiling temperature

$$T_3^\sigma < T_{FB,min} \quad (11.44)$$

leads to transition boiling. In addition, if the melt is in a liquid state, that is the melt solidification temperature is lower than the minimum film boiling temperature

$$T_3'' < T_{FB,\min} \quad (11.45)$$

violent explosion starts, *Board et al.* (1972), *Frost and Ciccarelli* (1988). One example is the experiment reported by *Board et al.* (1972), in which tin with melting temperature  $230^\circ\text{C}$  was dropped in water at  $60^\circ\text{C}$  having minimum film boiling temperature about  $250^\circ\text{C}$  at atmospheric pressure. 2 to 5 mm droplets of tin with initial temperature of  $800^\circ\text{C}$  dropped in  $20^\circ\text{C}$  water are reported to reach these conditions. The first following thermal interaction happens within 7 ms. Generally if the tin temperature was above  $400^\circ\text{C}$  and the water temperature was below  $60^\circ\text{C}$  the droplets always undergo thermal interaction. An experimentally observed dependence of the projected area of the tin fragments (initial temperature  $375$  to  $600^\circ\text{C}$ ) to the initial projected area of the molten drop is given by *Cho and Gunther*, Fig. 1 in (1973). It decreases starting at about 4-times of the initial area at about  $5^\circ\text{C}$  water temperature to 2-times at  $70^\circ\text{C}$ .

Instabilities caused by bubble formation, departure, and micro-shocks caused by liquid entering the volumes that are made free after the bubbles departure and local thermal stresses caused by the local differences in the temperature at the particle surface are the reason for the fragmentation. For larger subcooling of the coolant cyclic nature of the pressure spikes are reported by many researchers.

The minimum film boiling temperature is a function of the local pressure

$$T_{FB,\min} = T_{FB,\min}(p) < T_{2,cr} \quad \text{for } p < p_{2,cr} \quad (11.46)$$

and is limited by the critical temperature,

$$T_{FB,\min} = T_{2,cr} \quad \text{for } p \geq p_{2,cr} \quad (11.47)$$

see *Schröder-Richter* (1990). Theoretical dynamic stability condition is provided by *Matsumura and Nariai* (1996) analysis.

#### 11.4.2.3 Bubble collapse in subcooled liquid

Bubbles in subcooled *infinite* liquid having the same center of mass velocity as the liquid collapse *symmetrically*. This is not the case for *bubbles in asymmetric* flow field like

- bubbles attached to surfaces or in the vicinity of surfaces,
- bubbles attached to a droplet or in the vicinity of droplets,
- bubbles having relative velocity with respect to the liquid which is always the case in multiphase flows.

Bubbles in asymmetric flow, e.g. in the vicinity of a wall, elongate in the direction normal to the wall and develop a jet towards the wall. The velocity, length and diameter are found to be

$$V_{2,jet} = 13 \left( \frac{\Delta p}{\rho_2} \right)^{1/2} \quad (11.48)$$

$$\ell_{2,jet} = 0.4929R_{10}, \quad (11.49)$$

$$D_{2,jet} = 0.1186R_{10}, \quad (11.50)$$

as reported by *Plesset* and *Chapman* in 1971. *Gibson* (1968) found experimentally that the constant in Eq. (11.48) is 7.6. *Gibson* and *Blake* (1982) indicate that this constant is a function of the ratio of the initial distance of the bubble center from wall to the initial radius. For ratio of 1.5 the constant is 11 and for 1, 8.6. *Voinov* and *Voinov* (1975) found that the constant could be as high as 64 if the initial bubble had a slightly excentric shape. The pressure exerted by the jet is either the “water hammer pressure”,

$$p_{2,jet,WH} = \rho_2 a_{2,sound} V_{2,jet} \frac{\rho_3 a_{3,sound}}{\rho_2 a_{2,sound} + \rho_3 a_{3,sound}} \quad (11.51)$$

or the stagnant pressure,

$$p_{2,jet} = \frac{1}{2} \rho_2 V_{2,jet}^2. \quad (11.52)$$

The duration of the water hammer pulse is of order of  $D_{2,jet} / a_{2,sound}$  whilst that of the stagnant pressure is  $\ell_{2,jet} / V_{2,jet}$  - see the discussion by *Buchman* (1973). It has been known for a long time that collapsing bubbles in the neighborhood of a solid surface can lead to pitting of the surface. That the damage is caused by liquid jets on the bubbles was first suggested by *Kornfeld* and *Suvorov* (1944). Experiments by *Benjamin* and *Ellis* (1966) have confirmed that jets do indeed form on bubbles collapsing near a solid wall.

Note that a pressure excursion may bring initially saturated water to a sub-cooled state, which may result in self triggering of the system.

#### 11.4.2.4 Entrapment

Melt reaching the bottom or an obstacle in a liquid state may serve as a trigger by the mechanism of the so called entrapment - see *Mitsumura* et al. (1997). The entrapment is defined as inclusion of coolant into the melt. The intensive contact heat transfer leads to local explosive evaporation of the liquid. Depending on the amount of the water involved the entrapment may result in a very strong trigger.

Entrapment is the geometry typically considered as the initial state for volcano eruptions - see *Zimanowski* et al.(1995). Laboratory experiments with silicate melts and water injected into the melt are intensively studied. *Buetner* and *Zimanowski* reported in (1998) a summary of the results of their own investigations. The authors reported that static water injection may lead to virtually stable layering. Imposing of pressure pulse - trigger - results in violent explosion. The energy gain depends on the pulse straight intensity. The authors reported experiments with triggers ranging between about  $4 \times 10^{12}$  and  $10^{12} \text{ MPa/s}$

with rise time between 1 and 7  $\mu\text{s}$ . The maximum energy gain was obtained for about  $2 \times 10^{12} \text{ MPa/s}$  with rise time about 4  $\mu\text{s}$ . Local thermal efficiencies of maximum 48.7% are reported. Because only one small part was able to react during the expansion process, the global efficiency resulted in 2%.

### 11.4.3 The mechanism of the thermal fragmentation

#### 11.4.3.1 Film collapse dynamics

The arriving pressure wave has an effect on the vapor film depending on its *time signature*. If the time necessary for crossing the distance of the particle size is much smaller than the duration of the pressure pulse, we can assume that the film collapse is governed by the difference between the water bulk pressure and the vapor pressure. Different approaches are thinkable to compute the collapse time of a vapor film with thickness  $\delta_{1F}$ . The contact discontinuity velocity for the case of negligible mass transfer is given by the mass and momentum jump conditions at the interface

$$V_{1\sigma} = V_1 + \frac{p_2 - p_1}{\rho_1(V_2 - V_1)} \quad (11.53)$$

valid for plane geometry. Even for plane geometry this approach gives constant velocity and no surface acceleration. It can, therefore, not explain the interfacial instabilities which are resulting from non-zero acceleration of the interface. That is why modeling the bubble collapse dynamics is required to compute the surface averaged interfacial acceleration. *Board* et al. (1972) expressed the hypothesis that the cyclic nature of thermal fragmentation in subcooled water observed in the experiments is due to bubble growth and collapse. *Bankoff* et al. succeeded in 1983 to reproduce very well the collapse time and the cyclic behavior of the process using the bubble collapse theory.

The following system of non-linear ordinary differential equations describes the bubble dynamics.

$$R \frac{d^2 R}{d\tau^2} + \frac{3}{2} \left( \frac{dR}{d\tau} \right)^2 = \frac{1}{\rho_2} \left( p_1 - p_2 - \frac{2\sigma}{R} \right), \quad R_3 \leq R \quad (11.54)$$

$$\frac{dp_1}{d\tau} = \frac{3R^2}{(R^3 - R_3^3)} a_1^2 \left\{ [(\rho w)_{M21} - (\rho w)_{M12}] \left[ 1 + C_{n1} \frac{R_{M1} - R_{n1}}{R_1} \right] + \frac{c_{pM1}}{c_{p1}} \frac{T_2^{\sigma 1} - T_1}{T_1} \right\} - \rho_1 \frac{dR}{d\tau}, \quad (11.55)$$

$$\frac{dT_1}{d\tau} = \frac{1}{\rho_1 c_{p1}} \left\{ \frac{dp_1}{d\tau} + \frac{3R^2}{(R^3 - R_3^3)} \left[ \dot{q}_1'' + (\rho w)_{M21} (h_{M1}^{\sigma 2} - h_{M1}) \right] \right\}, \quad (11.56)$$

$$\frac{dC_{n1}}{d\tau} = -\frac{C_{n1}}{\rho_1} \frac{3R^2}{(R^3 - R_3^3)} \left[ (\rho w)_{M21} - (\rho w)_{M12} \right]. \quad (11.57)$$

The first equation is the momentum equation for incompressible fluid known as the *Rayleigh* equation. Note that for fast pressure change, which can be linearized by

$$p_2 = p_{20} + \frac{dp_2}{d\tau} \tau, \quad (11.58)$$

the *Rayleigh* equation is

$$R \frac{d^2 R}{d\tau^2} + \frac{3}{2} \left( \frac{dR}{d\tau} \right)^2 = \frac{1}{\rho_2} \left( p_1 - p_{20} - \frac{2\sigma}{R} - \frac{dp_2}{d\tau} \tau \right). \quad (11.59)$$

The second equation is the mass conservation equation of the gas film combined with the energy conservation equation of an ideal gas mixture. The third equation is the energy conservation equation of an ideal gas mixture. The last equation is the mass conservation equation of the non-condensable gas components. The dependent variable vector in this case is  $(R, p_1, T_1, C_{n1})$ .

For the case of no non-condensable gases in the film we have  $C_{n1} = \text{const} = 0$  and the pressure and temperature equations simplify to

$$\frac{dp_1}{d\tau} = \frac{3R^2}{(R^3 - R_3^3)} a_1^2 \left\{ [(\rho w)_{M21} - (\rho w)_{M12}] \frac{T'(p_1)}{T_1} - \rho_1 \frac{dR}{d\tau} \right\}, \quad (11.60)$$

$$\frac{dT_1}{d\tau} = \frac{1}{\rho_1 c_{p1}} \left\{ \frac{dp_1}{d\tau} + \frac{3R^2}{(R^3 - R_3^3)} \left[ \dot{q}_1'' + (\rho w)_{M21} c_{pM1} (T'(p_1) - T_1) \right] \right\}. \quad (11.61)$$

Constitutive relations are required here in order to estimate the condensation and the evaporation mass flow rate from the liquid surface, and the total heat flux into the vapor. Thin thermal boundary layer solution of the *Fourier* equation is applicable to compute the heat flux from the interface into the water

$\rho_2 c_{p2} (T_3^\sigma - T_2) \sqrt{\frac{3a_2}{\pi\tau}}$ . The heat flux transferred from the hot melt surface through

the vapor film is  $\lambda_1 \frac{T_3 - T_3^\sigma}{R_1 - R_3}$ . The net flux of evaporation is computed from the

*Hertz* (1882) equation modified by *Knudsen* (1915) and *Langmuir* (1913), *Langmuir et al.* (1927).

$$(\rho w)_{M21} - (\rho w)_{M12} = c \left( \frac{p'(T_3^\sigma)}{\sqrt{2\pi R_{M1} T_3^\sigma}} - \frac{p_{M1}}{\sqrt{2\pi R_{M1} T_1}} \right) \quad (11.62)$$

In addition, for no sound physical reason, the assumption is made in the literature that the probability of escape for liquid molecule at the interface is equal to the probability of capture for a vapor molecule at the interface - the  $c$ -constant in the above equation. For pressures below 0.1 bar measurements for  $c$  reported by *Fedorovich* and *Rohsenow* (1968) for liquid metals tightly clustered about unity. For larger pressure

$$c = 0.1 \text{ to } 1 \quad (11.63)$$

is a good approximation - see the discussion by *Mills* (1967) and *Mills* and *Seban* (1967). For water the discussion and the measurements by [70, 73, 11] give

$$c = 0.35 \text{ to } 1. \quad (11.64)$$

Thus from the energy jump condition at the water surface the interface temperature is governed by

$$\begin{aligned} c \left( \frac{p'(T_3^\sigma)}{\sqrt{2\pi R_{M1} T_{di}}} - \frac{p_{M1}}{\sqrt{2\pi R_{M1} T'(p_1)}} \right) \\ = \frac{1}{h''(p_1) - h'(p_1)} \left[ \lambda_1 \frac{T_3 - T_3^\sigma}{R_1 - R_3} - \rho_2 c_{p2} (T_3^\sigma - T_2) \sqrt{\frac{3a_2}{\pi\tau}} \right]. \end{aligned} \quad (11.65)$$

It is interesting to note that for large film thickness,  $R_1 - R_3$ , the condensation predominates,

$$\lambda_1 \frac{T_3 - T_3^\sigma}{R_1 - R_3} < \rho_2 c_{p2} (T_3^\sigma - T) \sqrt{\frac{3a_2}{\pi\tau}}, \quad (11.66)$$

and the pressure decreases. If the film thickness decreases sufficiently to have

$$\lambda_1 \frac{T_3 - T_3^\sigma}{R_1 - R_3} > \rho_2 c_{p2} (T_3^\sigma - T) \sqrt{\frac{3a_2}{\pi\tau}}, \quad (11.67)$$

the pressure starts to increase. This physics combined with the momentum equation (11.54) (*Rayleigh*) describes the experimentally observed cyclic nature of the bubble collapse in subcooled liquid.

### 11.4.3.2 Interfacial instability due to bubble collapse

During the bubble collapse the vapor/water interface is subject to instability. As shown by the experiments performed by *Ciccarelli* (1992), the pressure differences leading to surface oscillations do not lead to symmetric melt drop



compression and successive hydraulic explosion as assumed by *Drumheller* (1979), but to the following mechanism. The surface instabilities during the bubble collapse will cause melt-coolant contact at predominant places. The result is contact heat transfer, local explosion of highly superheated coolant pressing the melt at the initial contact points and causing them to erupt on the non-contact places. This mechanism leads to eruption of melt particles into the surrounding liquid causing a cloud of additional bubble production. The cloud is observed optically by several authors, e.g. *Buetner* and *Zimanowski* (1998). Successive condensation due to the resultant local pressure spike leads to collapse of the voided region for subcooled coolant. Then the process may repeat. This is known in the literature as a *cyclic nature of the thermal fragmentation*. The cyclic nature of the thermal fragmentation is observed in *Kim et al.* (1989), *Inoue and Aritomi* (1989), *Nelson and Duda* (1981), *Arakeri et al.* (1978), *Yuen et al.* (1994). The droplet surface topology during the instability interactions is not directly visible from usual photographs, *Henry and Fauske* (1996), but clearly demonstrated by the x-ray photographs by *Ciccarelli* (1992). The work by *Ciccarelli* provided the experimental evidence for the hypothesis which was asked for a long time. Analytical understanding of the process is provided by direct numerical simulation of the interaction and gives surprisingly similar results - see the work by *Koshizuka et al.* 1997.

For saturated water only one cycle is usually experimentally observed. It is obvious that one cycle will cause fragmentation only of a surface droplet layer with limited thickness. Therefore this effect is a *surface entrainment effect*. The residual part of the hot droplets will remain not fragmented.

The most important part of this observation is that the whole process is driven by the energy transferred by the melt during the contact time at the contact melt/coolant spots.

At the beginning of the bubble collapse,

$$R \frac{d^2 R}{d\tau^2} \gg \frac{3}{2} \left( \frac{dR}{d\tau} \right)^2, \quad (11.68)$$

$$R \sim R_3, \quad (11.69)$$

the interface acceleration is

$$\frac{d^2 R}{d\tau^2} \approx \frac{1}{R_3 \rho_2} \left( p_1 - p_2 - \frac{2\sigma}{R_3} \right) \quad (11.70)$$

and therefore

$$\lambda_{RT} \sim \pi \left[ \frac{12\sigma_2}{\left| \frac{1}{R_3 \rho_2} \left( p_1 - p_2 - \frac{2\sigma}{R_3} \right) \right| (\rho_2 - \rho_1)} \right]^{1/2}, \quad (11.71)$$

and

$$V_{2,jets} = 2\pi \left[ 3\sigma_2 \frac{1}{R_3 \rho_2} \left( p_1 - p_2 - \frac{2\sigma}{R_3} \right) \frac{\rho_2 - \rho_1}{(\rho_2 + \rho_1)^2} \right]^{1/4}. \quad (11.72)$$

### 11.4.3.3 Contact heat transfer

The purpose of this section is to estimate the local efficiency of possible contact heat transfer from fragmented melt to water after arrival of a trigger shock wave. After the pressure pulse collapses locally the vapor film, the wavy liquid interface touches the droplet. The heat transfer coefficients on those spots is much higher than the heat transfer in film boiling. *Inoue* and *Aritomi* (1989) obtained the empirical expression for the local heat transfer coefficient as a function of the time elapsed from the contact initiation

$$h_{TB} \approx 10^5 \left[ 1 - (2\tau / \Delta\tau_H)^2 \right] W / (m^2 K), \quad (11.73)$$

where  $\Delta\tau_H \approx 30 \times 10^{-6} s$ . The average heat transfer coefficient within the contact time  $\Delta\tau_H$  is  $\overline{h_{TB}} \approx (2/3) \times 10^5 W / (m^2 K)$ . It causes significant drop cooling at these spots and simultaneous superheating of the coolant liquid.

Analytical estimation of the local heat transfer as a function of time is possible in the following way.

#### 11.4.3.3.1 Non-solidifying droplet

For contact spots much smaller than the droplet interface we can assume a plane geometry and use the solution of the *Fourier* equation

$$\frac{\partial T}{\partial \tau} = a \frac{\partial^2 T}{\partial x^2}, \quad (11.74)$$

with initial conditions  $T = T_3$  inside the particle and  $T = T_2$  inside the coolant, requiring that  $T$  and  $\lambda \frac{\partial T}{\partial x}$  be continuous at the interface. The spatial coordinate starts at the interface and points into the droplet. The short time solution of the temperature field inside the *non-solidifying* droplet is

$$T(x) = \frac{T_3 \lambda_3 \sqrt{a_2} + T_2 \lambda_2 \sqrt{a_3} + \lambda_2 \sqrt{a_3} (T_3 - T_2) \operatorname{erf} \left( \frac{x}{2\sqrt{a_3 \tau}} \right)}{\lambda_2 \sqrt{a_3} + \lambda_3 \sqrt{a_2}}. \quad (11.75)$$

The instantaneous interface temperature is

$$T_{3\sigma} = \frac{T_3 \sqrt{\rho_3 c_{p3} \lambda_3} + T_2 \sqrt{\rho_2 c_{p2} \lambda_2}}{\sqrt{\rho_2 c_{p2} \lambda_2} + \sqrt{\rho_3 c_{p3} \lambda_3}}. \quad (11.76)$$

This relation is sometimes written in the literature in the form

$$\frac{T_{3\sigma} - T_2}{T_3 - T_{3\sigma}} = \sqrt{\frac{\rho_3 c_{p3} \lambda_3}{\rho_2 c_{p2} \lambda_2}}, \quad (11.77)$$

see e.g. *Fauske* (1973).

The instantaneous heat flux with corrector for spherical geometry is

$$\begin{aligned} \dot{q}_{\sigma 2}'' &= \rho_2 c_{p2} (T_{3\sigma} - T_2) \sqrt{\frac{3a_2}{\pi \tau}} \\ &= \sqrt{\frac{3}{\pi}} \frac{1}{1/\sqrt{\rho_2 c_{p2} \lambda_2} + 1/\sqrt{\rho_3 c_{p3} \lambda_3}} \frac{T_3 - T_2}{\sqrt{\tau}}. \end{aligned} \quad (11.78)$$

This is valid as far as the heat conduction within non-disintegrated water is possible. The water disintegrates due to homogeneous nucleation if the interface temperature is larger than the homogeneous nucleation temperature,

$$T_3^\sigma > T_{2,spin}. \quad (11.79)$$

That is why injecting water in liquid materials like steel or uranium dioxide always results in explosive interactions. The opposite, injection of molten materials in water not always results in explosive interaction.

For systems which have demonstrated propagating vapor explosions, the corresponding propagation velocity has been observed to be of the order of 100 m/s with a rise time for the shock wave of order of

$$\Delta \tau_{23} \approx 0.001s. \quad (11.80)$$

Obviously, the contact time cannot exceed this scale. It is interesting to know what the maximum of the energy is that can be transferred during this time. The heat flux averaged over this time is limited by

$$\begin{aligned} \dot{q}_{32,average}'' &= \sqrt{\frac{3}{\pi}} \frac{T_3 - T_2}{1/\sqrt{\rho_2 c_{p2} \lambda_2} + 1/\sqrt{\rho_3 c_{p3} \lambda_3}} \frac{1}{\Delta \tau_{12}} \int_0^{\Delta \tau_{23}} \frac{d\tau}{\sqrt{\tau}} \\ &= 2\sqrt{\frac{3}{\pi}} \frac{T_3 - T_2}{1/\sqrt{\rho_2 c_{p2} \lambda_2} + 1/\sqrt{\rho_3 c_{p3} \lambda_3}} \frac{\sqrt{\Delta \tau_{23}}}{\Delta \tau_{23}}. \end{aligned} \quad (11.81)$$

Over the period of time  $\Delta \tau_{23}$  the ratio of the released energy

$$\pi D_3^2 2 \sqrt{\frac{3}{\pi}} \frac{T_3 - T_2}{1/\sqrt{\rho_2 c_{p2} \lambda_2} + 1/\sqrt{\rho_3 c_{p3} \lambda_3}} \sqrt{\Delta \tau_{23}}$$

to the available energy inside a single droplet

$$\frac{\pi}{6} D_3^3 \rho_3 \{c_{p3} [T_3 - T'(p)] + h'_3 - h_3^m\} \quad (11.82)$$

is

$$\begin{aligned} \eta_{\text{efficiency}} &= \chi \frac{\pi D_3^2 2 \sqrt{\frac{3}{\pi}} \frac{T_3 - T_2}{1/\sqrt{\rho_2 c_{p2} \lambda_2} + 1/\sqrt{\rho_3 c_{p3} \lambda_3}} \sqrt{\Delta \tau_{23}}}{\frac{\pi}{6} D_3^3 \rho_3 \{c_{p3} [T_3 - T'(p)] + h'_3 - h_3^m\}} \\ &= 12 \sqrt{\frac{3}{\pi}} \frac{T_3 - T_2}{T_3 - T'(p) + \frac{h'_3 - h_3^m}{c_{p3}}} \frac{\chi \sqrt{\frac{\lambda_3}{\rho_3 c_{p3}} \Delta \tau_{23}}}{\left(1 + \sqrt{\frac{\rho_3 c_{p3} \lambda_3}{\rho_2 c_{p2} \lambda_2}}\right) \frac{1}{D_3}}. \end{aligned} \quad (11.83)$$

Here the  $\chi$  is the ratio of the contact surface to the total surface of a single drop being between zero and one depending on the mode of contact disturbances. Comparing this expression with the one reported by *Henry and Fauske* in 1996

$$3 \left[ 1 + \frac{T'(p) - T_{2,spin}}{T_3 - T'(p)} \right] \frac{\sqrt{\frac{\lambda_3}{\rho_3 c_{p3}} \Delta \tau_{12}}}{D_3}, \quad (11.84)$$

we see that the coolant properties are neglected by these authors relying on the assumption that the surface temperature is equal to the homogeneous nucleation temperature  $T_{2,spin}$  and the latent heat of solidification is also neglected. These assumptions are not necessary and are omitted in our analysis.

#### 11.4.3.3.2 Solidifying droplet

In the above derivation it is assumed that no freezing occurs at the surface, that is the surface temperature is always greater than the solidus temperature. Freezing at the surface is associated with release of the latent heat of melting. An approximate method to take this effect into account is to increase the effective temperature difference  $T_3 - T_2$  by  $\frac{h'_3 - h_3^m}{c_{p3}}$ , as proposed by *Buchman* in 1973. Thus the final expression for the efficiency is

$$\eta_{\text{efficiency}} = 12 \sqrt{\frac{3}{\pi}} \frac{T_3 - T_2 + \frac{h'_3 - h''_3}{c_{p3}}}{T_3 - T'(p) + \frac{h'_3 - h''_3}{c_{p3}}} \frac{\chi \sqrt{\frac{\lambda_3}{\rho_3 c_{p3}} \Delta \tau_{23}}}{\left(1 + \sqrt{\frac{\rho_3 c_{p3} \lambda_3}{\rho_2 c_{p2} \lambda_2}}\right)} \frac{1}{D_3} \quad (11.85)$$

$$\approx 12 \sqrt{\frac{3}{\pi}} \frac{\sqrt{\frac{\lambda_3}{\rho_3 c_{p3}} \Delta \tau_{23}}}{1 + \sqrt{\frac{\rho_3 c_{p3} \lambda_3}{\rho_2 c_{p2} \lambda_2}}} \frac{\chi}{D_3}. \quad (11.86)$$

For  $UO_2$   $T_3 = 3000K$ ,  $T_2 = 30^\circ C$ ,  $\chi = 1$ ,  $\Delta \tau_{23} \approx 0.001s$  and atmospheric pressure we have

$$\eta_{\text{efficiency}} = \frac{0.000133}{D_3}. \quad (11.87)$$

For the same conditions for  $Al_2O_3$  we have

$$\eta_{\text{efficiency}} = \frac{0.000129}{D_3}. \quad (11.88)$$

It interesting to note some valuable information contained in this expression:

a) The smaller the size of the particles before the thermal interaction the higher the efficiency, which is also confirmed by the experiments. The thermal efficiency of the heat transfer from particles with size smaller than  $0.1 \text{ mm}$  can be considered as 100%. The final size of the solidified fragments after steam explosion experiments is in order of  $D_{3\infty} \approx (1 \text{ to } 100) \times 10^{-6} m$ . It was measured by several experimentalists, e.g. *Kim et al.* (1989),  $(150 \text{ to } 250) \times 10^{-6} m$ , see in *Corradini* (1982) for  $Fe-Al_2O_3$  systems,  $(1 \text{ to } 700) \times 10^{-6} m$ , in KROTOS experiments, *Huhtiniemi et al.* (1997). Obviously the fine fragmented melt in steam explosion is able to release its thermal energy completely if the contact with the water is possible. Experimental data reported by *Buxton et al.* in 1979 for  $Al_2O_3$  and  $Fe$  thermite give thermal efficiency of the order of 0.1 to 1.4%. Recently *Corradini* (1996) summarized the Alumina-Water interaction data obtained from nine KROTOS explosion experiments *Hohmann et al.* (1995) in confined geometry. Again all of the data give thermal efficiency between 0.1 and 3%. The reason for not having global thermal efficiency of 100% is the fact that only small part of the melt participates effectively in the interaction.

b) For particles larger than  $0.1 \text{ mm}$  the energy transferred during the liquid-liquid contact is limited by the amount stored inside the thermal boundary layer of the large premixed particles before the explosion. For  $1 \text{ mm}$  particle size and  $\chi = 1$  the thermal efficiency for  $UO_2$  is 13.3% and for  $Al_2O_3$  is 12.9%. This

demonstrates how important it is to know the particle size distribution during the interaction process. Non-explosive interactions produce debris in order of 1 to 3 mm, *Corradini* (1982), 3.8 to 4.8 mm, FARO experiments with 80w%  $\text{UO}_2$  and 20w%  $\text{ZrO}_2$ , *Magalon et al.* (1997). This is in fact the range of particle size which should be used to estimate the efficiency of postulated non-explosive melt-water interactions for real reactor systems.

c) The water subcooling has virtually no effect on the local thermal efficiency.

d) The mode of contact,  $\chi$ , greatly influences the local thermal efficiency. If there is locally no water,  $\alpha_2 = 0$ , no steam can be produced and therefore  $\chi = 0$ . Another interesting aspect resulting from this fact is that to transfer the thermal energy completely into evaporation of water in a control volume by some hypothetical mechanism, i.e.

$$\alpha_{2,st} \rho_2 (h_1'' - h'') = \alpha_3 \rho_3 (h_3' - h'''), \quad (11.89)$$

we need a optimum liquid volume fraction of about

$$\alpha_{2,st} = \frac{1 - \alpha_1}{1 + \frac{\rho_2 (h_1'' - h'')}{\rho_3 (h_3' - h''')}}. \quad (11.90)$$

We call this liquid volume fraction “*stoichiometric*” in analogy to the chemical combustion processes where the maximum of the released energy can not be increased by providing more fuel or more oxidizer than the stoichiometric one. If the melt mixture is “*oversaturated*”, that is

$$\alpha_2 > \alpha_{2,st}, \quad (11.91)$$

all the melt can virtually discharge its thermal energy. If the melt is “*undersaturated*”, that is

$$\alpha_2 < \alpha_{2,st}, \quad (11.92)$$

only part of the melt,

$$\chi = \frac{\alpha_2}{\alpha_{2,st}} = \frac{\alpha_2}{1 - \alpha_1} \left[ 1 + \frac{\rho_2 (h_1'' - h'')}{\rho_3 (h_3' - h''')} \right], \quad \text{for } \alpha_1 < 1 \quad (11.93)$$

can virtually discharge its thermal energy. Both conditions can be written as

$$\chi = \min \left\{ 1, \frac{\alpha_2}{1 - \alpha_1} \left[ 1 + \frac{\rho_2 (h_1'' - h'')}{\rho_3 (h_3' - h''')} \right] \right\} \quad \text{for } \alpha_1 < 1. \quad (11.94)$$

For corium-water mixtures we obtain

$$\chi = \min \left\{ 1, \frac{\alpha_2}{1 - \alpha_1} \left[ 1 + \frac{1\,000 \times 2\,257\,200}{8\,105.9 \times 305\,350} \right] \right\} = \min \left( 1, 1.912 \frac{\alpha_2}{1 - \alpha_1} \right). \quad (11.95)$$

For a mixture consisting of melt and water only the *stoichiometric* liquid volume fraction turns out to be 0.523. In other words, if the volume of the water in a control volume is less than 52% the complete release of the thermal energy is simply impossible. Increasing the vapor void fraction decreases this value to

$$0.523/(1 - \alpha_1). \quad (11.96)$$

**Conclusions:** There are three important thermal limitations on the fast melt-water heat transfer.

- 1) The contact time is limited;
- 2) The heat conduction in the thermal boundary layer is limited;
- 3) The local availability of water in the mixture is limited

**Crust straight:** If the contact temperature is lower than the solidus temperature the droplet starts to solidify at the surface. *Cronenberg* found in 1973 that the crystallization is much faster than heat transfer. For plane geometry the growth of the crusts is governed by the solution obtained by *Carslaw* and *Jaeger* see Eq. (39) in *Carslaw and Jaeger* (1959), p 289,

$$\delta(\tau) = \psi 2\sqrt{a_3'''} \tau, \quad (11.97)$$

where  $\psi$  satisfies the following equation

$$\begin{aligned} & \frac{(T_3''' - T_2) \lambda_2 \sqrt{a_3'''} \exp(-\psi^2)}{\lambda_3''' \sqrt{a_2} + \lambda_2 \sqrt{a_3'''}} \operatorname{erf}(\psi) - \frac{\lambda_3 \sqrt{a_3'''} (T_3 - T_3''') \exp\left(-\psi^2 \frac{a_3'''}{a_3}\right)}{\lambda_3''' \sqrt{a_3} \operatorname{erfc}\left(\psi \frac{\sqrt{a_3'''}}{\sqrt{a_3}}\right)} \\ & = \psi \sqrt{\pi} \frac{\Delta h_{3,melt}}{c_{p3}'''} . \end{aligned} \quad (11.98)$$

Thus any interactions leading to break up of the crust have to provide a local pressure larger than the ultimate pressive strength ( $Al \approx 10^8 \text{ Pa}$ ,  $UO_2 \approx 2 \times 10^9 \text{ Pa}$ ). If the break is caused by shearing, the shear stress should be larger than the ultimate shear strength.

It is important to note that for many systems of practical interest there is solidification at the cold spot. However, the explosion post-test debris analysis in KROTOS shows perfectly spherical fine debris which runs quickly on inclined surface of paper. This seems to contradict this prediction of local solidification. The surrounding of the micro-crust is liquid and the entrained droplets retain in fact the large part of the superheating energy so that after a while in a film boiling the complete melting is recovered and the further solidification mechanism is that of radiating micro-droplets in film boiling and having almost ideal spherical geometry.

#### 11.4.3.4 Liquid coolant fragmentation

After the melt-coolant contact heat transfer the coolant boundary layer becomes metastable and expands dramatically due to homogeneous nucleation. This causes fragmentation of the coolant and highly turbulent oscillation of the liquid-liquid interface causing further fragmentation of the liquid metal droplet and of the coolant. *Henry and Fauske (1996)* pointed out the importance of the fine *water* fragmentation at the water surface, the oscillation of the resulting fine spray, and the improvement of the heat transfer even under established vapor film conditions.

#### 11.4.3.5 The maximum of the contact time

The purpose of this section is to estimate an upper limit of the possible contact time. We postulate that the absolute maximum is proportional to the time which is required to bring all of the liquid to homogeneous nucleation temperature by contact heat transfer.

Consider a water film surrounding the fragments, with a thickness proportional to the size of the fragments

$$\delta_{2F} \approx \delta_{2F}^* D_{3\infty}, \quad (11.99)$$

where  $\delta_{2F}^* > 0$ . The ratio of the volume of the sphere consisting of (a) one particle and (b) the surrounding film, to the volume of the particle itself is

$$(\alpha_3 + \alpha_{2F}) / \alpha_3 = (D_3 + 2\delta_{2F})^3 / D_3^3 = (1 + 2\delta_{2F}^*)^3. \quad (11.100)$$

Therefore the liquid volume fraction of the non-stable film is

$$\alpha_{2F} = \alpha_3 \left[ (1 + 2\delta_{2F}^*)^3 - 1 \right]. \quad (11.101)$$

In fact the film thickness is limited by the maximum packing density given by

$$\alpha_{2F} \leq 0.52 - \alpha_3 \quad (11.102)$$

or

$$\delta_{2F}^* \leq \delta_{2F,\max}^*, \quad (11.103)$$

where

$$\delta_{2F,\max}^* = \frac{1}{2} \left[ \left( \frac{0.52}{\alpha_3} \right)^{1/3} - 1 \right]. \quad (11.104)$$

An estimate of the time constant is obtained by the condition that the average temperature of the liquid equals the homogeneous nucleation temperature,



$$\begin{aligned} & \frac{\pi}{6} D_3^3 \left[ (1 + \delta_{2F}^*)^3 - 1 \right] \rho_2 c_{p2} (T_{2,nc} - T_2) \frac{1}{\Delta \tau_{23}} \\ &= \pi D_3^2 (1 + \delta_{2F}^*)^2 2 \sqrt{\frac{3}{\pi}} \frac{T_3 - T_2}{1/\sqrt{\rho_2 c_{p2} \lambda_2} + 1/\sqrt{\rho_3 c_{p3} \lambda_3}} \frac{\sqrt{\Delta \tau_{23}}}{\Delta \tau_{23}}. \end{aligned} \quad (11.105)$$

Solving with respect to the liquid *Fourier* number, we finally obtain

$$\frac{\Delta \tau_{23}}{D_3^2} \frac{\lambda_2}{\rho_2 c_{p2}} \approx \frac{\pi}{432} \left\{ \frac{\left[ (1 + \delta_{2F}^*)^3 - 1 \right]}{(1 + \delta_{2F}^*)^2} \left( 1 + \sqrt{\frac{\rho_2 c_{p2} \lambda_2}{\rho_3 c_{p3} \lambda_3}} \right) \frac{T_{2,nc} - T_2}{T_3 - T_2} \right\}^2. \quad (11.106)$$

Thus the maximum of the contact time is given by replacing of  $\delta_{2F}^*$  with  $\delta_{2F,\max}^*$ . The real contact time will surely be smaller than the maximum one. To estimate it one needs additional mechanistic arguments.

#### 11.4.3.6 Marangoni effect

Next we discuss the role of the *Marangoni* effect on the thermo - mechanical fragmentation. The surface tension for liquid metals increases with decreasing temperature,  $d\sigma_3/dT_3 < 0$ , in

$$\sigma_3 \approx \sigma_{30} + \frac{d\sigma_3}{dT_3} (T_{30} - T_3). \quad (11.107)$$

Examples of the temperature gradient of the surface tension for different substances  $d\sigma/dT$  in  $\text{kg}/(\text{s}^2\text{K})$  are given below, compare with *Brennen* (1995), p. 132.

Water	$2.02 \times 10^{-4}$	Oxygen	$1.92 \times 10^{-4}$
Uranium Dioxide	$1.11 \times 10^{-4}$	Methane	$1.84 \times 10^{-4}$
Sodium	$0.90 \times 10^{-4}$	Butane	$1.06 \times 10^{-4}$
Mercury	$3.85 \times 10^{-4}$	Carbon Dioxide	$1.84 \times 10^{-4}$
Hydrogen	$1.59 \times 10^{-4}$	Ammonia	$1.85 \times 10^{-4}$
Helium-4	$1.02 \times 10^{-4}$	Toluene	$0.93 \times 10^{-4}$
Nitrogen	$1.92 \times 10^{-4}$	Freon-12	$1.18 \times 10^{-4}$

Therefore, the cooling of the spots causes significant tangential forces at the surface,

$$\tau_3^\sigma \approx \frac{\Delta \sigma_3}{\delta_C} = - \frac{d\sigma_3}{dT_3} \Delta T_3^\sigma / \delta_C. \quad (11.108)$$

$\delta_C$  ( $\approx \text{const } D_3, \text{const} < 1$ ) is the distance between the neighboring hot and cold places, i.e. 1/2 of the surface wavelength along which the temperature change

$\Delta T_3^\sigma$  takes place. These forces induce a thermo-capillary flow in the drop that is resisted by the viscosity of the drop, i.e.

$$\tau_3^\sigma = \eta_3 \frac{V_{Mar}}{\delta_3} = -\frac{d\sigma_3}{dT_3} \Delta T_3^\sigma / \delta_C, \quad (11.109)$$

$\delta_3$  is some characteristic thickness of the wavy surface. *Ostrach* (1982) solved with respect to  $V_{Mar}$  and obtained the characteristic *thermo-capillary velocity* caused by these forces

$$V_{Mar} \approx -\frac{d\sigma_3}{dT_3} \frac{\Delta T_3^\sigma}{\eta_3} (\delta_3 / \delta_C). \quad (11.110)$$

The surface wave needs the time

$$\tau_{br,TM} \approx \delta_C / V_{Mar} \quad (11.111)$$

to collapse and to create a droplet (a kind of micro jet). The dimensional analysis provides an estimate for the thickness of the disturbed surface layer

$$\delta_3 \approx \left( \nu_3 \tau_{br,TM} \right)^{1/2} \approx \left( \nu_3 \delta_C / V_{Mar} \right)^{1/2}. \quad (11.112)$$

After substituting  $\delta_3$  in Eq. (11.110) with the RHS of Eq. (11.112) and solving with respect to  $V_{Mar}$  one obtains

$$V_{Mar} \approx \left( -\frac{1}{\rho_3} \frac{d\sigma_3}{dT_3} \Delta T_3^\sigma \right)^{2/3} (\nu_3 \delta_C)^{-1/3}. \quad (11.113)$$

Therefore the velocity induced by thermo-capillary forces can be significant. These forces transport material from the hot to the cold spots. This is an important example of the well known *Marangoni* effect, originally discovered by *Thomson* (1855). *Marangoni* (1871) found that the presence of a surface tension gradient along the interface causes convective currents or vortices close to the interface. The transported mass accelerates the growing of the surface waves induced by *Taylor* instability and causes fragmentation - see the discussion by *Henkel* (1987) p 34. We call this mechanism *thermo-mechanical fragmentation* in order to distinguish it from the pure acceleration induced fragmentation called pure mechanical fragmentation.

#### 11.4.3.7 Coolant interface classification

Injecting water in transparent liquid salt with temperature higher than the nucleation temperature of the water *Zimanovski* et al. (1995) observed classification of the interface of the salt and cracks characteristic for solid materials. The cracks are caused due to the enormous local pressure increase due to the water fragmentation by homogeneous nucleation. The explanation that the final fragments have smooth

surface is that the energy release from the melt is not enough to solidify the melt fragments and they fly away from the interaction zone in liquid state.

#### 11.4.3.8 Particle size after thermal fragmentation

The third condition for thermo-mechanical liquid metal fragmentation is that the initial droplet size,  $D_3$ , is considerably greater than the size of the final fragments,  $D_{3\infty}$ ,

$$D_3 \gg D_{3\infty} . \quad (11.114)$$

As already mentioned before, the final size of the solidified fragments being of the order of  $D_{3\infty} \approx (1 \text{ to } 100) \times 10^{-6} m$ , is measured by several experimentalists, e.g. Kim et al. (1989),  $(150 \text{ to } 250) \times 10^{-6} m$ , see in Corradini (1996) for Fe-Al<sub>2</sub>O<sub>3</sub> systems,  $(1 \text{ to } 700) \times 10^{-6} m$ , in KROTOS experiments, Huhtiniemi et al. (1997). For comparison remember that non-explosive interactions produces debris in order of 1 to 3 mm, Corradini (1996), 3.8 to 4.8 mm, FARO experiments with 80w%UO<sub>2</sub> and 20w% ZrO<sub>2</sub>, Magalon et al. (1997). Inoue and Aritomi (1989) estimated  $D_{3\infty} \approx 50 \text{ to } 60 \times 10^{-6} m$  assuming that the Taylor instability before solidification is responsible for the scale of the fragments which is of the order of magnitude observed experimentally. The fastest growing wavelength Taylor (1950) is

$$D_{3\infty} \approx \delta_{3Taylor} = \pi \left[ 24 \frac{\sigma_3}{\frac{d}{d\tau}(\Delta V_{13})(\rho_3 - \rho_1)} \right]^{1/2} , \quad (11.115)$$

or

$$D_{3\infty} \approx \delta_{3Taylor} = \pi \left[ 24 \frac{\sigma_3}{\frac{d}{d\tau}(\Delta V_{23})(\rho_3 - \rho_2)} \right]^{1/2} , \quad (11.116)$$

where  $\frac{d}{d\tau}(\Delta V_{13})$  and  $\frac{d}{d\tau}(\Delta V_{23})$  are the accelerations of the unstable surfaces between gas and droplets and between liquid and droplet, respectively.

It appears that the Taylor instability starts the fragmentation and the Marangoni effect finishes it. Therefore we can assume that the final diameter of the newly created droplet,  $D_{3\infty}$ , should be between the Taylor wavelength and the dimension computed by the following consideration. The static pressure in the liquid droplets exceeds the environment pressure by approximately the pressure difference caused by the complete collapsed surface wave (the stagnant pressure of the wave) and therefore

$$\Delta p \approx \frac{1}{2} \rho_3 V_{Mar}^2. \quad (11.117)$$

The static force balance on the newly formed droplet gives

$$D_{3\infty} \approx 4\sigma_3 / \Delta p \approx 4\sigma_3 / \left( \frac{1}{2} \rho_3 V_{Mar}^2 \right). \quad (11.118)$$

## 11.5 Particle production rate during the thermal fragmentation

Next we compute the particle production rate. If the liquid is saturated  $T_2 \approx T'(p)$  no further fragmentation cycle can be expected in the microscopic time scale because the produced bubble did not collapse. If the liquid is sub-cooled,  $T_2 < T'(p)$ , the successive condensation causes the collapse of the so formed bubble and the residual hot fragment is subject to new fragmentation - new cycle of surface entrainment.

It is obvious that this mechanism will cause fragmentation only for a surface droplet layer with some thickness  $\delta_3$ . Therefore, as already mentioned, this effect is a *surface entrainment effect*. The residual part of the hot droplets will remain not fragmented. This is observed by several authors, e.g. Kim et al. (1989). The *cyclic nature of the fragmentation* is reported in Kim et al. (1989), Inoue and Aritomi (1989), Nelson and Duda (1981), Arakeri et al. (1978), Zyskowski (1975). Inoue and Aritomi estimated by comparisons with experiments that a fraction  $f_1$  of the initial drop mass  $m_3$  participates in the first fragmentation cycle, where  $f_1 \approx 0.2$ . Therefore, after the first cycle we have a number of  $(D_3 / D_{3\infty})^3 f_1$  fragments originating from one droplet and accelerated into the surrounding liquid. The second fragmentation is again a surface effect, as the first one, and takes only a part  $f_2$  of the residual mass of the first fragmentation  $(1 - f_1)m_3$ . Inoue and Aritomi (1989), estimated this part as  $f_2 \approx 0.8$  by comparison with experiments. Therefore, after the second fragmentation cycle we have  $(D_3 / D_{3\infty})^3 (1 - f_1) f_2$  additional fragments per one particle. Obviously, after  $K$  cycles of fragmentation we have

$$n_{3\infty} = n_3^+ \left\{ 1 + (D_3 / D_{3\infty})^3 \left[ f_1 + (1 - f_1) f_2 \sum_{k=2}^K (1 - f_2)^{k-2} \right] \right\} \quad (11.119)$$

particles per unit mixture volume, where  $K$  is the number of the finished fragmentation cycles. The production of particles per unit mixture volume rate for the time  $\Delta\tau_{br}$  is therefore

$$\dot{n}_{3,sp} = (n_{3\infty} - n_3) / \Delta\tau_{br} = n_3 f_{3,frag} , \quad (11.120)$$

where

$$f_{3,frag} = \left( f_3^+ \left\{ 1 + (D_3 / D_{3\infty})^3 \left[ f_1 + (1 - f_1) f_2 \sum_{k=2}^K (1 - f_2)^{k-2} \right] \right\} - 1 \right) / \Delta\tau_{br} \quad (11.121)$$

is the fragmentation frequency of a single particle.

Most of the authors observe a delay time interval needed for the mechanical distortions of the film *Dullforce* et al. (1986), *Bjorkquist* (1975), *Bjornard* et al. (1974). The time needed for the mechanical film distortion,  $\Delta\tau_{mfd}$ , is observed by *Kim* et al. (1989) as

$$\Delta\tau_{mfd} < 200 \times 10^{-6} s , \quad (11.122)$$

and the time needed for one fragmentation event is

$$\Delta\tau_{br} \approx 5 \times 10^{-6} s . \quad (11.123)$$

The time needed for the following bubble collapse is obviously a function of the water subcooling

$$\Delta\tau_{collapse} \approx f [T_2 - T'(p)] . \quad (11.124)$$

The time for one fragmentation cycle is the sum of the above times. It is estimated by *Inoue* and *Aritomi* in (1989) to be

$$\Delta\tau_k = \Delta\tau_{collapse} + \Delta\tau_{fr} \approx 30 \times 10^{-6} s . \quad (11.125)$$

Therefore the number of the finished fragmentation cycles is

$$K = \text{integer} \left( (\Delta\tau - \Delta\tau_{mfd}) / \Delta\tau_k \right) \quad \text{for } T_2 < T'(p) \quad (11.126)$$

$$K = 1 \quad \text{for } T_2 \approx T'(p) . \quad (11.127)$$

Thus, the breakup time required to compute the production rate is

$$\Delta\tau_{br} = \Delta\tau_{mfd} + K \Delta\tau_k . \quad (11.128)$$

The thermo - mechanical fragmentation needs further attention. The experimental work provided up to now gives the *superposition of the effects of the mechanical and thermo - mechanical fragmentation but not quantitative information on the separate phenomena*. From the point of view of computational analysis, fine spatial discretization is necessary in order to model accurately the local pressure gradient and therefore to predict the trigger conditions.

## 11.6 Tang's thermal fragmentation model

Tang [89] considered the thermal fragmentation as a process of surface entrainment of particles with entrainment mass flow rate

$$(\rho w)_{32,thermal} = const \rho_3 V_{3,jets} F_1(\alpha_1) F_2(\tau_{br}), \quad (11.129)$$

governed by *Rayleigh-Taylor* instabilities at the water - vapor interface caused by the pressure difference at both sides of the interface,  $\Delta p$ . This pressure difference causes bubble collapse governed by the *Rayleigh* equation at the beginning of the bubble collapse where the velocity of the bubble surface is zero and the initial acceleration is

$$\frac{d^2 R}{d\tau^2} = \frac{p_1 - p_2}{R \rho_2}. \quad (11.130)$$

The interface is subject to instability with the growing rate

$$V_{2,jets} \approx const \left( \frac{d^2 R}{d\tau^2} \lambda_{RT} \right)^{1/2} \approx const \left( \frac{p_1 - p_2}{R \rho_2} \lambda_{RT} \right)^{1/2}. \quad (11.131)$$

The instability wavelength is assumed to be proportional to the particle size  $\lambda_{RT} \approx R$  and therefore

$$V_{2,jets} \approx const \left( \frac{d^2 R}{d\tau^2} \lambda_{RT} \right)^{1/2} \approx const \left( \frac{p_1 - p_2}{\rho_2} \right)^{1/2}. \quad (11.132)$$

The reaction of the melt is again expressed in terms of surface instability with growing rate proportional to those of the water instability. Therefore melt jets erupt from the melt surface with

$$V_{3,jets} \approx const V_{2,jets}. \quad (11.133)$$

The entrainment mass source per unit time and unit mixture volume is consequently

$$\mu_{32,thermal} = (F/V)_3 (\rho w)_{32,thermal} = const \alpha_3 \rho_3 \left( \frac{\Delta p}{\rho_2 D_3^2} \right)^{1/2} F_1(\alpha_1) F_2(\tau_{br}). \quad (11.134)$$

The constant is proposed to take values smaller than 0.12. The function

$$F_2(\tau_{br}) = 1 - \Delta\tau/\tau_{br} \quad \text{for} \quad \Delta\tau < \tau_{br} \quad (11.135)$$

and

$$F_2(\tau_{br}) = 0 \quad \text{for} \quad \Delta\tau \geq \tau_{br} \quad (11.136)$$

limits the fragmentation process within the fragmentation time of  $\tau_{br} \approx 0.002$ . *Yerkess* (1997) uses the *Kim* and *Corradini* model (1988) and derived from the KROTOS experiments the following corrections

$$const = 0.002, \quad (11.137)$$

$$F_1(\alpha_1) = 0.5 - \arctan \left[ \frac{100(\alpha_1 - 0.35)}{\pi} \right], \quad (11.138)$$

$$\tau_{br} = 0.0012s. \quad (11.139)$$

For the prediction of the KROTOS experiments *Yerkess* assumed that the external trigger pressure pulse should be greater than some threshold value

$$p_2 > p_{2,th} \quad (11.140)$$

where

$$p_{2,th} \sim 2 \times 10^5 Pa. \quad (11.141)$$

The definition of the pressure difference is simple in the single drop case with stepwise pressure increase. This makes it difficult to apply this model in general purpose computer code where quite different pressure histories, resulting in different  $\Delta p$ , can be the reason for successive thermal fragmentation. *Brayer* et al. (1997) overcome this difficulty by using the time average pressure from many previous time steps as initial pressure.

Recently *Koshizuka* et al. (1997) clarified the problem whether water jets can penetrate heavier melt droplets. Using direct numerical simulation the authors conclude that it depends on the density ratio. For heavier melt they found that penetration of water into the melt is impossible for velocities of 5 m/s. Note, that cavitation of bubbles in subcooled liquid may lead to considerably higher velocities.

*Yuen* et al. (1994) noted that this approach does not explain how these microscopic jets can survive in the heating environment and penetrate the melt droplet surface. The *Marangoni* effect will counteract the water penetration into the melt at the contact point. The melt water contact will for sure transfer energy and cause nucleation explosion in the contact places. This will accelerate much more two-phase mist volume in all possible directions and aggravate the melt eruptions from contact surroundings as clearly demonstrated by the experiments of *Ciccarelli* (1992). Further, the volumetric displacement will be for sure associated with the number of contact points depending of the maximum growing wavelength during the *Rayleigh-Taylor* instabilities.

At least one improvement of this model is possible: There is no need to assume  $\lambda_{RT} \approx R$ . In this case setting again the melt jet velocity proportional to the coolant micro jet velocity

$$\begin{aligned}
 V_{3,jets} &\approx \text{const } V_{2,jets} \\
 &= \text{const } 2\pi \left[ 3\sigma_2 \frac{1}{R_3\rho_2} \left( p_1 - p_2 - \frac{2\sigma}{R_3} \right) \frac{\rho_2 - \rho_1}{(\rho_2 + \rho_1)^2} \right]^{1/4}, \quad (11.142)
 \end{aligned}$$

we obtain

$$\begin{aligned}
 \mu_{32,thermal} &= (F/V)_3 (\rho w)_{32,thermal} \\
 &= \text{const } 12\pi 6^{1/4} \alpha_3 \rho_3 \left[ \frac{\sigma_2}{\rho_2 D_3^5} \left( p_1 - p_2 - \frac{2\sigma}{R_3} \right) \frac{\rho_2 - \rho_1}{(\rho_2 + \rho_1)^2} \right]^{1/4}. \quad (11.143)
 \end{aligned}$$

Comparing this expression we see that  $\mu_{32,thermal} \propto (p_1 - p_2)^{1/4}$  instead of  $(p_1 - p_2)^{1/2}$  and  $\mu_{32,thermal} \propto \frac{1}{D_3^{5/4}}$  instead of  $\mu_{32,thermal} \propto \frac{1}{D_3}$  as obtained by *Tang* (1993).

## 11.7 Yuen's thermal fragmentation model

The thermal fragmentation model proposed by *Yuen et al.* (1994) is applied by the authors to already existing mechanically pre-fragmented melt droplets. The further fragmentation is considered as a sheet stripping and wave crest stripping governed by the water-melt velocity difference and their properties. The latter is very important. The dependence on the pressure gradients is taken into account as a dependence on the resulting velocity differences. This is an implicit statement saying *what ever the reason for the origination of the relative velocity between water and melt corresponding to Weber number greater than 100 is, the thermal fragmentation takes place*. Note that in accordance with the *Ciccarelli* experiment this is correct *Ciccarelli* (1992) if the fragmentation time constant is shortened for the thermal fragmentation by factor of about two. This is also supported by the experiments performed in *Bürger et al.* (1991, 1993).

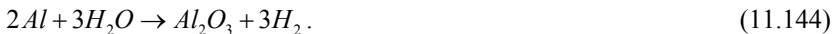
The new idea is that the fine fragments interact not with all of the water in the computational cell but with an amount proportional to the fine fragmentation rate. The proportionality factor was *empirically* chosen to be 7 based on volume. This amount is considered to immediately reach the fine particles/water thermal equilibrium, which may result in complete evaporation of the entrained water and superheating of the steam. Further interaction of the fine particles with the water is not considered. We call this phenomenon vapor shielding.



## 11.8 Oxidation

Liquid metals can oxidize in steam/water environment with different intensity. Three consequences of the oxidation are very important: a) Production of hydrogen; b) Heat release; c) Covering the fragment with oxide having given permeability for the reactant materials and melting temperature which may be higher than the metal melt temperature. As an example we consider the oxidation the aluminum next.

**Aluminum:** Molten aluminum interacts with water *Lida and Frederikse (1997)* as follows



The melting temperature of aluminum is 933.2 K *Kammor (1995)* and the melting temperature of the aluminum oxide (alumina) is 2324.15 K *Shpillrain et al. (1973)*. Consequently, if the initial temperature of the molten aluminum is less than 2324.15 K oxide layer forms and crystallizes very quickly *Turbill and Fisher (1949)*. The speed of the chemical reaction is then controlled by the diffusion processes at both sides of the interaction front: diffusion of molten metal into the oxide and diffusion of steam through the steam - hydrogen boundary layer and again partially into the oxide. It is known that for this system the interaction front is close to the outer surface *Merzhanov et al. (1977)*. The participating thermal processes are the heat transfer by film boiling and radiation at the external surface and the heat transfer into the both materials oxide and metal. The film boiling at sphere is well understood as demonstrated in Chapter 21 and in *Kolev (1997)* by comparison with about 2000 experimental data points in different regimes, as well the transient heat conduction in multi-layers sphere - see in *Carslaw and Jaeger (1959)*. Theoretical considerations containing the available models for the above discussed processes are presented in *Uludogan and Corradini (1995)*. The most important result of this study was the ignition temperature of aluminum as a function of the particle size. Figure 16 in *Uludogan and Corradini (1995)* shows in log-normal scale a linear dependence between about 1440 and 1720 K for particle sizes varying between 0.001 and 10 mm. These results are fairly close to the results obtained previously by *Epstein (1991)*. These results are consistent with the experimental observation reported from the TREAT experiments (rapid heating) *Ellison et al. (1993)* in which temperatures of 1473 to 2273.15 K are necessary to burn the aluminum alloy under water. This result is also consistent with the experiments performed on the THERMIR facility at Winfrith which show that just pouring the 1123.15 K molten charge into subcooled water was not able to initiate a steam explosion *Taleyarkhan (1990)*.

## 11.9 Superposition of thermal fragmentation

### 11.9.1 Inert gases

Because the thermal fragmentation is associated with film condensation and with local melt/coolant contact any mechanism suppressing condensation in the film acts as a suppressive for steam explosion. There are two experimentally observed mechanisms:

- a) entrapment of non-condensables if fragmented melt is falling through a atmosphere of non-condensable gases before entering the coolant as reported by *Akiyoshi et al. (1990)* or artificially introduced bubbles of non-condensable gases *Zimanowski et al. (1995)*, and
- b) melt oxidation leading to generation of inert gases inside the vapor film, *Nelson et al. (1991)*, *Corradini (1996)*.

Increasing the content of the non-condensable gases in the vapor film reduces the coolant/vapor interface oscillation, *Kim and Corradini (1986)*, and the reduces the maximum peak of the produced pulses *Akiyoshi et al.* - see fig. 8 in *Kim and Corradini (1986)*.

It is very interesting to note that recently the FARO experiments shows that heating  $\text{UO}_2$  up to melting temperature makes the oxide under-stoichiometric. During the melt-water interaction steam reduction is possible and  $\text{H}_2$  production up to 0.150 kg per 175 kg melt is possible, releasing 300 to 500 kJ per mole of reacted  $\text{UO}_2$  – see *Matzke (1998)*.

### 11.9.2 Coolant viscosity increase

Because the thermal fragmentation is associated with the stability of the coolant/vapor interface, increasing the viscosity of the coolant increases the stability of the coolant/vapor interface.

*Bang and Kim (1995)* changed the water viscosity by adding *polyethylene oxide polymer*. 800ppm solutions have 2.7-times larger viscosity then pure water, see fig. 2 in *Bang and Kim (1995)*. The authors reported that for subcooled boiling the increase of the coolant viscosity decreases the minimum film boiling temperature and suppresses the instabilities caused by transition of the film boiling temperatures. With the used external trigger with amplitude 50 kPa 300ppm solution suppressed completely the explosion.

For water the viscosity, nominally at atmospheric pressure 0.001 kg/(ms), can be increased to 0.04 and 0.24 kg/(ms) by adding *cellulose gum* into the water 0.1 and 0.4 w/o, respectively as reported by *Kim et al. (1989)*. The authors reported the following:

“...The mechanism of suppressing steam explosion is the mechanism of suppressing the trigger. The increase of coolant viscosity  $>0.05 \text{ kg/(ms)}$  at fixed trigger pressure (and impulse) results in complete explosion

suppression. As the trigger pressure was increased the explosion could be triggered for intermediate viscosities, but suppression still remained for high viscosities  $>0.15 \text{ kg/(ms)}$ . The explosion conversion ratio varies from 0 to 6 %.”

This in fact confirms the findings reported previously by *Nelson and Guay* in 1986. The latter authors found that adding *glycerol* in water requires 70 w/o in order to suppress explosions, which is rather large. The same effect can be reached by adding of 0.5 w/o cellulose gum.

### 11.9.3 Surfactants

Surfactants are substances changing the coolant/vapor interface properties. An examples of an-ionic surfactant is sodium- dodecyl- benzene- sulphonate  $\text{C}_{12}\text{H}_{25}\text{C}_6\text{H}_4\text{SO}_3\text{Na}$  which is available as UFSAN-65. An example of a non-ionic surfactant is the ethoxilated- nonyle- phenol,  $\text{C}_9\text{H}_{19}\text{C}_6\text{H}_4\text{O}(\text{C}_2\text{H}_4\text{O})_9\text{H}$ , available as Emulgator U-9. They possess long molecules being at the one end hydrophilic and at the other end hydrophobic. The hydrophilic end is always inside the bulk of the water and the hydrophobic tends to attach to the vapor side across the interface. The major effects of the dense surfactant population (1 to 5 ppm) at the interface as reported in *Becker and Linland* (1991) are

- a) decrease of surface tension (in small window of the concentration change),
- b) local increase of water viscosity,
- c) local increase of liquid density,
- d) imposes a rigid surface on the bubble.

*Becker and Linland* (1991) explained the stabilizing effect with the surface concentration *Marangoni* effect increasing the stability of the vapor/water interface. *Becker and Linland* drew the attention to these substances in *Becker and Linland* (1991) especially because of their property to suppress steam explosions reporting the following:

“...As a matter of fact the surfactants have been used successfully in two metallurgical factories in Norway. In these factories copper granulate and ferrous alloys granulate are produced by pouring molten material into about 5 m deep pools of water, where the melts fragments hydro-dynamically, sinks through the water, freezes and finally is collected as granulate at the bottom of the vessels. In the copper granulate factory 800 kg of copper is poured each time, while in the other factories the content of one batch is 8 000 kg. Before, strong steam explosions with severe damage to equipment and buildings occurred in both plants, but after the systematic use of surfactants was introduced no steam explosions have taken place in the copper factory, despite the fact that more than 10 000 pourings have been carried out until ...(April 1991). With regards to the ferrous alloy plant only mild interactions with water splashing out of the vessel have occurred on a few occasions. The number of pourings in this

latter plants have now (April 1991) exceeded 20 000 since the surfactants were introduced.”

Unfortunately small scale experiments performed later confirmed *statistically* the general trend by allowing occasionally steam explosions *Becker and Linland* (1991). *Kowal et al.* (1993) confirmed that a small concentration *on average* reduces the severity of steam explosions (*g*-quantities of 800°C-tin in water) by reducing the resulting pressure peak by 65% compared to pure water. There was no evidence in their study that surfactants can completely suppress steam explosions. *Chapman et al.* (1997) performed experiments with *kg*-quantities of 1000°C-tin in water and again did not find the evidence that the surfactants mitigate steam explosions.

#### 11.9.4 Melt viscosity

Since the pioneer work by *Ohnesorge* in 1936 it is well known that increasing the liquid viscosity reduces the fragmentation. In several experiments particulate liquids with particle *Ohnesorge* number larger than 4 are not observed to fragment - see Fig. 8.8.

### Nomenclature

#### *Latin*

$a$	normal interface acceleration pointing from the heavier to the lighter continuum, $m/s^2$
$a_m$	pressure pulse propagation velocity through the mixture, $m/s$
$a_2$	coolant sound velocity, $m/s$
$C_{n1}$	mass concentration of the non-condensable gases in the gas-vapor film, <i>dimensionless</i>
$c_p$	specific heat at constant pressure, $J/(kgK)$
$D_3$	hot spheres diameter, $m$
$D_{2,jet}$	jet diameter toward the wall in collapsing bubble, $m$
$d$	differential
$f_3^+$	part of the particles $n_3$ per unit mixture volume experiences melt/water fragmentation, <i>dimensionless</i>
$g$	gravitational acceleration, $m/s^2$
$h$	specific enthalpy, $J/kg$
$h_{TB}$	local heat transfer coefficient, $W/(m^2K)$

---

$\overline{h_{TB}}$	average heat transfer coefficient within the contact time $\Delta\tau_H$ , $W/(m^2K)$
$h_{FB}$	Film boiling heat transfer coefficient, $W/(m^2K)$
$k_{SB}$	<i>Stefan-Boltzman</i> constant,
$L_{pool\_depth}$	water reservoir water depth, $m$
$\ell_{2,jet}$	length jet toward the wall in collapsing bubble, $m$
$n_3$	hot spheres particle number, <i>dimensionless</i>
$p$	pressure, $Pa$
$p_{2,cr}$	critical pressure, $Pa$
$p_{2,th}$	threshold pressure, $Pa$
$p_{2,jet,WH}$	pressure exerted by the jet - “water hammer pressure”, $Pa$
$p_{2,jet}$	$= \frac{1}{2} \rho_2 V_{2,jet}^2$ stagnant jet pressure, $Pa$
$\dot{q}_3^{\sigma 2}$	heat flux emitted from the surface, $W/m^2$
$\dot{q}_{32,average}''$	time-averaged heat flux, $W/m^2$
$R$	bubble radius, $m$
$R_{10}$	initial size of the collapsing bubble, $m$
$R_{M1}$	vapor gas constant, $J/(kgK)$
$r$	ratio of the film thickness for natural convection only, <i>dimensionless</i>
$s_3$	locally average field specific entropy, $J/(kgK)$
$s''$	liquidus entropy of the molten drop, $J/(kgK)$
$T'(p)$	saturation temperature as a function of pressure $p$ , $K$
$T_3^\sigma$	droplet surface temperature, $K$
$T_{FB,min}$	minimum film boiling temperature, $K$
$T_{2,cr}$	critical temperature, $K$
$T_{2,spin}$	homogeneous nucleation temperature, $K$
$V_{2,jets}$	coolant micro jet velocity, velocity jet toward the wall in collapsing bubble, $m/s$
$V_{Mar}$	characteristic thermo-capillary velocity, $m/s$
$\langle w_1 \rangle_1$	vapor velocity averaged over the film thickness computed for particle having large size compared to the film thickness, $m/s$

**Greek**

$\alpha$	volume fraction, <i>dimensionless</i>
$\alpha_{2,st}$	optimum “ <i>stoichiometric</i> ” liquid volume fraction, <i>dimensionless</i>
$\Delta \mathbf{V}_{23}$	relative velocity vector particle-water, $m/s$

$\Delta V_{32}$	$= \sqrt{\Delta u_{32}^2 + \Delta v_{32}^2 + \Delta w_{32}^2}$ , magnitude of the relative velocity vector particle-water, $m/s$
$\Delta u_{32}$ , $\Delta v_{32}$ , $\Delta w_{32}$	components of the relative velocity vector particle-water in the three coordinate directions, $m/s$
$\Delta p_{pulse}$	pulse pressure increase, $Pa$
$\Delta \tau_{pulse}$	pulse duration, $s$
$\Delta \tau_{life\_time}$	time necessary to reach the bottom of the reservoir, $s$
$\Delta \tau_{crust}$	time necessary to cool down the liquid particle up to formation of the surface crust, $s$
$\Delta w_{32}$	average velocity with which the droplet crosses the water, $m/s$
$\Delta \tau_{br}$	fragmentation time, $s$
$\Delta \tau_{br}^*$	$= \frac{\Delta \tau_{br}}{\frac{D_3}{ \Delta V_{3c} } \sqrt{\frac{\rho_3}{\rho_c}}}$ , fragmentation time, <i>dimensionless</i>
$\Delta \tau_H$	time elapsed from the contact initiation, $s$
$\delta_{1F}$	film thickness at the equator, $m$
$\delta_{1F,nc}$	film thickness for natural convection only, $m$
$\delta_{1F,fc}$	film thickness for forced convection only, $m$
$\delta_{1F}^*$	$= \frac{\delta_{1F}}{D_3}$ dimensionless film thickness
$\delta_C$	distance between the neighboring hot and cold places, $m$
$\eta_{efficiency}$	efficiency, <i>dimensionless</i>
$\lambda_0$	initial disturbance wavelength, $m$
$\lambda$	wavelength, $m$
$\lambda_{RT}$	wavelength of the fastest growing oscillation, $m$
$\lambda$	thermal conductivity, $W/(mK)$
$\Delta \tau_{RT}$	growing time constant of the fastest growing oscillation, $s$
$\mu_{21}$	mass generated due to film boiling per unit mixture volume and unit time, $kg/(m^3s)$
$\rho$	density, $kg/m^3$
$(\rho w)_{M21}$	evaporation mass flow rate, $kg/(sm^2)$
$(\rho w)_{M12}$	condensation mass flow rate, $kg/(sm^2)$
$(\rho w)_{32,thermal}$	entrainment mass flow rate due to thermo-mechanical fragmentation,
$kg/(sm^2)$	

---

$\sigma$	surface tension, $N/m$
$\tau$	time, s
$\tau_3^\sigma$	tangential shear at the surface, $N/m^2$
$\nabla$	gradient

### ***Subscripts***

1	gas
2	liquid
3	particles
$IF$	vapor (gas) film
$m$	mixture
$M$	vapor
$n$	inert gas

### ***Superscripts***

'	saturated steam
''	saturated liquid
'''	saturated solid phase

## **References**

- Akiyoshi R, Nishio S, Tanasawa I (1990) A study of the effect of non-condensable gas in the vapor film on vapor explosion, *Int. J. Heat Mass Transfer*, vol 33 no 4 pp 603-609
- Ando M, Caldarola L (1982) Triggered fragmentation experiments at Karlsruhe, in Müller U and Günter C (eds), *Post Accident Debris Cooling*, Proc. of the Fifth Post Accident Heat Removal information Exchange meeting, NRC Karlsruhe, G. Braun Karlsruhe, pp 13-21
- Ando K (1984) Experiment zur getriggerten Fragmentation an einem schmelzflüssigen Kupfertröpfchen in Wasser, *KfK* 3667
- Arakeri VH et al. (1978) Thermal interaction for molten tin dropped into water, *Int. J. Heat Mass Transfer*, vol 21 pp 325-333
- Bang KH, Kim MK (1995) Boiling characteristics of dilute polymer solutions and implications for the suppression of vapor explosions, *Proceedings of the Seventh International Topical Meeting on Nuclear Reactor Thermal Hydraulics NURETH-7*, New York, USA, NUREG/CP-0142, pp 1677-1687
- Bankoff SG, Kovarik F, Yang JW (1983) A model for fragmentation of molten metal oxides in contact with water, *Proc. Int. Mtg. on LWR Severe Accident Evaluation*, Cambridge, MA pp TS-6.6-1 to 6.6-8
- Bankoff SG, Yang JW (October 10-13, 1989) Studies Relevant to in-Vessel Steam Explosions, *Proceedings Fourth International Topical Meeting on Nuclear Reactor Thermal-Hydraulics*, Karlsruhe. Müller U, Rehme K and Rust K (eds), G. Braun, Karlsruhe, p 312

- Becker KM, Linland KP (April 1991) The effect of surfactants on hydrodynamic fragmentation and steam explosions, KTK-NEL-50, Rev. Ed.
- Belman R, Pennington RH (1954) Effect of surface tension and viscosity on Taylor instability, *Quart. Appl. Maths*, vol 12 pp 151-162
- Benjamin TB, Ellis A T (1966) *Phil. Trans. R. Soc. A*, vol 260 pp 221-240
- Bjorkquist GM (1975) An experimental investigation of molten metal in water, TID-26820
- Bjornard TA et al. (1974) The pressure behavior accompanying the fragmentation of tin in water, *Transaction of American Nuclear Society*, vol 29 p 247
- Board S J, Farmer CL, Poole DH (October 1972) Fragmentation in thermal explosions, Berkeley Nuclear Laboratories, RD/B/N2423, CFR/SWP/P (72) p 81
- Brayer C, Berthoud G (19<sup>th</sup>-21<sup>th</sup> May 1997) First vapor explosion calculations performed with MC3D thermal-hydraulic code, OECD/CSNI Specialist Meeting on Fuel Coolant Interactions, JAERI-Tokai Research Establishment, Japan
- Brennen CE (1995) *Cavitation and bubble dynamics*. Oxford University Press, Oxford, New York
- Buchman DJ (1973) Penetration of a solid layer by a liquid jet, *J. Phys.D: Appl. Phys.*, vol 6 pp 1762-1771
- Buetner R, Zimanowski B (1998) Physics of thermohydraulic explosions, *Physical Review E*, vol 57 no 5
- Bürger M et al. (1991) Examination of thermal detonation codes and included fragmentation models by means of triggered propagation experiments in a tin/water mixture, *Nucl. Eng. Des.*, vol 131 pp 61-70
- Bürger M, Cho SH, von Berg E, Schatz A (January 5-8, 1993) Modeling of drop fragmentation in thermal detonation waves and experimental verification, Specialist's Meeting on Fuel-Coolant Interactions, Santa Barbara, California, USA
- Buxton LD, Nelson LS, Benedick WB (1979) Steam explosion triggering in efficiency studies, Forth CSNI Specialists Meeting on Fuel-Coolant Interaction in Nuclear Reactor Safety, Bournemouth, UK, pp 387-408
- Carslaw HS, Jaeger JC (1959) *Conduction of heat in solids*, Oxford Science Publications, Second edition, Oxford University Press
- Chapman R, Pineau D, Corradini M (May 22-25, 1997) Mitigation of vapor explosions in one-dimensional large scale geometry with surfactant coolant additives, *Proc. of the Int. Seminar on Vapor Explosions and Explosive Eruptions*, Sendai, Japan, pp 47-58
- Chen X, Yuen WW, Theofanous T (1995) On the constitutive description of microinteractions concept in steam explosions, *Proceedings of the Seventh International Topical Meeting on Nuclear Reactor Thermal Hydraulics NURETH-7*, New York, USA, NUREG/CP-0142.
- Cho DH, Gunther WH (June 1973) Fragmentation of molten materials dropped into water, *Trans. of the Am. Nucl. Soc.*, vol 16 no 1 pp 185-186
- Ciccarelli G (1992) Investigation of vapor explosions with single molten metal drops in water using x-ray, PhD Thesis, McGill University, Montreal, Quebec, Canada
- Corradini M (1982) Analysis and Modelling of Large Scale Steam Explosion Experiments, *Nucl. Sci. Eng.*, vol 82 pp 429-447
- Corradini ML (March 10-14, 1996) Vapor explosion phenomena: scaling considerations, *Proc. of the ASME-JSME 4th International Conference on Nuclear Engineering*, New Orleans, Louisiana U.S.A., vol 1 Part A, ASME 1996, pp 309-316



- Cronenberg AW (August 29, 1973) Solidification phenomena and fragmentation, in Sachs RG and Kyger JA, Reactor development program progress report, ANL-RDP-18, Liquid Metal Fast Breeder Reactors (UC-79), p 7.19
- Drumheller DS (1979) The initiation of melt fragmentation in fuel-coolant interactions, Nucl. Sc. Engineering, vol 72 pp 347-356
- Dullforce TA, Buchanan D, Peckover R S (1986) Self-triggering of small scale fuel-coolant interaction: I. Experiments, Journal of Physics D: Applied Physics, vol 9 pp 1295-1303
- Ellison PG, Hyder ML, Monson PR, DeWald AB Jr, Long TA, and Epstein M (April-June 1993) Aluminium-uranium fuel-melt behavior during severe nuclear reactor accidents, Nuclear Safety, vol 34 no 2 pp 196-212
- Epstein M (Aug. 1991) Underwater vapor phase burning of aluminium particles and on aluminium ignition during steam explosions, WSRC-RP-91-1001, Westinghouse Savannah River Co.
- Epstein M, Fauske K (August 4-7, 1985) Steam film instability and the mixing of core-melt jets and water, ANS Proceedings, National Heat Transfer Conference, Denver, Colorado, pp 277-284
- Fauske HK (1973) On the mechanism of uranium dioxide-sodium explosive interactions, Nuclear Science and Engineering, vol 51 pp95-101
- Fedorovich ED, Rohsenow W M (1968) The effect of vapor subcooling on film condensation of metals, Int. J. of Heat Mass Transfer, vol 12 pp 1525-1529
- Fletcher DF, Thyagaraja A (June 1989) A mathematical model of melt/water detonation, Appl. Math. Modelling, vol 13 pp 339-347
- Froehlich G (1991) Propagation of fuel-coolant interactions in multi-jet experiments with molten tin, Nuclear Engineering and Design, vol 131 pp 209-221
- Frost D L, Ciccarelli G (July 24-27, 1988) Propagation of explosive boiling in molten tin - water mixtures, Proc. Nat. Heat Transfer Conference, HDT - 96, Vol.2, Ed. H. R. Jacobs, Houston, Texas, pp 539-574
- Gelfand BE, Gubin SA et al. (1977) Influence of gas density on breakup of bubbles, Dokl. USSR Ac. Sci., vol 235 no 2 pp 292-294
- Gibson DC (1968) Cavitation adjacent to plane boundaries. Proc. Australian Conf. On Hydraulic and Fluid Machinery, pp 210-214
- Gibson DC and Blacke JR (1982) The growth and collapse of bubbles near deformable surface. App. Sci. Res., vol 38 pp 215-224
- Henkel P (1987) Hüllrohrmaterialbewegung während eines Kühlmittelverluststörfalls in einem schnellen, natriumgekühlten Reaktor, Dissertation, Kernforschungszentrum Karlsruhe
- Henry RE, Fauske HK (March 10-14, 1996) A different approach to fragmentation in steam explosions, Proc. of the ASME-JSME 4th International Conference on Nuclear Engineering, New Orleans, Louisiana U.S.A., vol 1 Part A, ASME 1996, pp 309-316
- Hertz H (1882) Wied. Ann., vol 17 p 193
- Hohmann H, Magalon D, Huhtiniemi I, Annunziato A, Yerkess A (October 1995) Recent results in FARO/KROTOS test series, Trans.23rd WRSIM, Bethesda MD
- Huhtiniemi I, Magalon D, Hohmann H (19<sup>th</sup>-21<sup>th</sup> May 1997) Results of recent KROTOS FCI tests: alumina vs. corium melts, OECD/CSNI Specialist Meeting on Fuel Coolant Interactions, JAERI-Tokai Research Establishment, Japan

- Inoue A, Aritomi M (October 10-13, 1989) An Analytical model on vapor explosion of a high temperature molten metal droplet with water induced by a pressure pulse, Proceedings Fourth International Topical Meeting on Nuclear Reactor Thermal-Hydraulics, Karlsruhe. Müller U, Rehme K and Rust K (eds), G. Braun, Karlsruhe, p 274
- Kammer C (1995) Aluminium-Taschenbuch, Bd.1 Grundlagen und Werkstoffe, Herausgeber: Aluminium-Zentrale Düsseldorf, Aluminium-Verlag Düsseldorf
- Kim BJ, Corradini ML (1986) Recent film boiling calculations: implication on fuel-coolant interactions, Int. J. Heat Mass Transfer, vol 29 pp 1159-1167
- Kim B, Corradini M (1988) Modeling of small scale single droplet fuel/coolant interactions, Nucl. Sci. Eng., vol 98 pp 16-28
- Kim H, Krueger J, Corradini ML (October 10-13, 1989) Single droplet vapor explosions: effect of coolant viscosity, Proceedings Fourth International Topical Meeting on Nuclear Reactor Thermal-Hydraulics, Karlsruhe. Müller U, Rehme K and Rust K (eds), G. Braun, Karlsruhe, p 261
- Knowles JB (1985) A mathematical model of vapor film destabilization, Report AEEW-R-1933
- Knudsen M (1915) Ann. Physik, vol 47 p 697
- Kolev NI (19th-21st May 1997) Verification of the IVA4 Film boiling model with the data base of Liu and Theofanous, Proceedings of OECD/CSNI Specialists Meeting on Fuel-Coolant Interactions (FCI), JAERI-Tokai Research Establishment, Japan
- Kornfeld M, Suvorov L (1944) J. Appl. Physics, vol 15 pp 495-506
- Koshizuka S, Ikeda H, Oka Y (May 22-25, 1997) Effect on Spontaneous Nucleation on Melt Fragmentation in Vapor Explosions, Proc. of the Int. Seminar on Vapor Explosions and Explosive Eruptions, Sendai, Japan, pp 185-192
- Kowal MG, Dowling MF, Abdel-Khalik S I (1993) An experimental investigation of the effects of surfactants on the severity of vapor explosions, Nuclear Science and Engineering, vol 115 pp 185-192
- Langmuir I (1913) Physik. Z., vol 14 p 1273
- Langmuir I, Jones HA, Mackay GMJ (1927) Physic. Rev., vol 30 p 201
- Lide DR, Frederikse HPR (eds) (1997) CRC Handbook of chemistry and physics, 8th Edition, CRC Press, New York 1997
- Magalon D, Huhtiniemi I, Hohmann H (19<sup>th</sup>-21<sup>th</sup> May 1997) Lessons learnt from FARO/TERMOS corium melt quenching experiments, OECD/CSNI Specialist Meeting on Fuel Coolant Interactions, JAERI-Tokai Research Establishment, Japan
- Marangoni CGM (1871) Über die Ausbreitung der Tropfen einer Flüssigkeit auf der Oberfläche einer anderen. Ann. Phys., vol 143 p 337
- Matsumura K, Nariai H (March 10-14, 1996) The occurrence condition of spontaneous vapor explosions, Int. Conf. on Nuclear Engineering ICONE-4, New Orleans, Louisiana, vol 1 - Part A, ASME, pp 325-332
- Matzke H (28-29 September 1998) Status of FARO debris analysis by ITU, Karlsruhe, 9th FARO Expert Meeting, Ispra
- Medhekar S, Amarasooriya WH, Theofanous TG (October 10-13, 1989) Integrated analysis of steam explosions, Proceedings Fourth International Topical Meeting on Nuclear Reactor Thermal-Hydraulics, Karlsruhe. Müller U, Rehme K and Rust K (eds), G. Braun, Karlsruhe, p 319-326
- Merzhanov AG, Grigoriev YM, Gal'chenko YA (1977) Aluminium ignition, Combustion Flame, vol 29 p 1

- Mills AF (1967) The condensation of steam at low pressure, Techn. Report Series No. 6, Issue 39. Space Sciences Laboratory, University of California, Berkeley
- Mills AF, Seban RA (1967) The condensation coefficient of water, J. of Heat Transfer, vol 10 pp 1815-1827
- Mitsumura K, Nariai H, Egashira Y, Ochimizu M (May 22-25, 1997) Experimental study on the base triggering spontaneous vapor explosions for molten tin-water system, Proc. of the Int. Seminar on Vapor Explosions and Explosive Eruptions, Sendai, Japan, pp 27-32
- Naylor P (1985) Film boiling destabilization, Ph.D. Thesis, University of Exeter
- Nelson LS, Buxton LD (1980) Steam explosion triggering phenomena: stainless steel and corium-e simulants studied with a floodable arc melting apparatus, SAN77 - 0998, NUREG/CR-01222, Sandia National Laboratories
- Nelson LS, Duda PM (1981) Steam explosion experiments with single drops of iron-oxide melted with CO<sub>2</sub> laser, SAND81-1346, NUREG/CR-2295, Sandia National Laboratory
- Nelson LS, Guay KP (1986) Suppression of steam explosion in tin and FeAl<sub>2</sub>O<sub>3</sub> melts by increasing the viscosity of the coolant, High Temperature and High Pressures, vol 18 pp 107-111
- Nelson LS, Hyndman DA, Duda PM (July 21-25, 1991) Steam explosions of single drops of core-melt simulants: Triggering, work output and Hydrogen generation, Proc. of the Int. Top. Meeting on Safety of Thermal Reactors, Portland, Oregon, pp 324-330
- Ohnesorge W (1936) Die Bildung von Tröpfchen an Düsen und die Auflüssiger Strahlen, Z. Angew. Math. Mech., vol 16 pp 335-359
- Ostrach S (1982) Low gravity fluid flows, Ann. Rev. Fluid Mech., vol 14 pp 313-345
- Peppler W, Till W, Kaiser A (Sept. 1991) Experiments on Thermal Interactions: Tests with Al<sub>2</sub>O<sub>3</sub> Droplets and Water, Kernforschungszentrum Karlsruhe, KfK 4981
- Pilch M, Erdman CA, Reynolds AB (Aug. 1981) Acceleration induced fragmentation of liquid drops, Charlottesville, VA: Department of Nucl. Eng., University of Virginia, NUREG/CR-2247
- Plesset MS, Chapman RB (1971) Collapse of an initially spherical vapor cavity in the neighborhood of solid boundary, J. of Fluid Mechanics, vol 47 no 2 pp 283-290
- Saito M, Sato K, Imahori S (July 24-July 27, 1988) Experimental study on penetration behaviours on water jet into Freon-11 and liquid nitrogen, ANS Proc. Nat. Heat Transfer Conference, HTC-vol 3. Jacobs HR (ed), Houston, Texas
- Schröder-Richter D, Bartsch G (1990) The Leidenfrost phenomenon caused by a thermo-mechanical effect of transition boiling: A revisited problem of non-equilibrium thermodynamics, in Witte LC and Avedisian CT (eds) HTD-vol 136, Fundamentals of phase change: Boiling and condensation. Book No.H00589-1990, pp 13-20
- Shpillrain EE, Yakimovich KA, Tsitsarkin AF (1973) Experimental study of the density of liquid alumina up to 2750 C, High Temperures - High Pressures, vol 5 pp 191-198
- Spencer BW et al. (August 4-7, 1985) Corium quench in deep pool mixing experiments, ANS Proceedings, National Heat Transfer Conference, Denver, Colorado, pp 267-276
- Taleyarkhan R (Febr. 1990) Steam-explosion safety consideration for the advanced neutron source reactor at the Oak Ridge National Laboratory, ORNL/TM-11324
- Tang J (1993) A complete model for the vapor explosion process, PhD Thesis, University of Wisconsin, Madison WI
- Taylor G (1950) The instability of liquid surfaces when accelerated in a direction perpendicular to their planes. I., Proceedings of the Royal Society of London, Series A. Mathematical and Physical Sciences, vol 201 pp 192-196

- Thomson J (July-December 1855) On certain curious motions observable at the surfaces of wine and other alcoholic liquors, *Philosophical Magazine and Journal of Science*, vol X - Fourth Series, pp 330-333
- Uludogan A, Corradini ML (Feb. 1995) Modeling of molten metal/water interactions, *Nuclear Technology*, vol 109 pp 171-186
- Voinov OV and Voinov VV (1975) Numerical method of calculating non-stationary motions of ideal incompressible fluid with free surface. *Sov. Phys. Dokl.* Vol 20 pp 179-18091.
- Yerkess (1997) TEXAS-IV Dynamic fragmentation model, private communication, 8th FARO Expert Meeting, Ispra, Italy
- Young MF (1990) Application of the IFCI Integrated fuel-coolant interaction code to a fits-type pouring mode experiment, SAND89-1692C
- Young MF (Sept. 1987) IFCI: An integrated code for calculation of all phases of fuel coolant interaction, NUREG/CR-5084, SAND87-1048
- Yuen WW, Chen X, Theofanous TG (1994) On the fundamental micro-interactions that support the propagation of steam explosions, *NED*, vol 146 pp 133-146
- Zimanowski B, Fröhlich G, Lorenz V (1995) Experiments on steam explosion by interaction of water with silicate melts, *NED* vol 155 pp 335-343
- Zimmer HJ, Peppler W, Jacobs H (October 10-13, 1989) Thermal fragmentation of molten alumina in sodium, *Proceedings Fourth International Topical Meeting on Nuclear Reactor Thermal-Hydraulics*, Karlsruhe. Müller U, Rehme K and Rust K (eds) G. Braun, Karlsruhe, p 268
- Zyskowski W (1975) Thermal interaction of molten copper with water, *Int. J. of Heat and Mass Transfer*, vol 18 pp 271-287

## 12 Nucleation in liquids

*After reviewing the literature for description of the nucleation in superheated liquids the following conclusions and recommendations have been drawn. The maximum superheating in technical systems is a function of the depressurization velocity and of the produced turbulence. The maximum superheating can be predicted by the Algamiir and Lienhard and by the Bartak correlations within an error band of 48.5%. Flashing in short pipes and nozzles leads to critical flows driven by the pressure difference equal to the entrance pressure minus the flashing inception pressure. For the prediction of the maximum achievable superheating which represents the Spinoidal line the Skripov correlation is recommended. The wetting angle is an important property of the polished surface characterizing its capability to activate nucleation sites. For the prediction of the activated nucleation sites the correlation obtained by Wang and Dhir is recommended. The establishing of a vapor film around a heated surface having temperature larger than the minimum film boiling temperature takes a finite time. Availability of small bubbles of non-condensing gases reduces the superheating required to initiate evaporation. Evaporation at lower than the saturation temperature is possible.*

### 12.1 Introduction

Liquids having temperature larger than the saturation temperature corresponding to the local pressure are called superheated liquids. Superheated liquids are unstable and start to disintegrate. This process is in generally called *flashing*. The process of rupturing a *continuous* liquid by decrease in pressure at roughly constant liquid temperature is often called *cavitation* - a word proposed by *Froude*. The process of rupturing a *continuous* liquid by increase the temperature at roughly constant pressure is often called *boiling*. The fluctuation of molecules having energy larger than that characteristic for a stable state causes the formation of clusters of molecules, which after reaching some critical size are called nuclei. The theory of the nucleation provides us with information about the generation of nuclei per unit time and unit volume of the liquid as a function of the local parameter.

## 12.2 Nucleation energy, equation of *Kelvin and Laplace*

Let us abstract from a superheated *non-stable liquid a spherical volume*, having an initial radius  $R_{10}$ , a volume  $\frac{4}{3}\pi R_{10}^3$ , pressure  $p$ , temperature  $T_2$  and density  $\rho_2 = \rho_2(p, T_2)$ . After some time the selected sphere liquid volume increases due to the *evaporation* to the radius  $R_1$  (respectively to the volume  $\frac{4}{3}\pi R_1^3$ ) and reaches a pressure  $p'(T_2)$ . The pressure inside the bubble is assumed to be uniform because of the small bubble size. The density of the evaporated steam inside the sphere is  $\rho'' = \rho''[p'(T_2)] = \rho''(T_2)$ . The *initial and the end spheres have the same mass* per definition, therefore

$$\left(\frac{R_{10}}{R_1}\right)^3 = \frac{\rho''}{\rho_2}. \quad (12.1)$$

Consequently, the initial volume of the sphere is changed by

$$\frac{4}{3}\pi(R_1^3 - R_{10}^3) = \frac{4}{3}\pi R_1^3 \left(1 - \frac{\rho''}{\rho_2}\right). \quad (12.2)$$

During this expansion a *mechanical work*

$$\begin{aligned} 4\pi \int_{R_{10}}^{R_1} [p'(T_2) - p] r^2 dr &\approx \frac{4}{3}\pi(R_1^3 - R_{10}^3)[p'(T_2) - p] \\ &= \frac{4}{3}\pi R_1^3 \left(1 - \frac{\rho''}{\rho_2}\right)[p'(T_2) - p] \end{aligned} \quad (12.3)$$

is performed and transferred into total kinetic energy of the surrounding liquid *Skripov et al. (1980)*. In other words, this work is introduced into the liquid. For the creation of a sphere with a free surface additional work

$$\int_0^{R_1} \frac{2\sigma}{r} 4\pi r^2 dr = 4\pi R_1^2 \sigma \quad (12.4)$$

is needed. The surface tension of water in  $N/m$ ,  $\sigma$ , in contact with its vapor is given in *Lienhard (1976)* with great accuracy by

$$\sigma = 0.2358 \left[1 - \frac{T'(p)}{T_c}\right]^{1.256} \left\{1 - 0.625 \left[1 - \frac{T'(p)}{T_c}\right]\right\}, \quad (12.5)$$

where the  $T_c$  is the thermodynamic critical temperature (for water  $T_c = 647.2$  K). For the region of 366 to 566 K the above equation can be approximated by

$$\sigma = 0.14783(1 - T/T_c)^{1.053} \quad (12.6)$$

with an error of  $\pm 1\%$ . The surface tension is a function of the surface temperature, which can strongly vary in transients. The surface tension is usually measured at macroscopic surfaces. Whether the so obtained information is valid for the microscopic metastable bubbles is not clear. Next we assume that this relationship holds also for microscopic surfaces.

Thus, the work necessary to create a single bubble with radius  $R_1$  is

$$\Delta E_1 = 4\pi R_1^2 \sigma - [p'(T_2) - p] \frac{4}{3} \pi R_1^3 \left(1 - \frac{\rho''}{\rho_2}\right) = 4\pi \sigma \left(R_1^2 - \frac{2}{3} \frac{R_1^3}{R_{1c}}\right), \quad p'(T_2) > p \quad (12.7)$$

We see that this work depends on the bubble radius and has a maximum

$$\Delta E_{1c} = \frac{16\pi\sigma^3}{3[p'(T_2) - p]^2 \left(1 - \frac{\rho''}{\rho_2}\right)^2} = \frac{4}{3} \pi \sigma R_{1c}^2 \approx \frac{4}{3} \pi \sigma \left[ \frac{T'(p)}{T_2 - T'(p)} \frac{2\sigma}{\rho''(h'' - h')} \right]^2 \quad (12.8)$$

for

$$R_{1c}^2 = \frac{3\Delta E_{1c}}{\sigma 4\pi} = \left\{ \frac{2\sigma}{[p'(T_2) - p](1 - \rho''/\rho_2)} \right\}^2. \quad (12.9)$$

The corresponding bubble volume is then

$$V_{1c} = \frac{4}{3} \pi \left( \frac{3\Delta E_{1c}}{\sigma 4\pi} \right)^{3/2}. \quad (12.10)$$

The Equation (12.9) is known as the *Laplace* and *Kelvin* equation. *Gibbs* (1878) noted that the expression for the maximum "... does not involve any geometrical magnitudes".

## 12.3 Nucleus capable to grow

The above consideration did not lead to any conclusion whether a bubble with size  $R_{1c}$  will further grow or collapse. It says only that at that size the mechanical energy needed to create a bubble at the initial state  $R_1 = 0$  and at the final state  $R_{1\infty} > R_{1c}$  possesses a maximum at  $R_{1c}$  and no more. There are many papers in which this size is taken to represent the bubble size, at which the bubble is further capable to grow, which as we will show below is not true.

Next we consider the conservation of the liquid mechanical energy in order to describe the bubble growth from the beginning through the critical radius. The mass conservation equation of the liquid can be approximated by

$$\frac{1}{r^2} \frac{\partial}{\partial r} (r^2 u_2) \approx 0, \quad (12.11)$$

or integrating with the boundary condition

$$r = R_1, \quad u_2 = \frac{\partial R_1}{\partial \tau} \quad (12.12)$$

$$u_2 = \text{const} / r^2 = \frac{\partial R_1}{\partial \tau} (R_1 / r)^2. \quad (12.13)$$

It gives the liquid velocity as a function of the radius if the liquid is assumed to be incompressible during the bubble expansion. The total kinetic energy of the liquid environment estimated using the above equation is therefore

$$\begin{aligned} \int_{R_1}^{\infty} \frac{1}{2} \rho_2 u_2^2 dVol_2 &= \frac{1}{2} \rho_2 \left( \frac{\partial R_1}{\partial \tau} \right)^2 R_1^4 4\pi \int_{R_1}^{\infty} \frac{dr}{r^2} = 2\pi \rho_2 \left( \frac{\partial R_1}{\partial \tau} \right)^2 R_1^4 \int_{R_1}^{\infty} d \left( -\frac{1}{r} \right) \\ &= 2\pi \rho_2 \left( \frac{\partial R_1}{\partial \tau} \right)^2 R_1^3. \end{aligned} \quad (12.14)$$

During the bubble growth the work performed by the bubble expansion is transferred in total kinetic energy of the liquid environment, i.e.

$$2\pi \rho_2 \left( \frac{\partial R_1}{\partial \tau} \right)^2 R_1^3 = -4\pi \sigma \left( R_1^2 - \frac{2}{3} \frac{R_1^3}{R_{lc}} \right) \equiv \Delta E_1$$

or

$$\left( \frac{\partial R_1}{\partial \tau} \right)^2 = \frac{2\sigma}{\rho_2} \left( \frac{2}{3} \frac{1}{R_{lc}} - \frac{1}{R_1} \right). \quad (12.15)$$

The constant  $2/3$  valid for bubble growth in a bulk liquid should be replaced by  $\pi/7$  if a spherical bubble grows on a flat surface.

Equation (12.15) is a very important result. We see that real bubble growth is possible *if and only if*

$$R_1 > \frac{3}{2} R_{lc}. \quad (12.16)$$

For the case of  $R_1 \gg R_{lc}$  Eq. (12.15) transforms into

$$\left( \frac{\partial R_1}{\partial \tau} \right)^2 = \frac{4}{3} \frac{\sigma}{\rho_2 R_{lc}}. \quad (12.17)$$



This mechanism of bubble growth is called *inertially controlled bubble growth*. For low pressure where the assumption  $\rho''/\rho_2 = 0$  is reasonable the above equation reduces to one obtained for the first time by *Besand* (1859) and in a more elegant way by *Rayleigh* (1917). This mechanism controls the bubble growth within the first  $10^{-8}$  s of the life of the stable bubble.

It follows from the above consideration that for the creation of a bubble with a critical unstable diameter  $3/2 R_{1c}$ , a surplus of internal energy of the liquid is needed greater than  $E_{1c}$ , and for creation of bubble that is capable to grow, a surplus of internal energy of the liquid - greater than  $(9/4) E_{1c}$ .

## 12.4 Some useful forms of the *Clausius-Clapeyron* equation, measures of superheating

Usually the liquid superheating is expressed by the temperature difference  $T_2 - T'(p)$ . Sometimes the pressure difference  $\Delta p = p'(T_2) - p$  corresponding to the superheating of the liquid with respect to the saturation temperature  $T_2 - T'(p)$  is also used as a measure for the liquid superheating. Using the *Clausius - Clapeyron* equation

$$\frac{dT}{dp} = \frac{v'' - v'}{s'' - s'} = \frac{\rho' - \rho''}{s'' - s'} \frac{1}{\rho' \rho''} = T'(p) \frac{\rho' - \rho''}{h'' - h'} \frac{1}{\rho' \rho''} \quad (12.18)$$

integrated between the initial state  $[p, T'(p)]$  and the final state  $[p'(T_2), T_2]$  for

$$\frac{\rho' - \rho''}{h'' - h'} \frac{1}{\rho' \rho''} \approx \text{const} \quad (12.19)$$

one obtains

$$p'(T_2) - p = (h'' - h') \frac{\rho' \rho''}{\rho' - \rho''} \ln \left[ 1 + \frac{T_2 - T'(p)}{T'(p)} \right]. \quad (12.20)$$

With this result the critica bubbles size can be approximated by

$$R_{1c} \approx 2\sigma / \left\{ (h'' - h') \rho' \ln \left[ 1 + \frac{T_2 - T'(p)}{T'(p)} \right] \right\}. \quad (12.22)$$

For  $T_2 - T'(p) \ll T'(p)$  we have for the tensile pressure difference

$$p'(T_2) - p = (h'' - h') \frac{\rho' \rho''}{\rho' - \rho''} \frac{T_2 - T'(p)}{T'(p)}, \quad (12.23)$$

and for the critical bubble size

$$R_{lc} \approx \frac{T'(p)}{T_2 - T'(p)} \frac{2\sigma}{\rho''(h'' - h')} \quad (12.24)$$

Thus one can use as a measure of liquid superheating either the *tension pressure difference*  $p'(T_2) - p$  or the *liquid superheat*  $T_2 - T'(p)$ .

Equation (12.23) makes it possible to compute the liquid superheating corresponding to the radius  $R_{lc}$  from Eq. (12.9)

$$[T_2 - T'(p)]/T'(p) = \frac{2\sigma}{R_{lc}} \frac{(\rho' - \rho'')\rho_2}{(\rho_2 - \rho'')\rho'\rho''} \frac{1}{h'' - h'} \approx 2 \frac{\sigma}{R_{lc}} \frac{1}{\rho''(h'' - h')} \quad (12.25)$$

or corresponding to  $3 R_{lk}/2$

$$[T_2 - T'(p)]/T'(p) = \frac{4}{3} \frac{\sigma}{R_{lc}} \frac{(\rho' - \rho'')\rho_2}{(\rho_2 - \rho'')\rho'\rho''} \frac{1}{h'' - h'} \approx \frac{4}{3} \frac{\sigma}{R_{lc}} \frac{1}{\rho''(h'' - h')} \quad (12.26)$$

For the atmospheric pressure Eq. (12.23) gives

$$T_2 - T'(p) = 6.4197 \times 10^{-5} / D_{lc} \quad (12.27)$$

A nonlinear expression is obtained also for low pressure for which the density difference between liquid and vapor is very large. In this case Eq.(12.18) simplifies to  $dT/dp = v''/(T\Delta h)$ . This equation is known since 1828 in France as the *August* equation. Assuming the vapor behave as a perfect gas results in  $dp/p = (\Delta h/R)dT/T^2$ , where  $R$  is the vapor gas constant for the specific substance. Integrating between an initial state  $[p, T'(p)]$  and a final state  $[p'(T_2), T_2]$  and rearranging results in useful expression for computing the relation between *tension pressure difference*  $p'(T_2) - p$  and the *liquid superheat*  $T_2 - T'(p)$  of metastable liquid,

$$\frac{p'(T_2) - p}{p} = \exp \left[ \frac{\Delta h}{RT_2} \frac{T_2 - T'(p)}{T'(p)} \right] - 1 \quad (12.28)$$

With this result the *Laplace* and *Kelvin* equation reads

$$R_{lc} \approx \frac{2\sigma}{\left\{ \exp \left[ \frac{\Delta h}{RT_2} \frac{T_2 - T'(p)}{T'(p)} \right] - 1 \right\} p(1 - \rho''/\rho_2)} \quad (12.29)$$

One should carefully use the approximations of the *Laplace* and *Kelvin* equation. At low pressure the apporroximations are good as shown in Fig.12.1. In this case at higher superheat Eq. (12.29) is much close to the accurate equation.

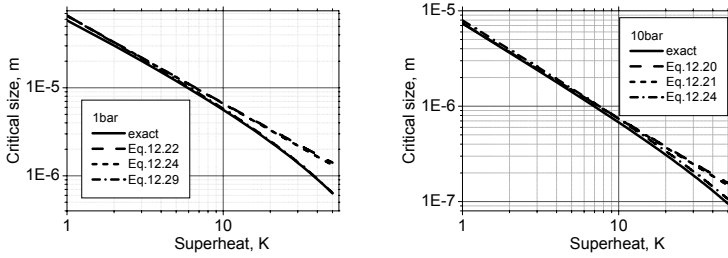


**Fig. 12.1** Critical bubbles size at low pressure as a function of the liquid superheat

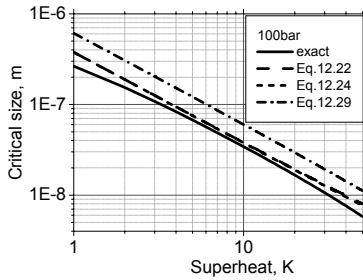


**Fig. 12.2** Critical bubbles size at high pressure as a function of the liquid superheat

At high pressure the approximations may deviate substantially from the exact solution as shown in Fig. 12.2.

The dimensionless number constructed as follows

$$Gb_2 = \frac{\Delta E_{lc}}{kT_2} = \frac{\Delta S_{lc}}{k} = \frac{16\pi\sigma^3}{kT_2 3[p'(T_2) - p]^2 (1 - \rho''(T_2)/\rho_2)^2} \quad (12.30)$$

is called the *Gibbs* number. Here  $k = 13.805 \times 10^{-24} \text{ J/K}$  is the *Boltzmann* constant. The *Gibbs* number is frequently used as a dimensionless measure of superheating. The greater the superheating the smaller the *Gibbs* number.  $Gb_2$  converging to infinity means no superheating. For  $T_2 = T_c$ ,  $\sigma = 0$  and  $Gb_2 = 0$ .

However, it should be noted that neither of the measures discussed above tells us at what  $\Delta T$  liquid starts boiling or flashing.

## 12.5 Nucleation kinetics

### 12.5.1 Homogeneous nucleation

Now we discuss the dependence between liquid superheating and production rates of bubbles with critical size called nuclei. Consider a continuous liquid characterized by average state parameters  $p$  and  $T_2$ . An observer measures along long time  $\Delta\tau$  the time  $\Delta\tau_n$  in which a mass  $\Delta m_{2c}$  of the continuum departs from the normal, average, state. The entropy change necessary for this fluctuation is  $\Delta m_{2c} \Delta s_{2c} = \Delta S_{2c}$ . Volmer (1939) p. 81 following Boltzman and Einstein assumed that

$$\Delta\tau_n / \Delta\tau \approx \text{const } e^{-\Delta S_{2c}/k} = \text{const } e^{-Gb_2} \quad (12.31)$$

where  $k$  is the Boltzmann constant. It means, that the smaller the needed entropy change for the fluctuation the higher the probability of this fluctuation. This is the leading idea for describing such processes. It did not change with the years. Actually it is known from experimental observations that the greater the superheating the greater the probability of origination of bubbles with critical size. The probability of origination of a single bubble is defined as

$$\text{probability of origination of single bubble} = \frac{\text{nucleation events}}{\text{molecular colisions}}. \quad (12.32)$$

Thus

$$\frac{\text{nucleation events}}{\text{molecular colisions}} = \exp(-Gb_2) \quad (12.33)$$

Obviously for  $T_2 = T_c$  and  $\sigma_2 = 0$ , the probability of origination of a single bubble  $\exp(-Gb_2) = 1$ . Nuclei with critical size can originate in the bulk liquid. This phenomenon is called *homogeneous* nucleation. Nuclei with critical size can originate also at the wall. This phenomenon is called *heterogeneous* nucleation. The theories modeling the nucleation in the bulk liquid are called homogeneous nucleation theories. The theories modeling the nucleation at surfaces are called heterogeneous nucleation theories. Next we give the main result of the homogeneous nucleation theory.

Kaishew and Stranski computed in 1934 the number of the created nuclei per unit time in unit volume of the liquid as follows

$$\begin{aligned} \dot{n}_{\text{cin}} &= N_2 \left\{ \frac{6\sigma}{[2 + p/p'(T_2)]\pi m_2} \right\}^{1/2} \exp(-Gb_2) \\ &= \exp \left\{ \ln \left[ \rho_2 \left( \frac{N_A}{m_\mu} \right)^{3/2} \left\{ \frac{6\sigma}{[2 + p/p'(T_2)]\pi m_2} \right\}^{1/2} \right] - Gb_2 \right\}. \end{aligned} \quad (12.34)$$

Here  $N_2 = \rho_2/m_2 = \rho_2 N_A/m_\mu$  ( $\approx 3.3 \times 10^{28}$  for water) is the number of the molecules in one cubic meter,  $m_2 = m_\mu/N_A$  is the mass of a single molecule,  $m_\mu$  is the *kg-mole* mass (18 kg for water),  $N_A = 6.02 \times 10^{26}$  (1/*kg-mole*) is the number of molecules in one kilogram-mole mass, the *Avogadro* number, and

$$\left\{ \frac{6\sigma}{[2 + p/p'(T_2)]\pi m_2} \right\}^{1/2} \quad (12.35)$$

is the frequency with which each single liquid molecule interacts with its neighbors. The logarithmic expression is not very sensitive with respect to  $p$  and  $T_2$  and ranges over

$$\ln \left[ \rho_2 \left( \frac{N_A}{m_\mu} \right)^{3/2} \left\{ \frac{6\sigma}{[2 + p/p'(T_2)]\pi m_2} \right\}^{1/2} \right] \approx 80 \text{ to } 83 \quad (12.36)$$

for water.

## 12.5.2 Heterogeneous nucleation

### 12.5.2.1 Characteristics of the surfaces and of the liquid-surface contact

The technical surfaces possess roughness as a result of the manufacturing procedure. The structure of the roughness is an important characteristic of the nucleation processes at the surface. Another important characteristic is the molecular interaction between the surface and the liquid. It is usually characterized by the so called contact angle. The angle between the tangent to the interface and the wall  $\theta$  is called contact angle. Hydrophobic surfaces,  $\theta > 0$ , causes heterogeneous nucleation at much reduced pressure difference (tensile strength). In this section we give some examples of the characteristics of surfaces influencing the heterogeneous nucleation kinetics.

At real surfaces there are several cavities. For ordinary machined surfaces the cavities have sizes from 2 to 6  $\mu\text{m}$  with density in the range of

$$n_w'' \approx (10 \text{ to } 250) \times 10^4 \text{ m}^{-2} \quad (12.37)$$

For mirror finished copper surfaces as described in *wang and Dhir* (1993) the physically existing cavities have been found to have surface densities depending on the equivalent cavity size in the range

$$n_w'' \approx 9 \times 10^{-9} / D_{cav}^2 \quad \text{for } D_{cav} \geq 5.8 \times 10^{-6} \text{ m} \quad (12.38)$$

$$n_w'' \approx 10.3 \times 10^4 + 1.5 \times 10^{-25.2} / D_{cav}^{5.2} \quad \text{for } 3.5 \times 10^{-6} \leq D_{cav} \leq 5.8 \times 10^{-6} \text{ m} \quad (12.39)$$

$$n_w'' \approx 2.2135 \times 10^7 + 3.981 \times 10^{-26.4} / D_{cav}^{5.4} \quad \text{for } D_{cav} \leq 3.5 \times 10^{-6} \text{ m} . \quad (12.40)$$

These are surface properties, which depend on the surface manufacturing only.

The following tables give some information on how the contact angle can change for different wall materials and different surface preparation procedures.

**Table 12.1** Static contact angles  $\theta$  for distilled water at polished surfaces.

Steel	$\pi / 3.7$	<i>Siegel and Keshock (1964)</i>
Steel, Nickel	$\pi / 4.74$	<i>Bergles and Rohsenow (1964)</i>
Nickel	$\pi / 4.76$ to $\pi / 3.83$	<i>Tolubinsky and Ostrovsky (1966)</i>
Nickel	$\pi / 4.74$ to $\pi / 3.83$	<i>Siegel and Keshock (1964)</i>
Chrome-Nickel Steel	$\pi / 3.7$	<i>Arefeva and Aladev (1958)</i>
Silver	$\pi / 6$ to $\pi / 4.5$	<i>Labuntsov (1963)</i> for $p = 1$ to 150 bar
Zinc	$\pi / 3.4$	<i>Arefeva and Aladev (1958)</i>
Bronze	$\pi / 3.2$	<i>Arefeva and Aladev (1958)</i>
Zr-4	$\pi / 3.16$	<i>Basu et al. (2002)</i>
Note the contradictory data for copper in the literature		
Copper	$\pi / 4$	<i>Arefeva and Aladev (1958)</i>
Copper	$\pi / 3$	<i>Gaertner and Westwater (1960)</i>
Copper	$\pi / 2$	<i>Wang and Dhir (1993)</i>
Stainless steel 304 (25°C)	$\theta_{25} \approx \pi / 2.25$	<i>Hirose et al. (2006)</i>
Zircaloy (25°C)	$\theta_{25} \approx \pi / 2.46$	<i>Hirose et al. (2006)</i>
Aluminum (25°C)	$\theta_{25} \approx \pi / 2$	<i>Hirose et al. (2006)</i>

**Table 12.2** Static contact angle  $\theta$  for distilled water at thermally or chemically treated polished surfaces

Copper heated to 525 K and exposed to air one hour:	$\pi / 5.14$	<i>Wang and Dhir (1993)</i>
Copper heated to 525 K and exposed to air two hour:	$\pi / 10$	<i>Wang and Dhir (1993)</i>
Chrome-Nickel Steel chemically treated:	$\pi / 2.9$	<i>Arefeva and Aladev (1958)</i>

*Hirose et al.* (2006) found that the wetting angle is a function of the wall temperature. He correlated measurements within  $\pm 12.5\%$  uncertainty band for nitrogen and argon and water-stainless steel 304, water-zircaloy and water-aluminum for pressures 1 to 151 bar and temperatures 20 to 300°C by the expression

$$\theta = \theta_{25} \tanh(2.55 \times T^{*1.72}) \text{ for } T^* > 0.3,$$

$$\theta = \theta_{25} \tanh(2.55 \times 0.3^{1.72}) \text{ for } T^* < 0.3,$$

where  $T^* = \frac{T_{cr} - T_w}{T_{cr} - (273.15 + 25)}$ ,  $T_{cr}$  is the critical water temperature and  $T_w$  is the wall temperature and  $\theta_{25} = \theta(25^\circ\text{C})$ . Note that there is no zero wettability at the critical temperature. This is important finding. The work by *Hirose et al.* (2006) shows that measurements for wetting angles can be compared to each other if they are made at the same wall temperature.

In case of nucleation at walls the segment of a bubble attached at the cavity possesses

$$\text{surface area} = \phi 4\pi R_{lc}^2 \quad (12.41)$$

which is less than the nucleation surface by a factor of  $\phi$ . Therefore less energy is needed for the creation of bubbles at walls

$$\Delta E_{lc}^* = \phi \Delta E_{lc}, \quad (12.42)$$

than inside the liquid. Consequently, the superheating which can be achieved in technical systems is much smaller than in spontaneous bulk nucleation systems.  $\phi$  is frequently called in the literature the work reduction factor.

*Tolubinski* (1980) computed the work reduction factor,  $\phi$ , for an idealized wall surface having *plane geometry* without cavities as follows

$$\phi = \frac{1}{4}(1 + \cos \theta)^2 (1 - \cos \theta). \quad (12.43)$$

Using the values from the Table 12.1 we have  $\phi$ 's in the range of 0.078 to 0.25.

The work reduction factor for surface with cavities calculated by *Kottowski* (1973) is

$$\phi = \frac{1}{4} [2 - 3 \sin(\theta - \Phi) + \sin^3(\theta - \Phi)]. \quad (12.44)$$

Here  $\Phi$  is the cavity angle if the cavity is idealized as a cone.

### 12.5.2.2 Nucleation theories and experimental observations

*Blander and Katz* (1975) computed for the heterogeneous nucleation the number of the nucleations per unit liquid volume and unit time in a pipe with wetted diameter  $D_{hy}$  as follows

$$\dot{n}_{cin} = \frac{4}{D_{hy}} N_2^{2/3} \frac{1 + \cos \theta}{2} \left\{ \frac{6\sigma}{[2 + p/p'(T_2)] \pi m_2 \varphi} \right\}^{1/2} \exp(-\varphi G b_2) =$$

$$\exp \left\{ \ln \left[ \frac{4}{D_{hy}} \rho_2^{2/3} \left( \frac{N_A}{m_\mu} \right)^{7/6} \frac{1 + \cos \theta}{2} \left\{ \frac{6\sigma}{[2 + p/p'(T_2)] \pi m_2 \varphi} \right\}^{1/2} \right] - \varphi G b_2 \right\} \quad (12.45)$$

Instead of  $N_2$  in the *Kaishew* and *Stranski* equation  $N^{2/3}$  is used because the nucleation occurs at the wall instead in the bulk.

The problem with the homogeneous and heterogeneous nucleation theories is that they did not describe appropriate nucleation rates in real liquid. *Rohatgi and Reshotko* (1975), *Algami* and *Lienhard* (1981) data comparisons indicated substantial deviation from the above theories in a real technical systems.

*Rohatgi and Reshotko* (1975) tried to match the *Simoneau's* experimental data (1975) with an expression

$$\dot{n}_{cin} = (2.236 \text{ to } 4.472) \times 10^3 \left( \frac{2\sigma}{\pi m_2 \varphi} \right)^{1/2} \exp(-\varphi G b_2) \quad (12.46)$$

where

$$\varphi = 5 \times 10^{-6}. \quad (12.47)$$

As it will be discussed below *Algami* and *Lienhard* (1981) found

$$\varphi = 0.055 \text{ to } 2 \times 10^{-7} \quad (12.48)$$

for different depressurization speeds. *Algami* and *Lienhard* (1981) found that depending on the depressurization speed the nucleation process can be delayed. They use the work reduction factor  $\varphi$  to correlate experimental data with the following relationship

$$\varphi = 0.1058 (T_2 / T_c)^{28.46} \left\{ 1 + 14 \left[ \left( \gamma_v \frac{\delta p}{\delta \tau} + \mathbf{V} \gamma \cdot \text{grad } p \right) / 10^{11} \right]^{0.8} \right\} \quad (12.49)$$

taking values as already mentioned of  $0.055$  to  $2 \times 10^{-7}$  for different depressurization rates. The correlation is valid for decompression speeds within



$$0.004 \leq (dp/d\tau)10^{-11} \leq 1.803 \quad (12.50)$$

in channels with constant cross section in the temperature range

$$0.62 \leq T_2/T_c \leq 0.935. \quad (12.51)$$

Here the decompression rate  $dp/d\tau$  is measured in  $Pa/s$ .

For some practical applications it is useful to compute the time required to cover strongly superheated walls with nuclei. This is in fact the time which is required to establish film boiling at walls heated at temperatures above the film boiling temperature. Next we discuss briefly this problem. If the growth of the nucleus is neglected and the initial conditions are assumed to remain constant the nucleation number density originating during the time interval  $\Delta\tau$  is

$$n_1 = \int_0^{\Delta\tau} \dot{n}_{1cin} d\tau = \dot{n}_{1cin} \Delta\tau. \quad (12.52)$$

If the nuclei are spherical in shape and their centers form a triangular array at the wall the maximum number of nucleation sites per unit volume in a pipe is

$$n_{1,max} = \frac{4}{D_h} \frac{2}{\sqrt{3}} \frac{1}{D_{lc}^2} \quad (12.53)$$

and the time required to reach it is

$$\Delta\tau_{max} = \frac{4}{D_h} \frac{2}{\sqrt{3}} / (D_{lc}^2 \dot{n}_{1cin}). \quad (12.54)$$

If the cause for the superheating is depressurization with a  $dp/d\tau$  starting from the saturation state the number of the produced particles is

$$n_1 = \int_0^{\Delta\tau} \dot{n}_{1cin} d\tau = n_1 = \frac{1}{dp/d\tau} \int_0^{\Delta p} \dot{n}_{1cin} dp \quad (12.55)$$

If  $\Delta p$  corresponding to experimentally observed superheating is known and  $n_1$  is set equal to  $n_{1,max}$  the critical work reduction factor can be estimated. This procedure was used by *Algami* and *Lienhard* (1981). The authors found as already mentioned

$$\varphi = 0.055 \text{ to } 2 \times 10^{-7} \quad (12.56)$$

for different depressurization speeds. Obviously only the functional form derived from the nucleation theories is useful to fit experimental data but not the theoretical formula itself. One of the reasons, why this is so may be the neglecting of nucleus growth of the already existing bubble generations during the nucleation.

Next we improve the computation by allowing each generation to grow. During a time interval  $N \Delta\tau$ ,  $N$ -generation of nuclei, or  $n_{1,n=1N}$  nuclei per unit flow volume are produced

$$n_{1,n} = \int_0^{\Delta\tau} \dot{n}_{1cin} d\tau, \quad n = 1, N. \quad (12.57)$$

Each generation has its own bubble growth history. If we assume that the bubble growth is thermally controlled following the following relationship

$$\frac{dD_{1,n}}{d\tau} = \frac{B}{\sqrt{\tau}} \quad (12.58)$$

where  $B$  is a function of local parameter the bubble size of the  $n$ -th generation after the time  $N \Delta\tau$  is

$$D_{1,n} = D_{1c} + \sum_{k=1}^{N-n+1} \int_0^{\Delta\tau} \frac{dD_{1,n}}{d\tau} d\tau = D_{1c} + 2(N-n+1)B\Delta\tau^{1/2}. \quad (12.59)$$

Thus the total number of nuclei and bubbles after  $N$  time steps of  $\Delta\tau$  is

$$n_1 = \sum_{n=1}^N n_{1,n} = N \int_0^{\Delta\tau} \dot{n}_{1cin} d\tau. \quad (12.60)$$

The cross section at the wall surface covered by attached bubbles per unit flow volume is

$$F_1 / Vol = \frac{\pi}{4} \sum_{n=1}^N n_{1,n} D_{1,n}^2, \quad (12.61)$$

which for deformable bubble can not be larger than  $4/D_h$ , where  $D_h$  is the hydraulic diameter of the pipe, i.e.

$$\frac{4}{D_h} \approx \frac{\pi}{4} \sum_{n=1}^N n_{1,n} D_{1,n}^2. \quad (12.62)$$

Analogous conditions can be derived for a hot sphere with diameter  $D_3$  immersed in liquid

$$D_3^2 \approx \frac{1}{4} \sum_{n=1}^N D_{1,n}^2. \quad (12.63)$$

By known nucleation and bubble growth laws and prescribed time step  $\Delta\tau$ , the above equation defines the number of bubble generation,  $N$ , and therefore the time needed to cover the surface with bubbles and nuclei,  $N \Delta\tau$ . At this time the maximum possible superheating is reached. At the end of this process the void fraction generated within  $N \Delta\tau$  is

$$\alpha_1 = \frac{4}{3} \pi \sum_{n=1}^N n_{1,n} D_{1,n}^3 \quad (12.64)$$

and volume-averaged bubble size is then

$$D_1^{*3} = \left( \frac{3}{4\pi} \alpha_1 / n_1 \right)^{1/3}. \quad (12.65)$$

After this moment the bubble production frequency is governed by combined thermal interaction and mechanical entrainment phenomena, which will be considered later.

## 12.6 Maximum superheat

*Skripov* et al. (1980) p. 136, 143, found that rapid decompressions can bring the water into a state of maximum superheating defined by  $Gb_2 = 6.8$  to  $9.6$ , which means

$$p'(T_2^{spin}) - p = (1.57 \text{ to } 1.32) \frac{\sigma^{3/2}}{(kT_2)^{1/2} [1 - \rho''(T_2)/\rho'(T_2)]}. \quad (12.66)$$

*Lienhard* found in 1976 the following explicit approximation of the homogeneous nucleation temperature which can be taken as a spinoidal temperature

$$T_2^{spin} = T'(p) + \left\{ 0.905 - \frac{T'(p)}{T_c} + 0.095 \left[ \frac{T'(p)}{T_c} \right]^8 \right\} T_c. \quad (12.67)$$

Under rapid decompression we understand decompression with

$$dp/d\tau \geq 2 \times 10^{11} \text{ Pa/s}. \quad (12.68)$$

In addition we should mention that *Hutcherson* et al. (1983) classified the boundary between "fast" and "slow" depressurization as about  $400 \times 10^6 \text{ Pa/s}$ . The line in the  $p$ - $T$  diagram, defined by the Eq. (12.66) or (12.67) is called the spinoidal line. The database defining the spinoidal line for water is given by *Skripov* (1980) p. 144 Table 6.4. *Lienhard* (1981) proposed for the constant the value 1.349 corresponding to  $Gb_2 \approx 9.2$ . For n-pentane, n-hexane, n-nephane, ether and benzene *Eberhard* and *Schnyders* reported in 1973  $Gb_2 \approx 11.5$ . The authors observed experimentally negative pressure up to  $\approx 0.4 p_c$ .

In technical systems the superheating is a function of several parameters not considered in our previous discussion. Next we discuss some of them.

The question of the maximal achievable superheating in technical systems has attracted the attention of the engineers since 1947. Probably *Burnell* [10] was the first who investigated in 1947 experimentally the flow of boiling water through orifices. The inlet conditions are corresponding to saturated water at  $p \approx (0.34 \text{ to } 12.7) \times 10^5 \text{ Pa}$ . *Burnell* found that a superheating of  $\Delta p_{Fi}^* = p'(T_2) - p_{Fi}$  is necessary to observe flashing inception at the throat. The flashing inception at the throat

reduces dramatically the mass flow rate compared to the prediction of the *Bernoulli* equation for subcooled water. *Burnell* found that the product of the initial saturated pressure multiplied by the critical bubble radius is constant

$$p'(T_2)R_{lc} \approx \text{const} \quad (12.69)$$

and therefore

$$\begin{aligned} \Delta p_{Fi}^* &= p'(T_2) - p_{Fi} = 2\sigma_2(T_2)/R_{lc} \approx 2\sigma_2(T_2)p'(T_2)/\text{const} \\ &\approx f(\sigma_2)p'(T_2) \end{aligned} \quad (12.70)$$

and

$$f(\sigma_2) = 0.264 \frac{\sigma_2 [T'(p)]}{\sigma_2' [T'(12.066 \times 10^5 \text{ Pa})]} \quad (12.71)$$

where the surface tension of the saturation condition was computed as follows

$$\sigma_2'(T_2) = 0.07548 [1 - 1.85 \times 10^{-3} (T_2 - 273.15)] \text{ in } N/m. \quad (12.72)$$

Thus the critical bubble radius in this region is

$$R_{lc} = 2\sigma_2(T_2)/\Delta p_{Fi}^*. \quad (12.73)$$

*Algami* and *Lienhard* correlated several experimental data for the reached water superheating with a standard deviation of  $\pm 10\%$  with the following value of the dimensionless critical work  $Gb_2 = 28.2 \pm 5.8$  which after using Eqs. (12.30) and (12.49) results in the following relationship for flashing inception,

$$\begin{aligned} \Delta p_{Fi}^* &= \left\{ \frac{16\pi\sigma^3}{3kT_c [1 - \rho''(T_2)/\rho'(T_2)]^2 \frac{T_2}{T_c} \frac{Gb_2}{\phi}} \right\}^{1/2} \\ &= \Delta p_{Fi}^o \sqrt{1 + 14 \left[ (\gamma_v \partial p / \partial \tau + \mathbf{V} \gamma \cdot \text{grad } p) / 10^{11} \right]^{0.8}} \end{aligned} \quad (12.74)$$

where

$$\Delta p_{Fi}^o = 0.253 \frac{[\sigma(T_2)]^{3/2} (T_2/T_c)^{13.73}}{(kT_c)^{1/2} [1 - \rho''(T_2)/\rho'(T_2)]} \quad (12.75)$$

is the pressure difference corresponding to the maximum possible superheating in an isobar system and  $T_2$  is the initial temperature before the pressurization. For

$$T_2 = 273.15 + 100 \text{ K}, \Delta p_{Fi}^* > 0.2 \times 10^5 \text{ Pa}, \quad (12.76)$$

and for

$$T_2 \approx 273.15 + 300 K, \Delta p_{Fi}^* < 9.5 \times 10^5 Pa \quad (12.77)$$

For  $T_2 > 273.15 + 300K$   $\Delta p_{Fi}^*$  decreases to zero due to vanishing surface tension as the critical point is approached. In fact Eq. (12.75) is the modified *Skripov* equation. Instead of the constant the expression  $0.253(T_2 / T_c)^{13.73}$  is used.

*Bartak* (1990) correlated the data of several authors including his own data with the following correlation

$$\Delta p_{Fi}^* = \left\{ \frac{16\pi\sigma^3}{3kT_2 [1 - \rho''(T_2)/\rho'(T_2)]^2 \frac{T_2}{T_c} \frac{Gb_2}{\varphi}} \right\}^{1/2} \quad (12.78)$$

where

$$\frac{Gb_2}{\varphi} = f_1 f_2, \quad (12.79)$$

$$\log f_1 = 11 - 0.0274(T_2 - 273.15), \quad (12.80)$$

$$f_2 = 36 / \left[ (\gamma_v \partial p / \partial \tau + \mathbf{V} \gamma \cdot \text{grad } p) / 10^6 \right]^{0.37}, \quad (12.81)$$

with a mean relative error of 16%. It is valid for water in the temperature range from 373.15 to 583.15 K and depressurization rates of  $4 \times 10^8$  to  $2 \times 10^{11}$  Pa/s. *Bartak* reported that the *Algamir* and *Lienhard* correlation 65 approximates his own data with 21% mean relative error. In fact *Baratak's* correlation predict more then 30% higher values than the *Algamir* and *Lienhard* correlation. Consequently, it can be concluded that the achievable prediction accuracy is within the error band of about 48.5%.

If the maximum possible superheating under given conditions is reached, the maximum nucleation density is reached too. Note that the reduction factor, Eq. (12.48) obtained by *Algamir* and *Lienhard* can be used to compute the heterogeneous nucleation densities using the *Blander* and *Katz* Equation (12.45) only together with the assumption of no bubble growth during the nucleation process.

*Jones* found in 1979 that the turbulization of the flow could reduce the maximum superheating

$$\Delta p_{Fi} = \Delta p_{Fi}^* - 27 \frac{1}{2} \rho_2 V_2'^2, \quad (12.82)$$

where the turbulent pulsation velocity in a straight pipe is 7.2 % from the local flow velocity

$$\sqrt{V'^2} = 0.072 V_2 \text{ or } V_2'^2 = 5.184 \times 10^{-3} V_2^2 \quad (12.83)$$

For a converging nozzle the local fluctuation velocity can be expressed as a function of the entrance velocity  $V_{2o}$  using the continuity equation

$$V_2'^2 = 5.184 \times 10^{-3} V_{2o}^2 (F_o / F)^2. \quad (12.84)$$

Comparing with experimental data *Abuqf* et al. (1983) found that the turbulent pulsation velocity varies in accordance with

$$V_2'^2 = 5.184 \times 10^{-3} V_{2o}^2 (F_o / F)^n, \quad (12.85)$$

where

$$n = 1.75 \text{ for } F / F_o \geq 1/6, \quad (12.86)$$

and for stronger contraction

$$n = 1.4 \text{ for } F / F_o < 1/6. \quad (12.87)$$

*Jones* (1982) shows that for  $G > 15\,000 \text{ kg/(m}^2\text{s)}$  no superheating is observed. To what extent the superheating reduction explained by *Jones* (1979) with turbulization is separable from the convective transport of nuclei by high-liquid velocities is not clear.

## 12.7 Critical mass flow rate in short pipes, orifices and nozzles

The most important outcome of the heterogeneous nucleation theory for the engineering design practice is the possibility to compute in a simple manner the critical mass flow rate in short pipes, orifices and nozzles for saturated and subcooled water. Probably *Burnell* was the first approximating critical flow in nozzles with saturated and subcooled inlet condition modifying the *Bernoulli* equation as follows

$$G^* = \sqrt{2\rho_2(p_o - p_{Fi})} \quad (12.88)$$

where the critical pressure is set to the flashing inception pressure

$$p_{Fi} = p'(T_2) - \Delta p_{Fi}. \quad (12.89)$$

*Jones* (1982) described successfully critical mass flow rate in nozzles modifying Eq. (12.88) to

$$G^* = (0.93 \pm 0.04) \sqrt{2\rho_2(p_o - p_{Fi})} \quad (12.90)$$

The error of this approach was reported to be  $\pm 5\%$  for inlet conditions of  $p = (28 \text{ to } 170) \times 10^5 \text{ Pa}$  and  $T_2 = 203 \text{ to } 288^\circ\text{C}$  and use of the *Algair* and *Lienhard* correlation. *Fincke* (1984) found for the discharge coefficient instead of 0.93 the value 0.96 and reported that this coefficient does not depend on the *Reynolds* number.

## 12.8 Nucleation in the presence of non-condensable gases

In the liquids usually used in technology there are *dissolved inert gases* and *microbubbles*. It is known that at  $p = 10^5 \text{ Pa}$ ,  $T_{20} = 298.15 \text{ K}$  the amount of dissolved gases and microbubbles in the coolant is  $\alpha_{10} \cong 0.005$ , for boiling water reactors, and  $\alpha_{10} \cong 0.001$ , for pressurized water reactor *Malnes* and *Solberg* (1973). *Brennen* (1995) p. 20 reported that it takes weeks of deaeration to reduce the concentration of air in the water tunnel below  $3 \text{ ppm}$  (saturation at atmospheric pressure is about  $15 \text{ ppm}$ ).

This amount is dissolved in a form of

$$n_{10} = \alpha_{10} / (\pi D_{10}^3 / 6) \quad (12.91)$$

bubbles per unit volume, so that before starting the nucleation  $n_{10}$  nucleation sites already exist. Here the initial bubble diameter is in any case less than the bubble diameter computed after equating the buoyancy force and the surface force

$$D_{10} < \sqrt{6} \lambda_{RT}. \quad (12.92)$$

Note that the so called free stream nuclei number density is subject to distribution depending on the nucleation size, e.g.  $n_{10} \sim R_{10}^{-4}$ ,  $R_{10} > 5 \times 10^{-6}$  as reported by *Brennen* (1995).

Let us suppose that at  $p_0$ ,  $T_{20}$  we have no water steam in the single bubble *Besand* (1859) and therefore the mass of the single bubble is

$$m_{\Sigma n_{10}} = p_{\Sigma n_1} \frac{\frac{4}{3} \pi R_{10}^3}{R_{\Sigma n_1} T_{20}} = (p + \frac{2\sigma}{R_{1\sigma}}) \frac{\frac{4}{3} \pi R_{10}^3}{R_{\Sigma n_1} T_{20}} = (p + \frac{2\sigma}{R_{1\sigma}}) \frac{\alpha_{10} / n_{10}}{R_{\Sigma n_1} T_{20}}. \quad (12.93)$$

Further let us assume that the steam evaporating from the surface into the bubble is saturated. The initial internal bubble pressure  $\frac{3}{4} \frac{m_{\Sigma n_{10}} R_{\Sigma n_1} T'}{\pi R_1^3}$  increases with

$p'(T_2)$  and equals the external pressure  $p + \frac{2\sigma}{R_1}$

$$p'(T_2) - p = \frac{2\sigma}{R_1} - \frac{3}{4} \frac{m_{\Sigma n_{10}} R_{\Sigma n_1} T'}{\pi R_1^3}, \quad T_2 > T'(p). \quad (12.94)$$

With increasing liquid superheating the bubble radius increases to its critical size

$$R_{1c} = 3 \sqrt{\frac{m_{\Sigma n_{10}} R_{\Sigma n_1} T'(p)}{8\pi\sigma}}, \quad (12.95)$$

Blake (1949), Neppiras and Noltingk (1951), corresponding to the superheating

$$T_2 - T'(p) = \frac{2^{5/2}}{3\sqrt{\pi}} \sigma^{3/2} \sqrt{T'(p)} \frac{(\rho' - \rho'')\rho_2}{(\rho_2 - \rho'')\rho'\rho''} \frac{1}{h'' - h'} \frac{1}{\sqrt{m_{\sum n_{1o}} R_{\sum n_1}}} \quad (12.96)$$

This is the maximum possible superheating. Thereafter the bubble loses its stability and starts to increase in size. We see that the presence of dissolved gases in the liquid decreases the superheating necessary for starting the intensive evaporation. A considerable amount of dissolved gases can lead to flashing initiation at temperatures *lower than the saturation temperature*.

For the first time steps, where the nucleation occurs, the instantaneous source terms are

$$\mu_{21} = \rho'' V_{1c} \dot{n}_{1cin} \quad (12.97)$$

$$\dot{q}_2^{m1\sigma} = -\mu_{21} (h'' - h_{M2}) \quad (12.98)$$

## 12.9 Activated nucleation site density – state of the art

Not all cavities at the wall serve as a nucleation sites. It is experimentally observed that the increase of the wall superheating activates an increasing number of nucleation sites, Fig. 12.3. Many authors tried to represent this observation by setting

$$n''_{lw} \approx \text{const} / D_{1c}^n \quad (12.99)$$

where the exponent  $n$  varies from 2 to 6. If nucleation sites forms a triangular array and are touching each other their maximum number per unit surface corresponding to the local superheating is

$$n''_{lw, \max} = 2 / (\sqrt{3} D_{1c}^2) \quad (12.100)$$

Note that at atmospheric pressure this expression reduces to

$$n''_{lw, \max} = 0.20 \times 10^9 \Delta T^2 \quad (12.101)$$

Labuntsov assumed in 1963 that the active nucleation sites density is a part of this value

$$n''_{lw, \max} = \text{const} \ 2 / (\sqrt{3} D_{1c}^2) \quad (12.102)$$

Later in 1977 this equation was used by Avdeev et al. (1979) for modeling of flashing flows

$$n''_{lw, \max} = 20 \times 10^{-5} / D_{1c}^2 \quad (12.103)$$



which for atmospheric pressure gives an activated site density four order of magnitude lower than the thinkable maximum. The constant  $20 \times 10^{-5}$  was estimated by comparison of the critical mass flow rates with those experimentally measured. For atmospheric pressure Eq. (12.92) results in

$$n''_{1w,\max} = 4.85 \times 10^4 \Delta T^2. \quad (12.104)$$

*Johov* (1969) plotted data for water and non-water liquids for the nucleation site density as a function of the critical diameter. The data have been in the region  $400 \leq n''_{1w} \leq 4 \times 10^8$ . The data correlated with

$$n''_{1w} = 4 \times 10^{-12} / D_{1c}^3, \quad (12.105)$$

$[= 15.12 \Delta T^3]$  for  $p = 0.1 \text{ MPa}$ , with considerable data spreading within two orders of magnitude.

*Mikic and Rohsenow* (1969) proposed the expression

$$n''_{1w} = c (D_1^* / D_{1c})^{3.5}, \quad (12.106)$$

where  $D_1^*$  is the diameter for which  $n''_{1w}$  would be 1 per unit area, and  $c$  is a dimensional constant ( $1/m^2$ ) depending on the cavity size distribution. Here  $n''_{1w}$  is interpreted as the number of the active bubble sites, per unit area, having sizes greater than  $D_1^*$ . For a triangular array

$$D_1^* = (2 / \sqrt{3})^{1/2}. \quad (12.107)$$

*Hutcherson et al.* (1983) uses instead of the critical nucleation size the bubble departure size and obtained good agreement with experimental data for the initial depressurization of a vessel blow down assuming

$$n''_{1w} D_{1d}^2 \approx 0.01 \times 2 / \sqrt{3} \quad (12.108)$$

using the *Fritz* equation for the bubble departure diameter  $D_{1d}$ .

$$D_{1d} \equiv D_{1d,Fritz} = 1.2\theta \left\{ \frac{\sigma}{g[\rho_2 - \rho''(p)]} \right\}^{1/2}. \quad (12.109)$$

For the case of nucleate boiling at the wall, *Kocamustafaogullari and Ishii* (1983) proposed the following correlation to predict the active nucleation sites density

$$n''_{1w} D_{1d}^2 = \left[ (D_{1d} / D_{1c})^{4.4} 2.157 \times 10^{-7} (1 + 0.0049 \bar{p})^{4.13} / \bar{p}^{3.2} \right] \quad (12.110)$$

where

$$\bar{\rho} = (\rho' - \rho'') / \rho'', \quad (12.111)$$

$$D_{1d} = 0.0012 \bar{\rho}^{0.9} D_{1d, Fritz} \quad (12.112)$$

and the size of the activated sites,  $D_{1c}$ , is computed using Eq. (12.9) with a temperature difference  $S [T_w - T'(p)]$ . Here  $S$  is the so called *Chen* superposition factor for taking into account the effective superheating of the wall boundary layer.  $S = 1$  for free convection pool boiling and  $\leq 1$  for forced convection boiling. The authors reported good agreement with data for pressures  $p = 0.1$  to  $19.8$  MPa and for both subcooled and pool boiling.

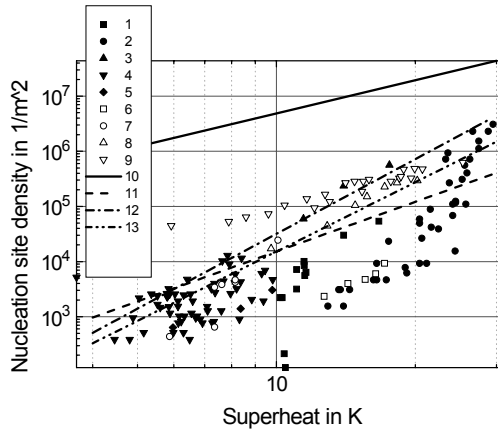


**Fig. 12.3** Active nucleation site density as a function of superheat. Saturated water at 0.1 MPa. Data: 1) Gaertner 1965, 4/0 polished copper, 2) Gaertner and Westwater 1960, 4/0 polished copper, 20 p.c. nickel salt-water solution, 3) Sultan and Judd 1978, diamond grid 600 polished copper, 4) Yamagata et al. 1955, fine polished brass, 5) Jakob and Linke 1933, polished steel, 6) Cornwell and Brown 1978, 4/0 polished copper, 7) Kurihara and Myers 1960, 4/0 polished copper, 8) Rallis and Jawurek 1964, nickel wire, 9) Faggani et al. 1981, polished 316 steel horizontal cylinder. Prediction with correlations proposed by 10) Avdeev et al. (1977), 11) Johov (1969), 12) Cornwell and Brown (1978) and 13) Kocamustafaogullari and Ishii (1983)

*Jones* (1992) found

$$n''_{1w} D_{1d}^2 = 10^{-7} (D_{1d} / D_{1c})^4 \quad (12.113)$$

for critical flashing flow in a nozzle using the equilibrium between drag and surface forces in the viscous boundary layer to compute departure diameter. *Riznic* and *Ishii* (1989) demonstrated the applicability of this correlation for flashing adiabatic flow using  $D_{1c}$  computed with the equation by *Kocamustafaogullari* and *Ishii* for the temperature difference  $T_2 - T'(p)$ .

*Cornwell* and *Brown* (1978) reported experimental data for pool boiling of saturated water at atmospheric pressure on a copper surface correlated by

$$n''_{1w} \approx \Delta T^{4.5} \approx 1.36 \times 10^{-19} / D_{lc}^{4.5} . \quad (12.114)$$

Plotting the available data for nucleation site density as a function of superheating for boiling water at atmospheric pressure, Fig. 12.1, gives an average trend that can be represented by

$$n''_{1w} \approx \Delta T^{4.18} \approx 2.988 \times 10^{-18} / D_{lc}^{4.18} . \quad (12.115)$$

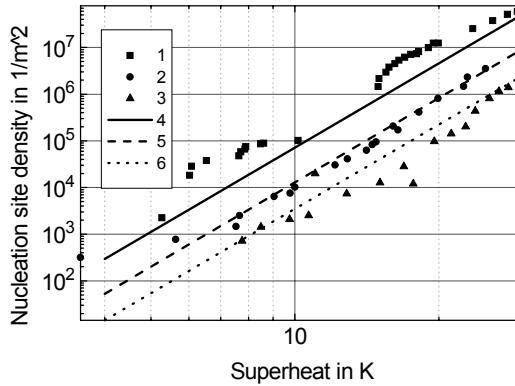


**Fig. 12.4** Active nucleation site density as a function of superheating. Saturated water at 0.1 MPa. Wang and Dhir (1993) data for three different static contact angles 1) 90°, 2) 35° and 3) 18°. Prediction of the same data with their correlation 4), 5), and 6), respectively. Larger static contact angle results of larger active nucleation site density by the same superheating

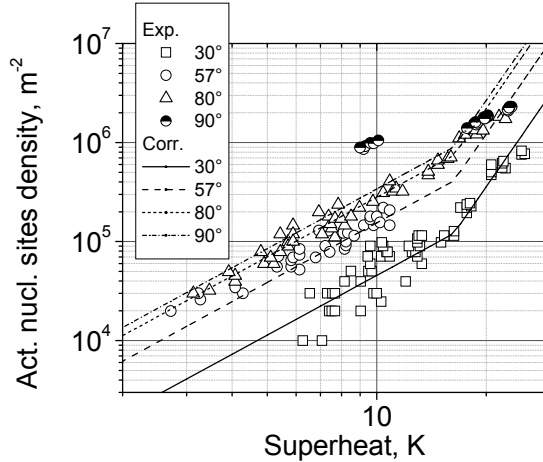


**Fig. 12.5** Active nucleation site density as a function of superheating. Saturated water at 0.1 MPa. Basu et al. (2002) data for different static contact angles: 30°, 57°, 80°, 90°.  $124 < G < 886 \text{ kg}/(\text{m}^2 \text{ s})$ ,  $6.6 < \Delta T_{sub} < 52.5 \text{ K}$ ,  $25 < q''_{w2} < 960 \text{ kW}/\text{m}^2$ . Prediction of the same data with their correlation respectively

The minimum of the nucleation site density can be represented by

$$n''_{1w} \approx (\Delta T / 3.729)^{2.593} \text{ for } \Delta T \leq 21.1, \quad (12.116)$$

and

$$n''_{1w} \approx 100(\Delta T / 16.135)^{16.53} \text{ for } 21.19 \leq \Delta T \leq 40. \quad (12.117)$$

Comparing the predictions for  $n''_{1w}$  by the different above mentioned methods with each other shows discrepancies of several orders of magnitude in different regions which leads to the conclusion that the knowledge in this field is unsatisfactory for practical application.

An important step in this field was made by *Wang and Dhir* (1993). *Wang and Dhir* (1993) succeeded to quantify the effect of the static contact angle  $\theta$ , and correlated their data for active nucleation sites density as a function of the wall superheating as follows

$$n''_{1w} = 5 \times 10^{-27} (1 - \cos \theta) / D_{lc}^6 = 714.3 \Delta T^6, \quad (12.118)$$

where the constant has a dimension  $m^4$  - see Fig. 12.4. The uncertainty in measuring the static contact angle was  $\pm 1/60$  rad; the uncertainty of the measured nucleation site density was estimated to  $\pm 20\%$ . The data are collected for atmospheric pool boiling of water with static contact angle of  $\pi/90$ ,  $\pi/35$  and  $\pi/18$  rad. The authors discovered that only cavities having a nearly spherical form and mouth angle less than the static contact angle serve as nucleation sites. The mouth angle is the angle between the boiling surface and the internal surface of the cavity forming the mouth. The region of changing the heat flux covers the entire nucleate boiling region.

Note that Eq. (12.118) should be used together with the experimentally observed relationship between the averaged nearest-neighbor distance and the nucleation site density,

$$\ell \approx 0.84 / n''_{1w}. \quad (12.119)$$

In 2002 *Basu et al.* (2002) proposed a replace for the Eq. (12.118)

$$n''_{1w} = 3400(1 - \cos \theta) \Delta T^2 = 2.183 \times 10^{-5} (1 - \cos \theta) / D_{lc}^2 \quad (12.120)$$

for  $\Delta T_{inb} < \Delta T < 16.298K$ , and

$$n''_{1w} = 0.34(1 - \cos \theta) \Delta T^{5.3} = 2.048 \times 10^{-23} (1 - \cos \theta) / D_{lc}^{5.3} \quad (12.121)$$

for  $16.298K \leq \Delta T$ . Here  $\Delta T_{inb}$  is the superheat required for initiation of the nucleate boiling. The correlation reproduces data given Fig. 12.5 for  $\theta = \pi/2$  and  $\theta = \pi/6$  within  $\pm 40\%$ . The correlation is valid in the range  $124 < G < 886 kg/(m^2 s)$ , inlet subcooling  $6.6 < \Delta T_{sub} < 52.5K$ ,  $25 < \dot{q}''_{w2} < 960 kW/m^2$ , and  $\pi/6 < \theta < \pi/4$ .

*Shoji* et al. performed experiments in 2005 with conical, cylindrical and spherical form. From the wall temperature fluctuation at the cavity they found that the conical cavities are not holding bubble nucleus so effective as the cylindrical or spherical cavity do which is fact conformation of the *Wang* and *Dhir* finding. At the same heat flux the conical cavity showed much larger magnitude of the temperature fluctuations compared to the other forms and waiting time reduction with increasing heat flux.

*Benjamin* and *Balakrishnan* reported in 1997 the only correlation taking into account the thermal properties of the wall and its roughness as follows

$$n_{1w}'' = 218.8 \frac{\text{Pr}_2^{1.63}}{\gamma \delta_w^{*0.4}} \Delta T^3. \quad (12.122)$$

The liquid *Prandtl* number, the dimensionless roughness and the dimensionless factor defining the transient interface temperature are defined as follows

$$\text{Pr}_2 = c_{p2} \eta_2 / \lambda_2, \quad (12.123)$$

$$\delta_w^* = 14.5 - 4.5 \frac{\delta_w p}{\sigma_2} + \left( \frac{\delta_w p}{\sigma_2} \right)^{0.4}, \quad (12.124)$$

$$\gamma = \left[ \lambda_w \rho_w c_{pw} / (\lambda_2 \rho_2 c_{p2}) \right]^{1/2}. \quad (12.125)$$

$\delta_w$  is the arithmetic averaged deviation of the roughness surface counter from the averaged line. The correlation is valid within  $1.7 < \text{Pr}_2 < 5$ ,  $4.7 < \gamma < 93$ ,  $0.02 < \delta_w < 1.17 \text{ mm}$ ,  $5 < \Delta T < 25 \text{ K}$ ,  $13 \times 10^{-3} < \sigma < 59 \times 10^{-3} \text{ N/m}$ ,  $2.2 < \delta_w^* < 14$ . Table 12.3 provides useful information about the roughness of differently polished materials.

**Table 12.3.** Roughness of differently polished materials

Material	Finish	Roughness in $\mu\text{m}$	Reference
Cooper	3/0 emery paper	0.14	<i>Griffith</i> and <i>Wallis</i> (1960)
Cooper	4/0 emery paper	0.07	<i>Kurihara</i> and <i>Myers</i> (1960)
Cooper	4/0 emery paper	0.07	<i>Gaertner</i> and <i>Westwater</i> (1960)
Cooper	4/0 emery paper	0.07	<i>Gaertner</i> (1965)
Cooper	Mirror finish	<0.02	<i>Wang</i> and <i>Dhir</i> (1993)
Nickel	4/0 emery paper	0.045	<i>Zuber</i> (1963)
Stainless steel	1/0 emery paper	0.2	<i>Benjamin</i> et al. (1997)
Aluminium	2/0 emery paper	1.17	<i>Benjamin</i> et al. (1997)
Aluminium	3/0 emery paper	0.89	<i>Benjamin</i> et al. (1997)
Aluminium	4/0 emery paper	0.52	<i>Benjamin</i> et al. (1997)

Many authors reported that the wall nucleation is not dependent on the liquid sub-cooling but only on the wall superheating with respect to the saturation line e.g. *Judd and Hwang* (1976).

There is no attempt to describe theoretically the activated nucleation sites per unit surface as a function of the local superheating.

## 12.10. Conclusions and recommendations

1. The maximum superheating in technical systems is a function of the depressurization velocity and of the produced turbulence.
2. The maximum superheating can be predicted by the *Algamir* and *Lienhard* and by the *Bartak* correlations within an error band of 48.5%.
3. Flashing in short pipes and nozzles leads to critical flows driven by the pressure difference equal to the entrance pressure minus the flashing inception pressure.
4. For the prediction of the maximum achievable superheating which represents the spinoidal line the *Skripov* correlation is recommended.
5. The wetting angle is an important property of the polished surface characterizing its capability to activate nucleation sites.
6. For the prediction of the activated nucleation sites the correlation obtained by *Wang* and *Dhir* is recommended.
7. The establishing of a vapor film around a heated surface having temperature larger than the minimum film boiling temperature takes a finite time.
8. Availability of small bubbles of non-condensing gases reduces the superheating required to initiate evaporation. Evaporation at lower than the saturation temperature is possible.

## Nomenclature

$B$	thermally controlled bubble growth parameter
$D_{cav}$	equivalent cavity size, $m$
$D_h$	hydraulic diameter, $m$
$D_{1,n}$	bubble diameter belonging to $n$ -th bubble generation, $m$
$D_{1c}$	critical bubble diameter, $m$
$D_{1d}$	bubble departure diameter, $m$
$d$	differential, <i>dimensionless</i>
$F_1/Vol$	cross section at the wall surface covered by attached bubbles per unit flow volume, $1/m$
$G^*$	critical mass flow rate, $kg/(m^2s)$
$Gb_2$	$= \frac{\Delta E_{1kr}}{kT_2}$ , <i>Gibbs number, dimensionless</i>

$h$	specific enthalpy, $J/kg$
$k$	$= 13.805 \times 10^{-24}$ , Boltzmann constant, $J/K$
$m_2$	$= m_\mu / N_A$ , mass of single molecule, $kg$
$m_\mu$	$kg$ -mole mass (18 $kg$ for water), $kg/mole$
$N_2$	$= \rho_2 / m_2 = \rho_2 N_A / m_\mu$ ( $\approx 3.3 \times 10^{28}$ for water), number of the molecules per unit volume, $1/m^3$
$N_A$	$= 6.02 \times 10^{26}$ , Avogadro number, number of molecules in one kilogram-mole mass, $1/kg$
$\dot{n}_{1cin}$	number of the created nuclei per unit time in unit volume of the liquid, $1/(m^3s)$
$n''_w$	cavity per unit surface, $1/m^2$
$n''_{1w}$	bubble generating (active) cavity per unit surface, $1/m^2$
$n_1$	bubble number density, $1/m^3$
$n_{1,n}$	bubble number density belonging to $n$ -th bubble generation, $1/m^3$
$n_{1,max}$	maximum number of nucleation sites per unit volume in a pipe, $1/m^3$
$p$	pressure, $Pa$
$\dot{q}_2^{m1\sigma}$	thermal energy consumed from the liquid per unit time and unit flow volume, $W/m^3$
$R$	gas constant, $J/(kgK)$
$R_1$	bubble radius, $m$
$R_{10}$	initial bubble radius, $m$
$R_{1c}$	critical bubble radius, $m$
$R_{1\infty}$	final radius of the bubble, $m$
$r$	radius, $m$
$s$	specific entropy, $J/(kgK)$
$T$	temperature, $K$
$u$	radial velocity, $m/s$
$\mathbf{V}$	velocity vector, $m/s$
$V_{1c}$	volume of the bubble with critical size
$v$	specific volume, $m^3/kg$
$Vol$	volume, $m^3$

### Greek

$\alpha_1$	bubble volumetric fraction, $m^3/m^3$
$\gamma_v$	volume occupied by the flow divided by the volume of the system, <i>dimensionless</i>
$\gamma$	cross section flowed by the flow divided by the total cross section of the system, <i>dimensionless</i>

$\Delta$	finite difference
$\Delta E_1$	work necessary to create a single bubble with radius $R_1$ , $J$
$\Delta E_{1c}$	work necessary to create a single bubble with radius $R_{1c}$ , $J$
$\Delta E_{1c}^*$	$= \phi \Delta E_{1c}$ , energy for the creation of a single bubble at a wall, $J$
$\Delta p_{Fi}^*$	$= p'(T_2) - p_{Fi}$ , flashing inception pressure difference, $Pa$
$\Delta \tau$	time interval, $s$
$\theta$	static contact angle, $rad$
$\lambda_{RT}$	<i>Rayleigh-Taylor</i> wavelength, $m$
$\mu_{21}$	evaporating mass per unit time and unit flow volume, $kg/(m^3s)$
$\rho$	density, $kg/m^3$
$\sigma$	surface tension, $N/m$
$\tau$	time, $s$
$\Phi$	cavity angle if the cavity is idealized as a cone, $rad$
$\phi$	work reduction factor, <i>dimensionless</i>

### Superscripts

'	saturated liquid
"	saturated vapor
<i>spin</i>	spinoidal line

### Subscripts

1	vapor, gas
2	liquid
<i>c</i>	critical state
<i>s</i>	at constant entropy
<i>Fi</i>	flashing inception
$\sum_{nlo}$	sum of all non-condensing gases
<i>M</i>	evaporating chemical component

## References

- Abuaf N, Jones OC Jr, Wu BJC (May 1983) Critical flashing flows in nozzles with sub-cooled inlet conditions, *J. of Heat Transfer*, vol 105 pp 379-383
- Algamir M, Lienhard JH (1981) Correlation of pressure undershoot during hot-water depressurisation. *J. of Heat Transfer*, vol 103 no 1 p 60
- Arefeva EI, Aladev IT (July 1958) O wlijanii smatchivaemosti na teploobmen pri kipenii, *Injenerno - Fizicheskij Jurnal*, vol 1 no 7 pp 11 - 17, in Russian
- Avdeev AA, Maidanik VN, Selesnev LI, Shanin VK (1977) Calculation of the critical flow rate with saturated and subcooled water flashing through a cylindrical duct, *Teploenergetika*, vol 24 no 4 pp 36-38



- Bartak J (1990) A study of the rapid depressurization of hot water and the dynamics of vapor bubble generation in superheated water, *Int. J. Multiphase Flow*, vol 16 no 5 pp 789-798
- Basu N, Warriar GR and Dhir VK (2002) Onset of nucleate boiling and active nucleation site density during subcooled flow boiling, *J. Heat Transfer*, vol 124 pp 717-728
- Benjamin RJ and Balakrishnan AR (1997) Nucleation site density in pool boiling of saturated pure liquids: effect of surface microroughness and surface and liquid physical properties, *Exp. Thermal Fluid Sci.*, vol 15 pp 32-42
- Benjamin RJ and Balakrishnan AR (1997) Nucleation site density in pool boiling of binary mixtures: effect of surface microroughness and surface and liquid physical properties, *Can. J. Chem. Eng.*, vol 75 pp 1080-1089
- Bergles AE and Rohsenow WM (1964) The determination of forced convection surface-boiling heat transfer, *ASME J. Heat Transfer*, vol 1 pp 365-372
- Besand WH (1859) *Hydrostatics and hydrodynamics*, Deighton Bell, Cambridge, p 170
- Blake FG (1949) The onset of cavitation in liquids. I. Acoustic Res. Lab., Harvard Univ., Tech. Memo. no 12
- Blander M, Katz JL (1975) Bubble nucleation in liquids. *AIChE*, vol 21 pp 833-838
- Brennen CE (1995) *Cavitation and bubble dynamics*. Oxford University Press, Oxford, New York
- Burnell JG (Dec.12, 1947) Flow of boiling water through nozzles, orifices and pipes, *Engineering*, pp 572-576
- Cornwell K, Brown RD (1978) Boiling surface topology, *Proc. 6th Int. Heat Transfer Conf. Heat Transfer*, Toronto, vol 1 pp 157-161
- Eberhard JG and Schnyders MC (1973) Application of the mechanical stability condition to the prediction of the limit of superheat for normal alkanes, ether and water. *J. Phys. Chem.* Vol 77 no 23 pp 2730-2736
- Faggiani S, Galbiati P, Grassi W (1981) Active site density, bubble frequency and departure on chemically etched surfaces, *La Termotecnica*, vol 29 no 10 pp 511-519
- Fincke JR (August 5 - 8, 1984) Critical flashing flow of subcooled fluids in nozzles with contour discontinuities, *Basic Aspects of Two Phase Flow and Heat Transfer*, 22nd Nat. Heat Transfer Conference and Exhibition, Niagara Falls, New York, HTD - vol 34 p 85-93
- Gaertner RF (Feb. 1965) Photographic study of nucleate pool boiling on a horizontal surface, *transaction of the ASME, Journal of Heat Transfer*, vol 87 pp 17 - 29
- Gaertner RF, Westwater JW (1960) Population of active sites in nucleate boiling heat transfer, *Chem. Eng. Progr. Symp. Ser.*, vol 30 no 30 pp 39-48
- Gibbs JW (1878) *Thermodynamische Studien* (Leipzig 1892), *Amer. J. Sci. and Arts*, vol 16 pp 454-455
- Griffith P and Wallis GB (1960) The role of the surface conditions in nucleate boiling, *Chem. Eng. Prog. Symp.*, vol 56 pp 49-63
- Hirose Y, Hayashi T, Hazuku T and Takamasa T (July 17-20, 2006) Experimental study on contact angle of water droplet in high temperature conditions, *Proc. of ICONE14, Int. Conf. on Nucl. Engineering*, Miami, Florida, USA
- Hutcherson MN, Henry RE, Wollersheim DE (Nov. 1983) Two-phase vessel blowdown of an initially saturated liquid - Part 2: Analytical, *Trans. ASME, J. Heat Transfer*, vol 105 pp 694-699
- Jakob M, Linke W (1933) Der Wärmeübergang von einer waagerechten Platte an siedendes Wasser, *Forsch. Ing. Wes.*, vol 4 pp 75-81

- Johov KA (1969) Nucleations number during steam production, Aerodynamics and Heat Transfer in the Working Elements of the Power Facilities, Leningrad, in Russian, Proc. CKTI, vol 91 pp 131- 135
- Jones OC Jr (1979) Flashing inception in flowing liquids, non-equilibrium two-phase flow, in Chan JC and Bankoff SG (eds), ASME, New York, pp 29-34
- Jones OC Jr (1982) Towards a unified approach for thermal non-equilibrium in gas- liquid systems, Nucl. Eng. and Design, vol 69 pp 57-73
- Jones OC (1992) Non-equilibrium phase change 1. Flashing inception, critical flow, and void development in ducts, Boiling Heat Transfer, Lahey RT Jr (ed) Elsevier Science Publishers BV, pp 189-234
- Jones OC (1992) Nonequilibrium phase change 2. Relaxation models, general applications, and post heat transfer, in Lahey RT Jr (ed) Boiling heat transfer, Elsevier Science Publishers BV, pp 447-482
- Judd RL and Hwang (Nov. 1976) A comprehensive model for nucleate pool boiling heat transfer including microlayer evaporation, Transactions of ASME, Journal of Heat Transfer, pp 623-629
- Kaishew R, Stranski IN (1934) Z. Phys. Chem., vol 26 p 317
- Kocamustafaogullari G, Ishii M (1983) Interfacial area and nucleation site density in boiling systems, Int. J. Heat Mass Transfer, vol 26 pp 1377-1389
- Kottowski HM (1973) Nucleation and superheating effects on activation energy of nucleation, in Progress in Heat and Mass Transfer, Dwyer OE (ed) Pergamon, New York, vol 7 pp 299-324
- Kurihara HM, Myers JE (March 1960) The effect of superheat and surface roughness on boiling coefficients, AIChE Journal, vol 6 no 1 pp 83 - 91
- Labuntsov DA (1963) Approximate theory of heat transfer by developed nucleate boiling (Russ.), Izvestiya AN SSSR, Energetika i transport, no 1
- Lienhard JH (1976) Correlation for the limiting liquid superheat, Chem. Eng. Sci., vol 31 pp 847-849
- Lienhard JH (1981) Homogeneous nucleation and the spinoidal line, J. of Heat Transfer, vol 103 p 72
- Lienhard JH (2005), A Heat Transfer Textbook, Phlogiston Press, Cambridge Massachusetts
- Malnes D, Solberg K (May 1973) A fundamental solution to the critical two-phase flow problems, applicable to loss of coolant accident analysis. SD-119, Kjeller Inst., Norway
- Mikic BB, Rohsenow WM (May 1969) A new correlation of pool-boiling data including the effect of heating surface characteristics, Transactions of the ASME, J. Heat Transfer, vol 91 pp 245-250
- Neppiras EA and Noltingk BE (1951) Cavitation by ultrasonic: theoretical conditions for onset of cavitation. Proc. Phys. Soc., London, vol 64B pp 1032-1038
- Rallis CJ, Jawurek HH (1964) Latent heat transport in saturated nucleate boiling, Int. J. Heat Transfer, vol 7 pp 1051-1068
- Rayleigh L (1917) On the pressure developed in a liquid during the collapse of spherical cavity, Phil. Mag., vol 34 p 94
- Riznic J, Ishii M (1989) Bubble number density and vapor generation in flashing flow, Int. J. Heat Mass Transfer, vol 32 pp 1821-1833
- Rohatgi US, Reshotko E (1975) Non-equilibrium one dimensional flow in variable area channels. In Lahey RT and Wallis GB (eds) Non-equilibrium two phase flows, ASME, New York

- Shoji M, Zhang L and Chatpun S (April 17-21, 2005) Nucleation site interaction in pool nucleate boiling, 6<sup>th</sup> World Conference on Experimental Heat Transfer, Fluid Mechanics, and Thermodynamics, Matsushima, Miyagi, Japan
- Siegel R, Keshock EG (July 1964) Effects of reduced gravity on nucleate boiling bubble dynamics in saturated water, *AIChE Journal*, vol 10 no 4 pp 509-517
- Simoneau RJ (1975) Pressure distribution in converging diverging nozzle during two phase choked flow of subcooled nitrogen. Lahey RT and Wallis GB (eds) *Non-equilibrium two phase flows*, ASME, New York
- Skripov VP et al. (1980) Thermophysical properties of liquids in meta - stable state, Moskva - Atomisdat, in Russian
- Sultan M, Judd RL (Feb. 1978) Spatial distribution of active sites and bubble flux density, *Transactions of the ASME, Journal of Heat Transfer*, vol 100 pp 56-62
- Tolubinski IS (1980) Boiling heat transfer, Kiev, Naukova Dumka, in Russian
- Tolubinsky VI, Ostrovsky JN (1966) On the mechanism of boiling heat transfer (vapor bubbles growth rate in the process of boiling in liquids, solutions, and binary mixtures), *Int. J. Heat Mass Transfer*, vol 9 pp 1463-1470
- Volmer M (1939) *Kinetik der Phasenbildung*, Dresden und Leipzig, Verlag von Theodor Steinkopf
- Wang CH, Dhir VK (Aug. 1993) Effect of surface wettability on active nucleation site density during pool boiling of water on a vertical surface, *ASME Journal of Heat Transfer*, vol 115 pp 659-669
- Yamagata K, Hirano F, Nishikawa K, Matsuoka H (1955) Nucleate boiling of water on the horizontal heating surface, *Mem. Fac. Engng; Kyushu Univ.*, vol 15 p 97
- Zuber N (1963) Nucleate boiling: The region of isolated bubbles and the similarity with natural convection, *Int. J. Heat Mass Transfer*, vol 6 pp 53-79



## 13 Bubble growth in superheated liquid

*This review presents the achievements of the theory of bubble growth in superheated liquids. The thermally controlled bubble growth solutions are summarized and the derivation of the Mikic equation is discussed in some more details. Then the link between the solutions for the bubble growth and the mass source terms for the averaged conservation equations for two-phase flow are presented. The way to derive non-averaged mass source terms and time-averaged mass source terms is given. The effect of the steam superheating is discussed. Brief discussion of diffusion controlled bubble growth initially containing non-condensable gases is also given.*

### 13.1 Introduction

The *spontaneous flashing of superheated liquid* is associated with the *bubble growth* in the liquid. The mechanism of the *bubble growth* is described already by *Jakob* in 1932 in the following way:

"...it can be imagined that during the small explosion which starts the growth of a bubble, the interface temperature, because of the consumed heat for vaporization, drops immediately from the superheat temperature to the saturation temperature, for example from 110°C to 100°C. As a consequence of the heat transfer from the liquid to the vapor bubble the liquid envelope is being cooled progressively from the inside toward the outer boundary; a temperature boundary layer is created with a constantly decreasing temperature drop. This thermal boundary layer increases in thickness until the thermal wave, which advances from the vapor bubble interface into the liquid, has reached the outer limit of the hydrodynamics boundary layer. The decrease in thickness of the hydrodynamics boundary layer because of the evaporation at the interface is, initially, a small fraction of the total thickness..."

The rigorous mathematical description of the processes in a system of spherical coordinates with the origin equivalent with the center of the mass of the nucleation site, needs the solution of a system of mass, momentum, and energy conservation equations for the corresponding initial and boundary conditions, see by *Nigmatulin* (1978), *Beylich* (1991) among others. An important result of such a solution is the *bubble radius as a function of time* and of the local thermodynamic parameters describing the non-equilibrium of the mixture. A general analytical solution of these problems is not known to the author. For practical applications

there are several approximate solutions obtained under different simplifying assumptions. The most successful compromise between strict formulation and sound simplifying assumption was made by *Mikic et al.* (1970). In what follows we present the arguments used by *Mikic*.

### 13.2 The thermally controlled bubble growth

Consider infinite liquid with temperature  $T_2$  which is superheated with respect to the saturation temperature by the system pressure  $p$ , i.e.

$$T_2 > T'(p). \quad (13.1)$$

The liquid side bubble interface temperature is  $T_2^{l\sigma}$ .

$$T_2^{l\sigma} < T_2, \quad (13.2)$$

Due to the intensive steam production from the bubble surface and the fact that vapor sound velocity is larger than the bubble interface velocity, it can be assumed that the pressure inside the bubble is uniform and that the *vapor temperature in the bubble is equal to the surface temperature*

$$T_1 = T_2^{l\sigma}. \quad (13.3)$$

The pressure inside the bubble can be assumed to be the saturation pressure at the vapor temperature and therefore

$$p'(T_1) = p'(T_2^{l\sigma}). \quad (13.4)$$

The change of the bubble mass with the time is equal to the mass evaporating from the surface per unit time, i.e.

$$\frac{d}{d\tau} \left( \frac{4}{3} \pi R_1^3 \rho_1 \right) = 4\pi R_1^2 (\rho w)_{21}, \quad (13.5)$$

see *Bosnjakovic* (1930). This is the vapor mass conservation equation. Here  $(\rho w)_{21}$  is the mass flow rate from the surface into the bubble. This equation is used in the literature in different forms e.g.

$$\frac{1}{3} \frac{d}{d\tau} \left[ \left( R_1 \rho_1^{1/3} \right)^3 \right] = R_1^2 (\rho w)_{21} \quad (13.6)$$

or

$$\frac{d}{d\tau} \left[ \left( R_1 \rho_1^{1/3} \right) \right] = (\rho w)_{21} / \rho_1^{2/3} \quad (13.7)$$

or in integrated form

$$R_1 = (\rho_{10} / \rho_1)^{1/3} R_{10} \left\{ 1 + \frac{1}{R_{10} \rho_{10}} \int_0^{\Delta \tau} [(\rho w)_{21} / \rho_1^{2/3}] d\tau \right\}, \quad (13.8)$$

which is appropriate to take into account the density change with the time, or

$$\frac{dR_1}{d\tau} = (\rho w)_{21} / \rho_1 - \frac{R_1}{3\rho_1} \frac{d\rho_1}{d\tau}. \quad (13.9)$$

The enthalpy of the liquid experiencing evaporation before crossing the interface is  $h'(T_2^{1\sigma})$  and after crossing the interface  $h''(T_2^{1\sigma})$ . Thus the energy jump condition at the interface, assuming no heat transfer between the bubble and the interface,  $\dot{q}_1^{n2\sigma} = 0$ , is

$$(\rho w)_{21} [h''(T_2^{1\sigma}) - h'(T_2^{1\sigma})] = -\dot{q}_2^{n1\sigma}. \quad (13.10)$$

Solving with respect to the evaporation mass flow rate and substituting into the mass conservation equation (13.9) we obtain

$$\frac{dR_1}{d\tau} = -\dot{q}_2^{n1\sigma} / \left\{ \rho_1 [h''(T_2^{1\sigma}) - h'(T_2^{1\sigma})] \right\} - \frac{R_1}{3\rho_1} \frac{d\rho_1}{d\tau} \quad (13.11)$$

The heat transferred from the superheated bulk liquid to the surface is controlled by the *Fourier* equation, in spherical coordinates (see *J. Fourier*, (1822))

$$\frac{\partial T}{\partial \tau} = -a_2 \frac{1}{r^2} \frac{\partial}{\partial r} \left( r^2 \frac{\partial T}{\partial r} \right) \quad (13.12)$$

solved for the initial and boundary conditions

$$\tau = 0, \quad r = R_1, \quad T = T_2^{1\sigma}, \quad (13.13)$$

$$\tau = 0, \quad r > R_1, \quad T = T_2, \quad (13.14)$$

$$r = R_1, \quad T = T_2^{1\sigma}, \quad (13.15)$$

$$r = \infty, \quad T = T_2. \quad (13.16)$$

The text book solution for *thin thermal boundary layer*, *Carlsow and Jaeger* (1959), is used to compute the temperature gradient at the bubble surface and to compute the resulting heat flux as a function of time

$$\begin{aligned} \dot{q}_{i2}'' &= -\lambda_2 \frac{\partial T}{\partial r} \Big|_{r=R_1} = -\rho_2 c_{p2} (T_2 - T_2^{1\sigma}) \sqrt{\frac{3a_2}{\pi\tau}} \\ &= -\rho_2 c_{p2} [T_2 - T'(p)] \sqrt{\frac{3a_2}{\pi\tau}} \left[ 1 - \frac{T_2^{1\sigma} - T'(p)}{T_2 - T'(p)} \right]. \end{aligned} \quad (13.17)$$

Usually the so obtained heat flux is substituted in Eq. (13.11) and the resulting equation is rewritten in the form

$$\frac{dR_1}{d\tau} = \frac{1}{2} \frac{B}{\sqrt{\tau}} \left[ 1 - \frac{T_2^{1\sigma} - T'(p)}{T_2 - T'(p)} \right] - \frac{R_1}{3\rho_1} \frac{d\rho_1}{d\tau} \quad (13.18)$$

where

$$B = Ja \sqrt{\frac{12a_2}{\pi}}. \quad (13.19)$$

The group

$$Ja = \frac{\rho_2 c_{p2} [T_2 - T'(p)]}{\rho_{10} [h''(T_2^{1\sigma}) - h'(T_2^{1\sigma})]} \quad (13.20)$$

is named *Jakob* number in honor of the German scientist considering for the first time this problem in Jakob (1932). *Fritz* and *Ende* obtained in 1936 Eq. (13.18) for  $\rho_1 \approx \text{const}$  and plane geometry. For processes with dramatic pressure change the vapor compressibility is important and  $d\rho_1/d\tau$  cannot be neglected. Equation (13.18) controls the bubble growth if the surface temperature  $T_2^{1\sigma}$  is known. If the surface temperature is assumed to be saturation temperature at the system pressure

$$T_2^{1\sigma} = T'(p), \quad (13.21)$$

the obtained solution for  $\rho_1 \approx \text{const}$  is the so called thermally controlled bubble growth solution obtained by *Plesset* and *Zwick* in 1954

$$\frac{dR_1}{d\tau} = \frac{1}{2} \frac{B}{\sqrt{\tau}}. \quad (13.22)$$

There are several authors contributing to this topic. Their results are summarized in Appendix 13.1.

### 13.3 The *Mikic* solution

Note that in accordance with the assumption that the pressure inside the bubble is equal to the saturation pressure as a function of the interface temperature, there is no pressure difference between bubble and environment, which is not true. Improved solution can be obtained if one allows a surface temperature different from the saturation temperature at the system pressure. In this case one needs one more equation to close the description. *Mikic* uses the following way: The mass conservation equation of the liquid can be approximated by



$$\frac{1}{r^2} \frac{\partial}{\partial r} (r^2 u_2) \approx 0, \quad (13.23)$$

or integrating with the boundary condition

$$r = R_1, \quad u_2 = \frac{\partial R_1}{\partial \tau}, \quad (13.24)$$

$$u_2 = \text{const} / r^2 = \frac{\partial R_1}{\partial \tau} (R_1 / r)^2. \quad (13.25)$$

It gives the liquid velocity as a function of the radius if the liquid were incompressible during the bubble expansion. During the bubble growth the work performed by the bubble expansion

$$4\pi \int_0^{R_1} (p_1 - p) r^2 dr \approx \frac{4}{3} \pi R_1^3 (1 - \frac{\rho''}{\rho_2}) (p_1 - p), \quad (13.26)$$

is transferred in total kinetic energy of the liquid environment

$$\begin{aligned} \int_{R_1}^{\infty} \frac{1}{2} \rho_2 u_2^2 dVol_2 &= \frac{1}{2} \rho_2 \left( \frac{dR_1}{d\tau} \right)^2 R_1^4 4\pi \int_{R_1}^{\infty} \frac{dr}{r^2} = 2\pi \rho_2 \left( \frac{dR_1}{d\tau} \right)^2 R_1^4 \int_{R_1}^{\infty} d\left(-\frac{1}{r}\right) \\ &= 2\pi \rho_2 \left( \frac{dR_1}{d\tau} \right)^2 R_1^3, \end{aligned}$$

i.e.

$$\left( \frac{dR_1}{d\tau} \right)^2 = \frac{2}{3} \left( 1 - \frac{\rho''}{\rho_2} \right) (p_1 - p) / \rho_2 = \frac{2}{3} \left( 1 - \frac{\rho''}{\rho_2} \right) (p'(T_2^{1\sigma}) - p) / \rho_2 = \frac{2}{3} \frac{2\sigma}{R_{lc}} / \rho_2, \quad (13.27)$$

which is the second needed equation. The constant  $2/3$  valid for bubble growth in a bulk liquid should be replaced by  $\pi/7$  if a spherical bubble growing on a flat surface is considered. In fact this is the mechanical energy conservation equation. If one assumes that the interface temperature is equal to the liquid temperature

$$T_2^{1\sigma} = T_2, \quad (13.28)$$

and therefore the bubble pressure is the saturation pressure at the liquid temperature the above equation describes alone the bubble growth. This is the limiting case giving the fastest bubble growth with the liquid superheating. This solution is named inertially controlled solution and was obtained for the first time by *Besand* (1859) and in the above described more elegant way by *Rayleigh* (1917) for  $\rho'' / \rho_2 = 0$ . The solution is valid within the first  $10^{-8}$  s of the life of the bubble.

In reality the bubble in a superheated liquid behaves between the both above described limiting mechanisms, so the bubble growth is governed by the equations (13.22) and (13.27) simultaneously. To transfer the pressure difference

$p'(T_2^{1\sigma}) - p$  in the last equation into a temperature difference  $T_2^{1\sigma} - T'(p)$  one can use the linearized equation of *Clausius* and *Clapeyron*

$$\frac{p'(T_2^{1\sigma}) - p}{T_2^{1\sigma} - T'(p)} = \left( \frac{dp}{dT} \right)_{sat}, \quad (13.29)$$

where

$$\left( \frac{dp}{dT} \right)_{sat} = \frac{1}{T'(p)} \frac{h''(p) - h'(p)}{v''(p) - v'(p)}, \quad (13.30)$$

or

$$[p'(T_2^{1\sigma}) - p] / \rho_2 = [T_2^{1\sigma} - T'(p)] \frac{1}{\rho_2} \left( \frac{dp}{dT} \right)_{sat}. \quad (13.31)$$

The result is

$$\begin{aligned} \left( \frac{dR_1}{d\tau} \right)^2 &= \frac{2}{3} \left( 1 - \frac{\rho''}{\rho_2} \right) [T_2^{1\sigma} - T'(p)] \frac{1}{\rho_2} \left( \frac{dp}{dT} \right)_{sat} \\ &= \frac{2}{3} \frac{1}{\rho_2} \left( \frac{dp}{dT} \right)_{sat} \left( 1 - \frac{\rho''}{\rho_2} \right) [T_2 - T'(p)] \frac{T_2^{1\sigma} - T'(p)}{T_2 - T'(p)} \end{aligned} \quad (13.32)$$

or

$$\left( \frac{dR_1}{d\tau} \right)^2 = A^2 \frac{T_2^{1\sigma} - T'(p)}{T_2 - T'(p)}, \quad (13.33)$$

where

$$A^2 = \frac{2}{3} \frac{1}{\rho_2} \left( \frac{dp}{dT} \right)_{sat} \left( 1 - \frac{\rho''}{\rho_2} \right) [T_2 - T'(p)]. \quad (13.34)$$

Eliminating the temperature difference from the both equations, Eqs. (13.22) and (13.33), *Mikic* et al. obtained the following final form of the equation describing best the available experimental data

$$\frac{1}{A^2} \left( \frac{dR_1}{d\tau} \right)^2 + \frac{2\sqrt{\tau}}{B} \frac{dR_1}{d\tau} - 1 + \frac{2\sqrt{\tau}}{B} \frac{R_1}{3\rho_1} \frac{d\rho_1}{d\tau} = 0, \quad (13.35)$$

or after solving for  $dR_1 / d\tau$  and substituting  $(dR_1 / d\tau) / A = dR_1^+ / d\tau^+$

$$\frac{dR_1^+}{d\tau^+} = \left( \tau^+ + 1 - \frac{2}{3} R_1^+ \frac{\tau_1^{+1/2}}{\rho_1^+} \frac{d\rho_1^+}{d\tau^+} \right)^{1/2} - (\tau^+)^{1/2}, \quad (13.36)$$

where

$$R^+ = AR_1 / B^2, \quad (13.37)$$

$$\tau^+ = A^2 \tau / B^2. \quad (13.38)$$

Substituting the time derivative of the bubble radius from Eq. (13.36) into Eq. (13.33) we compute the surface temperature

$$T_2^{1\sigma} = T'(p) + [T_2 - T'(p)] \left[ \left( \tau^+ + 1 - \frac{2}{3} R_1^+ \frac{\tau_1^{+1/2}}{\rho_1^+} \frac{d\rho_1^+}{d\tau^+} \right)^{1/2} - (\tau^+)^{1/2} \right]^2 \quad (13.39)$$

which is necessary to compute the enthalpies of the transferred mass before and after crossing the interface.

Integrating the equation (13.35) for  $R_1^+ = R_{1o}$  at  $\tau^+ = 0$ , and  $\rho_1 = \text{const}$ , Mikic et al. obtained the general bubble growth relation

$$R_1^+ - R_{1o}^+ = \frac{2}{3} \left[ (\tau^+ + 1)^{3/2} - (\tau^+)^{3/2} - 1 \right], \quad (13.40)$$

which for  $\tau^+ \ll 1$  simplifies to the *Rayleigh* solution, and for  $\tau^+ \gg 1$  to the thermally controlled bubble growth solution.

The validity of the Eq. (13.40) is confirmed experimentally by *Lien and Griffith* (1969) for superheated water over the pressure range 0.0012 to 0.038 MPa, superheating range 8 to 15 K, and  $58 \leq Ja \leq 2690$ . The comparison with experimental data made by *Tolubinskii* (1980) shows that in a earlier stadium of the bubble growth  $\tau^+ < 10^{-3}$  ( $\tau \leq 10^{-8}$  s) the bubble growth is inertially dominated. For  $\tau^+ > 10^{-3}$  the *Mikic et al.* solution is the best one. For the time  $\tau^+ > 10$  all of the heat diffusion controlled solutions tend to the asymptotic solution, the so called thermally controlled bubble growth.

*Olek et al.* (1990) obtained a general counterpart solution to that of *Mikic et al.* (1970) using the hyperbolic heat conduction equation, instead of the classical *Fourier* (parabolic) equation. The new solution is important for bubble growth in fluids like Helium II.

## 13.4 How to compute the mass source terms for the averaged conservation equations?

### 13.4.1 Non-averaged mass source terms

In what follows we show how to link the results obtained in the previous chapter with the macroscopic flow description from Volume 1 of this monograph.

The evaporated mass per unit mixture volume and unit time is equal to the product of the number of the bubbles per unit mixture volume and the mass change of a single bubble. Therefore

$$\mu_{21} = \rho''(T_2^{1\sigma}) n_1 dV_1 / d\tau = \rho''(T_2^{1\sigma}) n_1 4\pi R_1^2 dR_1 / d\tau, \quad (13.41)$$

or replacing

$$R_1 = \left( \frac{3}{4\pi} \frac{\alpha_1}{n_1} \right)^{1/3}, \quad (13.42)$$

$$\mu_{21} = 3^{1/3} (4\pi)^{2/3} \rho''(T_2^{1\sigma}) n_1^{2/3} \alpha_1^{1/3} R_1 dR_1 / d\tau. \quad (13.43)$$

Replacing  $dR_1 / d\tau$  with one of the expressions from Appendix 13.1 we have for the non-averaged mass source term for the thermally controlled bubble growth

$$\mu_{21} = C \rho''(T_2^{1\sigma}) n_1^{2/3} \alpha_1^{1/3} B^2 = C \rho''(T_2^{1\sigma}) n_1^{2/3} \alpha_1^{1/3} \left( \frac{B}{Ja} \right)^2 \left[ \frac{\rho_2 c_{p2}}{\rho''(h'' - h')} \right]^2 [T_2 - T'(p)]^2, \quad (13.44)$$

with constant  $C$  ranging from 2.2 to 14.89. It is very interesting to note that the evaporation source term depends on the void fraction, on the bubble number density, on the liquid temperature, and on the system pressure. All of these values change during a single time interval.

The heat taken away from the liquid and used for the evaporation per unit mixture volume and unit time is

$$\dot{q}_2^{m1\sigma} = -\mu_{21} [h''(T_2^{1\sigma}) - h'(T_2^{1\sigma})], \quad (13.45)$$

or for the thermally controlled bubble growth

$$\dot{q}_2^{m1\sigma} = -const \ n_1^{2/3} \alpha_1^{1/3} \frac{\rho_2 c_{p2} \lambda_2}{\rho''(h'' - h')} [T_2 - T'(p)]^2. \quad (13.46)$$

We see that it is nearly proportional to the square root of the difference between the liquid temperature and the saturation temperature. This is the non-averaged energy source term. The use of the non-averaged source terms is justified for time steps considerably smaller than the characteristic time interval needed to reach the equilibrium. Otherwise the averaged source terms have to be used. Further we discuss how to compute the averaged source terms.

### 13.4.2 The averaged mass source terms

For a constant number of bubbles during the time step, the *volume difference* between the end and the beginning of the time step, *multiplied* by the *steam density*

and the *bubble number per unit mixture volume*, gives the *integral mass evaporating* during the considered time step per unit mixture volume. Dividing this mass by the time step we obtain the averaged mass source term

$$\mu_{21} = \rho'' n_{10} V_1 / \Delta \tau, \quad \alpha_1 = 0, \quad (13.47)$$

for the first integration step when the bubble growth just starts and

$$\mu_{21} = n_{10} \frac{\rho_1 V_1 - \rho_{10} V_{10}}{\Delta \tau} = \frac{\rho_{10} n_{10} V_{10}}{\Delta \tau} \left( \frac{\rho_1 V_1}{\rho_{10} V_{10}} - 1 \right) = \frac{\rho_{10} \alpha_{10}}{\Delta \tau} \left[ \frac{\rho_1}{\rho_{10}} \left( \frac{R_1}{R_{10}} \right)^3 - 1 \right], \quad \alpha_1 > 0 \quad (13.48)$$

for the next time steps. Using Eq. (13.40) we obtain for  $\alpha_{1a} = 0$

$$\mu_{21} = \frac{\rho'' n_{10}}{\Delta \tau} \left( \frac{4}{3} \pi R_1^3 \right) = \frac{\rho'' n_{10}}{\Delta \tau} \frac{4}{3} \pi \left\{ \frac{B^2}{A} \frac{2}{3} \left[ (\tau^+ + 1)^{3/2} - (\tau^+)^{3/2} - 1 \right] \right\}^3 \quad (13.49)$$

and for  $\alpha_{1a} > 0$

$$\mu_{21} = \frac{\rho'' \alpha_{10}}{\Delta \tau} \left[ \left\{ 1 + \frac{2}{3} \left[ (\tau^+ + 1)^{3/2} - (\tau^+)^{3/2} - 1 \right] / R_{10}^+ \right\}^3 - 1 \right] \quad (13.50)$$

where

$$\tau^+ = \frac{\Delta \tau}{B^2 / A^2}. \quad (13.51)$$

For the thermally controlled bubble growth the third power of the radii ratio reduces to

$$\left( \frac{R_1}{R_{10}} \right)^3 = \left[ 1 + (\Delta \tau / \tau^*)^{1/2} \right]^3. \quad (13.52)$$

The time interval measured from the beginning of the bubble growth to the beginning of the time step can easily be calculated

$$\tau^* = (R_{10} / B)^2 = \left[ \left( \frac{3 \alpha_{10}}{4 \pi n_{10}} \right)^{1/3} / B \right]^2. \quad (13.53)$$

Having in mind, that for the spontaneous evaporation  $\mu_{12} = 0$  and  $\dot{q}_1^{n2\sigma} = 0$ , we obtain the corresponding energy source term from the energy jump condition on the bubble surface, i.e. Eq. (13.45).

### 13.5 Superheated steam

The above derived formalism is strictly valid if the bubble surface temperature is equal to the gas temperature  $T_1$ ,

$$T_2^{1\sigma} = T_1. \quad (13.54)$$

In the following we denote the evaporation rate for this case with  $\mu'_{21}$ . In general it is possible to have superheated or subcooled steam with respect to the surface temperature due to the history of the gas - liquid mixing process. In such cases there is a small amount of heat transferred from the bubble to the surface if  $T_1 > T_2^{1\sigma}$  or from the surface to the bubble, if  $T_1 < T_2^{1\sigma}$ , due to a mechanism similar to natural convection inside the cavity. In this case the above theory should be revised. An approximate correction of the theory can be introduced as follows:

$$\dot{q}_2^{m1\sigma} = -\mu'_{21} [h''(T_2^{1\sigma}) - h'(T_2^{1\sigma})], \quad (13.55)$$

$$\mu_{12} = 0, \quad (13.56)$$

$$\dot{q}_1^{m2\sigma} = a_{21} h_{NC} (T_2^{1\sigma} - T_1) \quad (13.57)$$

$$\mu_{21} = \mu'_{21} - \dot{q}_1^{m2\sigma} / [h''(T_2^{1\sigma}) - h'(T_2^{1\sigma})], \quad (13.58)$$

where the heat transfer coefficient due to natural e.g. convection in a cavity is

$$h_{NC} = \text{const} \frac{\lambda_1}{D_1} (Gr_1 Pr_1)^m, \quad (13.59)$$

$$Gr_1 = g |\rho_1 - \rho_1''(T_2^{1\sigma})| \rho_1 D_1^3 / \eta_1^2, \quad (13.60)$$

$$Pr_1 = \eta_1 c_{p1} / \lambda_1, \quad (13.61)$$

$$\text{const} \approx 0.59 \div 0.9, \quad (13.62)$$

$$m \approx 1/4. \quad (13.63)$$

The second term in Eq. (13.58) is usually neglected as very small compared to the first one. This term becomes important only for mass transfer processes on the bubble surface in saturated or nearly saturated liquid.

### 13.6 Diffusion controlled evaporation into mixture of gases inside the bubble

Consider a bubble consisting of a mixture of vapor and non-condensable gases. The partial pressure of the vapor is  $p_{M1}$ . If the interface pressure  $p'(T_2)$  is larger than the partial vapor pressure there is an evaporation mass flux from the interface into the bubble. The emitted steam molecules from the surface enter the boundary layer of the bubble by diffusion. The non-averaged instantaneous mass source term is

$$\begin{aligned}\mu_{21} &= a_{21}(\rho w)_{21} = -a_{12}\beta \frac{C_{M1}\rho_1}{p_{M1}}[p_{M1} - p'(T_2)] \\ &= -a_{21}\alpha_c \frac{M_{M1}}{M_1} \ln \frac{p - p'(T_2)}{\sum p_{n1}} / (c_{p1} Le^{2/3}) \text{ see in VDI-Waermeatlas (1984)}\end{aligned}\quad (13.64)$$

where

$$\beta = \frac{p_{M1}}{C_{M1}\rho_1[p'(T_2) - p_{M1}]} \alpha_c \frac{M_{M1}}{M_1} \ln \frac{p - p'(T_2)}{\sum p_{n1}} / (c_{p1} Le^{2/3}), \quad (13.65)$$

$$p_{M1} < p'(T_2) < p, \quad (13.66)$$

$$Le_1 = \lambda_1 / (\rho_1 c_{p1} D_{M \rightarrow \sum n}) \quad (13.67)$$

$$M_1 = \frac{\sum p_{n1}}{p} \sum M_{n1} + \frac{p - \sum p_{n1}}{p} M_{M1} \quad (13.68)$$

$$(\sum M_{n1} = 28.96 \text{ kg for air, } M_{M1} = 18.96 \text{ kg for water steam}) \quad (13.69)$$

$p'$  is the partial pressure of the steam in the boundary layer, where the steam is supposed to be saturated at a temperature nearly equal to the liquid temperature

$$p' = p'(T_2). \quad (13.70)$$

During the evaporation the liquid is cooled by

$$\dot{q}_2^{m1\sigma} = -\mu_{21}(h'' - h_{M2}). \quad (13.71)$$

Because this process is relatively slow in most of the practical cases averaging in the time steps of the source terms is not necessary.

## 13.7 Conclusions

1. After the origination of bubbles with stable bubble size the evaporation of the superheated liquids is controlled by the bubble growth. The bubble growth is over a very short time controlled by the inertia and is well described by the *Besand* and *Rayleigh* solution. For the time after the inertia-controlled period the thermally controlled bubble growth controls the evaporation. From nine known models for this region the model by *Mikic* is recommended. The *Mikic* model interpolates properly between inertia controlled and thermally controlled regions.
2. Thermally controlled bubble growth at heated walls is described by modifying the solutions for thermally controlled bubble growth in the bulk.
3. Evaporation processes are the driving forces for pressure excursions. The pressure change has an important feedback on the bubble growth by changing the driving temperature difference controlling the energy transfer between the bulk and the interface. For pressure change with semi-constant pressure change velocity over a given time step the bubble growth is best approximated by the solution of *Jones* and *Zuber*.

### Appendix 13.1 Radius of a single bubble in a superheated liquid as a function of time

---

Thermally controlled bubble growth:  $\frac{dR_1}{d\tau} = \frac{1}{2} \frac{B}{\sqrt{\tau}}$ ,  $R_1 = B\sqrt{\tau}$ ,  $R_1 \frac{dR_1}{d\tau} = B^2 / 2$

where  $Ja = \frac{\rho_2 c_{p2} (T_2 - T')}{\rho'' (h'' - h')}$ ,  $a_2 = \frac{\lambda_2}{\rho_2 c_{p2}}$  and  $B$  is given below.

---

*Bosnjakovic* (1930), *Fritz* and *Ende* (1936) for plane geometry:

$$B = Ja \sqrt{\frac{4a_2}{\pi}}.$$

*Plesset* and *Zwick* (1954) for  $Ja < 100$ :

$$B = Ja \sqrt{\frac{12a_2}{\pi}}.$$

*Foster* and *Zuber* (1954), *Dergarabedian* see in *Tolubinskii* (1980) for  $Ja < 100$ :

$$B = Ja \sqrt{\pi a_2}.$$



*Labuntsov* et al. (1964) approximate the analytical solution obtained by *Scriven* (1959) for bubble growth in uniformly heated liquid with an error of 2%

$$B = Ja \sqrt{\frac{12a_2}{\pi}} \left[ 1 + \frac{1}{2} \left( \frac{\pi}{6Ja} \right)^{2/3} + \frac{\pi}{6Ja} \right]^{1/2}.$$

The *Labuntsov* approximation give close results to the *Foster* and *Zuber* (1954) solution.

*Olek* et al. (1990):

$$B = \sqrt{\frac{a_2}{\pi}} Ja \left[ 1 + \left( 1 + \frac{2\pi}{Ja} \right)^{1/2} \right].$$

*Cole* and *Schulman* (1966):

$$B = Ja \sqrt{\frac{\pi a_2}{4}}.$$

*Cooper* - see in wang (1969) for H<sub>2</sub>O:

$$B = 1.57 Ja \sqrt{\frac{a_2}{Pr_2}}.$$

*Mikic* and *Rohsenow* (1969)

$$B = 0.83 Ja \sqrt{\pi a_2}.$$

*Prisnjakov* (1970) for  $Ja < 500$ :

$$B = Ja \sqrt{\frac{16a_2}{9\pi}}.$$

Bubble growth at heated wall: no complete analytical description, empirical correlations recommended for practical use.

*Jagov* (1971)

$$B = \left( \gamma Ja + \sqrt{\gamma^2 Ja^2 + 2\beta a_2 Ja} \right) a_2^{1/2},$$

$\gamma = 0.3$ ,  $\beta = 6$ , valid for  $10^{-1} < Ja < 1000$ . For  $Ja \ll 1$ , high pressure, the *Jagov*'s expressions is equivalent with the *Labuntsov* et al. result from (1964), validated for water boiling at silver surface at  $p = 1$  to 100 bar.

$$B = \sqrt{2\beta a_2 Ja},$$

where

$$\beta = \frac{2(\cos \frac{\theta}{2}) \ln(\delta_v / \delta_m)}{(1 + \cos \theta)^2 (2 - \cos \theta)} \approx \frac{25.3 \cos(\theta/2)}{(1 + \cos \theta)^2 (2 - \cos \theta)},$$

$\theta \approx \pi 35/180$ ,  $\delta_m \approx 10^{-9}$  to  $10^{-10} m$ , is the averaged distance between the liquid molecules, and  $\delta_v \approx 10^{-4} m$  is the thickness of viscous boundary layer of the boiling surface.  $\beta \approx 5.6$  to  $6.7$ ,  $\beta = 6$  recommended. For  $Ja \gg 1$ , high pressure, the *Jagov's* expression tends to  $B = 2\gamma Ja a_2^{1/2}$  characteristic for bubble growth in bulk liquid.

*Piening* (1971) for  $8 \times 10^{-2} < Ja < 500$ :

$$B = \sqrt{a_2 Ja}.$$

*Kutateladze* (1982) p.120 for bubble growth at heated wall:

$$B \approx \text{const} \sqrt{a_2 Ja}.$$

*Hutcherson et al.* (1983):

$$B = \sqrt{12 a_2 Ja / \pi}.$$

*Wang* (1989) for  $p \neq \text{const}$ :

$$R_1 = (\rho_{10} / \rho_1)^{1/3} R_{10} \left[ 1 + \frac{1}{R_{10} \rho_{10}} \int_0^{\Delta \tau} [(\rho w)_{21} / \rho_1^{2/3}] d\tau \right],$$

where

$$(\rho w)_{21, \text{wall}} = \beta (\rho w)_{21, \text{inf init liquid see}},$$

$$\beta = \frac{2(1 + \cos \theta) + \sin^2 \theta}{2 + \cos \theta (2 + \sin^2 \theta)}, \quad \theta = 1.05 \text{ to } 1.31 \text{ rad}.$$

*Cole and Shulman* (1966):

$$B = \frac{5}{2} Ja^{3/4} \sqrt{a_2}.$$

*Galim and Kirilov* (1987)

$$B = \sqrt{2\beta a_2 Ja \varphi(Ja) \psi \left( \sqrt{\frac{\lambda_w \rho_w c_{pw}}{\lambda_2 \rho_2 c_{p2}}} \right)}, \quad \varphi(Ja) = 1 + \frac{\gamma^2}{\beta} Ja + \frac{\gamma}{\beta} \sqrt{2\beta Ja + \gamma Ja^2},$$

$\beta = 6$ ,  $\gamma = 0.3$ ,  $\psi$  unknown.

Jones and Zuber (1978), Kroshilin et al. (1986) for  $p \neq \text{const}$  in uniformly heated liquid

The heat flux at the bubble surface  $\dot{q}_2^{n1\sigma}$  is computed using the *Carlsow* and *Jaeger* (1959) solution of the *Fourier* equation for heat slab with variable temperature difference at the one boundary

$$T_2 = \text{const}, \quad \Delta T(\tau) = T_2 - T_2^{1\sigma}(\tau), \quad \Delta T(0) = T_2 - T'(p_0),$$

$$\dot{q}_2^{n1\sigma} = -k_s \frac{\lambda_2}{\sqrt{\pi a_2}} \left[ \frac{\Delta T(0)}{\sqrt{\tau}} + \int_0^\tau \frac{\Delta T(\eta)}{\sqrt{\tau - \eta}} d\eta \right]$$

$k_s$  is the sphericity correction =  $\pi/2$  for *Foster - Zuber*,  $\sqrt{3}$  for *Plesset - Zwick*. For linear pressure decrease during the time step  $\Delta\tau$ ,

$$\Delta T(\eta) = b\eta,$$

where

$$b = - \left( \frac{dT}{dp} \right)_{\text{sat}} \frac{dp}{d\tau} = - \left( \frac{dT}{dp} \right)_{\text{sat}} \frac{p - p_a}{\Delta\tau},$$

the heat flux is

$$\dot{q}_2^{n1\sigma} = - \frac{k_s}{\sqrt{\pi}} \sqrt{\lambda_2 \rho_2 c_{p2}} \left[ \frac{\Delta T(0)}{\sqrt{\tau}} + \frac{4}{3} b \tau^{3/2} \right].$$

Neglecting the expression containing the density change and substituting into the mass transport equations with

$$(\rho w)_{21} = -\dot{q}_2^{n1\sigma} / (h'' - h').$$

we obtain

$$\frac{R_1}{R_{10}} = 1 + \frac{k_s}{\sqrt{\pi}} \frac{1}{\rho_1 (h'' - h') R_{10}} \sqrt{\lambda_2 \rho_2 c_{p2}} \int_0^{\Delta\tau} \left[ \frac{\Delta T(0)}{\sqrt{\tau}} + \frac{4}{3} b \tau^{3/2} \right] d\tau.$$

After the integration the result is

$$\frac{R_1}{R_{10}} = 1 + \frac{2k_s}{\sqrt{\pi}} \frac{1}{\rho_1 (h'' - h') R_{10}} \sqrt{\lambda_2 \rho_2 c_{p2}} \left( \Delta\tau^{1/2} + \frac{4}{15} b \Delta\tau^{5/2} \right).$$

The equation rewritten in dimensionless form is

$$R_1 = R_{10} \left[ 1 + \frac{2k_s}{\sqrt{\pi}} \left( Ja_T Fo^{1/2} + \frac{4}{15} \frac{R_{10}^2}{a_2} Ja_p Fo^{5/2} \right) \right],$$

where

$$Ja_T = \frac{\rho_2 c_{p2}}{\rho_{10} (h'' - h')} [T_2 - T'(p_0)],$$

$$Ja_p = b \frac{\rho_2 c_{p2}}{\rho_{10} (h'' - h')} \frac{R_{10}^2}{a_2},$$

$$Fo = a_2 \tau / R_{10}^2.$$

The result obtained by *Jones* and *Zuber* is slightly different

$$R_1 = (\rho_{10} / \rho_1)^{1/3} R_{10} \left\{ 1 + \frac{2k_s}{\sqrt{\pi}} \left[ Ja_T Fo^{1/2} + \frac{2}{3} Ja_p Fo^{3/2} \right] \right\}.$$

The time-averaged evaporation mass per unit time and unit mixture volume is therefore

$$\mu_{21} = \frac{\rho_{10} \alpha_{10}}{\Delta \tau} \left\{ \left\{ 1 + \frac{2k_s}{\sqrt{\pi}} \left[ Ja_T Fo^{1/2} + \frac{2}{3} Ja_p Fo^{3/2} \right] \right\}^3 - 1 \right\} \quad \text{for } \alpha_1 > 0$$

---

Inertia controlled bubble growth,  $\Delta \tau \leq 10^{-8}$  s, *Besand* (1859), *Rayleigh* (1917).

---

$$\frac{dR_1}{d\tau} = \left\{ \frac{2}{3} [p'(T_2) - p] / \rho_2 \right\}^{1/2} = \left\{ \frac{2}{3} \frac{1}{\rho_2} \left( \frac{dp}{dT} \right)_{sat} [T_2 - T'(p)] \right\}^{1/2}$$

$$R_1 = \left\{ \frac{2}{3} \frac{1}{\rho_2} \left( \frac{dp}{dT} \right)_{sat} [T_2 - T'(p)] \right\}^{1/2} \tau$$

---

Inertia and thermal controlled bubble growth, *Mikic* et al. (1970):

---

$$R_1^+ - R_{10}^+ = \frac{2}{3} \left[ (\tau^+ + 1)^{3/2} - \tau^{+3/2} - 1 \right]$$

where

$$R_1^+ = R_1 (B^2 / A), \quad \tau^+ = \frac{\tau}{B^2 / A^2}$$

$$Ja = \frac{\rho_2 c_{p2} [T_2 - T'(p)]}{\rho_1 [h''(T_2^{1\sigma}) - h'(T_2^{1\sigma})]}, \quad B = \left( \frac{12}{\pi} a_2 \right)^{1/2} Ja$$

$$A^2 = c \frac{1}{\rho_2} \left( \frac{dp}{dT} \right)_{sat} [T_2 - T'(p)],$$

$$\left( \frac{dp}{dT} \right)_{sat} = \frac{1}{T'(p)} \frac{h''(p) - h'(p)}{v''(p) - v'(p)}$$

$c = 2/3$  for bubble growth in infinite continuum,

$c = \pi/7$  for bubble growth on a wall surface.

Instantaneous mass transfer per unit time and unit mixture volume:

$$\mu_{21} = (36\pi)^{1/3} n_1^{1/3} \alpha_1^{2/3} \rho'' A \left[ (\tau^+ + 1)^{1/2} - (\tau^+)^{1/2} \right].$$

## Nomenclature

### Latin

$a$	liquid thermal diffusivity, $m^2/s$
$a_{21}$	interfacial area density between the liquid 2 and the vapor 1, $1/m$
$C$	mass concentration, $kg/kg$
$c_p$	specific heat at constant pressure, $J/(kgK)$
$D_{M \rightarrow \sum n}$	diffusion constant for the species $M$ into the mixture $\sum n$ , $1/m$
$D_{cav}$	equivalent cavity size, $m$
$D_h$	hydraulic diameter, $m$
$D_{1,n}$	bubble diameter belonging to $n$ -th bubble generation, $m$
$D_{1c}$	critical bubble diameter, $m$
$D_{1d}$	bubble departure diameter, $m$
$d$	differential, <i>dimensionless</i>
$F_1 / Vol$	cross section at the wall surface covered by attached bubbles per unit flow volume, $1/m$
$g$	gravitational acceleration, $m/s^2$
$Ja$	$= \frac{\rho_2 c_{p2} [T_2 - T'(p)]}{\rho_{10} [h''(T_2^{1\sigma}) - h'(T_2^{1\sigma})]},$ Jakob number, <i>dimensionless</i>
$G^*$	critical mass flow rate, $kg/(m^2s)$
$Gb_2$	$= \frac{\Delta E_{lkr}}{kT_2},$ Gibbs number, <i>dimensionless</i>

---

$Gr_1$	$= g \left  \rho_1 - \rho_1''(T_2^{1\sigma}) \right  \rho_1 D_1^3 / \eta_1^2$ , bubble <i>Grashoff</i> number, <i>dimensionless</i>
$h$	specific enthalpy, $J/kg$
$h_{NC}$	heat transfer coefficient by natural circulation, $W/(m^2K)$
$k$	$= 13.805 \times 10^{-24}$ , <i>Boltzmann</i> constant, $J/K$
$Le_1$	$= \lambda_1 / (\rho_1 c_{p1} D_{M \rightarrow \Sigma_n})$ , gas <i>Lewis</i> number, <i>dimensionless</i>
$m_2$	$= m_\mu / N_A$ , mass of single molecule, $kg$
$m_\mu$	$kg\text{-}mol$ mass (18 $kg$ for water), $kg/mole$
$N_2$	$= \rho_2 / m_2 = \rho_2 N_A / m_\mu$ ( $\approx 3.3 \times 10^{28}$ for water), number of the molecules per unit volume, $1/m^3$
$N_A$	$= 6.02 \times 10^{26}$ , <i>Avogadro</i> number, number of molecules in one kilogram-mole mass, $1/kg\text{-}mole$
$\dot{n}_{1cin}$	number of the created nuclei per unit time in unit volume of the liquid, $1/(m^3s)$
$n_w''$	cavity per unit surface, $1/m^2$
$n_{1w}''$	bubble generating (active) cavity per unit surface, $1/m^2$
$n_1$	bubble number density, $1/m^3$
$n_{1,n}$	bubble number density belonging to $n$ -th bubble generation, $1/m^3$
$n_{1,max}$	maximum number of nucleation sites per unit volume in a pipe, $1/m^3$
$Pr_1$	$= \eta_1 c_{p1} / \lambda_1$ , gas <i>Prandtl</i> number, <i>dimensionless</i>
$p$	pressure, $Pa$
$\dot{q}_2^{n1\sigma}$	thermal energy flow density coming from the vapor interface and introduced into the bulk liquid, $W/m^3$
$\dot{q}_1^{n2\sigma}$	thermal energy flux coming from the liquid interface and introduced into the bulk vapor, $W/m^2$
$\dot{q}_2^{n1\sigma}$	thermal energy flux coming from the vapor interface and introduced into the bulk liquid, $W/m^2$
$R$	gas constant, $J/(kgK)$
$R_1$	bubble radius, $m$
$R_{10}$	initial bubble radius, $m$
$R_{1c}$	critical bubble radius, $m$
$R_{1\infty}$	final radius of the bubble, $m$
$r$	radius, $m$
$s$	specific entropy, $J/(kgK)$
$T$	temperature, $K$
$u$	radial velocity, $m/s$
$\mathbf{V}$	velocity vector, $m/s$
$V_{1c}$	volume of the bubble with critical size

---

$v$	specific volume, $m^3/kg$
$Vol$	volume, $m^3$

**Greek**

$\alpha_1$	bubble volumetric fraction, $m^3/m^3$
$\beta$	diffusion coefficient
$\gamma_v$	volume occupied by the flow divided by the volume of the system, <i>dimensionless</i>
$\gamma$	cross section flowed by the flow divided by the total cross section of the system, <i>dimensionless</i>
$\Delta$	finite difference
$\Delta E_1$	work necessary to create a single bubble with radius $R_1$ , $J$
$\Delta E_{1c}$	work necessary to create a single bubble with radius $R_{1c}$ , $J$
$\Delta E_{1c}^*$	$= \phi \Delta E_{1c}$ , energy for the creation of a single bubble at a wall, $J$
$\Delta p_{Fi}^*$	$= p'(T_2) - p_{Fi}$ , flashing inception pressure difference, $Pa$
$\Delta \tau$	time interval, $s$
$\eta$	dynamic viscosity of liquid, $kg/(ms)$
$\theta$	static contact angle, $rad$
$\lambda_{RT}$	<i>Rayleigh-Taylor</i> wavelength, $m$
$\lambda$	thermal conductivity, $W/(mK)$
$\mu_{21}$	evaporating mass per unit time and unit flow volume, $kg/(m^3s)$
$\mu_{12}$	condensing mass per unit time and unit flow volume, $kg/(m^3s)$
$\rho$	density, $kg/m^3$
$(\rho w)_{21}$	evaporation mass flow rate, $kg/(m^2s)$
$\sigma$	surface tension, $N/m$
$M_{M1}$	kg-mole mass of the condensing gases, $kg/mol$
$\sum M_{n1}$	kg-mole mass of the non condensing gases, $kg/mol$
$M_1$	kg-mole mass of the gas mixture, $kg/mol$
$\tau$	time, $s$
$\Phi$	cavity angle if the cavity is idealized as a cone, $rad$
$\phi$	work reduction factor, <i>dimensionless</i>

**Superscripts**

'	saturated liquid
"	saturated vapor
<i>spin</i>	spinoidal line

$1\sigma$	interface with vapor
$2\sigma$	interface with liquid

### ***Subscripts***

1	vapor, gas
2	liquid
$c$	critical state
$s$	at constant entropy
$sat$	saturated
$Fi$	flashing inception
$\sum_{n1o}$	sum of all non-condensing gases
$M$	evaporating or condensing chemical component
$n$	inert (non condensing) chemical component

### **References**

- Besand WH (1859) Hydrostatics and hydrodynamics, Deighton Bell, Cambridge, p 170
- Beylich AE (January 1991) Dynamics and thermodynamics of spherical vapor bubbles, International Chemical Engineering, vol 31 no 1 pp 1-28
- Bosnjakovic F (1930) Techn. Mech. Thermodyn, vol 1 p 358
- Carlson HS, Jaeger JC (1959) Conduction of heat in solids, Oxford
- Cole R, Schulman HL (1966) Bubble growth rates of high Jacob number, Int. J. Heat Mass Transfer, vol 9 pp 1377-1390
- Foster HK, Zuber N (1954) J. Appl. Physics, vol 25 pp 474-478
- Fourier J (1822) Theory Analytique de la Chaleur
- Fritz W, Ende W (1936) Ueber den Verdampfungsvorgang nach kinematographischen Aufnahmen an Dampfblasen. Phys. Z., vol 37 pp 391-401
- Galin HM and Kirilov PL (1987) Teplomassoobmen, Moskva, Energoatomisdat
- Hutcherson MN, Henry RE, Wollersheim DE (Nov. 1983) Two - phase vessel blow down of an initially saturated liquid - Part 2: Analytical, Trans. ASME, vol. 105 pp 694-699
- Jagov VV (1971) Issledovanie kipenija jidkosteij v oblasti niskih davlenij, PhD Thesis, Moskva
- Jakob M (1932) Z. d. Ver. Dtsch. Ing., vol 76 p 1161
- Jones OC Jr, Zuber N (Aug. 1978) Bubble growth in variable pressure fields, Journal of Heat Transfer, vol 100 pp 453-458
- Kroshilin AE, Kroshilin VE, Nigmatulin BI (May - June 1986) Growth of a vapor bubble in a superheated liquid volume for various laws governing the pressure variation in the liquid, Teplofizika Vysokih Temperatur, vol 24 no 3 pp 533 - 538
- Kutateladze SS (1982) Analiz podobija v teplofiske (Similarity analysis in thermal physics), Nauka, (in Russian)
- Labuntsov DA, Kol'chugin VA, Golovin VS et al (1964) Teplofiz. Vys. Temp., vol 3 pp 446 - 453
- Lien Y, Griffith P (1969) Bubble growth in reduced pressure, Ph. D. Thesis, Massachusetts Institute of Technology, Cambridge



- 
- Mikic BB, Rohsenow WM, Griffith P (1970) On bubble growth rates, *Int. J. Heat Mass Transfer*, vol 13 pp 657-666
- Mikic BB, Rohsenow WM (1969) Bubble growth rates in non uniform temperature fields, *Progr. Heat Mass Transfer*, vol 2 pp 283-293
- Nigmatulin RI (1978) Basics of the mechanics of the heterogeneous fluids, Moskva, Nauka, In Russian.
- Olek S, Zvirin Z, Elias E (1990) Bubble growth prediction by the hyperbolic and parabolic heat conduction equations, *Waerme- and Stoffuebertragung*, vol 25 pp 17-26
- Piening J (1971) *Der Wärmeübergang an eine an der Heizwand wachsende Dampfblase beim Sieden*. Dissertation, Berlin TU 1971
- Plesset MS, Zwick S (April 1954) The growth of bubbles in superheated liquids, *J. of Applied Physics*, vol 25 no 4 pp 493-500
- Prisnjakov VF (January 1970) Bubble growth in liquids, *Journal of Engineering Physics*, vol 18 no 1 pp 584-588
- Rayleigh L (1917) On the pressure developed in a liquid during the collapse of spherical cavity, *Phil. Mag.*, vol 34 p 94
- Scriven LE (1959) On the dynamics of phase growth, *Chem. Engng. Sci.*, vol 10 no 1 pp 113
- Tolubinskii IS (1980) Boiling heat transfer, Kiev, Naukova Dumka, in Russian
- VDI-Waermeatlas, 4. Auflage 1984, VDI-Verlag
- Wang Z (December 1989) Transient level swell and liquid carryover phenomena of a vapor-liquid pool, PhD Dissertation, Northwestern University, Evanston, Illinois, USA



## 14 Condensation of a pure steam bubble in a subcooled liquid

*This is a review Chapter about the different methods for description of bubble collapse due to vapor condensation in subcooled liquid. First we consider the case of stagnant bubbles. The solutions for moving bubbles are then presented. The available experimental data are then discussed. Then the link between the solutions for the bubble growth and the mass source terms for the averaged conservation equations for two-phase flow is presented. The way to derive non-averaged mass source terms and time-averaged mass source terms is given. The very interesting case of disappearance of the bubbles from the size distribution spectrum due to condensation is discussed in some details. The influence of the liquid turbulence on the bubble condensation in pipes is discussed too. Then a brief description of the vapor condensation from gas mixtures inside bubbles surrounded by subcooled liquid is given for the two limiting cases a) thermally controlled collapse and b) diffusion controlled collapse.*

### 14.1 Introduction

Injecting steam in subcooled water causes condensation. If a pressure wave crosses a water-steam system in thermodynamic equilibrium condensation also happens. One of the basic condensation mechanisms in multi-phase systems is the condensation of a single bubble in subcooled water. Several authors study condensation of a saturated bubble in a subcooled liquid. As for the evaporation, the theoretical results of the approximate integration of the process governing a system of PDEs describe the radius as a function of time. Unlike the evaporation, the condensation is associated with a given *initial bubble size*. There are two classes of solutions: a) for a stagnant bubble and b) for a bubble in motion with respect to the surrounding liquid. The motion increases the heat transfer between the bubble interface and the bulk liquid and therefore increases the condensation.

### 14.2 Stagnant bubble

Table 14.1 contains some of the results known from the literature, obtained with the assumption that there is no relative motion of the bubble with respect to the surrounding liquid.

**Table 14.1.** Size of a bubble condensing in a subcooled liquid as a function of time by  $\Delta V = 0$ 

---


$$\tau_H = \frac{4}{\pi} Ja^2 Fo, \quad Ja = \frac{\rho_2 c_{p2} [T'(p) - T_2]}{\rho'' \frac{h'' - h'}{h'' - h'}}, \quad Fo = \frac{a_2 \tau}{R_{1o}^2}$$


---

*Forschuetz and Chao (1965)* for  $\tau \leq \frac{\pi R_{1o}^2}{4Ja^2 a_2}$

$$\frac{R_1}{R_{1o}} = 1 - \sqrt{\tau_H}.$$

*Plesset and Zwick (1954):*

$$\tau_H = \frac{2}{3} \left( \frac{R_{1o}}{R_1} \right) + \frac{1}{3} \left( \frac{R_1}{R_{1o}} \right)^2 - 1, \quad \tau_{99\%} = 65 \frac{\pi R_{1o}^2}{4Ja^2 a_2}.$$

*Prisnjakov (1970)* for  $\tau \leq \frac{1}{4\varepsilon^2} \frac{\pi R_{1o}^2}{4Ja^2 a_2}$ :

$$\frac{R_1}{R_{1o}} = 1 - 2\varepsilon \sqrt{\tau_H}, \quad \varepsilon = 1 / \left[ 1 - \frac{\rho''}{\rho_2} + 2 \frac{h_2}{h'' - h'} \right].$$

*Zuber (1961)* for  $\tau \leq 4\tau_m$ :

$$\frac{R_1}{R_{1m}} = \left( \frac{\tau}{\tau_m} \right)^{1/2} \left[ 2 - \left( \frac{\tau}{\tau_m} \right)^{1/2} \right].$$

$\tau_m$  time when the bubble reaches its maximum radius  $R_{1m}$ . For bubble growing and collapsing on a heated wall in subcooled water

$$\tau_m = \frac{1}{\pi a_2} \left( \lambda_2 \frac{T_w - T'}{\dot{q}_w''} \right)^2, \quad R_m = \frac{b}{\pi} Ja \sqrt{\pi a_2 \tau_m}, \quad b \approx 1 \div \sqrt{3},$$

$$Ja = \frac{(T_w - T') c_{p2} \rho_2}{(h'' - h') \rho''}.$$


---

*Bucher and Nordman (1978)* show that the best fitting of the experimental data is obtained with *Zuber's* equation from Table 14.1.

## 14.3 Moving bubble

The influence of the relative velocity on the temperature profile around the bubble and therefore on the condensation process can be taken into account by using the results of several authors describing the heat transfer around a solid sphere as summarized in Table 14.2.

**Table 14.2.** Averaged heat transfer coefficient on the surface of solid sphere moving in a liquid

---


$$Pe_2 = \frac{D_1 \Delta V_{12}}{a_2}, \quad a_2 = \frac{\lambda_2}{\rho_2 c_{p2}}, \quad Pr_2 = \frac{\eta_2}{\rho_2 a_2}, \quad Re_1 = \frac{D_1 \rho_2 \Delta V_{12}}{\eta_2}, \quad Nu_1 = \frac{D_1 h_k}{\lambda_2},$$

$$Fo = \frac{a_2 \tau}{R_{10}^2}, \quad Re_{10} = \frac{D_{10} \rho_2 \Delta V_{12}}{\eta_2}, \quad Fo \leq 1/(Nu_1 Ja)$$


---

Potential flow  $\left( \frac{\partial R_1}{\partial \tau} \ll \Delta V \right), \quad Re_1 \ll 1:$

*Soo* (1969) for  $Pe_2 \ll 1$ :

$$Nu_1 = 2 + \frac{9}{16} Pe_2 + \frac{9}{64} Pe_2^2 + \dots$$

*Nigmatulin* (1978) for  $Pe_2 \gg 1$ :

$$Nu_1 = \frac{0.65}{\left( 1 + \frac{\eta_1}{\eta_2} \right)^{1/2}} Pe_2^{1/2}, \quad \eta_1 / \eta_2 \leq 1.$$

*Hunt* (1970) for a single-component system:

$$Nu_1 = \frac{2}{\pi^{1/2}} (c Pe_2)^{1/2},$$

where  $c = 1$ .

For a two-component system *Isenberg* and *Sideman* (1970) take into account viscous effects in the *Hunt* equation using  $c = 0.25 \, Pr_2^{-1/3}$  resulting in

$$Nu_1 = \frac{1}{\pi^{1/2}} Re_{12}^{1/2} Pr_2^{1/3}.$$

*Kendouch* (1976) for bubbles in a swarm:

$$Nu_1 = \frac{2}{\pi^{1/2}} Pe_2^{1/2} (1 - \alpha_1)^{-1/2}.$$

Wilson (1965) for  $Re_1 < 1$ :

$$Nu_1 = 2 + 0.37 Re_1^{3/5} Pr_2^{1/3}.$$

Nigmatulin (1978) for  $Re_1 < 1$  or  $Pe_2 < 10^3$  (e.g. for  $D_{H_2O} < 0.1$  mm):

$$Nu_1 = 2 + \frac{0.65 Pe_2^{1.7}}{1 + Pe_2^{1.3}}, \quad \eta_1 / \eta_2 \cong 0.$$

Brauer et al. (1976) for bubbles without internal circulation:

$$Nu_1 = 2 + \frac{0.65 Pe_2^{1.7}}{\left[1 + (0.84 Pe_2^{1.6})^3\right]^{1/3} (1 + Pe_2^{1.2})}.$$

Soo (1969) for  $1 < Re_1 < 7 \times 10^4$ ,  $0.6 < Pr_2 < 400$ :

$$Nu_1 = 2 + (0.55 \text{ to } 0.7) Re_1^{1/2} Pr_2^{1/3}.$$

Akiyama (1973):  $Nu_1 = 0.37 Re_1^{0.6} Pr_2^{1/3}$ .

Zeitoun et al. (1995):  $Nu_1 = 2.04 Re_1^{0.61} Ja^{-0.308} \alpha_1^{0.328}$ .

There are a limited number of correlations, approximating directly experimental data for a *condensing moving bubble in a subcooled liquid*. Some of them are summarized in Table 14.3. Next we first show the analytical way to derive such an expression which can be successfully modified to correlate the data. Then, to illustrate the idea how the approximate form of the correlations in Table 14.3 is obtained we apply the theory using the heat transfer mechanism described by the correlation by *Hunt and Isenberg*.

The energy conservation equation with neglected convection and diffusion from the surrounding computational cells gives

$$\rho'' \frac{dR_1}{d\tau} = -h_c \frac{T' - T_2}{h'' - h_2}, \quad (14.1)$$

or

$$\frac{dR_1}{d\tau} = -\frac{h_c}{\rho''} \frac{T' - T_2}{h'' - h_2} = -\frac{Nu_1 \lambda_2 (T' - T_2)}{R_1 2 \rho'' (h'' - h_2)} = -c / R_1 = -\frac{a_2 Nu_1 Ja}{2 R_1}, \quad (14.2)$$

or

$$\frac{d}{dFo} \left( \frac{R_1}{R_{1o}} \right)^2 = -Nu_1 Ja. \quad (14.3)$$

Integrating the above equation for  $Nu_1 = const$  we obtain

$$\frac{R_1}{R_{1o}} = \left( 1 - \frac{2c\Delta\tau}{R_{1o}^2} \right)^{1/2} = \sqrt{1 - \Delta\tau / \Delta\tau_o} = (1 - Nu_1 Ja Fo)^{1/2} = (1 - Fo / Fo_o)^{1/2}. \quad (14.4)$$

The last form of the above notation contains the important information for the dimensionless time,  $Fo_o$ , within which the bubble collapses completely if the mixture still does not reached the saturation. The bubble collapses entirely

$$R_1 = 0, \quad (14.5)$$

within

$$\Delta\tau_o = R_{1o}^2 / (2c), \quad [Fo_o = 1 / (Nu_1 Ja)]. \quad (14.6)$$

After this time interval Eq. (14.4) is no longer valid. For the third power of the radii ratio we have

$$\left( \frac{R_1}{R_{1o}} \right)^3 = (1 - \Delta\tau / \Delta\tau_o)^{3/2} = (1 - Fo / Fo_o)^{3/2} \quad (14.7)$$

If we drop the assumption  $Nu_1 = const$  and use the *Hunt* and *Isenberg's* equation from Table 14.2 we obtain

$$\left( \frac{R_1}{R_{1o}} \right)^3 = (1 - Fo / Fo_o)^2, \quad (14.8)$$

where

$$Fo_o = 1 / \left( \frac{3}{2} \frac{1}{2\sqrt{\pi}} Re_{1o}^{1/2} Pr_2^{1/3} Ja \right), \quad (14.9)$$

see the first equation in Table 14.3. It differs from the *Moalem* and *Sideman* correlation only in the constant.

As seen from Table 14.3 all the correlations are based on the above form modifying the exponents except the correlation by *Dushkin* and *Kolomenzev*.

**Table 14.3.** Bubble size of saturated steam condensing in a subcooled liquid  $\Delta V \neq 0$ . Approximation of experimental data.  $Fo_o$  is the dimensionless lifetime of condensing bubble

---

**Theory**

---

$Nu_1 \neq f(r_1)$ , and Eq. (14.3)

$$\frac{R_1}{R_{1o}} = (1 - Nu_1 Ja Fo)^{1/2} = (1 - Fo / Fo_o)^{1/2}, Fo = 1 / (Nu_1 Ja)$$

$Nu_1 = \text{Hunt and Isenberg Table 14.2, and Eq. (14.3) + } \Delta V \neq f(R_1)$

$$\begin{aligned} \frac{R_1}{R_{1o}} &= \left(1 - \frac{3}{2} \frac{1}{2\sqrt{\pi}} Re_{1o}^{1/2} Pr_2^{1/3} Ja Fo\right)^{2/3} \\ &= (1 - 0.423 Re_{1o}^{1/2} Pr_2^{1/3} Ja Fo)^{2/3} = (1 - Fo / Fo_o)^{2/3}, \\ Fo_o &= 1 / (0.423 Re_{1o}^{1/2} Pr_2^{1/3} Ja). \end{aligned}$$

---

**Experiment**

---

*Mayinger and Nordmann (1979)* for  $4 < Ja < 300$ ,  $p = 0.2$  to  $5$  bar:

$$\begin{aligned} \frac{R_1}{R_{1o}} &= \left[1 - \frac{5}{3} \frac{10^3}{2} \left(\frac{\rho_1}{\rho_2}\right)^{0.79} Re_{1o}^{1/3} Pr_2^{2/3} Ja^{1.27} Fo\right]^{3/5} \\ &= \left[1 - 0.833 \times 10^3 \left(\frac{\rho_1}{\rho_2}\right)^{0.79} Re_{1o}^{1/3} Pr_2^{2/3} Ja^{1.27} Fo\right]^{3/5} = (1 - Fo / Fo_o)^{3/5}, \\ Fo_o &= 1 / \left[0.833 \times 10^3 \left(\frac{\rho_1}{\rho_2}\right)^{0.79} Re_{1o}^{1/3} Pr_2^{2/3} Ja^{1.27}\right]. \end{aligned}$$

---

**Condensation of bubbles in a pool behind nozzles**

---

$$\begin{aligned} \text{Akiyama (1973) for } \Delta V_{12} &= 1.18 \left[ \frac{\sigma g (\rho_2 - \rho'')}{\rho_2^2} \right]^{1/4} \\ \frac{R_1}{R_{1o}} &= \left(1 - 0.259 Re_{1o}^{0.6} Pr_2^{1/3} Ja Fo\right)^{1/1.4} = (1 - Fo / Fo_o)^{1/1.4}, \\ Fo_o &= 1 / (0.259 Re_{1o}^{0.6} Pr_2^{1/3} Ja). \end{aligned}$$

---

*Brucker and Sparrow (1977)* for  $\Delta T = 15$  to  $100K$ ,

$p = (10.3 \text{ to } 62.1) \times 10^5 Pa$ ,

$Pe_2 = 2000 \text{ to } 3000$ ,  $Nu_1 \pm 50\%$  :



$$\frac{R_1}{R_{1o}} = \left(1 - 0.259 Re_{1o}^{0.6} Ja Fo\right)^{1/1.4} = \left(1 - Fo / Fo_o\right)^{1/1.4},$$

$$Fo_o = 1 / \left(0.259 Re_{1o}^{0.6} Ja\right).$$

*Moalem and Sideman (1973):*

$$\frac{R_1}{R_{1o}} = \left(1 - \frac{2}{3} \frac{1}{\sqrt{\pi}} Re_{1o}^{1/2} Pr_2^{1/2} Ja Fo\right)^{2/3}$$

$$= \left(1 - 0.846 Re_{1o}^{1/2} Pr_2^{1/2} Ja Fo\right)^{2/3} = \left(1 - Fo / Fo_o\right)^{2/3},$$

$$Fo_o = 1 / \left(0.846 Re_{1o}^{1/2} Pr_2^{1/2} Ja\right).$$

*Dushkin and Kolomenzev (1989)* for  $0.8 \times 10^6 \leq p \leq 2 \times 10^6$  Pa,  $15 \leq T' - T_2 \leq 25$  K,  $2 \times 10^{-3} \leq D_{1o} \leq 4 \times 10^{-3}$  m, or  $0.1 < Ja < 20$ ,  $0 < Fo < 0.2$ ,  $10^3 < Pe_2 < 10^5$ ,  $0.1 \leq \frac{R_1}{R_{1o}} \leq 1$ ,  $\alpha_1 = 0.2$  to  $0.7$ ,  $Re_1 = 10^4$  to  $10^6$ ,  $566 \leq \alpha_1 \rho_1 w_1 \leq 1698$  kg/(m<sup>2</sup>s),  $11317 \leq \alpha_2 \rho_2 w_2 \leq 56588$  kg/(m<sup>2</sup>s) approximate experimental data of several authors for a vertical upwards flow, and their own data for downward flow of Freon-22 in a tube with  $D_h = 0.015$  with

$$\frac{R_1}{R_{1o}} = \exp \left[ -\frac{4}{3} \left( Pe_2^{0.43} + 1 \right) Ja Fo \right].$$

*Chen and Maynger (1989)*, experiment  $2 < Pr_2 < 15$ ,  $1 < Ja < 120$ .

$$\frac{R_1}{R_{1o}} = \left(1 - 0.56 Re_{1o}^{0.7} Pr_2^{1/2} Ja Fo\right)^{0.9} = \left(1 - Fo / Fo_o\right)^{0.9},$$

$$Fo_o = 1 / \left(0.56 Re_{1o}^{0.7} Pr_2^{1/2} Ja\right).$$

At *Jacob* numbers above 70 inertia controlled phenomena start to dominate.

*Bucher and Nordman (1978)* compared experimental data with the predictions of the equations from Table 14.3 and found that the *Akiyama* equation shows the best results up to 1978.

## 14.4 Non-averaged source terms

The non-averaged source terms required for microscopic flow description are given below. First the evaporation mass per unit volume and unit time is equal to zero,

$$\mu_{21} = 0. \quad (14.10)$$

There is no heat transfer between the bubble interface and the vapor

$$\dot{q}_1^{m2\sigma} = 0. \quad (14.11)$$

Only the heat transfer between the interface and the bulk liquid

$$\dot{q}_2^{m1\sigma} = a_{12} h_c [T'(p) - T_2], \quad (14.12)$$

controls the condensed mass per unit mixture volume and unit time

$$\mu_{12} = \dot{q}_2^{m1\sigma} / [h_{M1} - h'(p)]. \quad (14.13)$$

Here the instantaneous heat transfer coefficient between the interface and the bulk liquid is

$$h_c = \frac{\lambda_2}{D_1} Nu_1, \quad (14.14)$$

where the *Nusselt* number is a function of the local parameter of the flow.

In what follows we show how to link the empirically obtained results for the change of the radius of the condensing bubble with the macroscopic flow description. The condensed mass per unit mixture volume and unit time is equal to the product of the number of the bubbles per unit mixture volume and the mass change of a single bubble.

$$\mu_{12} = -\rho''(p) n_1 dV_1 / d\tau = -\rho''(p) n_1 4\pi R_1^2 dR_1 / d\tau \quad (14.15)$$

or replacing

$$R_1 = \left( \frac{3}{4\pi} \frac{\alpha_1}{n_1} \right)^{1/3}, \quad (14.16)$$

$$\mu_{12} = -3^{2/3} (4\pi)^{1/3} \rho''(p) n_1^{1/3} \alpha_1^{2/3} \frac{dR_1}{d\tau} = 4.84 \rho''(p) n_1^{1/3} \alpha_1^{2/3} \frac{dR_1}{d\tau}, \quad (14.17)$$

where for  $dR_1 / d\tau$  one can use one of the expressions from Table 14.2 or 14.3. The heat absorbed by the liquid during the condensation per unit mixture volume and unit time is

$$\dot{q}_2^{m1\sigma} = \mu_{12} [h''(p) - h'(p)]. \quad (14.18)$$

## 14.5 Averaged source terms

In order to calculate the averaged mass source term we proceed as follows.

The integral expression for the averaged condensation within the time interval  $\Delta\tau$ , where  $\Delta\tau < \Delta\tau_o$ , is

$$\mu_{12} = \rho'' n_1 \frac{V_{1o} - V_1}{\Delta\tau} = \frac{\rho'' n_1 V_{1o}}{\Delta\tau} \left( 1 - \frac{V_1}{V_{1o}} \right) = \frac{\rho'' \alpha_1}{\Delta\tau} \left( 1 - \left( \frac{R_1}{R_{1o}} \right)^3 \right). \quad (14.19)$$

If the time interval is selected larger than the lifetime of the bubble,  $\Delta\tau \geq \Delta\tau_o$  we have

$$\mu_{12} = \rho'' \alpha_1 / \Delta\tau. \quad (14.20)$$

The last relationship is practically the condition for the entire condensation of the available steam within the time step  $\Delta\tau$ . Having in mind that during the condensation

$$\mu_{21} = 0 \quad (14.21)$$

$$\dot{q}_1^{m2\sigma} = 0, \quad (14.22)$$

we obtain from the energy jump condition on the bubble surface the averaged energy source term

$$\dot{q}_2^{m1\sigma} = \mu_{12} (h_{M1} - h'). \quad (14.23)$$

The above relationship is strictly valid if the bubble surface temperature

$$T_2^{1\sigma} = T'(p_{M1}) \quad (14.24)$$

is equal to the gas temperature  $T_1$ . We note the condensation rate in this case with  $\mu'_{12}$ . In general there is a small amount of heat transfer from the bubble to the surface if  $T_1 > T'(p_{M1})$  or from the surface to the bubble if  $T_1 < T'(p_{M1})$  due to a mechanism similar to natural convection inside the cavity. In this case we have

$$\dot{q}_2^{m1\sigma} = \mu'_{12} [h_{M1} - h'(p)]. \quad (14.25)$$

$$\mu_{21} = 0, \quad (14.26)$$

$$\dot{q}_1^{m2\sigma} = a_{21} h_{NC} [T'(p_{M1}) - T_1]. \quad (14.27)$$

$$\mu_{12} = \mu'_{12} + \dot{q}_1^{m2\sigma} / [h_{M1} - h'(p)], \quad (14.28)$$

where  $h_{NC}$  is the heat transfer coefficient due to natural convection in a cavity. The second term in Eq. (14.28) is usually neglected as very small compared to the first one. This term becomes important only for mass transfer processes on the bubble surface in saturated or nearly saturated liquid.

## 14.6 Change of the bubble number density due to condensation

Now let us answer the question what happens to the particle number density during the condensation of bubbles? Suppose the bubbles size distribution obeys the *Nukama-Tanasawa* law (1938)

$$P(D_1) = 4 \left( \frac{D_1}{D'_1} \right)^2 e^{-2(D_1/D'_1)}. \quad (14.29)$$

Here  $P(D_1)$  is the probability that a bubble has its size between  $D_1$  and  $D_1 + \delta D_1$ .  $D'_1$  is the most probable particle size, i.e. the size where the probability function has its maximum value. The particle sizes may take values between zero and a maximum value

$$0 < D_1 < D_{1max}. \quad (14.30)$$

Thus, if we know  $D'_1$  and  $D_{1max}$  the particle distribution is uniquely characterized. *Mac Vean*, see in *Wallis* (1969), found that a great deal of data could be correlated by assuming that

$$D'_1 = D_1/2 \quad (14.31)$$

where  $D_d$  is the volume averaged particle size. The relationship between  $D_d$  and the maximum particle size,  $D_{1max}$ , is reported as

$$D_{1max} \approx (2.04 \text{ to } 3.13) D_1, \quad (14.32)$$

see *Pilch* et al. (1981), *Kataoka* et al. (1983), among others. Suppose that the distribution remains unchanged during the time step  $\Delta\tau$ . For that time the volume-averaged diameter changes as

$$\Delta D_1 = D_{10} - D_1 = D_{10} (1 - R_1 / R_{10}) = D_{10} \left[ 1 - \left( 1 - \frac{\mu_{12} \Delta\tau}{\rho_1 \alpha_1} \right)^{1/3} \right] \quad (14.33)$$

and all particles having sizes

$$0 \leq D_1 \leq 2\Delta D_1 \quad (14.34)$$

namely

$$n_1 \int_0^{2\Delta D_1} P(D_1) dD_1 = 2n_1 \left\{ 1 - e^{-4\Delta D_1 / D'_1} \left[ 1 + 4 \frac{\Delta D_1}{D'_1} \left( 1 + 2 \frac{\Delta D_1}{D'_1} \right) \right] \right\} \quad (14.35)$$

disappear. The averaged particle sink per unit time and unit mixture volume is consequently

$$\dot{n}_1 \approx -(n_1 / \Delta \tau) 2 \left\{ 1 - e^{-4\Delta D_1 / D'_1} \left[ 1 + 4 \frac{\Delta D_1}{D'_1} \left( 1 + 2 \frac{\Delta D_1}{D'_1} \right) \right] \right\}, \quad (14.36)$$

for  $\Delta D_1 \leq D'_1$ . The latter condition means that approximately within the interval  $2\Delta D_1$  the averaged bubble size is  $\Delta D_1$ .

## 14.7 Pure steam bubble drifting in turbulent continuous liquid

In a bubble flow or in a churn-turbulent flow with considerable turbulence, the bubbles are moving practically with the *same* velocity as the liquid. The mechanism governing the condensation is quite different compared to the mechanism described in the previous Sections. There are several authors assuming that the heat released during the condensation is transported *by exchange of turbulent eddies* between the boundary layer and the bulk liquid. The characteristic time of one cycle, estimated by dimensional analysis of the turbulent characteristics of the continuous velocity field, is of the order of

$$\Delta \tau = \text{const} (l_{e2}^2 / \varepsilon_2)^{1/2} \quad (14.37)$$

for high frequency pulsations in accordance with the *statistical theory of turbulence*. Replacing the characteristic size of the turbulent eddies in the liquid with

$$l_{e2} = \text{const} (v_2^3 / \varepsilon_2)^{1/4} \quad (14.38)$$

we obtain for the time constant

$$\Delta \tau = \text{const} (v_2 / \varepsilon_2)^{1/2}. \quad (14.39)$$

After replacing the dissipated specific kinetic energy of the turbulent pulsations with

$$\alpha_2 \rho_2 \varepsilon_2 = \frac{1}{2} \frac{\rho^2}{\rho_2} \left[ u^3 \Phi_{2ou}^2 \left( \frac{\lambda_{Ru}}{D_{hu}} + \frac{\zeta_u}{\Delta r} \right) + v^3 \Phi_{2ov}^2 \left( \frac{\lambda_{Rv}}{D_{hv}} + \frac{\zeta_\theta}{r^\kappa \Delta \theta} \right) + w^3 \Phi_{2ow}^2 \left( \frac{\lambda_{Rw}}{D_{hw}} + \frac{\zeta_w}{\Delta z} \right) \right] \quad (14.40)$$

we obtain

$$\Delta\tau = \text{const} \frac{\rho_2}{\rho} \left[ \frac{2\alpha_2 v_2}{\left[ u^3 \Phi_{2ou}^2 \left( \frac{\lambda_{Ru}}{D_{hu}} + \frac{\zeta_u}{\Delta r} \right) + v^3 \Phi_{2ov}^2 \left( \frac{\lambda_{Rv}}{D_{hv}} + \frac{\zeta_\theta}{r^\kappa \Delta \theta} \right) + w^3 \Phi_{2ow}^2 \left( \frac{\lambda_{Rw}}{D_{hw}} + \frac{\zeta_w}{\Delta z} \right) \right]} \right]^{1/2} \quad (14.41)$$

The heat flux on the bubble surface can be determined to the accuracy of a constant as

$$\dot{q}_2^{n\sigma} = \text{const}(T' - T_2) \sqrt{\frac{\lambda_2 \rho_2 c_{p2}}{\Delta\tau}}, \quad (\text{const} = \frac{2}{\sqrt{\pi}} \text{ plane}), \quad (14.42)$$

where  $\Delta\tau$  is the time interval in which the high frequency eddy is in contact with the bubble surface. During this time, the heat is transported from the surface to the eddy by molecular diffusion. Thereafter the eddy is transported into the bulk flow again, and its place on the surface is occupied by another one. In this way the heat released during the condensation is transported from the bubble to the turbulent bulk liquid. We substitute  $\Delta\tau$  from Eq. (14.41) into Eq. (14.42) and obtain

$$\dot{q}_2^{n\sigma} = \text{const}(T' - T_2) \lambda_2 Pr_2^{1/2} \sqrt{\frac{\rho}{\eta_2 v_2^{1/2} \alpha_2^{1/2}}} \times \left[ \frac{u^3 \Phi_{2ou}^2 \left( \frac{\lambda_{Ru}}{D_{hu}} + \frac{\zeta_u}{\Delta r} \right) + v^3 \Phi_{2ov}^2 \left( \frac{\lambda_{Rv}}{D_{hv}} + \frac{\zeta_\theta}{r^\kappa \Delta \theta} \right) + w^3 \Phi_{2ow}^2 \left( \frac{\lambda_{Rw}}{D_{hw}} + \frac{\zeta_w}{\Delta z} \right)} \right]^{1/4}. \quad (14.43)$$

The constant can be determinate by comparison with a result obtained by *Avdeev* in (1986) for one-dimensional flow without local resistance ( $\xi = 0$ ). *Avdeev* used the known relationship for the *friction coefficient of turbulent flow*

$$\lambda_{Rw} = 0.184 Re_2^{-0.2} \quad (14.44)$$

where

$$Re_2 = \frac{D_{hw} w_2}{\nu_2}, \quad (14.45)$$

compared the so obtained equation with experimental data, and estimated the constant in

$$\dot{q}_2^{n1\sigma} = \text{const } 0.184^{1/4} (T' - T_2) \frac{\lambda_2}{D_{hw}} Pr_2^{1/2} Re_2^{0.7} (\Phi_{2ow}^2 / \alpha_2)^{1/4} \quad (14.46)$$

as

$$\text{const } 0.184^{1/4} = 0.228 \quad (14.47)$$

or

$$\text{const} = 0.348. \quad (14.48)$$

The final relationship recommended by *Avdeev* for one-dimensional flow

$$Nu = 0.228 Pr_2^{1/2} Re_2^{0.7} (\Phi_{2ow}^2 / \alpha_2)^{1/4} \quad (14.49)$$

describes his own data within  $\pm 30\%$  error band for  $D_1 / D_{hw} > 80 / Re_2^{0.7}$ . Note that in the *Avdeev* equation  $\rho / \rho_2$  is set to one. Thus, the so estimated constant can be successfully applied to three-dimensional flows. For comparison let us write the relationships obtained by *Hancox* and *Nikol* (see in Hughes et al. (1981))

$$Nu = 0.4 Pr_2 Re_2^{2/3} \quad (14.50)$$

and *Labunzov* (see in Labunzov (1974))

$$Nu = \frac{\lambda_{Rw} / 8}{1 - 12 \sqrt{\frac{\lambda_{Rw}}{8}}} Pr_2 Re_2 \frac{D_1}{D_h} \cong \frac{0.023}{1 - 1.82 Re_2^{-0.1}} \frac{D_1}{D_h} Pr_2 Re_2^{0.8}. \quad (14.51)$$

We see that in the three equations obtained independently from each other the dependence on  $Re_2$  is  $Re_2^{0.7 \text{ to } 0.8}$ , and the dependence on  $Pr_2$  is  $Pr_2^{0.5 \text{ to } 1}$ . In case of  $Re_2 \approx 0$  the energy dissipated behind the bubbles should be taken into account.

## 14.8 Condensation from a gas mixture in bubbles surrounded by subcooled liquid

In the *presence of a non-condensing gas*, the temperature of the bubble surface  $T'_k$  is not equal to the saturation temperature  $T'$  at the system pressure  $p$ . During the condensation the partial pressure of the inert components increases with the decreasing bubble size due to the simultaneously decreasing partial steam pressure until  $T'_k$  becomes equal to the liquid temperature and the condensation ceases. Note that in this case the *bubble remains with a stable equilibrium volume*. Because in accordance with *Dalton's law* the non-condensing mixture occupies the whole bubble volume at the beginning of the condensation as well at its end the ratio of the end volume to the initial volume is inversely proportional to the densities of the non-condensing mixture in both states, respectively

$$\left(\frac{R_{1\infty}}{R_1}\right)^3 = \frac{\sum \rho_{n1o}}{\sum \rho_{n1\infty}} = \frac{1}{\sum \rho_{n1\infty}} \rho_{1o} (1 - C_{M1o}) = \frac{R_{n1}^* T_{1o}}{p - p'(T_2)} \rho_{1o} (1 - C_{M1o}) \approx \frac{\sum p_{n1o}}{p - p'(T_2)} \quad (14.52)$$

This expression is necessary for the estimation of the *maximum duration of the bubble collapse*.

There are different approaches to estimate the condensing mass per unit mixture volume and unit time.

### 14.8.1 Thermally controlled collapse

One of them assumes that the non-condensing components are *uniformly* distributed through the whole bubble volume and the condensation is controlled, as in one-component bubble condensation, by the heat transport from the bubble surface to the bulk liquid. The only difference is that the surface temperature, assumed in the single-component case to be equal to the saturation temperature at the steam partial pressure, is not equal to the saturation temperature at the system pressure. Thus, the equation describing the change of the bubble radius for a one-component bubble can simply be corrected as follows

$$\begin{aligned} \frac{dR_1}{d\tau} &= -\frac{h_c}{\rho''} \frac{T'_c - T_2}{h'' - h_2} = -\frac{Nu_1 \lambda_2 (T'_c - T_2)}{R_1 2 \rho'' (h'' - h_2)} = -c_T \frac{Nu_1 \lambda_2 (T' - T_2)}{R_1 2 \rho'' (h'' - h_2)} \\ &= -\frac{a_2 Nu_1 Ja}{2R_1} = -c_T c / R_1, \end{aligned} \quad (14.53)$$

where

$$c_T = \frac{T'_c - T_2}{T' - T_2} \quad (14.54)$$

is the dimensionless surface temperature. Thus, the derivation of the averaged source terms is similar to the derivation shown in Section 14.4 for single-component bubble condensation.

### 14.8.2 Diffusion controlled collapse

Another approach considers the *concentration profile* in the neighborhood of the bubble surface and models the condensation as a diffusion process. The non-averaged mass condensing per unit mixture volume and unit time is

$$\mu_{12} = a_{12}(\rho w)_{12} = -a_{12} \beta \frac{C_{M1} \rho_1}{p_{M1}} [p_{M1} - p'(T_2)]$$



$$= -a_{21}\alpha_c \frac{M_{M1}}{M_1} \ln \frac{[p - p'(T_2)]}{\sum p_{n1}} / (c_{p1} Le^{2/3}), \text{ see in VDI-Waermeatlas. (1984)} \quad (14.55)$$

where

$$\beta = \frac{P_{M1}}{C_{M1}\rho_1 [p'(T_2) - p_{M1}]} \alpha_c \frac{M_{M1}}{M_1} \ln \frac{p - p'(T_2)}{\sum p_{n1}} / (c_{p1} Le^{2/3}), \quad (14.56)$$

$$p'(T_2) < p_{M1}, \quad (14.57)$$

$$Le = \lambda_1 / (\rho_1 c_{p1} D_{M \rightarrow \sum n}), \quad (14.58)$$

$$M_1 = \frac{\sum p_{n1}}{p} \sum M_{n1} + \frac{p - \sum p_{n1}}{p} \sum M_{M1}, \quad (14.59)$$

$p'$  is the partial steam pressure in the boundary layer, where the steam is supposed to be saturated, having a temperature nearly equal to the liquid temperature

$$p' = p'(T_2). \quad (14.60)$$

The released heat during the condensation is transported into the liquid

$$\dot{q}_2^{m1\sigma} = \mu_{12} [h_{M1} - h'(p)]. \quad (14.61)$$

## Nomenclature

$a$	thermal diffusivity, $m^2/s$
$a_2$	$= \frac{\lambda_2}{\rho_2 c_{p2}}$ , liquid thermal diffusivity, $m^2/s$
$a_{21}$	interfacial area density between the liquid 2 and the vapor 1, $1/m$
$C$	mass concentration, $kg/kg$
$c_p$	specific heat at constant pressure, $J/(kgK)$
$D_{M \rightarrow \sum n}$	diffusion constant for the species $M$ into the mixture $\sum n$ , $1/m$
$D_{cav}$	equivalent cavity size, $m$
$D_h$	hydraulic diameter, $m$
$D_{1,n}$	bubble diameter belonging to $n$ -th bubble generation, $m$
$D_{1c}$	critical bubble diameter, $m$
$D_{1d}$	bubble departure diameter, $m$
$D_1$	bubble diameter, $m$

$D_{1\max}$	maximum bubble diameter, $m$
$D'_1$	most probable bubble size, $m$
$d$	differential, <i>dimensionless</i>
$F_1 / Vol$	cross section at the wall surface covered by attached bubbles per unit flow volume, $1/m$
$ Fo$	$= \frac{a_2 \tau}{R_{10}^2}$ , <i>Fourier number</i> – condensation time scale, <i>dimensionless</i>
$ Fo_o$	time within which the bubble collapses completely, <i>dimensionless</i>
$ g$	gravitational acceleration, $m/s^2$
$ Ja$	$= \frac{\rho_2 c_{p2} [T_2 - T'(p)]}{\rho_{10} [h''(T_2^{1\sigma}) - h'(T_2^{1\sigma})]}$ , <i>evaporation Jacob number</i> , <i>dimensionless</i>
$ Ja$	$= \frac{\rho_2 c_{p2} [T'(p) - T_2]}{\rho'' \frac{h'' - h'}{h'' - h'}}$ , <i>condensation Jacob number</i> , <i>dimensionless</i>
$ G^*$	critical mass flow rate, $kg/(m^2s)$
$ Gb_2$	$= \frac{\Delta E_{1kr}}{kT_2}$ , <i>Gibbs number</i> , <i>dimensionless</i>
$ Gr_1$	$= g [\rho_1 - \rho_1''(T_2^{1\sigma})] \rho_1 D_1^3 / \eta_1^2$ , <i>bubble Grashoff number</i> , <i>dimensionless</i>
$ h$	specific enthalpy, $J/kg$
$ h_{NC}$	heat transfer coefficient by natural circulation, $W/(m^2K)$
$ h_c$	heat transfer coefficient by forced convection, $W/(m^2K)$
$ k$	$= 13.805 \times 10^{-24}$ , <i>Boltzmann constant</i> , $J/K$
$ Le_1$	$= \lambda_1 / (\rho_1 c_{p1} D_{M \rightarrow \Sigma_n})$ , <i>gas Lewis number</i> , <i>dimensionless</i>
$ l_{e2}$	$= const (v_2^3 / \varepsilon_2)^{1/4}$ , <i>characteristic size of the turbulent eddies in the liquid</i> , $m$
$ m_2$	$= m_\mu / N_A$ , <i>mass of single molecule</i> , $kg$
$ m_\mu$	<i>kg-mol mass</i> (18 $kg$ for water), $kg/mole$
$ Nu_1$	$= \frac{D_1 h_k}{\lambda_2}$ , <i>bubble Nusselt number</i> , <i>dimensionless</i>
$ N_2$	$= \rho_2 / m_2 = \rho_2 N_A / m_\mu$ ( $\approx 3.3 \times 10^{28}$ for water), <i>number of the molecules per unit volume</i> , $1/m^3$
$ N_A$	$= 6.02 \times 10^{26}$ , <i>Avogadro number</i> , <i>number of molecules in one kilogram mole mass</i> , $1/kg\text{-mole}$
$ \dot{n}_{1cin}$	<i>number of the created nuclei per unit time in unit volume of the liquid</i> , $1/(m^3s)$
$ n''_w$	<i>cavity per unit surface</i> , $1/m^2$
$ n''_{1w}$	<i>bubble generating (active) cavity per unit surface</i> , $1/m^2$
$ n_1$	<i>bubble number density</i> , $1/m^3$

---

$\dot{n}_1$	bubble number density change per unit time, $1/(m^3s)$
$n_{1,n}$	bubble number density belonging to $n$ -th bubble generation, $1/m^3$
$n_{1,\max}$	maximum number of nucleation sites per unit volume in a pipe, $1/m^3$
$P(D_1)$	probability that a bubble has its size between $D_1$ and $D_1 + \delta D_1$ , <i>dimensionless</i>
$Pr_1$	$= \eta_1 c_{p1} / \lambda_1$ , gas <i>Prandtl</i> number, <i>dimensionless</i>
$Pr_2$	$= \frac{\eta_2}{\rho_2 a_2}$ , liquid <i>Prandtl</i> number, <i>dimensionless</i>
$Pe_2$	$= \frac{D_1 \Delta V_{12}}{a_2}$ , bubble <i>Peclet</i> number, <i>dimensionless</i>
$p$	pressure, <i>Pa</i>
$Re_1$	$= \frac{D_1 \rho_2 \Delta V_{12}}{\eta_2}$ , bubble <i>Reynolds</i> number, <i>dimensionless</i>
$Re_{1o}$	$= \frac{D_{1o} \rho_2 \Delta V_{12}}{\eta_2}$ , bubble <i>Reynolds</i> number based on the initial bubbles size, <i>dimensionless</i>
$\dot{q}_2^{m1\sigma}$	thermal energy flow density coming from the vapor interface and introduced into the bulk liquid, $W/m^3$
$\dot{q}_1^{m2\sigma}$	thermal energy flow density coming from the liquid interface and introduced into the bulk vapor, $W/m^3$
$\dot{q}_1^{n2\sigma}$	thermal energy flux coming from the liquid interface and introduced into the bulk vapor, $W/m^2$
$\dot{q}_2^{n1\sigma}$	thermal energy flux coming from the vapor interface and introduced into the bulk liquid, $W/m^2$
$R$	gas constant, $J/(kgK)$
$R_1$	bubble radius, $m$
$R_{10}$	initial bubble radius, $m$
$R_{1c}$	critical bubble radius, $m$
$R_{1\infty}$	final radius of the bubble, $m$
$r$	radius, $m$
$s$	specific entropy, $J/(kgK)$
$T$	temperature, $K$
$u$	radial velocity, $m/s$
$\mathbf{V}$	velocity vector, $m/s$
$V_{1c}$	volume of the bubble with critical size, $m^3$
$V_1$	volume of the bubble, $m^3$
$V_{10}$	initial volume of the bubble, $m^3$

$v$	specific volume, $m^3/kg$
$Vol$	volume, $m^3$

**Greek**

$\alpha_1$	bubble volumetric fraction, $m^3/m^3$
$\alpha_2$	liquid volumetric fraction, $m^3/m^3$
$\beta$	diffusion coefficient
$\gamma_v$	volume occupied by the flow divided by the volume of the system, <i>dimensionless</i>
$\gamma$	cross section flowed by the flow divided by the total cross section of the system, <i>dimensionless</i>
$\Delta$	finite difference
$\Delta E_1$	work necessary to create a single bubble with radius $R_1$ , $J$
$\Delta E_{1c}$	work necessary to create a single bubble with radius $R_{1c}$ , $J$
$\Delta E_{1c}^*$	$= \phi \Delta E_{1c}$ , energy for the creation of a single bubble at a wall, $J$
$\Delta p_{Fi}^*$	$= p'(T_2) - p_{Fi}$ , flashing inception pressure difference, $Pa$
$\Delta \tau$	time interval, $s$
$\Delta \tau_o$	time within which the bubble collapses completely, $s$
$\varepsilon$	dissipation rate for kinetic energy from turbulent pulsations, irreversibly dissipated power by the viscous forces due to turbulent pulsations, $W/kg$
$\xi$	local friction coefficient
$\eta$	dynamic viscosity of liquid, $kg/(ms)$
$\theta$	static contact angle, $rad$
$\lambda_{RT}$	<i>Rayleigh-Taylor</i> wavelength, $m$
$\lambda$	thermal conductivity, $W/(mK)$
$\lambda_R$	<i>Darcy</i> friction coefficient
$\mu_{21}$	evaporating mass per unit time and unit flow volume, $kg/(m^3s)$
$\mu_{12}$	condensing mass per unit time and unit flow volume, $kg/(m^3s)$
$\rho$	density, $kg/m^3$
$(\rho w)_{21}$	evaporation mass flow rate, $kg/(m^2s)$
$\sigma$	surface tension, $N/m$
$M_{M1}$	kg-mole mass of the condensing gases, $kg/mole$
$\sum M_{n1}$	kg-mole mass of the non-condensing gases, $kg/mole$
$M_1$	kg-mole mass of the gas mixture, $kg/mole$
$\tau$	time, $s$
$\tau_H$	$= \frac{4}{\pi} Ja^2 Fo$ , condensation time scale, <i>dimensionless</i>

---

$\Phi$	cavity angle if the cavity is idealized as a cone, <i>rad</i>
$\Phi_{2o}^2$	two-phase friction multiplier, <i>dimensionless</i>
$\varphi$	work reduction factor, <i>dimensionless</i>

### ***Superscripts***

'	saturated liquid
"	saturated vapor
<i>spin</i>	spinoidal line
$1\sigma$	interface with vapor
$2\sigma$	interface with liquid

### ***Subscripts***

1	vapor, gas
2	liquid
<i>c</i>	critical state
<i>s</i>	at constant entropy
<i>sat</i>	saturated
<i>Fi</i>	flashing inception
$\sum_{n1o}$	sum of all non-condensing gases
<i>M</i>	evaporating or condensing chemical component
<i>n</i>	inert (non condensing) chemical component
<i>u, v, w</i>	in the positive direction of the velocity components <i>u, v</i> and <i>w</i>
<i>R</i>	friction

## **References**

- Akiyama A (1973) Bubble collapse in subcooled boiling, *Bul. JSME*, vol 16 no 93 pp 570-575
- Akiyama M (1973) Bubble collapse in subcooled boiling, *Bulletin of the JSME*, vol 16 pp 570-575
- Avdeev AA (1986) Growth and condensation velocity of steam bubbles in turbulent flow, *Teploenergetika*, in Russian, vol 1 pp 53 - 55
- Brauer et al H (1976) *Chem. Ing. Tech.*, vol 48 pp 737 - 741
- Brucker GG, Sparrow EM (1977) Direct contact condensation of steam bubbles in water of high pressure, *Int. J. Heat Mass Transfer*, vol 20 pp 371-381
- Bucher B, Nordman D (1978) Investigations of subcooled boiling problems in two- phase transport and reactor safety, *Veziroglu RN, Kakac S (eds) Hemisphere, Washington, D.C.*, vol 1 pp 31-49
- Chen YM, Maynger F (August 6 - August 9, 1989) Measurement of heat transfer at the phase interface of condensing bubbles, *ANS Proceedings Nat. Heat Transfer Conference, Philadelphia, Pensilvania*, vol 4 pp 147-152

- Dushkin AL, Kolomenzev AI (1989) Steam bubble condensation in subcooled liquid, High Temperature Physics, , in Russian, vol 27 no 1 pp 116-121
- Forschuetz L, Chao BT (May 1965) On the mechanics of vapor bubble collapse, Transactions of the ASME, Journal of Heat Transfer, pp 209-220
- Hughes ED, Paulsen MP, Agee LJ (Sept. 1981) A drift-flux model of two-phase flow for RETRAN. Nuclear Technology, vol 54 pp 410-420
- Hunt DL (1970) The effect of delayed bubble growth on the depressurization of vessels Containing high temperature water. UKAEA Report AHSB(S) R 189
- Isenberg J, Sideman S (June 1970) Direct contact heat transfer with change of phase: Bubble condensation in immiscible liquids, Int. J. Heat Mass Transfer, vol 13 pp 997-1011
- Kataoka I, Ishii M, Mishima K (June 1983) Transactions of the ASME, vol 105 p 230-238
- Kendouch AA (1976) Theoretical and experimental investigations into the problem of transient two-phase flow and its application to reactor safety, Ph.D.Thesis, Department of Thermodynamics and Fluid Mechanics, University of Strathclyde, U.C.
- Labunzov DA (1974) State of the art of the nuclide boiling mechanism of liquids, Heat Transfer and Physical Hydrodynamics, Moskva, Nauka, in Russian, pp 98-115
- Mayinger F, Nordmann D (1979) Temperature, pressure and heat transfer near condensing bubbles, Proc.of the Heat and Mass Transfer, Dubrovnik, Hemisphere Publ.Corp., New York, vol 1
- Moalem D, Sideman S (1973) The effect of motion on bubble collapse, Int. J. Heat Mass Transfer, vol 16 pp 2321-2329
- Nigmatulin RI (1978) Basics of the mechanics of the heterogeneous fluids, Moskva, Nauka, in Russian
- Nukiyama S, Tanasawa, Y (1938) Trans. Soc. Mech. Engrs. (Japan), vol 4 no 14 p 86
- Pilch M, Erdman CA, Reynolds AB (August 1981) Acceleration induced fragmentation of liquid drops, Charlottesville, VA: Department of Nucl. Eng., University of Virginia, NUREG/CR-2247
- Plesset MS, Zwick SA (April 1954) The growth of bubbles in superheated liquids, J. of Applied Physics, vol 25 no 4 pp 493-500
- Prisnjakov VF (January 1970) Bubble growth in liquids, Journal of Engineering Physics, vol 18 no 1 pp 584-588
- Soo SL (1969) Fluid dynamics of multiphase systems, Massachusetts, Woltham VDI-Waermeatlas, 4. Auflage 1984, VDI-Verlag
- Wallis GB (1969) One-dimensional two-phase flow, McGraw-Hil, New York
- Wilson JF (1965) Primary separation of steam from water by natural separation. US/EURATOM Report ACNP-65002
- Zeitoun O, Shoukri M and Chatoorgoon V (1995) Interfacial heat transfer between steam bubbles and subcooled water in vertical upward flow, Journal of Heat Transfer, vol 117 pp 402-407
26. Zuber N (1961) The dynamics of vapor bubbles in non uniform temperature fields, Int. J. Heat Mass Transfer, vol 2 pp 83-98

## 15 Bubble departure diameter

*The tangential shear due to the volume- and time-averaged pulsation velocity caused by the thermally controlled bubble growth and successive cyclic departure is found to be responsible for the natural switch from the regime of isolated bubble growth and departure into the regime of mutual interaction bubble growth and departure as the temperature difference between the bubble interface and the surrounding liquid increases. The proposed theoretical model, based only on the first principles, agrees well with the experimental data for boiling water to which it was compared. The new model successfully predicts the isolated and the mutual interaction bubble departure size, and the quantitative description of the natural transition between the two regimes is the essentially new feature of this work. This Chapter is a slightly abbreviated version of the work published primarily in Kolev (1994).*

### 15.1 How accurately can we predict bubble departure diameter for boiling?

After 60 years of world wide research on boiling there are still "classical" problems of practical importance that have been not satisfactorily resolved. Such a problem is the analytical description of the bubble departure diameter during boiling or flashing. We demonstrate this problem as follows. Consider saturated water pool boiling at atmospheric pressure on a heated horizontal surface. The experimental data from the literature Gaertner and Westwater (1960), Gaertner (1965), Tolubinsky and Ostrovsky (1966), Siegel and Keshock (1964), van Stralen et al. (1975), Roll and Mayers (1964), are depicted on Figure 15.1 as a function of the wall superheating. Note that data for bubble sizes measured away from the surface and sometimes reported as bubble departure diameters are excluded. Now we try to predict the data behavior. For the prediction of the bubble departure diameter we use some of the frequently cited theories from Fritz (1935), van Krevelen and Hofstijzer (1950), Kocamustafaogullari and Ishii (1983), Cole and Rohsenow (1969), Moalem et al. (1977), Klausner et al. (1993). The results presented in Figs. 15.1 and 15.2 are disappointing. None of these theories predicts even an appropriate data trend. In particular, none of the existing theories gives an explanation of why the bubble departure diameter starts to decrease after a certain superheating is exceeded. The interested reader will find reviews on modeling by Hsu and Graham [8] up to 1975, by van Stralen and Cole up to 1979, and by Klausner et al. (1993) Zeng et al. (1993), Zeng et al. (1993).

for more recent work. These works and the references given there present the state of the art in this field and will not be repeated here.

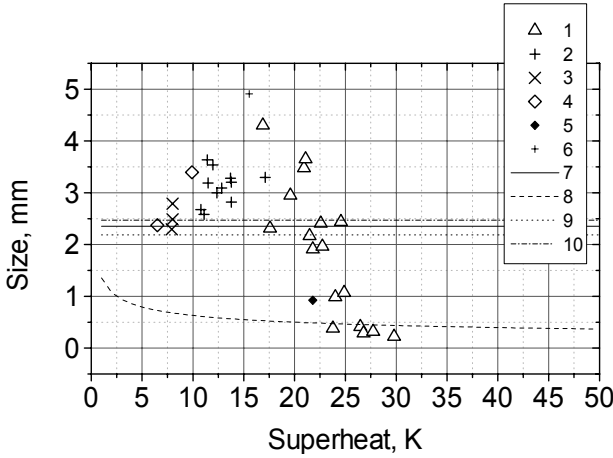


**Fig. 15.1** Bubble departure diameter as a function of superheating. Saturated water pool boiling at 0.1 MPa pressure. Data: 1 Gaertner and Westwater (1960), 2 Gaertner (1965), 3 Tolubinsky and Ostrovsky (1966), 4 Siegel and Keshock (1964), 5 van Stralen et al (1975), 6 Roll and Mayers (1964). Theories: 7 Fritz (1935), 8 van Krevelen and Hoftijzer (1950), 9 Kocamustafaogullari and Ishii (1983), 10 Cole and Rohsenow (1969)

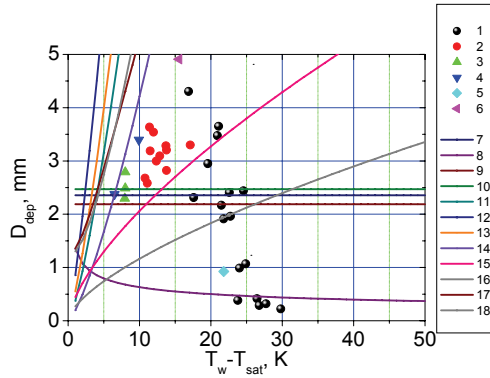


**Fig. 15.2** Bubble departure diameter as a function of superheating. Saturated water pool boiling at 0.1 MPa pressure. Data: 1 Gaertner and Westwater (1960), 2 Gaertner (1965), 3 Tolubinsky and Ostrovsky (1966), 4 Siegel and Keshock (1964), 5 van Stralen et al. (1975), 6 Roll and Mayers (1964). Theories: 7 Fritz (1935), 8 van Krevelen and Hoftijzer (1950), 9 Kocamustafaogullari and Ishii (1983), 10 Cole and Rohsenow (1969), 11 Moalem et al. (1977), 12 Klausner et al.  $n = 1/2$  (1993), 13 Klausner et al.  $n = 1/3$  (1993), 14 Ruckenstein (1961), 15 Voloshko and Vurgaft (1970), 16 Golorin et al (1978), 17 Kutateladze and Gogonin (1979), 18 Jensen and Memmel (1986)



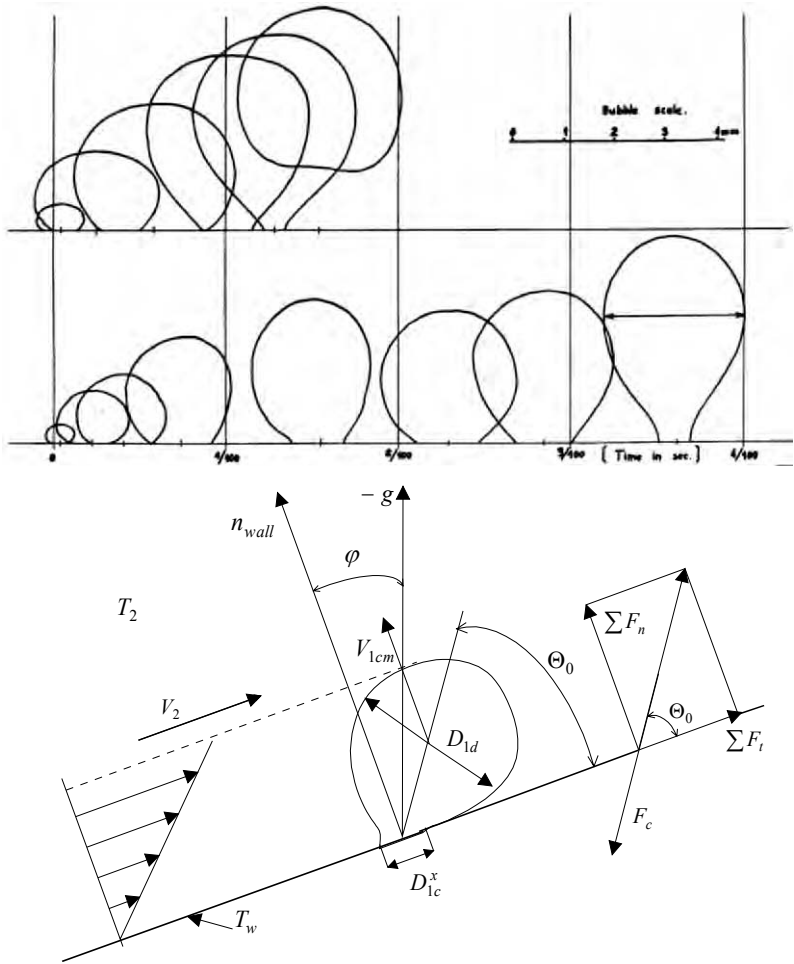


**Fig. 15.3** a) Morin's (1964) observations of water bubble detachment in pool at heated horizontal copper wall: a) 5°C subcooling; b) no subcooling; c) Model of a bubble detachment in heated wall in flow boiling used in this work

We present in this Section a new model for the prediction of the bubble departure diameter as a function of the local flow parameter, which agrees well with data for pool and flow boiling at atmospheric and elevated pressures. We show that the mutual interaction during bubble growth and departure introduces enough shear stress to cut off the adjacent bubbles at an earlier stage of their growth.

## 15.2 Model development

Consider bubble growth at a heated surface as shown in Fig. 15.3. The surface vector and the upwards-directed vertical form an angle  $\varphi$ . There is a flow from left to right with an average velocity  $V_2$ . The derived expressions rely on the following assumptions:

- 1) The bubble is capable to grow after reaching the size given by Eq. (12.16)

$$D_{1c}^* = \frac{3}{2} D_{1c} \quad (15.1)$$

where  $D_{1c}$  is the critical bubble size.

- 2) The bubble growth is thermally controlled. The expression governing the bubble growth is of the type given in Appendix 13.1

$$D_1 = 2B\tau^n \quad (15.2)$$

or

$$dD_1 / d\tau = 2nB\tau^{n-1}. \quad (15.3)$$

It is generally agreed that the exponent  $n$  is of order of  $1/2$  for saturated liquids. For the purpose of data comparison we use in this work *Labuntsov's* approximation of the *Scriven* solution Labuntsov (1974),  $n = 1/2$  and

$$B = c Ja a_2^{1/2}, \quad (15.4)$$

where

$$c = (12/\pi)^{1/2} \left[ 1 + \frac{1}{2} \left( \frac{\pi}{6Ja} \right)^{2/3} + \frac{\pi}{6Ja} \right]^{1/2}. \quad (15.5)$$

- 3) The base bubble diameter at the wall is equal to  $D_{1c}^*$  for high pressure. For low pressure, the base diameter initially grows and thereafter collapses, so that at the moment of detachment it again approximates  $D_{1c}^*$ .

- 4) At the moment of detachment the bubble is deformed such that its diameter measured parallel to the surface is larger than the volume-averaged bubble departure diameter  $D_{1d}$ .

- 5) The presence of the wall increases the drag coefficient of the bubble in the tangential drag force compared to the case of a bubble in an infinite medium.

- 6) The bubble axis inclination,  $\theta_0$ , coincides with the main force inclination with respect to the wall.

7) At the moment of departure, the elongation of the bubble base to a cylindrical form with the axis coincident with the bubble axis is the reason for the tangential surface tension force component.

Some useful consequences of assumption 2 which will be used later are given below. At the moment of detachment,  $\Delta\tau_{1d}$ , the bubble radius is

$$R_{1d} = B \Delta\tau_{1d}^n \quad (15.6)$$

the bubble center of mass (c.m.) velocity normal to the wall is

$$V_{1cm} = dR_{1d} / d\tau = nB\Delta\tau_{1d}^{n-1} \quad (15.7)$$

and the c.m. temporal acceleration normal to the wall is

$$dV_{1cm} / d\tau = n(n-1)B\Delta\tau_{1d}^{n-2} \quad (15.8)$$

Consequently the total acceleration is

$$\begin{aligned} \left( \frac{dV_1}{d\tau} + V_1 \frac{dV_1}{dy} \right)_{cm} &= dV_{1cm} / d\tau + V_{1cm}^2 / R_{1d} = n(n-1)B\Delta\tau_{1d}^{n-2} + n^2 B\Delta\tau_{1d}^{n-2} \\ &= nB\Delta\tau_{1d}^{n-2} (2n-1). \end{aligned} \quad (15.9)$$

For  $n = 1/2$ , which, as already mentioned, is the case for bubble growth in saturated liquid, the total bubble acceleration is zero, and therefore the bubble does not exert any dynamic forces like inertia and virtual mass force. This is a very surprising result. It simply means that at the moment of departure only the static mechanical equilibrium governs the bubble departure.

Before writing the momentum equation we compute the force components in normal and tangential directions. The buoyancy force components are

$$F_{b,n} = \frac{\pi}{6} D_{1d}^3 (\rho_2 - \rho_1) g \sin \varphi \quad (15.10)$$

and

$$F_{b,t} = \frac{\pi}{6} D_{1d}^3 (\rho_2 - \rho_1) g \cos \varphi. \quad (15.11)$$

For computation of the normal drag force resisting the bubble growth, we modify the Eq. (2.20) derived by *Ishii and Zuber* (1978) for bubbles in infinite liquid

$$F_{d,n} = 3\pi\eta_2 c_{form} D_{1d} V_{1cm} \left[ 1 + 0.1(c_{form} D_{1d} V_{1cm} \rho_2 / \eta_2) \right]^{3/4}. \quad (15.12)$$

The product

$$D_{1d} V_{1cm} = 2nB^2 \Delta\tau_{1d}^{2n-1}, \quad (15.13)$$

which for  $n = 1/2$

$$D_{1d} V_{1cm} = B^2 \quad (15.14)$$

is obviously a function of superheating only. Consequently

$$F_{d,n} = 3\pi\eta_2 c_{form} B^2 [1 + 0.1(c_{form} B^2 \rho_2 / \eta_2)]^{3/4}. \quad (15.15)$$

The form coefficient,  $c_{form}$ , takes into account the ratio of the bubble size parallel to the wall to the volume-averaged bubble size as well the departure of the c.m. bubble velocity normal to the wall due to complicated bubble growth and deformation at the moment of detachment. It was found through the data comparison for pool boiling only that

$$c_{form} \approx 2. \quad (15.16)$$

The drag force parallel to the wall is

$$F_{d,t} = 0.3\pi\rho_2 (c_{wall} D_{1d} V_{21d})^2. \quad (15.17)$$

Here  $V_{21d}$  is the boundary layer velocity at distance  $R_{1d}$  from the wall. We compute this velocity using the *Reichardt* (1951) universal velocity profile for  $y \ll D_{1d}/2$

$$\frac{V_{21d}}{w^*} = 2.5 \ln(1 + 0.4y^+) + 7.8 \left[ 1 - \exp(-y^+/11) - \frac{y^+}{11} \exp(-0.33y^+) \right].$$

in exactly the same manner as described in *Klausner et al.* (1993). Here  $y^+ = y w^* / \nu$  is the dimensionless distance from the wall and  $w^*$  is the friction velocity. The deviation from the idealized profile in the real flow, caused by the bubbles themselves, the bubble deformation, and the wall influence are pooled into the wall correction coefficient, which was found to be

$$c_{wall} = 2 \quad (15.18)$$

through comparison with flow boiling data for negligible mutual interaction. The lift force caused by the rotation of the non-uniform velocity field at the wall is

$$F_{l,n} = \pi \frac{1}{2} \rho_2 (D_{1d} V_{21d})^2 c_{lift}, \quad (15.19)$$

where

$$c_{lift} = 3.877 \beta^{1/2} (0.014 \beta^2 + \text{Re}_{12}^{-2})^{1/4},$$

$$\text{Re}_{12} = V_{21d} D_1 / \nu_2,$$

$$\beta = \frac{D_1/2}{V_{21d}} \left| \frac{dV_{21d}}{dy} \right|,$$

$$\frac{dV_{2ld}}{dy} = \frac{w^{*2}}{\nu} \left\{ \frac{1}{1+0.4y^+} + \frac{7.8}{11} \left[ \exp(-y^+/11) + (0.33y^+ - 1) \exp(-0.33y^+) \right] \right\}$$

is computed in accordance with *Klausner et al.* (1993).

Finally we consider a force never before considered in the literature in the momentum equation describing bubble departure - the drag force caused by the growth of the neighboring bubbles

$$F'_{d,t} = 0.3\pi\rho_2(D_{1d}\bar{\bar{V}}_2')^2. \quad (15.20)$$

For an incompressible liquid denoted with subscript 2 the mass conservation equation for the liquid velocity gives  $u_2 = (dR_1/d\tau)(R_1/r)^2$  in the region between  $R_1$  and  $R_{2,inf}$ , where  $R_{2,inf}$  is half of the average center-to-center spacing. *Zuber* (1963) obtained the volume average liquid velocity as follows

$$\bar{\bar{V}}_2' = \frac{1}{R_{2,inf} - R_1} \int_{R_1}^{R_{2,inf}} R_1^2 \frac{dR_1}{d\tau} \frac{dr}{r^2} = \frac{R_1}{R_{2,inf}} \frac{dR_1}{d\tau} = 2R_1 \frac{dR_1}{d\tau} / D_{2,inf} = B^2 / D_{2,inf} \quad (15.21)$$

where

$$B^2 = 2R_1 \frac{dR_1}{d\tau}. \quad (15.22)$$

for  $n = 1/2$ . For the idealized case of a triangular array at a plane surface, the influence circle has a diameter  $D_{2,inf} = \left( \frac{2}{\sqrt{3}} \frac{1}{n_{1w}''} \right)^{1/2} \approx 1.074 / n_{1w}^{1/2}$ ,

but the experimentally observed distribution of the active nucleation sites is a *Poisson* distribution *Gaertner* (1963), *Sultan and Judd* (1978), *Wang and Dhir* (1993). It gives an average distance between two neighboring bubbles sites of

$$\left( D_{2,inf}^2 \right)^{1/2} = \left( \frac{1}{\pi n_{1w}''} \right)^{1/2} \approx 0.56 / n_{1w}^{1/2} \quad (15.23)$$

More recent measurements by *Wang and Dhir* (1993) give  $\left( D_{2,inf}^2 \right)^{1/2} \approx 0.84 / n_{1w}^{1/2}$ .

For the purpose of the data comparisons we use in this work Eq. (15.23). The *time-averaged fluctuation velocity* (called sometimes micro-convection velocity) during  $\Delta\tau_w + \Delta\tau_d$  is therefore

$$\bar{\bar{V}}_2' = (B^2 / D_{2,inf}) \frac{\Delta\tau_d}{\Delta\tau_w + \Delta\tau_d} = B^2 \frac{\Delta\tau_d}{\Delta\tau_w + \Delta\tau_d} (\pi n_{1w}'')^{1/2}, \quad (15.24)$$

which is generally applicable to different situations of bubble production at walls such as boiling, flashing, and gas injection through perforated plates. Note that

nucleation at inner and outer walls of a cylinder with diameter  $D_h$  is characterized by

$$D_{2,\text{inf}} = \left( \frac{1}{\pi n_{1w}''} \right)^{1/2} (1 \pm D_{1d} / D_h), \quad (15.23a)$$

where the minus sign is valid for the inner surface. Consequently

$$\begin{aligned} \bar{\bar{V}}_2' &= (B^2 / D_{2,\text{inf}}) \frac{\Delta \tau_d}{\Delta \tau_w + \Delta \tau_d} = B^2 \frac{\Delta \tau_d}{\Delta \tau_w + \Delta \tau_d} (\pi n_{1w}'')^{1/2} / (1 \pm D_{1d} / D_h) \\ &= D_{1d}^2 f_{1w} (\pi n_{1w}'')^{1/2} / (1 \pm D_{1d} / D_h). \end{aligned} \quad (15.24a)$$

Consequently, with increased wall superheating, bubbles in a pipe interact more strongly than bubbles at a plane, and bubbles at an outer cylinder wall interact less intensively than bubbles at a plane. The higher the value of  $D_{1d}/D_h$  the stronger is the influence of the geometry. For large values of superheating,  $\Delta \tau_{1d} / (\Delta \tau_{1w} + \Delta \tau_{1d})$  approximates 1. For small values, this force is not important. Thus the approximation of the exact equation

$$\bar{\bar{V}}' = B^2 (\pi n_{1w}'')^{1/2} \quad (15.25)$$

can be used to compute the bubble departure diameter. Now we compute the bubble inclination angle using assumption 6

$$\theta_0 = \arctan \left[ (F_{b,n} - F_{d,n} + F_{1,n}) / (F_{b,t} + F_{d,t} + F_{d,t}') \right] \quad (15.26)$$

and write the static force balance along the axis of the bubble divided by  $\pi$

$$\begin{aligned} & \frac{1}{6} D_{1d}^3 (\rho_2 - \rho_1) g \sin(\varphi + \theta_0) + \frac{1}{2} \rho_2 (D_{1d} V_{21d})^2 c_{\text{lift}} \sin \theta_0 \\ & + 0.3 \rho_2 (c_{\text{wall}} D_{1d} V_{21d})^2 \cos \theta_0 + 0.3 \rho_2 (D_{1d} \bar{\bar{V}}_2')^2 \cos \theta_0 \\ & = D_{1c}^* \sigma + 3 \eta_2 c_{\text{form}} B^2 \left[ 1 + 0.1 (c_{\text{form}} B^2 \rho_2 / \eta_2) \right]^{3/4} \sin \theta_0 \end{aligned}$$

or simply

$$(D_{1d} / D_{1d,nc})^3 + (D_{1d} / D_{1d,fc})^2 = 1 \quad (15.27)$$

where

$$D_{1d,nc} = \left\{ 6A / \left[ (\rho_2 - \rho_1) g \sin(\varphi + \theta_0) \right] \right\}^{1/3}, \quad (15.28)$$

$$D_{1d,fc} = \left\{ A / \left[ \rho_2 V_{21d}^2 \left( \frac{1}{2} c_{lift} \sin \theta_0 + 0.3 c_{wall}^2 \cos \theta_0 \right) + 0.3 \rho_2 \bar{V}_2'^2 \cos \theta_0 \right] \right\}^{1/2}, \quad (15.29)$$

and

$$A = D_{1c}^* \sigma + 3 \eta_2 c_{form} B^2 \left[ 1 + 0.1 (c_{form} B^2 \rho_2 / \eta_2) \right]^{3/4} \sin \theta_0. \quad (15.30)$$

Note that the inclination angle for forced convection is a real one. For pool boiling it is the cone angle within which the fluctuation of the spatial inclination occurs. The angular position within this angle changes chaotically. That is why one experimentally sees fluctuation but never inclination of the vapor column. It explains the well known oscillating of the bubble columns. Note that the bubbles at a surface never start and grow simultaneously - such an idealized picture should give zero interaction force, which is never the real case.

Obviously we have two transcendental equations with two unknowns  $D_{1d}$  and  $\theta_0$  which are solved by iteration. It is important to note that after each iteration-step the new inclination is computed as an average value between the previous and the new computed values. This ensures a stable algorithm that converges to the desired accuracy after a maximum of seven iterations. For low superheating and low flow velocities,  $D_{1d}$  approximates  $D_{1d,nc}$ , and for large superheating and large flow velocities,  $D_{1d}$  approximates  $D_{1d,fc}$ . It is important to note that the surface tension and the latent heat of vaporization are functions of the wall temperature for boiling and of the liquid temperature for flashing.

Note that the contribution of the macro-convection in boiling heat transfer is generally accepted. Consequently we have to take it into account also in the momentum balance.

## 15.3 Comparison with experimental data

We have confined our attention to water data only because this model is operating in computer code IVA in all of its variants, which has water as one of the three flow components Kolev (1993). For further information on this code see the references given in Kolev (1993). The prediction of bubble departure diameter is a part of the analytical modeling of transient sources and sinks of bubbles and droplets in addition to the information presented in Kolev (1993), which is used in IVA3. Figure 15.4 presents a comparison of the prediction of the new theory with the already discussed data for saturated water pool boiling at a horizontal surface. Without considering the mutual bubble interaction the trend of the curve for superheating is lower than 15 K continuous to an asymptotic value of about 5 mm as shown in Fig. 4 in Kolev (1994). The line on Fig. 15.4 represents the new model considering the mutual bubble interaction.

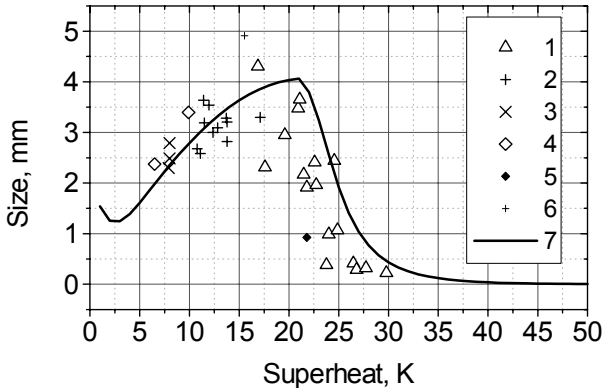


**Fig. 15.4** Bubble departure diameter as a function of superheating. Saturated water pool boiling at 0.1 MPa pressure. Data 1: Gaertner and Westwater (1960), 2 Gaertner (1965), 3 Tolubinski and Ostrovsky (1966), 4 Siegel and Keshock (1964), 5 van Stralen et al. (1975), 6 Roll and Mayers (1964), 7 IVA5 model with bubble interactions

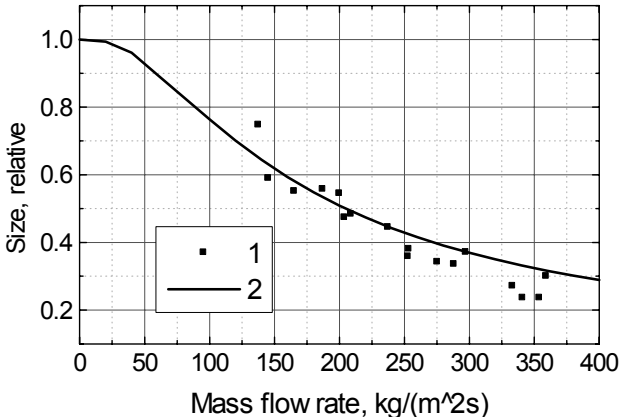


**Fig. 15.5** Bubble departure diameter as function of mass flow rate. Saturated water flow boiling at 0.1 MPa pressure.  $D_{hy} = 0.019\text{ m}$ ,  $T_w - T_2 = 15\text{ K}$ . 1 Data of Koumoutsos et al. (1968), 2 IVA5 model without bubble interaction

The particle number density for the *Gaertner* and *Westwater* (1960) data, presented in Fig. 12.1 and approximated by Eqs. (12.107) and (12.108) is used for this comparison. In the original publication, *Gaertner* and *Westwater* (1960) called the bubble departure diameter "lift off diameter", and in a later work by *Gaertner*



(1963) it is called "bubble column stem" diameter. However, the proportionality constant between both diameters is around one. Note that the *Gaertner* and *Westwater* data for particle number density and bubble departure diameter as a function of the wall superheating are confirmed also by the later measurements by *Iida* and *Kobayasi* (1970), who measured particle number density and the thickness of the thermal boundary layer for pool boiling. Figure 12.1 presents the nucleation site density as a function of superheating also by other authors *Gaertner* (1965), *Labuntsov* (1974), *Yamagata* et al. (1955), *Jakob* (1932), *Cornwell* and *Brown* (1978), *van Stralen* and *Cole* (1979), *Rallis* and *Jawurek* (1964). This is done to classify the *Gaertner* and *Westwater* data as the data giving the lowest possible nucleation site density for saturated pool boiling of water. The consideration of the mutual bubble interaction has a striking effect that can not be overlooked. This interaction is responsible for the decrease of the bubble diameter when the nucleation site density exceeds some value, that is, when the wall superheating exceeds some value. This regime causes a change of the character of the *Nukiyama* diagram containing data for saturated water pool boiling at atmospheric pressure on polished surfaces *Gaertner* (1965), *van Stralen* and *Cole* (1979), *Yamagata* et al. (1955), *Sultan* and *Judd* (1978), *Wiebe* (1970), *Gaertner* and *Westwater* (1960), *Borishanskii* et al. (1961), *Jakob* and *Fritz* (1935), *Cornwell* and *Brown* (1978), *Vachon* et al. (1968), *Nishikawa* et al. (1984). As shown in Fig. 15.7 and is in fact quite different from boiling with negligible interaction, which in the boiling literature is called the regime of isolated bubbles. Our theory predicts a smooth transition between the two regimes, which is the expected behavior in nature.

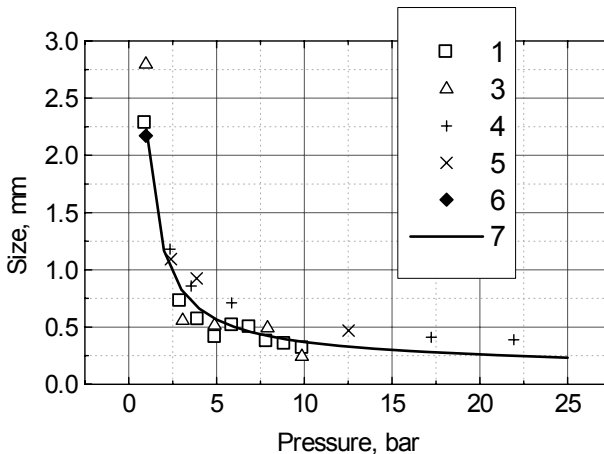


**Fig. 15.6** Bubble departure diameter as a function of pressure. Saturated water pool boiling, superheat = 7.2 K. Data of Tolubinsky and Ostrovsky: 1 Permalloy, 2 brass, 3 copper. Data of Semeria: 4 wire  $D = 0.8\text{mm}$ , 5 plate. 6 Model IVA5 with bubble interaction

*Shoji* et al. confirmed again in 2005 by carefully performing experiments that decreasing of the spacing between two neighboring nucleation sites decreases the bubble departure diameter definitely and vice versa: the authors found that for  $D_{2,\text{inf}}/D_{1d} > 3$  the influence is almost negligible.

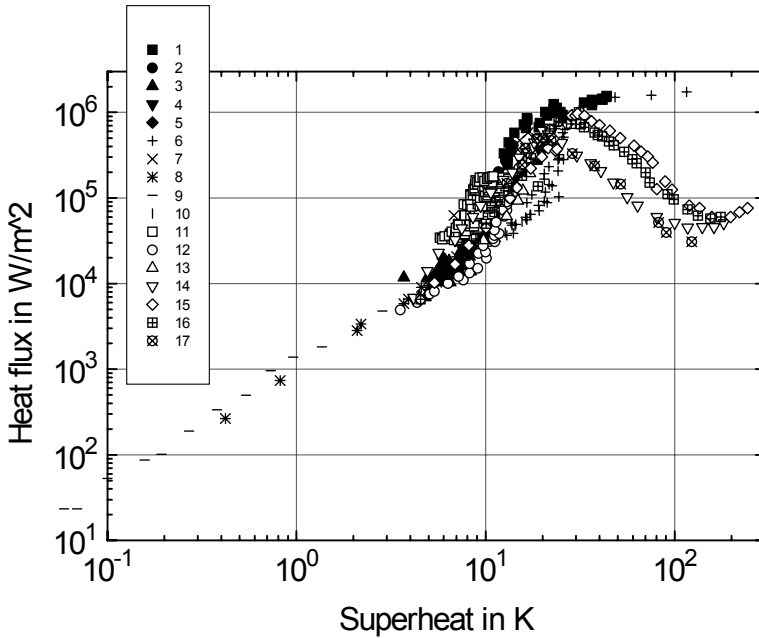


**Fig. 15.7** Heat flux as a function of superheat. Saturated water at 0.1 MPa. 1) Gaertner 1965, 4/0 polished copper, 2) Kurihara and Myers 1960, 4/0 polished copper, 3) Yamagata et al. 1955, fine polished brass, 4) Sultan and Judd 1978, diamond grid 600 polished copper, 5) Wiebe 1970, diamond 600 polished copper, 6) Gaertner and Westwater 1960, 4/0 polished copper, 20 p.c. nickel salt-water solution, 7) Borishanskii et al. 1961, steel, 5 to 8 p.c. error, 8) Fritz 1935, polished steel, 9) Jakob and Linke 1933, polished steel, 10) Cornwell and Brown 1978, 4/0 polished copper, 11) Vachon et al. 1968, emery grid 600 polished 304 stainless steel, 12) Nishikawa et al. 1984, emery grid No.0/10 polished copper, 13) Rallis and Jawurek 1964, nickel wire, 14) Wang and Dhir (1993) nuclide and transition boiling. Contact angle 90 deg, 15) Wang and Dhir (1993) nuclide and transition boiling. Contact angle 18 deg, 16) Wang and Dhir (1993) nuclide and transition boiling. Contact angle 35 deg, 17) Wang and Dhir (1993) nuclide and transition boiling. Contact angle 35 deg. Liaw data

In Fig. 15.5 we compare the prediction of our theory with *flow boiling* data given in Koumoutsos et al. (1968). On the abscissa is entered the bubble departure diameter divided by the bubble departure diameter for pool boiling. The trend of the data is reasonably reproduced. Figure 8 in Kolev (1994) shows the same data compared also with predictions using theories of other authors Levy (1967), Yang and weisman (1991), Jones (1992), Jones (1992) and with prediction of our theory neglecting the normal force components. We find from this comparison that neglecting the normal force component is allowed for mass flow rates larger than  $150 \text{ kg/m}^2\text{s}$ . The theory of Jones [1992] gives unbounded values for small mass flow rate, and the Yang and Weisman modification Yang and Weisman

(1991) of *Levy's* theory *Levy* (1967) underpredicts the data as shown in Fig. 8 in *Kolev* (1994).

Figure 15.6 gives a comparison with data at elevated pressures reported in Refs. [36, 31]. In this case also, the trend of the data is properly reproduced by our theory.

*Shoji et al.* (2005) demonstrated that for cylindrical cavity serving as nucleation sites the cavity diameter (5 to 100 $\mu\text{m}$ ) does not influence the bubble departure sizes. But the decrease of the depth of the cavity (80, 40, 20 $\mu\text{m}$ ) decreases the wall superheat at constant power and reduces the bubble departure diameter: 8.5K 1.85mm, 7.5K, 1.5mm, 5.8K, 1.3mm. 4W distributed on a circle with 12mm was the heat source in this experiment. This slope corresponds to those obtained by other authors in this temperature region as shown in Fig. 15.4.

From the above discussion the following conclusions are in order:

1. The mutual interaction of the growing and departing bubbles causes significant shear at the surface and forces the bubbles to detach at an earlier stage of their growth.
2. The proposed theory successfully describes quantitatively the natural transition between the isolated bubble boiling and boiling with mutual bubble interaction with changing temperature difference.

## 15.4 Significance

The proposed method can be used in various fields of engineering practice, a few of them being

1. Flashing in channel flow due to depressurization and critical flow - Chapter 17.
2. Boiling in pools and channels - Chapter 16.
3. Modeling of multi-phase flow in system computer codes.
4. Reexamination of all approaches for analytical description of boiling heat transfer using the bubble departure diameter as an input variable.
5. Reexamination of all approaches for analytical description of bubble diameter produced by gas injection into a liquid through perforated plates - Section 10.7.

## 15.5 Summary and conclusions

The *tangential shear* due to the volume- and time- averaged *pulsation velocity* caused by the thermally controlled bubble growth and successive cyclic departure is found to be responsible for the natural switching from the regime of *isolated* bubble growth and departure into the regime of *mutually interacting* bubble growth and departure as the temperature difference between the bubble interface and the surrounding liquid increases. The proposed theoretical model, based only on the first principles, agrees well with the experimental data for boiling water to which it was compared. The new model, which successfully predicts the isolated

and the mutually interacting bubble departure sizes, and the quantitative description of the natural transition between the two regimes are the essentially new features of the work presented in this Chapter.

## 15.6 Extension of the theory to sub-cooled liquids

The theory presented above successfully describes the bubble departure in saturated liquid. In this section we will extend the theory to sub-cooled boiling following the already introduced method of combined thermal analysis with force equilibrium.

*Ünal* proposed in 1976 to consider the sub-cooled boiling bubble growth as superposition of evaporation feed by the conduction from the wall and partial condensation at the bubble top. Using the imagination of *Zuber* (1961) that the superheated micro-layer is created before the explosion of the nucleus and neglecting the nucleation diameter as a small compared to any later bubble size after the origination we can write the following equation for the growth of the bubble mass

$$\frac{d}{d\tau} \left( \rho'' \frac{\pi}{6} D_1^3 \right) = \frac{\pi D_1^2}{\Delta h} \left[ -\dot{q}_2^{n1\sigma} - c_1 \left( h_{2,w=0}^{1\sigma} + h_{2,w \neq 0}^{1\sigma} \right) (T' - T_2) \right], \quad (15.31)$$

which for constant vapor density results in

$$\frac{dR_1}{d\tau} = -\frac{\dot{q}_2^{n1\sigma}}{\rho'' \Delta h} - c_1 \left( h_{2,w=0}^{1\sigma} + h_{2,w \neq 0}^{1\sigma} \right) \frac{(T' - T_2)}{\rho'' \Delta h}. \quad (15.32)$$

For bubble growth at a wall the expression obtained by *Labuntsov* et al. in 1964 can be used

$$-\frac{\dot{q}_2^{n1\sigma}}{\rho'' \Delta h} = \frac{B_{\text{sup}}}{2\sqrt{\tau}}, \quad (15.33)$$

where

$$B_{\text{sup}} = 2.5 \sqrt{2a_2 \beta Ja_{2w}}, \quad (15.34)$$

$Ja_{2w} = \frac{\rho_2 c_{p2} (T_w - T')}{\rho'' \Delta h}$ , and  $\beta \approx 6$ . We assume that the disc with a cross section  $\pi D_1^2/4$  receive the evaporation mass flow rate corresponding to  $\dot{q}_2^{n1\sigma}$ . The constant  $c_1$  reflects the part of the bubble surface  $\pi D_1^2$  contacting the sub-cooled liquid e.g.  $c_1 = 1/2$ . The condensation is assumed to be driven by a superposition of molecular heat conduction

$$h_{2,w=0}^{1\sigma} \frac{(T' - T_2)}{\rho'' \Delta h} = Ja_{2,sub} \sqrt{\frac{1}{\pi} \frac{a_2}{\tau}}, \quad (15.35)$$

$$Ja_{2,sub} = \frac{\rho_2 c_{p2} (T' - T_2)}{\rho'' \Delta h}, \quad (15.36)$$

*Forschluetz* and *Chao* (1965), and eddies renewal due to turbulence

$$\frac{h_{2,w=0}^{1\sigma} D_h}{\lambda_2} = 0.228 Re_2^{0.8} Pr_2^{1/2} \left( \Phi_{20}^2 / \alpha_2 \right)^{1/4}, \quad (15.37)$$

*Avdeev* (1986). Replacing the heat flux components in the mass conservation equation results in

$$\frac{dR_1}{d\tau} = \frac{B}{2\sqrt{\tau}} - A, \quad (15.38)$$

where

$$B = B_{sup} - \sqrt{\frac{a_2}{\pi}} Ja_{2,sub}, \quad (15.39)$$

$$A = 0.228 \frac{1}{2} \frac{a_2}{D_h} Ja_{2,sub} Re_2^{0.8} Pr_2^{1/2} \left( \Phi_{20}^2 / \alpha_2 \right)^{1/4}. \quad (15.40)$$

Note that there is a driving mechanism for a bubble growth in sub-cooled liquid only if

$$2.5\sqrt{2\beta\pi Ja_{2w}} > Ja_{2,sub}. \quad (15.41)$$

The radius of the bubble as a function of time is then

$$R_1 \approx R_{1c} + B\sqrt{\tau} - A\tau. \quad (15.42)$$

The radius possesses a maximum

$$R_{1m} \approx R_{1c} + \frac{1}{4} \frac{B^2}{A} \quad (15.43)$$

at

$$\tau_{1m} = \frac{1}{4} \left( \frac{B}{A} \right)^2. \quad (15.44)$$

If the maximum of the diameter is smaller then the bubble departure diameter the bubble will stay at the surface, else the bubble will depart with the bubble departure diameter. The bubble growth equation can be rewritten in dimensionless form as proposed by *Zuber* in 1961

$$\frac{R_l - R_{lc}}{R_{lm} - R_{lc}} = 2 \sqrt{\frac{\tau}{\tau_{lm}}} - \frac{\tau}{\tau_{lm}}. \quad (15.45)$$

Note that the form of the equation is as obtained by *Zuber* but not the contents of the different terms. As expected for a given radius there are two solutions for the time

$$\frac{\tau}{\tau_{lm}} = \left( 1 \pm \sqrt{1 - \frac{R_l - R_{lc}}{R_{lm} - R_{lc}}} \right)^2. \quad (15.46)$$

The center of mass velocity corresponding to this bubble growth mechanism is then

$$V_{lcm} = \frac{dR_l}{d\tau} = \frac{R_{lm} - R_{lc}}{\tau_{lm}} \left[ \left( \frac{\tau}{\tau_{lm}} \right)^{-1/2} - 1 \right]. \quad (15.47)$$

The temporal bubble acceleration is

$$\frac{\partial V_{lcm}}{\partial \tau} = -\frac{1}{2} \frac{R_{lm} - R_{lc}}{\tau_{lm}^2} \left( \frac{\tau}{\tau_{lm}} \right)^{-3/2}. \quad (15.48)$$

The total bubble acceleration is

$$\frac{\partial V_{lcm}}{\partial \tau} + V_{lcm} \frac{V_{lcm}}{R_l - R_{lc}} = \frac{R_{lm} - R_{lc}}{\tau_{lm}^2} \left\{ \frac{R_{lm} - R_{lc}}{R_l - R_{lc}} \left[ \left( \frac{\tau}{\tau_{lm}} \right)^{-1/2} - 1 \right]^2 - \frac{1}{2} \left( \frac{\tau}{\tau_{lm}} \right)^{-3/2} \right\}. \quad (15.49)$$

Neglecting the virtual mass force we apply now the equations (15.26) and (15.27) by using the already described mechanism of the bubble growth and collapse. The result for horizontal plane at 1 bar pressure and varying sub-cooling is presented in Fig. 15.8.

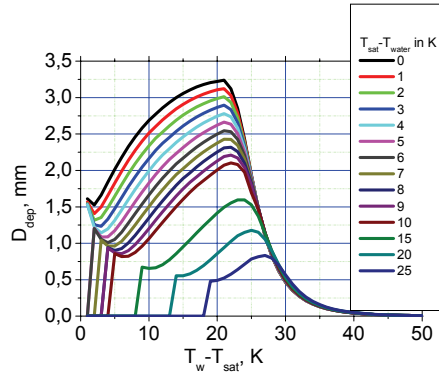


**Fig. 15.8** Bubble departure diameter at horizontal surface without flow as function of the wall superheating at 1 bar. Parameter – water sub-cooling. Stagnant liquid

For zero sub-cooling we reproduce well the experimental data as already discussed in the pervious section. For increasing sub-cooling the bubble departure diameter decreases. The zero-values are artificially set to indicate in the graph that in the particular combination of superheating and sub-cooling there are no conditions for bubble departure at all.

## 15.7 Influence of the wall material

*Morin* (1964) measuring the temperature in the wall just below the growing bubble found that there is cyclic decrease and increase corresponding to the growing cycle.

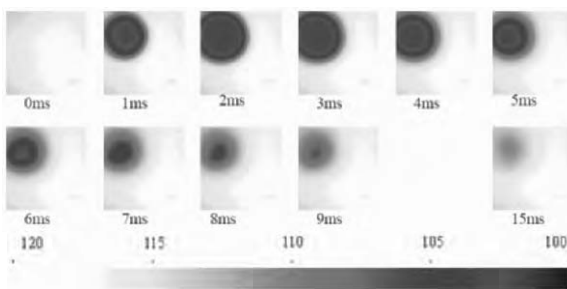


**Fig. 15.9** Wall temperature distribution under the growing bubble at 100kW/m², *Golobic et al.* (2006)

Better heat conduction materials react faster on the changing heat exhausting conditions due to evaporation of the liquid around the bubble contact line with the

wall. 42 years later *Golobic et al.* (2006) reported two dimensional temperature distribution around the nucleation center as given in Fig. 15.9. Therefore the theory reported above can farther be improved by considering this phenomenon.

## Nomenclature

### Latin

$a_2$	liquid thermal diffusivity, $m^2/s$
$B^2$	$= 2R_1 dR_1 / d\tau$ , $m^2/s$
$D_l$	bubble diameter, $m$
$D_{1c}$	critical diameter, $m$
$D_{1d}$	bubble departure diameter, $m$
$D_{2,inf}$	$= 2R_{2,inf}$ , $m$
$D_{1d,fc}$	bubble departure diameter for strongly predominant forced convection, $V_{21d} \gg \bar{V}_2'$ , $m$
$D_{1d,nc}$	bubble departure diameter for natural circulation, $V_{21d} \ll \bar{V}_2'$ , $m$
$D$	total differential, <i>dimensionless</i>
$G$	mass flow rate, $kg/(m^2s)$
$g$	gravitational acceleration, $m/s^2$
$h'$	saturated liquid specific enthalpy, $J/(kgK)$
$h''$	saturated steam specific enthalpy, $J/(kgK)$
$Ja$	$= \frac{[T_2 - T'(p)]c_{p2}}{h''(p) - h'(p)} \frac{\rho'}{\rho''}$ , <i>Jacob number, dimensionless</i>
$n_{1w}''$	active nucleation site density, $1/m^2$
$p$	pressure, $Pa$
$p_c$	critical pressure, $Pa$
$R_1$	bubble radius, $m$
$R_{2,inf}$	half of the average center-to-center spacing, $m$
$T'(p)$	saturation temperature at system pressure $p$ , $K$
$T_2$	liquid temperature, $K$
$T_w$	wall temperature, $K$
$V_{1cm}$	center-of-mass bubble velocity at the moment of detachment, $m/s$
$V_{21d}$	tangential velocity in the boundary layer of thickness $D_{1d}$ , $m/s$
$u_2$	liquid velocity in the region between $R_1$ and $R_{2,inf}$ , $m/s$
$\bar{V}_2'$	volume-averaged fluctuation velocity, $m/s$
$\bar{\bar{V}}_2'$	time- and volume-averaged fluctuation velocity over $\Delta\tau_w + \Delta\tau_d$ , $m/s$



**Greek**

$\partial$	partial differential, <i>dimensionless</i>
$\Delta\rho_{21}$	$= \rho_2 - \rho_1$ , $kg/m^3$
$\Delta\tau_d$	time need from the origination of bubble with critical size to the bubble departure from the wall, <i>s</i>
$\Delta\tau_w$	delay time, <i>s</i>
$\eta_2$	dynamic viscosity of liquid, $kg/(ms)$
$\varphi$	angle between the flow direction and the upwards-directed vertical, - $\mathbf{n}_g$ , <i>rad</i>
$\rho_1$	gas density, $kg/m^3$
$\rho_2$	liquid density, $kg/m^3$
$\rho''$	saturated steam density, $kg/m^3$
$\rho'$	saturated liquid density, $kg/m^3$
$\bar{\rho}$	$= (\rho' - \rho'') / \rho$ , <i>dimensionless</i>
$\sigma$	surface tension, <i>N/m</i>
$\tau_{2w}$	$= \frac{\xi}{8} G^2 / \rho$ shear stress, <i>N / m<sup>2</sup></i>
$\tau$	time, <i>s</i>
$\theta_0$	angle between the bubble axis and the wall, <i>rad</i>

**References**

- Avdeev AA (1986) Growth and condensation velocity of steam bubbles in turbulent flow, Teploenergetika, in Russian, vol 1 pp 53 – 55
- Borishanskii V, Bobrovich G, Minchenko F (1961) Heat transfer from a tube to water and to ethanol in nucleate pool boiling, Symposium of Heat Transfer and Hydraulics in Two-Phase Media, Kutateladze SS (ed) Gosenergoizdat, Moscow
- Cole R, Rohsenow WM (1969) Correlation of bubble departure diameters for boiling of saturated liquids, Chem. Eng. Prog. Symp. Ser. , vol 65 no 92 pp 211-213
- Cornwell K, Brown RD (1978) Boiling surface topology, Proc. 6th Int. Heat Transfer Conf., Toronto, vol 1 pp 157-161
- Forschuetz L, Chao BT (May 1965) On the mechanics of vapor bubble collapse, Transactions of the ASME, Journal of Heat Transfer, pp 209-220
- Fritz W (1935) Berechnung des maximalen Volumens von Dampfblasen, Phys. Z., vol 36 no 11 pp 379-384.
- Gaertner RF (1963) Distribution of active sites in the nucleate boiling of liquids, Chem. Eng. Prog. Symp. Series, no 41 vol 59 pp 52-61
- Gaertner RF (Feb. 1965) Photographic study of nucleate pool boiling on a horizontal surface, Transaction of the ASME, Journal of Heat Transfer, pp 17- 29
- Gaertner RF, Westwater JW (1960) Population of active sites in nucleate boiling heat transfer, Chem. Eng. Progr. Symp. Ser, vol 30 pp 39-48

- Golobic I, Petkovsek J, Baselj M, Papez A and Kenning DBR (7-12 May 2006) Experimental determination of the transient wall temperature distribution close to growing vapor bubbles, ECI International Conference on Boiling Heat Transfer Spoleto
- Golorin VS, Kol'chugin BA, and Zakharova EA (1978) Investigation of the mechanism of nucleate boiling of ethyl alcohol and benzene by means of high-speed motion-picture photography, *Heat Transfer-Sov. Res.*, vol 10 no 4 pp 79-98
- Hsu YY, Graham RW (1976) Transport processes in boiling and two - phase systems, Hemisphere Publishing Corporation, Washington - London, Mc Graw - Hill Book Company, New York
- Iida Y, Kobayasi K (1970) An experimental investigation on the mechanism of pool boiling phenomena by a probe method, 4th Int. Heat Transfer Conf., Paris – Versailles, vol 5 no 3 B13 pp 1-11
- Ishii M, Zuber N (1978) Relative motion, interfacial drag coefficients in dispersed two - phase flow of bubbles, drops and particles, Paper 56a, AIChE 71st Ann. Meeting, Miami
- Jakob M (1932) Kondensation und Verdampfung, *Zeitschrift des Vereins deutscher Ingenieure*, vol 76 no 48 pp 1161-1170
- Jakob M, Fritz W (1931) *Forsch. Ing.-Wes.*, vol 2 p 435
- Jakob M, Linke W (1933) Der Waermeuebergang von einer waagerechten Platte an siedendes Wasser, *Forsch. Ing. Wes.*, vol 4 pp 75-81
- Jensen MK and Memmel GJ (1986) Evaluation of Bubble Departure Diameter Correlations, *Proc. Eighth Int. Heat Transf. Conf.*, vol 4 pp 1907-1912
- Jones OC (1992) Nonequilibrium phase change --1. Flashing inception, critical flow, and void development in ducts, in Lahey RT Jr (ed) *Boiling Heat Transfer*, Elsevier Science Publishers B.V., pp 189 - 234
- Jones OC (1992) Nonequilibrium Phase Change --2. Relaxation models, general applications, and post heat transfer, in Lahey RT Jr (ed) *Boiling Heat Transfer*, Elsevier Science Publishers B.V., pp 447-482
- Klausner JF, Mei R, Bernard DM, Zeng LZ (1993) Vapor bubble departure in forced convection boiling, *Int. J. of Heat and Mass Transfer*, vol 36 no 3 pp 651-662
- Kocamustafaogullari G, Ishii M (1983) Interfacial area and nucleation site density in boiling systems, *Int. J. Heat Mass Transfer*, vol 26 no 9 pp 1377-1389
- Kolev NI (1993) The code IVA3 for modeling of transient three-phase flows in complicated 3D geometry, *Kerntechnik*, vol 58 no 3 pp 147-156
- Kolev NI (1993) Fragmentation and coalescence dynamics in multi-phase flows, *Experimental Thermal and Fluid Science*, Elsevier, vol 6 pp 211-251
- Kolev NI (1994) The influence of mutual bubble interaction on the bubble departure diameter, *Experimental Thermal and Fluid Science*, Elsevier, vol 8 pp 167-174
- Kolev NI (October 5-8 1993) IVA3 NW: Computer code for modeling of transient three phase flow in complicated 3D geometry connected with industrial networks, *Proc. of the Sixth International Topical Meeting on Nuclear Reactor Thermal Hydraulics*, Grenoble, France
- Koumoutsos N, Moissis R, Spyridonos A (May 1968) A study of bubble departure in forced-convection boiling, *Journal of Heat Transfer, Transactions of the ASME* pp 223-230
- Kurihara HM, Myers J E (March 1960) The effect of superheat and surface roughness on boiling coefficients, *A. I. Ch. E. Journal*, vol 6 no 1 pp 83-91

- Kutateladze SS and Gogonin II (1979) Growth rate and detachment diameter of a vapour bubble in free convection boiling of saturated liquids, *High Temperature*, vol 17 pp 667-671
- Labuntsov DA (1974) State of the art of the nucleate boiling mechanism of liquids, *Heat Transfer and Physical Hydrodynamics*, Moskva, Nauka, in Russian, pp. 98-115
- Labuntsov DA, Kol'chugin VA, Golovin VS et al (1964) *Teplofiz. Vys. Temp.*, vol 3 pp 446 – 453
- Levy S (1967) Forced convection subcooled boiling prediction of vapor volume fraction, *Int. J. Heat Mass Transfer*, vol 10 pp 951-965
- Moalem D, Yijl W, van Stralen SJD (1977) Nucleate boiling at a liquid-liquid interface, *letters heat and mass transfer*, vol 4 pp 319-329
- Morin R (1964) Wall temperature fluctuations during bubble generation in boiling, in *Convective heat transfer in two-phase and one-phase flows*, Energiya, Moskva. eds. Boris-hanskii VM and Paleev II
- Nishikawa K, Fujita Y, Uchida S, Ohta H (1984) Effect of surface configuration on nucleate boiling heat transfer, *Int. J. Heat and Mass Transfer*, vol 27 no 9 pp 1559-1571
- Rallis C J, Jawurek HH (1964) Latent heat transport in saturated nucleate boiling, *Int. J. Heat Transfer*, vol 7 pp 1051-1068
- Reichardt H (Juli 1951) Vollständige Darstellung der turbulenten Geschwindigkeiten in glatten Leitungen, *Z. angew. Math. Mech.*, Bd. 31 Nr. 7, S. 208-219
- Roll JB, Mayers JC (July 1964) The effect of surface tension on factors in boiling heat transfer, *A.I.Ch.E. Journal*, pp 330-344
- Ruckenstein E (1961) A physical model for nucleate boiling heat transfer from a horizontal surface, *Bul. Institutului Politech. Bucuresti*, vol. 33, no. 3. pp. 79-88, 1961 ; *Appl. Mech. Rev.*, vol. 16, Rev. 6055, 1963.
- Semeria RF (1962) Quelques resultats sur le mecanisme de l'ebullition, 7, *J. de l'Hydraulique de la Soc. Hydrotechnique de France*
- Shoji M, Zhang L and Chatpun S (April 17-21, 2005) Nucleation site interaction in pool nucleate boiling, 6<sup>th</sup> World Conference on Experimental Heat Transfer, Fluid Mechanics, and Thermodynamics, Matsushima, Miyagi, Japan
- Siegel R, Keshock EG (July 1964) Effects of reduced gravity on nucleate boiling bubble dynamics in saturated water, *A.I.Ch.E. Journal*, vol 10 no 4 pp 509-517
- Sultan M, Judd RL (Feb. 1978) Spatial distribution of active sites and bubble flux density, *Journal of Heat Transfer, Transactions of the ASME*, vol 100 pp 56-62
- Tolubinsky VI, Ostrovsky JN (1966) On the mechanism of boiling heat transfer (vapor bubbles growth rise in the process of boiling in liquids, solutions, and binary mixtures), *Int. J. Heat Mass Transfer*, vol 9 pp 1463-1470
- Ünal HC (1976) Maximum bubble diameter, maximum bubble-growth time and bubble-growth rate during the subcooled nucleate flow boiling of water up to 17.7 MN/m<sup>2</sup>, *Int. J. Heat Mass Transfer* vol 19 pp 643-649
- Vachon RI, Tanger GE, Davis DL, Nix GH (May 1968) Pool boiling on polished chemically etched stainless-steel surfaces, *Transactions of ASME, Journal of Heat Transfer*, pp 231-238
- van Krevelen DW, Hoftijzer PJ (1950) Studies of gas- bubble formulation, calculation of interfacial area in bubble contactor, *Chem. Eng. Progr. Symp. Ser.*, vol 46 no 1 pp. 29-35
- van Stralen S, Cole R (1979) *Boiling Phenomena*, Hemisphere, USA

- van Stralen SJD, Sluyter WM, Sohal MS (1975) Bubble growth rates in nucleate boiling of water at subatmospheric pressures, *Int. J. Heat and Mass transfer*, vol 18 pp 655-669
- Voloshko AA and Vurgaft AV (November 1970) Dynamics of vapor-bubble break off under free-convection boiling conditions, *Heat Transfer-Soviet Research*, vol 2 no 6 pp 136-141
- Wang CH, Dhir VK (Aug. 1993) Effect of surface wettability on active nucleation site density during pool boiling of water on a vertical surface, *ASME Journal of Heat Transfer*, vol 115 pp 659-669
- Wiebe JR (1970) Temperature profiles in subcooled nucleate boiling, M. Eng. thes., Mechanical Engineering Department, McMaster University, Canada
- Yamagata K, Hirano F, Nishikawa K, Matsuoka H (1955) Nucleate boiling of water on the horizontal heating surface, *Mem. Fac. Engng, Kyushu Univ*, vol 15 p 97
- Yang JY, Weisman J (1991) A phenomenological model of subcooled flow boiling in the detached bubble region, *Int. J. Multiphase Flow*, vol 17 no 1 pp 77-94
- Zeng LZ, Klausner JF, Mei R (1993) A unified model for the prediction of bubble detachment diameters in boiling systems - 1. Pool boiling, *Int. J. of Heat and Mass Transfer*, vol 36 no 9 pp 2261 - 2270
- Zeng L Z, Klausner JF, Bernard DM, Mei R (1993) A unified model for the prediction of bubble detachment diameters in boiling systems - 2. Flow boiling, *Int. J. of Heat and Mass Transfer*, vol 36 no 9 pp 2271 - 2279
- Zuber N (1961) The dynamics of vapor bubbles in non uniform temperature fields, *Int. J. Heat Mass Transfer*, vol 2 pp 83-98
- Zuber N (1963) Nucleate boiling. The region of isolated bubbles and the similarity with natural convection, *Int. J. Heat and Mass Transfer*, vol 6 pp 53-78

## 16 How accurately can we predict nucleate boiling?

In this Chapter we present a new theory of nucleate pool boiling based on turbulence in the boundary layer induced by bubble growth and departure which incorporates the effect of the static contact angle and explains the large spread of the available experimental data. In addition an exiting feature of the new theory is demonstrated - the capability to predict the critical heat flux with the same correlation which was never reported before in the literature as far as the author knows. This is a slightly modified version of the work previously published in *Kolev (1995)*.

### 16.1 Introduction

Nucleate boiling is probably the most investigated phenomenon in the thermal sciences over 60 years. Data are collected, e.g. *Jakob and Fritz (1931)*, *Jakob and Linka (1933)*, *Yamagata et al. (1955)*, *Kurihara and Myers (1960)*, *Gaertner and Westwater (1960)*, *Gaertner (1965)*, *Borishanskii et al. (1961)*, *Rallis and Jawurek (1964)*, *Vachon et al. (1968)*, *Wiebe (1970)*, *Sultan and Judd (1978)*, *Cornwell and Brown (1978)*, *Nishikawa et al (1984)*. see also Appendix 16.2, and many theoretical models exist, e.g. *Van Stralen and Cole (1979)*, *Rohsenow (1952)*, *Fritz (1935)*, *Vachon et al. (1968)*, *Yang and Weisman (1991)*, *Mikic and Rohsenow (1969)*, *Cole and Rohsenow (1969)*, *Zuber (1959)*, *Zuber (1960)*, *Judd and Hwang (1976)*, *Zuber (1963)*, *Von karman (1921)*, *Pohlhausen (1921)*, *Brauer (1971)*, *Forster (1955)*, *Zuber (1958)*, *Chen (1966)*, *Jakob (1949)* *Kocamustafaogullari and Zshii (1983)*, *Tolubinsky and Ostrovsky (1966)*. The practical needs are satisfied usually by empirical correlations. In these correlations the heat flux at the wall is proportional to the wall superheating with respect to the saturation temperature to a power  $n$

$$\dot{q}_{NB}'' = h_{NB}(p) [T_w - T'(p)]^n$$

which varies between 2 and 4. The coefficient  $h_{NB}$  is found to be mainly a function of the system pressure. Some of the frequently used correlations in the literature are summarized below.

1) *Thom (1966)* :  $n = 2$ ,

$$h_{NB\_Thom} = 1942 \exp(p / 4.35 \times 10^6).$$

2) *Micheev and Miheeva* (1973) :  $n = 3$ , valid in  $1 \times 10^5 \leq p \leq 200 \times 10^5 \text{ Pa}$ ,

$$h_{NB\_Micheev} = \frac{0.07845 p^{0.53}}{(1 - 4.5 \times 10^{-8} p)^3}.$$

3) *Jens and Lottes* (1951),  $n = 4$ , valid in  $p \leq 140 \times 10^5 \text{ Pa}$ ,  $\dot{q}_{NB}'' < 1.1 \times 10^6 \text{ W/m}^2$ ,  $G < 10^4 \text{ kg/(m}^2\text{s)}$ ,

$$h_{NB\_Jens-Lottes} = 2.567 \exp(p/1.55 \times 10^6).$$

4) *Borishanskii et al* (1964),  $n = 10/3$ , valid in steel/water,  $9.81 \times 10^4 \leq p \leq 196.2 \times 10^5 \text{ Pa}$ , measurement error  $\mp 5\%$ ,

$$h_{NB\_Borishanskii} = 2.28^{10/3} \left[ (p/10^4)^{0.14} + 2.53 \times 10^{-6} (p/10^4)^2 \right]^{10/3}.$$

The data by *Borischanski* are reproduced with rms. 13.7%. His data can be reproduced with rms. 10 %, by

$$h_{NB\_Borishanskii} = \left\{ 10^{[-24.60379 + 13.14641 \log_{10} p - 2.30694 (\log_{10} p)^2 + 0.13636 (\log_{10} p)^3]} \right\}^{10/3}.$$

The same data are reproduced with rms. 11.2% with a correlation that is appropriate also for other fluid:  $n = 3$ ,

$$h_{NB\_Borishanskii} = \left\{ 238 \frac{(p_c/10^4)^{1/3}}{T_c^{5/6} M^{1/6}} \left( \frac{p}{p_c} \right)^{0.1} \left[ 1 + 4.65 \left( \frac{p}{p_c} \right)^{1.16} \right] \right\}^3.$$

Here  $M$  is the molar weight in kg-mole and  $c$  indicates the critical state.

6) *Arefeva and Aladev* (1958),  $n = 4$ , valid for  $0.7 < \theta < 1.08$ , 1bar

$$h_{NB\_Arefeva-Aladev} = (2.559\theta - 0.727)^4.$$

*Arefeva and Aladev* (1958),  $n = 3/2$  valid for  $1.6 < \theta < 2.41$  and 1bar,

$h_{NB\_Arefeva-Aladev} = 3287.26$ . Note the differences in the predictions among the different correlations as demonstrated in Fig. 16.1 for water at 1bar pressure.

It seems that the question of how accurately we can predict the heat flux as a function of the wall superheating for simple pool boiling is banal and boring. However, let us consider this problem in more detail.

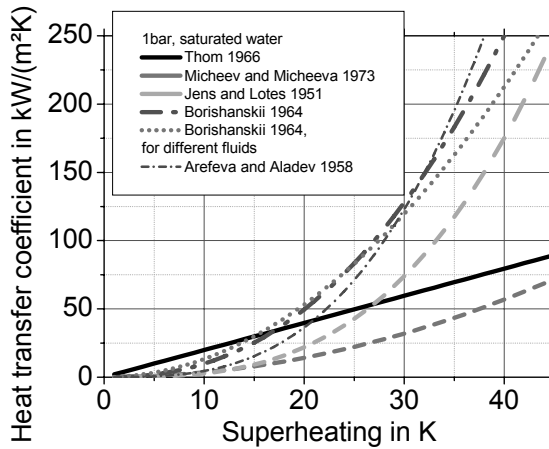


**Fig. 16.1** Heat transfer coefficient for pool boiling of water at 1bar computed using different correlations

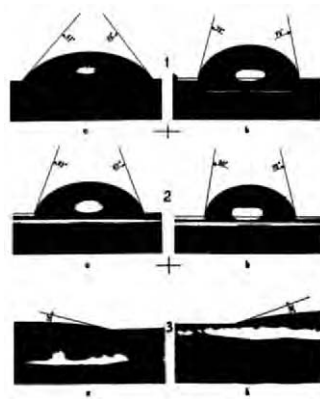


**Fig. 16.2** To the definition of the contact (wetting) angle: Water drops at solid surfaces: 1) stainless steel; 2) copper; 3) glass; a) surface just polished with emery paper; b) same surface after treated with trichloroethylene, Morin (1964)

Figure 16.3 depicts the heat flux as a function of the wall superheating for water at atmospheric pressure at plane surfaces taken from Jakob and Fritz (1931), Jakob and Linka (1933), Yamagata et al. (1955), Kurihara and Myers (1960), Gaertner and Westwater (1960), Gaertner (1965), Borishanskii et al. (1961), Rallis and Jawurek (1964), Vachon et al. (1968), Wiebe (1970), Sultan and Judd (1978), Cornwell and Brown (1978), Nishikawa et al. (1984) for mirror polished surfaces (data for specifically prepared rough surfaces are excluded).

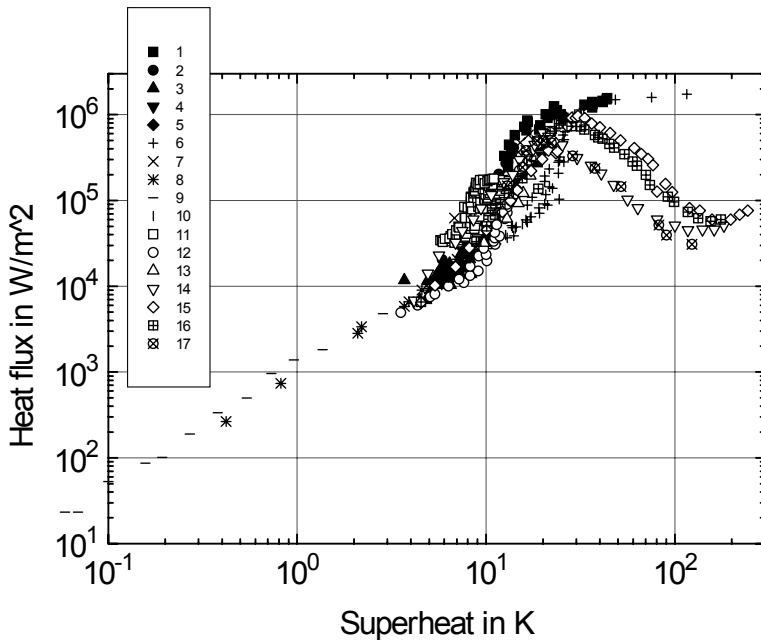


**Fig. 16.3** Heat flux as a function of superheat. Saturated water at 0.1 MPa. 1) Gaertner 1965, 4/0 polished copper, 2) Kurihara and Myers 1960, 4/0 polished copper, 3) Yamagata et al. 1955, fine polished brass, 4) Sultan and Judd 1978, diamond grid 600 polished copper, 5) Wiebe 1970, diamond 600 polished copper, 6) Gaertner and Westwater 1960, 4/0 polished copper, 20 p.c. nickel salt-water solution, 7) Borishanskii et al. 1961, steel, 5 to 8 p.c. error, 8) Jakob and Fritz 1931, polished steel, 9) Jakob and Linke 1932, polished steel, 10) Cornwell and Brown 1978, 4/0 polished copper, 11) Vachon et al. 1968, emery grid 600 polished 304 stainless steel, 12) Nishikawa et al. 1984, emery grid No.0/10 polished copper, 13) Rallis and Jawurek 1964, nickel wire, 14) Wang and Dhir (1993) nucleate and transition boiling. Contact angle 90 deg, 15) Wang and Dhir (1993) nucleate and transition boiling. Contact angle 18 deg, 16) Wang and Dhir (1993) nucleate and transition boiling. Contact angle 35 deg, 17) Wang and Dhir (1993) nucleate and transition boiling. Contact angle 35 deg. Liaw data

By taking a close look at these data we see that while the reported error for temperature measurements is about 5 to 6 % and for heat transfer measurements about 1 to 14 % in each particular experiment the spreading of different authors data is over two orders of magnitude which cannot be explained with measurements error. This spreading corresponds to the data for the nucleation site density (reported measurement error about 1 to 20 %) as a function of wall superheat presented in Fig. 16.4 for the same data set as far as available Avdeev et al. (1977), Brauer (1971), Chen (1966), Cole and Rohsenow (1969), Fagginani et al. (1981), Gaertner and westwater (1960), Gaertner (1963). The state of the art of the modeling of this phenomenon is well represented by van Stralen and Cole (1979), Rohsenow (1952), Fritz (1935), Vachon et al. (1968), Yang and Weisman (1991), Mikic and Rohsenow (1969), Cole and Rohsenow (1969), Zuber (1959), Zuber (1960), Judd and Hwang (1976), Zuber



(1963), von Karman (1921), Pohlhausen (1921), Brauer (1971), Forster and Zuber (1955), Zuber (1958), Chen (1966), Jakob (1949), Kocamustafagullari and Ishii (1983), Tolubinsky and Ostrovsky (1966). Examining the main basic physical ideas on which these models rely (see Appendix 16.1) we surprisingly find that none of them predicts the main reason for the observed data spreading.

There are many qualitative hypotheses in the literature for the reason of the observed data spreading but none of them are used to quantitatively improve our predictive capability. Illustration how static contact angle influence the form of the solid-liquid-steam contact is demonstrated in Fig. 16.2.

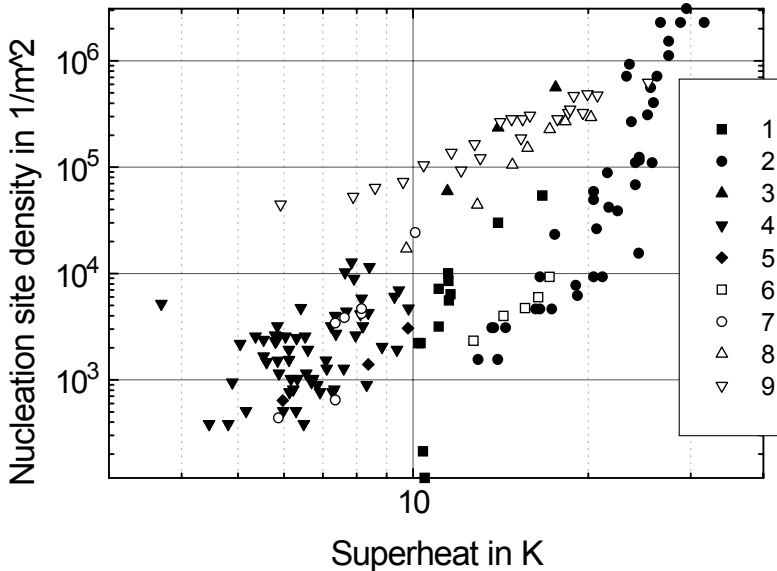


**Fig. 16.4** Active nucleation site density as a function of superheat. Saturated water at 0.1 MPa. 1) Gaertner 1965, 4/0 polished copper, 2) Gaertner and Westwater 1960, 4/0 polished copper, 20 p.c. nickel salt-water solution, 3) Sultan and Judd 1978, diamond grid 600 polished copper, 4) Yamagata et al. 1955, fine polished brass, 5) Jakob and Linke 1933, polished steel, 6) Cornwell and Brown 1978, 4/0 polished copper, 7) Kurihara and Myers 1960, 4/0 polished copper, 8) Rallis and Jawurek 1964, nickel wire, 9) Faggani et al. 1981, polished 316 steel horizontal cylinder

Wang and Dhir (1993) published interesting experimental work showing clearly the effect of the static contact angle on the active nucleation site density as a function of the wall superheat. We transform the new data in the coordinates of Fig. 16.4 and plot them in Fig. 16.4. Comparing Figs. 16.4 and 16.5 it is obvious that variation of the static contact angle could account for a substantial part of the observed data spread in Fig. 16.4 and consequently in Fig. 16.3. This conclusion is supported by the following consideration. Nucleation site density is reported to be measured with about 1 to 20 % error. Static contact angle (if measured at all) is

measured with  $\pm 3$  rad error. Distilled water being in contact with different polished solid surfaces not especially chemically treated possesses different static contact angles as indicated in Tables 12.1 and 12.2. Since in Fig. 16.3 we have data sets for different static contact angles varying between very small values, as is the case with the *Gaertner* and *Westwater's* data, and  $\pi/2$ , as it seems to be the case for copper-water data, the data sets must differ from each other.

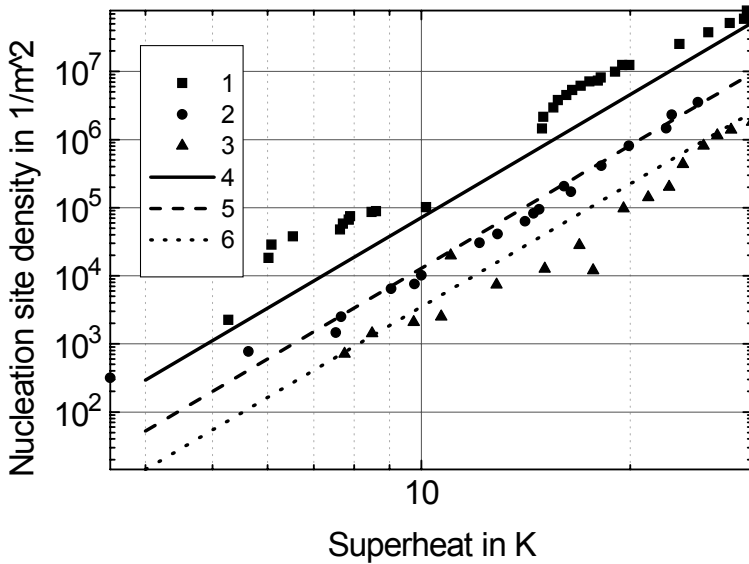


**Fig. 16.5** Active nucleation site density as a function of superheat. Saturated water at 0.1 MPa. Wang and Dhir (1993) data for three different static contact angles 1) 90, 2) 35 and 3) 18 deg. Prediction of the same data with their correlation 4), 5), and 6), respectively. Larger static contact angle results of larger active nucleation site density by the same superheating

*Wang* and *Dhir* correlated their data for active nucleation sites density as a function of the wall superheat as follows

$$n_{lw}'' = 5 \times 10^{-27} (1 - \cos \phi) / D_{lc}^6 \quad (16.1)$$

where the constant has a dimension  $m^4$ , the critical diameter is a function of the local superheating

$$D_{lc} = \frac{4\sigma}{[p'(T_2) - p] \left(1 - \frac{\rho''}{\rho_2}\right)} = \frac{4\sigma}{(h'' - h') \rho' \ln \left[1 + \frac{T_w - T'(p)}{T'(p)}\right]} \approx \frac{T'(p)}{T_w - T'(p)} \frac{4\sigma}{\rho''(h'' - h')} \quad (16.2)$$

and  $\sigma = \sigma(T_w)$ .

Note that all saturation properties in this paper are computed as a function of the wall temperature. The results of the prediction of  $n''_{1w}$  for the three different static contact angles ( $\varphi = 90, 35$  and  $18 \text{ deg}$ ) as function of the wall superheating and the experimental data which they correlate are presented in Fig. 16.5. For the prediction we use the measured wall superheating  $T_w - T'(p)$ . For comparison see the previous correlations not taking into account the influence of the static contact angle published in Cornwell and Brown (1978), Labuntsov (1963), Mickic and Rohsenow (1969), Avdeev et al. (1977), Hutcherson et al. (1983), Kocamustafaogullari and Ishii (1983), Riznic and Ishii (1989), Johov (1969), Jones (1992), Jones (1992) and summarized in Appendix 16.2 - some of them are depicted together with data in Fig 16.6. The quantitative dependence on the static contact angle reported by Wang and Dhir was not previously known. It strongly supports the qualitative arguments published in 1958 by Arefeva and Aladev (1958) p.12 which are briefly summarized below:

“ ... Boiling of liquid is associated with liquid fragmentation by liquid detachment from the wall. Consequently steam must appear for lower wall superheats at places where the work for liquid detachment is lower. Quantitative measure for the influence of the wall on heat transfer is the rate of wetting i.e. the static contact angle. Therefore, (a) the nucleation site density and consequently the heat transfer coefficient increases with increasing static contact angle, and (b) increasing static contact angle decreases the critical heat flux...”

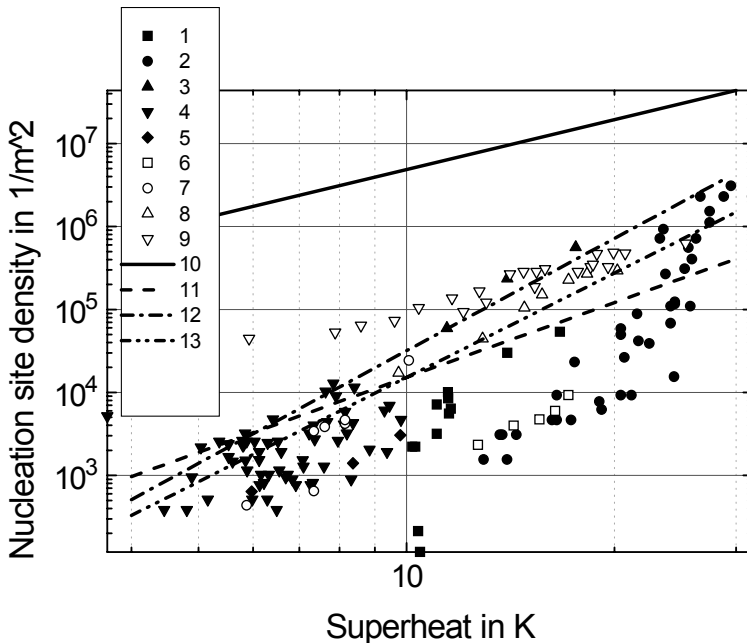


**Fig. 16.6** Active nucleation site density as a function of superheat. Saturated water at 0.1 MPa. 1) to 9) Data from Fig. 16.3. Prediction with correlations proposed by 10) Avdeev et al. (1977), 11) Johov (1969), 12) Cornwell and Brown (1978) and 13) Kocamustafaogullari and Ishii (1983)

Another important result of the measurements by *Wang* and *Dhir* is the relationship between the averaged nearest - neighbor distance and the nucleation site density

$$\left(D_{2,\text{inf}}^2\right)^{1/2} \approx 0.84 / n_{1w}''^{1/2} \quad (16.3)$$

which is obtained with better statistics than the earlier relation reported by *Gaertner* (1963) and *Sultan and Judd* (1978)  $\approx 1 / (\pi n_{1w}'')^{1/2}$ . In what follows we shall demonstrate the importance of the experimental findings of *Wang* and *Dhir* for the prediction of heat transfer in nucleate boiling.

In this Chapter, we present a new theory of nucleate pool boiling based on bubble growth and departure induced turbulence in the boundary layer which incorporates the effect of the static contact angle and explains the large spreading of the available experimental data. In addition an exciting feature of the new theory is demonstrated - the capability to predict the critical heat flux with the same correlation. This was not previously reported in the literature as far as the author knows.

## 16.2 New phenomenological model for nucleate pool boiling

### 16.2.1 Basic assumptions

1. Wall superheating larger than a given value is necessary to initiate pool boiling. For smaller wall superheating the heat is transferred by natural convection, *Jakob* (1932)

$$\dot{q}_{w2,nc}'' = 2.417 \lambda_2 \left( \text{Pr}_2 g \beta_2 / \nu_2^2 \right)^{1/4} (T_w - T_2)^{21/16} \quad (16.4)$$

Here indices “2” indicates bulk liquid values.

2. The heat flux from the wall into the boiling mixture during nucleate pool boiling is caused by boundary layer turbulence due to bubble growth and departure.  
3. The turbulent length scale is of the order of the *Rayleigh - Taylor* instability wavelength

$$\ell_2^t = \pi \lambda_{RT}, \quad (16.5)$$

where  $\lambda_{RT} = \left\{ \sigma / [g(\rho' - \rho'')] \right\}^{1/2}$  is the capillary *Laplace* constant. The imagination that boiling at a heated wall is in fact counter-current gas liquid flow led *Zuber* (1958) and *Zuber et al.* (1958, 1961) to the conclusion that the instability of such flow is controlled by the *Rayleigh-Taylor* instability wavelength. This imagination led to a successful theory for critical heat flux. *Rohsenow* (1952) and *Tolubinsky* (1966) used  $\lambda_{RT}$  as a length scale to correlate data also for sub-critical nucleate boiling heat transfer. Thus, we proceed with the imagination that not only the continuous steam stream counter current to the liquid but also the train of bubbles counter current to the liquid produce macroscopic instability of order of the *Rayleigh-Taylor* instability

wavelength. As will be demonstrated later by comparison with data this assumption seems quite appropriate. We found that neither the average distance between two departing bubbles, nor the bubble departure diameter is appropriate as a macroscopic length scale of turbulence for this process.

4. The nucleation site distribution obeys the *Poisson* distribution law and the experimentally observed averaged site to site space  $D_{2,inf}$  is given by Eq. (16.3).

5. The bubble growth at the wall is thermally controlled. The expression governing the bubble growth is

$$D_1 = 2B\tau^n \quad (16.6)$$

As shown in Appendix 13.1 it is generally agreed that the exponent is of the order of 1/2 for saturated liquids. For the purpose of data comparison we use in this work the *Labuntsov* approximation (1974, 1963) of the *Scriven* solution for bubble growth in a bulk liquid,

$$B = cJa'a'^{1/2} \quad (16.7a)$$

where

$$c = (12/\pi)^{1/2} \left[ 1 + \frac{1}{2} \left( \frac{\pi}{6Ja'} \right)^{2/3} + \left( \frac{\pi}{6Ja'} \right)^{1/2} \right]^{1/2} \quad (16.8)$$

and  $n = 1/2$ . Alternatively the *Labuntsov* et al. (1964) solution for bubble growth at heated wall

$$B = \sqrt{2\beta a'Ja'} \quad (16.7b)$$

where

$$\beta \approx \frac{25.3 \cos(\theta/2)}{(1 + \cos \theta)^2 (2 - \cos \theta)},$$

validated for water boiling at silver surface at  $p = 1$  to 100 bar, can also be used.

6. The order of magnitude of the minimum waiting time will be computed in accordance with the proposal by *Han* and *Griffith* (1965)

$$\Delta\tau_{1w} \approx \Delta\tau_{1w,\min} = \delta_{2,\min}^2 / (\pi a') \quad (16.9)$$

where

$$\delta_{2,\min} = 12(T_w - T_2)T'(p)\sigma / \left\{ [T_w - T'(p)]^2 \rho''(h'' - h') \right\} \quad (16.10)$$

is the minimum of the thermal boundary layer thickness.

7. The bubble departure diameter  $D_{1d}$  and consequently the bubble departure time

$$\Delta\tau_{1d} = \frac{1}{4} D_{1d}^2 / B^2, \quad (16.11)$$

are controlled by the force balance in accordance with the model

$$\left(D_{1d} / D_{1d,nc}\right)^3 + \left(D_{1d} / D_{1d,fc}\right)^2 = 1 \quad (16.12)$$

presented recently in *Kolav* (1994). The reader will find in *Kolav* (1994) the detailed derivation of Eq. (16.12) and the method for computation of the bubble departure diameter for natural convection only,  $D_{1d,nc}$ , and for forced convection only,  $D_{1d,fc}$ , which will not be repeated here. Further the model was compared in *Kolav* (1994) with the available data for saturated water for pool and flow boiling at low and elevated pressures and good agreement was found. The most exiting feature of this model is the taking into account of the influence of the mutual bubble interaction on the bubble departure diameter, something which was experimentally observed but never theoretically explained before.

The frequency of bubble departure from the wall is therefore

$$f_{1w} = 1 / (\Delta\tau_{1d} + \Delta\tau_{1w}), \quad (16.13)$$

It should not be confused with the average frequency of the turbulent pulsation in the wall boundary layer.

### 16.2.2 Proposed model

The proposed model is strictly valid for pool boiling of saturated liquid. Nevertheless the main ideas used here can be easily extended for nucleate flow boiling of saturated liquid and pool and flow boiling of subcooled liquid as it will be discussed in Section 16.4.

Before jumping apart from the wall, the turbulent eddies stay at the wall during the time  $1 / f'_{1w}$  and receives heat from the wall by heat conduction. Therefore, the average heat flux at the wall follows the analytical solution of the *Fourier* equation averaged over the period  $\Delta\tau = 1 / f'_{1w}$

$$\begin{aligned} \dot{q}''_{w2,nb}(\Delta\tau) &= \frac{1}{\Delta\tau} \int_0^{\Delta\tau} \dot{q}''_w(\tau) d\tau = 2 \left( \frac{\lambda' \rho' c'_p}{\pi \Delta\tau} \right)^{1/2} (T_w - T_2) \\ &= (2 / \pi^{1/2}) (f'_{1w} a')^{1/2} \rho' c'_p (T_w - T_2) \end{aligned} \quad (16.14)$$

The idea to use the time-averaged heat flux at the wall stems from *Mikic* and *Rohsenow* (1969). In contrast to these authors we use here the turbulence renewal period rather than the bubble departure time. The time- and space-averaged pulsation velocity is

$$\bar{\bar{V}}'_2 = (B^2 / D_{2,inf}) \frac{\Delta\tau_d}{\Delta\tau_w + \Delta\tau_d} = \frac{1}{0.84} B^2 n_{1w}^{1/2} \frac{\Delta\tau_{1d}}{\Delta\tau_{1w} + \Delta\tau_{1d}}. \quad (16.15)$$

The above time- and space-averaged pulsation velocity is in fact the space-averaged micro-convection velocity, first computed by *Forster* and *Zuber* (1955),

see also Zuber (1959) p. 12, which is then time averaged. The most unexpected effect introduced by the additional time averaging is the capability of the finally obtained equation to predict the critical flux as it will be demonstrated later. The fluctuation frequency is therefore a function of the bubble departure frequency

$$f'_{1w} = \bar{V}'_2 / \ell'_2 = \frac{1}{0.84} B^2 n''_{1w}{}^{1/2} \frac{\Delta \tau_{1d}}{\Delta \tau_{1w} + \Delta \tau_{1d}} / \ell'_2 \quad (16.16)$$

Substituting Eq. (16.16) in (16.14) we obtain

$$\dot{q}''_{w2,nb} = \frac{2}{\sqrt{\pi 0.84}} \left( \frac{\lambda' \rho' c'_p}{\ell'_2 (1 + \Delta \tau_{1w} / \Delta \tau_{1d})} \right)^{1/2} n''_{1w}{}^{1/4} B (T_w - T_2).$$

Using Eq. (16.7a) results in

$$\dot{q}''_{w2,nb} = \frac{c_1 c}{\left[ \ell'_2 (1 + \Delta \tau_{1w} / \Delta \tau_{1d}) \right]^{1/2}} \frac{\lambda' \rho' c'_p}{\rho'' \Delta h} n''_{1w}{}^{1/4} (T_w - T_2)^2. \quad (16.17a)$$

In Eq. 16.17a  $c_1 = 2 / (\pi 0.84)^{1/2}$  is of order of unity. For the data comparison the value of

$$c_1 = 1.4626 \quad (16.18)$$

was used. Because  $\Delta \tau_{1w}$  is a very rough estimate for the averaged waiting time and therefore the ratio  $\Delta \tau_{1w} / \Delta \tau_{1d}$  is only approximately analytically known we introduce the empirical constant  $c_2 \Delta \tau_{1w} / \Delta \tau_{1d}$

$$\dot{q}''_{w2,nb} = \frac{c_1 c}{\left[ \ell'_2 (1 + c_2 \Delta \tau_{1w} / \Delta \tau_{1d}) \right]^{1/2}} \frac{\lambda' \rho' c'_p}{\rho'' \Delta h} n''_{1w}{}^{1/4} (T_w - T_2)^2. \quad (16.19)$$

The effect of  $c_2$  will be demonstrated by data comparison. As will be shown

$$c_2 = 0.3 \quad (16.20)$$

is appropriate. Finally, replacing Eq. (16.1) in the form

$$n''_{1w} = 5 \times 10^{-27} (1 - \cos \varphi) / D_{1c}^6 = 5 \times 10^{-27} (1 - \cos \varphi) \left[ \frac{\rho'' \Delta h}{4 \sigma T'(p)} (T_w - T_2) \right]^6 \quad (16.21)$$

we obtain

$$\dot{q}''_{w2,nb} = \frac{c_1 c \left[ 5 \times 10^{-27} (1 - \cos \varphi) \right]^{3/2}}{\left[ \ell'_2 (1 + c_2 \Delta \tau_{1w} / \Delta \tau_{1d}) \right]^{1/2}} \left[ \frac{\rho'' \Delta h}{4 \sigma T'(p)} \right]^{-3/2} \frac{\lambda' \rho' c'_p}{\rho'' \Delta h} (T_w - T_2)^{7/2}. \quad (16.22a)$$

Note the power of the temperature difference if a bubble growth equation for bulk flow is used is  $7/2 = 3.5$ . If we use equation (16.7b) for bubble growing at a wall we obtain

$$\dot{q}_{w2,nb}'' = \frac{2\sqrt{2\beta}}{\sqrt{\pi}0.84} \left[ \frac{5 \times 10^{-27} (1 - \cos \varphi)}{\ell_2' (1 + \Delta \tau_{1w} / \Delta \tau_{1d})} \right]^{3/2} \left[ \frac{\rho'' \Delta h}{4\sigma T'(p)} \right]^{3/2} \lambda' \left( \frac{\rho' c_p'}{\rho'' \Delta h} \right)^{1/2} (T_w - T_2')^3, \quad (16.22b)$$

a power equal to 3. Therefore theoretical basics dictate the dependence

$$\dot{q}_{w2,nb}'' \propto (T_w - T_2')^{3 \text{ to } 7/2}.$$

The mass of steam generated per unit time and unit flow volume is therefore

$$\mu_{21,gen} = \frac{4}{D_h} \dot{q}_{w2,b}'' / (h'' - h_2). \quad (16.23)$$

The corresponding number of bubbles generated with bubble departure diameter per unit flow volume is

$$\dot{n}_{1w} = \mu_{21} / \left( \rho_1 \frac{\pi}{6} D_{1d}^3 \right). \quad (16.24)$$

From that moment the bubbles start their own history inside the bulk flow and undergo condensation or further evaporation as well as collisions, coalescence or fragmentation.

## 16.3 Data comparison

Comparison of the prediction of Eq. (16.22) with all data available to the author for atmospheric pool boiling of water at a horizontal surface is shown on Figs. 16.7, 16.8. We see from Figs. 16.7 and 16.8 that the data in the region of pool boiling are well reproduced by Eq. (16.22) including the important effect of the static contact angle. In order to demonstrate the effect of the additional time averaging we set

$$\Delta \tau_{1d} / (\Delta \tau_{1d} + \Delta \tau_{1w}) \approx 1 \quad (16.25)$$

which is equivalent to  $c_2 = 0$ ,

$$\dot{q}_{w2,nb}'' = c_1 c \left[ 5 \times 10^{-27} (1 - \cos \varphi) \right]^{3/2} \ell_2'^{t-1/2} \left[ \frac{\rho'' \Delta h}{4\sigma T'(p)} \right]^{3/2} \frac{\lambda' \rho' c_p'}{\rho' \Delta h} (T_w - T_2')^{7/2}. \quad (16.26)$$

and compare only with the original data set reported by *Wang* and *Dhir*. The result is shown in Fig. 16.9.



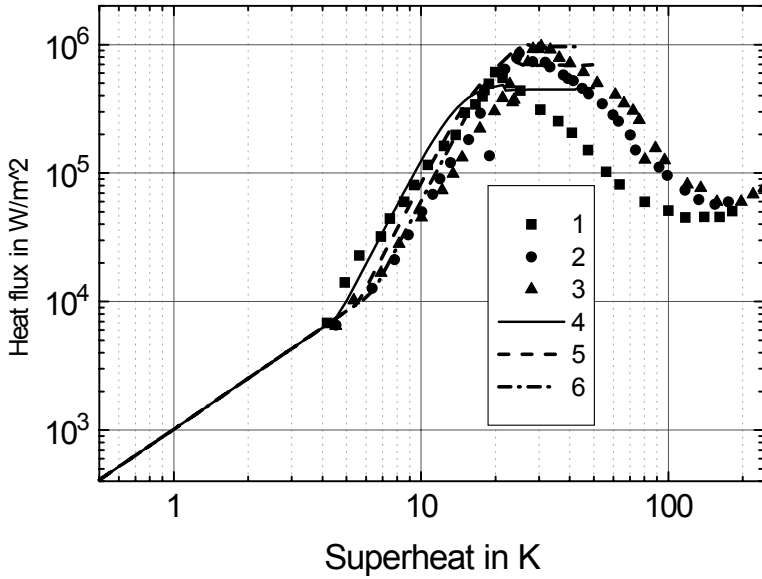


**Fig. 16.7** Heat flux as a function of superheat. Saturated water at 0.1 MPa.  $n_w'' = 5 \times 10^3 (1 - \cos \theta) / (10^5 D_{lc})^6$ . Comparison of the prediction of the new theory with the experimental data by Wang and Dhir for three different static contact angles: 1) Exp.- 90 deg; 2) Exp.-35 deg; and 3) Exp.-18 deg, 4) Kolev-90 deg; 5) Kolev-35 deg; and 6) Kolev-18 deg. The larger the static contact angle the smaller the critical heat flux

From the comparison of Fig. 16.9 with Fig. 16.7 we see also that the ratio  $\Delta \tau_{1w} / \Delta \tau_{1d}$  introduced by the time average is getting important in the region of high superheating where the predicted heat flux no longer increases with increasing superheating. Surprisingly, the obtained equation seems to predict critical heat flux without additional correlation. The mechanism which works in this case is the dramatic increase of the nucleation site density for high temperature differences which causes a dramatic decrease of the bubble departure diameter and therefore a dramatic decrease of the bubble departure time. As a result, we reach the critical heat flux, a critical heat flux that does not increase any more with increasing temperature difference. The surprising effect here is that we predict accurately the nucleate boiling heat transfer and the critical heat flux with a *single theory*. The theory predicts also the observed decreasing critical heat flux with increasing contact angle that is with decreasing wettability. This effect is observed also by *Ramilison*,

$$\dot{q}_{CHF}'' / \dot{q}_{CHF,Zuber}'' = 0.0336(\pi - \theta)^3 k^{0.125} \quad (16.27)$$

where  $k$  is the RMS surface roughness.

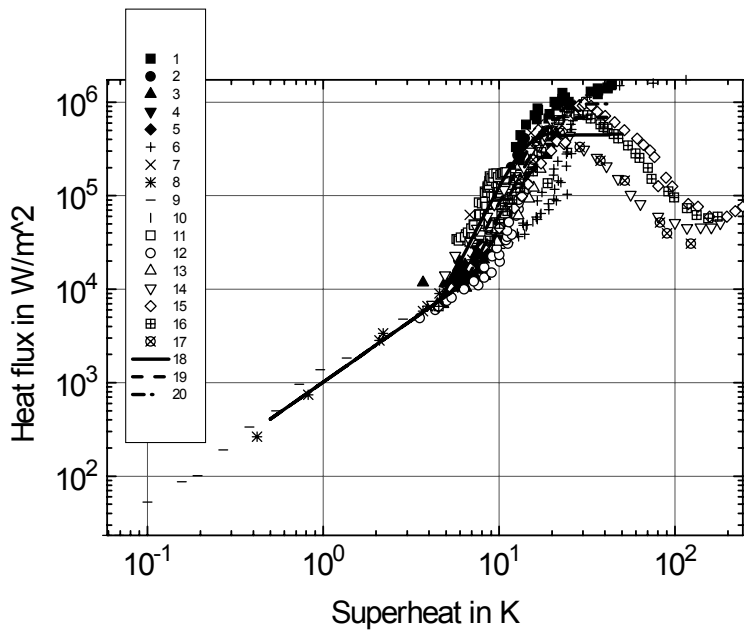


**Fig. 16.8** Experimental data for heat flux as a function of superheat for saturated water at 0.1 MPa - 1) to 17) as in Fig. 16.1. Prediction of the new theory for three different static contact angles: 18) Kolev-90 deg; 19) Kolev-35 deg; and 20) Kolev-18 deg

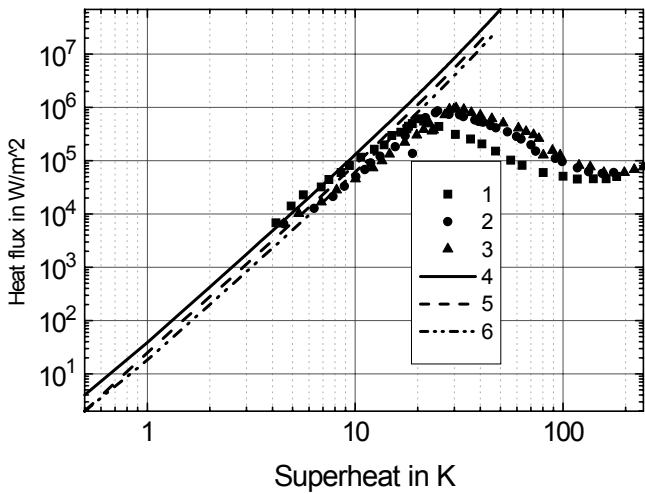


**Fig. 16.9** Wang and Dhiri experimental data for heat flux as a function of superheat for saturated water at 0.1 MPa and for three different static contact angles: 1) 90 deg; 2) 35 deg; and 3) 18 deg. 4), 5), 6) Prediction of the new theory for the corresponding static contact angles without taking into account the time averaging that is with  $c_2 = 0$

Note the difference to the so called “hydrodynamic theory of critical heat flux” proposed first by *Kutateladse* (1954, 1962) and later by *Zuber* (1958), *Zuber* and *Tribus* (1958) and *Zuber et al.* (1965). A brief summary of this theory is given in Section 20.4.1. The hydrodynamic theory of critical heat flux is intended to predict only the critical heat flux up to which the nucleate boiling regime is possible but it was not aimed to predict heat transfer in nucleate boiling itself. Note the two completely different approaches to the boiling crises by comparing this theory with the theory presented in Section 20.4.1. We showed here that the micro-scale of the nucleation processes, bubble growth and departure, and the turbulence generated by this process naturally lead to self saturation of the boundary layer with bubbles and dramatically changes of the phenomenon. In contrast, *Kutateladse* and *Zuber* analyzed the macro-scale of the instability above the layer where the micro-physics happens. That is the reason why their analysis gives an absolute upper limit which is about 5 times larger than the observed critical heat flux. This is reflected in the necessity of introducing an empirical constant of about 1/5 – see Section 20.4.1.

Recently *Kim et al.* (2006) confirmed that micro-particles in water increase the critical heat flux. For the explanation of the observed phenomena the authors considered the hydrodynamic stability theory, *Kutateladse* (1954, 1962), *Zuber* (1958, 1958) the micro-layer theory, *Haramura* and *Katto* (1983) and the hot/dry spot theory *Theofanus et al.* (2002). All these theories are shown not to take into account the nucleation kinetics at the surface and its relation to active nucleation sites. Only the here presented theory was capable to explain the change of the CHF with the change of the active nucleation site density as presented in Fig. 16.10. In this figure Eq. 16.21 is used in the form  $n_{1w}'' = C(1 - \cos \varphi)(T_w - T_2)^6$ .

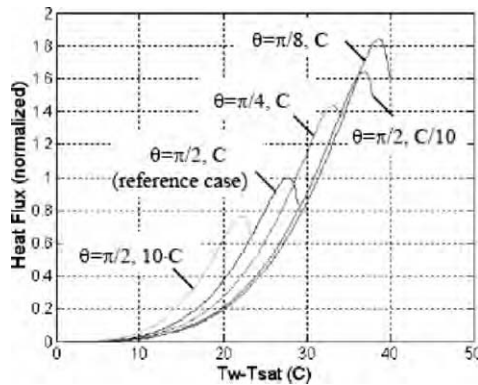


**Fig. 16.10** Effect of the contact angle and the active nucleation site density on the boiling curve, *Kim et al.* (2006)

### 16.3.1 Nucleation site density at high pressures

The theory discussed here was based on expression for the nucleation site density derived at 1 bar experimentally. For high pressure systematic data for water do not

exists. One intermediate solution for deriving an expression for the nucleation site density is to equalize the nucleate boiling heat flux defined by the simplified Eq. 16.17

$$\dot{q}_{w2,nb}'' = \frac{2}{\sqrt{\pi 0.84}} \left( \frac{\lambda' \rho' c'_p}{\pi \lambda_{RT}} \right)^{1/2} n_{1w}''^{1/4} B (T_w - T_2) \quad (16.28)$$

to one of the empirical expressions given in the introduction

$$\dot{q}_{NB}'' = h_{NB}(p) [T_w - T'(p)]^n \quad (16.29)$$

and solving with respect to the active nucleation site density. The result is

$$n_{1w}'' = 4.29 \lambda_{RT}^2 \left\{ h_{NB}(p) \frac{[T_w - T'(p)]^{n-1}}{B \sqrt{\lambda' \rho' c'_p}} \right\}^4. \quad (16.30)$$

For  $B = \sqrt{2\beta a' Ja'}$  we obtain

$$n_{1w}'' = \frac{4.29}{(2\beta)^2} \lambda_{RT}^2 \left\{ h_{NB}(p) \frac{[T_w - T'(p)]^{n-1}}{\lambda' \sqrt{Ja'}} \right\}^4. \quad (16.31)$$

Using the correlation by *Borishanskii* in 16.31 that is appropriate for different fluids and introducing the multiplier  $3.57^{-4} (1 - \cos \theta)^{1.5}$  we obtain the results presented in Fig. 16.11a. Therefore we obtain a prediction method which is as accurate as the empirical correlation by *Wang* and *Dhir* at low pressure and possesses a physically based potential for prediction of the active nucleation sites up to 196.2 bar.

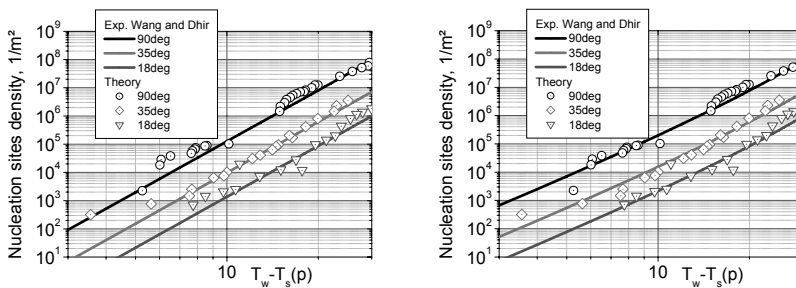


**Fig. 16.11** Active nucleation site density as a function of superheat. Saturated water at 0.1 MPa. Wang and Dhir (1993) data for three different static contact angles 1) 90, 2) 35 and 3) 18 deg. a) Prediction of the same data with Eq. (16.31) and the *Borishanskii* et al. (1964) correlation for pool boiling; b) Prediction with the *Kocamustafaogullari* and *Ishii* (1983) empirical correlation multiplied by  $44.54(1 - \cos \theta)^{1.5}$

Note that the idea to use expression for the heat flux in pool boiling in the form  $\dot{q}_{w2,nb}'' = f(p)n_{1w}''^m (T_w - T_2)^n$ , data approximation in the form  $\dot{q}_{w2,nb}'' = f(T_w - T_2)$ , equalizing them and solving with respect to  $n_{1w}''$  was proposed first by *Kocamustafaogullari* and *Ishii* (1983). These authors expressed already in that time the opinion, that their approach is preliminary until detailed measurements for the nucleation site density and other internal boiling characteristics are available. It is interesting to note, that if their correlation is multiplied by  $44.54(1 - \cos\theta)^{1.5}$ , it predicts even somewhat better slope of the low pressure data as shown in Fig. 16.11b.

## 16.4 Systematic inspection of all the used hypotheses

1) The used hypotheses for the development of the bubble departure theory presented in Chapter 15 are checked against data for saturated water pool boiling for

- a) wall superheating up to 40 K,
- b) mass flow rates up to 360 kg/(m<sup>2</sup>s) and
- c) pressure up to 24 bar,

and good agreement was obtained. The trends of the dependence of the bubble departure diameter on superheating, mass flow rate and pressure are also well predicted. Thus, I could expect that the theory will hold also outside this region.

2) There are only two constants in Eq. (16.17):

- a) The theoretical value of  $c_1 = 1.23$  is corrected with 19 % to 1.4626 after comparison with experimental data, which is not unusual in the heat transfer theory at all.
- b) The  $c_2$  constant is empirically introduced to account for uncertainties in the prediction of the ratio  $\Delta\tau_{1w}/\Delta\tau_{1d}$ . It was demonstrated that for superheatings giving heat flux up  $\approx 70$  % from the critical heat flux this correction is unimportant. It becomes important if one uses the new theory to improve heat flux predictions for superheatings giving heat fluxes  $\approx 70$  % from the critical heat flux.

3) The new heat transfer theory is strictly valid for pool boiling of saturated liquid. The bubble departure theory and therefore the theory for prediction of the fluctuation velocity in the boundary layer are correct also for flow boiling at saturated liquid. The ideas used in this Chapter to reach Eq. (16.17) can be also used to extend its validity to flow boiling. The main questions which should be addressed in this case is whether the characteristic length scale of turbulence in the wall boundary layer will very much change for flow boiling with respect to  $\pi\lambda_{RT}$ . If no, the same theory should be used. If yes, additional investigation is *necessary* in which the flow induced fluctuations in the wall boundary layer

should be superimposed to the bubble departure generated fluctuations. This remains to be done.

4) The extension of the theory for subcooled nucleate boiling requires modification of the bubble departure model published in *Kolev* (1994). The road is: replace the bubble growth model for saturated water with a bubble growth model for subcooled water. This remains to be done.

## 16.5 Significance

1. The economical design of heat exchangers working with pool boiling depends on the accuracy of the prediction models. I believe that the proposed method will find application in this field.
2. The appropriate quantitative separation of the effects of single sub-mechanisms into a single correlation for the prediction of pool boiling has never succeeded before in spite of the fact that it was frequently tried. The prediction of the heat transfer in pool boiling together with the prediction of the critical heat flux for water boiling at atmospheric pressure seems to be indicative that Eq. (16.22) quantitatively predicts the appropriate separate effects.

## 16.6 Conclusions

1. The turbulence induced by the bubble growth and departure is the main heat transfer mechanism during pool boiling.
2. The static contact angle is a very important parameter explaining the large spread of the experimental data for pool boiling.
3. The new theory consists of sound verified sub theories and models
  - the bubble departure diameter, confirmed by data comparison Chapter 15,
  - the active nucleation site density provided by *Wang and Dhir* (1993),
  - the mean site to site distance provided by *Wang and Dhir* (1993),

and the hypothesis of bubble growth and departure introduced turbulence in the boundary layer as the main heat transfer mechanism. These are new features that do not follow from the preceding works *van Stralen and Cole* (1979), *Rohsenow* (1952), *Fritz* (1935), *Vachon et al.* (1968), *Yang and Weisman* (1991), *Mikic and Rohsenow* (1969), *Cole and Rohsenow* (1969), *Zuber* (1959), *Zuber* (1960), *Jueld and Hwang* (1976), *Zuber* (1963), *von Karman* (1921), *Pohlhausen* (1921), *Brauer* (1971), *Forster and Zuber* (1955), *Zuber* (1958), *Chen* (1966), *Jakob* (1949), *Kocamustafaogullari and Ishii* (1983), *Tolubinsky and Ostrovsky* (1966).

4. Equation (16.22) predicts the existing experimental data including the effect of the static contact angle with sufficient accuracy. It is recommended for general use. Surprisingly, Eq. (16.22) also seems to predict the critical heat flux, which was demonstrated for water at atmospheric pressure.

5. Increasing static contact angle leads to decreasing critical heat flux.
6. From the simplified Eq. (16.26) one should easily estimate that if the measurement error for wall superheat is of order of 5 to 6 % the error of the comparison with the experimental data with known static contact angle will be about 21 %. Heat transfer data with unknown static contact angle are not appropriate for validation of any nucleate boiling heat transfer theory.

From the above conclusions we can derive some practical recommendations for the application of the new theory.

1. Equating the predictions of Eq. (16.4) and (16.22) computes the wall temperature  $T_{w,NBI}$  necessary to initiate nucleate boiling

$$T_{w,NBI} = T_2 + \left\{ \frac{2.417 \lambda_2 (Pr_2 g \beta_2 / \nu_2^2)^{1/4}}{c_1 c \left[ 5 \times 10^{-27} (1 - \cos \varphi) \right]^{1/4} \ell_2^{t-1/2} \left[ \frac{\rho'' \Delta h}{4 \sigma T'(p)} \right]^{3/2} \frac{\lambda' \rho' c'_p}{\rho'' \Delta h}} \right\}^{8/35} \quad (16.22)$$

2. If the actual wall temperature is less than  $T_{w,NBI}$  we have natural circulation heat transfer. In this case Eq. (16.4) describes the heat transfer number.
3. If the wall temperature is larger than  $T_{w,NBI}$  we have two possibilities to compute the heat flux:
  - a) Use existing correlation for prediction of the critical heat flux, predict the heat flux by the simplified theory, Eq. (16.26), if the predicted heat flux is below the critical one the prediction of Eq. (16.26) is the desired one. Note that in this case the error is increasing in the region between 70 and 100 % of the critical heat flux.
  - b) Use the complete theory for prediction of the heat flux, that is Eqs. (16.19) and (16.21) together with the complete algorithm described in Chapter 15 for prediction of the bubble departure diameter.
- 4) In accordance with the measurements by *Arefeva* and *Aladev* (1958) the influence of the contact angle on the heat flux is observed in the region between  $\varphi = 0$  and  $\pi/2$ . Beyond this contact angle nucleate boiling heat transfer does not depend on the contact angle. That is why we recommend to use the present theory in the region  $\varphi = 0$  and  $\pi/2$ . For larger contact angles we recommend to use  $\varphi = \pi/2$  until data for the nucleation site density as a function of superheating are available for static contact angles larger  $\pi/2$ .

## 16.7 Extension to forced convection with nucleate boiling

The cross section averaged time scale of the fluctuation of *small* eddies in developed pipe flow is therefore

$$\Delta\tau_{\mu e,2,\infty} \approx b\sqrt{\nu_2/\varepsilon_{2,\infty}},$$

and therefore the frequency of turbulent pulsations is of order of  $f'_{2,\infty} = 1/\Delta\tau_{\mu e,2,\infty}$ . There is a superposition of the frequencies in turbulent flow caused by developed turbulence and by the departing bubbles. Therefore

$$f_{1w} = 1/(\Delta\tau_{1d} + \Delta\tau_{1w}) + 1/\Delta\tau_{e,2,\infty}$$

and

$$\begin{aligned} \dot{q}''_{w2,nb}(\Delta\tau) &= \frac{1}{\Delta\tau} \int_0^{\Delta\tau} \dot{q}''_w(\tau) d\tau = 2 \left( \frac{\lambda_2 \rho_2 c_{p2}}{\pi \Delta\tau} \right)^{1/2} (T_w - T_2) \\ &= (2/\pi^{1/2}) \left( \frac{1}{\Delta\tau_{1d} + \Delta\tau_{1w}} + \frac{1}{\Delta\tau_{e,2,\infty}} \right)^{1/2} a_2^{1/2} \rho_2 c_{p2} (T_w - T_2). \end{aligned}$$

Here using the results of *Chandesris et al. (2005)* for computation of the developed steady state turbulent kinetic energy and its dissipation in pipes we obtain

$$\varepsilon_{2,\infty} = \frac{\lambda_{fr}}{D_h} \frac{1}{2} \bar{w}^3 \left( 1 - y_{\lim}^+ \sqrt{\frac{\lambda_{fr}}{8}} \right),$$

where  $y_{\lim}^+ = 8, 7, 16$ ,  $c_k = 0.0306, 0.0367, 0.0368$  for channels, pipes and rod bundles, respectively. The extension of this result to multi-phase flow requires appropriate model for computation of the effective friction. The pressure loss due to friction is usually expressed in term of the pressure loss of fictive flow consisting of the same mass flow  $\rho \bar{w} = \sum_{l=1}^{l_{\max}} \alpha_l \rho_l \bar{w}_l$  but having the properties of the continuum. The so computed pressure loss is then modified by the so called two-phase friction multiplier  $\Phi_{co}^2$  or *Martinelli-Nelson* multiplier,

$$\left( \frac{dp}{dz} \right)_{fr} = f_w = \frac{\lambda_{fr,co} \Phi_{co}^2}{D_h} \frac{1}{2} \frac{(\rho \bar{w})^2}{\rho_c} = \frac{4\tau_w}{D_h}.$$

Here  $\tau_w = \frac{\lambda_{fr,co} \Phi_{co}^2}{8} \frac{(\rho \bar{w})^2}{\rho_c}$  is the wall share stress. *co* stays for “continuum only”. The effective friction coefficient is  $\lambda_{fr,eff} = \lambda_{fr,co} \Phi_{co}^2$ . The multi-phase friction velocity is then  $w^* = \sqrt{\frac{\tau_w}{\rho_c}} = \frac{(\rho \bar{w})}{\rho_c} \sqrt{\frac{\lambda_{fr,co} \Phi_{co}^2}{8}}$ . The effective boundary



layer dimensionless velocity and wall distance are  $w^+ = \frac{(\rho w)}{\rho_c w^*}$  and  $y^+ = y \frac{w^*}{\nu}$ ,

respectively. The presence of vapor in the liquid for instance increases considerably the friction pressure loss. Recovering the profiles from averaged parameters is difficult. In any case the boundary layer thickness in which the irreversible viscous dissipation happens should be smaller. Therefore we introduce intuitively

$$y_{\text{lim}}^+ = \alpha_c y_{\text{lim},co}^+$$

in

$$\varepsilon_{2,\infty} = \frac{1}{\alpha_c} \frac{\lambda_{fr,co} \Phi_{c0}^2}{D_{hyd}} \frac{1}{2} \frac{(\rho \bar{w})^3}{\rho_c^3} \left( 1 - \alpha_c y_{\text{lim},co}^+ \sqrt{\frac{\lambda_{fr,co} \Phi_{c0}^2}{8}} \right).$$

In the limiting case of continuum only we have  $y_{\text{lim}}^+ = y_{\text{lim},co}^+$ . Here the division with the continuous volume fraction reflects the assumption that all of the dissipation is putted into the continuum.

In the limiting case of no boiling we obtain after rearrangement

$$\frac{\dot{q}_w'' D_h}{(T_w - T_2) \lambda_2} = \frac{2^{3/4}}{\pi^{1/2} b^{1/2}} \left[ \frac{\lambda_{fr,2o} \Phi_{2o}^2}{\alpha_2} \left( 1 - \alpha_2 y_{\text{lim}}^+ \sqrt{\frac{\lambda_{fr,2o} \Phi_{2o}^2}{8}} \right) \right]^{1/4} \text{Re}^{3/4} \text{Pr}_2^{1/2}.$$

This is the general form in which  $\text{Re} = D_h (\rho \bar{w}) / \eta_2$ . Comparison with the *Sani's* (1960) experimental data for single phase flow by using the *Blasius* correlation for friction  $\lambda_{fr} = 0.3164 / \text{Re}^{1/4}$ , dictates the approximated value for  $b = 98.32$  resulting in mean error of 6.4% and increasing divergence for lower *Prandtl* numbers. Note the similarity to the *Dittus-Boelter* (1930) correlation

$$\frac{\dot{q}_w'' D_h}{(T_w - T) \lambda_2} = 0.024 \text{Re}^{0.8} \text{Pr}_2^{0.4},$$

which approximates the *Sani's* data with mean error of 3%. Note also the similarity to the *Avdeev's* result

$$\frac{\dot{q}_w'' D_h}{(T_w - T) \lambda_2} = 0.228 \text{Pr}_2^{1/2} \text{Re}_2^{0.7} (\Phi_{2ow}^2 / \alpha_2)^{1/4}.$$

It describes his own data for recondensation in subcooled boiling at heated pipe walls within  $\pm 30\%$  error band for  $D_1 / D_{hw} > 80 / \text{Re}_2^{0.7}$ . The amplification of the numerical coefficient by *Avdeev* takes into account that the bubble condensation interface is larger than the heated surface.

## Appendix 16.1 State of the art of nucleate pool boiling modeling

Detailed information on this topic can be found in *van Stralen* (1979). We confine our attention to some basic ideas on which some of the frequently used correlations in the literature rely.

*Rohsenow* (1952) computed the heat flux from the wall during nucleate boiling of saturated liquid as  $\dot{q}_{w2}'' = G_{1d} [h'' - h'(T_w)]$ , where  $G_{1d}$  is the mass flow rate of departing bubbles from the surface.  $G_{1d} = \dot{q}_{w2}'' / [h'' - h'(T_w)]$  is used in the *Reynolds* number defined as  $Re_{1d} = G_{1d} D_{1d} / \eta_2 = D_{1d} \dot{q}_{w2}'' / \{ [h'' - h'(T_w)] \eta_2 \}$  for postulating the heat transfer dependence  $St_{1d} = Nu_{1d} / (Pr_2 Re_{1d}) \approx f(Re_{1d}, Pr_2)$ , where the *Nusselt* number is defined as  $Nu_{1d} = h_w D_{1d} / \lambda_2$ . *Rohsenow* uses the *Fritz* equation (1935)  $D_{1d} = 1.2 \phi \lambda_{RT}$  for the estimation of the bubble departure size. *Rohsenow* finally obtained

$$1 / St_{1d} = c_{p2} [T_w - T'(p)] / \Delta h \approx const [\dot{q}_w'' \lambda_{RT} / (\eta_2 \Delta h)]^{1/3} Pr_2^m$$

where the constant and the exponent are fitted against experimental data for water:  $m = 1$ ,  $const = 0.006$  to  $0.013$ , for other liquids:  $m = 1.7$ ,  $const = 0.0025$  to  $0.015$ . Additional values for  $const$  and  $m$  are reported by *Vachon* et al. (1968) for different fluid - surface combinations and different surface preparations.

The definitions by *Rohsenow* are used later by *Kurihara* and *Myers* (1960) in the form  $h_{w2} D_{1d} / \lambda_2 = const (G_{1d} D_{1d} / \eta_2)^m Pr_2^n$ , where for saturated pool boiling the authors assumed that all produced steam is removed from the wall boundary layer, i.e.  $G_{1d} = (\pi / 6) D_{1d} \rho_1 f_{1w} n_{1w}''$ . The authors assumed further  $D_{1d} f_{1w} \approx const$ . The comparison with experimental data for a constant pressure gives  $m \approx 1/3$ , which cancels the effect of the bubble departure diameter. Finally the authors obtained

$$h_{w2} = 820 \lambda_2 (\rho_1 / \eta_2)^{1/3} n_{1w}''^{1/3} Pr_2^{-0.89}$$

Note that  $D_{1d} f_{1w}$  is not a constant as assumed by *Kurihara* and *Myers* but a function of the pressure.

*Mikic* and *Rohsenow* (1969) computed the temperature as a function of time and distance  $y$  from the wall

$$T = T_2 + (T_w - T_2) \operatorname{erfc} \left\{ y / \left[ 2(a_2 \tau)^{1/2} \right] \right\}$$

and the heat flux at the wall in the liquid

$$\dot{q}_w''(\tau) = -\lambda_2 \left. \frac{dT}{dy} \right|_{y=0} = \lambda_2 (T_w - T_2) / [(\pi a_2 \tau)^{1/2}]$$

Thereafter they performed time averaging of the heat flux during the time interval  $\Delta \tau$

$$\dot{q}_w''(\Delta \tau) = \frac{1}{\Delta \tau} \int_0^{\Delta \tau} \dot{q}_w''(\tau) d\tau = 2 \left( \frac{\lambda_2 \rho_2 c_{p2}}{\pi \Delta \tau} \right)^{1/2} (T_w - T_2)$$

The averaged heat flux over the total surface is computed assuming that the heat conduction from the wall into the liquid happens only inside a circle around the nucleation site with the diameter as the bubble departure diameter

$$\dot{q}_w'' = \frac{\pi}{4} D_{1d}^2 n_{1w}'' \dot{q}_w''(\Delta \tau)$$

In addition, the authors computed the bubble departure diameter in accordance with the correlation by *Cole and Rohsenow* (1969)  $D_{1d} = c_2 \lambda_{RT} Ja^{*5/4}$ , where  $Ja^* = \rho_2 c_{p2} T'(p) / (\rho_1 \Delta h)$ , and  $c_2 = 1.5 \times 10^{-4}$  for water, and  $4.65 \times 10^{-4}$  for other liquids. The time averaging is performed during the bubble departure period only  $\Delta \tau = \Delta \tau_{1d} = 1 / f_{1d}$ . Here the relationship obtained by *Zuber* (1959, 1960) for free bubble rise in a pool,  $f_{1d} D_{1d} \approx 0.6 [\sigma g (\rho_2 - \rho_1) / \rho_2^2]^{1/4}$ , was used, where  $f_{1d}$  is the bubble removal frequency from the wall boundary layer, rather than the bubble departure frequency. The bubble number density was postulated to be  $n_{1w}'' = c (D_1^* / D_{1c})^{3.5}$  where the critical bubble size is

$$D_{1c} = 4 \sigma T'(p) / \{ \rho_1 \Delta h [T_w - T'(p)] \}.$$

The constants  $c D_1^{*3.5}$  are estimated by fitting experimental data.

*Judd and Hwang* (1976) extended this model by postulating that the area of influence of a single bubble is  $C \approx 1.7$  times the projected bubble area at departure and the heat transfer outside the area of influence is due to natural convection. The final expression by *Judd and Hwang* is

$$\dot{q}_{w2}'' = C \frac{\pi}{4} D_{1d}^2 n_{1w}'' \dot{q}_{w2}''(\Delta \tau) + (1 - C) \frac{\pi}{4} D_{1w}^2 n_{1w}'' \dot{q}_{w2,nc}'' ,$$

or

$$\dot{q}_{w2}'' - \dot{q}_{w2,nc}'' = C \frac{\pi}{4} D_{1d}^2 n_{1w}'' [\dot{q}_{w2}''(\Delta \tau) - \dot{q}_{w2,nc}''] ,$$

where the natural convection heat flux is

$$\dot{q}_{w2,nc}'' = 0.18 \lambda_2 [Pr_2 g \beta_2 / \nu_2^2]^{1/3} (T_w - T_2)^{4/3} ,$$

and  $\beta_2 = -\frac{1}{\rho_2} \left( \frac{\partial \rho_2}{\partial T_2} \right)$  is the volumetric thermal expansion coefficient. The data of of several investigators can be approximated using 0.272 instead 0.18 as proposed by *Zuber* (1963). Note that *Jacob* used earlier the equation

$$\dot{q}_{w2,nc} \delta_{2,th} / [\lambda_2 (T_w - T_2)] = const [(T_w - T_2) \delta_{2,th}^3 g \beta_2 / \nu_2^2 Pr_2]^{1/4},$$

where the thermal boundary layer thickness was assumed to be

$$\delta_{2,th} \approx const / \Delta T^4,$$

and

$$\dot{q}_{w2,nc} = 2.417 \lambda_2 [Pr_2 g \beta_2 / \nu_2^2]^{1/4} (T_w - T_2)^{21/16}.$$

Bubble growth and departure causes liquid fluctuation parallel to the wall, the so called micro-convection. This leads some authors to the idea to modify the well-known *Karman - Pohlhausen* equation (1921)

$$Nu = h_{w2} \ell / \lambda_2 = 0.664 Re^{1/2} Pr_2^{1/3}$$

for computing the averaged heat transfer at the wall for viscous flow. Note that the heat flux in the above equation is averaged along the distance length  $\ell$ , and that  $\ell$  is used as a scale in the *Nusselt* and *Reynolds* numbers. The velocity used in the *Reynolds* number is the bulk velocity of the flow parallel to the horizontal plate. The corresponding equation for turbulent flow is

$$Nu = h_{w2} \ell / \lambda_2 = 0.037 Re^{4/5} Pr_2^{1/3}$$

see *Brauer* (1971), p.182, Eq. 3.38.

*Forster* and *Zuber* (1955) applied the *Pohlhausen* equation using as averaging length scale the bubble departure diameter  $D_{1d}$

$$h_{w2,mic} D_{1d} / \lambda_2 = const Re^m Pr_2^n$$

The authors averaged the bubble growth velocity along an averaged distance between two neighboring bubbles,  $D_{2,inf}$ , for thermally controlled bubble growth and obtained

$$\bar{V}' = 2R_1 \frac{dR_1}{d\tau} = B^2 / D_{2,inf}.$$

where  $B = \sqrt{\pi a_2} Ja_2$ . This velocity is called micro convection velocity. The *Reynolds* number was computed to

$$Re = \bar{V}' D_{1d} / \nu_2 = (B^2 / \nu_2) (D_{1d} / D_{2,inf})$$

and substituted into the *von Karman - Pohlhausen* equation with

$$Re = B^2 / \nu_2$$

setting  $D_{1d}/D_{2,inf} \approx 1$ . The ratio  $D_{1d}/D_{2,inf} < 1$  was taken into account by the constant

$$const = 0.003$$

for the polar fluids *n*-pentane, benzene, ethanol and for water. The exponents are found to be  $m = 0.62$ ,  $n = 1/3$ . For the bubble departure diameter the authors used the thermally controlled bubble growth mechanism

$$D_{d1} \approx 2B\Delta\tau_{1d}^{1/2},$$

where the order of magnitude of the departure time

$$\Delta\tau_{1d} \approx \left\{ \sigma / [p'(T_{2i}) - p] \right\} \left\{ \rho_2 [p'(T_{2i}) - p] \right\}^{1/2}$$

is estimated from the mechanical energy equation setting the bubble growth work equal to the kinetic energy of the bubble environment

$$(dR_i / d\tau)^2 \approx (R_{1d} / \Delta\tau_{1d})^2 = (2/3)(1 - \rho'' / \rho_2) \Delta\rho / \rho_2.$$

The authors themselves considered the use of this time constant as “not the only one that may be significant”. The verification of this equation is made with data for superheat and heat flux at the point of burn out for different pressure. The exponents were questioned later by *Katz*, see the *Katz* comments to *Zuber*’s work in (1958), and new exponents are proposed in order to obtain agreement with experimental data for ethanol/chromium with  $const = 300$ , benzene with  $const = 1$ , and *n*-pentane with  $const = 0.3$ , where  $m = 1.05$  and  $n = -7$  was used for all three cases. Nevertheless, in a later work *Chen* (1966) uses the *Forster* and *Zuber* equation with  $m = 1/2$ ,  $n = 1/3$  to successfully describe the part of heat transfer due to nucleate boiling in forced convection.

In a later work *Zuber* (1960) comes back to the *von Karman - Pohlhausen* equation using again  $D_{1d}$  as a length scale but replacing the average distance between the neighboring bubbles by assuming a quadratic arrangement  $1/D_{2,inf} = n_{1w}''^{1/2}$ . Here,  $n_{1w}''$  is the nucleation site density in sites per square meter. Thus *Zuber* finally writes  $h_{w,mic} D_{1d} / \lambda_2 = const Re^{1/2} Pr_2^{1/3}$  where  $Re = B^2 D_{1d} / (\nu_2 D_{2,inf}) = B^2 D_{1d} n_{1w}''^{1/2} / \nu_2$ . This time, the  $B^2 = \frac{4}{\pi} a_2 Ja_2^2$  function is computed in accordance with *Bosnjakovic* (1930). The intention of *Zuber* in (1959) was not to derive a correlation but to show the dependence  $h_{w,mic} \approx n_{1w}''^{1/4}$  which was experimentally observed. Nevertheless, *Zuber* computed the heat flux at the wall during nucleate boiling as

$$\dot{q}_w'' = \dot{q}_{w,mic}'' \left( 1 - \frac{\pi}{4} D_{1d}^2 n_{1w}^{1/2} \right) + \dot{n}_{1w}'' f_{1w} \Delta h \frac{\pi}{6} D_{1d}^3 \rho_1$$

In more recent work, *Kocamustafaogullari and Ishii* (1983) use the idea of micro-convection in the following way

$$h_{w,mic} D_{2,inf} / \lambda_2 = 13.18 Re^m Pr_2^n \left( D_{1d} / D_{2,inf} \right)^p,$$

where  $m = 1/4$ ,  $n = -0.14$ ,  $p = -1/4$ . The distance between the neighboring bubbles is used as a characteristic which is consistent with the length along which the fluctuation velocity was averaged. It gives a simple expression for the *Reynolds* number  $Re = \bar{V}_2' D_{2,inf} / \nu_2 = B^2 / \nu_2$ . The authors used again the *Bosnjakovic*

model for thermally controlled bubble growth at a wall  $B^2 = \frac{4}{\pi} a_2 Ja_2^2$  and quadratic nucleation arrangement  $1/D_{2,inf} = n_{1w}''^{1/2}$ . Substituting into the starting equation and rearranging the authors came to

$$h_{w,mic} = 14 Ja^{1/2} Pr_2^{-0.39} \frac{\lambda_2}{D_{1d}^{1/4}} n_{1w}''^{3/8}$$

The constant and the powers are determined by comparison with experimental data where the bubble departure diameter was computed using a modified form of the *Fritz* equation.

*Labuntsov* (2000) assumed that the nucleation site density is a function of the critical bubble radius  $n_{1w}'' = const / R_{1c}^2$ . Using the dimensionless micro convection velocity  $V_{2,\mu c}^* = R_1 (dR_1 / d\tau) / R_{1c}$ , computing the thickness of the laminar boundary layer at  $y^+ = 10$ ,  $y = 10 \nu_1 / V_{2,\mu c}^*$  and assuming that the heat conduction through this layer is controlling the heat transfer he obtained

$$\dot{q}_w'' = const \frac{\lambda_2^2 (T_w - T')^3}{\nu_2 \sigma_{12} T'}.$$

Later on he introduced empirically the pressure dependence and proposed the following expression for the heat transfer coefficient at nucleate boiling

$$h_w = 0.075 \left( \frac{\lambda_2^2 q_w''}{\nu_2 \sigma_{12} T'} \right)^{1/3} \left[ 1 + 10 \left( \frac{\rho''}{\rho' - \rho''} \right)^{2/3} \right].$$

*Tolubinsky and Ostrovsky* (1966) generalized great number of data for water and other liquids by the correlation

$$h_w \lambda_{RT} / \lambda_2 = 75 \left[ \frac{\dot{q}_{w1}'' / (\Delta h \rho_1)}{D_{1d} f_{1w}} \right]^{0.7} Pr_2^{-0.2}$$

$\lambda_{RT}$  where the bubble departure velocity  $D_{1d}f_{1w} = 0.36 \times 10^{-3} (p_c / p)^{1.4}$ . The data are fitted within an error band of  $\pm 25\%$ .

Some conclusions seem to be in order after knowing the above discussed approaches to the modeling of nucleate pool boiling:

- Obviously, heat conduction and micro-convection simultaneously exist in pool boiling.
- The appropriate scale in the *von Karman - Pohlhausen* equation for micro-convection is the average distance between two neighboring bubbles. Nevertheless, the micro-convection is much more similar to turbulent heat transfer than to forced convection.
- The bubble removal frequency from the wall boundary layer is not necessarily equal to the bubble departure frequency.
- Besides the spatial averaging of the pulsation velocity, a time averaging during the bubble generating period  $1/f_{1w}$  is necessary.
- None of the theories takes into account the influence of the static contact angle on the heat transfer.
- All models put the unknown phenomena in empirical constants so that none of the theories is able to predict separate phenomena like bubble departure diameter, nucleation site density etc. appropriately.

## Nomenclature

$a_2$	liquid thermal diffusivity, $m^2/s$
$a'$	saturation liquid thermal diffusivity, $m^2/s$
$B^2$	$= 2R_1 dR_1 / d\tau$ , $m^2/s$
$c_{p2}$	specific heat of liquid, $J/(kgK)$
$D_1$	bubble diameter, $m$
$D_{1c}$	critical size, $m$
$D_{1d}$	bubble departure diameter, $m$
$D_{1d,fc}$	bubble departure diameter for strongly predominant forced convection, $m$
$D_{1d,nc}$	bubble departure diameter for natural circulation, $m$
$D_{2,inf}$	average center to center spacing, $m$
$f_{1w}$	bubble departure frequency, $1/s$
$f'_{1w}$	boundary layer turbulence fluctuation frequency, $1/s$
$G$	mass flow rate, $kg/(m^2s)$
$g$	gravitational acceleration, $m/s^2$
$h', h''$	specific saturation enthalpies for water and steam, $J/(kgK)$
$\Delta h$	$= h'' - h'$ , $J/kg$
$Ja$	$= \rho_2 c_{p2} [T_2 - T'(p)] / (\rho_1 \Delta h)$ , <i>Jacob number</i> , dimensionless
$Ja'$	$= \rho' c'_p [T_2 - T'(p)] / (\rho'' \Delta h)$ , <i>Jacob number</i> , dimensionless

$n''_{1w}$	Active nucleation site density, $1/m^2$
$p$	pressure, $Pa$
$p'$	saturated pressure, $Pa$
$Pr_2$	$= \eta_2 / (\rho_2 a_2)$ , <i>Prandtl</i> number, dimensionless
$\dot{q}''_{w2,nc}$	heat flux from the wall into the liquid during natural convection without boiling, $W/m^2$
$\dot{q}''_{w2,nb}$	heat flux from the wall into the liquid during pool boiling, $W/m^2$
$R_1$	bubble radius, $m$
$R_{2,inf}$	$= D_{2,inf} / 2$ , $m$
$T'(p)$	saturation temperature at system pressure $p$ , $K$
$T_2$	liquid temperature, $K$
$T_w$	wall temperature, $K$
$\bar{V}'_2$	the volume-averaged fluctuation velocity, $m/s$
$\bar{\bar{V}}'_2$	the volume-averaged fluctuation velocity time averaged over $\Delta\tau_w + \Delta\tau_d$ , $m/s$

### Greek

$\beta_2$	$= -\frac{1}{\rho_2} \left( \frac{\partial \rho_2}{\partial T_2} \right)_p$ , thermal expansion coefficient, $1/K$
$\delta_{2,min}$	minimum of the thermal boundary layer thickness, $m$
$\Delta\rho_{21}$	$= \rho_2 - \rho_1$ , $kg/m^3$
$\Delta\tau_d$	time needed from the origination of a bubble with critical size to the bubble departure from the wall, $s$
$\Delta\tau_w$	delay time, $s$
$\eta_2$	dynamic viscosity of liquid, $kg/(ms)$
$\lambda_2$	thermal conductivity of liquid, $W/(mK)$
$\lambda_{RT}$	$= \left( \frac{\sigma}{g\Delta\rho_{21}} \right)^{1/2}$ , <i>Rayleigh - Taylor</i> instability wavelength, $m$
$\nu_2$	cinematic viscosity of liquid, $m^2/s$
$\rho_1$	gas density, $kg/m^3$
$\rho_2$	liquid density, $kg/m^3$
$\rho''$	saturated steam density, $kg/m^3$
$\rho'$	saturated liquid density, $kg/m^3$
$\sigma$	surface tension, $N/m$
$\tau$	time, $s$
$\theta_0$	angle between the bubble axis and the wall, $rad$
$\varphi$	static contact angle between “liquid drop” and the wall, $rad$



## References

- Arefeva EI and Aladev IT (July 1958) O wlijanii smatchivaemosti na teploobmen pri kipenii, Injenerno - Fizitcheskij Jurnal, in Russian, vol 1 no 7 pp 11-17
- Avdeev AA, Maidanik VN, Selesnev LI and Shanin VK (1977) Calculation of the critical flow rate with saturated and subcooled water flushing through a cylindrical duct, *Teploenergetika*, vol 24 no 4 pp 36-38
- Borishanskii V, Kozyrev A and Svetlova L (1964) Heat transfer in the boiling water in a wide range of saturation pressure, *High Temperature*, vol 2 no 1 pp 119-121
- Borishanskii, V, Bobrovich G, Minchenko F (1961) Heat transfer from a tube to water and to ethanol in nucleate pool boiling, Symposium of Heat Transfer and Hydraulics in Two-Phase Media, Kutateladze SS (ed) Gosenergoizdat, Moscow, pp 75-93
- Brauer H (1971) Stoffaustausch, Verlag Sauerländer
- Chandesris M, Serre G and Sagaut (2005) A macroscopic turbulence model for flow in porous media suited for channel, pipe and rod bundle flows, 4<sup>th</sup> Int. Conf. On Computational Heat and Mass Transfer, Paris
- Chen JC (July 1966) Correlation for boiling heat transfer to saturated fluids in convective flow, *Ind. & Eng. Chem. Progress Design and Development*, vol 5 no 3 pp 322-329
- Cole R, Rohsenow WM (1969) Correlation of bubble departure diameters for boiling of saturated liquids, *Chem. Eng. Prog. Symp. Ser.*, no 92 vol 65 pp 211-213
- Cornwell K, Brown RD (1978) Boiling surface topology, *Proc. 6th Int. Heat Transfer Conf. Heat Transfer 1978 - Toronto*, vol 1 pp 157-161
- Dittus FV and Boelter LMK (1930) Univ. of Calif. Publ. In Engng. Vol 2 no 13 p 443
- Faggiani S, Galbiati P and Grassi W (1981) Active site density, bubble frequency and departure on chemically etched surfaces, *La Termotecnica*, vol 29 no 10 pp 511-519
- Forster HK, Zuber N (1955) Dynamics of vapor bubbles and boiling heat transfer, *AIChE J.*, vol 1 no 4 pp 531-535
- Fritz W (1935) Berechnung des maximalen Volumens von Dampfblasen, *Phys. Z.*, vol 36 no 11 pp 379-384
- Gaertner RF (1963) Distribution of active sites in the nucleate boiling of liquids, *Chem. Eng. Prog. Symp. Series*, no 41 vol 59 pp 52-61
- Gaertner RF (Feb. 1965) Photographic study of nucleate pool boiling on a horizontal surface, *Transaction of the ASME, Journal of Heat Transfer*, vol 87 pp 17 - 29
- Gaertner RF, Westwater JW (1960) Population of active sites in nucleate boiling heat transfer, *Chem. Eng. Progr. Symp. Ser.*, no 30 vol 30 pp 39-48
- Han CY, Griffith P (1965) The mechanism of heat transfer in nucleate pool boiling, Part I, Bubble initiation, growth and departure, *Int. J. Heat Mass Transfer*, vol 8 pp 887-904
- Haramura Y and Katto Y (1983) A new hydrodynamic model of CHF applicable widely to both pool and forced convection boiling on submerged bodies in saturated liquids, *Int. J. of Heat and Mass Transfer*, vol 26 pp 389-399
- Hutcherson MN, Henry RE and Wollersheim DE (Nov. 1983) Two-phase vessel blowdown of an initially saturated liquid - Part 2: Analytical, *Trans. ASME, J. Heat Transfer*, vol 105 pp 694-699
- Jakob M (1932) Kondensation und Verdampfung, *Zeitschrift des Vereins Deutscher Ingenieure*, vol 76 no 48 pp 1161-1170
- Jakob M (1949) Heat transfer, Wiley, New York, vol 1 ch 29

- Jakob M and Fritz W (1931) Versuche ueber den Verdampfungsvorgang, Forsch. Ing. - Wes., vol 2 p 435
- Jakob M and Linke W (1933) Der Wärmeübergang von einer waagerechten Platte an siedendes Wasser, Forsch. Ing. Wes., vol 4 pp 75-81
- Jens WH and Lottes PA (1951) Analysis of heat transfer, burnout, pressure data and density data for high pressure water. USAEC Rep. ANL-4627
- Johov KA (1969) Nucleations number during steam production, Aerodynamics and Heat Transfer in the Working Elements of the Power Facilities, Proc. CKTI, Leningrad, in Russian, vol 91 pp 131- 135
- Jones OC (1992) Nonequilibrium phase change --1. Flashing inception, critical flow, and void development in ducts, in boiling heat transfer, Lahey RT Jr (ed) Elsevier Science Publishers B.V., pp 189 - 234
- Jones OC (1992) Nonequilibrium phase change --2. Relaxation models, general applications, and post heat transfer, Lahey RT Jr (ed) Boiling Heat Transfer, Elsevier Science Publishers B.V., pp 447-482
- Judd RL, Hwang KS (Nov. 1976) A comprehensive model for nucleate pool boiling heat transfer including microlayer evaporation, Transaction of the ASME, Journal of Heat Transfer, vol 98 pp 623-629
- Kim SJ, Truong B, Buongiorno J, Hu LW, Bang IC (June 4-8, 2006) Study of two-phase heat transfer in nanofluids for nuclear applications, Proceedings of ICAPP '06 Reno, NV USA, Paper 6005
- Kocamustafaogullari G and Ishii M (1983) Interfacial area and nucleation site density in boiling systems, Int. J. Heat Mass Transfer, vol 26 pp 1377-1389
- Kolev NI (1994) The influence of mutual bubble interaction on the bubble departure diameter, Experimental Thermal and Fluid Science, vol 8 pp 167-174
- Kolev NI (1995) How accurate can we predict nucleate boiling, Experimental Thermal and Fluid Science, Experimental Thermal and Fluid Science, vol 10 pp 370-378
- Kurihara HM, Myers JE (March 1960) The effect of superheat and surface roughness on boiling coefficients, AIChE Journal, vol 6 no 1 pp 83-91
- Kutateladse SS (1954) A hydrodynamic theory of changes in the boiling process under free convection conditions, Izv. Akad. Nauk SSSR, Otd. Tech. Nauk, vol 4 pp 529-536, 1951; AEC-tr-1991
- Kutateladse SS (1962) Basics on heat transfer theory, in Russian, Moscow, Mashgis, p 456
- Labuntsov DA (1963) Approximate theory of heat transfer by developed nucleate boiling (Russ.), Izvestiya AN SSSR, Energetika i transport no 1
- Labuntsov DA (1974) State of the art of the nucleate boiling mechanism of liquids, Heat Transfer and Physical Hydrodynamics, Moskva, Nauka, in Russian, pp 98-115
- Labuntsov DA (2000) Physical fundamentals of power engineering. Selected works on heat transfer, hydrodynamics and thermodynamics, MPEI publisher, Moscow
- Labuntsov DA, Kol'chugin VA, Golovin VS et al (1964) Teplofiz. Vys. Temp., vol 3 pp 446-453
- Miheev MA and Miheeva IM (1973) Basics of heat transfer, Moskva, Energija, in Russian, p 320
- Mikic BB, Rohsenow WM (May 1969) A new correlation of pool-boiling data including the effect of heating surface characteristics, Transactions of the ASME, J. Heat Transfer, vol 91 pp 245-250

- Morin R (1964) Wall temperature fluctuations during bubble generation in boiling, in *Convective heat transfer in two-phase and one-phase flows*, Energiya, Moskva. eds. Borishanskii VM and Paleev II
- Nishikawa K, Fujita Y, Uchida S, Ohta H (1984) Effect of surface configuration on nucleate boiling heat transfer, *Int. J. Heat and Mass Transfer*, vol 27 no 9 pp 1559-1571
- Pohlhausen K (1921) Zur nährungsweisen Integration der Differentialgleichung der laminaren Grenzschicht, *Z. angew. Math. Mech.*, vol 1 pp 252-268
- Rallis CJ, Jawurek HH (1964) Latent heat transport in saturated nucleate boiling, *Int. J. Heat Transfer*, vol 7 pp 1051-1068
- Riznic J and Ishii M (1989) Bubble number density and vapor generation in flushing flow, *Int. J. Heat Mass Transfer*, vol 32 pp 1821-1833
- Rohsenow WM (1952) A method of correlating heat transfer data for surface boiling of liquids, *Trans. ASME*, vol 74 pp 969-975
- Sani RL (4 January 1960) Down flow boiling and non-boiling heat transfer in a uniformly heated tube, University of California, URL-9023, Chemistry-Gen. UC-4, TID-4500 (15<sup>th</sup> Ed.)
- Siegel R and Keshock EG (July 1964) Effects of reduced gravity on nucleate boiling bubble dynamics in saturated water, *AIChE Journal*, vol 10 no 4 pp 509-517
- Sultan M, Judd RL (Feb. 1978) Spatial distribution of active sites and bubble flux density, *Transactions of the ASME, Journal of Heat Transfer*, vol 100, pp 56-62
- Theofanus TG et al. (2002) The boiling crisis phenomenon. Part II: dryout dynamics and burnout, *Experimental Thermal and Fluid Science*, vol 26 pp 793-810
- Thom IRS et. al. (1966) Boiling in subcooled water during up heated tubes or annuli. *Proc. Instr. Mech. Engs.*, vol 180 3C pp 1965-1966
- Tolubinsky VI, Ostrovsky JN (1966) On the mechanism of boiling heat transfer (vapor bubbles growth rate in the process of boiling in liquids, solutions, and binary mixtures), *Int. J. Heat Mass Transfer*, vol 9 pp 1463-1470
- Vachon RI, Tanger GE, Davis DL, Nix GH (May 1968) Pool boiling on polished chemically etched stainless-steel surfaces, *Transactions of ASME, Journal of Heat Transfer*, vol 90 pp 231-238
- Vachon RI, Nix GH, Tanger GH (May 1968) Evaluation of the constants for the Rohsenow pool - boiling correlation, *Transactions of the ASME Journal of Heat Transfer*, vol 90 pp 239-247
- van Stralen S, Cole R (1979) *Boiling Phenomena*, Hemisphere, USA
- von Karman T (1921) Über laminare und turbulente Reibung, *Z. angew. Math. Mech.*, vol 1 pp 233-252
- Wang CH, Dhir VK (Aug. 1993) Effect of surface wettability on active nucleation site density during pool boiling of water on a vertical surface, *ASME Journal of Heat Transfer*, vol 115 pp 659-669
- Wiebe JR (1970) Temperature profiles in subcooled nucleate boiling, M. Eng. thesis, Mechanical Engineering Department, McMaster University, Canada
- Yamagata K, Hirano F, Nishikawa K, Matsuoka H (1955) Nucleate boiling of water on the horizontal heating surface, *Mem. Fac. Engng; Kyushu Univ*, vol 15 p 97
- Yang JK, Weisman J (1991) A phenomenological model of subcooled flow boiling in the detached bubble region, *Int. J. Multiphase Flow*, vol 17 no 1 pp 77-94
- Zuber N (1959) Hydrodynamic aspect of boiling heat transfer, U.S. Atomic Energy Commission Rept., AECU - 4439, Tech. Inf. Serv. Oak Ridge, Tenn

- Zuber N (1963) Nucleate boiling, The region of isolated bubbles and the similarity with natural convection, *Int. J. Heat Mass Transfer*, vol 6 pp 53-78
- Zuber N (April 1958) On the stability of boiling heat transfer, *Transactions of the ASME*, vol 80 pp 711-720
- Zuber N (Jan. 1960) Hydrodynamic aspect of nucleate pool boiling, Part I - The region of isolated bubbles, *Research Laboratory Ramo - Wooldridge*, RW-RL-164, 27
- Zuber N and M Tribus (1958) Further remarks on the stability of boiling heat transfer, report 58-5, Department of Engineering, University of California, Los Angeles
- Zuber N, Tribus M and Westwater JW (1961) The hydrodynamic crisis in pool boiling of saturated and subcooled liquids, *International Developments in Heat Transfer*, Proc. Int. Heat Transfer Conf., Boulder, Colorado, Part 2, no 27 pp 230-236

## 17 Heterogeneous nucleation and flashing in adiabatic pipes

*A new model of heterogeneous nucleation at walls during flashing and boiling is presented. The model is based on a new method for computation of the bubble departure diameter in flows accounting for mutual bubble interactions and the limitation of the bubble production due to the limited amount of energy supplied into the boundary layer by turbulence induced by bubble growth and departure. The final model together with fragmentation and coalescence models is incorporated into the system code IVA and verified by comparison with data. This Chapter is a short version of the primary published work in Kolev (1995).*

### 17.1 Introduction

Modern theories of multi-phase flows account for the dynamic generation of particles of one phase inside the other. Bubbles generation at walls during boiling or flashing is a typical example discussed in Chapter 16. The number of the bubbles generated per unit time and unit surface, and the bubble departure diameter, are the most important parameters in this process, which influence the later process of bubble growth and/or collapse into the bulk liquid. There have been some publications on this field in the last decade whose main result is the so called figure-of-merit model. This model produces agreement with data by introducing fitting parameters in the general model without verifying the sub-models. Examples are Refs. *Shin and Jones* (1993), *Blinkov et al.* where the model used for bubble departure diameter is not appropriate for strong superheating *Kolev* (1994). In this Chapter we extend the validity of the results obtained in Chapters 15 and 16 to adiabatic flashing of superheated liquids in pipes. The final model together with fragmentation and coalescence models is incorporated into the system code IVA4 and verified by comparison with data for flashing flows in converging-diverging nozzles and pipe blow-down of water. IVA4 is computer code describing multi-phase non-equilibrium flows by means of three velocity fields in industrial networks and/or three-dimensional facilities. The system of partial differential equations, 21 PDE's for 3D and 15 PDE's for 1D network, solved by this code contains Eq. (1.62) from Volume 1 which is the local volume-averaged mass conservation equation subsequently time averaged

$$\frac{\partial}{\partial \tau}(\alpha_\ell \rho_\ell \gamma_v) + \nabla \cdot (\alpha_\ell \rho_\ell \gamma \mathbf{V}_\ell) = \mu_\ell \quad (17.1)$$

and Eq. (1.102) from Volume 1 which is the local volume- and time-averaged conservation equation for the number of the particles per unit flow volume without diffusion terms

$$\frac{\partial}{\partial \tau} (n_\ell \gamma_v) + \nabla \cdot (n_\ell \gamma \mathbf{V}_\ell) = \dot{n}_{\ell,kin} + \dot{n}_{\ell,frag} - n_{\ell,coal} \cdot \quad (17.2)$$

Knowing the local volume- and time-averaged particle number density  $n_\ell$  and the volumetric fraction  $\alpha_\ell$ , the characteristic local volume- and time-averaged particle size  $D_\ell$  is computed from the equation

$$n_\ell \frac{\pi}{6} D_\ell^3 = a_\ell \quad (17.3)$$

that is strictly valid for spherical bubble. Next we confine our attention only to origination of the steam velocity field, designated by 1, in water, designated by 2.

## 17.2 Bubbles generated due to nucleation at the wall

Heterogeneous nucleation theory is sometimes recommended to describe nucleation at walls *Skripov et al.* (1980). This theory gives the probability of nucleation for given local conditions *Kaishev and Stranski* (1934) and *volmer* (1939), but does not predict these conditions. As far the author knows there is no other attempt to describe the nucleation at walls theoretically as those presented in Chapters 15 and 16. The turbulence in the boundary layer is an important energy exchange mechanism also during flashing of superheated liquids in adiabatic pipes. This follows from the fact that no more energy for bubble generation at the wall can be consumed than is supplied by the turbulence transfer from the bulk into the boundary layer. That is why we propose to use Eqs. (16.22) to (16.24) also for flashing in adiabatic pipes with driving temperature difference  $T_2 - T'$  instead  $T_w - T'$ :

$$\dot{q}_{w2,b}'' = \dots \text{Eq. (16.22)}, \quad (17.4)$$

$$\mu_{21,gen} = \frac{4}{D_h} \dot{q}_{w2,b}'' / (h'' - h_2), \quad (17.5)$$

and

$$\dot{n}_{1w} = \mu_{21} / \left( \rho_1 \frac{\pi}{6} D_{1d}^3 \right). \quad (17.6)$$

From the moment of bubble detachment from the wall the bubble starts its own history inside the bulk flow and undergoes condensation or further evaporation as

well as collisions, coalescence or fragmentation. In the next section we consider an example of such history for superheated liquids.

### 17.3 Bubble growth in the bulk

Consider a constant number of bubbles per unit mixture volume,  $n_l$ , during the time step  $\Delta\tau$ . As discussed in Chapter 13, the mass difference between the end and the beginning of the time step in a single bubble multiplied by the bubble number per unit mixture volume, gives the mass evaporated in the bulk per unit mixture volume and unit time.

$$\mu_{21,bulk} = n_l \frac{\pi}{6} (\rho_l D_l^3 - \rho_{l0} D_{l0}^3) / \Delta\tau = \frac{\rho_{l0} \alpha_{l0}}{\Delta\tau} \left[ \frac{\rho_l}{\rho_{l0}} \left( \frac{R_l}{R_{l0}} \right)^3 - 1 \right] \quad \alpha_{l0} > 0 \quad (17.7)$$

As already mentioned from the sixteen analytical solutions of the bubble growth problem obtained for different degrees of simplicity known to the author - see Appendix 13.1, the bubble growth model proposed by *Mikic et al* (1970) is used as the best one:

$$\mu_{21,bulk} = \frac{\rho'' \alpha_{l0}}{\Delta\tau} \left[ \left\{ 1 + \frac{2}{3} \left[ (\tau^+ + 1)^{3/2} - (\tau^+)^{3/2} - 1 \right] / R_{l0}^+ \right\}^3 - 1 \right] \quad (17.8)$$

where

$$\tau^+ = \Delta\tau / (B^2 / A^2), \quad (17.9)$$

$$A^2 = \frac{2}{3} \frac{1}{\rho_2} (dp / dT)_{sat} (1 - \rho'' / \rho_2) [T_2 - T'(p)], \quad (17.10)$$

$$R^+ = AR_l / B^2. \quad (17.11)$$

Thus the steam generation is a superposition of the nucleation at the wall and of the bubble growth inside the bulk flow

$$\mu_{21} = \mu_{21,bulk} + \mu_{21,gen}. \quad (17.12)$$

### 17.4 Bubble fragmentation and coalescence

A review of the existing fragmentation and coalescence models for gases and liquids was given in Chapters 7 to 10. For the computation presented below we use the following gas fragmentation model. The volume and time average number

of generated particles per unit time and unit mixture volume due to dynamic fragmentation is

$$\dot{n}_{1,frag} = (n_{1\infty} - n_1) / \Delta\tau_{fr} \text{ for } n_{1\infty} > n_1 \text{ and } \Delta\tau \leq \Delta\tau_{fr}, \quad (17.13)$$

$$\dot{n}_{1,frag} = (n_{1\infty} - n_1) / \Delta\tau \text{ for } n_{1\infty} > n_1 \text{ and } \Delta\tau > \Delta\tau_{fr}, \quad (17.14)$$

$$\dot{n}_{1,frag} = 0 \text{ for } n_{1\infty} \leq n_1, \quad (17.15)$$

where  $\Delta\tau$  is the time step,  $n_1$  is local bubble density concentration, and

$$n_{1\infty} = 6\alpha_1 / (\pi D_{1\infty}^3) \quad (17.16)$$

is the stable bubble number density concentration after fragmentation. Equation (17.14) gives in fact steady state fragmentation for large time steps. The stable bubble diameter is computed in accordance with the *Achmad's* equations (8.173) and (8.172),

$$D_{1\infty} = \lambda_{RT} [9\alpha_1 / (1 - \alpha_1)]^{1/3} \quad (17.17)$$

for  $\alpha_1 > 0.1$ , and

$$D_{1\infty} = 0.9\lambda_{RT} / \left\{ 1 + 1.34 \left[ (1 - \alpha_1) V_2 \right]^{1/3} \right\} \quad (17.18)$$

for  $\alpha_1 < 0.1$ , see in *Ahmad* (1970).

The fragmentation time is set equal to the natural fluctuation period of bubble flow, Eq. (8.177)

$$\Delta\tau_{fr} = \left( \frac{6}{\pi\sqrt{2}} \right)^{1/3} \alpha_1^{1/3} / \Delta V_{12}^*, \quad (17.19)$$

where the relative velocity is a superposition of the difference between the mean velocity and the turbulent fluctuation velocity,

$$\Delta V_{12}^* = |V_1 - V_2| + V_2' \quad (17.20)$$

$$V_2' \approx 0.3|V_2| \text{ for } \alpha_1 < 0.3 \quad (17.21)$$

and

$$V_2' \approx 0.7|V_2| \text{ for } \alpha_1 \geq 0.3 \quad (17.22)$$

The volume and time average bubble disappearance per unit time and unit mixture volume due to collision and coalescence is computed in accordance with Eq. (7.22),

$$\dot{n}_{coal} = n_1 [1 - \exp(f_{coal} / \Delta\tau)] / \Delta\tau, \quad (17.23)$$



where  $\Delta\tau$  is the time averaging period. Here the instantaneous coalescence frequency of a single bubble is

$$f_{coal} = P_{coal} f_{col} \quad (17.24)$$

where the collision frequency is computed in accordance with Eq. (7.29),

$$f_{col} = 4.5\alpha_1^{1/2} \Delta V_{12}^* / D_1 \quad (17.25)$$

and the coalescence probability  $P_{coal}$  is set to 1 for superheated liquid in order to approximate the effect of non-uniform particle distribution in the cross section. In case of no liquid superheating we use Eq. (7.45),

$$P_{coal} \approx 0.032 (\Delta\tau_{col} / \Delta\tau_{coal})^{1/3} \quad \text{for } \Delta\tau_{col} / \Delta\tau_{coal} \geq 1, \quad (17.26)$$

where

$$\Delta\tau_{col} / \Delta\tau_{coal} = 1.56 \left( \frac{D_1 \sigma_2}{3\rho_1 + 2\rho_2} \right)^{1/2} / V_2'. \quad (17.27)$$

## 17.5 Film flashing bubble generation in adiabatic pipe flow

Boiling and flashing are governed by the same physical phenomena. Having accepted that there is departure from nucleate boiling in heated channels we have also to accept that the departure from nucleate bubble generation is also possible in adiabatic pipe flow. The steam volumetric fraction in the boundary layer with a thickness  $D_{ld}$  is

$$\alpha_{ld} = (\pi / 6) n_{lw}'' D_{ld}^2 \quad (17.28)$$

If  $\alpha_{ld} > 0.52$  the bubbles touch each other and a film is formed. We call this bubble generation mechanism *film* flashing because it is controlled by bubble entrainment from the vapor layer. If there is no flow velocity imposed, we have

$$D_{ld} \approx 2\pi\lambda_{RT}, \quad (17.29)$$

$$f_{lw} \approx V_{1Ku} / D_{ld}, \quad (17.30)$$

where

$$V_{1Ku} = 1.41 \left[ g\sigma(\rho_2 - \rho_1) / \rho_2^2 \right]^{1/4}, \quad (17.31)$$

is the free rising bubble velocity (*Kutateladze* velocity). For forced convection we assume that the stability criterion

$$We_{1d} \approx 12 \quad (17.32)$$

controls the bubble entrainment size, and therefore

$$D_{1d} \approx 12\sigma / (\rho_2 \Delta V_{21}^2), \quad (17.33)$$

$$f_{1w} \approx \Delta V_{21} / D_{1d}. \quad (17.34)$$

For both cases we have

$$\dot{n}_{1w} = \frac{4}{D_h} n_{1w} f_{1w}, \quad (17.35)$$

$$\mu_{21,gen} \approx \rho_1 \dot{n}_{1w} (\pi D_{1d}^3 / 6), \quad (17.36)$$

and

$$\dot{q}_{\sigma 2,gen}''' = -\mu_{21,gen} (h'' - h_2). \quad (17.37)$$

## 17.6 Verification of the model

As already mentioned, the model developed in the preceding Sections was incorporated into the code IVA4. Its predicting capabilities will now be verified taking the flashing flow in converging - diverging nozzles and the blow-down in pipes as examples. It is very important in such calculations to ensure that the code properly predicts the single-phase steady state and transient flows.

The results of three BNL experiments for water flow in a converging-diverging nozzle *Abuaf* et al. (1981) are presented in Fig. 17.1, together with the results calculated with our model. We see good agreement for pressure distribution as well as for the predicted mass flow rate as function of inlet/outlet pressure difference.

The *Kellner* and *Gissler* experiment (1984) used for the next comparison produced pressure wave propagation in single pipes with five bends and one dead end. The imposed pressure function at the entrance of the pipe is shown in Fig. 17.2a. The comparison of the predicted and the measured responses presented on Figs. 17.2b through 17.2d shows good agreement.

Now we proceed to the BNL converging-diverging nozzle experiment *Abuaf* et al. (1981) with an entrance condition which causes flashing flow behind the nozzle throat. The results of the computation are presented in Figs. 17.3 through 17.6. We see that our model

- a) predicts the data for pressure distribution data well,
- b) slightly over predicts the data for the volumetric void fraction distribution, resulting in
- c) some under prediction of the mass flow as a function of the measured pressure difference.

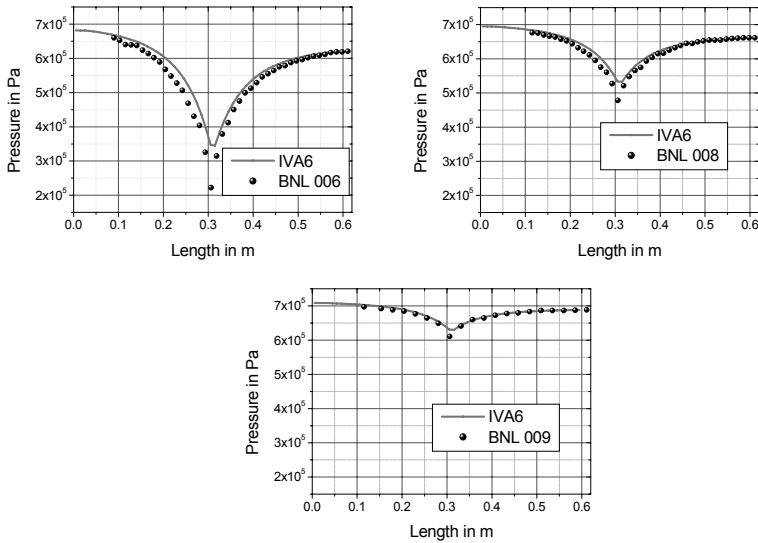


**Fig. 17.1** Comparison of IVA4-NW predictions with BNL experimental data for pressure distribution. Single phase flow. Runs 6, 8, 9.  $p_{in} = 682, 695, 709$  kPa,  $p_{out} = 627, 665, 692$  kPa,  $T_{in} = 27^\circ\text{C}$ ,  $G_{exp} = 7010, 4710, 3130$  kg/(m<sup>2</sup>s),  $G_{com} = 6319, 4362, 2991$  kg/(m<sup>2</sup>s).

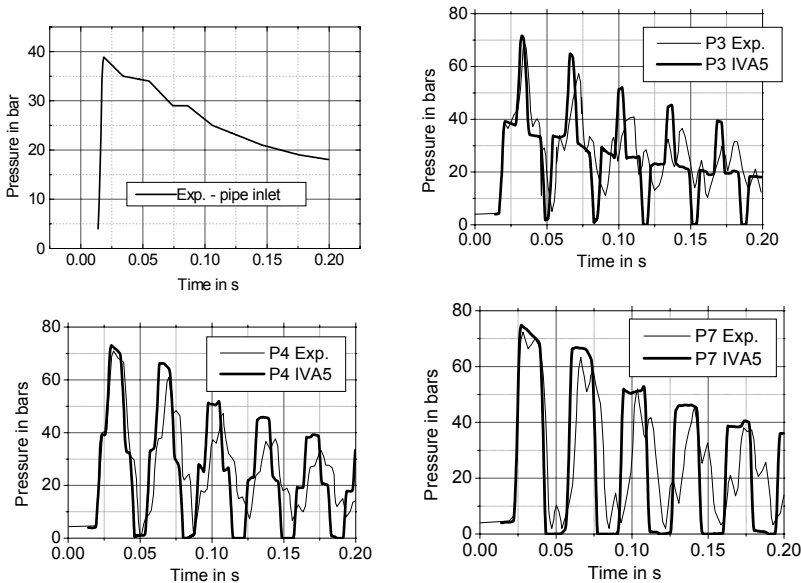


**Fig. 17.2** a) Pressure at the pipe entrance as a function of time as measured by Kellner and Gissler (1984). Pipe length 13.12 m, diameter 0.1 m, 4 bends at 4.8, 10.2, 12.6, 13.64 m from the entrance. Initial conditions: water at atmospheric temperature and pressure. b) at 4.08 m from the pipe entrance. Comparison of IVA5 prediction with the experimental data by Kellner and Gissler (1984). c) at 8.18 m from the pipe entrance. d) at 12.5 m from the pipe entrance

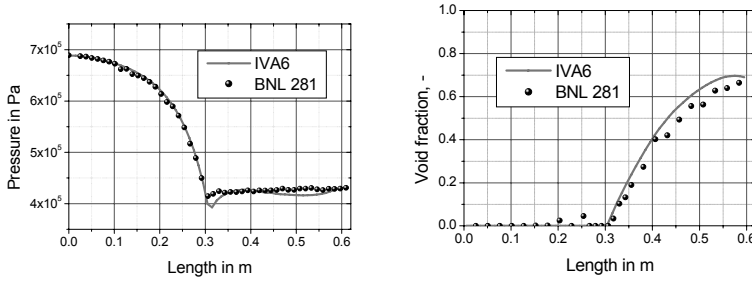


**Fig. 17.3** Comparison of IVA4 prediction with BNL experimental data for pressure distributions and area averaged void fractions for Runs 281 - 283.  $p_{in} = 688 \text{ kPa}$ ,  $T_{in} = 148.8^\circ\text{C}$ ,  $G_{in} = 5730 \text{ kg/(m}^2\text{s)}$ ,  $p_{out} = 431 \text{ kPa}$ ,  $p_c = 452 \text{ kPa}$ ,  $T_c = 148.8^\circ\text{C}$ ,  $G_{com} = 5533 \text{ kg/(m}^2\text{s)}$

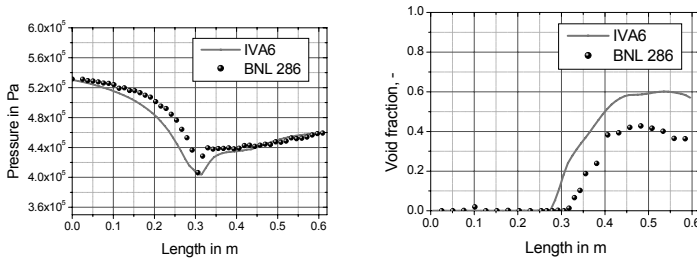


**Fig. 17.4** Comparison of IVA4 predictions with BNL experimental data for pressure distributions and area average void fractions for Runs 286 - 288.  $p_{in} = 530 \text{ kPa}$ ,  $T_{in} = 149.2^\circ\text{C}$ ,  $G_{in} = 3580 \text{ kg/(m}^2\text{s)}$ ,  $p_{out} = 459 \text{ kPa}$ ,  $p_c = 456 \text{ kPa}$ ,  $T_c = 149.2^\circ\text{C}$ ,  $G_{com} = 2706 \text{ kg/(m}^2\text{s)}$

Next we simulate the pipe blow-down experiment documented in *Edwards and O'Brien (1970)*, *Kolev (1995)*. A horizontal pipe is initially filled with water slightly subcooled under the initial pressure. One end of the pipe is quickly opened. The pressure drops below the saturation pressure at the water temperature and the heterogeneous nucleation starts. After producing enough bubble sizes the pressure increases up to the saturation pressure corresponding to the initial temperature for a long time due to intensive flashing inside the pipe. Then it starts to decrease to the external pressure.

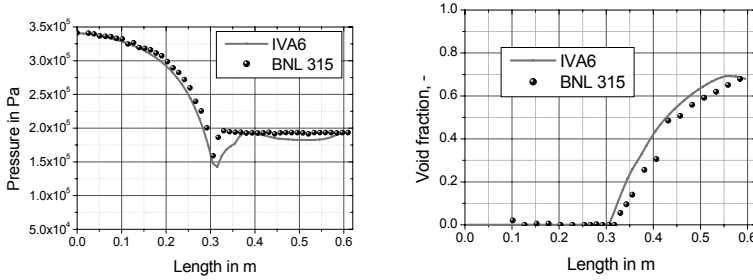


**Fig. 17.5** Comparison of IVA4 predictions with BNL experimental data for pressure distributions and area average void fractions for Runs 313 - 315.  $p_{in} = 341 \text{ kPa}$ ,  $T_{in} = 121^\circ\text{C}$ ,  $G_{in} = 4410 \text{ kg/(m}^2\text{s)}$ ,  $p_{out} = 193 \text{ kPa}$ ,  $p_c = 200 \text{ kPa}$ ,  $T_c = 119^\circ\text{C}$ ,  $G_{com} = 4202 \text{ kg/(m}^2\text{s)}$

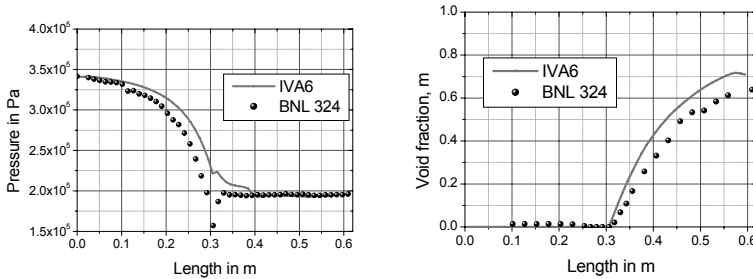


**Fig. 17.6** Comparison of IVA4 predictions with BNL experimental data for pressure distributions and area average void fractions for Runs 324 - 325.  $p_{in} = 341 \text{ kPa}$ ,  $T_{in} = 121^\circ\text{C}$ ,  $G_{in} = 4410 \text{ kg/(m}^2\text{s)}$ ,  $p_{out} = 196 \text{ kPa}$ ,  $p_c = 200 \text{ kPa}$ ,  $T_c = 121.8^\circ\text{C}$ ,  $G_{com} = 4004 \text{ kg/(m}^2\text{s)}$

The results are given in Figs. 17.7 through 17.11. We see that the nucleation theory applied here results in an appropriate pressure prediction (Fig. 17.7). The somewhat faster emptying of the pipe in the computation in the later stage of the process (Fig. 17.8) is caused by the several interactions in the computer code like drag forces, flow pattern recognition, etc., which will not be discussed here. We see also that the computed water temperature (Fig. 17.10) decreases faster than in reality. This is evidence that more energy is released from the liquid for evaporation in the model than in reality. This is consistent with the predicted void fraction at a given position (Fig. 17.9). The large void fraction increase in the first 0.1 s is not predicted by the model. This experimental observation is in contrast with the behavior observed behind the throat of the NL - nozzle.

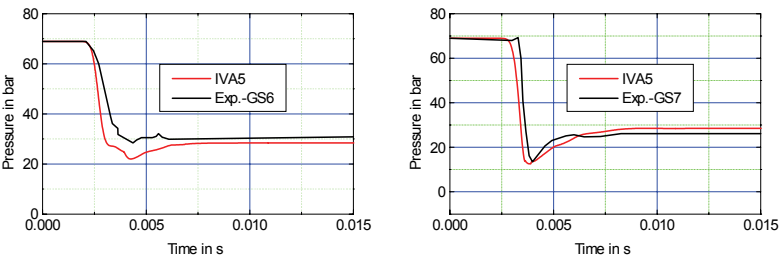


**Fig. 17.7** Pressure at 0.072 and 0.914 *m* from the dead end of pipe as a function of time. Comparison IVA5 prediction with experimental data by Edwards and O'Brien. Pipe diameter 0.0732 *m*, length 4.096 *m*

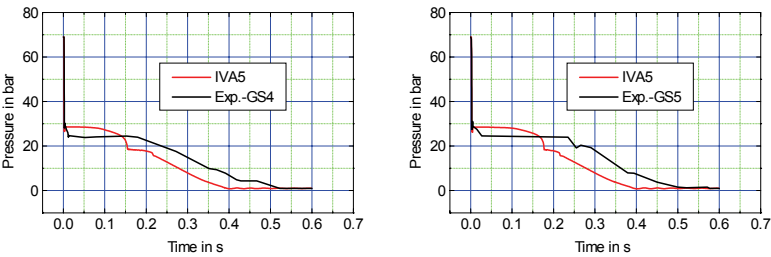


**Fig. 17.8** Pressure at 2.024 and 2.469 *m* from the dead end of pipe as a function of time. Comparison IVA5 prediction with experimental data by Edwards and O'Brien. Pipe diameter 0.0732 *m*, length 4.096 *m*

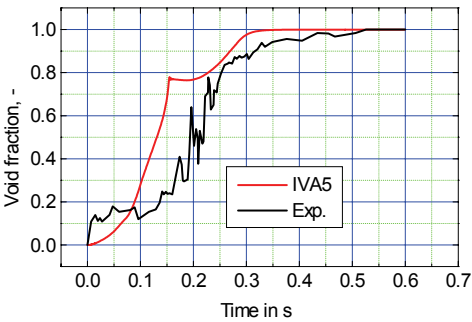


**Fig. 17.9** Steam volume fraction at 1.469 *m* from the dead end of the pipe as a function of time. Comparison IVA5 prediction with experimental data by Edwards and O'Brien. Pipe diameter 0.0732 *m*, length 4.096 *m*

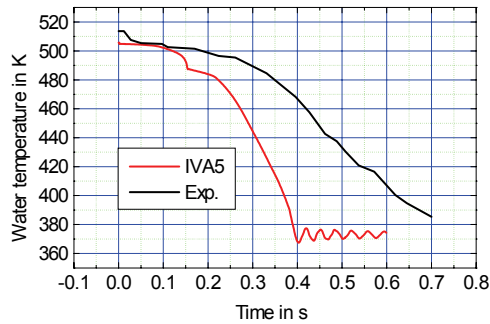


**Fig. 17.10** Water temperature at 1.469 *m* from the dead end of the pipe as a function of time. Comparison IVA4 prediction with experimental data by Edwards and O'Brien. Pipe diameter 0.0732 *m*, length 4.096 *m*

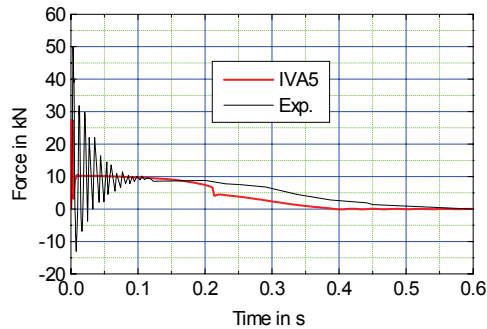


**Fig. 17.11** Force as a function of time: a) IVA4 prediction without fluid-structure interactions; b) Edwards - O'Brien measurements reflecting fluid structure interactions.

The IVA5 force processor computes pipe forces due to hydrodynamics only as discussed in Chapter 8 of Volume 1. The result is presented in Fig. 17.11a. It corresponds to the pressure history. The oscillating character of the measurements, (Fig. 17.11b), is due to the fluid structure interactions. These interactions are not simulated by our computation.

## 17.9 Significance and conclusions

The proposed nucleation and flashing model consists of sub-models, which were verified separately with the available data sets for each particular sub-phenomenon like

- the bubble departure diameter, taking into account the mutual bubble interactions at high superheatings, confirmed by data comparison in Chapter 15, *Kolev* (1993),
- the active nucleation site density, provided by *Wang and Dhir* (1993) measurements,
- the mean site-to-site distance provided by *Wang and Dhir* (1993) measurements,
- heat transfer between wall-fluid interface and bulk liquid caused mainly by bubble-growth and departure

introduced turbulence in the boundary layer verified in Chapter 16, *Johov* (1969) etc. As far the author knows this is the first boiling and flashing model which gives reasonable agreement with data for complex flashing flows in addition to the good agreement in separated tests. The model has the advantage to predict properly the separation between steam generation due to bubble production and bubble growth. I believe that it will be successfully applied in multi-phase flow modeling.

## Nomenclature

$a_2$	liquid thermal diffusivity, $m^2/s$
$B^2$	$= 2R_1 dR_1 / d\tau$ , $m^2 / s$
$D_h$	hydraulic diameter, $m$
$D_l$	particle size of velocity field $l$ , $m$
$D_1$	bubble diameter, $m$
$D_{1\infty}$	stable bubble diameter under the local flow conditions, $m$
$D_{1c}$	critical size, $m$
$D_{1d}$	bubble departure diameter, $m$
$D_{1d,fc}$	bubble departure diameter for strongly predominant forced convection, $m$
$D_{1d,nc}$	bubble departure diameter for natural convection, $m$
$D_{2,inf}$	average center-to-center spacing, $m$
$f_{1w}$	bubble departure frequency, $1/s$
$f'_{1w}$	boundary layer turbulence fluctuation frequency, $1/s$
$f_{coal}$	coalescence frequency, $1/s$
$f_{col}$	collision frequency of single bubble, $1/s$
$P_{coal}$	coalescence probability, dimensionless
$G$	gravitational acceleration, $m/s^2$
$h', h''$	specific saturation enthalpies for water and steam, $J/kg$
$\Delta h$	$= h'' - h'$ , $J/kg$
$Ja_2$	$= \rho_2 c_{p2} [T_2 - T'(p)] / (\rho_1 \Delta h)$ , <i>Jacob number, dimensionless</i>
$n_l$	particle number density of velocity field $l$ , time averaged, $1/m^3$
$n_{1\infty}$	stable particle number density concentration after fragmentation, $1/m^3$
$n''_{1w}$	active nucleation site density, $1/m^2$



$\dot{n}_{l,kin}$	particles of velocity field $l$ originating per unit time and unit mixture volume due to change of the state of aggregate, local volume and time averaged, $1/(s\ m^3)$
$\dot{n}_{lw}$	bubbles originating at the wall per unit time and unit mixture volume, local volume and time averaged, $1/(s\ m^3)$
$\dot{n}_{l,frag}$	particles of velocity field $l$ originating per unit time and unit mixture volume due to fragmentation, local volume and time averaged, $1/(s\ m^3)$
$\dot{n}_{l,coal}$	particles of velocity field $l$ disappearing per unit time and unit mixture volume due to coalescence, local volume and time averaged, $1/(s\ m^3)$
$p$	pressure, $Pa$
$p'$	saturated pressure, $Pa$
$Pr_2$	$= \eta_2 / (\rho_2 a_2)$ , Prandtl number, <i>dimensionless</i>
$\dot{q}_{2\sigma,gen}'''$	the energy consumed for the bubble generation until departure per unit mixture volume and unit time, $W/m^3$
$\dot{q}_{2\sigma,gen}''$	heat flux from the wall into the liquid during film flashing bubble generation in adiabatic pipe flow boiling, $W/m^2$
$\dot{q}_{w2,b}''$	heat flux from the wall into the liquid during pool boiling, $W/m^2$
$R_1$	bubble radius, $m$
$R_{10}$	bubble radius at the beginning of the time step $\Delta\tau$ , $m$
$R_{2,inf}$	$= D_{2,inf} / 2$ , $m$
$T'(p)$	saturation temperature at system pressure $p$ , $K$
$T_2$	liquid temperature, $K$
$T_w$	wall temperature, $K$
$V_1$	surface average and time average velocity of velocity field $l$ , $m/s$
$V_{IKu}$	free rising bubble velocity, Kutateladze velocity, $m/s$
$\bar{V}'_2$	volume-averaged fluctuation velocity, $m/s$
$\bar{\bar{V}}'_2$	volume-averaged fluctuation velocity time averaged over $\Delta\tau_w + \Delta\tau_d$ , $m/s$

### Greek

$\alpha_1$	volume concentration of velocity field $l$ , <i>dimensionless</i>
$\alpha_{1d}$	the steam volumetric fraction in the boundary layer having thickness of $D_{1d}$ , <i>dimensionless</i>
$\gamma_v$	volume porosity, <i>dimensionless</i>
$\gamma$	surface permeability, <i>dimensionless</i>
$\Delta\rho_{21}$	$= \rho_2 - \rho_1$ , $kg/s$
$\Delta\tau_d$	time elapsed from the origination of bubble with the critical size to the bubble departure from the wall, $s$
$\Delta\tau_w$	delay time, $s$

$\Delta\tau_{1d}$	bubble departure time, <i>s</i>
$\eta_2$	dynamic viscosity of liquid, <i>kg/(ms)</i>
$\lambda_{RT}$	$= \left( \frac{\sigma}{g\Delta\rho_{21}} \right)^{1/2}$ , <i>Rayleigh - Taylor</i> instability wavelength
$\ell_2^t$	turbulent length scale, <i>m</i>
$\nu_2$	kinematic viscosity of liquid, <i>m<sup>2</sup>/s</i>
$\rho_l$	density of velocity field <i>l</i> , <i>kg/m<sup>3</sup></i>
$\rho_1$	gas density, <i>kg/m<sup>3</sup></i>
$\rho_2$	liquid density, <i>kg/m<sup>3</sup></i>
$\rho''$	saturated steam density, <i>kg/m<sup>3</sup></i>
$\rho'$	saturated liquid density, <i>kg/m<sup>3</sup></i>
$\mu_1$	mass introduced into the velocity field <i>l</i> per unit mixture volume and unit time, local volume and time average, <i>kg/(m<sup>3</sup>s)</i>
$\mu_{21,gen}$	steam generation per unit mixture volume and unit time due to bubble generation at the wall, local volume and time average, <i>kg/(m<sup>3</sup>s)</i>
$\mu_{21,bulk}$	mass evaporated in the bulk per unit mixture volume and unit time, <i>kg/(m<sup>3</sup>s)</i>
$\sigma$	surface tension, <i>N/m</i>
$\tau$	time, <i>s</i>
$\varphi$	contact angle between "liquid drop" and the wall, <i>rad</i>

## References

- Abuaf N, Wu BJC, Zimmer GA and Saha P (June 1981) A study of nonequilibrium flashing of water in a converging diverging nozzle, Vol.1 Experimental, vol 2 Modeling, NUREG/CR-1864, BNL-NUREG-51317,
- Ahmad SY (1970) Axial distribution of bulk temperature and void fraction in heated channel with inlet subcooling, *J. Heat Transfer*, vol 92 p 595
- Blinkov VN, Jones OC and BI Nigmatulin (1993) Nucleation and Flashing in Nozzles - 2. Comparison with Experiments Using a Five - Equation Model for Vapor Void Development, *Int. J. Multiphase Flow*, vol 19 no 6 pp. 965-986
- Edwards AR, O'Brien TP (1970) Studies of phenomena connected with the depressurization of water reactors, *The Journal of The British Nuclear Energy Society*, vol 9 nos 1-4 pp 125-135
- Kaishev R and Stranski IN (1934) *Z. Phys. Chem.*, vol 26 p 317
- Kellner H, Gissler (07.02.1984) Programsystem SAPHYR: Anwendungsbeispiel II, Notiz Nr.70.02748.4, Interatom GmbH
- Kolev NI (1994) The influence of mutual bubble interaction on the bubble departure diameter, *Experimental Thermal and Fluid Science*, vol 8 no 2 pp 167-174

- 
- Kolev NI (1995) The Code IVA4: Nucleation and flashing model, *Kerntechnik*, vol 60, no 6 pp 157-164. Also in: (Apr.3-7, 1995) Proc. Second Int. Conf. On Multiphase Flow, Kyoto; (Aug.13-18, 1995) ASME & JSME Fluid Engineering Conference International Symposium on Validation of System Transient Analysis Codes, Hilton Head (SC) USA; (October 9-11, 1995) Int. Symposium on Two-Phase Flow Modeling and Experimentation, ERGIFE Place Hotel, Rome, Italy
- Mikic BB, Rohsenow WM and Griffith P (1970) On bubble growth rates, *Int. J. Heat Mass Transfer*, vol 13 pp 657-666
- Shin TS and Jones OC (1993) Nucleation and flashing in nozzles - 1, A distributed nucleation model, *Int. J. Multiphase Flow*, vol 19 no 6 pp 943-964
- Skipov VP et al. (1980) Thermophysical properties of liquids in metastable state, Moskva, Atomisdat, in Russian
- Volmer M (1939) *Kinetik der Phasenbildung*, Dresden und Leipzig, Steinkopf,



## 18 Boiling of subcooled liquid

### 18.1 Introduction

The description of the forced convection boiling of subcooled liquid started with using the equilibrium thermodynamics of two-phase flow. In this framework empirical correlations are obtained by generalizing experimental data using the *equilibrium steam mass flow rate concentration* in the flow,

$$X_{eq} = \frac{h - h'(p)}{h''(p) - h'(p)}, \quad (18.1)$$

where the specific mixture enthalpy is defined as the *mixture enthalpy of the non-inert components*

$$\begin{aligned} h &= \left[ \sum_l \left( 1 - \sum_n C_{nl} \right) \alpha_l \rho_l w_l h_{Ml} \right] / \left[ \sum_l \left( 1 - \sum_n C_{nl} \right) \alpha_l \rho_l w_l \right] \\ &= \left[ \sum_l \left( 1 - \sum_n C_{nl} \right) X_l h_{Ml} \right] / \left[ \sum_l \left( 1 - \sum_n C_{nl} \right) X_l \right] \end{aligned} \quad (18.2)$$

and the *mass flow rate* in the axial direction is defined as follows

$$G = \sum (\alpha \rho w)_l. \quad (18.3)$$

### 18.2 Initiation of visible boiling on the heated surface

*Treshchev* reported in (1969) measurements for the number of the vapor-formation centers on a flat surface for pressures between 5.25 and 50 *bars*, water temperature from 80 to 250°C, heat fluxes between 0.4 to 5 *MW* and flow velocities up to 2 *m/s*. The heat flux at which a nucleation is observed at the surface is correlated by

$$\dot{q}_{w0,50bar}'' = 15.4 \times 10^3 \left[ T'(p) - T_2^* \right] w^{0.8}.$$

The exponent 0.8 resembles the dependence of the heat transfer coefficient for single phase flow on velocity. The corresponding equilibrium quality at which the nucleation starts is then

$$X_{1eq}^* = -\frac{c_{p2} [T'(p) - T_2^*]}{h'' - h'} = -6.49 \times 10^{-5} \frac{c_{p2} \dot{q}_{w0}''}{(h'' - h') w^{0.8}}.$$

Here the subscript \* means onset of nucleate boiling (ONB). For larger heat fluxes the number of active nucleation seats per unit surface is

$$n_w'' = \frac{1}{3} 10^{-5} \left( \frac{\Delta h \rho''}{10^3} \right)^{1.7} \exp(-2.1 \times 10^{-8} \Delta h \rho'') [T'(p) - T_2^*]^{0.6} \\ \times (\dot{q}_w'' - \dot{q}_{w0,50bar}'') \exp(-1.25 \times 10^{-3} \sqrt{\dot{q}_w'' - \dot{q}_{w0,50bar}''}).$$

The data for the initiation of the nucleation can be correlated using dimensionless numbers within an error band of 30% as follows:

$$St = \frac{\dot{q}_{w0}''}{Gc_{p2} [T'(p) - T_2^*]} = 0.01286 - 5.4553 \times 10^{-8} Pe_2 \quad \text{for } Pe_2 \leq 166\,000,$$

$$St = 0.0038 \quad \text{for } Pe_2 > 166\,000,$$

where  $Pe_2 = GD_{hy} c_{p2} / \lambda_2$ . The performance of the correlation is given in Fig. 1.

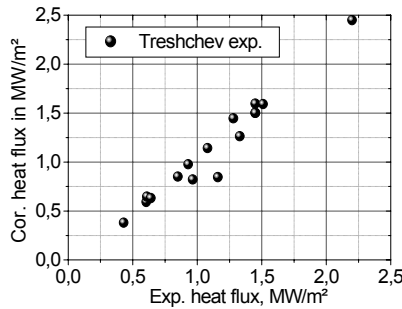


**Fig. 1** Correlated versus measured heat fluxes at the moment of initiation of the nucleation

Note that the above information reported by *Treshchev* is based on local conditions at the surface. *Basu et al.* (2002) reported that the local onset of the nucleate boiling is dependent also on the wetting angle  $\theta$  as follows

$$T_2^* = T'(p_1) - T'(p), \\ p_1 - p = 4\sigma_2 / D_{lc}, \\ D_{lc} = \left[ \frac{8\sigma_2 T'(p) \lambda_2}{\rho_1 \Delta h q_{w2}''} \right]^{1/2} \left[ 1 - \exp\left(-\theta^3 - \frac{1}{2}\theta\right) \right].$$

*Sekoguchi et al.* (1972) correlated their experimental data for the dependence of the local equilibrium steam mass flow concentration in the flow, defining the *initiation of the visible nucleate boiling*,  $X_{1eq}^*$ , as a function of the wall heat flux and the local parameters by

$$X_{1eq}^* = -13.5 \left[ \frac{\dot{q}_w''}{G(h'' - h')} \right]^{0.65},$$

valid in  $0.3 < \dot{q}_w'' / [G(h'' - h')] < 1$ .

*Saha and Zuber* (1974) approximated a number of experimental data by

$$X_{1eq}^* = -0.0022 \frac{D_h c_{p2}}{\lambda_2} \frac{\dot{q}_w''}{h'' - h'} \quad Pe_2 \leq 70\,000, \quad (18.4)$$

or recomputed in terms of liquid temperature at which the subcooled nucleate boiling starts,

$$T_2^* = T'(p) - 0.0022 \dot{q}_w'' D_h / \lambda_2 \quad \text{or} \quad Nu =: \frac{\dot{q}_w''}{T'(p) - T_2^*} \frac{D_h}{\lambda_2} = 454, \quad (18.5)$$

and

$$X_{1eq}^* = -\frac{154}{G} \frac{\dot{q}_w''}{h'' - h'} \quad Pe_2 > 70\,000 \quad (18.6)$$

or

$$T_2^* = T'(p) - 154 \frac{\dot{q}_w''}{c_{p2} G} \quad \text{or} \quad St =: \frac{\dot{q}_w''}{G c_{p2} [T'(p) - T_2^*]} = 0.0065 \quad (18.7)$$

where

$$Pe_2 = G D_h c_{p2} / \lambda_2, \quad (18.8)$$

and  $T_2^*$  is, as already mentioned, the liquid temperature corresponding  $X_{1eq}^*$ . The above correlation approximates experimental data in the region:  $1 \times 10^5 < p < 138 \times 10^5 \text{ Pa}$ ,  $95 < G < 2760 \text{ kg/(m}^2\text{s)}$ ,  $280\,000 < \dot{q}_w'' < 1\,890\,000 \text{ W/m}^2$  for channels with rectangular and circular cross sections. For Freon the correlation is valid in  $3.2 \times 10^5 < p < 8.5 \times 10^5 \text{ Pa}$ ,  $101 < G < 2073 \text{ kg/(m}^2\text{s)}$ ,  $6\,300 < \dot{q}_w'' < 5\,360\,000 \text{ W/m}^2$ .

Comparing the form of Eq. (18.6) with the *Treshchev's* equation we recognize the similarity. Note the differences for the application of the both correlation: The *Treshchev's* correlation is based on local parameters and the *Saha and Zuber* correlation is based on cross section averaged parameters.

*Chan* (1984) analyzed the net vapor generation point in horizontal flow boiling in a tube with  $D_h = D_{heat} = 10.7 \text{ mm}$ , and length of 2 m at 4 bar pressure and came to the conclusion that the constant in Eq. (18.5) has to be equal to 380. The *Peclet* numbers of his experiments varied between  $10^4$  and  $4 \times 10^4$ .

*Kawara et al.* (1998) reported that at low void fraction the *Saha* and *Zuber* correlation is not accurate. The proposed the modification:

$$Nu \frac{\dot{q}_w''}{0.88 \times 10^7} = 454, \quad Pe_2 \leq 70\,000,$$

$$St \frac{\dot{q}_w''}{0.88 \times 10^7} = 0.0065, \quad Pe_2 > 70\,000.$$

My own analysis, *Kolev* (2005), based on the *NUPEC* data (2004) demonstrated that at low void fraction the use of the *Hughes et al.* (1981) model, that will be described in the next section is superior to the use of the *Saha* and *Zuber* model in combination with the *Levy* (1967) relaxation model.

## 18.3 Local evaporation and condensation

### 18.3.1 Relaxation theory

There are different approaches proposed in the literature to describe the local evaporation and condensation processes. One of the oldest is that by *Levy*. In one of his earlier publications in this field *Levy* (1967) approximates the profile of the experimentally observed steam mass flow concentration in the flow with the following simple expressions

$$X_1 = X_{1eq} - X_{1eq}^* \exp(X_{1eq} / X_{1eq}^* - 1) \quad (18.9)$$

where  $X_{eq}$  is the *equilibrium steam mass flow concentration* in the flow defined by Eq. (18.1) for the case of no inert components

$$\sum X_i h_i = X_{1eq} h'' + (1 - X_{1eq}) h' = X_{1eq} (h'' - h') + h'. \quad (18.10)$$

Now let us compute the net vapor generation rate defined by the profile described with Eq. (18.9). For one-dimensional steady state flow in a channel with constant cross section we write the mixture mass conservation, the vapor mass conservation and the mixture energy conservation equations as follows

$$G = const, \quad (18.11)$$

$$\mu_{21} - \mu_{12} = G \frac{dX_1}{dz} \quad (18.12)$$

$$\frac{d}{dz} \left( \sum X_i h_i \right) = \frac{4}{D_{heat}} \frac{\dot{q}_w''}{G} \quad (18.13)$$



Having in mind the definition equation (18.10) for  $X_{1eq}$

$$d\left(\sum X_1 h_1\right) = d\left[X_{1eq}(h'' - h') + h'\right] = (h'' - h')dX_{1eq} \quad (18.14)$$

Eq. (18.13) can be rewritten as follows

$$\frac{dX_{1eq}}{dz} = \frac{4}{D_{heat}} \frac{\dot{q}_w''}{G(h'' - h')} \quad (18.15)$$

Thus from mass conservation equation of the gas phase (18.12) and using Eq. (18.15) we obtain

$$\mu_{21} - \mu_{12} = G \frac{dX_1}{dz} = G \frac{dX_1}{dX_{1eq}} \frac{dX_{1eq}}{dz} = \frac{4}{D_{heat}} \frac{\dot{q}_w''}{h'' - h'} \frac{dX_1}{dX_{1eq}}, \quad (18.16)$$

or after differentiating the *Levy* approximation, Eq. (18.9),

$$\mu_{21} - \mu_{12} = \frac{4}{D_{heat}} \frac{\dot{q}_w''}{h'' - h'} \left[ 1 - \exp\left(\frac{X_1}{X_{1eq}^*} - 1\right) \right] \quad \text{for } X_1 > X_{1eq}^* \quad (18.17)$$

Obviously in accordance with this approach the heat flux at the wall causing all the net evaporation is

$$\dot{q}_{net\_evaporation}'' = \dot{q}_w'' \left[ 1 - \exp\left(\frac{X_1}{X_{1eq}^*} - 1\right) \right], \quad (18.18)$$

and the heat flux introduced into the bulk liquid due to recondensation is

$$\dot{q}_2^{\sigma 1} = \dot{q}_w'' - \dot{q}_w'' \left[ 1 - \exp\left(\frac{X_1}{X_{1eq}^*} - 1\right) \right] = \dot{q}_w'' \exp\left(\frac{X_1}{X_{1eq}^*} - 1\right). \quad (18.19)$$

Therefore the effectively condensed mass per unit time and unit mixture volume is

$$\mu_{12} = \frac{4}{D_{heat}} \frac{\dot{q}_2^{\sigma 1}}{h'' - h'} = \frac{4}{D_{heat}} \frac{\dot{q}_w''}{h'' - h'} \exp\left(\frac{X_1}{X_{1eq}^*} - 1\right). \quad (18.20)$$

From equation (18.20) and (18.17) we compute the evaporated mass per unit time and mixture volume as

$$\mu_{21} = \frac{4}{D_{heat}} \frac{\dot{q}_w''}{h'' - h'}. \quad (18.21)$$

This approach does not answer the question about the magnitude of the heat transfer coefficient. One is forced to arbitrarily assume some wall superheat, e.g. 5 K and compute the total heat transfer coefficient by dividing wall heat flux by this value.

An alternative to Eq. (18.9) is the relaxation profile proposed by *Achmad* (1970)

$$X_1 = \frac{X_{1eq} - X_{1eq}^* \exp(X_{1eq} / X_{1eq}^* - 1)}{1 - X_{1eq}^* \exp(X_{1eq} / X_{1eq}^* - 1)}, \quad (18.22)$$

which results in

$$\dot{q}_2^{\sigma 1} = \dot{q}_w'' \left\{ 1 - \frac{1 - (1 - X_{1eq} + X_{1eq}^*) \exp(X_{1eq} / X_{1eq}^* - 1)}{[1 - X_{1eq}^* \exp(X_{1eq} / X_{1eq}^* - 1)]^2} \right\}. \quad (18.23)$$

Note that there are other proposals for the approximations  $X_1 = X_1(X_{1eq}, X_{1eq}^*)$  - see *Kolev* (1986).

Thus, the relaxation theory provided a simple expression for the recondensation process which does not take into account the influence of the local flow pattern and therefore of the interfacial area density. This approach is successfully used for description of steady state boiling in a channel with constant cross sections.

### 18.3.2 Boundary layer treatment

The treatment of the boundary layers is the more sophisticated method for description of the evaporation and condensation processes. Let us illustrate this approach with the method proposed by *Hughes* et al. (1981), based on one proposal by *Lellouche* (1974) and *Lellouche* and *Zolotar* - see in *Hughes* et al. (1981). The authors consider the heat transfer at the wall as a superposition of the heat flux causing boiling for saturated liquid and a convective heat flux from the wall into the bulk liquid

$$\dot{q}_w'' = \dot{q}_{NB}'' + \dot{q}_2^{\sigma w} = h_{NB\_Thom} (T_w - T')^2 + h_{convective} (T_w - T_2). \quad (18.24)$$

Here in accordance with *Thom* (1966) the saturated boiling heat flux  $\dot{q}_{NB}''$  is a quadratic function of the wall superheat with a coefficient being a function only of the system pressure

$$h_{NB\_Thom} = 1942 \exp(p / 4.35 \times 10^6) \quad (18.25)$$

and the convective heat transfer coefficient is that derived by *Dittus* and *Boelter* in 1937 for single-phase liquid flow

$$h_{convective} = 0.023 Re_2^{0.8} Pr_2^{0.4} \frac{\lambda_2}{D_h}, \quad (18.26)$$

where

$$Re_2 = \rho_2 w_2 D_h / \eta_2, \quad (18.27)$$

$$Pr_2 = c_{p2} \eta_2 / \lambda_2, \quad (18.28)$$

are the *Reynolds* and the *Prandtl* numbers respectively. The heat flux released by the recondensation into the bulk flow is in accordance with *Hancox* and *Nicoll* - see in *Hughes et al.*, (1981)

$$\dot{q}_2^{\sigma_1} = h_2^{\sigma_1} (T' - T_2) \quad \text{for} \quad X_1 > X_{1eq}^*, \quad (18.29)$$

where

$$h_2^{\sigma_1} = 0.4 Re_2^{0.662} Pr_2 \frac{\lambda_2}{D_h}. \quad (18.30)$$

The liquid temperature defining the initiation of the visible nucleate boiling,  $T_{2,NBI}$ , and the corresponding wall temperature are computed from the condition that the evaporation heat flux equals the condensation one

$$h_{NB\_Thom} (T_w - T')^2 = h_2^{\sigma_1} (T' - T_{2,NBI}) \quad (18.31)$$

and Eq. (18.24)

$$\dot{q}_w'' = h_{NB\_Thom} (T_w - T')^2 + h_{convective} (T_w - T_{2,NBI}). \quad (18.32)$$

Solving with respect to the liquid subcooling the authors obtained

$$T' - T_{2,NBI} = \frac{h_{NB\_Thom}}{h_2^{\sigma_1}} (T_w - T')^2$$

$$= \left[ \frac{\sqrt{h_{convective}^2 \frac{h_2^{\sigma_1}}{h_{NB\_Thom}} + 4(h_2^{\sigma_1} + h_{convective}) \dot{q}_w'' - h_{convective} \sqrt{\frac{h_2^{\sigma_1}}{h_{NB\_Thom}}}}}{2(h_2^{\sigma_1} + h_{convective})} \right]^2 \quad (18.33)$$

The wall temperature is obtained after solving the slightly rearranged Eq. (18.32)

$$\dot{q}_w'' = h_{NB\_Thom} (T_w - T')^2 + h_{convective} (T' - T_2) \quad (18.34)$$

with respect to the wall superheating

$$T_w - T' = \sqrt{\frac{\dot{q}_w'' - h_{convective} (T' - T_2)}{h_{NB\_Thom}}} \quad \text{for} \quad T_2 > T_{2,NBI}. \quad (18.35)$$

The evaporated mass per unit time and unit mixture volume is then

$$\mu_{21} = \frac{4}{D_{heat}} \frac{h_{NB\_Thom} (T_w - T')^2}{h'' - h'}. \quad (18.36)$$

The condensed mass per unit time and unit volume is

$$\mu_{12} = \frac{4}{D_{heat}} \frac{h_2^{\sigma 1} (T' - T_2)}{h'' - h'} . \quad (18.37)$$

The heat introduced into the bulk liquid due to recondensation is

$$\dot{q}_2^{\sigma 1} = \frac{4}{D_{heat}} h_2^{\sigma 1} (T' - T_2) . \quad (18.38)$$

The heat introduced from the wall into the bulk liquid due to forced convection is

$$\dot{q}_2^{\sigma w} = \frac{4}{D_{heat}} h_{convection} (T_w - T_2) . \quad (18.39)$$

*Hughes* reports very good agreement with experimental data for void fraction in a vertical heated channel using the *Lellouche's* drift flux correlation. *Kolev* (1986) compared the predictions of this approach with a number of data for void fractions in a vertical boiling channel in the region  $38 < G < 2000 \text{ kg}/(\text{m}^2 \text{s})$ ,  $T' - T_2 < 132 \text{ K}$ ,  $1 < p < 140 \text{ bar}$ ,  $20.3 < \dot{q}_w'' < 1723 \text{ kW}/\text{m}^2$ ,  $0.686 < L < 1.835$ ,  $0.0044756 < D_h < 0.0269 \text{ m}$  using the *Chexal* and *Lellouch's* drift flux correlation, and reported a very good agreement. The agreement was worse for very low mass flow rates.

Note that the condensation of the generated vapor happens on larger interfacial area density  $6\alpha_1/D_1$  then  $4/D_{hy}$  to which the condensation heat transfer coefficient is related. Therefore the constant in empirically obtained correlations like  $h_2^{\sigma 1} = 0.4 Re_2^{0.662} Pr_2 \frac{\lambda_2}{D_h}$  has to be function actually of  $\frac{3}{2} \alpha_1 \frac{D_{hy}}{D_1}$ . Based on experiments with condensation into subcooled water after a heated section in pipe *Avdeev* (1986) obtained

$$h_2^{\sigma 1} = 0.228 Re_2^{0.7} Pr_2^{1/2} (\Phi_{2o}^2 / \alpha_2)^{1/4} \frac{\lambda_2}{D_h} , \pm 30\% , D_1 / D_{hw} > 80 / Re_2^{0.7} .$$

If the boiling heat transfer is described in general with  $\dot{q}_{NB}'' = h_{NB} (T_w - T')^n$  the equation defining the temperature at which the initiation of nucleate boiling

$$\left( h_2^{\sigma 1} + h_{convection} \right) (T' - T_{2,NBI}) + h_{convection} \left[ \frac{h_2^{\sigma 1}}{h_{NB}} (T' - T_{2,NBI}) \right]^{1/n} - \dot{q}_w'' = 0$$

has to be solved by iterations.

## Nomenclature

### Latin

$C_{nl}$	mass concentration of the inert component $n$ inside the gas mixture, <i>dimensionless</i>
$c_p$	specific heat at constant pressure, $J/(kgK)$
$D_{hy}$	hydraulic diameter (4 times flow cross-sectional area / wet perimeter), $m$
$D_{heat}$	heated diameter (4 times flow cross-sectional area / heated perimeter), $m$
$G$	$= \sum (\alpha \rho w)$ , mass flow rate in the axial direction, $kg/(m^2s)$
$h$	specific enthalpy, $J/kg$
$h_{NB\_Thom}$	saturated boiling heat transfer coefficient, $W/(m^2K)$
$h_{convective}$	convective heat transfer coefficient, $W/(m^2K)$
$h_2^{\sigma 1}$	heat flux coefficient by the recondensation into the bulk flow based on the heated surface, $W/(m^2K)$
$Nu$	$\frac{\dot{q}_w''}{T'(p) - T_2^*} \frac{D_h}{\lambda_2}$ , Nusselt number, <i>dimensionless</i>
$h$	specific mixture enthalpy - mixture enthalpy of the non-inert components, $J/kg$
$L$	length, $m$
$p$	pressure, $Pa$
$Pe_2$	$= GD_{hy} c_{p2} / \lambda_2$ , Peclet number, <i>dimensionless</i>
$Pr_2$	$= c_{p2} \eta_2 / \lambda_2$ , liquid Prandtl number, <i>dimensionless</i>
$Re_2$	$= \rho_2 w_2 D_h / \eta_2$ , liquid Reynolds number, <i>dimensionless</i>
$St$	$\frac{\dot{q}_w''}{c_{p2} [T'(p) - T_2^*]}$ , Stanton number, <i>dimensionless</i>
$T_2^*$	liquid temperature corresponding $X_{1eq}^*$ , $K$
$\dot{q}_w''$	wall heat flux, $W/m^2$
$\dot{q}_{net\_evaporation}''$	heat flux at the wall causing all the net evaporation, $W/m^2$
$\dot{q}_{NB}''$	saturated boiling heat flux, $W/m^2$
$\dot{q}_2^{\sigma w}''$	convective heat flux from the wall into the bulk liquid, $W/m^2$
$\dot{q}_2^{\sigma 1}''$	heat flux released by the recondensation into the bulk flow, $W/m^2$
$X_l$	mass flow rate concentration of the velocity field $l$ inside the multi-phase mixture, <i>dimensionless</i>
$X_{1eq}^*$	local equilibrium steam mass flow concentration in the flow, defining the initiation of the visible nucleate boiling, <i>dimensionless</i>

---

$X_{eq}$	equilibrium steam mass flow rate concentration in the flow, <i>dimensionless</i>
$w$	axial velocity, $m/s$

**Greek**

$\alpha$	volume fraction, <i>dimensionless</i>
$\lambda$	thermal conductivity, $W/(mK)$
$\rho$	density, $kg/m^3$
$\mu_{21}$	evaporation mass per unit time and unit mixture volume, $kg/(m^3s)$
$\mu_{12}$	condensation mass per unit time and unit mixture volume, $kg/(m^3s)$

**Subscript**

'	saturated liquid
"	saturated steam
1	gas
2	liquid
$M1$	non-inert component in the gas mixture
$n1$	inert component in the gas mixture

**References**

- Achmad SI (1970) Raspredelenie srednomassovoj temperatury zidkosti I istinnogo obemnogo parosoderzanie vodoi obogrevaemogo kanala s nedogrevom na vchode, Teploperedaca, vol 4
- Avdeev AA (1986) Growth and condensation velocity of steam bubbles in turbulent flow, Teploenergetika, in Russian, vol 1 pp 53 – 55
- Basu N, Warrior GR and Dhir VK (Aug. 2002) Onset of nucleate boiling and active nucleation site density during subcooled flow boiling, Transactions of ASME, J. Heat Transfer, vol 127 pp 717728
- Chan AMC (1984) Point on net vapor generation and its movement in transient horizontal flow boiling, Proc. of the 22th Nat. Heat Transfer Conference, Niagara Falls, New York, Dhir VK and Schrock VE (eds)
- Dittus FW, Boelter LMK (1937) Heat transfer in automobile radiators of the tubular type, University of California Publications in Engineering, vol 2 no 13 p 443
- Hughes ED, Paulsen MP, Agee LJ (Sept. 1981) A drift-flux model of two-phase flow for RETRAN. Nuclear Technology, vol 54 pp 410-420
- Kawara Z, Kataoka I, Serizawa A, Ko YJ and Takahashi O (August 23-28, 1998) Analysis of forced convective CHF based on two-fluid and three-fluid model, Heat Transfer 19998, Proc. Of the 11th IHTC, Kyongju, Korea, vol 2 pp 103-108
- Kolev NI (August 5-8, 1986) Transiente Zweiphasenstromung, Springer Verlag
- Kolev NI (September 12-15, 2005) Do we have appropriate constitutive sets for sub-channel and fine-resolution 3D-analyses of two-phase flows in rod bundles? *Mathematics and Computation, Supercomputing, Reactor Physics and Nuclear and*

- 
- Biological Applications* Palais des Papes, Avignon, France, on CD-ROM, American Nuclear Society, LaGrange Park, IL (2005)
- Lellouche GS (1974) A model for predicting two-phase flow, BNL-18625
- Levy S (1967) Int. J. Heat Mass Transfer, vol 10 pp 351-365
- OECD/NRC Benchmark based on NUPEC BWR Full-size Fine-mesh Bundle Tests (BFBT), Assembly Specifications and Benchmark Database, October 4, 2004, Incorporated Administrative Agency, Japan Nuclear Energy Safety Organization, JNES-04N-0015
- Saha P, Zuber N (1974) Proc. Int. Heat Transfer Conf. Tokyo, Paper 134.7
- Sekoguchi K, Nishikawa K, Nakasatomi M, Hirata N and Higuchi H (1972) Flow boiling in subcooled and low quality regions – heat transfer and local void fraction, B4.8, pp 180-184
- Thom IRS et. al. (1966) Boiling in subcooled water during up heated tubes or annuli. Proc. Instr. Mech. Engs., vol 180 3C pp 1965-1966
- Treshchev GG (1969) The number of vapor-formation centers in surface boiling, in Convective Heat Transfer in Two-Phase and One-Phase Flows, Borishanskii VM and Pallev II, eds., translated from Russian by the Israel Program of Scientific Translations





## 19 Natural convection film boiling

### 19.1 Minimum film boiling temperature

*Groeneveld* and *Stewart* (1982) derived from their measurements the following expression for the minimum film boiling temperature.

For  $p \leq 90 \times 10^5 \text{ Pa}$

$$T_{w,MFB} = 557.85 + 0.0441 \times 10^{-3} p - 3.72 \times 10^{-12} p^2 - \max \left( 0, \frac{10^4 X_{1,eq}}{2.82 + 0.00122 \times 10^{-3} p} \right), \quad (19.1)$$

and for  $p > 90 \times 10^5 \text{ Pa}$

$$T_{w,MFB} - T'(p) = 76.722 \frac{p_c - p}{p_{cr} - 90 \times 10^5}. \quad (19.2)$$

Equation (19.2) guarantees that the minimum film boiling temperature at critical pressure is equal to the critical temperature. This correlation provides the best agreement with data compared to the prediction of seven other correlations reviewed by the authors in *Groeneveld* and *Stewart* (1982). The mass flow rates in the experiments are varied between 110 and 2750  $\text{kg}/(\text{m}^2\text{s})$  with no effect on the minimum film boiling temperature. This correlation is valid for pressure between 1 and 220 *bar*, mass flux 50 and 4000  $\text{kg}/(\text{m}^2\text{s})$ , equilibrium vapor mass flow fraction –19 and 64% for vertical up-flow in circular pipe.

The minimum heat flux is defined as follows

$$q''_{w,MFB} = h_{FB} [T_{w,MFB} - T'(p)], \quad (19.3)$$

$h_{FB}$  is the film boiling heat transfer coefficient.

*Schroeder-Richter* and *Bartsch* (1990) interpreted the minimum film boiling phenomenon as a phase interface normal velocity discontinuity governed by the *Rankine* and *Hugoniot* equation *Rankine* (1870) and *Hugoniot* (1887),

$$h_2 - h_1 - \frac{1}{2}(p_2 - p_1) \left( \frac{1}{\rho_2} + \frac{1}{\rho_1} \right) = 0 \quad (19.4)$$

assuming that the liquid side boundary layer properties are those at saturation at the minimum film boiling temperature and the vapor side properties are those at saturation at system pressure

$$h''(p) - h'(T_{w,MFB}) - \frac{1}{2} \left[ p - p'(T_{w,MFB}) \right] \left[ \frac{1}{\rho''(p)} + \frac{1}{\rho'(T_{w,MFB})} \right] = 0. \quad (19.5)$$

*Henry* (1974) related the minimum stable film boiling temperature to the homogeneous nucleation temperature and the wall properties

$$T_{w,MFB} = T_{hm} + (T_{hm} - T_2) \sqrt{\frac{(\lambda \rho c_p)_2}{(\lambda \rho c_p)_w}}. \quad (19.6)$$

*Henry* gives the homogeneous nucleation temperature as a curve fit to those used by *Thurgood* and *Kelley* (1979),

$$T_{hm} = \frac{5}{9} \left( \begin{aligned} &459.67 + 705.44 - 4.722 \times 10^{-2} p_{psi} \\ &+ 2.3907 \times 10^{-5} p_{psi}^2 - 5.8193 \times 10^{-9} p_{psi}^3 \end{aligned} \right), \quad (19.7)$$

where

$$p_{psi} = 3203.6 - 14.50377 \times 10^{-5} p. \quad (19.8)$$

## 19.2 Film boiling in horizontal upwards-oriented plates

Film boiling in horizontal upwards-oriented plates in a large pool is possible if the temperature of the wall is larger then the so called minimum film boiling temperature  $T_{w,MFB}$ ,

$$T_w > T_{w,MFB} \quad (19.9)$$

*Berenson* (1961) obtained the following expression for film boiling on a horizontal plane

$$h_{nc\_FB} = 0.425 \left[ \frac{\lambda_1^3 \rho_1 (\rho' - \rho'') (h'' - h') g}{\eta'' \Delta T \lambda_{RT}} \right]^{1/4}, \quad (19.10)$$

where

$$\lambda_{RT} = \left[ \frac{\sigma}{g(\rho' - \rho'')} \right]^{1/2}, \quad (19.11)$$

and

$$\Delta T = (T_w - T'). \quad (19.12)$$

The averaged vapor film thickness can be then expressed as

$$\delta_{1F} \approx \frac{\lambda_1}{h_{nc\_FB}} = 2.35 \left[ \frac{\eta_1 \lambda_1 \Delta T}{(h'' - h') \rho_1 g(\rho' - \rho'')} \lambda_{RT} \right]^{1/4}, \quad (19.13)$$

where vapor properties are computed as a function of the averaged vapor film temperature  $(T_w - T')/2$ .

Equating the critical heat flux predicted by the *Zuber's* correlation (1958) to the heat flux obtained for film boiling by the *Berenson* equation an expression for the minimum film boiling temperature can be obtained

$$\Delta T_{w,MFB} = 0.127 \frac{(h'' - h') \rho_{1F}}{\lambda_{1F}} \left[ \frac{g(\rho_2 - \rho_1)}{\rho_2 + \rho_1} \right]^{2/3} \left[ \frac{\sigma}{g(\rho_2 - \rho_1)} \right]^{1/2} \left[ \frac{\eta_2}{\rho_2 - \rho_1} \right]^{1/3} \pm 10\%. \quad (19.14)$$

*Leperriere* (1983) modified the *Berenson* equation to obtain a correlation for forced convection film boiling in channels with very low mass flux

$$h_{Be,mod} = h_{Berenson} \left( 1 + 25.5 \frac{T_w - T'}{T_2} \right) (1 - \alpha_{1h})^{0.5}, \quad (19.15)$$

where the homogeneous local vapor volume fraction is

$$\alpha_{1h} = \frac{X_{1,eq} / \rho''}{X_{1,eq} / \rho'' + (1 - X_{1,eq}) / \rho'}. \quad (19.16)$$

## 19.3 Horizontal cylinder

For natural convection film boiling on a horizontal cylinder *Bromley* (1950)

$$h_{nc\_FB} = 0.62 \left[ \frac{\lambda_{1F}^3 \rho_{1F} (\rho' - \rho'') g (h'' - h') \left[ 1 + 0.4 \frac{c_p'' (T_w - T')}{h'' - h'} \right]}{\eta'' D_h \Delta T} \right]^{1/4}, \quad (19.17)$$

obtained a very similar result as those by *Berenson* with the exception of the empirical constant. The modification of the latent heat of vaporization takes into account the superheating of the vapor. The analytical derivation of this equation is very similar to those for planes presented in Chapter 21 in details. Later in 1962 *Breen* and *Westwater* (1962) found better agreement with experimental data modifying the *Berenson* result by using instead 0.62 the function

$$(0.59 + 0.069 \lambda_{RT}^* / D_h) (D_h / \lambda_{RT}^*)^{1/4}, \quad (19.18)$$

where

$$\lambda_{RT}^* = 2\pi \left[ \frac{3\sigma}{(\rho_2 - \rho'')g} \right]^{1/2}. \quad (19.19)$$

and instead 0.4, 0.34.

## 19.4 Sphere

For natural convection film boiling on a sphere *Bromley* (1950) computed a different constant in the Eq. (19.17)

$$h_{nc\_FB} = 0.76 \left[ \frac{\lambda_{1F}^3 \rho_{1F} (\rho' - \rho'') g (h'' - h') \left[ 1 + 0.4 \frac{c_p'' (T_w - T')}{h'' - h'} \right]}{\eta'' D_3 \Delta T} \right]^{1/4}. \quad (19.20)$$

For better agreement with data for liquid nitrogen *Frederking* and *Clark* recommended in 1963 the following correlation

$$h_{nc\_FB} = 0.14 \left[ \frac{\lambda_{1F}^3 g \rho_{1F} (\rho' - \rho'') (h'' - h')}{\eta'' D_3 (T_w - T')} \left[ 1 + 0.5 \frac{c_p'' (T_w - T')}{h'' - h'} \right] \right]^{1/3}. \quad (19.21)$$

We devote a special Section 21.2 to this subject.

## Nomenclature

### *Latin*

- $c_p$  specific heat at constant pressure,  $J/(kgK)$   
 $D_{hy}$  hydraulic diameter (4 times flow cross-sectional area / wet perimeter),  $m$

---

$g$	gravitational acceleration, $m/s^2$
$h$	specific enthalpy, $J/kg$
$h_{FB}$	film boiling heat transfer coefficient, $W/(m^2K)$
$h_{nc\_FB}$	natural convection film boiling heat transfer coefficient, $W/(m^2K)$
$p$	pressure, $Pa$
$p_{psi}$	$= 3203.6 - 14.50377 \times 10^{-5} p$ , $psi$
$p_{cr}$	critical pressure, $Pa$
$q''_{w,MFB}$	minimum film boiling heat flux, $W/m^2$
$T_{w,MFB}$	minimum film boiling temperature, $K$
$T_{hn}$	homogeneous nucleation temperature, $K$
$X_{eq}$	equilibrium steam mass flow rate concentration in the flow, <i>dimensionless</i>

### Greek

$\alpha$	volume fraction, <i>dimensionless</i>
$\alpha_{1h}$	$= \frac{X_{1,eq} / \rho''}{X_{1,eq} / \rho'' + (1 - X_{1,eq}) / \rho'}$ , homogeneous local vapor volume fraction, <i>dimensionless</i>
$\Delta$	finite difference
$\delta_{1F}$	averaged vapor film thickness
$\lambda$	thermal conductivity, $W/(mK)$
$\lambda_{RT}$	$= \left[ \frac{\sigma}{g(\rho' - \rho'')} \right]^{1/2}$ , Rayleigh-Taylor instability wavelength, $m$
$\rho$	density, $kg/m^3$
$\sigma$	surface tension, $N/m$
$\mu_{21}$	evaporation mass per unit time and unit mixture volume, $kg/(m^3s)$
$\mu_{12}$	condensation mass per unit time and unit mixture volume, $kg/(m^3s)$

### Subscript

'	saturated liquid
"	saturated steam
1	gas
2	liquid
1F	vapor film

## References

- Berenson PJ (Aug. 1961) Film boiling heat transfer from a horizontal surface, *J. Heat Transfer*, p 351
- Breen BP and Westwater JW (1962) Effect of diameter of horizontal tubes on film heat transfer, *Chem. Eng. Prog.*, vol 58, no 7 p 67
- Bromley LA (1950) Heat transfer in stable film boiling, *Chem. Eng. Process*, vol 46 no 5 p 221
- Frederking THK and Clark JA (1963) Natural convection film boiling on a sphere, *Adv. Cryogen. Eng.*, vol 8, pp 501-506
- Groeneveld DC, Stewart JC (1982) The minimum boiling temperature for water during film boiling collapse, *Proc. 7th International Heat Transfer Conference, Munich, FRG*, vol 4 pp 393-398
- Henry RE (1974) A correlation for minimum film boiling temperature, *AIChE Symposium Series*, vol 138 pp 81-90
- Hugoniot PH (1887) Memoire sur la propagation du mouvement dans les corps et specialement dans les gases parfaits, *Journal de l'École Polytechnique*
- Leperriere A (1983) An analytical and experimental investigation of forced convective film boiling, *M. A. Sc. Thesis, University of Ottawa, Ottawa*
- Rankine WJM (1870) On the thermodynamic theory of waves of finite longitudinal disturbances, *Philosophical Transactions of the Royal Society*
- Schroeder-Richter D, Bartsch G (1990) The Leidenfrost phenomenon caused by a thermo-mechanical effect of transition boiling: A revisited problem of non-equilibrium thermodynamics, *HTD-Vol.136, Fundamentals of Phase Change: Boiling and Condensation*, Witte LC and Avedisian CT (eds) Book No. H00589 – 1990 pp 13-20
- Thurgood MJ, Kelley JM (December 1979) Battelle Pacific Northwest Laboratories
- Zuber N (1958) On the stability of boiling heat transfer, *Trans. ASME*, vol 80 pp 711-720

## 20 Forced convection boiling

### 20.1 Convective boiling of saturated liquid

*Chen* 1963, *Hetstrony* (1982) correlated over 600 data within an error band of 12% for convective heat transfer during forced convection boiling in a tube by superposition of single-phase liquid convection heat flux  $h_c(T_w - T_2)$  and of nucleate boiling heat flux  $h_{NB}(T_w - T')$  in the following way

$$\dot{q}_w'' = h_c(T_w - T_2) + h_{NB}(T_w - T'). \quad (20.1)$$

The mutual influence of both mechanisms is taken into account by modifying the corresponding correlations. The original *Dittus-Boelter* equation

$$h_c = 0.023 \frac{\lambda_1}{D_h} F \times Re_2^{0.8} Pr_2^{0.4}, \quad (20.2)$$

applied as if the liquid is flowing alone in the tube

$$Re_2 = X_2 G D_h / \eta_2, \quad (20.3)$$

$$Pr_2 = c_{p2} \eta_2 / \lambda_2, \quad (20.4)$$

is modified by the multiplier  $F = \Phi_2^{0.89}$  which is a function of the friction pressure drop ratio of the two phase and liquid only flow,  $\Phi_2^2 = \left( \frac{dp}{dz} \right)_{fr} / \left( \frac{dp}{dz} \right)_2$ . For

practical use the approximation is recommended

$$F = 2.35(1/X_{tt} + 0.213)^{0.736}, \quad 1/X_{tt} > 0.1 \quad (20.5)$$

$$F = 1, \quad 1/X_{tt} \leq 0.1 \quad (20.6)$$

where the *Martinelli* factor is computed as follows

$$1/X_{tt} = \left( \frac{X_1}{1 - X_1} \right)^{0.9} \left( \frac{\rho_2}{\rho_1} \right)^{1/2} \left( \frac{\eta_1}{\eta_2} \right)^{0.1}. \quad (20.7)$$

The nucleate boiling heat transfer coefficient as proposed by *Forster* and *Zuber* (1955)

$$h_{NB} = c_1 (T_w - T')^{0.24}, \quad (20.8)$$

where

$$c_1 = c \Delta p^{0.75}, \quad (20.9)$$

$$\Delta p = p' [\min(T_w, 647)] - p,$$

$$c = 0.00122 S \left( \frac{\lambda' c'_p}{\sigma} \right)^{1/2} Pr_2^{-0.29} \rho'^{1/4} \left[ \frac{c'_p \rho'}{\rho'' (h'' - h')} \right]^{0.24}, \quad (20.10)$$

Eq. 17 in *Chen* (1963), is modified by the multiplier  $S$ .  $S$  is the ratio of the effective superheat to the total superheat of the wall. It is a function of a modified *Reynolds* number computed as follows

$$Re_{Tp} = Re_2 F^{1.25} 10^{-4}, \quad (20.11)$$

$$S = (1 + 0.12 Re_{Tp}^{1.14})^{-1}, \quad \text{for } Re_{Tp} \leq 32.5, \quad (20.12)$$

$$S = (1 + 0.42 Re_{Tp}^{0.78})^{-1}, \quad \text{for } 32.5 \leq Re_{Tp} \leq 70, \quad (20.13)$$

$$S = 0.0797 \exp(1 - Re_{Tp} / 70), \quad \text{for } 70 > Re_{Tp}, \quad (20.14)$$

*Bjornard* and *Grifith* (1977). *Groeneveld* et al. (1989) use instead of the last expression simply  $S = 0.1$ . The correlation was verified in the region  $X_1 = 0$  to 0.71,  $p = (1.013 \text{ to } 69.) \times 10^5 \text{ Pa}$ ,  $G = 54 \text{ to } 4070 \text{ kg/(m}^2\text{s)}$ ,  $\dot{q}_w'' = 44 \text{ to } 2400 \text{ kW/m}^2$ . Thus the effective heat transfer coefficient is

$$h = \dot{q}_w'' / (T_w - T'). \quad (20.15)$$

The wall temperature by enforced heat flux is

$$T_w = (\dot{q}_w'' + h_c T_2 + h_{NB} T') / (h_c + h_{NB}). \quad (20.16)$$

Because the nucleate boiling heat transfer coefficient is also function of the wall temperature few iterations are necessary to solve the equation

$$\dot{q}_w'' = h_c (T_w - T_2) + c_1 (T_w - T')^{1.24}, \quad (20.17)$$

with respect to the wall temperature. The evaporated mass per unit time and mixture volume of the flow is then

$$\mu_{21} = \frac{4}{D_{heat}} \dot{q}_w'' / (h'' - h'). \quad (20.18)$$



## 20.2 Forced convection film boiling

### 20.2.1 Tubes

The forced convection film boiling description started with using the equilibrium thermodynamics of two-phase flow. In this framework the empirical correlations are obtained by generalizing experimental data using the *equilibrium steam mass flow rate concentration* in the flow,

$$X_{eq} = \frac{h - h'(p)}{h''(p) - h'(p)} \quad (20.19)$$

where the specific mixture enthalpy is defined as the *mixture enthalpy of the non-inert components*

$$h = \left[ \sum_l \left( 1 - \sum_n C_{nl} \right) \alpha_l \rho_l w_l h_{Ml} \right] / \left[ \sum_l \left( 1 - \sum_n C_{nl} \right) \alpha_l \rho_l w_l \right] \quad (20.20)$$

and the *mass flow rate* in the axial direction is defined as follows

$$G = \sum (\alpha \rho w)_l . \quad (20.21)$$

*Dougall* and *Rohsenow* proposed one of the oldest correlations in 1963 modifying the well-known single-phase heat transfer correlation of *Dittus* and *Boelter* from 1937

$$h_{fc\_FB} = 0.023 \frac{\lambda_1}{D_h} Re_l^{0.8} Pr_{lw}^{0.4} . \quad (20.22)$$

Here the *Reynolds* number is defined by using as a characteristic velocity the center of mass velocity

$$w_{eq} = G / \rho_{eq} , \quad (20.23)$$

assuming that the density of the mixture is equal to the equilibrium density

$$\frac{1}{\rho_{eq}} = \frac{1 - X_{eq}}{\rho'} + \frac{X_{eq}}{\rho''} , \quad (20.24)$$

and the properties of the mixture are those of the saturated vapor

$$Re_{l\_mix} = \frac{D_h w_{eq}}{\eta'' / \rho''} = D_h G \frac{\rho''}{\eta''} \left[ \frac{1 - X_{eq}}{\rho'} + \frac{X_{eq}}{\rho''} \right] . \quad (20.25)$$

The *Prandtl* number for steam

$$Pr_{lw} = c_{p1} \eta_l / \lambda_1 , \quad (20.26)$$

is computed with the properties at the wall temperature

$$c_{p1}, \eta_1, \lambda_1 = f \left[ \max(647, T_w), p \right]. \quad (20.27)$$

Note that the heat flux is then related to the saturation temperature at the local system pressure rather to the real vapor temperature

$$q_w'' = h_{fc\_FB} [T_w - T'(p)]. \quad (20.28)$$

The heat is then assumed to be completely used for evaporation of the continuous liquid

$$\mu_{21} = \frac{4}{D_{heat\ w}} \frac{q_w''}{h''(p) - h'(p)}, \quad (20.29)$$

$$\mu_{31} = 0, \quad (20.30)$$

if the continuous liquid is available, i.e. if  $\alpha_2 > 0$ . If there is no continuous liquid  $\alpha_2 = 0$  but all the liquid is in dispersed flow  $\alpha_3 > 0$  we have

$$\mu_{21} = 0, \quad (20.31)$$

$$\mu_{31} = \frac{4}{D_{heat\ w}} \frac{q_w''}{h''(p) - h'(p)}. \quad (20.32)$$

*Polomik* proposed in 1967 a modification of the *Dougall* and *Rohsenow* correlation in order to take into account the liquid subcooling

$$h_{fc\_FB} = 0.023 \frac{\lambda_1}{D_h} Re_{1\_mix}^{0.8} Pr_{1w}^{0.40} \left( \frac{T_2}{T_w} \right)^{0.5}. \quad (20.33)$$

As noted in 1994 by *Andreani* and *Yadigaroglu* p. 15 this correlation provides surprisingly good agreement with data for substantial thermal non-equilibrium.

In the same year as *Dougall* and *Rohsenow*, *Miropolskij* (1963) collected several experimental data in the region of  $40 \times 10^5 \leq p \leq 220 \times 10^5 \text{ Pa}$ ,  $400 \leq G \leq 2000 \text{ kg/(m}^2\text{s)}$ ,  $0 \leq X_{eq} \leq 1$ ,  $0.008 < D_h < 0.029 \text{ m}$  and successfully reproduced them by the following correlation

$$h_{fc\_FB} = 0.023 \frac{\lambda_1}{D_h} Re_{1\_mix}^{0.8} Pr_{1w}^{0.80} Y. \quad (20.34)$$

Note the difference in the exponent of the *Prandtl* number compared to the *Dougall* and *Rohsenow* correlation and the multiplier

$$Y = 1 - 0.1 \left( \frac{\rho'}{\rho''} - 1 \right)^{0.4} (1 - X_{eq})^{0.4}. \quad (20.35)$$

*Groneveld* and *Delorme* 1976 correlated their own measurements by modifying a correlation obtained by *Hadaller* and *Banerjee* (1969) for vapor only

$$h_{fc\_FB} = \max \left( 3.66, 0.008348 \frac{\lambda_1}{D_{hy}} Re_{1\_mix}^{0.8774} Pr_{1w}^{0.6112} \right), \quad (20.36)$$

where the properties for the vapor *Prandtl* number are computed for an averaged temperature as follows

$$c_{p1}, \eta_1, \lambda_1 = f \left\{ \max [647, (T_w + T_1) / 2], p \right\}. \quad (20.37)$$

The authors limited the prediction of this correlation by the value of the modified *Berenson* equation

$$h_{fc\_FB} = \max(h_{nc\_FB\_Berenson}, h_{nc\_FB}). \quad (20.38)$$

*Groeneveld* et al. successfully reproduced by this approach in 1989 their experimental data in the following region  $D_{hy} = 0.0005$  to  $0.0247$  m,  $p = (1.013$  to  $204.99)10^5$  Pa,  $G = 12.1$  to  $6874$  kg/(m<sup>2</sup>s),  $X_{eq} = -0.12$  to  $3.094$ . The predicted heat fluxes are in the region  $\dot{q}_w'' = 2660$  to  $2\,700\,200$  W/m<sup>2</sup>.

### 20.2.2 Annular channel

For prediction of the forced convection film boiling heat transfer coefficient in an *annular channel* in 1977 *Groeneveld* uses the *Miropolskij* multiplier in the following equation

$$h_{fc\_FB} = 0.052 \frac{\lambda_1}{D_h} Re_1^{0.688} Pr_{1w}^{1.26} / Y^{1.06}. \quad (20.39)$$

The authors reproduced successfully data in the following region:  $450 \times 10^3 \leq \dot{q}_w'' \leq 2250 \times 10^3$  W/m<sup>2</sup>,  $800 \leq G \leq 4100$  kg/(m<sup>2</sup>s),  $34 \times 10^5 < p < 100 \times 10^5$  Pa,  $0.1 < X_{eq} < 0.9$ . This equation is known as *Groeneveld's* Eq. 5-7 in the literature. *Bjornard* and *Griffith* recommended in 1977 the following modification of the correlation

$$h_{fc\_FB} = 0.052 \frac{\lambda_1}{D_h} Re_1^{0.688} Pr_{1w}^{1.26} / Y^{1.06} \quad \text{for } p > 13.8 \text{ bar}, \quad (20.40)$$

$$h_{fc\_FB} = 0.052 \frac{\lambda_1}{D_h} Re_1^{0.688} Pr_{1w}^{1.26} \quad \text{for } p < 13.8 \text{ bar}, \quad (20.41)$$

where

$$Re_1 = w_1 D_1 / \nu_1, \quad (20.42)$$

which removes the singularity of the *Y* factor and is appropriate for direct application in the framework of the non-equilibrium models. Further the authors proposed to combine the film boiling correlation from the type given above valid for high void fractions with natural circulation film boiling in liquid pool by weighting with the void fraction.

*Condie-Bengston* - see in *Andreani* and *Yadigaroglu* (1994), reported the correlation

$$h_{fc\_FB} = 0.0524 \frac{\lambda_1}{D_h} \frac{D_h^{0.1905}}{\lambda_1^{0.5407}} \frac{Pr_{1w}^{2.2598}}{(1 + X_{eq})^{2.0514}} Re_1^{[0.6249 + 0.2043 \ln(X_{eq} + 1)]} \quad (20.43)$$

valid for the following region:  $34 \times 10^3 \leq \dot{q}_w'' \leq 2.074 \times 10^3 \text{ W/m}^2$ ,  $16.5 \leq G \leq 5.234 \text{ kg/(m}^2\text{s)}$ ,  $4.2 \times 10^5 < p < 215 \times 10^5 \text{ Pa}$ ,  $-0.12 < X_{eq} < 1.73$ .

### 20.2.3 Tubes and annular channels

*Groeneveld* generalized in the same work (1977) the equation for both *tubes* and *annular channels* as follows

$$h_{fc\_FB} = 0.00327 \frac{\lambda_1}{D_h} Re^{0.901} Pr_{1w}^{1.32} / Y^{1.50} \quad (20.44)$$

This equation is known as *Groeneveld's* Eq. 5-9 in the literature. It is reported to be valid in the following region:  $120 \times 10^3 \leq \dot{q}_w'' \leq 2.250 \times 10^3 \text{ W/m}^2$ ,  $700 \leq G \leq 5300 \text{ kg/(m}^2\text{s)}$ ,  $34 \times 10^5 < p < 215 \times 10^5 \text{ Pa}$ ,  $X_{eq} < 0.9$ .

### 20.2.4 Vertical flow around rod bundles

For vertical flow around rod bundles *Loomis* and *Schumway* (1983) reported the following correlation

$$h_{fc\_FB} = const \frac{\lambda_1}{D_h} (1 - 0.76\alpha_1) \left[ \frac{h'' - h'}{(T_w - T_1)c_{p1}} \right]^{0.25} \frac{\lambda_{RT} G}{\eta_2} \frac{\rho_2 - \rho_1}{\rho_1} \quad (20.45)$$

where

$$\lambda_{RT} = \left[ \frac{1}{g} \frac{\sigma}{(\rho_2 - \rho_1)} \right]^{1/2} \quad (20.46)$$

and the constant is

$$const = 18(\pm 0.4) 10^{-4}. \quad (20.47)$$

The correlation is valid in the following region:  $p \cong 1.27 \times 10^5 \text{ Pa}$ ,  $31.55 \leq G \leq 70.9 \text{ kg/(m}^2\text{s)}$ ,  $0.1 \leq \alpha_1 \leq 1$ . Note that the correlation is applied in the framework of non-equilibrium thermodynamics, which means that

$$q_1''^{\sigma w} = h_{fc\_FB} (T_w - T_1). \quad (20.48)$$

## 20.3 Transition boiling

*Ramu and Weisman* (1974) proposed the following correlation for transition boiling in tubes

$$h_{TB} = \frac{1}{2} S h_{CHF\_Addoms} \left\{ \begin{array}{l} \exp[-0.01404(\Delta T - \Delta T_{CHF\_Addoms})] \\ + \exp[-0.12564(\Delta T - \Delta T_{CHF\_Addoms})] \end{array} \right\} + h_{fc\_FB}, \quad (20.49)$$

where

$$\Delta T = T_w - T'(p). \quad (20.50)$$

$\Delta T_{CHF\_Addoms}$  is given in Table 20.1.

The component of the forced convection film boiling is computed using the *Dougall and Rohsenow* (1963) proposal

$$h_{fc\_FB} = 0.023 \frac{\lambda_1}{D_h} Re^{0.800} Pr_{1w}^{0.40}, \quad (20.51)$$

$$Re = \frac{D_h w_{eq}}{\eta'' / \rho''} = D_h G \frac{\rho''}{\eta''} \left[ \frac{1 - X_{eq}}{\rho'} + \frac{X_{eq}}{\rho''} \right]. \quad (20.52)$$

The *Prandtl* number for steam

$$Pr_{1w} = c_{p1} \eta_1 / \lambda_1, \quad (20.53)$$

is computed with the properties at the wall temperature

$$c_{p1}, \eta_1, \lambda_1 = f[\max(647, T_w), p]. \quad (20.54)$$

$S$  is the ratio of the effective superheat to the total superheat of the wall from the *Chen* correlation, Eqs.(20.11) to (20.14), (1963).

**Table 20.1.** The critical heat flux and the corresponding temperature difference as a function of pressure – *Addoms* data (1948)

$p$	$h_{CHF\_Addoms}$	$\Delta T_{CHF\_Addoms}$
2 75800	86 877	18.9
4 13700	91 874	18.9
41 37000	227 139	16.6
68 95000	397 478	13.9
96 53000	438 930	12.2
169 96175	408 835	6.1
184 78600	384 986	5.0
195 12850	369 087	4.4
204 78150	348 077	3.9
210 02170	323 661	3.3

The correlation was verified in the region  $1.72 \times 10^5 < p < 2.06 \times 10^5 \text{ Pa}$ ,  $20 < G < 50 \text{ kg/(m}^2\text{s)}$ ,  $30 < \dot{q}_w'' < 260 \text{ W/m}^2$ ,  $0 < X_{eq} < 0.5$ .

As noted by *Groeneveld et al.* (1989) transition-boiling correlations generally provide incorrect asymptotic trends outside their region of validity. An alternative approach uses simply a linear interpolation between the maximum and the minimum points of a log-log plot of  $\dot{q}_w''$  vs.  $\Delta T_w$ , i.e.

$$\frac{\dot{q}_{TB}''}{\dot{q}_{\min\_FB}''} = \left( \frac{\dot{q}_{CHF}''}{\dot{q}_{\min\_FB}''} \right)^m, \quad \text{where} \quad m = \frac{\ln(\Delta T_{\min\_FB} / \Delta T_w)}{\ln(\Delta T_{\min\_FB} / \Delta T_{CHF})} \quad (20.55)$$

or

$$\frac{\Delta T_w}{\Delta T_{\min\_FB}} = \left( \frac{\Delta T_{CHF}}{\Delta T_{\min\_FB}} \right)^n, \quad \text{where} \quad n = \frac{\ln(\dot{q}_{TB}'' / \dot{q}_{\min\_FB}'')}{\ln(\dot{q}_{CHF}'' / \dot{q}_{\min\_FB}'')} \quad (20.56)$$

Film boiling in a large pool exists if  $T_w > \Delta T_{\min\_FB}$ , where  $\Delta T_{\min\_FB}$  is the minimum film boiling temperature.

Note that once the value of the critical heat flux is known, the corresponding temperature is obtained from the definition equation of the heat flux for forced convection nucleate boiling as follows

$$\Delta T_{CHF} = T_{CHF} - T'(p) = \dot{q}_{CHF}'' / h_{fc\_FB} \quad (20.57)$$

*Guo and Leung* (2005) proposed to approximate the 11 163 transition boiling data for pipes by the following relation

$$\frac{h_{TB} - h_{FB}}{h_{CHF} - h_{FB}} = \exp \left[ -a \left( \frac{T_{w,TB} - T'}{T_{w,CHF} - T'} - 1 \right)^b \right],$$

valid up to 170bar. The constants are proprietary but Fig. 5 in *Guo and Leung* (2005) allows the estimate of  $a \approx 0.8$  and  $b \approx 0.6$ .

## 20.4 Critical heat flux

Natural or forced convection nucleate boiling is a very effective cooling mechanism. Increasing the local heat flux or decreasing the cooling mass flow rate may lead in technical facilities to film boiling in which the heat is transferred to the liquid through a vapor film. This is not an effective heat transfer mechanism. The effect on the material interface is manifested by a temperature jump. At high mass flow rates the jump is not as strong as at low mass flow rates. We distinguish two different mechanisms of occurrence of film boiling. The first one happens at low void fractions and is mainly caused by increasing the bubble population at the

heated surface so that they merge together and build a film. The mechanical flow pattern is continuous liquid and dispersed void. This regime is known as departure from nucleate boiling or abbreviated DNB. Different is the mechanism at high void fractions. The mechanical flow pattern is continuous liquid film at the wall and dispersed droplet carried by the void. In this case simply the film dries out and the wall experiences an intimate contact with the steam. This regime is known as the *dry out* regime.

### 20.4.1 The hydrodynamic stability theory of free convection DNB

*Kutateladze* established in 1951 the hydrodynamic stability theory. The main idea on which this theory relies is as follows: The vapor film with thickness above the heated surface governed by the capillary constant

$$\delta_{1F} \approx \left( \frac{\sigma}{g\Delta\rho_{21}} \right)^{1/2},$$

experiences a buoyancy force per unit wall surface equal to  $g\Delta\rho_{21}\delta_{1F}$ . The equilibrium between the dynamic pressure forces  $\rho_1 V_{1ev}^2$ , and the buoyancy force is distorted if the film is not stable. The transition point is controlled by the conditions

$$\rho_1 V_{1ev}^2 / \left[ g\Delta\rho_{21} \left( \frac{\sigma}{g\Delta\rho_{21}} \right)^{1/2} \right] \approx const,$$

or

$$V_{1ev} \approx const \left[ \frac{g\sigma(\rho_2 - \rho_1)}{\rho_1^2} \right]^{1/4}.$$

*Kutateladze* set the critical mass flow rate proportional to the critical velocity

$$\dot{q}_{CHF}'' / \Delta h \approx const \left[ \frac{g\sigma(\rho_2 - \rho_1)}{\rho_1^2} \right]^{1/4}$$

and found from experiments  $const \approx 0.16$ . Later the constant was replaced by the dimensionless group

$$const \approx 0.05 \left[ 10^4 (g\lambda_{RT}\rho_1 / p)^{1/2} \right]^{2/3}.$$

The obtained result is valid for saturated liquid. Subcooling increases the CHF. *Kutateladze* found in 1962 the following relationship

$$\frac{\dot{q}_{CHF,sub}''}{\dot{q}_{CHF,sat}''} = 1 + 0.065 \left( \frac{\rho_2}{\rho_1} \right)^{4/5} \frac{c_{p2}(T' - T_2)}{h'' - h'}.$$

This relationship was verified for  $p = (1 \text{ to } 20) \times 10^5 \text{ Pa}$ ,  $\frac{c_{p2}(T' - T_2)}{h'' - h'} \leq 0.6$  and  $\rho_2 / \rho_1 = 45 \text{ to } 1650$ . A very similar expression was obtained in the same year by *Irvey and Morris* (1962),

$$\frac{\dot{q}_{CHF,sub}''}{\dot{q}_{CHF,sat}''} = 1 + 0.1 \left( \frac{\rho_2}{\rho_1} \right)^{3/4} \frac{c_{p2}(T' - T_2)}{h'' - h'}.$$

The main ideas behind the hydrodynamic theory of boiling by *Zuber* (1958) and *Zuber and Tribus* (1958) is slightly different from those of *Kutateladze*. *Zuber* considered the *Rayleigh - Taylor* instability as responsible for the film instability. If the vapor film possesses a wavy vapor-liquid interface the characteristic wavelength is

$$\lambda_{RT}^* \approx 2\pi \left( \frac{\sigma}{g\Delta\rho_{21}} \right)^{1/2}.$$

Vapor jets are then formed with a distance between the axis equal to  $\lambda_{RT}^*$ . The jets are arranged equidistantly in rectangular grid and take a cross section  $\alpha_{w1}$  part of the total surface. The vertical disturbed surface of the jets is unstable - *Helmholtz* instability. The waves are traveling with velocity

$$c^2 = \frac{\sigma n_c}{\rho_2 + \rho_1} - \frac{\rho_2 \rho_1}{(\rho_2 + \rho_1)^2} (V_1 - V_2)^2,$$

where  $n_c$  is the wave number. In critical conditions  $c \approx 0$  and  $n_c \approx 2\pi / \lambda_{RT}^*$  therefore

$$V_1 - V_2 = \left( \frac{\rho_2 + \rho_1}{\rho_2} \right)^{1/2} \left[ \frac{g\sigma(\rho_2 - \rho_1)}{\rho_1^2} \right]^{1/4}$$

The rising vapor mass flux is equal to the liquid flux (continuity) and therefore

$$\alpha_{w1}\rho_1 V_1 = -\alpha_{w2}\rho_2 V_2$$

or

$$V_1 - V_2 = V_1 \frac{\alpha_{w2}\rho_2 + \alpha_{w1}\rho_1}{\alpha_{w2}\rho_{w2}}.$$

Thus the critical velocity of the rising vapor jets is



$$V_1 = \frac{\alpha_{w2}\rho_{w2}}{\alpha_{w2}\rho_{w2} + \alpha_{w1}\rho_{w1}} \left( \frac{\rho_2 + \rho_1}{\rho_2} \right)^{1/2} \left[ \frac{g\sigma(\rho_2 - \rho_1)}{\rho_1^2} \right]^{1/4}.$$

Thus the critical heat flux is finally

$$\begin{aligned} \frac{\dot{q}_{CHF}''}{\rho_1(h'' - h')} &\approx j_1 = \alpha_{1d} V_1 = \alpha_{1d} \frac{\alpha_{w2}\rho_{w2}}{\alpha_{w2}\rho_{w2} + \alpha_{w1}\rho_{w1}} \left( \frac{\rho_2 + \rho_1}{\rho_2} \right)^{1/2} \left[ \frac{g\sigma(\rho_2 - \rho_1)}{\rho_1^2} \right]^{1/4} \\ &\approx \frac{\pi}{24} \left( \frac{\rho_2}{\rho_2 + \rho_1} \right)^{1/2} \left[ \frac{g\sigma(\rho_2 - \rho_1)}{\rho_1^2} \right]^{1/4} \end{aligned}$$

which is in fact the *Kutateladze* equation with multiplier  $\frac{\pi}{24} \left( \frac{\rho_2}{\rho_2 + \rho_1} \right)^{1/2}$  instead of the constant. For low flow,  $G \leq 100 \text{ kg/(m}^2\text{s)}$ , Zuber et al. (1961) modified later this correlation to

$$\frac{\dot{q}_{CHF}''}{\rho_1(h'' - h')} \approx 0.23164 (0.96 - \alpha_1) \left( \frac{\rho_2}{\rho_2 + \rho_1} \right)^{1/2} \left[ \frac{g\sigma(\rho_2 - \rho_1)}{\rho_1^2} \right]^{1/4}.$$

Note the two completely different approaches to the boiling crises by comparing this theory with the theory presented in Chapter 16. We showed in Chapter 16 that the micro-scale of the nucleation processes, bubble growth and departure, and the turbulence generated by this process naturally lead to self-saturation of the boundary layer with bubbles and dramatically change the mechanism of the heat transfer. In contrast, *Kutateladze* and *Zuber* analyzed the macro-scale above the layer where the micro-physics happens. That is the reason why their analysis gives an absolute upper limit which is about 5 times larger than the observed critical heat flux. This is reflected in the necessity of introducing an empirical constant of about 1/5.

## 20.4.2 Forced convection DNB and DO correlations

For flow in heated pipes and channels the mass flow rate influences the CHF. There are more than 500 empirical correlations for description of this process demonstrating that the final understanding of this phenomena is not yet reached. We give here three of the successful empirical correlations. *Smolin* et al. [25] considered separately the different flow pattern and for each particular flow pattern proposed a correlation for prediction of the CHF. For equilibrium mass flow fraction less than the one defined by

$$X_0 = 1.5 \frac{\rho_1}{\rho_2 + \rho_1} - 0.1 \quad (\text{bubble to film flow transition})$$

the flow is bubbly. In this case *Smolin et al.* propose to use the *Kutateladze* correlation in the form

$$\frac{\dot{q}_{CHF,0}''}{\rho_1(h''-h')} = 0.18 \left( \sqrt{\frac{\nu''}{\nu'}} - 1 \right) \left[ \frac{g\sigma(\rho_2 - \rho_1)}{\rho_1^2} \right]^{1/4}.$$

For

$$X_{eq} \geq X_0$$

we have inverted annular flow called film boiling. In this case the pipe geometry, the mass flow rate and the equilibrium mass flow concentration influence the CHF

$$\dot{q}_{CHF,2}'' = \dot{q}_{CHF,0}''' / \exp \left[ 0.2 \left( \frac{D_h}{\rho'\sigma} \right)^{1/3} G^{2/3} (X_{eq} - X_0) \right].$$

For

$$X_{eq} < 0,$$

$$\dot{q}_{CHF}'' = \dot{q}_{CHF,2}''.$$

*Saturated liquid boiling:* For saturated liquid boiling

$$X_{eq} \geq 0,$$

$$\dot{q}_{CHF}''' = \min(\dot{q}_{CHF,2}'', \dot{q}_{CHF,3}'', \dot{q}_{CHF,3}''),$$

the minimum of the CHF in the following regimes is taken:

Fine dispersed flow,

$$\dot{q}_{CHF,3}'' = 0.22(h''-h') \frac{\eta''}{\eta'} \left[ \frac{\eta''\rho''\rho'}{D_h(\rho'-\rho'')} \right]^{1/3} G^{2/3} (1-X_{eq})^2 / [X_{eq}(\rho'-\rho'') + \rho'']^{1/3};$$

Drying of the heated wall,

$$\dot{q}_{CHF,2}''' = \frac{(h''-h')(\rho'-\rho'')}{45} \left( \frac{\sigma g}{\rho''} \right)^{1/4} \ln \left[ \frac{0.9(\rho''\sigma)^{1/2} \left( \frac{\nu''}{\nu'} \right)^{2/3} (1-X_{eq})^{1/3}}{\eta'^{2/3} G^{2/3} D_h^{1/6} X_{eq}} \right];$$

Continuous vapor: For bubbly flow

$$X_{eq} < X_0,$$

and

$$p \leq 98 \times 10^5$$

we have boiling of subcooled liquid

$$\begin{aligned} \dot{q}_{CHF}'' &= \dot{q}_{CHF,0}'' \\ &+ 8.4 \times 10^{-3} (h'' - h') \sqrt{\rho''} \left\{ [\sigma g (\rho' - \rho'')]^{1/4} \left( \frac{\eta'}{\eta''} \right) \right\}^{1.25} \left[ \frac{G}{\rho'} \left( \frac{\rho' - \rho''}{\sigma g} \right)^{1/4} \right]^{2/3} (X_0 - X_{eq}) \end{aligned} \quad (1)$$

For

$$p > 98 \times 10^5$$

$$\dot{q}_{CHF,2}'' \text{ at } X_{eq}=X_0 = \dot{q}_{CHF,0}''$$

film to fine dispersed flow transition (hydraulic theory)

$$\dot{q}_{CHF,3}'' \text{ at } X_{eq}=X_0 = 0.22 (h'' - h') \frac{\eta''}{\eta'} \left[ \frac{\eta'' \rho'' \rho'}{D_h (\rho' - \rho'')} \right]^{1/3} G^{2/3} \frac{(1 - X_0)^2}{[X_0 (\rho' - \rho'') + \rho'']^{1/3}}$$

If

$$\dot{q}_{CHF,2}'' \text{ at } X_{eq}=X_0 \geq \dot{q}_{CHF,3}'' \text{ at } X_{eq}=X_0 ,$$

then

$\dot{q}_{CHF}'' = \text{Eq. (1)}$ , boiling of subcooled or saturated liquid. Otherwise,

$$\dot{q}_{CHF,2}'' \text{ at } X_{eq}=X_0 < \dot{q}_{CHF,3}'' \text{ at } X_{eq}=X_0 ,$$

the CHF is

$$\begin{aligned} \dot{q}_{CHF}'' &= \dot{q}_{CHF,3}'' \text{ at } X_{eq}=X_0 \\ &+ 0.01 (h'' - h') \left( \frac{\rho'}{\rho''} \right)^{1/2} [\sigma g (\rho' - \rho'')]^{1/4} \left[ G \left( \frac{\rho' - \rho''}{\sigma g} \right)^{1/4} \right]^{1/2} (X_0 - X_{eq}) \end{aligned}$$

*Smolin et al.* (1977) verified the above set of correlations for  $30 \times 10^5 \leq p \leq 200 \times 10^5 \text{ Pa}$ ,  $G \leq 7500 \text{ kg/(m}^2\text{s)}$ ,  $T' - T_2 < 75 \text{ K}$ ,  $0.004 < D_h < 0.025 \text{ m}$ ,  $1 \text{ m} < L$ .

Data for film boiling heat transfer in rod bundles are reported by *Morris et al.* (1985).

*Biasi et al.* proposed in 1967 the following correlation valid for tubes and  $100 < G < 6000 \text{ kg/(m}^2\text{s)}$ ,  $0.003 < D_h < 0.0375 \text{ m}$ ,  $0.2 < L < 6 \text{ m}$ ,  $2.7 \times 10^5 < p < 140 \times 10^5 \text{ Pa}$ ,  $1/(1 + \rho_2 / \rho_1) < X_{eq} < 1$ :

$$\dot{q}_{CHF}'' = \max \left\{ 1000, \frac{1.883 \times 10^7}{D_h^* G^{*1/6}} (FP / G^{*1/6} - X_{eq}), \frac{3.78 \times 10^7}{D_h^* G^{*0.6}} H P (1 - X_{eq}) \right\},$$

where

$$\begin{aligned} G^* &= G/10, D_h^* = D_h/100, p^* = p/10^5, D_h > 0.01, n = 0.4, D_h \leq 0.01, n = 0.6, \\ \text{FP} &= 0.7249 + 0.099 p^*/\exp(0.032 p^*), \\ \text{HP} &= -1.159 + 0.149 p^*/\exp(0.019 p^*) + 8.99 p^*/(10 + p^{*2}). \end{aligned}$$

This correlation is not recommended for rod bundle geometry *Yoder et al. (1985)*.

*Bowring (1972)* proposed the following correlation validated by comparison with 3800 experimental data points in the region:  $2 \times 10^5 < p < 190 \times 10^5 \text{ Pa}$ ,  $136 < G < 18\,600 \text{ kg/(m}^2\text{s)}$ ,  $0.002 < D_h < 0.045 \text{ m}$ ,  $0.15 < L < 3.7 \text{ m}$ . The reported rms error is 7%.

$$\begin{aligned} \dot{q}_{CHF}'' &= [A - B(h'' - h')X_{eq}] / C \\ A &= 2.317(h'' - h')B F_1 / (1 + 0.0143 F_2 D_h^{0.5} G), \\ B &= 0.25 D_h G, \\ C &= 0.077 F_3 D_h G / [1 + 0.347 F_4 (G/1356)^{SN}], \\ SN &= 2 - 0.5 \bar{p}, \\ \bar{p} &= 0.145 10^{-6} p. \end{aligned}$$

$$\begin{aligned} \bar{p} &\leq 1 \\ F_1 &= \{\bar{p}^{18.942} \exp[20.89(1 - \bar{p})] + 0.917\} / 1.917, \\ F_1 F_2 &= \{\bar{p}^{1.3610} \exp[2.444(1 - \bar{p})] + 0.309\} / 1.309, \\ F_1 &= F_1 / (F_1 F_2) \\ F_3 &= \{\bar{p}^{17.023} \exp[16.658(1 - \bar{p})] + 0.667\} / 1.667, \\ F_4 F_3 &= \bar{p}^{1.649}, \\ F_4 &= (F_4 F_3) F_3. \end{aligned}$$

$$\begin{aligned} \bar{p} &> 1 \\ F_1 &= \{\exp[0.648(1 - \bar{p})]\} / \bar{p}^{0.368}, \\ F_2 &= \{F_1 \exp[0.245(1 - \bar{p})]\} / \bar{p}^{0.448}, \\ F_3 &= \bar{p}^{0.219}, \\ F_4 F_3 &= \bar{p}^{1.649}, \\ F_4 &= (F_4 F_3) F_3 \end{aligned}$$

### 20.4.3 The 1995 and 2005 look-up tables

A look-up table for critical heat flux (CHF) has been developed jointly by AECL Research (Canada) and IPPE (Obninsk, Russia) *Groeneveld et al.* (1996)

$$q''_{CHF} = q''_{CHF}(p, G, X_{1,eq}, D_{hy}).$$

It is based on an extensive data base of CHF values obtained in tubes with a vertical upward flow of steam-water mixture. While the data base covers a wide range of flow conditions, the look-up table is designed to provide CHF values for 8 mm tubes at discrete values of pressure, mass flux and dry-out quality covering the ranges 0.1 to 20.0 MPa, 0.0 to 8000 kg/(m<sup>2</sup>s) and -0.5 to +1.0 respectively. Linear interpolation is used to determine the CHF for conditions between the tabulated values, and an empirical correction factor is introduced to extend this CHF table to tubes of diameter values other than 8 mm,

$$\dot{q}''_{CHF} = \dot{q}''_{CHF-8mm} \left( \frac{1000 D_{hy}}{8} \right)^{-1/2}.$$

Compared against the combined AECL-IPPE world data bank (consisting of 22946 data points after excluding duplicate data and obviously erroneous data), the 1995 look-up table predicts the data with overall average and root-mean-square errors of 0.69% and 7.82%, respectively. An assessment of various CHF tables and several empirical correlations shows that the 1995 table consistently provides the best prediction accuracy and is applicable to the widest range of conditions.

*Groeneveld et al.* (2005) issued the improved variant of their first table known as the 2005-look up table containing 20% more data. The rms. error was reduced to 7.1%.

**Problem:** Check whether it is possible to use the 2005-look up table primary designed for heated pipes also for heated rod bundles.

**Solution:** I performed this check in 2006, Kolev (2006). I exploit deliberately a set of simplifying assumptions usually used in the 60's:

1. Fictive sub-channels corresponding to the number of rods are so defined as to be equivalent in geometry;
2. Equal mass flow rate to each sub-channel;
3. The critical heat flux occurs at the exit of the hot channel as a function of the exit parameters; The phenomenon is similar to pipe flow; Therefore the *Groeneveld's* look up table is expected to give the right dependence on mass flow rate, quality and sub-cooling;
4. Uniform boundary conditions for all channels;
5. Grid turbulization as well as the axial power distribution is not specifically treated.

The procedure I use is: Unless  $\left| \frac{q''_{crit,i}(z_{max}) - q''_i(z_{max})}{q''_{crit,i}(z_{max})} \right| < \varepsilon$  increase  $q$  with a  $\Delta q$  starting with  $q_0$ . Here the power of the hot channel is  $q_i = f_{lat,i} q / n_{rods}$ , where per definition the bundles power is the sum of the sub-channel powers  $q = \sum_{i=1}^{n_{rods}} q_i$  and the lateral distribution factor obeys  $\frac{1}{n_{rods}} \sum_{i=1}^{n_{rods}} f_{lat,i} = 1$ . The exit equilibrium mass flow quality is  $X_{1,i} = \frac{1}{\Delta h} \left( \frac{q_i}{\dot{m}_i} - \Delta h_{sub} \right) = \frac{1}{\Delta h} \left( f_{lat,i} \frac{q}{\dot{m}} - \Delta h_{sub} \right)$ . Here by virtue of assumption 2 I use  $\dot{m}/\dot{m}_i = n_{rods}$ . The local heat flux at the exit of the hot channel  $I$ ,  $q''_i(z_{max}) = f_{z_{max},i} \frac{f_{lat,i} q / n_{rods}}{\pi D_{rod} L_{rod}}$ , is compared with the local critical heat flux. The critical heat flux at the exit of channel  $i$  is defined by the 2005-look-up-table  $q''_{crit,i}(z_{max}) = f(p, G, X_{1,i}, D_{hyd})$ . Dividing this value by the lateral hot channel factor and recomposing the averaged flux into bundle power we obtain the final result  $q = \frac{q''_{crit,i}(z_{max})}{f_{lat,i}} \pi D_{rod} L_{rod} n_{rods}$ . Note that the last expression is based on the intuitive assumption that this value may represent the averaged heat flux in the hot channel. It is only a *hypothesis*. It is very interesting to compare the prediction of this “primitive” approach with experimental data and to see how it works.

**8x8 NUPEC BWR bundle tests:** First I simulate three data sets for experiments with the 8x8 NUPEC BWR bundle tests (Fig. 20.1) as proposed in the international benchmark by Neykov et al. (2005). The *first* and the *second* tests are performed with the same axial power distribution but with different lateral power peaking pattern. They serve for analysis of the influence of the lateral power distribution. The *first* and the *third* tests are performed with the same lateral power peaking pattern but with different axial power distribution. They serve for analysis of the influence of the axial power distribution.

The measured versus the predicted bundle power is presented in Figs. 20.1c), 20.2 and 20.3.

Comparing Figs. 20.1a and 20.2 we see that for flatter lateral profiles this method slightly systematically under predicts the measurements.

Comparing Figs. 20.2 and 20.3 we see that for the two different axial power profiles this method predicts almost similarly the measurements.

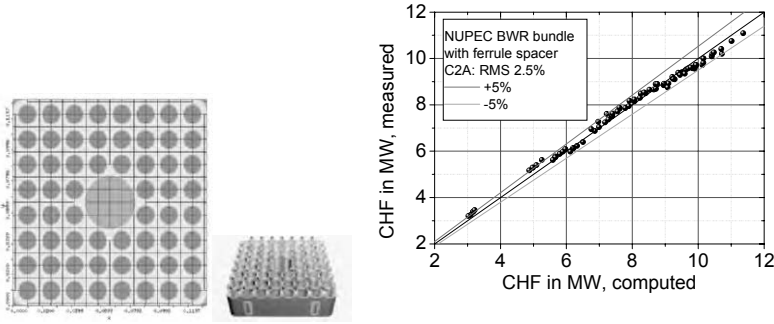


**Fig. 20.1** Geometry of the 8x8 NUPEC CHF bundle tests: a) cross section; b) ferrule spacer; c) Measured versus computed critical bundle power for *cosine* profile with  $f_{z,\max} = 1.4$  and lateral peaking pattern characterized by  $f_{xy} = 0.89$  to  $1.3$ . Data by NUPEC:  $p = 5.48$  to  $8.67 \text{ MPa}$ ,  $\Delta h_{2,\text{sub}} = 22.61$  to  $137.26 \text{ kJ/kg}$ ,  $\dot{m} = 9.98$  to  $65.52 \text{ t/h}$ .

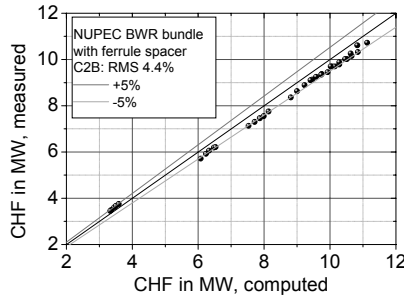


**Fig. 20.2** Measured versus computed critical bundle power for *cosine* profile with  $f_{z,\max} = 1.4$  and lateral peaking pattern characterized by  $f_{xy} = 0.99$  to  $1.18$ . Data by NUPEC:  $p = 7.14$  to  $7.20 \text{ MPa}$ ,  $\Delta h_{2,\text{sub}} = 21.06$  to  $128.57 \text{ kJ/kg}$ ,  $\dot{m} = 9.93$  to  $64.85 \text{ t/h}$ .

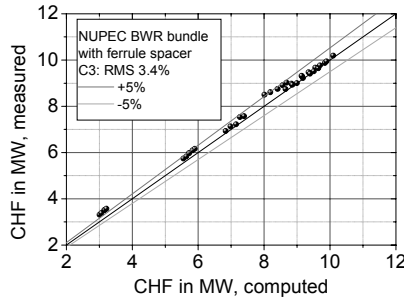


**Fig. 20.3** Measured versus computed critical bundle power for *inlet peak* profile with  $f_{z,\max} = 1.4$  and lateral peaking pattern characterized by  $f_{xy} = 0.89$  to  $1.3$ . Data by NUPEC:  $p = 7.10$  to  $7.19 \text{ MPa}$ ,  $\Delta h_{2,\text{sub}} = 21.7$  to  $125.74 \text{ kJ/kg}$ ,  $\dot{m} = 9.93$  to  $65.02 \text{ t/h}$ .

Having in mind the 2005-look up table possesses rms. error of 7.1% the above predictions with rms. error of 2.5, 4.4 and 3.4% can hardly be made better.

**AREVA ATRIUM10 BWR tests:** Figures 20.4 and 20.5 presents the measured versus the predicted bundle power for a specific tests for AREVA BWR bundles ATRIUM 10.

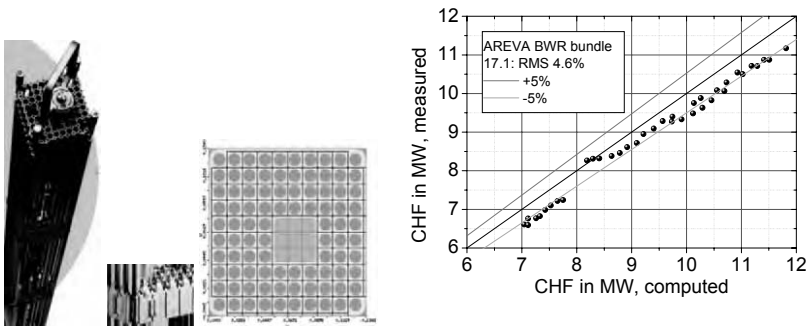


**Fig. 20.4** a) BWR ATRIUM™ 10 bundle with ULTRAFLOW™ spacer; b) Measured versus computed critical bundle power for *cosine* profile with  $f_{z,\max} = 1.4$  and lateral peaking pattern characterized by  $f_{xy} = 0.751$  to 1.255: rms. 4.6%, slight systematic under prediction. Data by Fleiss et al. (1992):  $p = 69\text{bar}$ ,  $\Delta h_{2,\text{sub}} = 23$  to 184 kJ/kg,  $\dot{m} = 6.3$  to 18.90 kg/s.

There are slight differences in the geometry. For both cases we see rms. error of 4.6 and 3.95%, respectively, which again lies inside the accuracy of the 2005-look up table. Again, prediction with better accuracy can hardly be achieved.

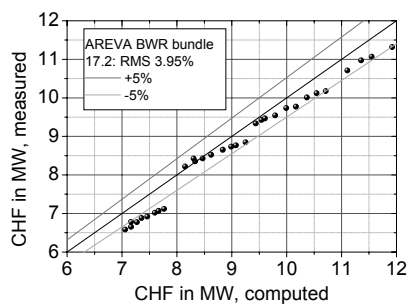


**Fig. 20.5** Measured versus computed critical bundle power for *cosine* profile with  $f_{z,\max} = 1.4$  and lateral peaking pattern characterized by  $f_{xy} = 0.731$  to 1.251: rms. 3.95%, slight systematic under prediction. Data by Fleiss et al. (1992):  $p = 68.8$  to 69.5 bar,  $\Delta h_{2,\text{sub}} = 23$  to 188 kJ/kg,  $\dot{m} = 6.33$  to 15.7 kg/s.



**AREVA tests for PWR bundles with FOCUS grids:** Unlike the previous four data sets this one is for pressures up to 165bar. The bundle contains 5x5 rods and 5 grids. Again, the simple method predicts the CHF with rms. error of 7.24 which is within the accuracy of the 2005-look up table, see Fig. 20.6.

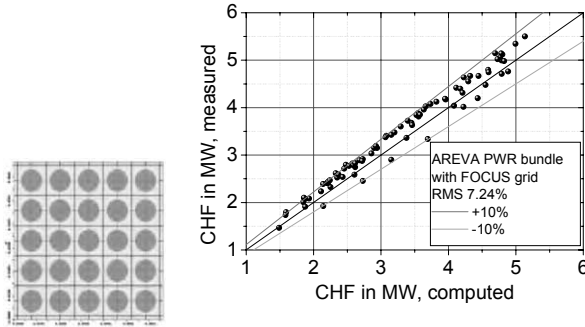


**Fig. 20.6** AREVA PWR bundle with FOCUS grid: Computed versus measured bundle power: rms. 7.5%, slight systematic under prediction. Data by *Vogel et al. (1991)*:  $p = 69.3$  to  $166.6\text{bar}$ ,  $T_{2,\text{in}} = 179.4$  to  $329.5^\circ\text{C}$ ,  $G = 1186.6$  to  $3629\text{ kg/(m}^2\text{s)}$ ,  $q = 1.4643$  to  $5.5015\text{MW}$ .

## Conclusion

The surprising result of this example is that the bundle critical power for 5 data sets of three different bundles and different power distributions are predicted by a simple method described above using the 2005-look-up-table within the accuracy reported by the authors of this table. Therefore, unless better prediction method is developed it is good idea to use the above method as the best predictive instrument. The influence of the grid design can in addition be taken into account by empirical coefficient derived from experiment.

The influence of the axial non uniformity of the heat flux on the CHF for pipes was investigated experimentally by *Yang et al. (2006)* among others. It was found that as long as the mass fluxes are large the influence is not strong. At large mass flows and low smaller sub cooling the influence is within  $\pm 7\%$ . This confirms the conclusions of the above presented study. Similarly for the case of large sub cooling.

For small mass flows and small superheating the deviation from the data obtained with uniform flow can be up to 50%, by *Yang et al. (2006)*. This is the reason for the considerable interest on developing more accurate methods based on sophisticated description of the local physical phenomena.

## Nomenclature

### Latin

$C_{nl}$	mass concentration of the inert component $n$ inside the gas mixture, <i>dimensionless</i>
$c_p$	specific heat at constant pressure, $J/(kgK)$
$c$	wave travel velocity, $m/s$
$D_{heat}$	heated diameter (4 times flow cross-sectional area / heated perimeter), $m$
$D_{rod}$	rod diameter, $m$
$D_{hy}$	hydraulic diameter (4 times flow cross-sectional area / wet perimeter), $m$
$f_{lat,i}$	lateral power distribution factor, $\frac{1}{n_{rods}} \sum_{i=1}^{n_{rods}} f_{lat,i} = 1$ , <i>dimensionless</i>
$f_{z_{max},i}$	axial power distribution factor at the exit of the bundle for sub-channel $i$ , <i>dimensionless</i>
$G$	$= \sum (\alpha \rho w)_i$ , mass flow rate in the axial direction, $kg/(m^2s)$
$g$	gravitational acceleration, $m/s^2$
$h$	specific enthalpy, $J/kg$
$h$	specific mixture enthalpy - mixture enthalpy of the non-inert components, $J/kg$
$\Delta h$	evaporation enthalpy, $J/kg$
$\Delta h_{sub}$	sub-cooling enthalpy difference, $J/kg$
$h_c$	convective heat transfer coefficient, $W/(m^2K)$
$h_{NB}$	nucleate boiling heat transfer coefficient, $W/(m^2K)$
$h_{nc\_FB}$	natural convection film boiling heat transfer coefficient, $W/(m^2K)$
$h_{nc\_FB\_Berenson}$	natural convection film boiling heat transfer coefficient by Berenson, $W/(m^2K)$
$h_{fc\_FB}$	forced convection film boiling coefficient, $W/(m^2K)$
$h_{CHF}$	critical heat transfer coefficient, $W/(m^2K)$
$L_{rod}$	rod length, $m$
$p$	pressure, $Pa$
$q$	$:= \sum_{i=1}^{n_{rods}} q_i$ bundle power, $W$
$\Delta q$	bundle power increment, $W$
$q_0$	initial bundle power, $W$
$\dot{q}_w''$	wall heat flux, $W/m^2$
$\dot{q}_{TB}''$	transition boiling heat flux, $W/m^2$

---

$\dot{q}_{CHF}''$	critical heat flux, $W/m^2$
$\dot{q}_{CHF,sub}''$	critical heat flux for subcooled liquid, $W/m^2$
$\dot{q}_{CHF,sat}''$	critical heat flux for saturated liquid, $W/m^2$
$\dot{q}_{min\_FB}''$	minimum film boiling heat flux, $W/m^2$
$q_{crit,i}''$	critical heat flux in sub-channel $i$ , $W/m^2$
$q_i''$	heat flux in sub-channel $i$ , $W/m^2$
$\dot{m}_i$	mass flow through a sub-channel $i$ , $kg/s$
$\dot{m}$	total mass flow through a bundle, $kg/s$
$n_c$	wave number, -
$n_{rods}$	number of rods in the bundle, dimensionless
$Pr_{1w}$	$= c_{p1}\eta_1 / \lambda_1$ , gas <i>Prandtl</i> number at wall temperature, <i>dimensionless</i>
$Pr_2$	$= c_{p2}\eta_2 / \lambda_2$ , liquid <i>Prandtl</i> number, <i>dimensionless</i>
$Re$	$= X_2 G D_{hy} / \eta_2$ , liquid <i>Reynolds</i> number, <i>dimensionless</i>
$Re_1$	$= w_1 D_1 / \nu_1$ , steam <i>Reynolds</i> number, <i>dimensionless</i>
$Re_{l\_mix}$	$= \frac{D_h w_{eq}}{\eta'' / \rho''}$ , mixture <i>Reynolds</i> number based on vapor viscosity, <i>dimensionless</i>
$Re_{Tp}$	modified <i>Reynolds</i> number, <i>dimensionless</i>
$S$	ratio of the effective superheat to the total superheat of the wall, <i>dimensionless</i>
$T$	temperature, $K$
$T_{w,MFB}$	minimum film boiling temperature, $K$
$\Delta T_{CHF}$	temperature difference corresponding to the critical heat flux, $K$
$\Delta T_{min\_FB}$	minimum film boiling temperature, $K$
$X_l$	mass flow rate concentration in the flow of the velocity field $l$ , <i>dimensionless</i>
$X_{tt}$	<i>Martinelli</i> factor, <i>dimensionless</i>
$X_{eq}$	equilibrium steam mass flow rate concentration in the flow, <i>dimensionless</i>
$X_{1,i}$	homogeneous equilibrium mass flow ratio of vapor, <i>dimensionless</i>
$w$	axial velocity, $m/s$
$w_{eq}$	$= G / \rho_{eq}$ center of mass velocity, $m/s$
$z_{max}$	axial coordinate defining the exit of the bundle, $m$

**Greek**

$\alpha$	volume fraction, <i>dimensionless</i>
$\delta_{1F}$	$\approx \left( \frac{\sigma}{g\Delta\rho_{21}} \right)^{1/2}$ , capillary constant, <i>m</i>
$\varepsilon$	small number
$\Phi_{20}^2$	the ratio of the two phase friction pressure drop to the pressure drop of the liquid field flowing alone in the channel, <i>dimensionless</i>
$\eta$	dynamic viscosity of liquid, <i>kg/(ms)</i>
$\lambda$	thermal conductivity, <i>W/(mK)</i>
$\lambda_{RT}$	$= \left[ \frac{\sigma}{g(\rho' - \rho'')} \right]^{1/2}$ , <i>Rayleigh-Taylor</i> instability wavelength, <i>m</i>
$\rho$	density, <i>kg/m<sup>3</sup></i>
$\rho_{eq}$	homogeneous mixture equilibrium density, <i>kg/m<sup>3</sup></i>
$\sigma$	surface tension, <i>N/m</i>
$\mu_{21}$	evaporation mass from the liquid film per unit time and unit mixture volume, <i>kg/(m<sup>3</sup>s)</i>
$\mu_{31}$	evaporation mass from the droplets per unit time and unit mixture volume, <i>kg/(m<sup>3</sup>s)</i>
$\mu_{12}$	condensation mass per unit time and unit mixture volume, <i>kg/(m<sup>3</sup>s)</i>

**Subscript**

'	saturated steam
"	saturated liquid
1	gas
2	liquid
w	wall
M1	non-inert component in the gas mixture
n1	inert component in the gas mixture
1F	vapor film
2o	liquid only, as the liquid mass flow is occupying the total cross section

**References**

- Addoms JN (1948) D. Sc. Thesis, M. I. T.  
 Andreani A, Yadigaroglu G (1994) Prediction methods for dispersed flow film boiling, Int. J. Multiphase Flow, vol 20 pp 1-51

- Biasi L, Clerici GC, Garribba S, Sala R, Tozzi A (1967) Studies on burnout. Part 3: A new correlation for round ducts and uniform heating and its comparison with world data, *Energ. Nucl.*, vol 14 pp 530-536
- Bjornard TA, Griffith P (1977) PWR blow-down heat transfer, *Thermal and Hydraulic Aspects of Nuclear Reactor Safety*, American Society of Mechanical Engineers, New York, vol 1 pp 17-41
- Bowring RW (1972) Simple but accurate round tube, uniform heat flux, dryout correlation over the pressure range 0.7 to 17 MN/m<sup>2</sup> (100 to 2500 psia). AEEW-R-789
- Chen JC (1963) A correlation for film boiling heat transfer to saturated fluids in convective flow, *ASME Publication-63-HT-34*, p 2-6
- Dittus FW, Boelter LMK (1937) Heat transfer in automobile radiators of the tubular type, *University of California Publications in Engineering*, vol 2 no 13 p 443
- Dougall RS, Rohsenow WM (1963) Film boiling on the inside of vertical tubes with upward flow of the fluid of low qualities, MIT-TR-9079-26, Massachusetts Institute of Technology
- Fleiss, Knapp, Which (1992) STS-17.2, STS-17.1: Messung der Siedeübergangsleistungen und Druckverluste am ATRIUM-10-9Q-Testbündel, e321/92/43, e321/92/44, Karlstein, proprietary
- Forster HK, Zuber N (1955) Dynamic of the vapor bubbles and boiling heat transfer, *AIChE Journal*, vol 1 no 4 pp 531-535
- Groeneveld DC (Mar. 26-28, 1977) Post-dryout heat transfer at reactor operating conditions. Nat. Topical Meet. Water Reactor Safety, Salt Lake City, Utah, American Nuclear Society, Conf. 730304, Rept. AECL-4513, Atomic Energy of Canada Ltd
- Groeneveld DC, Chen SC, Leung LKH, Nguyen C (1989) Computation of single and two-phase heat transfer rates suitable for water-cooled tubes and subchannels, *Nuclear Engineering and Design*, vol 114 pp 61-77
- Groeneveld DC, Delorme GGJ (1976) Prediction of thermal non-equilibrium in the post-dryout regime, NED, vol 36 pp 7-26
- Groeneveld DC, Leunga LKH, Kirillov PL, Bobkov VP, Smogalev IP, Vinogradov VN, Huang XC, Royer E (1996) The 1995 look-up table for critical heat flux in tubes, *Nuclear Engineering and Design*, vol 163 pp 1 -23
- Groeneveld DC, Shan JQ, Vasi AZ, Leung LKH, Durmayaz A, Yang J, Cheng SC and Tanase A (Oct. 2-6, 2005) The 2005 CHF look-up table, The 11<sup>th</sup> Int. Top. Meeting on Nuclear Thermal-Hydraulics (NURETH11) Avignon, France
- Guo Y and Leung LKH (Oct. 2-6, 2005) Developing film boiling heat transfer in tubes, The 11<sup>th</sup> Int. Top. Meeting on Nuclear Thermal-Hydraulics (NURETH11) Avignon, France
- Hadaller G, Banerjee S (1969) Heat transfer to superheated steam in round tubes, AECL Unpublished Report WDI-147
- Hettrony G (ed) (1982) Handbook of multiphase systems, Hemisphere Publ. Corp., Washington etc., McGraw-Hill Book Company, New York
- Irvey HJ, Morris DJ (1962) On the relevance of the vapor - liquid exchange mechanism for subcooled boiling Heat Transfer at High Pressure, AEEW-R127
- Kolev NI (26-27 April 2006) IVA Simulations to the OECD/NRC Benchmarks based on NUPEC BWR Full-size Fine-mesh Bundle Tests, 3th Workshop on OECD/NRC Benchmark based on NUPEC BWR full-size fine-mesh bundle tests (BFBT)-(BFBT-3), Pisa, Italy

- Kutateladze SS (1951) A hydrodynamic theory of changes in the boiling process under free convection conditions. *Izv. Akad. Nauk SSSR, Otd. Tech. Nauk*, vol 4 pp 529-536; AEC-tr-1991 (1954)
- Kutateladze SS (1962) *Osnovy teorii teploobmena*, Moskva, Mashgis, p 456
- Loomis GG, Schumway RW (Oct. 1983) Low-pressure transient flow film boiling in vertically oriented rod bundles, *Nucl. Technology*, vol 63 pp 151-163
- Miropolskij ZL (1963) Heat transfer in film boiling of steam-water mixture in steam generating tubes, *Teploenergetika*, vol 10 no 5 pp 49-53
- Morris DG, Mullins CB, Yoder GL (Apr. 1985) An experimental study of rod bundle dispersed-flow film boiling with high pressure water, *Nucl. Tech.*, vol 69 pp 82-93
- Neykov B, Aydogan F, Hochreiter L, Ivanov K, Utsuno H, Fumio K, Sartori E, Martin M (November 2005) NUPEC BWR full-size fine-mesh bundle test (BFBT) nenchmark, vol 1: Specifications, US NRC, OECD Nuclear Energy Agency, NEA/NSC/DOC (2005) 5
- Polomik EE (October 1967) Transient boiling heat transfer program. Final summary report on program for February 1963- October 1967, GEAP-5563
- Ramu K, Weisman J (1974) A method for the correlation of transition boiling heat transfer data, *Heat Transfer 1974*, 5th Int. Heat Transfer Conf., Tokyo, vol 4 pp 160-164
- Smolin VN, Shpanskii SV, Esikov VI, Sedova TK (1977) Method of calculating burnout in tubular fuel rods when cooled by water and a water-steam mixture. *Teploenergetika*, vol 24 no 12 pp 30-35
- Vogel, Bruch, Wang (19. Aug. 1991) SIEMENS Test Section 52 (DTS52) Description of experiments, KWZ BT23 1991 e 244, Erlangen, proprietary
- Yang J, Groeneveld DC, Leung LKH, Cheng SC and El Nakla MA (2006) An experimental and analytical study of the effect of the axial power profile on CHF, *Nuclear Engineering and Design*, vol 236 pp 1384-1395
- Yoder GL Jr, Morris DG and Mullins CB (1985) Rod bundle burnout data and correlation comparison, *Nuclear Technology*, vol 68 pp 355-369
- Zuber N (1958) On the stability of boiling heat transfer, *Trans. ASME*, vol 80 pp 711-720
- Zuber N et al. (1961) The hydrodynamic crisis in pool boiling of saturated and subcooled liquids, *Int. Heat Transfer Conf.*, Boulder, Colorado, International Developments in Heat Transfer, Part 2 no 27 pp 230-236
- Zuber N, Tribus M (1958) Further remarks on the stability of boiling heat transfer, Report 58-5, Department of Engineering, University of California, Loss Angeles

## 21 Film boiling on vertical plates and spheres

*Section 21.1 of this Chapter presents a closed analytical solution for mixed-convection film boiling on vertical walls. Heat transfer coefficients predicted by the proposed model and experimental data obtained at the Royal Institute of Technology in Sweden by Okkonen et al. are compared. All data predicted are inside the  $\pm 10\%$  error band, with mean averaged error being below 4% (using slightly modified analytical solution). The solution obtained is recommended for practical applications. The method presented here is used in Section 22.2 as a guideline for developing a model for film boiling on spheres. The new semi-empirical film boiling model for spheres used in IVA computer code is compared with the experimental data base obtained by Liu and Theofanous. The data are predicted within  $\pm 30\%$  error band. This Chapter is a slightly changed variant of the work previously published in Kolev (1997), Kolev (1998).*

### 21.1 Plate

#### 21.1.1 Introduction

In nature, film boiling is the controlling heat transfer mechanism during lava-water interaction. In the cryogenic technology rocket engines, it is the inevitable heat transfer mechanism in many cases. Film boiling heat transfer is of particular interest for analysis of accident processes in industry. The theory of film boiling heat transfer has become a classical part of heat and mass transfer textbooks but is often presented in the context of an unwanted heat transfer regime which has to be avoided by design. The close scrutiny paid to accident processes in the industry requires critical re-evaluation of film boiling theory in order to yield a reliable prediction tool for engineering purposes. In particular, calculation of the components of the heat removed by film boiling that leads to vapor heating, liquid heating, evaporation mass flow rate, average vapor volume attached to the surface is very important for increasing the accuracy of the overall flow field prediction of melt interacting with water. As an example of the necessity for improvement of theory, it should be recalled that there is still a need for a closed analytical solution for mixed natural and forced-convection film boiling. In this Chapter a complete analytical solution for film boiling on a vertical wall will first be presented. After this, the attempt will be made to extend the model for spheres. Comparison with experimental data will indicate the success and the limitations of the theoretical results. Where necessary, empirical correction factors are introduced to give more accurate prediction of existing experimental data.

### 21.1.2 State of the art

Film boiling literature was reviewed by *Sakurai* in 1990, and more recently by *Liu* and *Theofanous* in 1995. There is no need to repeat this here.

In his pioneering work of 1916 *Nusselt* presented a closed model of laminar film condensation on vertical surfaces. The idea used was that the condensation is controlled by the heat conduction through the falling liquid film. This model is so easily applied to film boiling under natural convection on vertical plates, postulating that the heat transfer is controlled by the heat conduction through the vapor film that it deserves to be called the *Nusselt theory for laminar condensation and film boiling on vertical walls due to natural convection*.

*Natural-convection film boiling* was first investigated by *Bromley* in 1950. He applied *Nusselt's* idea from 1916. *Frederking* et al. demonstrated in 1965 that the treatment of vertical plates, spheres and horizontal cylinders results in the same expression multiplied by a numerical constant to characterize the appropriate one of the above geometries. Subsequent to this, many theoretical studies related to this subject have been published. The main physical ideas on which the published models rely are similar to those published by *Bromley* et al. (1950, 1953) for natural and mixed convection, and by *Witte* in 1968 for forced convection.

A rigorous formulation of the steady-state problem for *natural convection* was given by *Nishikawa* et al. (1966, (1976)). Several numerical solutions of the problem defined with some simplifying assumptions are available, e.g. *Dhir* and *Purohit* (1978). An accurate numerical solution is compared with an extensive set of data for cylinders and spheres by *Sakurai* et al. in (1990, 1986). *Sakurai* et al. proposed the most accurate correlation for cylinder geometry known to the author. This forms a good approximation of the accurate numerical solution and compares favorably with experimental data for saturated and subcooled water at atmospheric and elevated pressure, with radiation effects also considered. The same correlation has been recently recommended by *Liu* and *Theofanous* (1995) after comparison with an extensive experimental database.

Subsequent to *Witte's* analytical solution (1968) for simplified *forced-convection* steady-state problems in 1968, there have only been numerical solutions provided for this problem in the literature, e.g. *Fodemski* et al. (1982), *Liu* and *Theofanous* (1995).

A third group within the literature covers the conditions of the *stagnation point*. Assuming that the stagnation point condition is valid in the front half of the sphere, *Epstein* and *Heuser* derived in (1980) a correlation which additionally takes into account the liquid subcooling. A numerical solution to this problem is proposed by *Fodemski* (1992), *Kolev* (1995).

The effect of radiation and subcooling or superheating on the film conduction heat flux is taken into account in different ways. Some authors superposed the separate effects, recommending some reduction of the radiative component *Sakurai* (1990). The natural way to take these effects into account is to consider them within the formalism describing the local film thickness. The resulting system of differential equations is solved numerically, e.g. by *Sparrow* (1964),



*Fodemski* (1982), *Liu* and *Theofanous* (1995). There is no simple analytical solution to this problem available in the literature.

A numerical solution of the combined natural and forced-convection film boiling problem for spheres in saturated, subcooled or superheated water with radiation is possible as demonstrated in the literature, but requires a very large amount of computation effort if implemented in system computer codes. To analyze the interaction of fragmenting liquid metal in water, a simple method is needed which has the capability (a) to reproduce the available data for the heat transfer coefficient for natural and forced- convection, (b) to separate the effect of radiation, subcooling or superheating in order to compute the heat flux component consumed to cool the hot structure, to heat or cool the liquid, and to produce steam. Dynamic system characteristics can then be predicted by using such a model which provides heat and mass source terms for the macroscopic differential equation governing the flow. Some of the existing models for this case satisfy one or two of the above conditions, but not all of them. It was for this reason that the author developed a new simplified approach which permits separation of the different effects of radiation, subcooling or superheating and computes the particular heat flux components.

### 21.1.3 Problem definition

Consider the geometry presented in Fig. 21.1. Liquid of temperature  $T_2$  flows along a vertical heated wall. The surface temperature of the wall  $T_{3\sigma}$  is so high that a stable vapor film is formed. The evaporation at the liquid-vapor interface forces the interface temperature to be equal to the saturation temperature at the system pressure  $T'(p)$ . The thickness of the vapor film  $\delta_1(z)$  varies with the height  $z$ . We introduce two coordinate systems having the same axial coordinate  $z$ . The horizontal distance from the wall to the vapor film is  $r_1$ . The horizontal distance from the vapor-liquid interface with the liquid is  $r_2$ . The vapor velocity has only a vertical component  $w_1(r_1)$ . The liquid in the boundary layer has a vertical component of  $w_2(r_2)$ . Various different heat fluxes can immediately be identified first. The radiation heat flux can be split into three different components:  $\dot{q}_{r1}''$  is the radiation heat flux from the interface to the vapor.  $\dot{q}_{r2}''$  is the radiation heat flux from the wall to the bulk liquid.  $\dot{q}_{r\sigma 2}''$  is the radiation heat flux absorbed from the vapor-liquid interface. The partitioning depends mainly on the temperature of the emitting wall. For temperatures below 1000 K almost all radiation energy is dissipated at the liquid interface. This is not the case for the short wavelength light corresponding to higher temperatures. At the present time, it is not clear whether the liquid-vapor interface instabilities create a boundary layer transparent to light or not. The heat flux  $\dot{q}_{FB}''$  is due to conduction through the vapor film. The heat flux  $\dot{q}_{3\sigma 1}''$  is from the wall into the vapor, due the

convective heating of the vapor from the saturation interface temperature to some averaged vapor film temperature. This contribution is frequently neglected in the film boiling literature. In the case of subcooled liquid there is heat flux  $\dot{q}_{\sigma 2}''$  from the liquid interface into the liquid due to conduction and convection.

The problem to be solved is to compute all components of the wall heat flux.

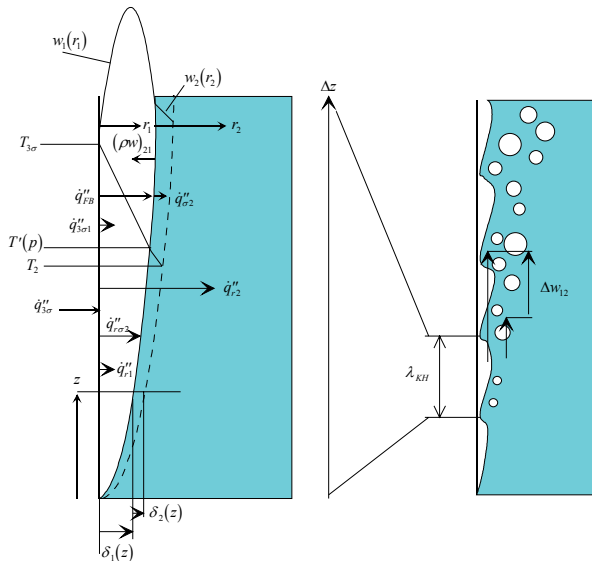


**Fig. 21.1** a) Geometry definition for film boiling on vertical wall. b) Instability of film boiling

### 21.1.4 Simplifying assumptions

The following simplifying assumptions are introduced:

- 1) The vapor and the liquid are incompressible.
- 2) The following simplified momentum equations describe flows in the vapor and liquid boundary layers respectively:

$$\eta_1 \frac{\partial^2 w_1}{\partial r_1^2} = \frac{\partial p}{\partial z} + \rho_1 g, \quad (21.1)$$

$$\eta_2 \frac{\partial^2 w_2'}{\partial r_2'^2} = \frac{\partial p}{\partial z} + \rho_2 g \approx 0. \quad (21.2)$$

Since the last equation simplifies to  $\frac{\partial p}{\partial z} \approx -\rho_2 g$  one can write

$$\eta_1 \frac{\partial^2 w_1}{\partial r_1^2} = -(\rho_2 - \rho_1) g, \quad (21.3)$$

$$\eta_2 \frac{\partial^2 w_2'}{\partial r_2^2} = 0. \quad (21.4)$$

The above two equations can be integrated analytically to give

$$w_1(r_1) = -\frac{1}{2\eta_1}(\rho_2 - \rho_1)gr_1^2 + C_1r_1 + C_3 \quad (21.5)$$

$$w_2'(r_2) = C_2r_2 + C_4. \quad (21.6)$$

The constants are determined from the following boundary conditions

$$1) \text{ at } r_1 = 0, \quad w_1 = 0, \quad (21.7)$$

$$2) \text{ at } r_1 = \delta_1 \text{ and } r_2 = 0, \quad w_1 = w_2', \quad (21.8)$$

$$3) \text{ at } r_1 = \delta_1 \text{ and } r_2 = 0, \quad \eta_1 \frac{\partial w_1}{\partial r_1} = \eta_2 \frac{\partial w_2'}{\partial r_2}, \quad (21.9)$$

$$4) \text{ at } r_2 = \delta_2, \quad w_2' = w_2. \quad (21.10)$$

The solutions to Eqs. (21.5) and (21.6) are

$$w_1 = \frac{\Delta\rho g \delta_1^2}{2\eta_1} \left[ \frac{r_1}{\delta_1} \frac{f + 2\xi}{f + \xi} - \left( \frac{r_1}{\delta_1} \right)^2 \right] + \frac{r_1}{\delta_1} \frac{f}{f + \xi} w_2, \quad (21.11)$$

$$w_2' = \left( 1 - \frac{r_2}{\delta_2} \right) \left[ \frac{\Delta\rho g \delta_1^2}{2\eta_2} \frac{f\xi}{f + \xi} + \frac{f}{f + \xi} w_2 \right] + \frac{r_2}{\delta_2} w_2 \quad (21.12)$$

where

$$f = \eta_2 / \eta_1, \quad (21.13)$$

$$\xi = \delta_2 / \delta_1. \quad (21.14)$$

For the case of zero liquid velocity Eqs. (21.11) and (21.12) reduce to those reported by *Liu and Theofanous* (1995).

In this Chapter the assumption is made that the layers thickness ratio is not a function of the axial coordinate.

The cross-section averaged vapor velocity profile is

$$\langle w_1 \rangle_1 = \frac{1}{\delta_1} \int_0^{\delta_1} w_1 dr_1 = \int_0^1 \left\{ \frac{\Delta \rho g \delta_1^2}{2\eta_1} \left[ \frac{r_1}{\delta_1} \frac{f+2\xi}{f+\xi} - \left( \frac{r_1}{\delta_1} \right)^2 \right] + \frac{r_1}{\delta_1} \frac{f}{f+\xi} w_2 \right\} d \frac{r_1}{\delta_1} \quad (21.15)$$

or

$$\langle w_1 \rangle_1 = \frac{\Delta \rho g \delta_1^2}{12\eta_1} \frac{f+4\xi}{f+\xi} + \frac{1}{2} \frac{f}{f+\xi} w_2. \quad (21.16)$$

The temperature profile in the vapor layer is assumed to be linear,

$$T_1 - T' = \Delta T_{sp} \left( 1 - \frac{r_1}{\delta_1} \right). \quad (21.17)$$

This assumption results from the observation that the cyclic instabilities do not allow thick films to exist. The order of magnitude is tenths of a *mm*. To permit further treatment, the following average is required

$$\begin{aligned} \langle w_1 (T_1 - T') \rangle_1 &= \frac{1}{\delta_1} \int_0^{\delta_1} w_1 (T_1 - T') dr_1 \\ &= \Delta T_{sp} \left[ \langle w_1 \rangle_1 - \int_0^1 \left\{ \frac{\Delta \rho g \delta_1^2}{2\eta_1} \left[ \left( \frac{r_1}{\delta_1} \right)^2 \frac{f+2\xi}{f+\xi} - \left( \frac{r_1}{\delta_1} \right)^3 \right] + \left( \frac{r_1}{\delta_1} \right)^2 \frac{f}{f+\xi} w_2 \right\} d \frac{r_1}{\delta_1} \right]. \end{aligned} \quad (21.18)$$

The last equation can, after integration, be written in the form:

$$\langle w_1 (T_1 - T') \rangle_1 = \frac{1}{2} \Delta T_{sp} \frac{\Delta \rho g \delta_1^2}{12\eta_1} \frac{f+3\xi}{f+\xi} + \frac{1}{6} \Delta T_{sp} \frac{f}{f+\xi} w_2. \quad (21.19)$$

The Reynolds similarity hypothesis for the liquid boundary layer is used:

$$T_2^* - T_2 = \Delta T_{sc} \left( 1 - \frac{r_2}{\delta_2} \right). \quad (21.20)$$

This means that the velocity boundary layer is similar to the temperature boundary layer. This hypothesis holds for liquids with  $Pr \approx 1$ . For the energy conservation of the liquid boundary layer the following average is required

$$\langle w_2 (T_2' - T_2) \rangle_2 = \frac{1}{\delta_2} \int_0^{\delta_2} w_2 (T_2' - T_2) dr_2$$

$$\begin{aligned}
&= \Delta T_{sc} \int_0^1 \left\{ \left( 1 - \frac{r_2}{\delta_2} \right) \left[ \frac{\Delta \rho g \delta_1^2}{2\eta_2} \frac{f\xi}{f+\xi} + \frac{f}{f+\xi} w_2 \right] + \frac{r_2}{\delta_2} w_2 \right\} d \frac{r_2}{\delta_2} \\
&- \Delta T_{sc} \int_0^1 \left\{ \left( \frac{r_2}{\delta_2} - \left( \frac{r_2}{\delta_2} \right)^2 \right) \left[ \frac{\Delta \rho g \delta_1^2}{2\eta_2} \frac{f\xi}{f+\xi} + \frac{f}{f+\xi} w_2 \right] + \left( \frac{r_2}{\delta_2} \right)^2 w_2 \right\} d \frac{r_2}{\delta_2} \\
&= \Delta T_{sc} \left( \frac{2\Delta \rho g \delta_1^2}{12\eta_2} \frac{f\xi}{f+\xi} + \frac{1}{6} \frac{3f+\xi}{f+\xi} w_2 \right). \tag{21.21}
\end{aligned}$$

### 21.1.5 Energy balance at the vapor-liquid interface, vapor film thickness, average heat transfer coefficient

In this section the layer thickness ratio  $\xi$  is taken as known. A separate section deals with calculation of the layer thickness ratio.

We assume that no energy can be accumulated at the vapor-liquid interface. As a consequence, the energy entering the interface due to conduction from the wall through the vapor, minus the energy removed convectively for heating of the vapor plus the radiation energy dissipated into the surface, minus the energy removed from the interface into the liquid will then evaporate a certain amount of steam at the surface:

$$\begin{aligned}
& \left( \lambda_1 \Delta T_{sp} / \delta_1 + \dot{q}_{r\sigma 2}'' - \lambda_2 \Delta T_{sc} / \delta_2 \right) dA_3 - d \left[ \rho_1 c_{p1} \left\langle w_1 \left[ T_1(r_1) - T' \right] \right\rangle_1 A_1 \right] \\
&= d \left( \rho_1 \Delta h \left\langle w_1 \right\rangle_1 A_1 \right). \tag{21.22}
\end{aligned}$$

The film cross-section at the position defined by the coordinate  $z$  is expressed by

$$A_1 = \delta_1 L, \tag{21.23}$$

where  $L$  is the transversal dimension of the plate. The infinitesimal wall surface is expressed by

$$dA_3 = L dz. \tag{21.24}$$

By appropriate substitution within the energy jump condition the following is then obtained

$$\begin{aligned}
& \lambda_1 \frac{\Delta T_{sp}}{\delta_1} \left( 1 + \frac{\dot{q}_{r\sigma 2}''}{\lambda_1 \Delta T_{sp} / \delta_1} - \frac{\lambda_2 \Delta T_{sc} / \delta_2}{\lambda_1 \Delta T_{sp} / \delta_1} \right) dz \\
&= \rho_1 \Delta h d \left\{ \frac{\left\langle w_1 \right\rangle_1 + c_{p1} \left\langle w_1 \left[ T_1(r_1) - T' \right] \right\rangle_1}{\Delta h} \delta_1 \right\}. \tag{21.25}
\end{aligned}$$

Introducing the following abbreviations

$$Sp = c_{p1} \Delta T_{sp} / \Delta h, \quad (21.26)$$

$$r_r = \frac{\dot{q}_{r\sigma 2}''}{\lambda_1 \Delta T_{sp} / \delta_1} \approx const, \quad (21.27)$$

$$C_2 = \frac{\lambda_2 \Delta T_{sc}}{\lambda_1 \Delta T_{sp}}, \quad (21.28)$$

$$\xi = \delta_2 / \delta_1, \quad (21.29)$$

$$f_{nc} = \frac{f + 4\xi}{f + \xi} \frac{1 + \frac{1}{2} Sp \frac{f + 3\xi}{f + 4\xi}}{1 + r_r - C_2 / \xi}, \quad (21.30)$$

$$f_{fc} = \frac{f}{f + \xi} \frac{1 + \frac{1}{3} Sp}{1 + r_r - C_2 / \xi}, \quad (21.31)$$

Eq. (21.25) is finally obtained in the form:

$$\frac{\lambda_1 \Delta T_{sp}}{\rho_1 \Delta h} dz = \frac{\Delta \rho g}{12 \eta_1} f_{nc} \frac{3}{4} d\delta_1^4 + \frac{1}{4} f_{fc} w_2 d\delta_1^2. \quad (21.32)$$

Before integrating the last equation it is assumed that the ratio of the radiative flux and the local film conduction heat flux is constant, Eq. (21.27). At first glance this assumption would seem arbitrary but as will be discussed later, this turns out to be a good assumption. Integrating with the initial condition  $z = 0$ ,  $\delta_1 = 0$  the local vapor film thickness as a function of the axial coordinate is then obtained

$$z = \frac{\rho_1 \Delta h \Delta \rho g}{\lambda_1 \Delta T_{sp} \eta_1} f_{nc} \left( \frac{\delta_1}{2} \right)^4 + \frac{\rho_1 \Delta h w_2}{\lambda_1 \Delta T_{sp}} f_{fc} \left( \frac{\delta_1}{2} \right)^2. \quad (21.33)$$

Comparing the above equation to Eq. (21.6) by *Bui* and *Dhir* (1985) it is evident that they are equivalent only when the conditions  $f_{nc} = 1$  and  $f_{fc} = 1$  hold, with the reason behind this not directly evident.

Calculation of the average heat transfer coefficients for the limiting case of pure natural convection is given in Appendix 21.1. An estimate of the average heat transfer coefficients for the limiting case of predominant forced convection is given in Appendix 21.2. In order to simplify Eq. (21.33) the resulting average heat transfer coefficients are introduced

$$h_{nc} = c_{nc} \left[ \frac{\lambda_1^3 \rho_1 \Delta h \Delta \rho g}{\Delta T_{sp} \eta_1 \Delta z} f_{nc} \right]^{1/4}, \quad (21.34)$$

$$h_{fc} = c_{fc} \left[ \frac{\rho_1 \lambda_1 \Delta h w_2}{\Delta T_{sp} \Delta z} f_{fc} \right]^{1/2}, \quad (21.35)$$

where

$$c_{nc} = 2/3, \quad (21.36)$$

and

$$c_{fc} = 1. \quad (21.37)$$

Eqs. (21.34) and (21.35) can be written in terms of dimensionless numbers as follows

$$Nu_{nc} = c_{nc} \left( Gr_1 \frac{Pr_1}{Sp} f_{nc} \right)^{1/4}, \quad (21.38)$$

$$Nu_{fc} = c_{fc} \left( Re_1 \frac{Pr_1}{Sp} f_{fc} \right)^{1/2}. \quad (21.39)$$

As it will be demonstrated later  $h_{nc}$  is the heat transfer coefficient for the case of zero liquid velocity, that is natural convection only, and  $h_{fc}$  is the heat transfer coefficient for predominant forced convection. Equation (21.33) can thus be rewritten in the following form

$$\left( \frac{\delta_1 h_{nc}}{\lambda_1 2 c_{nc}} \right)^4 + 2r^* \left( \frac{\delta_1 h_{nc}}{\lambda_1 2 c_{nc}} \right)^2 - \frac{z}{\Delta z} = 0 \quad (21.40)$$

where

$$r^* = \frac{1}{2} \left( \frac{h_{fc} c_{nc}}{h_{nc} c_{fc}} \right)^2 = \frac{1}{2} \left( \frac{\rho_1}{\Delta \rho} \frac{Pr_1}{Sp} \frac{f_{fc}^2}{f_{nc}} \right)^{1/2} Fr_2, \quad (21.41)$$

and the *Froude* number is defined as

$$Fr_2 = \frac{w_2}{\sqrt{\Delta z g}}. \quad (21.42)$$

The film thickness as a function of the axial coordinate is therefore

$$\frac{\delta_1 h_{nc}}{\lambda_1 2 c_{nc}} = \left[ \left( r^{*2} + \frac{z}{\Delta z} \right)^{1/2} - r^* \right]^{1/2}. \quad (21.43)$$

At location  $z = \Delta z$ , vapor thickness is at its maximum, i.e.

$$\frac{\delta_{1,\max} h_{nc}}{\lambda_1 2c_{nc}} = \left[ (r^{*2} + 1)^{1/2} - r^* \right]^{1/2}. \quad (21.44)$$

The averaged film boiling heat transfer coefficient is therefore

$$\begin{aligned} h &= \frac{\dot{q}_{FB}''}{\Delta T_{sp}} = \frac{1}{\Delta z} \int_0^{\Delta z} \frac{\lambda_1}{\delta_1} dz = \frac{h_{nc}}{2c_{nc}} \int_0^1 \left[ \left( r^{*2} + \frac{z}{\Delta z} \right)^{1/2} - r^* \right]^{-1/2} d \frac{z}{\Delta z} \\ &= \frac{h_{nc}}{2c_{nc}} \frac{4}{3} \left[ (r^{*2} + 1)^{1/2} + 2r^* \right] \left[ (r^{*2} + 1)^{1/2} - r^* \right]^{1/2} \\ &= h_{nc} \left[ (r^{*2} + 1)^{1/2} + 2r^* \right] \left[ (r^{*2} + 1)^{1/2} - r^* \right]^{1/2}. \end{aligned} \quad (21.45)$$

When liquid velocity is equal to zero,  $r^*=0$ , the expected solution  $h = h_{nc}$  is obtained. Equation (21.45) is an important new result. This represents the average heat transfer coefficient for mixed convection as a function of the average flow properties, the heat transfer coefficient for natural convection and the *Froude* number. Note that this equation still contains one unknown variable: the layer thickness ratio  $\xi$ . The second equation is obtained in the next section by using the energy balance of the liquid boundary layer.

### 21.1.6 Energy balance of the liquid boundary layer, layer thickness ratio

The energy balance for the liquid boundary layer has the following form

$$(\lambda_2 \Delta T_{sc} / \delta_2) dA_3 = d \left[ \rho_2 c_{p2} \left\langle w_2 \left[ T_2'(r_2) - T_2 \right] \right\rangle_2 A_2 \right]. \quad (21.46)$$

As has already been mentioned, it is not clear at the present time whether the liquid-vapor interface instabilities create a boundary layer transparent to light or not. Observations with the naked eye indicate that the interface is rather "milky" and therefore probably not so transparent as a water-steam interface at rest. This point deserves special attention in the future.

The liquid boundary layer cross-section at the position defined by the coordinate  $z$  is

$$A_2 = \delta_2 L, \quad (21.47)$$

Substituting Eq. (21.21) for the average used in the last equation, the following is then obtained

$$dz = \frac{\rho_2 c_{p2}}{\lambda_2} \left( \frac{2\Delta\rho g}{12\eta_2} \frac{f\xi^3}{f+\xi} \delta_1 d\delta_1^3 + \frac{1}{6} \frac{3f+\xi}{f+\xi} \xi^2 w_2 \delta_1 d\delta_1 \right). \quad (21.48)$$



After integrating, this yields:

$$z = \frac{\rho_2 c_{p2}}{\lambda_2} \frac{\Delta \rho g}{\eta_2} \frac{f \xi^3}{f + \xi} 2 \left( \frac{\delta_1}{2} \right)^4 + \frac{1}{3} \frac{3f + \xi}{f + \xi} \xi^2 w_2 \frac{\rho_2 c_{p2}}{\lambda_2} \left( \frac{\delta_1}{2} \right)^2. \quad (21.49)$$

Since the form of Eq. (21.49) is the same as Eq. (21.33), the same transformation can be applied to obtain another expression for the average heat transfer coefficient. Equating the right hand sides of the Eqs. (21.33) and (21.49), the definition equation for computation of the layer thickness ratio is then obtained. The heat transfer coefficients as function of the liquid side properties will next be computed in a similar way to the previous section.

First, the following definition is made

$$h_{2,nc} = c_{2,nc} \left( \lambda_1^4 \frac{\rho_2 c_{p2}}{\lambda_2} \frac{\Delta \rho g}{\eta_2 \Delta z} 2 \frac{f \xi^3}{f + \xi} \right)^{1/4}, \quad (21.50)$$

$$h_{2,fc} = c_{2,fc} \left( \lambda_1^2 \frac{1}{3} \frac{3f + \xi}{f + \xi} \xi^2 w_2 \frac{1}{\Delta z} \frac{\rho_2 c_{p2}}{\lambda_2} \right)^{1/2}, \quad (21.51)$$

where

$$c_{2,nc} = 1, \quad (21.52)$$

and

$$c_{2,fc} = 1. \quad (21.53)$$

With this notation Eq. (21.49) divided by  $\Delta z$  gives

$$\left( \frac{\delta_1 h_{2,nc}}{\lambda_1 2 c_{2,nc}} \right)^4 + 2 r_2^* \left( \frac{\delta_1 h_{2,nc}}{\lambda_1 2 c_{2,nc}} \right)^2 - \frac{z}{\Delta z} = 0, \quad (21.54)$$

where

$$r_2^* = \frac{1}{2} \left( \frac{h_{2,fc} c_{2,nc}}{h_{2,nc} c_{2,fc}} \right)^2 = \frac{1}{2} \left[ \frac{1}{18} \frac{\xi (3f + \xi)^2}{f (f + \xi)} \frac{\rho_2}{\Delta \rho} Pr_2 \right]^{1/2} Fr_2. \quad (21.55)$$

Solving for the film thickness yields

$$\frac{\delta_1 h_{2,nc}}{\lambda_1 2 c_{2,nc}} = \left[ \left( r_2^{*2} + \frac{z}{\Delta z} \right)^{1/2} - r_2^* \right]^{1/2} \quad (21.56)$$

Using Eq. (21.54) the following is obtained for the average heat transfer coefficient

$$h = h_{2,nc} \left[ \left( r_2^{*2} + 1 \right)^{1/2} + 2r_2^* \right] \left[ \left( r_2^{*2} + 1 \right)^{1/2} - r_2^* \right]^{1/2}. \quad (21.57)$$

By comparing Eqs. (21.57) and (21.45) the definition equation for the film thickness ratio is obtained as follows:

$$\begin{aligned} h_{2,nc} & \left[ \left( r_2^{*2} + 1 \right)^{1/2} + 2r_2^* \right] \left[ \left( r_2^{*2} + 1 \right)^{1/2} - r_2^* \right]^{1/2} \\ & = h_{nc} \left[ \left( r^{*2} + 1 \right)^{1/2} + 2r^* \right] \left[ \left( r^{*2} + 1 \right)^{1/2} - r^* \right]^{1/2}. \end{aligned} \quad (21.58)$$

This is a transcendental equation with respect to the layer thickness ratio and must be solved by iteration. An analytical solution for natural circulation is available as an initial value. Setting the liquid velocity equal to zero yields  $h_{2,nc} = h_{nc}$ , which results in a cubic equation with respect to the unknown  $\xi$

$$(1 + r_r) C_1 f \xi^3 - f C_1 C_2 \xi^2 - \frac{8}{81} \left( 4 + \frac{3}{2} Sp \right) \xi - \frac{8}{81} \left( 1 + \frac{1}{2} Sp \right) f = 0. \quad (21.59)$$

In actual fact, Eq. (21.59) is obtained by combining Eqs. (21.34) and (21.50). Here the following new dimensionless parameters inevitably result

$$C_1 = \frac{\lambda_1}{\lambda_2} \frac{\nu_1}{\nu_2} \frac{c_{p2} \Delta T_{sp}}{\Delta h} = \frac{1}{f} \frac{a_1}{a_2} Sp. \quad (21.60)$$

An analytical solution is available as follows. Substitute

$$q = -\frac{1}{3} \left\{ \frac{1}{9} \left[ \frac{C_2}{1 + r_r} \right]^3 + \frac{4}{81} C_2 \frac{4 + \frac{3}{2} Sp}{(1 + r_r)^2 f C_1} + \frac{4}{27} \frac{1 + \frac{1}{2} Sp}{(1 + r_r) C_1} \right\}, \quad (21.61)$$

$$p = -\frac{1}{3} \left\{ \frac{8}{81} \frac{4 + \frac{3}{2} Sp}{(1 + r_r) f C_1} + \frac{1}{3} \left[ \frac{C_2}{(1 + r_r)} \right]^2 \right\}, \quad (21.62)$$

$$D = q^2 + p^3. \quad (21.63)$$

For  $D > 0$  the real solution is

$$\xi = \left( -q + D^{1/2} \right)^{1/3} + \left( -q - D^{1/2} \right)^{1/3} + \frac{C_2}{3(1 + r_r)}. \quad (21.64)$$

### 21.1.7 Averaged heat fluxes

The film boiling heat flux is given by Eq. (21.45)

$$\dot{q}_{FB}'' = h\Delta T_{sp}. \quad (21.65)$$

The average heat flux from the vapor-liquid interface into the liquid is

$$\dot{q}_{\sigma 2}'' = \frac{1}{\Delta z} \int_0^{\Delta z} \lambda_2 \frac{\Delta T_{sc}}{\delta_2} dz = \frac{\lambda_2 \Delta T_{sc}}{\lambda_1 \Delta T_{sp}} \frac{1}{\xi} \frac{1}{\Delta z} \int_0^{\Delta z} \lambda_1 \frac{\Delta T_{sp}}{\delta_1} dz = \frac{C_2}{\xi} \dot{q}_{FB}'' . \quad (21.66)$$

The heat flux required for heating saturated steam to a certain average temperature corresponding to the linear temperature profile is

$$\dot{q}_{\sigma 1}''(z) dA_3 = d \left[ \rho_1 c_{p1} \left\langle w_1 [T_1(r_1) - T'] \right\rangle_1 A_1 \right], \quad (21.67)$$

or after rearrangement

$$\dot{q}_{\sigma 1}''(z) = \frac{1}{2} \rho_1 c_{p1} \Delta T_{sp} \frac{\Delta \rho g}{12 \eta_1} \frac{f + 3\xi}{f + \xi} \frac{d\delta_1^3}{dz} + \frac{1}{6} \rho_1 c_{p1} \Delta T_{sp} w_2 \frac{f}{f + \xi} \frac{d\delta_1}{dz}. \quad (21.68)$$

The average value can be finally expressed by

$$\begin{aligned} \dot{q}_{\sigma 1}'' &= \frac{1}{\Delta z} \int_0^{\Delta z} \dot{q}_{\sigma 1}''(z) dz \\ &= \frac{1}{2} \rho_1 c_{p1} \Delta T_{sp} \frac{\Delta \rho g}{12 \eta_1 \Delta z} \frac{f + 3\xi}{f + \xi} \delta_{1,\max}^3 + \frac{1}{6} \frac{\rho_1 c_{p1} \Delta T_{sp} w_2}{\Delta z} \frac{f}{f + \xi} \delta_{1,\max} \\ &= \frac{1}{2} Sp \left[ \frac{1}{f_{nc}} \frac{f + 3\xi}{f + \xi} \left( \frac{h_{nc} \delta_{1,\max}}{2 c_{nc} \lambda_1} \right)^3 \frac{h_{nc}}{h} + \frac{4}{6} \frac{1}{f_{fc}} \frac{f}{f + \xi} \left( \frac{h_{fc} \delta_{1,\max}}{2 \lambda_1 c_{fc}} \right) \frac{h_{fc}}{h} \right] \dot{q}_{FB}'' . \quad (21.69) \end{aligned}$$

The film thickness at the upper end of the integration region is determined by Eq. (21.44).

For the case of the natural convection Eq. (21.69) reduces to

$$\dot{q}_{\sigma 1}'' = \frac{1}{2} Sp \frac{1}{f_{nc}} \frac{f + 3\xi}{f + \xi} \dot{q}_{FB}'' , \quad (21.70)$$

and for the case of predominant forced convection to

$$\dot{q}_{\sigma 1}'' = \frac{1}{3} Sp \frac{1}{f_{fc}} \frac{f}{f + \xi} \dot{q}_{FB}'' . \quad (21.71)$$

It is evident that the energy transferred to heat up the vapor film is proportional to the energy transferred from the wall to the liquid interface by conduction.

The evaporation mass flow rate is expressed by

$$(\rho w)_{21} = (\dot{q}_{FB}'' + \dot{q}_{\sigma 2}'' - \dot{q}_{\sigma 2}'' - \dot{q}_{3\sigma 1}'') / \Delta h. \quad (21.72)$$

For natural convection the following is obtained

$$(\rho w)_{21} = \left( 1 + r_r - \frac{C_2}{\xi} - \frac{1}{2} Sp \frac{1}{f_{nc}} \frac{f + 3\xi}{f + \xi} \right) \frac{\dot{q}_{FB}''}{\Delta h}. \quad (21.73)$$

This equation contains an interesting item of information. The condition  $(\rho w)_{21} = 0$  leads to a transcendental equation with respect to superheat, as  $r_r$  and  $\xi$  are also functions of  $\Delta T_{sp}$ .

The assumption that there is a linear temperature profile is not valid for higher degrees of superheat, because heating of the vapor will first bring the liquid interface to a certain average temperature but will then require more energy than could be supplied at the interface. Under such conditions only radiation heat flux has any influence on film boiling.

Thus, a complete analytical description of the heat transfer mechanism for film boiling is now available.

### 21.1.8 Effect of the interfacial disturbances

The interfacial disturbances enhance the heat transfer from the interface to the liquid. This effect was recognized by *Coury and Dukler* (1970), *Suryanarayana and Merte* (1972) and discussed by *Analytis and Yadiragolu* (1985) for vertical surfaces. More recent works by *Bui and Dhir* (1985), *Nigmatulin et al.* (1994), *Nishio and Ohtake* (1993) substantiate this finding. The effect is:

(a) As it is evident from Fig. 21.1 b, the interfacial instabilities do not allow the film to become very thick. The series of crests indicates that the characteristic length of the process is proportional to the instability wavelength  $\lambda_{KH}$ , rather than to the height of the heated surface so long as  $\Delta z > \lambda_{KH} / 2$ . The classical *Kelvin-Helmholtz* instability analysis applied to this problem defines this instability wavelength by the formula

$$\lambda_{KH} = 2\pi \sqrt{\frac{2\sigma\delta_{1,z=\lambda_{KH}}}{\rho_1 (\langle w_1 \rangle_1 - w_2)^2}} = 2\pi \sqrt{\frac{2\sigma\delta_{1,z=\lambda_{KH}}}{\rho_1 \left( \frac{\Delta\rho g \delta_{1,z=\lambda_{KH}}^2}{12\eta_1} \frac{f+4\xi}{f+\xi} - \frac{1}{2} \frac{f+2\xi}{f+\xi} w_2 \right)^2}} \quad (21.74)$$

which has to be solved together with Eq. (21.43) for

$$z = \Delta z = \lambda_{KH} / 2. \quad (21.75)$$

(b) We expect that the theory as presented up to this point will underpredict the influence of the subcooling. The instabilities at the surface produce periodical bubble entrainment which causes turbulent mixing in the liquid boundary layer and therefore additional enhancement of heat transfer into the liquid.

This effect can be included in the model by modifying the liquid thermal boundary layer thickness as follows. In place of  $C_2$  the following is used

$$C_2^* = C_2 \left( 1 + \frac{2}{5} Sp \right). \quad (21.76)$$

This is valid for

$$(1 + r_r) \xi / C_2 > 1, \quad (21.77)$$

with the boundary layer thickness left unchanged for all other conditions. For small degrees of superheating this modification is not important; it only starts to influence the computed heat transfer into the liquid in the case of higher degrees of superheat. The data comparison given in the next section provides the justification for this modification.

### 21.1.9 Comparison of the theory with the results of other authors

Equation (21.58) provides a new general method for layer thickness ratio computation. Equation (21.45) provides a new general method for computation of the averaged film boiling heat transfer coefficient for an arbitrary state of the liquid.

It is worth noting that for the case of natural convection the cubic Eq. (21.59) is obtained for the layer thickness ratio just as do *Sakurai* (1990), and *Liu and Theofanous* (1995), but with different coefficients.

Comparing Eq. (21.28) with Eqs. (21.68) and (21.64) the following is obtained

$$f_{nc} = 1 / \left[ \left( 1 + \frac{\dot{q}_{r\sigma 2}'' - \dot{q}_{\sigma 2}''}{\dot{q}_{FB}''} \right) \frac{f + \xi}{f + 4\xi} - \frac{\dot{q}_{3\sigma 1}''}{\dot{q}_{FB}''} \right] \quad (21.78)$$

or

$$f_{nc} \approx 1 / \left( 1 + \frac{\dot{q}_{r\sigma 2}'' - \dot{q}_{\sigma 2}'' - \dot{q}_{3\sigma 1}''}{\dot{q}_{FB}''} \right). \quad (21.79)$$

This is a very significant equation indicating a simple way to take into account the effects of vapor heating, liquid subcooling and radiation. As a result, Eq. (21.40) can be written in the form

$$\frac{\dot{q}_{nc}''}{\dot{q}_{nc,0}''} \approx \left( 1 + \frac{\dot{q}_{r\sigma 2}'' - \dot{q}_{\sigma 2}'' - \dot{q}_{3\sigma 1}''}{\dot{q}_{nc}''} \right)^{-1/4} \quad (21.80)$$

where

$$\dot{q}_{nc,0}'' = c_{nc} \left[ \frac{\lambda_1^3 \rho_1 \Delta h \Delta \rho g}{\Delta T_{sp} \eta_1 \Delta z} \right]^{1/4} \Delta T_{sp} . \quad (21.81)$$

Similarly for the case of forced convection the following is obtained

$$\frac{\dot{q}_{fc}''}{\dot{q}_{fc,0}''} \approx \left( 1 + \frac{\dot{q}_{r\sigma 2}'' - \dot{q}_{\sigma 2}'' - \dot{q}_{3\sigma 1}''}{\dot{q}_{fc}''} \right)^{-1/2} \quad (21.82)$$

where

$$\dot{q}_{fc,0}'' = c_{fc} \left[ \frac{\rho_1 \lambda_1 \Delta h w_2}{\Delta T_{sp} \Delta z} \right]^{1/2} \Delta T_{sp} , \quad (21.83)$$

is the heat flux for predominant forced convection and saturated liquid.

The notation can now be generalized as follows

$$\frac{\dot{q}_{FB}''}{\dot{q}_{FB,0}''} \approx \left( 1 + \frac{\dot{q}_{r\sigma 2}'' - \dot{q}_{\sigma 2}'' - \dot{q}_{3\sigma 1}''}{\dot{q}_{FB,0}''} \frac{\dot{q}_{FB,0}''}{\dot{q}_{FB}''} \right)^{-1/m} . \quad (21.84)$$

The value  $m = 2$  applies for predominant forced convection, and  $m = 4$  for natural convection. Note that for  $(\dot{q}_{r\sigma 2}'' - \dot{q}_{\sigma 2}'' - \dot{q}_{3\sigma 1}'')/\dot{q}_{FB}'' \gg 1$  we have  $\dot{q}_{FB}''/\dot{q}_{FB,0}'' \approx [(\dot{q}_{r\sigma 2}'' - \dot{q}_{\sigma 2}'' - \dot{q}_{3\sigma 1}'')/\dot{q}_{FB,0}'']^{-1/(m-1)}$ . This describes the way in which heat transfer from the surface to the vapor and from the interface to the liquid enhances the film boiling heat transfer component.

It is common practice to incorporate the surface-vapor term into a modified term for latent heat of vaporization. The natural-convection film boiling heat transfer coefficient can thus be expressed with the modified Eq. (21.34a) as follows

$$h_{nc} = c_{nc} \left[ \frac{\lambda_1^3 \rho_1 \Delta h^* \Delta \rho g}{\Delta T_{sp} \eta_1 \Delta z} f_{nc} \right]^{1/4} , \quad (21.34a)$$

where

$$\Delta h^* = \Delta h \left\{ (f + 4\xi)/(f + \xi) + 0.5[(f + 3\xi)/(f + \xi)] Sp \right\} \approx \Delta h(1 + 0.5Sp) , \quad (21.85)$$

It is evident that this practice yields a good approximation of the general result as the ratio  $\dot{q}_{3\sigma 1}''/\dot{q}_{FB}''$  is almost constant for given thermal conditions. The constant 0.5 has been also used by *Sakurai* (1990). Some authors have used other values instead of 0.5: 0.4 - *Bromley* (1952), 0.6 - *Frederking* et al. (1965)

or  $0.84 / \text{Pr}_l$  - Sparrow (1964). If these values are compared with Eq. (21.85) it is evident that the correct value for the linear temperature profile in the vapor is very close to a constant value of 0.5. For degrees of superheat exceeding  $700 \text{ K}$  at atmospheric pressure the term  $\dot{q}_{3\sigma 1}'' / \dot{q}_{FB}''$  is larger than 0.4, and cannot be neglected. The modification of the latent heat of vaporization as discussed here simplifies the general equation to

$$\frac{\dot{q}_{FB}''}{\dot{q}_{FB,0}''} \approx 1 / \left( 1 + \frac{\dot{q}_{r\sigma 2}'' - \dot{q}_{\sigma 2}''}{\dot{q}_{FB,0}''} \frac{\dot{q}_{FB,0}''}{\dot{q}_{FB}''} \right)^{1/m}. \quad (21.86)$$

For predominant forced convection ( $m = 2$  in Eq. (21.84)) the following is then obtained

$$\frac{\dot{q}_{FB}''}{\dot{q}_{FB,0}''} = \left[ 1 + \frac{1}{4} \left( \frac{\dot{q}_{r\sigma 2}'' - \dot{q}_{\sigma 2}''}{\dot{q}_{FB,0}''} \right)^2 \right]^{1/2} - \frac{1}{2} \frac{\dot{q}_{r\sigma 2}'' - \dot{q}_{\sigma 2}''}{\dot{q}_{FB,0}''}. \quad (21.87)$$

This equation can be solved numerically for natural convection. As already mentioned, the effect of subcooling or superheating is to either reduce or enhance the effect of radiation.

For the case of natural circulation, film boiling Eq. (21.86) reduces to an equation that was in fact already intuitively introduced by Bromley, see Eq. (9) in Bromley (1950), who considered it as "approximate". It was shown by Sparrow [(1964), p 234] that for natural-convection film boiling use of Eq. (21.85) permits the effect of the radiation on the conductive heat flux to be predicted to within a few per cent of the accuracy of the exact method. This means that Eq. (21.86) is a very practical approach for the general case of film boiling with radiation in subcooled or superheated liquid as demonstrated in Kolev (1995).

### 21.1.10 Verification using the experimental data

Experimental data for averaged heat transfer coefficients were obtained at the Royal Institute of Technology in Sweden by Okkonen et al. (1996). The data are for vertical heated walls with  $\Delta z = 1.5 \text{ m}$ . Water at atmospheric pressure and subcooling of  $\Delta T_{sc} = 3$  to  $42 \text{ K}$ , was used as a coolant. The wall superheat was considerable:  $\Delta T_{sp} = 487$  to  $1236 \text{ K}$ . The heat transfer coefficient was defined by Okkonen with respect to the wall-liquid temperature difference. This is recomputed here with respect to wall-saturation temperature difference for comparison purposes. Prediction is performed using Eqs. (21.75), (21.64), (21.30 and (21.34a). A comparison of the predicted data with the 43 data points gained by experiment is given in Fig. 21.2. It is evident that all data are predicted inside the error band of  $\pm 10\%$ , with a mean averaged error of less than  $\pm 4\%$  when the modified theory expressed by Eq. (21.76) is used.

It is interesting to note that for this data we have  $f \approx 25$  to  $39.6$ ,  $\xi \approx 0.35$  to  $2.3$ ,  $f_{nc} \approx 4.2$  to  $205$ .

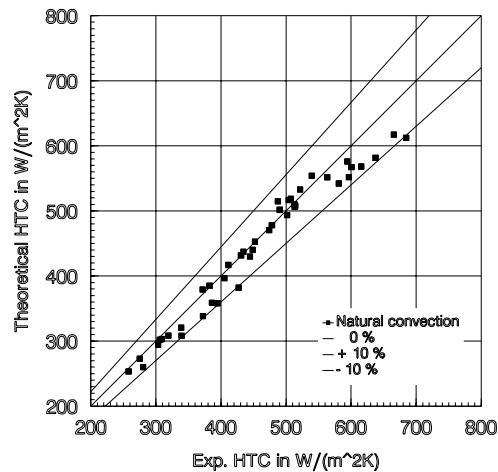


**Fig. 21.2** Comparison between the film boiling model and the data base of the Royal Institute of Technology (KTH - Sweden) - Okkonen et al. Vaeth's radiation model (FzK - Karlsruhe) incorporated.  $\Delta z = 1.5m$  vertical wall. Water at atmospheric pressure and subcooling  $\Delta T_{sc} = 3 - 42K$ . Wall superheat  $\Delta T_{sp} = 487 - 1236K$

### 21.1.11 Conclusions

The approximate mathematical description proposed in this work relates to mixed-convection film boiling on a vertical heated plate, in saturated or subcooled liquid. It takes into account the effect of radiation and leads to a new analytical solution. This solution compares well with the experimental data for natural-convection film boiling. The final result is recommended for practical application.

### 21.1.12 Practical significance

An analytical solution of the mass, momentum and energy conservation equations describing mixed-convection film boiling on vertical walls is now available. From this solution expressions are derived for the particular components of the removed heat that cause vapor heating, liquid heating, for evaporation mass flow rate, and for average vapor volume attached to the surface. This is a step forward in increasing the accuracy of the overall flow field prediction for melt interacting with water in severe accident analysis in industry. Design calculations for vertical surfaces cooled by film boiling can now be implemented with an accuracy of about 10%.



## 21.2 Sphere

### 21.2.1 Introduction

In Section 21.1 of this Chapter the method was described that led to a successful analytical description of film boiling on vertical plates. Here this method is extended to a method for description of mixed-convection film boiling at spheres.

### 21.2.2 Problem definition

Consider the geometry presented on Fig. 21.3. A hot sphere is flowed by liquid similarly to the case presented in Fig. 21.1. All geometry definitions are similar to those of the plate.

The problem to be solved is: compute all components of the heat flux emitted from the wall as indicated on Fig. 21.3.

### 21.2.3 Solution method

Encouraged by the successful model development for plane geometry we have repeated the same procedure for the spherical geometry. In addition to the assumption of a linear temperature profile in the liquid we considered also the case for a quadratic profile. The results are analytical solutions for natural and forced convection, respectively. A closed analytical solution for mixed convection could not be obtained. Therefore interpolation between both solutions was necessary to describe the mixed convection. The final result was more complicated than the plane solution. Data comparison shows that several empirical corrections are necessary to bring the model prediction within a 30% error band compared to experiments. An ad hoc application of the plane solution to spherical geometry was much better. Therefore we decided to modify the plane solution appropriately and to verify the solution on the data available. The motivation for this study comes from the *Meyer* and *Schumacher* experiment (1996).

### 21.2.4 Model

The interfacial area per unit volume of the flow

$$\frac{F_3}{Vol} = \frac{6\alpha_3}{D_3} \quad (21.88)$$

is necessary to compute power densities from heat fluxes at the surface. At the beginning of the computation we assume that the surface temperature is equal to the particle-averaged temperature  $T_{\sigma_3} = T_3$ . This assumption can be improved by repeating the procedure described below.



by introducing a multiplier depending on the superheating. The forced convection *Nusselt* number is computed by slightly modifying the method of *Gnielinski* (1978)

$$Nu_{\sigma_2,fc} = \max(Nu_{\sigma_2,fcl}, Nu_{\sigma_2,fct}), \quad (21.91)$$

where

$$Nu_{\sigma_2,fcl} = 0.664 Re_2^{1/2} Pr_2^{1/3}, \quad (21.92)$$

$$Nu_{\sigma_2,fct} = 0.037 \frac{Re_2^{0.8} Pr_2}{1 + \frac{2.443}{Re_2^{0.1}} (Pr_2^{2/3} - 1)}. \quad (21.93)$$

This method is verified for  $Re_2 < 2 \times 10^4$ ,  $0.7 < Pr_2 < 10^4$ . *Achenbach* (1993) reported data which demonstrate the validity of the above approach up to  $Re_2 < 7.7 \times 10^5$  and pressure up to 40 *bar*. Interface turbulence due to film boiling is taken into account by introducing a multiplier depending on the superheating

$$Nu_{\sigma_2,fc} = 1.5(1 + 5Sp^{*3}) Nu_{\sigma_2,fc}. \quad (21.94)$$

Again, as in the case of natural convection, the interface turbulence due to film boiling is taken into account by introducing an empirical multiplier  $1.5(1 + 5Sp^{*3})$  depending on the superheating. The coefficients are selected by comparison with experimental data as will be discussed later on.

For  $Re_2 < 0.001$

$$Nu_{\sigma_2} = Nu_{\sigma_2,nc} \quad (21.95)$$

otherwise

$$Nu_{\sigma_2} = \max(Nu_{\sigma_2,nc}, Nu_{\sigma_2,fc}). \quad (21.96)$$

The thermal power transferred from the interface into the bulk per unit flow volume is therefore

$$\dot{q}_{\sigma_2}'' = \omega_{\sigma_2} (T' - T_2), \quad (21.97)$$

$$\omega_{\sigma_2} = C_{gas} \frac{F_3}{Vol} \frac{\lambda_2}{D_3} Nu_{\sigma_2}. \quad (21.98)$$

Here the multiplier

$$C_{gas} = \left( \frac{\alpha_2}{\alpha_1 + \alpha_2} \right)^{1/3} \quad (21.99)$$

takes into account the presence of vapor in the flow outside the film. The power  $1/3$  rather the proposal by *Liu* and *Theofanous* (1995),  $1/4$ , is used in Eq. (21.99) for better reproduction of the experimental data for film boiling in two-phase flow with this particular model.

#### 21.2.4.2 Radiation from the sphere

For very high temperatures the radiation cannot be neglected. This is a very important topic which deserves separate and careful discussion. We will confine ourselves to referring to the formalism provided by *Lanzenberger* (1997), which gives three radiation components from the particle interface being functions of the volumetric fractions, partial vapor pressure and the temperatures of the emitter and receivers

$$[\dot{q}_{r1}''', \dot{q}_{r2}''', \dot{q}_{r\sigma 2}''']_L = f(\alpha_1, \alpha_2, \alpha_3, p_M, T_1, T_2, T_{3\sigma}). \quad (21.100)$$

For convenience we introduce a splitting factor for correction of the radiation heat redistribution in water due to surface instability based on the increase of the surface absorption

$$\dot{q}_{r\sigma 2}''' = [\dot{q}_{r\sigma 2}''']_L + c_{split} [\dot{q}_{r2}''']_L, \quad (21.101)$$

$$\dot{q}_{r2}''' = (1 - c_{split}) [\dot{q}_{r2}''']_L, \quad (21.102)$$

where

$$c_{split} = 0. \quad (21.103)$$

For superheated liquid

$$T_2 > T' \quad (21.104)$$

all the radiation reaching the liquid is deposited at the liquid interface facilitating an additional spontaneous flashing condition

$$\dot{q}_{r\sigma 2}''' = [\dot{q}_{r\sigma 2}''']_L + [\dot{q}_{r2}''']_L \quad (21.105)$$

$$\dot{q}_{r2}''' = 0. \quad (21.106)$$

For practical application *Vaeth's* model (1995) in IVA4 was replaced by the new model developed by *Lanzenberger* (1997). The new model solves correctly the radiation transport equation for particular geometries in the multi-phase flows without making use of some simplifying assumptions made by *Vaeth*. One of the results of the new model is, for instance, less radiation energy adsorbed in the steam. This is not significant for the discussed case, but in large-scale melt-water interaction is of importance. The comparisons with experimental data reported here are performed with the model of *Lanzenberger*.

### 21.2.4.3 Film boiling without radiation in saturated liquid

Here we consider film boiling without radiation in saturated liquid. In Section 21.2.4.3.4 the prediction of the model will be extended to take into account radiation and subcooling.

#### 21.2.4.3.1 Natural convection only

The heat transfer coefficient for natural-convection film boiling is computed by using a somewhat modified plane solution

$$h_{nc,1} = \frac{\lambda_l}{D_3} Nu_{nc,1} \quad (21.107)$$

where

$$Nu_{nc,1} = 0.7 f(\bar{D}_3) (f_{nc} Gr_1 Pr_1 / Sp)^{1/4}, \quad (21.108)$$

$$f_{nc} = \frac{f + 4\xi}{f + \xi} \left( 1 + \frac{1}{2} Sp \frac{f + 3\xi}{f + 4\xi} \right), \quad (21.109)$$

$$\xi = (-q + \Delta)^{1/3} + (-q - \Delta)^{1/3}, \quad \xi > 0, \quad (21.110)$$

$$\Delta = \sqrt{D} \quad \text{for } D \geq 0, \quad (21.111)$$

$$D = q^2 + p^3, \quad (21.112)$$

$$q = -\frac{1}{3} \frac{4}{27} \frac{1 + \frac{1}{2} Sp}{C_1}, \quad (21.113)$$

$$p = -\frac{1}{3} \frac{8}{81} \frac{4 + \frac{3}{2} Sp}{fC_1}. \quad (21.114)$$

From the comparison of the data by *Liu* and *Theofanous* (1995) for saturated liquid and different particle sizes we obtain correction function values around one.

$\bar{D}_3$	$f(\bar{D}_3)$
2.535	0.995
3.806	0.952
5.070	0.939
7.624	1.031

The natural instability length scale, the *Rayleigh-Taylor* wavelength, is used to normalize the particle size

$$\bar{D}_3 = D_3 / \lambda_{RT} . \quad (21.115)$$

For smaller values of  $\bar{D}_3$  of 2.535 we use  $\bar{D}_3 = 0.995$ . Finally the thermal power transferred by conduction through the vapor film per unit flow volume is

$$\dot{q}_{FB,nc}''' = \frac{F_3}{Vol} h_{nc,1} (T_{3\sigma} - T') . \quad (21.116)$$

Assuming that there is a vapor temperature profile automatically leads to the conclusion that there is some thermal power transfer into the vapor. We approximate this part

$$\dot{q}_{31,nc}''' = 0.3 Sp \frac{f + 3\xi}{f_{nc} (f + \xi)} \dot{q}_{FB,nc}''' , \quad (21.117)$$

For  $q^2 + p^3 < 0$  the layers thickness ratio is theoretically not defined. If using minimum film boiling theory strictly consistent with this work no further discussion is necessary. If not, e.g. empirical correlation for minimum film boiling is used, then we set

$$\dot{q}_{31,nc}''' = 0.3 Sp \dot{q}_{FB,nc}''' , \quad (21.118)$$

and  $f_{nc} = 1 + \frac{1}{2} Sp$ .

#### 21.2.4.3.2 Predominant forced convection

In earlier development *Vaeth* (1995) we used for this case the *Bromley-Witte* theory (1953, 1968),

$$\dot{q}_{FB,fc}''' = \frac{F_3}{Vol} h_{fc,1} (T_{3\sigma} - T') , \quad (21.119)$$

where

$$h_{fc,1} = \frac{\lambda_1}{D_3} 2.98 \left( \frac{Re_1}{Sp} \right)^{1/2} . \quad (21.120)$$

The comparison with the forced-convection film boiling data by *Liu and Theofanous* (1995) resulted in replacing this model by the model of *Epstein-Heuser* (1980):

$$h_{fc,1} = \frac{\lambda_1}{D_3} 0.60 \left( \frac{\rho_2}{\rho_1} \right)^{1/4} Re_1^{1/2} / Sp^{*1/4} \quad (21.121)$$

in which the constant is changed from 0.65 to 0.6. Again thermal power transfer into the vapor is approximated for  $D < 0$  by

$$\dot{q}_{31,fc}''' = 0.05 Sp \dot{q}_{FB,fc}''' \quad (21.122)$$

otherwise

$$\dot{q}_{31,fc}''' = 0.05 Sp \frac{f}{f_{fc}(f + \xi)} \dot{q}_{FB,fc}''' \quad (21.123)$$

Here

$$f_{fc} = \frac{f}{f + \xi} \left( 1 + \frac{1}{3} Sp \right) \quad (21.124)$$

is computed as Eq. (21.31) setting,  $C_2 = 0$ ,  $r_r = 0$ , and  $\xi$  is computed as for natural convection.

#### 21.2.4.3.3 Mixed convection

Mixed convection film boiling is known to exist in the region  $Fr \geq 0.2$ . For  $Fr < 0.2$  the natural-convection only solution

$$\dot{q}_{FB,0}''' = \dot{q}_{FB,nc}''' \quad (21.125)$$

$$\dot{q}_{31}''' = \dot{q}_{31,nc}''' \quad (21.126)$$

is the appropriate one. Otherwise, the approximation between natural- and forced-convection solutions is performed following *Liu and Theofanous (1995)*

$$\dot{q}_{FB,0}''' = \dot{q}_{FB,nc}''' \left[ 1 + \left( \frac{\dot{q}_{FB,fc}'''}{\dot{q}_{FB,nc}'''} \right)^5 \right]^{1/5} \quad (21.127)$$

$$\dot{q}_{31}''' = \dot{q}_{31,nc}''' \left[ 1 + \left( \frac{\dot{q}_{31,fc}'''}{\dot{q}_{31,nc}'''} \right)^5 \right]^{1/5} \quad (21.128)$$

Note that in the previous code development, *Vaeth (1995)*, we used

$$\dot{q}_{FB,0}''' = \max(\dot{q}_{FB,nc}''', \dot{q}_{FB,fc}''').$$

#### 21.2.4.3.4 Feedback of the radiation, subcooling and vapor heating on the vapor film conduction heat transfer

The experience with the plate solution is used here as a guideline. First we define the ratios

$$r_r = \frac{|\dot{q}_{r\sigma 2}'''| - \dot{q}_{\sigma 2}''' - \dot{q}_{31}'''}{\dot{q}_{FB,0}'''} , \quad (21.129)$$

$$r_r^* = \frac{1}{2} r_r , \quad (21.130)$$

influencing the film conduction through influencing the film thickness. Analytical solution of Eq.(21.84) is available for forced convection only,

$$x_{fc} = \sqrt{1 + r_r^{*2}} - r_r^* . \quad (21.131)$$

For natural convection Eq. (21.84) rewritten in the following form

$$x_{nc}^4 + r x_{nc}^3 + 1 = 0 \quad (21.132)$$

has to be solving by iteration. We start with the value for forced convection and iterate up to satisfying the equation with residuals less than 0.0001. Finally, we take the maximum of both values.

$$x = \max(x_{fc}, x_{nc}) , \quad (21.133)$$

$$\dot{q}_{FB}''' = C_{gas} x \dot{q}_{FB,0}''' . \quad (21.134)$$

The total thermal energy emitted by the interface of the particle is therefore

$$\dot{q}_{\sigma 3}''' = -\dot{q}_{FB}''' - \dot{q}_{31}''' - \dot{q}_{r1}''' - \dot{q}_{r2}''' - \dot{q}_{r\sigma 2}''' . \quad (21.135)$$

For implementation in computer codes it is important to check whether there is enough energy which has to be exhausted from the particles. The maximum of this energy can be defined as the energy required to heat up the particle from the liquid temperature to the actual particle temperature within the computational time step,

$$\dot{q}_{\sigma 3, \max}''' = \alpha_3 \rho_3 c_{p3} (T_{3\sigma} - T_2) / \Delta \tau . \quad (21.136)$$

Should the ratio  $f_{\max} = \dot{q}_{\sigma 3, \max}''' / \dot{q}_{\sigma 3}'''$  be larger than 1 the time step has to be corrected. If the time step is small enough we correct all components as follows  $\dot{q}_{fb}''' = \dot{q}_{fb}''' f_{\max}$ ,  $\dot{q}_{31}''' = \dot{q}_{31}''' f_{\max}$ ,  $\dot{q}_{r1}''' = \dot{q}_{r1}''' f_{\max}$ ,  $\dot{q}_{r2}''' = \dot{q}_{r2}''' f_{\max}$ ,  $\dot{q}_{r\sigma 2}''' = \dot{q}_{r\sigma 2}''' f_{\max}$ .

Finally the total film boiling heat transfer coefficient is

$$h_{FB} = -\dot{q}_{\sigma 3}''' / \left[ \frac{F_3}{Vol} (T_3 - T') \right] . \quad (21.137)$$

This definition is used for comparison with the experimental data. The energy crossing the liquid interface and entering the water bulk is composed of radiation and convective components

$$\dot{q}_{\sigma 2, total}''' = \dot{q}_{r2}''' + \dot{q}_{\sigma 2}''' . \quad (21.138)$$



Similarly the energy transferred from the particle into the gas film is composed by radiation and convective parts

$$\dot{q}_{3\sigma 1}''' = \dot{q}_{r1}''' + \dot{q}_{31}''' . \quad (21.139)$$

The energy jump condition at the liquid interface gives for the evaporated mass per unit time and unit flow volume the following expression

$$\mu_{21} = \frac{\dot{q}_{r\sigma 2}''' + \dot{q}_{FB}''' - \dot{q}_{\sigma 2}'''}{h'' - h'} . \quad (21.140)$$

#### 21.2.4.3.5 The interface temperature

The sphere interface temperature during film boiling may differ from the particle-averaged temperature, especially for large particles of poor heat conductors. The limitation come from the fact that only a limited amount can be supplied from the particle bulk to the particle surface. The analytical solution of the *Fourier* equation is the tool used here to estimate the interface temperature. The temperature profile is then averaged to estimate the averaged temperature and therefore the averaged temperature change during the time step. The task is to estimate the possible energy transfer due to the conditions during the time step considered and to compare it with that computed above. The final result is

$$T_{3\sigma} = T_3 + \dot{q}_{\sigma 3}''' / \omega_3 \quad (21.141)$$

where

$$\omega_3 = \alpha_3 \rho_3 c_{p3} \frac{\Delta \bar{T}_{3\sigma}}{\Delta \tau} \quad (21.142)$$

The averaged temperature difference is

$$\Delta \bar{T}_{3\sigma} = 1 - \frac{6}{\pi^2} \sum_{n=1}^{\infty} \frac{1}{n^2} / \exp\left(n^2 \frac{\Delta \tau}{\Delta \tau_3}\right), \quad (21.143)$$

where

$$\Delta \tau_3 = \frac{D_3^2}{4\pi^2 a_3} \quad (21.144)$$

is the time constant of the heat conduction into the spherical particle. The converging *Fourier* series is computed using  $n$  as big as necessary (but no larger than 100) to obtain improvement in the summation less than 0.00001. Because  $\dot{q}_{\sigma 3}'''$  is a function of the interface temperature itself some iterations may be required to finally obtain the released power density.

### 21.2.4.3.6 Averaged film thickness in the multiphase flows

To demonstrate the importance of the averaged film thickness in the multi-phase analysis, consider the question how much vapor is associated in the film and how much is in bubble form. The heat and mass transfer processes at the particle interface are completely described in the case of film boiling by the method presented already. The remaining part in bubble form is subject to additional water/vapor heat and mass transfer which will not be considered here. Analysis of the QUEOS *Kolev* (1996) experiments demonstrates that at the initial phase of penetration of hot particles in water almost the entire generated vapor is in the film. That means no additional vapor/water heat and mass transfer has to be modeled. For the later phase of interaction it starts to be active.

We approximate the averaged film thickness as follow. For  $\Delta V_{23} < 0.001$  we have natural-circulation film boiling leading to

$$\delta_{1F} = \delta_{1F,nc} = \left[ \frac{2D_3^2 \mu_{21} \eta_1}{\alpha_3 g \rho_1 (\rho_2 - \rho_1)} \right]^{1/3} \quad (21.145)$$

otherwise

$$\delta_{1F} = \delta_{1F,fc} = \frac{2}{9} \frac{D_3^2 \mu_{21}}{\alpha_3 \rho_1 \Delta V_{23}} \quad (21.146)$$

with the limitation

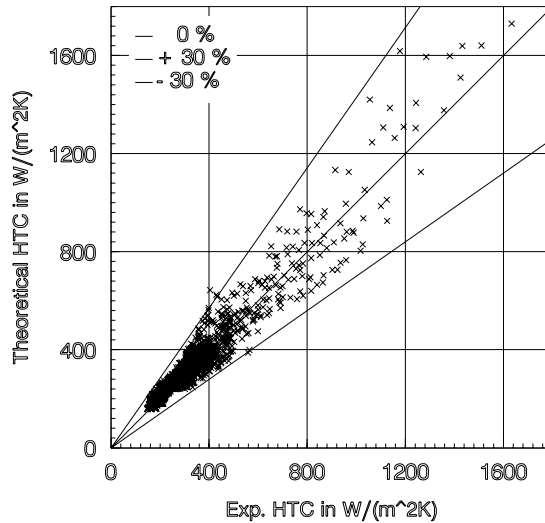
$$\delta_{1F} = \min(\delta_{1F,nc}, \delta_{1F,fc}). \quad (21.147)$$

## 21.2.5 Data comparison

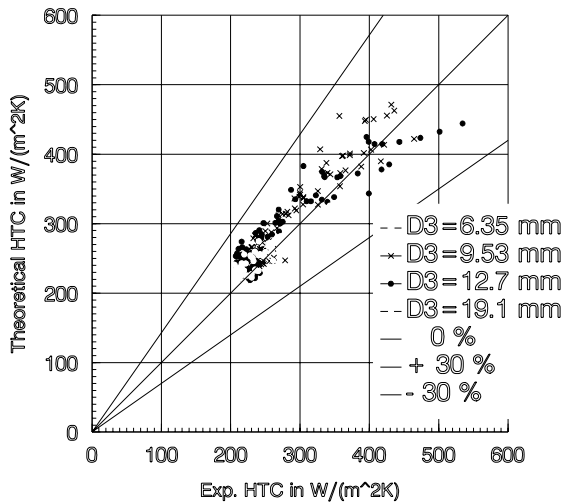
The sphere film boiling model presented here is implemented in the computer code IVA5. More information about the history of this development and the recent state is available in *Kolev* (1995) and *Kolev* (1996). This model is used for the data comparisons presented below. The new experimental data base provided by *Liu* and *Theofanous* in 1995 consists of single- and two-phase flow data. The single-phase data covers subcooling from 0 to 40 K, liquid velocity from 0 to 2.3 m/s, sphere superheat from 200 to 900 K and sphere diameter from 6 to 19 mm. The two-phase data are obtained for (a) upward flow having void fraction from 0.2 to 0.65, water velocity from 0.6 to 3.2 m/s, and steam velocity from 3 to 9 m/s, and (b) for downward flow having void fraction from 0.7 to 0.95, water velocity from 1.9 to 6.5 m/s, and steam velocity from 1.1 to 9 m/s.

Figure 21.4 presents the comparison between the predicted and calculated heat transfer coefficients for all data, *Kolev* (1997). The error band is found to be  $\pm 30\%$ . Figure 21.5 presents the comparison between the predicted and calculated heat transfer coefficients for single-phase saturated water and four different sphere diameters. The error band for this subset of data is found to be +20 to -15%. Figure 21.6

presents the comparison between the predicted and calculated heat transfer coefficients for subcooled water and 12.7 mm sphere diameter. The error band for this subset of data is found to be +20 to -30%.



**Fig. 21.4** Comparison between predicted and calculated heat transfer coefficients for all data. Error band:  $\pm 30\%$



**Fig. 21.5** Comparison between predicted and calculated heat transfer coefficients for single-phase saturated water and four different sphere diameters. Error band : +20 to - 15%

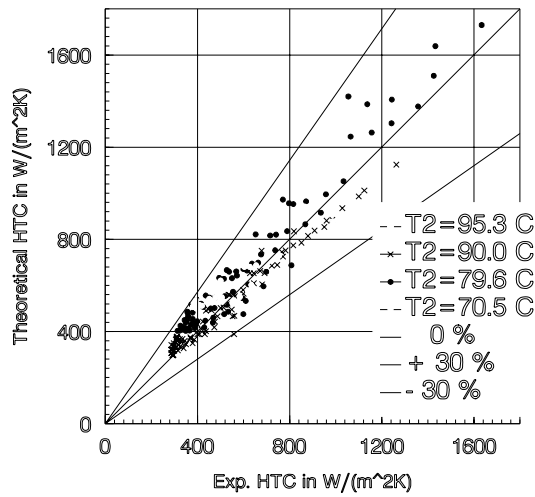


**Fig. 21.6** Comparison between predicted and calculated heat transfer coefficients for subcooled water and 12.7 mm sphere diameter. Error band: +20 to - 30%.

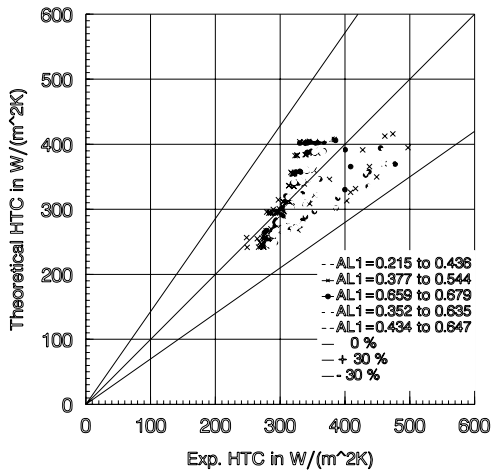


**Fig. 21.7** Comparison between the predicted and calculated heat transfer coefficients for saturated upward two phase flow, 12.7 mm sphere diameter, void fraction from 0.2 to 0.65, water velocity from 0.6 to 3.2 m/s, and steam velocity from 3 to 9 m/s. Error band: +30 to -20%

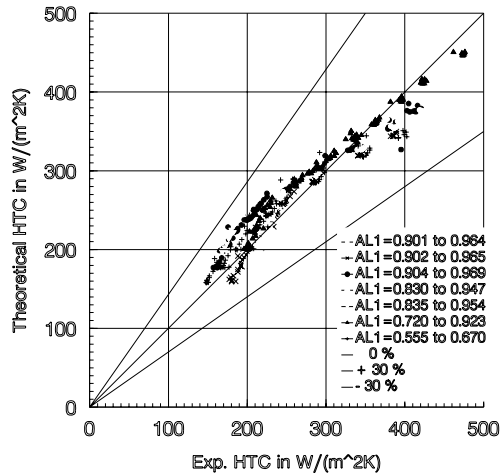


**Fig. 21.8** Comparison between the predicted and calculated heat transfer coefficients for saturated downward two phase flow, 12.7 mm sphere diameter, void fraction from 0.7 to 0.95, water velocity from 1.9 to 6.5 m/s, and steam velocity from 1.1 to 9 m/s. Error band: +20 to -20%

Figure 21.7 presents the comparison between the predicted and calculated heat transfer coefficients for saturated upward two-phase flow, 12.7 mm sphere diameter, void fraction from 0.2 to 0.65, water velocity from 0.6 to 3.2 m/s, and steam velocity from 3 to 9 m/s. The error band for this subset of data is found to be +30 to -20%.

Figure 21.8 presents the comparison between the predicted and calculated heat transfer coefficients for saturated downward two-phase flow, 12.7 mm sphere diameter, void fraction from 0.7 to 0.95, water velocity from 1.9 to 6.5 m/s, and steam velocity from 1.1 to 9 m/s. The error band for this subset of data is found to be +20 to -20%.

### 21.2.6 Conclusions

The semi-empirical film boiling model used in IVA5 computer code predicts the data base provided by *Liu* and *Theofanous* within  $\pm 30\%$ .

## Appendix 21.1 Natural convection at vertical plate

From Eq. (21.31) the local vapor film thickness as a function of the axial coordinate for natural-convection film boiling at a vertical plate is then obtained

$$\frac{1}{\delta_1} = \frac{1}{2} \left[ \frac{\rho_1 \Delta h \Delta \rho g}{\lambda_1 \Delta T_{sp} \eta_1 z} f_{nc} \right]^{1/4} \quad (\text{A21.1-1})$$

The film boiling heat flux averaged over the height  $\Delta z$  is therefore

$$\begin{aligned} \dot{q}_{FB}'' &= \frac{1}{\Delta z} \int_0^{\Delta z} \lambda_1 \frac{\Delta T_{sp}}{\delta_1} dz = \Delta T_{sp} \frac{1}{2} \left[ \frac{\lambda_1^3 \rho_1 \Delta h \Delta \rho g}{\Delta T_{sp} \eta_1} f_{nc} \right]^{1/4} \frac{1}{\Delta z} \int_0^{\Delta z} dz / z^{1/4} \\ &= \Delta T_{sp} \frac{2}{3} \left[ \frac{\lambda_1^3 \rho_1 \Delta h \Delta \rho g}{\Delta T_{sp} \eta_1 \Delta z} f_{nc} \right]^{1/4} \end{aligned} \quad (\text{A21.1-2})$$

The heat transfer coefficient is

$$h_{nc} = c_{nc} \left[ \frac{\lambda_1^3 \rho_1 \Delta h \Delta \rho g}{\Delta T_{sp} \eta_1 \Delta z} f_{nc} \right]^{1/4} \quad (\text{A21.1-3})$$

where

$$c_{nc} = 2/3. \quad (\text{A21.1-4})$$

Equation (A21.1-3) for  $f_{nc}=1$  reduces to the *Nusselt* equation for laminar film condensation at a cold wall *Nusselt* (1916) with correspondingly inverted subscripts.

## Appendix 21.2 Predominant forced convection only at vertical plate

Consider the predominant forced-convection film boiling at a vertical plate. Neglecting the natural convection terms as small against the predominant forced convection terms in Eq. (21.31), the following is then obtained

$$\frac{1}{\delta_1} = \frac{1}{2} \left[ \frac{\rho_1 \Delta h w_2}{\lambda_1 \Delta T_{sp} z} f_{fc} \right]^{1/2} \quad (\text{A21.2-1})$$

The film boiling heat flux averaged over the height  $\Delta z$  is therefore

$$\begin{aligned} \dot{q}_{FB}'' &= \frac{1}{\Delta z} \int_0^{\Delta z} \lambda_1 \frac{\Delta T_{sp}}{\delta_1} dz = \Delta T_{sp} \frac{1}{2} \left[ \frac{\rho_1 \lambda_1 \Delta h w_2}{\Delta T_{sp}} f_{fc} \right]^{1/2} \frac{1}{\Delta z} \int_0^{\Delta z} dz / z^{1/2} \\ &= \Delta T_{sp} \left[ \frac{\rho_1 \lambda_1 \Delta h w_2}{\Delta T_{sp} \Delta z} f_{fc} \right]^{1/2} \end{aligned} \quad (\text{A21.2-2})$$

The heat transfer coefficient is

$$h_{fc} = c_{fc} \left[ \frac{\rho_1 \lambda_1 \Delta h w_2}{\Delta T_{sp} \Delta z} f_{fc} \right]^{1/2} \quad (\text{A21.2-3})$$

where

$$c_{fc} = 1. \quad (\text{A21.2-4})$$

## Nomenclature

$a_1$	$= \frac{\lambda_1}{\rho_1 c_{p1}}$ , vapor temperature diffusivity, $m^2/s$
$a_2$	$= \frac{\lambda_2}{\rho_2 c_{p2}}$ , liquid temperature diffusivity $m^2/s$
$a_3$	$= \frac{\lambda_3}{\rho_3 c_{p3}}$ , particle temperature diffusivity, $m^2/s$
$C_1$	$= \frac{\lambda_1}{\lambda_2} \frac{v_1}{v_2} \frac{c_{p2} \Delta T_{sp}}{\Delta h}$ , superheat property number, -
$C_2$	$= \frac{\lambda_2 \Delta T_{sc}}{\lambda_1 \Delta T_{sp}}$ , superheat to subcooling ratio, -
$C_3$	$= \frac{\rho_2 \lambda_1}{\rho_1 \lambda_2} \frac{c_{p2} \Delta T_{sp}}{\Delta h} = \frac{a_1}{a_2} Sp$ , superheat property number, -
$c_{p1}$	vapor specific heat at constant pressure, $J/(kgK)$
$c_{p2}$	liquid specific heat at constant pressure, $J/(kgK)$
$c_{nc}$	numerical constant for heat transfer coefficient for pure natural convection, -
$c_{fc}$	numerical constant for heat transfer coefficient for pure forced convection,
$Fr$	$= \frac{ \Delta V_{23} }{\sqrt{g D_3}}$ , Froude number for sphere, -
$Fr_2$	$= \frac{w_2}{\sqrt{2 R_3 g}}$ , Froude number for sphere and cylinder, -
$Fr_2$	$= \frac{w_2}{\sqrt{\Delta z g}}$ , Froude number for vertical plane, -

- $f = \eta_2 / \eta_1$ , dynamic viscosity ratio, -  
 $Gr_1 = g(2R_3)^3 \rho_1 (\rho_2 - \rho_1) / \eta_1^2$ , *Grashoff* number for sphere and cylinder, -  
 $Gr_1 = g\Delta z^3 \rho_1 (\rho_2 - \rho_1) / \eta_1^2$ , *Grashoff* number for vertical plane, -  
 $Gr_2 = gD_3^3 \left| \frac{T' - T_2}{T_2} \right| \left( \frac{\rho_2}{\eta_2} \right)^2$ , *Grashoff* number for sphere, -  
 $g$  acceleration due to gravity,  $m/s^2$   
 $h$  heat transfer coefficient,  $W/(m^2K)$   
 $h_{nc}$  heat transfer coefficient for pure natural convection,  $W/(m^2K)$   
 $h_{fc}$  heat transfer coefficient for pure forced convection,  $W/(m^2K)$   
 $\dot{q}_{FB}''$  heat flux due to conduction through the vapor film,  $W/m^2$   
 $\dot{q}_{3\sigma 1}''$  heat flux from the wall into the vapor due to convective heating of the vapor from the saturation interface temperature to an averaged vapor film temperature,  $W/m^2$   
 $\dot{q}_{\sigma 2}''$  heat flux from the liquid interface into the liquid due to convection,  $W/m^2$   
 $\dot{q}_{r2}''$  radiation heat flux from the wall into the bulk liquid,  $W/m^2$   
 $\dot{q}_{3\sigma}''$  total heat flux from the wall,  $W/m^2$   
 $\dot{q}_{r\sigma 2}''$  radiation heat flux absorbed from the vapor-liquid interface,  $W/m^2$   
 $\dot{q}_{r1}''$  radiation heat flux from the interface into the vapor,  $W/m^2$   
 $Pr_1 = \frac{\eta_1 c_{p1}}{\lambda_1}$ , vapor *Prandtl* number, -  
 $Pr_2 = \frac{c_{p2} \eta_2}{\lambda_2}$ , liquid *Prandtl* number, -  
 $R_3$  radius of sphere or cylinder,  $m$   
 $Re_1 = \rho_1 \Delta w_{23} 2R_3 / \eta_1$ , *Reynolds* number, -  
 $Re_2 = |\Delta V_{23}| D_3 \rho_2 / \eta_2$ , liquid *Reynolds* numbers, -  
 $r^* = \left( \frac{h_{fc} c_{nc}}{h_{nc} c_{fc}} \right)^2 / 2 = \frac{2}{9} r^2$ , -  
 $r = h_{fc} / h_{nc}$ , -  
 $r_r = \frac{\dot{q}_{r\sigma 2}''}{\lambda_1 \Delta T_{sp} / \delta_1}$ , ratio of the radiation heat flux to the conduction heat flux  
 for plates, -  
 $r_r = \frac{|\dot{q}_{r\sigma 2}''' - \dot{q}_{\sigma 2}''' - \dot{q}_{31}'''|}{\dot{q}_{FB,0}'''}$ , for spheres, -  
 $r_r^* = \frac{1}{2} r_r$ , for spheres, -



$r_1$	distance from the wall, $m$
$r_2$	distance from the interface, $m$
$Nu$	$= h2R_3 / \lambda_1$ , <i>Nusselt</i> number for sphere and cylinder,
$Nu$	$= h\Delta z / \lambda_1$ , <i>Nusselt</i> number for vertical plane,
$p$	pressure, $Pa$
$p_M$	partial vapor pressure in a mixture of vapor and inert components, $Pa$
$Sp$	$= c_{p1}\Delta T_{sp} / \Delta h$ , superheat number, -
$Sp^*$	$= \frac{c_{p1}(T_{\sigma 3} - T')}{\Delta h * Pr_1}$ , modified superheat number, -
$T_2$	liquid temperature, $K$
$T_{3\sigma}$	temperature at the wall surface, $K$
$T'(p)$	vapor-liquid interface temperature equal to the saturation temperature of the liquid at the system pressure, $K$
$w_1(r_1)$	vapor film velocity as a function of the distance from the wall, $m/s$
$w_2(r_2)$	liquid boundary layer velocity as function of the distance from the interface, $m/s$
$z$	axial coordinate, $m$
$\langle \rangle_1$	$= \frac{1}{\delta_1} \int_0^{\delta_1} dr_1$ , cross-section average, -
$\alpha_1$	gas volume fraction in three-phase flow, -
$\alpha_2$	water volume fraction in three-phase flow, -
$\alpha_3$	volume fraction in three-phase flow, -
$\Delta T_{sp}$	$T_{3\sigma} - T'$ , wall superheat, $K$
$\Delta T_{sc}$	$T' - T_2$ , liquid subcooling, $K$
$\Delta h$	latent heat of evaporation, $J/kg$
$\Delta h^*$	$= (h'' - h') \left( 1 + \frac{1}{2} Sp \right)$ , modified latent heat of evaporation, $J/kg$
$\Delta z$	total height of the wall, $m$
$\Delta w_{12}$	vapor film - liquid velocity difference, $m$
$\Delta \theta$	infinitesimal change of the angular coordinate, $rad$
$\delta_1(z)$	vapor layer thickness as a function of the axial coordinate, $m$
$\delta_2(z)$	liquid boundary layer thickness as a function of the axial coordinate, $m$
$\delta_1(\theta)$	vapor layer thickness as a function of the angular coordinate, $m$
$\delta_2(\theta)$	liquid boundary layer thickness as a function of the angular coordinate, $m$
$\eta_1$	dynamic viscosity of vapor, $Pa \cdot s$

$\eta_2$	dynamic viscosity of liquid, $Pa\ s$
$\rho_1$	density of vapor, $kg/m^3$
$\rho_2$	density of liquid, $kg/m^3$
$(\rho w)_{21}$	evaporation mass flow rate, $kg/m^2$
$\sigma$	surface tension, $N/m$
$\omega_2$	heat transport coefficient liquid bulk/liquid surface, $W/(Km^3)$
$\omega_3$	heat transport coefficient particle bulk/particle surface, $W/(Km^3)$
$\theta$	angular coordinate, $rad$
$\lambda_{KH}$	<i>Kelvin-Helmholtz</i> instability wavelength, $m$
$\lambda_{RT}$	$= \sqrt{\frac{\sigma_2}{g(\rho_2 - \rho_1)}}$ , <i>Rayleigh- Taylor</i> wavelength, $m$
$\xi$	$= \delta_2 / \delta_1$ , film thickness ratio, -

### Subscripts

$nc$	natural convection
$fc$	forced convection
$l$	laminar
$t$	turbulent
$1$	gas
$2$	water
$3$	particles
$mn$	from field $m$ to field $n$
$FB$	film boiling
$\sigma$	surface

### References

- Achenbach E (1993) Heat and flow characteristics of packed beds, *Experimental Heat Transfer, Fluid Mechanics and Thermodynamics*, Kelleher MD et al. (eds.) Elsevier, pp 287-293
- Analytis GT, Yadiragolu G (Oct. 15-18, 1985) Analytical modeling of IAFB, Proc. of the Third Int. Topical Meeting on Reactor Thermal Hydraulics, Newport, Rhode Island, USA, Chiu C and Brown G (eds) vol 1 paper no 2.B
- Bromley LA (1950) Heat transfer in stable film boiling, *Chem. Eng. Prog.*, vol 46 no 5 pp 221-227
- Bromley LA (Dec. 1952) Effect of heat capacity of condensate, *Industrial and Engineering Chemistry*, vol 44 no12 pp 2966-2969
- Bromley LA, LeRoy NR, Rollers JA (Dec. 1953) Heat transfer in forced convection film boiling, *Industrial and Engineering Chemistry*, vol 45 pp 2639-2646

- Bui TD, and Dhir VK (November 1985) Film boiling heat transfer on isothermal vertical surface. ASME Journal of Heat Transfer, vol 107 pp 764-771
- Coury GE, Dukler AE (1970) Turbulent film boiling on vertical surfaces - A study including the interface waves, 4th International Heat Transfer Conference, Paper no B.3.6
- Dhir VK, Purohit GP (1978) Subcooled film-boiling heat transfer from spheres, Nuclear Engineering and Design, vol 47 pp 49 - 66
- Epstein M, Heuser GM (1980) Subcooled forced-convection film boiling in the forward stagnation region of a sphere or cylinder, Int. J. Heat Mass Transfer, vol 23 pp 179-189
- Fodemski TR (1992) Forced convection film boiling in the stagnation region of molten drop and its application to vapor explosions, Int. J. Heat Mass Transfer, vol 35 pp 2005-2016
- Fodemski TR, Hall WB (1982) Forced convection film boiling on a sphere immersed in (a) sub-cooled or (b) superheated liquid, Proc. 7th Int. Heat Transfer Conference, Muenchen, vol 4 pp 375 - 739
- Frederking THK, Chapman RC, Wang S (1965) Heat transport and fluid motion during cooldown of single bodies to low temperatures, International Advances in Cryogenic Engineering, Timmerhaus KD (ed) Plenum Press, New York, pp 353-360
- Gnielinski V (1978) Gleichungen zur Berechnung des Waerme und Stoffaustausches in durchstroemten ruhenden Kugelschuettingen bei mittleren und grossen Pecletzahlen. Verfahrenstechnik, vol 12 pp 363-366
- Kolev NI (1998) Film boiling on vertical plates and spheres, Experimental Thermal and Fluid Science, vol 18 (1998) pp 97-115
- Kolev NI (19th-21st May 1997) Verification of the IVA4 film boiling model with the data base of Liu and Theofanous, Proceedings of OECD/CSNI Specialists Meeting on Fuel-Coolant Interactions (FCI), JAERI-Tokai Research Establishment, Japan
- Kolev NI (27-29 September 1995) IVA4 Computer code: An universal analyzer for multi-phase flows and its applicability to melt water interaction, Proc. of the Technical committee meeting on advances in and experiences with accidents consequences analysis, held at Vienna, Austria, IAEA-TC-961, Vienna, Austria
- Kolev NI (April 3-7 1995) IVA4 Computer code: The model for film boiling on a sphere in subcooled, satutated and superheated water, Proc. Second Int. Conference On Multiphase Flow, Kyoto, Japan. Presented also in (14-15 Nov. 1994) "Workshop zur Kuehlmittel/Schmelze - Wechselwirkung", Koeln, Germany
- Kolev NI (June 2-6, 1997) Film boiling: vertical plates, Proceedings of 4th World Conference on Experimental Heat Transfer, Fluid Mechanics and Thermodynamics EXHFT 4, Brussels, Belgium
- Kolev NI (October 15-16, 1996) Three fluid modeling with dynamic fragmentation and coalescence fiction or daily practice? 7th FARO Experts Group Meeting Ispra. (5th-8th November 1996) Proceedings of OECD/CSNI Workshop on Transient thermal-hydraulic and neutronic codes requirements, Annapolis, MD, USA. (June 2-6, 1997) 4th World Conference on Experimental Heat Transfer, Fluid Mechanics and Thermodynamics, ExHFT 4, Brussels. (June 22-26, 1997) ASME Fluids Engineering Conference & Exhibition, The Hyatt Regency Vancouver, Vancouver, British Columbia, CANADA, Invited Paper
- Langzenberger K (1997) Radiation models for multi-phase flows. Part 1: Film boiling, Siemens report 1997, KWU NA-M/97/E024

- Liu C, Theofanous TG (August 1995) Film boiling on spheres in single- and two-phase flows Part 1: Experimental Studies ANS Proceedings, Part 2: A Theoretical Study, National Heat Transfer Conference, Portland
- Meyer L, Schumacher G (April 1996) QUEOS a simulation-experiment of the premixing phase of steam explosion with hot spheres in water base case experiments, Forschungszentrum Karlsruhe Technik und Umwelt, Karlsruhe, Wissenschaftliche Berichte FZKA 5612
- Nigmatulin NI et al. (1994) Interface oscillations and heat transfer mechanism at film boiling, Proc. of the Tenth International Heat Transfer Conference, Brighton, UK
- Nishikawa K, Ito T (1966) Two-phase boundary-layer treatment of free convection film boiling, Int. J. Heat Mass Transfer, vol 9 pp 103-115
- Nishikawa K, Ito T, Matsumoto K (1976) Investigation of variable thermophysical Property problem concerning pool film boiling from vertical plate with prescribed uniform temperature, Int. J. Heat Mass Transfer, vol 19 pp 1173-1182
- Nishio S, Ohtake H (1993) Vapor film unit model and heat transfer correlation for natural convection film boiling with wave motion under subcooled conditions. Int. J. Heat Mass Transfer, vol 36 no 10 pp 2541-2552
- Nusselt WZ (1916) Z. Ver. deut. Ing., vol 60 pp 541-569
- Okkonen T et al (August 3-6, 1996) Film boiling on a long vertical surface under high heat flux and water subcooling conditions, Proc. of the 31st Nat. Heat Transfer Conference, Houston, Texas
- Sakurai A (1990) Film boiling heat transfer, Proc. of the Ninth Intern. Heat Transfer Conference, Jerusalem, Israel, Hetstroni G (ed), vol 1 pp 157 - 187
- Sakurai A, Shiotsu M, Hata K (1986) Effect of subcooling on film boiling heat transfer from horizontal cylinder in a pool water, Proc. 8th Int. Heat Transfer Conf., vol 4 pp 2043 - 2048
- Sparrow EM (1964) The effect of radiation on film boiling heat transfer, Int. J. Heat and Mass Transfer, vol 7 pp 229 - 238
- Suryanarayana NV, Merte H (1972) Film boiling on vertical surfaces, J. Heat Transfer, vol 94 pp 337-383
- Vaeth L (March 1995) Radiative heat transfer for the transient three phase three component flow model IVA3, Kernforschungszentrum Karlsruhe GmbH, INR, Interner Bericht 32.21.02/10A, INR-1914, PSF-3212
- Witte LC (August 1968) Film boiling from a sphere, I&EC Fundamentals, vol 7 no 3 pp 517-518

## 22 Liquid droplets

### 22.1 Spontaneous condensation of pure subcooled steam – nucleation

Consider steam at local temperature  $T_1$  and local static pressure  $p$ . The saturation temperature at the system pressure is

$$T' = T'(p). \quad (22.1)$$

The saturation pressure as a function of the steam temperature is

$$p' = p'(T_1). \quad (22.2)$$

The subcooling is defined as a temperature difference

$$\Delta T_{1,sub} = T'(p) - T_1. \quad (22.3)$$

For steam temperature larger than the saturation temperature there is no condensation. One expects intuitively condensation if the local steam temperature is lower than the saturation temperature at the system pressure, that is if

$$\Delta T_{1,sub} > 0. \quad (22.4)$$

The originating nucleus releases energy at saturation temperature  $T'(p)$ . The released energy is then transferred into the subcooled vapor acting toward reducing subcooling and toward stopping condensation. Therefore, in nature subcooling is a necessary condition to observe condensation. The condensation itself starts around a preferred number of points in the unit volume  $n_3$ . Around these points the predominantly low energy molecules form microscopic drops called activated clusters - nucleus with size  $R_3$ . Very small clusters are not stable and degrade spontaneously. Clusters with larger sizes may become stable. Intuitively we expect increasing origination frequency of clusters if the subcooling of the vapor is larger. We also intuitively cannot imagine that arbitrary large meta-stable subcooling is sustainable in nature.

In order to describe nucleation it is necessary to answer the following questions:

- a) what is the nucleation size separating the stable from the unstable clusters,
- b) how does nucleation site density depend on the subcooling, and
- c) what is the maximum allowable subcooling in the steam.

The purpose of this Section is to give answers to these questions for pure vapors.

### 22.1.1 Critical nucleation size

The considerations leading to estimate of the critical nucleation size, probably first formulated by *Gibbs* in 1878, will be next summarized. Consider a subcooled non-stable spherical steam volume, which is just about forming a nucleus, having an initial radius  $R_{30}$ , and volume  $\frac{4}{3}\pi R_{30}^3$ , pressure  $p$ , temperature  $T_1$ , and density  $\rho_1 = \rho_1(p, T_1)$ . Note that this density is computed for unstable steam. For practical application attention should be paid to this point because usually the state equation is obtained for stable fluids and an extrapolation into the unstable region is not straightforward for all approximations of the equation of state. During the origination of the nucleus the sphere collapse from the initial radius to  $R_3$ , that is to the volume  $\frac{4}{3}\pi R_3^3$ . The final state is characterized by the same temperature  $T_1$  but the state is stable, that is, the local pressure inside the nucleus is  $p' = p'(T_1)$ . Because of the small nucleus size the pressure inside is considered to be uniform. The density is therefore  $\rho' = \rho'(T_1)$ . During the origination of the nucleus the initial and the end mass are the same. Therefore

$$\left(\frac{R_{30}}{R_3}\right)^3 = \frac{\rho'(T_1)}{\rho_1}. \quad (22.5)$$

Thus the initial volume of the sphere is changed by

$$\frac{4}{3}\pi(R_3^3 - R_{30}^3) = \frac{4}{3}\pi R_3^3 \left[1 - \frac{\rho'(T_1)}{\rho_1}\right]. \quad (22.6)$$

Volume reduction requires mechanical work. The amount of this work

$$\begin{aligned} 4\pi \int_{R_{30}}^{R_3} [p'(T_1) - p] r^2 dr &\approx \frac{4}{3}\pi(R_3^3 - R_{30}^3)[p'(T_1) - p] \\ &= \frac{4}{3}\pi R_3^3 \left[1 - \frac{\rho'(T_1)}{\rho_1}\right] [p'(T_1) - p] \end{aligned} \quad (22.7)$$

is reducing the internal energy of sphere. The initial sphere interface was not a real one. The final sphere interface is a real one. The interface is a prominent

characteristic of the origination of new liquid phase inside the steam. This well-defined surface requires additional mechanical work

$$4\pi \int_0^{R_3} \frac{4\sigma}{r} r^2 dr = 4\pi R_3^2 \sigma \quad (22.8)$$

to be created. The surface tension  $\sigma$  is a function of the local temperature which may strongly vary during transient processes. It is usually measured at macroscopic droplets. Whether the so obtained information is still valid for a very small nucleus is not clear. We will assume that the so measured surface tension holds also for very small droplets. One example of the dependence of the surface tension on the temperature is given here for water surrounded by its steam,

$$\sigma = 0.2358(1 - T_3 / T_c)^{1.256} [1 - 0.625(1 - T_3 / T_c)], \quad (22.9)$$

*Lienhard.* We see that if the droplet surface approaches the critical temperature for water,  $T_{c,H_2O} = 647.2K$ , the surface tension diminishes. Within the region 366 to 566 K the above equation can be approximated by

$$\sigma = 0.14783(1 - T_3 / T_c)^{1.053} \quad (22.10)$$

with an error of  $\pm 1\%$ .

Thus the work required to create a single nucleus

$$\Delta E_3 = 4\pi R_3^2 \sigma - \frac{4}{3} \pi R_3^3 \left( 1 - \frac{\rho'(T_1)}{\rho_1} \right) [p'(T_1) - p] = 4\pi \sigma \left( R_3^2 - \frac{2}{3} \frac{R_3^3}{R_{3c}} \right), \quad (22.11)$$

where

$$R_{3c} = 2\sigma / \left\{ \left[ 1 - \frac{\rho'(T_1)}{\rho_1} \right] [p'(T_1) - p] \right\}, \quad (22.12)$$

possesses a maximum at

$$\Delta E_{3c} = \frac{4}{3} \pi \sigma R_{3c}^2, \quad (22.13)$$

"...which does not involve any geometrical magnitudes", see Gibbs 1878. Equation (22.12) is known in the literature as the *Laplace* and *Kelvin* equation. Clusters with sizes smaller than the critical one are unstable and disappear quickly after creation absorbing the excess energy from the surrounding vapor. Droplets with sizes larger than the critical one remain stable and release heat into the surrounding vapor. Obviously to create a nucleus a deficiency of internal energy of the steam is necessary which has to be greater than the critical energy. The energy required to create a stable nucleus with critical size divided by the vapor temperature defines the entropy change of the system between the initial and final state.

$$\Delta S_{13c} = \Delta E_{3c} / T_1 . \quad (22.14)$$

The entropy change is made dimensionless by dividing by the *Boltzmann* constant  $k = 13.805 \times 10^{-24}$ . The resulting dimensionless number

$$Gb_1 = \frac{\Delta E_{3c}}{kT_1} , \quad (22.15)$$

is called the *Gibbs* number and is frequently used in the literature as a measure of the subcooling. We see that the larger the subcooling the smaller the *Gibbs* number. Two consequences of Eqs. (22.12 to 22.15) are of practical importance.

a) If the steam temperature approaches the critical temperature the surface tension diminishes and therefore the energy required for creation of a nucleus is zero, which means that all molecules are nuclei for themselves and the origination of liquid inside the steam is impossible. The *Gibbs* number in this case is also equal to zero.

b) Rapid decompression can lead to large subcooling. The maximum possible subcoolings experimentally observed are in the range of *Gibbs* numbers from 6.8 to 9.6, *Skripov* et al. (1980), p. 136. It follows from the Eqs. (22.12 to 22.14)

$$p'(T_{1,spin}) - p = (1.57 \text{ to } 1.32) \frac{\sigma^{3/2}}{(kT_{1,spin})^{1/2} \left( 1 - \frac{\rho'(T_{1,spin})}{\rho_1(p, T_{1,spin})} \right)} . \quad (22.16)$$

This equation is known as the *Furth* equation (1941). It describe a dependence in the  $p, T$ -plane called a *spinoidal line*.

### 22.1.2 Nucleation kinetics, homogeneous nucleation

Origination of nucleation clusters within the steam is called homogeneous nucleation. It has to be distinguished from the so called heterogeneous nucleation. In the heterogeneous nucleation the origination of the liquid drops happens at the surfaces of other materials, e.g. walls, solid particles etc. Statistical thermodynamics provides the mathematical tools for the derivation of an equation defining the generated nucleus per unit volume and unit time,  $\dot{n}_{3,kin}$ , as a function of the local parameters. If we observe over the time  $\Delta\tau$  a point in the space occupied by subcooled vapor, we will see that the stronger the subcooling the more frequently the system departs from the averaged state. With other words over an integral time  $\Delta\tau_{13}$  the system is outside of the averaged state. *Volmer* (1939) p.81 following *Boltzman* and *Einstein* defined the probability of departure from the averaged state as  $\Delta\tau_{13}/\Delta\tau$  and assumed that this probability is proportional to  $\exp(-Gb_1)$ , that is



$$\Delta \tau_{13} / \Delta \tau = \exp(-Gb_1). \quad (22.17)$$

This mathematical expression says that the smaller the needed entropy change for a departure from the averaged state, the higher the probability of its occurrence. The probability of departure from the averaged state is usually set equal to the probability of origination of a single nucleus, that is

$$\frac{\text{nucleation\_frequency}}{\text{molecular\_colisions\_frequency}} = \exp(-Gb_1). \quad (22.18)$$

*Zeldovich* (1962) obtained the final expression for the generated nuclei per unit volume and unit time in the form

$$\dot{n}_{3,kin} = c_T Ze_1 \left( \frac{1}{4} N_1 a_1 F_{3c} \right) N_1 \exp(-Gb_1), \quad (22.19)$$

- see also in *Fieder* et al. (1966). The assumptions used to derive this expression are at the same time the limitation of the model as discussed by *Ehrler* in VDI (1984):

- a) The clusters are distributed in the vapor and are assumed to have a degree of freedom characteristic for big molecules in the vapor;
- b) The nuclei are solid non-oscillating spheres with respect to the center of the mass of the system;
- c) Macroscopic properties like density and surface tension are applicable to clusters having sizes of the order of nanometers.

Here the nucleation frequency per unit volume is considered as proportional to the number of the clusters with critical size originating per unit time and unit volume,  $N_1 \exp(-Gb_1)$ , and the number of the molecules striking the cluster,  $\frac{1}{4} N_1 a_1 F_{3c}$ , and remaining there  $c_c \frac{1}{4} N_1 a_1 F_{3c}$ . The proportionality factor was found to be  $c_T Ze_1$ , where

$$Ze_1 = \sqrt{\frac{Gb_1}{3\pi n_{3c}^2}} \quad (22.20)$$

is the so called *Zeldovich* number (1942) and  $c_T$  is the so called temperature correction factor taking into account the heat transfer from the nucleus to the surrounding vapor. For pure water steam  $c_T \approx 0.001$ . The components of these two expressions are computed as follows. The molecular mass,  $m_\mu$ , and the *Avogadro* number,  $N_A = 6.02 \times 10^{23}$ , uniquely define the mass of a single molecule  $m_1 = m_\mu / N_A$ . The number of the vapor molecules per unit volume is therefore  $N_1 = \rho_1 / m_1$ . The thermal velocity of the vapor molecules is defined by

$$a_1 = \sqrt{\frac{8}{\pi}} R_1 T_1. \quad (22.21)$$

After its origination the surface  $F_{3c}$  of the cluster is struck by the following number of molecules per unit time  $\frac{1}{4} N_1 a_1 F_{3c}$ . Only a part of them,  $c_c \frac{1}{4} N_1 a_1 F_{3c}$  remain there, where  $c_c \approx 0.1$  for water-steam plus non-condensable gases, and  $c_c \approx 0.5$  to 1, for pure water steam. The number of the molecules in a single nucleus with critical size is

$$n_{3c} = \rho'(T_1) \frac{4}{3} \pi R_{3c}^3 / m_1. \quad (22.22)$$

For successful prediction of several experiments with steam flows in *Laval* nozzles *Deitsch* and *Philiphoff* (1981) p.153 provided the following modification of one expression obtained by *Frenkel* (1973)

$$\dot{n}_{3,kin} = \left( \frac{p}{kT_1} \right)^2 \frac{c_T}{\rho'(T_1)} \sqrt{\frac{2\sigma m_1}{\pi}} \exp(-\beta G b_1). \quad (22.23)$$

The modification contains the following empirical factor

$$\beta = 0.25 + 6.7 \left\{ \left[ p'(T_1) + \frac{1}{2} \rho_1 w^2 \right] / p_c \right\}^{1/3} \quad (22.24)$$

for  $c_T = 1$ . The validity of Eq. (22.23) is proven for pressures between 0.25 and 4 MPa.

The mass condensed per unit volume and time due to nucleation is

$$\mu_{13} = \rho'(T_1) \frac{d}{d\tau} (n_3 V_3) = \rho'(T_1) V_{3c} \dot{n}_{3,kin} + \rho'(T_1) n_3 \frac{dV_3}{d\tau}. \quad (22.25)$$

We see that it consists of two parts, one due to nucleation, and the other due to growth of the droplets. The energy released during the condensation into the surrounding vapor is therefore

$$\dot{q}_1^{m\sigma 3} = \dot{n}_{3,kin} \Delta E_{3c} + \rho'(T_1) n_3 \frac{dV_3}{d\tau} [h_1 - h'(T_1)]. \quad (22.26)$$

### 22.1.3 Droplet growth

*Small droplets:* For very small droplets with sizes comparable with the molecular free path length the kinetic gas theory provides the basis for computation of the heat and mass transfer. The net mass flow rate of condensation is then

$$(\rho w)_{13} = \frac{p_{M1}}{\sqrt{2\pi R_{M1} T_1}} - \frac{p'(T_3^{\sigma 1})}{\sqrt{2\pi R_{M1} T_3^{\sigma 1}}}. \quad (22.27)$$

or having in mind that

$$\dot{q}_3^{m\sigma 1} = a_{13} h_c (T_1 - T_3^{\sigma 1}) = a_{13} (\rho w)_{13} [h_1 - h'(T_1)],$$

we obtain for the effective heat transfer coefficient the following expression

$$h_c = (\rho w)_{13} \frac{h_1 - h'(T_1)}{T_1 - T_3^{\sigma 1}} = \frac{h_1 - h'(T_1)}{T_1 - T_3^{\sigma 1}} \left( \frac{p_{M1}}{\sqrt{2\pi R_{M1} T_1}} - \frac{p'(T_3^{\sigma 1})}{\sqrt{2\pi R_{M1} T_3^{\sigma 1}}} \right). \quad (22.28)$$

Mason (1951, 1957), Ludvig (1975) proposed the following equation describing the change of the droplet radius under such conditions

$$\rho_3 \frac{dR_3}{d\tau} = \frac{1 - \frac{R_{3c}}{R_3}}{R_3 + 1.59\ell_1} \frac{T'(p_{M1}) - T_1}{\frac{h'' - h'}{\lambda_1} + \frac{p - p_{M1}}{p} \frac{R_{M1} T'(p_{M1}) p_{M1}^2}{\rho_{M1} (h'' - h') D_{M \rightarrow \Sigma n}}}, \quad (22.29)$$

for  $R_3 > R_{3c}$  which is equivalent to the equation

$$\rho_3 \frac{dR_3}{d\tau} = \frac{\mu_{13}}{a_{13}} = \frac{\dot{q}_1^{m\sigma 3}}{h_{M1} - h'}, \quad (22.30)$$

where

$$h_c = (h_{M1} - h') \frac{1 - \frac{R_{3c}}{R_3}}{R_3 + 1.59\ell_1} \frac{T'(p_{M1}) - T_1}{\frac{h'' - h'}{\lambda_1} + \frac{p - p_{M1}}{p} \frac{R_{M1} T'(p_{M1}) p_{M1}^2}{\rho_{M1} (h'' - h') D_{M \rightarrow \Sigma n}}}, \quad (22.31)$$

is the heat transfer coefficient. Here

$$\ell_1 = \frac{\eta_1}{p} \sqrt{\frac{\pi R_{M1} T_1}{2m_{\mu, M1}}} \quad (22.32)$$

is the *free path of a steam molecule* and  $m_{\mu, M1}$  is the *mole weight*. For water we have  $m_{\mu, M1} = m_{\mu, H_2O} = 18$ . Note that this equation is valid for steam-air mixtures.

*Large droplets:* For *larger macroscopic droplets* heat conduction and convection govern the heat and mass transfer. In this case the droplet grows due to condensation at the surface which depends on the properties of the environment to absorb the released heat. For a droplet in stagnant steam the results obtained by the

modeling of *thermally controlled bubble growth* can be applied. Note that the continuous phase is the gas phase in this case. This means that in the relationship

$$R_3 = f \sqrt{a_1 \tau^*}, \quad (22.33)$$

where  $f = f(\dots, Ja)$ ,  $a_1 = \lambda_1 / (\rho_1 c_{p1})$ , and

$$Ja = \frac{\rho_1 c_{p1} (T' - T_1)}{\rho' (h'' - h')}. \quad (22.34)$$

is the *Jakob* number. Remember that the denominator of the *Jakob* number is obtained from the boundary condition on the droplet surface, namely the equality of the heat released by the condensation, and of the heat taken away by heat conduction from the environment. The mass corresponding to this heat changes the radius of the droplet. The numerator in the *Jakob* number is obtained from the energy conservation equation for the continuum.

Analogously for convective heat transfer we can compute a heat transfer coefficient for a moving droplet and the corresponding mass and energy source terms.

#### 22.1.4 Self-condensation stop

As already mentioned, the released heat during the condensation increases the gas temperature, which for closed systems may decrease the condensation to zero. For a closed control volume or negligible convection and the diffusion from the neighboring elementary cells, the approximate form of the energy conservation equation is

$$\alpha_1 \rho_1 c_{p1} \frac{dT_1}{d\tau} = \dot{q}_1^{m\sigma 3} = \frac{3\alpha_3}{R_3} h_c (T_3^{\sigma 1} - T_1) \quad (22.35)$$

or

$$\frac{dT_1}{d\tau} = \frac{T_3^{\sigma 1} - T_1}{\Delta \tau_1^*}, \quad (22.36)$$

where

$$\Delta \tau_1^* = \frac{\alpha_1 \rho_1 c_{p1} R_3}{3\alpha_3 h_c} \quad (22.37)$$

approximates the *time constant of the phenomena*. The product of the density and the specific heat at constant pressure for a gas is less than the analogous product for a liquid. That is why the time constant for the analyzed case is smaller compared to the time constant for processes controlled by the heat accumulation in a liquid. This fact is very important and has to be taken into account for the construction of stable solution algorithms especially for condensing flows.

Thus, under these circumstances the difference between the saturation temperature and the gas temperature decreases exponentially

$$T_3^{\sigma 1} - T_1 = (T_{30}^{\sigma 1} - T_{10}) e^{-\Delta \tau / \Delta \tau_1^*}. \quad (22.38)$$

Therefore, the *average* heat released during the condensation within the time step  $\Delta \tau$  per unit mixture volume and unit time is

$$\dot{q}_1^{m\sigma 3} = \frac{3\alpha_3}{R_3} h_c (T_3^{\sigma 1} - T_1) f, \quad (22.39)$$

where

$$f = \frac{\Delta \tau_1^*}{\Delta \tau} (1 - e^{-\Delta \tau / \Delta \tau_1^*}). \quad (22.40)$$

The corresponding *averaged* mass source term is

$$\mu_{13} = \frac{\dot{q}_1^{m\sigma 3}}{h_{M1} - h'}. \quad (22.41)$$

## 22.2 Heat transfer across droplet interface without mass transfer

Consider a family of mono-disperse droplet designated with  $d$ , moving in a continuum, designated with  $c$ , with relative velocity  $\Delta V_{cd}$ . We are interested in how much thermal energy is transferred between the surface of a droplet and the surrounding continuum. We will consider first the steady state case, thereafter the transient heat conduction problem within a droplet and finally we will give some approximate solutions for the effective interface temperature and the average energy transferred.

The energy transported between the drop velocity field and the continuum per unit time and unit mixture volume for a steady state case is frequently approximated by

$$\dot{q}_{cd}^m = a_{cd} h_{cd} (T_c - T_d) = 6\alpha_d \lambda_c Nu_d (T_c - T_d) / D_d^2. \quad (22.42)$$

Here  $a_{cd} = 6\alpha_d / D_d$  is the interfacial area density,  $h_{cd} = \lambda_c Nu_d / D_d$  is the heat transfer coefficient and  $Nu_d$  is the *Nusselt* number defined as given in Table 22.1. Table 22.1 contains analytically and experimentally obtained solutions for the *Nusselt* number as a function of the relative velocity and the continuum properties.

**Table 22.1** Heat transfer coefficient on the surface of moving solid sphere and water droplets

$$Nu_d = \frac{D_d h_c}{\lambda_c}, Pe_c = \frac{D_d |\Delta V_{cd}|}{a_c} = Re_d Pr_c, Re_d = \frac{D_d \rho_c |\Delta V_{cd}|}{\eta_c}, Pr_c = \frac{\eta_c}{\rho_c a_c} = \frac{\eta_c c_{pc}}{\lambda_c},$$

$$a_c = \frac{\lambda_c}{\rho_c c_{pc}}$$

$$Re_d \ll 1$$

Potential flow

$$Pe_c \ll 1$$

$$Nu_d = 2 + \frac{1}{2} Pe_c + \frac{1}{6} Pe_c^2 + \dots$$

Soo (1969)

$$Pe_c \gg 1$$

$$Nu_d = 0.98 Pe_c^{1/3} \quad \eta_d / \eta_c = \infty$$

Nigmatulin (1978)

$$Nu_d = \frac{2}{\pi^{1/2}} Pe_c^{1/3}$$

Boussinesq (1905),  
isothermal sphere

$$Nu_d = \left( \frac{3}{4\pi} \frac{1}{1 + \eta_d / \eta_c} Pe_c \right)^{1/2}$$

Levich (1962)

$$Nu_d = 0.922 + 0.991 Pe_c^{1/3}$$

Acrivos-Goddard (1965)

$$Nu_d = 4.73 + 1.156 Pe_c^{1/2}$$

Watt (1972) isothermal sphere

$$Re_d < 1,$$

$$Pe_c < 10^3$$

$$Nu_d = 2 + \frac{\frac{1}{3} Pe_c^{0.84}}{1 + \frac{1}{3} Pe_c^{0.51}} \quad \eta_d / \eta_c = \infty$$

Nigmatulin (1978)

$$Pe_c < 1$$

$$Nu_d = 2 + \frac{1}{2} Pe_c^{1/3}$$

Acrivos and Taylor (1962)

only the resistance in the gas is  
taken into account

$$1 < Re_d < 7 \times 10^4, \quad 0.6 < Pr_c < 400$$

$$Nu_d = 2 + (0.55 \text{ to } 0.7) Re_d^{1/2} Pr_c^{1/3} \quad \text{Soo (1969)}$$

Droplets and bubbles

Michaelides (2003)

$$0 < Re_d < 1, \quad Pe_c > 10$$

$$Nu_d = \left( \frac{0.651}{1 + 0.95 \eta_d / \eta_c} Pe_c^{1/2} + \frac{0.991 \eta_d / \eta_c}{1 + \eta_d / \eta_c} Pe_c^{1/3} \right) (1.032 + A) \\ + \frac{1.651(0.968 - A)}{1 + 0.95 \eta_d / \eta_c} + \frac{\eta_d / \eta_c}{1 + \eta_d / \eta_c}, \quad A = \frac{0.61 Re_d}{21 + Re_d}.$$

$$10 \leq Pe_c \leq 1000, \quad Re_d > 1$$

$$Nu_d = \frac{2 - \eta_d / \eta_c}{2} Nu_{d,0} + \frac{4 \eta_d / \eta_c}{6 + \eta_d / \eta_c} Nu_{d,2} \quad \text{for } 0 \leq \eta_d / \eta_c \leq 2$$

$$Nu_d = \frac{4}{\eta_d / \eta_c + 2} Nu_{d,2} + \frac{\eta_d / \eta_c - 2}{\eta_d / \eta_c + 2} Nu_{d,\infty} \quad \text{for } 2 < \eta_d / \eta_c < \infty$$

where

$$Nu_{d,0} = 0.651 Pe_c^{1/2} (1.032 + A) + 1.6 - A \quad \text{for } \eta_d / \eta_c = 0,$$

$$Nu_{d,\infty} = 0.852 Pe_c^{1/3} (1 + 0.233 Re_d^{0.287}) + 1.3 - 0.182 Re_d^{0.355} \quad \text{for } \eta_d / \eta_c = \infty,$$

$$Nu_{d,2} = 0.64 Pe_c^{0.43} (1 + 0.233 Re_d^{0.287}) + 1.41 - 0.15 Re_d^{0.287} \quad \text{for } \eta_d / \eta_c = 2.$$

Solid sphere undergoing a step temperature change, *Feng and Michaelides (1986)*

$$Nu_d = 2 \left\{ 1 + 2 Pe_c^2 \ln(2 Pe_c) + Pe_c \left[ \frac{1}{2} \operatorname{erf}(2 Pe_c \sqrt{\tau^*}) + \frac{\exp(-4 Pe_c^2 \tau^*)}{4 Pe_c \sqrt{\pi \tau^*}} \right] \right\}$$

Water droplets

$$Nu_d = 2 + 0.6 Re_d^{1/2} Pr_c^{1/3} \quad \text{Ranz and Marschal (1952)}$$

$$64 < Re_d < 250, \quad 0.00023 < D_d < 0.00113 m, \quad 1.03 \times 10^5 < p < 2.03 \times 10^5 Pa, \\ 2.8 < T_c - T_d < 36 K, \quad 2.7 < \Delta V_{cd} < 11.7 m/s$$

$$Nu_d = 2 + 0.738 Re_d^{1/2} Pr_c^{1/3} \quad \text{Lee and Ryley (1968)}$$

In nature the temperature of both media changes with the time. That is why we consider next the transient heat conduction problem inside the droplet associated with the heat transfer at the surface.

Consider the case for which the continuum temperature is  $T_c$  and the droplet temperature at the beginning of the time  $\Delta\tau$  is  $T_d$ . The *Fourier* equation

$$\frac{\partial T}{\partial \tau} = \frac{\lambda_d}{\rho_d c_{cd}} \left( \frac{\partial^2 T}{\partial r^2} + \frac{2}{r} \frac{\partial T}{\partial r} \right). \quad (22.43)$$

describes the temperature profile in the droplet. Usually the equation is written in terms of the dimensionless temperature

$$\bar{T} = \frac{T(r, \tau) - T_d}{T_d^{\sigma c} - T_d} \quad (22.44)$$

for  $r = 0$ ,  $R_d$ ,  $\tau = \tau, \tau + \Delta\tau$  in the following form

$$\frac{\partial \bar{T}}{\partial \tau} = a_d \left( \frac{\partial^2 \bar{T}}{\partial r^2} + \frac{2}{r} \frac{\partial \bar{T}}{\partial r} \right), \quad (22.45)$$

where  $a_d = \lambda_c / (\rho_c c_{pc})$  is the droplet thermal diffusivity. Text book analytical solution of the *Fourier* equation is available for the following boundary conditions:

- (a) Drop initially at uniform temperature:  $\bar{T}(r, 0) = 0$ ;
- (b) Drop surface at  $r = R_d$  immediately reaches the temperatures  $T_d^{\sigma c}$ ,  $\bar{T}(R_d, \tau) = 1$ ;
- (c) Symmetry of the temperature profile:  $\left. \frac{\partial \bar{T}}{\partial r} \right|_{r=0} = 0$ .

The solution is represented by the converging *Fourier* series

$$\bar{T}(r, \tau) = 1 - \frac{2}{\pi} \frac{R_d}{r} \sum_{n=1}^{\infty} \frac{(-1)^n}{n} \sin\left(n\pi \frac{r}{R_d}\right) \exp(-n^2 \tau / \Delta\tau_d) \quad (22.46)$$

where  $\Delta\tau_d = D_d^2 / (4\pi^2 a_d)$  is the characteristic time constant of the heat conduction process. The volume-averaged non-dimensional temperature is

$$\bar{T}_m = 1 - \frac{6}{\pi^2} \sum_{n=1}^{\infty} \frac{1}{n^2} \exp(-n^2 \tau / \Delta\tau_d), \quad (22.47)$$



Convection inside the droplet caused by the interfacial shear due to relative velocity can improve the thermal conductivity of the droplet  $a_d$  by a factor  $f \geq 1$ . Therefore

$$\bar{T}_m = 1 - \frac{6}{\pi^2} \sum_{n=1}^{\infty} \frac{1}{n^2} \exp\left(-fn^2\tau / \Delta\tau_d\right). \quad (22.48)$$

*Celata et al.* (1991) correlated their experimental data for condensation with the following expression for  $f$ ,

$$f = 0.53Pe_c^{*0.454}, \quad (22.49)$$

where a special definition of the *Peclet* number is used  $Pe_c^* = \frac{D_d |\Delta V_{cd}|}{a_c} \frac{\eta_c}{\eta_c + \eta_d}$ .

For a water droplet with  $D_d = 0.00002, 0.0002, 0.001m$  and  $T_c - T_d = 20K$  the time necessary to reach  $\bar{T}_m = 0.99$  is 0.00006, 0.00613, 0.612 s respectively. For values of  $\bar{T}_m$  greater than 0.95 (long contact times) the first term only of Eq. (22.48) is significant

$$\bar{T}_m \approx 1 - \frac{6}{\pi^2} \exp\left(-fn^2\tau / \Delta\tau_d\right). \quad (22.50)$$

One alternative solution of Eq. (22.48) can be obtained by the method of *Laplace* transformations which takes the form of a diverging infinite series. For values of  $\bar{T}_m$  less than 0.4 (short contact times) the first term only of this series

$$\bar{T}_m = \frac{3\sqrt{\pi}}{D_d \sqrt{a_d \tau}} \quad (22.51)$$

is significant. This equation applies for short contact times when the temperature gradient of the surface surroundings has not penetrated to the center of the sphere which consequently behaves as a semi-infinite body.

From the energy balance of the droplet velocity field we obtain the time-averaged energy transfer from the surface into the droplet per unit time and unit mixture volume

$$\dot{q}_d^{m\sigma c} = \alpha_d \rho_d c_{pd} \frac{1}{\Delta\tau} \int_0^{\Delta\tau} \frac{dT_{dm}}{d\tau} d\tau = \alpha_d \rho_d c_{pd} \frac{1}{\Delta\tau} (T_d^{\sigma c} - T_d) [\bar{T}_{dm}(\Delta\tau) - \bar{T}_{dm}(0)]$$

leading to

$$\alpha_d \rho_d c_{pd} \frac{\bar{T}_{dm}(\Delta\tau)}{\Delta\tau} (T_d^{\sigma c} - T_d) = \omega_d (T_d^{\sigma c} - T_d) \quad (22.52)$$

If the surface temperature differs from the continuum temperature there is a convective component of the energy transported from the continuum to the surface for  $T_c > T_d^{\sigma c}$  or from the surface to the continuum for  $T_c < T_d^{\sigma c}$ , namely

$$\dot{q}_c^{\sigma d} = 6\alpha_d \lambda_c Nu_d (T_d^{\sigma c} - T_c) / D_d^2 = \omega_c (T_d^{\sigma c} - T_c), \quad (22.53)$$

where  $Nu_d$  is the *Nusselt* number for convective heat transfer between a sphere and the continuum.

For  $T_c \approx \text{const}$  the effective interface temperature is obtained from the energy jump condition  $\dot{q}_d^{\sigma c} = -\dot{q}_c^{\sigma d}$  after solving for  $T_d^{\sigma c}$

$$T_d^{\sigma c} = \frac{\omega_d T_d + \omega_c T_c}{\omega_d + \omega_c}. \quad (22.54)$$

For the case when  $T_c \neq \text{const}$  the heat-transfer causes changes in the continuum temperature too. If we neglect the convection and the diffusion from the neighboring elementary cells, which is valid for a heat transfer time constant considerably smaller than the flow time constant, the continuum energy conservation can be approximated by

$$\alpha_c \rho_c c_{pc} \frac{dT_c}{d\tau} = 6\alpha_d \lambda_c Nu_d (T_d^{\sigma c} - T_c) / D_d^2 \quad (22.55)$$

or

$$\frac{dT_c}{d\tau} = \frac{T_d^{\sigma c} - T_c}{\Delta \tau_c^*}, \quad (22.56)$$

where

$$\Delta \tau_c^* = \frac{\alpha_c \rho_c c_{pc} D_d^2}{6\alpha_d \lambda_c Nu_d} \quad (22.57)$$

approximates the characterizing time constant of the continuum heating or cooling. Note that the product of the density and the specific heat at constant pressure for gas is less than the analogous product for liquid. That is why the time constant for gases as a continuum should be smaller compared to the time constant for liquids as a continuum. This makes the gas temperature very sensitive to the heat and mass transfer process.

Thus for some effective  $T_d^{\sigma c}$  the difference between the interface temperature and the continuum temperature decreases exponentially

$$\bar{T}_{cm}(\Delta \tau) = \frac{T_d - T_c}{T_d^{\sigma c} - T_c} = \exp\left(-\frac{\Delta \tau}{\Delta \tau_c^*}\right) \quad (22.58)$$

during the time interval  $\Delta \tau$ . Therefore, the time-averaged heat, transferred from the surface into the continuum per unit mixture volume and unit time is

$$\dot{q}_c^{m\sigma d} = 6\alpha_d \lambda_c Nu_d (T_d^{\sigma c} - T_c) f_c / D_d^2 = \omega_c (T_d^{\sigma c} - T_c) \quad (22.59)$$

where

$$f_c = \left[ 1 - \exp\left(-\frac{\Delta \tau}{\Delta \tau_c^*}\right) \right] \frac{\Delta \tau_c^*}{\Delta \tau}. \quad (22.60)$$

Note that for  $\Delta \tau \rightarrow 0$ ,  $f_c \rightarrow 1$ .

Thus, from the energy jump conditions  $\dot{q}_d^{m\sigma c} = -\dot{q}_c^{m\sigma d}$  we obtain the effective interface temperature by Eq. (22.12). Having this temperature we can compute the average heat power density  $\dot{q}_c^{m\sigma d}$  by Eq. (22.58).

## 22.3 Direct contact condensation of pure steam on subcooled droplet

Consider the case where the steam temperature is equal to the saturation temperature by the system pressure

$$T_1 = T'(p), \quad (22.61)$$

and the droplet temperature at the beginning of the time step considered is less than the saturation temperature

$$T_3 < T'(p). \quad (22.62)$$

The heat conduction from the surface, which has the saturation temperature, to the bulk of the droplet is the condensation controlling mechanism in this case. Therefore, the *Fourier* equation describes the temperature profile inside the droplet. *Ford and Lekic* (1973) considered additionally the following effects

- (a) convection inside the droplet;
- (b) limitation of the steam supply toward the droplet surface

and introduced the corrector  $f$  in Eq. (22.48),

$$\bar{T}_m \approx 1 - \exp(-f\tau / \Delta \tau). \quad (22.63)$$

From the energy balance of the droplet velocity field we obtain the time-averaged energy transfer from the surface into the droplet per unit time

$$\dot{q}_3^{m\sigma 1} = \alpha_3 \rho_3 c_{p3} [T'(p) - T_3] \bar{T}_{3m} (\Delta \tau) / \Delta \tau. \quad (22.64)$$

If the steam temperature differs from the saturation temperature there is a convective component of the energy transported from the steam to the surface for  $T_1 > T'(p)$  or from the surface to the steam for  $T_1 < T'(p)$ , namely

$$\dot{q}_1^{\sigma 3} = a_{13} \frac{\lambda'_1}{D_3} Nu_{13} (T' - T_1), \quad (22.65)$$

where  $Nu_{13}$  is the *Nusselt* number for convective heat transfer between sphere and steam. For the case when  $T_1 < T'(p)$  part of the released heat during the condensation increases the gas temperature. If we neglect the convection and the diffusion from the neighboring elementary cells, the energy conservation can be approximated by

$$\alpha_1 \rho_1 c_{p1} \frac{dT_1}{d\tau} = 6\alpha_3 \lambda_1 Nu_3 (T_3^{\sigma 1} - T_1) / D_3^2, \quad (22.66)$$

or

$$\frac{dT_1}{d\tau} = \frac{T_3^{\sigma 1} - T_1}{\Delta \tau_1^*}, \quad (22.67)$$

where

$$\Delta \tau_1^* = \frac{\alpha_1 \rho_1 c_{p1} D_3^2}{6\alpha_3 \lambda_1 Nu_3} \quad (22.68)$$

approximates the time constant of the steam heating. For nearly constant pressure, and therefore constant  $T'$ , the difference between the saturation temperature and the gas temperature decreases exponentially during the time interval  $\Delta \tau$ ,

$$\bar{T}_{cm}(\Delta \tau) = \frac{T_3^{\sigma 1} - T_1}{T_3^{\sigma 1} - T_{10}} = \exp\left(-\frac{\Delta \tau}{\Delta \tau_1^*}\right). \quad (22.69)$$

Therefore, the time-averaged heat transferred from the surface into the gas per unit mixture volume and unit time is

$$\dot{q}_1^{\sigma 3} = 6\alpha_3 \frac{\lambda'_1}{D_3^2} Nu_{13} (T' - T_1) \quad (22.70)$$

where

$$f = \left[ 1 - \exp\left(-\frac{\Delta \tau}{\Delta \tau_1^*}\right) \right] \frac{\Delta \tau_1^*}{\Delta \tau}. \quad (22.71)$$

Thus, from the assumption that there is no energy and mass accumulation the interface (energy and mass jump conditions) we obtain for the averaged condensing mass per unit mixture volume and unit time the following expression

$$\mu_{13} = \frac{\dot{q}_3^{m\sigma 1} - \dot{q}_1^{m\sigma 3}}{h'' - h'} . \quad (22.72)$$

## 22.4 Spontaneous flashing of superheated droplet

Next we consider a single droplet in a gas environment having pressure  $p$ . The averaged droplet temperature is  $T_3$ . The surface temperature of the droplet,  $T_3^{\sigma 1}$ , is *higher* than the saturated temperature  $T'(p)$ . In the first instant of the process considered here, the spontaneous emission of mass will be *explosive*. In the next moment the surface temperature would drop and reach the saturation temperature, if no heat is transferred from the bulk region of the droplet to the surface. The heat transferred from the bulk region to the surface maintains the surface temperature *higher* than the saturation temperature and causes further evaporation. The *thermal resistance inside the drop* has a delaying effect on the evaporation, because the heat conduction is the slower process compared to the mass emission from the surface.

The net mass flow rate of evaporation from the droplet surface can be calculated by solving numerically the *Boltzmann* kinetic equation for such conditions. This is a quite complicated task. For the practical application the theory first proposed by *Hertz* is used. *Hertz* (1882) computed the evaporation mass flow rate from a surface with temperature  $T_3^{\sigma 1}$  and surface pressure  $p'(T_3^{\sigma 1})$  multiplying the frequency of the molecules leaving unit surface  $N_1 a_1 / 4$  by the mass of a single molecule  $m_1$ . Here  $N_1$  is the number of vapor molecules in unit volume. The averaged thermal velocity of the molecules at temperature  $T_3^{\sigma 1}$  is

$$a_1 = \sqrt{\frac{8}{\pi} R_{M1} T_3^{\sigma 1}} . \quad (22.73)$$

The result is

$$(\rho w)_{31}^* = m_1 \frac{1}{4} N_1 a_1 . \quad (22.74)$$

Having in mind that

$$m_1 N_1 = \rho_1 \left[ p'(T_3^{\sigma 1}), T_3^{\sigma 1} \right] , \quad (22.75)$$

$$p'(T_3^{\sigma 1}) / \rho_1 \left[ p'(T_3^{\sigma 1}), T_3^{\sigma 1} \right] \approx R_{M1} T_3^{\sigma 1} , \quad (22.76)$$

*Hertz* obtain finally

$$(\rho w)_{31}^* = \frac{p'(T_3^{\sigma_1})}{\sqrt{2\pi R_{M1} T_3^{\sigma_1}}} . \quad (22.77)$$

Similarly *Hertz* computed the condensing mass flow rate from the steam with temperature  $T_1$  equal to the gas temperature and partial pressure  $p_{M1}$  multiplying the frequency of the molecules striking unit surface by the mass of a single molecule. The averaged thermal velocity of the molecules at temperature  $T_1$  across the plane surface in local thermodynamical equilibrium is

$$a_1 = \sqrt{\frac{8}{\pi} R_{M1} T_1} . \quad (22.78)$$

The result is

$$(\rho w)_{13}^* = \frac{p_{M1}}{\sqrt{2\pi R_{M1} T_1}} . \quad (22.79)$$

Assuming (i) reversible process, (ii)  $T_1 \approx T_3^{\sigma_1}$ , and (iii) condensation and evaporation flows do not affect each other, *Hertz* obtained finally

$$\begin{aligned} (\rho w)_{31} &= (\rho w)_{31}^* - (\rho w)_{13}^* = \frac{1}{\sqrt{2\pi R_{M1} T_1}} \left[ \sqrt{\frac{T_1}{T_3^{\sigma_1}}} p'(T_3^{\sigma_1}) - p_{M1} \right] \\ &\approx c \frac{1}{\sqrt{2\pi R_{M1} T_1}} \left[ p'(T_3^{\sigma_1}) - p_{M1} \right], \end{aligned} \quad (22.80)$$

where  $c$  is the so called accommodation coefficient being of order of

$$c = 0.1 \text{ to } 1 \quad (22.81)$$

as shown by *Volmer's* review in *Volmer* (1939). Later improvements by *Knudsen* (1915) and *Langmuir* (1913), *Langmuir et al.* (1927) led to the formula for the *net mass flow rate of the spontaneous evaporation*

$$(\rho w)_{31} = (\rho w)_{31}^* - (\rho w)_{13}^* = c_e \frac{p'(T_3^{\sigma_1})}{\sqrt{2\pi R_{M1} T_3^{\sigma_1}}} - c_c \frac{p_{M1}}{\sqrt{2\pi R_{M1} T_1}} . \quad (22.82)$$

Here  $c_e$  is the *probability of escape* for a liquid molecule at the interface, and  $c_c$  is the *probability of capture* for a vapor molecule at the interface. This relationship is known in the literature as the equation of *Hertz*, *Knudsen* and *Langmuir* (see in *Ranz and Marschal* (1952). For no sound physical reason, Eq. (22.81) is generally approximated in the literature by

$$(\rho w)_{31} = c \left( \frac{p'(T_3^{\sigma_1})}{\sqrt{2\pi R_{M1} T_3^{\sigma_1}}} - \frac{p_{M1}}{\sqrt{2\pi R_{M1} T_1}} \right) . \quad (22.83)$$

For pressures below 0.1 bar measurements reported by *Fedorovich* and *Rohsenow* (1968) for liquid metals tightly clustered about unity. For larger pressure Eq. (22.81) is a good approximation - see the discussion by *Mills* and *Mills* and *Seban* (1967). For water the discussion and the measurements in *Mills* and *Seban* (1967), *Nabavian* and *Bromley* (1963), *Berman* (1961) give

$$c = 0.35 \text{ to } 1. \quad (22.84)$$

*Knowles* (1985) derived an analytical expression taking into account the influence of the condensation due to the relative motion of the interface with respect to the steam. The result is

$$(\rho w)_{31} = c \left( \frac{p'(T_3^{\sigma 1})}{\sqrt{2\pi R_{M1} T_3^{\sigma 1}}} - f(\Delta|\mathbf{V}_{21}|) \frac{p_{M1}}{\sqrt{2\pi R_{M1} T_1}} \right), \quad (22.85)$$

where the so called *transport enhancement factor* approximating the analytical solution is

$$f(\Delta|\mathbf{V}_{21}|) = 1 + 1.7 \frac{\Delta|\mathbf{V}_{21}|}{\sqrt{2R_{M1} T_1}} + 0.7 \left( \frac{\Delta|\mathbf{V}_{21}|}{\sqrt{2R_{M1} T_1}} \right)^2 \quad (22.86)$$

for  $\frac{\Delta|\mathbf{V}_{21}|}{\sqrt{2R_{M1} T_1}} \geq -1$  and

$$f(\Delta|\mathbf{V}_{21}|) = 0 \quad (22.87)$$

otherwise. For completeness we give some other modifications given in the literature. *Schrage*, see in *Bankoff* (1980), used the following form:

$$(\rho w)_{d1} = \frac{2c}{2-c} \frac{1}{\sqrt{2\pi R_{M1} T_3^{\sigma 1}}} \left[ p'(T_3^{\sigma 1}) - p_{M1} - \frac{p'(T_3^{\sigma 1})}{2T_3^{\sigma 1}} (T_3^{\sigma 1} - T_1) \right], \quad (22.88)$$

Here a modified *accommodation* coefficient is used having values for water  $c_{H_2O} = 0.01$  to 1. *Samson* and *Springer* (1969) used the following form for very small droplets, for  $\ell_1 / D_d \gg 1$ ,

$$(\rho w)_{d1} = \frac{1}{\sqrt{2\pi R_{M1} T_1}} \left[ p'(T_d^{\sigma c}) - p_{M1} - \frac{p_{M1}}{2T_1} (T_d^{\sigma c} - T_1) \right], \quad (22.89)$$

and for large droplets,  $\ell_1 / D_d \ll 1$

$$(\rho w)_{d1} = \frac{1}{\sqrt{2\pi R_{M1} T_1}} \left[ p'(T_d^{\sigma c}) - p_{M1} \right]. \quad (22.90)$$

Here

$$\ell_1 = \frac{\eta_1}{p} \sqrt{\frac{\pi R_{M1} T_1}{2 M_{M1}}}, \quad (22.91)$$

is the free path of a steam molecule and  $M_{M1} = M_{H_2O} = 18$  is the mole weight. *Labunzov and Krjukov* (1977) used the following form:

$$(\rho w)_{d1} = 2 \left[ \rho''(T_{di}) - \rho_{M1}(T_1, p_{M1}) \right] \sqrt{\frac{R_{M1} T_{di} \rho_{M1}(T_1, p_{M1})}{2 \pi \rho''(T_{di})}}. \quad (22.92)$$

The spontaneously evaporating mass from the superheated velocity field per unit mixture volume is

$$\mu_{d1} = (6\alpha_d / D_d) (\rho w)_{d1}. \quad (22.93)$$

In the case of strong emission of steam from the surface into the surrounding gas the heat transfer from the surface to the surrounding continuum can be neglected and therefore

$$\dot{q}_1^{m\sigma 3} = 0. \quad (22.94)$$

The energy jump condition for this situation reads

$$\mu_{d1} \left[ h''(T_d^{\sigma c}) - h'(T_d^{\sigma c}) \right] = -\dot{q}_d^{m\sigma c}. \quad (22.95)$$

If we use the approximate solution of the *Fourier* equation we obtain the one equation with respect the unknown surface temperature, namely

$$\frac{6}{D_d} (\rho w)_{d1} \left[ h''(T_d^{\sigma c}) - h'(T_d^{\sigma c}) \right] = \rho_d c_{pd} (T_d - T_d^{\sigma c}) \frac{1}{\Delta \tau} \left[ 1 - \frac{6}{\pi^2} \exp\left(-\frac{\Delta \tau}{\Delta \tau_d}\right) \right]. \quad (22.96)$$

This equation can be solved by iteration starting with

$$T_d^{\sigma c} \approx T_d. \quad (22.97)$$

Having the surface temperature it is very easy to compute the mass source term from the Eqs. (22.85) and (22.93), and the corresponding heat power density from Eq. (22.95).

The spontaneous evaporation will cease if the droplet surface temperature reaches the saturation temperature corresponding to the system pressure. If the saturation temperature corresponding to the partial steam pressure  $T'(p_{M1})$  is lower than the surface temperature the slow evaporation continues due to molecular diffusion. This process will be considered in Section 22.5.



## 22.5 Evaporation of saturated droplets in superheated gas

Let us consider the evaporation of saturated droplets in superheated gas. *Lee and Ryley* (1968) found that the heat needed for the evaporation is convectively transported from the gas to the surface, and the emitted mass from the surface does not influence considerably this heat transfer process. In this case we have

$$\mu_{1d} = 0, \quad (22.98)$$

$$\dot{q}_3^{m\sigma 1} = 0. \quad (22.99)$$

During the droplet evaporation the gas is *cooled* with

$$\dot{q}_1^{m\sigma d} = -a_{d1} h_c [T_1 - T'(p)] = -(6\alpha_d / D_d) h_c [T_1 - T'(p)]. \quad (22.100)$$

This is the instantaneous power density. From the energy jump condition (no energy accumulation on the droplet interface) we obtain for the instantaneous evaporating mass per unit mixture volume and unit time

$$\mu_{31} = (6\alpha_d / D_d) h_c [T_1 - T'(p)] / [h''(p) - h_{Md}]. \quad (22.101)$$

Actually we are interested in the *averaged* values of the mass source term during the time step  $\Delta\tau$ . For their approximate estimation we use the following way. Because the mass change of the droplet is caused by the evaporated mass per unit time, we have the following form of the mass conservation equation for a single droplet

$$\rho' \frac{dR_d}{d\tau} = -h_c [T_1 - T'(p)] / [h''(p) - h_{Md}] \quad (22.102)$$

or

$$\begin{aligned} \frac{dR_d}{d\tau} &= -\frac{h_c}{\rho'} [T_1 - T'(p)] / [h''(p) - h_{Md}] \\ &= -\frac{Nu_{d1} \lambda_1}{\rho' 2R_d} [T_1 - T'(p)] / [h''(p) - h_{Md}] = -c / R_3. \end{aligned} \quad (22.103)$$

This is the relationship between the change of the radius, the *Nusselt* number, and the temperature difference driving the evaporation. Integrating the above equation we obtain

$$\frac{R_d}{R_{d0}} = \sqrt{1 - 2c\Delta\tau / R_{d0}^2} = \sqrt{1 - \Delta\tau / \Delta\tau^*}. \quad (22.104)$$

If sufficient internal energy of the gas is available the *evaporation* of the entire droplet  $R_d = 0$  happens after the time interval

$$\Delta\tau^* = R_{d0}^2 / (2c). \quad (22.105)$$

After this time interval the Eq. (22.103) is no longer valid.

The third power of the radii ratio

$$\left(\frac{R_d}{R_{d0}}\right)^3 = \left(1 - \frac{\Delta\tau}{\Delta\tau^*}\right)^{3/2}. \quad (22.106)$$

is necessary to compute the averaged value of the evaporated mass per unit mixture volume and unit time within the time interval  $\Delta\tau$

$$\mu_{d1} = \rho' n_d \frac{V_{d0} - V_d}{\Delta\tau} = \frac{\rho' n_d V_{d0}}{\Delta\tau} \left(1 - \frac{V_d}{V_{d0}}\right) = \frac{\rho' \alpha_d}{\Delta\tau} \left[1 - \left(\frac{R_d}{R_{d0}}\right)^3\right] \quad (22.107)$$

for  $\Delta\tau < \Delta\tau^*$  and

$$\mu_{d1} = \frac{\rho' \alpha_d}{\Delta\tau} \quad (22.108)$$

for  $\Delta\tau \geq \Delta\tau^*$ . The last equation is practically the equation of the entire evaporation of the available droplets inside the time interval  $\Delta\tau$ .

Having in mind that during the evaporation

$$\mu_{d1} = 0 \quad (22.109)$$

$$\dot{q}_d^{m\sigma c} = 0, \quad (22.110)$$

we obtain from the energy jump condition the following relationship

$$\dot{q}_1^{m\sigma d} = -\mu_{d1} [h''(p) - h'(p)]. \quad (22.111)$$

The above analysis was performed under the assumption that the *Nusselt* number does not depend on the radius during the considered time interval. In fact, the radius decreases in accordance with the relationship of *Lee* and *Ryley* (1968),

$$Nu_{d1} = 2 + 0.738 Re_{d1}^{1/2} Pr_1^{1/3} = 2 + 0.738 \left(2 |\Delta V_{1d}| / \nu_1\right)^{1/2} Pr_1^{1/3} D_d^{1/2} = 2 + c_3 R_d^{1/2}, \quad (22.112)$$

and therefore, the *Nusselt* number decreases too. This makes the process slower than that previously described (assuming the *Nusselt* number not depending on the radius). Taking into account this relationship

$$\frac{R_d}{2 + c_3 R_d^{1/2}} \frac{dR_d}{d\tau} = c_2, \quad (22.113)$$

*Lee* and *Ryley* (1968) obtained an analytical integral of the above equation, namely

$$\Delta \tau = \Delta \tau^* - \frac{1}{c_2} \left[ \frac{2}{3} \frac{\sqrt{R_d}}{c_3} - \frac{D_d}{c_3^2} + \frac{8\sqrt{D_d}}{c_3^3} - \frac{16}{c_3^4} \ln \left( \frac{2}{2 + c_3 D_d^{1/2}} \right) \right]. \quad (22.114)$$

For a known time interval  $\Delta \tau$  we can compute the corresponding droplet diameter after solving the above transcendental equation iteratively. The time required for the full droplet evaporation (if sufficient excess internal gas energy is available), i.e.  $R_d = 0$  is easily obtained

$$\Delta \tau^* = \frac{1}{c_2} \left[ \frac{2}{3} \frac{\sqrt{R_{d0}}}{c_3} - \frac{D_{d0}}{c_3^2} + \frac{8\sqrt{D_{d0}}}{c_3^3} - \frac{16}{c_3^4} \ln \left( \frac{2}{2 + c_3 D_{d0}^{1/2}} \right) \right]. \quad (22.115)$$

Finally for completeness let us mention the empirical correlation proposed by *Saha* (1980), describing the droplet evaporation in superheated steam in dispersed non-adiabatic flow, in dry out condition on the heated wall

$$\alpha_{1d} h_c = 6300 \alpha_d \frac{\lambda_1}{D_h^2} \left( 1 - \frac{p}{p_{kr}} \right)^2 \left( \frac{\rho_1 V_1^2 D_h}{\sigma} \right)^{1/2}. \quad (22.116)$$

*Condie* et al. (1984) show that this correlation overestimates the evaporation rate compared to the experimental data and recommend *Webb's* correlation (see *Condie* et al. (1984))

$$\alpha_{1d} h_c = 1.32 (1 - \alpha_1^*)^{2/3} \frac{\lambda_1}{D_h^2} \left( 1 - \frac{p}{p_{kr}} \right)^2 \left( \frac{\rho_1 V_1^2 D_h}{\sigma} \right)^{1/2} \quad (22.117)$$

approximating better a number of experimental data ( $\alpha_1^*$  is the homogeneous void fraction).

## 22.6 Droplet evaporation in gas mixture

Consider a gas mixture with inert mass concentration  $\sum C_{n1}$  and vapor concentration  $C_{M1}$ , having total pressure  $p$  and gas temperature  $T_1$  see Fig. 22.1. A family of mono-dispersed droplets is flowing through the gas with relative velocity  $\Delta V_{13}$ . At the beginning of the time interval considered,  $\Delta \tau$ , the droplets possess temperature  $T_3$  and diameter  $D_3$ . Consider the case when the droplet temperature  $T_3$  is greater than the saturation temperature  $T'$  corresponding to the partial vapor pressure  $p_{M1}$

$$T_3 > T'(p_{M1}). \quad (22.118)$$

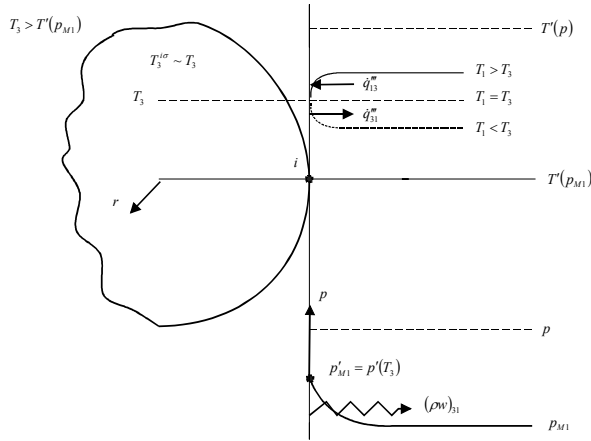


**Fig. 22.1** Evaporation of a water droplet in a two-component gas mixture

In this case the interface temperature  $T_{3\sigma}$  is somewhere between  $T'(p_{M1})$  and  $T_1$

$$T'(p_{M1}) < T_{3\sigma} < T_1. \quad (22.119)$$

The surface is emitting vapor molecules which are struggling through the gas mixture boundary layer. The molecules of the inert gas present considerable resistance to their movement. The transport through the boundary layer is diffusion controlled. The evaporation mass flow per unit surface and unit time is  $(\rho w)_{31}$ . The heat needed for the evaporation is absorbed partially from the bulk of the droplet by thermal diffusion. Heat is transferred from or to the surface to or from the surrounding gas due to convection. The purpose of this section is to describe a method for computation of the evaporation mass flow rate.

The vapor pressure of the immediate neighborhood of the interface is equal to the saturation pressure corresponding to the surface temperature

$$p_{M1\sigma} = p'(T_3^{\sigma 1}). \quad (22.120)$$

Therefore there is a pressure difference  $p_{M1\sigma} - p_{M1}$  across the diffusion boundary layer driving the mass flow rate  $(\rho w)_{31}$ . The simplest way to compute  $(\rho w)_{31}$  is to use the assumption for the similarity between temperature and concentration profile around the droplets and therefore the analogy between the heat and mass transfer, namely

$$(\rho w)_{31} = \rho_1 \beta (C_{M1\sigma} - C_{M1}) \quad (22.121)$$

where

$$\beta = -\frac{D_{M \rightarrow \Sigma n}}{C_{M1\sigma} - C_{M1}} (\nabla C_{M1})_{\sigma 3} \quad (\text{definition}) \quad (22.122)$$

$$C_{M1\sigma} = \frac{\rho_{M1\sigma}}{\sum \rho_{n1\sigma} + \rho_{M1\sigma}} = \frac{1}{1 + \sum \rho_{n1\sigma} / \rho_{M1\sigma}}, \quad (22.123)$$

$$\rho_{M1\sigma} = \rho''(T_{3\sigma}), \quad (22.124)$$

$$\sum \rho_{n1\sigma} = \frac{p - p'(T_3^{\sigma 1})}{R_{\Sigma n 1} T_3^{\sigma 1}}, \quad (22.125)$$

where

$$R_{\Sigma n 1} = 287.04 \quad (22.126)$$

is the gas constant for air.

In these case the mass transfer coefficient is computed from an appropriate heat transfer correlation, e.g. the correlation of *Ranz and Marschall* (1952) replacing the *Nu* and *Pr* numbers with *Sh* and *Sc* numbers respectively

$$Sh = \frac{\beta D_3}{D_{M \rightarrow \Sigma n}} = 2 + 0.6 Re_{13}^{1/2} Sc_1^{1/3}, \quad (22.127)$$

where

$$Re_{13} = \rho_1 D_1 \Delta V_{13} / \eta_1, \quad (22.128)$$

$$Sc_1 = \eta_1 / (\rho_1 D_{M \rightarrow \Sigma n}). \quad (22.129)$$

An additional simplifying assumption

$$T_{3\sigma} \approx T_3 \quad (22.130)$$

completes this model.

Having in mind that

$$\mu_{13} = 0, \quad (22.131)$$

$$\dot{q}_1^{m\sigma 3} = 0, \quad (22.132)$$

we obtain from the energy jump condition the heat extracted from the droplet during the slow evaporation per unit mixture volume and unit time

$$\dot{q}_3^{m\sigma 1} = -\mu_{31} [h''(p) - h_{M3}]. \quad (22.133)$$

In order to obtain the averaged value of the mass source term, we use the sum of the mass conservation equations for the inert components in the gas mixture, neglecting convection and diffusion from the neighbor control volumes,

$$\alpha_1 \rho_1 \frac{d}{d\tau} \sum C_{n1} = -\mu_{31} \sum C_{n1} = a_{13} \rho_1 \beta \sum C_{n1} (\sum C_{n1\sigma} - \sum C_{n1}) \quad (22.134)$$

or after the substitution

$$\bar{\tau} = \frac{\tau a_{13} \rho_1 \beta \sum C_{n1\sigma}}{\alpha_1}, \quad (22.135)$$

$$C = \frac{\sum C_{n1}}{\sum C_{n1\sigma}}, \quad (22.136)$$

$$\frac{dC}{d\bar{\tau}} = C(1-C). \quad (22.137)$$

The solution of this equation for  $\tau = 0$ ,  $C = C_0$  is

$$\frac{1-C}{1-C_0} = \frac{1}{1+C_0(e^{\bar{\tau}}-1)}. \quad (22.138)$$

Using the so obtained solution, we compute the *averaged* value of the evaporated mass per unit mixture volume and unit time within the time interval  $\Delta\tau$ ,

$$\mu_{31} = -a_{13} \rho_1 \beta (\sum C_{n1\sigma} - \sum C_{n1}) f, \quad (22.139)$$

where

$$f = \frac{1}{1-C_0} \left\{ 1 - \frac{1}{\Delta\bar{\tau}} \ln \left[ 1 - C_0 (1 - e^{\bar{\tau}}) \right] \right\} \leq 1, \quad (22.140)$$

This expression takes into account the *reduction of the driving forces* of the evaporation under the above discussed conditions.

There are other proposals in the literature how to compute  $(\rho w)_{31}$ . Following *Spalding* (1953) the diffusion mass flow rate at macroscopic surface is

$$(\rho w)_{31} = \rho_1 \beta \ln(1 + Sp) = \rho_1 \beta \ln C, \quad (22.141)$$

where

$$Sp = \frac{C_{M1\sigma} - C_{M1}}{1 - C_{M1\sigma}}, \quad (22.142)$$

is the *Spalding* mass transfer number and  $C_{M1\sigma}$  is the vapor mass concentration at the boundary layer.

*Clift* et al. (1978) use for the region  $0.25 < Sc_1 < 100$  and  $Re_{13} < 400$  the following correlation to compute

$$Sh = 1 + \left(1 + Re_{13} Sc_1\right)^{1/3} f(Re_{13}), \quad (22.143)$$

$$f(Re_{13}) = 1 \quad \text{for} \quad Re_{13} < 1, \quad (22.144)$$

$$f(Re_{13}) = Re_{13}^{0.077} \quad \text{for} \quad 1 < Re_{13} < 400. \quad (22.145)$$

Approximating numerical results *Chiang and Sirignano* (1990) use the following correlation

$$(\rho w)_{31} = \rho_1 \beta \frac{Sp}{(1 + Sp)^{0.7}}, \quad (22.146)$$

where  $\beta$  is computed by

$$Sh = 2 + 0.46 Re_{13}^{0.6} Sc_1^{1/3}. \quad (22.147)$$

The validity of this approach is recommended by the authors within the region  $0.3 < Sp < 4.5$ ,  $30 < Re_{13} < 250$ .

*Tanaka* (1980) uses the following equation

$$(\rho w)_{31} = \rho_1 \beta (C_{M1\sigma} - C_{M1}) 1.39 \frac{\left(\frac{\sum C_{n1\sigma}}{\sum C_{n1}}\right)^{0.52}}{\left(1 + \frac{\sum C_{n1\sigma}}{\sum C_{n1}}\right)^{0.48} \sum C_{n1}} \quad (22.148)$$

where the mass transfer coefficient  $\beta$  was computed by means of the *Ranz and Marchal* (1952) correlation.

*Abramson and Sirignano* (1989) used the *Spalding* correlation by computing the mass transfer coefficient taking into account the heat transfer from the droplet bulk to the surface by modifying the *Ranz and Marchal* equation for *Sh*-number as follows

$$Sh = 2 + B \frac{Sh_{RM} - 2}{(1 + Sp)^{0.7} \ln(1 + Sp)}, \quad (22.149)$$

where

$$B = \frac{c_{p3}(T_1 - T_3)}{h'' - h'}. \quad (22.150)$$

All properties for  $Re_{13}$ ,  $Sc_1$ , except  $\rho_1$  are computed at reference parameters,  $C_{ref}$ , defined as follows

$$C_{ref} = \frac{1}{n} [(n-1)C_{M1\sigma} + C_{M1}], \quad n = 3. \quad (22.151)$$

Next we try to remove the simplifying assumption  $T_3^{\sigma 1} \approx T_3$ .

The time-averaged heat transfer from the bulk of the droplet to the surface is

$$\dot{q}_3^{\sigma 1} = \alpha_3 \rho_3 c_{p3} (T_3^{\sigma 1} - T_3) \bar{T}_{3m} (\Delta \tau) / \Delta \tau. \quad (22.152)$$

The time-averaged convective heat transfer from the surface to the gas is

$$\dot{q}_1^{\sigma 3} = 6\alpha_3 \lambda_{1\sigma} Nu_{13} (T_3^{\sigma 1} - T_1) f_1 / D_3^2. \quad (22.153)$$

From the energy jump condition at the surface we have

$$\dot{q}_3^{\sigma 1} + \dot{q}_1^{\sigma 3} = -6\alpha_3 (\rho w)_{31} [h''(T_3^{\sigma 1}) - h'(T_3^{\sigma 1})] / D_3. \quad (22.154)$$

Solving this equation with respect to the surface temperature we obtain

$$T_3^{\sigma 1} = \frac{\rho_3 c_{p3} T_3 \bar{T}_{3m} (\Delta \tau) / \Delta \tau + 6\lambda_{1\sigma} Nu_{13} T_1 f_1 / D_3^2 - 6(\rho w)_{31} [h''(T_3^{\sigma 1}) - h'(T_3^{\sigma 1})] / D_3}{\rho_3 c_{p3} \bar{T}_{3m} (\Delta \tau) / \Delta \tau + 6\lambda_{1\sigma} Nu_{13} T_1 f_1 / D_3^2}. \quad (22.155)$$

$(\rho w)_{31}$ ,  $h''$  and  $h'$  are non-linear functions of  $T_3^{\sigma 1}$  and therefore the above equation should be solved by iterations. Having  $T_3^{\sigma 1}$  it is a simple matter to compute  $(\rho w)_{31}$ ,  $\dot{q}_3^{\sigma 1}$  and  $\dot{q}_1^{\sigma 3}$ .

The method to describe vapor condensation from a gas mixture on a liquid droplet is similar and will not be described separately.

## Nomenclature

### Latin

$a_1$	$= \sqrt{\frac{8}{\pi}} R_1 T_1$ , thermal velocity of the vapor molecules, <i>m/s</i>
$c_c$	$\approx 0.1$ for water steam plus non-condensable gases, $\approx 0.5$ to 1, for pure water-steam, part of the molecules striking the nucleus and remaining there, <i>dimensionless</i>
$c_T$	temperature correction factor taking into account the heat transfer from the nucleus to the surrounding vapor, <i>dimensionless</i>
$F_{3c}$	surface of the cluster, <i>m<sup>2</sup></i>
$Gb_1$	$= \frac{\Delta E_{3c}}{kT_1}$ , <i>Gibbs number, dimensionless</i>
$k$	$= 13.805 \times 10^{-24}$ is the <i>Boltzmann constant, J/K</i>



$m_\mu$	molar mean molecular mass, as many kilograms of a given substance as its molecular mass is, e.g. $m_{\mu,H_2O}=18$ , $m_{\mu,Air}=28.9$ , $kg/mol$
$m_1$	$= \frac{m_\mu}{N_A}$ mass of a single molecule, $kg$
$N_A$	$= 6.02 \times 10^{23}$ , <i>Avogadro</i> number, $1/mol$
$N_1$	$= \rho_1 / m_1$ , number of the vapor molecules per unit volume, $1/m^3$
$\dot{n}_{3,kin}$	generated nuclei per unit volume and unit time, $1/(m^3s)$
$n_3$	number of droplets per unit flow, $1/m^3$
$n_{3c}$	$= \rho'(T_1) \frac{4}{3} \pi R_{3c}^3 / m_1$ , number of the molecules in a single nucleus with critical size, $1/m^3$
$p$	local static pressure, $Pa$
$p'$	$= p'(T_1)$ , saturation pressure as a function of the steam temperature, $Pa$
$p_c$	critical pressure, for water $221.2 \times 10^5$ , $Pa$
$R_3$	droplet radius, $m$
$R_{30}$	radius of a subcooled non-stable spherical steam volume, $m$
$R_{3c}$	critical nucleus radius, $m$
$T_1$	steam at local temperature, $K$
$T'$	$= T'(p)$ , saturation temperature at the system pressure, $K$
$T_c$	critical temperature, $K$
$T_{c,H_2O}$	$= 647.2$ , critical temperature of water, $K$
$T_{1,spin}$	temperature at the spinoidal line, $K$
$w$	local velocity, $m/s$
$Ze_1$	$= \sqrt{\frac{Gb_1}{3\pi n_{3c}^2}}$ , <i>Zeldovich</i> number, <i>dimensionless</i>

### Greek

$\beta$	empirical coefficient, <i>dimensionless</i>
$\Delta E_3$	work required to create a single nucleus, $J$
$\Delta E_{3c}$	work required to create a stable single nucleus, $J$
$\Delta S_{13c}$	$= \Delta E_{3c} / T_1$ , entropy increase required to create a stable single nucleus, $J/K$
$\Delta T_{1,sub}$	$= T'(p) - T_1$ , subcooling, $K$
$\rho_1$	$= \rho_1(p, T_1)$ , steam density, $kg/m^3$
$\sigma$	surface tension, $Nm$

## References

- Abramson B, Sirignano WA (1989) Droplet vaporization model for spray combustion calculations, *Int. Heat Mass Transfer*, vol 32 pp 1605-1618
- Acrivos A, Goddard J (1965) Asymptotic expansion for laminar forced- convection heat and mass transfer, Part 1, *J. of Fluid Mech.*, vol 23 p 273
- Acrivos A, Taylor TD (1962) Heat and mass transfer from single spheres in stokes flow, *The Physics of Fluids*, vol 5 no 4 pp 387-394
- Bankoff SS (1980) Some Condensation Studies Pertinent to LWR Safety, *Int. J. Multiphase Flow*, vol 6 pp 51-67
- Berman LD (1961) Soprotivlenie na granize razdela fas pri plenochnoi kondensazii para nizkogo davleniya, *Tr. Vses. N-i, i Konstrukt In-t Khim. Mashinost*, vol 36 p 66
- Boussinesq M (1905) Calcul du pouvoir refroidissant des courant fluids, *J. Math. Pures Appl.*, vol 1 p 285
- Celata GP, Cumo M, D'Annibale F, Farello GE (1991) Direct contact condensation of steam on droplets, *Int. J. Multiphase Flow*, vol 17 no 2 pp 191-211
- Chiang CH, Sirignano WA (Nov. 1990) Numerical analysis of convecting and interacting vaporizing fuel droplets with variable properties, Presented at the 28th AIAA Aerospace Sciences Mtg, Reno
- Clift R, Ggarce JR, Weber ME (1978) Bubbles, drops, and particles, Academic Press, New York 1978
- Condie KG et al. (August 5-8, 1984) Comparison of heat and mass transfer correlation with forced convective non equilibrium post-CHF experimental data, *Proc. of 22nd Nat. Heat Transfer Conf. & Exhibition*, Niagara Falls, New York, in Dhir VK, Schrock VE (ed) *Basic Aspects of Two-Phase Flow and Heat Transfer*, pp 57-65
- Deutsch ME, Philiphoff GA (1981) Two phase flow gas dynamics, Moscu, Energoisdat, in Russian
- Fedorovich ED, Rohsenow WM (1968) The effect of vapor subcooling on film condensation of metals, *Int. J. of Heat Mass Transfer*, vol 12 pp 1525-1529
- Feng Z-G and Michaelides EE (1986) Unsteady heat transfer from a spherical particle at finite Peclet numbers, *ASME Journal of Fluids Engineering*, vol 118 pp 96-102
- Fieder J, Russel KC, Lothe J, Pound GM (1966) Homogeneous nucleation and growth of droplets in vapours. *Advances in Physics*, vol 15 pp 111-178
- Ford JD, Lekic A (1973) Rate of growth of drops during condensation. *Int. J. Heat Mass Transfer*, vol 16 pp 61-64
- Frenkel FI (1973) Selected works in gasdynamics, Moscu, Nauka, in Russian
- Furth R (1941) *Proc. Cambr. Philos. Soc.*, vol 37 p 252
- Gibbs JW (1878) *Thermodynamische Studien*, Leipzig 1982, *Amer. J. Sci. and Arts*, Vol.XVI, pp 454 - 455
- Hertz H (1882) *Wied. Ann.*, vol 17 p 193
- Knowles J B (1985) A mathematical model of vapor film destabilization, Report AEEW-R-1933
- Knudsen M (1915) *Ann. Physik*, vol 47 p 697
- Labunzov DA, Krjukov AP (1977) Processes of intensive flushing, *Thermal Engineering*, in Russian, vol 24 no 4 pp 8-11
- Langmuir I (1913) *Physik. Z.*, vol 14 p 1273
- Langmuir I (1927) Jones HA and Mackay GMJ, *Physic.*, rev vol 30 p 201

- Lee K, Ryley DJ (Nov. 1968) The evaporation of water droplets in superheated steam, *J. of Heat Transfer*, vol 90
- Levich VG (1962) *Physicochemical Hydrodynamics*, Prentice-Hall, Englewood Cliffs, NJ
- Lienhard JH A heat transfer textbook, Prentice-Hall, Inc., Englewood Cliffs, New Jersey 07632
- Ludvig A (1975) Untersuchungen zur spontaneous Kondensation von Wasserdampf bei stationärer Ueberschallstroemung unter Beruecksichtigung des Realgasverhaltens. Dissertation, Universitaet Karlsruhe (TH)
- Mason BJ (1951) Spontaneous condensation of water vapor in expansion chamber experiments. *Proc. Phys. Soc. London, Serie B*, vol 64 pp 773-779
- Mason BJ (1957) *The Physics of Clouds*. Clarendon Press, Oxford
- Michaelides EE (March 2003) Hydrodynamic force and heat/mass transfer from particles, bubbles and drops – The Freeman Scholar Lecture, *ASME Journal of Fluids Engineering*, vol 125 pp 209-238
- Mills AF The condensation of steam at low pressure, *Techn. Report Series No. 6, Issue 39*. Space Sciences Laboratory, University of California, Berkeley
- Mills AF, Seban RA (1967) The condensation coefficient of water, *J. of Heat Transfer*, vol 10 pp 1815-1827
- Nabavian K, Bromley LA (1963) Condensation coefficient of water; *Chem. Eng. Sc.*, vol 18 pp 651-660
- Nigmatulin RI (1978) Basics of the mechanics of the heterogeneous fluids, Moskva, Nauka, in Russian
- Ranz W, Marschal W Jr (1952) Evaporation from drops, *Ch. Eng. Progress*, vol 48 pp 141-146
- Ranz W, Marschal W Jr. (1952) Evaporation from drops, *Ch. Eng. Progress*, vol 48 pp 141-146
- Saha P (1980) *Int. J. Heat and Mass Transfer*, vol 23 p 481
- Samson RE, Springer GS (1969) Condensation on and evaporation from droplets by a moment method, *J. Fluid Mech.*, vol 36 pp 577-584
- Skripov WP, Sinizyn EN, Pavlov PA, Ermakov GW, Muratov GN, Bulanov NB, Bajdakov WG (1980) Thermophysical properties of liquids in metha-stable state, Moscu, Atomisdat, in Russia
- Soo SL (1969) *Fluid dynamics of multiphase systems*, Massachusetts, Woltham
- Spalding DB (1953) The combustion of liquid fuels, *Proc. 4th Symp. (Int.) on Combustion*, Williams & Wilkins, Baltimore MD, pp 847-864
- Tanaka M (Feb. 1980) Heat transfer of a spray droplet in a nuclear reactor containment. *Nuclear Technology*, vol 47 p 268
- Uatts (1972) Vlijanie krivisnji na teplo- I massootdachu ot izotemicheskoy sfere, *Teplopere-dacha*, no 1 p 1, Mir, in Russian
- VDI-Waermeatlas (1984) 4. Auflage VDI-Verlag
- Volmer M (1939) *Kinetik der Phasenbildung*, Dresden und Leipzig, Verlag von Theodor Steinkopff
- Zeldovich JB (1942) To the theory of origination of the new phase, cavitation, *Journal of Experimental and Theoretical Physics*, in Russian, vol 12 no 11/12 pp 525-538



## 23 Heat and mass transfer at the film-gas interface

### 23.1 Geometrical film-gas characteristics

There are different flow pattern leading to a film-gas interface in multi-phase flows. Stratified and annular flows in channels with different geometry, walls of large pools with different orientations and part of the stratified liquid gas configuration in large pools are the flow patterns of practical interest. The problem of the mathematical modeling of interface heat and mass transfer consists of (a) macroscopic predictions of the geometrical sizes and local averaged temperatures, velocities, concentrations and pressure and (b) microscopic modeling of the interface heat and mass transfer. The purpose of this Chapter is to review the state of the art for modeling of the interface heat and mass transfer for known geometry.

Next we summarize some important geometrical characteristics needed further.

The cross section occupied by gas and liquid in a channel flow is

$$F_1 = \alpha_1 F \quad (23.1)$$

and

$$F_2 = \alpha_2 F \quad (23.2)$$

respectively, where  $F$  is the channel cross section. Depending on the gas velocity the film structure can be

- (a) symmetric, or
- (b) asymmetric.

The symmetric film structure is characterized by uniformly distributed film on the wet perimeter in the plane perpendicular to the main flow direction. For this case the film thickness is

$$\delta_{2F} = D_h (1 - \sqrt{1 - \alpha_2}) / 2, \quad (23.3)$$

where  $D_h$  is the hydraulic diameter of the channel in a plane perpendicular to the main flow direction.

The liquid gas interface per unit flow volume that is called the interfacial area density is

$$a_{12} = \frac{4}{D_h} \sqrt{1 - \alpha_2} . \quad (23.4)$$

The hydraulic diameter of the gas is

$$D_{h1} = D_h \sqrt{1 - \alpha_2} . \quad (23.5)$$

Asymmetric film structure results in the case of dominance of the gravitation force. The flow can be characterized by three perimeters, one of the gas-wall contact,  $Per_{1w}$ , one of the gas-liquid contact,  $Per_{12}$ , and one of the liquid-wall contact,  $Per_{2w}$ . To these three perimeters correspond three shear stresses, one between the gas and wall,  $\tau_{1w}$ , one between gas and liquid,  $\tau_{12}$ , and one between the liquid and wall,  $\tau_{2w}$ . The hydraulic diameters for computation of the friction pressure loss of the both fluids can be defined as

$$D_{h1} = 4\alpha_1 F / (Per_{1w} + Per_{12}) , \quad (23.6)$$

$$D_{h1} = 4\alpha_2 F / (Per_{2w} + Per_{12}) . \quad (23.7)$$

Two characteristic *Reynolds* numbers can be defined by using these length scales

$$Re_1 = \frac{\rho_1 V_1 D_{h1}}{\eta_1} = \frac{\alpha_1 \rho_1 V_1}{\eta_1} \frac{4F}{Per_{1w} + Per_{12}} , \quad (23.8)$$

$$Re_2 = \frac{\rho_2 V_2 D_{h2}}{\eta_2} = \frac{\alpha_2 \rho_2 V_2}{\eta_2} \frac{4F}{Per_{2w} + Per_{12}} . \quad (23.9)$$

In the three-dimensional space it is possible that the liquid in a computational cell is identified to occupy the lower part of the cell. In this case the gas-liquid interfacial area density is

$$a_{12} = 1 / \Delta z . \quad (23.10)$$

The film thickness in this case is

$$\delta_{2F} = \alpha_2 \Delta z , \quad (23.11)$$

where the  $\alpha_2$  is the local liquid volume fraction in the computational cell. In the case of film attached at the vertical wall of radius  $r$  of a control volume in cylindrical coordinates

$$\delta_{2F} = r \left( 1 - \sqrt{1 - \alpha_2 \left[ 1 - (r_{i-1}/r)^2 \right]} \right). \quad (23.12)$$

For the limiting case of  $r_{i-1} = 0$  Eq. (23.12) reduces to Eq. (23.3). The interfacial area density in this case is

$$a_{12} = 2 \frac{1 - \delta_{2F}/r}{r \left[ 1 - (r_{i-1}/r)^2 \right]} = 2 \frac{\sqrt{1 - \alpha_2 \left[ 1 - (r_{i-1}/r)^2 \right]}}{r \left[ 1 - (r_{i-1}/r)^2 \right]}. \quad (23.13)$$

For the case of  $r_{i-1} = 0$  Eq. (23.13) reduces to Eq. (23.4). For such flow pattern the following film *Reynolds* number is used

$$Re_{2F} = \frac{\rho_2 V_2 \delta_{2F}}{\eta_2}.$$

## 23.2 Convective heat transfer

Next we consider a flow without mass transfer. Detailed consideration of the convective heat transfer is useful not only for flows without mass transfer but also for flow with mass transfer at the film-gas interface.

The gas and liquid temperatures are  $T_1$  and  $T_2$ , respectively. The interface temperature, which plays an important role in the mathematical description is  $T_2^{1\sigma}$ . The total heat transfer mechanism can be considered as

- (a) heat transfer from the interface into the gas,  $\dot{q}_1^{m2\sigma}$ , and
- (b) heat transfer from the interface into the bulk liquid  $\dot{q}_2^{m1\sigma}$ .

### 23.2.1 Gas side heat transfer

To model the heat transfer between interface and gas we can use known correlations for heat transfer from gas to solid surface

$$\dot{q}_1^{m2\sigma} = a_{12} h_1^{2\sigma} (T_1^{2\sigma} - T_1). \quad (23.14)$$

Here  $h_1^{2\sigma}$  is the heat transfer coefficient.

For laminar gas flow in channels,  $Re_1 < 1450$  in accordance with *Hausen*, see in (1958), the maximum *Nusselt* number is 3.66 corrected for the effect of the temperature gradients,

$$h_1^{2\sigma} = 3.66 \frac{\lambda_1}{D_{h1}} \left( \frac{T_1}{T_1^{2\sigma}} \right)^{1/4} \quad (23.15)$$

For turbulent gas flow in channels,  $Re_1 < 1450$  in accordance with *Mc Eligot*, see (1958), the *Nusselt* number is computed by modified similarity to momentum transfer

$$h_1^{2\sigma} = 0.021 \frac{\lambda_1}{D_{h1}} Re_1^{0.8} Pr_1^{0.4} \left( \frac{T_1}{T_1^{2\sigma}} \right)^{1/2} \quad (23.16)$$

Sometimes this correlation is used in the form

$$\beta_1 = \frac{h_{1\sigma}}{\rho_1 c_{p1}} = \frac{Nu_1}{Re_1 Pr_1} V_1 = Sr_1 V_1 \quad (23.17)$$

or

$$\beta_1 = 0.021 Pr_1^{-0.6} Re_1^{-1/5} \left( \frac{T_1}{T_1^{2\sigma}} \right)^{1/2} V_1. \quad (23.18)$$

Similar is the equation introduced by *Bunker* and *Carey* (1986) for gas side heat transfer namely

$$\beta_1 = 0.037 Pr_1^{-1/3} Re_1^{-1/5} V_1. \quad (23.19)$$

The order of magnitude of the constants in the above equations, 0.021 to 0.037, was derived by comparison with experiments.

In the case of natural circulation of gas at a vertical wall we can use the proposal made by *Rohsenow* and *Choi* (1961),

$$h_{1\sigma} \Delta z / \lambda_1 = 0.56 (Gr_1 Pr_1)^{1/4} \quad (10^4 < Gr_1 Pr_1 < 10^8 \text{ laminar}), \quad (23.20)$$

$$h_{1\sigma} \Delta z / \lambda_1 = 0.13 (Gr_1 Pr_1)^{1/3} \quad (10^8 < Gr_1 Pr_1 < 10^{10} \text{ transition}), \quad (23.21)$$

$$h_{1\sigma} \Delta z / \lambda_1 = 0.021 (Gr_1 Pr_1)^{2/5} \quad (10^{10} < Gr_1 Pr_1 \text{ turbulent}), \quad (23.22)$$

where the *Grashof* number

$$Gr_1 = g \left( -\frac{1}{\rho_1} \frac{\partial \rho_1}{\partial T_1} \right) \Big|_{T_1} (T_1 - T_1^{2\sigma}) \Delta z^3 / \nu_1^2 \approx g \left( \left| T_1 - T_1^{2\sigma} \right| / T_1 \right) \Delta z^3 (\rho_1 / \eta_1)^2 \quad (23.23)$$

is defined using the vertical size  $\Delta z$  of the considered wall.

For a horizontal plane the *Jakob* correlation (1933) for natural circulation can be used



$$h_1^{2\sigma} = 2.417 \lambda_1 \left[ g \left( |T_1 - T_1^{2\sigma}|^{20/16} / T_1 \right) (\rho_1 / \eta_1)^2 \text{Pr}_1 \right]^{1/4}. \quad (23.24)$$

The heat transfer coefficient for forced convection at a plane surface can be computed using the classical *Reynolds* analogy, assuming similarity of the velocity and temperature profiles and no distortion of the boundary layer due to mass transfer

$$\beta_1 = \frac{\dot{q}_1'^{2\sigma} / (T_1 - T_1^{2\sigma})}{\rho_1 c_{p1}} = \frac{1}{2} \lambda_{w1} V_1 \quad (23.25)$$

or

$$\beta_1 = \frac{h_{1\sigma}}{\rho_1 c_{p1}} = V_1 \lambda_{w1} / 2 \quad (23.26a)$$

or

$$Nu_{1z} = \text{Re}_{1z} \text{Pr}_1 \lambda_{w1} / 2 \quad (23.26b)$$

where

$$Nu_{1z} = h_{1\sigma} \Delta z / \lambda_1, \quad (23.27)$$

$$\text{Re}_{1z} = V_1 \Delta z / \nu_1. \quad (23.28)$$

For plane walls the average shear stress along  $\Delta z$  is

$$\tau_{w1} = \lambda_{w1} \frac{1}{2} \rho_1 V_1^2, \quad (23.29)$$

where for laminar flow

$$\text{Re}_{1z} < (1 \text{ to } 3) 10^5, \quad (23.30)$$

in accordance with *Prandtl* and *Blasius*

$$\lambda_{w1} = 1.372 / \text{Re}_{1z}^{1/2}, \quad (23.31)$$

and for turbulent flow - see in *Albring* (1970)

$$\lambda_{w1} = 0.072 / \text{Re}_{1z}^{1/5}. \quad (23.32)$$

For the laminar flow Eq. (23.31) substituted in Eq. (23.26) gives

$$Nu_{1z} = 0.686 \text{Re}_{1z}^{1/2} \text{Pr}_1, \quad (23.33)$$

which is very similar to the widely used *Pohlhausen* equation (1921)

$$Nu_{1z} = 0.664 \text{Re}_{1z}^{1/2} \text{Pr}_1^{1/3} \quad (23.34)$$

recommended by *Gnielinski* (1975) after comparison with data for the laminar flow. For turbulent flow Eq. (23.26) was improved by *Petukhov* and *Popov* (1963)

$$Nu_{1z} = (Re_{1z} Pr_1 \lambda_{w1} / 2) / \left[ 1 + 12.7 (\lambda_{w1} / 2)^{1/2} (Pr_1^{2/3} - 1) \right]. \quad (23.35)$$

The influence of the change of the gas properties at the wall can be taken into account in accordance with *Churchill* and *Brier* (1955) by multiplying the results by  $(T_1 / T_{1\sigma})^{0.12}$ . After comparing with a large number of data for turbulent flows *Gnielinski* recommended Eqs. (23.35) and (23.32). For comparison we give here the recently successfully used modification of the *Petukhov* and *Popov* result, by *Kim* and *Corradini* (1990)

$$Nu_{1z} = (Re_{1z} Pr_1 \lambda_{w1} / 2) / Pr_1^f, \quad (23.36)$$

where the turbulent *Prandtl* number is

$$Pr_1^f = c_1 + c_2 / Pr_1 \quad (23.37)$$

$$c_1 = 0.85, \quad (23.38)$$

$$c_2 = 0.012 \text{ to } 0.05 \text{ for } Re_{1z} = 2 \cdot 10^4, \quad (23.39)$$

$$c_2 = 0.005 \text{ to } 0.015 \text{ for } Re_{1z} = 10^5. \quad (23.40)$$

In pure vapor condensation the condensate film provides the only heat transfer resistance.

### 23.2.2 Liquid side heat transfer due to conduction

Next we consider the heat transfer from the interface into the bulk liquid. The liquid can be laminar or turbulent. For laminar liquid the heat is transferred from the interface into the liquid due to heat conduction described by the *Fourier* equation, (1822),

$$\frac{\partial T}{\partial \tau} = -a_2 \frac{\partial^2 T}{\partial y^2}, \quad (23.39)$$

where the positive  $y$  direction is defined from the interface into the bulk. The text book solution for the following boundary conditions

$$\tau \geq 0, y = 0, T = T \text{ (interface)}, \quad (23.40)$$

$$\tau = 0, y > 0, T = T_2 \text{ (bulk liquid)}, \quad (23.41)$$

$$\tau > 0, y \rightarrow 1, T = T_2 \text{ (bulk liquid)}, \quad (23.42)$$

is

$$T - T_2 = (T_2^{1\sigma} - T_2) \operatorname{erfc} \frac{y}{2(a_2\tau)^{1/2}}. \quad (23.43)$$

Using the temperature gradient

$$\frac{\partial T}{\partial \tau} = -\frac{T_2^{1\sigma} - T_2}{(\pi a_2\tau)^{1/2}} \exp[-y^2/(4a_2\tau)] \quad (23.44)$$

at  $y = 0$  we compute the heat flux at the interface

$$\begin{aligned} \dot{q}_2^{n1\sigma} &= -\lambda_2 \left. \frac{\partial T}{\partial y} \right|_{y=0} = \sqrt{\frac{2a_2}{\pi\tau}} \rho_2 c_{p2} (T_2^{1\sigma} - T_2) = \frac{B}{\sqrt{\tau}} \rho_2 c_{p2} (T_2^{1\sigma} - T_2) \\ &= \beta_2 \rho_2 c_{p2} (T_2^{1\sigma} - T_2). \end{aligned} \quad (23.45)$$

The averaged heat flux over the time period  $\Delta\tau$  is

$$\dot{q}_2^{n1\sigma} = B \rho_2 c_{p2} (T_2^{1\sigma} - T_2) 2/\sqrt{\Delta\tau} \quad (23.46)$$

Assuming  $T_1 \approx \text{const}$ ,  $T_2 \approx \text{const}$  and using the energy jump condition  $\dot{q}_1^{n2\sigma} + \dot{q}_2^{n1\sigma} = 0$  in or

$$h_1^{2\sigma} (T_1^{2\sigma} - T_1) + \frac{2B}{\sqrt{\Delta\tau}} \rho_2 c_{p2} (T_2^{1\sigma} - T_2) = 0, \quad (23.47)$$

and assuming  $T_2^{1\sigma} = T_1^{2\sigma}$  which is valid for the case of no mass transfer across the interface we obtain

$$T_2^{1\sigma} = \left( h_1^{2\sigma} T_1 + \frac{2B}{\sqrt{\Delta\tau}} \rho_2 c_{p2} T_2 \right) / \left( h_1^{2\sigma} + \frac{2B}{\sqrt{\Delta\tau}} \rho_2 c_{p2} \right). \quad (23.48)$$

Thus having  $T_2^{1\sigma}$  we compute for Eq. (23.46) the heat flux from the interface into the bulk liquid

$$\dot{q}_2^{n1\sigma} = h_{12}^* (T_1 - T_2) \quad (23.49)$$

where

$$\frac{1}{h_{12}^*} = \frac{1}{h_1^{2\sigma}} + \frac{1}{\frac{2B}{\sqrt{\Delta\tau}} \rho_2 c_{p2}}. \quad (23.50)$$

The heat transferred per unit control volume and unit time is

$$\dot{q}_2^{n1\sigma} = -\dot{q}_1^{n2\sigma} = a_{12} \dot{q}_2^{n1\sigma}. \quad (23.51)$$

### 23.2.3 Liquid side heat conduction due to turbulence

Let  $\Delta\tau_2$  be the average time in which a turbulent eddy stays in the neighborhood of the free surface before jumping apart called sometimes the renewal period. During this time the average heat flux from the interface to the eddies by heat conduction is

$$\dot{q}_2^{n\sigma} = \left(2B / \sqrt{\Delta\tau_2}\right) \rho_2 c_{p2} (T_2^{1\sigma} - T_2) = \beta_2 \rho_2 c_{p2} (T_2^{1\sigma} - T_2). \quad (23.52)$$

If the volume-averaged pulsation velocity is  $V_2'$  and the turbulent length scale in the film is  $\ell_{e2}$  the time in which the eddy stays at the interface is

$$\Delta\tau_2 = f(\ell_{e2}, V_2'). \quad (23.53)$$

Thus, the task to model turbulent heat conduction from the interface into the liquid is reduced to the task to model

- (i) pulsation velocity  $V_2'$  and
- (ii) turbulent length scale  $\ell_{e2}$ .

Usually  $\beta_2$  is written as a function of the dimensionless turbulent *Reynolds* number

$$Re_2' = \rho_2 V_2' \ell_{e2} / \eta_2, \quad (23.54)$$

and *Prandtl* number  $Pr_2$ ,

$$\beta_2 = \sqrt{\frac{2a_2}{\pi \Delta\tau_2}} = \sqrt{\frac{2}{\pi}} Pr_2^{-1/2} \sqrt{\frac{\eta_2}{\rho_2 \Delta\tau_2}} = \sqrt{\frac{2}{\pi}} Pr_2^{-1/2} Re_2'^{-1/2} \sqrt{\frac{V_2' \ell_{e2}}{\Delta\tau_2}}, \quad (23.55)$$

and is a subject of modeling work and verification with experiments. Once we know  $\beta_2$  we can compute some effective conductivity by the equation

$$\sqrt{\frac{2\lambda_{2eff}}{\rho_2 c_{p2} \pi \Delta\tau_2}} \rho_2 c_{p2} (T_{2\sigma} - T_2) = \beta_2 \rho_2 c_{p2} (T_{2\sigma} - T_2) \quad (23.56)$$

or

$$\lambda_{2eff} = \frac{\pi}{2} \rho_2 c_{p2} \Delta\tau_2 \beta_2^2, \quad (23.57)$$

and use Eq. (23.48) for both laminar and turbulent heat transfer.

### 23.2.3.1 High Reynolds number

One of the possible ways for computation of the renewal period  $\Delta\tau_2$  for high turbulent *Reynolds* numbers

$$Re'_2 > 500 \quad (23.58)$$

is the use the hypothesis by *Kolmogoroff* for isotropic turbulence

$$\Delta\tau_2 \approx c_1 \left( \nu_2 \ell_{e2} / V_2'^3 \right)^{1/2}, \quad (23.59)$$

where

$$\ell_{e2} \approx c_1 \delta_{2F}, \quad (23.60)$$

where  $c_1$  is a constant. In this region the turbulence energy is concentrated in microscopic eddies (mechanical energy dissipating motion). Substituting  $\Delta\tau_2$  from Eq. (23.61) into (23.57) we obtain

$$\beta_2 = \sqrt{\frac{2}{\pi}} Pr_2^{-1/2} Re_2'^{-1/4} V_2'. \quad (23.61)$$

The qualitative relationship  $\beta_2 Pr_2^{1/2} \approx Re_2'^{-1/4}$  was originally proposed by *Banerjee* et al. in (1968) and experimentally confirmed by *Banerjee* et al. (1990). *Lamont* and *Scot*, see in *Lamont* and *Yuen* (1982), describe successfully heat transfer from the film surface into the flowing turbulent film for high Reynolds numbers using Eq. (23.61) with a constant 0.25 instead of  $\sqrt{2/\pi}$ . Recently *Hobbhahn* (1989) obtained experimental data for condensation on a free surface, which are successfully described by Eq. (23.61) modified as follows

$$\beta_2 = 0.07 Pr_2^{-0.6} Re_2'^{-1/5} V_2' \quad (23.62)$$

where the discrepancy between the assumption made by the authors

$$\ell_{e2} \approx \delta_{2F} \quad (23.63)$$

and

$$V_2' \approx |V_2| + \sqrt{\rho_1 / \rho_2} |V_1 - V_2| \quad (23.64)$$

and the reality are compensated by the constant 0.07.

### 23.2.3.2 Low Reynolds number

For low turbulence *Reynolds* number

$$Re'_2 < 500 \quad (23.65)$$

the *Kolmogoroff* time scale is no longer applicable. In this region the turbulence energy is concentrated in macroscopic eddies (mechanical energy containing motion). The choice of the liquid film thickness, as a length scale of turbulence

$$\ell_{e2} \approx \delta_{2F} \quad (23.66)$$

is reasonable. Therefore the renewal period is

$$\Delta\tau_2 \approx \delta_{2F} / V'_2 \quad (23.67)$$

and Eq. (23.55) reduces to

$$\beta_2 = \sqrt{\frac{2}{\pi}} Pr_2^{-1/2} Re_2'^{-1/2} V'_2. \quad (23.68)$$

For low *Reynolds* numbers *Fortescue* and *Pearson* (1967) recommended instead of  $\sqrt{2/\pi}$  in Eq. (23.68) to use

$$\text{const} = 0.7(1 + 0.44 / \Delta\tau_2^*), \quad (23.69)$$

where

$$\Delta\tau_2^* = \Delta\tau_2 V'_2 / \ell_{e2} \approx 1, \quad (23.70)$$

which is  $> 0.85$ , as recommended by *Brumfield* et al. (1975).

*Theofanous* et al. (1976) show that most of their experimental data for condensation on channels with free surface can be described by using Eqs. (23.61) and (23.68) with the above discussed corrections introduced by *Lamont* and *Scot*, and *Fortescue* and *Person*, respectively.

### 23.2.3.3 Pulsation velocity

a) Time scale of turbulence pulsation velocity based on average liquid velocity.

A very rough estimate of the pulsation velocity is

$$V' = c_1 V_2 \approx (0.1 \text{ to } 0.3) V_2, \quad (23.71)$$

With this approach and

$$\ell_{e2} \approx c_2 \delta_{2F} \quad (23.72)$$

the two equations for  $\beta_2$  read

$$Re_{2F} < c_1 500, \quad (23.73)$$

$$\beta_2 = c_2^{-1/4} c_1^{3/4} \sqrt{\frac{2}{\pi}} Pr_2^{-1/2} Re_{2F}^{-1/4} V_2 = \text{const} Pr_2^{-1/2} Re_{2F}^{-1/4} V_2. \quad (23.74)$$

Comparing this equation with the *McEligot* equation we see that

$$const \approx 0.021 \text{ to } 0.037. \quad (23.75)$$

For

$$Re_2 < c_1 500, \quad (23.76)$$

$$\beta_2 = c_1^{1/2} \sqrt{\frac{2}{\pi}} Pr_2^{-1/2} Re_{2F}^{-1/2} V_2. \quad (23.77)$$

b) The scale of turbulence pulsation velocity based on friction velocity

Improvement of the above theory requires a close look to the reasons for the existence of turbulence in the liquid film. This is either the wall shear stress,  $\tau_{2w}$ , or the shear stress acting at the gas-liquid interface,  $\tau_{12}$ , or both simultaneously. The shear stress at the wall for channel flow is

$$\tau_{w2} = \frac{1}{4} \lambda_{w2} \frac{1}{2} \rho_2 V_2^2, \quad (23.78)$$

where

$$\lambda_{w2} = \lambda_{friction} \left( \frac{\rho_2 V_2 D_{h2w}}{\eta_2}, k_w / D_{h2w} \right). \quad (23.79)$$

Here

$$D_{h2w} = \frac{4\alpha_2 F}{Per_{2w}}. \quad (23.80)$$

is the hydraulic diameter of the channel for the liquid, and  $k_w / D_{h2w}$  is the relative roughness. The shear stress of the gas liquid interface in channel flow is

$$\tau_{12} = \frac{1}{4} \lambda_{12} \frac{1}{2} \rho_1 \Delta V_{12}^2, \quad (23.81)$$

where

$$\lambda_{w2} = \lambda_{friction} \left( \frac{\rho_1 V_{12} D_{h1}}{\eta_2}, \frac{\delta_{2F} / 4}{D_{h1}} \right). \quad (23.82)$$

Here

$$D_{h1} = \frac{4\alpha_1 F}{Per_{1w} + Per_{12}}, \quad (23.83)$$

is the hydraulic diameter of the "gas channel" and  $(\delta_{2F}/4)/D_{h1}$  is the relative roughness for the "gas channel" taken to be a function of the waviness of the film.

For vertical plane walls the average shear stress at the wall along  $\Delta z$  is

$$\tau_{w2} = \lambda_{w2} \frac{1}{2} \rho_2 V_2^2 \quad (23.84)$$

where for laminar flow

$$Re_{2z} < (1 \text{ to } 3)10^5 \quad (23.85)$$

in accordance to *Prandtl* and *Blasius*

$$\lambda_{w2} = 1.372 / Re_{2z}^{1/2} \quad (23.86)$$

and

$$Re_{2z} = V_2 \Delta z / \nu_2 \quad (23.87)$$

and for turbulent flow - see in *Albring* (1970)

$$\lambda_{w2} = 0.072 / Re_{2z}^{1/5} \quad (23.88)$$

Similarly the gas side averaged shear stress is computed using

$$Re_{1z} = \Delta V_{12} \Delta z / \nu_2 \quad (23.89)$$

Thus the effective shear stress in the film is

$$\tau_{2eff} = \frac{Per_{2w} \tau_{2w} + Per_{12} \tau_{12}}{Per_{2w} + Per_{12}} \quad (23.90)$$

Now we can estimate the time scale of the turbulence in the shear flow

$$\Delta \tau_2 \approx \left( \nu_2 \delta_{2F} / V_2'^3 \right)^{1/2}, \quad (23.91)$$

using the dynamic friction velocity

$$V_{2eff}^* = \sqrt{\tau_{2eff} / \rho_2} \quad (23.92)$$

Assuming that the pulsation velocity is of the order of magnitude of the friction velocity

$$V_2' \approx \text{const } V_{2eff}^*, \quad (23.93)$$

where the

$$\text{const} \approx 2.9, \quad (23.94)$$

we obtain for



$$Re_{2F}^* > \text{const } 500, \quad (23.95)$$

$$\beta_2 = \text{const}^{3/4} \sqrt{\frac{2}{\pi}} Pr_2^{-1/2} Re_{2F}^{*-1/4} V_{2eff}^*, \quad (23.96)$$

and for

$$Re_2 < \text{const } 500, \quad (23.97)$$

$$\beta_2 = \text{const}^{1/2} \sqrt{\frac{2}{\pi}} Pr_2^{-1/2} Re_{2F}^{*-1/2} V_{2eff}^*, \quad (23.98)$$

where

$$Re_{2F}^* = \frac{\rho_2 V_{2eff}^* \delta_{2F}}{\eta_2}. \quad (23.99)$$

More careful modeling of the turbulent length scale for the derivation of Eq. (23.98) was done by *Kim and Bankoff* (1983). The authors used the assumption

$$V_2' \approx V_{2eff}^*, \quad (23.100)$$

and modified Eq. (23.98) as follows

$$\beta_2 = 0.061 Pr_2^{-1/2} Re_2^{0.12} V_{2eff}^*, \quad (23.101)$$

where

$$\ell_{e2} = \left[ \frac{\sigma}{(\rho_2 - \rho_1) g} \right]^{1/2} 3.03 \times 10^{-8} Re_1^{*1.85} Re_2^{*0.006} Pr_2^{-0.23}, \quad (23.102)$$

for  $3000 < Re_1^* < 18000$  and  $800 < Re_2^* < 5000$ ,  $\lambda_{12} = 0.0524 + 0.92 \times 10^{-5} Re_2^*$  valid for  $Re_2^* > 340$ , and  $\tau_{12} \gg \tau_{2w}$ . Note the special definition of the *Reynolds* numbers as mass flow per unit width of the film

$$Re_1^* = \frac{\alpha_1 \rho_1 V_1}{\eta_1} \frac{F}{Per_{12}}, \quad (23.103)$$

$$Re_2^* = \frac{\alpha_2 \rho_2 V_2}{\eta_2} \frac{F}{Per_{12}}. \quad (23.104)$$

Assuming that the pulsation velocity is of order of the magnitude of the friction velocity as before but the time scale of the turbulence is

$$\Delta \tau_2 \approx (\nu_2 / \varepsilon_2)^{1/2} = \nu_2 / V_{2eff}^{*2}, \quad (23.105)$$

results for

$$Re_{2F}^* > \text{const } 500, \quad (23.106)$$

in

$$\beta_2 = \sqrt{\frac{2}{\pi}} Pr_2^{-1/2} V_{2eff}^* \cdot \quad (23.107)$$

This equation is recommended by *Jensen and Yuen* (1982) with a constant 0.14 instead  $\sqrt{2/\pi}$  for  $\tau_{12} \gg \tau_{2w}$ . *Hughes and Duffey* reproduced an excellent agreement with experimental data for steam condensation in horizontal liquid films by using Eq. (23.96) and the assumption

$$\tau_{2eff} = (\tau_{12} + \tau_{2w}) / 2. \quad (23.108)$$

Nevertheless one should bear in mind that Eq. (23.90) is more general.

An example of detailed modeling of the turbulence structure in the film during film condensation from stagnant steam on vertical cooled surfaces is given by *Mitrovich Rohsenow and Choi* (1961). For this case

$$\dot{q}_2^{m1\sigma} = h_2^{1\sigma} (T_2^{1\sigma} - T_w) \quad (23.109)$$

where

$$h_2^{1\sigma} \delta_{2F} / \lambda_2 = 1.05 Re_{2F}^{-0.33} \left[ 1 + C^{1.9} Re_{2F}^{1.267} Pr_2^{1.11} \right]^{0.526}, \quad (23.110)$$

$$C = 8.8 \cdot 10^{-3} / (1 + 2.29 \cdot 10^{-5} Ka_2^{0.269}), \quad (23.111)$$

$$Ka_2 = \rho_2 \sigma^3 / (g \eta_2^4). \quad (23.112)$$

Summarizing the results discussed above we can say the following:

(a) Gas in the two-phase film flow behaves as a gas in a channel. Therefore the gas side heat transfer can be considered as a heat transfer between gas and the "channel wall" taking into account that the "wall roughness" is influenced by the waves at the liquid surface.

(b) The liquid side heat transfer at the interface is due to molecular and turbulent heat conduction. The modeling of the turbulent heat conduction can be performed by modeling the time and length scale of the turbulence taking into account that turbulence is produced mainly

- (i) at the wall - liquid interface, and
- (ii) at the gas - liquid interface.

(c) Gas side heat transfer in a pool flow can be considered as a heat transfer at plane interface.

(d) The liquid side heat transfer from the interface into the bulk liquid is governed by the solution of the transient *Fourier* equation where in case of the turbulence the use of effective heat conductivity instead of the molecular conductivity is recommended.

### 23.3 Spontaneous flashing of superheated film

The considerations for the estimation of the spontaneous evaporation of the superheated film are identical to those presented in Chapter 22 Section 5 for the spontaneous evaporation of a superheated droplet. In order to calculate the source terms we simply replace the subscripts 3 with 2 and use the relationships from Chapter 22 Section 5.

Having in mind that

$$\mu_{12} = 0, \quad (23.113)$$

$$\dot{q}_1^{m2\sigma} = 0, \quad (23.114)$$

we obtain for the energy jump condition

$$(\rho w)_{21} [h''(T_2^{1\sigma}) - h'(T_2^{1\sigma})] = -\beta_2 \rho_2 c_{p2} (T_2^{1\sigma} - T_2), \quad (23.115)$$

or

$$T_2^{1\sigma} = T_2 - (\rho w)_{21} [h''(T_2^{1\sigma}) - h'(T_2^{1\sigma})] / (\beta_2 \rho_2 c_{p2}). \quad (23.116)$$

From this equation the interface temperature can be computed by iterations starting with  $T_2^{1\sigma} \approx T'(p)$ . The heat transfer from the interface to the bulk liquid is

$$\dot{q}_2^{m1\sigma} = \beta_2 \rho_2 c_{p2} (T_2^{1\sigma} - T_2), \quad (23.117)$$

and the evaporated mass per unit time and unit mixture volume is

$$\mu_{21} = a_{12} (\rho w)_{21}. \quad (23.118)$$

### 23.4 Evaporation of saturated film in superheated gas

If the flow consists of superheated gas,  $T_1 > T'(p)$ , and saturated liquid,  $T_2 = T'(p)$  the heat transferred from the gas to the interface by convection is

$$\dot{q}_2^{m1\sigma} = -a_{12} h_c [T_1 - T'(p)]. \quad (23.119)$$

The energy jump condition at the surface is

$$\mu_{21} = -\dot{q}_2^{m1\sigma} / [h''(p) - h'(p)] = a_{12} h_c [T_1 - T'(p)] / [h''(p) - h'(p)]. \quad (23.120)$$

The energy balance for the gas at  $p \approx \text{const}$  and negligible gas diffusion and convection from the neighboring cells is

$$\alpha_1 \rho_1 c_{p1} \frac{dT_1}{d\tau} = -\dot{q}_2^{n1\sigma} \frac{h_1 - h''(p)}{h''(p) - h'(p)} \approx -\dot{q}_2^{n1\sigma} \frac{c_{p1} [T_1 - T'(p)]}{h''(p) - h'(p)}, \quad (23.121)$$

or

$$\frac{dT_1}{d\tau} = [T_1 - T'(p)]^2 / \Delta\tau_1, \quad (23.122)$$

where

$$\Delta\tau_1 = [h''(p) - h'(p)] \alpha_1 \rho_1 / a_{12}.$$

We see from the above equation that the colder steam entering the bulk steam has a cooling effect on the bulk steam. For  $\tau = 0$ ,  $T_1 = T_{1a}$  the analytical solution gives

$$\frac{T_1 - T'(p)_1}{T_{1a} - T'(p)} = \frac{1}{1 - [T_1 - T'(p)] \frac{\Delta\tau}{\Delta\tau_1}}. \quad (23.123)$$

The averaged temperature difference  $T_l - T'(p)$  along the time  $\Delta\tau$  is

$$T_1 - T'(p) = -\frac{\Delta\tau_1}{\Delta\tau} \ln \left\{ 1 - [T_{1a} - T'(p)] \frac{\Delta\tau}{\Delta\tau_1} \right\}. \quad (23.124)$$

Thus, for evaporation of a saturated film in superheated gas the instantaneous heat and mass transfer is defined by Eqs. (23.119) and (23.120) and the average heat and mass transfer along the time  $\Delta\tau$  is computed as follows:

- (i) Compute the averaged heat temperature difference using Eq. (23.124);
- (ii) Compute the average heat transfer using Eq. (23.119);
- (iii) Compute the average mass transfer using the energy jump condition, Eq. (23.120).

## 23.5 Condensation of pure steam on subcooled film

Consider steam having temperature  $T_l$  interacting with a liquid film having temperature  $T_2$  where

$$T_2 < T'(p). \quad (23.125)$$

The steam side interface temperature is  $T_1^{2\sigma}$ . The heat transferred from the interface into the gas per unit time and unit mixture volume is

$$\dot{q}_1^{m2\sigma} = a_{12} h_c (T_1^{2\sigma} - T_1) \quad (23.126)$$

where  $h_c$  is computed as discussed in Section 23.1. The heat transferred from the interface into the bulk liquid is

$$\dot{q}_2^{m1\sigma} = a_{12} \beta_2 \rho_2 c_{p2} (T_2^{1\sigma} - T_2). \quad (23.127)$$

A simplified way to compute the condensing mass per unit time and unit mixture volume is to assume

$$T_2^{1\sigma} = T_1^{2\sigma} \approx T'(p). \quad (23.128)$$

Using the energy jump condition we obtain

$$\mu_{12} = a_{12} \left\{ h_c [T'(p) - T_1] + \beta_2 \rho_2 c_{p2} [T'(p) - T_2] \right\} / [h''(p) - h'(p)]. \quad (23.129)$$

An improvement of the description can be achieved by dropping the assumption (23.128). In this case one must compute the condensing mass flow rate  $(\rho w)_{12}$  as a function of the interface temperature using the kinetic theory as discussed in Section 22.1.2. Consequently we have

$$(\rho w)_{12} = f(T_2^{1\sigma}, T_1, p) \quad (23.130)$$

The energy jump condition

$$(\rho w)_{12} [h''(T_{2i}) - h'(T_{2i})] = h_c (T_1^{2\sigma} - T_1) + \beta_2 \rho_2 c_{p2} (T_2^{1\sigma} - T_2), \quad (23.131)$$

governs the interface temperature

$$T_2^{1\sigma} = \left\{ (\rho w)_{12} [h''(T_2^{1\sigma}) - h'(T_2^{1\sigma})] + h_c T_1 + \beta_2 \rho_2 c_{p2} T_2 \right\} / (h_c + \beta_2 \rho_2 c_{p2}). \quad (23.132)$$

Obviously  $T_2^{1\sigma}$  has to be obtained by iterations starting with  $T_2^{1\sigma} \approx T'(p)$ .

## 23.6 Evaporation or condensation in presence of non-condensable gases

In pure vapor condensation the condensate film provides the only heat transfer resistance, whereas if a small amount of non-condensable gas is present, then the main resistance to heat transfer is the gas/vapor boundary layer. Air mass fractions

as low as 0.5 % can reduce 50 % or more the condensation, see *Pohlhausen* (1921), *Potukho and popov* (1963), *Gnielinski* (1975), *Al-Diwani and Rose* (1973), *Siddique and Golay* (1994), *Uchida et al.* (1964).

Next we consider gas-film flow. The gas has temperature  $T_1$  and concentration of steam  $C_{M1}$ . The system pressure is  $p$  and the steam partial pressure in the bulk of the gas is  $p_{M1}$ . The liquid has temperature  $T_2$ , that is less than the saturation temperature  $T'(p)$  for the system pressure. This means that the liquid is subcooled and spontaneous flashing is not possible. In this case diffusion controlled evaporation or condensation at the interface is possible depending on the interface temperature satisfying the energy jump condition. If the partial pressure in the gas boundary layer  $p'(T_2^{1\sigma}) > p_{M1}$  steam is transported from the interface into the gas bulk. The opposite is the case if  $p'(T_2^{1\sigma}) < p_{M1}$ .

Thus for the analysis the estimation of the interface temperature is important. The way we propose here is:

- (1) Assume as a first estimation  $T_2^{1\sigma} \approx T_2$ ;
- (2) Compute the steam partial pressure at the interface  $p'(T_2^{1\sigma})$ ;
- (3) If  $p'(T_2^{1\sigma}) > p_{M1}$  compute the diffusion controlled evaporation mass flow rate

$$(\rho w)_{21} = -(\rho w)_{12}^*, \quad (23.133)$$

where

$$(\rho w)_{12}^* = h_c \frac{M_{M1}}{M_1} \ln \frac{p - p'(T_2^{1\sigma})}{\sum p_{n1}} / (c_{p1} Le^{2/3}), \quad (23.134)$$

see in VDI-Waermeatlas (1984).

- (4) If  $p'(T_2^{1\sigma}) < p_{M1}$  compute the diffusion controlled condensation mass flow rate

$$(\rho w)_{21} = (\rho w)_{12}^* \quad (23.135)$$

Here

$$M_1 = \frac{\sum p_{n1}}{p} M_{\Sigma n1} + \frac{p - \sum p_{n1}}{p} M_{M1} \quad (23.136)$$

is the mixture mole mass and  $M_{\Sigma n1}$  and  $M_{M1}$  are the mole masses of the inert components and of the steam, respectively, e.g.  $M_{\Sigma n1} = 28.96 \text{ kg/mol}$  for air and  $M_{M1} = 18.96 \text{ kg/mol}$  for water steam.

$$Le = \lambda_1 / \left( \rho_1 c_{p1} D_{M \rightarrow \sum n} \right) \quad (23.137)$$

is the *Lewis* number,  $D_{M \rightarrow \sum n}$  is the diffusion constant for steam in the gas mixture.

(5) Compute the gas and the liquid heat flux from the interface

$$\dot{q}_1^{n2\sigma} = f h_c (T_1^{2\sigma} - T_1), \quad (23.138)$$

$$\dot{q}_2^{n1\sigma} = \beta_2 \rho_2 c_{p2} (T_2^{1\sigma} - T_2). \quad (23.139)$$

Here  $f$  is a factor reflecting the gas side convective heat transfer. In the case of no mass transfer  $f=1$ .

For condensation the following proposal for computation of  $f$  was made in VDI-Waermeatlas (1984):

$$f = |F| / \left( 1 - e^{-|F|} \right), \quad (23.140)$$

where

$$F = (\rho w)_{12} c_{pM1} / h_c. \quad (23.141)$$

(6) Compute by iterations the interface temperature  $T_2^{1\sigma}$  from the energy jump condition

$$T_2^{1\sigma} = \left\{ (\rho w)_{12}^* \left[ h''(T_2^{1\sigma}) - h'(T_2^{1\sigma}) \right] + f h_c T_1 + \beta_2 \rho_2 c_{p2} T_2 \right\} / (f h_c + \beta_2 \rho_2 c_{p2}) \quad (23.142)$$

starting with  $T_2^{1\sigma} = T_2$ .

(7) Check again the initial hypothesis and compute the interfacial evaporation or condensation mass flow rate, respectively, and the heat fluxes using the final interfacial temperature  $T_2^{1\sigma}$ .

## Nomenclature

### Latin

$a$  =  $\lambda / (\rho c_p)$ , temperature conductivity,  $m^2/s$

$a_{12}$  =  $1/\Delta z$  gas liquid interfacial area density in Cartesian coordinates,  $1/m$

$D_{h1}$	hydraulic diameter for the gas, $m$
$D_{h2}$	hydraulic diameter for the liquid, $m$
$D_{h12}$	hydraulic diameter for computation of the gas friction pressure loss component in a gas-liquid stratified flow, $m$
$F$	channel cross section, $m$
$Gr_1$	$= g \left( -\frac{1}{\rho_1} \frac{\partial \rho_1}{\partial T_1} \right) \big _{T_1 - T_1^{2\sigma}} \Delta z^3 / \nu_1^2$ , gas site <i>Grashof</i> number, dimensionless
$h_1^{2\sigma}$	gas site interface heat transfer coefficient, $W/(m^2K)$
$k_w$	wall roughness, $m$
$Le$	$= \lambda_1 / \left( \rho_1 c_{p1} D_{M \rightarrow \Sigma n} \right)$ Lewis number, dimensionless
$D_{M \rightarrow \Sigma n}$	diffusion coefficient for steam in the gas mixture, $m^2/s$
$\ell_{e2}$	turbulent length scale in the film, $m$
$M_1$	mixture mole mass, $kg/1\_mol$
$M_{n1}$	mole masses as the inert components, $kg/1\_mol$
$M_{M1}$	mole masses of the steam, $kg/1\_mol$
$Nu_{1z}$	$= h_{1\sigma} \Delta z / \lambda_1$ , gas <i>Nusselt</i> number, dimensionless
$Per_w$	perimeter of the rectangular channel, $m$
$Per_{1w}$	wetted perimeters for the gas, $m$
$Per_{2w}$	wetted perimeters for the liquid, $m$
$Pr_1^t$	turbulent gas <i>Prandtl</i> number, dimensionless
$Pr_1$	gas <i>Prandtl</i> number, dimensionless
$Pr_2$	liquid <i>Prandtl</i> number, dimensionless
$p$	pressure, $Pa$
$\dot{q}_1^{m2\sigma}$	heat flux density from the interface into the gas, $W/m^3$
$\dot{q}_2^{m1\sigma}$	heat flux density from the interface into the bulk liquid, $W/m^3$
$Re_1$	$= \rho_1 w_1 D_{h1} / \eta_1$ , gas <i>Reynolds</i> number, dimensionless
$Re_2$	$= \rho_2 w_2 D_{h2} / \eta_2$ , liquid <i>Reynolds</i> number, dimensionless
$Re_1^*$	$= \frac{\alpha_1 \rho_1 V_1}{\eta_1} \frac{F}{Per_{12}}$ , modified gas <i>Reynolds</i> number, dimensionless
$Re_2^*$	$= \frac{\alpha_2 \rho_2 V_2}{\eta_2} \frac{F}{Per_{12}}$ , modified liquid <i>Reynolds</i> number, dimensionless
$Re_{2F}$	$= \frac{\rho_2 V_2 \delta_{2F}}{\eta_2}$ film <i>Reynolds</i> number, dimensionless
$Re_{1z}$	$= V_1 \Delta z / \nu_1$ , gas <i>Reynolds</i> number, dimensionless



---

$Re_2'$	$= \rho_2 V_2' \ell_{e2} / \eta_2$ , liquid turbulent <i>Reynolds</i> number, <i>dimensionless</i>
$Re_{2F}^*$	$= \frac{\rho_2 V_{2eff}^* \delta_{2F}}{\eta_2}$ , liquid turbulent <i>Reynolds</i> number based on the friction velocity, <i>dimensionless</i>
$r$	radius, <i>m</i>
$Sr_1$	$= \frac{Nu_1}{Re_1 Pr_1}$ , <i>Struhal</i> number, <i>dimensionless</i>
$T$	temperature, <i>K</i>
$T_2^{l\sigma}$	liquid side interface temperature, <i>K</i>
$V_1$	gas velocity, <i>m/s</i>
$V_2$	liquid velocity, <i>m/s</i>
$V_2'$	volume-averaged liquid pulsation velocity, <i>m/s</i>
$V_{2eff}^*$	$= \sqrt{\tau_{2eff} / \rho_2}$ , dynamic friction velocity, <i>m/s</i>
$w_1$	axial gas velocity, <i>m/s</i>
$w_2$	axial liquid velocity, <i>m/s</i>
$y$	distance, <i>m</i>
$z$	axial coordinate, <i>m</i>

### Greek

$\alpha_2$	local liquid volume fraction in the computational cell, <i>dimensionless</i>
$\beta_1$	$= \frac{h_{l\sigma}}{\rho_1 c_{p1}} = \frac{Nu_1}{Re_1 Pr_1} V_1 = Sr_1 V_1$ , weighted heat transfer coefficient, <i>m/s</i>
$\Delta$	finite difference, -
$\Delta \tau_2$	time for which the eddy stays at the interface, renewal period, <i>s</i>
$\delta_{2F}$	film thickness, <i>m</i>
$\eta$	dynamic viscosity of liquid, <i>kg/(ms)</i>
$\lambda$	thermal conductivity, <i>W/(mK)</i>
$\lambda_{2eff}$	effective conductivity, <i>W/(mK)</i>
$\lambda_{w1}$	friction coefficient, <i>dimensionless</i>
$\mu_{21}$	steam mass generation per unit mixture volume and unit time due to evaporation, <i>kg/(sm<sup>3</sup>)</i>
$\mu_{12}$	liquid mass generation per unit mixture volume and unit time due to condensation, <i>kg/(sm<sup>3</sup>)</i>
$\rho$	density, <i>kg/m<sup>3</sup></i>
$(\rho w)_{21}$	steam mass generation per unit surface and unit time due to evaporation, <i>kg/(m<sup>2</sup>s)</i>

$(\rho w)_{12}$	liquid mass generation per unit surface and unit time due to condensation, $kg/(m^2s)$
$\tau_{w1}$	$= \lambda_{w1} \frac{1}{2} \rho_1 V_1^2$ , shear stress, $N/m^2$
$\tau_{2w}$	liquid-wall shear stress, $N/m^2$
$\tau_{12}$	gas-liquid interface shear stress, $N/m^2$
$\tau$	time, $s$

### Subscripts

1	gas
2	liquid film
2F	liquid film
Ml	vapor inside the gas mixture
nl	inert components inside the gas

### References

- Albring W (1970) *Angewandte Stroemungslehre*, Verlag Theodor Steinkopf, Dresden, 4. Auflage,
- Al-Diwani HK and Rose JW (1973) Free convection film condensation of steam in presence of non condensing gases, *Int. J. Heat Mass Transfer*, vol 16 p 1959
- Banerjee S (1990) Turbulence structure and transport mechanisms at interfaces, *Proc. Ninth Int. Heat Transfer Conference*, Jerusalem, Israel, vol 1 pp 395-418
- Brumfield LK, Houze KN, and Theofanous TG (1975) Turbulent mass transfer at free, Gas-Liquid Interfaces, with Applications to Film Flows. *Int. J. Heat Mass Transfer*, vol 18 pp 1077-1081
- Bunker RS and Carey VP (1986) Modeling of turbulent condensation heat transfer in the boiling water reactor primary containment, *Nucl. Eng. Des.*, vol 91 pp 297-304
- Churchill SW, Brier JC (1955) Convective heat transfer from a gas stream at high temperature to a circular cylinder normal to the flow, *Chem. Engng. Progr. Simp. Ser.* 51, vol 17 pp 57-65
- Fortescue GE and Pearson JRA (1967), On gas absorption into a turbulent liquid, *Chem. Engng. Sci.*, vol 22 pp 1163-1176
- Fourier J (1822) *Theory analytique de la chaleur*
- Gnielinski V (1975) Berechnung mittlerer Waerme- und Stoffuebertragungskoeffizienten an laminar und turbulent ueberstroemenden Einzelkoerpern mit Hilfe einer einheitlichen Gleichung, *Forsch. Ing. Wes*, vol 41 no 5 pp 145-153
- Hausen H (1958) Darstellung des Waermeueberganges in Roehren durch verallgemeinerte Potenzgleichungen, *Verfahrenstechnik*, vol 9 no 4/5 pp 75-79
- Hobbbahn WK (Oct. 10-13, 1989) Modeling of condensation in light water reactor safety, *Proc. of the Fourth International Topical Meeting on Nuclear Reactor Thermal-Hydraulics*, Mueller U, Rehme K, Rust K, Braun G (eds) Karlsruhe, vol 2 pp 1047-1053

- Jakob M, Linke W (1933) Der Waermeübergang von einer waagerechten Platte an sidendes Wasser, *Forsch. Ing. Wes.*, vol 4 pp 75-81
- Jensen RJ and Yuen MC (1982) Interphase transport in horizontal stratified concurrent flow, U.S. Nuclear Regulatory Commission Report NUREG/CR-2334
- Kim HJ and Bankoff SG (Nov. 1983) Local heat transfer coefficients for condensation in stratified countercurrent steam - water flows, *Trans. ASME*, vol 105 pp 706-712
- Kim MH, Corradini ML (1990) Modeling of condensation heat transfer in a reactor containment, *Nucl. Eng. and Design*, vol 118 pp 193-212
- Lamont JC and Yuen MC (1982) Interfase transport in horizontal stratified concurrent flow, U. S. Nuclear Regulatory Commission Report NUREG/CR-2334
- Petukhov BS, Popov VN (1963) Theoretical calculation of heat exchange and friction resistance in turbulent flow in tubes of an incompressible fluid with variable physical properties. *High Temperature*, vol 1 pp 69-83
- Pohlhausen E (1921) Der Waermeaustausch zwischen festen Koerpern und Fluessigkeiten mit kkleiner Reibung und kleiner Waermeleitung, *Z. angew. Math. Mech.*, vol 1 no 2 pp 115 - 121
- Rohsenow WM, Choi H (1961) Heat, mass and momentum transfer, Prentice - Hall Publishers, New Jersey
- Siddique M, Golay MW (May 1994) Theoretical modeling of forced convection condensation of steam in a vertical tube in presence of non condensable gas, *Nuclear Technology*, vol 106
- Slattery JC 1990 Interfacial transport phenomena, Springer Verlag
- Theofanous TG, Houze RN and Brumfield LK (1976) Turbulent mass transfer at free, gas-liquid interfaces, with application to open- channel, bubble and jet flows, *Int. J. Heat Mass Transfer* vol 19 pp 613-624
- Uchida U, Oyama A, Togo Y (1964) Evolution of post - incident cooling system of light water reactors, *Proc. 3th Int. Conf. Peaceful Uses of Atomic Energy*, International Atomic Energy Agency, Vienna, Austria, vol 13 p 93
- VDI-Waermeatlas (1984) 4. Auflage, VDI-Verlag.



## 24 Condensation at cooled walls

### 24.1 Pure steam condensation

#### 24.1.1 Onset of the condensation

Consider gas flow in a pipe. The heat transfer coefficient at the wall for turbulent flow without correction of the properties in the wall boundary layer is

$$h_{convective} = 0.023 Re_1^{0.8} Pr_1^{0.4} \frac{\lambda_1}{D_{hy}}, \quad (24.1)$$

where the *Reynolds* and the *Prandtl* numbers are defined as a functions of the gas mixture properties

$$Re_1 = D_{hy} \rho_1 |w_1| / \eta_1, \quad (24.2)$$

$$Pr_1 = \eta_1 c_{p1} / \lambda_1. \quad (24.3)$$

For prescribed heat flux the wall temperature is

$$T_w = T_1 + \dot{q}_w'' / h_{convective}. \quad (24.4)$$

If the wall temperature is less then the saturation temperature at the partial pressure of the steam

$$T_w \leq T_{cond}, \quad (24.5)$$

where

$$T_{cond} = T'(p_{M1}), \quad (24.6)$$

condensation at the wall occurs.

#### 24.1.2 Gravitation films on plates

Gravitational films along inclined surfaces are common in nature and technology. That is why they attracted attention of scientists like *Nusselt* already in 1916. The source of the film is usually defined as the flow rate per unit of film width  $\dot{V}'$  in  $m^2/s$ . This amount is either prescribed or subject to analyses for instance in case of

mass transfer due to condensation, droplet deposition on the wall etc. If the source of the liquid is known then the independent values characterizing the film flow are  $(\nu_2, \sigma_2, \rho_2, g, \varphi)$ . Isothermal films without heat and mass transfer are easy to describe. For this purpose the conservation of momentum is solved for steady developed flow neglecting entrance effects. The solutions are presented in the form of dependence between the share stress, film thickness and flow rate per unit of film width,

$$f(\tau_{2w}, \delta_2, \dot{V}'_2) = 0, \quad (24.7)$$

called in the literature *triangular* relationships. In our case the wall share stress is easily obtained by setting the weight of the liquid attached to a surface divided by this surface,

$$\tau_{2w} = \text{weight} / (\Delta x \Delta z) = \rho_2 g \delta_2, \quad (24.8)$$

so that the relation defining the film thickness depends only on the volumetric flow rate per unit of film width

$$\delta_2 = f(\dot{V}', \dots). \quad (24.9)$$

We see that for given  $\dot{V}'$  the velocity profile of the film being either laminar or turbulent is determining the film thickness. In order to decide which type of the velocity profile we have to expect the classification of the different film flow regimes is helpful.

#### 24.1.2.1 Film flow regimes

The waviness of the surface depends (a) on the properties of the liquid collected a dimensionless group called *Kapiza* number

$$Ka_2 = \sigma_2^3 / (\rho_2^3 g \nu_2^4) \quad (24.10)$$

and (b) on the mass flow rate represented by the film *Reynolds* number

$$Re_{2\delta} = \dot{V}' / \nu. \quad (24.11)$$

Usually engineers consider laminar flow for Reynolds number less then 400 and turbulent for larger then 400. More precisely, a variety of wave types lead to different classifications of the flow regimes. *Ishigai* et al. (1972), based on the analysis of surface perturbations, discriminate five regimes in the flow of a vertical liquid film as given in Table 1. The table contains also the regimes for water at atmospheric conditions.

**Table 1** *Ishigai et al. (1972) classification of the film regimes*

Type	Region	Water at atmospheric conditions
Laminar	$\text{Re}_{2\delta} \leq 0.47Ka_2^{1/10}$	$\text{Re}_{2\delta} \leq 5.7$
First transient regime	$0.47Ka_2^{1/10} < \text{Re}_{2\delta} \leq 2.2Ka_2^{1/10}$	$5.7 < \text{Re}_{2\delta} \leq 27$
Stable wavy	$2.2Ka_2^{1/10} < \text{Re}_{2\delta} \leq 75$	$27 < \text{Re}_{2\delta} \leq 75$
Second transient regime	$75 < \text{Re}_{2\delta} \leq 400$	$75 < \text{Re}_{2\delta} \leq 400$
Fully turbulent	$400 < \text{Re}_{2\delta}$	$400 < \text{Re}_{2\delta}$

Note that the origination of the first waves was already observed by *Kapitza* in 1948 for  $\text{Re}_{2\delta} > 0.61Ka_2^{1/11}$ . *Brauer* (1971) reported for this limit  $\text{Re}_{2\delta} > 0.261Ka_2^{1/8}$ .

#### 24.1.2.2 Film thickness without mass transfer

We concentrate our attention to liquid films without evaporation, condensation, gas absorption or gas release. In this case the mass flow rate is delivered to the wall from external source.

**Steady state laminar films (Nusselt 1916):** For constant properties the solution of the steady state *Navier-Stokes* equation  $\nu_2 \frac{d^2 u_2}{dy^2} + g \cos \varphi = 0$  with boundary conditions  $u_2 = 0$  at  $y = 0$  (adherence at wall),  $du_2/dy = 0$  at  $y = \delta_2$  (absence of shear stresses on the free surface) is

$$u_2 = \frac{g \cos \varphi}{\nu_2} \left( y\delta_2 - \frac{1}{2} y^2 \right). \quad (24.12)$$

The volumetric flow rate per unit of film width is then

$$\dot{V}'_2 = \int_0^{\delta_2} u_2 dy = \frac{g\delta_2^3}{3\nu_2} \cos \varphi. \quad (24.13)$$

The film thickness then depends on the volumetric flow rate per unit of film width as follows

$$\delta_2 = \left( \frac{\dot{V}'_2 3\nu_2}{g \cos \varphi} \right)^{1/3} = \left( \frac{3\nu_2^2}{g \cos \varphi} \right)^{1/3} \text{Re}_{2\delta}^{1/3}. \quad (24.14)$$

This expression was confirmed by several authors to agree well with experimental data – see *Fulford* (1964), *Ganchev and Kozlov* (1973), *Alekseenk et al.* (1973),

*Tananaiko* and *Vorontsov* (1975), *Gimbutis* (1988), *Boyadjiev* and *Beschkov* (1984).

**Steady-state turbulent film flow on a smooth plate:** *Alekseenko* et al. (1996) assuming smooth surface postulated the validity of the *Blasius* law for wall shear stress

$$\tau_{2w} = \frac{0.045}{\frac{u_2 \delta_2}{v_2}} \frac{1}{2} \rho u_2^2. \quad (24.15)$$

Assuming that the 1/7th profile

$$\frac{u'}{u} = \left( \frac{y}{\delta} \right)^{1/7}, \quad (24.16)$$

represents the real turbulent velocity distribution in the film the authors obtained

$$u_2 = \frac{8}{7} \frac{\dot{V}'_2}{\delta_2}. \text{ Taking into account that the wall share stress is known, } \tau_{2w} = \rho_2 g \delta_2,$$

and replacing into the *Blasius* equation the authors come to the result

$$\delta_2 = 0.305 \frac{\dot{V}_2'^{7/12} v_2^{1/12}}{(g \cos \varphi)^{1/3}} = 0.305 \left( \frac{v_2^2}{g \cos \varphi} \right)^{1/3} \text{Re}_{2\delta}^{7/12}. \quad (24.17)$$

Correspondingly the shear stress is

$$\tau_{2w} = \rho_2 g \delta_2 = 0.305 \rho_2 (g \cos \varphi)^{2/3} v_2^{1/12} \dot{V}_2'^{7/12} = 0.305 \rho_2 (v_2 g \cos \varphi)^{2/3} \text{Re}_{2\delta}^{7/12}. \quad (24.18)$$

Note that *Brauer* (1971) recommend for the turbulent film the following empirical relation

$$\delta_2 = 0.302 \left( \frac{3v_2^2}{g \cos \varphi} \right)^{1/3} \text{Re}_{2\delta}^{8/15}, \quad (24.19)$$

which is obviously very close to the 1/7<sup>th</sup> profile solution. *Kutateladze* (1979) and *Dukler* and *Bergelin* (1952) have applied similar approaches using instead of 1/7<sup>th</sup> profiles logarithmic profiles for two-layered schemes. As can be seen from Fig. 1 for the data for shear stress as well as from the analysis by *Gimbutis* (1988) for the data for thickness, various approaches differ insignificantly and generalize fairly well the experimental results for  $\text{Re} > 500$ .



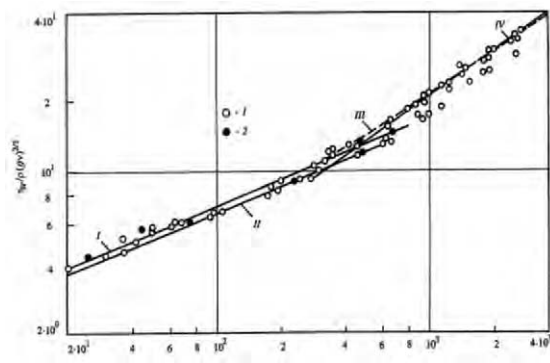


**Fig. 1** Wall shear stresses as a function of the film Reynolds number for water falling film on a vertical wall taken from Berman and Tumanov (1962). Prediction: I – Nusselt (1916); II – Kapitza (1948); III – Kutateladze (1979); IV – Alekseenko et al. (1996); Experiment by Alekseenko et al. (1996) – points 1, 2

**Conclusion:** For engineering applications it is recommended to compute the thickness of a falling film on inclined smooth walls as follows:

$$\delta_2 = \left( \frac{\dot{V}'_2 3\nu_2}{g \cos \varphi} \right)^{1/3} = \left( \frac{3\nu_2^2}{g \cos \varphi} \right)^{1/3} \text{Re}_{2\delta}^{1/3} \text{ for } \text{Re}_{2\delta} \leq 400, \quad (24.20)$$

$$\delta_2 = 0.305 \left( \frac{\nu_2^2}{g \cos \varphi} \right)^{1/3} \text{Re}_{2\delta}^{7/12} \text{ for } 400 > \text{Re}_{2\delta}. \quad (24.21)$$

### 24.1.2.3 Film thickness during condensation

Now we concentrate our attention to liquid films for which the source of mass is a *condensation process* from a steam being in saturation. The surface temperature of the film during the condensation is the saturation temperature at the environmental pressure  $T'$  and the wall temperature is  $T_w$ . Assuming linear temperature profile in the film the heat flux release by the condensation and removed into the wall is

$$\dot{q}_w^{n2\sigma} = \lambda_2 \frac{T' - T_w}{\delta_2} \quad (24.22)$$

and the heat transfer coefficient

$$h_{\text{stagnant}} = \lambda_2 / \delta_2. \quad (24.23)$$

Note that for this case the Reynolds number can be expressed by the averaged heat flux over the height  $H$  as follows

$$\text{Re}_{2\delta} = \frac{\rho_2 w_2 \delta_2}{\eta_2} = \frac{\dot{q}_w^{n2\sigma} H}{\eta_2 \Delta h}. \quad (24.24)$$

For prescribed wall temperature the Eqs. (24.20) or (24.21) together with (24.22-24) can be solved iteratively with respect to the heat flux and the film thickness. While for laminar flow this is accurate, for turbulent flow this is approximation because the thermal eddy diffusivity inside the film is not a constant. More sophisticated approaches are described below. The improvements take into account the variation of the thermal properties in the film, the waviness of the film that promote mass transfer, the turbulent structure of the film and some adjustments to experimental data.

**The Nusselt water skin theory for laminar condensation from 1916:** Assuming that the thermal resistance controlling the condensation is the heat conduction through the film and the flow in the film is laminar *Nusselt* obtained the following analytical solution for the averaged heat transfer coefficient for laminar condensation on vertical wall with high  $H$  from stagnant steam

$$h_{stagnant} := \frac{\dot{q}_w''^{2\sigma}}{T_{cond} - T_w} = \frac{2}{3} \sqrt{2} \left[ \frac{\rho'(\rho' - \rho'') \lambda'^3 g \cos \varphi \Delta h}{H \eta'(T_{cond} - T_w)} \right]^{1/4} f_{prop} f_{wave}, \quad (24.25)$$

or

$$T_w = T_{cond} - \left( -\dot{q}_w''^{2\sigma} C \right)^{4/3}, \quad (24.26)$$

where

$$C = \frac{2}{3} \sqrt{2} \left[ \frac{\rho'(\rho' - \rho'') \lambda'^3 g \cos \varphi \Delta h}{H \eta'} \right]^{1/4} f_{prop} f_{wave}, \quad (24.27)$$

$\Delta h = h'' - h'$  is the latent heat of vaporization and  $f_{prop} = 1$ ,  $f_{wave} = 1$ . In order to take into account the variation of the thermal properties inside the film and the wave structure for  $Re \leq 400$  *Labuntzov* (1957) proposed to correct the *Nusselt* solution by

$$f_{prop} = \left\{ \left[ \frac{\lambda_2(T_w)}{\lambda'} \right]^3 \frac{\eta'}{\eta(T_w)} \right\}^{1/8}, \quad (24.28)$$

and

$$f_{wave} = Re_{2\delta}^{0.04}, \quad (24.29)$$

respectively. Correction for the influence of the film subcooling is introduced by *Rohsenow et al.* (1985) p. 115 as follows:

$$\Delta h = h'' - h' + \frac{3}{8} c'_p (T' - T_w). \quad (24.30)$$

**Condensation from stagnant steam at turbulent liquid film:** For large vertical surfaces the heat transfer coefficient may exceed the computed one by 70% due to ripples that attain greatest amplitude even for  $Re_{\delta_2} < 400$ . Some authors write the *Nusselt* result in the form

$$\frac{h_{\text{saignant}}}{\lambda'} \left[ \frac{\eta'^2}{\rho'(\rho' - \rho'')g \cos \varphi} \right]^{1/3} = 0.95 Re_{2\delta}^{-1/3} \quad (24.31)$$

and surge for appropriate modification to make it valid for high film *Reynolds* numbers. For the turbulent region,  $Re_{\delta_2} > 400$ , *Labuntzov* uses in 1957 variable distribution of the eddy viscosity to describe the turbulent velocity profile. He approximate finally the analytical integral solution within  $1 \leq Pr_2 \leq 25$  and  $1.5 \times 10^3 \leq Re \leq 6.9 \times 10^4$  by

$$\frac{h_{\text{saignant}}}{\lambda'} \left[ \frac{\eta'^2}{\rho'(\rho' - \rho'')g \cos \varphi} \right]^{1/3} = 0.0325 Re_{2\delta}^{0.25} Pr_2^{0.5}, \quad (24.32)$$

reproducing experimental data of several authors within 12%. *Isachenko* extended in 1977 this result by taking into account also the upper laminar part to

$$\frac{h_{\text{saignant}}}{\lambda'} \left[ \frac{\eta'^2}{\rho'(\rho' - \rho'')g \cos \varphi} \right]^{1/3} = \frac{Re_{2\delta}}{2300 + 41 Pr_2^{0.5} (Re_{2\delta}^{3/4} - 89)}. \quad (24.33)$$

For comparison we give here also the *Kutateladze* correlation from 1963

$$\frac{h_{\text{saignant}}}{\lambda'} \left[ \frac{\eta'^2}{\rho'(\rho' - \rho'')g \cos \varphi} \right]^{1/3} = \frac{Re_{2\delta}}{389 + 18.5 Pr_2^{-0.4} (Re_{2\delta}^{5/6} - 47)}. \quad (24.34)$$

For  $Re_{\delta_2} > 2000$  the right hand side simplifies to  $0.054 Re_{2\delta} Pr_2^{0.4}$ . Note the differences in the *Prandtl* number dependence.

*Butterworth* proposed in 1981 for vertical plane in [6] the following set of correlations for the three regions:

1. Laminar film: *Nusselt* theory.
2. Wavy film:  $8.25 < Re_{\delta_2} < 400$ ,

$$\frac{h_{\text{saignant}}}{\lambda'} \left[ \frac{\eta'^2}{\rho'(\rho' - \rho'')g \cos \varphi} \right]^{1/3} = \frac{Re_{2\delta}}{1.465 Re_{2\delta}^{1.22} - 1.3}. \quad (24.35)$$

3. Turbulent film:  $Re_{\delta_2} > 400$ ,

$$\frac{h_{\text{saignant}}}{\lambda'} \left[ \frac{\eta'^2}{\rho'(\rho' - \rho'')g \cos \varphi} \right]^{1/3} = \frac{Re_{2\delta}}{2187 + 41 Pr'^{-1/2} (Re_{2\delta}^{3/4} - 89.4)}. \quad (24.36)$$

**Problem 1:** Consider a room filled with 100°C steam at 1bar. The vertical 10m walls of the room consist of 10cm steel followed by 95cm concrete with initial temperature 50°C. The external wall surface is considered as adiabatic. Compute the temperature profile in the wall, the film Reynolds number and the film thickness.

**Solution to problem 1:** We create a simple algorithm solving the Fourier equation for the direction normal to the wall. At the internal site we first postulate that the condensing film is laminar. Therefore we use Eq. (24.25) to compute the heat transfer coefficient, Eq. (24.24) to compute the Reynolds number and Eq. (24.20) to compute the film thickness. The results are presented in Figs. 2 and 3. We see that (a) after a half an hour the steam is heated almost to the saturation temperature but the concrete due to its bad heat conductivity follows slowly; (b) Within the first 100s the film Reynolds number exceed 400 which indicate that in this region the film is turbulent and the *Nusselt* theory is not appropriate; (c) In almost all the time the film is laminar with weave surface.

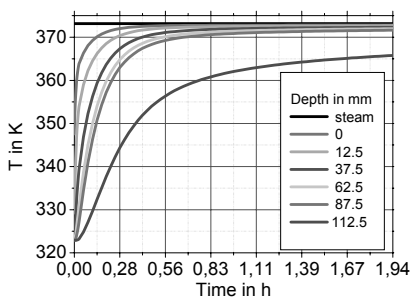


Fig. 2 Temperatures as a function of time

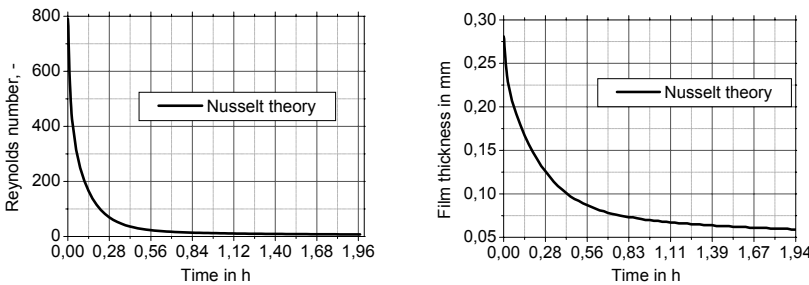
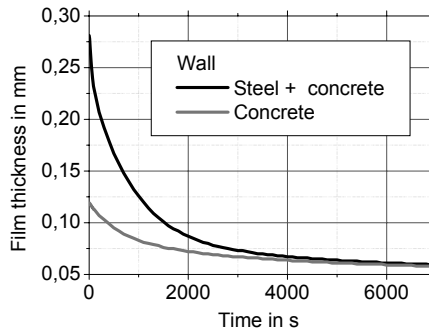


Fig. 3 a) Film Reynolds number as a function of time; b) Film thickness as a function of time



**Fig. 4** Film thickness as a function of time. Parameter: the thermal conductivity of the wall removing the condensation heat

**Problem 2:** Repeat the analysis for problem 1 by considering only a concrete wall.

**Solution to problem 2:** The solution is presented in Fig. 4. As expected the worst conduction of the concrete controls the rate of condensation resulting in smaller film thickness. The *Reynolds* number varying from 58 to 5.8 was less than 400. Therefore the application of the *Nusselt* theory in all the region of interest was correct.

### 24.1.2 Gravitation films on pipes

The coefficient in the *Nusselt* solution was set by *Isachenko* et al. (1981) to 0.728 for external condensation on horizontal pipes by using as a characteristic length the external wetted diameter of the pipe  $H = D_h$ . *Bird* et al. (1960) recommended the constant 0.725 for *external condensation on a horizontal single pipe* reporting  $\pm 10\%$  error compared with experiments. The correlation was also recommended for *bundles of horizontal pipes* *Bird* et al. (1960) p 417. The *Nusselt* equation was modified for condensation *inside inclined pipe* by using a constant 0.296 taking into account the partial occupation of the pipe cross section by the flowing condensate and  $H = D_h$  by *Collier* in 1972. *Chato* (1962) came to 0.68 instead to  $3/8$ , for  $H = D_h$ , and recommend for small inclinations  $\Delta z/\Delta x < 0.002$  the constant in the *Nusselt* equation to be

$$0.468 f \left[ \text{Pr}_2, \frac{c'_p (T'_k - T_w)}{h'' - h'} \right]$$

a function of the liquid *Prandtl* number given graphically in his work. For larger inclinations  $0.002 < \Delta z/\Delta x < 0.6$ , 0.3 is used instead 0.468.

## 24.2. Condensation from forced convection two-phase flow at liquid film

### 24.2.1 Down flow of vapor across horizontal tubes

As already mentioned, the *Nusselt* theory is valid also for condensation of stagnant vapor on a horizontal cylinder with the modification of the numerical coefficient to 0.728 by *Isachenko*. Several authors correlated their data by using as a measure the *Nusselt* heat transfer coefficient as follows:

$$\text{Fijii et al. (1979)} : \frac{h}{h_{Nu}} = 1.24 \left( \frac{w_1 D_{hy}}{\nu_2} \right) \left( \frac{h_{Nu} D_{hy}}{\lambda'} \right)^{-0.2} \quad (24.37)$$

$$\text{Berman and Tumanov (1962)} : \frac{h}{h_{Nu}} = 1 + 0.0095 \left( \frac{w_1 D_{hy}}{\nu_1} \right)^{11.8 / \sqrt{\frac{h_{Nu} D_{hy}}{\lambda'}}} \quad (24.38)$$

$$\text{Shekrladze and Geomelauri (1966)} : \frac{h}{h_{Nu}} = \left\{ \frac{1}{2} \left( \frac{h_{Sh}}{h_{Nu}} \right)^2 + \frac{1}{4} \left[ \left( \frac{h_{Sh}}{h_{Nu}} \right)^4 + 1 \right]^{1/2} \right\}^{1/2} \quad (24.39)$$

where

$$h_{Sh} = 0.9 \frac{\lambda_2}{D_{pipe}} \left( \frac{w_1 D_{hy}}{\nu_2} \right)^{1/2} \quad (24.40)$$

$$\text{Kutateladze (1962)} : \frac{h}{h_{Nu}} = 1 + 0.004 \left( \frac{w_1^2 \rho_1 h_{Nu}}{g \rho_2 \lambda_2} \right)^{0.8} \quad (24.41)$$

### 24.2.2 Collier correlation

For forced convection in inclined pipe in the case of a *laminar film* inside *Collier* (1972) proposed

$$h_{lam} = 0.825 \left[ \frac{\rho'(\rho' - \rho'') \lambda'^3 g \cos \varphi}{GD_h} \right]^{1/3} \quad (24.42)$$

and in the case of *turbulent film*

$$h_{turb} = 0.065 \frac{\lambda' \rho'^{1/2}}{\eta'} \frac{0.023 \rho' w_1^2}{Re_1^{1/4}} Pr^{1/2} \quad (24.43)$$

where the liquid properties are those of saturated liquid at the local pressure,

$$Pr' = \eta' c'_p / \lambda' . \quad (24.44)$$

In practical computations the maximum of all three expressions is taken,

$$h = \max(h_{\text{stagnant}}, h_{\text{lam}}, h_{\text{turb}}) , \quad (24.45)$$

which is in fact using the *Nusselt* theory in cases where the forced convection correlations gives lower values than the values for stagnant steam condensation.

### 24.2.3 Boyko and Krujilin approach

*Boyko* and *Krujilin* recommended in 1966 for forced convection condensation the following correlation

$$h = h_{20} \left[ 1 + X_1 \left( \frac{\rho'}{\rho''} - 1 \right) \right]^{1/2} , \quad (24.46)$$

where

$$h_{20} = 0.024 Re_{20}^{0.8} Pr'^{0.4} \frac{\lambda_2}{D_{hy}} , \quad (24.47)$$

$$Re_{20} = D_{hy} G / \eta_2 . \quad (24.48)$$

The correlation was verified with experimental data for  $12.3 < p < 88 \text{ bar}$ ,  $1 < X_1 < 0.26$ ,  $162\,000 < \dot{q}_w^{\sigma 2} < 1\,570\,000 \text{ W/m}^2$ . The constant 0.024 was recommended for steel pipes and 0.032 for copper pipes.

*Miropolskij* (1960) obtained experimentally for vertical steel tubes

$$h = 0.023 Re_2^{*0.8} Pr'^{0.4} \frac{\lambda'}{D_{hy}} \left[ 1 + 0.63 \left( \frac{\rho'}{\rho''} \right)^{0.67} X_1 \right] ,$$

where

$$Re_2^* = D_{hy} \rho' w_1 / \eta' .$$

This correlation has a mean error of 15% for pressures 7 to 220 atm, mass flow rates 400 to 2000 kg/(m<sup>2</sup>s) and heat fluxes 0.15 to  $6 \times 10^6 \text{ ccal/(m}^2\text{h)}$ . For copper tubes the coefficient was found to be 0.03.

#### 24.2.4 The *Shah* modification of the *Boyko* and *Krjulin* approach

*Shah* (1979) reported a modification of this correlation

$$h = h_{20} \left[ (1 - X_1)^{0.8} + \frac{3.8 X_1^{0.76} (1 - X_1)^{0.04}}{(p / p_{cr})^{0.38}} \right]. \quad (24.49)$$

The correlation is reported to reproduce 474 data points within  $0.002 < p / p_{cr} < 0.44$ ,  $21 < T'(p) < 310^\circ\text{C}$ ,  $3 < w_1 < 300\text{m/s}$ ,  $0 < X_1 < 1$ ,  $17.5 < G < 210.6\text{kg/s}$ , and  $158 < \dot{q}_w''^{\sigma 2} < 1\,893\,000\text{W/m}^2$  with mean deviation 15.4%.

The condensing mass per unit flow volume is then

$$\mu_{12} = \frac{4}{D_{hy}} \frac{\dot{q}_w''}{\Delta h}. \quad (24.50)$$

### 24.3 Steam condensation from mixture containing non-condensing gases

Consider forced convection in a pipe. Given is the gas temperature, the wall temperature and the local parameters. We ask for the mass transferred per unit time and mixture volume and for the power density removed from the wall. The overall heat transfer coefficient can be estimate also in this case by using the *Boyko* and *Krjulin* (1966) heat transfer correlation. What changes in this case is the driving temperature difference across the water film. There is convective heat transfer between the gas and the interface

$$h_{convective} (T_1 - T_1^{\sigma 2}), \quad (24.51)$$

where

$$h_{convective} = 0.023 Re_1^{0.8} Pr_1^{0.4} \frac{\lambda_1}{D_h}. \quad (24.52)$$

A diffusion controlled condensation mass flux is defined as follows

$$(\rho w)_{12} = \beta_{12} \rho_1 (C_{1M} - C_{1M}^{\sigma 2}), \quad (24.53)$$

where the condensation coefficient  $\beta_{12}$  is defined depending of geometry and local conditions. The procedure for its computation will be discussed later. Using the ideal gas approximation we may rewrite the definition equation in terms of the corresponding partial pressures, or alternatively using the local partial pressures and the gas temperature



$$(\rho w)_{12} = \beta_{12} \rho_1 (C_{1M} - C_{1M}^{\sigma^2}) = \beta_{12} \rho_1 \frac{p_{1M} - p'(T_1^{\sigma^2})}{p} = \frac{\beta_{12}}{R_1 T_1} [p_{1M} - p'(T_1^{\sigma^2})]. \quad (24.54)$$

The energy jump condition at the gas-liquid interface requires

$$h(T_1^{\sigma^2} - T_w) = (\rho w)_{12} \Delta h + h_{convective} (T_1 - T_1^{\sigma^2}). \quad (24.55)$$

This is a transcendental equation with respect to the interface temperature. The equation has to be solved by iterations. To construct a *Newton* iteration we rewrite Eq. (24.55) in the form

$$f(T_1^{\sigma^2}) = h(T_1^{\sigma^2} - T_w) - (\rho w)_{12} \Delta h - h_{convective} (T_1 - T_1^{\sigma^2}) = 0, \quad (24.56)$$

and search for the zeros. For this purpose we need the derivative

$$\frac{df(T_1^{\sigma^2})}{dT_1^{\sigma^2}} = h + \frac{d(\rho w)_{12} \Delta h}{dT} + h_{convective}, \quad (24.57)$$

which is used in

$$T_1^{\sigma^2} = T_{1,old}^{\sigma^2} - f / \frac{df(T_1^{\sigma^2})}{dT_1^{\sigma^2}}. \quad (24.58)$$

For small deviation of the interface temperature from the saturation temperature at the bulk vapor partial pressure the use of the *Clausius-Clapyron* equation is possible to transform pressure differences into temperature differences in both: the definition equation for the diffusion controlled mass transfer

$$(\rho w)_{12} \approx \beta_{12} \frac{\rho_1}{p} \frac{dp'}{dT} [T'(p_{1M}) - T_1^{\sigma^2}], \quad (24.59)$$

and the energy jump condition

$$h(T_1^{\sigma^2} - T_w) = \beta_{12} \frac{\rho_1}{p} \Delta h \frac{dp'}{dT} [T'(p_{1M}) - T_1^{\sigma^2}] + h_{convective} (T_1 - T_1^{\sigma^2}). \quad (24.60)$$

This allows direct computation of the interface temperature as follows

$$T_1^{\sigma^2} = \frac{hT_w + \beta_{12} \frac{\rho_1}{p} \Delta h \frac{dp'}{dT} T'(p_{1M}) + h_{convective} T_1}{h + \beta_{12} \frac{\rho_1}{p} \Delta h \frac{dp'}{dT} + h_{convective}}. \quad (24.61)$$

Also in this case the dependence of the mass transfer coefficient on the interface temperature still remains and has to be resolved by iterations. Note that the

iterative solution is very sensitive to the chosen initial values, and it has to be carefully controlled.

### 24.3.1 Computation of the mass transfer coefficient

#### 24.3.1.1 Gas flow in a pipe

*Bobe and Solouhin* (1972), see also in *Isuchenko* (1977) p. 136, correlated experimental data for steam condensation from gas-steam mixtures inside pipes as follows:

$$\beta_{12} = \beta_{12,0} \left( \frac{p_1 \sum^n}{p_{1M} - p_{1M}^{\sigma^2}} \right)^m, \quad (24.62)$$

where

$$\beta_{12,0} = 0.0191 \left( \frac{w_1 D_h}{v_1} \right)^{0.8} \left( \frac{v_1}{D_{\sum^{n \rightarrow M}}} \right)^{0.43} \frac{D_1 \sum^{n \rightarrow M}}{D_h} \left( \frac{p}{p_1 \sum^n} \right)^n \quad (24.63)$$

or

$$(\rho w)_{12} = \rho_1 \beta_{12,0} \left[ \frac{p_{1M} - p'(T_1^{\sigma^2})}{p} \right]^{1-m}, \quad (24.64)$$

where for  $0.1 < \frac{p_1 \sum^n}{p_{1M} - p'(T_1^{\sigma^2})} < 1$ ,  $n = 0.6$ ,  $m = 0.4$ , and for  $\frac{p_1 \sum^n}{p_{1M} - p_{1M}^{\sigma^2}} \geq 1$ ,  $n = 0.9$ ,  $m = 0.1$ . The derivative required for the iterative solution is then

$$\frac{d(\rho w)_{12}}{dT_1^{\sigma^2}} = -\beta_{12,0} (1-m) \frac{\rho_1}{p} \left[ \frac{p}{p_{1M} - p'(T_1^{\sigma^2})} \right]^m \frac{dp'(T_1^{\sigma^2})}{dT_1^{\sigma^2}}. \quad (24.65)$$

#### 24.3.1.2 Gas flow across a bundle of pipes

*Berman and Fuks* (1958) correlated experimental data for steam condensation from gas-steam mixtures flowing perpendicular to horizontal internally cooled tubes:

$$\beta_{12} = \text{const} \left( \frac{w_1 D_h}{v_1} \right)^{0.8} \frac{D_1 \sum^{n \rightarrow M}}{D_h} \left( \frac{p}{p_1 \sum^n} \right)^{0.6} \left( \frac{p}{p_{1M} - p_{1M}^{\sigma^2}} \right)^{1/3}, \quad (24.66)$$

or

$$(\rho w)_{12} = \text{const} \rho_1 \left( \frac{w_1 D_h}{\nu_1} \right)^{0.8} \left( \frac{p}{p_1 \Sigma^n} \right)^{0.6} \left( \frac{p_{1M} - p'(T_1^{\sigma 2})}{p} \right)^{2/3} \frac{D_1 \Sigma^{n \rightarrow M}}{D_h} \quad (24.67)$$

where  $\text{const} = 0.94$  for single pipe, 1.06 for the first row of pipes, 1.64 for the third and the subsequent row of pipes.

### 24.3.1.3 The Vierow and Shrock explicit correlation

The simplest method for taking into account the resistance of the non-condensable gases was proposed by *Vierow* and *Shrock* (1991). It consists of three steps: 1) Compute the condensation from stagnant pure steam; 2) Correct the expression for the influence of the gas mixture forced convection; 3) Modify the resulting heat transfer coefficient by a multiplier being a function of the inert mass concentration. In particular, the *Nusselt* theory is used in the first step to compute  $h_{\text{stagnant}}$ . In the second step the multiplier

$$f_1 = \min(2, 1 + 2.88^{-5} Re_1^{1.18}) \quad (24.68)$$

is used, where  $Re_1 = D_h \rho_1 |w_1| / \eta_1$ . In the third step an explicit correlation of experimental data is generated in the simple form by the second multiplier. Recently *Choi et al.* (2002) modified the originally proposed multiplier to

$$f_2 = 1 - 1.00962 C_{1n}^{0.13354} \quad \text{for} \quad 0.1 \leq C_{1n} \leq 0.65 \quad (24.69)$$

in order to obtain better approximation of their own data base for  $h_{\text{cond}} D_{\text{hy, film}} / \lambda_{\text{film}} < 30$  for stratified flow in inclined tubes ( $2.1^\circ$  and  $5^\circ$ ) – averaged percentage error 20 to 35%.

For comparison we give here the recent correlation proposed by *Goldbrunner* (2003) for condensation on films in pipes

$$\frac{h_2^{1\sigma} \delta_2}{\lambda_2} = 0.0388 \left( \frac{u_2^t \delta_2}{\nu_2} \right)^{1.53} Pr_2^{1/2} 0.5024 (1 - 1.5701 C_{1n}^{0.5987}), \quad (24.70)$$

where  $u_2^t = (\varepsilon_2 \nu_2)^{1/4}$ ,  $\varepsilon_2 = u_2 dp / dz$ , valid for horizontal water film flows in 80x64mm rectangular channel as follows. The standard deviation from the measurements reported was 22%.

parameters	co-current	counter-current
$p$ , bar	4 to 10	4 to 10
$N_2$ -mass conc., -	0 to 0.1	0 to 0.15
steam velocity, m/s	1.3 to 5.8	0.6 to 1.6
water velocity, m/s	0.25 to 0.30	0.25 to 0.30

## Nomenclature

### Latin

$a$	$= \lambda / (\rho c_p)$ , temperature conductivity, $m^2/s$
$a_{12}$	$= 1 / \Delta z$ gas-liquid interfacial area density in Cartesian coordinates, $1/m$
$C_{1M}$	vapor mass concentration inside the gas mixture, <i>dimensionless</i>
$C_{1n}$	mass concentration of the non-condensing gas $n$ inside the gas mixture, <i>dimensionless</i>
$C_{1M}^{\sigma^2}$	vapor mass concentration inside the gas mixture at the liquid interface, <i>dimensionless</i>
$D_{1\sum n \rightarrow M}$	diffusion gas coefficient for the vapor inside the mixture consisting of condensable and non-condensable gases, $m^2/s$
$D_{hy}$	pipe hydraulic diameter, $m$
$g$	acceleration due to gravity, $m/s^2$
$R_1$	mixture gas constant, $J/(kgK)$
$Re_{2\delta}$	$= \frac{\rho_2 w_2 4\delta_2}{\eta_2}$ , <i>Reynolds</i> number based on the hydraulic diameter of the film, <i>dimensionless</i>
$H$	height of the plate, $m$
$h$	specific enthalpy, $J/kg$
$h_{convective}$	convective heat transfer coefficient, $W/(m^2K)$
$h_{stagnant}$	heat transfer coefficient for stagnant steam, $W/(m^2K)$
$h_{stagnant\_steam/turbulent\_film}$	heat transfer coefficient for stagnant steam and turbulent condensate film, $W/(m^2K)$
$h_{Nu}$	heat transfer coefficient for stagnant steam in accordance with the <i>Nusselt</i> water skin theory, $W/(m^2K)$
$h_{lam}$	heat transfer coefficient for forced convection inclined pipe - laminar film, $W/(m^2K)$
$h_{turb}$	heat transfer coefficient for forced convection inclined pipe - turbulent film, $W/(m^2K)$
$h_{20}$	heat transfer coefficient for forced convection computed for flow having the mixture mass flow but consisting of liquid only, $W/(m^2K)$
$\dot{q}_w''$	wall heat flux from the interface into the gas, $W/m^2$
$p$	pressure, $Pa$
$p_{cr}$	critical pressure, $Pa$
$p_{1M}$	vapor partial pressure inside the gas mixture, $Pa$
$p_{1M}^{\sigma^2}$	vapor partial pressure inside the gas mixture at the liquid interface, $Pa$

$p_{1\Sigma^n}$	partial pressure of the non-condensing gases inside the gas mixture, <i>Pa</i>
$p'(T_1^{\sigma^2})$	vapor partial pressure inside the gas mixture at the liquid surface, <i>Pa</i>
$Re_1$	$= D_{hy} \rho_1  w_1  / \eta_1$ , gas <i>Reynolds</i> number, <i>dimensionless</i>
$Re_{20}$	$= D_{hy} G / \eta_2$ total flow <i>Reynolds</i> number based on the liquid viscosity, <i>dimensionless</i>
$Pr$	$= \eta c_p / \lambda$ , <i>Prandtl</i> number, <i>dimensionless</i>
$T$	temperature, <i>K</i>
$T_2^{1\sigma}$	liquid side interface temperature, <i>K</i>
$T_1^{\sigma^2}$	gas side interface temperature, <i>K</i>
$T_{cond}$	condensation initiation temperature, <i>K</i>
$V_1$	gas velocity, <i>m/s</i>
$V_2$	liquid velocity, <i>m/s</i>
$\dot{V}'$	Volumetric flow rate per unit of film width, <i>m<sup>2</sup>/s</i>
$w$	axial velocity, <i>m/s</i>
$X_l$	mass flow concentration of the field <i>l</i> inside the mixture, <i>dimensionless</i>

### Greek

$\beta_{12}$	condensation coefficient, <i>m/s</i>
$\delta$	film thickness, <i>m</i>
$\varphi$	angle between the positive flow direction and the upwards directed vertical, <i>rad</i>
$\Delta h$	$= h'' - h'$ , latent heat of vaporization, <i>J/kg</i>
$\eta$	dynamic viscosity of liquid, <i>kg/(ms)</i>
$\lambda$	thermal conductivity, <i>W/(mK)</i>
$\mu_{21}$	steam mass generation per unit mixture volume and unit time due to evaporation, <i>kg/(sm<sup>3</sup>)</i>
$\mu_{12}$	liquid mass generation per unit mixture volume and unit time due to condensation, <i>kg/(sm<sup>3</sup>)</i>
$\rho$	density, <i>kg/m<sup>3</sup></i>
$(\rho w)_{21}$	steam mass generation per unit surface and unit time due to evaporation, <i>kg/(m<sup>2</sup>s)</i>
$(\rho w)_{12}$	liquid mass generation per unit surface and unit time due to condensation, <i>kg/(m<sup>2</sup>s)</i>

**Subscripts**

1	gas
2	liquid film
2 <i>F</i>	liquid film
<i>Ml</i>	vapor inside the gas mixture
<i>nl</i>	inert components inside the gas

**Superscripts**

'	time fluctuation
'	saturated steam
"	saturated liquid

**References**

- Alekseenko SV, Nakoryakov VE and Pokusaev BG (1996) Wave flow of liquid films, Begell House, New York, English ed. Fukano T
- Alekseenko SV, Nakoryakov VE, Pokusaev BG and Khristoforov VV (1973) Shear stress at film falling down a vertical wall (in Russian), *Inzh. -Fiz. Zhurn.*, vol 24 no 5 pp 824-830
- Berman LD and Fuks SN (1958) *Teploenergetika*, vol 8 pp 66-74; (1959) *Teploenergetika*, vol 7 pp 74-83
- Berman LD and Tumanov VA (1962), Heat transfer during condensation of flowing steam in a tube bundle, *Teploenergetika*, vol 9 no 10 pp 77-83
- Bird RB, Stewart WE, Lightfoot EN (1960), *Transport phenomena*, John Wiley & Sons, New York
- Bobe LS and Solouhin VA (1972) Heat and mass transfer during steam condensation from steam-gas mixture by turbulent pipe flow, *Teploenergetika*, vol 9 pp 27-30.
- Boyadjiev C and Beschkov V (1984) *Mass Transfer in Liquid Film Flows*, Sofia, Publishing House of the Bulgarian Academy of Sciences
- Boyko LD and Krujilin GN (1966), *Izvestia akademii nauk SSSR Energetika I transport*, no 2 pp 113-128. See also Boyko LD (1966) *Teploobmen w elementach energeticheskikh ustanovak*, Nauka, Moskwa, pp 197-212
- Brauer H (1971) *Stofaustausch*, Verlag Sauerländer, Aarau und Frankfurt am Main
- Butterworth D (1981) *Condensers: Heat transfer and fluid flow, in heat exchanger*, Kakac S, Bergeles AE and Mayinger F (eds) Hemisphere, Washington, pp 89-314
- Chato JC (1962) Laminar condensation inside horizontal and inclined tubes, *ASHREE Journal*, vol 4 pp 52-60
- Choi KY, Chung HJ and No HC (2002) *Nuclear Engineering and design*, vol 211 pp 139-151
- Collier JG (1972) *Convection boiling and condensation*, London: McGraw-Hill Book Company Inc.
- Dukler AE and Berglin OP (1952) Characteristics of flow in falling liquid films, *Chem. Eng. Prog.*, vol 48 p558

- Fijii T, Honda H and Oda K (1979), Condensation of steam on horizontal tubes – influence of the oncoming velocity, Condensation heat transfer, 18<sup>th</sup> Nat. Heat Transfer Conf., San Diego August, pp 35-43
- Fulford GD (1964) The flow of liquids in thin films, *Advan. Chem. Eng.*, vol 5, pp 151-236.
- Ganchev BG and Kozlov VM (1973) Investigation into gravitational flow of liquid film along the walls of vertical channel with large length (in Russian), *Zhurn. Prikl. Mekh. Tekh. Fiz.*, vol 1 pp 128-135
- Gimbutis G (1988) Heat Transfer in Gravitational Flow of Liquid Film (in Russian), Vilnius, Mokslas, 232 p
- Goldbrunner M (Juli 2003) Kondensation bei stratifizierter Strömung in Gegenwart nichtkondensierbarer Gase, Final Report, Reaktor Safety Research Project No: 1501207, TU München
- Grigul U (1942) *Forsch Ing. Wes*, vol 13 pp 49-47; (1942) *Z. Ver. Dtsch. Ing.*, vol 86 pp 444
- Isachenko VP (1977) *Teploobmen pri kondensazii*, Moskva, Energia
- Isachenko VP, Osipova VA and Sukomel AS (1981) *Teploperedacha*, 4<sup>th</sup> Ed., Moskva, Energoisdat
- Isachenko VP (1977) *Teploobmen pri kondensacii*, Energia, Moskva
- Ishigai S, Nakanishi S, Koizumi T and Oyabi Z (1972) Hydrodynamics and heat transfer of vertical falling liquid films, *Bull. JSME*, vol 15 no 83 pp 594-602
- Kapitza PL (1948) Wave flow of thin layer of viscous fluid (in Russian), *Zhurn. Eksper. Teor. Fiz.*, vol 18 no 1 pp 3-28
- Kapitza PL (1948) *Zhur. Exper. Teoret. Fiz.*, vol 18 no 1
- Kitateladze SS (1962), Heat transfer in condensation and boiling, AEC-tr-3778 chaps 5-7
- Kutateladze SS (1963), *Fundamentals of heat transfer*, Academic, New York
- Kutateladze SS (1963), *Fundamentals of heat transfer*, Academic, New York
- Kutateladze, S.S., 1979, *Fundamentals of Heat Transfer Theory* (in Russian), M., Atomizdat.
- Labuntsov DA (1957), Heat transfer in film condensation of pure steam, *Teploenergetika*, vol 4 no 7 pp 72-80
- Labuntsov DA (1957), Heat transfer in film condensation of pure steam, *Teploenergetika*, vol 4 no 7 pp 72-80
- Miropolskij SL (1960) *Teplootdaza pri kondensazii para vysokogo davlenija vnutri trub*, *Teploenergetika*, no 3 pp 79-83
- Nusselt W (1916) Die Oberflächenkondensation des Wasserdampfes, *Zeitschrift VDI*, vol 60, pp 541-546
- Rohsenow WM, Hartnett JP and Ganic EN (1985) *Handbook of heat transfer fundamentals*, second edition, McGraw-Hill Book Company
- Rohsenow WM, Hartnett JP and Ganic EN (1985) *Handbook of heat transfer fundamentals*, second edition, McGraw-Hill Book Company
- Shah MM (1979) A general correlation for heat transfer during film condensation inside pipes, *Int. J. Heat Mass Transfer*, vol 22 pp 547-556
- Shekrladze IG and Gomelaury VI (1966), Laminar condensation on flowing vapor, *Int. J. Heat Mass Transfer*, vol 9 pp 581-591
- Tananaiko YuM and Vorontsov EG (1975) *Methods of Calculation and Investigation into Film Processes* (in Russian), Kiev, Tekhnika, 312 p
- Vierow KM and Shrock KE (1991) Condensation in a natural circulation loop with non condensable gases, Part 1 – Heat transfer, International Conference on Multi-Phase Flows, Tsukuba, Japan



































































































# 25 Discrete ordinate method for radiation transport in multi-phase computer codes

## 25.1 Introduction

Several applications in technology require radiation transport analysis (RTA). Examples are processes with combustion and interaction of high temperature molten material with water in the safety analysis in the nuclear industry and in the metallurgy. The RTA is always a part of the general flow simulation and of the analysis of the flow interaction with the structure. Radiation transport in high temperature media may be the governing process of energy transfer. This Chapter is not intended to replace the famous book of *Siegel and Howell* (1996) on this subject. The interested reader intending to reach a high level skill in this field has to go through this book. The Chapter rather gives some of the main ideas required to understand how the radiation transport theory can be implemented in multi-phase flow analysis. The Chapter is based on the experience gained by creating a radiation transport model for the computer code IVA *Kolev* (1999). This work started in 1998. In this year *Lanzenberger* (1997) created as far as I know the first computer code for modeling of 3D radiation transport in three-phase flow as a part of the IVA4 code development. The code uses the first order *step* scheme setting the positive wall coefficient equal to zero. Strictly speaking the code was developed for simulation of Cartesian coordinates without any obstacles inside the computational region. The further development of this technique in IVA6 went through the following direction: (a) rewriting the code from Fortran 77 to Fortran 90, improving macroscopic data and coupling with the IVA6 computer code; (b) changing the algorithm so that it allows one to handle internal obstacles.

### 25.1.1 Dimensions of the problem

For technical application on the ground we consider each beam as being linear. It can travel in an arbitrary direction through a single point. Therefore the first three dimensions are coming from the spatial description. The volume of interest is also three dimensional. It introduces another three dimensions in the problem. The electromagnetic radiation energy flow transported per unit time across unit normal surface is depending on the wavelength. The continuous spectrum is usually split in  $n$  groups with prescribed boundaries. This gives the other  $n$ -dimensions of the problem. In the discrete ordinate radiation transport method the governing energy

conservation equation is replaced by a set of equations for a finite number of ordinate directions, for a finite number of control volumes, and for finite number of spectral regions. It is the large number of dimensions that makes the RTA complicated.

### 25.1.2 Micro- versus macro-interactions

Any interactions of electromagnetic radiation with matter are described in physics by theoretical and experimental observation on a micro-scale. The engineer integrates the interactions over a control volume and prepares the information necessary for microscopic radiation transport on a macro-scale. If the characteristic interaction length is much smaller than the scale of the control volume, RTA on a macro-scale is not necessary because all the interaction happens inside the cell and no energy leaves the volume. An example is a relatively dense suspension of hot particles, which are shielding effectively the radiation inside large cells. If the characteristic interaction length is larger than the scale of the control volume then RTA is necessary because energy is leaving and entering the control volume. Examples are small concentrations of very hot spheres in water. The radiation energy may be transported up to 10 *m* in water up to full absorption. If the volume of interest is few cubic meters and the control volume of the discretization is of the order of liters the RTA is necessary.

### 25.1.3 The radiation transport equation (RTE)

The basic equation for the description of the radiation transport is the steady state energy conservation equation called radiation transport equation (RTE)

$$\begin{aligned} \frac{di'_\lambda(\mathbf{r}, \mathbf{s})}{ds} = & -a_\lambda i'_\lambda(\mathbf{r}, \mathbf{s}) - \sigma_{s\lambda} i'_\lambda(\mathbf{r}, \mathbf{s}) + a_\lambda i'_{\lambda b}(\mathbf{r}, \mathbf{s}) \\ & + \frac{\sigma_{s\lambda}}{4\pi} \int_{4\pi} i_\lambda(\mathbf{r}, \omega_i) \Phi(\lambda, \omega, \omega_i) d\omega_i . \end{aligned} \quad (25.1)$$

Here  $i'_\lambda(\mathbf{r}, \mathbf{s})$  is the spectral radiation intensity at the spatial location  $\mathbf{r}$  along the direction  $\mathbf{s}$  that is within an infinitesimal solid angle  $d\omega$ . Spectral – because it is associated with each particular wavelength  $\lambda$ . The dimensions of  $i'_\lambda$  are those of power flux through a square meter. It is in fact a heat flux.  $a_\lambda, \sigma_{s\lambda}$  are the spectral absorption and scattering coefficients,  $\Phi$  is the spectral scattering phase function and  $\omega_i$  is the scattering angle. The scattering phase function describes which amount of incident radiation is scattered in all other directions, Fig. 25.1.

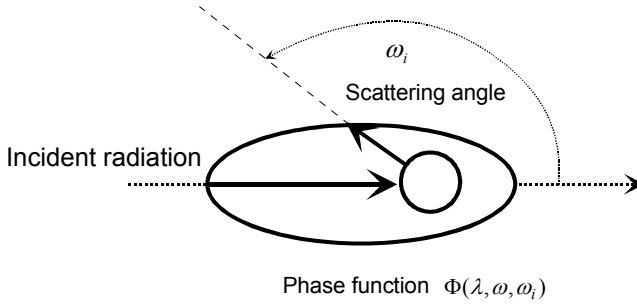


**Fig. 25.1** Scattering of incident radiation

The intensity of a ray passing through an infinitesimal volume is attenuated by absorption. This is reflected by the first term on the right hand side of Eq. (25.1). The intensity of a ray passing through an infinitesimal volume is attenuated also by scattering. It is taken into account in the second term on the RHS. The intensity is increased by the emitted intensity of the medium reflected by the third term on the RHS, and by the scattering from any other direction to the considered direction of the vector  $\mathbf{s}$ . For numerical integration of Eq. (25.1) it is convenient to introduce the so called spectral extinction coefficient

$$\beta_\lambda = a_\lambda + \sigma_{s\lambda} \quad (25.2)$$

and the source term

$$S' = a_\lambda i'_{\lambda b}(\mathbf{r}, \mathbf{s}) + \frac{\sigma_{s\lambda}}{4\pi} \int_{4\pi} i_\lambda(\mathbf{r}, \omega_i) \Phi(\lambda, \omega, \omega_i) d\omega_i \quad (25.3)$$

which simplify the notation

$$\frac{di'_\lambda(\mathbf{r}, \mathbf{s})}{ds} = -\beta_\lambda i'_\lambda(\mathbf{r}, \mathbf{s}) + S'. \quad (25.4)$$

In the discrete ordinate radiation transport method Eq. (25.4) will be replaced by a set of equations for a finite number of ordinate directions, for a finite number of control volumes, and for a finite number of spectral regions.

## 25.2 Discrete ordinate method

The spatial location in the space is defined by the position vector  $\mathbf{r}$ . In a polar coordinate system as presented in Fig. 25.2 with radius  $r = 1$ , azimuthal angle  $\varphi$ , and polar angle  $\theta$  the components of the unit vectors of  $\mathbf{s}$  in a Cartesian coordinate system with coordinates  $x$ ,  $y$  and  $z$  are defined as the direction cosines

$$\mathbf{s} = (\sin \theta \cos \varphi, \sin \theta \sin \varphi, \cos \theta) \equiv (s_x, s_y, s_z) \quad (25.5)$$

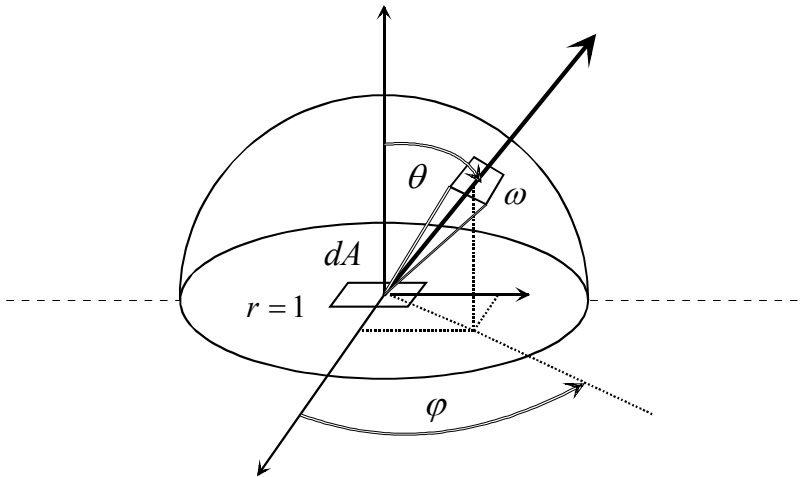


**Fig. 25.2** Unit hemisphere, solid angle  $\omega$ , angle  $\varphi$  and  $\theta$

The infinitesimal solid angle  $d\omega$  is equal to the infinitesimal area on the surface of the unit hemisphere

$$d\omega = \sin \theta d\theta d\varphi . \quad (25.6)$$

Integrating over all possible solid angle gives

$$\int_{\varphi=0}^{2\pi} \int_{\theta=-\pi/2}^{\pi/2} \sin \theta d\theta d\varphi = 4\pi . \quad (25.7)$$

The total surface area of the unit hemisphere is  $2\pi$ , and is denoted as the *total solid angle*. Let us divide the space into a discrete number of solid angles  $\Delta\omega_{a,b}$ , where

$$a = 1, a_{\max} , \quad (25.8)$$

$$b = 1, b_{\max} , \quad (25.9)$$

with  $a_{\max}$  and  $b_{\max}$  being even numbers. For equidistant discretization we have

$$\Delta\varphi = 2\pi / a_{\max} , \quad \varphi_a = \left( a - \frac{1}{2} \right) \Delta\varphi , \quad a = 1, a_{\max} \quad (25.10)$$

$$\Delta\theta = 2\pi / b_{\max} , \quad \theta_b = \left( b - \frac{1}{2} \right) \Delta\theta , \quad b = 1, b_{\max} , \quad (25.11)$$

and

$$\begin{aligned}
\Delta\omega_{a,b} &= \int_{\varphi_a - \Delta\varphi/2}^{\varphi_a + \Delta\varphi/2} \int_{\theta_b - \Delta\theta_b/2}^{\theta_b + \Delta\theta_b/2} \sin\theta \, d\theta \, d\varphi = 2\Delta\varphi_a \sin\theta_b \sin\frac{\Delta\theta_b}{2} \\
&= \Delta\varphi_a \left[ \cos\left(\theta_b - \frac{\Delta\theta_b}{2}\right) - \cos\left(\theta_b + \frac{\Delta\theta_b}{2}\right) \right]. \tag{25.12}
\end{aligned}$$

Here  $\varphi_a$  and  $\theta_b$  define the specific ordinate direction denoted with subscripts  $a, b$ . Other notation is

$$\mathbf{s}_{a,b} = (s_{x,a,b}, s_{y,a,b}, s_{z,a,b}). \tag{25.13}$$

There is an alternative notation used frequently in the literature

$$\mathbf{s}_{a,b} = (\mu_{a,b}, \eta_{a,b}, \xi_{a,b}). \tag{25.15}$$

### 25.2.1 Discretization of the computational domain for the description of the flow

The discretization of the computational domain for the description of the flow is performed by using a curvilinear coordinate system. In many practical cases either a Cartesian or a cylindrical coordinate system is used. We give here examples with the Cartesian systems for simplicity, but this is not a limitation of the approach. The discretization is structured and non-equidistant in each direction. Each control volume has 6 faces with surface  $A_m$ . The surfaces are numbered 1 for high  $i$ , 2 for low  $i$ , 3 for high  $j$ , 4 for low  $j$ , 5 for high  $k$  and 6 for low  $k$ . The orientation of each surface is defined by the outwards directed unit vector

$$\mathbf{e} = (e_x, e_y, e_z). \tag{25.16}$$

For Cartesian coordinate system the 6 surfaces have the surface vectors

$$\begin{aligned}
\mathbf{e}_1 &= (1, 0, 0), & \mathbf{e}_2 &= (-1, 0, 0), \\
\mathbf{e}_3 &= (0, 1, 0), & \mathbf{e}_4 &= (0, -1, 0), \\
\mathbf{e}_5 &= (0, 0, 1), & \mathbf{e}_6 &= (0, 0, -1). \tag{25.17-22}
\end{aligned}$$

For discretization of the cylindrical computational domain the 6 surfaces have the surface vectors given below

$$\mathbf{e}_m = (\cos\theta_m, \sin\theta_m, 0), \quad m=1,4, \quad \mathbf{e}_5 = (0, 0, 1), \quad \mathbf{e}_6 = (0, 0, -1). \tag{25.23-28}$$

The angles  $\theta_m$  are defined as follows  $\theta_1 = \theta$ ,  $\theta_1 = \pi + \theta$ ,  $\theta_1 = \frac{3}{4}\pi + \theta + \frac{1}{2}\Delta\theta$ ,  $\theta_1 = \frac{3}{4}\pi + \theta - \frac{1}{2}\Delta\theta$ . Here  $\theta$  is the azimuthal angle of the center of the control volume in the fluid domain.  $\Delta\theta$  is the size of the control volume in the azimuthal direction. Note the difference between these two angles and the angles used in the polar coordinate system for definition of the discrete ordinates.

### 25.2.2 Finite volume representation of the radiation transport equation

Integrating the RTE over the control volume  $dVol$  and over the angle  $\Delta\omega_{a,b}$  we obtain

$$\iint_{\Delta\omega_{a,b}} \int_{\Delta Vol} \frac{di'_\lambda(\mathbf{r}, \mathbf{s})}{ds} dVol d\omega = - \iint_{\Delta\omega_{a,b}} \int_{\Delta Vol} \beta_\lambda i'_\lambda(\mathbf{r}, \mathbf{s}) dVol d\omega + \iint_{\Delta\omega_{a,b}} \int_{\Delta Vol} S' dVol d\omega \quad (25.29)$$

or

$$\sum_{m=1}^6 i'_{\lambda,a,b,m} A_m \iint_{\Delta\omega_{a,b}} (\mathbf{s} \cdot \mathbf{e})_m d\omega + \beta_\lambda i'_{\lambda,a,b} \Delta Vol \Delta\omega_{a,b} = S'_{a,b} \Delta Vol \Delta\omega_{a,b}. \quad (25.30)$$

*Scalar product of the discrete directions vector and given surface vector:* Now we are interested in the estimation of the integral

$$\begin{aligned} D_{a,b} &= \iint_{\Delta\omega_{a,b}} \mathbf{s} \cdot \mathbf{e} d\omega = \int_{\varphi_a - \Delta\varphi/2}^{\varphi_a + \Delta\varphi/2} \int_{\theta_b - \Delta\theta_b/2}^{\theta_b + \Delta\theta_b/2} (\mathbf{s} \cdot \mathbf{e}) \sin\theta d\theta d\varphi = \\ &= \int_{\varphi_a - \Delta\varphi/2}^{\varphi_a + \Delta\varphi/2} \int_{\theta_b - \Delta\theta_b/2}^{\theta_b + \Delta\theta_b/2} (e_x \sin\theta \cos\varphi + e_y \sin\theta \sin\varphi + e_z \cos\theta) \sin\theta d\theta d\varphi \\ &= \left( e_x \int_{\varphi_a - \Delta\varphi/2}^{\varphi_a + \Delta\varphi/2} \cos\varphi d\varphi + e_y \int_{\varphi_a - \Delta\varphi/2}^{\varphi_a + \Delta\varphi/2} \sin\varphi d\varphi \right) \int_{\theta_b - \Delta\theta_b/2}^{\theta_b + \Delta\theta_b/2} \sin^2\theta d\theta \\ &\quad + e_z \Delta\varphi_a \int_{\theta_b - \Delta\theta_b/2}^{\theta_b + \Delta\theta_b/2} \cos\theta \sin\theta d\theta. \end{aligned} \quad (25.31)$$



Integrating we obtain

$$D_{a,b} = \left( e_x \cos \varphi_a + e_y \sin \varphi_a \right) 2 \sin \frac{\Delta \varphi_a}{2} \left[ \left( 1 - 2 \cos^2 \theta_b \right) \sin \frac{\Delta \theta_b}{2} \cos \frac{\Delta \theta_b}{2} + \frac{\Delta \theta_b}{2} \right] \\ + e_z \Delta \varphi_a 2 \cos \theta_b \sin \theta_b \cos \frac{\Delta \theta_b}{2} \sin \frac{\Delta \theta_b}{2}. \quad (25.32)$$

*Working form of the finite differential form of the RTE:* Using the above results the finite differential form of the RTE becomes

$$\sum_{m=1}^6 i'_{\lambda,a,b,m} A_m D_{a,b,m} + \beta_{\lambda} i'_{\lambda,a,b} \Delta Vol \Delta \omega_{a,b} = S'_{a,b} \Delta Vol \Delta \omega_{a,b}. \quad (25.33)$$

It is convenient to divide both sides by  $\Delta Vol \Delta \omega_{a,b}$ . The result is

$$\sum_{m=1}^6 a_{a,b,m} i'_{\lambda,a,b,m} + \beta_{\lambda} i'_{\lambda,a,b} = S'_{a,b}, \quad (25.34)$$

where

$$a_{a,b,m} = \frac{A_m}{\Delta Vol} \frac{D_{a,b,m}}{\Delta \omega_{a,b}}, \quad (25.35)$$

is geometry dependent only and is computed once at the beginning of the computation. Note that the ratio  $D_{a,b,m}/\Delta \omega_{a,b}$  is dimensionless and the coefficients  $a_{a,b,m}$  have dimension  $1/m$  which is the same as that of the extinction coefficient. For Cartesian coordinates using Eqs. (25.17-22) the above equation simplifies as follows

$$\left( i'_{\lambda,a,b,1} - i'_{\lambda,a,b,2} \right) \frac{A_1}{\Delta Vol} \frac{S_{x,a,b}}{\Delta \omega_{a,b}} + \left( i'_{\lambda,a,b,3} - i'_{\lambda,a,b,4} \right) \frac{A_3}{\Delta Vol} \frac{S_{y,a,b}}{\Delta \omega_{a,b}} \\ + \left( i'_{\lambda,a,b,5} - i'_{\lambda,a,b,6} \right) \frac{A_5}{\Delta Vol} \frac{S_{z,a,b}}{\Delta \omega_{a,b}} + \beta_{\lambda} i'_{\lambda,a,b} = S'_{a,b}. \quad (25.36)$$

The general form is preferred here.

Note that the spectral intensities  $i'_{\lambda,a,b,m}$  are defined at the cell boundaries and the spectral intensity  $i'_{\lambda,a,b}$  is defined in the cell center. There are numerous methods giving different approximations for the relationship between  $i'_{\lambda,a,b,m}$  and  $i'_{\lambda,a,b}$ . Three of them are discussed in the next section.

*Weighting factors: Step (donor cell), diamond and positive weighting:* The general form of the weighting factors for the first octant  $s_x > 0$ ,  $s_y > 0$ ,  $s_z > 0$

$$\begin{aligned} i'_{\lambda,a,b} &= f_x i'_{\lambda,a,b,1} + (1 - f_x) i'_{\lambda,a,b,2} = f_y i'_{\lambda,a,b,3} + (1 - f_y) i'_{\lambda,a,b,4} \\ &= f_z i'_{\lambda,a,b,5} + (1 - f_z) i'_{\lambda,a,b,6}, \end{aligned} \quad (25.37)$$

or

$$i'_{\lambda,a,b,1} = \frac{1}{f_x} i'_{\lambda,a,b} + \left(1 - \frac{1}{f_x}\right) i'_{\lambda,a,b,2}, \quad (25.38)$$

$$i'_{\lambda,a,b,3} = \frac{1}{f_y} i'_{\lambda,a,b} + \left(1 - \frac{1}{f_y}\right) i'_{\lambda,a,b,4}, \quad (25.39)$$

$$i'_{\lambda,a,b,5} = \frac{1}{f_z} i'_{\lambda,a,b} + \left(1 - \frac{1}{f_z}\right) i'_{\lambda,a,b,6}. \quad (25.40)$$

Substituting in the discretized RTE and solving with respect to the intensity in the center of the cell  $i'_{\lambda,a,b}$  we obtain finally

$$\begin{aligned} i'_{\lambda,a,b} &= \left\{ \begin{aligned} &S'_{a,b} - \left[ a_{a,b,2} + a_{a,b,1} \left(1 - \frac{1}{f_x}\right) \right] i'_{\lambda,a,b,2} \\ &- \left[ a_{a,b,4} + a_{a,b,3} \left(1 - \frac{1}{f_y}\right) \right] i'_{\lambda,a,b,4} - \left[ a_{a,b,6} + a_{a,b,5} \left(1 - \frac{1}{f_z}\right) \right] i'_{\lambda,a,b,6} \end{aligned} \right\} \\ &\times \left( a_{a,b,1} \frac{1}{f_x} + a_{a,b,3} \frac{1}{f_y} + a_{a,b,5} \frac{1}{f_z} + \beta_\lambda \right)^{-1}. \end{aligned} \quad (25.41)$$

*Step difference scheme:* Setting

$$f_x = f_y = f_z = 1 \quad (25.42)$$

results in a first order *step* difference scheme

$$i'_{\lambda,a,b,1} = i'_{\lambda,a,b}, \quad i'_{\lambda,a,b,3} = i'_{\lambda,a,b}, \quad i'_{\lambda,a,b,5} = i'_{\lambda,a,b}, \quad (25.43)$$

which resembles the *donor cell* scheme in the CFD. Consequently we have

$$\begin{aligned} i'_{\lambda,a,b} &= \frac{S'_{a,b} - a_{a,b,2} i'_{\lambda,a,b,2} - a_{a,b,4} i'_{\lambda,a,b,4} - a_{a,b,6} i'_{\lambda,a,b,6}}{\beta_\lambda + a_{a,b,1} + a_{a,b,3} + a_{a,b,5}} \\ &\equiv \frac{S'_{a,b} - a_{a,b,2} i'_{\lambda,a,b,i-1} - a_{a,b,4} i'_{\lambda,a,b,j-1} - a_{a,b,6} i'_{\lambda,a,b,k-1}}{\beta_\lambda + a_{a,b,1} + a_{a,b,3} + a_{a,b,5}}. \end{aligned} \quad (25.44)$$

Similar strategy is used for the other octants.

*The optimum marching strategy:* If the point *Gauss-Seidel* method is used to solve the above equation there is an optimum strategy of visiting the cells, and the ordinate directions – called the optimum marching strategy. The optimum marching strategy is direction dependent. First the octants are defined in which the discrete ordinate is, as given in the Table 25.1, and then the incident and the outlet walls of the cell. Then the marching strategy is defined in Tables 25.2 and 25.3.

**Table 25.1.** Definition of the octants. Incident and outlet walls in the cell

Angles	Octant	Incident wall cells i1,i2,i3	Outlet wall cells o1,o2,o3
$0 \leq \theta_b < \pi/2$			
$0 \leq \varphi_a < \pi/2$	1	2,4,6	1,3,5
$\pi/2 \leq \varphi_a < \pi$	2	1,4,6	2,3,5
$\pi \leq \varphi_a < 3\pi/2$	3	1,3,6	2,4,5
$3\pi/2 \leq \varphi_a < 2\pi$	4	2,3,6	1,4,5
$\pi/2 \leq \theta_b < \pi$			
$0 \leq \varphi_a < \pi/2$	5	2,4,5	1,3,6
$\pi/2 \leq \varphi_a < \pi$	6	1,4,5	2,3,6
$\pi \leq \varphi_a < 3\pi/2$	7	1,3,5	2,4,6
$3\pi/2 \leq \varphi_a < 2\pi$	8	2,3,5	1,4,6

**Table 25.2.** Marching strategy depending on the discrete ordinate direction

Octant	Marching strategy x-direction	y-direction	z-direction
1	$i = 2, i_{\max} - 1$	$j = 2, j_{\max} - 1$	$k = 2, k_{\max} - 1$
2	$i = i_{\max} - 1, 2, -1$	$j = 2, j_{\max} - 1$	$k = 2, k_{\max} - 1$
3	$i = i_{\max} - 1, 2, -1$	$j = j_{\max} - 1, 2, -1$	$k = 2, k_{\max} - 1$
4	$i = 2, i_{\max} - 1$	$j = j_{\max} - 1, 2, -1$	$k = 2, k_{\max} - 1$
5	$i = 2, i_{\max} - 1$	$j = 2, j_{\max} - 1$	$k = k_{\max} - 1, 2, -1$
6	$i = i_{\max} - 1, 2, -1$	$j = 2, j_{\max} - 1$	$k = k_{\max} - 1, 2, -1$
7	$i = i_{\max} - 1, 2, -1$	$j = j_{\max} - 1, 2, -1$	$k = k_{\max} - 1, 2, -1$
8	$i = 2, i_{\max} - 1$	$j = j_{\max} - 1, 2, -1$	$k = k_{\max} - 1, 2, -1$

**Table 25.3.** Marching strategy for the discrete ordinate

Octant	Marching strategy <i>a</i> -direction	<i>b</i> -direction
1	$a = 1, a_{\max} / 4$	$b = 1, b_{\max} / 2$
2	$a = a_{\max} / 4 + 1, a_{\max} / 2$	$b = 1, b_{\max} / 2$
3	$a = a_{\max} / 2 + 1, 3a_{\max} / 4$	$b = 1, b_{\max} / 2$
4	$a = 3a_{\max} / 4 + 1, a_{\max}$	$b = 1, b_{\max} / 2$
5	$a = 1, a_{\max} / 4$	$b = b_{\max} / 2 + 1, b_{\max}$
6	$a = a_{\max} / 4 + 1, a_{\max} / 2$	$b = b_{\max} / 2 + 1, b_{\max}$
7	$a = a_{\max} / 2 + 1, 3a_{\max} / 4$	$b = b_{\max} / 2 + 1, b_{\max}$
8	$a = 3a_{\max} / 4 + 1, a_{\max}$	$b = b_{\max} / 2 + 1, b_{\max}$

Therefore for each octant we have

$$i'_{\lambda,a,b} = \frac{S'_{a,b} - a_{a,b,i1}i'_{\lambda,a,b,i1} - a_{a,b,i2}i'_{\lambda,a,b,i2} - a_{a,b,i3}i'_{\lambda,a,b,i3}}{\beta_{\lambda} + a_{a,b,o1} + a_{a,b,o2} + a_{a,b,o3}}, \quad (25.45)$$

where  $i'_{\lambda,a,b,o1} = i'_{\lambda,a,b}$ ,  $i'_{\lambda,a,b,o2} = i'_{\lambda,a,b}$ ,  $i'_{\lambda,a,b,o3} = i'_{\lambda,a,b}$ .

This method has been in use for a long time. It is very simple in design and stable in performance regardless of the ordinate set chosen or the local radiative properties, but it is reported to be inaccurate *Mathews* (1999).

*Lathrop's diamond difference scheme:* Setting

$$f_x = f_y = f_z = \frac{1}{2} \quad (25.47)$$

results in the second order *Lathrop* diamond difference scheme. The diamond schemes are known to be unstable without additional improvement of the weighting coefficients *Mathews* (1999).

*Fiveland scheme:* *Fiveland* (1988) proposed to use

$$f_x = f_y = f_z = f \quad (25.48)$$

satisfying the following conditions

$$\Delta x < \frac{|s_{x,a,b}|}{\beta(1-f)}\phi, \quad \Delta y < \frac{|s_{y,a,b}|}{\beta(1-f)}\phi, \quad \Delta z < \frac{|s_{z,a,b}|}{\beta(1-f)}\phi, \quad (25.49-51)$$

where

$$\phi = \frac{f^3 + (1-f)^2 (2-5f)}{f}. \quad (25.53)$$

It is thinkable to use a set of non-equal weighting factors like

$$f_x = \max \left[ \left( 1 - \frac{|S_{x,a,b}|}{\beta \Delta x} \right), \frac{1}{2} \right], \quad (25.54)$$

$$f_y = \max \left[ \left( 1 - \frac{|S_{y,a,b}|}{\beta \Delta y} \right), \frac{1}{2} \right], \quad (25.55)$$

$$f_z = \max \left[ \left( 1 - \frac{|S_{z,a,b}|}{\beta \Delta z} \right), \frac{1}{2} \right], \quad (25.56)$$

to assure the positive scheme.

### 25.2.3 Boundary conditions

The radiation heat flux across the surface  $m$  is that computed by integrating over the discrete ordinates

$$\dot{q}_{\lambda,m}'' = \Delta Vol \sum_{b=1}^{b_{\max}} \sum_{a=1}^{a_{\max}} a_{a,b,m} \Delta \omega_{a,b} i'_{\lambda,a,b,m}. \quad (25.57)$$

The incident radiation heat flux from the inside of the computational cell is

$$\dot{q}_{\lambda,m-\text{incident}}'' = \Delta Vol \sum_{b=1}^{b_{\max}} \sum_{a=1}^{a_{\max}} a_{a_i,b_i,m} \Delta \omega_{a_i,b_i} i'_{\lambda,a_i,b_i,m}. \quad (25.58)$$

For Cartesian coordinate system the incident ordinate directions  $a_i, b_i$  are summarized in Table 25.4. At *diffusely emitting and reflecting* walls with temperature  $T_{w,m}$  and emissivity coefficient  $\varepsilon_w$  the emitting intensity is

$$i'_{\lambda,a_o,b_o,m} = \varepsilon_w \frac{\sigma T_{w,m}}{\pi} + (1 - \varepsilon_w) \frac{\dot{q}_{\lambda,m-\text{incident}}''}{\pi}. \quad (25.59)$$

The outlet ordinate directions are specified for each wall in Table 25.5 for a Cartesian coordinate system.

Setting

$$i'_{\lambda, a_o, b_o, m} = 0 \quad (25.60)$$

means a *transparent* wall. For *mirroring* walls we have

$$i'_{\lambda, a_{\max} - a + 1, b_{\max} - b + 1, m} = \varepsilon_w \frac{\sigma T_{w, m}}{\pi} + i'_{\lambda, a, b} \quad (25.61)$$

where  $a, b \in m - \text{incident}$ .

**Table 25.4.** Marching strategy for computation of the incident radiation at the cell walls required for definition of boundary conditions

Wall Nr.	Marching strategy, incident <i>a</i> -direction	<i>b</i> -direction
1	$a = 1, a_{\max} / 4$ $a = 3a_{\max} / 4 + 1, a_{\max}$	$b = 1, b_{\max}$
2	$a = a_{\max} / 4 + 1, 3a_{\max} / 4$	$b = 1, b_{\max}$
3	$a = 1, a_{\max} / 2$	$b = 1, b_{\max}$
4	$a = a_{\max} / 2 + 1, a_{\max}$	$b = 1, b_{\max}$
5	$a = 1, a_{\max}$	$b = 1, b_{\max} / 2$
6	$a = 1, a_{\max}$	$b = b_{\max} / 2 + 1, b_{\max}$

**Table 25.5.** Marching strategy for computation of the outlet radiation at the cell walls required for definition of boundary conditions

Wall Nr.	Marching strategy, outlet <i>a</i> -direction	<i>b</i> -direction
1 (e)	$a = a_{\max} / 4 + 1, 3a_{\max} / 4$	$b = 1, b_{\max}$
2 (w)	$a = 1, a_{\max} / 4$ $a = 3a_{\max} / 4 + 1, a_{\max}$	$b = 1, b_{\max}$
3 (n)	$a = a_{\max} / 2 + 1, a_{\max}$	$b = 1, b_{\max}$
4 (s)	$a = 1, a_{\max} / 2$	$b = 1, b_{\max}$
5 (u)	$a = 1, a_{\max}$	$b = b_{\max} / 2 + 1, b_{\max}$
6 (d)	$a = 1, a_{\max}$	$b = 1, b_{\max} / 2$

For mirroring the incident directions required are  $a = a_{\max} - a + 1$ ,  $b = b_{\max} - b + 1$

## 25.3 Material properties

### 25.3.1 Source terms – emission from hot surfaces with known temperature

The black body intensity in any direction is computed by integrating *Planck's* spectral distribution emissive power within the prescribed boundaries as follows

$$i'_{lb} = \frac{1}{\pi} \int_{\lambda_1}^{\lambda_2} \frac{2\pi C_1}{\lambda^5 \left( e^{\frac{C_2}{\lambda T}} - 1 \right)} d\lambda, \quad (25.62)$$

where

$$C_1 = 0.59552197 \times 10^{-16} m^2 / sr, \quad (25.63)$$

$$C_2 = 0.014338769 \times 10^{-16} mK. \quad (25.64)$$

Here index *b* stands for black body. We use three bands for the source terms. The boundaries are selected as follows

$$\lambda_1 = 7 \times 10^{-7} m, \lambda_2 = 1.2 \times 10^{-6} m, \quad (25.65, 66)$$

for the first band,

$$\lambda_1 = 1.2 \times 10^{-6} m, \lambda_2 = 1.8 \times 10^{-6} m, \quad (25.67, 68)$$

for the second band, and

$$\lambda_1 = 1.8 \times 10^{-6} m, \lambda_2 = 20 \times 10^{-6} m, \quad (25.69, 70)$$

for the third band. Other choices are of course possible. Thus the source term due to radiating melt particles assuming

$$\Phi(\lambda, \omega, \omega_i) = 1 \quad (25.71)$$

is

$$S' = f_{r,3} a_{3\lambda} i'_{lb}(T_3) + \frac{\sigma_{3s\lambda}}{4\pi} \sum_{a=1}^{a_{\max}} \sum_{b=1}^{b_{\max}} i'_{\lambda,a,b} = f_{r,3} a_{3\lambda} i'_{lb}(T_3) + \frac{\sigma_{3s\lambda}}{4\pi} i'_{\lambda,total}. \quad (25.72)$$

### 25.3.2 Spectral absorption coefficient of water

The experimentally measured index of refraction, *n*, and the index of absorption, *k*, as a function of the incident wave length are taken from *Hale* and *Marvin*

(1973) and *Zolotarev and Dyomin* (1977). The data of *Hale and Marvin* are used for wavelengths in the region of 0.7 to 7  $\mu\text{m}$  and the data of *Zolotarev and Dyomin* for the region of 7 to 17  $\mu\text{m}$ . The spectral absorption coefficient is then computed as follows

$$a_{\lambda}(\lambda) = \frac{4\pi k}{\lambda}. \quad (25.73)$$

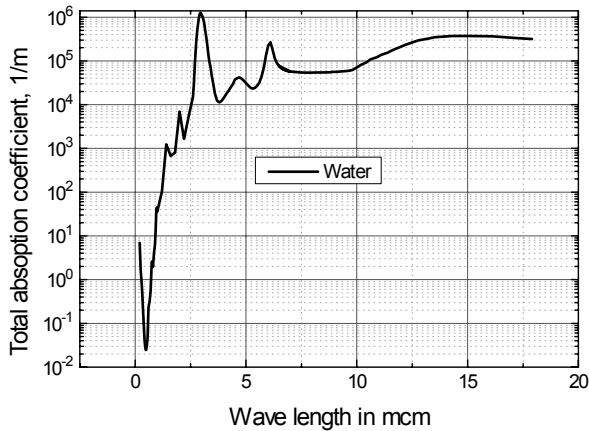


**Fig. 25.3** Spectral absorption coefficient for water as a function of the wavelength

The so obtained absorption coefficient is presented in Fig. 25.3. The argumentation that the spectral properties of water are not strong functions of water temperature and pressure summarized by *Fletcher* (1999) is acceptable. The total absorption coefficient is then computed as follows

$$a'(T_3) = \frac{\int_{\lambda_{\min}}^{\lambda_{\max}} i'_{lb}(T_3, \lambda) \left[ 1 - e^{-a_{\lambda}(\lambda)s} \right] d\lambda}{\int_{\lambda_{\min}}^{\lambda_{\max}} i'_{lb}(T_3, \lambda) d\lambda}. \quad (25.74)$$

We use for the limits the following values  $\lambda_{\min} = 0.7\mu\text{m}$  and  $\lambda_{\max} = 33\mu\text{m}$  and perform the integration numerically using 1000 steps. This is a very time consuming procedure. To avoid computation cost *Fletcher* (1985) tabulated the results obtained in similar manner for three different radiation surface temperatures, namely 1000, 2500 and 3500 K as a function of the water thickness  $s$ . *Vaeth* (1995) approximated the absorption coefficients obtained by *Fletcher* (1985) for three different radiation surface temperature, namely 1000, 2500 and



3500 K by an analytical function. We compared *Vaeth's* approximation with the analytically obtained coefficients and found that the coefficients for 3500 K are with about 30% lower and for 2500 K about 10% lower then those computed analytically. The modified *Vaeth* approximation is then recommended here

$$\begin{aligned}
 a(T_3, s) = & a(T_3 = 1000K, s) \frac{1}{15} \left[ 32 + 4 \frac{T_3}{1000} \left( -6 + \frac{T_3}{1000} \right) \right] \\
 & + a(T_3 = 2500K, s) \frac{1}{3} \left[ -7 + \frac{T_3}{1000} \left( 9 - 2 \frac{T_3}{1000} \right) \right] \\
 & + a(T_3 = 3500K, s) \frac{1}{5} \left[ 5 + \frac{T_3}{1000} \left( -7 + 2 \frac{T_3}{1000} \right) \right], \quad (25.75)
 \end{aligned}$$

where

$$a(T_3 = 1000K, s) = 1.395086 \ln \left( s^{0.01374877} + 1 \right), \quad (25.76)$$

$$a(T_3 = 2500K, s) = 1.1 \times 0.8641743 \ln \left( s^{0.1427472} + 1 \right), \quad (25.77)$$

$$a(T_3 = 3500K, s) = 1.3 \times 0.4948444 \ln \left( s^{0.2694667} + 1 \right). \quad (25.78)$$

Note that this correlation cannot be extrapolated for water thickness less than 1 mm because of the unacceptable error increase - see Fig. 25.5. Values for this region are given in Fig. 25.4, 25.6. We see that for water thickness between 1 and 30  $\mu\text{m}$  the error of the modified *Vaeth* approximation is less than 8%.

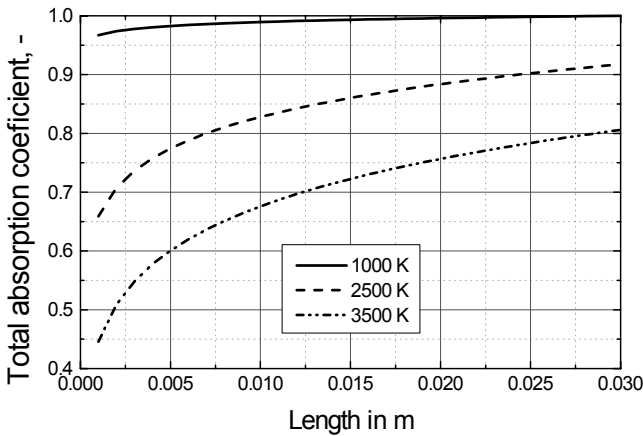


**Fig. 25.4** Analytically computed total absorption coefficient as a function of the water layer thickness. Parameter – temperature of the radiation sources

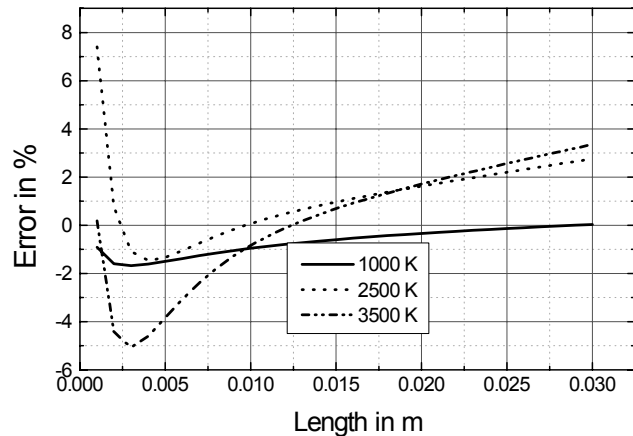


**Fig. 25.5** Error of the modified Vaeth approximation compared to the analytically computed total absorption coefficient as a function of the water layer thickness. Parameter – temperature of the radiation sources

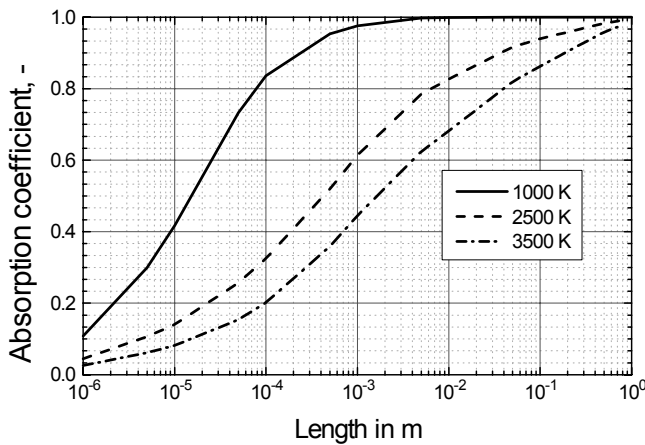


**Fig. 25.6** Analytically computed total absorption coefficient as a function of the water layer thickness. Parameter – temperature of the radiation sources

*Partitioning of the absorbed energy between the bulk and the surface:* Now let us estimate the band absorption coefficients for three different bands as presented in Figs. 25.7 a) through c). The figures demonstrated the strong heterogeneity of the absorption depending on the wavelength. Thermal radiation in the first band can

cover much longer distance without being absorbed than the radiation in the second and in the third band. In band no.2 the temperature dependence is not as strong as in the other two bands.

The problem of how much radiation energy is deposited at the surface and immediately transferred into evaporation mass is not solved up to now and has to be attacked in the future. Fig. 25.7 d) demonstrates that thermal radiation with wavelengths larger  $3 \mu\text{m}$  are completely absorbed within a  $0.5 \text{ mm}$  water layer. *Vaeth* (1995) proposed to consider all this energy deposited onto the surface which is obviously true only for lengths larger then  $0.5 \text{ mm}$ . The *Vaeth* approximation of the part of the energy deposited onto the surface is

$$f_{\text{surface}} = \min \left( 1, \frac{\left( \frac{T_3}{1000} \right)}{\left( \frac{T_3}{1000} \right)^2 - 0.4611115 \left( \frac{T_3}{1000} \right) + 0.8366274} \right). \quad (25.79)$$

If we arbitrary take all the deposit energy in  $0.01 \text{ mm}$  as surface energy the absorbed fractions of the incident energy analytically computed are 0.417, 0.141 and 0.0815 for the temperatures 1000, 2500 and 3500 K, respectively.

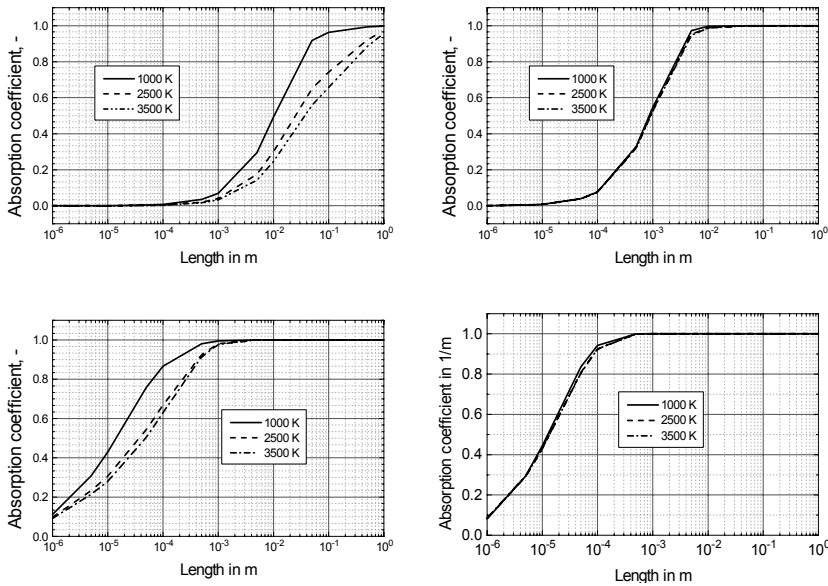


**Fig. 25.7** Analytically computed partial absorption coefficient as a function of the water layer thickness. Parameter – temperature of the radiation sources. a) Band no.1  $7 \times 10^{-7}$  to  $1.2 \times 10^{-6} \text{ m}$ ; b) Band no.2  $1.2 \times 10^{-6}$  to  $1.8 \times 10^{-6} \text{ m}$ ; c) Band no.3  $1.8 \times 10^{-6}$  to  $20 \times 10^{-6} \text{ m}$ ; d) Infrared  $3 \times 10^{-6}$  to  $200 \times 10^{-6} \text{ m}$ .

### 25.3.3 Spectral absorption coefficient of water vapor and other gases

Information about the total emissivity and absorptivity for carbon dioxide, water vapor and their mixtures is provided by *Steward and Kocaefer* (1986). Information about the gas emissivity for wide range of process conditions is provided by *Docherty* (1983).

## 25.4 Averaged properties for some particular cases occurring in melt-water interaction

During interaction of molten material with water some specific geometrical arrangement called flow pattern may happen. For some of them we provide the averaged properties across a control volume with finite size. We will consider three different cases as examples starting with the simplest and ending with a more complicated one:

- 1) Gas sphere inside a molten material.
- 2) Concentric spheres of water droplets, surrounded by vapor, surrounded by molten material.
- 3) Spherical particles of hot radiating material surrounded by a layer of vapor surrounded by water.

The first two cases are typical examples for local interaction. Whatever happens with the radiation transport it happens within the cavity. The third one is a typical example for interactions across the faces of the control volumes. It is the idealized film boiling case.

### 25.4.1 Spherical cavity of gas inside a molten material

Consider the case presented in Fig. 25.8.

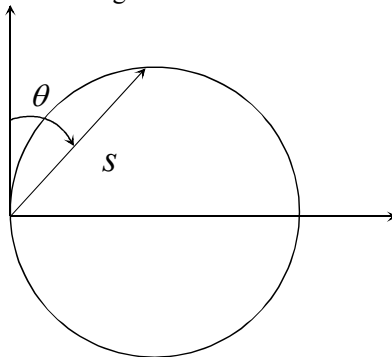


**Fig. 25. 8** Spherical cavity of gas inside a molten material

The gas cavity is surrounded completely by melt. Given is the diameter of the cavity  $D_1$ , the temperatures of the melt  $T_3$  and of the gas  $T_1$  and their radiation properties. The task is to estimate how much energy per unit time  $Q_A$  is transferred from the melt into the gas.

We select an arbitrary point at the interface and draw one axis going through the point an the center of the sphere and one vertical axis perpendicular to it. With respect to the vertical axis we define the angle  $\theta$ . All possible beam directions in the horizontal cross section are defined within the angle interval:  $\theta_1 = 0$ ,  $\theta_2 = \frac{\pi}{2}$ .

The beam length  $s$  is then depending only on the angle  $s = D_1 \sin \theta$ . The averaged beam length is then defined as follows

$$\bar{s} = \frac{\int_0^{2\pi} \int_{\theta_1}^{\theta_2} s_1 \cos \theta \sin \theta d\theta d\varphi}{\frac{1}{2}(\sin^2 \theta_2 - \sin^2 \theta_1)} = 2 \int_0^{\frac{\pi}{2}} s \cos \theta \sin \theta d\theta = \frac{2}{3} D_1. \quad (25.80)$$

The integration over the angle  $\varphi$  is in the boundaries 0 and  $2\pi$  because we have axis symmetry. Note in this case that  $\sin^2 \theta_2 - \sin^2 \theta_1 = 1$ . With this averaged beam length we compute the  $\alpha'_1(\bar{s})$  spectral-averaged absorption coefficient and the spectral-averaged emissivity coefficient of the vapor  $\varepsilon'_1(\bar{s})$ . The transferred power through the vapor sphere is therefore

$$Q = \pi D_1^2 \sigma \left\{ [1 - \alpha'_1(\bar{s})] \varepsilon_3 T_3^4 + \varepsilon'_1(\bar{s}) T_1^4 \right\}. \quad (25.81)$$

The absorbed power inside the sphere is

$$Q_A = \pi D_1^2 \sigma \left[ \alpha'_1(\bar{s}) \varepsilon_3 T_3^4 - \varepsilon'_1(\bar{s}) T_1^4 \right]. \quad (25.82)$$

### 25.4.2 Concentric spheres of water droplets, surrounded by vapor, surrounded by molten material

Consider a continuous melt with water and vapor enclosed inside the melt as presented in Fig.25.9.

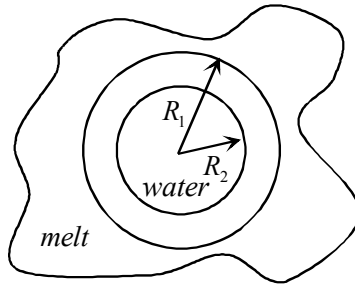


**Fig. 25.9** Sphere of water droplet, surrounded by vapor, surrounded by molten material

The volume fraction of the vapor  $\alpha_1$ , and of the water  $\alpha_2$  are known. The water diameter is known. We assume that the vapor is surrounding the water concentrically. The vapor diameter is then

$$D_1 = D_2 \sqrt[3]{1 + \frac{\alpha_1}{\alpha_2}}, \quad \alpha_2 > 0. \quad (25.83)$$

The melt radiates through the vapor and through the droplet. It is to be computed how much power radiated from the melt is absorbed by the vapor and how much is absorbed by the water droplet. Again we select an arbitrary point at the melt interface and draw an axis going through the point to the center of the sphere and one vertical axis perpendicular to it. With respect to the vertical axis we define the angle  $\theta$ . All possible beam directions in the horizontal cross section are defined

within the angle interval:  $\theta_1 = 0$ ,  $\theta_2 = \frac{\pi}{2}$  but in contrast with the previous case

there are two characteristic zones as shown in Fig. 25.10. In the first the beam crosses gas only and in the second gas, water, gas successively. We perform the integration within these two zones separately.

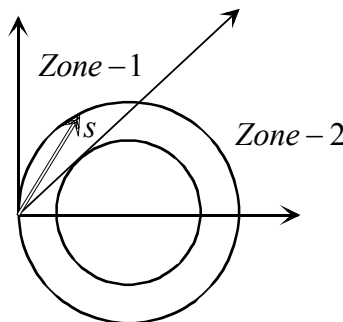


**Fig. 25.10** Zone 1 - beam crosses vapor only, zone 2 - beam crosses vapor-liquid-vapor

*First zone - vapor only:* This zone is defined within the angles

$$\theta_1 = 0, \theta_2 = \frac{\pi}{2} - \arcsin\left(\frac{D_2}{D_1}\right), \sin^2 \theta_2 - \sin^2 \theta_1 = 1 - \left(\frac{D_2}{D_1}\right)^2.$$

The beam length inside the zone is

$$s_{v,1,zone} = D_1 \sin \theta. \quad (25.84)$$

The averaged beam length is

$$\begin{aligned} \bar{s}_{v,1,zone} &= \frac{\int_0^{2\pi} \int_{\theta_1}^{\theta_2} s_1 \cos \theta \sin \theta d\theta d\varphi}{\frac{1}{2}(\sin^2 \theta_2 - \sin^2 \theta_1)} \\ &= 2 \frac{\int_0^{\frac{\pi}{2} - \arcsin\left(\frac{D_2}{D_1}\right)} s_{2,1,zone} \cos \theta \sin \theta d\theta}{1 - \left(\frac{D_2}{D_1}\right)^2} = \frac{2}{3} D_1 \left[ 1 - \left(\frac{D_2}{D_1}\right)^2 \right]^{1/2}. \end{aligned} \quad (25.85)$$

The transferred power through the vapor is

$$Q = \pi D_1^2 \sigma \left\{ [1 - \alpha'_v(\bar{s}_{v,1,zone})] \varepsilon_3 T_3^4 + \varepsilon'_v(\bar{s}_{v,1,zone}) T_1^4 \right\} \left( 1 - \frac{D_2^2}{D_1^2} \right). \quad (25.86)$$

The absorbed power inside the vapor is

$$Q_A = \pi D_1^2 \sigma \left\{ \alpha'_v(\bar{s}_{v,1,zone}) \varepsilon_3 T_3^4 - \varepsilon'_v(\bar{s}_{v,1,zone}) T_1^4 \right\} \left( 1 - \frac{D_2^2}{D_1^2} \right). \quad (25.87)$$

*Second zone – vapor/droplet:* The second zone is defined within the interval

$$\theta_1 = \frac{\pi}{2} - \arcsin\left(\frac{D_2}{D_1}\right) \text{ and } \theta_2 = \frac{\pi}{2}, \sin^2 \theta_2 - \sin^2 \theta_1 = \left(\frac{D_2}{D_1}\right)^2.$$

*Vapor:* The beam length inside the vapor is

$$s_{v,2,zone} = \frac{1}{2} D_1 \left[ \sin \theta - \left( \left(\frac{D_2}{D_1}\right)^2 - \cos^2 \theta \right)^{1/2} \right]. \quad (25.88)$$

The averaged beam length results then in

$$\begin{aligned}
\bar{s}_{v,2.zone} &= \frac{\int_{\theta_1}^{\theta_2} s_{v,2.zone} \cos \theta \sin \theta d\theta}{\frac{1}{2}(\sin^2 \theta_2 - \sin^2 \theta_1)} = \frac{2 \int_{\theta_1}^{\theta_2} s_{v,2.zone} \cos \theta \sin \theta d\theta}{\left(\frac{D_2}{D_1}\right)^2} \\
&= \frac{1}{3} D_1 \frac{1 - \left(\frac{D_2}{D_1}\right)^2 - \left(1 - \left(\frac{D_2}{D_1}\right)^2\right)^{3/2}}{\left(\frac{D_2}{D_1}\right)^2}. \quad (25.89)
\end{aligned}$$

The transferred power through the vapor is

$$Q = \pi D_1^2 \sigma \left\{ [1 - \alpha'_v(\bar{s}_{v,2.zone})] \varepsilon_3 T_3^4 + \varepsilon'_v(\bar{s}_{v,2.zone}) T_1^4 \right\} \left( \frac{D_2}{D_1} \right)^2. \quad (25.90)$$

The absorbed power inside the vapor is

$$Q_A = \pi D_1^2 \sigma \left\{ \alpha'_v(\bar{s}_{v,2.zone}) \varepsilon_3 T_3^4 - \varepsilon'_v(\bar{s}_{v,2.zone}) T_1^4 \right\} \left( \frac{D_2}{D_1} \right)^2. \quad (25.91)$$

*Water:* The beam length inside the water is

$$\Delta s_{w,2.zone} = D_1 \left[ \left( \frac{D_2}{D_1} \right)^2 - \cos^2 \theta \right]^{1/2}. \quad (25.92)$$

The averaged beam length is then

$$\Delta \bar{s}_{w,2.zone} = 2 \frac{\int_{\theta_1}^{\theta_2} s_{w,2.zone} \cos \theta \sin \theta d\theta}{\left(\frac{D_2}{D_1}\right)^2} = \frac{2}{3} D_2. \quad (25.93)$$

The transferred power through the water droplet is

$$Q = \pi D_1^2 \sigma \left\{ \begin{aligned} &[1 - \alpha'_w(\bar{s}_{w,2.zone})][1 - \alpha'_v(\bar{s}_{v,2.zone})] \varepsilon_3 T_3^4 \\ &+ [1 - \alpha'_w(\bar{s}_{w,2.zone})] \varepsilon'_v(\bar{s}_{v,2.zone}) T_1^4 \\ &+ \varepsilon'_w(\bar{s}_{w,2.zone}) T_2^4 \end{aligned} \right\} \left( \frac{D_2}{D_1} \right)^2. \quad (25.94)$$



The absorbed power by the water droplet is

$$Q_{Aw} = \pi D_1^2 \sigma \left\{ \begin{aligned} &\alpha'_w(\bar{s}_{w,2,zone})[1 - \alpha'_v(\bar{s}_{v,2,zone})]\varepsilon_3 T_3^4 \\ &+ \alpha'_w(\bar{s}_{w,2,zone})\varepsilon'_v(\bar{s}_{v,2,zone})T_1^4 - \varepsilon'_w(\bar{s}_{w,2,zone})T_2^4 \end{aligned} \right\} \left( \frac{D_2}{D_1} \right)^2. \quad (25.95)$$

The absorbed total power by the vapor is the sum of the absorbed power in the both vapor regions

$$Q_{Av} = \pi D_1^2 \sigma \left[ \begin{aligned} &\left\{ \alpha'_v(\bar{s}_{v,1,zone})\varepsilon_3 T_3^4 - \varepsilon'_v(\bar{s}_{v,1,zone})T_1^4 \right\} \left( 1 - \frac{D_2^2}{D_1^2} \right) \\ &+ \left\{ \alpha'_v(\bar{s}_{v,2,zone})\varepsilon_3 T_3^4 - \varepsilon'_v(\bar{s}_{v,2,zone})T_1^4 \right\} \left( \frac{D_2}{D_1} \right)^2 \end{aligned} \right]. \quad (25.96)$$

### 25.4.3 Clouds of spherical particles of radiating material surrounded by a layer of vapor surrounded by water –*Lanzenberger's* solution

Consider a cloud of equidistantly arranged hot spherical particles. The cloud is flying in a water and gas mixture. Compute the power radiated by a hot spherical particle and its environment. Compute what part of this energy is absorbed by water and what part is absorbed in the gas as a function of the characteristic scales inside the three-phase mixture. Compute the length required for almost complete length absorption.

The task can formally be described in the following way: Consider an artificially defined sphere with diameter  $D_2$  containing concentrically two other spheres as presented in Fig. 25.11. This resembles film boiling of hot particles in water. We use this structure as an abstract model for computing the radiation properties of the mixture consisting of particles, vapor and water. This elementary cell is called sometimes a *Wigner* cell. It contains as much vapor and water as the total vapor and water in the computational cell divided by the number of the particles inside the cell, respectively. We will first compute what happens inside the *Wigner* cell and how much radiation energy is leaving the cell. Then we will ask the question what happens with the radiation energy in consequently interacting *Wigner* cells.

The inner most sphere, having diameter  $D_3$ , is radiating. We call this sphere a “particle”. The space between the first and the second spherical surfaces is filled with vapor. The second sphere has diameter  $D_1$ . The space between the second and the external sphere (*Wigner* cell) is filled with water. Now consider a space

filled equidistantly with particles having volume fraction  $\alpha_3 > 0$  surrounded by vapor with volume fraction  $\alpha_1 > 0$  and water having volume fraction  $\alpha_2 > 0$ .

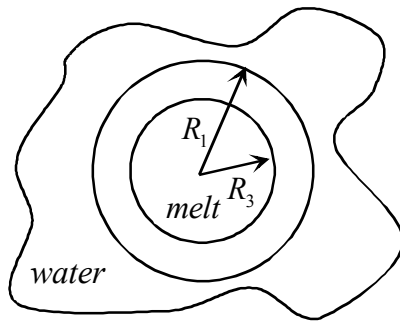


**Fig. 25.11** Radiating sphere concentrically surrounded by vapor and water

For homogeneously distributed particles we have

$$D_1 = D_2 \sqrt[3]{\alpha_1 + \alpha_3} = D_3 \sqrt[3]{1 + \frac{\alpha_1}{\alpha_3}}, \quad \alpha_3 > 0, \quad (25.97)$$

$$D_2 = \frac{D_3}{\sqrt[3]{\alpha_3}}, \quad \alpha_3 > 0. \quad (25.98)$$

Frequently used ratios in the following text are

$$\frac{D_1}{D_2} = (\alpha_1 + \alpha_3)^{1/3}, \quad (25.99)$$

$$\frac{D_3}{D_2} = \alpha_3^{1/3}. \quad (25.100)$$

In this section we will present *Lanzenberger's* results reported in (1997) simplifying in some places the resulting integrals for convenient use.

#### **25.4.3.1 Space-averaged beam lengths for the concentric spheres radiation problem**

The averaging procedure for computing the averaged beam length results from the radiation theory is

$$\bar{s} = \frac{\int_0^{2\pi} \int_{\theta_1}^{\theta_2} s(\varphi, \theta) \cos \theta \sin \theta d\theta d\varphi}{\int_0^{2\pi} \int_{\theta_1}^{\theta_2} \cos \theta \sin \theta d\theta d\varphi} = \frac{\int_{\theta_1}^{\theta_2} s(\theta) \cos \theta \sin \theta d\theta}{\frac{1}{2} (\sin^2 \theta_2 - \sin^2 \theta_1)}. \quad (25.101)$$

It gives the averaged beam length over the angles  $0 < \varphi < 2\pi$  and  $\theta_1 < \theta < \theta_2$ . The formal procedure contains (a) specification of  $\theta_1$  and  $\theta_2$ , (b) derivation of the relationship  $s_1(\varphi, \theta)$  and (c) finally integration in order to obtain  $\bar{s}$ . Two specific geometries presented in Fig. 25.12 and Fig. 25.13 represent all cases. The results of the computations are presented below:

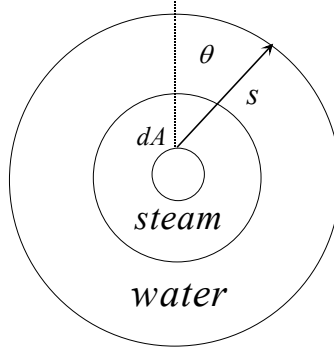


**Fig. 25.12** Radiating hot sphere through steam and water. The first Wigner cell.

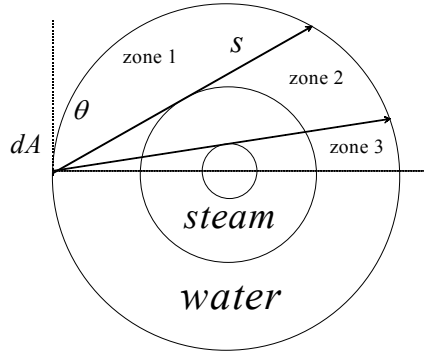


**Fig. 25.13** Radiation entering the second Wigner cell from outside sources

#### 25.4.3.1.1 Beam emitted from the particle surface

Angle interval:  $\theta_1 = 0$  and  $\theta_2 = \pi/2$ ,  $\sin^2 \theta_2 - \sin^2 \theta_1 = 1$ .

Vapor:  $0 < s < s_1$

$$\text{Beam length: } s_1 = \frac{1}{2} D_3 \left[ \left( \left( \frac{D_1}{D_3} \right)^2 - \sin^2 \theta \right)^{1/2} - \cos \theta \right]. \quad (25.102)$$

Averaged beam length:

$$\bar{s}_1 = 2 \int_0^{\pi/2} s_1 \cos \theta \sin \theta d\theta = \frac{1}{3} D_3 \left[ \left( \frac{D_1}{D_3} \right)^3 - \left( \left( \frac{D_1}{D_3} \right)^2 - 1 \right)^{3/2} - 1 \right]. \quad (25.103)$$

Water:  $s_1 < s < s_2$

Beam length:

$$s_2 - s_1 = \frac{1}{2} D_3 \left[ \left( \left( \frac{D_2}{D_3} \right)^2 - \sin^2 \theta \right)^{1/2} - \left( \left( \frac{D_1}{D_3} \right)^2 - \sin^2 \theta \right)^{1/2} \right]. \quad (25.104)$$

Averaged beam length:

$$\begin{aligned} \Delta \bar{s}_2 &= 2 \int_0^{\pi/2} (s_2 - s_1) \cos \theta \sin \theta d\theta \\ &= \frac{1}{3} D_3 \left\{ \left( \frac{D_2}{D_3} \right)^3 - \left( \frac{D_1}{D_3} \right)^3 + \left( \left( \frac{D_1}{D_3} \right)^2 - 1 \right)^{3/2} - \left( \left( \frac{D_2}{D_3} \right)^2 - 1 \right)^{3/2} \right\}. \end{aligned} \quad (25.105)$$

#### 25.4.3.1.2 Beam entering the external sphere (Wigner cell) surface

First zone - water only:

$$\text{Angle interval: } \theta_1 = 0, \theta_2 = \frac{\pi}{2} - \arcsin \left( \frac{D_1}{D_2} \right), \sin^2 \theta_2 - \sin^2 \theta_1 = 1 - \left( \frac{D_1}{D_2} \right)^2.$$

$$\text{Beam length: } s_{2,1,\text{zone}} = D_2 \sin \theta. \quad (25.106)$$

Averaged beam length:

$$\begin{aligned} \bar{s}_{2,1,\text{zone}} &= \frac{\int_0^{2\pi} \int_{\theta_1}^{\theta_2} s_1 \cos \theta \sin \theta d\theta d\varphi}{\frac{1}{2} (\sin^2 \theta_2 - \sin^2 \theta_1)} = \\ &= 2 \frac{\int_0^{\frac{\pi}{2} - \arcsin \left( \frac{D_1}{D_2} \right)} s_{2,1,\text{zone}} \cos \theta \sin \theta d\theta}{1 - \left( \frac{D_1}{D_2} \right)^2} = \frac{2}{3} D_2 \left[ 1 - \left( \frac{D_1}{D_2} \right)^2 \right]^{1/2}. \end{aligned} \quad (25.107)$$

Second zone:

Angle interval:  $\theta_1 = \frac{\pi}{2} - \arcsin\left(\frac{D_1}{D_2}\right)$  and  $\theta_2 = \frac{\pi}{2} - \arcsin\left(\frac{D_3}{D_2}\right)$ ,

$$\sin^2 \theta_2 - \sin^2 \theta_1 = \left(\frac{D_1}{D_2}\right)^2 - \left(\frac{D_3}{D_2}\right)^2.$$

*Region 1 – water:*

$$\text{Beam length: } s_{21,2.\text{zone}} = \frac{1}{2} D_2 \left[ \sin \theta - \left( \left( \frac{D_1}{D_2} \right)^2 - \cos^2 \theta \right)^{1/2} \right]. \quad (25.108)$$

Averaged beam length:

$$\begin{aligned} \bar{s}_{21,2.\text{zone}} &= \frac{\int_{\theta_1}^{\theta_2} s_{21,2.\text{zone}} \cos \theta \sin \theta d\theta}{\frac{1}{2} (\sin^2 \theta_2 - \sin^2 \theta_1)} = \frac{2 \int_{\theta_1}^{\theta_2} s_{21,2.\text{zone}} \cos \theta \sin \theta d\theta}{\left( \frac{D_1}{D_2} \right)^2 - \left( \frac{D_3}{D_2} \right)^2} \\ &= \frac{1}{3} D_2 \frac{\left( 1 - \left( \frac{D_3}{D_2} \right)^2 \right)^{3/2} - \left[ \left( \frac{D_1}{D_2} \right)^2 - \left( \frac{D_3}{D_2} \right)^2 \right]^{3/2} - \left( 1 - \left( \frac{D_1}{D_2} \right)^2 \right)^{3/2}}{\left( \frac{D_1}{D_2} \right)^2 - \left( \frac{D_3}{D_2} \right)^2}. \quad (25.109) \end{aligned}$$

*Region 2 – vapor:*

$$\text{Beam length: } \Delta s_{1,2.\text{zone}} = D_2 \left( \left( \frac{D_1}{D_2} \right)^2 - \cos^2 \theta \right)^{1/2}. \quad (25.110)$$

Averaged beam length:

$$\Delta \bar{s}_{1,2.\text{zone}} = 2 \frac{\int_{\theta_1}^{\theta_2} s_{21,2.\text{zone}} \cos \theta \sin \theta d\theta}{\left( \frac{D_1}{D_2} \right)^2 - \left( \frac{D_3}{D_2} \right)^2} = \frac{2}{3} D_2 \left[ \left( \frac{D_1}{D_2} \right)^2 - \left( \frac{D_3}{D_2} \right)^2 \right]^{1/2}. \quad (25.111)$$

*Region 3 – water:*

Beam length: The same as in region 1.

$$\text{Averaged beam length: } \Delta \bar{s}_{22,2,zone} = \bar{s}_{21,2,zone} . \quad (25.112)$$

*Third zone:*

$$\text{Angle interval: } \theta_1 = \frac{\pi}{2} - \arcsin\left(\frac{D_3}{D_2}\right) \text{ and } \theta_2 = \frac{\pi}{2}, \sin^2 \theta_2 - \sin^2 \theta_1 = \left(\frac{D_3}{D_2}\right)^2 .$$

*Region 1 –water only:*

$$\text{Beam length: } s_{2,3,zone} = \frac{1}{2} D_2 \left[ \sin \theta - \left( \left( \frac{D_1}{D_2} \right)^2 - \cos^2 \theta \right)^{1/2} \right] . \quad (25.113)$$

Averaged beam length:

$$\begin{aligned} \bar{s}_{2,3,zone} &= \frac{\int_{\theta_1}^{\theta_2} s_{2,3,zone} \cos \theta \sin \theta d\theta d\varphi}{\frac{1}{2} (\sin^2 \theta_2 - \sin^2 \theta_1)} = \frac{2 \int_{\theta_1}^{\theta_2} s_{2,3,zone} \cos \theta \sin \theta d\theta d\varphi}{\left( \frac{D_3}{D_2} \right)^2} \\ &= \frac{1}{3} D_2 \frac{1 - \left( \frac{D_1}{D_2} \right)^3 + \left[ \left( \frac{D_1}{D_2} \right)^2 - \left( \frac{D_3}{D_2} \right)^2 \right]^{3/2} - \left( 1 - \left( \frac{D_3}{D_2} \right)^2 \right)^{3/2}}{\left( \frac{D_3}{D_2} \right)^2} . \end{aligned} \quad (25.114)$$

*Region 2 –vapor only:*

$$\text{Beam length: } s_{1,3,zone} = \frac{1}{2} D_2 \left\{ \left[ \left( \frac{D_1}{D_2} \right)^2 - \cos^2 \theta \right]^{1/2} - \left[ \left( \frac{D_3}{D_2} \right)^2 - \cos^2 \theta \right]^{1/2} \right\} . \quad (25.115)$$

Averaged beam length:

$$\bar{s}_{1,3,zone} = \frac{\int_{\theta_1}^{\theta_2} s_{1,3,zone} \cos \theta \sin \theta d\theta}{\frac{1}{2} (\sin^2 \theta_2 - \sin^2 \theta_1)} = \frac{2 \int_{\theta_1}^{\theta_2} s_{1,3,zone} \cos \theta \sin \theta d\theta}{\left( \frac{D_3}{D_2} \right)^2}$$

$$= \frac{1}{3} D_2 \frac{\left( \left( \frac{D_1}{D_2} \right)^3 - \left( \frac{D_3}{D_2} \right)^3 - \left( \left( \frac{D_1}{D_2} \right)^2 - \left( \frac{D_3}{D_2} \right)^2 \right)^{3/2}}{\left( \frac{D_3}{D_2} \right)^2}. \quad (25.116)$$

### 25.4.3.2 Solution of the RTE

#### 25.4.3.2.1 Directional spectral intensity inside the vapor

Along the beam  $0 < s < s_1$  the analytical solution of the RTE equation without scattering gives the heat flux per unit solid angle, per unit wavelength and per unit area as a function of the beam length

$$i'_\lambda(\lambda, s, T_1, T_3) = i'_{3,\lambda}(\lambda, T_3) e^{-a_{1,\lambda}s} + i'_{1,\lambda}(\lambda, s, T_1) (1 - e^{-a_{1,\lambda}s}). \quad (25.117)$$

Across the infinitesimal cross section  $dA \cos \theta$ , for the infinitesimal solid angle  $d\omega$ , and within the wavelength region  $d\lambda$  we have

$$\begin{aligned} d^3 Q &= i'_\lambda(\lambda, s, T_1, T_3) dA \cos \theta d\omega d\lambda \\ &= \left[ i'_\lambda(\lambda, 0, T_3) e^{-a_{1,\lambda}s} + i'_{\lambda b}(\lambda, T_1) (1 - e^{-a_{1,\lambda}s}) \right] dA \cos \theta d\omega d\lambda. \end{aligned} \quad (25.118)$$

Integrated over all wavelengths of the emitting media we have

$$d^2 Q = \left[ \int_0^\infty i'_\lambda(\lambda, 0, T_3) e^{-a_{1,\lambda}s} d\lambda + \int_0^\infty i'_{\lambda b}(\lambda, T_1) (1 - e^{-a_{1,\lambda}s}) d\lambda \right] dA \cos \theta d\omega. \quad (25.119)$$

*Estimation of the first integral:* Having in mind the definition of the emissivity coefficient of the particle surface

$$\varepsilon_3(T_3) = \frac{\int_0^\infty i'_\lambda(\lambda, T_3) d\lambda}{\int_0^\infty i'_{\lambda b}(\lambda, T_3) d\lambda}, \quad (25.120)$$

and the definition of the vapor absorption coefficient of black body radiation with temperature  $T_3$

$$\begin{aligned}
 a'_1(T_3, s) &= \frac{\int_0^\infty i'_{\lambda b}(T_3, \lambda) [1 - e^{-a_{1,\lambda}s}] d\lambda}{\int_0^\infty i'_{\lambda b}(T_3, \lambda) d\lambda} \\
 &= 1 - \frac{\int_0^\infty i'_{\lambda b}(T_3, \lambda) e^{-a_{1,\lambda}s} d\lambda}{\int_0^\infty i'_{\lambda b}(T_3, \lambda) d\lambda} = 1 - \frac{\int_0^\infty i'_{\lambda b}(T_3, \lambda) e^{-a_{1,\lambda}s} d\lambda}{\frac{\sigma T_3^4}{\pi}} \quad (25.122)
 \end{aligned}$$

we obtain

$$\begin{aligned}
 \int_0^\infty i'_\lambda(\lambda, 0, T_3) e^{-a_{1,\lambda}s} d\lambda &= \varepsilon_3(T_3) \int_0^\infty i'_{\lambda b}(\lambda, T_3) e^{-a_{1,\lambda}s} d\lambda \\
 &= \varepsilon_3(T_3) [1 - a'_1(T_3, s)] \frac{\sigma T_3^4}{\pi}. \quad (25.123)
 \end{aligned}$$

*Estimation of the second integral:* For the second integral we use again the definition of the total emittance for vapor radiating with temperature  $T_1$

$$\int_0^\infty i'_{\lambda b}(\lambda, T_1) (1 - e^{-a_{1,\lambda}s}) d\lambda = \varepsilon_1(T_1, s) \frac{\sigma T_1^4}{\pi}. \quad (25.124)$$

Thus, after the integration over the total wavelength region we obtain

$$d^2Q = \left[ \varepsilon_3(T_3) [1 - a'_1(T_3, s)] \frac{\sigma T_3^4}{\pi} + \varepsilon_1(T_1, s) \frac{\sigma T_1^4}{\pi} \right] dA \cos \theta d\omega. \quad (25.125)$$

The first term gives the intensity at the point  $s$  coming from the particle with temperature  $T_3$ . The second term is the net contribution of the gas radiating with temperature  $T_1$  at point  $s$ .

#### 25.4.3.2.2 Directional spectral intensity inside the water

Along the beam  $s_1 < s < s_2$  the analytical solution of the RTE equation without scattering gives the heat flux per unit solid angle, per unit wavelength and per unit area as a function of the beam length

$$i'_\lambda(\lambda, s, T_1, T_2, T_3) = i'_\lambda(\lambda, s_1) e^{-a_{2,\lambda}s} + i'_{2,\lambda}(\lambda, s, T_2) (1 - e^{-a_{2,\lambda}s}). \quad (25.126)$$



Across the infinitesimal cross section  $dA \cos \theta$ , for the infinitesimal solid angle  $d\omega$ , and within the wavelength region  $d\lambda$  results in

$$\begin{aligned} d^3Q &= i'_\lambda(\lambda, s, T_1, T_2, T_3) dA \cos \theta d\omega d\lambda \\ &= \left[ i'_\lambda(\lambda, s_1) e^{-a_{2,\lambda}s} + i'_{2,\lambda}(\lambda, s, T_2) (1 - e^{-a_{2,\lambda}s}) \right] dA \cos \theta d\omega d\lambda. \end{aligned} \quad (25.127)$$

Integrated over all wavelengths of the emitting media results in

$$d^2Q = \left[ \int_0^\infty i'_\lambda(\lambda, s_1) e^{-a_{2,\lambda}s} d\lambda + \int_0^\infty i'_{2,\lambda}(\lambda, T_2) (1 - e^{-a_{2,\lambda}s}) d\lambda \right] dA \cos \theta d\omega.$$

*Estimation of the first integral:* The directional spectral intensity entering the water at point  $s_I$  is

$$i'_\lambda(\lambda, s_1, T_1, T_3) = i'_{3,\lambda}(\lambda, T_3) e^{-a_{1,\lambda}s_1} + i'_{b,\lambda}(\lambda, s_1, T_1) (1 - e^{-a_{1,\lambda}s_1}). \quad (25.128)$$

The total intensity at the same point is

$$i'(s_1, T_1, T_3) = \int_0^\infty i'_\lambda(\lambda, s_1) d\lambda = \varepsilon_3(T_3) [1 - a'_1(T_3, s_1)] \frac{\sigma T_3^4}{\pi} + \varepsilon_1(T_1, s_1) \frac{\sigma T_1^4}{\pi}. \quad (25.129)$$

Now note the special definition of the absorption coefficient in water required here

$$\bar{a}'_2(s, T_1, T_3) = \frac{\int_0^\infty i'_\lambda(\lambda, s_1) (1 - e^{-a_{2,\lambda}s}) d\lambda}{\int_0^\infty i'_\lambda(\lambda, s_1) d\lambda} \approx a'_2(s, T_3), \quad (25.130)$$

which can be replaced by the usual definition of the water absorption coefficient only as an *approximation*. Thus we obtain finally

$$\begin{aligned} &\int_0^\infty i'_\lambda(\lambda, s_1) e^{-a_{2,\lambda}s} d\lambda \\ &= [1 - a'_2(T_3, s)] \left\{ \varepsilon_3(T_3) [1 - a'_1(T_3, s_1)] \frac{\sigma T_3}{\pi} + \varepsilon_1(T_1, s_1) \frac{\sigma T_1}{\pi} \right\}. \end{aligned} \quad (25.131)$$

*Estimation of the second integral:* For the second integral we use again the definition of the total emittance of the water radiating with temperature  $T_2$

$$\int_0^\infty i'_{\lambda b}(\lambda, T_2) (1 - e^{-a_{2,\lambda}s}) d\lambda = \varepsilon_2(T_2, s) \frac{\sigma T_2^4}{\pi}. \quad (25.132)$$

Thus, after the integration over the total wavelength region we obtain

$$d^2 Q = \left[ 1 - a'_2(T_3, s) \right] \left\{ \begin{aligned} & \varepsilon_3(T_3) \left[ 1 - a'_1(T_3, s_1) \right] \frac{\sigma T_3^4}{\pi} \\ & + \varepsilon_1(T_1, s_1) \frac{\sigma T_1^4}{\pi} \end{aligned} \right\} + \varepsilon_2(T_2, s) \frac{\sigma T_2^4}{\pi} dA \cos \theta d\omega. \quad (25.133)$$

The first term gives the intensity at the point  $s$  coming from the particle with temperature  $T_3$  and crossing the vapor with temperature  $T_1$ . The second term is the net contribution of the water radiating with temperature  $T_2$  at point  $s$ .

#### 25.4.3.2.3 Total absorbed intensity

*Vapor:* The total absorbed directional intensity in the vapor is therefore that emitted by the particle minus that leaving the vapor sphere at  $s_1$

$$d^2 Q_{1a} = \left[ \varepsilon_3(T_3) a'_1(T_3, s_1) \frac{\sigma T_3^4}{\pi} - \varepsilon_1(T_1, s_1) \frac{\sigma T_1^4}{\pi} \right] dA \cos \theta d\omega. \quad (25.134)$$

*Water:* The total absorbed directional intensity in the water is therefore that entering from the internal sphere minus that leaving at  $s_2$ .

$$d^2 Q_{2a} = \left\{ \begin{aligned} & \varepsilon_3(T_3) \left[ 1 - a'_1(T_3, s_1) \right] a'_2(T_3, s_2) \frac{\sigma T_3^4}{\pi} \\ & + a'_2(T_3, s_2) \varepsilon_1(T_1, s_1) \frac{\sigma T_1^4}{\pi} - \varepsilon_2(T_2, s_2) \frac{\sigma T_2^4}{\pi} \end{aligned} \right\} dA \cos \theta d\omega. \quad (25.135)$$

#### Integration over the solid angle

The integration over the solid angle gives an expression in which optical properties have to be averaged over the solid angle. For the case of the absorption coefficient it will result in

$$\int_0^{2\pi} \int_{\theta_1}^{\theta_2} a'(T, s) \cos \theta \sin \theta d\theta d\varphi \approx \bar{a}'(T) \int_0^{2\pi} \int_{\theta_1}^{\theta_2} \cos \theta \sin \theta d\theta d\varphi, \quad (25.136)$$

where

$$\bar{a}'(T) = \frac{\int_0^{2\pi} \int_{\theta_1}^{\theta_2} a'(T, s) \cos \theta \sin \theta d\theta d\varphi}{\int_0^{2\pi} \int_{\theta_1}^{\theta_2} \cos \theta \sin \theta d\theta d\varphi}. \quad (25.137)$$

The computation of the averaged absorption coefficient is very expensive. That is why the following approximation will be used. The averaged optical property is set as the optical property being a function of the averaged beam distance. We illustrate this in the following example.

$$\bar{a}'(T) \approx a'(T, \bar{s}), \quad (25.138)$$

where

$$\bar{s} = \frac{\int_0^{2\pi} \int_{\theta_1}^{\theta_2} s(\theta, \varphi) \cos \theta \sin \theta d\theta d\varphi}{\int_0^{2\pi} \int_{\theta_1}^{\theta_2} \cos \theta \sin \theta d\theta d\varphi}. \quad (25.139)$$

The appropriate averaged beam lengths are already given in Section 25.4.3.1.

*Vapor:*

Performing the averaging of the optical properties over the solid angle results in

$$\begin{aligned} \int_0^{2\pi} \int_{\theta_1}^{\theta_2} a'_1(T_3, s_1) \cos \theta \sin \theta d\theta d\varphi &\approx a'_1(T_3, \bar{s}_1) \int_0^{2\pi} \int_{\theta_1}^{\theta_2} \cos \theta \sin \theta d\theta d\varphi \\ &= a'_1(T_3, \bar{s}_1) \pi (\sin^2 \theta_2 - \sin^2 \theta_1) \end{aligned} \quad (25.140)$$

$$\int_0^{2\pi} \int_{\theta_1}^{\theta_2} \varepsilon_1(T_1, s_1) \cos \theta \sin \theta d\theta d\varphi \approx \varepsilon_1(T_1, \bar{s}_1) \pi (\sin^2 \theta_2 - \sin^2 \theta_1). \quad (25.141)$$

In particular, integrating for  $\theta_1 = 0$  and  $\theta_1 = \pi/2$  we obtain

$$\int_0^{2\pi} \int_{\theta_1}^{\theta_2} a'_1(T_3, s_1) \cos \theta \sin \theta d\theta d\varphi \approx a'_1(T_3, \bar{s}_1) \pi, \quad (25.142)$$

$$\int_0^{2\pi} \int_{\theta_1}^{\theta_2} \varepsilon_1(T_3, s_1) \cos \theta \sin \theta d\theta d\varphi \approx \varepsilon_1(T_3, \bar{s}_1) \pi, \quad (25.143)$$

and consequently

$$d^2 Q_{1a} = [\varepsilon_3(T_3) a'_1(T_3, \bar{s}_1) \sigma T_3^4 - \varepsilon_1(T_1, \bar{s}_1) \sigma T_1^4] dA. \quad (25.144)$$

Integrating over the surface of the particle results in

$$Q_{1a} = \pi D_3^2 [\varepsilon_3(T_3) a'_1(T_3, \bar{s}_1) \sigma T_3^4 - \varepsilon_1(T_1, \bar{s}_1) \sigma T_1^4]. \quad (25.145)$$

The emitted total power from the particle is

$$Q_{3 \rightarrow \infty} = \pi D_3^2 \varepsilon_3(T_3) \sigma T_3^4. \quad (25.146)$$

The emitted power from the vapor interface into the water is

$$Q_{3 \rightarrow \infty} - Q_{1a} = \pi D_3^2 \sigma \left\{ \left[ 1 - a'_1(T_3, \bar{s}_1) \right] \varepsilon_3(T_3) T_3^4 + \varepsilon_1(T_1, \bar{s}_1) T_1^4 \right\}. \quad (25.147)$$

*Water:*

Similarly integrating for  $\theta_1 = 0$  and  $\theta_1 = \pi/2$  we obtain for the averages over the solid angle of the water optical properties

$$\int_0^{2\pi} \int_{\theta_1}^{\theta_2} a'_2(T_3, s_2) \cos \theta \sin \theta d\theta d\varphi \approx a'_2(T_3, \Delta \bar{s}_2) \pi, \quad (25.148)$$

$$\int_0^{2\pi} \int_{\theta_1}^{\theta_2} \varepsilon_2(T_3, s_2) \cos \theta \sin \theta d\theta d\varphi \approx \varepsilon_2(T_3, \Delta \bar{s}_2) \pi, \quad (25.149)$$

and consequently

$$d^2 Q_{2a} = \sigma \left\{ \begin{aligned} &\varepsilon_3(T_3) \left[ 1 - a'_1(T_3, \bar{s}_1) \right] a'_2(T_3, \Delta \bar{s}_2) T_3^4 \\ &+ a'_2(T_3, \Delta \bar{s}_2) \varepsilon_1(T_1, \bar{s}_1) T_1^4 - \varepsilon_2(T_2, \Delta \bar{s}_2) T_2^4 \end{aligned} \right\} dA. \quad (25.150)$$

Integrating over the surface of the particle results in

$$Q_{2a} = \pi D_3^2 \sigma \left\{ \begin{aligned} &\varepsilon_3(T_3) \left[ 1 - a'_1(T_3, \bar{s}_1) \right] a'_2(T_3, \Delta \bar{s}_2) T_3^4 \\ &+ a'_2(T_3, \Delta \bar{s}_2) \varepsilon_1(T_1, \bar{s}_1) T_1^4 - \varepsilon_2(T_2, \Delta \bar{s}_2) T_2^4 \end{aligned} \right\}. \quad (25.151)$$

The emitted power from the vapor sphere is

$$Q_{3 \rightarrow \infty} - Q_{1a} = \pi D_3^2 \sigma \left\{ \left[ 1 - a'_1(T_3, \bar{s}_1) \right] \varepsilon_3(T_3) T_3^4 + \varepsilon_1(T_1, \bar{s}_1) T_1^4 \right\}. \quad (25.152)$$

The difference between this power and that absorbed by the water is the power radiated from the water surface into the environment of the first cell

$$\begin{aligned} &Q_{3 \rightarrow \infty} - Q_{1a} - Q_{2a} \\ &= \pi D_3^2 \sigma \left\{ \begin{aligned} &\left[ 1 - a'_2(T_3, \Delta \bar{s}_2) \right] \left[ 1 - a'_1(T_3, \bar{s}_1) \right] \varepsilon_3(T_3) T_3^4 \\ &+ \left[ 1 - a'_2(T_3, \Delta \bar{s}_2) \right] \varepsilon_1(T_1, \bar{s}_1) T_1^4 + \varepsilon_2(T_2, \Delta \bar{s}_2) T_2^4 \end{aligned} \right\}. \end{aligned} \quad (25.153)$$

## Second cell

The power emitted by the first *Wigner* cell is entering the second one – Fig. 25.13. There are three characteristic space angle regions for computing the absorbed and the transmitted power in the second *Wigner* cell. We consider the three regions separately. The total directional intensity of the entering radiation is

$$\int_0^\infty i'_\lambda(\lambda, T_1) d\lambda = \frac{Q_{3 \rightarrow \infty} - Q_{1a} - Q_{2a}}{\pi D_2^2 \pi}. \quad (25.154)$$

*First zone: Water only*

$$i'_\lambda(\lambda, s) = i'_\lambda(\lambda) e^{-a_\lambda s} + i'_\lambda(\lambda, s) (1 - e^{-a_\lambda s}) \quad (25.155)$$

$$Q = \pi D_2^2 ([1 - \alpha'_w(\bar{s}_{11})] \frac{Q_1}{\pi D_2^2} + \varepsilon'_w(\bar{s}_{11}) \sigma T_2^4) \left( 1 - \frac{D_1^2}{D_2^2} \right), \quad (25.156)$$

$$Q_A = \pi D_2^2 (\alpha'_w(\bar{s}_{11}) \frac{Q_1}{\pi D_2^2} - \varepsilon'_w(\bar{s}_{11}) \sigma T_2^4) \left( 1 - \frac{D_1^2}{D_2^2} \right). \quad (25.157)$$

*Second zone:*

### Region 1: water

$$Q = \pi D_2^2 ([1 - \alpha'_w(\bar{s}_{21})] \frac{Q_1}{\pi D_2^2} + \varepsilon'_w(\bar{s}_{21}) \sigma T_2^4) \left( \frac{D_1^2}{D_2^2} - \frac{D_3^2}{D_2^2} \right) \quad (25.158)$$

$$Q_A = \pi D_2^2 (\alpha'_w(\bar{s}_{21}) \frac{Q_1}{\pi D_2^2} - \varepsilon'_w(\bar{s}_{21}) \sigma T_2^4) \left( \frac{D_1^2}{D_2^2} - \frac{D_3^2}{D_2^2} \right). \quad (25.159)$$

### Region 2: vapor

$$Q = \pi D_2^2 ([1 - \alpha'_v(\bar{s}_{22})] [1 - \alpha'_w(\bar{s}_{21})] \frac{Q_1}{\pi D_2^2} + [1 - \alpha'_v(\bar{s}_{22})] \varepsilon'_w(\bar{s}_{21}) \sigma T_2^4 + \varepsilon'_v(\bar{s}_{22}) \sigma T_1^4) \left( \frac{D_1^2}{D_2^2} - \frac{D_3^2}{D_2^2} \right) \quad (25.160)$$

$$Q_A = \pi D_2^2 (\alpha'_v(\bar{s}_{22}) [1 - \alpha'_w(\bar{s}_{21})] \frac{Q_1}{\pi D_2^2} + \alpha'_v(\bar{s}_{22}) \varepsilon'_w(\bar{s}_{21}) \sigma T_2^4 - \varepsilon'_v(\bar{s}_{22}) \sigma T_1^4) \left( \frac{D_1^2}{D_2^2} - \frac{D_3^2}{D_2^2} \right) \quad (25.161)$$

**Region 3: water**

$$Q = \pi D_2^2 ([1 - \alpha'_w(\bar{s}_{23})]Q^* + \varepsilon'_w(\bar{s}_{23})\sigma T_2^4) \left( \frac{D_1^2}{D_2^2} - \frac{D_3^2}{D_2^2} \right) \quad (25.162)$$

$$Q_A = \pi D_2^2 (\alpha'_w(\bar{s}_{23})Q^* - \varepsilon'_w(\bar{s}_{23})\sigma T_2^4) \left( \frac{D_1^2}{D_2^2} - \frac{D_3^2}{D_2^2} \right) \quad (25.163)$$

with

$$Q^* = [1 - \alpha'_v(\bar{s}_{22})][1 - \alpha'_w(\bar{s}_{21})] \frac{Q_1}{\pi D_2^2} + [1 - \alpha'_v(\bar{s}_{22})]\varepsilon'_w(\bar{s}_{21})\sigma T_2^4 + \varepsilon'_v(\bar{s}_{22})\sigma T_1^4 \quad (25.163)$$

*Third zone:*

**Region 1: water**

$$Q = \pi D_2^2 ([1 - \alpha'_w(\bar{s}_{31})] \frac{Q_1}{\pi D_2^2} + \varepsilon'_w(\bar{s}_{31})\sigma T_2^4) \frac{D_3^2}{D_2^2}, \quad (25.164)$$

$$Q_A = \pi D_2^2 (\alpha'_w(\bar{s}_{31}) \frac{Q_1}{\pi D_2^2} - \varepsilon'_w(\bar{s}_{31})\sigma T_2^4) \frac{D_3^2}{D_2^2}. \quad (25.165)$$

**Region 2: vapor**

$$Q = \pi D_2^2 ([1 - \alpha'_v(\bar{s}_{32})][1 - \alpha'_w(\bar{s}_{31})] \frac{Q_1}{\pi D_2^2} + [1 - \alpha'_v(\bar{s}_{32})]\varepsilon'_w(\bar{s}_{31})\sigma T_2^4 + \varepsilon'_v(\bar{s}_{32})\sigma T_1^4) \frac{D_3^2}{D_2^2}, \quad (25.166)$$

$$Q_A = \pi D_2^2 (\alpha'_v(\bar{s}_{32})[1 - \alpha'_w(\bar{s}_{31})] \frac{Q_1}{\pi D_2^2} + \alpha'_v(\bar{s}_{32})\varepsilon'_w(\bar{s}_{31})\sigma T_2^4 - \varepsilon'_v(\bar{s}_{32})\sigma T_1^4) \frac{D_3^2}{D_2^2}. \quad (25.167)$$

**25.4.4 Chain of infinite number of Wigner cells**

Knowing what happens inside a single cell we can now compute the energy that is transported  $Q_{T,1}$  and that is absorbed by the vapor  $Q_{av,1}$  and by the water  $Q_{aw,1}$  if such cells are virtually interacting in a subsequent chain. The *Lanzenberger* solution is given below

$$Q_{T,i} = a_T Q_{T,i-1} + b_T, \quad i = 2, n, \quad (25.168)$$

$$Q_{av,i} = a_v Q_{T,i-1} + b_v, \quad i = 2, n, \quad (25.169)$$

$$Q_{aw,i} = a_w Q_{T,i-1} + b_w, \quad i = 2, n, \quad (25.170)$$

$$Q_{T,2} = a_T Q_{T,1} + b_T, \quad (25.171)$$

$$Q_{T,3} = a_T a_T Q_{T,1} + a_T b_T + b_T, \quad (25.172)$$

$$Q_{T,4} = a_T a_T a_T Q_{T,1} + a_T a_T b_T + a_T b_T + b_T, \quad (25.173)$$

$$Q_{T,i} = a_T^{i-1} Q_{T,1} + b_T \sum_{m=2}^i a_T^{m-2}, \quad (25.174)$$

$$Q_{av,i} = a_v Q_{T,i-1} + b_v, \quad i \geq 2, \quad (25.175)$$

$$Q_{av,2} = a_v Q_{T,1} + b_v, \quad (25.176)$$

$$Q_{av,i} = a_v a_T^{i-1} Q_{T,1} + a_v b_T \sum_{m=2}^i a_T^{i-2} + b_v, \quad i \geq 3, \quad (25.177)$$

$$\begin{aligned} Q_{av} &= Q_{av,1} + Q_{av,2} + \sum_{i=3}^n Q_{av,i}, \\ &= Q_{av,1} + a_v Q_{T,1} + b_v + \sum_{i=3}^n a_v a_T^{i-1} Q_{T,1} + \sum_{i=3}^n a_v b_T \sum_{m=2}^i a_T^{i-2} + \sum_{i=3}^n b_v \\ &= Q_{av,1} + (n-1)b_v + a_v \left[ Q_{T,1} \left( 1 + \sum_{i=3}^n a_T^{i-1} \right) + b_T \sum_{i=3}^n \sum_{m=2}^i a_T^{i-2} \right]. \end{aligned} \quad (25.178)$$

### 25.4.5 Application of *Lanzenbergers's* solution

Consider a cloud of equidistantly arranged hot spherical particles. The cloud is flying in a water and gas mixture. Compute the radiated power by a hot spherical particle and its environment. Compute what part of this energy is absorbed by water and what in the gas as a function of the characteristic scales inside the three-phase mixture. Compute the length required for almost complete light absorption. Figure 25.15 presents the total absorption depth in three-phase particle-vapor-water flow as a function of the particle volume fraction. The gas volume fraction is 1%. The hot particle size is  $0.005m$ . We see from Figs. 25.14 and 25.15 an important behaviour: increasing the particle concentration leads to reduction of the length

necessary for complete absorbtion of the radiation. That is why for cases with large particle concentrations the discrete ordinate method is not necessary and a local in-cell description of the radiated energy is sufficient. This is not the case for small particle concentrations where the absorbtion length can be considerably larger than the cell size. In this case doing so as every thing happens in the cell leads to an overestimation of the local energy transport and therefore to larger local vapor production with all the consequences to the final macroscopic results.

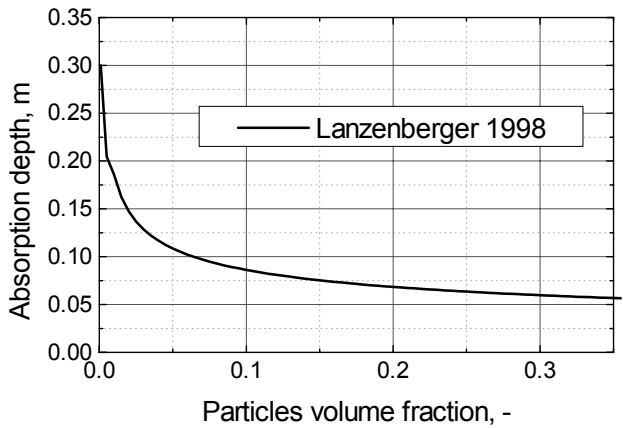


**Fig. 25.14** Total absorbtion depth in three-phase particle-vapor-water flow as a function of the particle volume fraction. Gas volume fraction 1%. Particle size  $0.005m$

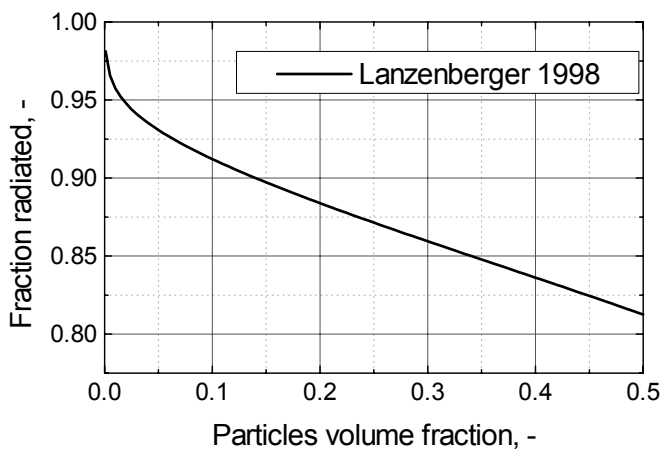


**Fig. 25.15** Radiated specific power of the cloud divided by the radiated specific power of a single particle as a function of the particles volume fraction



## Nomenclature

### Latin

$A_m$	surface area at side $m$ of the cell, $m^2$
$a_{\max}$	number of the discrete angle in the azimuthal direction
$a_\lambda(\lambda)$	$= \frac{4\pi k}{\lambda}$ , spectral absorption coefficient, $1/m$
$a_{a,b,m}$	$= \frac{A_m}{\Delta Vol} \frac{D_{a,b,m}}{\Delta \omega_{a,b}}$ , $m$ -surface geometry coefficient, $1/m$
$b_{\max}$	number of the discrete angles in the polar direction
$c_0$	$= 2.998 \cdot 10^8$ , speed of light in vacuum, $m/s$
$c$	speed of light, $m/s$
$D_{a,b,m}$	$\iint_{\Delta \omega_{a,b}} (\mathbf{s} \cdot \mathbf{e})_m d\omega$ , scalar product of the $(a,b)$ -directed unit vector and the outward directed $m$ -surface unit vector integrated over the angle $\Delta \omega_{a,b}$ , $sr$ .
$D_3$	diameter, $m$
$\mathbf{e}$	$= (e_x, e_y, e_z)$ , outward directed unit normal to a surface
$i'_\lambda(\mathbf{r}, \mathbf{s})$	spectral radiation intensity at the spatial location $\mathbf{r}$ along the direction $\mathbf{s}$ that is within an infinitesimal solid angle $d\omega$ , in other words heat flux per unit solid angle, per unit wavelength, and per unit area, $W/(m^3 sr)$
$k$	index of absorption
$n$	index of refraction - ratio of propagation velocity $c_0$ in vacuum related to the propagation velocity $c$ inside the medium
$\dot{q}''_{\lambda, m-incident}$	incident radiation heat flux from the inside of the computational cell, $W/m^2$
$\mathbf{r}$	position vector, $m$
$r$	radius, $m$
$\mathbf{s}$	direction vector
$T_{w,m}$	wall temperature at the $m$ -face of the control volume
$x$	$x$ -coordinate, $m$
$y$	$y$ -coordinate, $m$
$z$	$z$ -coordinate, $m$

**Greek**

$\Delta$	finite difference
$\Delta Vol$	cell volume, $m^3$
$\beta_\lambda$	$= a_\lambda + \sigma_{s\lambda}$ , spectral extinction coefficient, $1/m$
$\varepsilon_w$	wall emissivity coefficient
$\Phi$	spectral scattering phase function
$\varphi$	azimuthal angle, $rad$
$\sigma_{s\lambda}$	spectral scattering coefficients, $1/m$
$\sigma$	$= \frac{2C_1\pi^5}{15C_2^4} = 5.67051 \times 10^{-8}$ , <i>Stefan-Boltzmann</i> constant, $W/(m^2 K^4)$
$\theta$	polar angle, $rad$
$\omega$	solid angle, $rad$
$d\omega$	infinitesimal solid angle, $rad$

**Indies**

a	integer index for the discrete angle in the azimuthal direction
b	integer index for the discrete angle in the polar direction
b	black body
w	wall
x	in x-coordinate
y	in y-coordinate
z	in z-coordinate
1	vapor, gas
2	water
3	melt, solid particle

**References**

- Docherty P (6-10.9.1982) Prediction of gas emissivity for wide range of process conditions, Proc. of the 7<sup>th</sup> Heat Transfer Conference, Munich, Hemisphere Publ. Corp., Wash., vol 2 p 481-485
- Fiveland WA (1988) Three-dimensional radiative heat transfer solutions by discrete-ordinates method, Journal of Thermophysics and Heat Transfer, vol 2 no 4 pp 309-316
- Fletcher DF (1985) Assessment and development of the Bankoff and Han coarse mixing model, Culham Laboratory Report, CLM-R252
- Fletcher DF (1999) Radiation absorption during premixing, Nuclear Engineering and Design, vol 189 pp 435-440
- Hale GM and Marvin RQ (1973) Optical constants in water in the 200-nm to 200- $\mu m$  wavelength region, Appl. Opt., vol 12 no 3 pp 555-563

- Kolev NI (October 3-8, 1999) Verification of IVA5 computer code for melt-water interaction analysis, Part 1: Single phase flow, Part 2: Two-phase flow, three-phase flow with cold and hot solid spheres, Part 3: Three-phase flow with dynamic fragmentation and coalescence, Part 4: Three-phase flow with dynamic fragmentation and coalescence – alumina experiments, Proc of the Ninth International Topical Meeting on Nuclear Reactor Thermal Hydraulics (NURETH-9), San Francisco, California, , Log. Nr. 315
- Lanzenberger K (1997) Thermal radiation in multiphase flow - Application to the severe accident scenario of molten fuel coolant interaction (MFCI), Siemens AG, Power Generation (KWU), 1997 Karl Wirtz Prize for young scientists
- Mathews KA, (1999) On the propagation of rays in discrete ordinates, Nuclear Science and Engineering, vol 132 pp 155-180
- Siegel R and Howell JR (1996) Thermal radiation heat transfer, Third edition, Taylor & Francis, Washington
- Steward FR and Kocafefe YS (17.-22.8.1986) Total emissivity and absorptivity for carbon dioxide, water vapor and their mixtures, Proc. 8<sup>th</sup> Heat Transfer Conf., San Francisco, Springer Berlin, vol 2 p 735-740
- Vaeth L (Maerz 1995) Radiative heat transfer for the transient three-phase, three-component flow model IVA-KA, Forschungszentrum Karlsruhe, Internal report, INR-1914, PSF-3212
- Zolotarev VM and Dyomin AV (1977) Optical constants of water on wide wavelength range 0.1 Å to 1 μm, Optics and Spectroscopy, vol 43 no 2

# Index

- acceleration induced bubble fragmentation 207
- accommodation coefficient 584, 585
- activated nucleation site density 362
- active nucleation site density 443
- active nucleation site density as a function of superheat 364, 365, 443, 454
- active nucleation sites density 362, 366
- added mass force 73
- Altshul formula 84
- aluminum 331
- amount of melt surrounded by continuous water 298
- analogy between heat and mass transfer 169
- annular channels 509, 510
- annular dispersed flow 128
- annular film flow 12
- annular film flow with entrainment 12
- annular flow 16, 22, 50
- annular two-phase flow 149
- aspect ratio of a bubble 32
- Avdeev 408, 459
- average center-to-center spacing 423
- average mass conservation 188
- averaged beam length 661
- averaged film boiling heat transfer coefficient 538
- averaged film thickness 556
- averaged mass source term 383
- averaged vapor film thickness 501
- Avogadro number 571
  
- bag-and-stamen breakup 219
- bag and stamen breakup 216, 231
- bag breakup 216, 219, 229
- bag mode 218
- Baroczy correlation 99, 832
  
- black body 655
- black body intensity 655
- blow down 478
- boiling flow 100
- boiling of subcooled liquid 487, 517
- boiling with mutually bubble interaction 429
- Boltzmann constant 350
- Bowring 518
- breakup period for droplets in gas 225
- breakup time 222
- bubble coalescence mechanisms 197
- bubble collapse in subcooled liquid 310
- bubble condensing in a subcooled liquid 397
- bubble departure diameter 417, 447, 471
- bubble departure diameter as a function of pressure 427
- bubble departure diameter as a function of superheat 426
- bubble departure diameter as function of mass flow rate 426
- bubble departure diameter during boiling or flashing 417
- bubble departure frequency 449
- bubble disappearance 474
- bubble dynamics 312
- bubble entrainment from the vapor layer 475
- bubble entrainment size 476
- bubble flow 4, 9, 22, 23, 49, 122
- bubble flow in a annular channel 125
- bubble fragmentation 473
- bubble growth 375
- bubble growth in superheated liquid 375
- bubble growth in the bulk 473
- bubble inclination angle 420
- bubble rise velocity in pool 5

- bubbles generated due to nucleation at the wall 472
- bubbles in asymmetric flow field 310
- bubbles in turbulent liquid 258
- Bubble-to-slug flow transition 21
- bubbly flow 3, 135, 516
- bundles of horizontal pipes 631
  
- cap bubbles 34, 37
- catastrophic breakup 217, 231
- chain of infinite number of Wigner cells 677
- change of the bubble number density due to condensation 406
- channel flow 1, 161
- Channel flow – inclined pipes 13
- Channel flow – vertical pipes 9
- churn turbulent flow 5, 11, 38, 135
- churn-to-annular, dispersed flow transition 21
- churn-turbulent flow 122
- Clausius-Clapeyron equation 347
- cloud of equidistantly arranged hot spherical particles 665, 679
- coalescence 187, 196, 473
- coalescence escaping regime 264
- coalescence frequency 192, 266, 475
- coalescence probability 192, 262, 264, 299, 475
- coalescence probability of small droplets 266
- coalescence rate 192
- coalescence time 262
- Coddington and Macian 122
- Colebrook and Witte formula 85, 86
- collision frequency 191, 193, 475
- collision time 262
- condensation at cooled walls 623
- condensation from forced convection two-phase flow at liquid film 632
- condensation from stagnant steam at turbulent liquid film 629
- condensation inside a vertical pipe 631
- condensation of a pure steam bubble in a subcooled liquid 397
- condensation of pure steam on subcooled film 567
- condensing moving bubble in a subcooled liquid 400
- conservation equation of the droplets 199
- contact angle 351, 352
- contact heat transfer 297, 316
- contact time 263, 322
- contaminated systems 35
- convection inside the droplet 579, 581
- convective boiling of saturated liquid 505
- convective heat transfer 601
- converging disperse field 191
- converging-diverging nozzle 476
- coolant 297
- coolant fragmentation 322
- coolant interface classification 324
- coolant viscosity increase 332
- creeping flow 116
- critical bubble size 420
- critical heat flux 512, 515, 519
- critical mass flow rate 360
- critical mass flow rate in short pipes, orifices and nozzles 360
- critical nucleation size 568
- critical size 361
- critical Weber number 207
- cross-section averaged vapor velocity profile 534
- crust straight 321
  
- Darcy's law 47
- dense packed regime 45
- departure from nucleate boiling 513
- deposition correlations 156, 176
- deposition in annular two-phase flow 169
- deposition mass flow rate 170
- deposition rate 154, 159
- depressurization 355
- diffusely emitting and reflecting walls 653
- diffusion controlled collapse 410
- diffusion controlled evaporation 385
- diffusion mass flow rate at macroscopic surface 592
- diffusion velocities for algebraic slip models 109
- dimensional analysis for small scale motion 250
- direct contact condensation of pure steam on subcooled droplet 581
- direction cosines 645
- discrete ordinate method 645

- 
- discrete ordinate radiation transport method 644
  - disintegration of the continuum 189
  - dissolved inert gases 361
  - distorted bubble regime 34, 37
  - distorted particles 34, 37
  - distribution parameter 120
  - distribution parameter for annular flow 127
  - Dittus-Boelter equation 505
  - donor cell scheme 650
  - down flow of vapor across horizontal tubes 632
  - drag 110
  - drag coefficient 32, 41, 115, 121
  - Drag coefficient for single bubble 32
  - drag forces 31
  - drift flux correlation 121
  - drift flux models 119, 138
  - droplet evaporation in gas mixture 589
  - droplet growth 572
  - droplet mass conservation equation 200
  - droplet pulsation velocity 170
  - droplet size after the entrainment 161
  - droplets in turbulent liquid 257
  - droplets-gas system 39
  - dry out 513
  - duration of fragmentation 189
  - dynamic friction velocity 610
  
  - effective kinematic viscosity of turbulence 252
  - efficiency of coalescence of bubbles 262
  - emissivity and absorptivity for carbon dioxide 660
  - empirical flow map 18
  - entrainment 149
  - entrainment from liquid film for very high gas velocity 285
  - entrainment velocity 150
  - entrapment 311
  - entrapment triggers 309
  - equation of Kelvin and Laplace 344
  - equilibrium droplet concentration 154
  - equilibrium steam mass flow rate concentration 507
  - Ergun's equation 47
  - evaporation of saturated droplets in superheated gas 587
  
  - evaporation of saturated film in superheated gas 613
  - evaporation of the entire droplet 587
  - external condensation on horizontal single pipe 631
  - external triggers 307
  
  - family of particles in continuum 35
  - Fauske 322
  - film boiling 22, 507, 529
  - film boiling heat flux 541
  - film boiling heat transfer coefficient 499, 554
  - film boiling in horizontal upwards-oriented plates 500
  - film boiling model and data base 556
  - film boiling on a horizontal cylinder 501
  - film collapse dynamics 312
  - film flashing 475
  - film flashing bubble generation 475
  - film thickness 13, 155, 556, 625
  - film to fine dispersed flow transition 517
  - film velocity 141
  - film-gas force 51
  - film-gas interface in the multi-phase flows 599
  - film-wall force 50
  - final fragment velocity 219
  - fine dispersed flow 516
  - finite differential form of the RTE 649
  - finite volume representation of the radiation transport equation 648
  - Fiveland scheme 652
  - flashing in adiabatic pipes 471
  - flashing inception pressure 360
  - flow boiling 428
  - flow pattern transition criteria for non adiabatic flow 20
  - flow patterns 1, 2, 187
  - flow regime transition 4
  - Flow regime transition criteria 1
  - forced convection 487, 552
  - forced convection boiling 505
  - forced convection condensation 631
  - forced convection DNB and DO correlations 515
  - forced convection film boiling 507, 509, 511

- forced convection film boiling at vertical plate 560
- forced convection film boiling in channels with very low mass flux 501
- forced-convection film boiling data 552
- Fourier equation 578
- Fourier series 578
- fragmentation 189, 207
- fragmentation and coalescence 187
- fragmentation frequency 190
- fragmentation mechanism 275
- fragmentation modes 216
- fragmentation of melt in coolant 297
- free falling droplets in gas 12
- free falling sphere 112
- free particles regime 41
- free path of a steam molecule 573
- free rising bubble velocity 475
- free settling velocity 112, 138
- frequency of bubble departure 448
- frequency of coalescence of single bubble 197
- friction coefficient of turbulent flow 408
- friction pressure drop 83, 135
- friction pressure loss coefficient 83
- frictional pressure loss 102
- full-range drift flux correlations 128
- fully developed steady state flow 201
  
- gas jet disintegration in pools 289
- gas jet in a turbulent liquid stream 257
- gas side averaged shear stress 610
- gas-to-liquid velocity ratio 138
- Gauss-Seidel method 651
- generated nuclei 571
- geometrical film-gas characteristics 599
- geometry definition to film boiling at sphere 547
- Gibbs number 349, 570
- gradually applied relative velocities 215
- Groeneveld 510
- group of particles 119
  
- Hagen and Poiseuille law 84
- heat and mass transfer at the film-gas interface 599
- heat conduction due to turbulence 606
- heat flux as a function of superheat 428, 451
- heat flux as a function of superheat for saturated water 452
- heat flux as a function of the wall superheating 440
- heat released during the condensation 575
- heat transfer across droplet interface 575
- heat transfer between interface and gas 601
- heat transfer coefficient 506
- heat transfer coefficient on the surface of moving solid sphere and water droplets 576
- heat transfer coefficient on the surface of solid sphere moving in a liquid 399
- heat transfer from the interface into the bulk liquid 613
- heated channels 20, 100
- Helium II 381
- Henry and Fauske 322
- heterogeneous nucleation 350, 360, 471
- highly energetic collisions 238
- homogeneous local vapor volume fraction 501
- homogeneous nucleation 350, 357, 570
- homogeneous nucleation temperature 500
- homogeneous turbulence characteristics 249
- horizontal or inclined pipes 63
- hydraulic diameters 67
- hydrodynamic stability theory 513
- hydrodynamic theory of boiling 514
- hydrodynamic theory of critical heat flux 453
  
- inclined pipes 135
- inert gases 332
- inertially controlled bubble growth 347
- initiation of the visible nucleate boiling 489
- initiation of visible boiling 487
- inner scale or micro scale of turbulence 250
- instability of jets 275
- interaction of molten material with water 660
- interface solidification 308
- interfacial area density 51, 149

- 
- interfacial disturbances 542
  - interfacial instability due to bubble collapse 314
  - inverted annular flow 59, 516
  - isolated bubble boiling 427
  - isotropic turbulence 607
  
  - Jakob number 574
  - jet atomization 274
  - jet disintegration due to asymmetric waves 274
  - jet disintegration due to symmetric interface oscillations 274
  - jet fragmentation in pipes 287
  - jet of molten metal 282
  - jets causing film boiling 282
  
  - Kelvin-Helmholtz instability 208
  - Kelvin-Helmholtz gravity long wave theory 15
  - Kelvin-Helmholtz instability 542
  - Kolmogoroff 250
  - Kutateladze 5
  - Kutateladze terminal velocity 12, 117
  
  - laminar condensation on vertical wall 628
  - laminar film 625, 632
  - Lanzenberger's solution 665, 679
  - Laplace and Kelvin equation 345, 569
  - Laplace constant 101
  - Laplace number 219
  - large scale eddies 249
  - large scale motion 249
  - larger bubble sizes 5
  - Lathrop's diamond difference scheme 652
  - lava-water interaction 529
  - lean systems 302
  - Lellouche 122
  - length scale 1
  - Levich equation 255
  - lift force 67
  - liquid-liquid system 222
  - liquid and gas jet disintegration 275
  - liquid boundary layer 538
  - liquid droplets 567
  - liquid jet disintegration in pools 287
  - liquid-liquid systems 257
  - Liu and Theofanous 559
  - local drift velocity 120
  - local vapor film thickness 559
  - Lockhart and Martinelli 95
  - look-up table for critical heat flux 519
  
  - Mamaev 13, 135
  - Marangoni effect 323
  - Martinelli-Nelson method 102
  - Martinelli and Nelson 98
  - Martinelli factor 505
  - mass concentration of droplets 170
  - mass flow rate 507
  - mass transfer coefficient 636
  - maximal achievable superheating 357
  - maximum duration of the bubble collapse 410
  - maximum packing 35
  - maximum packing density 3
  - maximum superheat 357
  - mean free path 170
  - mean site-to-site distance 482
  - mechanical fragmentation 297
  - mechanism of the thermal fragmentation 312
  - melt 297
  - melt with water and vapor enclosed inside 661
  - mercury droplets in air 209
  - micro-convection velocity 423, 448
  - Mikic 378
  - minimum film boiling temperature 307, 499, 500
  - minimum heat flux 499
  - mirroring walls 654
  - mixed convection film boiling 553
  - mixed-convection film boiling at spheres 547
  - mixed-convection film boiling on vertical walls 546
  - mixture of gas, film and droplets 140
  - mole weight 573
  - mono-disperse 188
  - moving bubble 399
  - multi-group approach 189
  - mutual interaction of the growing and departing bubbles 429
  
  - natural convection 551
  - natural convection film boiling 499
  - natural convection film boiling at vertical plate 559



- natural convection film boiling on a sphere 502
- natural-convection film boiling 499
- nearest-neighbor distance 366
- net evaporation 491
- net mass flow rate of the spontaneous evaporation 584
- Newton's regime 40, 42
- Nigmatulin 172
- Nikuradze diagram 15, 93, 94
- non solidifying droplet 353
- non-averaged source terms 404
- non-condensable gases 332, 615
- non-condensing gas 409
- Non-oscillating particles 3
- non-stable liquid 344
- nucleate boiling 439
- nucleate boiling heat flux 505
- nucleate boiling heat transfer coefficient 506
- nucleate pool boiling 439
- nucleation 567
- nucleation energy 344
- nucleation frequency 571
- nucleation in liquids 343
- nucleation in presence of non-condensable gasses 361
- nucleation kinetics 350, 453
- nucleation sites density 423, 427
- nucleation theories 354
- nucleus capable to grow 345
- Nukiyama-Tanasawa law 406
- Nukuradze diagram 62
- number density after the fragmentation 190
  
- onset of the condensation 530
- optimum marching strategy 651
- oscillating particles 3
- Oseen equation 33
- over-entrained regime 153
- oversaturated 320
- oxidation 331
  
- particle production rate 229
- particle production rate during the thermal fragmentation 326
- particle production rate in case of entrainment 198
- particle sink velocity in pipes 188
  
- particle size after thermal fragmentation 325
- particle size formation in pipes 198
- particle size in the steady state flow 200
- particles in film boiling 22
- partitioning of the absorbed energy between the bulk and the surface 658
- penetration length 285
- permeability coefficients 48
- Pilch 219
- pipe forces 481
- pitting of the surface 311
- Planck's spectral distribution 655
- Poiseuille flow 47
- Poisson distribution law 447
- pool boiling of saturated liquid 455
- pool flows 2, 3
- porous media 21
- positive scheme 653
- potentially explosive mixtures 298
- Prandtl-Nikuradze 86
- pressure drop 83
- primary breakup 231, 233
- probability of capture 584
- probability of departure from the averaged state 571
- probability of escape 584
- probability of origination of a single bubble 350
- probability of origination of single nucleus 571
- production rate 190, 229
- propagation velocity 317
- pulsation velocity 608
- pure liquid 35
- pure natural convection 536
- pure steam bubble drifting in turbulent continuous liquid 407
- pure steam condensation 623
  
- radiated specific power of the cloud 680
- radiating sphere concentrically surrounded by vapor and water 665
- radiation from the sphere 550
- radiation transport analysis 643
- radiation transport equation 644
- Raleigh-Taylor wavelength 4, 843
- Rankine and Hugoniot equation 499
- Rayleigh equation 313
- rectangular channels 67

- 
- reduction of the driving forces of the evaporation 592
  - relative permeabilities 49
  - relative permeability multipliers 50
  - relative velocity 118
  - resistance of the non-condensable gases 637
  - resisting force between film and gas 66
  - Riccati 220
  - Richardson and Zaki 114
  - Richardson-Zaki 119
  - rippled film-to-micro film transition 21
  - rod bundles 23
  - roll wave regime 63
  
  - Sakagushi 138
  - saturated liquid boiling 516
  - scattering phase function 644
  - self condensation stop 574
  - shear stress at the wall 609
  - shear stress in the film 610
  - sheet stripping 217, 219, 231
  - single bubble terminal velocity 115
  - single particle terminal velocity 118
  - single-phase flow 83
  - single-phase liquid convection heat flux 505
  - sinuous jet breakup 274
  - size initialization by flow pattern transition 216
  - size of the entrained droplets 149, 161
  - size of the ligaments 277
  - slightly contaminated liquid 35
  - slip 138
  - slip models 138
  - slug bubble diameter 113
  - slug flow 10, 22, 24, 39, 50, 117, 135
  - slug flow in a tube 125
  - slug-to-churn flow transition 21
  - small bubble sizes 5
  - small scale motion 250
  - Smolin 517
  - Smoluchowski 194, 252
  - solid particles 40, 41, 45, 143
  - solid particles in a gas 40
  - solid particles in bubbly flow 43
  - solidifying droplet 318
  - Souter mean diameter 233
  - space averaged beam lengths for the concentric spheres radiation problem 666
  - Spalding mass transfer number 592
  - spectral absorption coefficient for water as a function of the wavelength 655
  - spectral absorption coefficient 655
  - spectral absorption coefficient of water 655
  - spectral absorption coefficient of water vapor 660
  - spectral averaged absorption coefficient 661
  - spectral averaged emissivity coefficient 661
  - spectral extinction coefficient 645
  - spectral radiation intensity 644
  - sphere interface temperature during film boiling 555
  - spherical cap 117
  - spherical cavity of gas inside a molten material 660
  - spinoidal line 570
  - spontaneous condensation of pure subcooled steam 567
  - spontaneous evaporation of the superheated film 613
  - spontaneous flashing of superheat liquid 375
  - spontaneous flashing of superheated droplet 583
  - stability criterion for bubbles in continuum 255
  - stable particle diameter after the fragmentation 189
  - stagnant bubble 397
  - static contact angles 443
  - statistical theory of turbulence 407
  - steam condensation from gas-steam mixtures flowing perpendicular to horizontal internally cooled tubes 636
  - steam condensation from gas-steam mixtures inside pipes 636
  - steam condensation from mixture containing non-condensing gases 634
  - step difference scheme 650
  - stoichiometric 320
  - stoichiometric liquid volume fraction 321
  - Stokes regime 3, 36, 39, 41
  - stratified flows 13, 14, 60, 64, 135
  - stratified horizontal flow 134
  - stratified wavy flow 13, 16, 18

- stratified-intermittent transition 18
- stripping of droplets 218
- stripping of the ligaments 218
- strong disturbance on the film-to-small ripples transition 21
- sub cooled boiling 100
- subcooled nucleate boiling 20
- suddenly applied relative velocity 215
- superheated steam 384
- surface entrainment effect 315, 326
- surface tension 569
- surface tension of water 344
- surface vectors 647
- surfactants 333
- suspension volumetric flux 138
  
- Taylor bubble 11, 126, 843
- temperature correction factor 571
- temperature profile in the vapor layer 534
- terminal speed of a spherical particle 112
- the Taylor bubble velocity 15
- thermal controlled bubble growth 390, 747
- thermal controlled collapse 410
- thermal fragmentation 325, 328
- thermal resistance inside the drop 583
- thermo-capillar velocity 324
- thermo-capillary flow in the drop 324
- thermo-mechanical fragmentation 301, 307, 324
- thick and thin vapor film 298
- thin thermal boundary layer 377
- three phase flow 141
- three velocity fields 140
- three-dimensional flow 36
- three-phase disperse flow 45
- three-phase flows 102
- threshold pressure 307
- time-averaged coalescence rate 192
- total absorption depth in three phase particle-vapor-water flow 680
- total solid angle 646
- transition boiling 309
- transition boiling in tubes 511
- transition conditions 20
- transition criteria 13
- transition to annular flow 18
- transition to bubble flow 19
- transition-boiling correlation 512
- transparent wall 654
  
- transport enhancement factor 585
- tubes 519
- turbulence dissipation rate 250
- turbulence induced droplet fragmentation in channels 259
- turbulence induced particle fragmentation and coalescence 249
- turbulence Reynolds number 249
- turbulent diffusion constant 170
- turbulent film 629, 632
- turbulent fluctuation velocity 474
- turbulent gas pulsation 169
- turbulent length scale 611
- turbulent viscosity 151
- two parallel plates 14
- two-phase friction pressure drop 95
  
- umbrella mode 218
- under-entrained regime 153
- undersaturated 320
- undisturbed particles 34, 37
  
- vapor collapse 298
- vapor thickness in film boiling 299
- vapor-coolant instability 297
- varicose mode of water jet breakup 278
- vertical flow around rod bundles 510
- vertical rod bundle 24
- vibration breakup 216, 218, 229
- Vierow and Shrock 637
- violent explosion 311
- virtual mass coefficient 49
- viscous limit 250, 251
- viscous regime 33, 37, 39, 42
  
- waiting time 449
- wakes behind particles 261
- wall friction force 115
- wall-gas 66
- wall-liquid forces 66
- Wang and Dhir 351
- wave crest stripping 217
- wave crests stripping 233, 235
- wavy film 629
- weighted mean velocity 119–120
- weighting factors 650
- Wigner cell 668
- work reduction factor 353
  
- Zaichik 152
- Zuber and Findlay model 120